DUDER-
STADT

NUCLEAR
REACTOR
ANALYSIS

# Nuclear Reactor Analysis

**James J. Duderstadt**

**Louis J. Hamilton**

Department of Nuclear Engineering
*The University of Michigan*
*Ann Arbor, Michigan*

Printed in the United States of America

10 9 8 7 6

## BOARD OF ADVISORS, ENGINEERING

*A. H-S. Ang*
University of Illinois

Civil Engineering—Systems and Probability

*Donald S. Berry*
Northwestern University

Transportation Engineering

*James Gere*
Stanford University

Civil Engineering and Applied Mechanics

*J. Stuart Hunter*
Princeton University

Engineering Statistics

*T. William Lambe*
*R. V. Whitman*
Massachusetts Institute of Technology

Civil Engineering—Soil Mechanics

*Perry L. McCarty*
Stanford University

Environmental Engineering

*Don T. Phillips*
Purdue University

Industrial Engineering

*Dale F. Rudd*
University of Wisconsin

Chemical Engineering

*Robert F. Steidel, Jr.*
University of California—Berkeley

Mechanical Engineering

*Richard N. White*
Cornell University

Civil Engineering—Structures

*To Anne and Jacqueline*

# Preface

The maturation of the nuclear power industry, accompanied by a redirection in emphasis from research and development to the large-scale installation of nuclear power systems, has induced a corresponding change in the growing demand for well-trained nuclear engineers. Earlier laboratory needs for research-oriented Ph. D. reactor physicists have been largely replaced by industrial requirements for more broadly trained nuclear engineers at the B. S. and M. S. levels who are capable of designing, constructing, and operating large nuclear power systems. Most universities are rapidly reorienting their own nuclear engineering programs in response to these changes.

Of central importance in such programs are those introductory courses in nuclear reactor analysis that first introduce the nuclear engineering student to the basis scientific principles of nuclear fission chain reactions and lay a foundation for the subsequent application of these principles to the nuclear design and analysis of reactor cores. Although several excellent texts have been written on the subject of nuclear reactor theory, we have found both the material and orientation of existing treatments somewhat outdated for today's nuclear engineering student. For example, the availability of large fast digital computers has had a very strong influence on the analytical techniques used in modern nuclear reactor design. In most cases such modern methods of reactor analysis bear little resemblance to the precomputer techniques of earlier years. And yet most existing texts on nuclear reactor theory dwell quite heavily on these outdated techniques, stressing analytical methods to the near exclusion of numerical techniques and digital computation.

Furthermore most introductory texts on nuclear reactor theory present a rather narrow view of nuclear reactor analysis by concentrating only on the behavior of the neutron population in the reactor core. However the neutronics analysis of a reactor core cannot be divorced from other nonnuclear aspects of core analysis such as thermal-hydraulics, structural design, or economic considerations. In any

practical design study, the interplay between these various facets of reactor analysis must be taken into account, and this should be reflected in modern nuclear engineering education programs.

We have attempted to write a reactor analysis text more tailored to the needs of the modern nuclear engineering student. In particular, we have tried to introduce the student to the fundamental principles governing nuclear fission chain reactions in a manner that renders the transition to practical nuclear reactor design methods most natural. This goal has led to a very considerable emphasis on numerical methods suitable for digital computation. We have also stressed throughout this development the very close interplay between the nuclear analysis of a reactor core and those nonnuclear aspects of core analysis, such as thermal-hydraulics or materials studies, which play a major role in determining a reactor design. Finally, we have included illustrations of the various concepts that we develop by considering a number of more practical problems arising in the nuclear design of various types of power reactors.

The text has been organized into four parts. In Part 1 we present a relatively elementary and qualitative discussion of the basic concepts involved in nuclear fission chain reactions, including a brief review of the relevant nuclear physics and a survey of modern power reactors. In Part 2 we develop in some detail a particularly simple and useful model of nuclear reactor behavior by assuming that the neutrons sustaining the fission chain reaction diffuse from point to point in the reactor in such a way that their energy and direction of motion can be ignored (one-speed diffusion theory). In Part 3 we generalize this model to develop the primary tool of nuclear reactor analysis, multigroup diffusion theory. In Part 4 we illustrate these methods of nuclear reactor analysis by considering several important applications in nuclear reactor design.

We include a wide variety of problems to further illustrate these concepts, since we have learned by past experience that such problems are essential for and adequate understanding of nuclear reactor theory. The degree of difficulty spanned by the problems is enormous, ranging from simple formula substitution to problems requiring extensive outside reading by the student. Since most universities have at their disposal large time-sharing computer systems, we have not hesitated to include problems that require rudimentary programming experience as well as access to digital computers. Also, since more and more nuclear engineering programs have access to libraries of the more common reactor design computer codes, we also include problems utilizing such codes. It is our hope that the volume and variety of problems are sufficient to provide the instructor with the opportunity to select those problems most appropriate to this particular needs.

The same broad scope also characterizes the material included in the text. We have attempted to prepare a text suitable for a wide variety of students, including not only senior-year B. S. or first-year M. S. nuclear engineering students, but for students from other disciplines as well, such as electrical and mechanical engineering, physics, and chemistry, who desire an exposure to the principles underlying nuclear reactor design and operation. Hence the text has been written with the intent of providing suitable material for a student with only a modest background in modern physics and applied mathematics, such as would be included in the curriculum of most undergraduate engineering or science students. To this end, much of the early material is presented in an essentially self-contained fashion.

However it is our intent that this text should also serve as a useful reference in more advanced courses or for practicing engineers, and therefore we include more advanced material when appropriate (particularly in later chapters). In such cases we provide numerous references to supplement our treatment. Certainly the entirety of the material presented would be overwhelming for a one- or even two-term course. (We have distributed the material among three terms at Michigan.) Rather we have sought to provide a text sufficiently flexible for a wide variety of applications. Hence we do not apologize for the scope and occasionally more rugged terrain covered by the text, since the instructor can always choose a less demanding route by selecting an appropriate subset of this material.

The units employed in this text are the International System of Units (SI), their derivatives, and several non-SI units (such as the electronvolt or the barn) which are recognized by the International Organization for Standardization for use in special fields. Unfortunately, the vast majority of nuclear engineering literature published in the United States prior to 1975 makes use of British units. To assist the reader in coordinating this literature with the SI units used in this text, we have included brief tables of the appropriate conversion factors in Appendix I.

As with any text at this level, very little of the material presented has originated with the authors, but rather has been accumulated and assimilated from an enormous variety of sources, some published, many unpublished. We generally attempt to present material in the fashion we have found most successful from our own teaching experience, frequently sacrificing originality for effectiveness of presentation. Throughout the text we attempt to acknowledge the sources of our material.

However, we would particularly like to acknowledge the impact made upon this work by several of our associates. In presentation, we have chosen to utilize the very appealing pedagogical approach of P. F. Zweifel by introducing as much of reactor analysis as possible within the one-speed diffusion approximation before continuing to discuss neutron energy-dependence. Our attempts to relate the basic concepts of nuclear reactor theory to practical reactor analysis have relied heavily upon numerous discussions, lecture materials, admonitions, and advice of Harvey Graves, Jr., to whom we are particularly grateful. We would also like to acknowledge the assistance of a group of truly exceptional former students (and now practicing nuclear engineers) including Thomas Craig, David Chapin, Lawrence Emmons, Robert Grossman, Ronald Fleming, Robert McCredy, William Martin, Philip Meyer, Sidney Karin, Russell Mosteller, William G. Price, Jr., Robert Steinke, and Paul J. Turinsky, as well as scores of other students who have suffered, sweated, and occasionally cursed their way through the many sets of lecture notes which led to this text.

It is particularly important to acknowledge the considerable assistance provided by other staff members at Michigan including A. Ziya Akcasu, David Bach, John Carpenter, Chihiro Kikuchi, Glenn Knoll, John Lee, Robert Martin, Richard K. Osborn, Fred Shure, and George C. Summerfield. Also we should acknowledge that much of the motivation and inspiration for this effort originated at Caltech with Harold Lurie and Noel Corngold and at Berkeley with Virgil Schrock. But, above all, we would like to thank William Kerr, without whose continued encouragement and support this work would have never been completed.

We also wish to express our gratitude to Miss Pam Hale for her Herculean

xii

efforts (and cryptographic abilities) in helping prepare the various drafts and manuscripts which led to this text.

*James J. Duderstadt*
*Louis J. Hamilton*

ANN ARBOR, MICHIGAN
FEBRUARY 1975

# Contents

**PART 1**

**Introductory Concepts
of Nuclear Reactor
Analysis**

# PART 2

## The One-Speed
## Diffusion Model
## of a Nuclear Reactor

# PART 3

## The Multigroup
## Diffusion Method

## PART 4

## An Introduction
## to Nuclear Reactor
## Core Design

# APPENDICES

# 1

# Introductory Concepts of Nuclear Reactor Analysis

# 1

# An Introduction to Nuclear Power Generation

It has been more than three decades since the first nuclear reactor achieved a critical fission chain reaction beneath the old Stagg Field football stadium at the University of Chicago. Since that time an extensive worldwide effort has been directed toward nuclear reactor research and development in an attempt to harness the enormous energy contained within the atomic nucleus for the peaceful generation of power. Nuclear reactors have evolved from an embryonic research tool into the mammoth electrical generating units that drive hundreds of central-station power plants around the world today. The recent shortage of fossil fuels has made it quite apparent that nuclear fission reactors will play a dominant role in meeting man's energy requirements for decades to come.

For some time electrical utilities have been ordering and installing nuclear plants in preference to fossil-fueled units. Such plants are truly enormous in size, typically generating over 1000 MWe (megawatts-electric) of electrical power (enough to supply the electrical power needs of a city of 400,000 people) and costing more than one billion dollars. It is anticipated that some 500 nuclear power plants will be installed in the United States alone by the year 2000 with an electrical generating capacity of about 500,000 MWe and a capital investment of more than $600 billion,[1] with this pattern being repeated throughout the world. The motivation for such a staggering commitment to nuclear power involves a number of factors that include not only the very significant economic and operational advantages exhibited by nuclear plants over conventional sources of power, but their substantially lower environmental impact and vastly larger fuel resources as well.[2-7]

The dominant role played by nuclear fission reactors in the generation of electrical power can be expected to continue well into the next century. Until at least A.D. 2000, nuclear power will represent the only viable alternative to

fossil-fueled plants for most nations.[2,3] The very rapid increase in fossil-fuel costs that has accompanied their dwindling reserves has led to a pronounced cost advantage for nuclear plants which is expected to widen even further during the next few decades.[4,6] Of course, there are other longer-range alternatives involving advanced technology such as solar power, geothermal power, and controlled thermonuclear fusion. However the massive practical implementation of such alternatives, if proven feasible, could probably not occur until after the turn of the century since experience has shown that it takes several decades to shift the energy industry from one type of fuel to another,[2] due both to the long operating lifetime of existing power machinery and the long lead times needed to redirect manufacturing capability. Hence nuclear fission power will probably be the dominant new source of electrical power during the productive lifetimes of the present generation of engineering students.

## I. NUCLEAR FISSION REACTORS

The term *nuclear reactor* will be used in this text to refer to devices in which controlled nuclear fission chain reactions can be maintained. (This restricted definition may offend that segment of the nuclear community involved in nuclear fusion research, but since even a prototype nuclear fusion reactor seems several years down the road, no confusion should result.) In such a device, neutrons are used to induce nuclear fission reactions in heavy nuclei. These nuclei fission into lighter nuclei (*fission products*), accompanied by the release of energy (some 200 MeV per event) plus several additional neutrons. These *fission neutrons* can then be utilized to induce still further fission reactions, thereby inducing a chain of fission events. In a very narrow sense then, a nuclear reactor is simply a sufficiently large mass of appropriately fissile material (e.g., $^{235}U$ or $^{239}Pu$) in which such a controlled fission chain reaction can be sustained. Indeed a small sphere of $^{235}U$ metal slightly over 8 cm in radius could support such a chain reaction and hence would be classified as a nuclear reactor.

However a modern power reactor is a considerably more complex beast. It must not only contain a lattice of very carefully refined and fabricated nuclear fuel, but must as well provide for cooling this fuel during the course of the chain reaction as fission energy is released, while maintaining the fuel in a very precise geometrical arrangement with appropriate structural materials. Furthermore some mechanism must be provided to control the chain reaction, shield the surroundings of the reactor from the intense nuclear radiation generated during the fission reactions, and provide for replacing nuclear fuel assemblies when the fission chain reaction has depleted their concentration of fissile nuclei. If the reactor is to produce power in a useful fashion, it must also be designed to operate both economically and safely. Such engineering constraints render the actual nuclear configuration quite complex indeed (as a quick glance ahead to the illustrations in Chapter 3 will indicate).

Nuclear reactors have been used for over 30 years in a variety of applications. They are particularly valuable tools for nuclear research since they produce copious amounts of nuclear radiation, primarily in the form of neutrons and gamma rays. Such radiation can be used to probe the microscopic structure and dynamics of matter (neutron or gamma spectroscopy).

The radiation produced by reactors can also be used to transmute nuclei into artificial isotopes that can then be used, for example, as radioactive tracers in industrial or medical applications. Reactors can use the same scheme to produce nuclear fuel from nonfissile materials. For example, $^{238}U$ can be irradiated by neutrons in a reactor and transmuted into the nuclear fuel $^{239}Pu$. This is the process utilized to "breed" fuel in the fast breeder reactors currently being developed for commercial application in the next decade.

Small, compact reactors have been used for propulsion in submarines, ships, aircraft, and rocket vehicles. Indeed the present generation of light water reactors used in nuclear power plants are little more than the very big younger brothers of the propulsion reactors used in nuclear submarines. Reactors can also be utilized as small, compact sources of long-term power, such as in remote polar research stations or in orbiting satellites.

Yet by far the most significant application of nuclear fission reactors is in large, central station power plants. A nuclear power plant is actually very similar to a fossil-fueled power plant, except that it replaces the coal or oil-fired boiler by a nuclear reactor, which generates heat by sustaining a fission chain reaction in a suitable lattice of fuel material. Of course, there are some dramatic differences between a nuclear reactor and, say, a coal-fired boiler. However the useful quantity produced by each is high temperature, high pressure steam that can then be used to run turbogenerators and produce electricity. At the center of a modern nuclear plant is the nuclear steam supply system (NSSS), composed of the nuclear reactor, its associated coolant piping and pumps, and the heat exchangers ("steam generators") in which water is turned into steam. (A further glance at the illustrations in Chapter 3 will provide the reader with some idea of these components.) The remainder of the power plant is rather conventional.

Yet we must not let the apparent similarities between nuclear and fossil-fueled power plants overshadow the very significant differences between the two systems. For example, in a nuclear plant sufficient fuel must be inserted into the reactor core to allow operation for very long periods of time (typically one year). The nuclear fuel cycle itself is extremely complex, involving fuel refining, fabrication, reprocessing after utilization in the reactor, and eventually the disposal of radioactive fuel wastes. The safety aspects of nuclear plants are also quite different, since one must be concerned with avoiding possible radiological hazards. Furthermore the licensing required by a nuclear plant before construction or operation demands a level of sophisticated analysis totally alien to fossil-fueled plant design.

Therefore even though the NSSS contributes only a relatively modest fraction of the total capital cost of a nuclear power plant (presently about 20%), it is of central concern since it not only dictates the detailed design of the remainder of the plant, but also the procedures required in plant construction and operation. Furthermore it is the low fuel costs of the NSSS that are responsible for the economic advantages presently enjoyed by nuclear power generation.

The principal component of the NSSS is, of course, the nuclear reactor itself. A rather wide variety of nuclear reactors are in operation today or have been proposed for future development. Reactor types can be characterized by a number of features. One usually distinguishes between those reactors whose chain reactions are maintained by neutrons with characteristic energies comparable to the energy of thermal vibration of the atoms comprising the reactor core (*thermal reactors*) and reactors in which the average neutron energy is more characteristic of the

much higher energy neutrons released in a nuclear fission reaction (*fast reactors*).

Yet another common distinction refers to the type of coolant used in the reactor. In the United States, and indeed throughout the world, the most popular of the present generation of reactors, the light water reactor (LWR) uses ordinary water as a coolant. Such reactors operate at very high pressures (approximately 70–150 bar) in order to achieve high operating temperatures while maintaining the water in its liquid phase. If the water is allowed to boil in the core, the reactor is referred to as a boiling water reactor (BWR), while if the system pressure is kept sufficiently high to prevent bulk boiling (155 bar), the reactor is known as a pressurized water reactor (PWR). Such reactors have benefited from a well-developed technology and performance experience achieved in the nuclear submarine program.

A very similar type of reactor uses heavy water ($D_2O$) either under high pressure as a primary coolant or simply to facilitate the fission chain reaction. This particular concept has certain nuclear advantages that allow it to utilize low-enrichment uranium fuels (including natural uranium). It is being developed in Canada in the CANDU series of power reactors and in the United Kingdom as steam generating heavy water reactors (SGHWR).

Power reactors can also utilize gases as coolants. For example, the early MAGNOX reactors developed in the United Kingdom used low-pressure $CO_2$ as a coolant. A particularly attractive recent design is the high-temperature gas-cooled reactor (HTGR) manufactured in the United States which uses high-pressure helium. Related gas-cooled reactors include the pebble-bed concept and the advanced gas cooled reactors (AGR) under development in Germany and the United Kingdom, respectively.

All of the above reactor types can be classified as thermal reactors since their fission chain reactions are maintained by low-energy neutrons. Such reactors comprise most of the world's nuclear generating capacity today, and of these the LWR is most common. It is generally agreed that the LWR will continue to dominate the nuclear power industry until well into the 1980s, although its market may tend to be eroded somewhat by the successful development of the HTGR or advanced heavy water reactors.

However as we will see in the next chapter, there is strong incentive to develop a fast reactor which will breed new fuel while producing power, thereby greatly reducing nuclear fuel costs. Such fast breeder reactors may be cooled by either liquid metals [the liquid metal-cooled fast breeder reactor (LMFBR)] or by helium [the gas-cooled fast breeder reactor (GCFR)]. Although fast breeder reactors are not expected to make an appreciable impact on the nuclear power generation market until after 1990, their development is actively being pursued throughout the world today.

Numerous other types of reactors have been proposed and studied—some even involving such exotic concepts as liquid or gaseous fuels. Although much of the analysis presented in this text is applicable to such reactors, our dominant concern is with the solid-fuel reactors cooled by either water, sodium, or helium, since these will comprise the vast majority of the power reactors installed during the next several decades.

## II. ROLE OF THE NUCLEAR ENGINEER

The nuclear engineer will play a very central role in the development and application of nuclear energy since he is uniquely characterized by his ability to

assist in both the nuclear design of fission reactors and their integration into large power systems. In the early days of the reactor industry a nuclear engineer was usually regarded as a Ph. D.-level reactor physicist primarily concerned with nuclear reactor core research and design. Today, however, nuclear engineers are needed not only by research laboratories and reactor manufacturers to develop and design nuclear reactors, but also by the electrical utilities who buy and operate the nuclear power plants, and by the engineering companies who build the power plants and service them during their operating lifetimes.

Hence an understanding of core physics is not sufficient for today's nuclear engineer. He must also learn how to interface his specialized knowledge of nuclear reactor theory with the myriad of other engineering demands made upon a nuclear power reactor and with a variety of other disciplines, including mechanical, electrical, and civil engineering, metallurgy, and even economics (and politics), just as specialists of these other disciplines must learn to interact with nuclear engineers. In this sense, he must recognize that the nuclear analysis of a reactor is only one facet to be considered in nuclear power engineering. To study and master it outside of the context of these other disciplines would be highly inadvisable. In the same sense, those electrical, mechanical, or structural engineers who find themselves involved in various aspects of nuclear power station design (as ever increasing numbers are) will also find some knowledge of nuclear reactor theory useful in the understanding of nuclear components and interfacing with nuclear design.

Future nuclear engineers must face and solve complex problems such as those involved in nuclear reactor safety, environmental impact assessment, nuclear power plant reliability, and the nuclear fuel cycle, which span an enormous range of disciplines. They must always be concerned with the economic design, construction, and operation of nuclear plants consistent with safety and environmental constraints. An increasing number of nuclear engineers will find themselves concerned with activities such as quality assurance and component standardization as the nuclear industry continues to grow and mature, and of course all of these problems must be confronted and handled in the public arena.

## III. SCOPE OF THE TEXT

Our goal in this text is to develop in detail the underlying theory of nuclear fission reactors in a manner accessible to both prospective nuclear engineering students and those engineers from other disciplines who wish to gain some exposure to nuclear reactor engineering. In every instance we attempt to begin with the fundamental scientific principles governing nuclear fission chain reactions and then carry these fundamental concepts through to the level of realistic engineering applications in nuclear reactor design. During this development we continually stress the interplay between the nuclear analysis of a reactor core and the parallel nonnuclear design considerations that must accompany it in any realistic nuclear reactor analysis.

We must admit a certain preoccupation with nuclear power reactors simply because most nuclear engineers will find themselves involved in the nuclear power industry. This will be particularly apparent in the examples we have chosen to discuss and the problems we have emphasized. However since our concern is always with emphasis of fundamental concepts over specific applications, most of the topics we develop have a much broader range of validity and would apply

equally well to the analysis of other types of nuclear reactors. And although our principal target is the prospective nuclear engineer, we would hope that engineers from other disciplines would also find this text useful as an introduction to the concepts involved in nuclear reactor analysis.

The present text develops in four progressive stages. Part 1 presents a very brief introduction to those concepts from nuclear physics relevant to nuclear fission reactors. These topics include not only a consideration of the nuclear fission process itself, but also a consideration of the various ways in which neutrons, which act as the carrier of the chain reaction, interact with nuclei in the reactor core. We next consider from a qualitative viewpoint the general concepts involved in studying nuclear chain reactions. Part 1 ends with an overview of nuclear reactor engineering, including a consideration of the various types of modern nuclear reactors, their principal components, and a qualitative discussion of nuclear reactor design.

Parts 2–4 are intended to develop the fundamental scientific principles underlying nuclear reactor analysis and to apply these principles for derivation of the most common analytical tools used in contemporary reactor design. By way of illustration, these tools are then applied to analyze several of the more common and significant problems facing nuclear engineers.

Part 2 develops the mathematical theory of neutron transport in a reactor. It begins with the most general description based on the neutron transport equation and briefly (and *very* qualitatively) reviews the standard approximations to this equation. After this brief discussion, we turn quickly to the development of the simplest nontrivial model of a nuclear fission reactor, that based upon one-speed neutron diffusion theory. This model is used to analyze both the steady state and time-dependent behavior of nuclear reactors, since although the model has very limited validity in practical reactor analysis, it does illustrate most of the concepts as well as the calculational techniques used in actual reactor design.

In Part 3, we develop the principal tool of modern nuclear reactor design, the multigroup diffusion model. Particular attention is devoted to the calculation of the multigroup constants appearing in these equations, as well as to the practical numerical solution of the equations themselves.

In Part 4, we attempt to give an overview of the methods used in nuclear reactor core design. In particular, we consider the application of the concepts and tools developed in the earlier sections to a variety of problems faced by the nuclear engineer, including criticality calculations, the determination of core power distributions and thermal-hydraulics analysis, burnup and control studies, and fuel-loading requirements. While certainly incomplete, we do feel that the problems we have chosen to examine are representative of those encountered in nuclear reactor design and serve to illustrate the concepts developed in the earlier chapters of the text.

## REFERENCES

1. *The Nuclear Industry*, USAEC Report WASH-1174–73, 1973. The USAEC publishes an annual report on the status of private nuclear industry within the United States. These reports provide a very comprehensive survey of the growth of the nuclear power industry.
2. Chauncey Starr, *Sci. Amer.* 225, 39 (1971).
3. Fourth International Conference on the Peaceful Uses of Atomic Energy (International Atomic Energy Agency, Geneva, 1972), Vol. 1.

4. A study of base-load alternatives for the Northeast Utilities System, Report to the Board of Trustees of Northeast Utilities, Arthur D. Little, Inc. (1973).
5. Nuclear Fuel Resources and Requirements, USAEC Report WASH-1243 (1973); *Nucl. Ind.* **21** (2) (1974); *Nucl. News* **17**, (5) (1974).
6. David J. Rose, *Science* **184**, 351 (1974).
7. An Assessment of Accident Risks in U. S. Commercial Nuclear Power Plants, USAEC Report WASH-1400 (1974).

Most current information concerning the nuclear power industry appears in a number of journal publications. Although the number of journals appearing in the field of nuclear science and engineering is quite voluminous, a brief list of journals of more general interest would include:

*Nuclear Engineering International* (Europressatom): A British journal distinguished by its elaborate, multicolored diagrams of nuclear power plants.

*Nuclear Industry* (Atomic Industrial Forum): A monthly news magazine written more from the viewpoint of the consumer of nuclear power products—namely, the electrical utilities.

*Nuclear News* (American Nuclear Society): A monthly news magazine published by the American Nuclear Society, the principal technical organization of nuclear engineering in the United States.

*Nuclear Safety* (Office of Information Services, U. S. Atomic Energy Commission): A journal highlighting recent developments in the field of nuclear reactor safety.

*Nuclear Science and Engineering* (American Nuclear Society): The principal technical research journal of nuclear engineering.

Other more research-oriented journals in the field of nuclear science and engineering include:

*Annals of Nuclear Science and Engineering* (formerly *Journal of Nuclear Energy*) (Pergamon, New York).

*Journal of Nuclear Science and Technology* (Atomic Energy Society of Japan).

*Nuclear Engineering and Design* (North-Holland, Amsterdam).

*Nuclear Technology* (American Nuclear Society).

*Soviet Atomic Energy* (Consultant's Bureau).

References on nuclear reactor theory include:

Bell, G. I., and Glasstone, S., *Nuclear Reactor Theory*, Reinhold, New York (1970).

Henry, Allan F., *Nuclear Reactor Analysis*, M.I.T. Press, Cambridge, Mass. (1975).

Glasstone, S. and Edlund, M. C., *The Elements of Nuclear Reactor Theory*, Reinhold, New York (1952).

Glasstone, S. and Sesonske, A., *Nuclear Reactor Engineering*, 2nd Edition, Van Nostrand, Princeton, N.J. (1975).

Lamarsh, J. R., *Introduction to Nuclear Reactor Theory*, Addison-Wesley, Reading, Mass. (1966).

Lamarsh, John R., *Introduction to Nuclear Engineering*, Addison-Wesley, Reading, Mass. (1975).

Meghreblian, R. V. and Holmes, D. K., *Reactor Analysis*, McGraw-Hill, New York (1960).

Murray, Raymond L., *Nuclear Energy*, Pergamon Press, New York (1975).

Weinberg, A. M. and Wigner, E. P., *The Physical Theory of Neutron Chain Reactors*, Chicago U. P. (1958).

Zweifel, P. F., *Reactor Physics*, McGraw-Hill, New York (1973).

# 2

## The Nuclear Physics of Fission Chain Reactions

The primary objective in the design and operation of a nuclear reactor is the utilization of the energy or radiation released by a controlled chain reaction of *nuclear fission* events maintained within the reactor core. Such fission reactions occur when a heavy atomic nucleus such as $^{235}U$ splits or fissions into two lighter nuclei with an attendant release of both energy and radiation. Yet just how are such fission reactions induced in a reactor? The rate at which such naturally occurring heavy nuclei will fission on their own (*spontaneous fission*) is very slow. It should also be apparent that one cannot simply smash two nuclei together to induce such a reaction, since the large electrical charges of heavy nuclei would lead to a very strong repulsion. A more attractive idea is to slam a neutral particle (which doesn't feel the nuclear charge) into a big, "overweight" nucleus and hope that this splits it. An ideal candidate for the incident particle is the neutron. Indeed experiments have shown that certain nuclei have an enormous appetite for neutrons, but after swallowing them suffer a case of violent indigestion that results in their fission. As an example of such a reaction, consider a neutron incident upon a $^{235}U$ nucleus:

$$Neutron + {}^{235}U \rightarrow fission\ products + more\ neutrons + energy.$$

The products of such a reaction (e.g., lighter nuclei, neutrons, and gammas) emerge with very large kinetic energy (some 200 MeV) which is then converted into heat as they slow down by banging into neighboring atoms in the reactor fuel. It is this heat energy that one utilizes to produce steam and eventually electrical power in a nuclear power plant.

Yet just as significantly the fission reaction kicks loose a few neutrons that may then go on to induce more fission reactions. Hence we can use the neutrons to

propagate a *chain* of fission reactions. In this sense, then, the neutron plays the role of the *chain carrier* while the fission reactions supply the desired energy.

However there are other possible nuclear reactions a neutron can undergo that do not lead to fission and hence are unproductive in nature. Indeed since there are usually two or three neutrons emitted in each fission reaction, it should be apparent that if each neutron resulted in another fission, the chain reaction would quickly grow without bound. One such parasitic reaction involves the capture of the neutron by a nucleus which then emits a gamma ray rather than fissioning. Another possible reaction involves the neutron simply bouncing or scattering off of a nucleus. After several such scattering reactions, the neutron might eventually leak out of the uranium core of the reactor. Such processes remove neutrons from the reactor and tend to inhibit the chain reaction.

Therefore one of the primary tasks of the nuclear engineer is to follow the neutron "economy" in a nuclear reactor in order to monitor and control the behavior of the fission chain reaction. That is, he must learn how to design the reactor so that there is a balance between the production of neutrons in fission reactions and the loss of neutrons due to capture or leakage. The study of such processes is known as either *nuclear reactor theory*, *nuclear reactor physics* or sometimes simply as *neutronics*. It is essentially the subject of this text.

However the achievement of a stable chain of fission reactions is only a part of the responsibility of the nuclear engineer. In addition he must learn how to extract and use the energy liberated in these fission reactions. This task involves the subjects of heat transfer, fluid flow, structural and materials analysis, and power systems analysis and interacts strongly with the nuclear analysis of a reactor core. It is discussed in the latter chapters of the text.

We first turn our attention to a development of the fundamental concepts involved in predicting the distribution of neutrons in a nuclear reactor in order to understand and design a fission chain reaction system. We need to consider essentially two different subjects: (a) the determination of the probabilities of occurrence of various neutron–nuclear reactions and (b) the derivation and solution of an equation that uses these probabilities to determine the neutron density and fission reaction rate in a nuclear reactor core.

The above discussion clearly indicates the importance of being able to determine the rate at which various types of neutron–nuclear reactions occur within the reactor. However it is important to keep in mind that there are enormous numbers of neutrons (typically $10^8$ per $cm^3$) and even larger numbers of nuclei ($10^{22}$ per $cm^3$) in the reactor core. Hence we really need concern ourselves only with the average behavior of the neutrons and nuclei in the reactor in a statistical sense. That is, we wish to calculate the *probabilities* that various types of neutron–nuclear interactions will occur. These reaction probabilities are expressed in terms of parameters called *nuclear cross sections*.

These cross sections represent the fundamental data utilized by the nuclear engineer in his analysis of a nuclear reactor, much in the same way that thermal or structural data are used by the mechanical engineer or circuit device parameters are used by the electrical engineer. Hence some familiarity with the physics underlying the determination and behavior of such cross sections is necessary for effective nuclear reactor analysis.

In this chapter we will review those aspects of nuclear physics that are particularly relevant to the study of fission chain reactions. It should be stressed that this

presentation is not intended to be complete. Indeed we would anticipate that most engineering students will have had some exposure to modern atomic and nuclear physics in earlier courses. (Students who find most of the material in this chapter to be totally alien territory would be well advised to consult one of the several excellent standard references on introductory nuclear physics[1-4] containing substantially more thorough discussions of these topics.) Unfortunately, however, most conventional treatments of these subjects do not place sufficient emphasis on the study of nuclear reactions in general, or neutron–nuclear reactions in particular, for our purposes (although there are several notable exceptions[5-6]).

We will begin with a brief introduction to spontaneous nuclear radioactive decay as an example of a nuclear reaction. We then consider nuclear collision reactions and introduce the concept of a nuclear cross section. Here we will devote particular attention to a qualitative discussion of cross sections characterizing neutron–nucleus reactions. Our final topic will be that of the nuclear fission reaction itself and the radiation emanating from such reactions.

## I. NUCLEAR REACTIONS

There are essentially two types of nuclear reactions of importance in the study of nuclear reactors: (a) spontaneous disintegrations of nuclei and (b) reactions resulting from the collision between nuclei and/or nuclear particles. An example of the first type of reaction would be the radioactive decay of fission products, since these are frequently unstable. Such disintegration reactions depend only on the properties of an individual nucleus. The neutron–nucleus collision events involved in the fission chain reaction are an example of the second type of reaction. These collision reactions depend not only on the properties of the colliding particles, for example, the neutron and the nucleus, but also the relative velocity with which they strike one another.

Before diving off into a discussion of nuclear reactions, let us first introduce some notation. We will denote the number of protons in an atomic nucleus by $Z$ (the *atomic number*), the number of neutrons by $N$, and the total number of nucleons (protons plus neutrons) by $A$ (the *mass number*). A specific nucleus will be denoted by a symbol such as $^A_Z X$, where $X$ is the chemical symbol for the atom of interest. For example, $^1_1 H$, $^{12}_6 C$, and $^{235}_{92} U$ are notations for three such nuclei. We will refer to various species of nuclei as *nuclides*. Nuclei characterized by the same atomic number $Z$ but different mass numbers $A$ are referred to as *isotopes* (e.g., $^{233}_{92} U$, $^{234}_{92} U$, $^{235}_{92} U$, and $^{238}_{92} U$). Since the nucleus is a quantum mechanical system, it may be found in any of a number of possible energy states. The general notation $^A_Z X$ refers to a nuclear ground state, while an asterisk is used to denote a nucleus in an excited state, $^A_Z X^*$. Long lived excited states of nuclei are referred to as nuclear *isomers* or *isomeric states* and are denoted by a superscript $m$ (e.g., $^{116m}_{49} In$).

### A. Radioactive Decay

Certain nuclei are unstable in the sense that they may spontaneously undergo a transformation into a different nuclide, usually accompanied by the emission of energetic particles. Such a spontaneous nuclear transformation is referred to as *radioactive decay*. The three most common types of radioactive decay found in

naturally occurring nuclides include *alpha decay*, in which the nucleus emits a helium nucleus $^4_2$He; *beta decay*, which corresponds to the conversion of a neutron in the nucleus into a proton, generally accompanied by the emission of an electron and a neutrino; and *gamma decay*, the transition of a nucleus from one excited state to a lower excited state with the accompanying emission of a photon. However other types of radioactive decay are possible in a nuclear reactor since many unstable nuclides are produced in fission which do not occur in nature. For example, certain nuclei such as $^{87}_{36}$Kr may decay by emitting a neutron. (We will later find that this particular type of decay process is extremely important for reactor operation.)

The fundamental law describing radioactive decay is based on the experimental observation that the probability that a nucleus will decay in a given time interval is essentially constant, independent of the age of the nucleus or its environment, dependent only on the type of the nucleus itself. Hence the time rate of change of the number of original nuclei of a given type must be proportional to the number of nuclei present at that time. Let us call the proportionality constant $\lambda$. Then if $N(t)$ is the number of original nuclei left at time $t$, we find

$$-\frac{dN}{dt} = \lambda N(t).$$ (2-1)

Here $\lambda$ is referred to as the *radioactive decay constant* characteristic of the nucleus and has units of inverse time. If we initially have $N_0$ nuclei present, then at any later time $t$ the number of nuclei present will be given by an exponential law:

$$N(t) = N_0 e^{-\lambda t}.$$ (2-2)

The rate at which nuclei are decaying is given by

$$\text{Rate} = \lambda N_0 e^{-\lambda t}.$$ (2-3)

From this time behavior, it is apparent that the probability that a given nucleus will decay in a time interval $t$ to $t + dt$ is just

$$p(t)dt = \lambda e^{-\lambda t} dt.$$ (2-4)

Since radioactive decay is a statistical phenomenon, we cannot predict with any certainty precisely when a given nucleus will decay. However we can calculate the *mean lifetime* $\bar{t}$ of the nucleus before decay using our expression for $p(t)$ from Eq. (2-4)

$$\bar{t} \equiv \int_0^\infty dt\, t\, p(t) = \lambda \int_0^\infty dt\, t\, e^{-\lambda t} = \frac{1}{\lambda}.$$ (2-5)

Hence on the average a given nucleus will decay after a time $1/\lambda$.

A closely related quantity is the length of time necessary for half of the original number of nuclei present to decay away. Such a time $T_{1/2}$ is referred to as *radioactive half-life* for the nucleus and can be calculated from its definition by noting

$$N(T_{1/2}) = N_0/2 = N_0 e^{-\lambda T_{1/2}},$$ (2-6)

or

$$T_{1/2} = \frac{\ln 2}{\lambda} = \frac{0.693}{\lambda}. \tag{2-7}$$

It is common practice to tabulate such radioactive half-lives of various unstable nuclei in preference to their mean lifetime $\bar{t}$ or decay constant $\lambda$.[8]
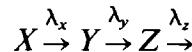
Yet another definition of some importance is that of the *activity* characterizing a sample of radioactive material. This quantity is simply the total number of disintegrations occurring per second $\lambda N(t)$. Activities are usually measured in units of *curies*, where one curie (Ci) is defined to be that quantity of radioactive nuclei for which the number of disintegrations per second is $3.70 \times 10^{10}$. (This is roughly the activity of 1 g of radium.)

Actually it is more common and far more useful to regard the dependent variable $N(t)$ as the atomic number density ($\#/cm^3$) of the nuclide of interest rather than the total number of nuclei present in the sample. We will adhere to this practice in our subsequent discussion.

Most radioactive decay processes are somewhat more complicated than those described by Eq. (2-1). For example, the decaying nuclide may itself be produced by some type of source, say, $R(t)$ nuclei/$cm^3 \cdot$sec. Then the nuclide balance equation becomes

$$\frac{dN}{dt} = -\lambda N(t) + R(t). \tag{2-8}$$

We can also write similar equations describing several nuclides, each of which decays into another. Consider, by way of example, the radioactive *decay chain*:

$$X \overset{\lambda_x}{\to} Y \overset{\lambda_y}{\to} Z \overset{\lambda_z}{\to}$$

Then the appropriate equations describing the number of nuclides of each type present are

$$\frac{dN_X}{dt} = -\lambda_X N_X + R_X,$$

$$\frac{dN_Y}{dt} = -\lambda_Y N_Y + \lambda_X N_X + R_Y, \tag{2-9}$$

$$\frac{dN_Z}{dt} = -\lambda_Z N_Z + \lambda_Y N_Y + R_Z,$$

where $R_X(t)$ is the production term for the $X$-nuclide, and so on. Since this is just a system of linear first-order differential equations with constant coefficients, it can easily be solved using standard techniques, and hence we will defer further discussion to the problems at the end of the chapter.

Very similar considerations also hold for the transition of nuclei between different excited states. Such states represent the quantum levels available to the nucleus. We can again characterize the probability that the nucleus will "decay" out of one excited state into a lower state by a decay constant $\lambda$, and once again also develop the concept of a mean lifetime for the excited state $\bar{t}$. A useful related

concept here is the uncertainty or *width* $\Gamma$ of the energy level characterizing the excited state. This width is related to the mean lifetime of the state by the Heisenberg uncertainty principle:

$$\Delta t \Delta E \gtrsim \hbar. \tag{2-10}$$

Hence the width of the state can be expressed in terms of its decay constant by
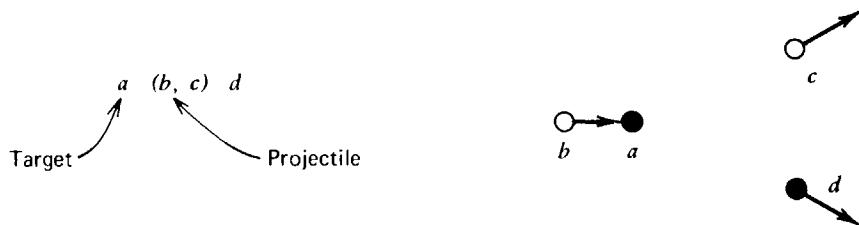
$$\Gamma = \Delta E \cong \hbar/\Delta t = \hbar\lambda. \tag{2-11}$$

## B. Nuclear Collision Reactions
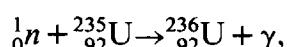
The study of nuclear collision reactions can be formulated in a manner very similar to that used to describe chemical reactions. Indeed, the familar notation for a chemical reaction

$$a + b \rightarrow c + d \tag{2-12}$$
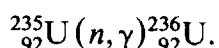
is frequently adopted to describe nuclear reactions. However since in nuclear reactions, one particle is usually considered to be a projectile while the other particle is taken as a target, one sometimes uses the more detailed notation



As an example, the reaction

$$_{0}^{1}n + _{92}^{235}U \rightarrow _{92}^{236}U + \gamma,$$

would be written as

$$_{92}^{235}U\,(n,\gamma)_{92}^{236}U.$$

The general class of such reactions would be simply denoted as $(n,\gamma)$ reactions.

Nuclear reactions are generally accompanied by either the absorption or emission of energy. One can calculate the energy released by (or required for) a given nuclear reaction by using the important result from the theory of relativity:

$$E = mc^2, \tag{2-13}$$

where $c$ is the speed of light and $m$ is the mass converted into energy in a reaction. The appropriate quantity to use for the variable $m$ that appears in this formula is the mass difference between the interacting particles before and after the collision.
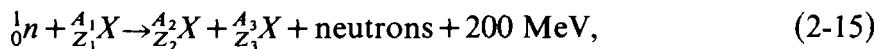
For the reaction $a(b,c)d$ we would calculate the reaction energy as

$$Q = [(M_a + M_b) - (M_c + M_d)]c^2. \qquad (2\text{-}14)$$
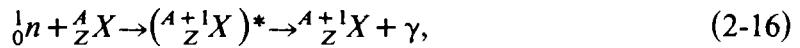
If $Q > 0$, then we say the reaction is *exothermic*, which corresponds to a release of energy in the reaction. If $Q < 0$, then the reaction is said to be *endothermic*, and energy must be supplied to the colliding nuclei in order to stimulate the reaction to occur. Obviously, nuclear fission is an example of an exothermic reaction.

There are a wide variety of possible nuclear reactions. The reactions of most interest in the analysis of a nuclear fission reactor involve interactions between neutrons and nuclei and include
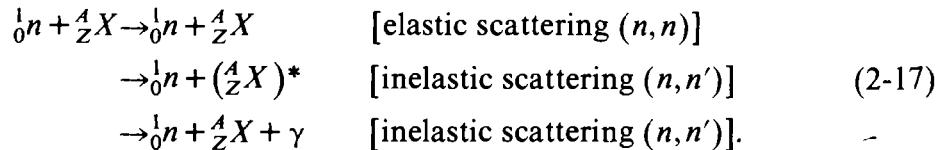
Nuclear fission $(n, \text{fission})$:

$$\frac{1}{0}n + \frac{A_1}{Z_1}X \rightarrow \frac{A_2}{Z_2}X + \frac{A_3}{Z_3}X + \text{neutrons} + 200 \text{ MeV}, \qquad (2\text{-}15)$$

Radiative capture $(n, \gamma)$:

$$\frac{1}{0}n + \frac{A}{Z}X \rightarrow (^{A+1}_{Z}X)^* \rightarrow ^{A+1}_{Z}X + \gamma, \qquad (2\text{-}16)$$

Scattering $(n, n)$ or $(n, n')$:

$$\frac{1}{0}n + \frac{A}{Z}X \rightarrow \frac{1}{0}n + \frac{A}{Z}X \qquad \text{[elastic scattering } (n,n)]$$

$$\rightarrow \frac{1}{0}n + (\frac{A}{Z}X)^* \qquad \text{[inelastic scattering } (n,n')] \qquad (2\text{-}17)$$

$$\rightarrow \frac{1}{0}n + \frac{A}{Z}X + \gamma \qquad \text{[inelastic scattering } (n,n')].$$

We have already discussed the nuclear fission reaction. In *radiative capture* the incident neutron is absorbed by the target nucleus to form a new nuclide of mass number $A + 1$. As we will see later, this "compound" nucleus is formed in an excited state. In a radiative capture reaction, it will eventually decay to its ground state by emitting a high-energy photon, that is, a gamma ray. An alternative type of capture reaction of some importance in reactor control is the $(n, \alpha)$ reaction which occurs in $^{10}_{5}B$, for example.

The third reaction of importance is *scattering*. In this reaction the neutron simply scatters off of the nucleus $(n, n)$, although in some cases, it may first combine with the nucleus to form a compound nucleus for a short time before being reemitted and will frequently leave the nucleus in an excited state from which it later decays by gamma emission.

The importance of the fission reaction to nuclear reactor operation is obvious. Both radiative capture and scattering are also extremely important since they influence the neutron economy and hence the chain reaction. We will concentrate specifically on neutron–nuclear reactions as we turn to a more quantitative treatment of nuclear reactions of importance in fission chain reactions.

## 1. MICROSCOPIC CROSS SECTIONS

The probability that a neutron–nuclear reaction will occur is characterized by a quantity called a *nuclear cross section*. Let us first define this quantity operation-

ally by considering a beam of neutrons, all traveling with the same speed and direction, which is incident normally upon and uniformly across the face of a target of material. If the target is sufficiently thin (say, one atomic layer thick), then no nuclei in the target will be shielded by other nuclei from the incident neutron beam (see Figure 2-1). In this case we would expect that the rate of neutron–nuclear reactions in the target will be proportional to both the incident neutron beam intensity $I$ (in units of number of neutrons/$cm^2 \cdot sec$) and the number of target atoms per unit area $N_A$ ($\#/cm^2$). If we call the constant of proportionality $\sigma$, we can write the rate at which reactions occur per unit area on the target as

$$\text{Rate} \equiv \underset{\left[\dfrac{\#}{cm^2 \cdot sec}\right]}{R} = \underset{[cm^2]}{\sigma} \quad \underset{\left[\dfrac{\#}{cm^2 \cdot sec}\right]}{I} \underset{\left[\dfrac{\#}{cm^2}\right]}{N_A}. \qquad (2\text{-}18)$$

We have indicated the units of each of these quantities since they imply that the proportionality factor $\sigma$ must have the units of an area.

If the incident neutrons and target nuclei could be visualized as classical particles, $\sigma$ would quite naturally correspond to the cross sectional area presented by each of the target nuclei to the beam. Hence $\sigma$ is known as the *microscopic cross section* characterizing the probability of a neutron–nuclear reaction for the nucleus. We might continue to think of $\sigma$ as the effective cross sectional area presented by the nucleus to the beam of incident neutrons. Since the nuclear radius is roughly $10^{-12}$ cm, the geometrical cross sectional area of the nucleus is roughly $10^{-24}$ $cm^2$. Hence we might expect that nuclear cross sections are of the order of $10^{-24}$ $cm^2$. In fact microscopic cross sections are usually measured in units of this size called *barns* (b). However this geometrical interpretation of a nuclear cross section can frequently be misleading since $\sigma$ can be much larger (or smaller) than the geometrical cross section of the nucleus due to resonance effects which, in turn, are a consequence of the quantum mechanical nature of the neutron and the nucleus. For example, the absorption cross section of $^{135}_{54}Xe$ for slow neutrons is almost one million times larger than its geometrical cross section.
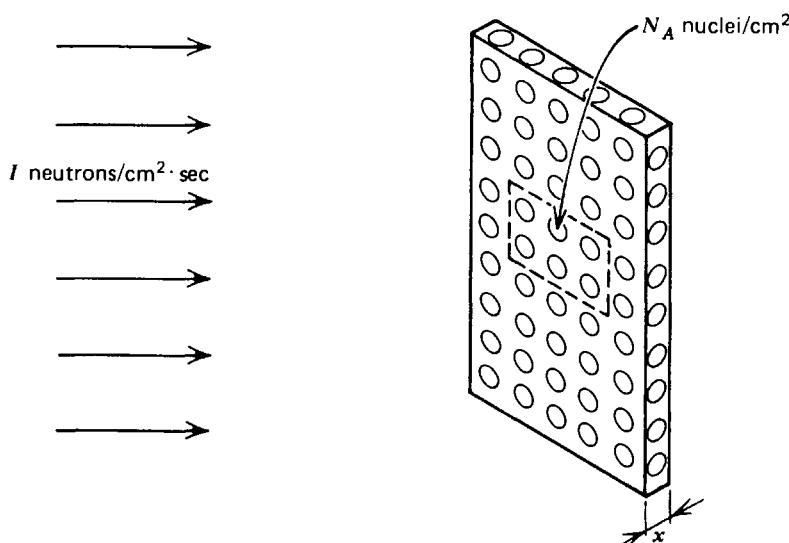


FIGURE 2-1.   A monoenergetic neutron beam incident normally upon a thin target.

We can give a slightly more formal definition of the microscopic cross section by rearranging Eq. (2-18) to write

$$\sigma = \frac{\text{Number of reactions/nucleus/sec}}{\text{Number of incident neutrons/cm}^2\text{/sec}} = \frac{(R/N_A)}{I} . \qquad (2\text{-}19)$$

In this sense, then, if the target has a total cross sectional area $\mathcal{C}$, all of which is uniformly exposed to the incident beam, then

$$\frac{\sigma}{\mathcal{C}} = \begin{array}{l}\text{Probability per nucleus that a neutron}\\ \text{in the beam will interact with it}\end{array} \qquad (2\text{-}20)$$

Thus far we have been discussing the concept of a nuclear cross section in a rather abstract sense without actually specifying the type of reaction we have in mind. Actually such cross sections can be used to characterize any type of nuclear reaction. We can define a microscopic cross section for each type of neutron-nuclear reaction and each type of nuclide. For example, the appropriate cross sections characterizing the three types of reactions we discussed earlier, fission, radiative capture, and scattering, are denoted by $\sigma_f$, $\sigma_\gamma$, and $\sigma_s$, respectively. We can also assign separate cross sections to characterize elastic scattering $\sigma_e$ in which the target nucleus remains in its ground state, and inelastic scattering $\sigma_{in}$ in which the target nucleus is left in an excited state. Since cross sections are related to probabilities of various types of reactions, it is apparent that

$$\sigma_s = \sigma_e + \sigma_{in}.$$

In a similar sense we can define the *absorption* cross section characterizing those events in which a nucleus absorbs a neutron. There are a number of possible types of absorption reactions including fission, radiative capture, $(n, \alpha)$ reactions, and so on. (Actually one could argue that fission is not really an absorption reaction since several neutrons are created in the fission reaction. It has become customary, however, to treat fission as an absorption event and then add back in the fission neutrons released in the reaction at another point, as we will see later.) Finally, we can introduce the concept of the *total* cross section $\sigma_t$ characterizing the probability that *any* type of neutron-nuclear reaction will occur. Obviously

$$\sigma_t = \sigma_s + \sigma_a = \sigma_e + \sigma_{in} + \sigma_f + \sigma_\gamma + \sigma_{n\alpha} + \cdots$$

A schematic diagram[9] of the heirarchy of cross sections along with their conventional notation is shown in Figure 2-2. Notice that in general one would define the absorption cross section to characterize any event other than scattering

$$\sigma_a = \sigma_t - \sigma_s.$$

In a similar fashion, one occasionally defines a *nonelastic* cross section as any event other than elastic scattering

$$\sigma_{ne} = \sigma_t - \sigma_e.$$

Thus far we have defined the concept of a microscopic cross section by considering a beam of neutrons of identical speeds incident normally upon the
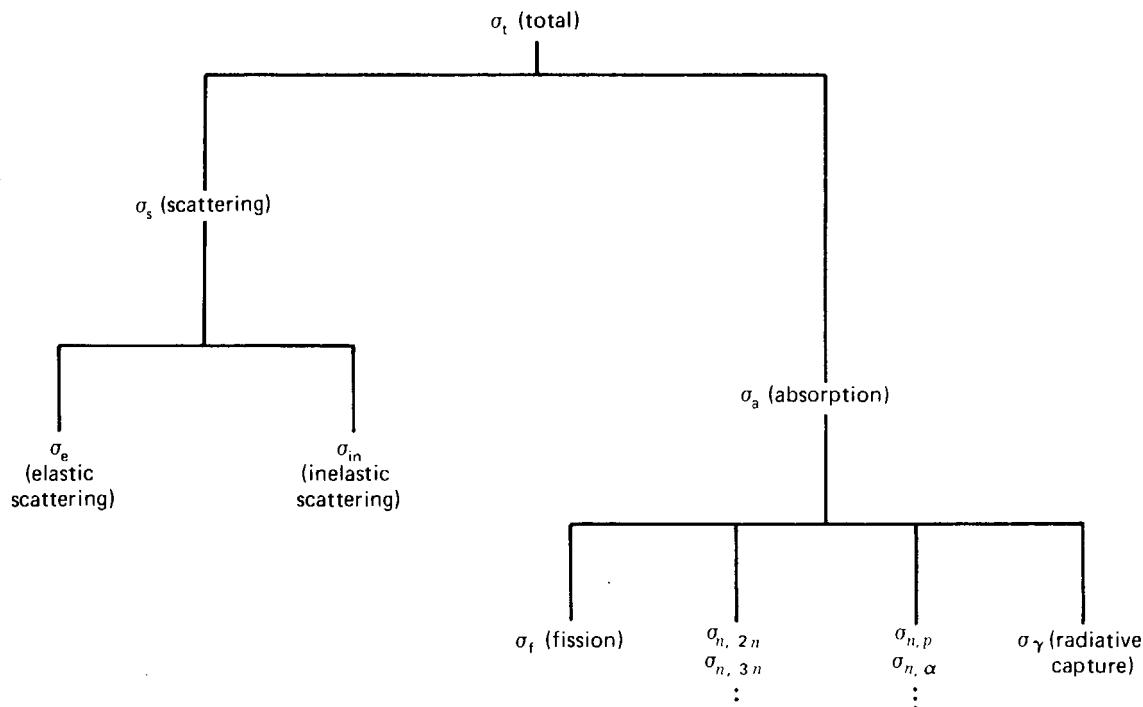
FIGURE 2-2. Neutron cross section heirarchy.

surface of a target. However it is certainly conceivable that such cross sections will vary, depending on the incident neutron speed (or energy) and direction. Indeed if the microscopic cross section for various incident neutron energies is measured, a very strong energy dependence of the cross section is found. The dependence of neutron cross sections on the incident beam angle is usually much weaker and can almost always be ignored in nuclear reactor applications. We will return later to consider in further detail the dependence of cross sections on incident neutron energy. First, however, it is useful to develop a quantity closely related to the microscopic cross section, that of the macroscopic cross section.

## 2. MACROSCOPIC CROSS SECTIONS

Thus far we have considered a beam of neutrons incident upon a very thin target. This was done to insure that each nucleus in the target would be exposed to the same beam intensity. If the target were thicker, the nuclei deeper within the target would tend to be shielded from the incident beam by the nuclei nearer the surface since interactions remove neutrons from the beam. To account for such finite thickness effects, let us now consider a neutron beam incident upon the surface of a target of arbitrary thickness as indicated schematically in Figure 2-3. We will derive an equation for the "virgin" beam intensity $I(x)$ at any point $x$ in the target. By virgin beam we are referring to that portion of the neutrons in the beam that have not interacted with target nuclei. Consider a differential thickness of target between $x$ and $x + dx$. Then since $dx$ is infinitesimally thin, we know that the results from our study of thin targets can be used to calculate the rate at which neutrons suffer interactions in $dx$ per $cm^2$. If we recognize that the number of target nuclei per $cm^2$ in $dx$ is given by $dN_A = N\,dx$, where $N$ is the number density of nuclei in the target, then the total reaction rate per unit area in $dx$ is just

$$dR = \sigma_t I\,dN_A = \sigma_t I N\,dx. \qquad (2\text{-}21)$$
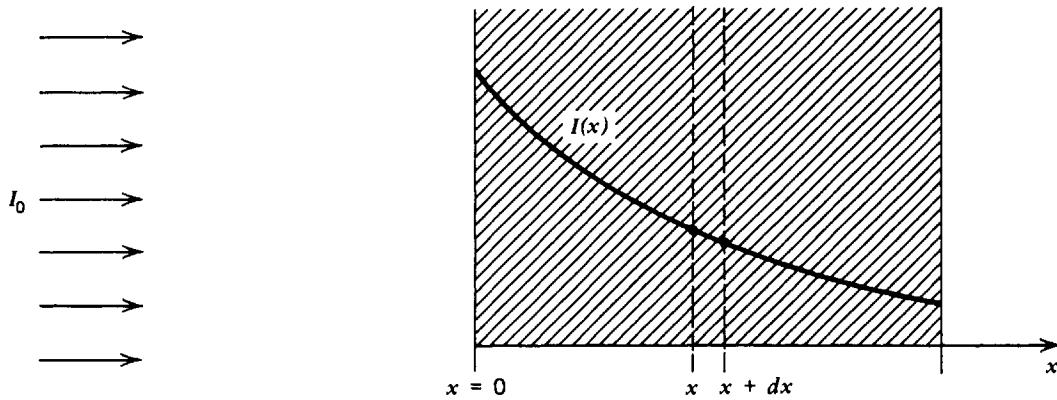
**FIGURE 2-3.** A monoenergetic neutron beam incident normally on a thick target.

Notice that, consistent with our prescription that *any* type of interaction will deflower an incident neutron, we have utilized the total microscopic cross section $\sigma_t$ in computing $dR$.

We can now equate this reaction rate to the decrease in beam intensity between $x$ and $x + dx$

$$-dI(x) = -[I(x + dx) - I(x)] = \sigma_t I N \, dx. \tag{2-22}$$

Dividing by $dx$ we find a differential equation for the beam intensity $I(x)$

$$\frac{dI}{dx} = -N\sigma_t I(x). \tag{2-23}$$

If we solve this equation subject to an incident beam intensity of $I_0$ at $x = 0$, we find an exponential attenuation of the incident beam of the form

$$I(x) = I_0 \exp(-N\sigma_t x). \tag{2-24}$$

The product of the atomic number density $N$ and the microscopic cross section $\sigma_t$ that appears in the exponential term arises so frequently in nuclear reactor studies that it has become customary to denote it by a special symbol:

$$\Sigma_t \equiv N\sigma_t = [\#/cm^3][cm^2] = [cm^{-1}]. \tag{2-25}$$

One refers to $\Sigma_t$ as the total *macroscopic cross section* characterizing the target material. The term "macroscopic" arises from the recognition that $\Sigma_t$ characterizes the probability of neutron interaction in a macroscopic chunk of material (the target), whereas the microscopic cross section characterizes the probability of interaction with only a single nucleus.

It should be noted that $\Sigma_t$ is not really a "cross section" at all, however, since its units are inverse length. A more appropriate interpretation can be achieved by reexamining Eq. (2-22) and noting that the fractional change in beam intensity occurring over a distance $dx$ is just given by

$$\frac{\left(\dfrac{-dI}{I}\right)}{dx} = \Sigma_t. \tag{2-26}$$

Hence, it is natural to interpret $\Sigma_t$ as the probability per unit path length traveled that the neutron will undergo a reaction with a nucleus in the sample. In this sense then

$$\exp(-\Sigma_t x) \equiv \text{probability that a neutron moves a distance } dx \text{ without any interaction;}$$

$$\Sigma_t \exp(-\Sigma_t x)\, dx \equiv \text{probability that a neutron has its first interaction in } dx$$
$$\equiv p(x)\, dx.$$

With this interaction probability, we can calculate the average distance a neutron travels before interacting with a nucleus in the sample

$$\bar{x} \equiv \int_0^\infty dx\, x p(x) \quad = \Sigma_t \int_0^\infty dx\, x \exp(-\Sigma_t x) \quad = \frac{1}{\Sigma_t}. \qquad (2\text{-}27)$$

It is customary to refer to this distance as the neutron *mean free path* since it essentially measures the average distance a neutron is likely to stream freely before colliding with a nucleus.

The reader has probably noticed the similarity of this analysis to our earlier treatment of radioactive decay. The spatial attentuation of a neutron beam passing through a sample of material and the temporal decay of a sample of radioactive nuclei are similar types of statistical phenomenon in which the probability of an event occurring that removes a neutron or nucleus from the original sample depends only on the number of neutrons or nuclei present at the position or time of interest. It should be stressed that both the mean free path and the mean lifetime for decay are very much average quantities. There will be statistical fluctuations about these mean values.

If we recall that $\Sigma_t$ is the probability per unit path length that a neutron will undergo a reaction, while the neutron speed $v$ is the distance traveled by the neutron in a unit time, then evidently

$$v\Sigma_t = \left[\frac{\text{cm}}{\text{sec}}\right][\text{cm}^{-1}] = [\text{sec}^{-1}] = \text{Frequency with which reactions occur.} \qquad (2\text{-}28)$$

This quantity is usually referred to as the *collision frequency* for the neutron in the sample. Its reciprocal, $[v\Sigma_t]^{-1}$, is therefore interpretable as the mean time between neutron reactions.

Thus far our discussion has been restricted to total macroscopic cross sections that characterize the probability that a neutron will undergo any type of reaction. We can generalize this concept by formally defining the macroscopic cross section for any specific reaction as just the microscopic cross section for the reaction of interest multiplied by the number density $N$ characterizing the material of interest. For example, the macroscopic fission cross section would be defined as

$$\Sigma_f \equiv N\sigma_f. \qquad (2\text{-}29)$$

In a similar fashion we can define

$$\Sigma_a \equiv N\sigma_a, \qquad \Sigma_s \equiv N\sigma_s. \qquad (2\text{-}30)$$

Notice also that

$$\Sigma_t = \Sigma_a + \Sigma_s. \tag{2-31}$$

It should be stressed that while one can formally define such macroscopic cross sections for specific reactions, our earlier discussion of neutron penetration into a thick target applies only to the total macroscopic cross section $\Sigma_t$. We could not extend this discussion, for example, to the calculation of the probability of neutron penetration to a depth $x$ prior to absorption by merely replacing $\Sigma_t$ in Eq. (2-24) by $\Sigma_a$, since it may be possible for the neutron to undergo a number of scattering reactions before finally suffering an absorption reaction. We can calculate these specific reaction probabilities only after a more complete consideration of neutron transport in materials (Chapters 4 and 5).

The concept of a macroscopic cross section can also be generalized to homogeneous mixtures of different nuclides. For example, if we have a homogeneous mixture of three different species of nuclide, $X$, $Y$, and $Z$, with respective atomic number densities $N_X$, $N_Y$, and $N_Z$, then the total macroscopic cross section characterizing the mixture is given by

$$\Sigma_t = N_X \sigma_t^X + N_Y \sigma_t^Y + N_Z \sigma_t^Z, \tag{2-32}$$

where $\sigma_t^X$ is the microscopic total cross section for nuclide $X$, and so on. It should be noted that such a prescription for determining the macroscopic cross section for a mixture arises quite naturally from our interpretation of such cross sections as probabilities of reactions.

As we mentioned earlier, all neutron–nuclear reaction cross sections (fission, radiative capture, scattering, etc.) depend to some degree on the energy of the incident neutron. If we denote the neutron energy by $E$, we acknowledge this dependence by including a functional dependence on $E$ in the microscopic cross section $\sigma(E)$ and hence by inference also in the macroscopic cross section $\Sigma(E)$.

However the macroscopic cross section can depend on additional variables as well. For example, suppose that the target material does not have a uniform composition. Then the number density $N$ will depend on the position r in the sample, and hence the macroscopic cross sections themselves will be space-dependent. In a similar manner, the number densities might depend on time— suppose, for example, that the nuclide of interest was unstable such that its number density was decaying as a function of time. Therefore in the most general case we would write

$$\Sigma(\mathbf{r}, E, t) = N(\mathbf{r}, t)\sigma(E) \tag{2-33}$$

to indicate the explicit dependence of the macroscopic cross section on neutron energy $E$, position r, and time $t$.

In summary then, nuclear cross sections can be used to characterize the probability of various types of neutron–nuclear reactions occurring. They obviously will be a very basic ingredient in any study of fission chain reactions. The determination of such cross sections is the task of the nuclear physicist and involves both experimental measurement and theoretical calculations. The enormous amount of cross section information required for nuclear reactor analysis is gathered by numerous nuclear research centers throughout the world. These cross section data

are compiled, evaluated, and then organized into data sets to be used by nuclear engineers. We will return in a later section to discuss in further detail such nuclear cross section data sets. For convenience, however, we have included in Appendix A a table of some of the more important cross sections characteristic of "thermal" neutrons—that is, of neutrons whose energies are comparable to the thermal energy of atoms in a reactor core at room temperature, $E = 0.025$ eV—which serves to illustrate typical orders of magnitudes of these quantities.

EXAMPLE: As a specific illustration, let us calculate the mean free path for a thermal neutron in graphite. According to the table in Appendix A, carbon is nearly a pure scatterer with microscopic cross sections $\sigma_s = 4.8$ b and $\sigma_a = 4.0 \times 10^{-3}$ b. If we assume a mass density of $1.60$ g/cm$^3$, we can calculate the atomic number density in graphite as $N = .0803 \times 10^{24}$ cm$^{-3}$. Consequently the macroscopic scattering and absorption cross sections are

$$\Sigma_s = N\sigma_s = 0.385 \, \text{cm}^{-1}, \quad \Sigma_a = N\sigma_a = 3.2 \times 10^{-4} \, \text{cm}^{-1},$$

and the total cross section is

$$\Sigma_t = 0.385 \, \text{cm}^{-1} \sim \Sigma_s.$$

The mean free path is therefore

$$\lambda = \frac{1}{\Sigma_t} = 2.6 \, \text{cm}.$$

Notice how small the absorption cross section in graphite is compared to its scattering cross section. Indeed since $\Sigma_s / \Sigma_a = 1.2 \times 10^3$, one can infer that a thermal neutron in graphite will make some 1200 scattering collisions on the average before being absorbed. This very low absorption cross section makes graphite an ideal material for nuclear reactor applications.

## C. Characteristics of Neutron–Nuclear Cross Sections

Before considering in detail the various types of neutron–nuclear reactions significant in nuclear reactor analysis, it is useful to give a brief discussion of some of the relevant physics underlying the behavior of these cross sections. There are two aspects involved in the analysis of neutron cross sections:
   (a) the kinematics of two-particle collisions and
   (b) the dynamics of nuclear reactions.
The kinematics of two-body collisions, that is, the application of the laws of conservation of momentum and energy to such collisions, should be very familiar to the reader from introductory courses in mechanics or modern physics. However consistent with our attempt to make this presentation as self-contained as possible, and being well aware of the short half-life of this type of information in the fast core memory of most students, we will review such kinematic calculations in Section 2-I-D.

The dynamics of nuclear reactions is concerned with the fundamental physical mechanisms involved in such collision events. The two mechanisms of most interest in nuclear reactor applications are those of *potential scattering*, in which the

neutron merely bounces off of the force field of the nucleus without actually penetrating the nuclear surface, and *compound nucleus formation*, in which the incident neutron is actually absorbed by the nucleus to form a new nucleus of mass number $A + 1$ which then decays by emitting a gamma, a neutron, or perhaps fissioning.

We will give a brief discussion of both of these interaction mechanisms, and then turn our attention to a specific survey of the various types of cross section behavior encountered in the more common materials utilized in nuclear reactors.
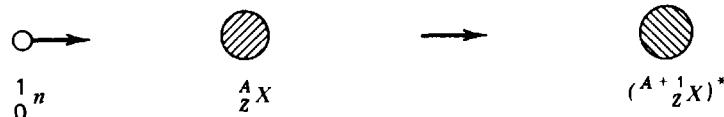
## 1. MECHANISMS OF NEUTRON–NUCLEAR INTERACTION

The simplest type of nuclear reaction occurring in a nuclear reactor is *potential scattering*, in which the neutron scatters elastically off the nuclear potential without ever penetrating the nucleus itself. This type of collision event is very similar to that which would occur between two hard spheres (e.g., billiard balls), and the cross section for such a reaction is essentially just the geometrical cross section of the nucleus. Potential scattering cross sections are characterized by a rather flat energy dependence from about 1 eV up to the MeV range.

Another common type of reaction encountered in a nuclear reactor is that in which the incident neutron is first absorbed by the nucleus $^A_Z X$ to create a new *compound nucleus* $^{A+1}_Z X$. This compound nucleus subsequently decays by emitting an energetic particle. Compound nucleus formation occurs in many neutron–nuclear reactions of interest to the reactor engineer, including fission, radiative capture, and certain types of scattering.

That such a mechanism must be involved in these reactions can be inferred from the relatively long times (at least on a nuclear time scale) for such events to occur. Whereas it would take a slow neutron (traveling at $10^5$ cm/sec) some $10^{-17}$ sec to cross the nucleus, neutron–nuclear reactions such as fission occur on a time scale of some $10^{-14}$ sec—or some 1000 transit times. Hence the incident neutron must first be absorbed by the original nucleus and rattle around a bit, distributing both its kinetic energy and the additional binding energy supplied by the added neutron to the other nucleons in the nucleus, before the compound nucleus finally decays. The long lifetime of the compound nucleus implies that the disintegration process is essentially independent of the original mode of formation; that is, the compound nucleus lasts long enough to "forget" most of the characteristics of the incident neutron (such as which direction it came from).

The formation of a compound nucleus actually corresponds to a so-called *resonance reaction*, in which the incident neutron energy matches one of the energy levels in the compound nucleus. To be more specific, consider a neutron incident upon a nuclide $^A_Z X$:



$^1_0 n \qquad\qquad ^A_Z X \qquad\qquad (^{A+1}_Z X)^*$

As we will see later when we develop the topic of collision kinematics, the energy available for such a reaction is the center of mass (CM) energy $E_c = (M/m + M)E$, where $m$ is the neutron mass, $M$ is the nuclear mass, and $E$ is the neutron kinetic energy in the laboratory system. The actual energy of the excited level of the

compound nucleus is much higher due to the additional binding energy of the added neutron $E_b$. If $E_c + E_b$ is very close to a nuclear energy level of the compound nucleus ${}^{A+1}_{Z}X$, one expects that the probability for compound nucleus formation will be much larger than if $E_c + E_b$ does not "match" this energy level. Hence we expect that the cross sections for such compound nuclear reactions will exhibit sharp peaks or *resonances* at those neutron energies $E$ for which this energy matching occurs. By way of illustration, we have shown the resonance structure in the low-energy cross section behavior of a number of nuclei in Figure 2-4.
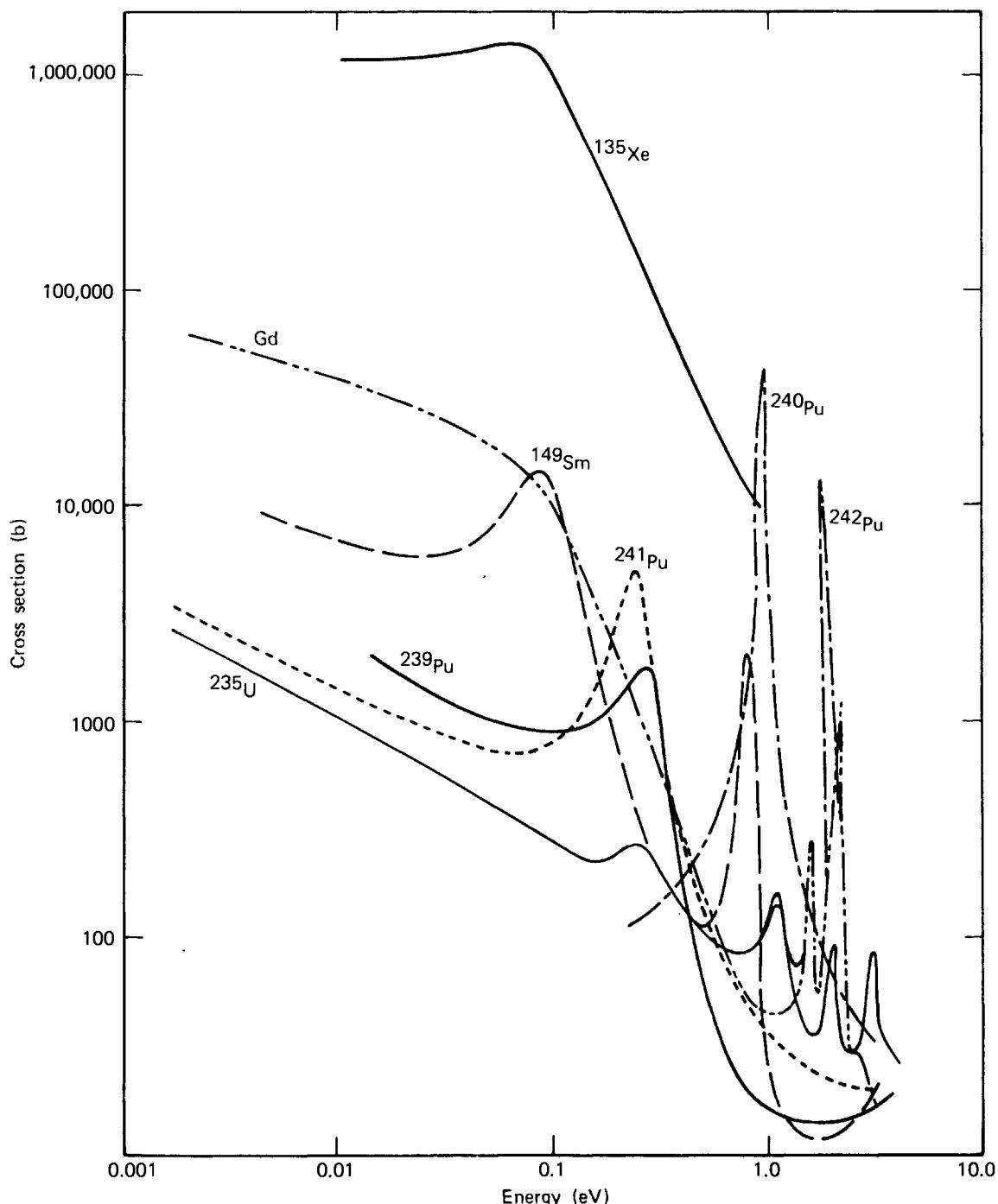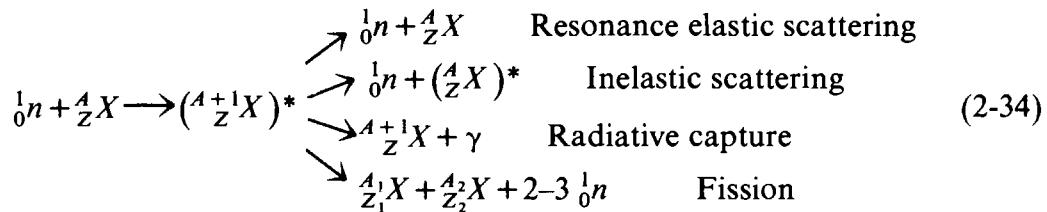


FIGURE 2-4.  Low-energy cross section behavior of several important nuclides.[12]

The second stage of a compound nucleus process is the decay of the compound nucleus. This decay may occur in a variety of ways, as indicated schematically below:

$$
{}_0^1n + {}_Z^A X \longrightarrow ({}_Z^{A+1}X)^* 
\begin{cases}
\nearrow & {}_0^1n + {}_Z^A X & \text{Resonance elastic scattering} \\
\nearrow & {}_0^1n + ({}_Z^A X)^* & \text{Inelastic scattering} \\
\searrow & {}_Z^{A+1}X + \gamma & \text{Radiative capture} \\
\searrow & {}_{Z_1}^{A_1}X + {}_{Z_2}^{A_2}X + 2\text{-}3 \, {}_0^1n & \text{Fission}
\end{cases}
\tag{2-34}
$$

Since we have argued that the final disintegration mode is essentially independent of the neutron absorption process which creates the compound nucleus, we might expect that the cross section energy dependence for compound nucleus reactions will exhibit certain similarities. These similarities will become apparent as we consider in more detail the specific neutron–nuclear reactions of importance in nuclear fission reactors.

## 2. A QUALITATIVE DISCUSSION OF NEUTRON CROSS SECTIONS

### (a.) RADIATIVE CAPTURE

*Radiative capture* reactions are quite significant for reactor analysis since they remove neutrons from the chain reaction. Such reactions proceed via compound nucleus formation in which the incident neutron is first absorbed to form the compound nucleus of mass number $A + 1$, and then this nucleus subsequently decays by emitting a cascade of high-energy gammas. For this reason, the functional dependence of the capture cross section on the neutron kinetic energy $E$ exhibits a resonance behavior at those energies at which the CM energy $E_c$ plus the neutron binding energy $E_b$ match an energy level of the compound nucleus. We have shown this resonance situation schematically for neutron capture in $^{238}U$ in Figure 2-5. In particular, we have indicated the energy level diagram for the compound nucleus $^{239}U$ for one of the low lying resonances at $E = 6.67$ eV. This resonance has a very narrow width of 0.027 eV and an extremely high peak (several thousand barns). The subsequent radiative decay of the compound $^{239}U$ nucleus is usually a cascade process, with the new nucleus jumping down through a number of energy levels accompanied by the emission of several gamma rays. Since the excited levels are typically in the MeV range, the total energy of the emitted gammas will be quite large.

For resonances (i.e., energy levels) which are spaced widely apart, it is possible to describe the energy dependence of the absorption cross section by a very simple expression known as the *Breit–Wigner single-level resonance formula*:[1-4]

$$
\sigma_\gamma(E_c) = \sigma_0 \frac{\Gamma_\gamma}{\Gamma}\left(\frac{E_0}{E_c}\right)^{1/2}\frac{1}{1+y^2}, \qquad y = \frac{2}{\Gamma}(E_c - E_0).
\tag{2-35}
$$

Here $E_0$ is the energy at which the resonance occurs (that is, the energy $E_c$ at which $E_c + E_b$ matches the energy level of the compound nucleus), $\Gamma$ is the so-called *total line width* of the resonance that essentially characterizes the width of the energy level and the full width at half-maximum (FWHM) of the resonance, while $\Gamma_\gamma$ is
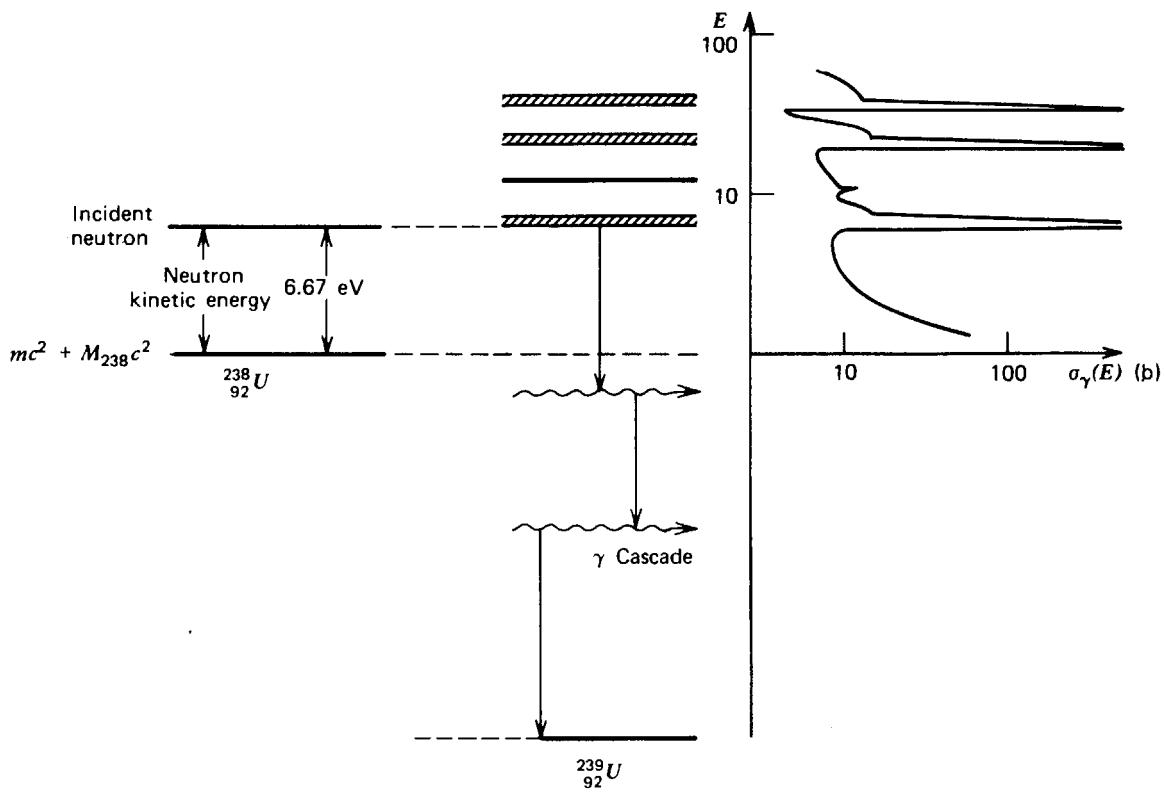
**FIGURE 2-5.** An energy-level diagram of the capture resonance in $U^{238}$ at $E = 6.67$ eV.

the *radiative line width* essentially characterizing the probability that the compound nucleus will decay via gamma emission. Here $\sigma_0$ is the value of the total cross section $\sigma_t(E)$ at the resonance energy $E_0$ and can be written in terms of the reduced neutron wavelength $\lambda_0$ at $E_0$ as

$$\sigma_0 = 4\pi \, \lambda_0^2 \frac{\Gamma_n}{\Gamma} g = 2.608 \times 10^6 \frac{(A+1)^2}{A^2 E_0(\text{eV})} \frac{\Gamma_n}{\Gamma} g, \qquad (2\text{-}36)$$

while $g = (2J + 1)/2(2I + 1)$ is a statistical spin factor given in terms of the nuclear spin $I$ and total spin $J$. $\Gamma_n$ is the *neutron line width* and varies in energy as

$$\Gamma_n \sim E^{1/2}. \qquad (2\text{-}37)$$

We have sketched the Breit–Wigner resonance shape versus the CM kinetic energy $E_c$ in Figure 2-6. It should be noted that since resonance absorption is primarily of importance in heavy nuclei, one can usually approximate $E_c \sim E$. For low energies $E \ll E_0$, the cross section behaves as essentially $1/E^{1/2}$ or $1/v$. For large energies $E \gg E_0$, the cross section drops off quite rapidly as $E^{-5/2}$. It is also important to note that such absorption cross sections are largest at low energies. (A list of several of the lower lying resonances of $^{238}U$ is given in Table 8-2.) The energy levels in heavy nuclei become relatively more closely spaced at higher energies. Indeed for energies above roughly 1 keV in heavy nuclei such as $^{238}U$, the absorption resonances become so closely spaced that they cannot be resolved by experimental measurements. The treatment of neutron absorption in such unresolved resonances is a very difficult but important task in nuclear reactor analysis.
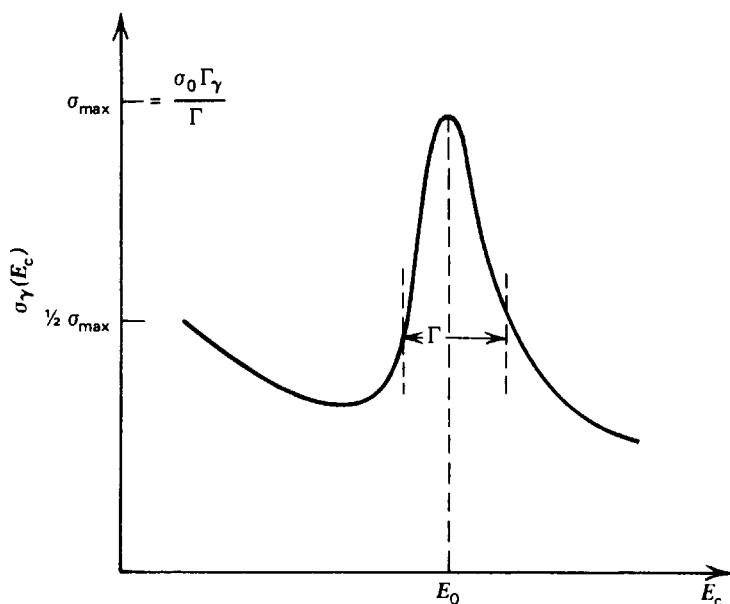
FIGURE 2-6. A single-level capture resonance.

### (b.) NUCLEAR FISSION

Nuclear fission is yet another reaction that proceeds by compound nucleus formation. Once again a compound nucleus is first formed by neutron absorption. This compound nucleus then decays by fissioning into two lighter nuclei. Since the mode of disintegration is relatively independent of the formation mechanism, we might again expect the cross sections for nuclear fission to exhibit a resonance structure very similar to that characterizing radiative capture. This is certainly the case for fission cross sections characterizing nuclei such as $^{233}U$, $^{235}U$, and $^{239}Pu$. However the fission cross sections for other heavy nuclei such as $^{232}Th$ and $^{238}U$ exhibit a somewhat different structure in that they are essentially zero until the incident neutron energy exceeds a threshold of roughly an MeV. To understand this latter behavior, we must examine in more detail the fission process itself, a task we shall defer until Section 2-II.

### (c.) SCATTERING

#### i.) Inelastic scattering

In an inelastic scattering reaction, the incident neutron is first absorbed by the nucleus to form a compound nucleus. This nucleus then subsequently decays by reemitting a neutron. However the final nucleus is left in an excited state. Such reactions usually occur only for relatively high neutron energies, say above 10 keV, since the neutron kinetic energy must exceed a certain threshold energy in order to excite the first excited state of the compound nucleus. We have depicted this reaction schematically in Figure 2-7.

Since much of the kinetic energy of the incident neutron may be converted into the energy of excitation of the target nucleus, it is possible for a neutron to lose a large amount of energy in an inelastic scattering reaction. It should be noted in particular that kinetic energy is not conserved in such an inelastic reaction.

#### ii.) Elastic resonance scattering

A very similar compound nucleus reaction involves first the absorption of the incident neutron, followed by the reemission of the neutron with the target nucleus
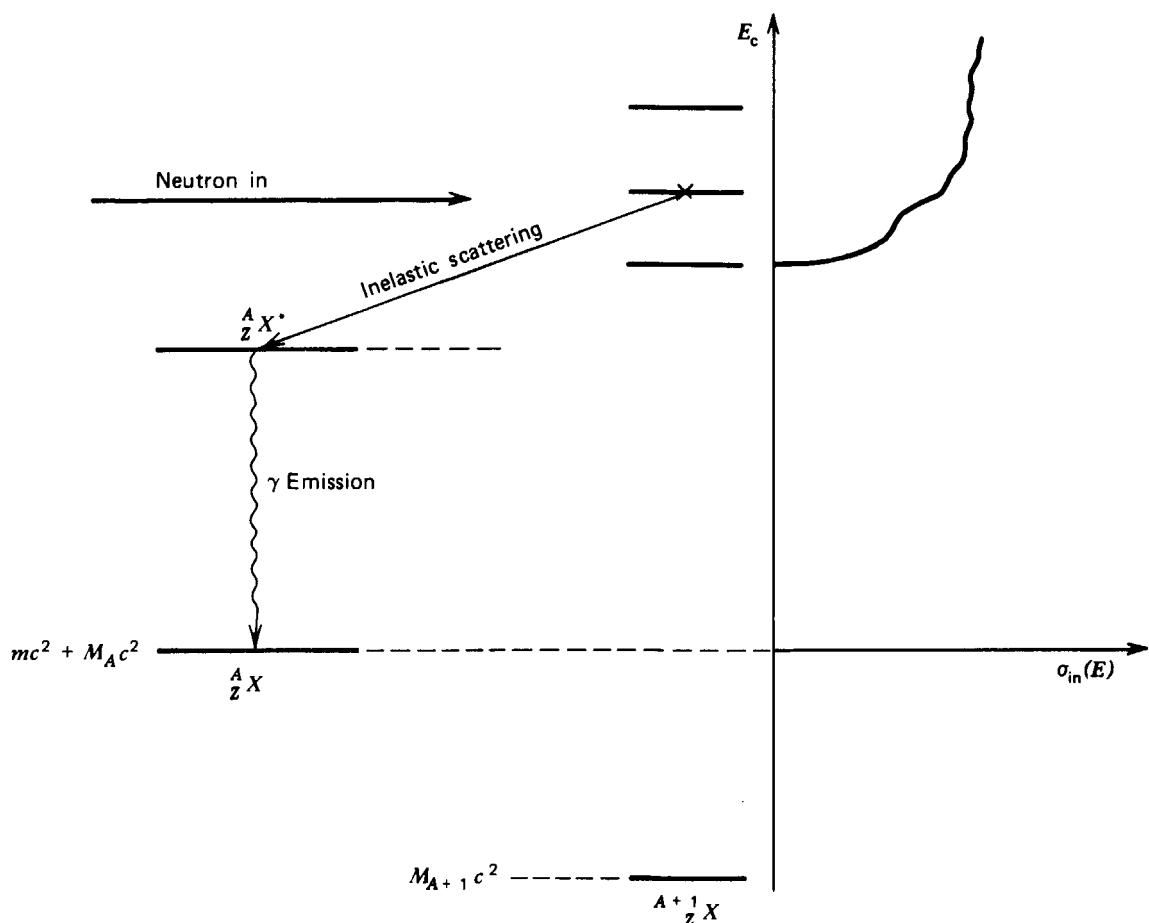
FIGURE 2-7.    A schematic of the energy-level diagram characterizing inelastic scattering.

returning to its ground state (see Figure 2-8). In contrast to inelastic scattering, kinetic energy is conserved in elastic events. As one finds with most compound nucleus reactions, there is again a resonance behavior in the corresponding scattering cross section. In this case, however, the cross section energy dependence is somewhat different from that observed in radiative capture or fission. The cross section may actually decrease before rising to a resonance maximum.

This structure arises because the process of resonance elastic scattering may interfere (in a quantum mechanical sense) with potential scattering. The appropriate modification of the Breit–Wigner formula to account for scattering interference is

$$\sigma_s(E_c) = \sigma_0 \frac{\Gamma_n}{\Gamma} \left( \frac{E_0}{E_c} \right)^{1/2} \frac{1}{1+y^2} + \sigma_0 \frac{2R}{\lambda_0} \frac{y}{1+y^2} + 4\pi R^2 \qquad (2\text{-}38)$$

|  resonance | interference | potential |
| --- | --- | --- |
| scattering | scattering | scattering |

where $R$ is the nuclear radius (given approximately by $R \sim 1.25 \times 10^{-13} A^{1/3}$ cm).

iii.) Potential scattering

The simplest type of nuclear interaction is *potential scattering*, in which the incident neutron scatters elastically off of the nuclear potential without penetrating the nuclear surface. Such "billiard-ball" collisions are characterized by an essen-
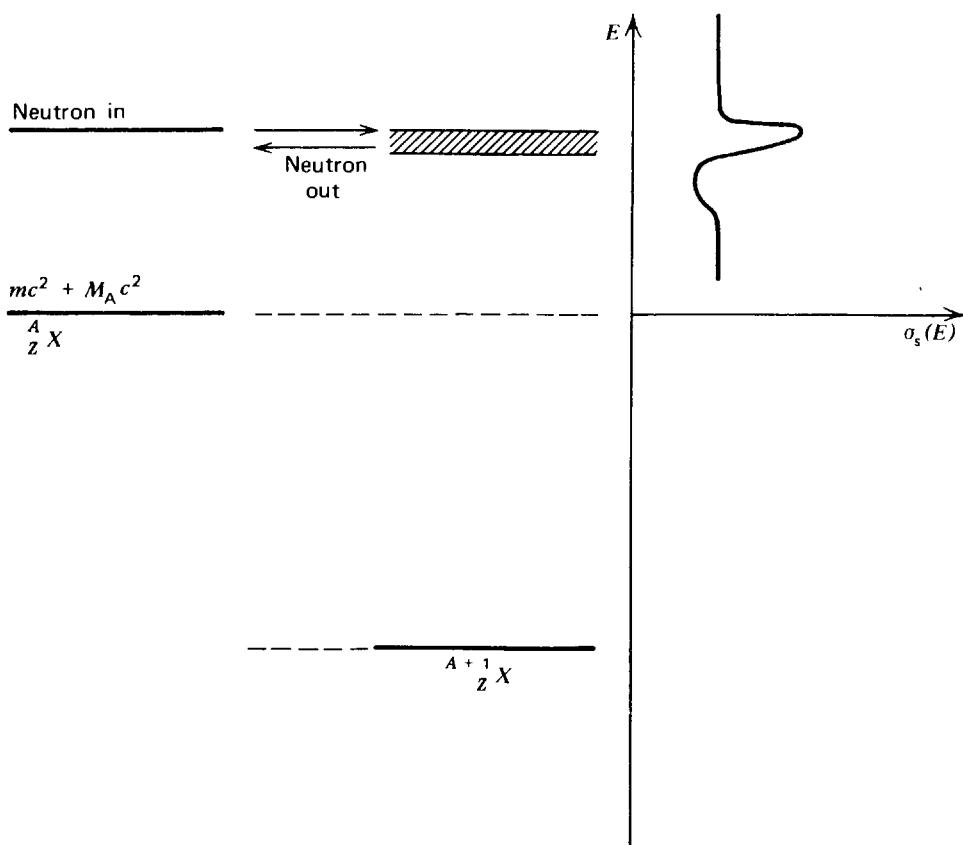
**FIGURE 2-8.** The energy-level diagram for resonance elastic scattering.

tially energy-independent cross section $\sigma_p$ which is of the order of magnitude of the geometric cross section of the nucleus for intermediate energies, $4\pi R^2$.

### (d) TOTAL NEUTRON CROSS SECTIONS

Recall that we defined the total cross section for neutron–nuclear reactions as the sum of the cross sections for each type of reaction

$$\sigma_t = \sigma_s + \sigma_\gamma + \sigma_f + \dots \qquad (2-39)$$

Such cross sections can be measured by performing transmission experiments such as those we used to operationally define the concept of a cross section. That is, one shoots a monoenergetic beam of neutrons of energy $E$ at a thin target and then measures the fraction of the incident beam that penetrates the sample.

It is of interest to see if we can understand the energy dependence of total cross sections in terms of the various different reactions and reaction mechanisms we have discussed earlier. To be specific, let us consider the total cross section of a common reactor material, graphite ($^{12}_6C$), which is shown over the energy range from $10^{-3}$ eV to 10 MeV in Figure 2-9. One can distinguish essentially five different regions of cross section behavior for this material. For very low energies, the cross section behaves as $E^{-1/2}$. At about $10^{-3}$ eV the cross section becomes very jagged and irregular. These spikes in the cross section smooth out by an energy of $10^{-1}$ eV, and the cross section from this energy up to $10^5$ eV is essentially constant. Above $10^5$ eV the cross section begins to show a detailed structure once again, until it eventually drops off above $10^7$ eV.
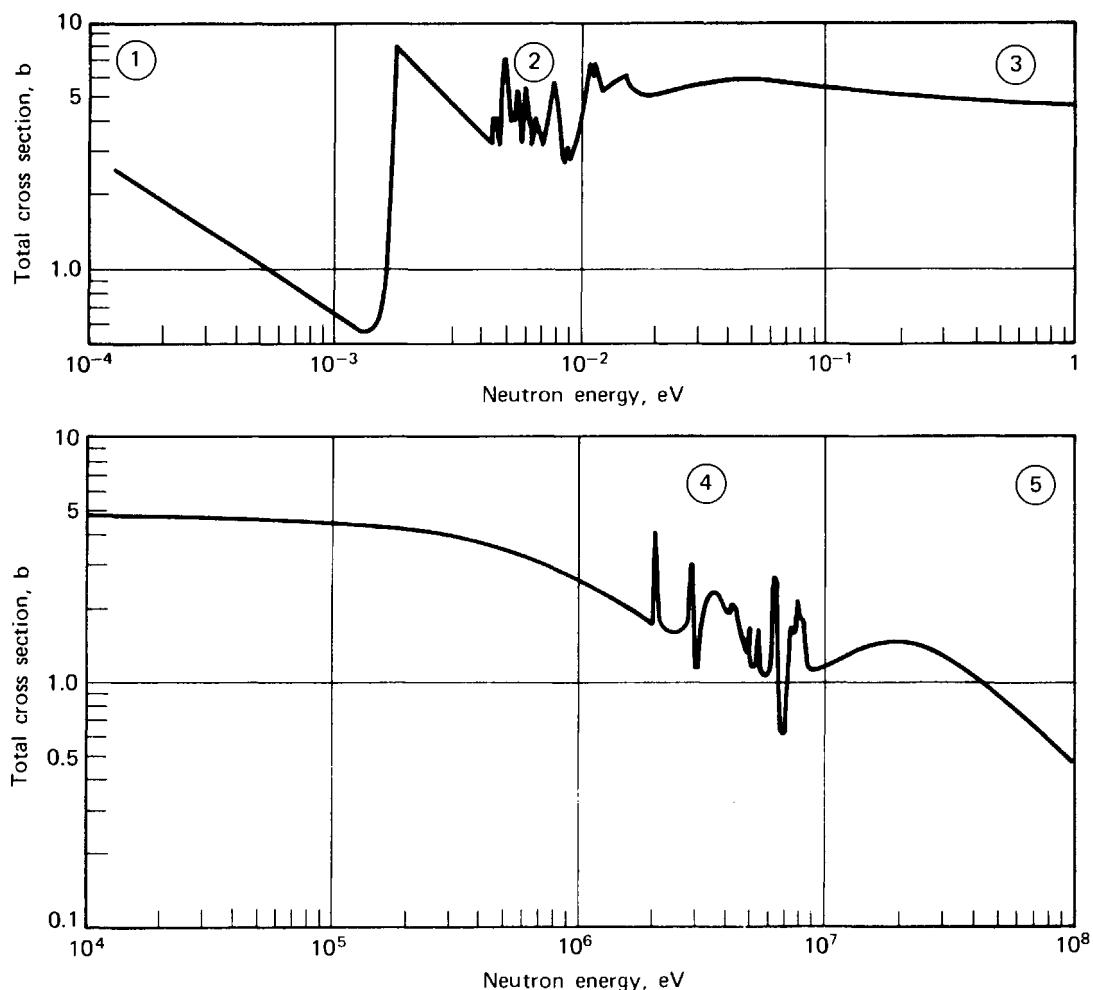
FIGURE 2-9. The total scattering cross section of $^{12}$C.

In an effort to explain each of these different types of behavior, let us begin with the smooth cross section variation for intermediate energies (region ③). In this energy range, the cross sections of most nuclei are dominated by potential scattering (except for heavy nuclei in which both resonance scattering and absorption may be dominant effects because of low-lying energy states). The cross section magnitude is essentially just the geometric area presented to the neutron by the nucleus (~5 b) and depends very little on neutron energy.

The jagged behavior in the MeV region ④ corresponds to resonance reaction mechanisms since now the incident neutron energy is comparable to that of the lowest energy levels in the compound nucleus $^{13}_{6}$C. Since the nuclear energy levels lie closer to the ground state for heavier nuclei, we would expect that such resonance structure would appear at progressively lower energies for the heavier nuclides. For example, we have already noted that a pronounced resonance occurs in $^{238}$U at 6.67 eV.

The falloff in the cross section at very high energies (region ⑤) is easily understandable in terms of the neutron wavelength

$$\lambda = \frac{h}{p} = \frac{h}{\sqrt{2mE}} = \frac{2.86 \times 10^{-9}}{\sqrt{E}\,(\text{eV})}\ \text{cm.} \qquad (2\text{-}40)$$

Since this wavelength decreases with increasing neutron energy, it is apparent that for sufficiently high energies, the probability of neutron interaction with the nucleus will similarly decrease. Such very high energy behavior has little relevance to nuclear reactor analysis, since neutrons in fission chain reactions rarely exceed 10 MeV in energy.

The irregular, jagged behavior at low energies in region ② is also a wavelength effect. For sufficiently small energies, the wavelength becomes comparable to the interatomic spacing, and the neutron interacts not with a single nucleus but rather with an aggregate of nuclei. If the material has a regular structure (such as the crystalline structure of graphite), the neutron will be diffracted, just as X-rays are diffracted when passing through a crystal. This is accompanied by a sensitive energy dependence as the neutron wavelength becomes comparable to multiples of the spacing between various crystal lattice planes. For sufficiently small energies, the wavelength becomes so large that diffraction becomes impossible, and the cross section becomes smoothly varying again.
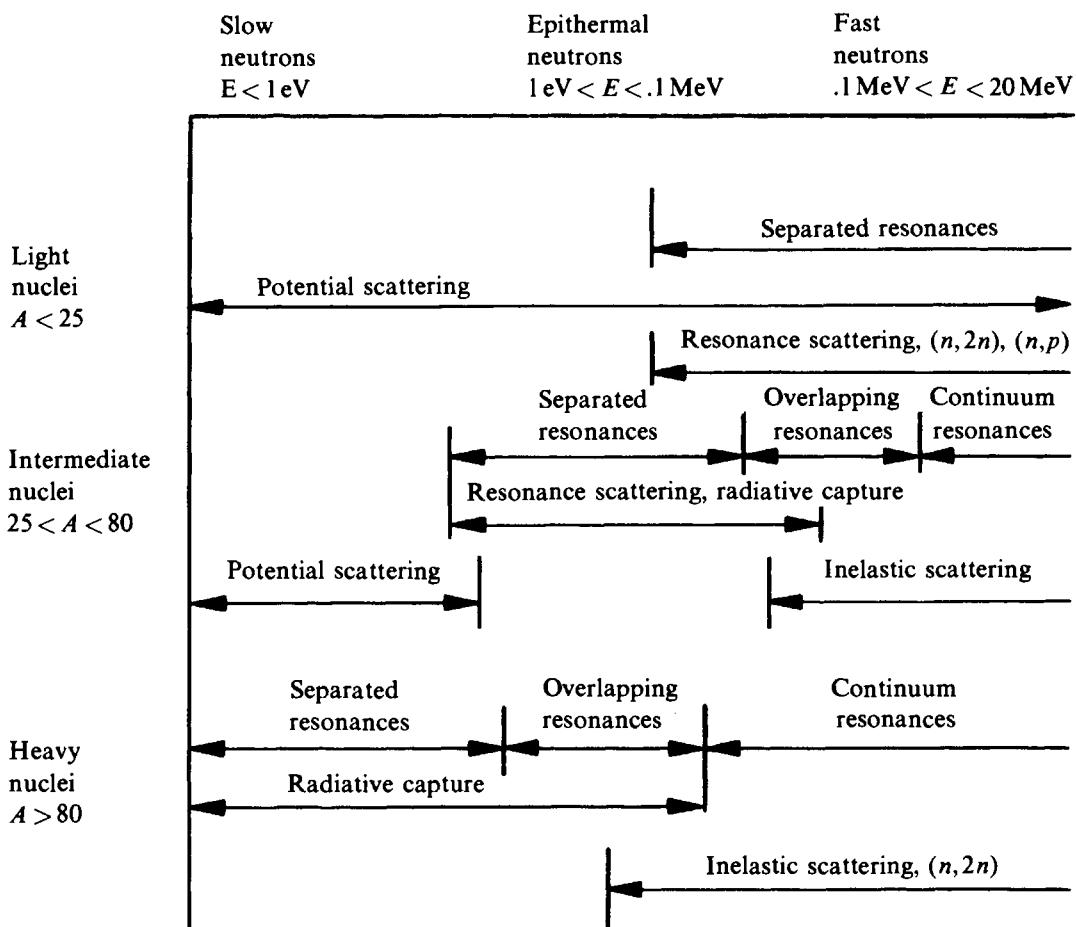
There are two other important effects which influence the neutron cross section behavior at very low energies (regions ① and ②). If the neutron energy is less than the chemical binding energy of atoms in the sample ($\sim 1$ eV), the neutron will no longer be interacting with a free nucleus, but rather with an aggregate of bound nuclei. It can interact and excite the internal modes of the sample, such as crystal lattice vibrations or molecular rotations. For these low energies, the thermal motion of the nuclei also becomes very important. If we recall that these thermal motions are essentially characterized by the sample temperature $T$ and that the atoms in thermal equilibrium at this temperature are characterized by a thermal energy $\frac{3}{2}kT$, where $k$ is the Boltzmann constant, $k = 8.6173 \times 10^{-5}$ eV/°K, then for neutron energies comparable to this thermal energy (at room temperature, $E = 0.025$ eV), the motion of the nuclei must be considered. We will return in the next section to discuss the modifications this requires in the neutron cross section. Suffice it to say at this point that such considerations imply that for small neutron energies, the cross section will behave as $1/E^{1/2}$.

Similar features are found in most neutron cross sections of interest in reactor analysis, although the particular energy regions in which such behavior arises will vary from nuclide to nuclide. For example, we have summarized the characteristics of nuclei of different mass numbers in Table 2-1.[10]

We will return later from time to time to discuss more specific features of neutron cross section behavior which are of particular significance for nuclear reactor applications.

## 3. NUCLEAR DATA SETS

The key ingredient in all reactor calculations is a knowledge of the various relevant neutron–nuclear cross sections. The complicated dependence of such cross sections on neutron energy and angle of incidence, combined with the large number of isotopes involved in nuclear reactor analysis implies that neutron cross section data can be quite massive. Such data have been accumulated over the past few decades by both experimental measurements and theoretical calculations. The tabulation of these data has grown from a single volume, BNL-325[11] (the so-called "barn book") in the 1950s to a six-volume set[12] in the 1960s to the point where nuclear data are most conveniently kept on magnetic tape or in computer memory. (Although it should be mentioned that a new third edition[13] of BNL-325 has recently been issued.)

TABLE 2-1   A Summary of Cross Section Behavior for Nuclei of Various Mass Number[10]

| | Slow neutrons E < 1 eV | Epithermal neutrons 1 eV < E < .1 MeV | Fast neutrons .1 MeV < E < 20 MeV |
|---|---|---|---|
| Light nuclei A < 25 | Potential scattering → | Separated resonances | Separated resonances / Resonance scattering, (n,2n), (n,p) |
| Intermediate nuclei 25 < A < 80 | Potential scattering | Separated resonances — Resonance scattering, radiative capture | Overlapping resonances / Continuum resonances / Inelastic scattering |
| Heavy nuclei A > 80 | Separated resonances / Radiative capture | Overlapping resonances | Continuum resonances / Inelastic scattering, (n,2n) |

Basic nuclear data appear in a wide variety of forms. For example, raw cross section data are usually provided by a variety of experiments, each characterized by a different degree of accuracy. Multiple sets of experimental data may exist giving different values for the same cross sections. Data may be provided by different theoretical calculations of varying accuracy. There are also numerous gaps where no cross section measurement or theory is available or applicable. The enormous volume of such varied nuclear data would overwhelm the nuclear engineer in his efforts to extract those cross sections of relevance to his particular needs.

Hence a number of years ago it was decided to consolidate and standardize all of the cross section information into one data set. To this end the Evaluated Nuclear Data File (ENDF)[14] was established to consolidate, organize, and present these data in a form convenient for nuclear applications. The ENDF system contains both neutron and photon cross section data along with data-processing computer programs which can manipulate the data into the most convenient form for the user. These data are stored in three computer library systems:

(1) CSISRS (Cross Section Information Storage and Retrieval System): This data set contains essentially unevaluated raw data from experimental measurements.

(2) ENDF/A: This data set contains both complete and incomplete sets of nuclear data as soon as they become available. For each isotope there

may be more than one data set for a particular reaction, or there may be none at all for certain reactions of interest.

(3) ENDF/B: The ENDF/B data set contains only complete, evaluated sets of nuclear data presented in a form that can be most conveniently utilized by the nuclear designer. Data for approximately 80 isotopes are included for all significant neutron-induced reactions in the energy range $10^{-5}$eV to 20 MeV. In particular, cross section data are provided for the reactions $(n,\gamma)$, $(n,\text{fission})$, $(n,p)$, $(n,\alpha)$, $(n,n)$, $(n,n')$, $(n,2p)$ and $(n,2n)$, as well as for the differential scattering cross sections (described in Section 2-I-D).

ENDF/B is therefore regarded as the standard source of nuclear data for use in nuclear reactor analysis in the United States. (There are comparable data sets in Europe and the Soviet Union.) The ENDF/B data set is continually being reevaluated and updated as new cross section measurements become available. Revised versions of the data set are issued at one- or two-year intervals.

The effort involved in preparing the ENDF/B set is enormous. It not only involves collecting and organizing the massive amount of nuclear data available from an enormous variety of sources, but evaluating these data, checking them for consistency, filling in the gaps in the data using existing theories (or educated guesses), testing the data against experimental measurements, and arranging the data in a convenient form for use.

The actual data contained in the ENDF/B set are usually not contained in tabular form, but rather in the form of numerous fitting parameters that can be assembled by a processing code into a fully evaluated set of cross section data for any material of interest. For example, the set contains resonance parameters such as level widths, resonance energies, and cross sections at resonance rather than a tabulated set of cross section data for various energies (which would require a prohibitively large storage). The resonance cross section can then be generated using these parameters in a Breit–Wigner type resonance formula.

We will return to discuss further details of how such data sets are manipulated into the forms useful for reactor calculations when we have developed a more complete understanding of the various methods used in nuclear reactor analysis. At the end of this chapter we have provided a list of the most useful sources of current neutron cross section data.[15]

## D. Some Generalizations of the Concept of the Cross Section

### 1. DIFFERENTIAL SCATTERING CROSS SECTIONS

Neutron cross sections provide a quantitative measure of the probability that various types of neutron–nuclear reactions will occur. For example, we have introduced $\sigma_a(E)$ to characterize the probability that a neutron with kinetic energy $E$ incident upon a nucleus will be absorbed. Similar cross sections have been introduced to describe reactions such as scattering.

It is frequently useful to introduce a generalization of the concept of a neutron cross section characterizing the scattering reaction. In such reactions the incident neutron will usually experience a change in both direction of motion and energy in the scattering event. (Just imagine a billiard-ball collision.) The microscopic scattering cross section will describe the probability that such a scattering collision occurs. However it provides no information about the change in neutron direction or

energy that occurs in such a collision. This latter information is very important in certain types of reactor studies. To characterize it, we must introduce the concept of the *differential scattering cross section*.

Before we develop these generalizations, let us offer both an explanation and an apology for the mathematical detail that follows. It has been our intent to keep the level of mathematics in these introductory chapters as low as possible. Unfortunately, however, to describe cross sections characterizing changes in neutron energy and direction, one must utilize a bit of vector notation. Frequently students tend to become somewhat intimidated by the notation customarily used to describe the treatment of the direction of neutron motion. We wish to reassure the reader that regardless of appearance, the actual level of mathematical analysis we will use is very rudimentary and essentially includes only vector algebra with an added dash of volume integration.

First we must introduce variables that characterize the motion of the incident neutron. The natural choice would be the neutron velocity **v**. Then the cross section we wish to define would describe the probability that a neutron incident with a velocity **v** would be scattered by a nucleus to a new velocity **v′**.

However in reactor analysis it will be more convenient to describe the neutron motion with slightly different variables. We will essentially decompose the neutron velocity vector into two components, one variable characterizing the neutron speed and a second variable for the neutron direction of motion. We use the kinetic energy of the neutron $E = \frac{1}{2}mv^2$ instead of the neutron speed itself. Then to specify the direction of neutron motion, we introduce a unit vector $\hat{\Omega}$ in the direction of the neutron velocity vector **v**:

$$\hat{\Omega} = \mathbf{v}/|\mathbf{v}| = \hat{e}_x \sin\theta \cos\phi + \hat{e}_y \sin\theta \sin\phi + \hat{e}_z \cos\theta. \qquad (2\text{-}41)$$

where we have chosen to represent this direction unit vector in spherical velocity-
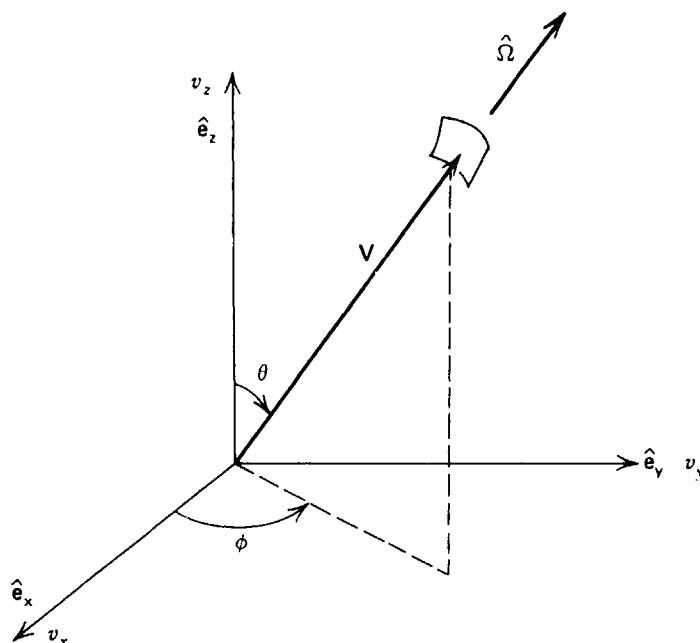


FIGURE 2-10.  The neutron direction unit vector $\hat{\Omega}$ in spherical coordinates.

space coordinates $(\theta, \phi)$ (see Figure 2-10). Notice that to describe the incident neutron velocity we now specify both its energy $E$ and its direction $\hat{\Omega}$.

At this point it is convenient to consider how one integrates over these variables (as we shall have cause to do later in this section). Suppose we wished to integrate over all possible neutron velocities. This integration could then be performed in either Cartesian or spherical velocity coordinates:

$$\int d^3 v f(\mathbf{v}) = \int_{-\infty}^{\infty} dv_x \int_{-\infty}^{\infty} dv_y \int_{-\infty}^{\infty} dv_z f(\mathbf{v}) = \int_0^{\infty} dv\, v^2 \int_0^{2\pi} d\phi \int_0^{\pi} d\theta \sin\theta f(\mathbf{v}). \quad (2\text{-}42)$$

However we have defined the unit vector in the direction of the velocity vector $\mathbf{v}$ as $\hat{\Omega}$. Hence we can identify the angular portion of the integration in Eq. (2-42) as just the integration over this direction:

$$\int_{4\pi} d\hat{\Omega} \equiv \int_0^{2\pi} d\phi \int_0^{\pi} \sin\theta\, d\theta. \quad (2\text{-}43)$$

In this sense we see that the differential $d\hat{\Omega}$ of the unit vector $\hat{\Omega}$ corresponds to a differential solid angle

$$d\hat{\Omega} = \sin\theta\, d\theta\, d\phi. \quad (2\text{-}44)$$

One final modification is useful here. We will usually choose to work with the neutron energy $E$ rather than the neutron speed. Hence rather than choosing to integrate functions of $\mathbf{v}$ over all neutron velocities, we will integrate functions of $E$ and $\hat{\Omega}$ over all possible neutron energies and directions:

$$\int d^3 v f(\mathbf{v}) \rightarrow \int_0^{\infty} dE \int_{4\pi} d\hat{\Omega} f(E, \hat{\Omega}). \quad (2\text{-}45)$$

So much for mathematical preliminaries. We will now proceed to introduce the concept of a cross section that characterizes the probability that a neutron is scattered from an initial energy $E$ and direction of motion $\hat{\Omega}$ to a final energy $E'$ and direction of motion $\hat{\Omega}'$. To make life simple, we will first do this for the situation in which we are only interested in the change in neutron energy in scattering. Imagine a beam of neutrons of incident intensity $I$, all of energy $E$, incident upon a thin target of surface atomic density $N_A$. Then the rate/cm$^2$ at which neutrons will be scattered from their original energy $E$ to a final energy $E'$ in the range $E'$ to $E' + dE'$ is proportional to the beam intensity $I$, the target surface density $N_A$, and the differential range $dE'$ of final energies. We will define the *microscopic differential scattering cross section* $\sigma_s(E \rightarrow E')$ as the appropriate proportionality parameter

$$\text{Rate/cm}^2 = \sigma_s(E \rightarrow E') dE' I N_A. \qquad \qquad (2\text{-}46)$$

Hence we find that $\sigma_s(E \rightarrow E')$ characterizes the probability that a scattering

collision changes the original neutron energy from $E$ to $E'$ in $dE'$. It is important to notice that this differential scattering cross section is a "distribution" in the sense that it is associated with a certain range of final energies, $E'$ to $E' + dE'$. Hence its dimensions are $cm^2/eV$.
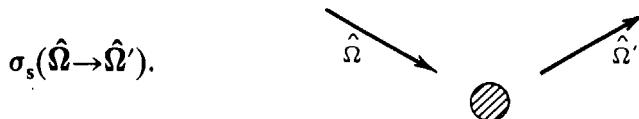
There is a very simple relationship between the differential scattering cross section $\sigma_s(E \to E')$ and our earlier definition of the microscopic scattering cross section $\sigma_s(E)$. If we recognize that the latter quantity is just related to the probability that a neutron of energy $E$ will suffer a scattering collision, regardless of the final energy $E'$ to which it is scattered, then it is apparent that $\sigma_s(E)$ is just the integral of the differential scattering cross section $\sigma_s(E \to E')$ over all final energies $E'$

$$\sigma_s(E) = \int_0^\infty dE' \, \sigma_s(E \to E').$$  (2-47)

Of course this relationship explains the origin of the term "differential."

It should be mentioned that occasionally one encounters a somewhat different notation for the differential scattering cross section which may be written as $d\sigma/dE$. We find the convention of denoting differential cross sections by a multiple variable argument [such as $(E \to E')$] to be more convenient for our purposes, and hence will use this notation throughout.

We can similarly introduce the concept of a differential scattering cross section describing the probability that a neutron scatters from an incident direction $\hat{\Omega}$ to a final direction $\hat{\Omega}'$ in a very similar manner:

$$\sigma_s(\hat{\Omega} \to \hat{\Omega}').$$
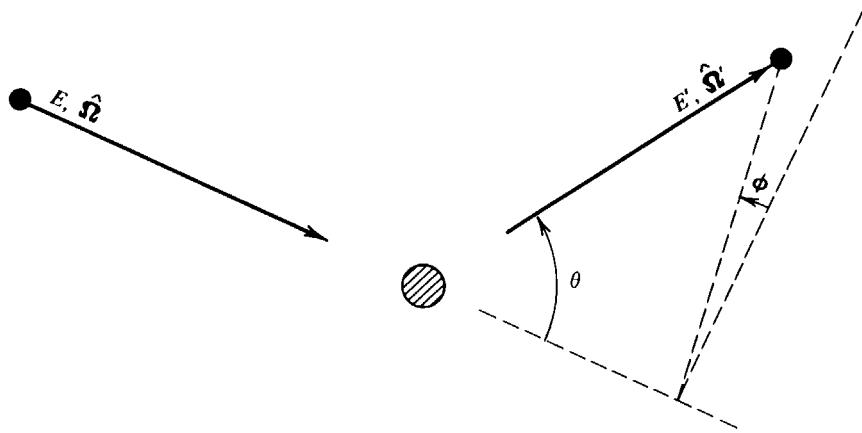
Once again, $\sigma_s(\hat{\Omega} \to \hat{\Omega}')$ is related to our earlier microscopic scattering cross section by an integration over all final directions

$$\sigma_s(\hat{\Omega}) = \int_{4\pi} d\hat{\Omega}' \, \sigma_s(\hat{\Omega} \to \hat{\Omega}') = \sigma_s.$$  (2-48)

Two comments are useful here. First, it should be mentioned that the dependence of the scattering cross section $\sigma_s(\hat{\Omega})$ on the *incident* neutron direction is usually ignored. Indeed very few microscopic scattering cross sections in reactor applications depend on the incident neutron direction because the nuclei in any macroscopic sample are usually randomly oriented, and thus any directional dependence averages out when averaged over all possible nuclear orientations. (One could imagine a sample in which most of the nuclei could be aligned—e.g., a ferromagnetic material—but such situations can safely be ignored in reactor analysis.)

In this case, however, even though the differential scattering cross section $\sigma_s(\hat{\Omega} \to \hat{\Omega}')$ will not depend on the incident neutron direction, it will depend on the *change* in neutron direction. This is most conveniently expressed in terms of a functional dependence on the angle through which the incident neutron is scattered —the so-called *scattering angle* $\theta$, or more conveniently, the cosine of this scattering
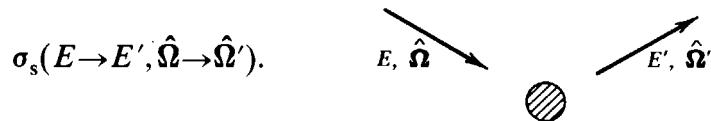
**FIGURE 2-11.** Definition of the scattering angle $\theta$.

angle, $\mu_0 \equiv \cos\theta$, which can be conveniently expressed as the dot product between the unit direction vectors $\mu_0 = \hat{\Omega} \cdot \hat{\Omega}'$. (Again, the dependence on azimuthal angle $\phi$ does not arise for materials in which the nuclei have a random orientation.) One occasionally denotes this functional dependence by writing

$$\sigma_s(\hat{\Omega} \to \hat{\Omega}') = \sigma_s(\hat{\Omega} \cdot \hat{\Omega}') = \sigma_s(\mu_0). \qquad (2\text{-}49)$$

We will continue to use the somewhat more formal notation by writing $\sigma_s(\hat{\Omega} \to \hat{\Omega}')$, even though we know that this differential cross section usually depends only on $\mu_0$.

Thus far we have developed the concept of differential scattering cross sections that characterize the probability of scattering from one energy to another or one direction to another. We can combine these concepts by defining a *double differential scattering cross section* that characterizes scattering from an incident energy $E$, direction $\hat{\Omega}$ to a final energy $E'$ in $dE'$ and $\hat{\Omega}'$ in $d\hat{\Omega}'$

$$\sigma_s(E \to E', \hat{\Omega} \to \hat{\Omega}').$$



Again, alternative notations are occasionally used such as $\sigma_s(E, \hat{\Omega} \to E', \hat{\Omega}')$ or $d^2\sigma_s / dE\, d\hat{\Omega}$.

We can again relate the double differential scattering cross section to the differential scattering cross section or the scattering cross section by integration over energy or angle:

$$\sigma_s(E \to E') = \int_{4\pi} d\hat{\Omega}' \, \sigma_s(E \to E', \hat{\Omega} \to \hat{\Omega}'), \qquad (2\text{-}50)$$

or

$$\sigma_s(E, \hat{\Omega} \to \hat{\Omega}') = \int_0^\infty dE' \, \sigma_s(E \to E', \hat{\Omega} \to \hat{\Omega}'), \qquad (2\text{-}51)$$

or

$$\sigma_s(E) = \int_{4\pi} d\hat{\Omega}' \int_0^\infty dE' \, \sigma_s(E \to E', \hat{\Omega} \to \hat{\Omega}').  \tag{2-52}$$

The concept of a differential scattering cross section can also be applied to macroscopic cross sections by merely multiplying by the atomic number density $N$:

$$\Sigma_s(E \to E', \hat{\Omega} \to \hat{\Omega}') \equiv N\sigma_s(E \to E', \hat{\Omega} \to \hat{\Omega}')$$

$$\Sigma_s(E \to E') \equiv N\sigma_s(E \to E')  \tag{2-53}$$

$$\Sigma_s(\hat{\Omega} \to \hat{\Omega}') \equiv N\sigma_s(\hat{\Omega} \to \hat{\Omega}')$$

Such differential cross sections are quite important in nuclear reactor analysis since they determine the manner in which neutrons move about in a reactor core, as well as the rate at which they leak out of the reactor. The measurement or calculation of such cross sections can become quite involved, and the amount of data necessary to adequately represent differential cross sections is usually rather voluminous. Such data are contained in evaluated cross section files such as ENDF/B, as well as in cross section compilations such as BNL-400.[16]

Although the calculation of such differential scattering cross sections is usually formidable, there is one instance of considerable importance to nuclear reactor analysis in which such cross sections can be calculated in a straightforward fashion merely by using the laws of conservation of energy and momentum. This is the situation in which neutrons scatter elastically from stationary nuclei. To prepare the way for the calculation of such cross sections, let us first decompose the differential scattering cross section into two factors:

$$\sigma_s(E \to E') = \sigma_s(E)P(E \to E').  \tag{2-54}$$

If we recall our earlier definition of the scattering cross section, $\sigma_s(E)$, then it becomes apparent that we can identify

$$P(E \to E')dE' = \begin{array}{l} \text{Probability that a neutron scattering with} \\ \text{initial energy } E \text{ will emerge with a new energy} \\ E' \text{ in the interval } E' \text{ to } E' + dE'. \end{array}$$

We can explicitly calculate this quantity for the situation in which neutrons of moderate energies $(E < 1 \text{ MeV})$ scatter elastically via potential scattering from stationary nuclei of low mass number A.

## 2. KINEMATICS OF NEUTRON SCATTERING FROM STATIONARY NUCLEI

The kinematics of any two-body collision process is simplified very considerably when analyzed within the center-of-mass (CM) coordinate frame. We have sketched the collision event before and after the collision in both the LAB and CM coordinate frames in Figure 2-12. Here, lower-case notation corresponds
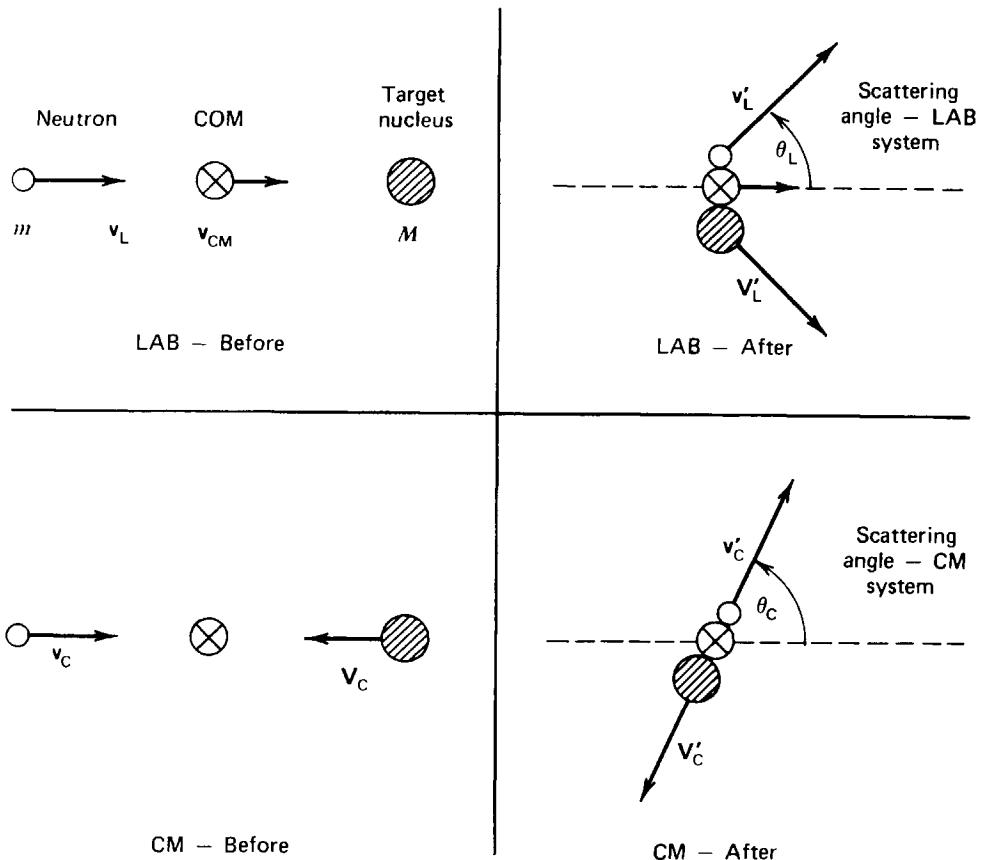
**FIGURE 2-12. Definition of collision coordinates in LAB and center-of-mass (CM) systems.**

to the neutron and upper-case notation to the nucleus. The subscripts L and C refer to LAB or CM frames, respectively.

The velocity of the CM frame is defined by

$$v_{CM} = \frac{1}{(m+M)}(mv_L + MV_L) = \left(\frac{1}{1+A}\right)v_L \qquad (2\text{-}55)$$

where we have assumed that the initial nucleus velocity $V_L$ is zero and noted that the nucleus–neutron mass ratio $M/m$ is essentially just the nuclear mass number $A$. If we note that the neutron and nucleus velocities in the CM frame are given by

$$v_C = v_L - v_{CM} = \frac{A}{A+1}v_L,$$
$$\qquad \qquad (2\text{-}56)$$
$$V_C = -v_{CM} = -\frac{1}{A+1}v_L,$$

then it is apparent that the total momentum in the CM frame is zero, as it must be.

We can relate the total kinetic energies in the LAB and CM frames by computing

$$\text{LAB: } E_L = \tfrac{1}{2}mv_L^2 + \tfrac{1}{2}MV_L^{2\,0},$$

$$\text{CM: } E_C = \tfrac{1}{2}mv_C^2 + \tfrac{1}{2}MV_C^2 = \tfrac{1}{2}\mu v_L^2. \qquad (2\text{-}57)$$

where we have introduced the reduced mass $\mu \equiv mM/(m+M)$. Hence we find the important relation between the energy in the CM and the LAB frames as

$$E_C = \frac{M}{m+M} E_L = \frac{A}{1+A} E_L. \qquad (2\text{-}58)$$

In particular it should be noted that the total energy in the CM system is always less than that in the LAB system. The energy difference is taken up by the center of mass motion itself.

Using conservation of momentum and energy, it is easy for one to demonstrate that the magnitudes of the CM velocities do not change in the collision:

$$v'_C = v_C = \frac{A}{A+1} v_L,$$

$$V'_C = V_C = \frac{1}{A+1} v_L; \qquad (2\text{-}59)$$

only their velocity vectors are rotated through the CM scattering angle $\theta_C$. This fact allows one to relate the scattering angles in the LAB and CM frames. Consider the vector diagram in Figure 2-13 illustrating the velocities and scattering angles in these two frames.

If we note from this diagram that

$$v'_L \sin \theta_L = v'_C \sin \theta_C,$$

$$v'_L \cos \theta_L = v_{CM} + v'_C \cos \theta_C, \qquad (2\text{-}60)$$

then we can relate the scattering angles in the CM and LAB frames by

$$\tan \theta_L = \frac{v'_C \sin \theta_C}{v_{CM} + v'_C \cos \theta_C} = \frac{\sin \theta_C}{\dfrac{1}{A} + \cos \theta_C}. \qquad (2\text{-}61)$$

This relationship is particularly useful since cross sections are usually calculated in the CM frame, but are measured and used in the LAB frame. If we denote the differential scattering cross sections characterizing scattering through angles $\theta_L$ and $\theta_C$ in the LAB and CM frames, $\sigma_L(\theta_L)$ and $\sigma_{CM}(\theta_C)$ respectively, we can use

$$\sigma_L(\theta_L) \sin \theta_L d\theta_L = \sigma_{CM}(\theta_C) \sin \theta_C d\theta_C \qquad (2\text{-}62)$$
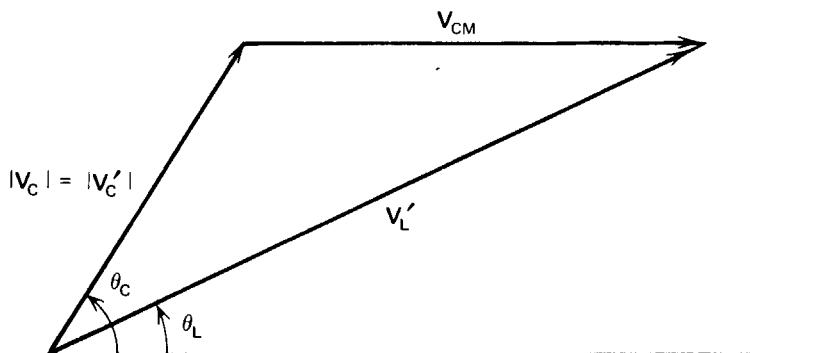


FIGURE 2-13.    Relation between the scattering angles in the LAB and CM frames.

to relate the LAB and CM differential scattering cross sections by

$$\sigma_L(\theta_L) = \sigma_{CM}(\theta_C) \frac{\left(\frac{1}{A^2} + \frac{2}{A}\cos\theta_C + 1\right)^{3/2}}{1 + \frac{1}{A}\cos\theta_C} . \tag{2-63}$$

Returning to our vector diagram in Figure 2-13 and using the law of cosines, we can find

$$\cos(180° - \theta_C) = \frac{v_C'^2 + v_{CM}^2 - v_L'^2}{2v_C v_{CM}} , \tag{2-64}$$

but using Eqs. (2-55) and (2-59), we can rewrite this as

$$\frac{1/2 m v_L'^2}{1/2 m v_L^2} = \frac{E'}{E} = \frac{A^2 + 1 + 2A\cos\theta_C}{(A+1)^2} . \tag{2-65}$$

It is useful to introduce a parameter related to the nuclear mass number $A$

$$\alpha \equiv \left(\frac{A-1}{A+1}\right)^2. \tag{2-66}$$

Then we can rewrite the *final* neutron energy after collision, $E_f \equiv E'$, in terms of the *incident* neutron energy, $E_i \equiv E$ as

$$E_f = \left[\frac{(1+\alpha) + (1-\alpha)\cos\theta_C}{2}\right] E_i. \tag{2-67}$$

Let us study this very important relation in more detail. First notice that it implies that the energy transfer from the neutron to the nucleus is directly related to the scattering angle in the CM frame. For example, if $\theta_C = 0$, then the neutron would lose no energy ($E_f = E_i$). This corresponds, of course, to no collision at all (a "miss"). The maximum energy loss occurs in a backscattering collision in which $\theta_C = 180°$. In this case, $E_f = \alpha E_i$. Hence the maximum energy that a neutron can lose in an elastic scattering collision with a stationary nucleus is $(1 - \alpha)E_i$. For example, in scattering collisions with hydrogen nuclei ($A = 1$), the neutron could conceivably lose all of its energy, while in a collision with a heavy nucleus such as $^{238}U$ it could lose at most 2% of its incident energy.

In summary, then, we have discovered two very important facts. First, a neutron cannot gain energy in an elastic collision with a stationary nucleus ($E_f$ is always less than $E_i$). Second, the neutron cannot emerge from an elastic scattering collision with an energy $E_f$ less than $\alpha E_i$.

We can now go one step further and actually calculate the scattering probability distribution, $P(E \to E')$, or in our present notation, $P(E_i \to E_f)$, for the case of elastic scattering from stationary nuclei. First we note from our preceding discussion that $P(E_i \to E_f)$ must vanish if the final energy $E_f$ does not fall within the range $\alpha E_i \leqslant E_f \leqslant E_i$. To calculate $P(E_i \to E_f)$ in this range, we will utilize the relationship Eq. (2-67).

If we recall that there is a one-to-one relationship between the neutron energy transfer and the scattering angle, we can infer that there must similarly be a relationship between the probability of the neutron experiencing a given energy transfer $E_i \to E_f$ and the probability that it will be scattered through a given scattering angle $\theta_C$. Yet the probability of scattering through an angle $\theta_C$ into $d\theta_C$ about $\theta_C$ is just given by

$$P(\theta_C)2\pi \sin\theta_C d\theta_C = \frac{\sigma_{CM}(\theta_C)}{\sigma_s} 2\pi \sin\theta_C d\theta_C. \tag{2-68}$$

Hence we can equate

$$P(E_i \to E_f)dE_f = -\frac{\sigma_{CM}(\theta_C)}{\sigma_s} 2\pi \sin\theta_C d\theta_C. \tag{2-69}$$

If we now differentiate Eq. (2-67)

$$dE_f = -\frac{E_i(1-\alpha)\sin\theta_C d\theta_C}{2}, \tag{2-70}$$

and substitute this into Eq. (2-69), we find the very important result

$$P(E_i \to E_f) = \frac{4\pi\sigma_{CM}(\theta_C)}{(1-\alpha)E_i\sigma_s}, \quad \alpha E_i \leqslant E_f \leqslant E_i. \tag{2-71}$$
$$0, \qquad \text{otherwise}$$

To complete the determination of $P(E_i \to E_f)$, we still need to know the differential scattering cross section in the CM frame. This knowledge must come from both a consideration of quantum mechanics and the detailed nuclear physics of the interaction. Fortunately, however, we can avoid such considerations since the CM potential scattering cross sections characterizing neutrons of interest in reactor applications (with energies $E < 10\,\text{MeV}$) do not depend on $\theta_C$ for light nuclei (say $A \leqslant 12$). That is, the scattering in the CM frame is isotropic such that

$$\sigma_{CM}(\theta_C) = \frac{\sigma_s}{4\pi} \tag{2-72}$$

Such behavior is known as "s-wave" scattering (a term which arises from quantum mechanics) and is the most common form of elastic scattering in nuclear reactors. For heavier nuclei, there will tend to be some mild angular dependence of $\sigma_{CM}(\theta_C)$, but since elastic scattering from such nuclei does not contribute appreciably to neutron energy loss in most nuclear reactor types, we will confine our attention here to s-wave elastic scattering from stationary nuclei. Then, using Eq. (2-72) in Eq. (2-71), we find that the scattering probability distribution for elastic s-wave scattering from stationary nuclei takes the form

$$P(E_i \to E_f) = \frac{1}{(1-\alpha)E_i}, \quad \alpha E_i \leqslant E_f \leqslant E_i. \tag{2-73}$$
$$0, \qquad \text{otherwise}$$

Notice in particular that the probability of scattering from an energy $E_i$ to a final energy $E_f$ is independent of the final energy $E_f$.

Using this probability distribution, we can compute the average final energy of a neutron suffering an elastic scattering collision as

$$\overline{E}_f \equiv \int_{\alpha E_i}^{E_i} dE_f \, E_f \, P(E_i \rightarrow E_f) = \left( \frac{1+\alpha}{2} \right) E_i. \tag{2-74}$$

Hence the average energy loss in such collisions is

$$\overline{\Delta E} = E_i - \overline{E}_f = \left( \frac{1-\alpha}{2} \right) E_i. \tag{2-75}$$

For example, neutrons suffering scattering collisions in hydrogen ($\alpha = 0$) will lose on the average half of their original energy in each collision. By way of contrast, in a scattering collision with a $^{238}$U nucleus, they will lose on the average less than 1% of their original energy.

We can now write the differential scattering cross section characterizing elastic (s-wave) scattering from stationary nuclei by substituting Eq. (2-73) into Eq. (2-54)

$$\sigma_s(E_i \rightarrow E_f) = \begin{cases} \dfrac{\sigma_s(E_i)}{(1-\alpha)E_i}, & \alpha E_i \leqslant E_f \leqslant E_i \\ 0, & \text{otherwise.} \end{cases} \tag{2-76}$$

This is about as far as we can go in determining the explicit form of $\sigma_s(E_i \rightarrow E_f)$ since the elastic scattering cross section $\sigma_s(E)$ itself depends on the details of the nuclear potential and is generally obtainable only by measurement. Fortunately $\sigma_s(E)$ characterizing potential scattering is only weakly dependent on energy and can frequently be taken as constant over a wide range of neutron energies.

Such elastic scattering plays a very important role in nuclear reactor behavior since it tends to slow the fast fission neutrons down to thermal energies. However inelastic scattering processes are also important, particularly in fast reactors where neutron moderation by light isotopes is minimized. Since kinetic energy is not a conserved quantity in an inelastic scattering collision (the nucleus is left in an excited state), we can no longer use simple kinematical arguments to determine $P(E_i \rightarrow E_f)$ for such processes. Rather one must rely on measurements of the differential scattering cross section or on nuclear models. Although such models are useful for qualitative estimates of neutron scattering, most detailed reactor studies simply use the measured cross section in essentially tabular form for the various different energy transfer combinations $E_i \rightarrow E_f$.

One final comment should be made concerning the "other half" of a scattering event, namely the nuclear recoil. Although this is of little concern to the neutron economist, it is of very considerable concern to the reactor designer since the recoil energy of a nucleus suffering a collision with a fast neutron will be sufficient to rip it completely out of its crystalline lattice. To be more specific, the average recoil energy of a nucleus suffering an elastic scattering collision with a neutron is just $\frac{1}{2}(1 - \alpha)E_i$ [recall Eq. (2-75)]. For fast neutrons, this recoil energy will be in the keV to low MeV range. Hence the recoiling nucleus will not only be torn out of its own

lattice position by the collision, but will possess sufficient recoil energy to dislocate other nuclei in the lattice, leading to significant radiation damage to the material. This is an extremely important process in materials exposed to the high radiation environment of a nuclear reactor core and must be taken into account in nuclear reactor design. We will return to consider it in more detail in Chapter 11.

## 3. EFFECTS OF NUCLEAR MOTION

Thus far we have studied neutron cross section behavior under the assumption that the target nuclei are at rest; but of course the nuclei are always in a state of thermal motion. Fortunately the speeds characterizing nuclear motions are often very much less than those of the neutrons, and for many purposes this nuclear motion can be neglected entirely.

There are two instances in which such thermal motion of the nuclei must be taken into account, however. If the neutron speeds are comparable to the nuclear speeds, then of course one can no longer treat the nuclei as stationary. This will occur when the neutron energy becomes comparable to the thermal energy of the nuclei, that is $v \cong V_{th} = (kT/M)^{1/2}$ or $E \cong kT$. Such a comparison indicates that for neutron energies less than roughly 1 eV, one must specifically account for the thermal motion of the nuclei. As we mentioned earlier, such low-energy neutrons are referred to as *thermal* neutrons.

There is also a situation in which the effects of nuclear motion must be taken into account even when the neutron speed is much larger than that of the nuclei. This arises when considering processes in which the cross sections exhibit sharp resonances. Since the width of these resonances may be quite narrow, much less than 1 eV in most cases of interest, even the modest speeds of nuclear thermal motion can significantly affect the energy dependence of the neutron cross section in the vicinity of the resonance. Such a phenomenon is known as the *Doppler effect*, since it is closely akin to the familiar frequency shift that accompanies variations in relative motions between source and receiver in sound propagation.

In this section we will first examine the effects of nuclear motion on neutron cross section behavior for both thermal neutrons and cross section resonances. We will then briefly discuss the modifications that occur in the differential scattering cross section when the thermal motion of the nuclei is taken into account.

### (a) THERMALLY AVERAGED INTERACTION RATES

Let us begin by considering an interaction between a neutron of velocity $\mathbf{v}$ and a nucleus moving at a velocity $\mathbf{V}$. If the atomic number density of such nuclei is $N$, then the interaction frequency for such reactions is given by

$$|\mathbf{v} - \mathbf{V}|\sigma(|\mathbf{v} - \mathbf{V}|)N, \qquad (2\text{-}77)$$

where we have noted that it is the relative speed, $|\mathbf{v} - \mathbf{V}|$, that occurs in this interaction frequency.

Of course not all of the nuclei in the target sample will be moving with the same velocity $\mathbf{V}$. In general they will have a distribution of velocities, and in fact, the interaction frequency we are really interested in is the average of Eq. (2-77) over these various nuclear velocities. Suppose we define the distribution of nuclear

velocities

$$\mathfrak{N}(\mathbf{V})d^3V \equiv \text{Number of target atoms/cm}^3 \text{ with velocities} \qquad (2\text{-}78)$$
$$\mathbf{V} \text{ in } d^3V \text{ about } \mathbf{V}.$$

Then the probability of a neutron interaction per neutron per second with a nucleus of any velocity is obtained by averaging Eq. (2-77) over $\mathfrak{N}(\mathbf{V})$

$$vN\bar{\sigma}(v) \equiv \int d^3V |\mathbf{v} - \mathbf{V}| \sigma(|\mathbf{v} - \mathbf{V}|) \mathfrak{N}(\mathbf{V}). \qquad (2\text{-}79)$$

Notice that we have essentially used this expression to define an averaged cross section $\bar{\sigma}(v)$ depending only on the neutron speed $v$. That is, we can write the appropriately averaged cross section characterizing neutrons moving with a speed $v$ through a sample of nuclei with a velocity distribution $\mathfrak{N}(\mathbf{V})$ as

$$\bar{\sigma}(v) = \frac{1}{vN} \int d^3V |\mathbf{v} - \mathbf{V}| \sigma(|\mathbf{v} - \mathbf{V}|) \mathfrak{N}(\mathbf{V}). \qquad (2\text{-}80)$$

It is important to remember that this is the cross section that would be measured in an experiment (such as the transmission experiment we described earlier). No experiment looks directly at the true neutron–nuclear reaction cross section, but rather measures an average of $\sigma(|\mathbf{v} - \mathbf{V}|)$ over the distribution of nuclear velocities. The same is true for applications of such cross sections to nuclear reactor analysis. Since any reactor is at a finite temperature, the nuclei comprising its core will be in thermal motion, and hence one must take care to always use cross sections that have been appropriately averaged over these nuclear velocities. Since this distribution function depends on the temperature characterizing the material of interest, the "thermally averaged" cross sections will similarly depend on temperature.

It is useful to consider the application of this result to two particularly simple examples of cross section behavior. We mentioned earlier that many nuclear cross sections behave essentially as $1/v$ (e.g., below a capture resonance). If nuclear motion is to be included, we would express such behavior as

$$\sigma(|\mathbf{v} - \mathbf{V}|) = \frac{\gamma}{|\mathbf{v} - \mathbf{V}|}. \qquad (2\text{-}81)$$

If we substitute this form into Eq. (2-80) and note that the nuclear velocity distribution function is normalized such that

$$\int d^3V \, \mathfrak{N}(\mathbf{V}, T) = N, \qquad (2\text{-}82)$$

then we find the averaged cross section becomes just

$$\bar{\sigma}(v, T) = \frac{\gamma}{v}. \qquad (2\text{-}83)$$

Hence in this instance the observed cross section depends on neutron speed $v$ in exactly the same way as the true cross section depends on relative speeds. Furthermore the observed cross section is independent of temperature.

A second example of interest is that in which the cross section $\sigma(|\mathbf{v} - \mathbf{V}|)$ is a very slowly varying function of relative speed. Since the nuclear velocity distribution is rather sharply peaked around $V = V_{th}$, we can approximate Eq. (2-80) by neglecting $\mathbf{V}$ in the relative speed in the integrand for neutron speeds $v \gg V_{th}$. In this case, we again find that

$$\bar{\sigma}(v, T) \cong \sigma(v) \qquad (2\text{-}84)$$

such that the true cross section and the observed cross section are again the same, and the observed cross section is temperature-independent. This behavior is frequently exhibited by the scattering cross section for many reactor materials.

It is also of interest to examine the behavior of the averaged cross section for small neutron speeds $v \ll V_{th}$. Then we can replace $|\mathbf{v} - \mathbf{V}|$ by $V$ in the integrand to find

$$\bar{\sigma}(v, T) \underset{v \to 0}{\longrightarrow} \frac{1}{vN} \int d^3V \, V\sigma(V) \mathfrak{N}(\mathbf{V}, T). \qquad (2\text{-}85)$$

Since the integral is now just a constant, independent of the neutron speed $v$, we find that the behavior of $\bar{\sigma}(v, T)$ as the neutron speed $v$ becomes very small is just

$$\bar{\sigma}(v, T) \sim \frac{C}{v} \quad \text{as } v \to 0. \qquad (2\text{-}86)$$

This explains the low-energy behavior we observed earlier in the total cross section for graphite. Of course this result can be explained physically by simply recognizing that for small neutron velocities, the neutron appears to be essentially stationary to the more rapidly moving nuclei. Hence the collision rate ceases to depend on the neutron speed and depends only on the nuclear speed distribution (i.e., the temperature of the scattering material).

Such averages over the thermal velocity distribution of the nuclei in a material must always be performed in measuring or utilizing cross sections characterizing thermal neutrons. However such an average is also extremely important in determining the correct effective cross sections to use when describing resonance behavior.

Life could become exceedingly complex indeed if a detailed estimate of the nuclear velocity distribution function $\mathfrak{N}(\mathbf{V})$ were required, since this depends on the complicated microscopic dynamics of atoms in the reactor (e.g., atomic vibrations in crystalline lattices or atomic motions in liquids). Fortunately it is sufficient for most purposes to represent the nuclear velocity distribution by the Maxwell–Boltzmann distribution characterizing an ideal gas in thermal equilibrium at a temperature $T$:

$$\mathfrak{N}(\mathbf{V}) = NM(\mathbf{V}, T) \equiv N \left( \frac{M}{2\pi kT} \right)^{3/2} \exp(-MV^2/2kT). \qquad (2\text{-}87)$$

Then one can write the thermally averaged cross section as

$$\bar{\sigma}(v, T) = \frac{1}{v} \int d^3V \, |\mathbf{v} - \mathbf{V}| \sigma(|\mathbf{v} - \mathbf{V}|) M(\mathbf{V}, T). \qquad (2\text{-}88)$$

We will make use of this particular average in the next section.

## (b) THE DOPPLER EFFECT ON CROSS SECTION RESONANCE BEHAVIOR

We have seen that the actual or true cross section depends on the relative speed between the neutron and the target nucleus. However since the nuclei themselves are in thermal motion, this relative speed may be either greater or less than the neutron speed. This difference in relative speeds gives rise to a "Doppler shift" effect in resonance cross section behavior.

We can take account of this effect by merely substituting the Breit-Wigner resonance cross section formulas into our expressions for the thermally averaged cross sections in Eqs. (2-80) or (2-88). For the purposes of this calculation it is usually adequate to assume that the nuclear velocities are described by a Maxwell-Boltzmann distribution $M(\mathbf{V})$.

Now recall that the single-level Breit-Wigner formula for a capture resonance gives the cross section

$$\sigma_\gamma(E_C) = \sigma_0 \frac{\Gamma_\gamma}{\Gamma} \left(\frac{E_0}{E_C}\right)^{1/2} \left[4\left(\frac{E_C - E_0}{\Gamma}\right)^2 + 1\right]^{-1}, \tag{2-89}$$

in terms of the center of mass energy $E_C$. Our task is to express $E_C$ in terms of the nuclear velocity vector $\mathbf{V}$ and then perform the integration over nuclear velocities indicated in the averaging formula Eq.(2-88). There is really nothing particularly complicated about this task, except for a bit of vector algebra and the fact that the integral that arises cannot be explicitly performed (rather, it must be performed numerically or tabulated).

Since this manipulation is not particularly enlightening, we will only outline the major steps here and refer the interested reader to more exhaustive treatments that exist in numerous places throughout the literature.[18-21] We begin by noting that for the case of a Maxwell-Boltzmann distribution of target nuclei, one can partially perform[20] the integration over nuclear velocity $\mathbf{V}$ to rewrite Eq. (2-88) as

$$\bar{\sigma}_\gamma(v, T) = \frac{1}{\sqrt{\pi}\, v_{th}^2 v} \int_0^\infty dv_r\, v_r^2 \sigma_\gamma(v_r) \left[\exp\left[-\frac{(v - v_r)^2}{2v_{th}^2}\right] - \exp\left[-\frac{(v + v_r)^2}{2v_{th}^2}\right]\right], \tag{2-90}$$

where $v_r = |\mathbf{v} - \mathbf{V}|$ while $v_{th} = (kT/m)^{1/2}$. If we substitute the Breit-Wigner formula (2-30) for $\sigma_\gamma(v_r)$ into this integral, we find an exact expression for the averaged cross section

$$\bar{\sigma}_\gamma(v, T) = \sigma_0 \frac{\Gamma_\gamma}{\Gamma} \frac{1}{\sqrt{\pi}\, v_{th}^2 v} \int_0^\infty \frac{dv_r\, v_r}{1 + y^2} \left[\exp\left[-\frac{(v - v_r)^2}{2v_{th}^2}\right] - \exp\left[-\frac{(v + v_r)^2}{2v_{th}^2}\right]\right]. \tag{2-91}$$

Here we have defined $y \equiv 2(E_C - E_0)/\Gamma$ where we recall that the CM energy is $E_C = \frac{1}{2}\mu v_r^2$. However this is where we get stuck, because unfortunately this integral cannot be evaluated analytically. Fortunately it is rather easy to compute the integral numerically. However before discussing such calculations, it is useful to

cast Eq. (2-91) into a slightly different form by defining the variables

$$x \equiv 2(E - E_0)/\Gamma \text{ and } \zeta \equiv \Gamma/\Gamma_D \qquad (2\text{-}92)$$

where $\Gamma_D$ is the so-called *Doppler width* of the resonance

$$\Gamma_D \equiv \left( \frac{4E_0 kT}{A} \right)^{1/2}. \qquad (2\text{-}93)$$

Then one can write

$$\bar{\sigma}_\gamma(E, T) = \sigma_0 \frac{\Gamma_\gamma}{\Gamma} \left( \frac{E_0}{E} \right)^{1/2} \Psi(\zeta, x), \qquad (2\text{-}94)$$

where

$$\Psi(\zeta, x) \equiv \frac{\zeta}{2} \int_{-2E/\Gamma}^{\infty} \frac{dy}{1+y^2} \left[ \exp\left[ -\frac{(v - v_r)^2}{2v_{th}^2} \right] - \exp\left[ -\frac{(v + v_r)^2}{2v_{th}^2} \right] \right]. \qquad (2\text{-}95)$$

In practice, the $\Psi(\zeta, x)$ would be calculated for each value of $\zeta$ and $x$ of interest using straightforward numerical integration techniques. To better understand the implications of such calculations, we have sketched the thermally averaged capture cross section as determined by Eq. (2-94) in Figure 2-14.

In particular, we have sketched the dependence of this cross section on energy for several different temperatures $T$. It should first be noted that as the temperature $T$ increases, the resonance broadens, while its peak magnitude decreases. For this reason, one frequently refers to resonance cross sections that have been averaged over the distribution of nuclear velocities as "Doppler-broadened" cross sections.

It should be stressed that we still have not introduced any additional assumptions or approximations into this derivation of the Doppler-broadened resonance cross section form Eq. (2-94). And in several modern computer codes, Doppler-
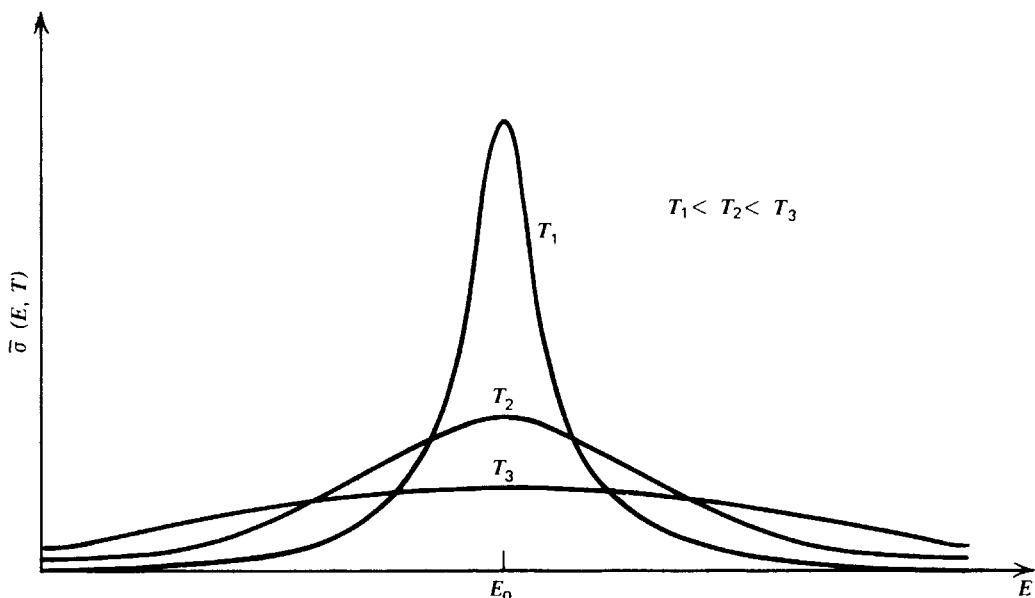


FIGURE 2-14. Doppler-broadening of a resonance with increasing temperature.

broadened cross sections are calculated directly from this expression.[19] However there is an alternative *approximate* expression for the Doppler-broadened Breit–Wigner resonance cross section first derived many years ago by Bethe and Placzek[18] which is more commonly found in textbooks. If one introduces the following approximations into $\Psi(\zeta,x)$:

(a) Neglect the second exponential in the integrand of $\Psi(\zeta,x)$.
(b) Replace $v' - v'_r$ by $(v'^2 - v'^2_r)/2v'$—which is equivalent to approximating

$$\sqrt{E_C} = \sqrt{E}\left(1 + \frac{E_C - E}{E}\right)^{1/2} \sim \sqrt{E}\left[1 + \frac{E_C - E}{2E}\right]. \qquad (2\text{-}96)$$

(c) Extend the lower limit of integration to $y = -\infty$;

then one finds

$$\Psi(\zeta,x) \sim \psi(\zeta,x) \equiv \frac{\zeta}{2\sqrt{\pi}} \int_{-\infty}^{\infty} dy\, \frac{\exp\left[-\frac{1}{4}(x-y)^2\zeta^2\right]}{1+y^2}, \qquad (2\text{-}97)$$

while

$$\bar{\sigma}_\gamma(E,T) \sim \sigma_0 \frac{\Gamma_\gamma}{\Gamma}\left(\frac{E_0}{E}\right)^{1/2} \psi(\zeta,x). \qquad (2\text{-}98)$$

The Bethe–Placzek cross section Eq. (2-98) is used very frequently in reactor calculations and for convenience we have tabulated $\psi(\zeta,x)$ in Table 2-2. The approximations used to obtain the Bethe–Placzek form break down for high-temperature target distributions and for low energy resonances. For example, a comparison for the 0.296 eV fission resonance of $^{239}$Pu at $T=2000°C$ shows a difference in broadening of 50% between the exact and approximate formulations.[22]

However since it is still traditional to utilize the Bethe–Placzek form in analyzing resonance behavior, we will include a brief analytical study of its behavior along with that of the exact expression. First notice that for low temperatures $T \rightarrow 0$ we can see from Eqs. (2-92) and (2-93) that $\zeta \rightarrow \infty$. Hence the integrand of both $\Psi(\zeta,x)$ and $\psi(\zeta,x)$ will vanish except in the neighborhood of $y \sim x$. We can therefore replace $y$ by $x$ in the denominator of the integrands to write

$$\Psi(\zeta,x) \sim \psi(\zeta,x) \sim \frac{\zeta}{2\sqrt{\pi}} \frac{1}{1+x^2} \int_{-\infty}^{\infty} dy\, \exp\left[-\frac{1}{4}(x-y)^2\zeta^2\right] = \frac{1}{1+x^2}. \qquad (2\text{-}99)$$

Hence for low temperatures we arrive at the usual Breit–Wigner form

$$\bar{\sigma}_\gamma(E,0) = \sigma_0 \frac{\Gamma_\gamma}{\Gamma}\left(\frac{E_0}{E}\right)^{1/2}\left[4\left(\frac{E-E_0}{\Gamma}\right)^2 + 1\right]^{-1}, \qquad (2\text{-}100)$$

which is a comforting, although certainly expected, result.

**TABLE 2-2     Tabulations of the Doppler Broadening Functions[†]**

The $\psi$ Function

| $\zeta$ | $x$ 0 | 0.5 | 1 | 2 | 4 | 6 | 8 | 10 | 20 | 40 |
|---|---|---|---|---|---|---|---|---|---|---|
| 0.05 | 0.04309 | 0.04308 | 0.04306 | 0.04298 | 0.04267 | 0.04216 | 0.04145 | 0.04055 | 0.03380 | 0.01639 |
| 0.10 | 0.08384 | 0.08379 | 0.08364 | 0.08305 | 0.08073 | 0.07700 | 0.07208 | 0.06623 | 0.03291 | 0.00262 |
| 0.15 | 0.12239 | 0.12223 | 0.12176 | 0.11989 | 0.11268 | 0.10165 | 0.08805 | 0.07328 | 0.01695 | 0.00080 |
| 0.20 | 0.15889 | 0.15854 | 0.15748 | 0.15331 | 0.13777 | 0.11540 | 0.09027 | 0.06614 | 0.00713 | 0.00070 |
| 0.25 | 0.19347 | 0.19281 | 0.19086 | 0.18324 | 0.15584 | 0.11934 | 0.08277 | 0.05253 | 0.00394 | 0.00067 |
| 0.30 | 0.22624 | 0.22516 | 0.22197 | 0.20968 | 0.16729 | 0.11571 | 0.07042 | 0.03880 | 0.00314 | 0.00065 |
| 0.35 | 0.25731 | 0.25569 | 0.25091 | 0.23271 | 0.17288 | 0.10713 | 0.05724 | 0.02815 | 0.00289 | 0.00064 |
| 0.40 | 0.28679 | 0.28450 | 0.27776 | 0.25245 | 0.17359 | 0.09604 | 0.04566 | 0.02109 | 0.00277 | 0.00064 |
| 0.45 | 0.31477 | 0.31168 | 0.30261 | 0.26909 | 0.17052 | 0.08439 | 0.03670 | 0.01687 | 0.00270 | 0.00064 |
| 0.50 | 0.34135 | 0.33733 | 0.32557 | 0.28286 | 0.16469 | 0.07346 | 0.03025 | 0.01446 | 0.00266 | 0.00063 |

The $\chi$ Function

| $\zeta$ | $x$ 0 | 0.5 | 1 | 2 | 4 | 6 | 8 | 10 | 20 | 40 |
|---|---|---|---|---|---|---|---|---|---|---|
| 0.05 | 0 | 0.00120 | 0.00239 | 0.00478 | 0.00951 | 0.01415 | 0.01865 | 0.02297 | 0.04076 | 0.05221 |
| 0.10 | 0 | 0.00458 | 0.00915 | 0.01821 | 0.03573 | 0.05192 | 0.06626 | 0.07833 | 0.10132 | 0.05957 |
| 0.15 | 0 | 0.00986 | 0.01968 | 0.03894 | 0.07470 | 0.10460 | 0.12690 | 0.14096 | 0.12219 | 0.05341 |
| 0.20 | 0 | 0.01680 | 0.03344 | 0.06567 | 0.12219 | 0.16295 | 0.18538 | 0.19091 | 0.11754 | 0.05170 |
| 0.25 | 0 | 0.02515 | 0.04994 | 0.09714 | 0.17413 | 0.21909 | 0.23168 | 0.22043 | 0.11052 | 0.05103 |
| 0.30 | 0 | 0.03470 | 0.06873 | 0.13219 | 0.22694 | 0.26757 | 0.26227 | 0.23199 | 0.10650 | 0.05069 |
| 0.35 | 0 | 0.04529 | 0.08940 | 0.16976 | 0.27773 | 0.30564 | 0.27850 | 0.23236 | 0.10437 | 0.05049 |
| 0.40 | 0 | 0.05674 | 0.11160 | 0.20890 | 0.32442 | 0.33286 | 0.28419 | 0.22782 | 0.10316 | 0.05037 |
| 0.45 | 0 | 0.06890 | 0.13498 | 0.24880 | 0.36563 | 0.35033 | 0.28351 | 0.22223 | 0.10238 | 0.05028 |
| 0.50 | 0 | 0.08165 | 0.15927 | 0.28875 | 0.40075 | 0.35998 | 0.27979 | 0.21729 | 0.10185 | 0.05022 |

[†]T. D. Beynon and I. S. Grant, *Nucl. Sci. Eng.* **17**, 547 (1963).

At the other extreme, the high temperature limit $T \to \infty$ implies that $\zeta \to 0$. In this case we find

$$\bar{\sigma}_\gamma(E,T) \to \sigma_0 \frac{\Gamma_\gamma}{\Gamma}\left(\frac{E_0}{E}\right)^{1/2} \frac{\zeta}{2\sqrt{\pi}} \int_{-\infty}^{\infty} \frac{dy}{1+y^2} \exp\left[-\frac{\zeta^2 x^2}{4}\right]$$

$$= \sigma_0 \frac{\Gamma}{\Gamma_D}\left(\frac{E_0}{E}\right)^{1/2} \frac{\sqrt{\pi}}{2} \exp\left[\frac{-(E-E_0)^2}{\Gamma_D^2}\right], \tag{2-101}$$

which is a Gaussian shape characterized by the Doppler width $\Gamma_D$ rather than the "natural" line width $\Gamma$. Hence as the temperature increases, the resonance broadens out from its natural width to eventually approach a width that depends on the temperature as $T^{\frac{1}{2}}$.

One other observation is important. If the Bethe–Placzek form is examined in greater detail, it becomes apparent that regardless of the temperature, the area under the resonance remains constant. We can demonstrate this by simply integrating over the resonance

$$\int_{\text{resonance}} dE\, \bar{\sigma}_\gamma(E,T) = \sigma_0 \frac{\Gamma_\gamma}{\Gamma} \int_{\text{resonance}} dx\, \psi(\zeta,x). \tag{2-102}$$

However since the contribution to the integral from the "wings" of the resonance (far-off resonance) are so small, we can approximately extend the range of integration to $\pm\infty$ so that we can explicitly perform the integral to find

$$\int dE\, \bar{\sigma}_\gamma(E,T) \cong \sigma_0 \frac{\Gamma_\gamma}{\Gamma} \int_{-\infty}^{\infty} \frac{dy}{1+y^2} \int_{-\infty}^{\infty} dx\, \exp\left[ -\tfrac{1}{4}(x-y)^2\zeta^2 \right] = \sigma_0 \Gamma_\gamma \frac{\pi}{2}, \tag{2-103}$$

a result which is temperature-independent.

It should be pointed out that such behavior is a consequence of the Bethe–Placzek approximation. More generally, the area under the Doppler-broadened resonance given by the exact expression Eq. (2-94) *will* in fact *change* with temperature.[22] However for the temperature range and resonances of interest in most reactor applications, this change is relatively small, and one can essentially assume that the area under the resonance is relatively insensitive to temperature changes. This fact will prove of some importance in our later study of reactor behavior, since it will imply that an increase in the temperature of the absorbing material will increase the rate at which neutrons are absorbed in the resonance range of the cross section.

Thus far we have only examined the effect of thermal nuclear motions on a capture resonance. However we could of course have also substituted in our expression for scattering cross sections in the vicinity of a resonance, Eq. (2-38), into the expression for thermally averaged cross sections Eq. (2-88) and labored through some algebra to again arrive at Doppler-broadened cross sections which again involve integrals that cannot be performed explicitly. We will avoid the agony of such manipulation and only state the result of such labors here:

$$\bar{\sigma}_s(E,T) = \sigma_0 \frac{\Gamma_n}{\Gamma} \psi(\zeta,x) + \frac{\sigma_0 R}{\lambda_0} \chi(\zeta,x) + 4\pi R^2, \tag{2-104}$$

where we have defined another tabulated function[21] $\chi(\zeta,x)$ (see Table 2-2) to characterize the interference term:

$$\chi(\zeta,x) \equiv \frac{\zeta}{\sqrt{\pi}} \int_{-\infty}^{\infty} dy\, \frac{y \exp\left[ -\tfrac{1}{4}\zeta^2(x-y)^2 \right]}{1+y^2}. \tag{2-105}$$

We will later utilize these expressions to study the absorption of neutrons in nuclear reactors. Although we have consistently denoted the thermally averaged cross sections with an over-bar, for instance, $\bar{\sigma}_s(E,T)$, we will usually omit this notation in future discussions and simply regard all resonance cross sections as having been Doppler-broadened.

(c) *DIFFERENTIAL SCATTERING CROSS SECTIONS WITH UPSCATTERING*

We will now discuss the modifications necessary in our study of the differential scattering cross section characterizing elastic potential scattering when effects of nuclear motion must be taken into account. Recall that in our earlier discussion we found that the neutron could not gain energy in an elastic collision with a stationary nucleus. It can only lose energy in such a collision. It is customary to refer to such a process as "downscattering," since the neutron will scatter down in energy.

We can make this more explicit by considering a particularly simple example in which an incident neutron scatters elastically from a stationary hydrogen nucleus (a proton). Then the scattering probability distribution is just

$$P(E_i \rightarrow E_f) = \begin{cases} 1/E_i, & E_f \leqslant E_i \\ 0, & E_f > E_i \end{cases} \tag{2-106}$$

That is, the scattering probability is independent of the final energy $E_f$ and vanishes for $E_f > E_i$ (corresponding to upscattering in energy).

Let us now consider the situation in which the neutron suffers elastic scattering collisions in a hydrogen gas at *finite* temperature $T$ in which the nuclei are in motion with a Maxwell–Boltzmann velocity distribution $M(\mathbf{V}, T)$. It is necessary to repeat our earlier consideration of two-body kinematics to include the motion of the target nucleus. One would then have to average the cross section characterizing such scattering over the nuclear velocity distribution $M(\mathbf{V}, T)$, just as we did in the previous sections. Since these tasks are rather tedious, we will simply note that the results of such calculations[23] are that for such a proton gas at temperature $T$, the differential scattering cross section is given by

$$\sigma_s(E_i \rightarrow E_f) = \begin{cases} \dfrac{\sigma_s^H}{E_i} \text{erf} \sqrt{\dfrac{E_f}{kT}}, & E_f \leqslant E_i \\[4mm] \dfrac{\sigma_s^H}{E_i} \exp\left(\dfrac{E_i - E_f}{kT}\right) \text{erf} \sqrt{\dfrac{E_i}{kT}}, & E_f > E_i \end{cases} \tag{2-107}$$

where the error function is defined by

$$\text{erf} \, x = \frac{2}{\sqrt{\pi}} \int_0^x dt \, e^{-t^2}. \tag{2-108}$$

We have plotted $P(E_i \rightarrow E_f)$ for several incident neutron energies $E_i$ in Figure 2-15. It should first be noted that unlike the situation in which the hydrogen nuclei were initially at rest, the scattering probability now depends on the final energy $E_f$. Furthermore this probability is not zero for $E_f > E_i$ for a finite temperature gas, hence implying that it is possible for the neutron to *gain* energy in a scattering collision. Such "upscattering" events are significant for incident neutron energies up to about $10kT$. Above this energy, the scattering probability begins to resemble that characterizing stationary nuclei (i.e., a $T = 0$ hydrogen gas).
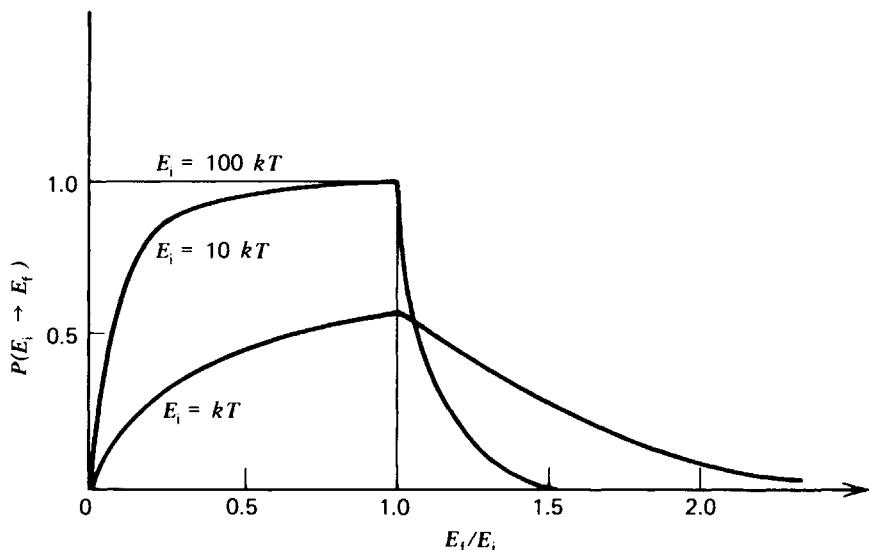
**FIGURE 2-15.** The scattering probability distribution $P(E_i \rightarrow E_f)$ characterizing neutron scattering from a proton gas at temperature $T$.

One could repeat this calculation for a free gas of arbitrary mass number $A$, but the expressions for the scattering probability and differential scattering cross section become quite complicated. Since there are also other effects important in low-energy neutron scattering such as chemical binding and diffraction, we will defer a more detailed discussion of thermal neutron cross section behavior until Chapter 9. However even this brief discussion should indicate the importance of accounting for the thermal motion of the target nuclei in measuring or using low-energy neutron cross sections.

## II. NUCLEAR FISSION

### A. Fission Physics

The binding energy per nucleon in atomic nuclei reaches a maximum of 8.7 MeV for nuclei mass numbers of about 50 (see Figure 2-16). Hence it is possible to produce more tightly bound nuclei and thereby release energy by either fusing together lighter nuclei (*nuclear fusion*) or inducing a heavy nucleus into fissioning into two nuclei of intermediate mass number (*nuclear fission*). The observed stability of heavy nuclei against spontaneous fission is due to the short-range nuclear forces within the nucleus giving rise to a potential energy barrier that must be overcome before the nucleus will fission. The size of this fission barrier is typically 6–9 MeV in most heavy nuclei of interest. Hence to induce nuclear fission, one must add a sufficient amount of energy to the heavy nucleus to overcome this fission barrier.

This can be done in a variety of ways. One could simply slam an energetic particle (with kinetic energy greater than the fission barrier) into the nucleus. An example of such a reaction would be photofission, in which a high-energy gamma strikes a heavy nucleus, thereby inducing fission. An alternative scheme would be to let the heavy nucleus capture a neutron. Then the binding energy of the added neutron itself might be sufficient to overcome the fission barrier and induce fission. This later process can in fact occur in certain heavy nuclei such as $^{233}U$, $^{235}U$,
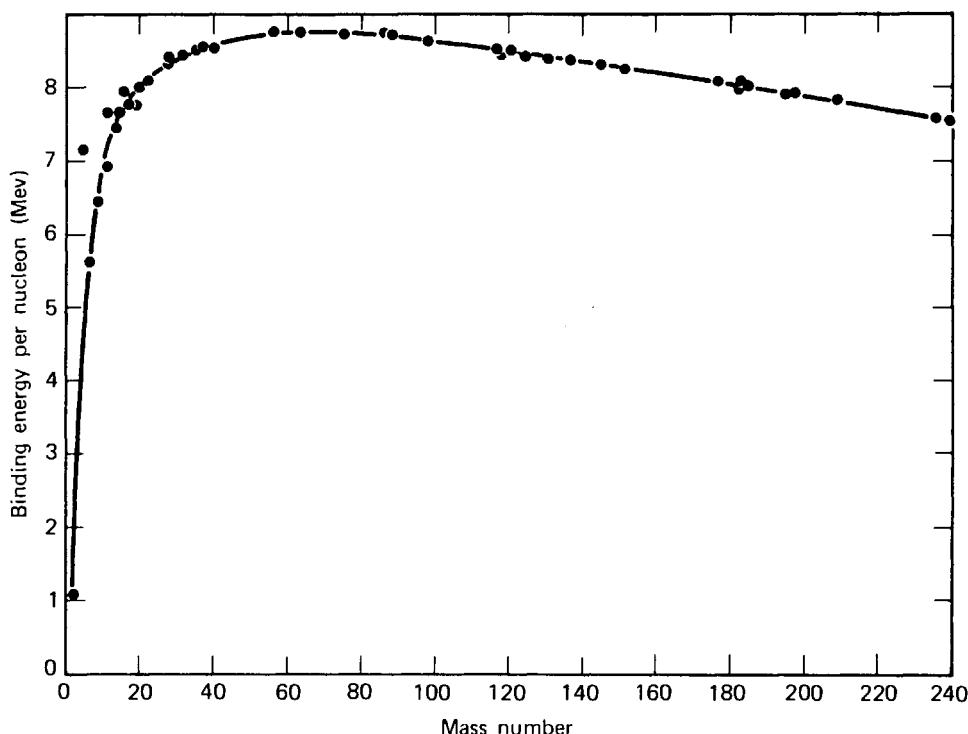
FIGURE 2-16.    Binding energy per nucleon versus mass number.

$^{239}$Pu, and $^{241}$Pu. Such nuclides that can be induced to fission with neutrons of essentially zero kinetic energy (or of more relevance to nuclear reactor applications, thermal neutrons having very small kinetic energies, at least compared to nuclear energies) are referred to as *fissile* nuclides. We will see later that such fissile nuclides represent the principal fuels used in fission chain-reacting systems.

With most heavy nuclides, the additional binding energy provided by a captured neutron is not sufficient to push the heavy nucleus over the fission barrier. Frequently, however, one can add a dash of extra energy to the neutron, for instance by giving it a kinetic energy of an MeV or so, and this is sufficient to lift the nucleus the rest of the way over the barrier to cause fission. Nuclides that can be fissioned with such "fast" neutrons are referred to as *fissionable*. Examples are $^{232}$Th, $^{238}$U, and $^{240}$Pu (as well as fissile nuclei such as $^{235}$U). Although such fissionable nuclides do play an important role as nuclear fuels they are unable to sustain by themselves a stable fission chain reaction and hence must always be used in combination with a fissile nuclide such as $^{235}$U or $^{239}$Pu.

There is also a small possibility that certain heavy nuclei will fission spontaneously via the barrier penetration mechanism familiar from quantum mechanics. However the probability for such an event is quite low in most nuclides of interest as nuclear fuels. For example, the half-life for spontaneous fission in $^{238}$U is some $6.5 \times 10^{15}$ years. However even this very slow spontaneous fission rate can be of importance in nuclear systems, since even a few neutrons can be rapidly multiplied to appreciable numbers in a growing chain reaction.

## B. Fission Cross Sections

We noted earlier that nuclear fission is a process that proceeds via compound nucleus formation, much as does radiative capture. Hence it is not surprising that fission cross sections show considerable resonance structure. In Figure 2-17 we
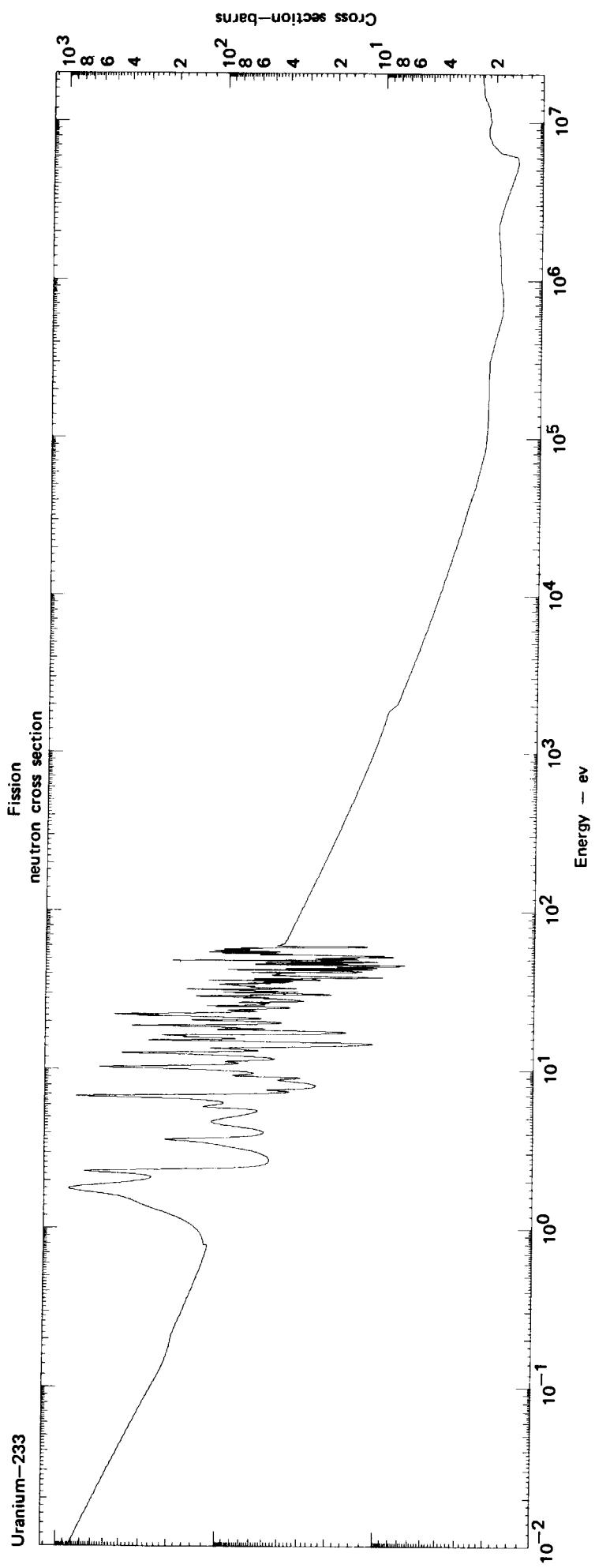
**FIGURE 2-17.** Fission cross sections of $^{233}$U, $^{235}$U, and $^{239}$Pu.

56
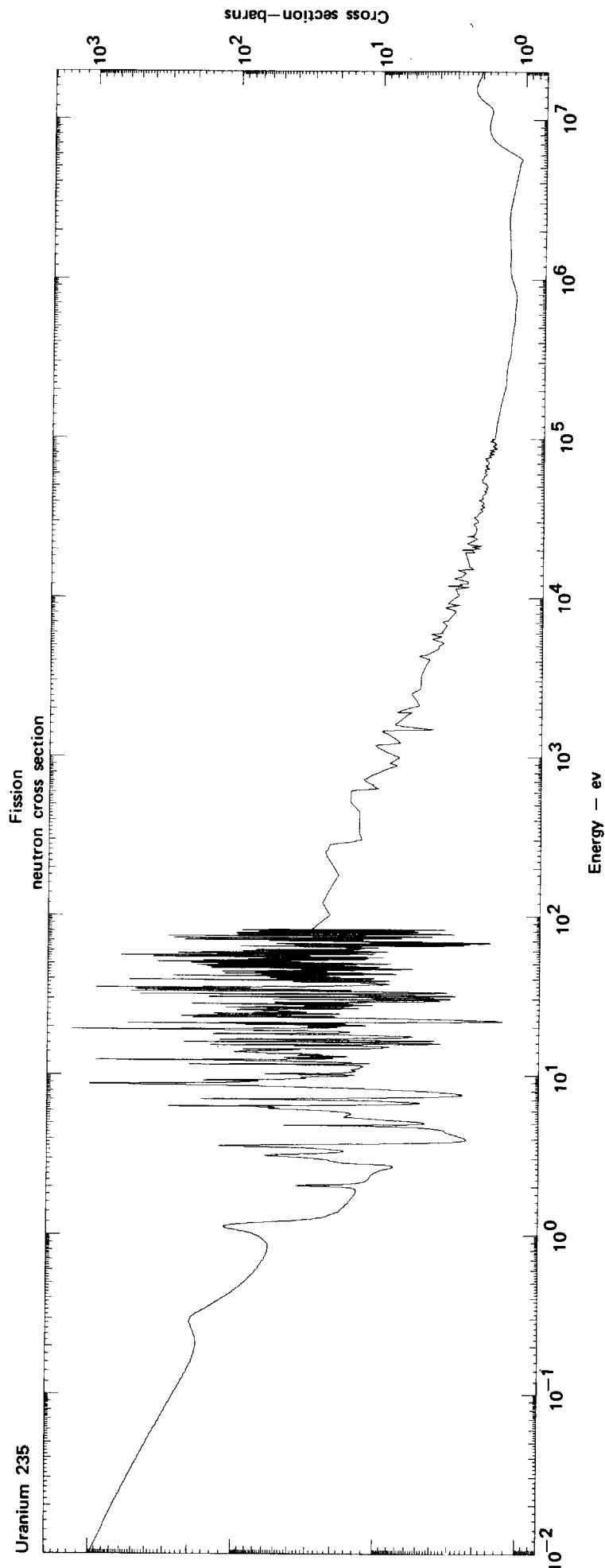
**FIGURE 2-17.** (*Continued*)
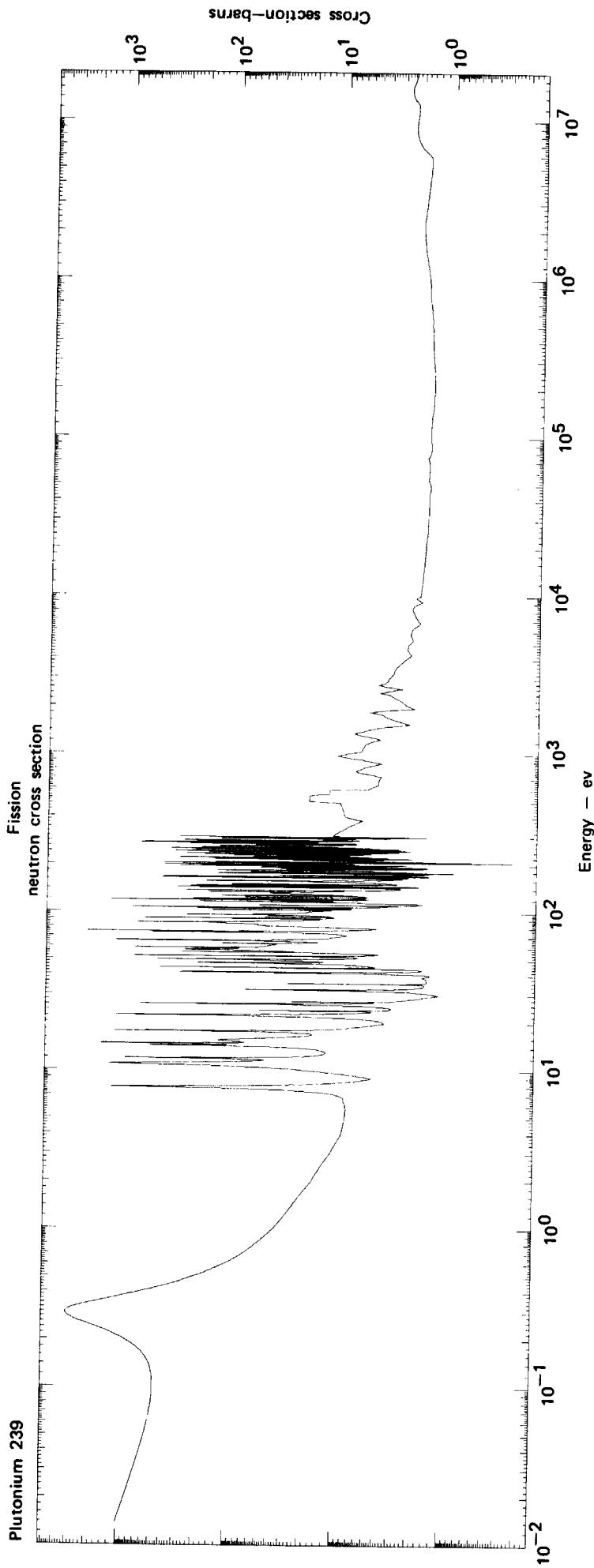
FIGURE 2-17. (Continued)

have shown the fission cross sections characterizing the principal fissile nuclides, $^{233}U$, $^{235}U$, and $^{239}Pu$, taken from ENDF/B-IV.

The indicated cross section behavior is very similar to that of radiative capture cross sections. However this would be expected since we have seen that compound nucleus formation via neutron absorption is essentially independent of the mode of compound nucleus disintegration or decay, for example, via fission or gamma emission. It is particularly important to note that the fission cross section is over two orders of magnitude larger for low-energy or thermal neutrons than for high-energy fast neutrons (above 1 keV). The thermal neutron fission cross sections are indeed enormous for these fissile isotopes, ranging up to thousands of barns in magnitude. Such behavior will prove of very considerable importance in our later studies of nuclear reactors.

We have also indicated the fission cross sections characterizing the principal fissionable nuclides of interest, $^{232}Th$, $^{238}U$, and $^{240}Pu$ (see Figure 2-18). This cross section behavior is somewhat different than that characterizing fissile nuclides since fissionable nuclides can only be fissioned by sufficiently high-energy neutrons. This implies that their fission cross sections will have a threshold energy, below which the cross section drops to zero. Even above this threshold energy (roughly 1 MeV), the fission cross sections are quite low, being less than two barns.

When a neutron is absorbed by a fissile isotope such as $^{235}U$, it may induce that isotope to fission. Yet it is also possible that the compound nucleus formed by the neutron absorption, $^{236}U^*$, might simply decay to its ground state by gamma emission. The relative balance between the probability of fission and radiative capture is an extremely important factor in nuclear reactor applications. We characterize this balance by the *capture-to-fission ratio*, defined by

$$\alpha \equiv \frac{\sigma_\gamma}{\sigma_f} .$$
(2-109)
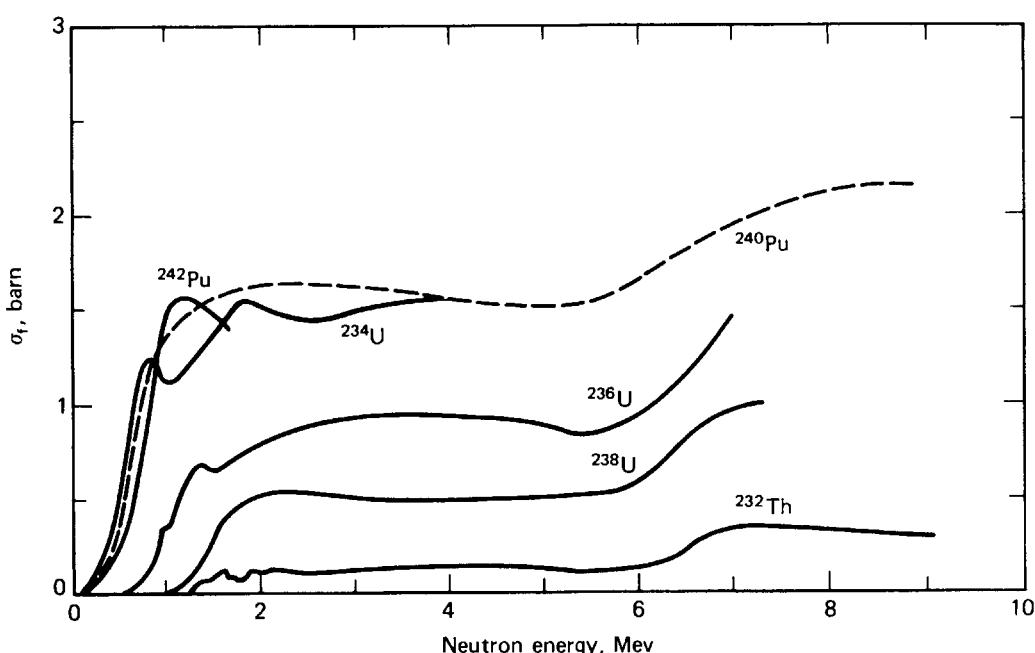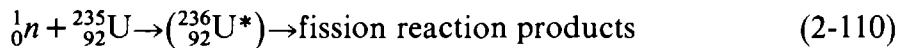


FIGURE 2-18.   Fission cross sections of principal fissionable isotopes.[12]

This ratio depends not only on the isotope of interest, but as well on the incident neutron energy $E$. It is plotted in Figure 2-19 for the three primary fissile nuclides. It can be seen that most neutron absorption in such isotopes leads to fission events (with the exception of a small range of $\alpha > 1$ for $^{235}U$). It should be noticed that $\alpha$ decreases quite appreciably above 0.1 MeV. This latter fact will prove to be of considerable importance when we discuss the concept of a fast breeder reactor.

## C. Nuclear Fission Reactions

A typical nuclear fission reaction such as

$$\mathrm{{}_{0}^{1}n + {}_{92}^{235}U \rightarrow ({}_{92}^{236}U^{*}) \rightarrow fission\ reaction\ products} \qquad (2\text{-}110)$$

spews out a variety of reaction products, including the fissioned nuclei or fission products and several neutrons as well as numerous gammas, betas, and neutrinos. And of course it also releases a very considerable amount of energy. Indeed a glance at the binding energy per nucleon before and after the fission reaction from Figure 2-16 suggests that energy on the order of 200 MeV will be released in each fission reaction.

The fission fragment nuclei produced by the fission reaction are both highly charged and highly energetic. They slow down via collisions with adjacent atoms, losing energy and charge (picking up electrons) in the process. This is in fact the principal mechanism by which the fission energy eventually appears as heat generated in the fuel material. However these fission products are usually quite unstable as well, being somewhat neutron-rich, and will subsequently decay, usually via beta emission. The energy released in such radioactive decay reactions can amount to as much as 4–5% of the total energy released in the fission reaction. Since such "decay heat" will appear with an appreciable time delay corresponding to the half-lives of the various nuclei involved, it can lead to difficulties unless properly anticipated in fission reactor design.
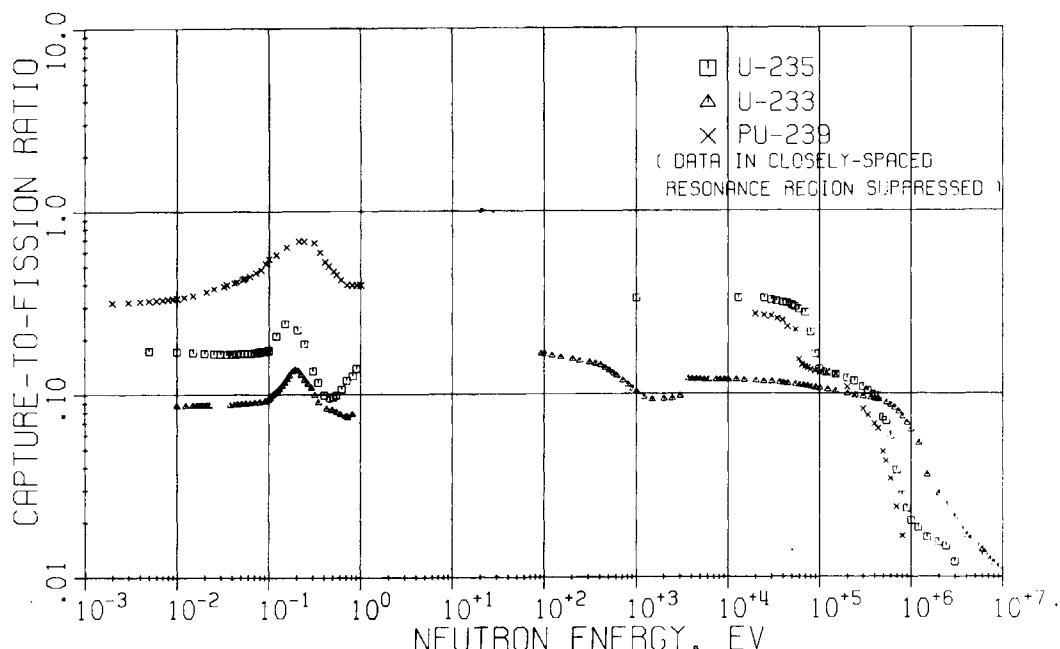


FIGURE 2-19.   Variation of $\alpha$ with energy for $^{233}U$, $^{235}U$, and $^{239}Pu$.

Yet just as significant as the energy released in the fission reaction is the fact that several neutrons are also produced in the reaction. These neutrons can be used to propagate a fission chain reaction. Most of these fission neutrons appear essentially instantaneously (within $10^{-14}$ sec) of the fission event. These neutrons are referred to as *prompt*. However a very few neutrons (less than 1%) appear with an appreciable time delay from the subsequent decay of radioactive fission products. Although only a very small fraction of the fission neutrons are delayed, these *delayed* neutrons are vital for the effective control of the fission chain reaction.

The total number of neutrons (both prompt and delayed) released in a fission reaction will vary. However in most nuclear applications we only need concern ourselves with the average number of neutrons released per fission, which we denote by $\nu$. This quantity will depend on both the nuclear isotope involved and the incident neutron energy, generally tending to increase with increasing neutron energy. We have shown $\nu(E)$ as a function of energy for the principal fissile isotopes in Figure 2-20.

The neutrons produced in the fission reaction emerge with a distribution of energies, with the average fission neutron energy being roughly 2 MeV. As with other fission parameters, this distribution will depend on the nuclear isotope involved, to a lesser degree on the incident neutron energy, and will differ for prompt and delayed neutrons. To characterize this variation in fission neutron energy, it is convenient to define the fission neutron energy spectrum, or more simply, the *fission spectrum*, $\chi(E)$, defined as

$$\chi(E)\,dE \equiv \text{Average number of fission neutrons emitted with}$$
$$\text{energy } E \text{ in } E \text{ to } E + dE \text{ per fission neutron.} \qquad (2\text{-}111)$$
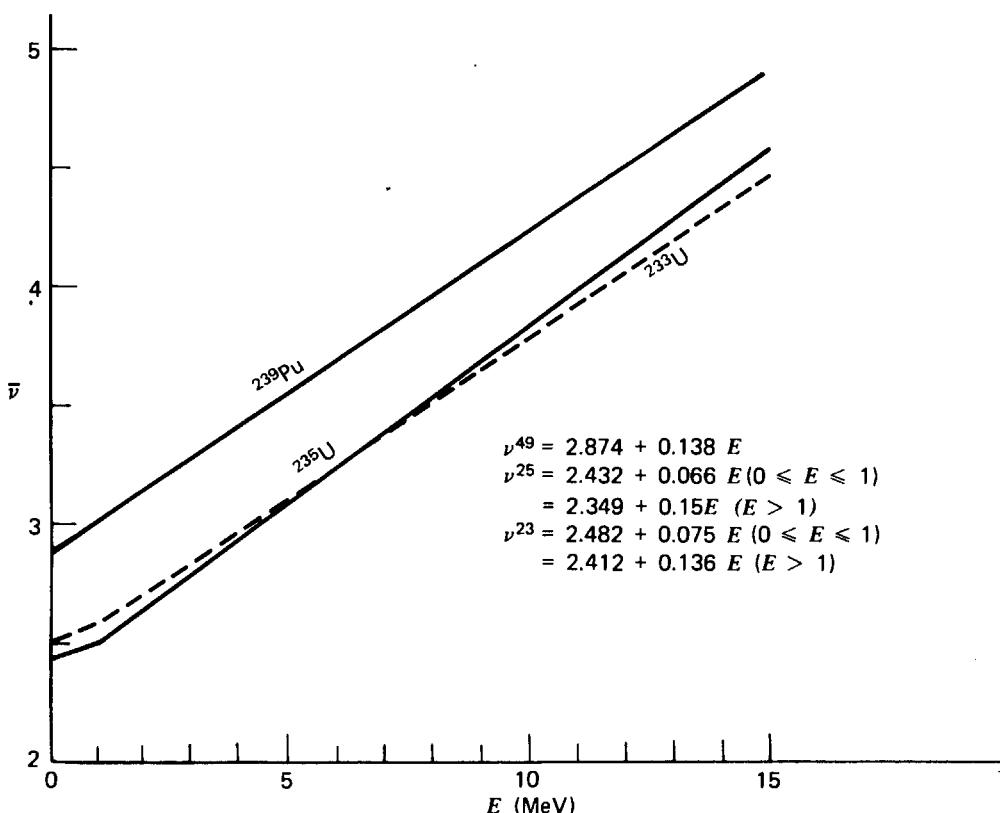


FIGURE 2-20.  Average neutron number per fission $\nu$ as a function of energy[24]
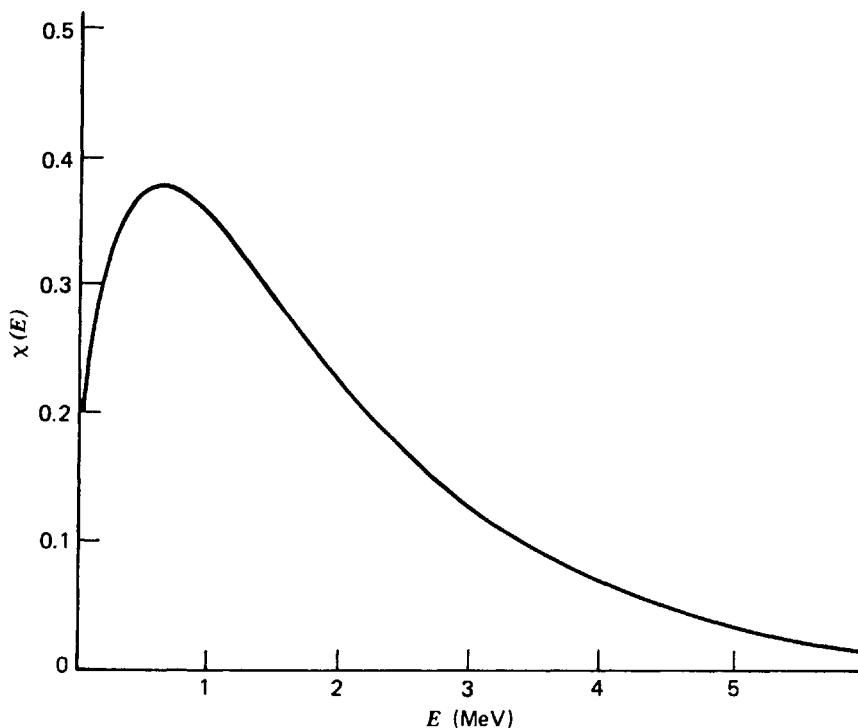
FIGURE 2-21. Fission spectrum for thermal neutron induced fission in $^{235}$U.

A typical prompt neutron fission spectrum is shown in Figure 2-21. One can also represent the fission spectrum by a simple empirical expression; for example, the prompt neutron fission spectrum of $^{235}$U is given by

$$\chi(E) = 0.453 \, e^{-1.036E} \sinh \sqrt{2.29E} \, . \tag{2-112}$$

This proves useful in performing simple estimates of fission chain reaction behavior. However more elaborate studies would simply use the fission spectra tabulated in a nuclear data set such as ENDF/B.

Because of the importance of delayed fission neutrons to nuclear reactor control, it is useful to introduce a few related concepts useful for their description. By way of example, consider a typical fission product decay scheme leading to the emission of a delayed neutron as sketched in Figure 2-22. It should be noted in particular that the decay sequence leading to the delayed neutron emission is first the beta decay of $^{87}$Br to $^{87}$Kr*, followed by the subsequent decay of $^{87}$Kr* to $^{86}$Kr via neutron emission. The effective time delay of this process is controlled by the beta-decay—in this case, the half-life is some 55 sec. We refer to the fission fragment whose beta-decay yields a daughter nucleus which subsequently decays via delayed neutron emission as a *delayed neutron precursor*. Of course a very large number (at least 45) of different delayed neutron precursor isotopes will be produced in a fission chain reaction. It has been customary (and found to be adequate) in reactor analysis to group these precursors into six classes characterized by approximate half-lives of 55, 22, 6, 2, 0.5, and 0.2-sec, respectively. Each precursor group will contain a number of different isotopes. For example, while the 55-sec precursor group is due almost entirely to one precursor, $^{87}$Br, there are at least two major contributors, $^{88}$Br and $^{137}$I, to the 22-sec group. The composition of the remaining groups are considerably more complex.
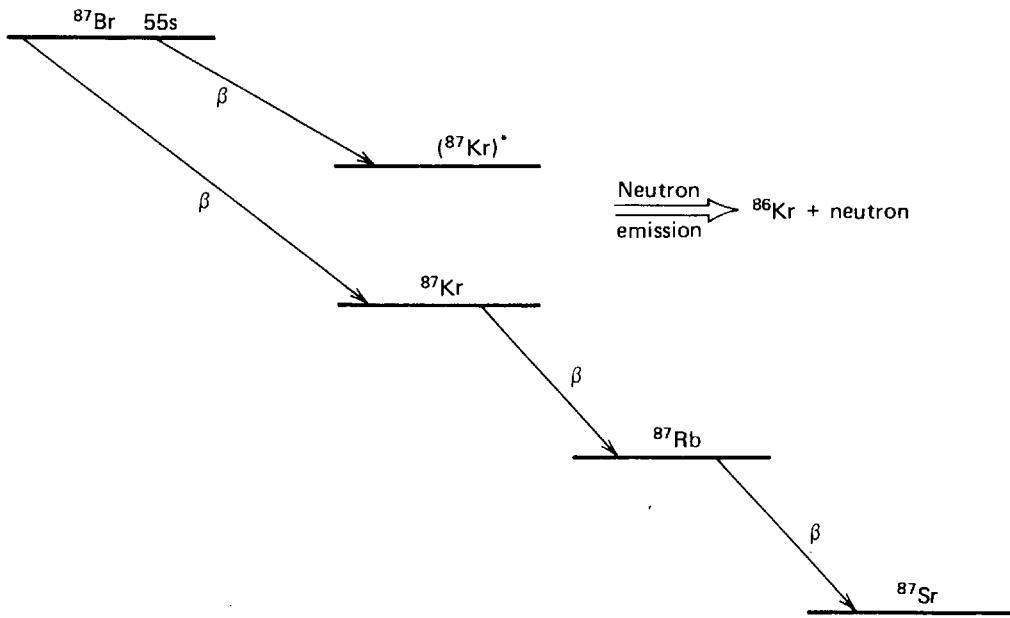
FIGURE 2-22.  Decay of the $^{87}$Br delayed neutron precursor.

Since the relative isotopic yield per fission will vary for different fuel isotopes, the detailed characteristics of the precursor groups will similarly be isotope-dependent. To this end, let us define:

$\lambda_i$ = Decay constant ($\beta$-decay) of $i$th precursor group

$\beta_i$ = Fraction of all fission neutrons (both prompt and delayed) emitted per fission that appear from $i$th precursor group

$\beta = \sum_i \beta_i$ = Total fraction of fission neutrons which are delayed.

In Table 2-3 we have listed the half-lives, relative yield fractions $\beta_i/\beta$, and total delayed neutron yields $\nu_d = \nu\beta$, for the precursor groups characterizing the principle fissionable isotopes recommended by ENDF/B-IV[25]. Although dependent on the fuel isotope, these data do not depend sensitively on the incident neutron energy below about 4 MeV and hence can be used for either thermal or fast reactor analysis.

The energy spectrum of delayed fission neutrons is considerably lower than that of prompt fission neutrons and again depends on both the delayed neutron group and fissioning isotope. We have given a rough composite delayed neutron fission spectrum in Figure 2-23 along with typical measured spectra for the 55-sec and 22-sec groups of $^{235}$U. More detailed spectrum data can be found in the review article of Cox.[25]

Actually there are additional processes that can contribute delayed neutrons to the chain reaction. Photoneutron reactions $(\gamma, n)$ are particularly important in reactors containing appreciable amounts of deuterium or beryllium. The decay times of these processes are even longer than those characterizing delayed fission neutrons (ranging up to 125 m).[25] However these photoneutrons can usually be accounted for in reactor analysis by simply including one or more additional groups of delayed neutrons such as those tabulated above. Furthermore one can

**TABLE 2-3   Delayed Neutron Yield and Half-Life Data**[25]

| $^{232}$Th: $\nu_d = 0.0527 \pm 0.0040$ $n/f$ | | | | $^{233}$U: $\nu_d = 0.0074 \pm 0.0004$ | | |
| Group | $T_{\frac{1}{2}}$ (sec) | Relative Yield | | Group | $T_{\frac{1}{2}}$ (sec) | Relative Yield |
|---|---|---|---|---|---|---|
| 1 | 56.030 | 0.034 | | 1 | 55.110 | 0.086 |
| 2 | 20.750 | 0.150 | | 2 | 20.740 | 0.274 |
| 3 | 5.740 | 0.155 | | 3 | 5.300 | 0.227 |
| 4 | 2.160 | 0.446 | | 4 | 2.290 | 0.317 |
| 5 | 0.571 | 0.172 | | 5 | 0.546 | 0.073 |
| 6 | 0.211 | 0.043 | | 6 | 0.221 | 0.023 |

| $^{235}$U: $\nu_d = 0.01668 \pm 0.00070$ $n/f$ | | | | $^{238}$U: $\nu_d = 0.0460 \pm 0.0025$ $n/f$ | | |
| Group | $T_{\frac{1}{2}}$ (sec) | Relative Yield | | Group | $T_{\frac{1}{2}}$ (sec) | Relative Yield |
|---|---|---|---|---|---|---|
| 1 | 54.51 | $0.038 \pm 0.004$ | | 1 | 52.38 | 0.013 |
| 2 | 21.84 | $0.213 \pm 0.007$ | | 2 | 21.58 | 0.137 |
| 3 | 6.00 | $0.188 \pm 0.024$ | | 3 | 5.00 | 0.162 |
| 4 | 2.23 | $0.407 \pm 0.010$ | | 4 | 1.93 | 0.388 |
| 5 | 0.496 | $0.128 \pm 0.012$ | | 5 | 0.493 | 0.225 |
| 6 | 0.179 | $0.026 \pm 0.004$ | | 6 | 0.172 | 0.075 |

| $^{239}$Pu: $\nu_d = 0.00645 \pm 0.00040$ $n/f$ | | | | $^{240}$Pu: $\nu_d = 0.0090 \pm 0.0009$ $n/f$ | | |
| Group | $T_{\frac{1}{2}}$ (sec) | Relative Yield | | Group | $T_{\frac{1}{2}}$ (sec) | Relative Yield |
|---|---|---|---|---|---|---|
| 1 | 53.75 | 0.038 | | 1 | 53.56 | 0.028 |
| 2 | 22.29 | 0.280 | | 2 | 22.14 | 0.273 |
| 3 | 5.19 | 0.216 | | 3 | 5.14 | 0.192 |
| 4 | 2.09 | 0.328 | | 4 | 2.08 | 0.350 |
| 5 | 0.549 | 0.103 | | 5 | 0.511 | 0.128 |
| 6 | 0.216 | 0.035 | | 6 | 0.172 | 0.029 |

| $^{241}$Pu: $\nu_d = 0.0157 \pm 0.0015$ $n/f$ | | |
| Group | $T_{\frac{1}{2}}$ (sec) | Relative Yield |
|---|---|---|
| 1 | 54.0 | 0.010 |
| 2 | 23.2 | 0.229 |
| 3 | 5.6 | 0.173 |
| 4 | 1.97 | 0.390 |
| 5 | 0.43 | 0.182 |
| 6 | 0.2 | 0.016 |
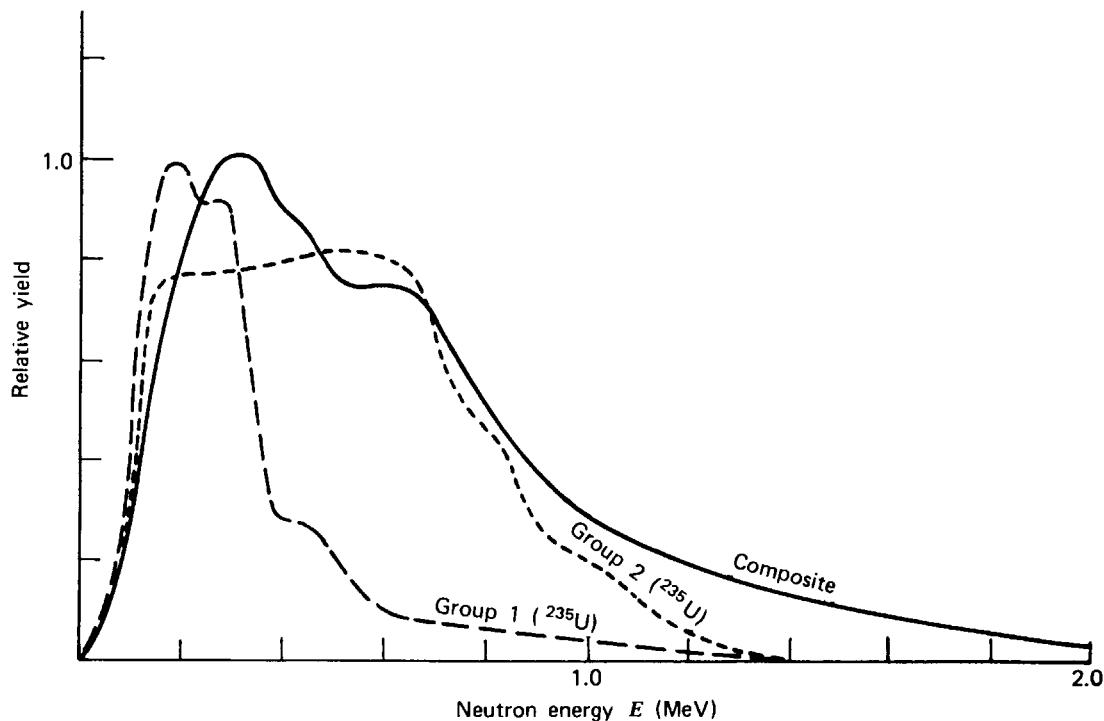
**FIGURE 2-23.** Composite delayed neutron spectrum.

also find delayed neutrons generated by neutron-absorption processes such as certain $(n,p)$ reactions, for example, $^{17}O(n,p)$ $^{17}N$, since $^{17}N$ decays by neutron emission with a half-life of 4.165 sec.

The energy released in a nuclear fission reaction is distributed among a variety of reaction products. We have classified these reaction products as to both range and emission time, and have indicated the approximate percentage of the fission energy (some 200 MeV) carried by each:

**TABLE 2-4    Energy Release in Nuclear Fission**

| Reaction Product | Energy (%) | Range | Time Delay |
|---|---|---|---|
| Kinetic energy of fission fragments | 80 | $< .01$ cm | instantaneous |
| Fast neutrons | 3 | 10–100 cm | instantaneous |
| Fission gamma energy | 4 | 100 cm | instantaneous |
| Fission product $\beta$ decay | 4 | short | delayed |
| Neutrinos | 5 | nonrecoverable | delayed |
| Nonfission reactions due to neutron capture | 4 | 100 cm | delayed |

The majority of the fission energy appears as the kinetic energy of the fission fragments and is deposited essentially at the point of fission in the nuclear fuel. Note, however, that some of the fission energy appears as kinetic energy of neutrons (3%) and gammas (4%) with relatively long ranges. This energy will be distributed over the core of the reactor and adjacent material such as shielding. In Figure 2-24 we have noted the types of emergent radiation.[28]

Furthermore it should be noted that some 4% of the fission energy appears in the form of heat generated by the decay of radioactive fission products. If the nuclear reactor were to be suddenly shut down, this decay heat would continue to be produced and would have to be removed; otherwise the reactor core temperature would rise dramatically, causing fuel element melting and failure. The removal of such decay heat is one of the most serious problems in reactor safety studies. Notice also that a sizable amount of energy (as much as 20 MeV per fission) may be liberated by the high-energy gammas produced in radiative capture $(n, \gamma)$ reactions.

It is customary to use an effective energy release per fission in determining the portion of the total energy of fission that can be recovered by a coolant and hence contributes to the thermal power output of the reactor. Although this energy will vary somewhat with the type of reactor and the detailed core composition, it is typically of the order of 192 MeV. (A more detailed tabulation of useful energy release per fission has been calculated using atomic mass data by James[26] and is given in Table 2-5.) Of this 192 MeV, some 168 MeV appears as fission fragment energy, while 7 MeV appears as beta energy. These short-range contributions deposit their energy in the nuclear fuel. If we also take into account the energy deposited in the fuel ($\sim$7%) due to fast neutrons and gammas, we find that some
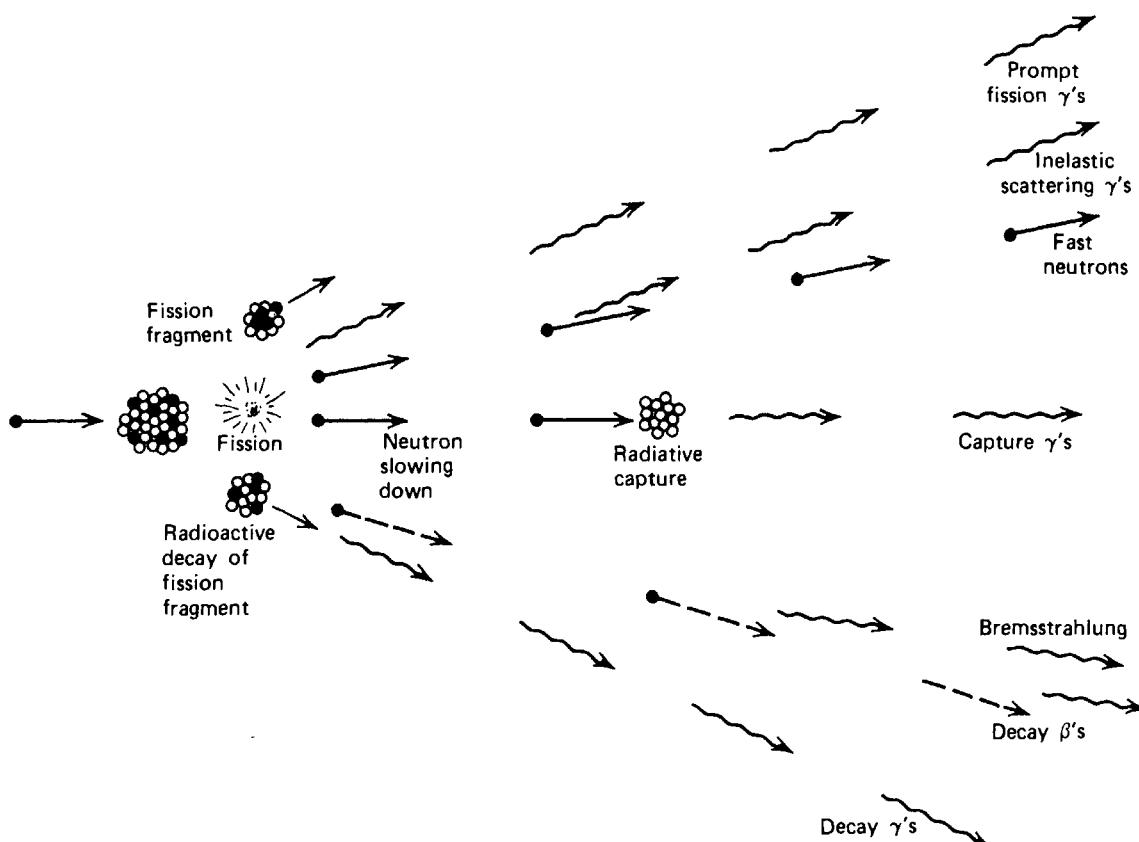


FIGURE 2-24.  Types of radiation produced in a fission chain reaction.

97% of the recoverable fission energy is deposited directly in the fuel material. The remainder is deposited in the coolant or structural materials by neutrons and gamma radiation, with less than 1% typically being deposited in shielding due to gamma radiation. Actually as we will see in Chapter 12, the energy deposited in other regions of the reactor is usually reassigned to the fuel in order to simplify the thermal analysis of the reactor.

**TABLE 2-5[26]  Effective Energy Released in Fission**

The effective energy released in and following fission of the principal fissile isotopes by thermal neutrons are:

$^{233}$U:     $190.0 \pm 0.5$ MeV/f

$^{235}$U:     $192.9 \pm 0.5$ MeV/f

$^{239}$Pu:   $198.5 \pm 0.8$ MeV/f

$^{241}$Pu:   $200.3 \pm 0.8$ MeV/f

The effective energy released following fission of the major fissionable isotopes by $^{235}$U fission spectrum neutrons are:

$^{232}$Th:   $184.2 \pm 0.9$ MeV/f

$^{234}$U:     $188.9 \pm 1.0$ MeV/f

$^{236}$U:     $191.4 \pm 0.9$ MeV/f

$^{238}$U:     $193.9 \pm 0.8$ MeV/f

$^{237}$Np:   $193.6 \pm 1.0$ MeV/f

$^{238}$Pu:   $196.9 \pm 0.8$ MeV/f

$^{240}$Pu:   $196.9 \pm 1.0$ MeV/f

$^{242}$Pu:   $200.0 \pm 1.9$ MeV/f

These values include all contributions except from neutrinos and very long-lived fission products.

## D. Fission Fuels

Our previous discussion has indicated that there are a number of possibilities available for fueling a fission chain-reacting system. In particular, we have noted that the principal nuclides[†] of concern in nuclear reactor applications are:

Fissile nuclides: $^{233}$U, $^{235}$U, $^{239}$Pu, $^{241}$Pu

while those susceptible to fast neutron fission are:
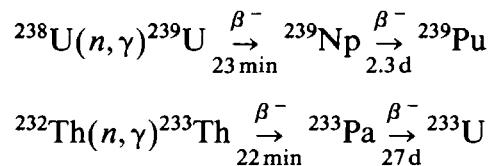
Fissionable nuclides: $^{232}$Th, $^{238}$U, $^{240}$Pu, $^{242}$Pu

Because of both the energy threshold that neutrons must exceed in order to induce fission in fissionable nuclides and the relatively large value of $\alpha$ characterizing such nuclides, only the first class of nuclides are capable of sustaining a fission chain reaction. Of these isotopes, only $^{235}$U is found in nature—and then, only as 0.711% of natural uranium (which is composed primarily of $^{238}$U). Although reactors can be fashioned out of natural uranium with even this low concentration of $^{235}$U if one

[†]A bit of conventional notation[27] for such nuclides remains as debris from the secrecy of the atomic weapons program during World War II. Two-digit code numbers are used to identify each isotope where the first digit is the atomic number minus 90 and the second digit is the last digit of the mass number. Hence $^{235}$U is denoted as "25," $^{238}$U as "28," $^{239}$Pu as "49," and so on.

is sufficiently clever, most present-day reactor types are fueled with uranium in which the percentage of $^{235}$U has been increased or *enriched* above its natural value. As we will see later, such uranium enrichment is an extremely complicated and expensive process.

There is yet another way to obtain fissile isotopes, however. It is found that when certain nuclides absorb neutrons, they then undergo a sequence of radioactive disintegrations that eventually result in the formation of a fissile isotope. The two most important examples of such neutron transmutation reactions are:

$$^{238}\text{U}(n,\gamma)^{239}\text{U} \xrightarrow[23\,\text{min}]{\beta^-} {}^{239}\text{Np} \xrightarrow[2.3\,\text{d}]{\beta^-} {}^{239}\text{Pu}$$

$$^{232}\text{Th}(n,\gamma)^{233}\text{Th} \xrightarrow[22\,\text{min}]{\beta^-} {}^{233}\text{Pa} \xrightarrow[27\,\text{d}]{\beta^-} {}^{233}\text{U}$$

Isotopes that can be transmitted into fissile nuclides via neutron capture are referred to as *fertile*. The fertile isotopes of most interest are $^{238}$U and $^{232}$Th, which are in abundant supply throughout the world.

Yet where does one find the neutrons necessary for this process? In a nuclear reactor. Indeed since most present-day reactors are fueled with low-enrichment uranium that may contain as high as 98% $^{238}$U, such transmutation processes will occur quite naturally as the fertile nuclei capture excess neutrons from the fission chain reaction. The key parameter in such processes is the number of neutrons produced in each fission reaction per neutron absorbed in the fuel nuclei. (Here we must remember that not all neutron absorptions in the fuel lead to fission—some result in radiative capture.) We will define

$$\eta \equiv \text{Average number of neutrons produced per neutron}$$
$$\text{absorbed in fuel.}$$

For a fuel composed of a single fissile isotope, we can write

$$\eta = \nu\sigma_f/\sigma_a = \nu/(1+\alpha). \tag{2-113}$$

Most fuels, however, contain a mixture of isotopes. In this case, we would use the macroscopic fission and absorption cross sections characterizing each isotope to write

$$\eta = \frac{\displaystyle\sum_j \nu_j \Sigma_f^j}{\displaystyle\sum_j \Sigma_a^j}. \tag{2-114}$$

The dependence of this very important quantity on energy $E$ is shown for the four principal fissile isotopes in Figure 2-25. It should be noted that $\eta(E)$ is generally of the order of 2 for low-energy neutrons, but increases with energy above 0.1 MeV as the capture-to-fission ratio $\alpha$ falls off. If we are to attempt to utilize the neutrons "left over" from the chain reaction to convert fertile isotopes into fissile material, it is apparent that we require $\eta(E)$ to be at least greater than 1, since one neutron per fission is needed to sustain the chain reaction. Of course, a
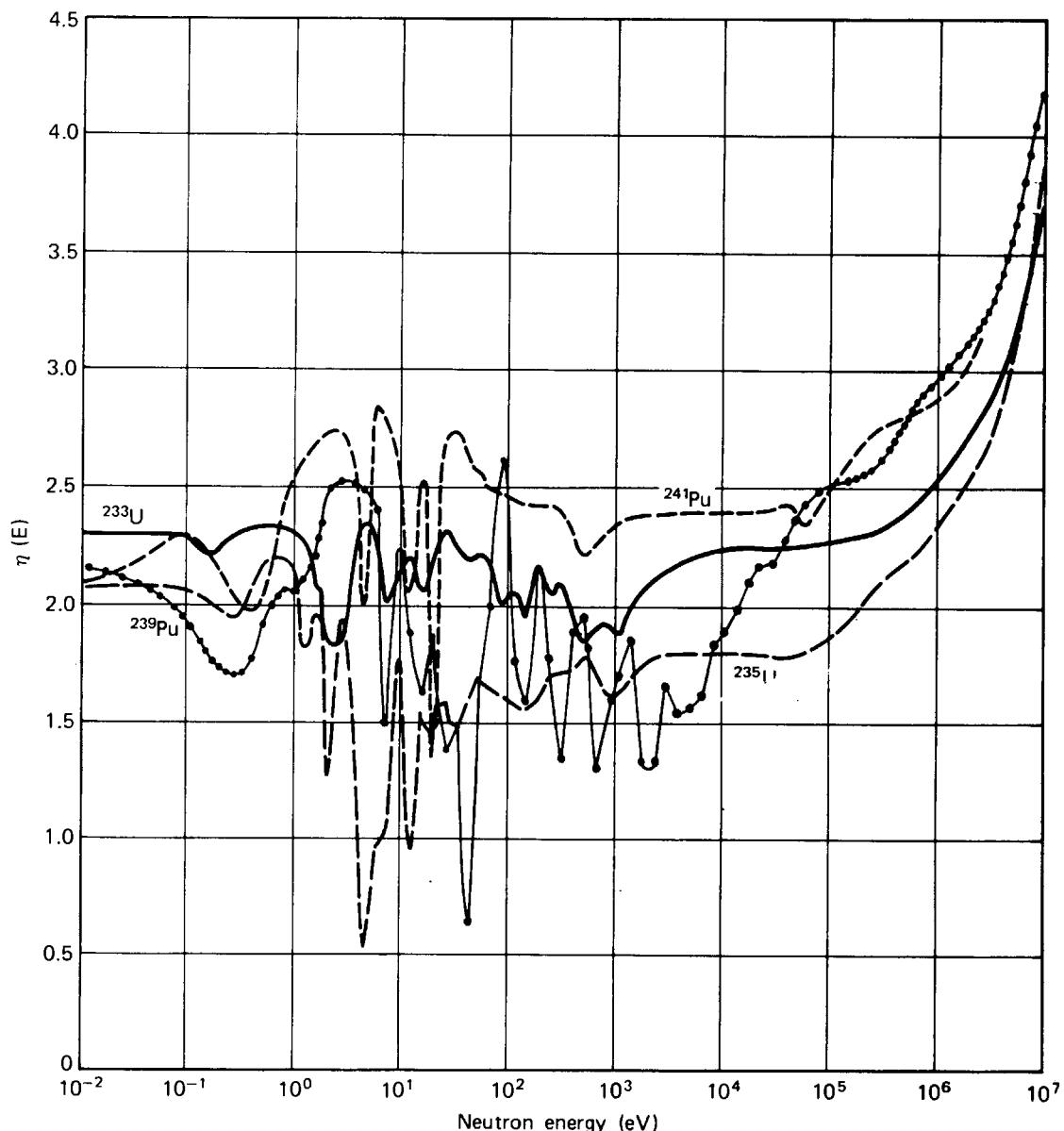
FIGURE 2-25.   Variation of $\eta$ with energy for $^{233}$U, $^{235}$U, $^{239}$Pu and $^{241}$Pu.

certain fraction of the fission neutrons will be absorbed in nonfuel materials, and others will leak out of the reactor and be lost to the chain reaction. Nevertheless it is apparent that $\eta(E)$ is sufficiently greater than unity to enable appreciable conversion using any of these isotopes.

Indeed it might even be possible to produce *more* fissile material than one depletes in maintaining the fission chain reaction. For this to occur, one would have to operate with fissile isotopes and neutron energies for which $\eta(E)$ was greater than two, since one neutron would be needed to maintain the chain reaction, while one neutron would be used to produce a new fissile nucleus to replace the one destroyed in the fission reaction. Any excess over this (and over the number of neutrons lost to the chain reaction via nonproductive capture or leakage) could then be used to produce or *breed* new fissile material.

It is apparent from Figure 2-25 that the most favorable situation for accomplishing this would involve relatively fast neutrons in the 0.1–1 MeV range. The most suitable fuel would be $^{239}$Pu. Such is the motivation behind the development of the

fast breeder reactor which operates with a chain reaction in a $^{239}Pu/^{238}U$ fuel mixture maintained by fast neutrons in order to achieve this large value of $\eta$.

However if we recall the energy dependence of the fission cross section itself, it is apparent that it is more difficult to use fast neutrons to sustain the chain reaction, since the cross sections for fast fission are some two orders of magnitude smaller than those characterizing thermal neutrons. This suggests that it might be easier to achieve a sustained chain reaction using slow neutrons, since then the probability of fission is appreciably larger. Yet we must remember that the neutrons produced in the fission reaction are quite energetic with average energies in the MeV range. Hence in order to take advantage of the large fission cross sections for slow neutrons, one must slow down the fast fission neutrons to thermal energies ($< 1$ eV). As we will see in the next chapter, this can be accomplished rather easily by using elastic scattering collisions.
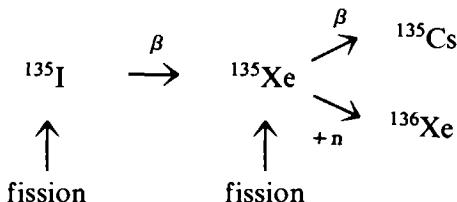
## REFERENCES

1. I. Kaplan, *Nuclear Physics*, 2nd Edition, Addison-Wesley, Reading, Mass. (1963).
2. O. Oldenberg and N. C. Rasmussen, *Modern Physics for Engineers*, McGraw-Hill, New York (1966).
3. M. G. Bowler, *Nuclear Physics*, Pergamon, New York (1973).
4. A. H. Foderaro, *The Elements of Neutron Interaction Theory*, M. I. T. Press, Cambridge (1971).
5. A. M. Weinberg and E. P. Wigner, *The Physical Theory of Neutron Chain Reactors*, University of Chicago Press (1958).
6. J. R. Lamarsh, *Introduction to Nuclear Reactor Theory*, Addison-Wesley, Reading, Mass. (1966).
7. A. deShalit and H. Feshbach, *Theoretical Nuclear Physics*, Wiley, New York (1974).
8. C. M. Lederer, J. M. Hollander, and I. Perlman, *Table of Isotopes*, 6th Edition, Wiley, New York (1968).
9. H. Goldstein, in *Fast Neutron Physics*, Vol. II ed. J. B. Marion and J. L. Fowler, Interscience, New York (1963), p. 2227.
10. K. H. Beckurts and K. Wirtz, *Neutron Physics*, Springer, Berlin (1964).
11. D. J. Hughes, et al., *Neutron Cross Sections*, BNL-325 (1955).
12. D. J. Hughes, et al., *Neutron Cross Sections*, 2nd Edition and Supplements, BNL-325 (1958, 1960, 1964, 1965).
13. *Neutron Cross Sections*, 3rd Edition, BNL-325 (1975).
14. H. C. Honeck, ENDF/B—Specifications for an Evaluated Nuclear Data File for Reactor Applications, BNL-50066 (1966); P. B. Heming, Development of ENDF/B System, in Proceedings of 3rd Conference on Neutron Cross Sections and Technology, USAEC CONF-71031 (1971), pp. 348–353.
15. A partial list of sources of neutron cross section data is given in the following references: CINDA 74 (and succeeding years), *An Index to the Literature of Microscopic Neutron Data*, International Atomic Energy Agency, Vienna (1974).
    R. J. Howerton, S. T. Perkins, C. P. Altamirano, and K. L. Hill, *A Bibliography of the Experimental Data of Neutron-Induced Reactions*, UCRL-50400, Vol. 2 (1970).
16. D. I. Garber, L. G. Stromberg, M. D. Goldberg, D. E. Cullen, and V. M. May, *Angular Distributions in Neutron Induced Reactions*, BNL-400, 3rd Edition (1970).
17. D. Okrent, R. Avery, and H. H. Hummel, Proceedings of the International Conference on Peaceful Application of Atomic Energy, Vol. 5 (1955), p. 357.
18. H. A. Bethe and G. Placzek, *Phys. Rev.* **51**, 450 (1937).
19. W. G. Pettus, *Nucl. Sci. Eng.* **31**, 168 (1968).

20. R. L. Murray, *Nucl. Sci. Eng.* **26**, 362 (1966).

21. L. Dresner, *Resonance Absorption in Nuclear Reactors*, Pergamon, (1960).

22. D. E. Cullen, *Nucl. Sci. Eng.* **54**, 498 (1974); D. G. Lindstrom, U. of Michigan, M.S. Thesis (1960).

23. E. P. Wigner and J. E. Wilkins, Jr., AECD-2275 (1944); M. M. R. Williams, *The Slowing Down and Thermalization of Neutrons*, North-Holland, Amsterdam (1966), p. 75.

24. G. R. Keepin, *Physics of Nuclear Kinetics*, Addison-Wesley, Reading, Mass. (1965).

25. S. A. Cox, USAEC Document ANL/NDM-5 (1974); L. Tomlinson, UKAEA AERE-R6993 (1972); R. J. Tuttle, *Nucl. Sci. Eng.* **56**, 37 (1975).

26. M. F. James, *J. Nucl. Energy* **23**, 517 (1969); **25**, 513 (1971).

27. S. Glasstone and M. C. Edlund, *The Elements of Nuclear Reactor Theory*, Van Nostrand, Princeton, N. J. (1952).

28. N. M. Schaeffer, *Reactor Shielding for Nuclear Engineers*, USAEC Document TID-25951 (1973).

## PROBLEMS

2-1. What target isotope must be used for forming the compound nucleus $^{24}_{11}\text{Na}$ when the incident projectile is: (a) a neutron, (b) a proton, or (c) an alpha particle?

2-2. A very important type of radioactive decay process in nuclear reactors is one in which fission products decay by neutron emission since such processes strongly influence the time behavior of the fission chain reaction. The slowest such decay process in most reactors is one characterized by a decay constant of 0.0126 $\text{sec}^{-1}$. Assuming that such a process controls the rate at which one can decrease the power level of a reactor, calculate the time necessary to decrease the reactor power level from 3800 MW (thermal) to 10 MW (thermal).

2-3. Consider an initially pure sample of radioactive material whose successive decay products are themselves radioactive with differing half-lives. Write the isotopic rate equations characterizing the concentration of various isotopes in the sample if the decay chain is of the form $1 \rightarrow 2 \rightarrow 3 \rightarrow 4 \rightarrow \ldots N$. Solve this set of equations in a stepwise fashion for the isotopic concentrations $N_1(t), N_2(t), \ldots$ In particular, determine the long-time composition of the sample if the half-life of one of the isotopes is very much longer than those characterizing other isotopes in the chain.

2-4. A fission product of very considerable importance in thermal reactor operation is $^{135}\text{Xe}$, which has an enormous thermal absorption cross section of $2 \times 10^6$ b. This nuclide can be produced either directly as a fission product or by beta decay of $^{135}\text{I}$, as indicated by the radioactive chains below:

$$^{135}\text{I} \xrightarrow{\beta} {}^{135}\text{Xe} \begin{array}{c} \xrightarrow{\beta} {}^{135}\text{Cs} \\ \searrow \\ {}_{+n} {}^{136}\text{Xe} \end{array}$$

$$\uparrow \qquad\qquad \uparrow$$
$$\text{fission} \qquad \text{fission}$$

Write the rate equations describing the concentration of $^{135}\text{I}$ and $^{135}\text{Xe}$ in a nuclear reactor. Then assuming a constant production rate of these isotopes from fission and transmutation rate by neutron capture, determine the steady-state or saturated concentration of $^{135}\text{Xe}$.

2-5. The measured line width of the gamma-ray resonance of $^{57}\text{Fe}$ is $3.4 \times 10^{-8}$ eV. Determine the lifetime of this excited state.

2-6. Boron is a common material used to shield against thermal neutrons. Estimate the thickness of boron required to attenuate an incident thermal neutron beam to 0.1% of its intensity. (Use the thermal cross section data in Appendix A.)

2-7. Suppose we consider a beam of neutrons incident upon a thin target with an intensity of $10^{12}$ neutrons/cm$^2$-sec. Suppose further that the total cross section for the nuclei in this target is 4 b. Using this information, determine how long one would have to wait, on the average, for a given nucleus in the target to suffer a neutron interaction.

2-8. A free neutron is unstable against beta decay with a half-life of 11.7 m. Determine the relative probability that a neutron will undergo beta-decay before being absorbed in an infinite medium. Estimate this probability for a thermal neutron in $H_2O$.

2-9. Determine the number of scattering collisions a thermal neutron will experience on the average before being absorbed in $H_2O$, $D_2O$, $^{238}U$, and cadmium, respectively.

2-10. How many mean free paths thick must a shield be designed in order to attenuate an incident neutron beam by a factor of 1000?

2-11. Using the data from BNL-325, compute the mean free paths of neutrons with the following energies in the specified materials: (a) 14 MeV neutrons in air, water, and uranium (characteristic of thermonuclear fusion neutrons), (b) 1 MeV neutrons in air, water, and uranium (fast breeder reactor neutrons), and (c) 0.05 eV neutrons in air, water, and uranium (thermal reactor neutrons).

2-12. Determine the kinetic energy at which the wavelength of a neutron is comparable to: (a) the diameter of a nucleus, (b) an atomic diameter, (c) the interatomic spacing in graphite, and (d) the diameter of a nuclear reactor core. (Only rough estimates are required.)

2-13. Suppose that the total cross section of rhodium has been measured and the following values have been obtained for the resonance parameters of a well-isolated resonance at $E_0 = 1.26$ eV: $\sigma_0 = 5000$ b, $\Gamma = 0.156$ eV, and $\sigma_s = 5.5$ b. Plot the value of the total cross section for values of the energy between 0.2 and 40 eV. Calculate the thermal absorption cross section and compare this with the measured value of 156 b. (Assume that resonance scattering can be neglected.)

2-14. At higher energies, the differential elastic scattering cross section in the CM system exhibits anisotropy (so-called "p-wave" scattering) of the form

$$\sigma_{CM}(\hat{\Omega} \cdot \hat{\Omega}') = \sigma_{CM}(\theta_C) = \frac{\sigma_s}{4\pi}(1 + a\cos\theta_C).$$

Plot the scattering probability $P(E_i \rightarrow E_f)$ against final energies $E_f$ for this more general cross section behavior for the three cases $a > 0$, $a = 0$, and $a < 0$. Give a physical interpretation of your sketches.

2-15. Using the Maxwell–Boltzmann distribution $M(V, T)$, calculate the most probable energy of the nuclei characterized by such a distribution. Also calculate the average thermal energy of these nuclei.

2-16. The partial widths of the first resonance in $^{236}U$ at 5.49 eV are $\Gamma_\gamma = .029$ eV and $\Gamma_n = .0018$ eV. Plot the Doppler-broadened capture cross section at the temperature of $0°K$, $20°C$, and $1000°C$. [Use the tabulated $\psi(\zeta, x)$ function.]

2-17. Show that the total area under a Doppler-broadened resonance is essentially independent of temperature.

2-18. Using the differential scattering cross section characterizing a proton gas at temperature $T$, compute the corresponding macroscopic scattering cross section $\Sigma_s(E)$. In particular, determine the behavior of this cross section for low energies $E$.

2-19. A neutron is absorbed in a $^{235}U$ nucleus at $t = 0$. Describe a probable life history of the resulting $^{236}U$ and its successors on the assumption that it undergoes fission. Give order of magnitude estimates of characteristic times at which various events occur. Describe the various particles injected into the system as a result of this fission.

2-20. Determine the fission-rate density necessary to produce a thermal power density of 400 kW/liter (typical of a fast breeder reactor core). Assume that the principal fissile isotope is $^{239}$Pu.

2-21. An indium foil is counted at 5:00 p.m. Tuesday and found to yield 346,573 CPM in a counter with a 50% efficiency for the 54-min In-116m activity. What is the probability that *none* of these radioactive In-116m nuclei will remain in the foil at 2:00 p.m. Thursday, the same week? (Note: $\ln(1-x)\sim -x, x \ll 1$) [Victims working this problem can thank Dr. Ronald Fleming.]

2-22. Compute and plot the parameter $\eta$ for uranium enriched in $^{235}$U as a function of its enrichment (atom percent $^{235}$U) at thermal neutron energies.

# 3

## Fission Chain
## Reactions and
## Nuclear Reactors
## --an Introduction

In order to sustain a stable fission chain reaction and thereby achieve a constant production rate of fission energy, one must design a nuclear reactor in such a way that the rates of neutron absorption and leakage are balanced by the rate of fission neutron production. In this chapter we will develop a very simple model of nuclear reactor behavior based on such a neutron balance principle in order to introduce a number of the concepts involved in studying fission chain reactions. General aspects of the design and operation of nuclear fission reactors can then be understood in terms of this model, and the principal components of such systems and their functions can be discussed (although, of course, the analysis and design of these components will require more elaborate models developed in later chapters of this text). We will be able to introduce and compare the various major types of nuclear reactors being utilized for electrical power generation throughout the world today. Finally the simple discussion in this chapter will allow us to outline the principal design functions of the nuclear engineer in order to lay an appropriate foundation for our further development of the more sophisticated methods required in modern nuclear reactor analysis.

## I. THE MULTIPLICATION FACTOR AND NUCLEAR CRITICALITY

### A. The Multiplication Factor

In Chapter 2 we indicated that an essential idea involved in tapping the energy released in nuclear fission was to use the fission neutrons from one fission reaction to induce yet another reaction. In this way one could propagate a chain of

such reactions by using the neutron as a chain carrier. It should be apparent that if we wish to maintain a stable or steady-state chain reaction, that is, one that does not grow or decay away with time, we must arrange things so that precisely one neutron from each fission will induce another fission event. The remaining fission neutrons will then either be absorbed in capture reactions or will leak out from the system. We must design the nuclear reactor to achieve this very delicate balance between fission reactions and neutron capture and leakage, as we indicate schematically in Figure 3-1.

We can express this requirement in mathematical form. Since the neutrons play the central role in maintaining the fission chain reaction, let us focus our attention on them for a moment. A given neutron will be "born" in a fission event and will then usually scatter about the reactor until it meets its eventual "death" in either an absorption reaction or by leaking out of the reactor. Certain numbers of these neutrons will be absorbed by fissile or fissionable nuclei and induce further fission, thereby leading to the birth of new fission neutrons, that is, to a new "generation" of fission neutrons. Suppose that we could somehow measure the number of neutrons in two successive fission neutron generations. We would then define the ratio of these numbers as the *multiplication factor* $k$ characterizing the chain reaction

$$k \equiv \text{Multiplication factor} \equiv \frac{\text{Number of neutrons in one generation}}{\text{Number of neutrons in preceding generation}}.$$

Actually since the number of fission neutrons in any generation is proportional to the number of fission events spawning that generation (recall that each fission reaction releases, on the average, $\nu$ fission neutrons), we could have just as easily defined $k$ using the number of fission events in each generation. However since we are primarily concerned with monitoring the number of neutrons present in the reactor in order to study the chain reaction, we will find it more convenient to use the definition above.

Now notice that if $k = 1$, the number of neutrons in any two consecutive fission generations will be the same, and hence the chain reaction will be time-independent. We refer to a system characterized by $k = 1$ as being *critical*.
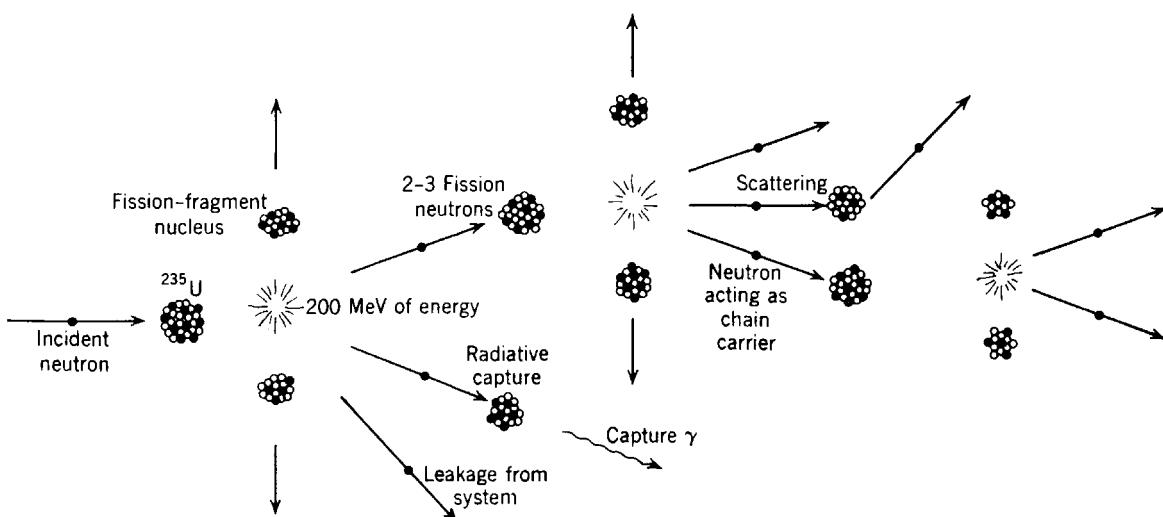


**FIGURE 3-1.    A simple schematic of a fission chain reaction.**

Obviously if we have been fortunate enough to have chosen just that reactor configuration and composition so that the reactor is critical with $k = 1$, then the number of neutrons in the reactor will always remain the same.

By a similar argument, we can conclude that if $k < 1$, the number of neutrons decreases from generation to generation, and hence the chain reaction dies out. We then refer to the system as being *subcritical*. Finally, if $k > 1$, then the chain reaction grows without bound as the number of neutrons in each successive generation is larger. Such a system is said to be *supercritical*.

In summary:

$$k < 1 \quad \text{subcritical}$$
$$k = 1 \quad \text{critical}$$
$$k > 1 \quad \text{supercritical.}$$

Hence the primary objective of the nuclear engineer is to design the nuclear reactor so that it is critical. One possible approach would be to choose a particular reactor material composition and configuration, then calculate $k$ for this choice, and if $k$ is not unity (and of course it usually won't be on the first try), readjust the reactor design until the *criticality condition*, $k = 1$, is achieved.

Actually life is a bit more complicated than this. Some method has to be provided by which the neutron population can be built up to appreciable levels in the core (about $10^9$ neutrons/cm$^3$) to yield the required power generation. In principle this could be done by merely inserting a source of neutrons into a critical assembly. Then any source neutrons appearing in the reactor would tend to induce fission reactions, thereby producing fission neutrons, which would have their progeny maintained by the chain reaction. However most neutron sources are sufficiently weak that it would take a very long time to build up an appreciable neutron population in a reactor using this method. Instead one can simply make $k$ temporarily greater than unity so that the reactor is supercritical, say by withdrawing some absorbing material to alter the balance between fission and absorption. The neutron population in the reactor will then grow. Once the desired neutron population has been reached, the reactor can be returned to critical, for example, by reinserting the absorbing material. A very similar procedure can be used to lower the neutron population in the reactor. The reactor is taken subcritical until the desired neutron population is reached and then restored to critical once again. Altering the multiplication factor $k$ characterizing a reactor in this way is known as *nuclear reactor control*. It is a very important aspect of nuclear reactor analysis.

It should now be apparent that the multiplication factor $k$ plays an extremely important role in determining nuclear reactor behavior. The calculation of the multiplication factor $k$ characterizing a given reactor configuration and composition is one of the primary objectives of nuclear reactor analysis, and much of our attention in this text will be devoted to developing various procedures for performing this calculation.

The definition of the multiplication constant $k$ in terms of successive fission neutron generations is sometimes known as the "life-cycle" point of view[1] because of its similarity to biological population growth. This definition is a bit awkward, however, since it is usually rather difficult to determine the neutron generation time. For example, some neutrons may induce fission immediately after their birth in a fission reaction. Others may first slow down to thermal energies before

inducing fission. Some neutrons may not induce fission reactions at all, but will instead be absorbed in nonproductive capture or leak out of the system.

A somewhat more practical definition of the multiplication factor $k$ can be given in terms of a neutron balance relation by defining

$$k \equiv \frac{\text{Rate of neutron production in reactor}}{\text{Rate of neutron loss (absorption plus capture) in reactor}} \equiv \frac{P(t)}{L(t)} \quad (3\text{-}1)$$

Here we have explicitly noted that the production and loss rates may change with time (e.g., due to fuel consumption).

We will find the "neutron balance" definition of multiplication a somewhat more useful concept, since it is consistent with the approach that we will use to develop more elaborate models of nuclear reactor behavior in later chapters. In particular, we can then define the neutron lifetime, $l$, in an unambiguous fashion as

$$l \equiv \frac{N(t)}{L(t)} \quad (3\text{-}2)$$

where $N(t)$ is the total neutron population in the reactor at a time $t$. This latter approach is also particularly convenient for studying the time behavior of the neutron population in a reactor.

## B. Simple Kinetics of Chain Reactions

Imagine that we could somehow count the number of neutrons $N(t)$ in a nuclear reactor at a time $t$. Then obviously the time rate of change of $N(t)$ is given by

$$\frac{dN}{dt} = \text{Production rate} - \text{Loss rate} = P(t) - L(t). \quad (3\text{-}3)$$

However if we use our definition of the multiplication factor $k$ as given by the neutron balance relation, we can write

$$\frac{dN}{dt} = \left[ \frac{P(t)}{L(t)} - 1 \right] L(t) = (k-1)L(t). \quad (3\text{-}4)$$

To proceed further we can use our definition of the neutron lifetime $l$ to write

$$\frac{dN}{dt} = \frac{(k-1)}{l} N(t). \quad (3\text{-}5)$$

If we assume that both $k$ and $l$ are time-independent (of course they will not be in general), then we can solve this simple ordinary differential equation for the neutron population at any time $t$, assuming that there are initially $N_0$ neutrons in the reactor at time $t = 0$, to find

$$N(t) = N_0 \exp\left[ \left( \frac{k-1}{l} \right) t \right]. \quad (3\text{-}6)$$

In particular, note that this very simple model of *nuclear reactor kinetics* agrees with our earlier definition of reactor criticality in terms of $k$ (see Figure 3-2). Yet this model also tells us that the growth or decay of the neutron population in a reactor obeys an exponential growth law. Such exponential growth is quite commonly found in the study of population dynamics. Indeed the study of the "neutron" population in a reactor core is mathematically rather similar to the study of biological populations, and hence the terminology of the latter field is frequently adopted in reactor physics (e.g., generation, birth, life, death, virgin, daughter).

We will later find that the power level of a nuclear reactor is essentially proportional to its neutron population. Hence we can also regard the time behavior of the reactor power level as being exponential with a time constant or *reactor period T* given by

$$T = \frac{l}{k-1} \, . \tag{3-7}$$

In particular it should be noted that as the multiplication factor $k$ approaches unity, the reactor period $T$ approaches infinity which corresponds to a time-independent neutron population or reactor power level.

However suppose that $k$ is not equal to unity. Then how rapidly might we expect the power level of the reactor to change? Suppose, for the sake of illustration, we increased $k$ to make the reactor ever so slightly supercritical by an amount of $k = 1.001$. Since the neutron lifetime in a typical power reactor is about $10^{-4}$ sec, we find this corresponds to a reactor period of $T = 0.1$ sec. Hence in one second the power level of the reactor will increase by a factor $e^{10} = 22,000$. Thus it appears that the reactor will respond very rapidly to changes in the multiplication factor. In fact, if a power reactor did indeed respond this rapidly, then it would be difficult to
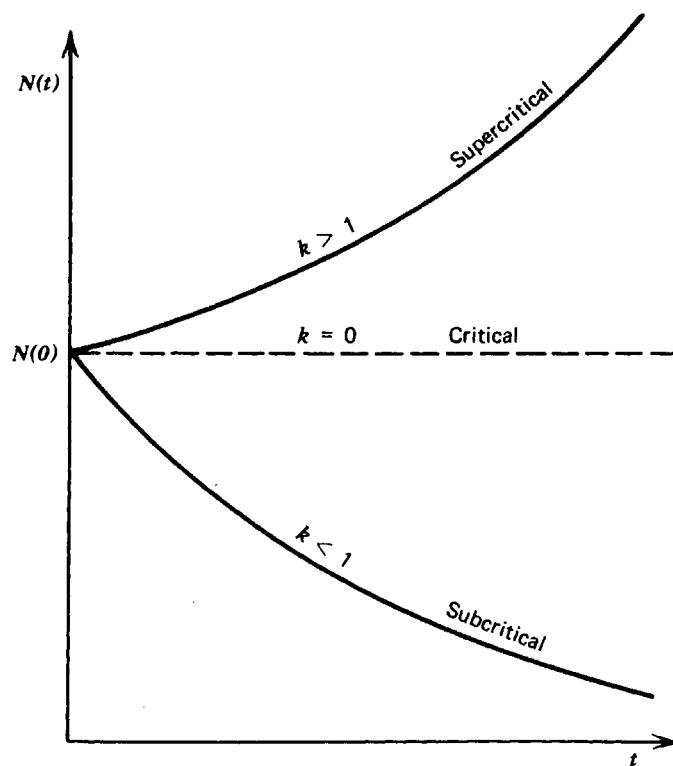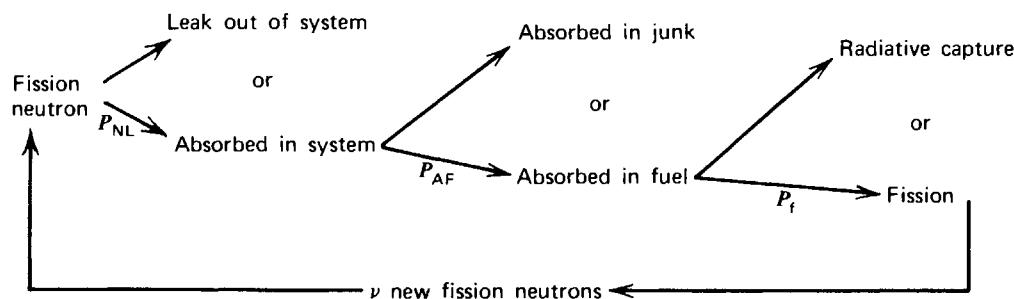


FIGURE 3-2.   Time behavior of the number of neutrons in a reactor.

control the reactor power level, for a 0.1% change in the multiplication factor is rather common. Fortunately we have omitted something from this simple model which tends to greatly increase the neutron lifetime $l$ and hence $T$, thereby slowing down the reactor time response. This is the effect of delayed neutrons on the chain reaction. However this is a tale for another time, so we will leave our study of reactor kinetics with the promise of returning later to patch up this model in order to provide a more optimistic picture of nuclear reactor time behavior.

## C. A Formal Calculation of $k$: The Four-Factor Formula

Let us now turn our attention to the calculation of the multiplication factor for, say, a pile of uranium that one wishes to make into a nuclear reactor. We probably should add some coolant to remove fission heat and perhaps some structural material to hold the core together. However we will assume that we can treat these materials as intimately and homogeneously mixed so that the composition of the reactor is uniform.

Now to calculate $k$ we must determine the possible fate of neutrons in a given fission generation. Fortunately this is rather easy to do since there are only two possible alternative destinies available to the neutron. First it might leak out of the reactor and be lost to the chain reaction. If it does not leak out, then it must eventually be absorbed.[†] This absorption may correspond to a nonproductive capture event in either the fuel or other materials, or the absorption may induce a fission reaction, in which case a new fission neutron generation is produced. We can represent these destinies schematically, as shown below:



To make this more formal, suppose we define the probabilities for each of these possible events as follows:

$$P_{NL} \equiv \frac{\text{Probability that neutron will not leak out of system before}}{\text{absorption}}$$

$$P_{AF} \equiv \frac{\text{Conditional probability that } if \text{ neutron is absorbed, it}}{\text{will be absorbed in the fuel}}$$

$$P_f \equiv \frac{\text{Conditional probability that } if \text{ neutron is absorbed in}}{\text{fuel, it will induce a fission reaction.}}$$

---

[†]Of course, yet a third alternative would be a decay of the neutron into a proton, electron, and neutrino, but since the half-life for decay of a free neutron is 11.7 minutes, and the typical neutron lifetime $l$ in the reactor is less than $10^{-3}$ sec, we can safely ignore this alternative.

These latter two conditional probabilities are easily calculated. The conditional probability for absorption in the fuel $P_{AF}$ can be expressed simply as the ratio of the macroscopic absorption cross sections for the fuel $\Sigma_a^F$, and for the fuel plus the rest of the material in the core $\Sigma_a$. (We will usually indicate with a superscript the material to which we are referring. The absence of the superscript will imply that the macroscopic cross section is the total for all of the materials in the system.) Thus we can write

$$P_{AF} = \frac{\Sigma_a^F}{\Sigma_a} .$$

(3-8)

It should be kept in mind that this expression has been introduced only for the situation in which the reactor has a uniform composition. Unfortunately for the reactor analyst all modern reactors have nonuniform compositions varying from point to point (e.g., due to fuel elements, coolant channels, support structure). In this more general case one can still use Eq. (3-8) if the macroscopic cross sections $\Sigma_a$ are regarded as spatial averages over the reactor. It should also be noted that we have not yet specified the neutron energy at which these cross sections are to be evaluated. Again, we will later find that the cross sections appearing in Eq. (3-8) must be appropriately averaged over energy, just as they are over space.

It is customary in reactor terminology to refer to this probability as the *thermal utilization* of the reactor and denote it by $P_{AF} \equiv f$. This term arose in the early analysis of thermal reactors in which essentially all fissions in the fuel were induced by thermal neutrons. In this case the cross sections in $f$ would be evaluated at thermal neutron energies and would represent the effectiveness of the fuel in competing with other materials in the reactor for the absorption of thermal neutrons, that is, the effectiveness with which the reactor utilized the thermal neutrons in the fuel. The expression in Eq. (3-8) actually applies to any type of reactor. However we will fall in line with convention and refer to it as the thermal utilization and denote it by "$f$."

The conditional probability for inducing a fission reaction in the fuel can also be expressed in terms of cross sections. In this case we simply take the ratio of the fission cross section to that of the absorption cross section (due to both fission and radiative capture) in the fuel material:

$$P_f = \frac{\Sigma_f^F}{\Sigma_a^F} = \frac{\sigma_f^F}{\sigma_a^F} .$$

(3-9)

We are now ready to utilize these probabilities to determine the multiplication factor $k$. The general scheme is to play a game of "follow the neutron." Suppose we start with $N_1$ neutrons present in the reactor in a given fission generation. Then with the help of the above probabilities and our diagram, we can compute the number of neutrons in the next generation as:

$$N_2 = \nu P_f P_{AF} P_{NL} N_1$$

(3-10)

or

$$N_2 = \eta f P_{NL} N_1 .$$

(3-11)

where we have recalled that $\eta = \nu(\sigma_f^F/\sigma_a^F)$ is the number of fission neutrons produced per absorption in the fuel. We can now use our definition of the multiplication factor $k$ as being the ratio of the number of neutrons in two successive fission generations to write

$$k = \frac{N_2}{N_1} = \eta f P_{NL}. \qquad (3\text{-}12)$$

The nonleakage probability $P_{NL}$ appearing in Eq. (3-12) and characterizing neutron leakage from the core is much more difficult to compute. It will require more elaborate mathematics (and in a realistic calculation, the use of a digital computer), and hence we will defer a discussion of it until later.

As a momentary detour, however, suppose our reactor were of infinite extent. Then since no neutrons could leak out, we immediately conclude that we must set the nonleakage probability $P_{NL} = 1$. The corresponding multiplication factor is then known as the *infinite medium multiplication factor* and denoted by

$$k_\infty = \eta f. \qquad (3\text{-}13)$$

Now of course no reactor is of infinite size. Nevertheless $k_\infty$ is a useful parameter in reactor analysis since it essentially characterizes the multiplication properties of the *material* in the reactor as distinct from the *geometry* of the reactor core. Of course since $P_{NL} < 1$ more generally for a finite reactor from which some neutron leakage can occur, we must have $k_\infty > 1$ in order to have any chance of achieving a critical chain reaction.

There are a couple of important modifications that must be introduced into this simple development in order to understand how the present generation of so-called "thermal" reactors works. We must account for the fact that the neutrons in a nuclear reactor have a distribution of energies. As we saw in Chapter 2, the fission neutrons are born at very high energies in the MeV range. However the fission cross section is largest at very low energies—indeed, at those energies corresponding to neutrons in thermal equilibrium with the reactor core at a temperature $T$, e.g., for $T = 300°C$, $E = kT = 0.05$ eV. Hence it is obviously to our advantage to try to slow down, or in the language of reactor physics, "moderate," the fast fission neutrons to take advantage of the fact that slow neutrons are more likely to induce fission reactions. This can be accomplished rather easily, simply by letting the fast neutrons collide with light nuclei, thereby losing some of their kinetic energy in elastic scattering collisions. The lighter the nucleus involved, the more kinetic energy per collision will be lost on the average by the neutron and hence the more effective the slowing down or moderation. In fact the best nucleus to use is hydrogen, which is fortunately quite commonly available in the form $H_2O$. Hence if we just let the fast neutrons rattle around in water for a bit, they will quickly slow down to the desired thermal energy. In this sense, we refer to water as a neutron *moderator*. Numerous other materials can be used as moderators in nuclear reactors, and we will discuss these in greater detail later.

The presence of such neutron moderation in a reactor suggests several modifications to our earlier calculation of the multiplication factor $k$. Suppose we first modify our diagram of the various possible neutron destinies to take into account neutron energy as shown in Figure 3-3. Now since most fissions will be induced by thermal neutrons, we will regard $f$ and $\eta$ as being evaluated at thermal neutron
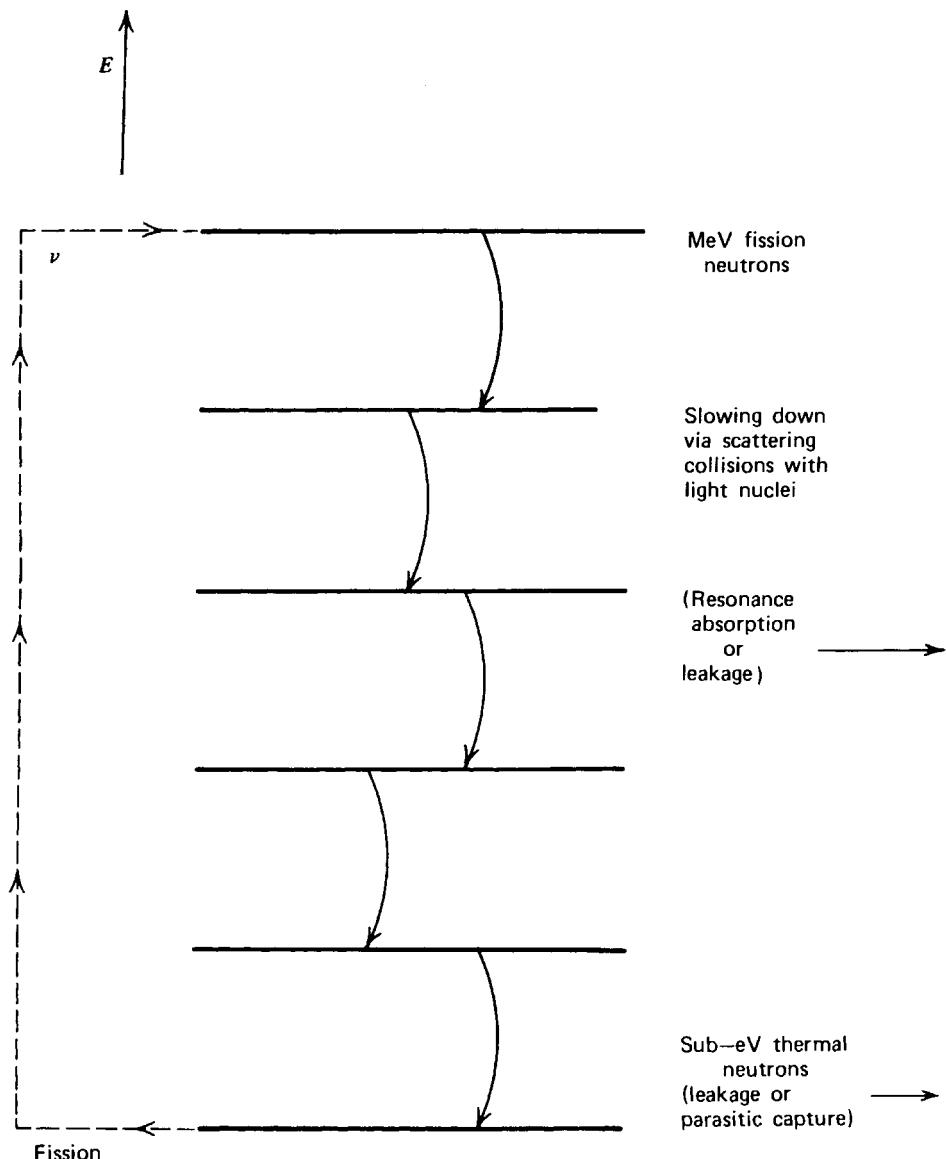
**FIGURE 3-3.** Processes characterizing a neutron generation in a thermal reactor.

energies. For example, $f$ would now refer to the ratio of *thermal* neutron absorptions in the fuel to total *thermal* neutron absorptions and thereby become more deserving of its designation as the "thermal" utilization. Similarly, $\eta$ is now identified as the average number of fission neutrons produced per absorption of a *thermal* neutron in the fuel.

Then to account for processes that occur while the neutron is slowing down to thermal energies, we will introduce two new quantities. We first define a factor that takes account of the fact that, although most fissions will be induced in fissile material by thermal neutrons, some fissions will be induced in both fissile and fissionable material by fast neutrons. Hence we will scale up our earlier expression for $k$ by a *fast fission factor* $\epsilon$:

$$\epsilon \equiv \frac{\text{Total number of fission neutrons (from both fast and thermal fission)}}{\text{Number of fission neutrons from thermal fissions}} \quad (3\text{-}14)$$

The fast fission factor $\epsilon$ is usually quite close to unity in a thermal reactor with typical values ranging between $\epsilon = 1.03$ and $\epsilon = 1.15$.

The second factor we will introduce will characterize the possibility that the neutron might be absorbed while slowing down from fission to thermal energies. Since most absorptions occurring during the slowing down process correspond to resonance capture in heavy nuclei such as $^{238}U$, we refer to this factor as the *resonance escape probability p*:

$$p \equiv \begin{array}{c} \text{Fraction of fission neutrons that manage to} \\ \text{slow down from fission to thermal energies} \\ \text{without being absorbed.} \end{array} \qquad (3\text{-}15)$$

Finally it is useful to modify our definition of the nonleakage probability to take account of the fact that there will be two distinct phases of neutron leakage that will require two rather different types of analysis in our later work. First the neutron may leak out while slowing down. Indeed since the neutron mean free path is relatively large for high energies, such fast neutron leakage may be quite appreciable. A second leakage process may occur after the neutron has managed to slow down to thermal energies. After slowing down, the neutron may continue to scatter and eventually leak out before it has had an opportunity to be absorbed. To take account of these two processes, we will break up our earlier nonleakage probability as follows:

$$P_{NL} = P_{FNL} P_{TNL} \qquad (3\text{-}16)$$

where

$$P_{FNL} \equiv \begin{array}{c} \text{Probability that fast neutron will not leak out} \\ \text{(fast nonleakage)} \end{array}$$

$$P_{TNL} \equiv \begin{array}{c} \text{Probability that thermal neutron will not leak out} \\ \text{(thermal nonleakage).} \end{array}$$

If we now insert these new definitions into our earlier expressions (3-12) and (3-13), we find that the infinite medium multiplication factor becomes

$$k_\infty = \eta f p \epsilon. \qquad (3\text{-}17)$$

This is known as the *four-factor formula*. Moreover one now writes

$$k = \eta f p \epsilon \, P_{FNL} P_{TNL}, \qquad (3\text{-}18)$$

which is known, surprisingly enough, as the *six-factor formula*.

EXAMPLE: To more vividly illustrate these ideas, we can list the values of each of the factors in the six-factor formula for a typical thermal reactor: $\eta = 1.65$, $f = 0.71$, $\epsilon = 1.02$, $p = 0.87$, $P_{FNL} = 0.97$, $P_{TNL} = 0.99 \Rightarrow k_\infty = 1.04 \Leftrightarrow k = 1.00$.

Hence provided we can calculate each of these factors, our criticality condition $k = 1$ can then be easily checked (in the above example we fudged up the parameters a bit to yield a critical system). Of course, the calculation of these factors is quite difficult in general. Indeed one cannot really separate the various

conditional probabilities as was done in these formulas. Instead alternative schemes based on iterative numerical methods must be used in practice to arrive at a criticality condition.

Nevertheless the four-factor and six-factor formulas are quite useful because they provide insight into the various mechanisms involved in nuclear fission chain reactions and on rare occasions may actually be of use in making crude estimates in nuclear design. They are also useful in illustrating the trends of parameter variation in a core design.

For example, although $\eta$ and $\epsilon$ are essentially fixed once the fuel has been chosen, the thermal utilization $f$ and resonance escape probability $p$ can be varied considerably by changing the ratio of fuel density to moderator density. All of these parameters can be varied by using a heterogeneous lattice of fuel elements surrounded by moderator rather than a uniform, homogeneous mixture of fuel and moderator.

One can also vary the nonleakage probabilities by simply making the reactor core larger, or surrounding the reactor by a material with large scattering cross section so that some of the neutrons leaking out will be scattered back into the reactor. Actually when leakage is changed, there will be some change in the parameters in the four-factor formula as well since these are actually averages over the various neutron energies in the reactor, and this distribution of energies will vary with the amount of leakage. Such considerations have given rise to a somewhat different notation for the multiplication factor characterizing a finite system which is occasionally referred to as the *effective multiplication factor* and denoted by $k_{eff}$

$$k_{eff} = k_{\infty} P_{FNL} P_{TNL}. \tag{3-19}$$

There are other prescriptions for defining the multiplication factor. In particular we will introduce one of these schemes later when we consider the analytical treatment of the neutron energy dependence in more detail. However for now we will continue to regard the multiplication factor as the ratio between either the number of neutrons in two successive fission generations or the neutron production and loss rates in the reactor.

We can use the six-factor formula for the multiplication factor to gain a bit more insight into the goals of reactor design and operation. There are several ways to adjust $k$ in the initial design of the reactor. One could first regard the size of the reactor as the design variable. Since the ratio of surface area to volume decreases as the reactor geometry is enlarged, one can control the relative importance of the leakage factors by adjusting the reactor size. For a given core composition (with $k_{\infty}$ greater than 1, of course) there will be a certain critical size at which $k = 1$. An alternative way to achieve the same reduction in leakage is to surround the reactor with a scattering material that acts as a neutron reflector. Most thermal reactor cores are so large that leakage represents a rather small loss mechanism (typically about 3% of the neutrons leak out from the core in large thermal reactors).

Usually the core size and geometry for a power reactor are dictated by thermal considerations, for instance, the size of the core necessary to produce a given power output while being provided with sufficient cooling so that the temperature of the reactor materials will not become excessively high. The primary design variable at the disposal of the nuclear engineer is the core composition. In particular he can vary the composition (enrichment) and shape of the fuel, the ratio of fuel to

moderator density, the type of moderator, coolant, and structural materials used, or the manner in which reactor multiplication is controlled. One would refer to the amount of fuel required to achieve a critical chain reaction as the *critical mass* of fuel.

In reality, however, a nuclear reactor is always loaded with much more fuel than is required merely to achieve $k = 1$. For example the LWR is typically loaded with sufficent fuel to achieve a multiplication of about $k = 1.25$. This extra multiplication is required for several reasons. First if the reactor is to operate at power for a period of time, one must provide enough excess fuel to compensate for those fuel nuclei destroyed in fission reactions during the power production. Since most contemporary reactors are run roughly one year between refueling, a sizable amount of excess fuel is needed to compensate for fuel burnup. A second motivation arises from the fact that the multiplication of a reactor tends to decrease as the reactor power level and temperature increase from ambient levels to operating levels. Additional multiplication is needed to compensate for this effect. Finally one must include enough extra multiplication to allow for reactor power level changes. For example, we have seen that if we wish to increase the reactor power level, we must temporarily adjust $k$ to a value slightly greater than 1 so that the reactor is supercritical. The reactor can then be returned to critical when the desired power level has been reached.

Of course when this excess multiplication is not being used, some mechanism has to be provided to cancel it out to achieve reactor criticality. This is the function of reactor control mechanisms. Such control is usually achieved by introducing into the reactor core materials characterized by large absorption cross sections. They will then tend to eat up the excess neutrons produced in the chain reaction. In terms of our six-factor formula such absorbing materials lower the value of the thermal utilization $f$, since they compete with the fuel for neutron absorption. A variety of types of reactor control are used in power reactors. For example, the neutron absorber might be fabricated into rods which can then be inserted into or withdrawn from the reactor at will to vary multiplication. Sometimes the absorber is fabricated directly into the fuel itself. Or it may be dissolved in the reactor coolant. When such control absorbers are used to hold down the excess multiplication introduced to compensate for fuel burnup, one refers to them as *shim* control. They may also be used to force the reactor subcritical in the case of an emergency; then they are known as *scram* control. Finally they may just be used to regulate the power level of the reactor; then they are referred to as *maneuvering* control elements.

The ease with which such control elements can control the fission chain reaction will depend on how rapidly the reactor responds to variations in multiplication. Since fuel burnup occurs over very long periods of time (typically weeks or months), a rapid response of shim control is not required—which is fortunate, because rather large amounts of multiplication must be manipulated (typically changes of 10–20% in $k$). The normal power variations in the reactor are due to much smaller changes in multiplication ($< 0.1\%$) and are characterized by essentially the reactor period $T$ which in turn is proportional to the neutron lifetime $l$. However we saw earlier that the lifetime of prompt fission neutrons was quite short, typically about $10^{-4}$ sec. The effective neutron lifetime is greatly increased by the presence of delayed neutrons, however. We recall that about 0.7% of the neutrons produced in fission are delayed anywhere from 0.6 to 80 sec since they arise from fission product radioactive decay. Hence the effective neutron lifetime is

actually the average of the prompt neutron lifetime and the average decay time of these delayed neutrons, properly weighted, of course, by their relative yield fractions. When this is taken into account, one finds that the effective neutron lifetime is almost two orders of magnitude longer, $l_{eff} \sim 10^{-1}$ seconds. Hence a multiplication of 0.1% would now correspond to a reactor period of $T = 10$ seconds, well within the control capability of a reactor control system.

## D. Conversion and Breeding

If we recall our earlier expression for the multiplication factor $k$ in Eq. (3-12), it is evident that since the thermal utilization $f$ and the nonleakage probability $P_{NL}$ are both less than 1, we require $\eta$ to be substantially greater than 1 if a critical fission chain reaction is to be possible. Fortunately as we can see from Figure 2-25, this condition is not only satisfied, but in fact for many energies one finds that $\eta > 2$. Hence we in fact appear to have an extra neutron. This "bonus" neutron can be put to good use if we recall that certain fertile isotopes can be transmuted into fissile material via neutron capture. In particular, $^{238}U$ can be transmuted into $^{239}Pu$, while $^{232}Th$ can be transmuted into $^{233}U$. Hence if we load the core of a reactor with such fertile material, we can use the extra neutron to produce a new fissile fuel material. This process is frequently referred to as *conversion*, and nuclear reactors whose principal job is to produce $^{239}Pu$ or $^{233}U$ are known as *converter reactors*.

Actually all modern power reactors are converter reactors in a sense, although this is not their primary function, since they contain substantial amounts of $^{238}U$ which will be transmuted into $^{239}Pu$ via neutron capture during normal operation. For example, a LWR will contain a fuel mixture of roughly 3% $^{235}U$ and 97% $^{238}U$ in a freshly loaded core. After a standard operating cycle (three years), this fuel will contain roughly 1% $^{235}U$ and 1% $^{239}Pu$ which can then be separated out of the spent fuel and refabricated into fresh fuel elements for reloading (so-called "plutonium recycling").

These considerations suggest that it might in fact be possible to fuel a reactor with $^{239}Pu$ and $^{238}U$ and then produce directly the fuel ($^{239}Pu$) needed for future operation. Indeed it might even be possible to produce more $^{239}Pu$ than is burned—that is, to "breed" new fuel. This is the essential idea behind the concept of a *breeder reactor*.

To discuss this concept in more detail, it is useful to define the *conversion ratio*

$$CR = \frac{\text{Average rate of fissile atom production}}{\text{Average rate of fissile atom consumption}}.$$

This quantity is also referred to as the *breeding ratio* (BR) if it is greater than one. If we have conversion then, consuming $N$ atoms of fuel during reactor operation will yield $CR \cdot N$ atoms of the new fissile isotopes. For example, most modern LWRs are characterized by a conversion ratio of $CR \cong 0.6$. By way of contrast, HTGRs are characterized by somewhat higher conversion ratios $CR \cong 0.8$ and hence are sometimes referred to as *advanced converter* reactors.

For breeding to occur we require that the conversion ratio be greater than unity, $CR = BR > 1$. Of course for this to happen we must have $\eta > 2$ since slightly more than one fission neutron is needed to maintain the chain reaction (some neutrons

will leak out or be absorbed in parasitic capture) while one neutron will be needed to replace the consumed fissile nucleus by converting a fertile into a fissile nucleus.

If we return to Figure 2-25 we can see that the only attractive breeding cycle for low-energy (i.e., thermal) neutrons would involve $^{233}U$, that is, the $^{232}Th/^{233}U$ process. To breed using $^{238}U/^{239}Pu$ requires that we use fast neutrons with energies greater than 100 keV. And of course this is the motivation behind the development of the *fast breeder reactor*.

At this point, it is useful to digress a bit and discuss the average energy of the neutrons sustaining the chain reaction in various types of nuclear reactors. As we have seen, the energies of neutrons in a reactor span an enormous range, from 10 MeV (usually the maximum energy of fission neutrons) down to as low as $10^{-3}$ eV after having suffered a number of scattering collisions with nuclei and slowing down. Furthermore the neutron cross sections depend sensitively on the neutron energy. As the examples in Chapter 2 indicated, the general trend is for cross sections to decrease with increasing energies. This feature is particularly true of absorption cross sections such as capture or fission.

The fact that the fission cross section $\sigma_f$ is largest at low energies implies that it is easiest to maintain a fission chain reaction using slow neutrons. Hence early nuclear reactors used low mass number materials such as water or graphite to slow down or moderate the fast fission neutrons. Such moderating materials slow the neutrons down to energies comparable to the thermal energies of the nuclei in the reactor core. Reactors characterized by an average neutron energy comparable to such thermal energies are referred to as *thermal reactors*. Such reactors require the minimum amount of fissile material for fueling and are the simplest reactor types to build and operate. Most nuclear power plants in this country and abroad utilize thermal reactors.

However we have also seen that there is a very definite advantage in keeping the neutron energy high, since the number of neutrons emitted per neutron absorbed in the fuel $\eta$ is largest for fast neutrons. Hence one can use the "extra" neutrons available in a fission chain reaction maintained by fast neutrons to convert or breed new fuel. However since $\sigma_f$ is smaller, one also needs much more fuel to sustain the chain reaction. Furthermore to keep the neutron energy high, one wants to utilize only high mass-number materials in the core to keep neutron slowing down to a minimum. Such reactors characterized by average neutron energies above 100 keV are known as *fast reactors*. It is felt by many that fast reactors will eventually replace the current generation of thermal power reactors because of their ability to breed fuel.

To make some of these ideas a bit more precise, we have compared the important nuclear parameters $\nu$, $\eta$, and $\sigma_f$ for typical nuclear fuels at energies characterizing both thermal and fast reactors. (To be more precise, these quantities have been calculated by averaging the energy-dependent nuclear parameters $\nu(E)$, $\eta(E)$, and $\sigma_f(E)$ over the neutron energy distributions found in typical LWRs and LMFBRs.) One should first note that the fission cross sections in fast reactors are some two orders of magnitude lower than those in thermal reactors. Hence even though fast reactors exhibit considerably higher conversion ratios (typically, CR $= BR \sim 1.2-1.5$) due to a larger value of $\eta$, their fissile inventory requirements may run as much as several times those required by thermal reactors just to maintain a critical chain reaction with fast neutrons. This table also indicates that while $^{235}U$ will yield a slightly higher conversion ratio than $^{239}Pu$ in thermal reactors, the use

of $^{239}$Pu does exhibit a sizable advantage in fast reactors since the capture-to-fission ratio $\alpha^{49}$ falls off quite markedly for large neutron energies. In Table 3-1 we have only indicated the nuclear fission properties of $^{238}$U in fast reactors, since this isotope is fissionable and hence contributes only a modest fraction of the fissions occurring in thermal reactors ($\sim$2-5%) in contrast to its rather large contribution in fast reactors ($\sim$20%).

TABLE 3-1   Energy-Averaged Fission Parameters Characterizing Thermal and Fast Reactors

| | Thermal Reactor (LWR) | | Fast Reactor (LMFBR) | | |
| | $^{235}$U | $^{239}$Pu | $^{235}$U | $^{239}$Pu | $^{238}$U |
|---|---|---|---|---|---|
| $\bar{\nu}$ | 2.4 | 2.9 | 2.6 | 3.1 | 2.6 |
| $\bar{\eta}$ | 2.0 | 1.9 | 2.1 | 2.6 | 0.3 |
| $\sigma_f$(b) | 280 | 790 | 1.9 | 1.8 | 0.06 |

We have mentioned only a few of the considerations involved in comparing the nuclear behavior of thermal versus fast reactors. As we develop more sophisticated methods of reactor analysis, we will return frequently to contrast the application of these methods for thermal and fast systems.

# II. AN INTRODUCTION TO NUCLEAR POWER REACTORS

## A. Nuclear Power Plants

The schematic illustration[4] of a typical large nuclear power plant appears in Figure 3-4. It is apparent from this illustration that the nuclear reactor itself is only one of a great many components in such a plant. Actually aside from the nuclear reactor and its associated coolant system, such power plants are remarkably similar to large fossil-fuel fired plants. Only the source of the heat energy differs, that is, nuclear fission versus chemical combustion. Hence most of the components of large central-station power plants are common to both nuclear and fossil units.

A very crude diagram of the major components of an electrical power plant is given in Figure 3-5. As we have sketched it in this diagram, the steam supply system could be either a fossil-fuel fired boiler or a nuclear reactor and its associated coolant loops.

All of the current large power plants operate on a steam cycle (a so-called Rankine cycle) in which the heat generated by combustion or nuclear fission is used to convert water into high-pressure, high-temperature steam. This steam is then allowed to expand against the blades of a *turbine*. In this way the latent energy of the steam is converted into the mechanical work of turning the turbine shaft. This shaft is connected to a large *electrical generator* that converts the mechanical turbine energy into electrical energy which can then be distributed to an electrical power grid. The low-pressure steam leaving the turbine must then be recondensed in a steam *condensor* into water so that it can be pumped back to the steam supply system to complete the cycle. The condensor requires large quantities of ambient
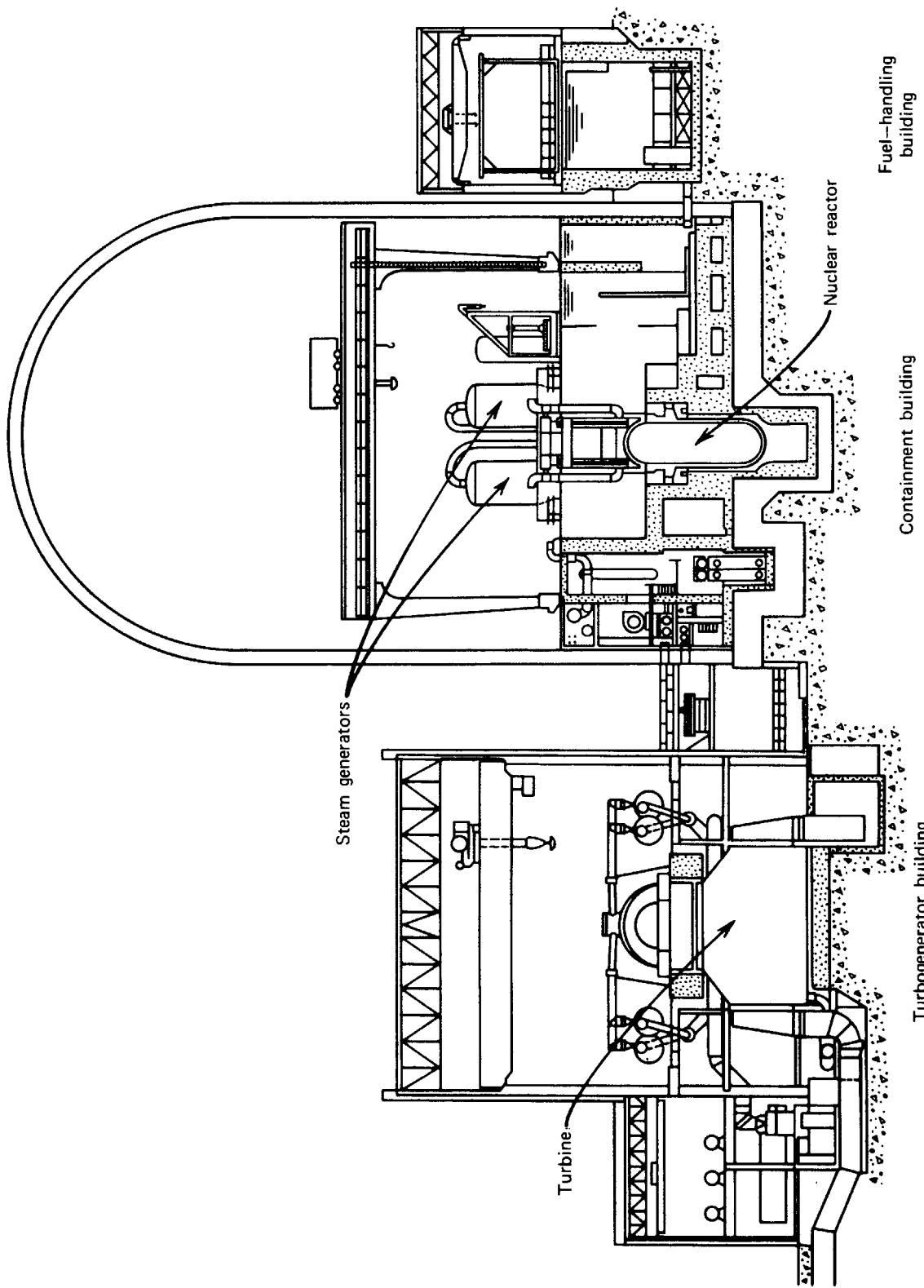
FIGURE 3-4. A schematic diagram of a nuclear power plant.[4]

89
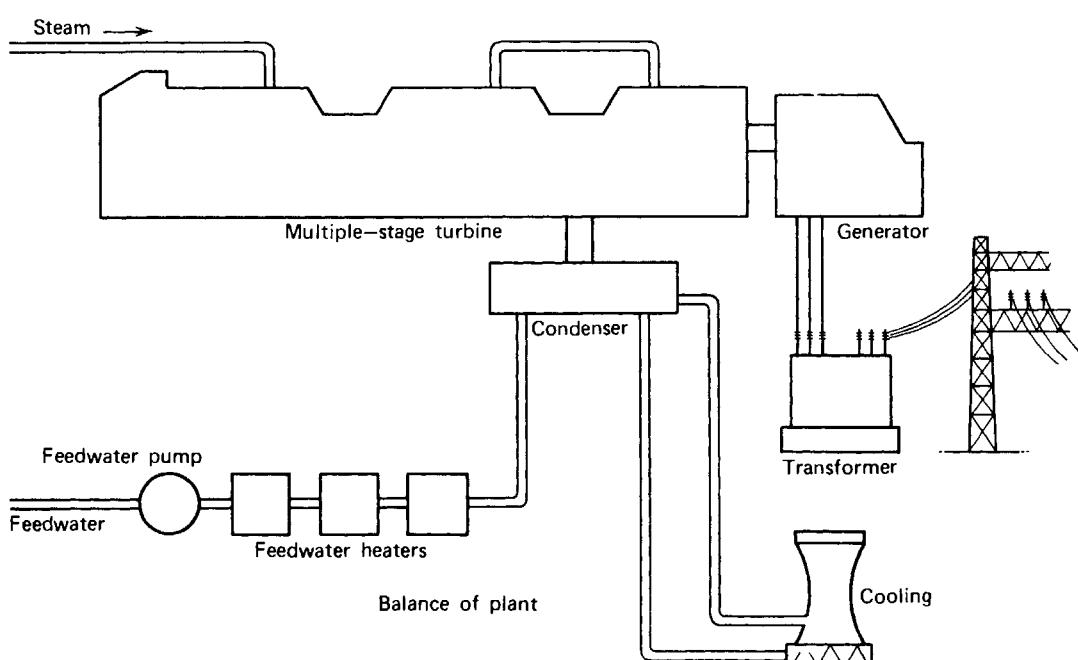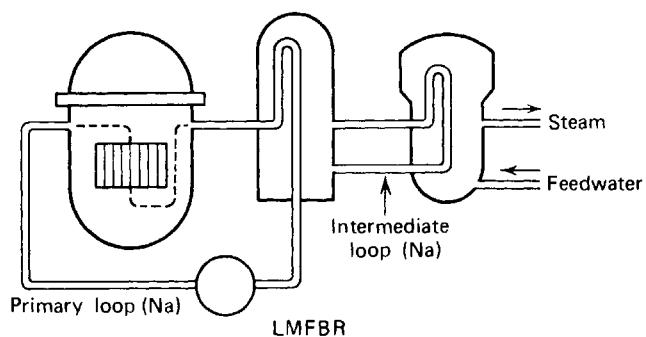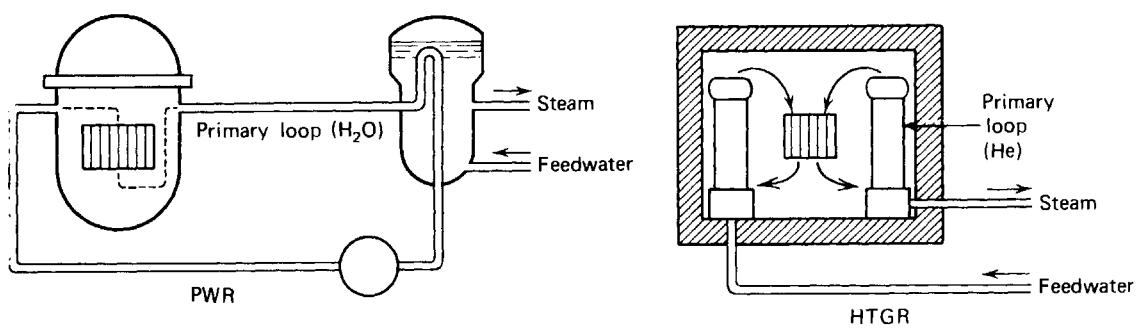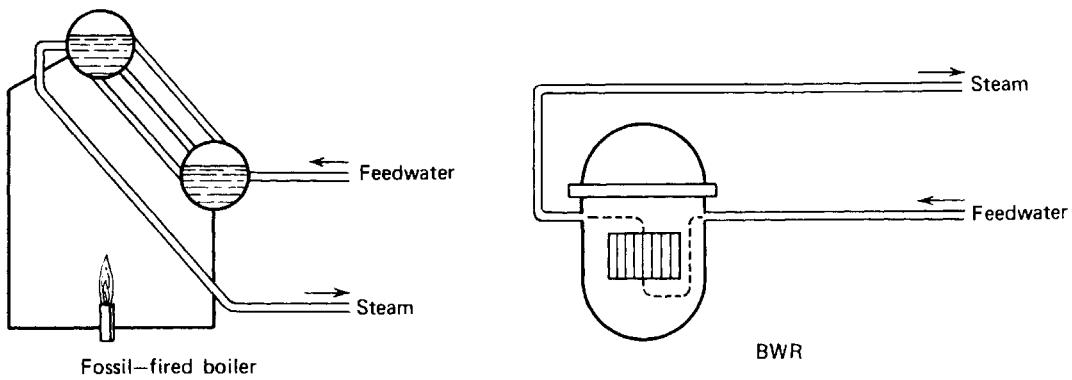
**FIGURE 3-5.** Comparison of different steam-supply systems.

temperature cooling water which is usually obtained from artificial *cooling ponds* or *cooling towers*.

This is of course a very oversimplified description of the major components of a power plant, but it does serve to illustrate that these components are quite similar for both nuclear and fossil-fueled stations. Actually as far as the steam cycle itself is concerned, the primary difference between the two types of plant is that the fossil-fueled boiler supplies slightly higher temperature, higher pressure steam, thereby reducing the design requirements on the turbine (although it should be mentioned that more advanced reactor types such as the HTGR supply system steam at conditions quite comparable to those of modern fossil-fueled units). Of course there are numerous other differences in the various subsystems of the plants, as well as in their operation. However the major features of the plants, aside from their steam supply system, are quite similar.

## B. The Nuclear Steam Supply System (NSSS)

The NSSS consists essentially of three major components: (a) a *nuclear reactor* supplying the fission heat energy, (b) several *primary coolant loops* and *primary coolant pumps* that circulate a coolant through the nuclear reactor to extract the fission heat energy, and (c) heat exchangers or *steam generators* that use the heated primary coolant to turn feedwater into steam. Several very simplified diagrams of NSSS components are given in Figure 3-5.

A variety of possible coolants can be used in the primary loops of the NSSS. Indeed nuclear reactor types are usually characterized by the type of coolant they use, such as LWRs or gas-cooled reactors. There are also a variety of possible NSSS configurations. For example, one may actually produce the steam in the reactor core itself. Or one may use a single-phase primary coolant such as water or helium to transfer the fission heat energy to a heat exchanger where it is used to produce steam (see Figure 3-5). In the liquid metal-cooled NSSS, an intermediate coolant loop must be utilized to isolate the steam generator from the very high induced radioactivity of the primary coolant loop passing through the reactor.

The most common coolant used in power reactors today is ordinary water, which serves as both coolant and moderating material in the reactor. There are two major types of LWR: pressurized water reactors (PWR) and boiling water reactors (BWR). In a PWR the primary coolant is water maintained under very high pressure ($\sim$155 bar) to allow high coolant temperatures without steam formation within the reactor. The heat transported out of the reactor core by the primary coolant is then transferred to a secondary loop containing the "working fluid" by a steam generator. Such systems typically contain from two to four primary coolant loops and associated steam generators.

In a BWR, the primary coolant water is maintained at a sufficiently low pressure ($\sim$70 bar) for appreciable boiling and steam formation to occur within the reactor core itself. In this sense the reactor itself serves as the steam generator, thereby eliminating the need for a secondary loop and heat exchanger. In both the PWR and BWR, the nuclear reactor itself and the primary coolant are contained in a large steel *pressure vessel* designed to accomodate the high coolant pressures and temperatures. In a PWR, this pressure vessel must be fabricated with thick steel walls to contain the very high primary coolant pressures. By way of contrast, the BWR pressure vessel need not be so thick, but must be much larger to contain both

the nuclear reactor and steam moisture-separating equipment.

A very closely related class of reactors utilizes $D_2O$ as moderator and either $D_2O$ or $H_2O$ as primary coolant. The most common type of such heavy water reactors, the CANDU-PHW, utilizes the pressure tube concept in which each coolant channel in the reactor is designed to accommodate the primary system pressure which is again kept high to prevent boiling. As with a PWR, the primary coolant thermal energy is transferred via a steam generator to a secondary loop containing light water as the working fluid. More recently, heavy water pressure tube reactors have been designed (e.g., the CANDU-BLW or SGHWR) which produce $H_2O$ steam directly in the core similar to a BWR.

Yet another type of reactor uses gas coolants. Although $CO_2$ has been used as the coolant in the MAGNOX class of natural uranium fueled, graphite moderated reactors for many years in the United Kingdom, most present interest is directed at HTGRs using helium under high pressure to cool a reactor fueled with enriched uranium and moderated by graphite. The helium coolant is then passed through steam generators to transfer the thermal energy on to a secondary loop containing water as a working fluid. It should also be mentioned that such HTGRs have the potential of being combined with gas turbines (rather than steam turbines), thereby eliminating the steam cycle altogether.

Gas coolants have also been proposed for use in fast breeder reactors (GCFRs). Because of the very high power densities required by such reactors, extremely high coolant flow rates would be required. Nevertheless the rather large breeding ratios (BR~ 1.5) achievable in the GCFR make it appear a very promising alternative to other fast reactor designs.

The final class of nuclear reactors utilizes liquid metals such as sodium as a primary coolant. Although sodium could be used in thermal reactors if alternative moderation were provided, its primary advantages occur in fast breeder reactors which require a primary coolant with low moderating properties and excellent heat-transfer characteristics. The LMFBR NSSS actually uses two sodium loops. A primary sodium loop is used to remove fission heat from the reactor; this coolant is then passed through an intermediate heat exchanger in which it transfers its heat energy to a secondary sodium loop, which, in turn, carries heat to a steam generator. The intermediate loop isolates the steam generator from the radioactivity induced in the primary sodium coolant.

The NSSS of a modern nuclear power plant is completely contained within a *reactor containment structure* designed to prevent the release of radioactivity to the environment in the even of a gross failure of the reactor coolant system. This nuclear island within the plant is usually fabricated out of steel-lined concrete and contains not only the reactor itself (and its associated pressure vessel), but also the primary coolant system including the primary pumps, steam generators, piping, and auxiliary systems. A glance back at the schematic diagram of a nuclear power plant in Figure 3-4 can quickly identify the containment building and the NSSS contained within it.

## C. The Nuclear Reactor Core

At the heart of the NSSS is the nuclear reactor. Far from being just a relatively simple "pile" of fuel and moderator à la Fermi, a modern power reactor is an enormously complicated system designed to operate under the most severe conditions of temperature, pressure, and intense radiation. To introduce the general
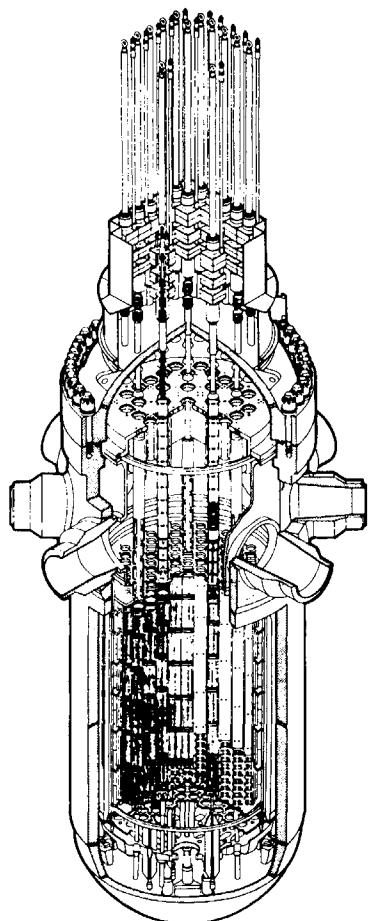
FIGURE 3-6.   A large pressurized water reactor.[4]

components of a typical power reactor, we will consider the specific example of a modern large PWR as illustrated in Figure 3-6.[4] The reactor proper consists of a *core* containing the fuel, coolant channels, structural components, control elements, and instrumentation systems. In this particular example, the core is a cylindrically shaped lattice roughly 350 cm in diameter by 370 cm in height consisting of long fuel *assemblies* or *bundles*. These assemblies consist of a large number of long, narrow *fuel rods* or *fuel elements*, which are metallic tubes containing the nuclear fuel in the form of ceramic pellets. Individual fuel elements and assemblies for such a PWR are shown in Figure 3-7.

In the reactor core one induces and maintains the nuclear fission reactions that produce the desired heat. The core itself is enclosed in a much larger container, a *reactor pressure vessel*, designed to withstand the enormous pressures of the coolant (up to 155 bar) as well as to isolate the reactor core from the remainder of the NSSS.

Most of our attention in this text will be directed at the nuclear analysis of the reactor core itself, since this is the principal responsibility of the nuclear engineer. However as we have mentioned earlier, we will try to develop this nuclear analysis within the context of other considerations influencing the design of the nuclear steam supply system.

Before we conclude this brief introduction to nuclear reactors, however, it is useful to make a short list of the various components of nuclear reactor systems as well as to introduce some of the standard nomenclature used in nuclear reactor engineering.

Fuel element     Fuel assembly
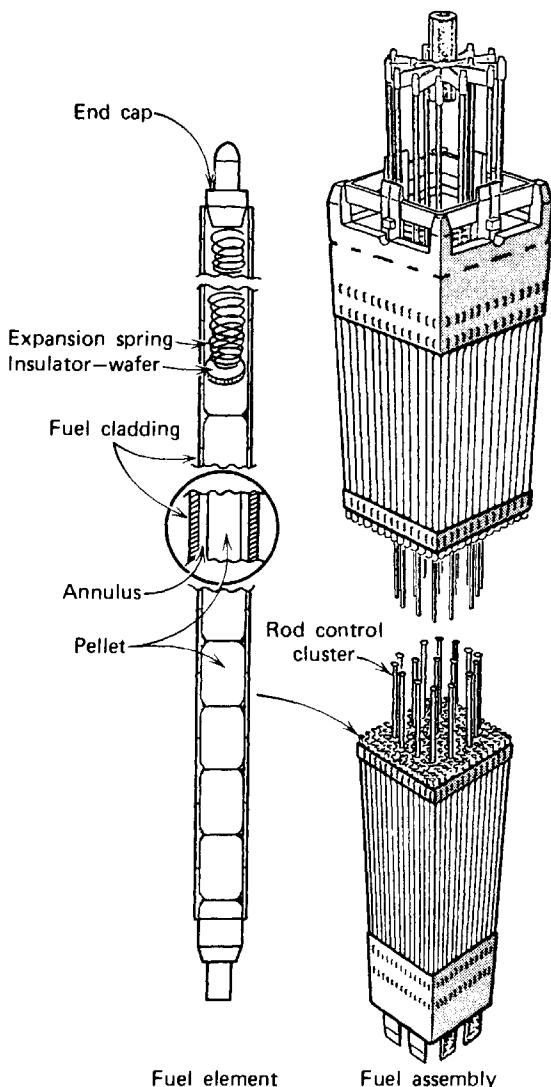
**FIGURE 3-7.   Fuel element; fuel assembly.**

(1) *Fuel*: Any fissionable material. This can be either fissile material such as $^{233}$U, $^{235}$U, $^{239}$Pu, or $^{241}$Pu or fissionable material such as $^{232}$Th, $^{238}$U, or $^{240}$Pu. Most modern power reactors utilize this fuel in a ceramic form— either as an oxide such as $UO_2$, a carbide such as UC, or a nitride, UN.

(2) *Fuel element*: The smallest sealed unit of fuel. In an LWR or LMFBR the fuel element is a metal tube containing ceramic pellets of fuel (such as $UO_2$). (See Figure 3-7.) In an HTGR the fuel element can be regarded as either a tiny (300 $\mu$m diameter) particle of uranium carbide coated with pyrolytic graphite layers, or as a cylindrical fuel pin composed of these fuel particles bound together with a graphite binder.

(3) *Fuel assembly* or *bundle*: The smallest unit combining fuel elements into an assembly. For example, in a LWR the fuel assembly is composed of several hundred fuel elements fastened together at top and bottom with coolant nozzle plates and with several spring clip assemblies along the length of the fuel (see Figure 3-7). In an HTGR the fuel assembly is a hexagonal block of graphite with holes into which the cylindrical fuel pins are inserted. Fuel is usually loaded into a reactor core or replaced one fuel assembly at a time. A typical power reactor core will contain hundreds of such fuel assemblies.

(4) *Moderator*: Material of low mass number which is inserted into the reactor to slow down or moderate neutrons via scattering collisions. Typical moderators include light water, heavy water, graphite, and beryllium.

(5) *Coolant*: A fluid which circulates through the reactor removing fission heat. The coolant can be either liquid, such as water or sodium, or gaseous, such as helium or carbon dioxide. It may also serve a dual role as both coolant and moderator, such as in the LWR.

(6) *Coolant channel*: One of the many channels through which coolant flows in the fuel lattice. This may be an actual cylindrical channel in the fuel assembly, as in the HTGR, or an equivalent channel associated with a single fuel rod, as in a LWR.

(7) *Structure*: The geometry and integrity of the reactor core is maintained by structural elements such as support plates, spacer grids, or the metallic tubes used to clad the fuel in some reactor designs. The structural materials may also serve a dual role by moderating neutrons such as the graphite in an HTGR.

(8) *Control elements*: Absorbing material inserted into the reactor to control core multiplication. Although most commonly regarded as movable rods of absorber, control elements may also consist of fixed absorbers or absorbing materials dissolved in the coolant. Common absorbing materials include boron, cadmium, gadolinium, and hafnium.

(9) *Reactor core*: The total array of fuel, moderator, and control elements.

(10) *Reactor blanket*: In a breeder or high conversion reactor the core is usually surrounded by a blanket of fertile material that more effectively utilizes the neutrons leaking out of the core.

(11) *Reflector*: A material characterized by a low absorption cross section used to surround the core in order to reflect or scatter leaking neutrons back into the core.

(12) *Shielding*: The reactor is an intense source of radiation. Not only must operating personnel and the public be shielded from this radiation, but reactor components must as well be protected. Hence absorbing material is introduced to attenuate both neutron and gamma radiation. Thermal shielding is used to attenuate the emergent core radiation to levels that do not result in significant heat generation and hence damage in reactor components. Biological shielding reduces the radiation still further to acceptable levels for operating personnel.

(13) *Support structure*: The support plates that serve to maintain the core geometry.

(14) *Reactor pressure vessel*: The high pressure containment for reactor and associated primary coolant system.

It is also useful to introduce at this point several quantities which are used to describe reactor performance. The units in which these quantities are usually expressed are denoted in brackets.

(1) *Reactor thermal power* [MWt]: The total heat produced in the reactor core.

(2) *Plant electrical output* [MWe]: Net electrical power generated by the plant.

(3) *Net plant efficiency* [%]: $\dfrac{\text{Plant electrical output}}{\text{Reactor thermal power}}$.

(4) *Plant capacity factor* [%]: $\dfrac{\text{Total energy generated over time period}}{(\text{Plant rating}) \times (\text{time})}$.

(5) *Plant load factor* [%]: $\dfrac{\text{Average plant electrical power level}}{\text{Peak power level}}$.

(6) *Plant availability factor* [%]: $\dfrac{\text{Integrated electrical energy output capacity}}{\text{Total rated energy capacity for period}}$.

(7) *Core power density* [kW/liter]: $\dfrac{\text{Reactor thermal power}}{\text{Total core volume}}$.

(8) *Linear power density* [kW/m]: Thermal heat generated per unit length of coolant channel.

(9) *Specific power* [kW/kg]: $\dfrac{\text{Reactor thermal power}}{\text{Total mass of fissionable material}}$.

(10) *Fissile loading* [kg]: Total mass of fissionable material.

(11) *Fuel enrichment* [%]: $\dfrac{\text{Mass of fissile material}}{\text{Mass of fissile and fertile material}}$.

(12) *Fuel burnup* [Megawatt-days/metric ton uranium $=$ MWD/TU]:

$$\dfrac{\text{Energy generated in fuel during core residence}}{\text{Total mass of fuel}}.$$

(13) *Fuel residence time*: $\dfrac{\text{Fuel burnup}}{(\text{Specific power}) \times (\text{capacity factor})}$.

These are the more common terms used in characterizing nuclear plant performance. We will introduce other more specific concepts and terminology later as we develop the more detailed theory of nuclear reactor behavior.

## III. NUCLEAR REACTOR DESIGN

### A. General Design Functions of the Nuclear Engineer

The design of a large nuclear power plant is an enormously complex task and involves the coordination of a remarkably diverse range of disciplines. Each major component of the plant requires a separate and distinct design analysis and is usually the responsibility of a specific engineering design team. For example, the design of the reactor pressure vessel or steam generators is usually performed by the reactor supplier, while the turbogenerator and switchgear design is the responsibility of the electrical equipment manufacturer. The coordination among these different design projects is extremely important, however, since the designs frequently interact to a very high degree.

The primary responsibility for the nuclear design of the reactor core rests with the nuclear engineer. This design must be accomplished within numerous con-

straints imposed on the reactor operation. The nuclear analysis and design of a reactor core is highly dependent on other areas of core design, including thermal-hydraulic design, structural analysis, economic performance, and so on. The criteria for a design effort are quite varied, encompassing considerations of performance, reliability, economics, and safety. These criteria are frequently contradictory in nature, and hence require optimization.

The complete nuclear design of a given core configuration is performed many times, initially to survey design parameters, identify constraints, then to refine the design while interacting with other facets of the plant design, and finally, to establish a reference design that provides a calculational base against which optimization calculations can be compared.[5]

This design process is very similar to that utilized in other fields of engineering. One first must attempt to define the various design constraints that include considerations of system performance in terms of both system reliability and economic performance and safety criteria. Next a preliminary design is proposed, drawing on available information such as plants already in operation, experimental mockups, and frequently, old-fashioned intuition. Such a design includes a set of specifications involving quantities such as fuel enrichment, coolant flow rates and temperatures, core configurations, reload patterns, and so on. A detailed analysis of this preliminary design is then performed in order to evaluate its predicted performance and ascertain whether it conforms to the constraints imposed on the system. For example, one would want to calculate the core power and temperature distribution, the pressure drop of the coolant as it passes through the core, coolant-flow conditions, and the fuel lifetime. When possible, these calculations are compared against experiments in order to validate the computational models used. A detailed evaluation of the preliminary design will then lead to more detailed designs and analyses as one attempts to optimize the tradeoff between system performance and design constraints. As a final design is approached, one attempts to define detailed system specifications.

The above procedures emphasize the importance of adequate models of a nuclear reactor in order to carry out the required parameter and optimization studies. These models must be realistic since nuclear reactors are far too expensive to be built without detailed and accurate design information. Unfortunately any calculation sufficiently realistic to be of use in reactor design is far too complex to be carried out by hand. Hence the digital computer plays a very key role in nuclear reactor design.[6]

A key task of the nuclear reactor engineer is to develop models of nuclear reactors that can then be analyzed on the computer. Such models result in large computer programs or "codes" which can then be used by other nuclear engineers in reactor design. Most of our emphasis in this text is on learning how to synthesize such approximate models of reactor behavior and then cast them in a form suitable for reactor design. In the language of nuclear engineering, then, this text should be regarded as a primer on *nuclear methods development*.

A word of caution should be inserted here, however. In the early days of reactor development it was hoped that one would eventually be able to accurately model nuclear reactor behavior utilizing only fundamental principles and measured nuclear data. However over the past three decades of reactor development experience it has become apparent that the accuracy of nuclear data and computationally feasible analytical methods are simply not sufficient to allow this.[6] Instead

nuclear reactor analysis has relied heavily on that very basic ingredient utilized in most other areas of engineering design known as the "enlightened fudge." That is, most nuclear analysis methods or computer codes contain empirical parameters that have been adjusted or calibrated by comparing the predictions of the methods with actual experimental measurements. While such empirical input is usually very successful in yielding accurate nuclear design information with a minimum amount of effort, the novice nuclear engineer should approach any existing nuclear analytical method or computer code with a high degree of skepticism, since methods calibrated to work well for one range of parameters may fail miserably when applied to new situations in which only limited experience is available.

The intimate relation between computers and reactor design cannot be overstressed. It is almost impossible for the present-day nuclear engineer to function without a reasonable background in computer techniques (both in programing and numerical analysis). Nevertheless the increasingly heavy reliance of the nuclear reactor industry on elaborate computational models of reactor performance makes it even more imperative that the nuclear engineer possess a very thorough background in the fundamental physical and mathematical concepts underlying these models, as well as a healthy dose of skepticism when he attempts to utilize their predictions in reactor analysis.

## B. Some Concluding Remarks

In these last three chapters we have attempted to introduce several simple but important concepts involved in nuclear fission chain reactions. We have also provided a brief overview of nuclear reactor systems and the function of the nuclear engineer in the design of such systems. With this background we now turn our attention to a development of the theory underlying the nuclear analysis of fission reactors. We have seen that the neutron plays the central role as the chain carrier perpetuating the chain reaction. The key problem of reactor theory, then, is to determine the distribution of neutrons in a reactor core. This will not only allow one to study the chain reaction process itself, but, as we will later find, since the neutron density is proportional to the rate at which fission reactions occur and hence proportional to the core power density, the neutron density is also the key to the subsequent thermal and mechanical analysis of the reactor. As we have mentioned earlier, there are essentially two aspects to this problem.

One must study the interaction of neutrons with matter—specifically, with the nuclei that make up the matter. This amounts to either experimental or theoretical determination of the probabilities that various neutron–nuclear interactions will occur—that is, a determination of the appropriate neutron–nuclear cross sections. This, however, is not the principal concern of the theory we will develop in this text but is more properly the domain of the nuclear physicist. Hence we tend to take microscopic cross section data as given (in a form to be discussed later), and turn our attention instead to the manner in which these data are utilized in nuclear reactor analysis.

Of comparable importance is the study of the transport or diffusion of neutrons within a nuclear reactor core as they stream around inside the core, suffering collisions with nuclei, occasionally being absorbed, inducing fission reactions, or leaking out through the surface of the core. It is this latter study that will allow us to develop models for calculating the distribution of neutrons within the reactor core.

Our theoretical approach is to begin with an essentially exact description of the neutron density in the reactor based on the so-called *neutron transport equation*. This equation, while relatively easy to derive, is extremely difficult to solve, and hence we will be concerned with developing various approximations to it that lend themselves more readily to practical application. We begin our actual study of nuclear reactor theory by using the simplest such approximation, that in which the neutron energy dependence is neglected by assuming all neutrons to be characterized as having a single speed, and describing their transport from point to point as a simple diffusion process. This very simple model suffices to develop most of the concepts, as well as to illustrate most of the practical computational techniques used in more detailed reactor analysis.

We next develop a more sophisticated model of the neutron density behavior based on breaking up the range of neutron energies into intervals or "groups" and then describing the diffusion of neutrons in each of these groups separately, accounting for the transfer of neutrons between groups caused by scattering. Such *multigroup diffusion* models are the principal tools used in modern reactor analysis, and we consider them in some detail.

In the final section of the book we illustrate these models by applying them to analyze several typical problems encountered in nuclear reactor design. In particular, we explore the relation between such nuclear analysis methods and the other types of analysis required in nuclear reactor core design.

## REFERENCES

1. A. M. Weinberg and E. P. Wigner, *The Physical Theory of Neutron Chain Reactors*, The University of Chicago Press (1958).
2. S. Glasstone and A. Sesonske, *Nuclear Reactor Engineering*, 2nd Ed., Van Nostrand, Princeton, N.J. (1975).
3. M. M. El-Wakil, *Nuclear Energy Conversion*, Intext, Scranton (1971).
4. There are a number of other useful sources on nuclear power systems. Each of the major suppliers of NSSS prepare detailed systems descriptions. For example, a very informative reference is

    Systems Summary of a Westinghouse Pressurized Water Reactor Nuclear Power Plant, Westinghouse Electric Corporation (1971).

    The most detailed descriptions of modern nuclear power plants can be found in the multivolume set of Preliminary Safety Analysis Reports (PSARs) or Final Safety Analysis Reports (FSARs) prepared for each nuclear plant. Of particular interest are the standard safety analysis reports prepared for each of the major NSSS types. For example:

    Babcock and Wilcox Standard Nuclear Steam System, B-SAR-241 (1974).

    BWR/6 Standard Safety Analysis Report, General Electric Company (1973).

    CESSAR, Combustion Engineering Standard Safety Analysis Report, System 80, Combustion Engineering (1973).

    GASSAR 6, General Atomic Standard Safety Analysis Report, GA-A13200 (1975).

    Clinch River Breeder Reactor Plant, Reference Design Report, Westinghouse Electric Corporation, 1974; PSAR (1975).

    RESAR-3, Reference Safety Analysis Report, Westinghouse Nuclear Energy Systems (1973).
5. A. Sesonske, *Nuclear Power Plant Design Analysis*, USAEC Document TID-26241 (1973).
6. J. Chernick, *Reactor Technol.* 13, 368 (1971).

## PROBLEMS

3-1 What is the maximum value of the multiplication factor that can be achieved in any conceivable reactor design?

3-2 Using the alternative definition of the multiplication factor based on the concept of neutron balance, repeat the derivation of the six-factor formula.

3-3 A spherical reactor composed of $^{235}U$ metal is operating in a critical steady state. Discuss what probably happens to the multiplication of the reactor and why, if the system is modified in the following ways (treat each modification separately, not cumulatively): (a) the reactor is rapidly compressed to one-half its original volume, (b) a large, fat reactor operator accidentally sits on the reactor, squashing it into an ellipsoidal shape, (c) a thick sheet of cadmium is wrapped around the outside of the reactor, (d) the reactor is suddenly immersed in a large container of water, (e) a source of neutrons is placed near the reactor, (f) another identical reactor is placed a short distance from the original reactor, and (g) one simply leaves the reactor alone for a period of time.

3-4 One defines the *doubling time* for a breeder reactor as the amount of time required for the original fissile loading of the reactor to double. Find an expression for the doubling time $t_d$ in terms of: (a) the original fissile loading $M_F$, (b) the power level of the reactor $P = w_f F_f$ where $F_f$ is the fission rate occurring in the reactor core, (c) and the breeding ratio BR.

3-5 A detailed comparison of typical power reactor core parameters is given in Appendix H. Choose one of the reactor types in this Appendix and perform the following calculations: (a) verify that the average linear power density, power density, and specific power given in the table are consistent with the core volume, thermal power rating, and fuel loading, (b) determine the discharge fuel burnup when the capacity factor of the nuclear unit is 80% and the fuel residence time is three years, (c) determine a range for core height and core diameter and sketch a core cross-section for one array of assemblies using the tabulated core data.

3-6 Calculate and plot $k_\infty$ as a function of enrichment from 0.7% $^{235}U$ to 100% $^{235}U$. Use the thermal cross section data of Appendix A and assume $p = \epsilon = 1$.

3-7 Derive a relationship between the waste heat rejected from a plant of a given output and the thermal efficiency of the plant. (Several years ago such waste heat was referred to as "thermal pollution." In a countermove, several of the more optimistic spokesmen for the nuclear power industry coined the phrase "thermal enrichment.") Using this expression, estimate the waste heat rejected by: (a) a modern fossil-fuel plant, (b) a LWR plant, (c) a HTGR plant, (d) an LMFBR plant, and (e) a fusion reactor plant, assuming that all of these plants are rated at 1000 MWe. Treat the efficiency of the plant as that for an ideal (Carnot) heat engine.

3-8 Consider an infinitely large homogeneous mixture of $^{235}U$ and a moderating material. Determine the ratio of fuel-to-moderator density that will render this system critical for the following moderators: (a) graphite, (b) beryllium, (c) water ($H_2O$), and (d) heavy water ($D_2O$). Use the thermal cross section data given in Appendix A.

3-9 Modify the simple description of the time behavior of the neutron population in a reactor given by Eq. (3-5) to account for the presence of a source in the reactor producing $S_0$ neutrons per second. In particular, determine the time behavior of the neutron population for each of the three cases: $k < 1$, $k = 1$, and $k > 1$.

# 2

# The One-Speed Diffusion Model of a Nuclear Reactor

# 4
# Neutron Transport

We now turn our attention to the central problem of nuclear reactor theory, the determination of the distribution of neutrons in the reactor. For it is the neutron distribution that determines the rate at which various nuclear reactions occur within the reactor. Furthermore by studying the behavior of the neutron population we will be able to infer the stability of the fission chain reaction. To determine the distribution of neutrons in the reactor we must investigate the process of *neutron transport*, that is, the motion of the neutrons as they stream about the reactor core, frequently scattering off of atomic nuclei and eventually either being absorbed or leaking out of the reactor. Most reactor studies treat the neutron motion as a *diffusion* process. In effect one assumes that neutrons tend to diffuse from regions of high neutron density to low neutron density, much as heat diffuses from regions of high to low temperature, or even more analogously, as one gas of molecules (corresponding to the neutrons) would diffuse through another (the nuclei) to reduce spatial variations in concentration.

Unfortunately, however, while the treatment of thermal conduction and gaseous diffusion as diffusion processes is usually found to be quite accurate, the treatment of neutron transport as a diffusion process has only limited validity. The reason for this failure is easily understood when it is noted that in most diffusion processes the diffusing particles are characterized by very frequent collisions that give rise to very irregular, almost random, zigzag trajectories. However, we have seen that the cross section for neutron–nuclear collisions is quite small (about $10^{-24}$ $cm^2$). Hence neutrons tend to stream relatively large distances between interactions (recall that the mean free path characterizing fast neutrons is typically on the order of centimeters). Furthermore, the dimensions characterizing changes in reactor core composition are usually comparable to a neutron mfp (e.g., a reactor fuel pin is typically about 1 cm in diameter).

Hence one frequently requires a more accurate description of neutron transport that takes into account the relatively long neutron mfp and neutron streaming. Such a description has been borrowed from the kinetic theory of rarefied gases (which are also characterized by long mfp)—more precisely, the kinetic theory of gas mixtures. The fundamental equation describing dilute gases was first proposed more than one century ago by Boltzmann, and even today the *Boltzmann equation* remains the principal tool of the gas dynamicist.[1] Its counterpart for the neutron "gas," the so-called *neutron transport equation*, is far younger (less than 40 years old), far simpler (e.g., it is a linear equation in contrast to the Boltzmann equation, which is nonlinear), but usually strikes far more terror in the hearts of fledgling nuclear engineers who are intimidated by its frightening reputation within the nuclear reactor community. Neutron transport theory has come to be associated with a hideous plethora of impenetrable mathematics, unwieldy formulas, and (eventually) the expenditure of enormous amounts of money on computer number-crunching.

This is most unfortunate because the neutron transport equation is much simpler to derive (requiring only the concept of neutron conservation plus a bit of vector calculus) and to understand than the neutron diffusion equation that we shall utilize in most of our development of reactor analysis. It is also a far more fundamental and exact description of the neutron population in a reactor—indeed, it is the fundamental cornerstone on which all of the various approximate methods used in nuclear reactor analysis are based.

It does have one major drawback, however. It is usually very difficult to solve the transport equation for any but the simplest modeled problems (and even these require an inordinate amount of analytical work). However that is quite all right, since it is not our intent to attack the transport equation head on. Rather the job of the reactor analyst is to develop suitable (i.e., calculationally feasible and accurate) approximations to it. Usually, however, only by comparing these various approximate theories to the transport equation from which they originated can one really assess their range of validity.

There is another reason for including an introduction to the neutron transport equation in even an elementary discussion of nuclear reactor analysis. Although neutron diffusion theory is usually found adequate for reactor applications, it owes its accuracy to various schemes that have been developed to "patch it up" using results from more accurate transport equation solutions. For example, we will find that the neutron diffusion equation is quite invalid near the boundary of a reactor, or near a highly absorbing material such as a fuel rod or a control element. Nevertheless we can continue to use diffusion theory to describe the reactor provided we fudge it a bit by inserting so-called "transport corrections" into the boundary conditions accompanying the diffusion equation.

So hopefully we have made a case for our inclusion of a very introductory discussion of neutron transport theory within an elementary text. We would caution the reader not to be intimidated by the notation or the apparent strangeness of the equation we will develop. He should find it rather easy to understand the derivation and interpretation of this equation.

Furthermore the effort he expends in understanding the material in this chapter will provide him with a much deeper and more thorough understanding of the approximate methods we will develop in later chapters.

With this strong note of encouragement, let us now add a qualification. We have attempted to develop these later approximations in a manner independent of this

chapter since we recognize that many nonnuclear engineers reading this text may not really need (or care) to understand the limitations and ranges of validity of nuclear analysis methods. Therefore if the reader is faint of heart in confronting the transport equation, and strong in faith in being able to accept the rather heuristic arguments necessary to develop these approximate theories (e.g., the neutron diffusion equation) without recourse to the transport equation, or perhaps just disinterested, he can proceed immediately to the development of neutron diffusion theory in the next chapter.

The more formal discussion in this chapter will also serve to introduce the standard numerical approximation schemes used to analyze the neutron behavior in nuclear reactors. As in other areas of physical analysis, we will find that the usual maxim applies: that the "brute force" numerical approach (i.e., discretize everything in sight and slap in on a computer) is conceptually the *simplest* approach to understand and computationally the most *expensive* calculation to perform. The more elegant approximate methods require far less computational effort but far more in the way of mental gymnastics in order to understand the significance and reliability of their predictions.

## I. INTRODUCTORY CONCEPTS

### A. Neutron Density and Flux

Our ultimate goal is to determine the distribution of neutrons in a nuclear reactor core. This requires accounting for the neutron motion about the core and neutron interactions with nuclei in the core. We will begin by defining the *neutron density* $N(\mathbf{r}, t)$ at any point $\mathbf{r}$ in the reactor core by
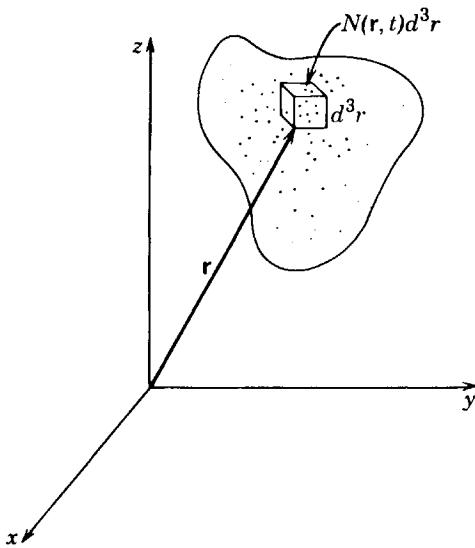
$$N(\mathbf{r}, t)\, d^3r \equiv \text{expected number of neutrons in}$$
$$d^3r \text{ about } \mathbf{r} \text{ at a time } t. \tag{4-1}$$

The word "expected" has been inserted into this definition to indicate that this will be a statistical theory in which only mean or average values are calculated. (The actual neutron density one would obtain from a series of measurements would fluctuate about this mean value, of course.) The neutron density $N(\mathbf{r}, t)$ is of interest because it allows us to calculate the *rate* at which nuclear reactions are occurring at any point in the reactor. To understand this, let us suppose for convenience that all the neutrons in the reactor have the same speed $v$. Now recall that one can express the frequency with which a neutron will experience a given neutron–nuclear reaction in terms of the macroscopic cross section characterizing that reaction $\Sigma$ and the neutron speed $v$ as

$$v\Sigma = \text{interaction frequency.} \tag{4-2}$$

Hence we can define the *reaction-rate density* $F(\mathbf{r}, t)$ at any point in the system by merely multiplying the neutron density $N(\mathbf{r}, t)$ by the interaction frequency $v\Sigma$:

$$F(\mathbf{r}, t)\, d^3r \equiv v\Sigma N(\mathbf{r}, t)\, d^3r \equiv \begin{array}{c} \text{expected rate at which} \\ \text{interactions are occurring} \\ \text{in } d^3r \text{ about } \mathbf{r} \text{ at time } t. \end{array} \tag{4-3}$$

FIGURE 4-1.   The neutron density $N(\mathbf{r}, t)$.

For example, if we consider a thermal neutron density of $N = 10^8 \text{ cm}^{-3}$ in a graphite medium then using the total cross section tabulated in Appendix A of $\Sigma_t = 0.385 \text{ cm}^{-1}$ and a corresponding neutron speed of $2.2 \times 10^5 \text{ cm/sec}$, we would find a reaction rate density of $8.47 \times 10^{12} \text{ reactions/cm}^3/\text{sec}$. In this particular case, most of these reactions would consist of scattering collisions.

These concepts can easily be extended to the case in which the neutron density is different for various neutron energies $E$ by defining

$$N(\mathbf{r}, E, t) d^3 r \, dE \equiv \begin{matrix} \text{expected number of neutrons in } d^3 r \\ \text{about } \mathbf{r}, \text{ energies in } dE \text{ about } E, \text{ at} \\ \text{time } t. \end{matrix} \qquad (4\text{-}4)$$

Notice that this "density" is defined with respect to both space and energy. One can also generalize the concept of reaction rate density to include energy dependence as

$$F(\mathbf{r}, E, t) d^3 r \, dE = v\Sigma(E)N(\mathbf{r}, E, t) d^3 r \, dE. \qquad (4\text{-}5)$$

The product $vN(\mathbf{r}, t)$ arising in Eqs. (4-3) and (4-5) occurs very frequently in reactor theory, and therefore it is given a special name:

$$\phi(\mathbf{r}, t) \equiv vN(\mathbf{r}, t) \equiv \text{neutron flux} \ [\text{cm}^{-2} \cdot \text{sec}^{-1}]. \qquad (4\text{-}6)$$

Although it will certainly prove convenient to work with $\phi(\mathbf{r}, t)$ rather than $N(\mathbf{r}, t)$ (since then one does not have to worry about including the neutron speed $v$ in the reaction rate densities), the tradition in nuclear engineering of referring to this quantity as the neutron "flux" is very misleading. For $\phi(\mathbf{r}, t)$ is not at all like the fluxes encountered in electromagnetic theory or heat conduction, since these latter fluxes are *vector* quantities, whereas $\phi(\mathbf{r}, t)$ is a *scalar* quantity. Actually the "neutron current" $\mathbf{J}(\mathbf{r}, t)$, which we shall introduce momentarily, corresponds more closely to the conventional interpretation of a "flux." To avoid unnecessary confusion over this unfortunate convention, the student would probably do best at this point to think of the neutron flux as simply a convenient mathematical variable

(speed x density) to use in computing reaction rates:

$$F(\mathbf{r}, E, t) = \Sigma(E)\phi(\mathbf{r}, E, t). \tag{4-7}$$

A bit later we will introduce a physical interpretation of the neutron flux.

## B. Angular Densities and Currents

The significance of the neutron density $N(\mathbf{r}, t)$ or flux $\phi(\mathbf{r}, t)$ in determining nuclear reaction rates leads us to search for an equation that describes these quantities. Unfortunately there is no exact equation that is satisfied by $N(\mathbf{r}, t)$ or $\phi(\mathbf{r}, t)$—only approximate equations. To understand why, we must generalize the concept of the neutron density somewhat.

First let us determine just which variables characterize the state of an individual neutron. Certainly these include the neutron position $\mathbf{r}$, energy $E$ (or speed $v = (2E/m)^{1/2}$), and the time $t$ at which the neutron is observed. Yet notice that to specify the state of the neutron, we must also give its direction of motion characterized by the unit vector $\hat{\Omega} = \mathbf{v}/|\mathbf{v}|$. (Actually one could worry about specifying other variables such as the neutron spin; but for reactor calculations, the variables $\mathbf{r}$, $E$, $\hat{\Omega}$, and $t$ provide a sufficient description of the state of the neutron.)

Let us now generalize the concept of density by defining the *angular neutron density* that depends on all of these variables

$$n(\mathbf{r}, E, \hat{\Omega}, t) \, d^3r \, dE \, d\hat{\Omega} \equiv \frac{\text{expected number of neutrons in}}{\begin{array}{l}d^3r \text{ about } \mathbf{r}, \text{ energy } dE \text{ about } E, \\ \text{moving in direction } \hat{\Omega} \text{ in solid} \\ \text{angle } d\hat{\Omega} \text{ at time } t.\end{array}} \tag{4-8}$$

[The term "angular" arises from the fact that $n(\mathbf{r}, E, \hat{\Omega}, t)$ depends on the velocity spherical coordinate angles $\theta$ and $\phi$ specifying the neutron direction $\hat{\Omega}$ (see Figure 4-2).] This is the most general neutron density function we need to define since it happens that one can derive an essentially exact equation, the neutron transport equation, for the angular neutron density $n(\mathbf{r}, E, \hat{\Omega}, t)$.

However before deriving this equation, it is useful to introduce several other definitions. We will first define the *angular neutron flux* in a manner similar to that in which we earlier defined the neutron flux, simply by multiplying the angular density by the neutron speed $v$:

$$\varphi(\mathbf{r}, E, \hat{\Omega}, t) \equiv vn(\mathbf{r}, E, \hat{\Omega}, t). \tag{4-9}$$

A related concept is the *angular current density*, defined by

$$\mathbf{j}(\mathbf{r}, E, \hat{\Omega}, t) \equiv v\hat{\Omega} n(\mathbf{r}, E, \hat{\Omega}, t) = \hat{\Omega}\varphi(\mathbf{r}, E, \hat{\Omega}, t). \tag{4-10}$$

Notice that since $\hat{\Omega}$ is a unit vector, the angular flux is actually nothing more than the magnitude of the angular current density

$$|\mathbf{j}| = |\hat{\Omega}|\varphi = \varphi. \tag{4-11}$$
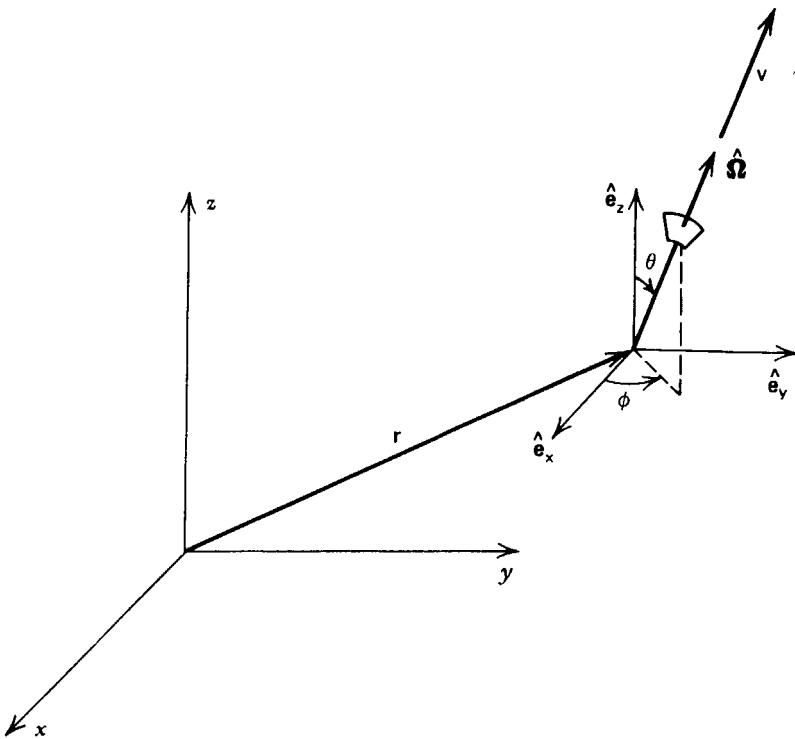
**FIGURE 4-2.** The position and direction variables characterizing a neutron.

The angular current density has a useful physical interpretation. Consider a small area $d\mathbf{A}$ at a point $\mathbf{r}$. [Here we will use the convention that $d\mathbf{A} = \hat{\mathbf{e}}_s d A$ where $\hat{\mathbf{e}}_s$ is the unit vector normal to the surface.] Then we can identify

$$\mathbf{j}(\mathbf{r}, E, \hat{\mathbf{\Omega}}, t) \cdot d\mathbf{A} \, dE \, d\hat{\mathbf{\Omega}} \equiv \begin{array}{l}\text{expected number of neutrons passing}\\\text{through an area } dA \text{ per unit time with}\\\text{energy } E \text{ in } dE, \text{ direction } \hat{\mathbf{\Omega}} \text{ in } d\hat{\mathbf{\Omega}}\\\text{at time } t.\end{array} \qquad (4\text{-}12)$$

We can also define an angular interaction rate

$$f(\mathbf{r}, E, \hat{\mathbf{\Omega}}, t) = v\Sigma(\mathbf{r}, E)n(\mathbf{r}, E, \hat{\mathbf{\Omega}}, t) = \Sigma(\mathbf{r}, E)\varphi(\mathbf{r}, E, \hat{\mathbf{\Omega}}, t). \qquad (4\text{-}13)$$

All of these angle-dependent quantities can be related to our earlier definitions in Section 4-I-A by simply integrating over the angular variables. For example:

$$N(\mathbf{r}, E, t) = \int_{4\pi} d\hat{\mathbf{\Omega}}\, n(\mathbf{r}, E, \hat{\mathbf{\Omega}}, t) , \qquad (4\text{-}14)$$
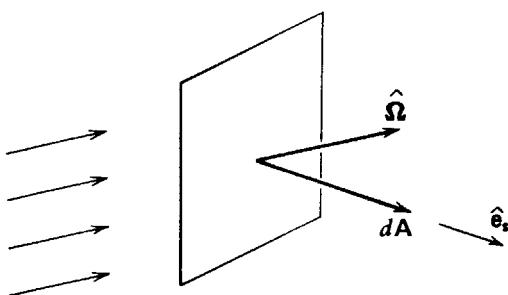


**FIGURE 4-3.** Neutrons incident on a differential element of area $dA$.

or

$$N(\mathbf{r},t) = \int_0^\infty dE\, N(\mathbf{r},E,t) = \int_0^\infty dE \int_{4\pi} d\hat{\Omega}\, n(\mathbf{r},E,\hat{\Omega},t) \quad . \tag{4-15}$$

Sometimes quantities such as $N(\mathbf{r},t)$ and $\phi(\mathbf{r};t)$ which do not depend on $\hat{\Omega}$ are referred to as *scalar* or *total densities* and *fluxes*, to distinguish them from $n(\mathbf{r},E,\hat{\Omega},t)$ and $\varphi(\mathbf{r},E,\hat{\Omega},t)$. We find this nomenclature cumbersome and will avoid it in our development.

Notice that if the angular density is independent of $\hat{\Omega}$ (i.e., it is *isotropic*) then we find that Eq. (4-14) demands the presence of a $4\pi$ normalization factor in the angular density

$$n(\mathbf{r},E,\hat{\Omega},t) = \frac{1}{4\pi} N(\mathbf{r},E,t). \tag{4-16}$$

More generally, however, $n(\mathbf{r},E,\hat{\Omega},t)$ will have a directional dependence—particularly if we are near a boundary or a source of neutrons, as a little geometrical reasoning applied to Figure 4-4 should indicate.

In a similar fashion, we find

$$\phi(\mathbf{r},E,t) = \int_{4\pi} d\hat{\Omega}\, \varphi(\mathbf{r},E,\hat{\Omega},t) \quad , \tag{4-17}$$

and

$$\phi(\mathbf{r},t) = \int_0^\infty dE\, \phi(\mathbf{r},E,t) = \int_0^\infty dE \int_{4\pi} d\hat{\Omega}\, \varphi(\mathbf{r},E,\hat{\Omega},t) \quad . \tag{4-18}$$

Finally, we can define the *neutron current density* $\mathbf{J}(\mathbf{r},E,t)$ in terms of the angular current density $\mathbf{j}(\mathbf{r},E,\hat{\Omega},t)$ as

$$\mathbf{J}(\mathbf{r},E,t) \equiv \int_{4\pi} d\hat{\Omega}\, \mathbf{j}(\mathbf{r},E,\hat{\Omega},t) \quad , \tag{4-19}$$

and

$$\mathbf{J}(\mathbf{r},t) \equiv \int_0^\infty dE\, \mathbf{J}(\mathbf{r},E,t) = \int_0^\infty dE \int_{4\pi} d\hat{\Omega}\, \mathbf{j}(\mathbf{r},E,\hat{\Omega},t) \quad . \tag{4-20}$$
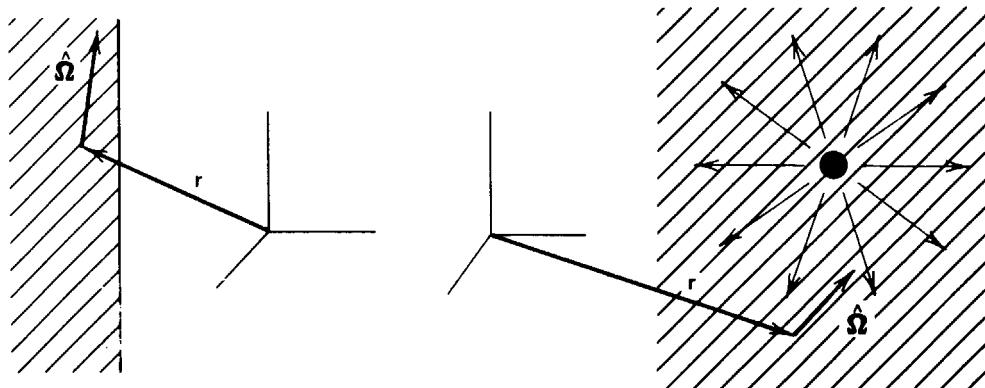


FIGURE 4-4. Anisotropies in the angular density $n(\mathbf{r},E,\hat{\Omega},t)$ near a boundary or a neutron source.

Notice that $\mathbf{J}(\mathbf{r},t)$ is actually what would be referred to as the "flux" in other fields of physics, since if we have a small area $dA$ at a position $\mathbf{r}$, then

$$\mathbf{J}(\mathbf{r},t)\cdot d\mathbf{A} = \frac{\text{net rate at which neutrons pass}}{\text{through a surface area } d\mathbf{A}.} \qquad (4\text{-}21)$$

The units of both $\mathbf{J}(\mathbf{r},t)$ and $\phi(\mathbf{r},t)$ are identical [$\text{cm}^{-2}\cdot\text{sec}^{-1}$]. However $\mathbf{J}$ is a vector quantity that characterizes the *net* rate at which neutrons pass through a surface oriented in a given direction, whereas $\phi$ simply characterizes the *total* rate at which neutrons pass through a unit area, regardless of orientation. Such an interpretation would suggest that $\mathbf{J}$ is a more convenient quantity for describing neutron *leakage* or *flow* (e.g., through the surface of the reactor core), while $\phi$ is more suitable for characterizing neutron *reaction rates* in which the total number of neutron interactions in a sample (e.g., a small foil) is of interest. Although the angular flux and current density are very simply related, we will find that there is no simple analogous relationship between $\mathbf{J}$ and $\phi$. These concepts may appear a bit confusing at first, but they will become more familiar after we have illustrated their application in both our further theoretical development and the problems at the end of the chapter.

A closely related concept is that of the *partial current densities*, $J_{\pm}(\mathbf{r},t)$ which correspond to the total rates at which neutrons flow through a unit area from left to right ($J_{+}$) or right to left ($J_{-}$). If we recall our earlier definition of $\mathbf{j}(\mathbf{r},E,\hat{\Omega},t)$, then it becomes apparent that

$$J_{\pm}(\mathbf{r},t) = \int_0^\infty dE \int_{2\pi^{\pm}} d\hat{\Omega}\,\hat{\mathbf{e}}_s\cdot\mathbf{j}(\mathbf{r},E,\hat{\Omega},t), \qquad (4\text{-}22)$$

where $2\pi^{\pm}$ is merely a convenient notation to indicate that the angular integration is performed only over directions with components along the surface normal ($2\pi^{+}$) or in the opposite direction ($2\pi^{-}$). For example, if we choose to define the polar coordinates that specify $\hat{\Omega}$ along the normal to the surface, then in the integration for $J_{+}$, $\phi$ would range from 0 to $2\pi$, while $\theta$ would range only from 0 to $\pi/2$.

It is evident from this definition that

$$\hat{\mathbf{e}}_s\cdot\mathbf{J}(\mathbf{r},t) = [J_{+}(\mathbf{r},t) - J_{-}(\mathbf{r},t)]. \qquad (4\text{-}23)$$

Hence $\mathbf{J}$ is sometimes referred to as the *net current density*, since it can be constructed as the difference of the partial current densities.
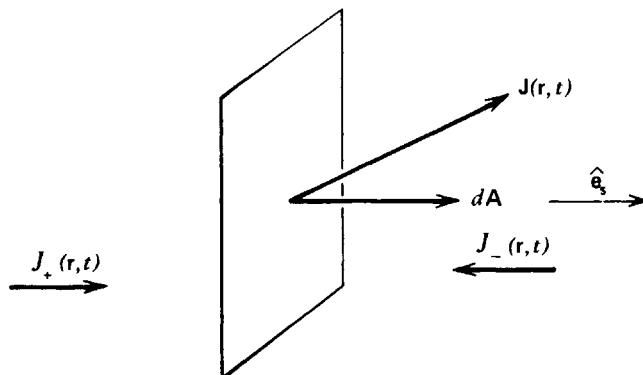


FIGURE 4-5.    Partial and total current densities.

## II. THE NEUTRON TRANSPORT EQUATION

We will now derive an exact equation for the angular neutron density in a system by simply balancing the various mechanisms by which neutrons can be gained or lost from an arbitrary volume $V$ within the system. That is, we will consider mechanisms that will change the number of neutrons in this volume that are characterized by a specific energy $E$ and are traveling in a specific direction $\hat{\Omega}$. It is convenient to use a bit of vector calculus here, but hopefully this will not obscure the simple physics behind this equation (which is just the mathematical expression of a "count-the-neutrons" game).

To this end, consider any old arbitrary volume $V$. The number of neutrons in $V$ with energy $E$ in $dE$ and traveling in a direction $\hat{\Omega}$ in $d\hat{\Omega}$ within this volume is just

$$\left[ \int_V n(\mathbf{r}, E, \hat{\Omega}, t) d^3r \right] dE \, d\hat{\Omega}.$$

(Since $n(\mathbf{r}, E, \hat{\Omega}, t)$, is a "density" in $E$ and $\hat{\Omega}$ space, we must multiply it by $dE$ and $d\hat{\Omega}$ in order to get a number.) The time rate of change of this number, then, is given by a balance relation

$$\frac{\partial}{\partial t} \left[ \int_V n(\mathbf{r}, E, \hat{\Omega}, t) d^3r \right] dE \, d\hat{\Omega} = \text{gain in } V - \text{loss from } V. \qquad (4\text{-}24)$$

If we assume that the arbitrary volume $V$ is chosen not to depend on time, we can bring the time differentiation inside the spatial integration

$$\frac{\partial}{\partial t} \left[ \int_V n(\mathbf{r}, E, \hat{\Omega}, t) d^3r \right] dE \, d\hat{\Omega} = \left[ \int_V \frac{\partial n}{\partial t} d^3r \right] dE \, d\hat{\Omega}. \qquad (4\text{-}25)$$

We will now classify the various ways that neutrons can appear or disappear from $V$, and then we will try to write mathematical expressions for each of these mechanisms in terms of the angular density $n(\mathbf{r}, E, \hat{\Omega}, t)$.

Gain mechanisms:
① Any neutron sources in $V$ (e.g., fissions).
② Neutrons streaming into $V$ through the surface $S$.
③ Neutrons of different $E'$, $\hat{\Omega}'$ suffering a scattering collision in $V$ that changes $E'$, $\hat{\Omega}'$ into the $E, \hat{\Omega}$ of interest.
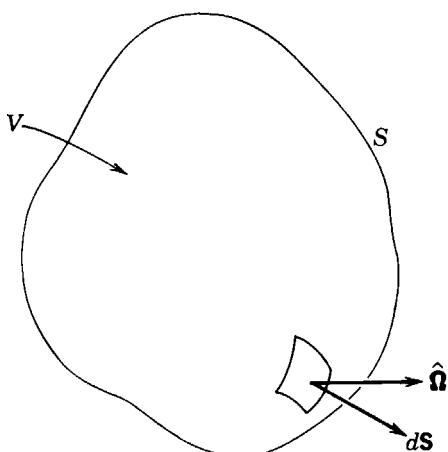


FIGURE 4-6. An arbitrary volume $V$ with surface area $S$.

Loss mechanisms:

④ Neutrons leaking out through the surface $S$.

⑤ Neutrons in $V$ suffering a collision. (It is obvious that an absorption interaction removes a neutron from $V$; and since by definition a scattering collision changes $E, \hat{\Omega}$ and since we are only keeping track of neutrons in $V$ with this specific energy and direction, a scattering collision also amounts to a loss of neutrons.)

We can now write a mathematical expression for each of these contributions. We will work progressively from the easiest to the more difficult:

① Source terms: If we define

$$s(\mathbf{r}, E, \hat{\Omega}, t) d^3r\, dE\, d\hat{\Omega} \equiv \begin{array}{l} \text{rate of source neutrons appearing} \\ \text{in } d^3r \text{ about } \mathbf{r}, dE \text{ about } E, \text{ and,} \\ d\hat{\Omega} \text{ about } \hat{\Omega} \end{array} \qquad (4\text{-}26)$$

then obviously

$$① = \left[ \int_V s(\mathbf{r}, E, \hat{\Omega}, t) d^3r \right] dE\, d\hat{\Omega}. \qquad (4\text{-}27)$$

[This term was really easy—we only needed to define a source density, $s(\mathbf{r}, E, \hat{\Omega}, t)$.]

⑤ Loss due to collisions in $V$: The rate at which neutrons suffer collisions at a point $\mathbf{r}$ is

$$f_t(\mathbf{r}, E, \hat{\Omega}, t) = v\Sigma_t(\mathbf{r}, E) n(\mathbf{r}, E, \hat{\Omega}, t). \qquad (4\text{-}28)$$

Hence integrating this collision rate over the volume $V$, we find

$$⑤ = \left[ \int_V v\Sigma_t(\mathbf{r}, E) n(\mathbf{r}, E, \hat{\Omega}, t) d^3r \right] dE\, d\hat{\Omega}. \qquad (4\text{-}29)$$

③ Gain due to neutrons scattering into $dE$ about $E$, $d\hat{\Omega}$ about $\hat{\Omega}$ from other energies $E'$ and directions $\hat{\Omega}'$: If we recall from Chapter 2 that the probability of scattering from $E', \hat{\Omega}'$ to $E, \hat{\Omega}$ is given in terms of the double-differential scattering cross section, then the rate at which neutrons scatter from $E', \hat{\Omega}'$ to $E, \hat{\Omega}$ is

$$\left[ \int_V v'\Sigma_s(E' \rightarrow E, \hat{\Omega}' \rightarrow \hat{\Omega}) n(\mathbf{r}, E', \hat{\Omega}', t) d^3r \right] dE\, d\hat{\Omega}. \qquad (4\text{-}30)$$

However we must consider contributions from any $E', \hat{\Omega}'$. Hence

$$③ = \left[ \int_V d^3r \int_{4\pi} d\hat{\Omega}' \int_0^\infty dE'\, v'\Sigma_s(E' \rightarrow E, \hat{\Omega}' \rightarrow \hat{\Omega}) n(\mathbf{r}, E', \hat{\Omega}', t) \right] dE\, d\hat{\Omega}. \qquad (4\text{-}31)$$

This is known as the *inscattering* term since it characterizes neutrons scattering from other energies or directions into $dE\, d\hat{\Omega}$.

②④ Leakage into or from the volume $V$: We will combine these terms together and calculate the net leakage through the surface $S$. If we use the concept of the angular current density $\mathbf{j}(\mathbf{r}, E, \hat{\Omega}, t)$, we can write the rate at which neutrons of

$E, \hat{\Omega}$ leak out of a piece of the surface, $dS$, as

$$\mathbf{j}(\mathbf{r}, E, \hat{\Omega}, t) \cdot d\mathbf{S} = v\hat{\Omega} n(\mathbf{r}, E, \hat{\Omega}, t) \cdot d\mathbf{S}. \tag{4-32}$$

Hence the leakage contribution over the entire surface area $S$ is

$$\text{④} - \text{②} = \int_S d\mathbf{S} \cdot v\hat{\Omega} n(\mathbf{r}, E, \Omega, t). \tag{4-33}$$

We can rewrite this in terms of a volume integral if we use Gauss's theorem

$$\int_S d\mathbf{S} \cdot \mathbf{A}(\mathbf{r}) = \int_V d^3r \, \nabla \cdot \mathbf{A}(\mathbf{r}), \tag{4-34}$$

to find

$$\left[ \int_S d\mathbf{S} \cdot v\hat{\Omega} n(\mathbf{r}, E, \hat{\Omega}, t) \right] dEd\hat{\Omega} = \left[ \int_V d^3r \nabla \cdot v\hat{\Omega} n(\mathbf{r}, E, \hat{\Omega}, t) \right] dEd\hat{\Omega}$$

$$= \left[ \int_V d^3r \, v\hat{\Omega} \cdot \nabla n(\mathbf{r}, E, \hat{\Omega}, t) \right] dEd\hat{\Omega}. \tag{4-35}$$

Here we have noted that

$$\nabla \cdot v\hat{\Omega} = v\hat{\Omega} \cdot \nabla \tag{4-36}$$

since $\hat{\Omega}$ does not depend on $\mathbf{r}$.
If we now combine all of these terms such that

$$\begin{array}{c} \text{rate of change of number} \\ \text{of neutrons in } V \end{array} = \text{①} + \text{②} + \text{③} - \text{④} - \text{⑤}, \tag{4-37}$$

then we find

$$\int_V d^3r \left[ \frac{\partial n}{\partial t} + v\hat{\Omega} \cdot \nabla n + v\Sigma_t n(\mathbf{r}, E, \hat{\Omega}, t) \right.$$

$$\left. - \int_0^\infty dE' \int_{4\pi} d\hat{\Omega}' v'\Sigma_s(E' \to E, \hat{\Omega}' \to \hat{\Omega}) n(\mathbf{r}, E', \hat{\Omega}', t) - s(\mathbf{r}, E, \hat{\Omega}, t) \right] dEd\hat{\Omega} = 0. \tag{4-38}$$

However we now apply the fact that the volume $V$ was quite arbitrarily chosen. Hence the only way for the integral to vanish for any $V$ is for its integrand to be identically zero—that is,

$$\int_{\text{any } V} d^3r f(\mathbf{r}) = 0 \Rightarrow f(\mathbf{r}) \equiv 0. \tag{4-39}$$

Hence we arrive at a balance relation

$$\frac{\partial n}{\partial t} + v\hat{\Omega} \cdot \nabla n + v\Sigma_t n(\mathbf{r}, E, \hat{\Omega}, t)$$

$$= \int_{4\pi} d\hat{\Omega}' \int_0^\infty dE' v'\Sigma_s(E' \to E, \hat{\Omega}' \to \hat{\Omega}) n(\mathbf{r}, E', \hat{\Omega}', t) + s(\mathbf{r}, E, \hat{\Omega}, t). \tag{4-40}$$

This is known as the *neutron transport equation*. Several general features of the equation should be noted: First, it is a linear equation in the unknown dependent variable $n(\mathbf{r}, E, \hat{\Omega}, t)$ with seven independent variables $(\mathbf{r} = x,y,z; E; \hat{\Omega} = \theta, \phi; t)$. Since it contains both derivatives in space and time as well as integrals over angle and energy, it is known as an "integrodifferential" equation.

However the presence of the derivatives suggest that we must also specify appropriate initial and boundary conditions for the angular density. Since only a single time derivative appears in the equation, we can simply choose the initial condition to be the specification of the initial value of the angular density for all positions, energies, and directions:

$$\text{Initial condition: } n(\mathbf{r}, E, \hat{\Omega}, 0) = n_0(\mathbf{r}, E, \hat{\Omega}), \text{ all } \mathbf{r}, E, \hat{\Omega}. \tag{4-41}$$

The boundary conditions will depend on the particular problem of interest. Suppose for purposes of illustration, that we consider the reactor to be surrounded by an infinite vacuum so that if a neutron leaks out, it can never be scattered back into the system. Actually to be more precise, we should also assume that the system geometry is characterized by a *nonreentrant surface* such that a neutron streaming out through the surface will never reenter the surface at another point (see Figure 4-7). Then our appropriate boundary condition would simply express the fact that there can be no neutrons entering the system from the outside. That is, we require the angular neutron density on the surface to vanish for all inward directions

$$n(\mathbf{r}_s, E, \hat{\Omega}, t) = 0 \qquad \text{if } \hat{\Omega} \cdot \hat{\mathbf{e}}_s < 0, \text{ for all } \mathbf{r}_s \text{ on } S, \tag{4-42}$$
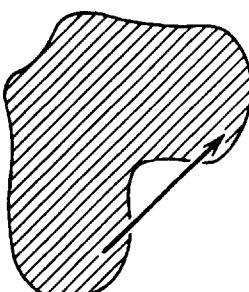
where $\mathbf{r}_s$ denotes a point on the surface $S$. There are other possible boundary conditions, but we will discuss these later.

It is convenient to rewrite the neutron transport equation along with its initial and boundary conditions in terms of the angular flux
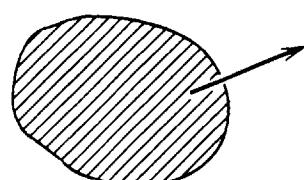
$$\frac{1}{v} \frac{\partial \varphi}{\partial t} + \hat{\Omega} \cdot \nabla \varphi + \Sigma_t(\mathbf{r}, E) \varphi(\mathbf{r}, E, \hat{\Omega}, t)$$

$$= \int_{4\pi} d\hat{\Omega}' \int_0^\infty dE' \Sigma_s(E' \to E, \hat{\Omega}' \to \hat{\Omega}) \varphi(\mathbf{r}, E', \hat{\Omega}', t) + s(\mathbf{r}, E, \hat{\Omega}, t), \tag{4-43}$$

$$\text{Initial condition: } \varphi(\mathbf{r}, E, \hat{\Omega}, 0) = \varphi_0(\mathbf{r}, E, \hat{\Omega}), \tag{4-44}$$

$$\text{Boundary condition: } \varphi(\mathbf{r}_s, E, \hat{\Omega}, t) = 0 \quad \text{if } \hat{\Omega} \cdot \hat{\mathbf{e}}_s < 0, \tag{4-45}$$
$$\text{all } \mathbf{r}_s \text{ on } S.$$



Reentrant surface                                    Nonreentrant surface

**FIGURE 4-7.    Examples of reentrant and nonreentrant surfaces.**
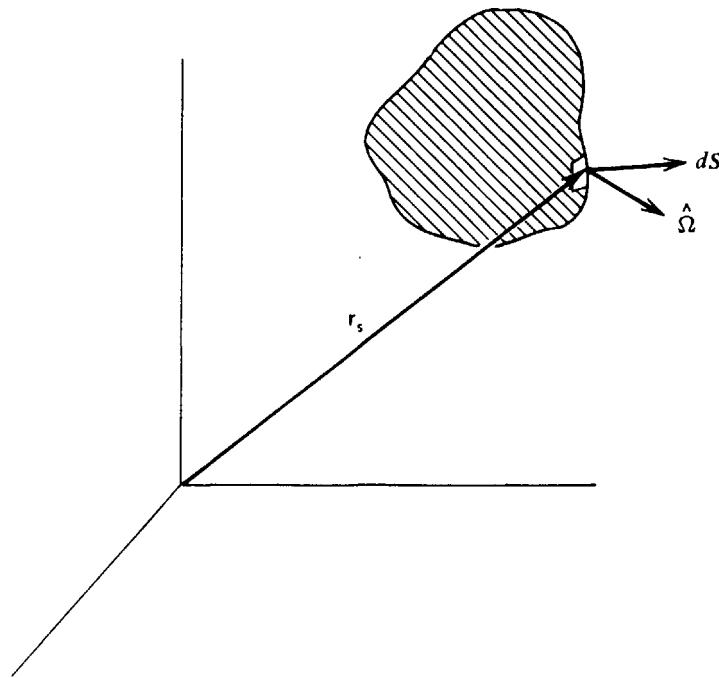
**FIGURE 4-8.** A free surface boundary.

EXAMPLE: Suppose we try to make this equation a little bit less abstract by applying it to the special case in which there is *plane symmetry*, that is, where the neutron flux depends only on a single spatial coordinate, say, $x$ (as shown in Figure 4-9). Then the directional derivative $\hat{\Omega} \cdot \nabla$ reduces to

$$\hat{\Omega} \cdot \nabla \varphi(x) = \left( \Omega_x \frac{\partial}{\partial x} + \Omega_y \frac{\partial}{\partial y} + \Omega_z \frac{\partial}{\partial z} \right) \varphi(x) = \Omega_x \frac{\partial \varphi}{\partial x}. \qquad (4\text{-}46)$$

For convenience, we will choose our angular coordinate system with its polar coordinate axis in the $x$-direction. Then $\Omega_x = \cos\theta$. The assumption of plane symmetry also implies that there is no dependence on the azimuthal angle $\phi$. Hence
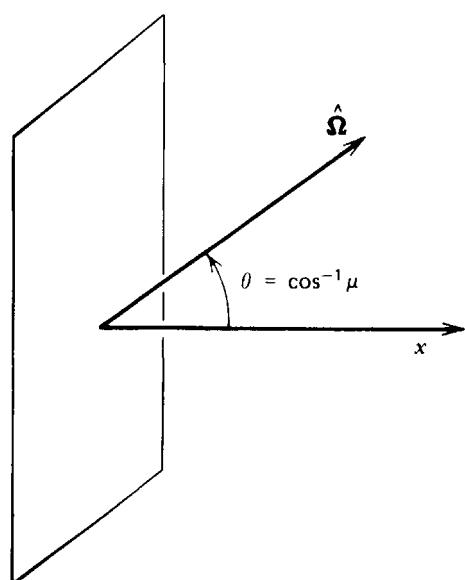


**FIGURE 4-9.** Coordinates characterizing plane symmetry.

the one-dimensional form of the transport equation becomes

$$\frac{1}{v}\frac{\partial \varphi}{\partial t} + \cos\theta \frac{\partial \varphi}{\partial x} + \Sigma_t \varphi(x, E, \theta, t)$$

$$= \int_0^\pi d\theta' \sin\theta' \int_0^\infty dE' \Sigma_s(E' \to E, \theta' \to \theta) \varphi(x, E', \theta', t) + s(x, E, \theta, t). \quad (4\text{-}47)$$

A final modification of the angular variable is useful. It is customary to rewrite this equation in terms of a new variable, $\mu \equiv \cos\theta$. Note that as $\theta$ ranges between 0 and $\pi$, $\mu$ ranges from 1 to $-1$. Hence the usual form of the one-dimensional transport equation is written as

$$\frac{1}{v}\frac{\partial \varphi}{\partial t} + \mu \frac{\partial \varphi}{\partial x} + \Sigma_t \varphi(x, E, \mu, t)$$

$$= \int_{-1}^{+1} d\mu' \int_0^\infty dE' \Sigma_s(E' \to E, \mu' \to \mu) \varphi(x, E', \mu', t) + s(x, E, \mu, t). \quad (4\text{-}48)$$

We can easily generalize Eq. (4-43) to include nuclear fission by including a component in the source term to account for fission neutrons. The rate at which neutrons with energy $E'$ and direction $\hat{\Omega}'$ induce fission events is just $\Sigma_f(E')$ $\varphi(r, E', \hat{\Omega}', t)$. If $\nu(E')$ is the average number of fission neutrons produced by a fission induced by a neutron of energy $E'$, then the total rate at which fission neutrons are born at a position $r$ is just

$$\int_{4\pi} d\hat{\Omega}' \int_0^\infty dE' \nu(E') \Sigma_f(E') \varphi(r, E', \hat{\Omega}', t). \quad (4\text{-}49)$$

These fission neutrons will have an energy distribution given by the fission spectrum $\chi(E)$. If we assume that they are emitted isotropically, then the fission source term we should include in the transport equation is just

$$s_f(r, E, \hat{\Omega}, t) = \frac{\chi(E)}{4\pi} \int_{4\pi} d\hat{\Omega}' \int_0^\infty dE' \nu(E') \Sigma_f(E') \varphi(r, E', \hat{\Omega}', t). \quad (4\text{-}50)$$

Actually we should qualify this argument a bit by admitting that we have assumed all of the fission neutrons to appear instantaneously at the time of fission. Hence $s_f$ is actually the source term corresponding to *prompt* fission neutrons. We will develop the modifications necessary for delayed fission neutrons in Chapter 6.

The neutron transport equation provides an essentially exact description of the neutron distribution within the reactor (at least, provided one is supplied with appropriate cross section information). Its solution would yield the angular flux $\varphi(r, E, \hat{\Omega}, t)$ containing essentially all the information (actually considerably *more*) we require concerning the nuclear behavior of the reactor. All we have to do is *solve* this equation.

Yet notice that: (a) the neutron transport equation has seven independent variables: $x$, $y$, $z$, $\theta$, $\phi$, $E$, $t$, (b) the dependence of the macroscopic cross sections on position $r$ is extremely complicated because of the complex, nonuniform structure of most reactor cores, and (c) as we have seen in Chapter 2, the cross section dependence on energy is also extremely complicated including resonance

structure, threshold effects, and so on. These considerations would immediately suggest that any attempt to solve the transport equation for a realistic system will involve heavy use of digital computers. Unfortunately no computer is sufficiently large enough (yet) to solve this equation in the general form in which we have derived it. This recognition implies that the major task of nuclear reactor analysis will be to introduce suitable approximations to the neutron transport equation which will allow us to solve it (at least on a computer), and yet still preserve enough reality that we can obtain a useful description of the nuclear reactor.

We will begin our discussion of such approximations to the transport equation by first briefly outlining the various "brute-force" procedures that can be used to reduce this equation to a discretized form more suitable for digital computation. We then will develop in a consistent fashion the principal approximations to the transport equation (such as neutron diffusion theory) used in nuclear reactor analysis.

## III. DIRECT NUMERICAL SOLUTION OF THE TRANSPORT EQUATION

Let us consider how one would attempt to solve the neutron transport equation directly using the aid of a digital computer. First we must recognize that digital computers are terrible at calculus (e.g., handling derivatives or integrals or such). Their real talent is in solving very large systems of algebraic equations. Hence our first task is to convert the transport equation into a system of algebraic equations more suitable for a digital computer. This is accomplished by "discretizing" each of the variables in the transport equation, that is, by replacing functions of continuous variables by a discrete set of values at a discrete set of points. The derivatives and integrals appearing in the transport equation must also be replaced by a corresponding discrete representation. In this way one arrives at a set of algebraic equations for the discrete representation of the dependent variable (in our case, the neutron flux $\varphi$).

The discretization of the transport equation—or, indeed, any such differential equation—can be accomplished by using either *discrete ordinates methods* or *function expansions*.[7,8] To illustrate these approaches, suppose we have an equation for a function, say $f(x)$, which contains derivatives and integrals:

$$F\left( f(x), \frac{df}{dx}, \frac{d^2f}{dx^2}, \dots, \int dx' f(x'), \dots \right) = 0. \tag{4-51}$$

In the *discrete ordinate* approach, one begins by representing the unknown $f(x)$ only by its values at a discrete set of points $x_i$ of the independent variable $x$. That is, one first discretizes the domain of variation of $x$ into a *mesh* of discrete points, each of which is labeled by a subscript $i$. Then we replace $f(x)$ by its value at each of these meshpoints

$$f(x) \rightarrow f(x_i) \equiv f_i, \quad i = 1, \dots, N. \tag{4-52}$$

(Of course, these values $f_i$ are still unknown.) Notice that what we have actually done is to replace a *function* $f(x)$ by a *column vector* $\underline{f}$

$$f(x) \rightarrow \underline{f} = col(f_1, f_2, \dots, f_N). \tag{4-53}$$

In this sense then, the system of algebraic equations we will arrive at for the unknown components of $\underline{f}$ can be written as a *matrix* equation.

We must next replace the various operations in the original equation by their discretized counterparts. For example, we would represent derivatives by *finite difference* formulas such as

$$\frac{df}{dx}\bigg|_{x=x_i} \cong \frac{f(x_i)-f(x_{i-1})}{x_i-x_{i-1}} = \frac{f_i-f_{i-1}}{x_i-x_{i-1}} \equiv \frac{\Delta f_i}{\Delta x_i}. \tag{4-54}$$

Integrals would be represented as sums or *numerical quadrature* formulas such as

$$\int_a^b dx f(x) \cong \sum_{i=1}^N w_i f(x_i) = \sum_{i=1}^N w_i f_i, \tag{4-55}$$

where the $w_i$ are known as the *quadrature weights*. A thorough description of such procedures can be found in any elementary textbook on numerical analysis,[7,8] although frequently it is more useful to derive such numerical approximations directly for the specific equation under investigation (as we will have occasion to do in Chapter 5).

Such procedures lead eventually to a set of coupled algebraic equations for the components $f_i$ that can be solved on a digital computer. Frequently these discrete values of the unknown $f(x)$ provide an adequate representation. However occasionally one wishes to reconstruct the original unknown $f(x)$ for all values of $x$ from the discrete values in $\underline{f}$. Then one must interpolate between the point values $f_i$ at $x_i$, for example by using polynomials. (See Figure 4-10.)

An alternative way to arrive at a discrete representation of an equation is to write the unknown function as an expansion in a finite number of known functions (frequently polynomials). If we call these expansion functions $p_l(x)$, then we would write

$$f(x) \cong \sum_{l=1}^N f_l p_l(x). \tag{4-56}$$

Hence once again we find that the function $f(x)$ is represented by a vector

$$f(x) \rightarrow col\,(f_1, f_2, f_3, \ldots, f_N) \equiv \underline{f}, \tag{4-57}$$

although in this case, the components of the vector are just the unknown expansion coefficients $f_l$. Notice that if we can determine these expansion coefficients, then we can easily reconstruct the unknown function $f(x)$ by merely using Eq. (4-56). Interpolation is not required as it is with the discrete ordinates approach.

EXAMPLE: When the dependent variable ranges between $-1$ and $+1$, a very convenient choice of expansion functions are the Legendre polynomials:

$$P_0(x)=1, P_1(x)=x, P_2(x)=(3-x^2)/2,\ldots \tag{4-58}$$

This choice of expansion functions is frequently used to represent the angular dependence of the neutron flux in one-dimensional problems in which $\mu=\cos\theta$ is
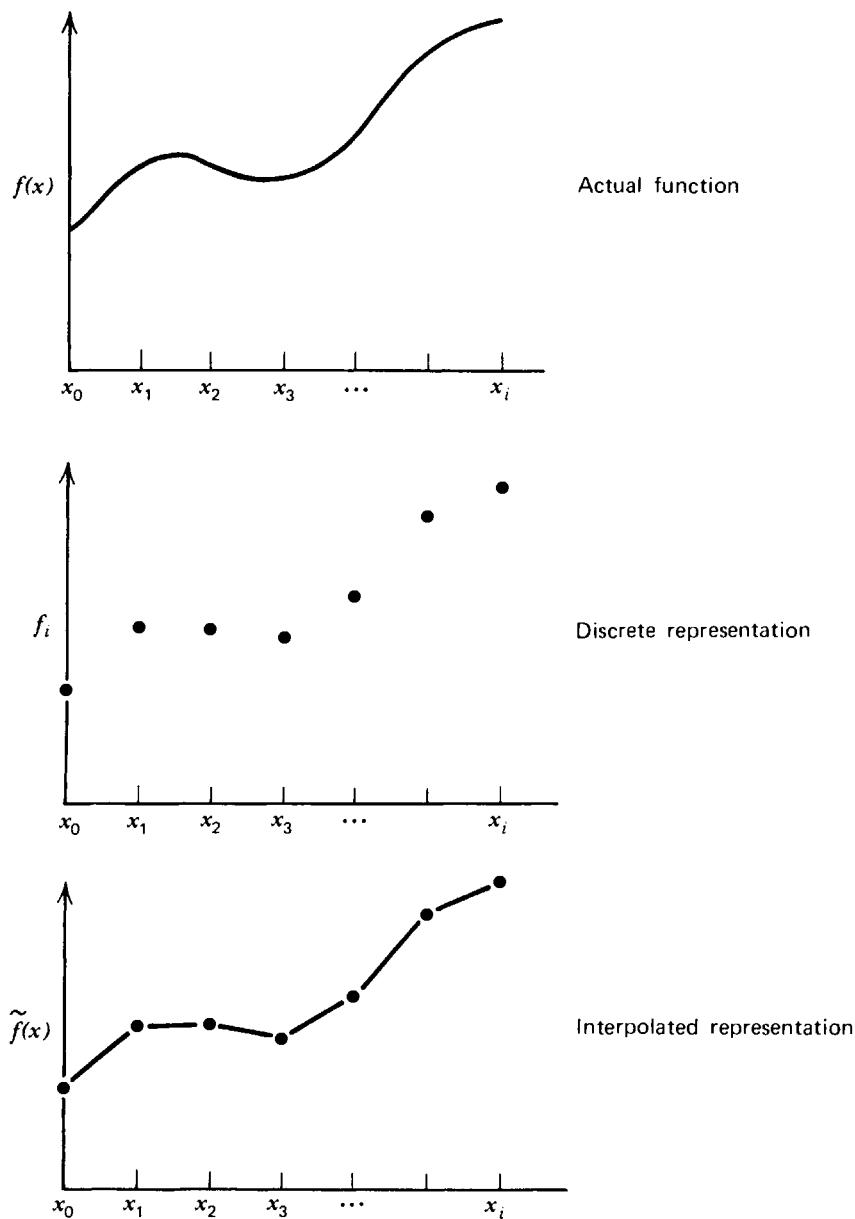
**FIGURE 4-10.** **Discrete ordinate representation of a function.**

the natural independent variable:

$$\varphi(x,\mu,E,t) = \sum_{l=1}^{N} \varphi_l(x,E,t) P_l(\mu).$$  (4-59)

(Here we might recall Eq. (4-48) as an example in which such an expansion would prove suitable.)

There are a variety of techniques one can now use to obtain a set of algebraic equations for the expansion coefficients from the original equation for $f(x)$. For example, it is frequently possible to substitute the expansion Eq. (4-56) into the original equation, multiply by each of the expansion functions $p_l(x)$, integrate over the independent variable $x$, and then use various properties of the $p_l(x)$ (such as the property of *orthogonality*, which we will discuss later) to arrive at a set of algebraic

equations for the $f_i$. One can also use more elaborate schemes such as the *calculus of variations* or so-called *weighted residual methods* to arrive at the set of algebraic equations. Since we will make only very limited use of such function expansions in our elementary development of numerical analysis methods in this text, we will refer the interested reader to several detailed descriptions[9,10] of these techniques for more information.

## A. Discretization of the Angular Dependence

Let us first consider how these techniques can be used to discretize the direction variable $\hat{\Omega}$ in the neutron transport equation. In the discrete ordinate approach,[11] we would first represent the independent variable by a discrete set of directions or rays $\hat{\Omega}_n, n = 1, \ldots, N$.

We then represent functions of $\hat{\Omega}$ by only their values at each of these mesh directions:

$$f(\hat{\Omega}) \rightarrow f(\hat{\Omega}_n) \equiv f_n, \quad n = 1, \ldots, N. \tag{4-60}$$

In such a discrete ordinate treatment of angle, the integral over $\hat{\Omega}$ becomes a summation:

$$\int_{4\pi} d\hat{\Omega} f(\hat{\Omega}) \cong \sum_{n=1}^{N} w_n f_n, \tag{4-61}$$

where the $w_n$ are appropriately chosen quadrature weights for the particular numerical integration scheme used to handle the angular integrals. In this scheme, the transport equation reduces to a coupled set of $N$ equations of the form:

$$\frac{1}{v} \frac{\partial \varphi_n}{\partial t} + \hat{\Omega}_n \cdot \nabla \varphi_n + \Sigma_t \varphi_n(\mathbf{r}, E, t)$$

$$= \sum_{n'=1}^{N} w_{n'} \int_0^\infty dE' \Sigma_s(E' \rightarrow E, \hat{\Omega}_{n'} \rightarrow \hat{\Omega}_n) \varphi_{n'}(\mathbf{r}, E', t) + s_n(\mathbf{r}, E, t) \tag{4-62}$$

where $n = 1, \ldots, N$ while

$$\varphi_n(\mathbf{r}, E, t) \equiv \varphi(\mathbf{r}, E, \hat{\Omega}_n, t). \tag{4-63}$$

This set of equations is commonly referred to as the $S_N$ *equations*[11,15] after early one-dimensional treatments utilizing trapezoidal quadrature corresponding to treating the angular variation of the flux as $N$ straight line segments.

One can also use functional expansions as an alternative scheme to discretize the angular variables. In the general case, this corresponds to expanding the angular dependence of the flux in a finite series of the spherical harmonics[3] $Y_{lm}(\hat{\Omega}) = Y_{lm}(\theta, \phi)$ familiar from quantum mechanics:[12,13]

$$\varphi(\mathbf{r}, E, \hat{\Omega}, t) = \sum_{l=0}^{N} \sum_{m=-l}^{+l} \varphi_{lm}(\mathbf{r}, E, t) Y_{lm}(\hat{\Omega}). \tag{4-64}$$

Then by substituting this expansion into the original transport equation, multiplying by spherical harmonics of different order, $Y_{l'm'}(\hat{\Omega})$, and integrating over the

angular variables, one can use orthogonality to obtain a coupled set of equations for the expansion coefficients $\varphi_{lm}(\mathbf{r},E,t)$. Since this set of equations is rather complicated when written out for general geometries, we will refer the interested reader to other sources for the general form of the equations.[3,4]

In one-dimension, an expansion in spherical harmonics corresponds to an expansion in Legendre polynomials, $P_l(\mu)$, where $\mu = \cos\theta$:

$$\varphi(x,E,\mu,t) = \sum_{l=0}^{N} \left(\frac{2l+1}{4\pi}\right)\varphi_l(x,E,t)P_l(\mu). \tag{4-65}$$

In this case the general form of the equations for the expansion coefficients is somewhat simpler and can be written as

$$\frac{1}{v}\frac{\partial\varphi_l}{\partial t} + \frac{(l+1)}{(2l+1)}\frac{\partial\varphi_{l+1}}{\partial x} + \frac{l}{(2l+1)}\frac{\partial\varphi_{l-1}}{\partial x} + \Sigma_t\varphi_l(x,E,t)$$

$$= \int_0^\infty dE'\Sigma_{s_l}(E'\to E)\varphi_l(x,E',t) + s_l(x,\mu,E), \tag{4-66}$$

where one defines the angular components of the differential scattering cross section as

$$\Sigma_{s_l}(E'\to E) \equiv 2\pi\int_{-1}^{+1} d\mu_0\,\Sigma_s(E'\to E,\mu_0)P_l(\mu_0), \quad \mu_0 \equiv \hat{\Omega}'\cdot\hat{\Omega}. \tag{4-67}$$

This set of equations is known, naturally enough, as the $P_N$ equations.[3,4]

In the particular case in which the expansion in spherical harmonics is truncated after two terms, that is $N = 1$, the expansion for the angular flux takes the form:

$$\varphi(\mathbf{r},E,\hat{\Omega},t) \cong \frac{1}{4\pi}\varphi_{00}(\mathbf{r},E,t) + \frac{3}{4\pi}\left[\varphi_{1x}(\mathbf{r},E,t)\Omega_x + \varphi_{1y}(\mathbf{r},E,t)\Omega_y + \varphi_{1z}(\mathbf{r},E,t)\Omega_z\right].$$

$$\tag{4-68}$$

We will find in the next section that this $P_1$ approximation to the angular flux is very closely related to neutron diffusion theory.

Hence we find that both discrete ordinate and functional expansion methods can be used to discretize the angular variables, giving rise to the $S_N$ or $P_N$ equations respectively. It might be mentioned that although the $P_1$ equations are used very frequently in nuclear reactor analysis (indeed, we shall have occasion to use them several times in our ensuing development), the higher order $P_N$ equations are rarely used in practical calculations. Rather one usually relies on the discrete ordinate approach if a more detailed treatment of the neutron directional dependence is required.

## B. Treatment of the Energy Variable
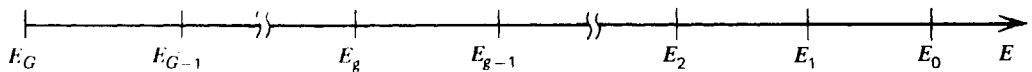
Very similar techniques can be used to discretize the energy variable $E$. Here, however, the discrete ordinate approach is far more common than function expansions. This can be easily understood when it is recognized that for the latter technique to be effective, the expansion functions must bear some resemblance to

the actual functional dependence of the neutron flux on the independent variable. The dependence of the angular flux on the neutron direction $\hat{\Omega}$ is usually rather weak, hence a set of general functions such as the spherical harmonics will provide an adequate description.

However, the neutron energy $E$ spans an enormous range from $10^{-3}$ eV up to $10^7$ eV. The dependence of the neutron distribution on energy is determined by quite different processes in different regions of energy. For example, at high energies the neutron energy dependence is dominated by the fission spectrum. At intermediate energies, neutron slowing down and resonance absorption are the dominant processes, while at low energies, neutron thermalization is important. To expand the neutron flux in a set of functions that adequately describe all of these processes is clearly hopeless. Indeed such function expansions are capable of describing neutron energy behavior only for a restricted range of neutron energies or a specific reactor type. (An example of such an expansion known as *energy* or *spectrum synthesis* is given in Chapter 13.)

One must be careful even when applying the discrete ordinate approach to the energy variable. The difficulties involved become quite apparent when the very detailed dependence of the neutron cross sections on energy is recalled. It clearly would be unthinkable simply to consider these cross sections tabulated at several discrete points as an adequate representation of this detailed structure.

Instead one first breaks up the neutron energy range into intervals or so-called *energy groups*:

$$\vdash\!\!\!\!\!\!\!\!\!\!\!\!-\!\!\!-\!\!\!-\!\!\!+\!\!\!\!\!\!-\!\!\!)\!\!\!-\!\!\!+\!\!\!\!\!\!\!\!-\!\!\!+\!\!\!\!\!\!-\!\!\!)\!\!\!-\!\!\!+\!\!\!\!\!\!\!\!-\!\!\!+\!\!\!\!\!\!\!\!-\!\!\!+\!\!\!\longrightarrow$$

$$E_G \qquad E_{G-1} \qquad E_g \qquad E_{g-1} \qquad E_2 \qquad E_1 \qquad E_0 \quad E$$

(Don't worry about the fact that these subscripts appear to run in the wrong direction—towards decreasing energy. It turns out that this is a more convenient labeling since neutrons tend to slow *down* in energy.) The neutron transport equation (or diffusion equation) is then integrated over each energy group in order to define appropriate average values of the various cross sections characterizing each group. For example, one would define the absorption cross section characterizing a group $g$ as

$$\Sigma_{a_g} \equiv \frac{\int_{E_g}^{E_{g-1}} dE \, \Sigma_a(E)\varphi(E)}{\int_{E_g}^{E_{g-1}} dE\varphi(E)} . \tag{4-69}$$

Of course these are only formal definitions of the cross sections characterizing the group, since the flux itself appears in their definition. However they do form the basis for the practical calculation of these quantities since one can insert approximations to the flux in order to calculate the group cross sections $\Sigma_{a_g}$. If we apply this scheme to the $S_N$ equations derived in the previous section, we find the coupled set of equations for the *group fluxes* $\varphi_n^g$:

$$\frac{1}{v_g}\frac{\partial \varphi_n^g}{\partial t} + \hat{\Omega}_n \cdot \nabla \varphi_n^g + \Sigma_{t_g}\varphi_n^g = \sum_{n'} w_{n'} \sum_{g'} \Sigma_{s_{n'\to n}}^{g'\to g} \varphi_{n'}^{g'} + s_n^g, \tag{4-70}$$

$$n = 1, \ldots, N \qquad g = 1, \ldots, G.$$

Such sets of equations are known as the *multigroup equations* (in this case, the *multigroup $S_N$ equations*) and play a very important role in nuclear reactor analysis. We will return in Chapter 7 to discuss their derivation in the case in which the angular flux is treated within the diffusion approximation.

## C. Treatment of Space and Time

The final step is to discretize the space and time variables. Although this can be done using function expansions (more specifically, expansions in the spatial or temporal modes of the system), such modal expansions are rarely used in general studies (although they are occasionally used in certain types of specific calculations in which the modes can be easily calculated). Instead one utilizes a direct discrete ordinate treatment in most cases. First the spatial variables $\mathbf{r} = (x, y, z)$ are decomposed into an appropriate spatial mesh. The various derivative terms are then replaced by finite difference equations defined on this mesh.

Finally the time variable is broken into discrete time steps, say $t_0, t_1, t_2, \ldots$ and the corresponding time derivatives are replaced by suitable difference formulas. The detailed mesh structure and difference formulas one utilizes depends on the type of problem one is investigating and will not be discussed here, since we will consider such topics in much greater detail in later chapters.

## D. Solution of the Discretized Equations

After using one scheme or another to discretize all of the variables in the neutron transport equation, we are left with a large system of algebraic equations for the components of the discretized representation of the flux, for example, $\varphi(x_i, y_j, z_k, E_g, \hat{\Omega}_n, t_s)$. Such algebraic equations can then be solved using routine numerical methods on a digital computer.

Unfortunately such a calculation becomes an immense undertaking if only a "brute force" discretization of the transport equation is applied. For example, consider "typical" mesh sizes of $100 \times 100 \times 100$ space points, 10 energy groups, and 10 angle points. Then for *each* time step we wish to calculate, we must solve $10^8$ simultaneous algebraic equations—a rather formidable task, even on a modern computer.

Hence the nuclear engineer cannot blindly depend on the computer to solve his problem, but rather he must first rely on *physical insight* (rather than brute force mathematics) to reduce the transport equation to more manageable form. He may be able to eliminate one or more of the independent variables in the transport equation. For example, one is usually interested in time-independent problems so that the time variable can be ignored. Frequently the reactor geometry can be modeled by a one- or two-dimensional calculation. The most useful class of approximations to the transport equation eliminate the angular variable $\hat{\Omega}$. The most popular (and useful) scheme for accomplishing this is to introduce the neutron diffusion approximation. Since neutron diffusion theory will constitute our primary tool in our study of nuclear reactor behavior, just as it does for the nuclear reactor industry, we will take some care in our derivation of the neutron diffusion equation.

## IV. THE DIFFUSION APPROXIMATION

### A. The Neutron Continuity Equation

For most reactor calculations, the details of the angular dependence of the flux are not necessary, and we really only need to calculate the angle-integrated flux:

$$\phi(\mathbf{r}, E, t) = \int_{4\pi} d\hat{\Omega}\, \varphi(\mathbf{r}, E, \hat{\Omega}, t) \,, \tag{4-71}$$

in order to calculate nuclear reaction rates and hence study the chain reaction (e.g., by calculating the multiplication factor $k$).

Surely we can formulate an equation for $\phi(\mathbf{r}, E, t)$ by simply integrating the transport equation over angle. Let's try and see what happens. That is, we will integrate each term of the transport equation (4-43) over the direction variable $\hat{\Omega}$:

$$\int_{4\pi} d\hat{\Omega}\, \frac{1}{v}\, \frac{\partial\varphi}{\partial t} + \int_{4\pi} d\hat{\Omega}\, \hat{\Omega}\cdot\nabla\varphi + \int_{4\pi} d\hat{\Omega}\, \Sigma_t\varphi$$
$$\underset{①}{} \qquad \underset{②}{} \qquad \underset{③}{}$$

$$= \int_{4\pi} d\hat{\Omega} \int_{4\pi} d\hat{\Omega}' \int_0^\infty dE'\, \Sigma_s(E'\to E, \hat{\Omega}'\to\hat{\Omega})\varphi(\mathbf{r}, E', \hat{\Omega}', t) + \int_{4\pi} d\hat{\Omega}\, s(\mathbf{r}, E, \hat{\Omega}, t)\,.$$
$$\underset{④}{} \qquad\qquad\qquad\qquad \underset{⑤}{}$$

$$\tag{4-72}$$

We can simplify each of these terms somewhat by the straightforward manipulations indicated below:

$$① = \int_{4\pi} d\hat{\Omega}\, \frac{1}{v}\, \frac{\partial\varphi}{\partial t} = \frac{1}{v}\, \frac{\partial}{\partial t} \int_{4\pi} d\hat{\Omega}\, \varphi = \frac{1}{v}\, \frac{\partial\phi}{\partial t}\,, \tag{4-73}$$

$$③ = \int_{4\pi} d\hat{\Omega}\, \Sigma_t\varphi = \Sigma_t \int_{4\pi} d\hat{\Omega}\, \varphi = \Sigma_t\phi, \tag{4-74}$$

$$⑤ = \int_{4\pi} d\hat{\Omega}\, s(\mathbf{r}, E, \hat{\Omega}, t) \equiv S(\mathbf{r}, E, t). \tag{4-75}$$

Here we have used our earlier expression Eq. (4-16) for the neutron flux $\phi$ in terms of the angular flux $\varphi$ and also simply defined a source term $S(\mathbf{r}, E, t)$. To evaluate the inscattering term ④ we first recall that $\Sigma_s(E'\to E, \hat{\Omega}'\to\hat{\Omega})$ usually depends only on the scattering angle cosine $\mu_0 = \hat{\Omega}'\cdot\hat{\Omega}$. This implies that

$$\int_{4\pi} d\hat{\Omega}\, \Sigma_s(E'\to E, \hat{\Omega}'\to\hat{\Omega}) = 2\pi \int_{-1}^{+1} d\mu_0\, \Sigma_s(E'\to E, \mu_0) = \Sigma_s(E'\to E), \tag{4-76}$$

where $\Sigma_s(E'\to E)$ is just the "single" differential scattering cross section defined in Eq. (2-46). Hence we can interchange the order of integrations over $\hat{\Omega}$ and $\hat{\Omega}'$ to

write:

$$
④ = \int_{4\pi} d\hat{\Omega}' \int_0^\infty dE' \left[ \int_{4\pi} d\hat{\Omega} \, \Sigma_s(E' \rightarrow E, \hat{\Omega}' \rightarrow \hat{\Omega}) \right] \varphi(\mathbf{r}, E', \hat{\Omega}', t)
$$

$$
= \int_0^\infty dE' \Sigma_s(E' \rightarrow E) \int_{4\pi} d\hat{\Omega}' \varphi(\mathbf{r}, E', \hat{\Omega}', t) \tag{4-77}
$$

$$
= \int_0^\infty dE' \Sigma_s(E' \rightarrow E) \phi(\mathbf{r}, E', t).
$$

So far everything is straightforward; but unfortunately the last term ② cannot be evaluated in terms of $\phi(\mathbf{r}, E, t)$. In fact we find that ② must be evaluated in terms of the neutron current **J** by using Eq. (4-19):

$$
② = \int_{4\pi} d\hat{\Omega} \; \hat{\Omega} \cdot \nabla \varphi = \nabla \cdot \int_{4\pi} d\hat{\Omega} \, \hat{\Omega} \varphi = \nabla \cdot \mathbf{J}(\mathbf{r}, E, t). \tag{4-78}
$$

If we now rewrite Eq. (4-72), it takes the form

$$
\frac{1}{v} \frac{\partial \phi}{\partial t} + \nabla \cdot \mathbf{J}(\mathbf{r}, E, t) + \Sigma_t(\mathbf{r}, E) \phi(\mathbf{r}, E, t) = \int_0^\infty dE' \Sigma_s(E' \rightarrow E) \phi(\mathbf{r}, E', t) + S(\mathbf{r}, E, t).
$$

$$
\tag{4-79}
$$

This is known as the *neutron continuity equation*, since it is just the mathematical statement of neutron balance.

It is important to note that this equation contains two unknowns, $\phi(\mathbf{r}, E, t)$ and $\mathbf{J}(\mathbf{r}, E, t)$, unlike the neutron transport equation, which only contained one unknown, the angular flux $\varphi(\mathbf{r}, E, \hat{\Omega}, t)$. Hence by removing the angular dependence we have in the process introduced another unknown, $\mathbf{J}(\mathbf{r}, E, t)$, and hence we now have an insoluble problem (i.e., one equation in two unknowns). The moral of this story is that you don't get something for nothing—that is, merely integrating out the angular dependence doesn't remove the complexities of the angular variation. It just shifts them by demanding that one obtain yet another equation relating $\phi(\mathbf{r}, E, t)$ and $\mathbf{J}(\mathbf{r}, E, t)$.

It is impossible to express $\mathbf{J}(\mathbf{r}, E, t)$ in terms of $\phi(\mathbf{r}, E, t)$ in a general and exact manner. This is more apparent if we recall the definitions Eqs. (4-17) and (4-19):

$$
\phi(\mathbf{r}, E, t) \equiv \int_{4\pi} d\hat{\Omega} \, \varphi(\mathbf{r}, E, \hat{\Omega}, t), \tag{4-17}
$$

$$
\mathbf{J}(\mathbf{r}, E, t) \equiv \int_{4\pi} d\hat{\Omega} \, \hat{\Omega} \varphi(\mathbf{r}, E, \hat{\Omega}, t). \tag{4-19}
$$

It is obvious that these two quantities are entirely different functions, although they can both be expressed in terms of an angular integral of the angular flux $\varphi(\mathbf{r}, E, \hat{\Omega}, t)$. Hence there is no reason why one would expect these functions to be simply related.

Undaunted by our failure to find a simple equation for $\phi(\mathbf{r}, E, t)$, suppose we shift our attention instead to developing an equation for the current density $\mathbf{J}(\mathbf{r}, E, t)$. By comparing the definitions in Eqs. (4-17) and (4-19) above, we are tempted to try

multiplying the transport equation by $\hat{\Omega}$ and then integrating once again over angle. Actually since the direction variable $\hat{\Omega}$ is a vector,

$$\hat{\Omega} = \underbrace{\hat{e}_x \sin\theta\cos\phi}_{\Omega_x} + \underbrace{\hat{e}_y \sin\theta\sin\phi}_{\Omega_y} + \underbrace{\hat{e}_z \cos\theta}_{\Omega_z},$$

(4-80)

we should multiply the transport equation by each component separately and integrate. For example, the $\Omega_x$ component would yield

$$\underbrace{\int_{4\pi} d\hat{\Omega}\, \Omega_x \frac{1}{v}\frac{\partial\varphi}{\partial t}}_{\textcircled{1}} + \underbrace{\int_{4\pi} d\hat{\Omega}\, \Omega_x \hat{\Omega}\cdot\nabla\varphi}_{\textcircled{2}} + \underbrace{\int_{4\pi} d\hat{\Omega}\, \Omega_x \Sigma_t \varphi}_{\textcircled{3}}$$

$$= \underbrace{\int_{4\pi} d\hat{\Omega}\, \Omega_x \int_{4\pi} d\hat{\Omega}' \int_0^\infty dE' \Sigma_s(E'\to E, \hat{\Omega}'\to\hat{\Omega})\varphi(\mathbf{r}, E', \hat{\Omega}', t)}_{\textcircled{4}} + \underbrace{\int_{4\pi} d\hat{\Omega}\, \Omega_x s(\mathbf{r}, E, \hat{\Omega}, t)}_{\textcircled{5}}$$

(4-81)

Each of these terms can be simplified in a manner similar to that used in deriving the neutron continuity equation [Eq. (4-79)]:

$$\textcircled{1} = \frac{1}{v}\frac{\partial}{\partial t}\int_{4\pi} d\hat{\Omega}\, \Omega_x \varphi = \frac{1}{v}\frac{\partial J_x}{\partial t},$$

(4-82)

$$\textcircled{3} = \Sigma_t \int_{4\pi} d\hat{\Omega}\, \Omega_x \varphi = \Sigma_t J_x,$$

(4-83)

$$\textcircled{5} = \int_{4\pi} d\hat{\Omega}\, \Omega_x s(\mathbf{r}, E, \hat{\Omega}, t) \equiv S_{1_x}(\mathbf{r}, E, t).$$

(4-84)

Now to handle the inscattering term $\textcircled{4}$, write

$$\textcircled{4} = \int_{4\pi} d\hat{\Omega}' \int_0^\infty dE' \left[\int_{4\pi} d\hat{\Omega}\, \Omega_x \Sigma_s(E'\to E, \hat{\Omega}'\to\hat{\Omega})\right]\varphi(\mathbf{r}, E', \hat{\Omega}', t).$$

(4-85)

Next we do something a bit sneaky. Since $\hat{\Omega}$ is a unit vector, we can write $\hat{\Omega}'\cdot\hat{\Omega}' = 1$. We will insert this into Eq. (4-85) so that we can rewrite it as:

$$\textcircled{4} = \int_0^\infty dE' \int_{4\pi} d\hat{\Omega}' \left[\int_{4\pi} d\hat{\Omega}\, \Omega_x \hat{\Omega}' \Sigma_s(E'\to E, \hat{\Omega}'\to\hat{\Omega})\right]\cdot\hat{\Omega}'\varphi(\mathbf{r}, E', \hat{\Omega}', t).$$

(4-86)

Now we recall again that $\Sigma_s(E'\to E, \hat{\Omega}'\to\hat{\Omega})$ depends only on the cosine of the scattering angle $\mu_0 = \hat{\Omega}'\cdot\hat{\Omega}$. Thus we can write

$$\textcircled{4} = 3\int_0^\infty dE' \int_{4\pi} d\hat{\Omega}' \left[\int_{4\pi} d\hat{\Omega}\, \Omega_x \Omega_x' \Sigma_s(E'\to E, \hat{\Omega}'\cdot\hat{\Omega})\right]\Omega_x'\varphi(\mathbf{r}, E', \hat{\Omega}', t).$$

(4-87)

We will define

$$\int_{4\pi} d\hat{\Omega}\, \Omega_x \Omega_x' \Sigma_s(E'\to E, \hat{\Omega}'\cdot\hat{\Omega}) = \frac{1}{3}\int_{4\pi} d\hat{\Omega}\, \hat{\Omega}\cdot\hat{\Omega}' \Sigma_s(E'\to E, \hat{\Omega}'\cdot\hat{\Omega})$$

$$= \frac{2\pi}{3}\int_{-1}^{+1} d\mu_0 \mu_0 \Sigma_s(E'\to E, \mu_0) \equiv \frac{1}{3}\Sigma_{s_1}(E'\to E),$$

(4-88)

so that ④ finally becomes

$$④ = \int_0^\infty dE' \Sigma_{s_1}(E' \to E) \int_{4\pi} d\hat{\Omega}' \, \Omega_x' \varphi(\mathbf{r}, E', \hat{\Omega}', t) = \int_0^\infty dE' \Sigma_{s_1}(E' \to E) J_x(\mathbf{r}, E', t).$$

$$(4\text{-}89)$$

We are almost finished. Thus far each of our terms has been expressed in terms of the current density $J_x$, except for the source term $S_{1x}$ which is a known term. But wait! We still haven't considered the streaming term:

$$② = \int_{4\pi} d\hat{\Omega} \, \Omega_x \hat{\Omega} \cdot \nabla \varphi = \nabla \cdot \int_{4\pi} d\hat{\Omega} \, \Omega_x \hat{\Omega} \varphi(\mathbf{r}, E, \hat{\Omega}, t). \qquad (4\text{-}90)$$

A quick glance at the integral term confirms our fears; once again the streaming term has kicked out yet another new unknown. To see this more clearly, we can combine these results along with similar results for $\Omega_y$ and $\Omega_z$ to write Eq. (4-81) as an equation for the current density **J**:

$$\frac{1}{v} \frac{\partial \mathbf{J}}{\partial t} + \nabla \cdot \int_{4\pi} d\hat{\Omega} \, \hat{\Omega} \hat{\Omega} \varphi(\mathbf{r}, E, \hat{\Omega}, t) + \Sigma_t \mathbf{J}(\mathbf{r}, E, t)$$

$$= \int_0^\infty dE' \Sigma_{s_1}(E' \to E) \mathbf{J}(\mathbf{r}, E', t) + \mathbf{S}_1(\mathbf{r}, E, t). \qquad (4\text{-}91)$$

However just as with the neutron continuity equation [Eq. (4-79)], we find that integrating over $\hat{\Omega}$ yields one equation but two unknowns, $\mathbf{J}(\mathbf{r}, E, t)$ and

$$\overset{\leftrightarrow}{\Pi}(\mathbf{r}, E, t) \equiv \int_{4\pi} d\hat{\Omega} \, \hat{\Omega} \hat{\Omega} \varphi(\mathbf{r}, E, \hat{\Omega}, t). \qquad (4\text{-}92)$$

[Here we have taken the luxury of using a symbolic notation of writing two vectors together, $\hat{\Omega}\hat{\Omega}$. If this bothers you, just interpret this as a convenient notation for taking each of the various combinations of components $\Omega_x \Omega_x, \Omega_x \Omega_y, \ldots, \Omega_z \Omega_z$ separately to construct a quantity with nine components, $\Pi_{xx}, \Pi_{xy}, \ldots, \Pi_{zz}$. Such quantities are referred to as *tensors* (or, in this case, *dyadics*), but we won't need to get so formal here.] It should be evident that we can get a new equation for $\overset{\leftrightarrow}{\Pi}(\mathbf{r}, E, t)$ by multiplying the transport equation by $\hat{\Omega}\hat{\Omega}$ and integrating, but this new equation will contain yet another unknown,

$$\int_{4\pi} d\hat{\Omega} \, \hat{\Omega} \hat{\Omega} \hat{\Omega} \varphi(\mathbf{r}, E, \hat{\Omega}, t).$$

Hence all we are doing by multiplying by $[\hat{\Omega}]^n$ and integrating is generating an infinite set of coupled equations (which we can't solve). [Incidently, it should be apparent that the culprit is the "streaming" or "leakage" term $\hat{\Omega} \cdot \nabla \varphi$ which contains a factor of $\hat{\Omega}$ and hence generates the new unknowns in each equation.]

The only way to cut off this chain of equations is to introduce an approximation. We shall do this by assuming that the angular flux is only *weakly dependent* on angle, and in so doing, we will generate the neutron diffusion equation. However it is useful to first discuss several simplifications that can frequently be introduced into the neutron transport equation.

## B. Common Simplifications to the Neutron Transport Equation

### 1. THE ONE-SPEED APPROXIMATION

It is frequently convenient to suppress the neutron energy dependence by assuming that one can characterize the neutrons by a single energy or speed. We will find in Chapter 7 that if one chooses the appropriate effective cross sections, such a representation will in fact frequently yield a reasonable description of the reactor. However for now we will introduce the *one-speed approximation* in a rather artificial manner by simply assuming that the neutron energy does not change in a scattering collision. This can be inserted into the transport equation [Eq. (4-43)] in a rather convenient manner by simply assuming a differential scattering cross section of the form

$$\Sigma_s(E' \to E, \hat{\Omega}' \to \hat{\Omega}) = \Sigma_s(E, \hat{\Omega}' \to \hat{\Omega}) \, \delta(E' - E), \qquad (4\text{-}93)$$

where $\delta(E' - E)$ is the Dirac $\delta$-function defined by the property

$$\int dx' f(x') \delta(x - x') = f(x) \qquad (4\text{-}94)$$

for any sufficiently well-behaved function $f(x)$. [See Appendix C for a more detailed discussion of animals such as the $\delta$-function.] Using this definition, the inscattering term in Eq. (4-43) becomes

$$\int_{4\pi} d\hat{\Omega}' \int_0^\infty dE' \, \Sigma_s(E' \to E, \hat{\Omega}' \to \hat{\Omega}) \varphi(\mathbf{r}, E', \hat{\Omega}', t) = \int_{4\pi} d\hat{\Omega}' \, \Sigma_s(E, \hat{\Omega}' \to \hat{\Omega}) \varphi(\mathbf{r}, E, \hat{\Omega}', t).$$

$$(4\text{-}95)$$

Since all of the terms in the transport equation are now evaluated at the same energy, we may as well eliminate the explicit dependence on energy to write the *one-speed neutron transport equation* as

$$\frac{1}{v} \frac{\partial \varphi}{\partial t} + \hat{\Omega} \cdot \nabla \varphi + \Sigma_t(\mathbf{r}) \varphi(\mathbf{r}, \hat{\Omega}, t) = \int_{4\pi} d\hat{\Omega}' \, \Sigma_s(\hat{\Omega}' \to \hat{\Omega}) \varphi(\mathbf{r}, \hat{\Omega}', t) + s(\mathbf{r}, \hat{\Omega}, t). \quad (4\text{-}96)$$

This equation is still far too complicated to solve (even using brute force numerical techniques) in realistic geometries. So we'll introduce yet another simplification.

### 2. ISOTROPIC SOURCES AND SCATTERING

One major simplification that can be introduced into the transport equation arises when one assumes both isotropic neutron sources

$$s(\mathbf{r}, \hat{\Omega}, t) = \frac{1}{4\pi} S(\mathbf{r}, t) \qquad (4\text{-}97)$$

and isotropic scattering (in the LAB system)

$$\Sigma_s(\hat{\Omega}' \to \hat{\Omega}) = \frac{1}{4\pi} \Sigma_s. \qquad (4\text{-}98)$$

The assumption of isotropic neutron sources is usually not too restrictive since most sources such as fission are indeed essentially isotropic. Unfortunately although neutron scattering is usually isotropic in the CM system, it is far from isotropic in the LAB system, particularly for low mass number scatterers such as hydrogen. Undeterred by such physical considerations, we will assume for the moment that isotropic scattering is present. Then the one-speed transport equation simplifies still further to

$$\frac{1}{v}\frac{\partial \varphi}{\partial t} + \hat{\Omega}\cdot\nabla\varphi + \Sigma_t\varphi(\mathbf{r},\hat{\Omega},t) = \frac{\Sigma_s}{4\pi}\int_{4\pi} d\hat{\Omega}'\varphi(\mathbf{r},\hat{\Omega}',t) + \frac{S(\mathbf{r},t)}{4\pi}. \qquad (4\text{-}99)$$

However even this equation is extremely difficult to solve in general.

### 3. OTHER SIMPLIFICATIONS

Thus far we have mutilated the energy and angular dependence of the transport equation in the interest of mathematical expediency—and still have not arrived at anything we can hope to solve (at least analytically). So in frustration we now turn our attention to the remaining time and spatial variables. First we will completely eliminate the time variable by agreeing to consider only steady-state transport problems. Then Eq. (4-99) simplifies to

$$\hat{\Omega}\cdot\nabla\varphi + \Sigma_t\varphi(\mathbf{r},\hat{\Omega}) = \frac{\Sigma_s}{4\pi}\int_{4\pi} d\hat{\Omega}'\varphi(\mathbf{r},\hat{\Omega}') + \frac{S(\mathbf{r})}{4\pi}. \qquad (4\text{-}100)$$

Next, we will assume that the system under study has uniform composition such that the cross sections do not depend on position. Finally we will simplify the system geometry, for example, by considering only planar or spherical symmetry. In the case of planar symmetry we arrive at a rather simple-looking equation

$$\mu\frac{\partial \varphi}{\partial x} + \Sigma_t\varphi(x,\mu) = \frac{\Sigma_s}{2}\int_{-1}^{+1} d\mu'\varphi(x,\mu') + \frac{S(x)}{2}. \qquad (4\text{-}101)$$

This equation can actually be solved *analytically*[6]—but only with rather sophisticated mathematical techniques beyond the scope of this text. So even after a number of rather questionable approximations, one arrives at an equation that can still only be solved with great difficulty.

After this rather pessimistic glance at the difficulties involved in solving the transport equation, let us remark that there is one very important class of transport problems that can be solved exactly with only a minimal expenditure of effort—those involving neutron transport in a purely absorbing medium.

### 4. NEUTRON TRANSPORT IN A PURELY ABSORBING MEDIUM

Frequently we are interested in neutron transport in a medium in which scattering can be ignored. This might occur in a vacuum, for example (or more realistically, a gas-filled region of a reactor). Or it might apply in a very highly absorbing medium such as a fuel element or a control rod. In these cases, the

transport equation becomes

$$\hat{\Omega} \cdot \nabla \varphi(\mathbf{r}, E, \hat{\Omega}) + \Sigma_a(\mathbf{r}, E) \varphi(\mathbf{r}, E, \hat{\Omega}) = s(\mathbf{r}, E, \hat{\Omega}). \qquad (4\text{-}102)$$

We have omitted the time dependence here since it is rarely of relevance when such transport problems are of interest.

This equation can be solved exactly for any source distribution since it can be converted into a simple first-order differential equation. Consider first the case of neutron transport in a vacuum in which $\Sigma_a \equiv 0$:

$$\hat{\Omega} \cdot \nabla \varphi(\mathbf{r}, E, \hat{\Omega}) = s(\mathbf{r}, E, \hat{\Omega}). \qquad (4\text{-}103)$$

However $\hat{\Omega} \cdot \nabla$ is just the directional derivative in the direction $\hat{\Omega}$. If we define a variable $R$ that measures distance along this direction (see Figure 4-11) then

$$\hat{\Omega} \cdot \nabla \rightarrow -\frac{\partial}{\partial R}, \qquad (4\text{-}104)$$

where $R$ is measured in the $-\hat{\Omega}$ direction, and we find

$$\frac{\partial \varphi}{\partial R} = -s(\mathbf{r}, E, \hat{\Omega}). \qquad (4\text{-}105)$$

If we now integrate with respect to this variable, we find

$$\varphi(\mathbf{r}, E, \hat{\Omega}) = \int_0^\infty dR\, s(\mathbf{r} - R\hat{\Omega}, E, \hat{\Omega}). \qquad (4\text{-}106)$$

Notice that this expression simply equates the neutron angular flux at position $\mathbf{r}$ in direction $\hat{\Omega}$ to the total number of source neutrons emitted in this $\hat{\Omega}$ (obtained by integrating back along $-\hat{\Omega}$).

EXAMPLE: Consider an isotropic point source located at the origin (for convenience, we will suppress the energy dependence for this example). The math-
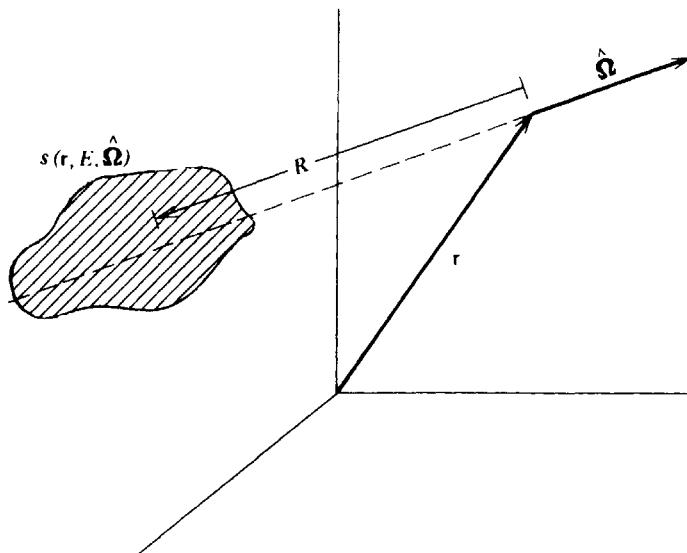


FIGURE 4-11. Neutron transport in a vacuum.

ematical representation for such a source is just

$$s(\mathbf{r}, \hat{\Omega}) = \frac{S_0}{4\pi} \delta(\mathbf{r}),\qquad(4\text{-}107)$$

where $\delta(\mathbf{r} - \mathbf{r}')$ is just the three-dimensional version of the Dirac $\delta$-function (see Appendix C) defined by

$$\int d^3r' f(\mathbf{r}') \delta(\mathbf{r} - \mathbf{r}') = f(\mathbf{r}).\qquad(4\text{-}108)$$

Hence we find

$$\varphi(\mathbf{r}, \hat{\Omega}) = S_0 \int_0^\infty dR\, \frac{\delta(\mathbf{r} - R\hat{\Omega})}{4\pi}.\qquad(4\text{-}109)$$

This still looks a bit strange. [Actually it can be shown that $\varphi(\mathbf{r}, \hat{\Omega})$ vanishes unless one is looking along the direction $\mathbf{r}$, as one would expect from Figure 4-12.] Suppose we compute instead the neutron flux itself:

$$\phi(\mathbf{r}) = \int_{4\pi} d\hat{\Omega}\, \varphi(\mathbf{r}, \hat{\Omega}) = \frac{S_0}{4\pi} \int_0^\infty dR \int_{4\pi} d\hat{\Omega}\, \delta(\mathbf{r} - R\hat{\Omega}).\qquad(4\text{-}110)$$

If we multiply the integrand by $R^2/R^2$, we can identify a volume integration (in spherical coordinates) over the dummy vector $\mathbf{R}$:

$$\phi(\mathbf{r}) = \frac{S_0}{4\pi} \int_0^\infty R^2 dR \int_{4\pi} d\hat{\Omega}\, \frac{\delta(\mathbf{r} - \mathbf{R})}{R^2} = \frac{S_0}{4\pi} \int d^3R\, \frac{\delta(\mathbf{r} - \mathbf{R})}{R^2}.\qquad(4\text{-}111)$$

Yet using the definition of $\delta(\mathbf{r} - \mathbf{r}')$ given by Eq. (4-108), we find that the flux resulting from an isotropic point source at the origin is just

$$\phi(\mathbf{r}) = \frac{S_0}{4\pi r^2},\qquad(4\text{-}112)$$

that is, $\phi$ falls off with distance as $1/r^2$ because of the ever increasing surface area $(4\pi r^2)$ over which the $S_0$ source neutrons/sec must be isotropically distributed.
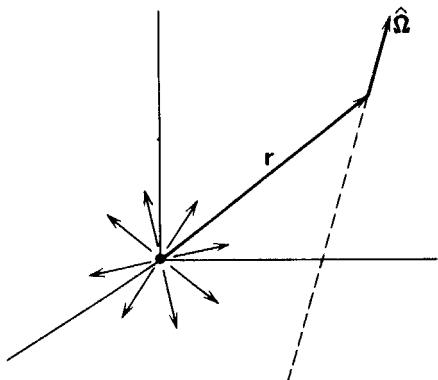


FIGURE 4-12. A point source emitting neutrons isotropically at the origin of an infinite medium.

Now return to Eq. (4-102), which characterizes transport in a purely absorbing medium. Suppose this medium is homogeneous, that is, $\Sigma_a$ is not a function of position. Then we can use an integrating factor $\exp[\Sigma_a \mathbf{r} \cdot \hat{\Omega}]$ to rewrite Eq. (4-102) as

$$\hat{\Omega} \cdot \nabla[\varphi \exp(\Sigma_a \mathbf{r} \cdot \hat{\Omega})] = s \exp(\Sigma_a \mathbf{r} \cdot \hat{\Omega}).$$ (4-113)

However we can integrate this equation just as we did Eq. (4-103) to find

$$\varphi(\mathbf{r}, E, \hat{\Omega})\exp(\Sigma_a \mathbf{r} \cdot \hat{\Omega}) = \int_0^\infty dR\, s(\mathbf{r} - \hat{\Omega}R, E, \hat{\Omega})\exp[\Sigma_a(\mathbf{r} - R\hat{\Omega}) \cdot \hat{\Omega}],$$ (4-114)

or canceling out the integrating factor from both sides

$$\varphi(\mathbf{r}, E, \hat{\Omega}) = \int_0^\infty dR\, s(\mathbf{r} - R\hat{\Omega}, E, \hat{\Omega})\exp(-\Sigma_a R).$$ (4-115)

This solution again has a very plausible interpretation when it is recognized that $\exp(-\Sigma_a R)$ is just the attenuation that would occur between the source point and the observation point $\mathbf{r}$. Notice that this immediately reduces to our vacuum result for the case in which $\Sigma_a \equiv 0$.

We can also obtain an exact solution for the situation in which $\Sigma_a$ depends on position. We need only use a slightly more complicated attenuation factor

$$\exp(-\Sigma_a R) \rightarrow \exp[-\alpha(\mathbf{r}, \mathbf{r} - R\hat{\Omega})],$$ (4-116)

where $\alpha(\mathbf{r}, \mathbf{r}')$ is known as the *optical thickness* or *optical depth* of the media and is defined by

$$\alpha(\mathbf{r}, \mathbf{r}') \equiv \int_0^R ds\, \Sigma_a\left(\mathbf{r} - s\frac{\mathbf{R}}{R}\right), \quad \mathbf{R} \equiv \mathbf{r}' - \mathbf{r}.$$ (4-117)

Note that $\alpha$ is essentially a measure of the effective absorption between points $\mathbf{r}'$ and $\mathbf{r}$.

EXAMPLE: Consider once again our point source, only this time assume that it is imbedded at the origin of an infinitely large medium characterized by a uniform absorption cross section $\Sigma_a$. Then repeating our earlier analysis using Eq. (4-115) yields

$$\phi(\mathbf{r}) = \frac{S_0 \exp(-\Sigma_a r)}{4\pi r^2},$$ (4-118)

which is similar to our vacuum result, with the exception of an additional attenuation factor $\exp(-\Sigma_a r)$ due to the absorption.

This very important result can be easily generalized to the situation in which the source is located at an arbitrary point $\mathbf{r}'$ by merely shifting the coordinate system origin to find

$$\phi(\mathbf{r}) = \frac{S_0 \exp(-\Sigma_a |\mathbf{r} - \mathbf{r}'|)}{4\pi |\mathbf{r} - \mathbf{r}'|^2}.$$ (4-119)
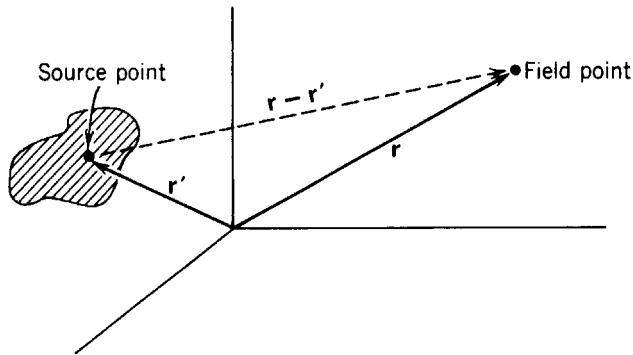
FIGURE 4-13.  Coordinates characterizing a disturbed source $s(r,E,\hat{\Omega})$.

We can finally use this result to synthesize the neutron flux resulting from an arbitrary distribution of isotopic sources, $S(\mathbf{r})$, in an infinite absorbing medium as

$$\phi(\mathbf{r}) = \int d^3r' \; \frac{\exp(-\Sigma_a|\mathbf{r}-\mathbf{r}'|)}{4\pi|\mathbf{r}-\mathbf{r}'|^2} S(\mathbf{r}'). \tag{4-120}$$

## C. The One-Speed Diffusion Equation

We now turn our attention toward the development of an approximate description of neutron transport more amenable to calculation than the neutron transport equation itself. To make life simple, we will first work within the one-speed approximation represented by Eq. (4-96). Let us first note the explicit forms taken by the neutron conservation equation and the corresponding equation for the current density $\mathbf{J}$ in the one-speed case:

$$\frac{1}{v}\frac{\partial\phi}{\partial t} + \nabla\cdot\mathbf{J} + \Sigma_t\phi(\mathbf{r},t) = \Sigma_s\phi(\mathbf{r},t) + S(\mathbf{r},t), \tag{4-121}$$

$$\frac{1}{v}\frac{\partial\mathbf{J}}{\partial t} + \nabla\cdot\int_{4\pi} d\hat{\Omega}\;\hat{\Omega}\hat{\Omega}\varphi(\mathbf{r},\hat{\Omega},t) + \Sigma_t\mathbf{J}(\mathbf{r},t) = \bar{\mu}_0\Sigma_s\mathbf{J}(\mathbf{r},t) + \mathbf{S}_1(\mathbf{r},t). \tag{4-122}$$

Here we have noted explicitly the simplifications that occur in the inscattering term when the one-speed approximation is introduced. More specifically,

$$\int_0^\infty dE'\,\Sigma_s(E'\to E)\phi(\mathbf{r},E',t) \to \Sigma_s\phi(\mathbf{r},t), \tag{4-123}$$

and

$$\int_0^\infty dE'\,\Sigma_{s_1}(E'\to E)\mathbf{J}(\mathbf{r},E',t) \to \Sigma_{s_1}\mathbf{J}(\mathbf{r},t). \tag{4-124}$$

But

$$\Sigma_{s_1} = 2\pi\int_{-1}^{+1} d\mu_0\,\mu_0\Sigma_s(\hat{\Omega}'\cdot\hat{\Omega}) = \bar{\mu}_0\Sigma_s \tag{4-125}$$

where we have defined the average scattering angle cosine $\bar{\mu}_0$ as

$$\bar{\mu}_0 \equiv \langle \hat{\Omega} \cdot \hat{\Omega}' \rangle = \frac{2\pi}{\Sigma_s} \int_{-1}^{+1} d\mu_0 \mu_0 \Sigma_s(\mu_0)$$

$$= \frac{1}{4\pi \Sigma_s} \int_{4\pi} d\hat{\Omega} \int_{4\pi} d\hat{\Omega}' \, \hat{\Omega} \cdot \hat{\Omega}' \Sigma_s(\hat{\Omega} \cdot \hat{\Omega}'). \qquad (4\text{-}126)$$

As an aside, it should be noted that one can easily calculate $\bar{\mu}_0$ for the case of elastic scattering from stationary nuclei when s-wave scattering is present. For then we know that in the CM system, $\sigma_{CM}(\theta_C) = \sigma_s/4\pi$. Hence if we use $\sigma_{CM}(\theta_C)d\hat{\Omega}_C = \sigma_L(\theta_L)d\hat{\Omega}_L$, we find

$$\bar{\mu}_0 = \frac{2\pi}{\Sigma_s} \int_0^\pi \sin\theta_C d\theta_C \cos\theta_L \Sigma_{CM}(\theta_C)$$

$$= \frac{1}{2} \int_0^\pi \sin\theta_C \cos\theta_L d\theta_C. \qquad (4\text{-}127)$$

But recall

$$\cos\theta_L = \frac{1 + A\cos\theta_C}{\sqrt{A^2 + 2A\cos\theta_C + 1}}. \qquad (4\text{-}128)$$

If we substitute this into Eq. (4-127) and perform the integration, we find the very simple result

$$\bar{\mu}_0 = \frac{2}{3A}. \qquad (4\text{-}129)$$

Now that we have justified the forms of Eqs. (4-121) and (4-122) let us consider how we might eliminate the annoying appearance of the third unknown, $\int d\hat{\Omega}\,\hat{\Omega}\hat{\Omega}\varphi(\mathbf{r},\hat{\Omega},t)$. We will accomplish this by assuming that the angular flux is only weakly dependent on angle. To be more specific, we will expand the angular flux in angle as

$$\varphi(\mathbf{r},\hat{\Omega},t) = \varphi_0(\mathbf{r},t) + \varphi_{1x}(\mathbf{r},t)\Omega_x + \varphi_{1y}(\mathbf{r},t)\Omega_y + \varphi_{1z}(\mathbf{r},t)\Omega_z + \cdots, \qquad (4\text{-}130)$$

and neglect all terms of higher than linear order in $\hat{\Omega}$. Actually a slightly different notation for the unknown functions $\varphi_0$, $\varphi_{1x}$, $\varphi_{1y}$, $\varphi_{1z}$ is useful. Write Eq. (4-130) as

$$\varphi(\mathbf{r},\hat{\Omega},t) \cong \frac{1}{4\pi}\phi + \frac{3}{4\pi}[J_x\Omega_x + J_y\Omega_y + J_z\Omega_z]$$

$$\cong \frac{1}{4\pi}\phi(\mathbf{r},t) + \frac{3}{4\pi}\mathbf{J}(\mathbf{r},t)\cdot\hat{\Omega}. \qquad (4\text{-}131)$$

Notice that we have labeled the unknown expansion coefficients as the flux and current. That this notation is perfectly consistent can be seen by noting from Eq. (4-131) that

$$\int_{4\pi} d\hat{\Omega}\,\varphi(\mathbf{r},\hat{\Omega},t) = \phi(\mathbf{r},t)\frac{1}{4\pi}\int_{4\pi} d\hat{\Omega} + \frac{3}{4\pi}\mathbf{J}(\mathbf{r},t)\cdot \int_{4\pi} d\hat{\Omega}\,\hat{\Omega} = \phi(\mathbf{r},t), \qquad (4\text{-}132)$$

and

$$\int_{4\pi} d\hat{\Omega}\,\hat{\Omega}\varphi(\mathbf{r},\hat{\Omega},t) = \phi(\mathbf{r},t)\frac{1}{4\pi}\int_{4\pi} d\hat{\Omega}\,\hat{\Omega} + \frac{3}{4\pi}\left[ J_x(\mathbf{r},t)\int_{4\pi} d\hat{\Omega}\,\Omega_x\hat{\Omega} \right.$$

$$\left. + J_y(\mathbf{r},t)\int_{4\pi} d\hat{\Omega}\,\Omega_y\hat{\Omega} + J_z(\mathbf{r},t)\int_{4\pi} d\hat{\Omega}\,\Omega_z\hat{\Omega} \right]. \qquad (4\text{-}133)$$

However one can easily demonstrate (see Problem 4-14) that the integral of the product of any two components of $\hat{\Omega}$ gives

$$\int_{4\pi} d\hat{\Omega}\,\Omega_i\Omega_j = \begin{cases} \dfrac{4\pi}{3} & i=j \\[2mm] 0 & i \neq j \end{cases} \quad i,j = x,y,z. \qquad (4\text{-}134)$$

Hence

$$\int_{4\pi} d\hat{\Omega}\,\hat{\Omega}\varphi(\mathbf{r},\hat{\Omega},t) = \mathbf{J}(\mathbf{r},t). \qquad (4\text{-}135)$$

Of course Eqs. (4-132) and (4-135) are identical to our original definitions of the flux and current earlier in Eqs. (4-17) and (4-19).

We will now use the approximate form of the angular flux in Eq. (4-131) to evaluate the second term in Eq. (4-122):

$$\nabla\cdot\int_{4\pi} d\hat{\Omega}\,\hat{\Omega}\hat{\Omega}\varphi(\mathbf{r},\hat{\Omega},t) = \nabla\cdot\int_{4\pi} d\hat{\Omega}\,\hat{\Omega}\hat{\Omega}\left[ \frac{1}{4\pi}\phi + \frac{3}{4\pi}\mathbf{J}\cdot\hat{\Omega} \right]. \qquad (4\text{-}136)$$

Next note that the integral of the product of any odd number of components of $\hat{\Omega}$ vanishes by symmetry:

$$\int_{4\pi} d\hat{\Omega}\,\Omega_x^l\Omega_y^m\Omega_z^n = 0 \quad \text{if } l, m, \text{ or } n \text{ is odd.} \qquad (4\text{-}137)$$

If we use both Eqs. (4-134) and Eq. (4-137) we can evaluate

$$\nabla\cdot\int_{4\pi} d\hat{\Omega}\,\hat{\Omega}\hat{\Omega}\varphi = \frac{1}{3}\nabla\phi(\mathbf{r},t). \qquad (4\text{-}138)$$

Hence by assuming that the angular flux depends only weakly on angle—more specifically, that the angular flux is only *linearly anisotropic*—we have managed to express the third unknown appearing in Eq. (4-122) in terms of the neutron flux $\phi(\mathbf{r},t)$. We have now achieved our goal of obtaining a closed set of two equations for two unknowns, $\phi(\mathbf{r},t)$ and $\mathbf{J}(\mathbf{r},t)$:

$$\frac{1}{v}\frac{\partial\phi}{\partial t} + \nabla\cdot\mathbf{J} + \Sigma_a(\mathbf{r})\phi(\mathbf{r},t) = S(\mathbf{r},t), \qquad (4\text{-}139)$$

$$\frac{1}{v}\frac{\partial\mathbf{J}}{\partial t} + \frac{1}{3}\nabla\phi + \Sigma_{tr}(\mathbf{r})\mathbf{J}(\mathbf{r},t) = \mathbf{S}_1(\mathbf{r},t). \qquad (4\text{-}140)$$

We have noted here that

$$\Sigma_a(\mathbf{r}) = \Sigma_t(\mathbf{r}) - \Sigma_s(\mathbf{r}), \qquad (4\text{-}141)$$

and defined the *macroscopic transport cross section*

$$\Sigma_{tr}(\mathbf{r}) = \Sigma_t(\mathbf{r}) - \bar{\mu}_0 \Sigma_s(\mathbf{r}). \tag{4-142}$$

(We will comment on this definition in a moment.) These two equations are known in nuclear reactor analysis as the $P_1$ *equations* (in the one-speed approximation) since the approximation of linearly anisotropic angular dependence in Eq. (4-131) in one-dimensional plane geometry is equivalent to expanding the angular flux in Legendre polynomials in $\mu = \cos\theta$ and retaining only the $l = 0$ and $l = 1$ terms

$$\varphi(x,\mu,t) = \phi(x,t)\tfrac{1}{2}P_0(\mu) + J(x,t)\tfrac{3}{2}P_1(\mu), \tag{4-143}$$

hence the name $P_1$ approximation. Notice that this could be easily generalized to obtain the $P_N$ *approximation*.

In principle we could now use the $P_1$ equations to describe the distribution of neutrons in a nuclear reactor. However it is customary to introduce two more approximations in order to simplify these equations even further. First we will assume that the neutron source term $s(\mathbf{r}, \hat{\Omega}, t)$ is isotropic. This implies, of course, that the source term $S_1(\mathbf{r}, t)$ vanishes in the equation for the current density. As we mentioned earlier, this approximation is usually of reasonable validity in nuclear reactor studies.

As our second approximation, we will assume that we can neglect the time derivative $v^{-1} \partial \mathbf{J}/\partial t$ in comparison with the remaining terms in Eq. (4-140). This would imply, for example, that

$$\frac{1}{|\mathbf{J}|} \frac{\partial |\mathbf{J}|}{\partial t} \ll v\Sigma_t, \tag{4-144}$$

that is, that the rate of time variation of the current density is much slower than the collision frequency $v\Sigma_t$. Since $v\Sigma_t$ is typically of order $10^5 \text{ sec}^{-1}$ or larger, only an extremely rapid time variation of the current would invalidate this assumption. We will later find that such rapid changes are very rarely encountered in reactor dynamics. Hence we are justified in rewriting Eq. (4-140) as

$$\frac{1}{3}\nabla\phi(\mathbf{r},t) + \Sigma_{tr}(\mathbf{r})\mathbf{J}(\mathbf{r},t) = 0. \tag{4-145}$$

We can solve Eq. (4-145) for the neutron current density in terms of the neutron flux

$$\mathbf{J}(\mathbf{r},t) = -\frac{1}{3\Sigma_{tr}(\mathbf{r})}\nabla\phi(\mathbf{r},t). \tag{4-146}$$

If we define the *neutron diffusion coefficient* $D$ by

$$D(\mathbf{r}) = [3\Sigma_{tr}(\mathbf{r})]^{-1} = [3(\Sigma_t - \bar{\mu}_0\Sigma_s)]^{-1}, \tag{4-147}$$

then we can rewrite Eq. (4-146) as

$$\mathbf{J}(\mathbf{r},t) = -D(\mathbf{r})\nabla\phi(\mathbf{r},t). \tag{4-148}$$

Hence we have found that in certain situations the neutron current density is proportional to the spatial gradient of the flux. This very important relation arises

quite frequently in other areas of physics where it is known as *Fick's law*. It is also occasionally referred to as the *diffusion approximation*.

Before we consider the physical implications of this relationship, let us use it to simplify the $P_1$ equations. If we substitute this into Eq. (4-139) we find

$$\frac{1}{v}\frac{\partial \phi}{\partial t} - \nabla \cdot D(\mathbf{r})\nabla \phi + \Sigma_a(\mathbf{r})\phi(\mathbf{r},t) = S(\mathbf{r},t). \tag{4-149}$$

This very important equation is known as the *one-speed neutron diffusion equation*, and it will play an extremely significant role in our further studies of nuclear reactors. We will discuss its solution in considerable detail in Chapter 5, and we will use it as the basis of a very simple but very useful model of nuclear reactor behavior.

Let us now return to consider the diffusion approximation [Eq. (4-148)] in more detail. Notice that it implies that a spatial variation in the neutron flux (or density) will give rise to a current of neutrons flowing from regions of high to low density. Physically this is understandable since the collision rate in high neutron density regions will be higher with the corresponding tendency for neutrons to scatter more frequently away toward lower densities. The rate at which such diffusion occurs
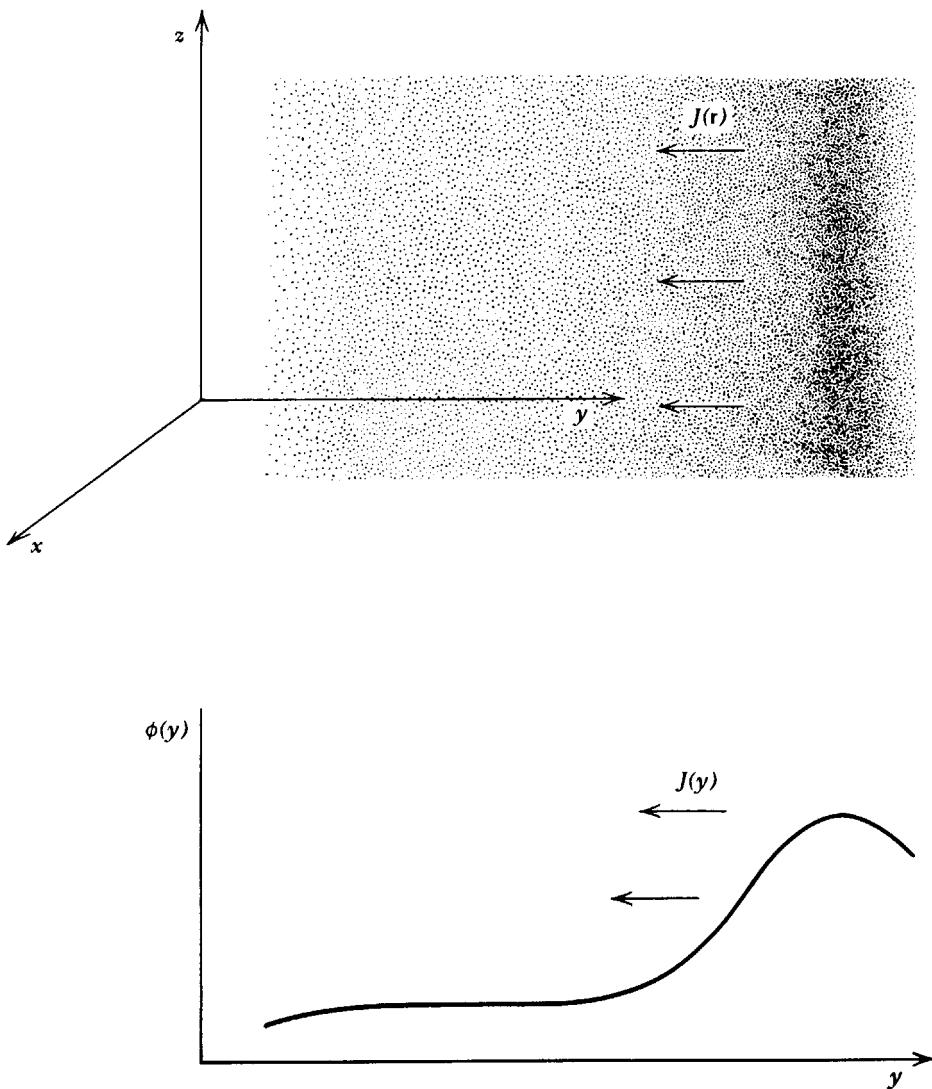


FIGURE 4-14. A schematic representation of Fick's law.

depends on the diffusion coefficient which, in turn, is inversely proportional to the transport cross section $\Sigma_{tr}$.

It is convenient to introduce the concept of a *transport mean free path*

$$\lambda_{tr} \equiv (\Sigma_{tr})^{-1} = (\Sigma_t - \bar{\mu}_0 \Sigma_s)^{-1}. \tag{4-150}$$

The transport mfp can be regarded as a corrected mfp accounting for anisotropies in the scattering collision process. Since $\bar{\mu}_0$ is almost always positive—that is, biased in the direction of *forward scattering*—the transport mfp $\lambda_{tr}$ will always be somewhat larger than the actual mfp, $\lambda = (\Sigma_t)^{-1}$. This essentially accounts for the fact that neutrons experiencing forward scattering tend to be transported somewhat further in a sequence of collisions than those being isotropically (or backward) scattered.

Hence since $D = \lambda_{tr}/3$, we see that diffusion is also enhanced in a material with pronounced forward scattering (e.g., hydrogen), although this of course also depends on the magnitude of the macroscopic cross sections.

It is important to keep in mind that the diffusion approximation is actually a consequence of four different approximations: (a) the angular flux can be adequately represented by only a linearly anisotropic angular dependence [Eq. (4-131)], (b) the one-speed approximation, (c) isotropic sources, and (d) the neutron current density changes slowly on a time scale compared to the mean collision time [Eq. (4-144)]. Actually only the first of these approximations is really crucial. The remaining approximations can be relaxed provided we are willing to work with the $P_1$ equations rather than the neutron diffusion equations (as one frequently is).

It is natural to ask when the angular flux is sufficiently weakly dependent on angle so that the diffusion approximation is valid. More detailed studies of the transport equation itself indicate that the assumption of weak angular dependence is violated in the following cases: (a) near boundaries or where material properties change dramatically from point to point over distances comparable to a mean free path, (b) near localized sources, and (c) in strongly absorbing media. In fact strong angular dependence can be associated with neutron fluxes having a strong spatial variation. Usually if one is over several mean free paths from any sources or boundaries in a weakly absorbing medium, the flux is slowly varying in space, and diffusion theory is valid.

## D. The Energy-Dependent Diffusion Equation

Let us now try to repeat this analysis for the case in which the neutron energy dependence is retained. Again we will approximate

$$\varphi(\mathbf{r}, E, \hat{\Omega}, t) \cong \frac{1}{4\pi} \phi(\mathbf{r}, E, t) + \frac{3}{4\pi} \mathbf{J}(\mathbf{r}, E, t) \cdot \hat{\Omega}, \tag{4-151}$$

so that we can evaluate

$$\nabla \cdot \int_{4\pi} d\hat{\Omega} \, \hat{\Omega}\hat{\Omega}\varphi(\mathbf{r}, E, \hat{\Omega}, t) \cong \frac{1}{3}\nabla\phi(\mathbf{r}, E, t). \tag{4-152}$$

If we now use this in the pair of Eqs. (4-79) and (4-91), we arrive immediately at

the *energy-dependent $P_1$ equations*

$$\frac{1}{v}\frac{\partial \phi}{\partial t}+\nabla\cdot\mathbf{J}+\Sigma_t(\mathbf{r},E)\phi(\mathbf{r},E,t)=\int_0^\infty dE'\,\Sigma_s(E'\to E)\phi(\mathbf{r},E',t)+S(\mathbf{r},E,t),\quad (4\text{-}153)$$

$$\frac{1}{v}\frac{\partial \mathbf{J}}{\partial t}+\frac{1}{3}\nabla\phi+\Sigma_t(\mathbf{r},E)\mathbf{J}(\mathbf{r},E,t)=\int_0^\infty dE'\,\Sigma_{s_1}(E'\to E)\mathbf{J}(\mathbf{r},E',t)+\mathbf{S}_1(\mathbf{r},E,t).$$

$$(4\text{-}154)$$

Continuing our analogy with the derivation of the one-speed diffusion equation, we will again assume: (a) isotropic source $\mathbf{S}_1\equiv 0$ (b) $|\mathbf{J}|^{-1}\partial|\mathbf{J}|/\partial t\ll v\Sigma_t(\mathbf{r},E)$ so that Eq. (4-154) can be rewritten as

$$\Sigma_t(\mathbf{r},E)\mathbf{J}(\mathbf{r},E,t)-\int_0^\infty dE'\,\Sigma_{s_1}(E'\to E)\mathbf{J}(\mathbf{r},E',t)=-\frac{1}{3}\nabla\phi(\mathbf{r},E,t).\quad (4\text{-}155)$$

However we can now see a problem that appears to prevent a straightforward generalization of Fick's law to include energy dependence. For we cannot bring $\mathbf{J}(\mathbf{r},E',t)$ out of the scattering integral since it depends on the integration variable $E'$.

Of course, if we were allowed to assume isotropic scattering in the LAB system, then $\Sigma_{s_1}(E'\to E)\equiv 0$ and we could find

$$\mathbf{J}(\mathbf{r},E,t)\cong-\frac{1}{3\Sigma_t(\mathbf{r},E)}\nabla\phi(\mathbf{r},E,t).\quad (4\text{-}156)$$

But the assumption of isotropic scattering is far too gross for most reactor calculations.

We could proceed formally by merely defining an energy-dependent diffusion coefficient

$$D(\mathbf{r},E)=\frac{1}{3}\left[\Sigma_t(\mathbf{r},E)-\frac{\int_0^\infty dE'\,\Sigma_{s_1}(E'\to E)J_i(\mathbf{r},E',t)}{J_i(\mathbf{r},E,t)}\right]^{-1},\quad (4\text{-}157)$$

which would automatically yield

$$\mathbf{J}(\mathbf{r},E,t)=-D(\mathbf{r},E)\nabla\phi(\mathbf{r},E,t).\quad (4\text{-}158)$$

Of course, this approach is highly artificial because as defined in Eq. (4-157) $D(\mathbf{r},E)$ still depends on $\mathbf{J}(\mathbf{r},E,t)$.

One common procedure for avoiding this difficulty is to neglect the anisotropic contribution to energy transfer in a scattering collision by setting

$$\Sigma_{s_1}(E'\to E)=\Sigma_{s_1}(E)\delta(E'-E)\quad (4\text{-}159)$$

so that

$$\int_0^\infty dE'\,\Sigma_{s_1}(E'\to E)J_i(\mathbf{r},E',t)=\bar{\mu}_0\Sigma_s(E)J_i(\mathbf{r},E,t).\quad (4\text{-}160)$$

Then we find a natural generalization of the diffusion coefficient:

$$D(\mathbf{r},E) = \frac{1}{3}[\Sigma_t(\mathbf{r},E) - \bar{\mu}_0 \Sigma_s(\mathbf{r},E)]^{-1}. \tag{4-161}$$

Actually none of these derivations of an energy-dependent diffusion equation are particularly satisfying because we have ignored the fact that in neutron transport processes, spatial transport, directional changes, and energy changes are intimately mixed. We can only provide a more satisfactory derivation of Eq. (4-158) after we have discussed comparable approximations characterizing neutron energy transfer in scattering collisions. Such a derivation must await our discussion of neutron slowing down in Chapter 8.

For the present, we will simply *assume* that the generalization of Fick's law to include energy-dependence is given by Eq. (4-158) with an energy dependent diffusion coefficient as defined by Eq. (4-161). If we now substitute this into Eq. (4-153), we arrive at the *energy-dependent diffusion equation*

$$\frac{1}{v}\frac{\partial \phi}{\partial t} - \nabla \cdot D(\mathbf{r},E)\nabla\phi + \Sigma_t(\mathbf{r},E)\phi(\mathbf{r},E,t)$$

$$= \int_0^\infty dE' \Sigma_s(E' \to E)\phi(\mathbf{r},E',t) + S(\mathbf{r},E,t). \tag{4-162}$$

This equation plays a very important role in nuclear reactor analysis since it is frequently taken as the starting point for the derivation of the multigroup diffusion equations. These latter equations represent the fundamental tool used in modern nuclear reactor analysis.

## E. Diffusion Theory Boundary Conditions

Since the neutron diffusion equation has derivatives in both space and time, it is apparent that one must assign suitable boundary and initial conditions to complete the specification of any particular problem. Since the diffusion equation itself is only an approximation to the more exact transport equation, we might suspect that we can use the transport theory boundary conditions as a guide in our development of appropriate diffusion boundary conditions. It will suffice to consider this development within the one-speed approximation.

Recall that the transport theory boundary conditions we discussed earlier were:

$$\text{Initial condition: } \varphi(\mathbf{r},\hat{\Omega},0) = \varphi_0(\mathbf{r},\hat{\Omega}), \tag{4-163}$$

$$\text{Boundary condition: } \varphi(\mathbf{r}_s,\hat{\Omega},t) = 0 \quad \text{for } \hat{\Omega}\cdot\hat{e}_s < 0, \text{ all } \mathbf{r}_s \text{ on } S. \tag{4-164}$$

We can obtain the appropriate initial condition for the diffusion equation by merely integrating the transport condition over angle to obtain:

$$\text{Initial condition: } \phi(\mathbf{r},0) = \phi_0(\mathbf{r}) \tag{4-165}$$

The boundary conditions are a bit harder to come by. Actually we will require several types of boundary condition, depending on the particular physical problem of interest. We will group these boundary conditions into one of several classes:

## 1. GENERAL MATHEMATICAL CONDITIONS ON THE FLUX

Although strictly speaking they are not boundary conditions, we should first mention those mathematical properties that the function $\phi(\mathbf{r}, t)$ must exhibit in order to represent a physically realizable neutron flux. For example, $\phi(\mathbf{r}, t)$ must be a real function. Furthermore since both the neutron speed $v$ and density $N$ cannot be negative, we must require that $\phi(\mathbf{r}, t)$ be greater than or equal to zero. In most cases we can also require that $\phi(\mathbf{r}, t)$ be bounded. However we should add here that one occasionally encounters pathological models of physical neutron sources that cause $\phi(\mathbf{r}, t)$ to diverge. An example would be the familiar point source. Another situation is the so-called *Milne problem*, in which one studies the behavior of the flux near a vacuum boundary fed by a source of infinite magnitude located at infinity. There will also be certain symmetry conditions that we can place on $\phi(\mathbf{r}, t)$ resulting from geometrical considerations, such as plane or axial symmetry. These conditions will become more understandable as we consider specific examples later in Chapter 5.

## 2. BOUNDARIES AT INTERFACES

Consider next an interface between two regions of differing cross sections. Now clearly the correct transport boundary condition is that

$$\varphi_1(\mathbf{r}_s, \hat{\Omega}, t) = \varphi_2(\mathbf{r}_s, \hat{\Omega}, t) \text{ for all } \hat{\Omega}, \tag{4-166}$$

where $\varphi_1$ is the angular flux in region 1, while $\varphi_2$ is the angular flux in region 2. This condition ensures conservation of neutrons across the boundary and can easily be derived directly from the transport equation.

Unfortunately we cannot satisfy this boundary condition exactly using diffusion theory. At best, we can only ensure that angular moments of Eq. (4-166) are satisfied. And since diffusion theory yields only the first two moments of the angular flux, $\phi(\mathbf{r}, t)$ and $\mathbf{J}(\mathbf{r}, t)$, at best we can demand

$$\int_{4\pi} d\hat{\Omega}\,\varphi_1(\mathbf{r}_s, \hat{\Omega}, t) = \int_{4\pi} d\hat{\Omega}\,\varphi_2(\mathbf{r}_s, \hat{\Omega}, t) \Rightarrow \phi_1(\mathbf{r}_s, t) = \phi_2(\mathbf{r}_s, t), \tag{4-167}$$
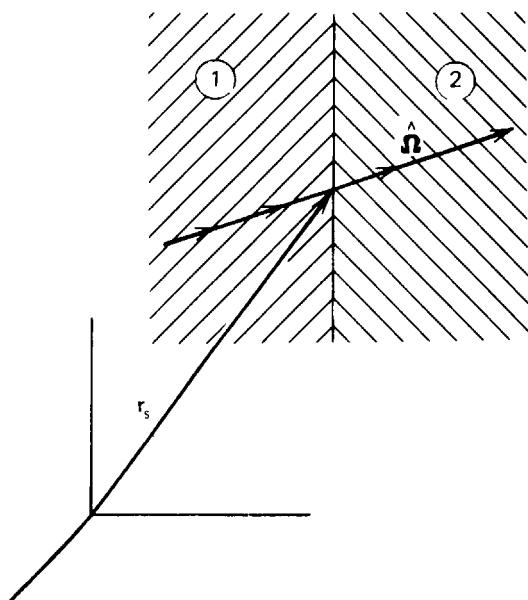


FIGURE 4-15. An interface boundary.

and

$$\int_{4\pi} d\hat{\Omega}\hat{\Omega}\varphi_1(\mathbf{r}_s,\hat{\Omega},t) = \int_{4\pi} d\hat{\Omega}\hat{\Omega}\varphi_2(\mathbf{r}_s,\hat{\Omega},t) \Rightarrow \mathbf{J}_1(\mathbf{r}_s,t) = \mathbf{J}_2(\mathbf{r}_s,t). \qquad (4\text{-}168)$$

Hence the interface diffusion theory boundary conditions are simply those corresponding to continuity of flux and current density across the interface:

$$\phi_1(\mathbf{r}_s,t) = \phi_2(\mathbf{r}_s,t)$$

$$-D_1\nabla\phi_1(\mathbf{r}_s,t) = -D_2\nabla\phi_2(\mathbf{r}_s,t). \qquad (4\text{-}169)$$

We will occasionally find it mathematically expedient to imagine an infinitestimally thin source of neutrons $S$ at an interface boundary. Then the interface boundary conditions are modified to read:

$$\phi_1(\mathbf{r}_s,t) = \phi_2(\mathbf{r}_s,t)$$

$$\hat{\mathbf{e}}_s \cdot \mathbf{J}_2(\mathbf{r}_s,t) - \hat{\mathbf{e}}_s \cdot \mathbf{J}_1(\mathbf{r}_s,t) = S(t), \qquad (4\text{-}170)$$

where $\hat{\mathbf{e}}_s$ is the unit normal to the surface.

## 3. VACUUM BOUNDARIES

Recall that our transport theory boundary condition was merely a mathematical statement that there could be no incoming neutrons at a free or vacuum boundary

$$\varphi(\mathbf{r}_s,\hat{\Omega},t) = 0 \qquad \begin{array}{l} \text{for } \hat{\Omega} \cdot d\mathbf{S} < 0, \\ \text{all } \mathbf{r}_s \text{ on } S. \end{array} \qquad (4\text{-}171)$$
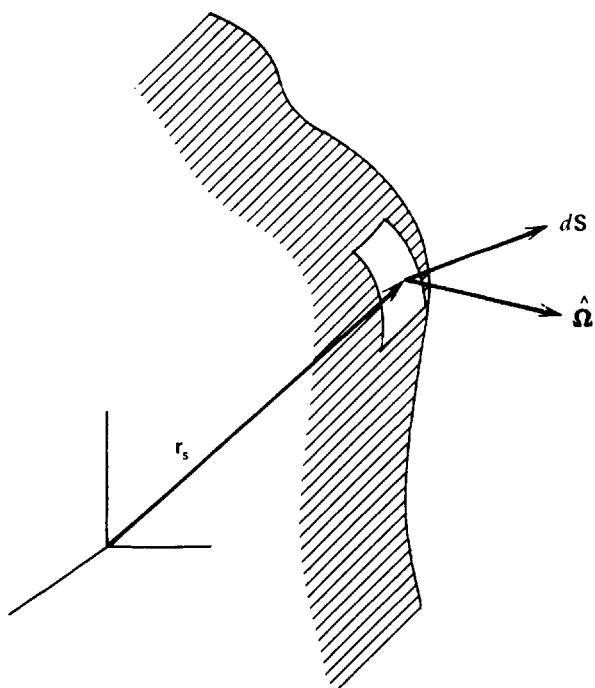


FIGURE 4-16.   A vacuum boundary.

Once again diffusion theory will only be able to approximate this boundary condition. Notice in particular that the boundary condition is given only over half of the range of solid angle (corresponding to incoming neutrons). Hence suppose we again seek to satisfy the transport boundary condition in an "integral" sense by demanding

$$\int_{2\pi^-} d\Omega \hat{e}_s \cdot \hat{\Omega}\varphi(r_s,\hat{\Omega},t) = \int_{2\pi^-} d\Omega \hat{e}_s \cdot j(r_s,\hat{\Omega},t) \equiv J_-(r_s,t) = 0. \qquad (4\text{-}172)$$

where we have recognized that this integral condition is equivalent to demanding that the inwardly directed partial current $J_-$ vanish on the boundary.

Unfortunately diffusion theory is capable of only approximating even this integral condition, since it cannot yield the exact form for $J_+$. Indeed if we use the $P_1$ approximation [(4-131)] for the angular flux, we find that the partial current densities $J_\pm$ are approximated in diffusion theory by

$$J_\pm(r,t) = \int_{2\pi^\pm} d\Omega \hat{e}_s \cdot \hat{\Omega}\varphi(r,\hat{\Omega},t) \cong \frac{1}{4}\phi(r,t) \mp \frac{D}{2}\hat{e}_s \cdot \nabla\phi(r,t). \qquad (4\text{-}173)$$

Hence our diffusion theory approximation to the transport boundary condition Eq. (4-171) is just

$$J_-(r_s,t) = \frac{1}{4}\phi(r_s,t) + \frac{D}{2}\hat{e}_s \cdot \nabla\phi(r_s,t) = 0. \qquad (4\text{-}174)$$

For convenience consider this boundary condition applied to a one-dimensional geometry with the boundary at $x = x_s$

$$J_-(x_s) = \frac{1}{4}\phi(x_s) + \frac{D}{2}\left.\frac{d\phi}{dx}\right|_{x_s} = 0$$

or

$$\frac{1}{\phi(x_s)}\left.\frac{d\phi}{dx}\right|_{x_s} = -\frac{1}{2D}. \qquad (4\text{-}175)$$

Notice that this relation implies that if we "extrapolated" the flux linearly beyond the boundary, it would vanish at a point

$$\tilde{x}_s \equiv x_s + 2D = x_s + \tfrac{2}{3}\lambda_{tr}. \qquad (4\text{-}176)$$

For this reason, one frequently replaces the vacuum boundary condition

$$J_-(x_s) = 0, \qquad (4\text{-}177)$$

by the slightly simpler condition

$$\phi(\tilde{x}_s) = 0, \qquad (4\text{-}178)$$

where $\tilde{x}_s$ is referred to as the "extrapolated" boundary. More advanced transport theory calculations of the extrapolated boundary indicate that one should choose

$$\tilde{x}_s = x_s + z_0, \qquad (4\text{-}179)$$
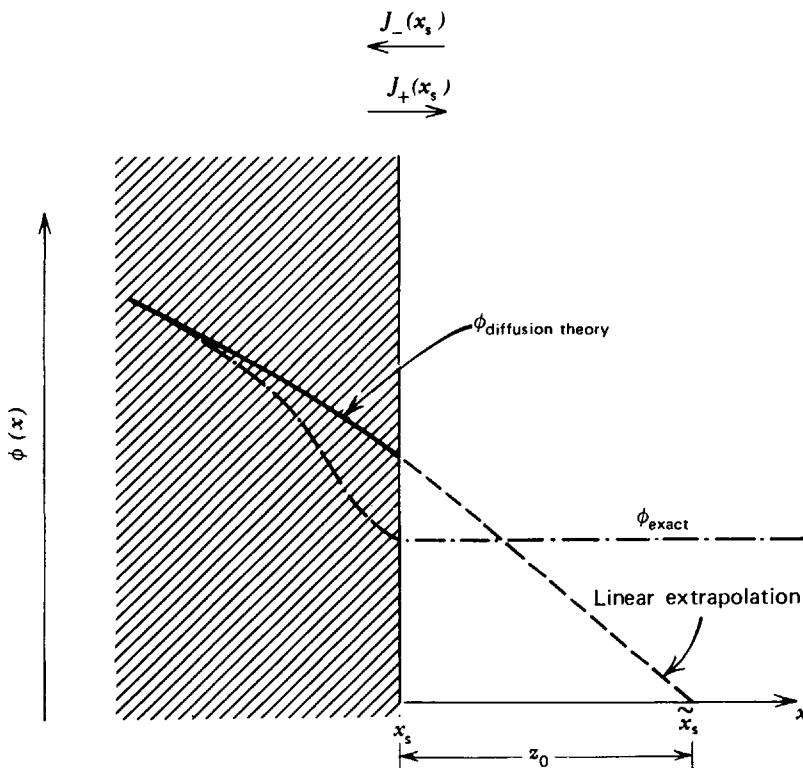
FIGURE 4-17. The behavior of approximate and exact representations of the neutron flux near a vacuum boundary.

where the "extrapolation length" $z_0$ for plane geometries is given by

$$z_0 = 0.7104\lambda_{tr}.$$ (4-180)

More complicated extrapolation length formulas can be derived for curved boundaries,[14] although they are rarely necessary since Eq. (4-180) suffices unless the radius of curvature of the boundary is comparable to a mean free path.

It should be remembered that the true flux does *not* vanish even outside the boundary. The diffusion theory flux is a poor representation of the true flux near the boundary (as we saw earlier, diffusion theory is not valid near a boundary). The boundary conditions we have derived are intended to yield the proper flux only in the *interior* of the reactor, that is, several mean free paths away from the reactor boundary.

These boundary conditions complete our description of neutron transport within the diffusion approximation. The neutron diffusion equation will play a very fundamental role in our development of nuclear reactor analysis methods. We will begin our study of nuclear reactor behavior using one-speed diffusion theory, since while this description has only limited quantitative validity, it does allow us to illustrate rather easily the principal concepts of nuclear reactor theory, as well as to develop the mathematical techniques used in more sophisticated models. With this background, we will then develop and apply the principal tool of the nuclear reactor designer, multigroup diffusion theory.

## REFERENCES

1. W. G. Vincenti and C. H. Kruger, Jr., *Introduction to Physical Gas Dynamics*, Wiley, New York (1965); K. Huang, *Statistical Mechanics*, Wiley, New York (1963).
2. P. F. Zweifel, *Reactor Physics*, McGraw-Hill, New York (1973).
3. A. M. Weinberg and E. P. Wigner, *The Physical Theory of Neutron Chain Reactors*, University of Chicago Press (1958).
4. G. I. Bell and S. Glasstone, *Nuclear Reactor Theory*, Van Nostrand, Princeton, N. J. (1970).
5. K. M. Case, F. de Hoffmann, and G. Placzek, *Introduction to the Theory of Neutron Diffusion*, Vol. I, Los Alamos Scientific Laboratory Report (1953).
6. K. M. Case and P. F. Zweifel, *Linear Transport Theory*, Addison-Wesley, Reading, Mass., (1967); B. Davison, *Neutron Transport Theory*, Oxford University Press, (1958).
7. E. Isaacson and H. B. Keller, *Analysis of Numerical Methods*, Wiley, New York (1966).
8. B. Carnahan, H. A. Luther, and J. O. Wilkes, *Applied Numerical Methods*, Wiley, New York (1969).
9. W. M. Stacey, Jr., *Modal Approximations: Theory and an Application to Reactor Physics*, M.I.T. Press, Cambridge (1967).
10. M. Becker, *The Principles and Applications of Variational Methods*, M.I.T. Press, Cambridge (1964).
11. G. I. Bell and S. Glasstone, *Nuclear Reactor Theory*, Van Nostrand, Princeton, N. J., (1970), pp. 214-249.
12. L. I. Schiff, *Quantum Mechanics*, 3rd Edition, McGraw-Hill, New York (1968).
13. A. Messiah, *Quantum Mechanics*, Vol. I., North-Holland, Amsterdam (1958).
14. *Reactor Physics Constants*, USAEC Document ANL-5800, 2nd Edition (1963).
15. K. D. Lathrop, *Reactor Technol.* 15, 107 (1972).

## PROBLEMS

4-1  We have defined the angular neutron density $n(\mathbf{r}, E, \hat{\Omega}, t)$ in terms of the neutron energy $E$ and the direction of motion $\hat{\Omega}$, but one could as well define an angular density that depends instead on the neutron velocity $\mathbf{v}$, $n(\mathbf{r}, \mathbf{v}, t)$. Calculate the relationship between these two dependent variables.

4-2  Two thermal neutron beams are injected from opposite directions into a thin sample of $^{235}U$. At a given point in the sample, the beam intensities are $10^{12}$ neutrons/cm²· sec from the left and $2 \times 10^{12}$ neutrons/cm²·sec from the right. Compute: (a) the neutron flux and current density at this point and (b) the fission reaction rate density at this point.

4-3  Suppose that the angular neutron density is given by

$$n(\mathbf{r}, \hat{\Omega}) = \frac{n_0}{4\pi}(1 - \cos\theta),$$

where $\theta$ is the angle between $\hat{\Omega}$ and the $z$-axis. If $A$ is the area perpendicular to the $z$-axis, then what is the number of neutrons passing through the area $A$ per second: (a) per unit solid angle at an angle of 45° with the $z$-axis, (b) from the negative $z$ to the positive $z$ direction, (c) net, and (d) total?

4-4  In a spherical thermal reactor of radius $R$, it is found that the angular neutron flux can be roughly described by

$$\phi(\mathbf{r}, E, \hat{\Omega}) = \frac{\phi_0}{4\pi} E \exp\left(-\frac{E}{kT}\right) \frac{\sin(\pi r/R)}{r}.$$

Compute the total number of neutrons in the reactor.

4-5 Demonstrate that in an isotropic flux, the partial current density in any direction is given by $J_+ = \phi/4$.

4-6 One of the principal assumptions made in the derivation of the neutron transport equation is that there are no external forces acting on the neutrons, that is, that the neutrons stream freely between collisions. Suppose we were to relax this assumption and consider such a force acting on the neutrons (say, a constant gravitational force in the z-direction). Then we might expect additional terms to appear that involve this force. Derive this more general transport equation.

4-7 Explain briefly whether or not the transport equation as we have derived it adequately describes the spatial and angular distribution of neutrons: (a) in a flux of the order of $100/\text{cm}^2 \cdot \text{sec}$, (b) scattering in a single crystal, (c) passing through a thin pure absorber, and (d) originating within a very intense nuclear explosion in which the explosion debris are moving outward with very high velocities.

4-8 Develop the particular form of the transport equation in spherical and cylindrical geometries. To simplify this calculation, utilize the one-speed form of the transport equation (4-100) in which time dependence has been ignored.

4-9 An interesting model of neutron transport involves transport in a one-dimensional rod. That is, the neutrons can move only to the left [say, described by an angular density $n_-(x,E,t)$] or to the right $[n_+(x,E,t)]$. One need only consider forward scattering events described by $\Sigma_s^+(E' \to E)$ or backward scattering events described by $\Sigma_s^-(E' \to E)$. Perform the following: (a) derive the transport equations for $n_+$ and $n_-$, (b) make the one-speed approximation in this set of equations, that is,

$$\Sigma_t(E) = \Sigma_a(E) + \Sigma_s^+(E) + \Sigma_s^-(E) = \Sigma_a + \Sigma_s^+ + \Sigma_s^-,$$

$$\Sigma_s^\pm(E' \to E) = \Sigma_s^\pm \delta(E' - E),$$

and (c) describe the boundary and initial conditions necessary to complete the specification of the problem if the rod is characterized by a length $L$.

4-10 Consider the following differential equation:

$$\frac{d^2f}{dx^2} + x^2 f(x) = 2x(4 - x),$$

where $f(x)$ is defined on the interval $0 \leqslant x \leqslant 4$. Discretize this equation by first breaking up the independent variable range into four segments of equal length. Next use a finite-difference approximation to the $d^2f/dx^2$ term to rewrite the differential equation as a set of algebraic equations for the discretized unknown $f(x_i) = f_i$. For convenience, assume boundary conditions such that $f(0) = 0 = f(4)$. Solve this set of equations for the $f_i$ and then plot this solution against $x$ using straight-line interpolation.

4-11 Consider the steady-state one-speed transport equation assuming isotropic scattering and sources in a one-dimensional plane geometry

$$\mu \frac{\partial \varphi}{\partial x} + \Sigma_t \varphi(x,\mu) = \frac{\Sigma_s}{2} \int_{-1}^{+1} d\mu' \varphi(x,\mu') + \frac{S(x)}{2}.$$

Expand the solution to this equation in the first two Legendre polynomials

$$\varphi(x,\mu) \cong \varphi_0(x)\tfrac{1}{2}P_0(\mu) + \varphi_1(x)\tfrac{3}{2}P_1(\mu),$$

$$P_0(\mu) = 1, \ P_1(\mu) = \mu.$$

Substitute this expansion into the transport equation, multiply by $P_0(\mu)$ and $P_1(\mu)$ respectively, and integrate over $\mu$ to obtain a set of equations for the unknown expansion coefficients $\varphi_0(x)$ and $\varphi_1(x)$. (These are just the $P_1$ equations.)

4-12 Use Simpson's rule to write a numerical quadrature formula for the angular integral $\int_{-1}^{+1} d\mu \varphi(x,\mu)$ for $N$ equal mesh intervals.

4-13 Develop the multigroup form of the transport equation as follows: First break the energy range $0 \leqslant E \leqslant 10$ MeV into $G$ intervals or groups. Now integrate each of the terms in the transport equation, Eq. (4-43), over the energies in a given group, say $E_g \leqslant E \leqslant E_{g-1}$. (Remember that the group indexing runs backwards such that $0 = E_G < E_{G-1} < \cdots E_g < E_{g-1} < \cdots E_1 < E_0 = 10$ MeV.) Now by defining the *group fluxes* as the integral of the flux over each group, and the cross sections characterizing each group as in Eq. (4-69), determine the set of $G$ equations representing the transport equation.

4-14 By writing out the components of the direction unit vector $\hat{\Omega}$ in polar coordinates, demonstrate explicitly that

$$\int_{4\pi} d\hat{\Omega}\, \Omega_i = 0 \quad \text{and} \quad \int_{4\pi} d\hat{\Omega}\, \Omega_i \Omega_j = \begin{cases} \dfrac{4\pi}{3} & i = j \\ 0 & i \neq j \end{cases}.$$

4-15 Demonstrate that $\int_{4\pi} d\hat{\Omega}\, \Omega_x^l \Omega_y^m \Omega_z^n = 0$ if $l$, $m$, or $n$ is odd.

4-16 Verify Eq. (4-138) using the identity in Problem 4-15.

4-17 Explicitly demonstrate by integration that $\bar{\mu}_0 = 2/3A$ for elastic scattering from stationary nuclei when such scattering is assumed to be isotropic in the CM system.

4-18 Consider an isotropic point source emitting $S_0$ monoenergetic neutrons per second in an infinite medium. Assume that the medium is characterized by an absorption cross section $\Sigma_a$, but only by negligible scattering. Determine the rate at which neutron absorptions occur per unit volume at any point in the medium.

4-19 Compute the neutron flux resulting from a plane source emitting neutrons isotropically at the origin of an infinite absorbing medium. Hint: Just represent the plane source as a superposition of point sources.

4-20 In a laser-induced thermonuclear fusion reaction, a tiny pellet is imploded to super high densities such that it ignites in a thermonuclear burn. In such a reaction some $10^{17}$ 14 MeV neutrons will be emitted essentially instantaneously (within $10^{-11}$ sec). Compute the neutron flux at a distance of 1 m from the reaction as a function of time, assuming that the chamber in which the reaction occurs is evacuated.

4-23 Compute the thermal neutron diffusion coefficients characterizing water, graphite, and natural uranium. Then compute the extrapolation length $z_0$ characterizing these materials.

4-24 Assuming that the diffusion approximation [Eq. (4-131)] is valid, compute the partial current densities in the $z$ direction defined by Eq. (4-22). Use the one-speed approximation.

4-25 Consider the time-dependent one-speed $P_1$ equations assuming isotropic sources and plane symmetry. Eliminate the current density $J(x,t)$ to obtain one equation for the neutron flux $\phi(x,t)$. Compare this equation with the one-speed neutron diffusion equation and indicate what differences you might expect in solutions to the two equations.

4-26 Try to construct solutions to the one-speed transport equation in an infinite sourceless medium:

$$\mu \frac{\partial \varphi}{\partial x} + \Sigma_t \varphi(x,\mu) = \frac{\Sigma_s}{2} \int_{-1}^{+1} d\mu' \, \varphi(x,\mu')$$

by seeking solutions of the form $\varphi(x,\mu) = \chi(\mu) \exp(-x/\nu)$ where $\nu$ and $\chi(\mu)$ are to be determined.

4-27 Consider the time-independent one-speed transport equation under the assumption of isotropic sources and scattering

$$\hat{\Omega} \cdot \nabla \varphi + \Sigma_t \phi(\mathbf{r}, \hat{\Omega}) = \frac{\Sigma_s}{4\pi} \int_{4\pi} d\hat{\Omega}' \varphi(\mathbf{r}, \hat{\Omega}') + \frac{S(\mathbf{r})}{4\pi} .$$

By regarding the right-hand side of this equation as an effective source, use the result [Eq. (4-120)] to derive an integral equation for the neutron flux $\phi(\mathbf{r})$.

# 5

## The One-Speed
## Diffusion Theory Model

In this chapter we will develop the one-speed diffusion model of neutron transport. This model plays an extremely important role in reactor theory since it is sufficiently simple to allow detailed calculations and also sufficiently realistic to allow us to study many of the more important concepts arising in nuclear reactor analysis. Of course any model characterizing all of the neutrons in a reactor by a single speed (or energy) and treating their transport from point to point as a diffusion process cannot be expected to yield accurate quantitative estimates. Nevertheless if the cross sections appearing in this theory are properly chosen, one can use the one-speed diffusion model to make preliminary design estimates. Moreover many of the mathematical techniques we will use to solve and analyze this model are in fact identical to those applied to the more sophisticated models (e.g., multigroup diffusion theory) used in modern nuclear reactor design.

The rigorous mathematical derivation of the one-speed diffusion model from the neutron transport equation has been given in Chapter 4. In this chapter we will give a more heuristic physical derivation of the one-speed diffusion equation and then apply this equation to study nuclear reactor behavior. The solution of the diffusion equation draws upon many familiar topics from a field that has become known as mathematical physics, including methods for solving boundary value problems involving both ordinary and partial differential equations.[1-3] For most problems of practical interest in nuclear reactor studies, one must employ methods from numerical analysis as well to allow the solution of the diffusion equation on a high-speed computer. We would expect that many of these topics (e.g., separation of variables methods in the solution of partial differential equations or Gaussian elimination for solving systems of algebraic equations) are already quite familiar to the advanced undergraduate. However we will continue our effort to make this

presentation as self-contained as possible by briefly reviewing such methods when they arise (although numerous references will also be provided). Throughout this development we would again caution the reader to avoid letting the smokescreen generated by these various mathematical techniques obscure the fundamental physical concepts governing the behavior of the neutron population in the reactor.

# I. THE ONE-SPEED DIFFUSION EQUATION

## A. Derivation of the Diffusion Equation

We will suppress the neutron energy dependence by assuming that all of the neutrons can be characterized by a single kinetic energy. Such a *one-speed* (or *one-group*) *approximation* greatly simplifies the mathematical study of nuclear reactor behavior. Of course such an approximation is also highly suspect, particularly in light of the fact that neutron energies typically encountered in a reactor span a range from $10^{-3}$ to $10^7$ eV, and neutron cross sections depend sensitively on energy over most of this range. We will later be able to show, surprisingly enough, that if one regards the one-speed approximation as an average description and chooses the appropriate average cross sections, then in fact the one-speed model can actually be used to obtain a quantitative description of a nuclear reactor.

As yet a further justification for our exhaustive study of the one-speed approximation, we would remark that most energy-dependent theories (e.g., multigroup diffusion theory) are solved by performing a sequence of one-speed calculations for each successive energy group. Hence the methods we develop for analyzing our one-speed model will later be extended directly to more sophisticated descriptions.

We will characterize the neutron distribution in the reactor by the neutron density $N(\mathbf{r},t)$ which gives the number of neutrons per unit volume at a position $\mathbf{r}$ at time $t$. Actually we will find it more convenient to work with the neutron flux, $\phi(\mathbf{r},t) = vN(\mathbf{r},t)$, since then we can compute the rate at which various types of neutron–nuclear reactions occur per unit volume by merely multiplying the flux by the corresponding macroscopic cross section. For example, the rate at which fission reactions occur per cm$^3$ at a point $\mathbf{r}$ would be given by $\Sigma_f(\mathbf{r})\phi(\mathbf{r},t)$.

We will derive an equation for the neutron flux by merely writing down a mathematical statement of the fact that the time rate of change of the number of neutrons in a given volume must be simply the difference between the rate at which neutrons are produced in the volume and the rate at which they are lost from the volume due to absorption or leakage.
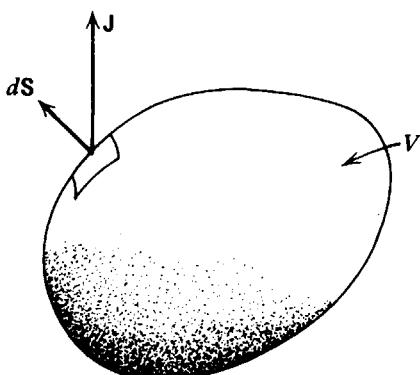


FIGURE 5-1. A control volume for monitoring neutron balance.

To be more precise, consider an arbitrary volume $V$ of surface area $S$ located anywhere within the reactor. We will examine this "control" volume carefully to determine how the neutron population within it changes. Evidently the total number of neutrons in $V$ at a time $t$ can be obtained by simply integrating over the volume

$$\int_V d^3r\, N(\mathbf{r},t) = \int_V d^3r\, \frac{1}{v}\phi(\mathbf{r},t). \tag{5-1}$$

Hence the time rate of change of the number of neutrons in $V$ must be just

$$\frac{d}{dt}\left[\int_V d^3r\, \frac{1}{v}\phi(\mathbf{r},t)\right] = \int_V d^3r\, \frac{1}{v}\frac{\partial\phi}{\partial t}$$

$$= \text{Production in } V - \text{absorption in } V$$

$$- \text{net leakage from } V. \tag{5-2}$$

We can easily write down mathematical expressions for the gain and loss terms. If we define a neutron source density $S(\mathbf{r},t)$, then

$$\text{Production in } V = \int_V d^3r\, S(\mathbf{r},t). \tag{5-3}$$

Since the absorption rate density at any point in $V$ is just $\Sigma_a(\mathbf{r})\,\phi(\mathbf{r},t)$, it is obvious that the total rate of neutron loss due to absorption in $V$ is just

$$\text{Absorption in } V = \int_V d^3r\, \Sigma_a(\mathbf{r})\,\phi(\mathbf{r},t). \tag{5-4}$$

The term describing neutron leakage out of or into $V$ is a bit more difficult. If $\mathbf{J}(\mathbf{r},t)$ is the neutron current density, then the net rate at which neutrons pass out through a small surface element $d\mathbf{S}$ at position $\mathbf{r}_s$ is $\mathbf{J}(\mathbf{r}_s,t)\cdot d\mathbf{S}$. Hence the total net leakage through the surface of $V$ is just

$$\text{Net leakage from } V = \int_S d\mathbf{S}\cdot\mathbf{J}(\mathbf{r},t). \tag{5-5}$$

Now we could combine all of these terms back into Eq. (5-2) as they stand, but first it is convenient to convert Eq. (5-5) into a volume integral similar to the other terms. The common way to convert such surface integrals into volume integrals is to use Gauss's theorem to write

$$\int_S d\mathbf{S}\cdot\mathbf{J}(\mathbf{r},t) = \int_V d^3r\, \nabla\cdot\mathbf{J}(\mathbf{r},t). \tag{5-6}$$

If we now substitute each of these mathematical expressions into Eq. (5-2), we find

$$\int_V d^3r\left[\frac{1}{v}\frac{\partial\phi}{\partial t} - S + \Sigma_a\phi + \nabla\cdot\mathbf{J}\right] = 0. \tag{5-7}$$

But recall that we chose our volume $V$ to be arbitrary. That is, Eq. (5-7) must hold for any volume $V$ that we would care to examine. However the only way this can occur is if the integrand itself were to vanish. Hence we find we must require

$$\frac{1}{v}\frac{\partial \phi}{\partial t} = -\nabla \cdot \mathbf{J} - \Sigma_a \phi + S. \tag{5-8}$$

Of course this equation is still quite exact (aside from the one-speed approximation), but it is also quite formal since it contains two unknowns, $\phi(\mathbf{r}, t)$ and $\mathbf{J}(\mathbf{r}, t)$. To proceed further, we need yet another relationship between these two variables. Unfortunately there is no exact relationship between $\phi(\mathbf{r}, t)$ and $\mathbf{J}(\mathbf{r}, t)$. One must resort to an approximate relation. Now it is well known from other fields of physics such as gaseous diffusion that the current density is approximately proportional to the negative spatial gradient of the density, or in our case, the flux. That is, particles will tend to flow from regions of high to low density at a rate proportional to the negative density gradient. Stated mathematically, one finds that

$$\mathbf{J}(\mathbf{r}, t) \cong -D(\mathbf{r})\nabla\phi(\mathbf{r}, t), \tag{5-9}$$

where the constant of proportionality $D(\mathbf{r})$ is known as the *diffusion coefficient*, while Eq. (5-9) is referred to as *Fick's law*. Of course to postulate such a relationship between current density and flux implies nothing about its range of validity. Indeed we do not even know what the diffusion coefficient $D$ is. This situation is very common in macroscopic descriptions of physics, and relationships such as Eq. (5-9) are usually referred to as "transport laws" (not to be confused with the transport equation—we are talking the language of the physicist now) while the proportionality coefficients are known as "transport coefficients." Examples are numerous and include Fourier's law of thermal conduction (thermal conductivity), Stokes' law of viscosity (shear viscosity), Ohm's law (electrical resistivity), to name only a few. In all cases, one is forced to go to a microscopic description in order to evaluate the transport coefficient and examine the range of validity of the transport law.

However this is of course exactly what we did by deriving the *diffusion approximation* [Eq. (5-9)] from the neutron transport equation in Chapter 4. There we found that

$$D = (3\Sigma_{tr})^{-1} = [3(\Sigma_t - \bar{\mu}_0\Sigma_s)]^{-1}, \tag{5-10}$$

where $\bar{\mu}_0$ is the average cosine of the scattering angle in a neutron scattering collision. Furthermore, we found that Eq. (5-9) was valid provided it was used to describe the neutron flux several mfp away from the boundaries or isolated sources, the medium was only weakly absorbing, and provided the neutron current was changing slowly on a time scale comparable to the mean time between neutron–nuclei collisions. It is important to keep these limitations in mind as we apply this approximation in nuclear reactor analysis.

Henceforth we will accept the diffusion approximation [Eq. (5-9)] as providing a valid expression for the neutron current density in terms of the neutron flux. If we substitute Eq. (5-9) into Eq. (5-8), we arrive at the *one-speed neutron diffusion*

*equation*

$$\frac{1}{v} \frac{\partial \phi}{\partial t} = \nabla \cdot D(\mathbf{r}) \nabla \phi - \Sigma_a(\mathbf{r}) \phi(\mathbf{r}, t) + S(\mathbf{r}, t). \tag{5-11}$$

This equation will form the basis of much of our further development of nuclear reactor theory.

## B. Initial and Boundary Conditions

We must augment this equation with suitable initial and boundary conditions. Although these conditions have been developed in a more rigorous fashion from neutron transport theory in Chapter 4, we will remotivate them here using plausible physical arguments.

The appropriate initial condition involves specifying the neutron flux $\phi(\mathbf{r}, t)$ for all positions $\mathbf{r}$ at the initial time, say $t = 0$:

$$\text{Initial condition: } \phi(\mathbf{r}, 0) = \phi_0(\mathbf{r}), \quad \text{all } \mathbf{r}. \tag{5-12}$$

The boundary conditions are a bit more complicated and depend on the type of physical system we are studying. The principal types of boundary conditions we will utilize include the following:

### 1. VACUUM BOUNDARY

At the outside boundary of a reactor, one would like to construct a boundary condition corresponding to the fact that no neutrons can enter the reactor through this surface from outside. Implicit in this fact is the assumption that the reactor is surrounded by an infinitely large vacuous region. Of course no reactor is surrounded by a vacuum, but rather by air, concrete, and a host of other materials. It is frequently convenient to assume that the reflection of neutrons back into the reactor from such materials is negligible so that nonreentrant boundary conditions apply.

There is only one problem; diffusion theory is incapable of exactly representing a nonreentrant boundary condition. The closest one can come would be to demand that the inwardly directed partial current

$$J_-(\mathbf{r}_s) = \frac{1}{4} \phi(\mathbf{r}_s) + \frac{D(\mathbf{r}_s)}{2} \hat{\mathbf{e}}_s \cdot \nabla \phi(\mathbf{r}_s) \tag{5-13}$$

vanish on the boundary (clearly an approximation, since this expression for $J_-$ already is approximate). Actually we really shouldn't worry much about a consistent free surface boundary condition within the diffusion approximation, for we have already indicated that diffusion theory is not valid near the boundary anyway. It can only be expected to hold several mfp inside the boundary.

Hence what we should really look for is a "fudged-up" boundary condition which, although it may have little physical relevance at the boundary, does in fact yield the correct neutron flux deep within the reactor where diffusion theory is valid. More detailed transport theory studies indicate that the proper boundary

condition to choose is one in which the diffusion theory flux $\phi(r, t)$ vanishes at a distance

$$z_0 = 0.7104\lambda_{tr} \tag{5-14}$$

outside of the actual boundary of the reactor. This *extrapolated boundary* is usually denoted symbolically with a tilde. For instance, if the physical surface is at $r_s$, then the flux will be taken to vanish on the extrapolated boundary $\phi(\tilde{r}_s, t) = 0$.

A side comment here is appropriate. For most reactor materials, $\lambda_{tr}$ is quite small, usually being of the order of several centimeters or less. When it is recognized that most reactor cores are quite large (several meters in diameter), then it is understandable that one frequently ignores the extrapolation length $z_0$ and simply assumes the flux vanishes on the true boundary.

Furthermore few realistic reactor geometries are surrounded by a free surface. Rather they are surrounded by coolant flow channels or plenums, structural materials, thermal shields or such. Hence while the concept of a free surface is useful pedagogically for painting a picture of an idealized reactor geometry surrounded by a vacuum of infinite extent, it is rarely employed in modern nuclear reactor analysis.

## 2. INTERFACES (MATERIAL DISCONTINUITIES)

The structure of a nuclear reactor core is extremely complex, containing regions of fuel, structural material, coolant, control elements, and so on. Hence while one rarely encounters situations in which the material cross sections $\Sigma(r)$ depend continuously on position, one frequently is faced with what might be termed "sectionally uniform" cross sections that change abruptly across an interface separating regions of differing material composition. Our usual procedure in treating such discontinuities in material properties will be to solve the diffusion equation in each region separately and then attempt to match these solutions at the interface using appropriate boundary conditions.

Once again the diffusion equation is not strictly valid within several mfp of the interface. However in this case one can argue that conservation of neutron transport across the interface demands continuity of both the normal component of the neutron current density $J(r, t)$ and the neutron flux $\phi(r, t)$.

This condition is occasionally modified to account for the physically fictitious but mathematically expedient convenience of including an infinitesimally thin neutron absorber or source at the interface. Then while the neutron flux is still continuous across the interface, the normal component of the current experiences a jump:

$$\hat{e}_s \cdot [J(r_s^+) - J(r_s^-)] = S, \tag{5-15}$$

where $\hat{e}_s$ is the interface surface normal, while $S$ would represent a source term (if positive) or an absorption term (if negative). (See Figure 4-15.)

## 3. OTHER TYPES OF BOUNDARY CONDITIONS

It is frequently convenient to impose other types of boundary conditions upon the neutron flux. For example, we know the flux must be nonnegative, real, and finite. Actually in our mathematical modeling of neutron sources we will

occasionally encounter a situation in which the neutron flux becomes singular at a localized source (e.g., a point source). However since such sources are mathematical idealizations, this singular behavior doesn't bother us, and in general we will demand that the flux be finite away from such sources. This condition is particularly useful in geometries in which certain dimensions are infinite.

We will also occasionally be able to use symmetry properties to discard physically irrelevant solutions of the diffusion equation. For example, in one-dimensional slab geometries, we can choose the coordinate origin at the centerline of the slab, and then use symmetry to eliminate solutions with odd parity [i.e., $\phi(-x) = -\phi(x)$].

Other types of boundary conditions are encountered in practice. A very common problem in reactor calculations involves the determination of the flux in a small subregion of the reactor fuel lattice, a so-called *unit cell* repeated throughout the lattice. For example, such a cell might contain a single fuel rod surrounded by coolant (a *fuel cell*) or several fuel assemblies along with a control element (a *control cell*). Since these unit cells are repeated in a regular fashion throughout the core lattice, one can argue that there should be no net transfer of neutrons between cells, that is, that the neutron current density $\mathbf{J}(\mathbf{r})$ vanish on the cell boundaries. This is an example of a boundary condition on the current. In such cell calculations it is also frequently necessary to obtain a diffusion theory solution in the vicinity of a strong absorber (e.g., a fuel rod or control element). The appropriate boundary condition at the interface between the diffusing medium and the absorber is handled much like that characterizing a free surface. That is, one uses a transport-corrected boundary condition on the flux or current to yield the proper diffusion theory solution at a distance of several mfp from the interface. We will
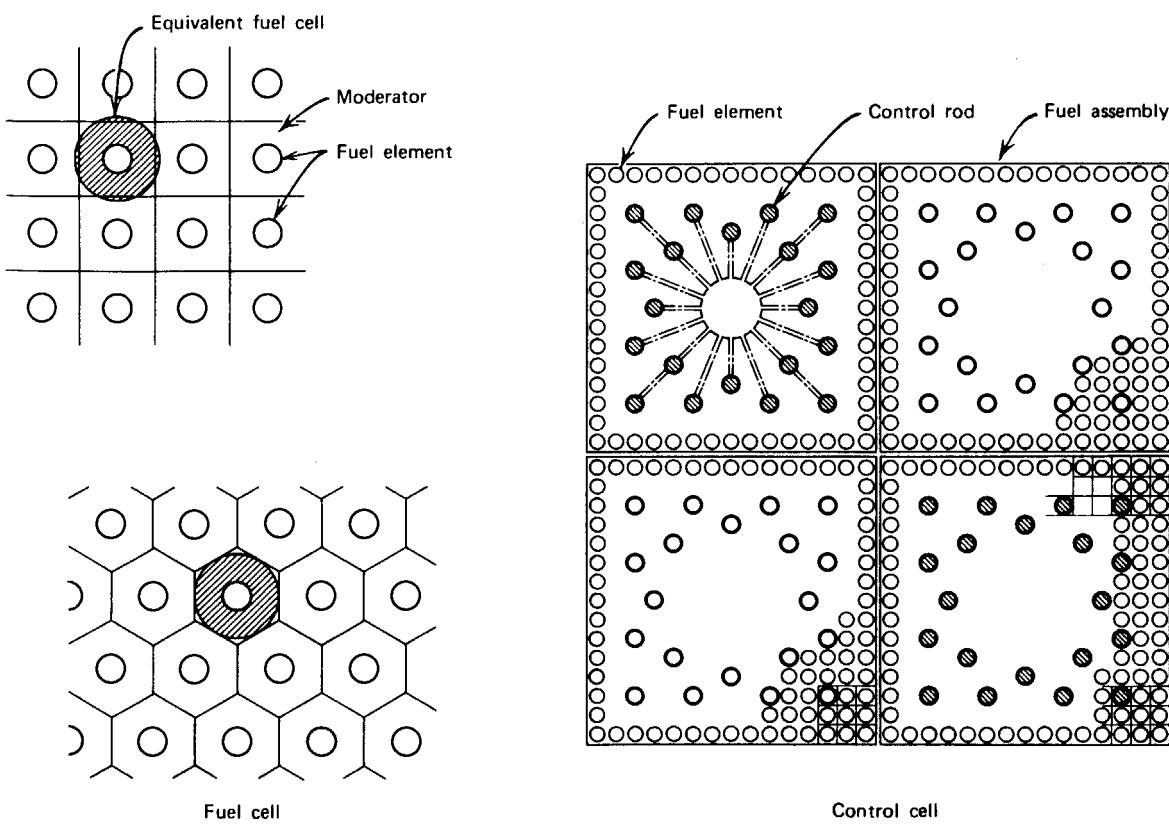


FIGURE 5-2.   Typical unit fuel and control cells.

give explicit examples of such boundary conditions when we consider cell calculations in Chapter 10.

We should reemphasize that the application of neutron diffusion theory in reactor analysis is successful in large part because the diffusion equation and its boundary conditions have been modified using more exact transport theory corrections. For example, $D = [3(\Sigma_t - \bar{\mu}_0 \Sigma_s)]^{-1}$ contains a correction to account for anisotropic scattering. Furthermore the boundary conditions on the flux or current at a free surface or adjacent to a highly absorbing region contain transport corrections to yield the proper neutron flux deeper within the diffusing region. Such transport corrections frequently yield diffusion theory estimates that are far more accurate than one would normally expect, especially when we recall the rather strong approximations required to derive the neutron diffusion equation.

## C. A Summary of the One-Speed Diffusion Model

To summarize then, the model we will initially use to describe the neutron population in a nuclear reactor consists of the neutron diffusion equation:

$$\frac{1}{v} \frac{\partial \phi}{\partial t} - \nabla \cdot D(\mathbf{r}) \nabla \phi + \Sigma_a(\mathbf{r}) \phi(\mathbf{r}, t) = S(\mathbf{r}, t) \tag{5-16}$$

along with suitable initial conditions:

$$\phi(\mathbf{r}, 0) = \phi_0(\mathbf{r}), \quad \text{all } \mathbf{r} \tag{5-17}$$

and boundary conditions:

(a) Free surface: $\phi(\tilde{\mathbf{r}}_s, t) = 0$ [or $J_-(\mathbf{r}_s, t) = 0$]
(b) Interface: $\phi$ and normal component of $\mathbf{J}$ continuous across interface, (5-18)
(c) $0 \leqslant \phi(\mathbf{r}, t) < \infty$ (except in the neighborhood of localized sources).

Here the diffusion coefficient $D = \lambda_{tr}/3 = [3(\Sigma_t - \bar{\mu}_0 \Sigma_s)]^{-1}$ while the extrapolation length characterizing a free surface boundary condition is $z_0 = 0.7104 \, \lambda_{tr}$.

The neutron diffusion equation [Eq. (5-16)] may be classified as an example of a linear partial differential equation of the *parabolic* type.[4] This type of equation has been thoroughly studied by mathematicians and physicists alike for years, since it also describes processes such as heat condition, gas diffusion, and even a wave function (notice, if we stick an "$i$" in front of the time derivative, we have essentially just the Schrödinger equation familiar from quantum mechanics). As we proceed to apply this equation to nuclear reactor analysis, we will review several of the more popular schemes available for solving such equations.

In many cases we will deal with situations for which the medium in which the neutrons are diffusing is uniform or homogeneous such that $D$ and $\Sigma_a$ do not depend on position. Then the one-speed diffusion equation simplifies to

$$\frac{1}{v} \frac{\partial \phi}{\partial t} - D \nabla^2 \phi + \Sigma_a \phi(\mathbf{r}, t) = S(\mathbf{r}, t). \tag{5-19}$$

The explicit form taken by this equation will depend on the specific coordinate system in which we choose to express the spatial variable $\mathbf{r}$. For convenience, we have included the explicit forms taken by the *Laplacian operator*, $\nabla^2$, in the more common coordinate systems in Appendix B.[5]

We will frequently consider situations in which the flux is not a function of time. Then Eq. (5-19) becomes

$$- D \nabla^2 \phi(\mathbf{r}) + \Sigma_a \phi(\mathbf{r}) = S(\mathbf{r}).$$ (5-20)

This equation is known as the *Helmholtz equation* and is also a very familiar beast in mathematical physics. It is useful to divide by $- D$ to rewrite Eq. (5-20) as

$$\nabla^2 \phi(\mathbf{r}) - \frac{1}{L^2} \phi(\mathbf{r}) = - \frac{S(\mathbf{r})}{D}$$ (5-21)

where we have defined the *neutron diffusion length* $L$

$$L \equiv \sqrt{D/\Sigma_a} \ .$$ (5-22)

We will later find that $L$ is essentially a measure of how far the neutrons will diffuse from a source before they are absorbed.

We now turn our attention to the application of this model to some important problems in nuclear reactor theory. We will first study neutron diffusion in "nonmultiplying" media—that is, media containing no fissile material. Then we will turn to the study of the neutron flux in fissile material and begin our investigation of nuclear reactor core physics.

## II. NEUTRON DIFFUSION IN NONMULTIPLYING MEDIA

We will first apply Eq. (5-20) to study the diffusion of neutrons from a steady-state source in a nonmultiplying medium. All of the mathematical techniques we will use are standard methods which arise in the solution of ordinary or partial differential equation boundary value problems and are discussed in any text on mathematical physics or applied mathematics.[1-3]

### A. Elementary Solutions of the Diffusion Equation

#### 1. PLANE SOURCE IN AN INFINITE MEDIUM

Perhaps the simplest problem in neutron diffusion theory is that of an infinitely wide plane source located at the origin of an infinite, homogeneous medium. The source is assumed to be emitting neutrons isotropically at a rate of $S_0$ neutrons/cm$^2$·sec. Since both the source plane and the medium are of infinite extent, the neutron flux $\phi(\mathbf{r}) \rightarrow \phi(x)$ can only be a function of the distance $x$ from the source plane. Hence the diffusion equation [Eq. (5-21)] reduces to the one-dimensional form

$$\frac{d^2 \phi}{dx^2} - \frac{1}{L^2} \phi(x) = - \frac{S(x)}{D} = - \frac{S_0}{D} \delta(x)$$ (5-23)

where we have mathematically modeled the source by a Dirac $\delta$-function. Hence we just have an inhomogeneous ordinary differential equation to solve with a
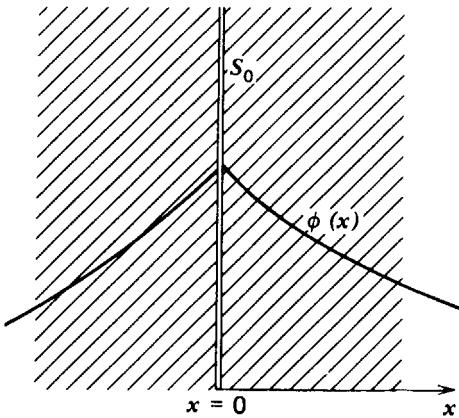
FIGURE 5-3. A plane source of neutrons in a infinite medium.

slightly weird source. Note that if we restrict $x \neq 0$, the source term disappears from Eq. (5-23):

$$\frac{d^2\phi}{dx^2} - \frac{1}{L^2}\phi(x) = 0, \qquad x \neq 0. \qquad (5\text{-}24)$$

Our approach will be to solve this homogeneous equation for $x \neq 0$, and then use a boundary condition at $x = 0$ to "fix up" these solutions.

We could obtain this boundary condition directly by integrating Eq. (5-23) from $x = 0 - \epsilon$ to $x = 0 + \epsilon$ across the source plane and then taking the limit as $\epsilon \to 0$ to find

$$-D\frac{d\phi}{dx}\bigg|_{+\epsilon} + D\frac{d\phi}{dx}\bigg|_{-\epsilon} = J_x(0^+) - J_x(0^-) = S_0. \qquad (5\text{-}25)$$

[See Problem 5-2]. However we might also merely note that this is just a special case of the more general interface boundary condition [Eq. (5-15)]. If we use the symmetry of the geometry to assert that $J_x(0^+) = -J_x(0^-) \equiv J(0)$, then our boundary condition at the source plane becomes just

$$\lim_{x \to 0^+} J(x) = \frac{S_0}{2}. \qquad (5\text{-}26)$$

This source boundary condition makes sense physically, since it merely says that the net neutron current at the origin on either side must be just half of the total source strength.

We are not through with boundary conditions yet. Since we have a second-order derivative, $d^2/dx^2$, we need another boundary condition. We will use the boundary condition of finite flux as $x \to \infty$.

Hence the mathematical problem to be solved is

$$\frac{d^2\phi}{dx^2} - \frac{1}{L^2}\phi(x) = 0, \qquad x > 0,$$

with boundary conditions:

$$\text{(a)} \qquad \lim_{x \to 0^+} -D\frac{d\phi}{dx} = \frac{S_0}{2}$$

$$\text{(b)} \qquad \lim_{x \to \infty} \phi(x) < \infty. \qquad (5\text{-}27)$$

We will then use symmetry to infer the solution for $x < 0$.

To solve this equation, we note the general solution

$$\phi(x) = A \exp\left(-\frac{x}{L}\right) + B \exp\left(\frac{x}{L}\right). \tag{5-28}$$

Applying the boundary conditions, we find

$$(b) \Rightarrow B = 0$$

$$(a) \Rightarrow \lim_{x \to 0} - D\left(-\frac{A}{L} \exp\left(-\frac{x}{L}\right)\right) = \frac{AD}{L} = \frac{S_0}{2}$$

or

$$A = \frac{S_0 L}{2D}.$$

Hence our solution is

$$\phi(x) = \frac{S_0 L}{2D} \exp\left(-\frac{x}{L}\right), \quad x > 0, \tag{5-29}$$

and by symmetry we can infer

$$\phi(x) = \frac{S_0 L}{2D} \exp\left(\frac{x}{L}\right), \quad x < 0. \tag{5-30}$$

Hence the neutron flux falls off exponentially as one moves away from the source plane with a characteristic decay length of $L$. As one might expect, the larger $L$ (i.e., the smaller $\Sigma_a$), the less the neutron flux is attenuated as we move into the medium. Notice also that the magnitude of the flux is proportional to the source. That is, doubling the source strength will double the neutron flux $\phi(x)$ at any position $x$, but this should have been anticipated since the neutron diffusion equation is linear and hence the principle of superposition holds.

The reader should be reminded that, while this solution may provide a reasonable description of the neutron flux in a medium (provided it is not too highly absorbing), it is certainly not valid within several mfp of the source plane itself. Indeed more accurate transport theory studies[6,7] indicate that the neutron flux does not look at all exponential near the source. In fact there are additional components to the solution. Fortunately if absorption is not too strong, these transport theory "transients" rapidly diminish as one moves several mfp away from the source plane, and the simple exponential behavior predicted by diffusion theory is found, with one mild modification. Transport theory predicts that the "relaxation length" characterizing the exponential decay is not $L = (D/\Sigma_a)^{1/2}$, but rather is given by the root of the transcendental expression

$$\frac{\Sigma_s L}{2} \ln\left[\frac{\Sigma_t L + 1}{\Sigma_t L - 1}\right] = \frac{1 + 3L^2 \Sigma_s \Sigma_a \bar{\mu}_0}{1 + 3L^2 \Sigma_t \Sigma_a \bar{\mu}_0}. \tag{5-31}$$

Fortunately if $\Sigma_a \ll \Sigma_t$ (as it must be for diffusion theory to be valid), one can
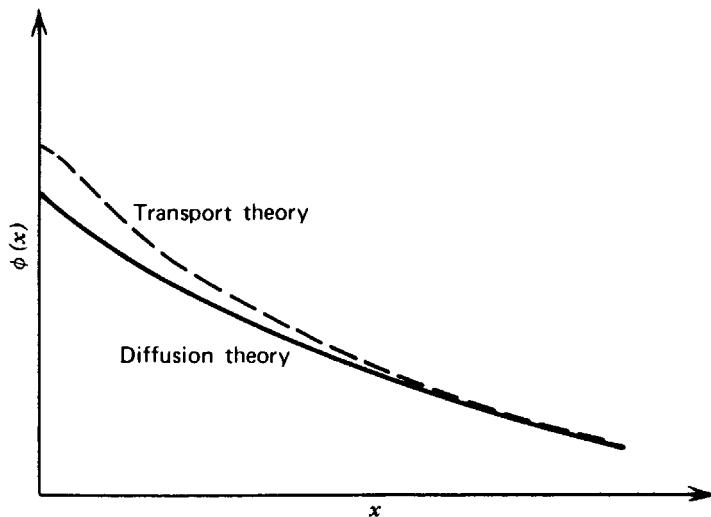
**FIGURE 5-4.** A comparison between the diffusion theory and transport theory solutions of the plane source problem.

expand Eq. (5-31) to find

$$L = \frac{1}{\sqrt{3\Sigma_{tr}\Sigma_a}} \left[ 1 + \frac{2}{5}\left(\frac{\Sigma_a}{\Sigma_t}\right) + 0\left(\frac{\Sigma_a}{\Sigma_t}\right)^2 \right]. \tag{5-32}$$

For example, in graphite $\Sigma_t = .385$ cm$^{-1}$ while $\Sigma_a = .00032$. Hence $\Sigma_a/\Sigma_t = 8.3 \times 10^{-4}$, which implies that the correction to $L$ given by higher terms in this expansion (that is, by transport theory) is only about 0.03% in this material.

## 2. POINT SOURCE IN AN INFINITE MEDIUM

As a variation on this theme, let us repeat this calculation for the case of an isotropic point source emitting $S_0$ neutrons/sec at the origin of an infinite medium. Since the source is isotropic, there can be no dependence of the neutron flux on angle. Hence the diffusion equation in spherical coordinates reduces to

$$\frac{1}{r^2}\frac{d}{dr}r^2\frac{d\phi}{dr} - \frac{1}{L^2}\phi(r) = 0, \qquad r > 0. \tag{5-33}$$

We will use our previous problem as a guide, and seek solutions such that the boundary conditions are

(a)     $\lim_{r \to 0} 4\pi r^2 J(r) = S_0$,

(b)     $\lim_{r \to \infty} \phi(r) < \infty$.

One can readily verify that the fundamental solutions to Eq. (5-33) are of the form $r^{-1}\exp(\pm r/L)$; hence we are led to seek

$$\phi(r) = A\frac{\exp(-r/L)}{r} + B\frac{\exp(r/L)}{r}. \tag{5-34}$$

Applying the boundary conditions, we find that (b) implies that we choose $B = 0$,

while (a) implies that $A = S_0/4\pi D$. Hence the solution is

$$\phi(r) = \frac{S_0 \exp(-r/L)}{4\pi r D} . \tag{5-35}$$

An interesting application of this result is to calculate the mean-square distance to absorption in a nonmultiplying medium. Note the number of neutrons absorbed between $r$ and $r + dr$ is just

$$\left( \frac{S_0 \exp(-r/L)}{4\pi r D} \right)(4\pi r^2 dr)(\Sigma_a) \tag{5-36}$$

and thus the probability that the neutron is absorbed in $dr$ is just

$$p(r)dr = \frac{r}{L^2} \exp\left(-\frac{r}{L}\right) dr. \tag{5-37}$$

We can then calculate

$$\langle r^2 \rangle = \int_0^\infty dr\, r^2 p(r) = 6L^2. \tag{5-38}$$

Hence the neutron-diffusion length $L$ has the interesting physical interpretation as being $1/\sqrt{6}$ of the root mean square (rms) distance to absorption

$$L^2 = \frac{1}{6} \langle r^2 \rangle . \tag{5-39}$$

That is, $L$ measures the distance to which the neutron will diffuse (on the average) away from the source before it is absorbed. It should be stressed that we have calculated the rms distance from the source to the point of absorption, not the total path length traveled by the neutron. This path length will be very much longer since the neutron suffers a great many scattering collisions before it is finally absorbed. For example, in graphite the thermal diffusion length is 59 cm. Hence the rms distance to absorption from a point source is $(\langle r^2 \rangle)^{1/2} = \sqrt{6}\, L = 144$ cm. If we recall that the mfp characterizing thermal neutrons in graphite is 2.5 cm and also recall that the average number of scattering collisions suffered by the neutron before absorption is 1500, then it is apparent that the average path length or track length traveled by the neutron is about 3700 cm, considerably larger than $\sqrt{6}\, L$.

One can actually use Eq. (5-39) to define the neutron diffusion length in situations in which diffusion theory would not apply (e.g., strongly anisotropic scattering or large absorption). Then one would first determine the flux $\phi(r)$ resulting from an isotropic point source using transport theory (or whatever description is relevant) and then calculate $L$ by using

$$L^2 = \frac{1}{6} \langle r^2 \rangle = \frac{\int d^3r\, r^2 \phi(\mathbf{r})}{\int d^3r\, \phi(\mathbf{r})} , \tag{5-40}$$

where the integral is taken over all space.

The cylindrical geometry problem of a line source at the origin of an infinite medium can be worked out in a very similar way. However to do so here would "deprive" the reader of an opportunity to try his own hand at such diffusion theory problems. Hence we have left the line source as an exercise in the problem set at the end of the chapter. We will instead turn our attention to problems in finite geometries.

## 3. FINITE SLAB GEOMETRIES

Let us now modify our isotropic plane source by assuming that it is imbedded at the center of a slab of nonmultiplying material of width $a$ surrounded on both sides by a vacuum (see Figure 5-5). We will set up this problem in a manner very similar to that for infinite plane geometry, except that we will add vacuum boundary conditions on either end of the slab.

$$\frac{d^2\phi}{dx^2} - \frac{1}{L^2}\phi(x) = 0, \qquad x \neq 0,$$

with boundary conditions:

(a)     $$\lim_{x \to 0^\pm} -D\frac{d\phi}{dx} = \frac{S_0}{2},$$

(b)     $$\phi\left(\pm\frac{\tilde{a}}{2}\right) = 0.$$

(5-41)

Here we have replaced the boundary condition at infinity by the vacuum boundary condition—in this case, using an extrapolated boundary $\tilde{a}/2 = a/2 + z_0$. If we again seek a general solution of the form of Eq. (5-28), then applying the boundary condition (b) implies

$$\phi\left(\frac{\tilde{a}}{2}\right) = 0 = A\exp\left(-\frac{\tilde{a}}{2L}\right) + B\exp\left(\frac{\tilde{a}}{2L}\right) \Rightarrow B = -A\exp\left(-\frac{\tilde{a}}{L}\right).$$
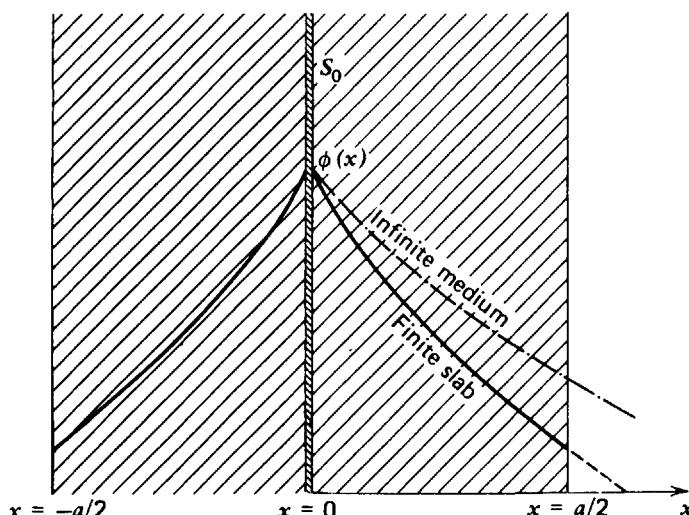


**FIGURE 5-5.** A plane source at the origin of a finite slab.

Then boundary condition (a) implies

$$A = \frac{SL}{2D}\left(1+\exp\left(-\frac{\tilde{a}}{L}\right)\right)^{-1}.$$

Our final solution is therefore

$$\phi(x) = \frac{SL}{2D} \frac{\exp\left(-\frac{x}{L}\right) - \exp\left(\frac{-(\tilde{a}-x)}{L}\right)}{1+\exp\left(-\frac{\tilde{a}}{L}\right)} = \frac{SL}{2D} \frac{\sinh\left[\frac{(\tilde{a}-2|x|)}{2L}\right]}{\cosh\left(\frac{\tilde{a}}{2L}\right)}. \qquad (5\text{-}42)$$

This solution is sketched in Figure 5-5. It looks somewhat similar to the infinite medium result [Eq. (5-29)], except for dropping off more rapidly near the boundaries due to neutron leakage. We should caution the reader once again that the solution is not valid within several mfp of the vacuum boundary (just as it is not valid near the source plane at the origin).

A variant on the above problem involves replacing the vacuum by a material of different composition than the slab itself (as sketched in Figure 5-6). The general procedure for attacking such multiregion problems is to seek solutions of the diffusion equation characterizing each region, and then match these solutions using interface boundary conditions. Once again we can use geometrical symmetry to allow us to restrict our attention to the range $0 < x < \infty$.

In region ① we will seek a solution of

$$\frac{d^2\phi_1}{dx^2} - \frac{1}{L_1^2}\phi_1(x) = 0, \qquad 0 < x < \frac{a}{2} \qquad (5\text{-}43)$$

where $L_1 = \sqrt{D_1/\Sigma_{a_1}}$ is the diffusion length characterizing region ①. Similarly in region ②

$$\frac{d^2\phi_2}{dx^2} - \frac{1}{L_2^2}\phi_2(x) = 0, \qquad \frac{a}{2} < x < \infty.$$
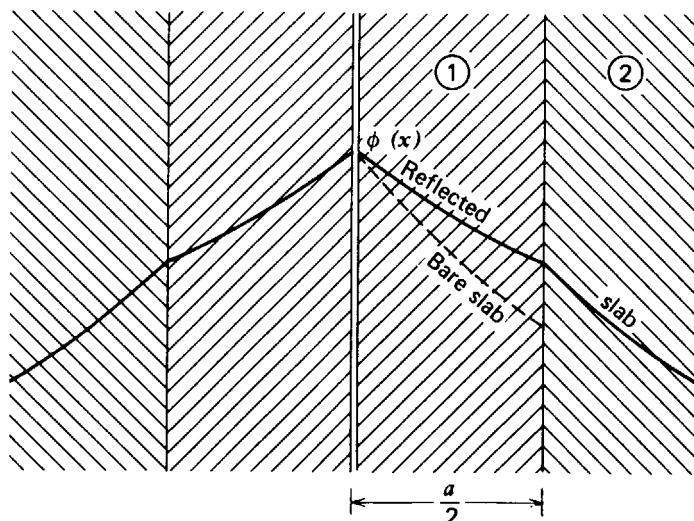


FIGURE 5-6.   A multiregion or reflected slab.

Now we will need several boundary conditions. We can use our earlier conditions [Eq. (5-27)]

(a) $\lim\limits_{x \to 0^+} J_1(x) = \dfrac{S_0}{2}$

(b) $\phi_2(x) < \infty$    as    $x \to \infty$.

In addition we will use the interface conditions

(c) $\phi_1\left(\dfrac{a}{2}\right) = \phi_2\left(\dfrac{a}{2}\right)$

(d) $J_1\left(\dfrac{a}{2}\right) = J_2\left(\dfrac{a}{2}\right)$   or   $-D_1 \dfrac{d\phi_1}{dx}\bigg|_{\frac{a}{2}} = -D_2 \dfrac{d\phi_2}{dx}\bigg|_{\frac{a}{2}}$.

Using our earlier work as a guide, we can seek general solutions

$$\phi_1(x) = A_1 \cosh \dfrac{x}{L_1} + B_1 \sinh \dfrac{x}{L_1} \qquad \text{in region } \textcircled{1}$$

$$\phi_2(x) = A_2 \exp\left(-\dfrac{x}{L_2}\right) + B_2 \exp\left(\dfrac{x}{L_2}\right) \qquad \text{in region } \textcircled{2}$$

and apply the boundary conditions to find (after a bit of algebra)

$$B_2 = 0, \qquad B_1 = -\dfrac{SL_1}{2D_1},$$

$$A_1 = \dfrac{SL_1}{2D_1} \dfrac{D_1 L_2 \cosh\left(\dfrac{a}{2L_1}\right) + D_2 L_1 \sinh\left(\dfrac{a}{2L_1}\right)}{D_2 L_1 \cosh\left(\dfrac{a}{2L_2}\right) + D_1 L_2 \sinh\left(\dfrac{a}{2L_1}\right)}, \qquad (5\text{-}44)$$

$$A_2 = \dfrac{SL_1 L_2}{2} \dfrac{\exp\left(\dfrac{a}{2L_2}\right)}{D_2 L_1 \cosh\left(\dfrac{a}{2L_2}\right) + D_1 L_2 \sinh\left(\dfrac{a}{2L_1}\right)}.$$

We have sketched the form of this solution in Figure 5-6. Several features of this solution are of some interest. Note that while the neutron flux is continuous across the interface, the derivative of the flux is not. This later discontinuity is, of course, a consequence of the fact that the diffusion coefficients in the two regions differ; hence to obtain continuity of *current J*, we must allow a jump in $d\phi/dx$ across the interface.

We have compared the solution for this problem with that obtained earlier for the slab surrounded by a vacuum. It should be noted that the flux in the central region falls off somewhat more slowly when the vacuum is replaced by a diffusing material. This can be readily understood by noting that the material surrounding the slab will tend to scatter neutrons back into the slab that would have otherwise

been lost to the vacuum. Such materials used to reduce neutron leakage are known as *reflectors*. Any material with a large scattering cross section and low absorption cross section would make a suitable neutron reflector. For example, the water channels surrounding LWR cores act as reflectors. In the HTGR, graphite blocks are added to the top and bottom of the reactor core to serve as neutron reflectors.

A concept very closely related to that of neutron reflectors is the *reflection coefficient* or *albedo*, defined as the ratio between the current out of the reflecting region to the current into the reflecting region:

$$\alpha \equiv \frac{J_{out}}{J_{in}} . \tag{5-45}$$

To make this concept more precise, suppose we want to attach a reflecting slab of thickness $a$ to a reactor core (or perhaps a medium with a neutron source in it such as the slab geometry we have just considered). If we are given a current density $J_{in} = J_+$ entering the reflecting slab surface, which we locate at $x = 0$ (see Figure 5-7) for convenience, then we can solve the diffusion equation characterizing the reflecting region:

$$\frac{d^2\phi}{dx^2} - \frac{1}{L^2}\phi(x) = 0, \qquad 0 < x < a \tag{5-46}$$

subject to boundary conditions $J_+(0) = J_{in}$, $\phi(\tilde{a}) = 0$. We can then solve for the flux $\phi(x)$ in the reflecting slab and use this solution to compute the albedo $\alpha$ as (see Problem 5-11):

$$\alpha = \frac{1 - \left(\frac{2D}{L}\right)\coth\left(\frac{a}{L}\right)}{1 + \left(\frac{2D}{L}\right)\coth\left(\frac{a}{L}\right)} . \tag{5-47}$$

It is of interest to plot the albedo for the slab reflector versus slab thickness as shown in Figure 5-8. For thin reflectors, very few of the neutrons are reflected and hence the albedo is small. As the reflector becomes very thick, the albedo
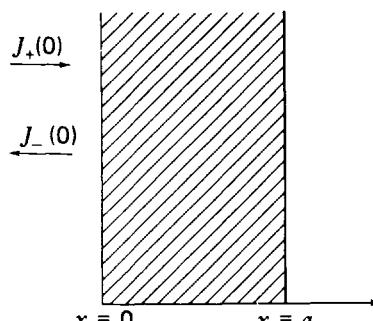


FIGURE 5-7. The albedo problem.
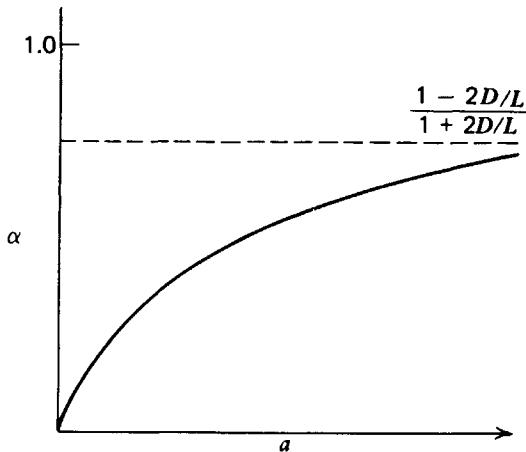
**FIGURE 5-8.** The albedo for a finite slab plotted versus slab thickness.

approaches an asymptotic limit dependent only upon the material properties $D$ and $L$:

$$\alpha \rightarrow \alpha_\infty = \frac{1 - \dfrac{2D}{L}}{1 + \dfrac{2D}{L}}. \tag{5-48}$$

For example, the albedos characterizing infinitely thick reflectors of graphite, $H_2O$, and $D_2O$ are 0.93, 0.82, and 0.97 respectively.

The albedo can be used to replace the detailed solution in the reflecting region by an equivalent boundary condition at the edge of the core using Eq. (5-45). That is, if we use our earlier definitions of the partial current densities $J_\pm$, then the effective boundary condition on the flux in the region $x < 0$ is just

$$\frac{1}{\phi} D \frac{d\phi}{dx} \bigg|_{x=0} = -\frac{1}{2} \left( \frac{1 - \alpha}{1 + \alpha} \right). \tag{5-49}$$

Used in this manner, the albedo becomes a very useful device for obtaining boundary conditions for reactor core calculations.

One can continue this game of solving the diffusion equation in various one-dimensional geometries indefinitely. As we mentioned earlier, it is simply an exercise in ordinary differential equations. A variety of two- and three-dimensional problems can also be studied. However since these latter problems involve partial differential equations, we will defer their treatment until after we have introduced the separation of variables approach for solving such equations in Section 5-III-C. If we really want to get masochistic, we can remove some of the symmetry in our earlier problems so that the original partial differential equation (5-20) would have to be solved directly—for example, a point source set off-center in a sphere. However there is very little in the way of new physics to be learned from such exercises. Hence we will bypass further examples in favor of moving directly to more general problems. In particular, we will study how our previous solutions for plane and point sources can be used to determine the neutron flux resulting from an arbitrary distribution of neutron sources.

## 4. GENERAL DIFFUSION PROBLEMS

Recall that the neutron flux resulting from an isotropic point source of strength $S_0$ located at the origin of an infinite medium was found to be

$$\phi(\mathbf{r}) = \frac{S_0 \exp\left(-\dfrac{r}{L}\right)}{4\pi r D} \, . \tag{5-50}$$

Suppose this source was located at the point $\mathbf{r}'$ instead. Then the flux could be found by a simple coordinate translation as

$$\phi(\mathbf{r}) = S_0 \frac{\exp\left(-\dfrac{|\mathbf{r}-\mathbf{r}'|}{L}\right)}{4\pi D |\mathbf{r}-\mathbf{r}'|} \, . \tag{5-51}$$

Next suppose we have several point sources at positions $\mathbf{r}'_i$, each of strength $S_i$. Then we can use the fact that the diffusion equation is linear to invoke the principle of superposition and write

$$\phi(\mathbf{r}) = \sum_i \frac{S_i \exp\left(-\dfrac{|\mathbf{r}-\mathbf{r}'_i|}{L}\right)}{4\pi D |\mathbf{r}-\mathbf{r}'_i|} \, . \tag{5-52}$$



Single point source

Several point sources

Distributed source
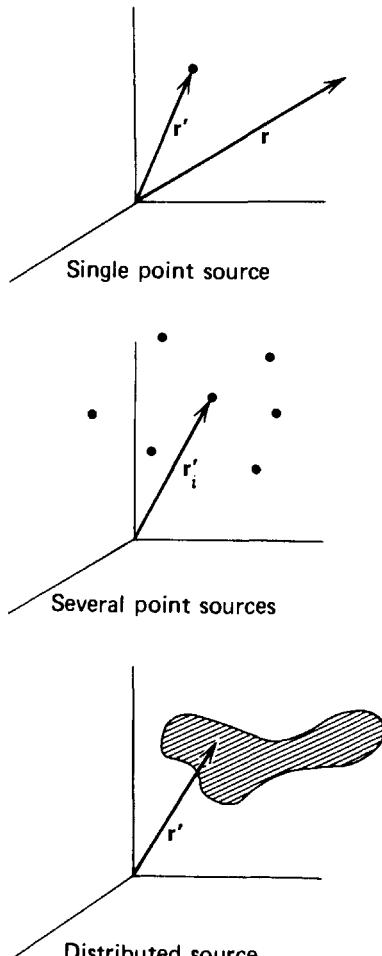
FIGURE 5-9.    Superposition of several point sources.

Finally suppose we have an arbitrary distribution of sources characterized by a source density $S(\mathbf{r})$. Then the flux resulting from this distributed source is just

$$\phi(\mathbf{r}) = \int d^3r' \frac{\exp\left(-\dfrac{|\mathbf{r}-\mathbf{r}'|}{L}\right)}{4\pi D |\mathbf{r}-\mathbf{r}'|} S(\mathbf{r}'). \tag{5-53}$$

This is frequently rewritten as

$$\phi(\mathbf{r}) = \int d^3r' \, G_{\text{pt}}(\mathbf{r},\mathbf{r}') S(\mathbf{r}'), \tag{5-54}$$

where

$$G_{\text{pt}}(\mathbf{r},\mathbf{r}') \equiv \frac{\exp\left(-\dfrac{|\mathbf{r}-\mathbf{r}'|}{L}\right)}{4\pi D |\mathbf{r}-\mathbf{r}'|} \tag{5-55}$$

is known as the *point diffusion kernel for an infinite medium*. [The expression *kernel*[8] is a mathematical term used to denote a function of several variables (including the variables of integration) in an integral of the form

$$\int dx' \, K(x,x') f(x'). \tag{5-56}$$

Here $K(x,x')$ would be the known kernel, while $f(x)$ might either be known [as the source density $S(\mathbf{r})$] or unknown as the flux $\varphi$ in the inscattering term of the transport equation

$$\int_{4\pi} d\hat{\Omega}' \int_0^\infty dE' \, \Sigma_s(E' \to E, \hat{\Omega}' \to \hat{\Omega}) \varphi(\mathbf{r}, E', \hat{\Omega}', t) \tag{5-57}$$

where $\Sigma_s(E' \to E, \hat{\Omega}' \to \hat{\Omega})$ is known as the *scattering kernel*.]

As a second example of such kernels, consider the flux resulting from a plane source at the origin

$$\phi(x) = \frac{SL}{2D} \exp\left(-\frac{|x|}{L}\right). \tag{5-58}$$

If this had been located at $x'$, then the flux at a position $x$ would be

$$\phi(x) = \frac{SL}{2D} \exp\left(-\frac{|x-x'|}{L}\right). \tag{5-59}$$

Hence in general, for $S \to S(x')dx'$, we find

$$\phi(x) = \int_{-\infty}^{\infty} dx' \left[ \frac{L}{2D} \exp\left(-\frac{|x-x'|}{L}\right) \right] S(x')$$

$$= \int_{-\infty}^{\infty} dx' \, G_{\text{pl}}(x,x') S(x'), \tag{5-60}$$

where we have identified the *plane source diffusion kernel for an infinite medium*

$$G_{\text{pl}}(x,x') = \frac{L}{2D} \exp\left(-\frac{|x-x'|}{L}\right). \tag{5-61}$$

Once again we will allow the reader the privilege of deriving the line source diffusion kernel. Actually both the plane source and line source kernels could have been superimposed from the point source diffusion kernel.

Notice that these kernels all depend only on the difference in spatial coordinates, that is, $r - r'$ or $x - x'$. Such *displacement kernels* arise because we have assumed an infinite, homogeneous medium. For such infinite geometries we can use these kernels to compute the neutron flux arising from any source distribution.

Unfortunately most geometries of interest are not uniform and are certainly not infinite. Hence we must generalize this discussion to determine the diffusion kernels characterizing other geometries and boundary conditions. Before attempting this generalization it is useful to step back a moment and try to obtain a general mathematical perspective of just what problem it is that we really wish to solve.

Actually all we are doing is trying to solve an inhomogeneous differential equation of the form

$$M\phi(x) = S(x), \tag{5-62}$$

where $M$ is a *differential operator* such as

$$M = \frac{d^2}{dx^2} - \frac{1}{L^2}. \tag{5-63}$$

(We will leave it as understood that one must also apply suitable boundary conditions.) There are a variety of techniques available to solve such inhomogeneous problems. The approach we have been using thus far is known as the Green's function method:[9]

### (a) GREEN'S FUNCTION METHODS

In this technique we first construct the solution to

$$M\phi_g(x) = \delta(x-x'). \tag{5-64}$$

Then if we call $\phi_g(x) = G(x,x')$ the "Green's function" for the operator $M$, we find that the general solution to Eq. (5-64) is just

$$\phi(x) = \int dx'\, G(x,x') f(x'). \tag{5-65}$$

[Proof:

$$M\phi = \int dx'\, \underbrace{MG(x,x')}_{\delta(x-x')} f(x') = f(x)] \tag{5-66}$$

EXAMPLE: Consider

$$M\phi = \left(\frac{d^2}{dx^2} - \frac{1}{L^2}\right)\phi(x) = -\frac{S(x)}{D} \tag{5-67}$$

for an infinite medium, $-\infty < x < +\infty$. Now define $G$ by

$$\frac{d^2G}{dx^2} - \frac{1}{L^2}G(x,x') = -\frac{\delta(x-x')}{D}.$$  (5-68)

However we have just solved this for

$$G(x,x') = G_{pl}(x,x') = \frac{L}{2D}\exp\left(-\frac{|x-x'|}{L}\right).$$  (5-69)

Hence the plane source kernel is just the Green's function for this operator, and we find

$$\phi(x) = \int_{-\infty}^{\infty} dx' \, G_{pl}(x,x')S(x').$$  (5-70)

It should not take much contemplation to convince the reader that this is just the scheme we have been using to construct infinite medium solutions by first determining the appropriate diffusion kernel or Green's function. The construction of the Green's function characterizing a finite geometry is not much more difficult, although one can no longer simply solve for the flux resulting from a source conveniently located at the origin, and then perform a coordinate translation to arrive at the Green's function. This latter complexity should be easily understood when it is recognized that shifting the source "off-center" in a finite geometry will destroy the symmetry of the problem. Hence one no longer finds a simple displacement kernel form for the Green's function. We will provide an alternative scheme for constructing these kernels later in this section.

(b) *VARIATION OF CONSTANTS*

Perhaps a more familiar scheme for the solution of inhomogeneous differential equations is *variation of constants*,[10] in which one first determines the linearly independent solutions $\phi_{hom}^{(j)}$ of the homogeneous equation

$$M\phi_{hom}^{(j)}(x) = 0,$$  (5-71)

and a *particular solution* of the inhomogeneous equation

$$M\phi_{part}(x) = S(x).$$  (5-72)

Since none of these solutions are required to satisfy the boundary conditions pertaining to the specific problem of interest, they are usually rather straightforward to find. Then one seeks the general solution to the problem as

$$\phi(x) = A_1\phi_{hom}^{(1)}(x) + A_2\phi_{hom}^{(2)}(x) + \phi_{part}(x)$$  (5-73)

and applies the boundary conditions to determine the unknown coefficients of the homogeneous solutions, $A_1$ and $A_2$.

EXAMPLE: Consider a uniform source $S(x) = S_0$ in an infinite medium. Then

$$\frac{d^2\phi}{dx^2} - \frac{1}{L^2}\phi(x) = -\frac{S_0}{D},$$  (5-74)

with boundary conditions such that $\phi(x) < \infty$ as $x \to \pm\infty$. The solutions to the homogeneous equation are $\exp(\pm x/L)$, and the particular solution is obviously $\phi(x) = S_0 L^2 / D$. Hence we will seek a general solution

$$\phi(x) = A \exp\left(-\frac{x}{L}\right) + B \exp\left(+\frac{x}{L}\right) + \frac{S_0 L^2}{D}. \tag{5-75}$$

Then applying the boundary conditions implies that both $A$ and $B$ must be zero, and hence the solution is

$$\phi(x) = \frac{S_0 L^2}{D}. \tag{5-76}$$

Usually for the method of variation of constants to be of use in more general problems, one must be able to guess $\phi_{part}(x)$ "by inspection." Hence for most problems, the Green's function technique or the method we will describe next is more convenient.

### (c) EIGENFUNCTION EXPANSION METHODS

One of the most powerful methods available for solving boundary value problems is to seek the solution as an expansion in the set of *normal modes* or *eigenfunctions* characterizing the geometry of interest. Rather than beginning with a general description of this very important scheme, we will introduce it by considering a specific example.

EXAMPLE: We will attempt to determine the neutron flux resulting from an arbitrary distributed source in a finite slab of width $a$. That is, we wish to solve

$$\frac{d^2\phi}{dx^2} - \frac{1}{L^2}\phi(x) = -\frac{S(x)}{D}, \qquad -\frac{a}{2} \leqslant x \leqslant \frac{a}{2}, \tag{5-77}$$

subject to the vacuum boundary conditions:

$$(a) \quad \phi\left(\frac{\tilde{a}}{2}\right) = 0$$

$$(b) \quad \phi\left(-\frac{\tilde{a}}{2}\right) = 0.$$

Since we have taken the source $S(x)$ to be arbitrary, we cannot assume symmetry to restrict our attention to the range $0 \leqslant x \leqslant \tilde{a}/2$.

Our approach to solving this problem may at first seem a bit irrelevant. We begin by considering a *homogeneous* problem very similar to Eq. (5-77):

$$\frac{d^2\psi}{dx^2} + B^2\psi(x) = 0, \tag{5-78}$$

with boundary conditions:

$$\psi\left(\frac{\tilde{a}}{2}\right) = 0 = \psi\left(-\frac{\tilde{a}}{2}\right).$$

Here $B^2$ is just an arbitrary parameter—at least for the moment. Let us now solve this associated homogeneous problem by noting the general solution

$$\psi(x) = A_1 \cos Bx + A_2 \sin Bx. \tag{5-79}$$

Our boundary conditions require

$$\psi\left(\pm\frac{\tilde{a}}{2}\right) = A_1\cos\left(\frac{B\tilde{a}}{2}\right) \pm A_2\sin\left(\frac{B\tilde{a}}{2}\right). \tag{5-80}$$

Adding and subtracting these equations, we find that we must simultaneously require

$$A_1\cos\left(\frac{B\tilde{a}}{2}\right) = 0,$$

and

$$A_2\sin\left(\frac{B\tilde{a}}{2}\right) = 0. \tag{5-81}$$

How do we achieve this? Certainly we cannot set $A_1$ and $A_2$ equal to zero since then we would have the "trivial" solution $\psi(x)\equiv 0$. Instead we must choose the parameter $B$ such that these conditions are satisfied. Of course there are many values of $B$ for which this will occur. For example, if we choose $A_2 = 0$, then any

$$B = B_n \equiv \frac{n\pi}{\tilde{a}}, \qquad n = 1, 3, 5, \ldots \tag{5-82}$$

will give rise to a solution

$$\psi_n(x) = A_n\cos\frac{n\pi x}{\tilde{a}}, \qquad n = 1, 3, 5, \ldots \tag{5-83}$$

which obviously satisfies both the differential equation [Eq. (5-78)] and the boundary conditions. Alternatively, we could have chosen $A_1 = 0$, in which case

$$B = B_n \equiv \frac{n\pi}{\tilde{a}}, \qquad n = 2, 4, 6, \ldots \tag{5-84}$$

yields solutions

$$\psi_n(x) = A_n\sin\frac{n\pi x}{\tilde{a}}, \qquad n = 2, 4, 6, \ldots \tag{5-85}$$

Hence our homogeneous problem can be solved only for certain values of the parameter $B$. One refers to the values of $B^2$ for which nontrivial solutions exist to the homogeneous problem as *eigenvalues*:

$$\text{Eigenvalues:} \quad B_n^2 = \left(\frac{n\pi}{\tilde{a}}\right)^2, \qquad n = 1, 2, \ldots \tag{5-86}$$

The corresponding solutions are referred to as the *eigenfunctions* of the problem:

$$\text{Eigenfunctions:} \quad \psi_n(x) = \begin{cases} A_n\cos\left(\dfrac{n\pi x}{\tilde{a}}\right), & n = 1, 3, 5, \ldots \\[2mm] A_n\sin\left(\dfrac{n\pi x}{\tilde{a}}\right), & n = 2, 4, 6, \ldots \end{cases} \tag{5-87}$$

The reader may have already encountered eigenvalue problems in a somewhat different form:

$$H\psi_n = \lambda_n \psi_n \qquad (5\text{-}88)$$

where $\psi_n$ is the eigenfunction corresponding to the eigenvalue $\lambda_n$. However by comparing this form with Eq. (5-78), one can easily identify $H = d^2/dx^2$, $\lambda \rightarrow - B^2$, and $\psi_n \rightarrow \psi_n(x)$.

Notice that in the example Eq. (5-78) we actually find two types of eigenfunctions: the cosine functions corresponding to odd $n$ and symmetric about the origin, and the sine functions corresponding to even $n$ and antisymmetric about the origin. Had we restricted ourselves to symmetric sources $S(x) = S(-x)$, we could have eliminated the antisymmetric solutions [Eq. (5-85)] from further consideration. We have sketched the first few eigenfunctions for the slab geometry in Figure 5-10.

In acoustics these eigenfunctions would be identified as the *normal modes* or *natural harmonics* of the system, and this terminology is frequently carried over to reactor analysis. Notice that the $A_n$ are still undetermined and are, in fact, arbitrary. These can be chosen in a number of ways, but for now we will just set $A_n = 1$ for convenience.

So now this auxiliary problem has given us an infinite set of solutions $\psi_n(x)$. What good are they? Well, they have a couple of very useful properties. First notice that the product of any two of these functions will vanish when integrated over the slab unless the functions are identical:

$$\int_{-\frac{\tilde{a}}{2}}^{\frac{\tilde{a}}{2}} dx\, \psi_m(x)\psi_n(x) = \begin{cases} 0, & \text{if } m \neq n \\ \dfrac{\tilde{a}}{2}, & \text{if } m = n. \end{cases} \qquad (5\text{-}89)$$

This property is known as *orthogonality* and proves to be of very considerable usefulness, as we will see in a moment.

The second property of the eigenfunctions $\psi_n(x)$ is that they form a *complete set* in the mathematical sense that any reasonably "well-behaved"[1] function $f(x)$ can be represented as a linear combination of the $\psi_n(x)$:

$$f(x) = \sum_{n=1}^{\infty} c_n \psi_n(x). \qquad (5\text{-}90)$$
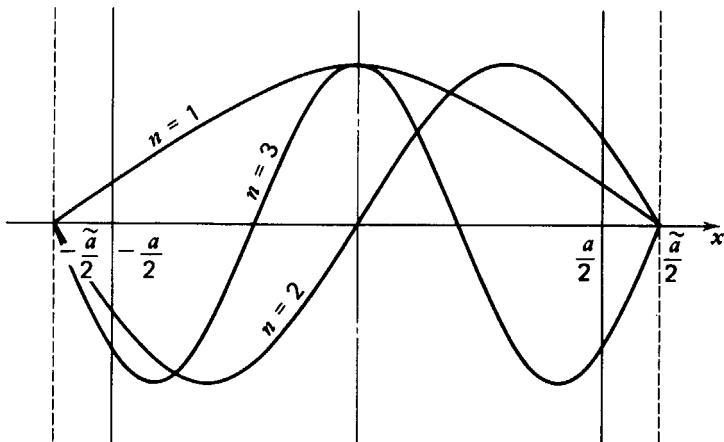


FIGURE 5-10.   The eigenfunctions for a slab geometry.

Of course, such a representation is only of formal interest unless some scheme is available for determining the expansion coefficients $c_n$, but this is where orthogonality comes in handy. Multiply Eq. (5-90) by $\psi_m(x)$ and integrate over $x$ to find

$$\int_{-\frac{a}{2}}^{\frac{a}{2}} dx\, \psi_m(x) f(x) = \sum_{n=1}^{\infty} c_n \int_{-\frac{a}{2}}^{\frac{a}{2}} dx\, \psi_m(x) \psi_n(x) = c_m \int_{-\frac{a}{2}}^{\frac{a}{2}} dx\, \psi_m^2(x)$$

or

$$c_m = \frac{2}{a} \int_{-\frac{a}{2}}^{\frac{a}{2}} dx\, f(x) \psi_m(x). \tag{5-91}$$

Hence given any function $f(x)$, we can evaluate the appropriate expansion coefficients $c_m$ by a simple integration. It should be mentioned that for the specific example of a finite slab we have been considering, an eigenfunction expansion is simply a Fourier series expansion and is probably already quite familar to most students.[1] However, the properties of orthogonality and completeness characterizing such trigonometric functions also hold for much more general eigenfunction expansions.

With this background, we are finally ready to return to solve our original boundary value problem. As we mentioned, the essential idea is to seek the solution as an expansion in the eigenfunctions $\psi_n(x)$:

$$\phi(x) = \sum_{n=1}^{\infty} c_n \psi_n(x). \tag{5-92}$$

We will also expand the source term in a similar fashion

$$S(x) = \sum_{n=1}^{\infty} s_n \psi_n(x). \tag{5-93}$$

Notice that since $S(x)$ is known, we can use orthogonality to determine the source expansion coefficients [as in Eq. (5-91)] as

$$s_n = \frac{2}{a} \int_{-\frac{a}{2}}^{\frac{a}{2}} dx\, S(x) \psi_n(x) \tag{5-94}$$

Of course since $\phi(x)$ is unknown, we cannot determine the $c_n$ in a similar fashion, but that is just what we can use the original equation [Eq. (5-77)] to accomplish. If we substitute Eqs. (5-92) and (5-93) into Eq. (5-77), we find

$$\sum_{n=1}^{\infty} c_n \left[ \frac{d^2\psi_n}{dx^2} - \frac{1}{L^2} \psi_n \right] = -\frac{1}{D} \sum_{n=1}^{\infty} s_n \psi_n. \tag{5-95}$$

However using Eq. (5-78), we can eliminate $d^2\psi_n/dx^2$ to find

$$\sum_{n=1}^{\infty} c_n \left( B_n^2 + \frac{1}{L^2} \right) \psi_n = \frac{1}{D} \sum_{n=1}^{\infty} s_n \psi_n. \tag{5-96}$$

Thus we are left with one equation for an infinite number of unknowns, the $c_n$. Fortunately orthogonality once again comes to our rescue. Multiply by $\psi_m(x)$, integrate over $x$, and use orthogonality to find

$$c_n = \frac{s_n/D}{B_n^2 + \frac{1}{L^2}} = \frac{s_n/\Sigma_a}{1 + L^2 B_n^2}.$$  (5-97)

Thus we find the flux for any source distribution as

$$\phi(x) = \frac{1}{\Sigma_a} \sum_{n=1}^{\infty} \frac{s_n}{1 + L^2 B_n^2} \psi_n(x),$$  (5-98)

where $\psi_n(x) = \cos(n\pi x/\tilde{a})$, $n$ odd and $\psi_n(x) = \sin(n\pi x/\tilde{a})$, $n$ even.

We can rewrite this in a bit more familiar form if we substitute Eq. (5-94) into Eq. (5-98) and rearrange things a bit:

$$\phi(x) = \int_{-\frac{a}{2}}^{\frac{a}{2}} dx' \left[ \frac{2}{\tilde{a}\Sigma_a} \sum_{n=1}^{\infty} \frac{\psi_n(x)\psi_n(x')}{1 + L^2 B_n^2} \right] S(x')$$

$$= \int_{-\frac{a}{2}}^{\frac{a}{2}} dx' \, G_{pl}(x,x') S(x').$$  (5-99)

Hence we have found an explicit representation of the plane diffusion kernel or Green's function for a finite slab as an eigenfunction expansion

$$G_{pl}(x,x') = \frac{2}{\tilde{a}\Sigma_a} \sum_{n=1}^{\infty} \frac{\psi_n(x)\psi_n(x')}{1 + L^2 B_n^2}.$$  (5-100)

Note in particular that the Green's function for a finite geometry is no longer a displacement kernel, that is, a function only of $x - x'$, as it was for infinite geometries.

This intimate relationship between Green's functions and eigenfunction expansions is actually a very general result. Suppose we consider the diffusion equation characterizing any homogeneous geometry:

$$\nabla^2 \phi - \frac{1}{L^2} \phi(\mathbf{r}) = -\frac{S(\mathbf{r})}{D},$$  (5-101)

subject to the usual vacuum boundary conditions on the extrapolated boundary:

Boundary conditions: $\phi(\tilde{\mathbf{r}}_s) = 0$, $\mathbf{r}_s$ on surface.

As before, we first construct the eigenfunctions as the nontrivial solutions to the associated homogeneous problem

$$\nabla^2 \psi_n + B_n^2 \psi_n(\mathbf{r}) = 0,$$

Boundary condition: $\psi_n(\tilde{\mathbf{r}}_s) = 0.$  (5-102)

One can demonstrate that these eigenfunctions are orthogonal in the sense that

$$\int_V d^3r\, \psi_m(\mathbf{r})\psi_n(\mathbf{r}) = 0, \quad n \neq m. \tag{5-103}$$

Since Eq. (5-102) is homogeneous, any solution $\psi_n(\mathbf{r})$ may be multiplied by a constant. We will scale each $\psi_n$ so that the eigenfunctions are *normalized* such that

$$\int_V d^3r\, \psi_n^2(\mathbf{r}) = 1. \tag{5-104}$$

[Our earlier slab eigenfunctions $\psi_n(x)$ would be normalized if we multiplied them by $(2/\tilde{a})^{1/2}$.] The set of orthogonal and normalized eigenfunctions $\{\psi_n(\mathbf{r})\}$ is said to be *orthonormal*. It can also be shown to be complete. Hence we can expand

$$\phi(\mathbf{r}) = \sum_n c_n\psi_n(\mathbf{r}),$$

$$\tag{5-105}$$

$$S(\mathbf{r}) = \sum_n s_n\psi_n(\mathbf{r}),$$

where

$$s_n = \int_V d^3r'\, \psi_n(\mathbf{r}')S(\mathbf{r}').$$

If we substitute these expansions into Eq. (5-101), we can use orthogonality as before to solve for

$$c_n = \frac{s_n/\Sigma_a}{1 + L^2B_n^2}. \tag{5-106}$$

Hence we find

$$\phi(\mathbf{r}) = \int_V d^3r'\, G(\mathbf{r},\mathbf{r}')S(\mathbf{r}'), \tag{5-107}$$

where

$$G(\mathbf{r},\mathbf{r}') = \frac{1}{\Sigma_a}\sum_n \frac{\psi_n(\mathbf{r})\psi_n(\mathbf{r}')}{1 + L^2B_n^2} \tag{5-108}$$

as a general result for any geometry (although the eigenfunctions or *spatial modes* $\psi_n(\mathbf{r})$ may be very hard to construct in practice).

## B. Numerical Methods for Solving the Neutron Diffusion Equation

### 1. INTRODUCTION

Thus far we have confined our attention to neutron diffusion in homogeneous (or perhaps regionwise homogeneous) media since in this case the one-speed diffusion equation could be solved analytically. However in any realistic reactor

calculation the heterogeneous nature of the core must be taken into account. One not only must consider nonuniformities corresponding to fuel pellets, cladding material, moderator, coolant, control elements, but spatial variations in fuel and coolant densities due to nonuniform core power densities and temperature distributions as well. Such complexities immediately force one to discard analytical methods in favor of a direct numerical solution of the diffusion equation. In fact even when an analytical solution of the diffusion equation is possible, it is frequently more convenient to bypass this in favor of a numerical solution, particularly when the analytical solution may involve numerous functions that have to be evaluated numerically in any event, or when parameter studies are required that may involve a great many such solutions.

The general procedure is to rewrite the differential diffusion equation in finite difference form and then solve the resulting system of difference equations on a digital computer. It is perhaps easiest to illustrate this approach by a very simple example (sufficiently simple, in fact, to enable analytical solution). Suppose we wish to solve
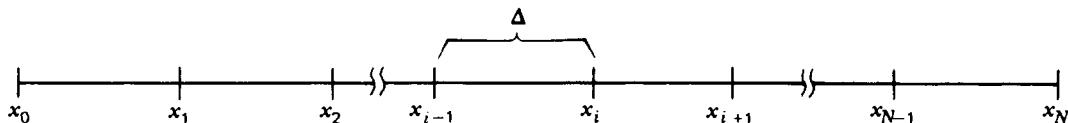
$$-D\frac{d^2\phi}{dx^2} + \Sigma_a\phi(x) = S(x) \tag{5-109}$$

subject to the boundary conditions characterizing a finite slab of width $a$:

$$\phi(0) = \phi(a) = 0.$$

(For convenience we will ignore the extrapolation length.)

We first discretize the spatial variable x by choosing a set of $N+1$ discrete points equally spaced a distance $\Delta = a/N$ apart (for convenience).



We now want to rewrite Eq. (5-109) at each of these discrete points $x_i$, but to do so we need an approximation for $d^2\phi/dx^2$. Suppose we Taylor expand $\phi$ at $x_{i\pm 1}$ in terms of its value at the point $x_i$:

$$\phi_{i+1} \equiv \phi(x_{i+1}) = \phi_i + \Delta\frac{d\phi}{dx}\bigg|_i + \frac{\Delta^2}{2}\frac{d^2\phi}{dx^2}\bigg|_i + \cdots$$

$$\phi_{i-1} \equiv \phi(x_{i-1}) = \phi_i - \Delta\frac{d\phi}{dx}\bigg|_i + \frac{\Delta^2}{2}\frac{d^2\phi}{dx^2}\bigg|_i - \cdots \tag{5-110}$$

If we add these expressions, we find

$$\frac{d^2\phi}{dx^2}\bigg|_i \cong \frac{\phi_{i+1} - 2\phi_i + \phi_{i-1}}{\Delta^2} \tag{5-111}$$

to within order $\Delta^2$. Hence if $\Delta$ is chosen sufficiently small, this *three-point central*

*difference formula* should be a reasonable approximation to the value of $d^2\phi/dx^2$ at the point $x_i$.

If we now use this difference formula to write Eq. (5-109) at any *mesh point* $x_i$, we find

$$-D\left(\frac{\phi_{i+1}-2\phi_i+\phi_{i-1}}{\Delta^2}\right)+\Sigma_a\phi_i=S_i, \quad i=1,2,\ldots \tag{5-112}$$

where again we have defined $S_i \equiv S(x_i)$. We can rearrange this *difference equation* to rewrite it as

$$-\underbrace{\frac{D}{\Delta^2}}_{a_{i,i-1}}\phi_{i-1}+\underbrace{\left(\frac{2D}{\Delta^2}+\Sigma_a\right)}_{a_{i,i}}\phi_i-\underbrace{\frac{D}{\Delta^2}}_{a_{i,i+1}}\phi_{i+1}=S_i \tag{5-113}$$

or

$$a_{i,i-1}\phi_{i-1}+a_{i,i}\phi_i+a_{i,i+1}\phi_{i+1}=S_i \tag{5-114}$$

$$i=1,\ldots,N-1$$

Hence we now have reduced Eq. (5-109) to a set of $N-1$ algebraic equations for $N+1$ unknowns $(\phi_0,\phi_1,\phi_2,\ldots,\phi_N)$. If we add on the boundary conditions at either end, say $\phi_0=0$, $\phi_N=0$, we can now imagine solving (or imagine the computer solving) this set of algebraic equations. In this particular case, the system of algebraic equations can be solved directly using Gaussian elimination.[11] More generally one must use iterative methods to solve the finite-difference equations.

This very simple example illustrates the two essential tasks involved in the numerical solution of the diffusion equation: (a) derivation of the corresponding difference equations and (b) formulation of a suitable algorithm for solving these equations on a digital computer. The methods used will vary from problem to problem. For example, whereas a direct solution of the difference equations [e.g., Eq. (5-114)] is possible for one-dimensional problems, iterative methods are required for two- and three-dimensional problems. Furthermore one generally desires to work with nonuniform meshes in reactor calculations, to account for the fact that the neutron flux may vary much more rapidly in certain regions than in others.

In this section we illustrate several of the techniques that are commonly applied in reactor analysis to the derivation and solution of difference equations. However just as in our earlier study of analytical techniques, we do not intend this discussion to be a detailed discussion of numerical methods in nuclear reactor calculations. Instead we refer the interested reader to the extensive literature on this topic.[12-16]
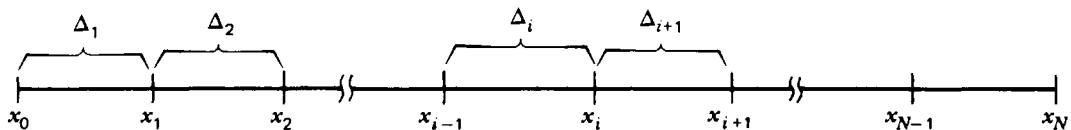
## 2. DERIVATION OF DIFFERENCE EQUATIONS FOR ONE-DIMENSIONAL DIFFUSION PROBLEMS

We will now consider the more general form of the one-dimensional diffusion equation in plane geometry
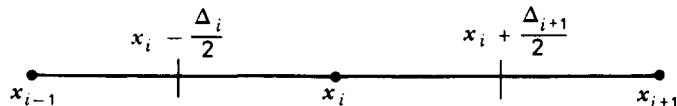
$$-\frac{d}{dx}D(x)\frac{d\phi}{dx}+\Sigma_a(x)\phi(x)=S(x) \tag{5-115}$$

subject to boundary or interface conditions that we will leave arbitrary for the moment. Actually we should remark here that this form of the diffusion equation is even a bit too general for most reactor applications. One rarely encounters reactor configurations in which the composition varies in a continuous way from point to point [i.e., $D(x)$ and $\Sigma_a(x)$]. Rather the system properties are assumed to be essentially uniform in various subregions of the reactor core (or can be suitably represented by spatially averaged or "homogenized" properties within each subregion). Hence the far more common situation is one in which the diffusion equation [Eq. (5-109)] with constant $D_j$ and $\Sigma_{aj}$ must be solved in a number of regions $j$. We will develop the difference equations for the general diffusion equation [Eq. (5-115)], however, since they are not really any more difficult to derive or solve, and in certain cases they are useful in avoiding technical difficulties arising in less general approaches (such as the handling of region interfaces).

As in our simple example we begin by setting up our discrete spatial mesh as shown below, although we will now allow for nonuniform mesh spacing.



There are a variety of schemes that can be used to generate a difference equation representation of Eq. (5-115) on this mesh. We have already considered a simple problem in which a Taylor series expansion was used to derive a central difference formula for $d^2\phi/dx^2$. A more common scheme is to integrate the original differential equation over an arbitrary mesh interval, and then to suitably approximate these integrals (after an occasional integration by parts) using simple mean values or difference formulas. By way of illustration, suppose we integrate Eq. (5-115) over a mesh interval $x_i - \Delta_i/2 < x < x_i + \Delta_{i+1}/2$ surrounding the mesh point $x_i$.



Let us choose the simplest scheme to approximate the integrals by expressing them as the value of the integrand evaluated at the meshpoint $x_i$ times the integration interval. For example,

$$\int_{x_i - \frac{\Delta_i}{2}}^{x_i + \frac{\Delta_{i+1}}{2}} dx\, \Sigma_a(x)\phi(x) \cong \Sigma_{a_i}\phi_i\left[\frac{\Delta_i}{2} + \frac{\Delta_{i+1}}{2}\right], \tag{5-116}$$

$$\int_{x_i - \frac{\Delta_i}{2}}^{x_i + \frac{\Delta_{i+1}}{2}} dx\, S(x) \cong S_i\left[\frac{\Delta_i}{2} + \frac{\Delta_{i+1}}{2}\right]. \tag{5-117}$$

The derivative term requires a bit more work. First write

$$\int_{x_i - \frac{\Delta_i}{2}}^{x_i + \frac{\Delta_{i+1}}{2}} dx \frac{d}{dx} D(x) \frac{d\phi}{dx} = D(x) \frac{d\phi}{dx} \Big|_{x_i - \frac{\Delta_i}{2}}^{x_i + \frac{\Delta_{i+1}}{2}} . \tag{5-118}$$

To handle $d\phi/dx$, we can use a simple two-point difference formula [which can be derived by subtracting Eqs. (5-110)]:

$$\frac{d\phi}{dx} \Big|_{x_i + \frac{\Delta_{i+1}}{2}} \cong \frac{\phi_{i+1} - \phi_i}{\Delta_{i+1}}$$



$$\frac{d\phi}{dx} \Big|_{x_i - \frac{\Delta_i}{2}} \cong \frac{\phi_i - \phi_{i-1}}{\Delta_i}$$



Furthermore we will use a centered average for $D$:

$$D\left(x_i + \frac{\Delta_{i+1}}{2}\right) = \frac{1}{2}[D_{i+1} + D_i] \equiv D_{i,i+1}, \qquad D\left(x_i - \frac{\Delta_i}{2}\right) = \frac{1}{2}[D_{i-1} + D_i] \equiv D_{i,i-1}. \tag{5-119}$$

Then we find that Eq. (5-118) can be written as

$$\int_{x_i - \frac{\Delta_i}{2}}^{x_i + \frac{\Delta_{i+1}}{2}} dx \frac{d}{dx} D(x) \frac{d\phi}{dx} \cong \frac{D_{i,i-1}}{\Delta_i} \phi_{i-1} - \left(\frac{D_{i,i+1}}{\Delta_{i+1}} + \frac{D_{i,i-1}}{\Delta_i}\right) \phi_i + \frac{D_{i,i+1}}{\Delta_{i+1}} \phi_{i+1}. \tag{5-120}$$

If we now combine Eqs. (5-116), (5-117), and (5-120), we arrive at a set of difference equations very similar to our earlier results

$$a_{i,i-1}\phi_{i-1} + a_{i,i}\phi_i + a_{i,i+1}\phi_{i+1} = S_i, \tag{5-121}$$

where

$$a_{i,i-1} = -\left(\frac{D_i + D_{i-1}}{\Delta_i}\right) \frac{1}{\Delta_i + \Delta_{i+1}},$$

$$a_{i,i} = \Sigma_{a_i} + \left(\frac{D_{i+1} + D_i}{\Delta_{i+1}} + \frac{D_{i-1} + D_i}{\Delta_i}\right) \frac{1}{\Delta_i + \Delta_{i+1}}, \tag{5-122}$$

$$a_{i,i+1} = -\left(\frac{D_{i+1} + D_i}{\Delta_i}\right) \frac{1}{\Delta_i + \Delta_{i+1}}.$$

Hence once again we have arrived at a set of $N-1$ three-point difference equations for the $N+1$ unknown discretized fluxes, $\phi_0, \phi_1, \ldots, \phi_N$. In the particular case in which the mesh size $\Delta_i$ is constant and the coefficients $D(x)$ and $\Sigma_a(x)$ do not

depend on $x$, we return to our earlier results [Eq. (5-113)] derived via a Taylor series expansion. Actually we should note that the coefficients $a_{ij}$ depend only on a single subscript, $j$. However double subscripting is useful, for we will rewrite these algebraic equations as a matrix equation.

Our final task is to append to these equations two additional equations taking into account the boundary conditions. Of course we could simply use the vacuum extrapolated boundary conditions, $\phi_0 = 0$, $\phi_N = 0$ as before (taking care to place the mesh points $x_0$ and $x_N$ on these extrapolated boundaries). More general boundary conditions (such as nonreentrant current) can be developed by taking the final two difference equations in the set as

$$a_{0,0}\phi_0 + a_{0,1}\phi_1 = S_0$$

and

$$a_{N,N-1}\phi_{N-1} + a_{N,N}\phi_N = S_N. \tag{5-123}$$

Such sets of three-point difference equations are characteristic of one-dimensional diffusion problems (indeed of any ordinary differential equation of second order). The coefficients $a_{ij}$ will depend upon the scheme used to derive the difference equations. Fortunately if the mesh spacing $\Delta$ is small, these differences will be insignificant in actual calculations. Since the spatial variation of the flux is essentially characterized by the diffusion length $L$, one generally chooses a mesh spacing $\Delta$ less than $L$.

Similar three-point difference equations will also arise in curvilinear geometries with one-dimensional symmetry. For convenience we will assume regionwise uniform properties. Then in cylindrical coordinates, the diffusion equation becomes

$$-D\left[\frac{d^2\phi}{dr^2} + \frac{1}{r}\frac{d\phi}{dr}\right] + \Sigma_a\phi(r) = S(r), \tag{5-124}$$

while in spherical coordinates, we find

$$-D\left[\frac{d^2\phi}{dr^2} + \frac{2}{r}\frac{d\phi}{dr}\right] + \Sigma_a\phi(r) = S(r). \tag{5-125}$$

Hence we can derive difference equations corresponding to these geometries, using either of the earlier techniques, to find for uniform mesh spacing[17]

$$a_{i,i-1}\phi_{i-1} + a_{i,i}\phi_i + a_{i,i+1}\phi_{i+1} = S_i, \tag{5-126}$$

where now

$$a_{i,i-1} = -\frac{D}{\Delta^2}\left[1 - \frac{c}{2i-1}\right],$$

$$a_{i,i} = \frac{2D}{\Delta^2} + \Sigma_a, \tag{5-127}$$

$$a_{i,i+1} = -\frac{D}{\Delta^2}\left[1 + \frac{c}{2i-1}\right],$$

next task is the determination of a suitable prescription or *algorithm* for solving this system of algebraic equations.

## 3. SOLUTION OF THREE-POINT DIFFERENCE EQUATIONS

Suppose we have developed an appropriate set of difference equations similar to Eq. (5-121). We must now solve for the discretized fluxes $\phi_i$. To be more explicit, let's first write out these equations in detail

$$
\begin{aligned}
a_{11}\phi_1 + a_{12}\phi_2 &= S_1 \\
a_{21}\phi_1 + a_{22}\phi_2 + a_{23}\phi_3 &= S_2 \\
a_{32}\phi_2 + a_{33}\phi_3 + a_{34}\phi_4 &= S_3 \qquad (5\text{-}132) \\
\vdots \\
a_{N-1,N-2}\phi_{N-2} + a_{N-1,N-1}\phi_{N-1} &= S_{N-1}
\end{aligned}
$$

It is useful to rewrite these equations in matrix form

$$
\begin{pmatrix}
a_{11} & a_{12} & & & \\
a_{21} & a_{22} & a_{23} & & \\
& a_{32} & a_{33} & a_{34} & \\
& & a_{43} & a_{44} & a_{45} \\
& & & & \ddots
\end{pmatrix}
\begin{pmatrix}
\phi_1 \\ \phi_2 \\ \phi_3 \\ \vdots \\ \phi_{N-1}
\end{pmatrix}
=
\begin{pmatrix}
S_1 \\ S_2 \\ S_3 \\ S_4 \\ \vdots \\ S_{N-1}
\end{pmatrix}
$$

or

$$
\underline{\underline{A}}\, \underline{\phi} = \underline{S}, \qquad (5\text{-}133)
$$

where $\underline{\underline{A}}$ is an $(N-1)\times(N-1)$ matrix, and $\underline{\phi}$ and $\underline{S}$ are $(N-1)$ dimension column vectors. (For a short review of matrix algebra, the reader should refer to Appendix F.) In particular the reader should note that the finite difference diffusion matrix $\underline{\underline{A}}$ is *tridiagonal*. This feature arises only for such one-dimensional geometries in which three-point difference equations arise. In two- and three-dimensional geometries, more complicated matrix structures are encountered.

Notice that the solution of this set of algebraic equations is tantamount to inverting the matrix $\underline{\underline{A}}$ to find

$$
\underline{\phi} = \underline{\underline{A}}^{-1}\underline{S}. \qquad (5\text{-}134)
$$

Such tridiagonal matrices can be inverted directly using Gaussian elimination (the "forward elimination—backward substitution" method).[18] The general scheme is to subtract $a_{i,i-1}/a_{i-1,i-1}$ times the $(i-1)$th row from the $(i)$th row to eliminate the $a_{i,i-1}$ element in the $(i)$th row. At each step, the $(i)$th row is then divided by its diagonal element, and the procedure is continued. For example, we have indicated

schematically the "forward elimination" on the first two equations in Eq. (5-132):

$$
\begin{pmatrix} a_{11} & a_{12} & 0 & \cdot \\ a_{21} & a_{22} & a_{13} & \cdot \\ \cdot & \cdot & \cdot & \end{pmatrix} \rightarrow \begin{pmatrix} 1 & \dfrac{a_{12}}{a_{11}} & 0 & \cdot \\ a_{21} & a_{22} & a_{23} & \cdot \\ \cdot & \cdot & \cdot & \cdot \end{pmatrix} \rightarrow \begin{pmatrix} 1 & \dfrac{a_{12}}{a_{11}} & 0 & \cdot \\ 0 & \left(a_{22} - \dfrac{a_{21}a_{12}}{a_{11}}\right) & a_{23} & \cdot \\ \cdot & \cdot & \cdot & \cdot \end{pmatrix}
$$

$$
\rightarrow \begin{pmatrix} 1 & \dfrac{a_{12}}{a_{11}} & 0 & \cdot \\ 0 & 1 & \dfrac{a_{23}}{\left(a_{22} - \dfrac{a_{21}a_{12}}{a_{11}}\right)} & \cdot \\ \cdot & \cdot & \cdot & \end{pmatrix} \rightarrow \begin{pmatrix} 1 & A_1 & 0 & \cdot \\ 0 & 1 & A_2 & \cdot \\ \cdot & \cdot & \cdot & \cdot \end{pmatrix} \tag{5-135}
$$

such that we eventually arive at a system of equations of the form

$$
\begin{pmatrix} 1 & A_1 & 0 & 0 & \cdot \\ 0 & 1 & A_2 & 0 & \cdot \\ 0 & 0 & 1 & A_3 & \cdot \\ \cdot & \cdot & \cdot & \cdot & \cdot \\ 0 & 0 & \cdot & 0 & 1 \end{pmatrix} \begin{pmatrix} \phi_1 \\ \phi_2 \\ \phi_3 \\ \\ \phi_{N-1} \end{pmatrix} = \begin{pmatrix} \alpha \\ \alpha \\ \alpha_3 \\ \\ \alpha_{N-1} \end{pmatrix} \tag{5-136}
$$

where

$$
A_n = \frac{a_{n,n+1}}{a_{n,n} + a_{n,n-1}A_{n-1}}, \qquad A_1 = \frac{a_{12}}{a_{11}}
$$

$$
\alpha_n = \frac{S_n - a_{n,n-1}\alpha_{n-1}}{a_{n,n} - a_{n,n-1}A_{n-1}}, \qquad \alpha_1 = \frac{S_1}{a_{11}}. \tag{5-137}
$$

We can now substitute back up the matrix to find

$$
\phi_{N-1} = \alpha_{N-1},
$$

$$
\phi_{N-2} = -A_{N-2}\phi_{N-1} + \alpha_{N-2}
$$

$$
= -A_{N-2}\alpha_{N-1} + \alpha_{N-2}, \tag{5-138}
$$

and so on.

Thus Gaussian elimination consisting of forward elimination and backward substitution can be used to directly solve the difference equations [Eqs. (5-132)]. This scheme is particularly important since it frequently appears as an integral part of the iterative methods used in two- and three-dimensional diffusion problems. For this reason it is useful to formalize Gaussian elimination a bit by noting that what we have in fact accomplished by forward elimination is the factorization of

the matrix $\underline{A}$ into a product of a lower ($\underline{L}$) and upper ($\underline{U}$) triangular matrix:[19]

$$\underline{A} = \begin{pmatrix} a_{11} & 0 & 0 & \cdot \\ a_{21} & (a_{22} - a_{21}A_1) & 0 & \cdot \\ 0 & a_{32} & (a_{33} - a_{32}A_2) & \cdot \\ \cdot & \cdot & \cdot & \cdot \end{pmatrix} \underbrace{\qquad\qquad}_{\underline{L}} \begin{pmatrix} 1 & A_1 & 0 & \cdot \\ 0 & 1 & A_2 & \cdot \\ 0 & 0 & 1 & \cdot \\ \cdot & \cdot & \cdot & \cdot \end{pmatrix} \underbrace{\qquad\qquad}_{\underline{U}} \qquad (5\text{-}139)$$

Hence our sequence of steps in Gaussian elimination begins with

$$\underline{A}\,\phi = \underline{L}\,\underline{U}\,\phi = \underline{S}. \qquad (5\text{-}140)$$

First we perform a forward elimination sweep to construct and invert $\underline{L}$

$$\underline{U}\phi = \underline{L}^{-1}\underline{S} = \underline{\alpha}, \qquad (5\text{-}141)$$

followed by a backward substitution to invert $\underline{U}$ and solve for

$$\phi = \underline{U}^{-1}\underline{L}^{-1}\underline{S} = \underline{U}^{-1}\underline{\alpha}. \qquad (5\text{-}142)$$

As an aside we should observe that while such methods for solving systems of linear algebraic equations are most easily understood and analyzed (mathematically) in matrix notation, they are most easily programmed when written as a simple algorithm such as Eq. (5-137). For example, one could simply construct a loop to generate and store all $A_n$ and $\alpha_n$ using Eq. (5-137) and then evaluate all $\phi_n$ using Eq. (5-138).

This algorithm for solving such sets of three-term equations (i.e., inverting tridiagonal matrices) is easily programmed and executed on a digital computer. The algorithm would also formally work for solving difference equations characterizing two- or three-dimensional diffusion problems, however it then encounters some severe computing limitations. To visualize this more clearly, we will now briefly comment on the numerical solution of multidimensional diffusion equations.

## 4. DERIVATION OF MULTIDIMENSIONAL DIFFERENCE EQUATIONS

Most detailed neutron diffusion calculations characterizing nuclear reactors require either two- or three-dimensional treatments. Such details are particularly important in studying power profiles in large reactors subject to nonuniform fuel loading and depletion. Hence we now must consider the numerical solution of the more general diffusion equation

$$-\nabla \cdot D(\mathbf{r})\nabla\phi + \Sigma_a(\mathbf{r})\phi(\mathbf{r}) = S(\mathbf{r}). \qquad (5\text{-}143)$$

Once again the geometry of interest is discretized into a mesh of cells such as the rectangular grids illustrated in Figure 5-11. Perhaps the most general way to derive
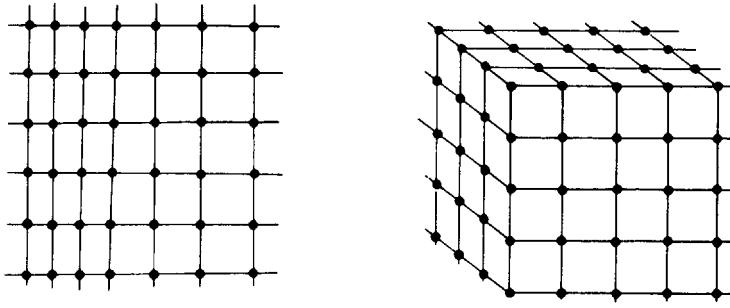
**FIGURE 5-11.** Rectangular two- and three-dimensional grids

difference equations for the mesh is to integrate the diffusion equation [Eq. (5-143)] over the spatial volume of a given mesh cell, using this to define the spatially averaged cell properties. In general one can write[20]

$$\frac{1}{V_i} \int_{V_i} d^3r\, \phi(\mathbf{r}) \equiv \phi_i, \tag{5-144}$$

$$\frac{1}{V_i} \int_{V_i} d^3r\, \Sigma_a(\mathbf{r})\phi(\mathbf{r}) \cong \Sigma_{a_i}\phi_i, \tag{5-145}$$

$$\frac{1}{V_i} \int_{V_i} d^3r\, [-\nabla \cdot D(\mathbf{r})\nabla\phi] \cong L_i\phi_i - \sum_{j=1}^{J} l_{ij}\phi_j. \tag{5-146}$$

$$\frac{1}{V_i} \int_{V_i} d^3r\, S(\mathbf{r}) \equiv S_i. \tag{5-147}$$

Here the sum is taken over the adjacent mesh point neighbors $j = 1, \ldots, J$ where $J = 2$, 4, or 6 in 1-, 2-, or 3-dimensional Cartesian geometries, while

$$L_i \equiv \sum_{j=1}^{J} l_{ij}, \tag{5-148}$$

where the mesh coupling coefficients $l_{ij}$ are determined by the particular mesh geometry and finite-difference scheme one chooses. For example, in Cartesian coordinates using essentially the approximation schemes represented by Eqs. (5-116) and (5-120), one would find

$$l_{ij} = D_{ij} / \Delta_{ij}^2 \tag{5-149}$$

where we define

$$D_{ij} \equiv \frac{1}{2}(D_i + D_j), \quad \Delta_{ij} \equiv \frac{\text{distance between mesh}}{\text{points } i \text{ and } j}. \tag{5-150}$$

The difference equations representing Eq. (5-143) then take the form

$$-\sum_{j=1}^{J} \frac{D_{ij}}{\Delta_{ij}^2}\phi_j + \left(\sum_{j=1}^{J} \frac{D_{ij}}{\Delta_{ij}^2} + \Sigma_{a_i}\right)\phi_i = S_i \tag{5-151}$$

where $i$ runs over all of the mesh points.

## 5. ITERATIVE SOLUTION OF
## MULTIDIMENSIONAL DIFFERENCE EQUATIONS

We now turn our attention to the solution of these difference equations. Our first task is to cast the set of equations into matrix form. This requires first assigning a single index to each mesh point. For example, in a two-dimensional mesh we could label the mesh points as

$$(i,j) \rightarrow k = i + (j-1)(N-1).$$

For a two-dimensional problem, the matrix structure takes the following form–in this case, for a five-by-four mesh point array

$$\left(-\frac{D_{7,2}}{(\Delta_{7,2})^2}\right)\left(-\frac{D_{7,6}}{(\Delta_{7,6})^2}\right)\left(\Sigma_{a_7} + \frac{D_{7,2}}{(\Delta_{7,2})^2} + \frac{D_{7,6}}{(\Delta_{7,6})^2} + \frac{D_{7,8}}{(\Delta_{7,8})^2} + \frac{D_{7,12}}{(\Delta_{7,12})^2}\right)\left(-\frac{D_{7,8}}{(\Delta_{7,8})^2}\right)\left(-\frac{D_{7,12}}{(\Delta_{7,12})^2}\right)\left(\phi_7\right) = \left(S_7\right)$$

$$(5\text{-}155)$$

Notice that the tridiagonal form we encountered in the one-dimensional case has now been augmented by two additional side-band diagonals—as we might have expected, since on closer examination we find the two-dimensional case yields a five-point difference equation.

Similarly, assigning a single index to each mesh point of a three-dimensional problem yields the matrix structure which corresponds to a seven-point difference equation.

$$= \quad (5\text{-}156)$$

Now let's consider how we might solve such systems—that is, invert such matrices. Since Gaussian elimination can be applied to any matrix (formally, at least), we might first consider applying this technique to obtain a direct inversion. Recall that for a one-dimensional diffusion equation, the forward elimination

sweep reduced the original tridiagonal matrix to a form with only two diagonals, while the backward substitution step completed the matrix inversion

$$
\begin{pmatrix} \diagdown \\ \diagdown \end{pmatrix} \xrightarrow[\text{sweep}]{\text{Forward}} \begin{pmatrix} \diagdown \end{pmatrix} \xrightarrow[\text{substitution}]{\text{Backward}} \begin{pmatrix} \diagdown \end{pmatrix}
\qquad (5\text{-}157)
$$

After a bit of examination, it becomes apparent that when a similar forward sweep is conducted on the five-diagonal matrix characterizing two-dimensional problems, the result is to fill in all of the zero entries between the main and outer diagonal.

$$
\begin{pmatrix} \diagdown \end{pmatrix} \longrightarrow \begin{pmatrix} \diagdown \end{pmatrix}
\qquad (5\text{-}158)
$$

This implies that one will require considerably more computer memory to allow such a direct inversion of the matrix. Such a direct algorithm is also rather complicated to program and leads to problems resulting from computer round-off error. For these reasons, it is far more efficient to use an iterative procedure to invert such matrices when $N$ is large, since such schemes attempt to preserve the sparse structure of the original matrix in their operations.

Let's illustrate the basic idea with a simple example: Suppose we wish to invert a matrix $\underline{A}$—that is, we wish to solve

$$
\underline{A}\,\phi = \underline{S}.
\qquad (5\text{-}159)
$$

We first compose $\underline{A}$ into its diagonal and off-diagonal elements

$$
\underset{\underline{A}}{\begin{pmatrix} \blacksquare \end{pmatrix}} = \underset{\underline{D}}{\begin{pmatrix} \diagdown \end{pmatrix}} - \underset{\underline{B}}{\begin{pmatrix} \blacksquare \end{pmatrix}}
\qquad (5\text{-}160)
$$

Now $\underline{D}$ can be easily inverted:

$$
\underline{D}^{-1} = \begin{pmatrix} a_{11}^{-1} & & & & 0 \\ & a_{22}^{-1} & & & \\ & & a_{33}^{-1} & & \\ & & & \ddots & \\ 0 & & & & a_{NN}^{-1} \end{pmatrix}
\qquad (5\text{-}161)
$$

Hence suppose we use Eq. (5-160) to rewrite Eq. (5-159) first as

$$\underline{\underline{D}}\,\underline{\phi} = \underline{\underline{B}}\,\underline{\phi} + \underline{S} \tag{5-162}$$

and then invert $\underline{\underline{D}}$ to find

$$\underline{\phi} = \underline{\underline{D}}^{-1}[\underline{\underline{B}}\,\underline{\phi}] + \underline{\underline{D}}^{-1}\underline{S}. \tag{5-163}$$

Now is where the iterative philosophy comes in. Suppose we guess $\underline{\phi}$ on the right-hand side—call the guess $\underline{\phi}^{(0)}$—and then use it to calculate a new guess, $\underline{\phi}^{(1)}$ as

$$\underline{\phi}^{(1)} = \underline{\underline{D}}^{-1}\underline{\underline{B}}\,\underline{\phi}^{(0)} + \underline{\underline{D}}^{-1}\underline{S}. \tag{5-164}$$

We can continue this iteration, calculating the $m+1$ guess as

$$\underline{\phi}^{(m+1)} = \underline{\underline{D}}^{-1}\underline{\underline{B}}\,\underline{\phi}^{(m)} + \underline{\underline{D}}^{-1}\underline{S}. \tag{5-165}$$

Hopefully, then, as $m$ becomes large, we converge to the true solution

$$\underline{\phi}^{(m)} \rightarrow \underline{\phi}. \tag{5-166}$$

Hence the general idea behind such iterative schemes is to generate improved guesses or iterates $\underline{\phi}^{(m)}$ by solving the original system of equations in an approximate, but efficient, manner. We continue such an iterative process until two successive iterates $\underline{\phi}^{(m)}$ and $\underline{\phi}^{(m+1)}$ are sufficiently close together, at which point the iteration is stopped and $\underline{\phi}^{(m+1)}$ is regarded as the solution. Notice that throughout the iterative process, we maintain the sparse structure of the original five-diagonal matrix $\underline{\underline{A}}$, thereby significantly reducing storage and calculational requirements.

The particular scheme we have presented is known as the *Jacobi–Richardson* or *Point–Jacobi method*, and although it is a very simple scheme, it has the drawback that it converges very slowly. The reader might very roughly think of the convergence rate of such iterative processes as being determined by how big a chunk of the original matrix he is willing to invert on each iteration. (More precisely, the convergence rate is determined by the size of the matrix *norm* of $\underline{\underline{D}}^{-1}\underline{\underline{B}}$.) In the Point–Jacobi method, only a relatively small bit of the matrix, its main diagonal, is inverted on each step and hence we might expect convergence to be slow. (As an extreme example, one bites off a much bigger chunk in Gaussian elimination—the whole matrix $\underline{\underline{A}}$—and hence only a single iteration is needed.) One can accelerate this convergence in several ways. First, one could attempt to invert a bigger chunk of $\underline{\underline{A}}$ on each iteration. It is also possible to use information about the next flux iterate during an iterative step. Finally, one can extrapolate from earlier flux iterates in order to more rapidly approach the true solution.

To understand how to improve the Jacobi iterative scheme, let's write it out

explicitly in terms of the algebraic system

$$
\boxed{a_{11}\phi_1^{(m+1)}} \quad + a_{12}\phi_2^{(m)} + \qquad a_{13}\phi_3^{(m)} + \cdots + \qquad a_{1N}\phi_N^{(m)} \quad = S_1
$$

$$
a_{21}\phi_1^{(m)} \quad + \boxed{a_{22}\phi_2^{(m+1)}} + \qquad a_{23}\phi_3^{(m)} + \cdots + \qquad a_{2N}\phi_N^{(m)} \quad = S_2
$$

solving only for these

$$
a_{N1}\phi_1^{(m)} \quad + a_{N2}\phi_2^{(m)} + \qquad a_{N3}\phi_3^{(m)} + \cdots + \quad \boxed{a_{NN}\phi_N^{(m+1)}} \quad = S_N
$$

(5-167)

Hence we can solve for the $m+1$ flux iterate immediately as

$$
\phi_i^{(m+1)} = \frac{1}{a_{ii}} \left[ S_i - \sum_{\substack{j=1 \\ \neq i}}^{N} a_{ij}\phi_j^{(m)} \right], \quad i = 1, 2, \ldots, N. \tag{5-168}
$$

It should be noted here that the Jacobi scheme does not use all of the available information during each iteration. For example, if the equations are solved in sequence from $i = 1$ to $i = N$, as they would be on a computer, then the solution of the first equation yields $\phi_1^{(m+1)}$; but to find $\phi_2^{(m+1)}$ using the second equation, $\phi_1^{(m)}$ is used rather than the improved estimate $\phi_1^{(m+1)}$. Similarly, solving the third equation for $\phi_3^{(m+1)}$ makes use of $\phi_1^{(m)}$ and $\phi_2^{(m)}$ rather than $\phi_1^{(m+1)}$ and $\phi_2^{(m+1)}$ which are known. If these estimates are used as soon as they are generated, a more efficient iterative scheme known as the *Gauss–Seidel* or *successive relaxation method* is obtained. In this case, the system of equations in each iteration is solved as

$$
\boxed{a_{11}\phi_1^{(m+1)}} + a_{12}\phi_2^{(m)} + a_{13}\phi_3^{(m)} + \cdots + a_{1N}\phi_N^{(m)} = S_1
$$

$$
\boxed{a_{21}\phi_1^{(m+1)} + a_{22}\phi_2^{(m+1)}} + a_{23}\phi_3^{(m)} + \cdots + a_{2N}\phi_N^{(m)} = S_2
$$

$$
\boxed{a_{31}\phi_1^{(m+1)} + a_{32}\phi_2^{(m+1)} + a_{33}\phi_3^{(m+1)}} + \cdots + a_{3N}\phi_N^{(m)} = S_3 \tag{5-169}
$$

$$
\boxed{a_{N1}\phi_1^{(m+1)} + a_{N2}\phi_2^{(m+1)} + a_{N3}\phi_3^{(m+1)} + \cdots + a_{NN}\phi_N^{(m+1)}} = S_N
$$

and the solution is

$$
\phi_i^{(m+1)} = \frac{1}{a_{ii}} \left[ S_i - \underbrace{\sum_{j=1}^{i-1} a_{ij}\phi_j^{(m+1)}}_{} - \underbrace{\sum_{j=i+1}^{N} a_{ij}\phi_j^{(m)}}_{} \right].
$$

From solution of    From previous       (5-170)
previous equations    ($m$th) iteration
in current ($m+1$)
iteration

This can be rewritten in matrix form by decomposing $\underline{\underline{A}}$ into the sum of an upper and lower triangular matrix:



$$\underline{\underline{A}} = \underline{\underline{L}} - \underline{\underline{U}} \tag{5-171}$$

Here $\underline{\underline{L}}$ contains elements of the main diagonal and below it, while $\underline{\underline{U}}$ contains elements above the main diagonal. Now we write Eq. (5-159) as

$$\underline{\underline{L}} \, \underline{\phi} = \underline{\underline{U}} \, \underline{\phi} + \underline{S}. \tag{5-172}$$

The Gauss–Seidel scheme described above amounts to inverting $\underline{\underline{L}}$ by forward elimination, stepping row by row down the matrix. Hence our iterative scheme is

$$\underline{\phi}^{(m+1)} = \underline{\underline{L}}^{-1} \underline{\underline{U}} \, \underline{\phi}^{(m)} + \underline{\underline{L}}^{-1} \underline{S}. \tag{5-173}$$

The fact that the Gauss–Seidel method utilizes the latest iterate elements of $\underline{\phi}^{(m+1)}$ when solving successive equations yields a factor of two better in error reduction per iteration than the Jacobi method.

It is possible to accelerate the convergence of the iteration scheme even further by introducing an *acceleration parameter* to extrapolate the iterative flux estimate. This procedure, known as the *successive overrelaxation* (*SOR*) *method*, can be illustrated by considering how one utilizes the $\phi^{(m)}$ iteration to determine the $\phi^{(m+1)}$ estimate. The first step in the calculation of $\phi_i^{(m+1)}$ is to compute the Gauss–Seidel estimate, which we will label as $\phi_i^{(m+1/2)}$ for convenience.

$$\underset{\substack{\big\backslash \\ \text{Gauss–Seidel} \\ \text{estimate}}}{\phi_i^{(m+\frac{1}{2})}} = \frac{1}{a_{ii}} \left[ S_i - \underset{\substack{\nearrow \\ \text{From SOR in} \\ \text{current iteration} \\ [(m+1)\text{st}]}}{\sum_{j=1}^{i-1} a_{ij}\phi_j^{(m+1)}} - \underset{\substack{\nearrow \\ \text{From SOR in} \\ \text{previous iteration} \\ [m\text{th}]}}{\sum_{j=i+1}^{N} a_{ij}\phi_j^{(m)}} \right] \tag{5-174}$$

Now $\phi_i^{(m+1)}$ is calculated as a linear combination of $\phi_i^{(m+\frac{1}{2})}$ and the previous SOR iterate

$$\phi_i^{(m+1)} = \omega\phi_i^{(m+\frac{1}{2})} + (1-\omega)\phi_i^{(m)}. \tag{5-175}$$

Here the extrapolation or acceleration parameter $\omega$ ranges between 1 and 2. Of course for $\omega = 1$ we return to the Gauss–Seidel method in which no extrapolation is used. The iterative algorithm for each element can then be written as

$$\phi_i^{(m+1)} = \frac{\omega}{a_{ii}} \left[ S_i - \sum_{j=1}^{i-1} a_{ij}\phi_j^{(m+1)} - \sum_{j=i+1}^{N} a_{ij}\phi_j^{(m)} \right] + (1-\omega)\phi_i^{(m)}. \tag{5-176}$$
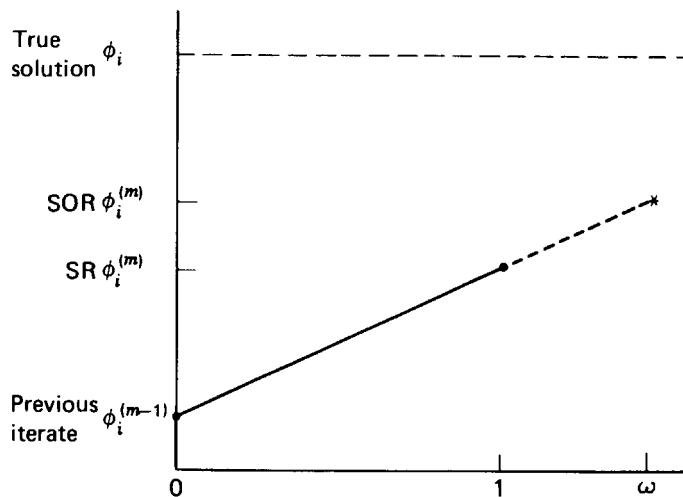
FIGURE 5-13. Flux extrapolation in the SOR method[20]

We have sketched in Figure 5-13 how the flux extrapolation can enhance convergence to the true solution $\underline{\phi}$.

The optimum value of $\omega$ giving the maximum rate of convergence can be related to characteristics of the original matrix $\underline{\underline{A}}$. In certain cases one can achieve a convergence rate as much as two orders of magnitude larger than the Jacobi method. It should be noted, however, that the estimate used for $\omega$ can strongly affect the convergence rate of this method, and it frequently must be determined by experience.

Very similar methods can be applied to three-dimensional diffusion problems. In this case the diffusion matrix $\underline{\underline{A}}$ has seven diagonal elements as indicated below



$$ \tag{5-177} $$

Again iterative methods are utilized in which the outer diagonal elements are handled in a manner similar to those used in two-dimensional problems. However there is some reduction in iterative convergence rates due to a loss of procedure implicitness caused by the additional diagonal elements.

Such iterative algorithms for the solution of the finite difference equations characterizing two- or three-dimensional diffusion problems are frequently referred to as *inner iterations*. This terminology arises from the fact that in nuclear reactor criticality calculations, the solution of the diffusion equation is itself imbedded in yet another iterative scheme—the so-called *outer* or *source iterations*—necessary to handle the presence of a fission term. We will study this latter scheme in Section 5-IV.

## 6. NODAL METHODS

There are many instances in nuclear reactor analysis in which one requires a full three-dimensional calculation of the neutron flux, for example, in core fuel depletion or control rod ejection studies. Although a direct numerical solution of the diffusion equation can be performed on a modern digital computer, it is extremely expensive to do so, particularly when a series of such calculations would be required for a parameter study. We desire a scheme for determining the three-dimensional core flux distribution that avoids the large storage and execution time requirements of a direct finite difference treatment of the diffusion equation.

Such a scheme is provided by so-called *nodal methods*.[22-23] The general idea is to decompose the reactor core into relatively large subregions or *node cells* in which the material composition and flux are assumed uniform (or at least treated in an average sense). One then attempts to determine the coupling coefficients characterizing node cell to node cell leakage and then to determine the node cell fluxes themselves.

To develop this approach in more detail, consider the neutron diffusion equation in its general time-independent form given by Eq. (5-143). Now we know that we can formally write the solution to this equation as

$$\phi(\mathbf{r}) = \int d^3r' \, G(\mathbf{r},\mathbf{r}') S(\mathbf{r}'), \tag{5-178}$$

where $G(\mathbf{r},\mathbf{r}')$ is the diffusion kernel or Green's function for the particular geometry of interest that satisfies

$$-\nabla \cdot D(\mathbf{r}) \nabla G(\mathbf{r},\mathbf{r}') + \Sigma_a(\mathbf{r}) G(\mathbf{r},\mathbf{r}') = S(\mathbf{r}-\mathbf{r}'). \tag{5-179}$$

Notice, in particular, that $G(\mathbf{r},\mathbf{r}')$ can be interpreted physically as the flux resulting at a position $\mathbf{r}$ from a unit point source at $\mathbf{r}'$.

Of course we usually cannot construct $G(\mathbf{r},\mathbf{r}')$—if we could, we would have already solved our problem. But suppose we ignore this annoyance for the moment. We will instead introduce the principal aspect of nodal methods by dividing the reactor core (or, more typically, one quadrant or octant of the core, since some symmetry is usually present) into N node cells as shown schematically in Figure
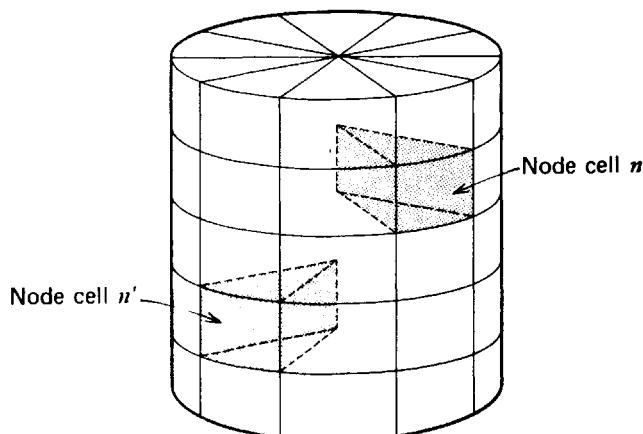


**FIGURE 5-14.** Nodal cell division of a reactor core

5-14. We now integrate Eq. (5-178) over the volume $V_n$ of the $n$th node cell

$$\int_{V_n} d^3r\,\phi(\mathbf{r}) = \int_{V_n} d^3r \int d^3r'\, G(\mathbf{r},\mathbf{r}')S(\mathbf{r}')$$

$$= \sum_{n'=1}^{N} \int_{V_n} d^3r \int_{V_{n'}} d^3r'\, G(\mathbf{r},\mathbf{r}')S(\mathbf{r}'). \qquad (5\text{-}180)$$

If we define the spatial averages over the nodal cells,

$$\phi_n \equiv \frac{1}{V_n}\int_{V_n} d^3r\,\phi(\mathbf{r}), \qquad (5\text{-}181)$$

$$S_n \equiv \frac{1}{V_n}\int_{V_n} d^3r\, S(\mathbf{r}), \qquad (5\text{-}182)$$

$$K_{nn'} \equiv \frac{\dfrac{1}{V_n}\displaystyle\int_{V_n} d^3r \int_{V_{n'}} d^3r'\, G(\mathbf{r},\mathbf{r}')S(\mathbf{r}')}{\dfrac{1}{V_{n'}}\displaystyle\int_{V_{n'}} d^3r'\, S(\mathbf{r}')}, \qquad (5\text{-}183)$$

then we can rewrite Eq. (5-180) as

$$\phi_n = \sum_{n'=1}^{N} K_{nn'}S_{n'}, \qquad (5\text{-}184)$$

or in matrix form

$$\underline{\phi} = \underline{\underline{K}}\,\underline{S}, \qquad (5\text{-}185)$$

where $\underline{\phi}$ and $\underline{S}$ are $N$-dimension column vectors and $\underline{\underline{K}}$ is an $N \times N$ matrix. Notice that the matrix elements $K_{nn'}$ can be interpreted as the probability of a neutron born in cell $n'$ diffusing to cell $n$. Hence $\underline{\underline{K}}$ is referred to as the *nodal transfer matrix* while $K_{nn'}$ are know as the *nodal coupling coefficients*.

Thus if we know $\underline{\underline{K}}$, we can easily determine the flux resulting from a given source $\underline{S}$ by a single matrix multiplication. But of course we don't know $\underline{\underline{K}}$ since we don't know $G(\mathbf{r},\mathbf{r}')$. The key to such nodal methods therefore lies in our ability to approximate or guess the coupling coefficients $K_{nn'}$.

Of course from a formal point of view, if the number of nodal cells $N$ is large, the nodal method becomes equivalent to the finite difference scheme and hence loses any calculational advantages. The real power of the nodal approach is realized only when the number of node cells $N$ is small, since then the cells are large enough that they become coupled via neutron diffusion only to nearby cells—that is, the transfer matrix $\underline{\underline{K}}$ is sparse (i.e., it has many zero elements). However choosing large node cells places the burden of the calculational effort on an estimate of the coupling coefficients $K_{nn'}$.

The determination of these coefficients is usually accomplished in a most empirical fashion (a nice way of saying they are *fudged*). Typically the $K_{nn'}$ are determined by assuming a flat nodal source and uniform composition in each cell

and allowing neutron transfer to only the six nearest neighbor cells. The transfer coefficients are represented as linear combinations of several simple trial functions (e.g., from one-dimensional slab geometry calculations). The blending coefficients in this representation are then determined by comparison with more accurate finite difference benchmark calculations and lots of experience, fiddling, and fudging.

If the transfer coefficients are properly chosen, then such nodal methods can be extremely useful in generating three-dimensional flux distributions when only limited accuracy is required. Unfortunately such empirical schemes for choosing the $K_{nn'}$ are quite problem-sensitive and require a good deal of experience on the part of the reactor analyst.

We will leave numerical methods for solving diffusion equations until later when we must generalize these methods to account for fission processes and energy-dependence. The above discussion has been an admittedly curse description of numerical methods for solving differential equations. There is a vast literature on this subject that provides the details of the methods we have so briefly outlined.[12-16] And perhaps the most valid argument for presenting only a brief sketch of such numerical methods lies in the recognition that these topics are of such vital importance to the practicing nuclear engineer, that he almost certainly will have had or will take further courses on numerical analysis in any event.

# III. ONE-SPEED DIFFUSION THEORY OF A NUCLEAR REACTOR

## A. Introduction

Thus far we have studied the diffusion of neutrons in nonmultiplying media as described by one-speed diffusion theory. We now wish to apply this theory to the study of nuclear reactors in which fissile material is present. Hence we must determine how to include nuclear fission in the one-speed diffusion equation (5-16).

To this end, let us first recall the sequence of events involved in a fission chain reaction. To be specific, we first consider the processes occurring in thermal nuclear reactors (see Figure 5-15). Fission neutrons are born at high energies in the MeV range. It is possible that such fast neutrons induce fission in either fissile ($^{235}U$ or $^{239}Pu$) or fissionable isotopes ($^{238}U$). It is far more likely that the fast fission neutrons will be moderated to lower energies by elastic scattering collisions with light moderator nuclei (e.g., $^{1}_{1}H$ or $^{12}_{6}C$). As the fission neutrons are slowed down, they pass through energies comparable to the absorption resonances in heavy nuclei such as $^{238}U$ and hence experience an appreciable probability of being absorbed. They may also leak out of the reactor core during this slowing down process. In a thermal reactor, however, over 85–90% of the neutrons will manage to slow down to thermal energies. They will then diffuse about the reactor core until they either leak from the core or are absorbed. If they are absorbed in the fuel, then they may induce a new fission, thereby repeating the cycle.

The processes involved in fast reactors are somewhat similar (see Figure 5-16). In such reactors an effort is made to prevent the fission neutrons from slowing down before they will have had a chance to induce fission. Low mass number material is avoided to reduce the energy loss via elastic scattering. However some moderation will occur, due both to elastic scattering from materials such as oxygen (remember, most fast reactor fuels are oxides) as well as inelastic scattering from materials such
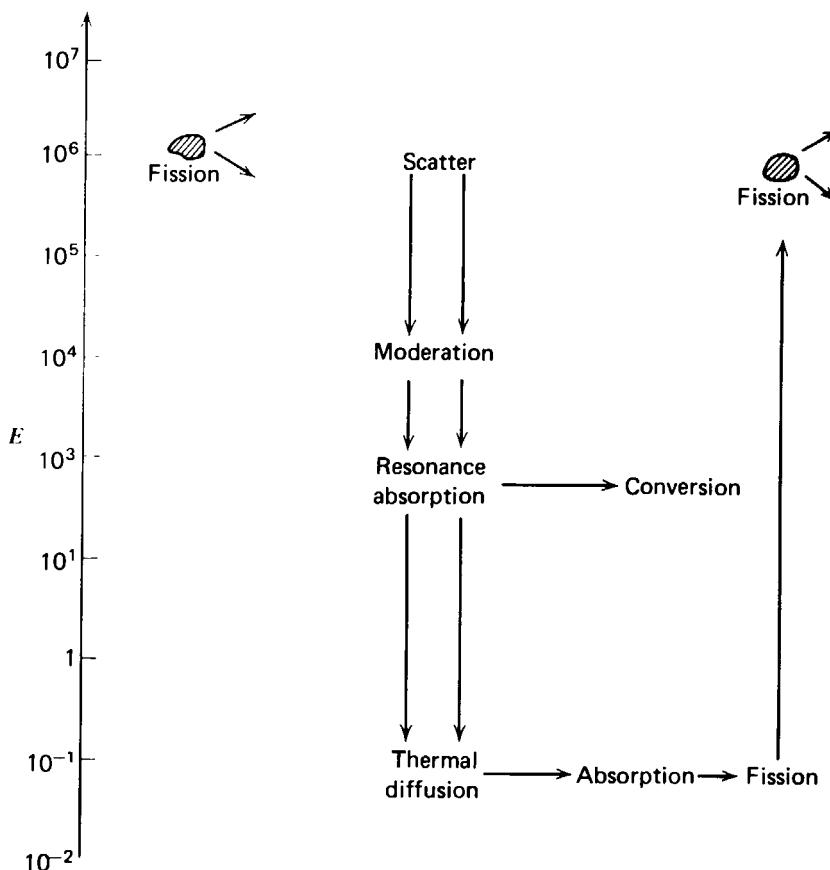
**FIGURE 5-15.** A schematic of the various processes involved in a thermal reactor

as sodium. In particular there will be a tendency for some of the neutrons to slow down to the energy range in which appreciable resonance absorption may occur, although most of the fission reactions will be induced by neutrons with energies above this range. Hence neutron moderation, leakage, and resonance absorption all play an important role in fast reactor physics, just as they do with thermal reactors.

It should be evident that the various processes occurring during this sequence are strongly energy dependent. We will apply our one-speed diffusion model to study such processes, however. Our motivation is partly pedagogical since this model is by far the simplest description of nuclear reactor behavior and allows us to introduce many concepts of nuclear reactor analysis in the simplest possible framework. However as we have noted earlier, the one-speed diffusion model can also provide a very useful qualitative description of certain reactor types (notably very thermal or very fast reactors) provided one uses the correct values for the cross sections $(\Sigma_a, \Sigma_f, \Sigma_{tr})$ which appear in the model.

## B. The Fission Source Term

We now direct our attention toward determining a way to include fission in the one-speed diffusion equation. We will assume that diffusion, absorption, and fission all occur at the same energy. Then a term to represent fissions can easily be derived by noting that if $\Sigma_f\phi(\mathbf{r}, t)$ is the fission reaction rate density, then the rate at which fission neutrons appear in the reactor—that is, the "fission source"—is given by

$$S_f(\mathbf{r}, t) = \nu\Sigma_f\phi(\mathbf{r}, t).$$

(5-186)
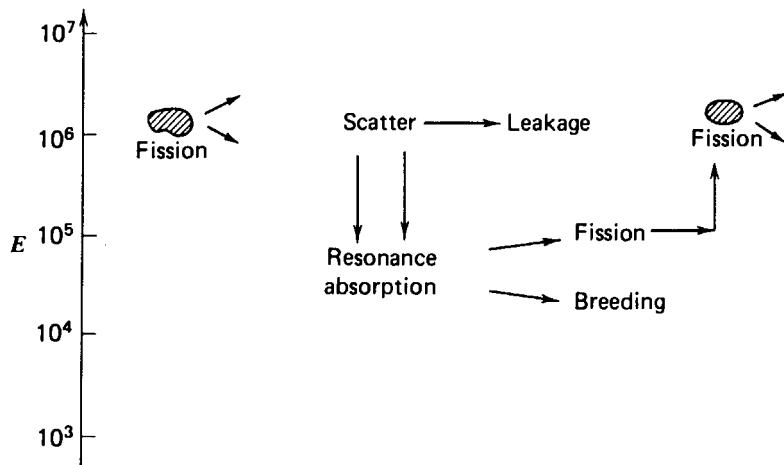
**FIGURE 5-16.    Neutron processes involved in a fast reactor**

If this is the only source of neutrons in the reactor,[†] then the appropriate diffusion equation becomes

$$\frac{1}{v}\frac{\partial\phi}{\partial t}-\nabla\cdot D\nabla\phi+\Sigma_a\phi(\mathbf{r},t)=\nu\Sigma_f\phi(\mathbf{r},t). \tag{5-187}$$

Note here that we can identify the various components of the macroscopic absorption cross section which appear in Eq. (5-187) as:

$$\Sigma_a=\Sigma_a^{\text{moderator}}+\Sigma_a^{\text{structure}}+\Sigma_a^{\text{coolant}}+\Sigma_a^{\text{fuel}}$$

and

$$\Sigma_a^{\text{fuel}}=\Sigma_\gamma^{\text{fuel}}+\Sigma_f^{\text{fuel}}. \tag{5-188}$$

## C. The Time-Dependent "Slab" Reactor

### 1. GENERAL SOLUTION

We will begin our study of nuclear reactor behavior as described by the one-speed diffusion equation by considering a uniform slab of fissile material characterized by cross sections $\Sigma_a$, $\Sigma_{tr}$, and $\Sigma_f$. This unrealistic appearing "slab reactor" is chosen to introduce many of the concepts of nuclear reactor analysis, since its one dimensional geometry greatly facilitates the detailed solution of the one speed diffusion equation.[‡] The appropriate mathematical description of the

---

[†] Actually we should hedge here a bit. Equation (5-187) actually represents only "prompt" neutrons, that is, those born instantaneously in fission. The "delayed" neutrons arising from fission product decay require a slightly different treatment. We will defer this modification until Chapter 6.

[‡] In this sense it is somewhat akin to the "vibrating string" or "simple harmonic oscillator" problems in physics that also get beaten to death since they contain most of the interesting physics—and yet are easy to solve.
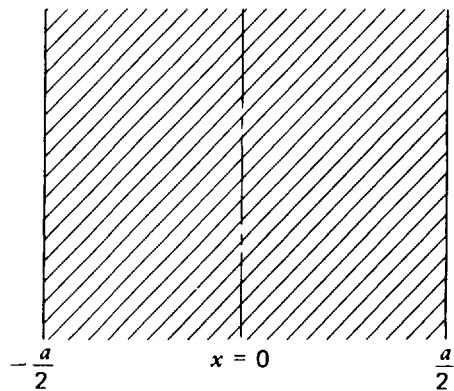
FIGURE 5-17. The slab reactor

neutron flux in such a reactor is

$$\frac{1}{v}\frac{\partial \phi}{\partial t} - D\frac{\partial^2 \phi}{\partial x^2} + \Sigma_a \phi(x,t) = \nu\Sigma_f \phi(x,t), \tag{5-189}$$

with initial condition: $\phi(x,0) = \phi_0(x) = \phi_0(-x)$ (symmetric),

and boundary conditions: $\phi\left(\frac{\tilde{a}}{2},t\right) = \phi\left(-\frac{\tilde{a}}{2},t\right) = 0.$

Notice that we have assumed that our initial flux is symmetric. We will find later that such an assumption will imply similar symmetry for all times, $\phi(x,t) = \phi(-x,t)$. This will simplify our manipulations somewhat.

Unlike our earlier studies of time-independent neutron diffusion, we are now faced with a *partial* differential equation to solve. There are a number of ways to attack such equations, but perhaps the simplest is to use *separation of variables*[1-3] by seeking a solution of the form

$$\phi(x,t) = \psi(x)T(t). \tag{5-190}$$

If we substitute this form into Eq. (5-189) and divide by $\psi(x)T(t)$, we find

$$\frac{1}{T}\frac{dT}{dt} = \frac{v}{\psi}\left[D\frac{d^2\psi}{dx^2} + (\nu\Sigma_f - \Sigma_a)\psi(x)\right] = \text{constant} \equiv -\lambda. \tag{5-191}$$

Here we have noted that since we have a function only of $x$ set equal to a function only of $t$, both terms must in fact be equal to a constant. We have named this constant $-\lambda$. However $\lambda$ is as yet unknown.

Hence the separation of variables given by Eq. (5-190) has reduced the original partial differential equation in two variables to two ordinary differential equations:

$$\frac{dT}{dt} = -\lambda T(t),$$

$$D\frac{d^2\psi}{dx^2} + (\nu\Sigma_f - \Sigma_a)\psi(x) = -\frac{\lambda}{v}\psi(x). \tag{5-192}$$

We can easily solve the time-dependent equation

$$T(t) = T(0)e^{-\lambda t}, \tag{5-193}$$

where $T(0)$ is an initial value which must be determined later. To solve the space-dependent equation, we must tack on the boundary conditions:

$$D\frac{d^2\psi}{dx^2} + \left(\frac{\lambda}{v} + \nu\Sigma_f - \Sigma_a\right)\psi(x) = 0,$$

$$\text{Boundary condition: } \psi\left(\frac{\tilde{a}}{2}\right) = \psi\left(-\frac{\tilde{a}}{2}\right) = 0. \tag{5-194}$$

Here $\lambda$ is still to be determined. However we recall the eigenvalue problem

$$\frac{d^2\psi_n}{dx^2} + B_n^2\psi_n(x) = 0,$$

$$\psi_n\left(\frac{\tilde{a}}{2}\right) = \psi_n\left(-\frac{\tilde{a}}{2}\right) = 0, \tag{5-195}$$

has symmetric solutions (we are only interested in symmetric solutions since $\phi_0(x)$ is symmmetric):

$$\text{eigenfunctions: } \psi_n(x) = \cos B_n x$$

$$\text{eigenvalues: } B_n^2 = \left(\frac{n\pi}{\tilde{a}}\right)^2, \qquad n = 1,3,5,\ldots \tag{5-196}$$

If we identify Eq. (5-194) as the same problem, it is apparent that we must choose

$$\lambda = v\Sigma_a + vDB_n^2 - v\nu\Sigma_f \equiv \lambda_n, \qquad n = 1,3,5,\ldots \tag{5-197}$$

These values of $\lambda_n$ are known as the *time eigenvalues* of the equation, since they characterize the time decay in Eq. (5-193). The general solution to Eq. (5-189) must therefore be of the form

$$\phi(x,t) = \sum_{\substack{n \\ \text{odd}}} A_n \exp(-\lambda_n t)\cos\frac{n\pi x}{\tilde{a}}. \tag{5-198}$$

This solution automatically satisfies the boundary conditions. To determine the $A_n$, we use the initial condition to write

$$\text{Initial condition: } \phi(x,0) = \phi_0(x) = \sum_{\substack{n \\ \text{odd}}} A_n \cos\frac{n\pi x}{\tilde{a}}. \tag{5-199}$$

Using orthogonality, we find

$$A_n = \frac{2}{\tilde{a}} \int_{-\frac{a}{2}}^{\frac{a}{2}} dx\, \phi_0(x)\cos\frac{n\pi x}{\tilde{a}}. \tag{5-200}$$

Thus we have found that the flux (for any symmetric initial distribution) can be represented as a superposition of modes, each mode weighted by an exponential

factor:

$$\phi(x,t)= \sum_{\substack{n \\ \text{odd}}} \left[ \frac{2}{\tilde{a}} \int_{-\frac{a}{2}}^{\frac{a}{2}} dx' \, \phi_0(x') \cos B_n x' \right] \exp(-\lambda_n t) \cos B_n x, \qquad (5\text{-}201)$$

where the time eigenvalues $\lambda_n$ are given by

$$\lambda_n = v\Sigma_a + vDB_n^2 - v\nu\Sigma_f, \qquad B_n = \frac{n\pi}{\tilde{a}}. \qquad (5\text{-}202)$$

Before we proceed to examine this solution in more detail, it is useful to make a few comments about the separation of variables approach. First notice that the separation parameter that arose was in fact identified as an eigenvalue. Thus separation of variables is essentially equivalent to an eigenfunction expansion. Indeed if we had the foresight to expand the spatial dependence of the flux in the eigenfunctions for the slab (using symmetry to restrict this expansion to odd $n$),

$$\phi(x,t)= \sum_{\substack{n \\ \text{odd}}} T_n(t) \cos \frac{n\pi x}{\tilde{a}}, \qquad (5\text{-}203)$$

where we have noted that the expansion coefficients now must be time-dependent, then we could have immediately arrived at an equation for the $T_n$

$$\frac{dT_n}{dt} = -\lambda_n T_n(t) \qquad (5\text{-}204)$$

by substituting Eq. (5-203) into the original equation (5-189) and using the orthogonality property of the eigenfunctions. This alternative approach is frequently useful when encountering problems in which sources are present, because the separation of variables approach we have presented applies only to homogeneous equations.

Finally, note that although we initially sought solutions $\psi(x)T(t)$ which were separable in $x$ and $t$, these solutions were eventually superimposed to yield a nonseparable function of space and time [cf. Eq. (5-201)]. Hence separation of variables does certainly not imply a separable solution. Interestingly enough, however, there is one very important situation in which such separability will occur, that involving the behavior of the neutron flux for very long times.

## 2. LONG TIME BEHAVIOR

Notice that one can order $B_1^2 < B_3^2 < \cdots B_n^2 = (n\pi/\tilde{a})^2 \cdots$. Hence the time eigenvalues must similarly be ordered such that $\lambda_1 < \lambda_3 < \lambda_5 < \lambda_7 < \cdots$. This means that the modes corresponding to larger $n$ decay out more rapidly in time. If we wait long enough, then only the *fundamental mode* remains:

$$\phi(x,t) \sim A_1 \exp(-\lambda_1 t) \cos B_1 x \qquad \text{as} \qquad t \to \infty. \qquad (5\text{-}205)$$

This implies that regardless of the initial shape of $\phi_0(x)$ the flux will decay into the
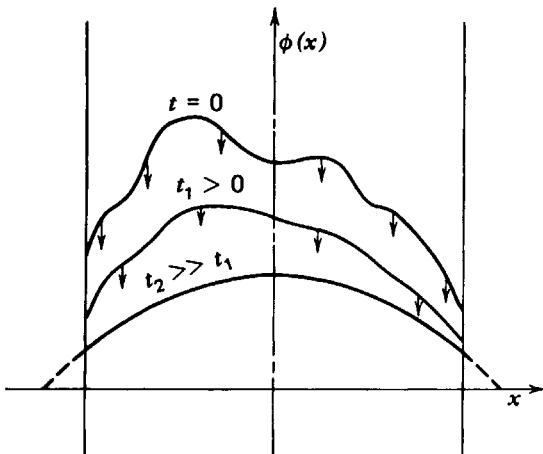
FIGURE 5-18.    Time decay of higher order spatial modes in the slab reactor

fundamental mode shape. Of course, we have implicitly assumed that $A_1$ will not be zero. The coefficient of the fundamental mode is just

$$A_1 = \frac{2}{\tilde{a}} \int_{-\frac{\tilde{a}}{2}}^{\frac{\tilde{a}}{2}} dx'\, \phi_0(x') \cos\frac{\pi x'}{\tilde{a}}.$$    (5-206)

Since $\phi_0(x)$ must be nonnegative in the slab to represent a physically realizable flux, then it is apparent that $A_1 > 0$.

Actually for sufficiently large $\Sigma_f$, $-\lambda_n$ may be positive corresponding to an exponentially *growing* flux. However the same argument will hold since $-\lambda_1 > -\lambda_3 > \cdots$. Hence regardless of whether the flux grows or decays, it will eventually approach a "persistent" or fundamental cosine distribution.

It is customary to refer to the value of $B_n^2$ characterizing this mode as

$$B_1^2 = \left(\frac{\pi}{\tilde{a}}\right)^2 \equiv B_g^2 \equiv geometric\ buckling.$$    (5-207)

This nomenclature is used since $B_n^2$ is a measure of the curvature of the mode shape

$$B_n^2 = -\frac{1}{\psi_n}\frac{d^2\psi_n}{dx^2}.$$    (5-208)

Since there will be a larger current density $J$ and hence leakage induced by a mode with larger curvature or buckling, we might expect that the mode with least curvature will persist in time the longest.

## 3. THE CRITICALITY CONDITION

Let us now see what is required to make the flux distribution in the reactor time-independent—that is, to make the fission chain reaction steady-state. We will define this situation to be that of reactor *criticality*:

Criticality ≡ when a time-independent neutron flux can be sustained in the reactor (in the absence of sources other than fission).

Notice that we have qualified this definition by specifically demanding that the flux be time-independent in the absence of a source. As we have seen in Chapter 3 (and will see later in the problem set at the end of this chapter), a source present in a critical system will give rise to an increase in flux that is linear in time.

If we write out the general solution for the flux

$$\phi(x,t) = A_1 \exp(-\lambda_1 t)\cos B_1 x + \sum_{\substack{n=3 \\ n \text{ odd}}}^{\infty} A_n \exp(-\lambda_n t)\cos B_n x, \qquad (5\text{-}209)$$

it is evident that the requirement for a time-independent flux is just that the fundamental time eigenvalue vanish

$$\lambda_1 = 0 = v(\Sigma_a - \nu\Sigma_f) + vDB_1^2, \qquad (5\text{-}210)$$

since then the higher modes will have negative $\lambda_n$ and decay out in time, leaving just

$$\phi(x,t) \to A_1 \cos B_1 x \neq \text{function of time.} \qquad (5\text{-}211)$$

If we rewrite this "criticality condition" using the notation $B_1^2 = B_g^2$, then we find we must require

$$\frac{\nu\Sigma_f - \Sigma_a}{D} = B_g^2. \qquad (5\text{-}212)$$

It has become customary to refer to

$$\frac{\nu\Sigma_f - \Sigma_a}{D} \equiv B_m^2 \equiv \text{material buckling} \qquad (5\text{-}213)$$

since it depends only on the material composition of the reactor core (whereas $B_g^2$ depends only on the core geometry). Hence our criticality condition can be written very concisely as

$$\text{(material composition)} \ B_m^2 = B_g^2 \ \text{(core geometry).} \qquad (5\text{-}214)$$

Thus to achieve a critical reactor, we must either adjust the size $(B_g^2)$ or the core composition $(B_m^2)$ such that $B_m^2 = B_g^2$. We also note

$$B_m^2 > B_g^2 \Rightarrow \lambda_1 < 0 \Rightarrow \quad \text{supercritical,}$$
$$B_m^2 = B_g^2 \Rightarrow \lambda_1 = 0 \Rightarrow \quad \text{critical,} \qquad (5\text{-}215)$$
$$B_m^2 < B_g^2 \Rightarrow \lambda_1 > 0 \Rightarrow \quad \text{subcritical.}$$

In particular notice that by increasing the core size we decrease $B_g^2$, while by increasing the concentration of fissile material we increase $\Sigma_f$ and hence $B_m^2$. Both of these modifications would therefore tend to enhance core multiplication.

Yet recall that in Chapter 3 we expressed the criticality condition in terms of the multiplication factor $k$. We can make the connection between these two criteria if we write the time eigenvalue as

$$\lambda_1 = v\Sigma_a(1 + L^2 B_g^2)\left(1 - \frac{\nu\Sigma_f/\Sigma_a}{1 + L^2 B_g^2}\right). \qquad (5\text{-}216)$$

Now recall that $(v\Sigma)^{-1}$ is the mean lifetime for a given neutron–nuclear reaction to occur. Hence $(v\Sigma_a)^{-1}$ must be just the mean lifetime of a neutron to absorption (ignoring leakage—that is, in an infinite medium). Furthermore, we can identify

$$\frac{\nu\Sigma_f}{\Sigma_a} = \frac{\nu\Sigma_f^{Fuel}}{\Sigma_a^{Fuel}} \frac{\Sigma_a^{Fuel}}{\Sigma_a} = \eta f = k_\infty. \tag{5-217}$$

Now the only remaining task is to identify $(1 + L^2 B_g^2)^{-1}$. Recall that the rate of neutron leakage is given by

$$\text{Leakage}_{\text{rate}} = \int_S d\mathbf{S}\cdot\mathbf{J} = \int_V d^3r\, \nabla\cdot\mathbf{J} = -\int_V d^3r\, D\nabla^2\phi, \tag{5-218}$$

where we have used both Gauss's theorem and the diffusion approximation. Hence we can write

$$\frac{\text{Rate of neutron absorption}}{\text{Rate of neutron absorption plus leakage}} = \frac{\int_V d^3r\Sigma_a\phi}{\int_V d^3r\Sigma_a\phi - \int_V d^3r D\nabla^2\phi}$$

$$= \frac{\Sigma_a\int_V d^3r\,\phi}{\Sigma_a\int_V d^3r\,\phi + DB_g^2\int_V d^3r\,\phi} = \frac{1}{\left(1 + L^2 B_g^2\right)}. \tag{5-219}$$

However we can identify this ratio as just

$$\text{Nonleakage probability} \equiv P_{\text{NL}} \equiv \frac{1}{1 + L^2 B_g^2}. \tag{5-220}$$

Therefore we can interpret

$$\frac{1}{(v\Sigma_a)(1 + L^2 B_g^2)} = P_{\text{NL}}\left(\frac{1}{v\Sigma_a}\right) \equiv l \equiv \frac{\text{neutron lifetime}}{\text{in a finite reactor}}, \tag{5-221}$$

since we have just reduced the lifetime to absorption in an infinite medium to take account of neutron leakage. If we now combine Eqs. (5-217) and (5-220), we find that the multiplication factor $k$ for this model becomes just

$$k = \eta f P_{\text{NL}} = \frac{\nu\Sigma_f/\Sigma_a}{1 + L^2 B_g^2}. \tag{5-222}$$

Thus we can identify our fundamental time eigenvalue as just the inverse of the reactor period

$$-\lambda_1 = \frac{k - 1}{l} = \frac{1}{T}. \tag{5-223}$$

If we also recall from Eq. (5-202) that

$$\lambda_1 = vD\left(B_g^2 - B_m^2\right), \tag{5-224}$$

then it is apparent that the various forms of the criticality condition are indeed equivalent:

$$\lambda_1 = 0 \Leftrightarrow B_g^2 = B_m^2 \Leftrightarrow k = 1. \tag{5-225}$$

In particular notice that by using $P_{\mathrm{NL}} = (1 + L^2 B_g^2)^{-1}$ we can avoid the analysis of the initial value problem and proceed directly to the criticality condition

$$k = \frac{\nu \Sigma_f / \Sigma_a}{1 + L^2 B_g^2} = 1. \tag{5-226}$$

We will return later to consider how these results can be applied to reactor criticality studies, but first we will extend them to more general reactor geometries.

## D. The Criticality Condition for More General Bare Geometries

Note that the only quantity characteristic of the reactor size or geometry that appears in $k$ or $P_{\mathrm{NL}}$ is the geometric buckling, $B_g^2$. For the case of a slab reactor of width $a$ we found $B_g^2 = (\pi / \tilde{a})^2$. We might suspect that for more general geometries we need only replace this by the geometric buckling characterizing the specific geometry under consideration. This suspicion is in fact easily verified, but only for so-called "bare" geometries in which the reactor composition is uniform. For the more complicated multiregion geometries, such as reactors composed of a core surrounded by a reflecting material, one can no longer derive simple expressions for $P_{\mathrm{NL}}$ or $k$ in terms of the reactor geometry and composition.

Consider, then, a bare reactor of uniform composition surrounded by a free nonreentrant surface characterized by vacuum boundary conditions. If the reactor is critical then the neutron flux must satisfy the steady-state diffusion equation

$$- D \nabla^2 \phi + \Sigma_a \phi(\mathbf{r}) = \nu \Sigma_f \phi(\mathbf{r}), \tag{5-227}$$

subject to the boundary condition $\phi(\tilde{\mathbf{r}}_s) = 0$ for $\tilde{\mathbf{r}}_s$ on the extrapolated surface. Of course in general there will be no solution to this equation unless we have happened to hit on just the right combination of composition and system size.

To see this more clearly, divide Eq. (5-227) by $- D$ so that it can be written as

$$\nabla^2 \phi + \left( \frac{\nu \Sigma_f - \Sigma_a}{D} \right) \phi(\mathbf{r}) = 0, \tag{5-228}$$

boundary condition: $\phi(\tilde{\mathbf{r}}_s) = 0.$

Sometimes Eq. (5-228) is written in a somewhat different form as

$$\nabla^2 \phi + \left( \frac{k_\infty - 1}{L^2} \right) \phi(\mathbf{r}) = 0, \tag{5-229}$$

boundary condition: $\phi(\tilde{\mathbf{r}}_s) = 0.$

Now notice that this equation is identical to that which generates the spatial eigenfunctions for this geometry

$$\nabla^2 \psi_n + B_n^2 \psi_n(\mathbf{r}) = 0, \tag{5-230}$$

boundary condition: $\psi(\tilde{\mathbf{r}}_s) = 0.$

We know that this latter equation has nontrivial solutions $\psi_n(\mathbf{r})$ only for certain values of the parameter $B^2$, the eigenvalues $B_n^2$. Hence by comparing Eqs. (5-228) and (5-230) we find that the steady-state diffusion equation for the flux $\phi(\mathbf{r})$ will only have nontrivial solutions when the core composition is such that $(\nu\Sigma_f - \Sigma_a)/D$ is equal to an eigenvalue $B_n^2$, and then the flux $\phi(\mathbf{r})$ will be given by the corresponding eigenfunction $\psi_n(\mathbf{r})$.

However since there are an infinite number of possible eigenvalues $B_n^2$, we might be tempted to think that there are an infinite number of values $(\nu\Sigma_f - \Sigma_a)/D \equiv B_m^2$ for which the reactor is critical. However it should be recalled that in the case of a slab geometry, only the lowest eigenvalue $B_1^2 = (\pi/\tilde{a})^2 \equiv B_g^2$ had a corresponding eigenfunction $\psi_1(x) = \cos\pi x/\tilde{a}$ that was everywhere positive. The eigenfunctions or spatial modes $\psi_n(x)$ corresponding to higher eigenvalues oscillated about zero. This same feature also characterizes the eigenfunctions $\psi_n(\mathbf{r})$ of more general geometries. Only the eigenfunction $\psi_1(\mathbf{r})$ corresponding to the smallest eigenvalue $B_1^2$ is everywhere nonnegative. Since the neutron flux can never be negative, it is apparent that the only solution to the eigenvalue problem Eq. (5-230) physically relevant is that corresponding to the smallest eigenvalue, $B_1^2 \equiv B_g^2$. Hence for the reactor to be critical we require

$$B_m^2 \equiv \left( \frac{\nu\Sigma_f - \Sigma_a}{D} \right) = B_1^2 \equiv B_g^2 \qquad (5\text{-}231)$$

just as for the slab.

Thus we can continue to use $P_{\mathrm{NL}} = (1 + L^2 B_g^2)^{-1}$ and $k = (\nu\Sigma_f/\Sigma_a)(1 + L^2 B_g^2)^{-1}$ for more general bare geometries provided we identify the geometric buckling $B_g^2$ as the smallest eigenvalue $B_1^2$ of the Helmhotz equation

$$\nabla^2\phi + B_g^2\phi(\mathbf{r}) = 0 \qquad (5\text{-}232)$$

subject to the boundary conditions that $\phi(\mathbf{r})$ vanish on the extrapolated boundary of the reactor. The corresponding critical flux distribution $\phi(\mathbf{r})$ is then given by the fundamental eigenfunction $\psi_1(\mathbf{r})$, which is everywhere nonnegative.

It should be pointed out that although the Helmhotz equation (5-232) will provide us with the flux shape in a critical reactor, it will tell us nothing about the magnitude of the flux. Since it is a homogeneous equation, if $\phi(\mathbf{r})$ is a solution, then any multiple of $\phi(\mathbf{r})$ is also a solution. Of course the magnitude of the flux was determined for us by the initial condition $\phi_0(\mathbf{r})$ when we studied reactor criticality by solving the full time-dependent diffusion equation (5-187). However this latter approach is far too cumbersome to use in practice.

Instead we merely note that a critical reactor can operate at any flux level—at least mathematically. (Of course one must provide for adequate core cooling, shielding, etc., but these factors are extraneous to our present model of the reactor so we won't worry about them here.) Hence we will merely assume that the magnitude of the flux is determined by the desired thermal power output of the core. If the usable energy produced per fission event is $w_f$, then the thermal energy deposited in the core per unit volume per second is just given in terms of the fission reaction rate density as

$$q(\mathbf{r}) = w_f\Sigma_f\phi(\mathbf{r}). \qquad (5\text{-}233)$$

This is just the local thermal power density at position r in the core. Hence the total power generated by the core is just the integral of the power density over the core volume

$$P = \int_V d^3r \, w_f \Sigma_f \phi(\mathbf{r}). \tag{5-234}$$

This relation can be used to determine the magnitude of the flux in terms of the core thermal power level.

Thus we now have developed a rather simple scheme to study the criticality of a nuclear reactor—at least a bare, uniform reactor. The only mathematical effort required is the solution of the Helmhotz equation characterizing the geometry of interest for the geometric buckling $B_g^2$ (the fundamental eigenvalue $B_1^2$) and the critical flux shape $\phi(\mathbf{r})$ [the fundamental spatial eigenfunction $\psi_1(\mathbf{r})$]. To illustrate how these quantities are determined, we will consider a simple yet very important example:

EXAMPLE: A Right Circular Cylindrical Core

The most common reactor core shape is that of a right circular cylinder of height $H$ and radius $R$. (Actually a sphere would be the more optimum geometry from the aspect of minimizing neutron leakage, but spheres are very inconvenient geometries to pass coolants through.) The appropriate form of the Helmholtz equation is then

$$\frac{1}{r} \frac{\partial}{\partial r} r \frac{\partial \phi}{\partial r} + \frac{\partial^2 \phi}{\partial z^2} + B^2 \phi(r, z) = 0, \tag{5-235}$$

subject to boundary conditions

$$\phi(\tilde{R}, z) = 0 = \phi\left(r, \pm \frac{\tilde{H}}{2}\right).$$

Since this is a homogeneous partial differential equation, we can seek its solution using separation of variables

$$\phi(r, z) = \mathcal{R}(r) \mathcal{Z}(z).$$

Then if we substitute this form into Eq. (5-235), we arrive at two ordinary
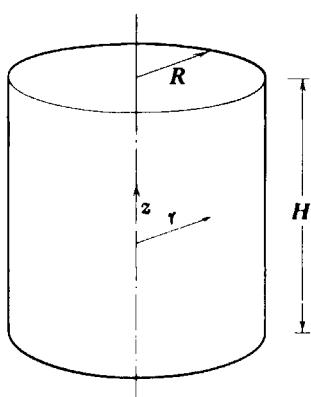


FIGURE 5-19. Finite cylindrical reactor core

differential equations

$$\frac{1}{r}\frac{d}{dr}r\frac{d\mathcal{R}}{dr} + \alpha^2\,\mathcal{R}(r) = 0, \qquad \mathcal{R}(\tilde{R}) = 0, \tag{5-236a}$$

$$\frac{d^2\mathcal{Z}}{dz^2} + \lambda^2\mathcal{Z}(z) = 0, \qquad \mathcal{Z}\left(\pm\frac{\tilde{H}}{2}\right) = 0, \tag{5-236b}$$

where the separation constants $\alpha^2$ and $\lambda^2$ are constrained by the relationship $B^2 = \alpha^2 + \lambda^2$. Each of these equations represents a separate eigenvalue problem that one can use to determine $\alpha$ and $\lambda$ (and hence $B^2$). The eigenfunctions and eigenvalues of the axial equation are well known to us

$$\mathcal{Z}_n(z) = \cos\left(\frac{n\pi z}{\tilde{H}}\right), \qquad \lambda_n^2 = \left(\frac{n\pi}{\tilde{H}}\right)^2, \qquad n = 1, 3, \ldots \tag{5-237}$$

To construct the eigenfunctions of the radial Eq. (5-236a), we first identify its general solution in terms of zeroth order Bessel functions (see Appendix D)

$$\mathcal{R}(r) = AJ_0(\alpha r) + CY_0(\alpha r). \tag{5-238}$$

Since $Y_0(\alpha r) \to \infty$ as $r \to 0$, we must set $C \equiv 0$. Applying our boundary condition at $r = \tilde{R}$, we find

$$\mathcal{R}(\tilde{R}) = AJ_0(\alpha\tilde{R}) = 0 \Rightarrow \alpha\tilde{R} = \nu_n, \tag{5-239}$$

where $\nu_n$ are the zeros of $J_0$. In particular, the smallest such zero is $\nu_0 = 2.405\ldots$ (kind of like $\pi$ to a Bessel function). Hence we find the eigenfunctions and eigenvalues generated by the radial equation (5-236a) are just

$$\mathcal{R}_n(r) = J_0\left(\frac{\nu_n r}{\tilde{R}}\right), \qquad \alpha_n^2 = (\nu_n/\tilde{R})^2, \qquad n = 0, 1, \ldots \tag{5-240}$$

Therefore, consistent with our prescription of seeking the smallest value of $B^2$ as our geometric buckling, we find

$$B_g^2 = \left(\frac{\nu_0}{\tilde{R}}\right)^2 + \left(\frac{\pi}{\tilde{H}}\right)^2, \tag{5-241}$$

corresponding to a spatial flux shape

$$\phi(r,z) = AJ_0\left(\frac{\nu_0 r}{\tilde{R}}\right)\cos\left(\frac{\pi z}{\tilde{H}}\right). \tag{5-242}$$

Since this is the geometry most frequently encountered in reactor design, it is useful to calculate the normalization factor $A$ in terms of the core power level $P$ by noting

$$P = \int_V d^3r\, w_f\Sigma_f\phi(\mathbf{r}) = w_f\Sigma_f 2\pi A \int_0^{\tilde{R}} dr\, rJ_0\left(\frac{\nu_0 r}{\tilde{R}}\right)\int_{-\frac{\tilde{H}}{2}}^{\frac{\tilde{H}}{2}} dz\cos\left(\frac{\pi z}{\tilde{H}}\right) = \frac{w_f\Sigma_f A4VJ_1(\nu_0)}{\pi\nu_0}. \tag{5-243}$$
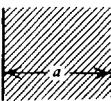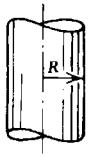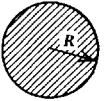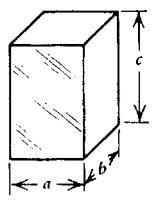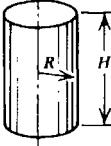
Thus we find

$$A = \frac{3.63P}{w_f \Sigma_f V}, \quad V = \pi \tilde{R}^2 \tilde{H}. \tag{5-244}$$

It should perhaps be mentioned that since reactor cores are fabricated from either square- or hexagonally-shaped fuel assemblies, one can only approximate such cylindrical geometries. However for most purposes one can assume the reactor core is essentially a right circular cylinder.

One can proceed in a very similar manner to analyze other bare core geometries. For convenience, we have tabulated the geometric buckling and critical flux profile in other common geometries in Table 5-1.

**TABLE 5-1 Geometric Bucklings and Critical Flux Profiles Characterizing Some Common Core Geometries**

| | | Geometric Buckling $B_g^2$ | Flux profile |
|---|---|---|---|
| Slab | | $\left(\frac{\pi}{\tilde{a}}\right)^2$ | $\cos\frac{\pi x}{\tilde{a}}$ |
| Infinite Cylinder | | $\left(\frac{\nu_0}{\tilde{R}}\right)^2$ | $J_0\left(\frac{\nu_0 r}{\tilde{R}}\right)$ |
| Sphere | | $\left(\frac{\pi}{\tilde{R}}\right)^2$ | $r^{-1}\sin\left(\frac{\pi r}{\tilde{R}}\right)$ |
| Rectangular Parallelepiped | | $\left(\frac{\pi}{\tilde{a}}\right)^2 + \left(\frac{\pi}{\tilde{b}}\right)^2 + \left(\frac{\pi}{\tilde{c}}\right)^2$ | $\cos\left(\frac{\pi x}{\tilde{a}}\right)\cos\left(\frac{\pi y}{\tilde{b}}\right)\cos\left(\frac{\pi z}{\tilde{c}}\right)$ |
| Finite Cylinder | | $\left(\frac{\nu_0}{\tilde{R}}\right)^2 + \left(\frac{\pi}{\tilde{H}}\right)^2$ | $J_0\left(\frac{\nu_0 r}{\tilde{R}}\right)\cos\left(\frac{\pi z}{\tilde{H}}\right)$ |

The reader should not be deceived into believing that such criticality calculations are always so straightforward. For we must remember that the expression we have derived for the nonleakage probability $P_{NL} = (1 + L^2 B_g^2)^{-1}$ holds only for uniform, bare reactor geometries (i.e., single-region cores). As we will find later, it is no longer possible to derive simple expressions for $P_{NL}$ or $k$ in terms of the reactor geometry and composition for multiregion (e.g., reflected) reactors.

These results can be used to determine the core geometry or composition that

will yield a critical reactor. For example, if the material composition is specified, one can compute the material buckling $B_m^2$ in terms of the macroscopic cross sections using Eq. (5-213). Then by using the criticality condition $B_m^2 = B_g^2$ (along with Table 5-1), one can infer the core dimensions that will yield a critical system.

In the more usual situation the nuclear designer will be given $B_g^2$ (rather than $B_m^2$) since the core dimensions are determined by limitations on core thermal performance (and not nuclear considerations). That is, the core must be built a sufficiently large size to avoid excessively high temperatures for a desired power output. The nuclear designer must then determine the fuel concentration or loading (i.e., $B_m^2$) that not only will result in a critical system, but will also allow the core to operate at a rated power for a given time period.

EXAMPLE:   As a specific example we will study the one-speed diffusion model of a bare, homogeneous cylindrical reactor with material composition representative of that of a modern PWR such as described in Appendix H. We will use "homogenized" number densities corresponding to a PWR core operating at full power conditions and containing a concentration of 2210 ppm of natural boron (as boric acid) dissolved in the water coolant for control purposes. The fuel is taken as $UO_2$ enriched to 2.78% $^{235}U$. In Table 5-2 we have listed the number densities and microscopic one-speed cross sections for this core. (Here the cross sections are actually averages over the neutron energy distribution in such a reactor core.)

TABLE 5-2   Number Density and Microscopic Cross Sections

| Material | $N\,(1/b\text{-cm})$ | $\sigma_{tr}(b)$ | $\sigma_a(b)$ | $\sigma_f(b)$ | $\nu$ |
|---|---|---|---|---|---|
| H | $2.748 \times 10^{-2}$ | 0.650 | 0.294 | 0 | 0 |
| O | $2.757 \times 10^{-2}$ | 0.260 | $1.78 \times 10^{-4}$ | 0 | 0 |
| Zr | $3.694 \times 10^{-3}$ | 0.787 | 0.190 | 0 | 0 |
| Fe | $1.710 \times 10^{-3}$ | 0.554 | 2.33 | 0 | 0 |
| $^{235}U$ | $1.909 \times 10^{-4}$ | 1.62 | 484.0 | 312.0 | 2.43 |
| $^{238}U$ | $6.592 \times 10^{-3}$ | 1.06 | 2.11 | 0.638 | 2.84 |
| $^{135}Xe$ | 0.000 | 1.21 | $2.36 \times 10^6$ | 0 | 0 |
| $^{10}B$ | $1.001 \times 10^{-5}$ | 0.877 | $3.41 \times 10^{-3}$ | 0 | 0 |

This data can be used to calculate the macroscopic cross sections tabulated in Table 5-3. Here we have also included the relative absorption rates in each material which serve as a measure of neutron balance within the core.

TABLE 5-3   Macroscopic Cross Sections

| Material | $\Sigma_{tr}(cm^{-1})$ | $\Sigma_a(cm^{-1})$ | $\nu\Sigma_f(cm^{-1})$ | Relative Absorption |
|---|---|---|---|---|
| H | $1.79 \times 10^{-2}$ | $8.08 \times 10^{-3}$ | 0 | 0.053 |
| O | $7.16 \times 10^{-3}$ | $4.90 \times 10^{-6}$ | 0 | 0 |
| Zr | $2.91 \times 10^{-3}$ | $7.01 \times 10^{-4}$ | 0 | 0.005 |
| Fe | $9.46 \times 10^{-4}$ | $3.99 \times 10^{-3}$ | 0 | 0.026 |
| $^{235}U$ | $3.08 \times 10^{-4}$ | $9.24 \times 10^{-2}$ | 0.145 | 0.602 |
| $^{238}U$ | $6.95 \times 10^{-3}$ | $1.39 \times 10^{-2}$ | $1.20 \times 10^{-2}$ | 0.091 |
| $^{10}B$ | $8.77 \times 10^{-6}$ | $3.41 \times 10^{-2}$ | 0 | 0.223 |
| | $3.62 \times 10^{-2}$ | 0.1532 | 0.1570 | 1.000 |

It should be noted that the transport cross sections used in this example have been artifically adjusted (reduced by almost an order of magnitude) to take some account of fast neutron leakage which would normally not be described by a one-speed model.

We can use these cross sections to calculate a number of important parameters characterizing the PWR core:

Diffusion coefficient: $D = 9.21$ cm

Infinite multiplication constant: $k_\infty = \nu\Sigma_f/\Sigma_a = 1.025$

Material buckling: $B_m^2 = (\nu\Sigma_f - \Sigma_a)/D = 4.13 \times 10^{-4}$ cm$^{-2}$

Extrapolation distance: $z_0 = 0.71\lambda_{tr} = 19.6$ cm

Leakage fraction for a critical core: $1 - P_{NL} = 0.025$ (5-245)

Next we will compute the critical core dimensions. If we assume that the core height is fixed at 370 cm by thermal considerations, then we can determine the radius at which a core with such a composition will be critical. First calculate the axial buckling $B_z^2$

$$B_z^2 = \left(\frac{\pi}{\tilde{H}}\right)^2 = 6.00 \times 10^{-5} \text{ cm}^{-2}.$$ (5-246)

Then using Eq. (5-241), we can determine the radial buckling $B_r^2$

$$B_r^2 = \left(\frac{\nu_0}{\tilde{R}}\right)^2 = B_m^2 - B_z^2 = 3.53 \times 10^{-4} \text{ cm}^{-2}.$$ (5-247)

Hence we can solve for the critical radius as

$$\tilde{R} = \left(\frac{\nu_0}{B_z}\right) - z_0 = 108 \text{ cm}.$$ (5-248)

(It should be noted that this is somewhat smaller than the radius of 180 cm for a typical PWR core. This illustrates the limitation of such a one-speed model for obtaining quantitative estimates in reactor analysis.)

### E. Reflected Reactor Geometries

To illustrate the complications that arise with multiregion core geometries, we will return to our slab reactor and add a reflector of nonmultiplying material of thickness $b$ to either side (see Figure 5-20). For the purposes of this analysis we will characterize the reactor core by superscript "C" and the reflector by "R." Rather than repeat our earlier analysis of the initial value problem for this geometry, we will proceed directly to examine the time-independent diffusion equations that must be satisfied by the fundamental mode flux shape. As in our earlier analysis of the nonmultiplying reflected slab, we will seek a solution in each region of the
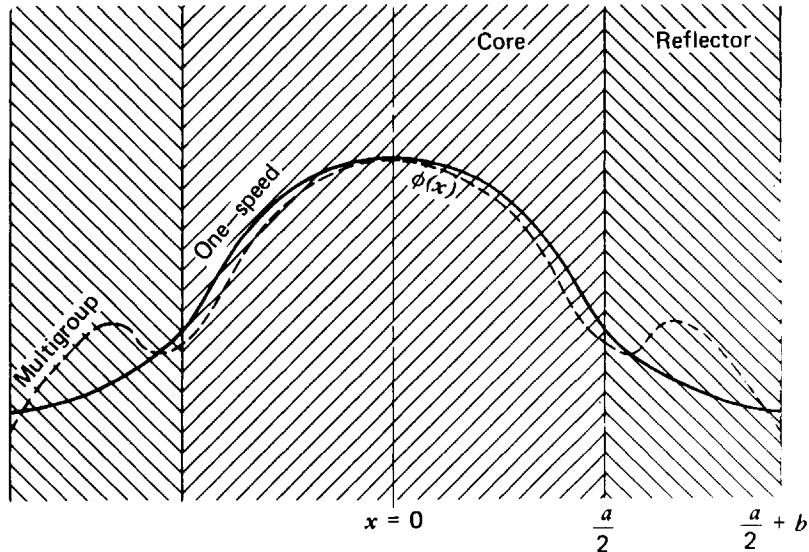
**FIGURE 5-20.** Reflected slab reactor

reactor and then use interface conditions to match these solutions. Hence we must solve

Core: $\qquad -D^{C}\dfrac{d^{2}\phi^{C}}{dx^{2}}+(\Sigma_{a}^{C}-\nu\Sigma_{f}^{C})\phi^{C}(x)=0, \qquad 0\leqslant x\leqslant\dfrac{a}{2},$

$$(5\text{-}249)$$

Reflector: $\quad -D^{R}\dfrac{d^{2}\phi^{R}}{dx^{2}}+\Sigma_{a}^{R}\phi^{R}(x)=0, \qquad\qquad \dfrac{a}{2}\leqslant x\leqslant\dfrac{a}{2}+\tilde{b},$

subject to the set of boundary conditions:

(a) $\qquad \phi^{C}\left(\dfrac{a}{2}\right)=\phi^{R}\left(\dfrac{a}{2}\right)$

(b) $\qquad J^{C}\left(\dfrac{a}{2}\right)=J^{R}\left(\dfrac{a}{2}\right)$

(c) $\qquad \phi^{R}\left(\dfrac{a}{2}+\tilde{b}\right)=0.$

Note that we have used the reactor symmetry to narrow our attention to the range of positive $x$. As we noted earlier in Section 5-III-D this problem will have no solution unless we choose the proper combination of core composition and size. We would anticipate that a criticality condition relating these core characteristics would emerge in the course of our analysis.

The general approach, as always, is to determine the general solutions in the core and reflector and then use the boundary conditions to determine the unknown coefficients. In the core the general solution will be

$$\phi^{C}(x)=A^{C}\cos B_{m}^{C}x, \qquad\qquad (5\text{-}250)$$

where we have utilized the symmetry of the core to discard the sine term. Here the material buckling characterizing the core is defined by

$$B_{m}^{C2}\equiv\dfrac{\nu\Sigma_{f}^{C}-\Sigma_{a}^{C}}{D^{C}}. \qquad\qquad (5\text{-}251)$$

while in the reflector we will seek a solution satisfying the vacuum boundary condition (c)

$$\phi^R(x) = A^R \sinh\left[\frac{\frac{a}{2} + \tilde{b} - x}{L^R}\right],$$

(5-252)

where the reflector diffusion length $L^R = (D^R / \Sigma_a^R)^{\frac{1}{2}}$. We now apply the interface boundary conditions to find

$$A^C \cos\left(\frac{B_m^C a}{2}\right) = A^R \sinh\left(\frac{\tilde{b}}{L^R}\right),$$

$$D^C B_m^C A^C \sin\left(\frac{B_m^C a}{2}\right) = \frac{D^R}{L^R} A^R \cosh\left(\frac{\tilde{b}}{L^R}\right).$$

(5-253)

Dividing these expressions, we can cancel $A^C$ and $A^R$ to find

$$D^C B_m^C \tan\left(\frac{B_m^C a}{2}\right) = \frac{D^R}{L^R} \coth\left(\frac{\tilde{b}}{L^R}\right).$$

(5-254)

Notice that this equation represents a relation between reactor composition $(D^C, B_m^C, D^R, L^R)$ and size $(a, b)$ that must be satisfied if a solution to the steady-state diffusion equations (5-249) is to exist. Hence this is just the reactor criticality condition for this particular geometry. Admittedly, it doesn't look anything like our earlier condition, $B_m^2 = B_g^2$, that characterized a bare reactor. In fact the criticality condition for a reflected reactor is transcendental–one cannot obtain an explicit solution for the critical size or composition. Instead, either numerical or graphical techniques must be used. The latter technique is more useful for our present discussion. Rewrite Eq. (5-254) as

$$\left(\frac{B_m^C a}{2}\right) \tan\left(\frac{B_m^C a}{2}\right) = \frac{D^R a}{2D^C L^R} \coth\left(\frac{\tilde{b}}{L^R}\right).$$

(5-255)

If we plot the LHS against $(B_m^C a / 2)$, we can then determine the solution of this transcendental equation graphically by noting where it intersects the value of the RHS, as shown in Figure 5-21. [Actually since there will be many such intersections, we are only interested in the lowest value of $(B_m^C a / 2)$.] From this graph we notice that the critical value of $B_m^C$ must be such that

$$\frac{B_m^C a}{2} < \frac{\pi}{2} \quad \text{or} \quad B_m^{C2} < \left(\frac{\pi}{\tilde{a}}\right)^2$$

(5-256)

in contrast to the bare (unreflected) core in which $B_m^{C2} = (\pi / \tilde{a})^2$. Hence we see that the width $a$ required for criticality is somewhat smaller when a reflector is added, but we would expect this since a reflector is added primarily to reduce neutron leakage.

It is conventional to define the difference between bare and reflected core dimensions as the *reflector savings* $\delta$:

$$\delta = a \text{ (bare)} - a \text{ (reflected)}.$$

(5-257)
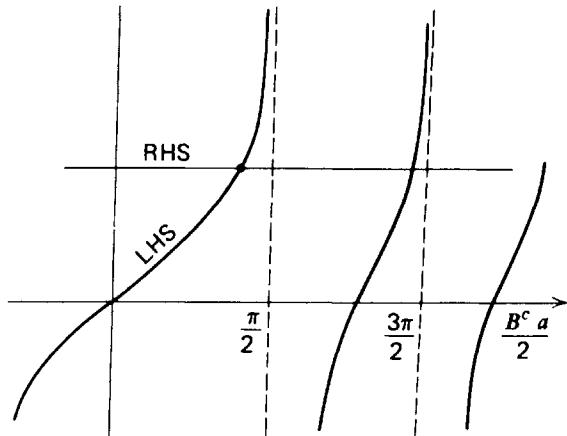
**FIGURE 5-21.  Graphical solution for reflected reactor criticality**

For example, the reflector savings for our slab reactor can be written as

$$\delta = \frac{1}{B_m^C} \tan^{-1}\left[ \frac{D^C B_m^C L^R}{D^R} \tanh\left( \frac{\tilde{b}}{L^R} \right) \right].$$
(5-258)

For a thick reflector $b \gg L^R$ this simplifies to

$$\delta \cong \frac{D^C}{D^R} L^R,$$
(5-259)

which is essentially a measure of the maximum reflector savings that can be realized.

Reflectors serve another function besides reducing neutron leakage. They tend to flatten the flux and hence the power distribution in the reactor core. Unfortunately one-speed diffusion theory is not adequate to describe this effect, which results in a peaking of the thermal flux in the reflector region (see Figure 5-19), so we must defer a further discussion of reflected cores until we have developed multigroup diffusion theory.

## IV. REACTOR CRITICALITY CALCULATIONS

### A.  Introduction

Let us now turn to the very important topic of determining the composition or size of a reactor that will yield criticality. It should be apparent after the last example that in most practical reactor designs one cannot simply determine the geometric buckling for a core geometry and then use $B_m^2 = B_g^2$ to arrive at criticality.

One "brute force" procedure would be to determine the lowest time eigenvalue of

$$-\nabla \cdot D(\mathbf{r})\nabla\phi + (\Sigma_a - \nu\Sigma_f)\phi(\mathbf{r}) = \frac{\lambda}{v}\phi(\mathbf{r}),$$
(5-260)

and then keep adjusting things until $\lambda = 0$. However this is rather awkward, and

moreover would tend to introduce errors in an unnatural manner when we generalize our analysis to include energy dependence.

Instead suppose we write our diffusion equation as

$$-\nabla \cdot D\nabla\phi + \Sigma_a\phi(\mathbf{r}) = \nu\Sigma_f\phi(\mathbf{r}), \tag{5-261}$$

$$\text{boundary condition:} \quad \phi(\tilde{\mathbf{r}}_s) = 0$$

(which, of course, is the steady-state equation we solved analytically in the earlier simple examples). Unfortunately this equation has *no* solution in general—unless we just happen to hit on the exact combination of core composition and geometry such that the reactor is critical (a highly unlikely possibility on a computer).

What we can do is introduce an arbitrary parameter "$k$" into this equation as:

$$-\nabla \cdot D\nabla\phi + \Sigma_a\phi(\mathbf{r}) = \frac{1}{k}\nu\Sigma_f\phi(\mathbf{r}). \tag{5-262}$$

Then for *some* value of $k$, we assert that this equation will always have a solution. The idea is to pick a core size and composition and solve the above equation while determining $k$. If $k$ should happen to be unity, we have chosen the critical size and composition. If $k \neq 1$, however, we must choose a new size and composition and repeat the calculation. As one might expect, $k$ turns out to indeed be the multiplication factor we defined earlier in Chapter 3, as we will demonstrate later.

We could give a formal mathematical proof that Eq. (5-262), or its generalizations will always have a solution for some $k$, but it is more convenient to simply argue physically that since varying $k$ will vary the effective fuel concentration $N_F \to N_F/k$, one can always achieve a critical system by making $k$ sufficiently small.

Sometimes a slightly different formulation is used in which one pretends that $\nu$, the number of neutrons emitted per fission, is in fact variable. (Of course it isn't, but it is a useful device to regard it as adjustable for the moment.) Now physically we know that there must be some value of $\nu$, call it $\nu_C$, that will yield a nontrivial solution to

$$-\nabla \cdot D\nabla\phi + \Sigma_a\phi = \nu_C\Sigma_f\phi, \tag{5-263}$$

regardless of what composition or geometry we have chosen. Hence the idea is to determine this $\nu_C$, then readjust composition and geometry until we have forced

$$\nu_C \to \nu_{actual} = \nu. \tag{5-264}$$

If we compare this approach to our earlier scheme in which we calculate $k$, it is evident that

$$k = \nu/\nu_C. \tag{5-265}$$

From a mathematical point of view, each of these approaches introduces a new parameter into the steady-state diffusion equation, either $k$ or $\nu_C$, which can then be regarded as an *eigenvalue* in a subsequent analysis. Once this eigenvalue has been calculated, one can return and readjust composition and geometry in an effort to force this eigenvalue to a desired value (e.g., $k \to 1$ or $\nu_C \to \nu$). Hence the criticality

calculation is converted into a sequence of eigenvalue problems for the *criticality eigenvalue* (sometimes also called the *multiplication eigenvalue*).

Of course, in general there will be a set of criticality eigenvalues $k_n$ corresponding to the eigenvalue problem represented by Eq. (5-262). For example, our earlier analysis for the bare slab reactor indicated the existence of the set of eigenvalues: $k_n = (\nu\Sigma_f/\Sigma_a)(1 + L^2 B_n^2)^{-1}$ where $B_n^2 = (n\pi/\tilde{a})^2$, $n = 1,2\ldots$. Only the largest such eigenvalue (in this case, $k_1$) will correspond to an everywhere-nonnegative flux distribution $\phi(\mathbf{r})$ and hence to a critical reactor configuration. We will refer to the largest criticality eigenvalue $k_1$ as the *effective multiplication factor* and denote it by $k_{eff}$. As we will see below, $k_{eff}$ can be identified as the multiplication factor $k$ for the reactor core defined earlier in terms of fission neutron generations in Chapter 3.

## B. Numerical Criticality Searches

We have seen in Section 5-III how one can obtain a criticality condition for a bare, uniform reactor. Let us now see how the criticality search is conducted in practical reactor calculations in which numerical methods must be used to solve the one-speed diffusion equation. To simplify our manipulations, let us first rewrite the criticality eigenvalue problem (5-262) in operator notation as

$$M\phi = \frac{1}{k}F\phi, \qquad (5\text{-}266)$$

where we identify

$$M\circ \equiv -\nabla \cdot D(\mathbf{r})\nabla\circ + \Sigma_a(\mathbf{r})\circ \equiv \text{Destruction operator}$$
$$\text{(leakage plus absorption)}$$

$$F\circ \equiv \nu\Sigma_f(\mathbf{r})\circ \equiv \text{Production operator}$$
$$\text{(fission)}$$

We will leave the boundary conditions on $\phi(\mathbf{r})$ as understood.

Of course in any numerical solution, finite-difference methods will lead to a representation of the neutron diffusion equation (5-266) as a matrix eigenvalue problem for the eigenvalue $k^{-1}$. The solution of such eigenvalue problems can be accomplished using a common technique from numerical analysis known as the *power method*. We will introduce this scheme using physical arguments.

First notice that if we assumed that the "fission source" term $S \equiv F\phi$ on the RHS of Eq. (5-266) was known, then the remaining part of the equation would be effectively just the diffusion equation for the neutron flux resulting from this source in a nonmultiplying medium. We presumably already know how to solve this problem (cf. Section 5-II), but we do not really know the fission source $F\phi$ since it involves $\phi$ itself. Hence we will do the next best thing and try to guess it by making an initial estimate of

$$S(\mathbf{r}) \equiv F\phi \cong S^{(0)}(\mathbf{r}), \qquad k \cong k^{(0)}. \qquad (5\text{-}267)$$

We next solve for the flux $\phi^{(1)}$ resulting from this source estimate:

$$M\phi^{(1)} = -\nabla \cdot D\nabla\phi^{(1)} + \Sigma_a\phi^{(1)} = \frac{1}{k^{(0)}}S^{(0)} \qquad (5\text{-}268)$$

using our earlier procedures. With this solution, we can now explicitly calculate the fission source resulting from this flux $\phi^{(1)}$ as

$$S^{(1)} = F\phi^{(1)} = \nu\Sigma_f\phi^{(1)}. \tag{5-269}$$

This can then be taken as a new estimate of the fission source and used to generate a new flux, $\phi^{(2)}$, and so on—provided we can also generate improved estimates of $k$. That is, we can iteratively solve for an improved source estimate $S^{(n+1)}$ from an earlier estimate $S^{(n)}$ by solving

$$M\phi^{(n+1)} = \frac{1}{k^{(n)}} S^{(n)} \tag{5-270}$$

for $\phi^{(n+1)}$ and then computing

$$S^{(n+1)} = F\phi^{(n+1)}. \tag{5-271}$$

However we also need a prescription for generating improved estimates of $k^{(n)}$.

This prescription can be obtained by returning to our original eigenvalue problem (5-266). As $n$ becomes large, we would anticipate that (if our fission source iteration scheme really works), $\phi^{(n+1)}$ will converge to the true eigenfunction $\phi(\mathbf{r})$ that satisfies Eq. (5-266). That is, for large $n$

$$M\phi^{(n+1)} \cong \frac{1}{k^{(n+1)}} F\phi^{(n+1)}. \tag{5-272}$$

The convergence of $\phi^{(n)}$ to $\phi(\mathbf{r})$ and $k^{(n)}$ to $k$ can be proven mathematically. It can also be motivated physically by recognizing that if indeed we have adjusted $k$ such that a steady-state or self-sustaining flux profile were possible, then regardless of the initial fission source estimate, successive fission neutron generations will eventually fall into this distribution.

Now for finite $n$, it is highly unlikely that $\phi^{(n+1)}$ and $k^{(n+1)}$ will satisfy Eq. (5-266) exactly. Nevertheless if we integrate Eq. (5-272) over all space, we should be able to obtain a reasonable estimate for $k^{(n+1)}$ as

$$k^{(n+1)} \cong \frac{\int d^3r\, F\phi^{(n+1)}}{\int d^3r\, M\phi^{(n+1)}}. \tag{5-273}$$

However $F\phi^{(n+1)}$ is just the $(n+1)$st estimate of the fission source, while we can use Eq. (5-270) to write $M\phi^{(n+1)}$ in terms of the $n$th estimate of this source to find

$$k^{(n+1)} \cong \frac{\int d^3r\, S^{(n+1)}(\mathbf{r})}{\frac{1}{k^{(n)}} \int d^3r\, S^{(n)}(\mathbf{r})}. \tag{5-274}$$

We can now use this relationship to compute a new guess of $k^{(n+1)}$ from $\phi^{(n+1)}$ and $k^{(n)}$.

We should note that this prescription is quite consistent with our earlier interpretation of $k$ as the multiplication factor—that is, the ratio of the number of neutrons in two consecutive fission generations—if we note that a factor of $k^{(n)}$ must be inserted in the denominator since $[k^{(n)}]^{-1}S^{(n)}$ is in fact the effective fission source that generates $S^{(n+1)}$.

We can now use Eqs. (5-270), (5-271), and (5-274) as the basis of an iterative algorithm to determine both $k$ and $\phi$. For large $n$, we expect that $\phi$ will converge to the fundamental eigenfunction of Eq. (5-266) corresponding to the largest eigenvalue $k_{eff}$ to which $k^{(n)}$ converges. (Recall we have agreed to denote this largest eigenvalue by $k_{eff}$.) In practice one continues this iteration until the error in $k$ and/or $S$ decreases below some specified amount:

$$\left|\frac{k^{(n)}-k^{(n-1)}}{k^{(n)}}\right|<\epsilon_1 \quad \text{and/or} \quad \max_r\left|\frac{S^{(n)}-S^{(n-1)}}{S^{(n)}}\right|<\epsilon_2. \tag{5-275}$$

Notice that by scaling the source term appearing in the diffusion equation (5-266) by a factor of $1/k^{(n)}$ in each iteration, we will prevent the rapid growth or decrease of successive source iterates (causing possible overflow or underflow) in the event that a number of iterations are required when $k$ is not close to unity. That is, dividing the source term by $k^{(n)}$ removes the dependence of the flux iterate $\phi^{(n+1)}$ on $n$ [at least as $\phi^{(n+1)}$ approaches the true solution].

This iterative scheme to determine the effective multiplication factor $k_{eff}$ and the corresponding flux $\phi(\mathbf{r})$ is known as the *power iteration* or *source iteration* method. The iterations themselves are known as *outer* or *source iterations*.

In addition to such outer or source iterations, one will also be required to perform *inner iterations* to solve the diffusion problem

$$M\phi^{(n+1)}=\frac{1}{k^{(n)}}S^{(n)}, \tag{5-276}$$

when two- or three-dimensional calculations are necessary. The general strategy then takes the form sketched in Figure 5-22.

## C. Source Extrapolation

Needless to say, there is strong incentive to perform as few iterations as possible in converging to the desired accuracy. For that reason, one usually attempts to accelerate the source iteration convergence by extrapolating ahead to a new source guess. This is accomplished by introducing an extrapolation parameter (much as is used in relaxation methods). For example, in a one-parameter extrapolation, one would use as the source definition

$$S^{(n)}=S^{(n-1)}+\alpha\left(\frac{1}{k^{(n)}}F\phi^{(n)}-S^{(n-1)}\right) \tag{5-277}$$

where $0\leqslant\alpha\leqslant 1$. A two-parameter extrapolation takes the form

$$S^{(n)}=S^{(n-1)}+\alpha\left(\frac{1}{k^{(n)}}F\phi^{(n)}-S^{(n-1)}\right)+\beta\left(S^{(n-1)}-S^{(n-2)}\right) \tag{5-278}$$

where $1\leqslant\alpha\leqslant 2$, $0\leqslant\beta\leqslant 1$ and can be chosen by using methods based on Chebyshev polynomial interpolation.[13]
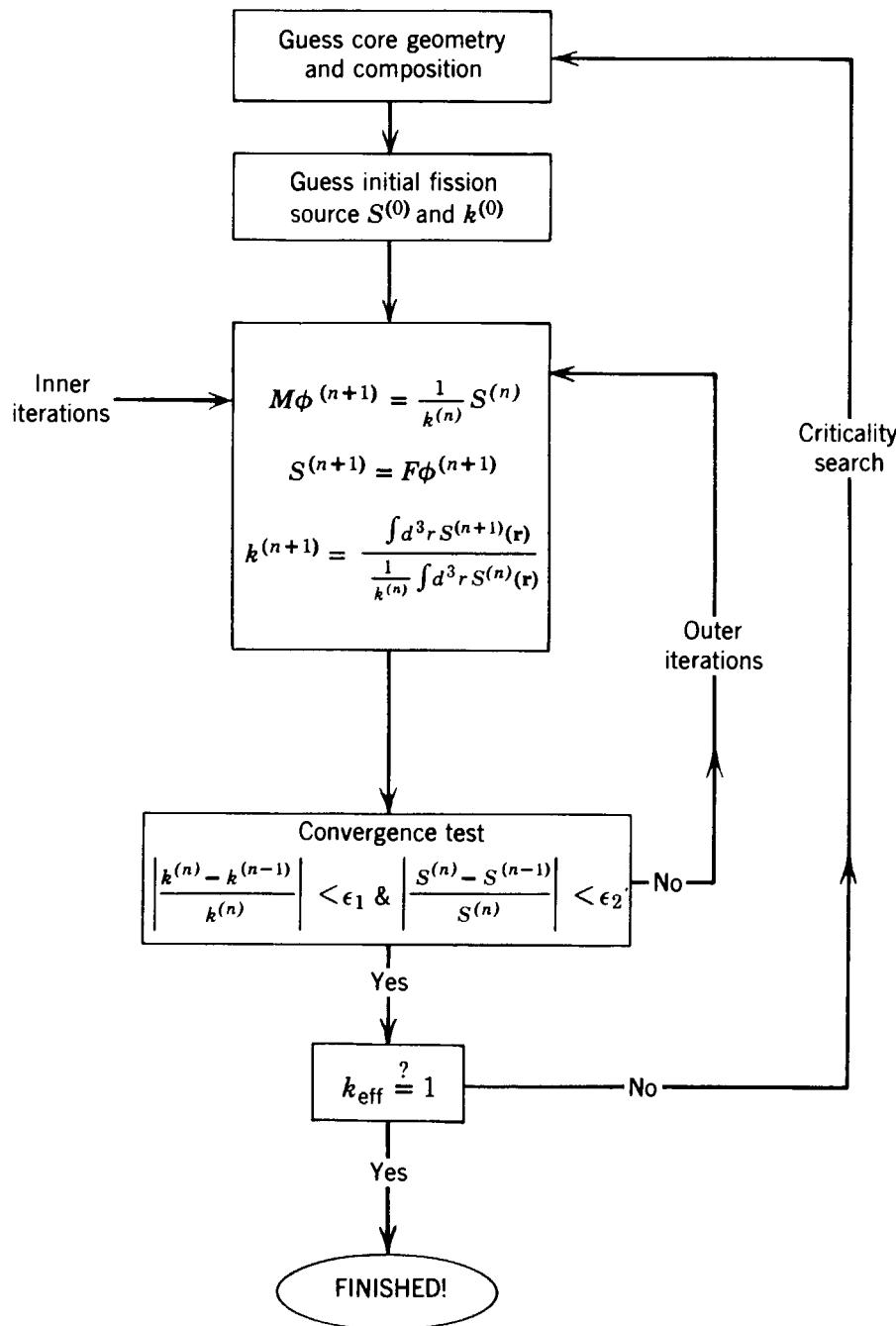
**FIGURE 5-22.** Calculation strategy for reactor criticality calculation

## V. PERTURBATION THEORY

It is frequently of interest to compute the change in core multiplication caused by a small change in the core geometry or composition. Fortunately if this change or "perturbation" is sufficiently small, one does not have to repeat the original criticality calculation, but instead can use well-known techniques of *perturbation theory* to express the corresponding change in multiplication in terms of the fluxes characterizing the unperturbed core.

By way of example, consider a very simple one-speed diffusion model of a bare, homogeneous reactor in which the criticality relation is

$$k = \frac{\nu \Sigma_f / \Sigma_a}{1 + L^2 B^2} = 1.$$

(5-279)

Now suppose we were to uniformly modify or perturb the absorption cross section to a new value

$$\Sigma_a' = \Sigma_a + \delta\Sigma_a, \tag{5-280}$$

where we will assume that the perturbation $\delta\Sigma_a$ is small—that is,

$$\delta\Sigma_a \ll \Sigma_a. \tag{5-281}$$

Then the value of $k'$ corresponding to the perturbed core can be written as

$$k' = \frac{\nu\Sigma_f/\Sigma_a'}{1 + L'^2 B^2} \cong k\left(1 - \frac{\delta\Sigma_a}{\Sigma_a} \frac{1}{1 + L^2 B^2}\right), \tag{5-282}$$

where we have expanded $k'$ in $\delta\Sigma_a/\Sigma_a$ and have neglected all terms of higher than first order in the perturbation $(\delta\Sigma_a)$. This has allowed us to express the perturbed multiplication factor $k'$ in terms of the unperturbed multiplication $k$ and the perturbation $\delta\Sigma_a$.

These general features appear in applications of perturbation theory to more general problems in nuclear reactor analysis in which the perturbations may be localized or in which the multigroup diffusion equations are used as the basic model of the core behavior. Although the general ideas are essentially as simple as those in the example above, it is necessary to introduce a few mathematical preliminaries. (For more details, the reader is referred to Appendix E.)

We will describe the multiplication of the core by the criticality eigenvalue problem [Eq. (5-266)]:

$$M\phi \equiv -\nabla\cdot D(\mathbf{r})\nabla\phi(\mathbf{r}) + \Sigma_a(\mathbf{r})\phi(\mathbf{r}) = \frac{1}{k}\nu\Sigma_f(\mathbf{r})\phi(\mathbf{r}) \equiv \frac{1}{k}F\phi \tag{5-283}$$

where we will leave it as understood that the solution of this equation, $\phi(\mathbf{r})$, must satisfy appropriate boundary conditions such as $\phi(\tilde{\mathbf{r}}_s) = 0$ on the surface of the core.

Now suppose we define the *inner product* $(f,g)$ between any two functions $f(\mathbf{r})$ and $g(\mathbf{r})$ as

$$(f,g) \equiv \int_V d^3r\, f^*(\mathbf{r})g(\mathbf{r}), \tag{5-284}$$

where $f^*(\mathbf{r})$ denotes the complex conjugate of $f(\mathbf{r})$, and $V$ is the core volume.

We can now use this inner product to define the operator $M^\dagger$ *adjoint* to the operator $M$ as that operator $M^\dagger$ for which

$$(M^\dagger f, g) = (f, Mg) \tag{5-285}$$

for every $f(\mathbf{r})$ and $g(\mathbf{r})$ satisfying the boundary conditions $f(\tilde{\mathbf{r}}_s) = 0 = g(\tilde{\mathbf{r}}_s)$.

We can use this definition to explicitly construct the adjoint of an operator. Consider for example the operator $F\circ = \nu\Sigma_f\circ$ which simply corresponds to multiply-

ing a function by $\nu\Sigma_f(\mathbf{r})$. If we write

$$(f,Fg) = \int_V d^3r f^* \nu\Sigma_f g = \int_V d^3r (\nu\Sigma_f f)^* g$$

$$= (\nu\Sigma_f f, g) = (F^\dagger f, g),\qquad (5\text{-}286)$$

where we have merely shuffled $\Sigma_f(\mathbf{r})$ around in the integral (noting that $\Sigma_f$ is real) to identify

$$F^\dagger \circ \equiv \nu\Sigma_f(\mathbf{r})\circ.\qquad (5\text{-}287)$$

Notice that in this case, $F^\dagger$ and $F$ are in fact *identical*. We refer to such operators as being *self-adjoint*.

For a more complicated example, consider the spatial derivatives in the diffusion operator $M$:

$$(f, \nabla\cdot D\nabla g) = \int_V d^3r f^* \nabla\cdot D\nabla g.\qquad (5\text{-}288)$$

Now if we use the vector identity

$$\nabla\cdot a\mathbf{b} = a\nabla\cdot\mathbf{b} + \mathbf{b}\cdot\nabla a,\qquad (5\text{-}289)$$

we can rewrite this as

$$(f, \nabla\cdot D\nabla g) = \int_V d^3r\, \nabla\cdot[f^* D\nabla g] - \int_V d^3r [\nabla f^* \cdot D\nabla g].\qquad (5\text{-}290)$$

Using Gauss's law, we can convert the first term into an integral over the surface:

$$\int_V d^3r \nabla\cdot[f^* D\nabla g] = \int_S d\mathbf{S}\cdot f^* D\nabla g.\qquad (5\text{-}291)$$

However since we require that $f$ and $g$ vanish on the surface, this term vanishes. If we repeat this procedure we find we can rewrite

$$(f, \nabla\cdot D\nabla g) = \int_V d^3r [\nabla\cdot D\nabla f]^* g = (\nabla\cdot D\nabla f, g).\qquad (5\text{-}292)$$

Hence we find that

$$\nabla\cdot D\nabla^\dagger\circ = \nabla\cdot D\nabla\circ\qquad (5\text{-}293)$$

Thus we have again encountered a self-adjoint operator.

From these examples, it is apparent that the operator $M\circ = -\nabla\cdot D\nabla\circ + \Sigma_a\circ$ is also self-adjoint, $M^\dagger = M$. We will continue to distinguish between the adjoint and direct operators $M^\dagger$ and $M$ however, since for more general multigroup diffusion calculations, $M$ will not be self-adjoint (as we will find in Chapter 7). We will

define the adjoint flux $\phi^\dagger$ as the corresponding solution of

$$M^\dagger\phi^\dagger = \frac{1}{k}F^\dagger\phi^\dagger. \tag{5-294}$$

(Although again we keep in mind that $M^\dagger = M$ and $F^\dagger = F$ implies that $\phi^\dagger = \phi$ for the one-speed diffusion model of a reactor.)

To understand the application of these concepts, let us go back to the criticality equation (5-283). Now suppose we were to perturb the macroscopic absorption cross section, say by adding a localized absorber, to a new value

$$\Sigma_a'(r) = \Sigma_a(r) + \delta\Sigma_a(r). \tag{5-295}$$

We will assume that this perturbation $\delta\Sigma_a(r)$ is small and attempt to calculate the corresponding change in $k$ as governed by the perturbed criticality problem

$$M'\phi' = \frac{1}{k'}F\phi'. \tag{5-296}$$

Note here that the perturbation in the core absorption appears as a perturbation $\delta M$ in the diffusion operator

$$M' = M + \delta M, \qquad \delta M\circ \equiv \delta\Sigma_a(r)\circ. \tag{5-297}$$

To calculate the change in $k$, first take the scalar product of Eq. (5-296) with the adjoint flux $\phi^\dagger$ characterizing the unperturbed core, that is, satisfying Eq. (5-294),

$$(\phi^\dagger, M\phi') + (\phi^\dagger, \delta M\phi') = \frac{1}{k'}(\phi^\dagger, F\phi'). \tag{5-298}$$

Now using the definition Eq. (5-285) of the adjoint operator, we find

$$(\phi^\dagger, M\phi') = (M^\dagger\phi^\dagger, \phi') = \left(\frac{1}{k}F^\dagger\phi^\dagger, \phi'\right) = \frac{1}{k}(\phi^\dagger, F\phi'). \tag{5-299}$$

Hence we find

$$\left(\frac{1}{k'} - \frac{1}{k}\right) = \frac{(\phi^\dagger, \delta M\phi')}{(\phi^\dagger, F\phi')}. \tag{5-300}$$

We could now calculate $\delta k = k' - k$. However it is far more convenient to define the core *reactivity*

$$\rho \equiv \frac{k-1}{k}, \tag{5-301}$$

which essentially measures the deviation of the core multiplication from unity. Then since the perturbation in reactivity is just

$$\Delta\rho = \rho' - \rho = \frac{k'-1}{k'} - \frac{k-1}{k} = \left(\frac{1}{k} - \frac{1}{k'}\right), \tag{5-302}$$

we can use Eq. (5-300) to find the change in reactivity due to the addition of an absorption cross section $\delta\Sigma_a(\mathbf{r})$

$$\Delta\rho = -\frac{(\phi^\dagger, \delta\Sigma_a\phi')}{(\phi^\dagger, F\phi')} \,. \tag{5-303}$$

As it stands, this expression is still quite exact, but also still quite formal since it involves the perturbed flux, $\phi'$, which we usually don't know (and usually don't want to calculate).

However this is where the idea of "perturbation theory" comes in. For if the perturbation $\delta\Sigma_a$ is small, then presumably the corresponding perturbation in the flux $\delta\phi \equiv \phi' - \phi$ is similarly small. Hence we can write

$$\Delta\rho = -\frac{(\phi^\dagger, \delta\Sigma_a\phi)}{(\phi^\dagger, F\phi)} - \frac{(\phi^\dagger, \delta\Sigma_a\delta\phi)}{(\phi^\dagger, F\phi)} + \frac{(\phi^\dagger, \delta\Sigma_a\phi)(\phi^\dagger, F\delta\phi)}{(\phi^\dagger, F\phi)^2} + \cdots \tag{5-304}$$

Then neglecting second and higher order quantities in the perturbation—that is, using *first order perturbation theory*—we find

$$\Delta\rho \cong -\frac{(\phi^\dagger, \delta\Sigma_a\phi)}{(\phi^\dagger, F\phi)} \,. \tag{5-305}$$

Since the one-speed diffusion operator is self-adjoint, we know $\phi^\dagger = \phi$, and hence we find

$$\Delta\rho \cong -\frac{\displaystyle\int_V d^3r\,\phi(\mathbf{r})\delta\Sigma_a(\mathbf{r})\phi(\mathbf{r})}{\displaystyle\int_V d^3r\,\phi(\mathbf{r})\nu\Sigma_f(\mathbf{r})\phi(\mathbf{r})} \,. \tag{5-306}$$

It should be noted that all of this analysis was exact until we neglected second-order terms in Eq. (5-304). Thus, we have calculated a first-order estimate of the reactivity change $\Delta\rho$ due to introducing a localized absorber $\delta\Sigma_a(\mathbf{r})$ in terms of the unperturbed flux distribution.

EXAMPLE: Consider a bare slab reactor characterized by one-group constants $D$, $\Sigma_a$, and $\nu\Sigma_f$. We will perturb this reactor by imagining that an additional absorber is uniformly inserted in the region $0 < x < h$. One might consider this to be a model of a bank of control rods inserted to a depth $h$ in the core. Of course to allow the application of perturbation theory, we must assume this absorption to be relatively small.

Hence our perturbation is

$$\delta\Sigma_a(x) = \begin{cases} \delta\Sigma_a, & 0 < x < h \\ 0, & h < x < a. \end{cases} \tag{5-307}$$

If we note that the unperturbed flux in this reactor is

$$\phi(x) = \phi_0 \sin \frac{\pi x}{a},$$  (5-308)

then we compute the reactivity change due to an insertion of the absorber to a depth $h$ as:

$$\Delta\rho(h) = -\frac{\int_0^a \delta\Sigma_a \phi^2 \, dx}{\nu\Sigma_f \int_0^a \phi^2 \, dx} = -\frac{2}{\pi} \frac{\delta\Sigma_a}{\nu\Sigma_f} \left[ \frac{\pi h}{2a} - \frac{1}{4} \sin \frac{2\pi h}{a} \right]$$  (5-309)

It is customary to refer to the reactivity change due to such an absorber as the "worth" of the absorber. (This concept will be defined more precisely in Chapter 14.) Hence the reactivity worth can be sketched for various insertion depths $h$ as shown in Figure 5-23.

It is also of interest to compute the "differential worth" defined as

$$\frac{d\rho}{dh} = -\frac{\delta\Sigma_a}{a\nu\Sigma_f} \left[ 1 - \cos \frac{2\pi h}{a} \right].$$  (5-310)

Note that the differential worth is at a maximum when the edge of the absorbing region (e.g., the tip of the control rods) is in the region of largest flux in the center of the core (see Figure 5-23). Such an analysis, while certainly of interest in illustrating general trends, is of limited usefulness in detailed control studies because of the highly absorbing nature of most control elements. Such elements very strongly perturb the flux in their vicinity, hence invalidating the use of perturbation theory. We will consider alternative methods required for computing control rod worth in Chapter 14.

One can obtain more general expressions for the reactivity change induced by perturbations in the core parameters. For example, if we were to simultaneously perturb

$$\Sigma_f' = \Sigma_f + \delta\Sigma_f, \qquad \Sigma_a' = \Sigma_a + \delta\Sigma_a, \qquad D' = D + \delta D,$$  (5-311)

the corresponding reactivity change then would be

$$\Delta\rho = \frac{\int_V d^3r \left[ (\nu\delta\Sigma_f - \delta\Sigma_a)\phi^2 - \delta D |\nabla\phi|^2 \right]}{\int_V d^3r \, \nu\Sigma_f \phi^2}.$$  (5-312)

The adjoint flux $\phi^\dagger(\mathbf{r})$ has a rather interesting physical interpretation. Suppose we imagine an absorber inserted into the reactor core at a point $\mathbf{r}_0$ such that

$$\delta\Sigma_a(\mathbf{r}) = \alpha\delta(\mathbf{r} - \mathbf{r}_0).$$  (5-313)

Here $\alpha$ is the effective strength of the absorber. (If we were to imagine that the $\delta$-function was, in fact, a mathematical idealization of an absorber of volume $V_A$, then $\alpha = \Sigma_a^A V_A$.) Now strictly speaking, perturbation theory should not be valid for such a singular perturbation, but we will dismiss such concerns with a wave of
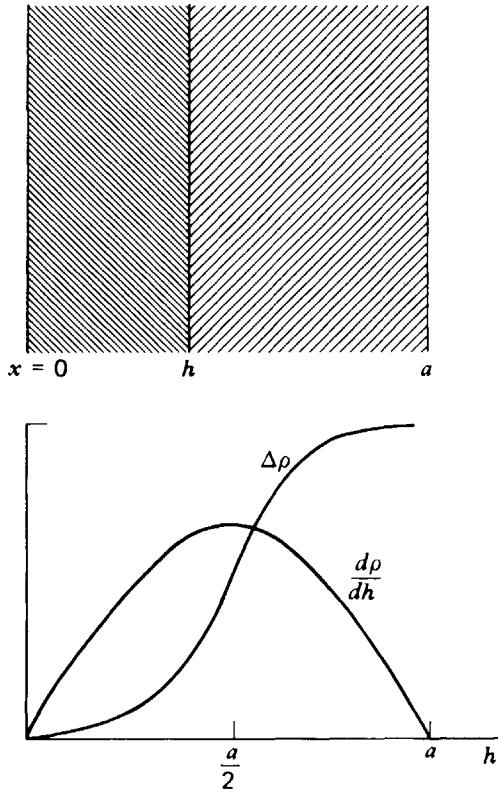
FIGURE 5-23. Relative and differential control rod bank worth

the hand and use our earlier result to find the corresponding reactivity change as

$$\Delta\rho = -\frac{\int_V d^3r\,\phi^\dagger(\mathbf{r})\delta\Sigma_a(\mathbf{r})\phi(\mathbf{r})}{\int_V d^3r\,\phi^\dagger(\mathbf{r})\nu\Sigma_f(\mathbf{r})\phi(\mathbf{r})}$$

$$= -\frac{\alpha}{\mathcal{C}}\phi^\dagger(\mathbf{r}_0)\phi(\mathbf{r}_0), \tag{5-314}$$

where we have denoted the denominator by a constant $\mathcal{C}$ (since it is independent of the perturbation). If we recognize that $\alpha\phi(\mathbf{r}_0)$ is just the absorption rate at $\mathbf{r}_0$, we then find

$$\phi^\dagger(\mathbf{r}_0) \sim \frac{-\Delta\rho}{\alpha\phi(\mathbf{r}_0)} \tag{5-315}$$

is simply proportional to the change in reactivity per neutron absorbed at $\mathbf{r}_0$ per second. In this sense, then, the adjoint flux $\phi^\dagger(\mathbf{r})$ is a measure of how effective an absorber inserted at a position $\mathbf{r}$ is in changing the reactivity of the core. Evidently if $\phi^\dagger(\mathbf{r})$ is large at $\mathbf{r}$, the core multiplication will be quite sensitive to the absorption of neutrons at that point. Hence $\phi^\dagger(\mathbf{r})$ is sometimes referred to as the *neutron importance* or the *importance function*.

We can see this from a somewhat different perspective if we consider the flux induced in a subcritical reactor by an arbitrary source $S(\mathbf{r})$ as governed by

$$(M - F)\phi = -\nabla\cdot D\nabla\phi + (\Sigma_a - \nu\Sigma_f)\phi = S. \tag{5-316}$$

Consider the adjoint problem

$$(M^\dagger - F^\dagger)\phi^\dagger = -\nabla \cdot D\nabla\phi^\dagger + (\Sigma_a - \nu\Sigma_f)\phi^\dagger = S^\dagger. \qquad (5\text{-}317)$$

(Of course for one-speed diffusion theory, $M = M^\dagger$ is self-adjoint, but we will retain the generality for a bit.) Notice that we have allowed the source $S^\dagger(r)$ appearing in the adjoint equation to differ from that in Eq. (5-316).

Now suppose we multiply Eq. (5-316) by $\phi^\dagger$ and integrate over $r$, then multiply Eq. (5-317) by $\phi$ and integrate, and then subtract these two results to find

$$(\phi^\dagger, (M - F)\phi) - ((M^\dagger - F^\dagger)\phi^\dagger, \phi) = (\phi^\dagger, S) - (S^\dagger, \phi). \qquad (5\text{-}318)$$

However by the definition of the adjoint $M^\dagger - F^\dagger$, the LHS is zero. Hence we find:

$$\int_V d^3r\,\phi^\dagger(r)S(r) = \int_V d^3r\,S^\dagger(r)\phi(r). \qquad (5\text{-}319)$$

Since this must hold for any choice of $S(r)$ and $S^\dagger(r)$, we will use it to our advantage by specifying $S(r)$ as a unit point source at $r_0$:

$$S(r) = \delta(r - r_0), \qquad (5\text{-}320)$$

and $S^\dagger(r)$ as the cross section $\Sigma_d(r)$ characterizing an imagined detector placed in the core. Then we find

$$\phi^\dagger(r_0) = \int_V d^3r\,\Sigma_d(r)\phi(r). \qquad (5\text{-}321)$$

Hence in this instance the adjoint flux is simply the response of a detector in the core to a unit point source inserted at a position $r_0$. Once again we find that $\phi^\dagger(r_0)$ is a measure of the *importance* of a neutron event (in this case, the production, rather than the absorption, of a neutron) at a point $r_0$ in contributing to the response of a detector with cross section $\Sigma_d(r)$ (as opposed to reactivity).

For the simple one-speed diffusion model we have been studying, the adjoint flux $\phi^\dagger(r)$ is identical to the flux itself. Hence perturbations affecting the creation or destruction of neutrons will have the most pronounced affect in those regions in which the flux is largest. This is not true, however, for the more general multigroup diffusion model, as we will see in Chapter 7.

## REFERENCES

1. J. W. Dettman, *Mathematical Methods in Physics and Engineering*, McGraw-Hill, New York (1969).
2. B. Friedman, *Principles and Techniques of Applied Mathematics*, Wiley, New York (1956).
3. G. Arfken, *Mathematical Methods for Physicists*, 2nd Edition, Academic, New York (1970).
4. P. M. Morse and H. Feshbach, *Methods of Theoretical Physics*, Vol. I, McGraw-Hill, New York (1953), p. 173.
5. Ibid., pp. 115-117.
6. B. Davison, *Neutron Transport Theory*, Oxford U. P. (1958), pp. 51-55.

7. K. M. Case and P. F. Zweifel, *Linear Transport Theory*, Addison-Wesley, Reading, Mass. (1967).

8. G. Arfken, *Mathematical Methods for Physicists*, 2nd Edition, Academic, New York (1970), pp. 733–739.

9. Ibid., pp. 748–768.

10. E. A. Coddington, *Ordinary Differential Equations*, Prentice-Hall, Englewood Cliffs, N. J. (1961), p. 67.

11. B. Carnahan, H. A. Luther, and J. O. Wilkes, *Applied Numerical Methods*, Wiley, New York (1969).

12. M. Clark, Jr., and K. F. Hansen, *Numerical Methods of Reactor Analysis*, Academic, New York (1964).

13. E. Wachspress, *Iterative Solution of Elliptic Systems*, Prentice-Hall, Englewood Cliffs, N. J. (1966).

14. R. S. Varga, *Matrix Iterative Analysis*, Prentice-Hall, Englewood Cliffs, N. J. (1962).

15. H. Greenspan, et al., *Computing Methods in Reactor Physics*, Gordon and Breach, New York (1968).

16. G. E. Forsythe and C. B. Moler, *Computer Solution of Linear Algebraic Systems*, Prentice-Hall, Englewood Cliffs, N. J. (1967).

17. T. Craig, SLODOG, A Modified One-group, One-dimensional Diffusion Code, University of Michigan Nuclear Engineering Report (1968).

18. E. Wachspress, *Iterative Solution of Elliptic Systems*, Prentice-Hall, Englewood Cliffs, N. J. (1966), p. 22.

19. Ibid., p. 24, 25.

20. R. G. Steinke, A Review of Direct and Iterative Strategies for Solving Multi-dimensional Finite Difference Problems, University of Michigan Nuclear Engineering Report (1971).

21. W. R. Cadwell, et al., PDQ–An IBM-704 Code to Solve the Two-dimensional Few-group Neutron Diffusion Equations, WAPD-TM-70 (1957) and related reports, WAPD-TM-179, WAPD-TM-230, WAPD-TM-364, WAPD-TM-678.

22. D. L. Delp, et al., FLARE, A Three Dimensional Boiling Water Reactor Simulator, General Electric Company Report, GEAP 4598 (1964).

23. E. G. Adensam, et al., Computer Methods for Utility Reactor Physics Analysis, *Reactor and Fuel Processing Technology*, Vol. 12, No. 2 (1969).

24. E. Wachspress, *Iterative Solution of Elliptic Systems*, Prentice-Hall, Englewood Cliffs, N. J. (1966). p. 83.

25. R. Froehlich, in Mathematical Models and Computational Techniques for Analysis of Nuclear Systems, USAEC CONF-730414-P2 (1973), p. VII-1.

## PROBLEMS

5-1 Compare the derivation of the one-speed neutron diffusion equation with that for the equation of thermal conduction, taking care to point out the assumptions and approximations used in each case. Refer to any text on heat transfer such as those listed at the end of Chapter 12.

5-2 By considering a plane source or absorber of neutrons located at the origin of an infinite medium, derive the interface condition Eq. (5-15) on the neutron current density by modeling the source term in the one-dimensional diffusion equation as $S\delta(x)$ and then integrating this equation over an infinitesimal region about origin.

5-3 Compute the rms distance $(\langle x^2 \rangle)^{1/2}$ a neutron will travel from a plane source to absorption using one-speed diffusion theory. Compare this result with the rms distance to absorption in a strongly absorbing medium (in which neutron scattering can be neglected). In particular, plot the rms distance to absorption in water in which boron has been dissolved against the boron concentration to determine whether the

diffusion theory result for $(\langle x^2 \rangle)^{1/2}$ ever approaches the result characterizing a purely absorbing medium. (Use the thermal cross section data in Appendix A.)

5-4 It is possible to derive an expression for the relaxation or diffusion length $L$ from the one-speed transport equation characterizing a homogeneous medium

$$\mu \frac{\partial \varphi}{\partial x} + \Sigma_t \varphi(x,\mu) = \frac{\Sigma_s}{2} \int_{-1}^{+1} d\mu' \varphi(x,\mu')$$

(we have assumed isotropic scattering for convenience). Seek a solution of the form $\varphi(x,\mu) = \chi(\mu) \exp(-x/L)$ to this equation in order to eliminate the $x$-dependence. The resulting homogeneous equation for $\chi(\mu)$ can be reduced to an algebraic equation for $L$ by eliminating $\int_{-1}^{+1} d\mu \chi(\mu)$. By following this procedure, derive a transcendental equation for the diffusion length $L$:

$$1 - \frac{\Sigma_s L}{2} \ln \left[ \frac{\Sigma_t L + 1}{\Sigma_t L - 1} \right] = 0 .$$

5-5 Using the assumption that $\Sigma_a \ll \Sigma_s$, expand $L$ as a power series in $\Sigma_a / \Sigma_t$, substitute this expansion into the equation above, and evaluate the coefficients of the expansion in order to derive Eq. (5-32) and obtain the transport corrections to the diffusion length $L = (D/\Sigma_a)^{1/2}$.

5-6 Determine the neutron flux in a sphere of nonmultiplying material of radius $R$ if an isotropic point source of strength $S_0$ neutrons per second is placed at the center of the sphere. Assume the sphere is surrounded by a vacuum.

5-7 The Milne problem: Imagine a diffusing medium in the half space $x > 0$ with a source of infinite magnitude at infinity such that the boundary condition on the flux is that $\phi(x) \sim S_0 \exp(x/L)$ as $x \to \infty$. Perform the following calculations:

(a) Using one-speed diffusion theory and the boundary condition of zero reentrant current, determine the flux in the medium.
(b) Repeat the solution of this problem using the extrapolated boundary concept.
(c) Determine the conditions under which these two boundary conditions might be expected to yield similar results.

5-8 Consider a slab of nonmultiplying material with a plane source at its origin emitting $S_0$ neutrons/cm²·sec. By solving this problem first with the condition of zero-reentrant current and then extrapolated boundaries, compare the absorption rate in the slab predicted by these two approaches. Also calculate the rate at which neutrons leak from the slab in each case.

5-9 Consider a thermal neutron incident on a slab-shaped shield of concrete 1 m in thickness, and determine the probability that: (a) the neutron will pass through the shield without a collision, (b) it will ultimately diffuse through the shield, and (c) it will be reflected back from the shield. (For convenience, treat the concrete as if it had the composition of 10% $H_2O$, 50% calcium, and 40% silicon.)

5-10 Consider an infinite nonmultiplying medium containing a uniformly distributed neutron source. If one inserts an infinitesimally thin sheet of absorber at the origin, determine the neutron flux throughout the medium.

5-11 Derive the expression given by Eq. (5-47) for the albedo characterizing a slab of material of thickness $a$. In particular plot this albedo for a slab of water for various thicknesses. (Use thermal cross section data.) Comment on the behavior of the albedo as given by Eq. (5-47) for both very thin and very thick slabs.

5-12 One defines the *blackness coefficient* characterizing a region as

$$\beta \equiv \frac{J_+(a) - J_-(a)}{J_+(a)} ,$$

where $a$ denotes the surface of the region. Yet another useful parameter characterizing interfaces is the ratio of the current density $J$ to the flux at the interface

$$\gamma \equiv \frac{J(a)}{\phi(a)}.$$

Determine the relation between these parameters and the albedo, assuming that diffusion theory can be used to describe the material adjacent to the region of interest. (It should be remarked that one frequently uses these concepts to characterize very highly absorbing regions such as fuel elements or control rods in which diffusion theory will usually not be valid in the highly absorbing region.)

5-13   In reactor analysis it is frequently of interest to determine the neutron flux in a so-called *unit fuel cell* of the reactor, that is, a fuel element surrounded by a moderator. As a model of such a cell characterizing a cylindrical fuel element, consider a fuel pin of radius $a$ surrounded by a moderator of thickness $b$. For reasons that will become more apparent in Chapter 10, one assumes that the fission neutrons that slow down to thermal energies appear as a source uniformly distributed over the moderator—but not directly in the fuel. Furthermore it is assumed that there is no net transfer of neutrons from cell to cell—that is, the neutron current vanishes on the boundary of the cell (although the neutron flux will not vanish there).

Determine the neutron flux in this cell geometry. In particular, determine the thermal utilization characterizing the cell by computing the fraction of those neutrons slowing down that is absorbed in the fuel.

5-14   Consider a one-dimensional slab model of a fuel cell in which the center region consists of the fuel, and the outer regions consist of a moderating material in which neutrons slow down to yield an effective uniformly distributed source of thermal neutrons $S_0$ neutrons/cm$^3 \cdot$sec. Determine the neutron flux in this cell. In particular, compute the so-called *self-shielding factor* $f_s$ defined as the ratio between the average flux in the fuel to the average flux in the cell.

5-15   Consider two isotropic point sources located a distance $a$ apart in an infinite nonmultiplying medium. Determine the neutron flux and current density at any point in a plane midway between the two sources.

5-16   Determine the infinite medium Green's functions or diffusion kernels characterizing cylindrical and spherical geometries.

5-17   By representing a plane source as a superposition of isotropic point sources, construct the plane source kernel $G_{pl}(x,x')$ by using the point source kernel $G_{pt}(r,r')$.

5-18   Obtain an expression for the plane source diffusion kernel characterizing a *finite* slab of width $a$ by solving for the neutron flux resulting from a unit plane source at a position $x'$ in the slab. This can be most easily accomplished by seeking a separate solution on either side of the source plane which satisfies the vacuum boundary conditions at either end, and then matching these solutions at the source plane using the interface condition of continuity of flux and a discontinuity in the current density given by the source strength.

5-19   Consider a neutron source emitting a monodirectional beam of neutrons into an infinite medium. Using one-speed diffusion theory, calculate the neutron flux in the medium. For convenience, locate your coordinate system with its origin at the source and align the $x$-axis along the source beam. Since the source is highly anisotropic, you cannot apply diffusion theory directly. Rather, compute the distribution of first scattering collisions of the source neutrons along the $x$-axis, and then assume that each of these collisions acts in effect as an isotropic point source of neutrons for the subsequent diffusion theory analysis (assuming that such scattering is isotropic).

5-20   Use the method of variation of constants to determine the flux in a finite slab that contains a uniformly distributed neutron source.

5-21   Construct the spatial eigenfunctions of the Helmholtz equation in spherical geometry.

5-22 Construct the spatial eigenfunctions of the Helmholtz equation in infinite cylindrical geometry.

5-23 Construct the spatial eigenfunctions of the Helmholtz equation characterizing a parallelepiped geometry.

5-24 Demonstrate explicitly that the eigenfunctions for the slab geometry are indeed orthogonal.

5-25 Consider a slab of nonmultiplying material containing a uniformly distributed neutron source. Determine the neutron flux in the slab: (a) by directly solving the diffusion equation and (b) using eigenfunction expansions. Demonstrate that these solutions are indeed equivalent.

5-26 Determine the neutron flux in a long parallelepiped column of nonmultiplying material caused by a uniform source distributed across the face of the column. In particular determine the spatial behavior of the flux far from the source plane. Describe how one might measure the neutron diffusion length in the column by studying the spatial behavior of the flux.

5-27 The objective of this problem is to write a computer code to calculate the flux in a uniform nonmultiplying slab containing an arbitrary source distribution. Perform the following steps:

(a) Derive the finite difference form of the appropriate one-speed diffusion equation using vacuum boundary conditions. Use 30 mesh points and equal mesh spacing.

(b) Write the equations in matrix form, $\underline{\underline{A}} \, \phi = \underline{S}$.

(c) Derive the steps necessary to solve this equation using the simultaneous relaxation method. (Gaussian elimination would be better, but less instructive.)

(d) Write the necessary computer program. Input should consist of slab thickness, $D$, $\Sigma_a$, and $S_i$. Output should include a tabulation of $x_i$, $\phi_i$, and $S_i$. Pay particular attention to your convergence criterion and initial flux guess $\phi_i^{(0)}$ for the inner iterations of the SR method.

(e) "Check out" your code by solving at least two problems with known analytical solutions (e.g., cosine source or uniform source). Show how the inner iterations of your program converge by plotting $\phi_i^{(n)}$ for various values of $n$.

5-28 Repeat the analysis of the time-dependent slab reactor given in Section 5-3, but with the addition of a plane source of neutrons of strength $S_0$ located at the origin of the slab. In particular determine the long time behavior of the reactor when it is critical.

5-29 Determine the geometric buckling $B_g^2$ and critical flux profile in the following bare reactor geometries: (a) sphere, (b) infinite cylinder, and (c) parallelepiped.

5-30 We can define the *power-peaking factor* for a given reactor core as the ratio between the maximum power density and the average power density in the core. Recognizing that the power density is proportional to the neutron flux in the one-speed approximation, compute the power-peaking factor for three common geometries: (a) sphere, (b) cube, and (c) finite cylinder.

5-31 A homogeneous one-speed bare reactor has a cylindrical configuration. Determine: (a) the radius and length of the reactor as functions of the buckling so that the volume of the critical reactor, and hence its mass, is a minimum and (b) the minimum volume as a function of buckling.

5-32 'Jezebel is a bare, fast, spherically shaped critical reactor constructed of pure $^{239}$Pu metal (density 15.4 g/cm$^3$). Calculate the critical radius and critical mass of the reactor using the one-group data: $\nu = 2.98$, $\sigma_f = 1.85$ b, $\sigma_\gamma = 0.26$ b, and $\sigma_{tr} = 6.8$ b.

5-33 There has been considerable interest in the possibility of super heavy nuclei with mass numbers $A > 300$. Such nuclei would be characterized by large values of $\nu$ ($\sim 6$–$10$). Using the results of Problem 5-32, study the effect of varying $\nu$ on the critical radius and mass of a bare sphere of such material.

5-34 Two infinite slabs, each of thickness $a$ in the $x$ direction, are separated by an inner region of thickness $2a$ and are bounded by vacuum on their outer surfaces. The slab material is of composition to give $k_\infty = 1.2$ and thermal diffusion length of 50 cm.

Determine the thickness $a$ for criticality when: (a) inner region is vacuum and (b) inner region is a medium with $k_\infty = 1$ and same $D$ and $L$ as the outer slabs.

5-35 A bare spherical reactor is made with $^{235}U$ uniformly dispersed in graphite ($\rho = 1.7$) with an atomic ratio $N_C/N_{25} = 10^4$. For the cross section values given below, calculate the critical size and mass of the reactor according to one-group diffusion theory. If the reactor is modified by placing a cavity (vacuum) of half the total radius in its center, find the critical size for this case. Recalculate the critical radius if the center void is filled instead by a perfect absorber. Use as data: $\sigma_s^C = 4.3$ b, $\sigma_a^C = 0.003$ b, $\sigma_\gamma^{25} = 105$ b, $\sigma_f^{25} = 584$ b, and $D = 0.9$ cm.

5-36 A bare spherical reactor is to be constructed of a homogeneous mixture of $D_2O$ and $^{235}U$. The composition is such that for every uranium atom there are 2000 heavy water molecules (i.e., $N_{D_2O}/N_{25} = 2000$). Calculate: (a) the critical radius of the reactor using one-speed diffusion theory (Data: $\eta^{25} = 2.06$, $D_{D_2O} = 0.87$ cm, $\Sigma_a^{D_2O} = 3.3 \times 10^{-5}$ cm$^{-1}$, $\sigma_a^{D_2O} = 0.001$ b, and $\sigma_a^{25} = 678$ b.) and (b) the mean number of scattering collisions made by a neutron during its lifetime in this reactor.

5-37 There is strong motivation to obtain as flat a power distribution as possible in a reactor core. One manner in which this may be accomplished is to load a reactor with a nonuniform fuel enrichment. To model such a scheme, consider a bare, critical slab reactor as described by one-speed diffusion theory. Determine the fuel distribution $N_F(x)$ which will yield a flat power distribution $P(x) = w_f \Sigma_f(x)\phi(x) = $ constant. For convenience, assume that fuel only absorbs neutrons and that it does not significantly scatter them. Also assume that all other materials in the core are uniformly distributed.

5-38 A one-dimensional slab reactor system consists of three regions: vacuum for $x < 0$; a multiplying core for $0 < x < a$; and an infinite nonmultiplying reflector for $x > a$. Calculate the core thickness $a$ that will yield a critical system.

Suppose $a$ cannot be made large enough to achieve criticality. Then determine the flux at all points when an external source $S_0$ is uniformly distributed throughout the reflector region $x > a$.

5-39 Consider a bare slab reactor with material composition such that $\Sigma_a = 0.066$ cm$^{-1}$, $D = 0.90$, and $\nu\Sigma_f = 0.070$ cm$^{-1}$. Modify the one-speed diffusion computer code developed in Problem 5-27 so that you can calculate the width $a$ that will yield criticality.

One possible procedure is to guess an initial slab width $a$ and then perform a source iteration calculation to determine $k_{eff}$. To simplify the calculation, choose $S^{(0)}(x) = 1.0$ = constant. The integrated fission source that appears in the estimate of $k^{(n)}$ given by Eq. (5-274) can be performed using simple trapezoidal quadrature

$$\int_0^a dx\, S(x) = \sum_{i=0}^{N} \left( \frac{S_i + S_{i+1}}{2} \right) \Delta x$$

where $\Delta x$ is the mesh spacing. Again use 30 mesh points and require a convergence criterion on $k^{(n)}$ of

$$\left| \frac{k^{(n+1)} - k^{(n)}}{k^{(n+1)}} \right| < \epsilon = 10^{-2}.$$

After each criticality calculation, readjust the slab width $a$ and recalculate $k_{eff}$. After several such calculations, plot $k_{eff}$ against $a$ to determine the critical slab width $a^*$. Compare this with the analytical expression for $a^*$.

5-40 Investigate the convergence of the inner and outer iterations in the one-speed diffusion code developed in Problem 5-39 for the following modifications:

(a) Use the outer iteration source $S^{(n)}(x)$ as the initial estimate in the inner iterations.

(b) Determine the sensitivity of both inner and outer iterations to the convergence criteria.

(c) Attempt to accelerate the outer iterations by source extrapolation.

5-41 Verify the general first-order perturbation theory result Eq. (5-312).

5-42 Why is the adjoint system introduced in developing the perturbation equations? Illustrate your answer with an example showing that only the use of the adjoint system will yield the desired result.

5-43 Describe a reasonable experimental procedure by which one could measure the variation of neutron importance within a reactor core.

5-44 Calculate the error in the critical mass of a bare homogeneous spherical reactor due to a 1% error in $k$. Assume that only the core size would be adjusted to give criticality.

5-45 Calculate the relative worth of a control rod bank inserted axially into a cylindrical reactor core.

5-46 Consider a critical bare slab reactor of thickness $a$ which is composed of a homogeneous mixture of fuel and moderator. Estimate the reactivity change if a thickness $\delta x$ of the fuel-moderator mixture at a position $x$ is replaced by pure moderator. What $\delta x$ at a distance from the centerline of $x = 0.4\,a$ is required to give the same reactivity change as a perturbation thickness $\delta x_0$ at the center of the slab?

5-47 Variational methods can be used in a manner very similar to perturbation theory to estimate the multiplication of a given core configuration using only crude guesses of the flux in the core. For example, a useful variational expression for the multiplication of a core described by a one-speed diffusion theory is

$$k^{-1} = \frac{\int d^3r\,\phi(\mathbf{r})M\phi(\mathbf{r})}{\int d^3r\,\phi(\mathbf{r})F\phi(\mathbf{r})}.$$

Compare the accuracy of such a scheme for a slab of width $a$ where the estimates of the flux or "trial functions" $\phi(x)$ are taken as simple quadratic polynomials that vanish on the boundaries of the slab [i.e., $\phi(x) = 1 - (2x/a)^2$].

# 6

## Nuclear Reactor Kinetics

For a nuclear reactor to operate at a constant power level, the rate of neutron production via fission reactions should be exactly balanced by neutron loss via absorption and leakage. Any deviation from this balance condition will result in a time-dependence of the neutron population and hence the power level of the reactor. This may occur for a number of reasons. For example, the reactor operator might desire to change the reactor power level by temporarily altering core multiplication via control rod adjustment. Or there may be longer term changes in core multiplication due to fuel depletion and isotopic buildup. More dramatic changes in multiplication might be caused by unforeseen accident situations, such as the failure of a primary coolant pump or a blocked coolant flow channel or the accidental ejection of a control rod.

It is important that one be able to predict the time behavior of the neutron population in a reactor core induced by changes in reactor multiplication. Such a topic is known as *nuclear reactor kinetics*. However, we should recognize that the core multiplication is never completely under the control of the reactor operator. Indeed since multiplication will depend on the core composition, it will also depend on other variables not directly accessible to control such as the fuel temperature or coolant density distribution throughout the reactor, but these variables depend, in turn, on the reactor power level and hence the neutron flux itself. The study of the time-dependence of the related processes involved in determining the core multiplication as a function of the power level of the reactor is known as *nuclear reactor dynamics* and usually involves a detailed modeling of the entire nuclear steam supply system. Although we briefly discuss several of the more important "feedback" mechanisms involved in determining core multiplication later in this chapter, our dominant concern is with predicting the time behavior of the neutron flux in the reactor for a given change in multiplication.

The principal applications of such an analysis are not only to the study of operating transients in reactors, but also to the prediction of the consequences of accidents involving changes in core multiplication, and to the interpretation of experimental techniques measuring reactor parameters by inducing time-dependent changes in the neutron flux. One can roughly distinguish between two different types of analysis depending on the time scale characterizing changes in the neutron population or core properties. For example, one is interested in relatively short-term changes possibly ranging from fractions of a second up to minutes in length when analyzing normal changes in reactor power level (e.g., startup or shutdown) or in an accident analysis. By way of contrast, changes in core composition due to fuel burnup or isotope buildup usually occur over periods of days or months. Needless to say, the analysis required for each class of time behavior is quite different.

The reader will recall that we have already considered a particularly simple example of nuclear reactor kinetics when we discussed the time behavior of the neutron flux in a slab reactor model in Chapter 5. Although this earlier analysis was useful for deriving the condition for reactor criticality, it is not valid for an accurate description of nuclear reactor kinetics, since it assumed that all fission neutrons appeared promptly at the instant of fission. As we demonstrate in the next section, it is essential that one explicitly account for the time delay associated with delayed neutrons in describing nuclear reactor kinetics.

Fortunately the one-speed diffusion model we have been using to study reactor criticality is also capable of describing qualitatively the time behavior of a nuclear reactor, provided we include the effects of delayed neutrons. Indeed such a model is frequently *too* detailed for practical implementation in reactor kinetics analysis due to excessive computation requirements, particularly when the effects of phenomena such as temperature feedback are included. For that reason, we will begin our study of nuclear reactor kinetics by reducing the one-speed diffusion model still further with the assumption that the spatial dependence of the flux in the reactor can be described by a single spatial mode shape (the fundamental mode). Under this assumption, we can remove the spatial dependence of the diffusion model and arrive at a description involving only ordinary differential equations in time. This model is sometimes known as the *point reactor kinetics model*, although this is somewhat of a misnomer since the model does not really treat the reactor as a point but rather merely assumes that the spatial flux shape does not change with time. Although we will rely heavily on the point reactor kinetics model in our study of nuclear reactor time behavior, we will indicate its generalizations to include a nontrivial spatial dependence as well as feedback mechanisms.

There are two other aspects of nuclear reactor kinetics that we will not touch upon in this chapter. The first topic involves the study of nuclear reactor control and includes not only the analysis of the various schemes used to adjust core multiplication but those mechanisms by which changes in the core power level can affect multiplication as well. The second topic involves the study of long-term changes in the core power distribution due to fuel depletion and the buildup of highly absorbing fission products in the reactor core.

However the study of both of these subjects involves only a steady-state analysis of the neutron flux in the reactor—or, at most, a sequence of steady-state criticality calculations. Only the time-dependence of the slowly varying changes in core composition such as those due to fuel depletion must be explicitly considered. Therefore such topics can be more appropriately developed in later chapters.

# I. THE POINT REACTOR KINETICS MODEL

## A. The Importance of Delayed Neutrons in Reactor Kinetics

In our earlier treatment of the simple bare slab reactor (Section 5-III-C), we found that the neutron flux in such a system could be written as a superposition of spatial modes (or eigenfunctions) characteristic of the reactor geometry, each weighted with an exponentially varying time-dependence:

$$\phi(\mathbf{r},t) = \sum_n A_n \exp(-\lambda_n t)\, \psi_n(\mathbf{r}). \tag{6-1}$$

Here the spatial eigenfunctions were determined as the solution to the eigenvalue problem [Eq. (5-232)]:

$$\nabla^2 \psi_n + B_n^2 \psi_n(\mathbf{r}) = 0, \qquad \psi_n(\tilde{\mathbf{r}}_s) = 0, \tag{6-2}$$

while the time eigenvalues $\lambda_n$ were given by

$$\lambda_n = vDB_n^2 + v\Sigma_a - v\nu\Sigma_f. \tag{6-3}$$

These eigenvalues are ordered as $-\lambda_1 > -\lambda_2 > \cdots$. Hence for long times the flux approaches an asymptotic form

$$\phi(\mathbf{r},t) \sim A_1 \exp(-\lambda_1 t)\, \psi_1(\mathbf{r}) = A_1 \exp\left[\left(\frac{k-1}{l}\right)t\right]\psi_1(\mathbf{r}), \tag{6-4}$$

where we identify

$$l \equiv \left[v\Sigma_a\left(1 + L^2 B_g^2\right)\right]^{-1} \equiv \text{mean lifetime of neutron in reactor,}$$

$$k \equiv \frac{\nu\Sigma_f/\Sigma_a}{1 + L^2 B_g^2} = \frac{k_\infty}{1 + L^2 B_g^2} \equiv \text{multiplication factor.} \tag{6-5}$$

It would be natural to inquire as to just how long one would have to wait until such asymptotic behavior sets in. We can determine this rather easily by assuming that the reactor is operating in a critical state such that $\lambda_1 = 0$, and then estimating $\lambda_n$. If we recall that for a slab $B_n^2 = n^2 \,(\pi/\tilde{a})^2$, then

$$\lambda_n = -vD\left(B_n^2 - B_m^2\right) = -vD\left(B_n^2 - B_g^2\right) = -vD\,(n^2 - 1)\left(\frac{\pi}{\tilde{a}}\right)^{2.} \tag{6-6}$$

Now in a typical thermal reactor, $\tilde{a} \sim 300$ cm, $v \sim 3 \times 10^5$ cm/sec, and $D \sim 1$ cm. Hence the higher order $\lambda_n$ are of the order of 100–1000 sec$^{-1}$, which implies that the higher order spatial modes die out very rapidly indeed.

We can utilize this fact to bypass our earlier separation of variables solution of the one-speed diffusion equation [Eq. (5-187)] by merely assuming a space–time separable flux of the form

$$\phi(\mathbf{r},t) = vn(t)\psi_1(\mathbf{r}), \tag{6-7}$$

where $\psi_1(\mathbf{r})$ is the fundamental mode or eigenfunction of the Helmholtz equation,

Eq. (6-2). If we substitute this form into the one-speed diffusion equation, we find that $n(t)$ satisfies

$$\frac{dn}{dt} = \left(\frac{k-1}{l}\right)n(t). \tag{6-8}$$

In this sense, $n(t)$ can be interpreted as the total number of neutrons in the reactor at time $t$ [if we normalize $\int d^3 r \psi_1(\mathbf{r}) = 1$]. Actually since the normalization of $n(t)$ is arbitrary, we could also scale the dependent variable $n(t)$ to represent the total instantaneous power $P(t)$ being generated in the reactor core at any particular time. That is, we could let

$$n(t) \rightarrow P(t) = w_f v \Sigma_f n(t), \tag{6-9}$$

where $w_f$ is the usable energy released per fission event. Since the reactor power level is usually a more convenient variable to monitor, we will frequently express the reactor time-dependence in terms of $P(t)$.

Equation (6-8) represents a somewhat simplified form of a more general set of equations, which we shall derive in a moment, that are commonly referred to as the *point reactor kinetics equations*. This term arises since we have separated out the spatial dependence by assuming a time-independent spatial flux shape $\psi_1(\mathbf{r})$. In this sense we have derived a "lumped parameter" description of the reactor in which the neutron flux time behavior is of the form of the product of a *shape factor* $\psi_1(\mathbf{r})$ and a time-dependent *amplitude factor* $n(t)$,

$$\phi(\mathbf{r},t) = v n(t)\psi_1(\mathbf{r}) = v n_0 \exp\left[\left(\frac{k-1}{l}\right)t\right]\psi_1(\mathbf{r}), \tag{6-10}$$

characterized by a time constant

$$T \equiv \frac{l}{k-1} \equiv \text{reactor period.} \tag{6-11}$$

This model is of course identical to that developed in our qualitative discussion of chain-reaction kinetics in Section 3-I-B except that one-speed diffusion theory has now given us an explicit expression for the neutron lifetime $l$ [Eq. (6-5)].

However there is, of course, something very important missing from this model. For by assuming a fission term in Eq. (5-186) of the form $v\Sigma_f \phi(\mathbf{r},t)$, we have implied that all fission neutrons appear promptly at the time of fission. But we know that a very small fraction ($\beta \sim 0.7\%$) of such neutrons are emitted with appreciable time delay (recall the discussion of Section 2-II). Although these delayed neutrons are only of minor significance in steady-state critical reactors, they are extremely important for reactor time behavior. For if we recall that the prompt neutron lifetime $l$ is typically of the order $10^{-4}$ sec in a thermal reactor ($10^{-7}$ sec in a fast reactor), then it is apparent that the reactor period predicted by this model would be far too small for effective reactor control.

We can give a crude estimate of the influence of delayed neutrons on the reactor time behavior by noting that the effective lifetime of such neutrons is given by their prompt neutron lifetime $l$ plus the additional delay time $\lambda_i^{-1}$ characterizing the $\beta$-decay of their precursor. If we weight both prompt and delayed neutrons by their respective yield fractions, we can estimate an average neutron lifetime $\langle l \rangle$

characterizing all fission neutrons as

$$\langle l \rangle = (1-\beta)l + \sum_{i=1}^{6} \beta_i \left[ \frac{1}{\lambda_i} + l \right]. \tag{6-12}$$

Using the delayed neutron data given in Table 2-3, we find that this average lifetime is typically $\langle l \rangle \sim 0.1$ sec, which is considerably longer than the prompt neutron lifetime $l \sim 10^{-6} - 10^{-4}$ sec. Hence delayed neutrons substantially increase the time constant of a reactor so that effective control is possible.

This fact suggests a related idea; suppose we consider a reactor that is very slightly subcritical when only prompt neutrons are considered. Suppose further that the fraction $\beta$ of delayed neutrons provides just enough extra multiplication to achieve criticality. This fraction will, in fact, control the criticality—and hence the time constant. However if $k - 1 \geqslant \beta$, the reactor will be critical (or supercritical) on prompt neutrons alone, and the reactor period should become very short, since the delayed neutrons are not needed to sustain the chain reaction. Obviously we should design a reactor such that this situation will never occur.

## B. Derivation of the Point Reactor Kinetics Equations

In actual fact, one cannot proceed so heuristically. We must first set up a set of equations describing the time dependence of the delayed neutrons. To this end, we must define the precursor atomic number density:

$C_i(\mathbf{r}, t)d^3r \equiv$ expected number of "fictitious" precursors of
$i$th kind in $d^3r$ about $\mathbf{r}$ that *always* decay by $\tag{6-13}$
emitting a delayed neutron.

Note that $C_i(\mathbf{r}, t)$ is only some fraction of the true precursor isotope concentration, since only a fraction of the $i$th isotope nuclei eventually decays by delayed neutron emission. For example, the $^{87}$Br precursor described in Section 2-II is characterized by a fictitious precursor concentration

$$C_{Br}(\mathbf{r}, t) = (.029)\ (.7)\ Br(\mathbf{r}, t). \tag{6-14}$$

One can immediately write down a balance relation for these precursor concentrations by referring to our earlier discussion of radioactive decay to identify

$$\left[ \begin{array}{l} \text{Number of precursors} \\ \text{decaying in} \\ d^3r/\text{sec} \end{array} \right] = \lambda_i C_i(\mathbf{r}, t)d^3r, \tag{6-15}$$

$$\left[ \begin{array}{l} \text{Number of precursors} \\ \text{being produced} \\ \text{in } d^3r/\text{sec} \end{array} \right] = \beta_i \nu \Sigma_f \phi(\mathbf{r}, t)d^3r. \tag{6-16}$$

[This latter relation assumes the precursors don't migrate or diffuse before decay-

ing.] Hence our precursor concentration balance equation is just

$$\frac{\partial C_i}{\partial t} = -\lambda_i C_i(\mathbf{r},t) + \beta_i \nu \Sigma_f \phi(\mathbf{r},t). \tag{6-17}$$

Now our old friend, the one-speed diffusion equation, can still be used to describe the flux—provided we treat the delayed neutron contribution to the fission source explicitly by writing it as

$$S_f(\mathbf{r},t) = (1-\beta)\nu\Sigma_f\phi(\mathbf{r},t) + \sum_{i=1}^{6} \lambda_i C_i(\mathbf{r},t). \tag{6-18}$$

Hence our system of equations describing the neutron flux in a reactor *including delayed neutrons* is

$$\frac{1}{v}\frac{\partial\phi}{\partial t} - D\nabla^2\phi + \Sigma_a\phi(\mathbf{r},t) = (1-\beta)\nu\Sigma_f\phi(\mathbf{r},t) + \sum_{i=1}^{6}\lambda_i C_i(\mathbf{r},t),$$

$$\frac{\partial C_i}{\partial t} = -\lambda_i C_i(\mathbf{r},t) + \beta_i\nu\Sigma_f\phi(\mathbf{r},t), \qquad i = 1,\ldots,6. \tag{6-19}$$

We will apply these once again to the asymptotic situation in which both the flux and precursor concentrations can be written as separable functions of space and time

$$\phi(\mathbf{r},t) = vn(t)\psi_1(\mathbf{r}),$$

$$C_i(\mathbf{r},t) = C_i(t)\psi_1(\mathbf{r}), \tag{6-20}$$

where $\psi_1(\mathbf{r})$ is the fundamental mode of Eq. (6-2).If we substitute these forms into Eq. (6-19) and use our expressions for the prompt neutron lifetime $l$ and multiplication factor $k$ for a bare, uniform reactor as given by Eq. (6-5), we arrive at a set of ordinary differential equations for $n(t)$ and $C_i(t)$:

$$\frac{dn}{dt} = \frac{k(1-\beta)-1}{l}n(t) + \sum_{i=1}^{6}\lambda_i C_i(t),$$

$$\frac{dC_i}{dt} = \beta_i\frac{k}{l}n(t) - \lambda_i C_i(t), \qquad i = 1,\ldots,6. \tag{6-21}$$

These are known as the point reactor kinetics equations and represent a generalization of Eq. (6-8) to include the effects of delayed neutrons. One frequently rewrites these equations in a somewhat different form by introducing two definitions. First we must define the *mean neutron generation time*:

$$\Lambda \equiv \frac{l}{k} \equiv \frac{\textit{mean generation time}\text{ between birth of neutron}}{\text{and subsequent absorption inducing fission.}} \tag{6-22}$$

If $k \sim 1$, then $\Lambda$ is essentially just the prompt neutron lifetime $l$. Next we define a very important quantity known as the *reactivity*, which essentially measures the

deviation of core multiplication from its critical value $k = 1$,

$$\rho(t) \equiv \frac{k(t) - 1}{k(t)} \equiv reactivity. \tag{6-23}$$

Notice here that we have explicitly indicated that $k$ and hence $\rho$ may be functions of time. We will comment more on this in a moment.

These definitions allow us to rewrite Eqs. (6-21) in perhaps their most conventional form

$$\frac{dn}{dt} = \left[ \frac{\rho(t) - \beta}{\Lambda} \right] n(t) + \sum_{i=1}^{6} \lambda_i C_i(t),$$

$$\frac{dC_i}{dt} = \frac{\beta_i}{\Lambda} n(t) - \lambda_i C_i(t), \qquad i = 1, \ldots, 6. \tag{6-24}$$

Hence we now have a set of seven coupled ordinary differential equations in time that describe both the time-dependence of the neutron population in the reactor and the decay of the delayed neutron precursors. Unfortunately the solution of this system of equations is not as straightforward as it might first appear for several reasons. First the reactivity $\rho(t)$ is usually a function of time and in fact frequently depends on the neutron population $n(t)$ itself. Hence the equations will generally be nonlinear. Furthermore the time constants characterizing the nuclear processes represented by the equations range all the way from $\Lambda \sim 10^{-6}$–$10^{-4}$ sec to the lifetime of the longest lived precursor, usually about 80 sec. These widely different time scales complicate even a direct numerical solution of Eqs. (6-24) since the time step size allowed in most standard numerical schemes (e.g., Runge–Kutta or predictor–corrector) is primarily controlled by the smallest time constant —in our case, the prompt neutron lifetime. Since reactor dynamics usually occur on a time scale characterized by the delayed neutrons, such direct approaches tend to be quite inefficient and more sophisticated methods are frequently required.

## C. Limitations of the Point Reactor Kinetics Model

A number of questionable assumptions have entered into the derivation of these equations, such as the one-speed diffusion approximation, and a time-independent spatial shape. Fortunately the point reactor kinetics equations can be derived in a much more general fashion in which such assumptions are not necessary.[1] Such derivations usually proceed from the transport equation itself and are also usually very formal. They lead, however, to the set [Eq. (6-24)] in which only the definitions of $\beta$, $\Lambda$, and $\rho$ are changed. Hence provided one uses the more general expressions for these parameters, the point reactor kinetics equations can be regarded as having a much broader domain of validity.

One major modification that must be introduced into the equations is to take some account of energy-dependent effects. These arise primarily because the delayed neutrons appear with somewhat lower energies than do the prompt fission neutrons (recall Figures 2-21 and 2-23). Hence in a thermal reactor, they do not have to slow down quite so far and therefore are characterized by a somewhat higher probability of inducing thermal fission (by as much as 20%). Of course, this may work in just the opposite direction in fast reactors, since delayed neutrons

usually appear with energies below the fast fission threshold. We can take account of these effects by characterizing each delayed neutron group by a slightly different fast nonleakage probability and a resonance escape probability, say $P^i_{FNL}$ and $p^i$. Then we would merely modify the definition of the parameters appearing in the point reactor kinetics equations as

$$k \to \eta f p \epsilon P_{TNL} P_{FNL}, \qquad (6\text{-}25)$$

$$\lambda_i \to \lambda_i p^{\,i} P^{\,i}_{FNL}, \qquad (6\text{-}26)$$

$$\beta_i \to \bar{\beta}_i \equiv \frac{\beta_i p^{\,i} P^{\,i}_{FNL}}{(1-\beta)pP_{FNL} + \sum_i \beta_i p^{\,i} P^{\,i}_{FNL}} = \frac{\beta_i p^{\,i} P^{\,i}_{FNL}}{\langle pP_{FNL} \rangle}, \qquad (6\text{-}27)$$

$$\beta \to \bar{\beta} \equiv \sum_{i=1}^{6} \bar{\beta}_i. \qquad (6\text{-}28)$$

In large thermal power reactors, $\bar{\beta}_i$ is typically several percent larger than the physical value $\beta_i$ (although in small research reactors, $\bar{\beta}_i$ may be as much as 20–30% larger than $\beta_i$). It should also be kept in mind that the delayed neutron yield fractions $\bar{\beta}_i$ must be calculated as suitable weighted averages over the relevant mixture of fuel isotopes. In fact one will find that in most thermal spectrum reactors these averaged delayed neutron fractions will decrease with core life since the most common bred materials, $^{239}Pu$ and $^{233}U$, have somewhat lower delayed neutron yields than $^{235}U$.

In $^{239}Pu/^{238}U$-fueled fast reactors, the situation becomes much more complicated since there are as many as six fissioning isotopes, each characterized by six different precursor groups. To handle 36 delayed neutron precursor concentration equations would be very complicated indeed. Fortunately the recent trend toward direct experimental measurement of isotopic yields as opposed to precursor group data should allow one to eventually solve directly for the isotopic concentrations of the major precursor isotopes (e.g., $^{87}Br$, $^{88}Br$, and $^{137}I$) and only lump the minor isotopes into effective precursor groups. This would then eliminate the problem of isotopic averaging for several fissionable isotopes, and decouple the data used in the kinetics calculation more effectively from the particular reactor core composition.

Perhaps the most serious approximation involved in the point reactor kinetics equations involves the assumption that the flux can be adequately represented by a single, time-independent spatial mode $\psi_1(r)$. It should first be noted that this shape function is actually not the fundamental mode characterizing a critical system, but rather the fundamental mode characterizing the reactor core that has been subjected to a reactivity change away from critical. Nevertheless it is common to utilize a shape function $\psi_1(r)$ characterizing a critical core configuration if the reactor is close to a critical state or on a truly asymptotic period.

When the changes in core composition are sufficiently slow, as in fuel depletion or fission-product poisoning studies, one can perform an instantaneous steady-state criticality calculation of the shape function $\psi_1(r)$, even though this shape will slowly change with time. Such a scheme is known as the *adiabatic approximation*.[2]

More elaborate procedures exist for including a time variation in the shape function.[3] However for rapidly varying transients in which spatial effects are

important, one is usually forced to solve the time-dependent neutron diffusion equation directly (at considerable expense). We will return to discuss such spatially dependent kinetics problems later in this chapter.

Of course one could proceed in a much more empirical fashion by noting that the point reactor kinetics equations hold for more general situations than we have considered, but then simply to postulate that the correct values for the parameters $\beta$, $\Lambda$, and $\rho$ are available (perhaps from experimental measurement). In this sense, all detailed considerations of the flux spatial shape are avoided (or, rather, swept under the carpet).

Let us now briefly examine the reactivity $\rho(t) = [k(t) - 1]/k(t)$ appearing in the point reactor kinetics equations. We know that the multiplication factor $k$, and hence $\rho$, depends on the size and composition of the reactor. In our specific one-speed diffusion model of a bare reactor core, we have found an explicit form for $k$ [Eq. (6-5)]. Hence by changing the size or composition—say by inserting or withdrawing a rod of absorbing material or adjusting a poison concentration—we can change $\rho$ and hence control the reactor. In this sense, $\rho$ will in general be a function of time partly under the control of the reactor operator.

However for any reactor operating at power, $\rho$ will also depend on the flux itself due to several factors. First, the power level will influence the temperature of the components of the reactor core. However the atomic concentrations of materials in the core depend sensitively on their temperature. As the temperature changes, they may contract or expand or change phase. This in turn will cause a change in the macroscopic cross sections—and hence in the reactivity. Furthermore temperature changes may directly affect the microscopic cross sections (e.g., via the Doppler effect). Finally, the atomic concentration of materials in the core will vary as fission products are produced or fuel nuclei are fissioned and depleted. This will also strongly influence the reactivity.

Such processes whereby the reactor operating conditions will affect the criticality of the core are known as *feedback effects* and play an extremely important role in reactor operation. Stated mathematically, such feedback effects imply that the reactivity must be regarded as a nonlinear function of the power level $\rho[n(t), t]$. Hence the point reactor kinetics equations are actually a coupled set of nonlinear ordinary differential equations that are extremely difficult to analyze analytically, with the exception of certain very simplified model cases.

Although we will eventually discuss the physics of several of the more prominent feedback mechanisms, we will initially limit our study to those cases in which $\rho(t)$ is a specified function of time (and hence the point reactor kinetics equations are linear). Such a situation is commonly referred to as the *zero-power point reactor model*, since it ignores the feedback that would occur due to variations in the reactor power level. Although limited in this sense, this model does reveal quite a bit about the time behavior of the neutron population in a reactor.

## II. SOLUTION OF THE POINT REACTOR KINETICS EQUATIONS

### A. Solution With One Effective Delayed Group

We will first apply the point reactor kinetics equations to the situation in which the reactivity is a prescribed function of time. In fact we will begin with the

very simple situation in which we imagine a reactor operating at some given power level $P_0$ prior to a time, say $t=0$, at which point the reactivity is changed to a nonzero value $\rho_0$. Rather than attempting to solve the full set of point reactor kinetics equations for this situation, we will first consider the case in which all delayed neutrons are represented by one effective delayed group, characterized by a yield fraction

$$\beta = \sum_i \beta_i \tag{6-29}$$

and an averaged decay constant

$$\lambda = \langle\lambda\rangle \equiv \left[ \frac{1}{\beta} \sum_i \frac{\beta_i}{\lambda_i} \right]^{-1}. \tag{6-30}$$

The point reactor kinetics equations for this simplified case become

$$\frac{dP}{dt} = \left[ \frac{\rho_0 - \beta}{\Lambda} \right] P(t) + \lambda C(t),$$

$$\frac{dC}{dt} = \frac{\beta}{\Lambda} P(t) - \lambda C(t), \qquad t \geqslant 0. \tag{6-31}$$

Note that we have chosen to work with the instantaneous reactor power level $P(t)$ as our dependent variable. The precursor concentration is then slightly modified to $C = C_{new} = w_f \Sigma_f C_{old}$. Now prior to $t=0$, the reactor is operating at a steady-state power level $P_0$. Hence we find that for $t<0$ we must require

$$\frac{dP}{dt} = \frac{dC}{dt} = 0 \implies C_0 = \frac{\beta}{\lambda\Lambda} P_0. \tag{6-32}$$

This relationship yields the appropriate initial conditions that accompany Eq. (6-31):

$$P(0) = P_0, \quad C(0) = \frac{\beta}{\lambda\Lambda} P_0. \tag{6-33}$$

This simple initial value problem can be solved in a variety of ways (the easiest being by Laplace transforms as discussed in Appendix G). We will use a more pedestrian approach by merely seeking exponential solutions of the form

$$P(t) = Pe^{st}, \quad C(t) = Ce^{st}, \tag{6-34}$$

where $P$, $C$, and $s$ are to be determined. Then if we substitute these forms into Eq. (6-31), we find the algebraic equations

$$sP = \left( \frac{\rho_0 - \beta}{\Lambda} \right) P + \lambda C,$$

$$sC = \frac{\beta}{\Lambda} P - \lambda C. \tag{6-35}$$

This set of homogeneous equations has a solution if and only if

$$\left[ s - \left( \frac{\rho_0 - \beta}{\Lambda} \right) \right][s + \lambda] - \frac{\lambda\beta}{\Lambda} = 0,$$

or

$$\Lambda s^2 + (\lambda\Lambda + \beta - \rho_0)s - \rho_0\lambda = 0. \tag{6-36}$$

Hence we have arrived at a characteristic equation for the parameter $s$. In particular we find that there are two possible values for $s$

$$s_{1,2} = \frac{1}{2\Lambda}\left[ -(\beta - \rho_0 + \lambda\Lambda) \pm \sqrt{(\beta - \rho_0 + \lambda\Lambda)^2 + 4\Lambda\lambda\rho_0} \right] \tag{6-37}$$

and hence our general solutions will be of the form

$$P(t) = P_1\exp s_1 t + P_2\exp s_2 t,$$
$$C(t) = C_1\exp s_1 t + C_2\exp s_2 t. \tag{6-38}$$

To determine the unknown coefficients we can apply both the initial conditions and the equations (6-35) to obtain four algebraic equations for the four unknowns $P_1$, $P_2$, $C_1$, and $C_2$. Since these results are still rather cumbersome, we will examine the solution in the case in which $(\beta - \rho_0 + \lambda\Lambda)^2 \gg 4\Lambda\lambda\rho_0$ (or $\lambda\Lambda/\beta \ll 1$) and $|\rho_0| \ll \beta$. Then the two roots are approximately given by

$$s_1 \cong \frac{\lambda\rho_0}{\beta - \rho_0}, \qquad s_2 \cong -\left( \frac{\beta - \rho_0}{\Lambda} \right), \tag{6-39}$$

while the power $P(t)$ becomes

$$P(t) \cong P_0\left[ \left( \frac{\beta}{\beta - \rho_0} \right)\exp\left( \frac{\lambda\rho_0}{\beta - \rho_0} \right)t - \left( \frac{\rho_0}{\beta - \rho_0} \right)\exp-\left( \frac{\beta - \rho_0}{\Lambda} \right)t \right]. \tag{6-40}$$

We have sketched this solution in Figure 6-1 for both positive and negative reactivity insertion of an amount $|\rho_0| = 0.0025$ into a reactor characterized by $\beta = 0.0075$, $\lambda = 0.08$ sec$^{-1}$, and $\Lambda = 10^{-3}$ sec. In particular, it should be noted that after a very rapid initial transient ($s_2^{-1} \sim .2$ sec), the reactor time response becomes exponential with a period of $T = s_1^{-1} \sim 25$ sec. This time constant characterizing the more slowly varying asymptotic behavior is occasionally referred to as the *stable reactor period*.

## B. The Inhour Equation

The reciprocal time constants $s_1$ and $s_2$ characterizing the single delayed group model were given as the roots of a quadratic equation (6-36) in terms of $\rho_0$, $\beta$, $\lambda$, and $\Lambda$. We can generalize this result to the situation in which there are several groups of delayed neutrons by first rewriting Eq. (6-36) in a slightly different form.
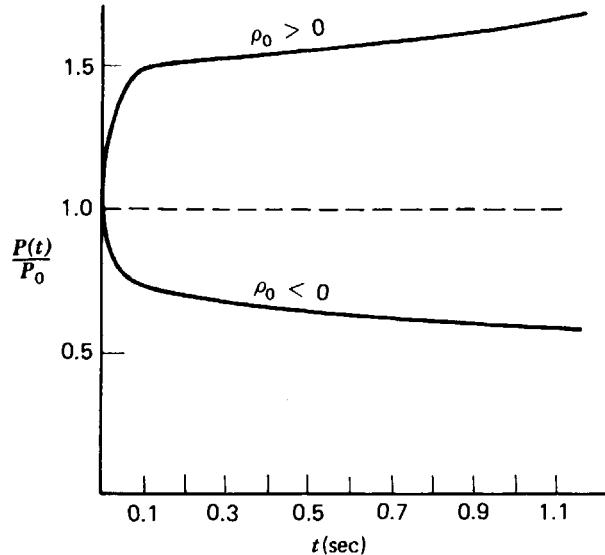
**FIGURE 6-1.** Reactor power level behavior following a positive step reactivity insertion

Using our definitions of $\rho$ and $\Lambda$ in Eqs. (6-22) and (6-23), we can rewrite Eq. (6-36) as

$$\rho_0 = \frac{sl}{sl+1} + \frac{1}{sl+1}\left(\frac{s\beta}{s+\lambda}\right). \tag{6-41}$$

This equation will determine the decay constants $s$ for any constant reactivity $\rho_0$. To generalize to six delayed groups, we write

$$\rho_0 = \frac{sl}{sl+1} + \frac{1}{sl+1}\sum_{i=1}^{6}\frac{s\beta_i}{s+\lambda_i} \equiv \rho(s). \tag{6-42}$$

This equation, which expresses the decay constants $s_j$ as the roots of a seventh-order polynomial, is known in reactor theory as the *inhour equation*. [This terminology arises from the very early attempts to express reactivity in units of "inverse hours" or *inhours*, which were defined as the amount of reactivity required to make the reactor period equal to one hour. Reactivity is more commonly expressed today either in decimals or percentages or pcm (per cent mille = $10^{-5}$) of $\Delta k/k$. We will later introduce another unit called the *dollar*, in which $\rho$ is measured in units of the delayed neutron fraction $\beta$.]

The roots of Eq. (6-42) are most conveniently studied using graphical techniques. In Figure 6-2 we have plotted the right-hand side of Eq. (6-42) for various values of $s$. The intersection of these curves with the line $\rho = \rho_0$ yields the seven decay constants $s_j$ characterizing the time-behavior

$$P(t) = \sum_{j=1}^{7} P_j \exp s_j t. \tag{6-43}$$

The root lying farthest to the right, $s_0$, is identified as the reciprocal reactor period, $s_1 = T^{-1}$. It is apparent from Figure 6-2 that only this root will ever be positive. The remaining roots $s_j$, $j > 1$, can then be identified as transients that die out rapidly after a reactivity $\rho_0$ is inserted into the reactor.
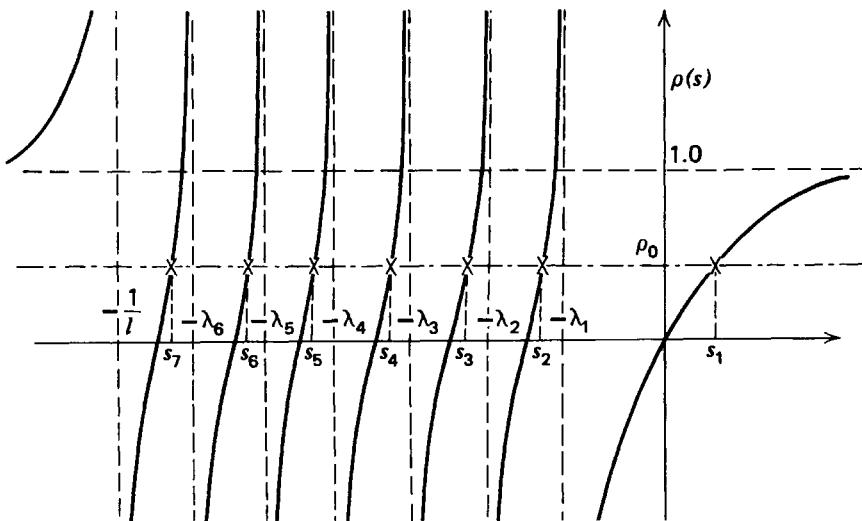
**FIGURE 6-2.** A graphical determination of the roots to the inhour equation

It should be noted that the range of $\rho_0$ is bounded by unity,

$$-\infty < \rho = \frac{k-1}{k} < 1. \tag{6-44}$$

In the limiting cases we find

$$\rho_0 = 0 \Rightarrow s_1 = 0 \qquad \text{(critical)}$$

$$\rho_0 \rightarrow 1 \Rightarrow s_1 \rightarrow \infty \qquad \text{(supercritical)}$$

$$\rho_0 \rightarrow -\infty \Rightarrow s_1 \rightarrow -\lambda_1 \qquad \text{(subcritical)}$$

This last limit is particularly interesting because it implies that no matter how much negative reactivity we introduce, we cannot shut the reactor down any faster than on a period $T = 1/\lambda_1$ determined by the longest-lived delayed neutron precursor. In $^{235}$U fueled thermal reactors, $\lambda_1^{-1} \sim 80$ sec.

Several other limiting cases are of particular interest:

(1) Small reactivity insertions $(\rho_0 \ll \beta)$: Then we can assume that the magnitude of $s_0$ is small such that

$$|s_0| \ll \lambda_1 < \lambda_2 \ldots < l^{-1}.$$

Hence in the inhour equation (6-42) we can neglect $s_1$ in comparison with $l^{-1}$ and $\lambda_i$ to write

$$\rho_0 \cong s_1 l + s_1 \sum_{i=1}^{6} \beta_i / \lambda_i.$$

Thus the reactor period is given by

$$T = \frac{1}{s_1} = \frac{1}{\rho_0} \left[ l + \sum_{i=1}^{6} \frac{\beta_i}{\lambda_i} \right] \cong \frac{\langle l \rangle}{\rho_0} \cong \frac{\langle l \rangle}{k-1}. \tag{6-45}$$

However this is of course identical to the result suggested by our earlier heuristic argument. Hence for small reactivities the reactor period is determined essentially by the average neutron lifetime $\langle l \rangle$ including delayed neutrons.

(2) Large positive reactivity insertions $(\rho_0 \gg \beta)$: In the opposite extreme of large reactivity insertion, we can assume $s_1 \gg \lambda_i$ to write the inhour equation (6-42) as

$$\rho_0 \cong \frac{s_1}{s_1 + l^{-1}} + \frac{l^{-1}}{s_1 + l^{-1}} \sum_{i=1}^{6} \beta_i = \frac{s_1 + \beta l^{-1}}{s_1 + l^{-1}}. \tag{6-46}$$

Hence we can solve for the reactor period as

$$T = \frac{1}{s_1} \cong \frac{l}{k(\rho_0 - \beta)} \cong \frac{l}{k - 1}, \tag{6-47}$$

which is just the result we would have obtained by totally ignoring delayed neutrons. Thus for large positive reactivity insertions, the reactor response is determined essentially by the prompt neutron lifetime $l$.

(3) $\rho_0 = \beta$: This is essentially the "break point" between a reactor kinetic response controlled by delayed neutrons and that governed by prompt neutrons alone. If we refer to the point reactor kinetics equations (6-24), it is apparent that for the reactor to be critical on prompt neutrons alone, we would require $\rho_0 = \beta$. For $\rho_0 < \beta$ the delayed neutron contribution is needed for reactor criticality, and hence the time response of the reactor will be determined to a large extent by the time delay characterizing the precursor $\beta$-decay. Some common terminology is to refer to the range $0 < \rho < \beta$ as *delayed critical*, while $\rho \geqslant \beta$ is referred to as *prompt critical* or *prompt supercritical*. Obviously it is very important to avoid this latter situation in reactor operation, since the reactor time response would be very rapid if prompt criticality were exceeded.

Actually the transition between these two classes of time response is not quite so abrupt. In Figure 6-3[4] we have shown the asymptotic reactor period $T = s_1^{-1}$ plotted versus $\rho_0$ for positive reactivity insertions in $^{233}U$, $^{235}U$, and $^{239}Pu$-fueled cores. The rather dramatic decrease in the reactor period in the neighborhood of prompt critical $\rho_0 = \beta$ should be noted.

The significance of the prompt critical condition has led to the custom of measuring reactivity in units of $\beta$. More precisely, a $\rho = \beta$ is referred to as one *dollar* ($) of reactivity. For example, a reactivity of $.40 would correspond to $\rho = 0.4\beta = 0.0028$ $\Delta k / k = 280$ pcm for a $^{235}U$-fueled thermal reactor.

## C. The Inverse Method[5]

There are very few problems for which it is possible to obtain an exact solution for $P(t)$ given a specific $\rho(t)$. Actually it is frequently more appropriate to invert the problem by determining that $\rho(t)$ which will yield a desired $P(t)$ behavior, since this is more in line with the philosophy of reactor control.
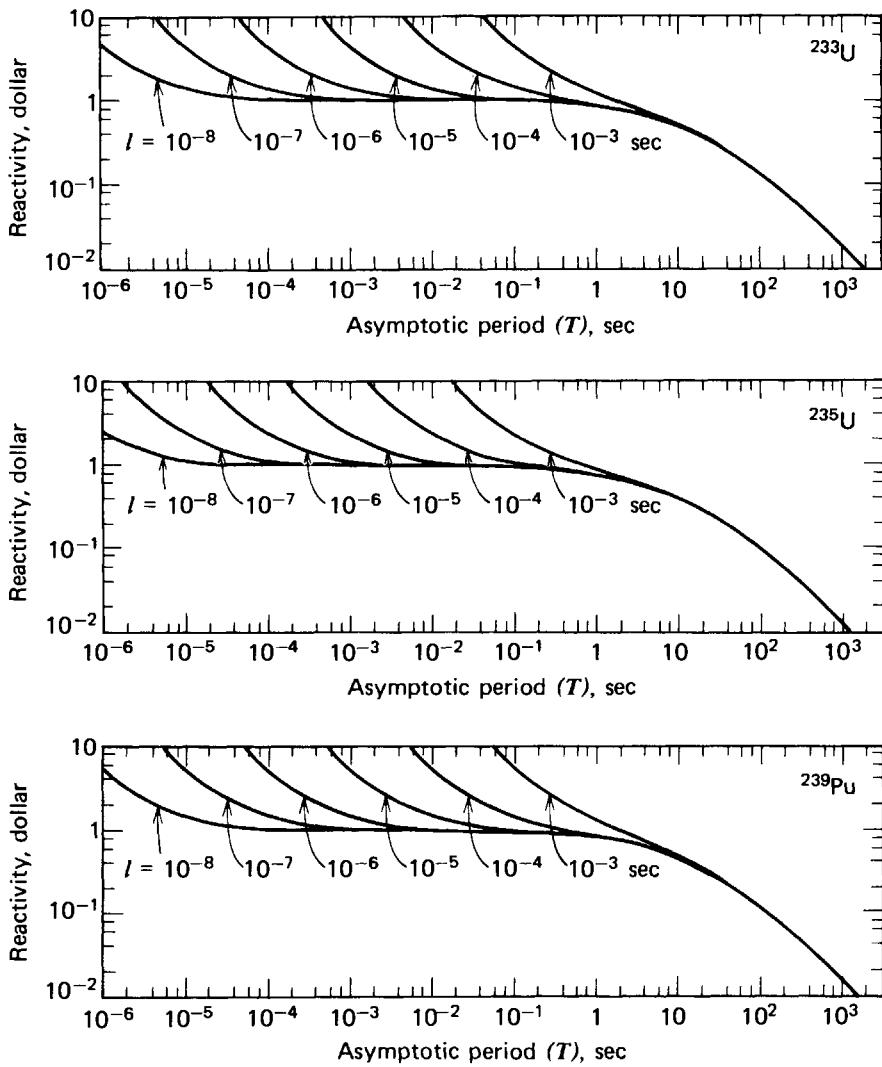
FIGURE 6-3.    Reactor period versus reactivity for fissile isotope delayed-neutron data[4]

In order to solve for $\rho(t)$ in terms of $P(t)$, let us derive yet another form of the point reactor kinetics equation. Suppose we begin by formally solving the equations for the precursor concentrations in terms of $P(t)$:

$$C_i(t) = \int_{-\infty}^{t} dt' \; \frac{\beta_i}{\Lambda} P(t') \; \exp - \lambda_i(t - t') = \int_{0}^{\infty} d\tau \; \frac{\beta_i}{\Lambda} \exp(-\lambda_i \tau) P(t - \tau), \quad (6\text{-}48)$$

where we have implicitly assumed that $C_i(t)$ $\exp \lambda_i t \rightarrow 0$ as $t \rightarrow -\infty$ and then let $\tau = t - t'$ to obtain the second integral. [Note that if we wish to take explicit account of initial conditions on $C_i(t)$, say at a time $t = t_0$, then we would merely separate out the contribution in the first form of the integral in Eq. (6-48) from $t = -\infty$ to $t = t_0$ to represent $C_i(t_0)$.] We will now substitute this into the first of the point reactor kinetics equations to write

$$\frac{dP}{dt} = \left[ \frac{\rho(t) - \beta}{\Lambda} \right] P(t) + \int_{0}^{\infty} d\tau \left[ \sum_{i=1}^{6} \frac{\lambda_i \beta_i}{\Lambda} \exp - \lambda_i \tau \right] P(t - \tau). \quad (6\text{-}49)$$

If we define the *delayed neutron kernel* $D(\tau)$

$$D(\tau) \equiv \sum_{i=1}^{6} \frac{\lambda_i \beta_i}{\beta} \exp - \lambda_i \tau, \tag{6-50}$$

(noting that $D(\tau) d\tau$ is just the probability that a delayed neutron will be emitted in a time $d\tau$ following a fission event at $\tau = 0$) then we arrive at an "integro-differential" form of the point reactor kinetics equations

$$\frac{dP}{dt} = \left[ \frac{\rho(t) - \beta}{\Lambda} \right] P(t) + \frac{\beta}{\Lambda} \int_{0}^{\infty} d\tau \, D(\tau) P(t - \tau). \tag{6-51}$$

We can now rearrange this equation to yield $\rho(t)$ in terms of $P(t)$:

$$\rho(t) = \beta + \Lambda \frac{d}{dt} [\ln P(t)] - \beta \int_{0}^{\infty} d\tau \, D(\tau) \frac{P(t - \tau)}{P(t)}. \tag{6-52}$$

This particular relationship is important for two reasons: (a) it can be used in principle to determine the time-dependence of the applied reactivity required to yield a specific power variation—that is, to program the control rod motion and (b) the interpretation of the measured power responses in transient analyses of reactivity changes can be used to provide information about the feedback mechanism in the reactor. Several specific applications of this relationship are of considerable interest:

## 1. PERIODIC POWER VARIATION

Suppose we seek the reactivity that will yield a sinusoidally varying power of the form

$$P(t) = P_0 + P_1 \sin \omega t. \tag{6-53}$$

(Note that we must require $P_0 > P_1$ since a negative power would offend our physical intuition.) Inserting this expression into Eq. (6-52) and performing a few manipulations (left for the reader's enjoyment to the exercises at the end of the chapter), we arrive at

$$\rho(t) = \frac{P_1}{P_0} |Y(i\omega)| \frac{\sin(\omega t - \phi)}{1 + \frac{P_1}{P_0} \sin \omega t}, \tag{6-54}$$

where

$$\phi = \arg\{Y(i\omega)^{-1}\}. \tag{6-55}$$

and $Y(i\omega)$ is a function which looks suspiciously like a chunk of the inhour

equation

$$Y(i\omega) = i\omega \left[ \Lambda + \sum_{i=1}^{6} \frac{\beta_i}{i\omega + \lambda_i} \right]. \tag{6-56}$$

(It will cross our path again.) Notice in particular that the reactivity insertion that gives rise to a purely sinusoidal power variation is periodic—but *not* sinusoidal (at least for large power variations). One can show, in fact, that $\rho(t)$ has a negative bias. This fact proves of some importance in reactor oscillator experiments in which an absorbing material is oscillated within the core and the core power response is then measured in an effort to infer system parameters (e.g., $\beta$ and $\Lambda$).

## 2. REACTIVITY AFTER A POSITIVE POWER TRANSIENT

As a second application of Eq. (6-52), suppose we determine the reactivity present following a power transient in which the reactor power increases from its initial value $P_0$ at $t = 0$, and then decreases back to $P_0$ at a later time $t_0$

$$\rho(t_0) = \Lambda \frac{1}{P_0} \frac{dP}{dt} \bigg|_{t_0} - \beta \int_0^{t_0} d\tau\, D(\tau) \left[ \frac{P(t_0 - \tau) - P_0}{P_0} \right]. \tag{6-57}$$

Now we know that for a positive transient, $P(t_0 - \tau) > P(t_0) = P_0$ and hence the integral is always positive. Furthermore it is apparent that at $t = t_0$, the slope $dP/dt|_{t_0} \leqslant 0$. Thus we can infer that the reactivity following a positive power excursion must, in fact, be negative. That is, the reactor must be taken subcritical to return the power to its original level.

## 3. RAMP REACTIVITY INSERTION

Suppose the reactor power level is found to increase very rapidly from an initial level $P_0$ as $P_0 \exp(\alpha t^2)$ for $t > 0$. Then using Eq. (6-52) we can find that for long times $t$,

$$\rho(t) \cong \beta + 2\Lambda \alpha t. \tag{6-58}$$

Hence $\rho(t)$ approaches a linear function of time—that is, a ramp insertion of reactivity above prompt critical. We can turn this calculation around to infer that the response of the reactor power $P(t)$ to a ramp insertion $\rho(t) \cong \gamma t$ should behave as $\exp[\gamma t^2 / 2\Lambda]$ for long times. This conclusion has particular relevance for certain classes of fast reactor accident models in which fuel melting is assumed to lead to core reassembly in a prompt supercritical configuration with a ramp reactivity insertion. Obviously the power increase resulting from such an occurrence would be very rapid indeed.

## D. Approximate Solutions

As we have seen, exact solutions of the point reactor kinetics equations are known for only a few special reactivity insertions. Hence we now turn our attention to approximate schemes for solving these equations in the absence of feedback.

## 1. CONSTANT DELAYED NEUTRON PRODUCTION RATE APPROXIMATION

In certain problems, such as when the reactor is shut down by rapid insertion of the safety rods, we are interested in the response of the reactor power to a given reactivity insertion in short time intervals following a time $t_0$. During such short time intervals we can ignore the change in the rate of production of delayed neutrons, replacing $C_i(t)$ by $C_i(0)$. Hence in this approximation, the point reactor kinetics equation becomes

$$\frac{dP}{dt} = \left[ \frac{\rho(t) - \beta}{\Lambda} \right] P(t) + Q(t), \tag{6-59}$$

where the effective source of delayed neutrons $Q(t)$ is now presumed known and given by

$$Q(t) = \sum_{i=1}^{6} \lambda_i C_i(0). \tag{6-60}$$

However we now just have a first-order inhomogeneous differential equation that we can easily integrate for any given $\rho(t)$.

A rather interesting application of this result is to the case of a reactor scram in which control rods are rapidly inserted into the reactor core to shut the reactor down in an emergency situation such as the loss of primary coolant flow. Since the rod insertion takes a finite time, we cannot really treat the reactor scram as a step reactivity change (as in Section 6-II-1). A more reasonable model is to assume a negative ramp insertion, that is, $\rho(t) = -\gamma t$. If we substitute this into Eq. (6-59) and solve this equation subject to the initial condition imposed by steady-state power operation prior to the scram,

$$\sum_{i=1}^{6} \lambda_i C_i(0) = \frac{\beta}{\Lambda} P_0, \tag{6-61}$$

then we find that the power level decreases as

$$P(t) = P_0 \left\{ \exp - \frac{1}{\Lambda} \left( \frac{\gamma t^2}{2} + \beta t \right) + \frac{1}{\Lambda} \int_0^t dt' \exp - \frac{1}{\Lambda} \left[ \frac{\gamma}{2} (t - t')^2 - \beta (t - t') \right] \right\}.$$

$$\tag{6-62}$$

After the scram rods have been fully inserted, the negative reactivity becomes constant, and one can determine $P(t)$ for subsequent time using our earlier solutions of the point reactor kinetics equation for constant $\rho(t) = -\rho_0$.

## 2. THE PROMPT JUMP APPROXIMATION

In our earlier study of the response of the reactor power $P(t)$ to a step change in reactivity, we found that there was initially a very rapid transient behavior on a time-scale characteristic of the prompt neutron lifetime, followed by a more slowly varying response governed by delayed neutron behavior. Since this transient is so rapid, a very useful approximation to make for systems below prompt critical is

one in which the prompt neutron lifetime is essentially taken to be zero such that the power level jumps instantaneously to its asymptotic behavior (recall Figure 6-1). This so-called *prompt jump approximation* is effected by merely neglecting the time derivative $dP/dt$ in the point reactor kinetics equation

$$0 = [\rho(t) - \beta]P(t) + \Lambda \sum_{i=1}^{6} \lambda_i C_i(t)$$

$$\frac{dC_i}{dt} = \frac{\beta_i}{\Lambda}P(t) - \lambda_i C_i(t).$$

(6-63)

Since the delayed neutron production cannot respond immediately to a step change in reactivity, this model predicts that a reactivity jump from $\rho_1$ to $\rho_2$ causes an instantaneous change in reactor power from $P_1$ to $P_2$ as given by

$$\frac{P_2}{P_1} = \frac{\beta - \rho_1}{\beta - \rho_2}.$$

(6-64)

The prompt jump approximation is frequently used in numerical studies of the point reactor kinetics equations since it eliminates the very short time scale due to $\Lambda$ which plagues finite difference methods. However it is also of use in simplifying analytical estimates based on the one-effective delayed group model, since in this case the precursor concentration $C(t)$ can be eliminated to find a simple first-order differential equation for the power $P(t)$

$$[\rho(t) - \beta]\frac{dP}{dt} + \left[\frac{d\rho}{dt} + \lambda\rho(t)\right]P(t) = 0.$$

(6-65)

If $\rho(t)$ is given, we can again solve for $P(t)$ as

$$P(t) = P(0)e^{A(t)},$$

(6-66)

where

$$A(t) = \int_0^t d\tau \left[\frac{\dot{\rho}(\tau) + \lambda\rho(\tau)}{\beta - \rho(\tau)}\right].$$

(6-67)

For example, for a ramp insertion $\rho(t) = \gamma\beta t$, the prompt jump approximation implies

$$P(t) = P(0)e^{-\lambda t}[1 - \gamma t]^{-\left(1 + \frac{\lambda}{\gamma}\right)}.$$

(6-68)

The prompt jump approximation is frequently found to yield an adequate description of reactor kinetic behavior. Numerical solutions of the point reactor kinetics equations have demonstrated the approximation is valid to within about 1% up to reactivity insertions of $\rho_0 = \$0.50.$[6]

## 3. SMALL AMPLITUDE APPROXIMATION (LINEARIZATION)

Suppose that we assume that small reactivity variations will produce only small changes in the reactor power from its equilibrium value $P_0$. We already know that this assumption is not true for a critical reactor since even a slight positive step in reactivity gives rise to an exponentially increasing power response that eventually grows beyond any bound. However the assumption will still be valid if we consider only short times following the step insertion. Furthermore for certain classes of reactivity changes such as a periodic reactivity insertion with an appropriate negative bias, the resulting power variations remain small for all times. In this case, the point reactor kinetics equations reduce from a set of linear ODEs with variable coefficients to a set of linear ODEs with constant coefficients.

Consider again the integrodifferential form of the point reactor kinetics equations

$$\frac{dP}{dt} = \left[ \frac{\rho(t) - \beta}{\Lambda} \right] P(t) + \frac{\beta}{\Lambda} \int_0^\infty d\tau \, D(\tau) P(t - \tau). \tag{6-69}$$

If we now let $p(t)$ denote the power variations about a reference level $P_0$

$$P(t) = P_0 + p(t), \tag{6-70}$$

then substitution of Eq. (6-70) into Eq. (6-69) and use of the identity

$$\int_0^\infty d\tau \, D(\tau) = 1 \tag{6-71}$$

yields (after a bit of manipulation)

$$\frac{dp}{dt} = \frac{\rho(t)}{\Lambda} P_0 + \frac{\rho(t) p(t)}{\Lambda} + \frac{\beta}{\Lambda} \int_0^\infty d\tau \, D(\tau) [p(t - \tau) - p(t)]. \tag{6-72}$$

Thus far our analysis has been exact, merely consisting of a bit of algebraic manipulation. We now introduce our key approximation by assuming that $\rho(t)$ and $p(t)$ are sufficiently small that we can neglect the second-order term $\rho(t) \, p(t)$ to write

$$\frac{dp}{dt} = \frac{\rho(t)}{\Lambda} P_0 + \frac{\beta}{\Lambda} \int_0^\infty d\tau \, D(\tau) [p(t - \tau) - p(t)]. \tag{6-73}$$

This approximation is sometimes (incorrectly) referred to as the *linearization approximation*. Actually both the original point reactor kinetics equation as well as Eq. (6-72) are already linear, provided we are given $\rho(t)$. All we have done is to remove $\rho(t)$ as a time-dependent coefficient in the equation and replace it by a time-dependent inhomogeneous term $\rho(t) P_0 / \Lambda$.

Equation (6-73) forms the basis of nuclear reactor stability analysis, since it relates the response of the reactor power to a small change in reactivity. At this point one can essentially turn the mathematical analysis of this equation over to the systems (or control) engineer who will then proceed to hack away at it using the powerful tools of linear systems analysis.[7] It is not our intent here to venture very far into this topic.

However with the recognition that many readers of this text (particularly electrical engineers) will already be acquainted with methods of linear systems analysis, we do feel it useful to provide a very short discussion of this topic in an effort to bridge the gap to reactor kinetics.[8,9] (Other readers may wish to bypass the remaining discussion of this section.)

The key tool used in linear systems analysis is the Laplace transform (defined and discussed in Appendix G). We will define the Laplace transform $\tilde{f}(s)$ of a function $f(t)$ by

$$\tilde{f}(s) = \int_0^\infty dt\, e^{-st} f(t).$$  (6-74)

Then we can easily Laplace transform the "linearized" reactor kinetics equation (6-73) and solve for

$$\tilde{p}(s) = P_0 Z(s)\tilde{\rho}(s)$$  (6-75)

where we have defined the *zero power transfer function* $Z(s)$
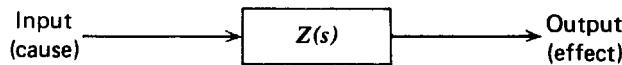
$$Z(s) \equiv \frac{1}{s}\left[\Lambda + \sum_{j=1}^6 \frac{\beta_j}{s+\lambda_j}\right]^{-1} \equiv \frac{1}{Y(s)}.$$  (6-76)

Hence to determine the behavior of the reactor power, we need only study the poles of $Z(s)$ and $\tilde{\rho}(s)$. However there is a great deal more we can do by employing the very powerful methods of linear systems analysis. In particular we can study the stability of the reactor when it is operating at power (i.e., when we introduce feedback).

The concept of a transfer function is much more general. The response (or output) of any physical system to a signal (or input) applied to it can be expressed in terms of such transfer functions. More precisely, we define

$$\text{Transfer function} = \frac{\text{Laplace transform of response}}{\text{Laplace transform of input}} \equiv Z(s).$$  (6-77)
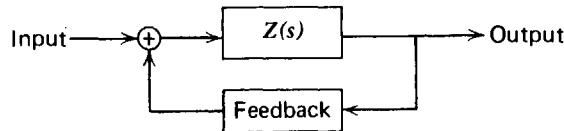
This can be conveniently represented by a "block diagram."



In our case, the input is the reactivity $\rho(t)$, while the output is the fractional power change $p(t)/P_0$. Of course other choices are possible, such as the inlet coolant temperature and pressure.

The transfer function defined for a linear system in this way is sometimes called the "open-loop" transfer function, since we have assumed that the output (power level) does not affect the input (reactivity) in any way. Later we will consider the

case in which we allow feedback effects:



(That is, we "close" the feedback loop.)

It should be noted that the concept of a transfer function allows one to use the principle of superposition to write the total output resulting from several inputs as the sum of the individual output from each of the inputs. In particular since $\mathcal{L}\{\delta(t)\} = 1$, the response to a $\delta$-function reactivity input is just the inverse Laplace transform of the transfer function itself.

$$\frac{p(t)}{P_0} = \mathcal{L}^{-1}\{Z(s)\} = \frac{1}{\Lambda} + \sum_{j=2}^{7} \frac{\exp s_j t}{s_j \left[\Lambda + \sum_{i=1}^{6} \frac{\beta_i \lambda_i}{(s_j + \lambda_i)^2}\right]} \equiv \mathcal{X}(t). \tag{6-78}$$

Here, $\mathcal{X}(t)$ is the so-called *unit impulse response*, that is, the power response to a unit impulse reactivity insertion. The $s_j$ are the roots of the inhour equation, while we have noted that for a critical system, $s_0 = 0$.

One can now use the convolution theorem (Appendix G) to reexpress Eq. (6-75) in the "time domain" as

$$p(t) = P_0 \int_0^t d\tau \, \mathcal{X}(t - \tau) \rho(\tau). \tag{6-79}$$

Note that $\mathcal{X}(t - \tau)$ is just the Green's function for the linearized point reactor kinetics equation. Hence it is not surprising that $\mathcal{X}(t)$ plays an extremely important role in the study of nuclear reactor kinetics. In particular one can infer the stability properties of a linear system by studying $\mathcal{X}(t)$.

One defines such a linear system to be *stable* if its response to any bounded input is also bounded. It is possible to show (see Problem 6-27) that a necessary and sufficient condition for stability is for

$$\int_0^\infty |\mathcal{X}(t)| \, dt < \infty. \tag{6-80}$$

In this regard it is interesting to note that since the zero power reactor response function $\mathcal{X}(t) \to \Lambda^{-1}$ as $t \to \infty$, the integral of $\mathcal{X}(t)$ over all time is *not* bounded. This then implies that a critical reactor without feedback is *unstable* with respect to bounded reactivity inputs. However as we will see later, there are always sufficient negative reactivity feedback mechanisms present in reactors to render them stable under almost any conceivable operating conditions.

As an example of the use of the reactor transfer function, let us determine the response of the reactor to a sinusoidal reactivity input

$$\rho(t) = \delta\rho \sin \omega t. \tag{6-81}$$

Then if we note that the Laplace transform of this input is just

$$\tilde{\rho}(s) = \frac{\delta\rho\omega}{s^2 + \omega^2}, \tag{6-82}$$

we can easily invert Eq. (6-75) to find

$$\frac{p(t)}{P_0} = \delta\rho |Z(i\omega)| \sin(\omega t + \phi) + \omega\delta\rho \sum_{j=1}^{7} \frac{\exp s_j t}{\left(\omega^2 + s_j^2\right)\frac{dY}{ds}\Big|_{s_j}}, \tag{6-83}$$

where $\phi(\omega) = \arg[Z(i\omega)]$ is known as the *phase shift* of the transfer function, while $|Z(i\omega)|$ is known as the system *gain*. The first term in Eq. (6-83) arises from the poles of $\tilde{\rho}(s)$ on the imaginary axis at $s = \pm i\omega$, while the remaining terms are due to the poles of $Z(s)$. These latter poles are just the roots $s_j$ of the inhour equation $Y(s_j) = 0$. Of course for the critical system we are considering, $s_7 < s_6 < \cdots < s_1 = 0$. Hence as $t \to \infty$, only the oscillating terms and the $s_1 = 0$ term remain, and we find the asymptotic behavior of the power oscillations as

$$\frac{p(t)}{P_0} = \delta\rho |Z(i\omega)| \sin(\omega t + \phi) + \frac{\delta\rho}{\omega\Lambda}. \tag{6-84}$$

Notice in particular that there is a shift in the average power level of $P_0 \delta\rho/\omega\Lambda$.

If a reactor operating at a steady-state power level is subjected to a sinusoidal perturbation in reactivity, the power will oscillate with the source frequency, but with a phase shift $\phi(\omega) \equiv \arg\{Z\}$ (actually a phase lag) and an amplitude proportional to $G(\omega) \equiv |Z(i\omega)|$. Hence we can obtain the values of $Z(s)$ on the imaginary axis in the complex $s$-plane by measuring experimentally the amplitude and relative phase of power oscillations as functions of frequency, induced by a sinusoidal reactivity insertion with constant amplitude. This is the basis of the zero-power pile-oscillator experiment. We have sketched the gain and phase shift of the zero power transfer function for a $^{235}U/^{238}U$-fueled system in Figure 6-4.

## F. Some General Comments on Applications of the Point Reactor Kinetics Equations

The point reactor kinetics equations are commonly applied to analyze most short-term transients in nuclear reactor behavior. The popularity of the point reactor kinetics model is not due necessarily to its validity (which is limited), but rather the fact that alternative methods that also treat the spatial dependence of the flux are usually prohibitively expensive to use in the large variety of problems typically encountered in a core design effort.
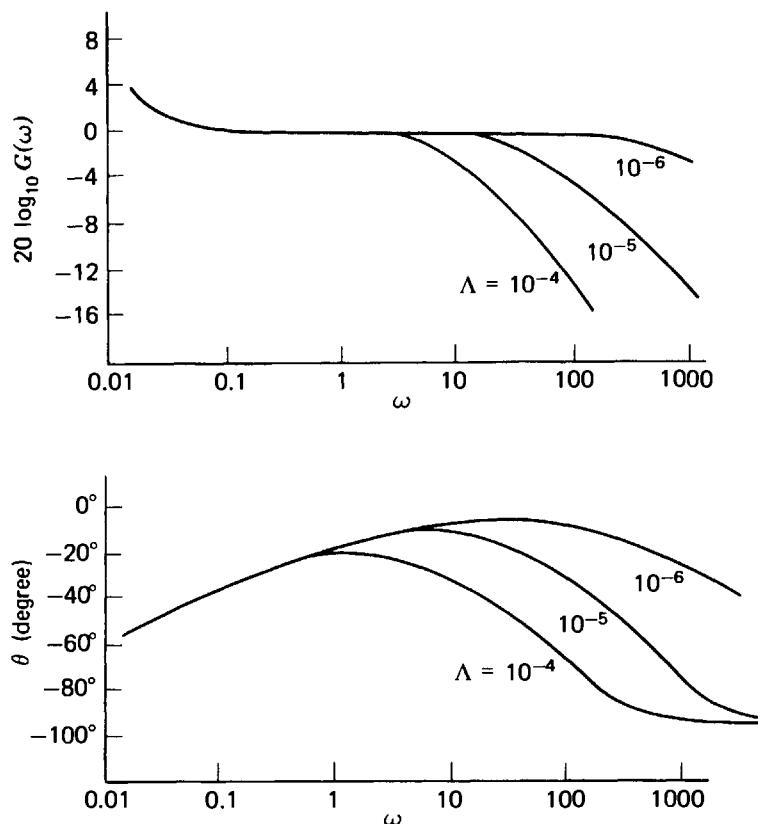
FIGURE 6-4.    Gain and phase shift of the zero-power reactor transfer function

Most experimental measurements on reactors involving a reactivity change can be analyzed via the point reactor kinetics equations. Indeed since such experiments are usually performed at zero power, it is frequently not necessary to append to the point reactor kinetics equations suitable models of reactivity feedback. Although we will briefly review a variety of experimental techniques commonly used to measure reactor kinetics parameters later in this chapter, we would merely mention here as an example experiments in which the reactivity worth of control rods are measured by withdrawing a rod and then determining the resulting asymptotic reactor period. The inhour equation can then be used to relate this period to the worth of the control rod.

Normal operating transients in nuclear power reactors are usually very easy to analyze, since they are typically rather slow. This is because the rate of change of reactor power level in a large plant is limited not by neutronic considerations, but rather by the rate of temperature change allowable in nonnuclear plant components. For such slow transients (typically a 5% change in power per minute or less for maneuvering) reactivity insertions are kept far below prompt critical, and hence the prompt jump approximation, in which the mean generation time $\Lambda$ is set equal to zero, is adequate. Furthermore on such a time scale the spatial power shape usually remains in a fundamental mode and hence the point reactor kinetics equations are valid. The solution of the point reactor kinetics equations for such slow transients does necessitate consideration of reactivity feedback, however. Frequently one finds the point reactor kinetics equations augmented with transient

models of the remainder of the plant suffices for on-line system performance studies in the plant itself (using hybrid digital–analog process computers).

The most stringent application of the point reactor kinetics equations is in the analysis of hypothetical reactor accident situations in which reactivity insertions may be quite large (several \$) and power transients very rapid. Indeed one frequently encounters situations in which such equations are not valid. Typically one uses them to provide a parameter study of the effects of various input data such as reactivity insertions on reactor behavior under the postulated accident conditions. Occasionally spatially dependent kinetics calculations are performed to check the predictions of the point reactor model. Obviously an effort is always made to generate conservative predictions.

For most severe transients in thermal reactors, such as a loss of coolant accident or the ejection of a control rod, the usual transient thermal–hydraulics models are adequate to supplement the core neutronics calculations. However in fast systems very severe transients may lead to fuel melting and slumping with an appreciable change in core configuration. Indeed such core rearrangements may produce large positive reactivities, leading to very large energy release, followed by core disassembly (that is, a small nuclear explosion). Such severe accidents, although quite remote in probability, must nevertheless be studied in reactor analysis. They require not only models of the core neutronics (e.g., the point reactor kinetics equations) and thermal-hydraulics, but as well models of the physical motion of the core due to melting and disassembly. Needless to say, such analyses can become very complicated indeed.

# III. REACTIVITY FEEDBACK AND REACTOR DYNAMICS

## A. Mathematical Description of Feedback

Thus far we have assumed that the reactivity $\rho(t)$ appearing in the point reactor kinetics equations is a given function of time. However we know, in fact, that it depends on the neutron flux (or power level) itself. This dependence arises because the reactivity depends on macroscopic cross sections, which themselves involve the atomic number densities of materials in the core:

$$\Sigma(\mathbf{r},t) = N(\mathbf{r},t)\sigma(\mathbf{r},t). \tag{6-85}$$

Now it is easily understandable how the atomic density $N(\mathbf{r},t)$ can depend on the reactor power level, since: (a) material densities depend on temperature $T$, which in turn depends on the power distribution and hence the flux and (b) the concentrations of certain nuclei is constantly changing due to neutron interactions (buildup of poison or burnup of fuel). However it should also be noted that we have explicitly written the microscopic cross sections as explicit functions of $\mathbf{r}$ and $t$. This must be done since the cross sections that appear in our one-speed diffusion model are actually averages of the true energy-dependent microscopic cross sections over an energy spectrum characterizing the neutrons in the reactor core. And

this neutron energy spectrum will itself depend on the temperature distribution in the core, and hence the reactor power level.

Such reactivity variation with temperature is the principal feedback mechanism determining the inherent stability of a nuclear reactor with respect to short-term fluctuations in power level. Evidently our first task in constructing a model of temperature feedback is to determine the temperature distribution in the core. Of course, one could begin by writing the fundamental equations of heat and mass transport characterizing the reactor. That is, one could write the equations of thermal conduction and convection using the fission energy deposition as the source of heat generation. The motion of the coolant through the core would then be described by the equations of hydrodynamics. As we will find in our detailed development of thermal–hydraulic core analysis in Chapter 12, this fundamental approach results in a formidable set of nonlinear partial differential equations unless further simplifications are introduced.

Hence it has become customary to avoid the complexity of a direct solution of the full set of thermal–hydraulic equations by replacing the spatially dependent description by a "lumped parameter" model similar in philosophy to the point reactor kinetics model. The reactor core is typically characterized by several average temperatures, such as an average fuel temperature, moderator temperature, and coolant temperature. One then models a simple dependence of the reactivity on these temperature variables.

Of course one must append to the original point reactor kinetics model equations describing the changes of these core temperatures produced by changes in the reactor power level. Typically such calculations are based on a model of a single average fuel element and its associated coolant channel, and describes the conduction of fission heat out of the fuel element and into the coolant, and then its subsequent convection out of the reactor core. We will consider such models in some detail in Chapter 12.

Our more immediate concern in this chapter, however, is to study how the results of such thermal–hydraulic models, namely the core component average temperatures such as $T_F$ (fuel) and $T_M$ (moderator or coolant), can be used in suitable models of reactivity feedback. To this end let us return to consider our point reactor kinetics model. We will write the reactivity $\rho(t)$ as a sum of two contributions

$$\rho(t) = \delta\rho_{ext}(t) + \delta\rho_f[P]. \tag{6-86}$$

The $\delta\rho$ notation signifies that the reactivity is measured with respect to the equilibrium power level $P_0$ [for which $\rho \equiv 0$]. Furthermore, $\delta\rho_{ext}(t)$ represents the "externally" controlled reactivity insertion such as by adjusting a control rod. $\delta\rho_f[P]$ denotes the change in reactivity corresponding to inherent feedback mechanisms. This latter component is written generally as a functional of the reactor power level.

When the reactor is operating at a steady-state power level $P_0$, then there will be a certain feedback reactivity $\rho_f[P_0]$. Since in almost all cases this will correspond to a negative reactivity, it is customary to refer to $\rho_f[P_0]$ as the *power defect* in reactivity. To sustain the criticality of the system, we must supply a counteracting external reactivity $\rho_0$ (such as by withdrawing control rods) such that

$$\rho_0 + \rho_f[P_0] = 0. \tag{6-87}$$

In this sense then, we define our incremental reactivities as

$$\delta\rho_{\text{ext}}(t) = \rho_{\text{ext}}(t) - \rho_0,$$

$$\delta\rho_f[P] = \rho_f[P] - \rho_f[P_0].$$
(6-88)

It is also useful to recall our definition of the incremental power

$$p(t) \equiv P(t) - P_0.$$
(6-89)

From Eq. (6-88) we note that $\delta\rho_f[p = 0] = \delta\rho_f[P_0] = 0$.

We can now sketch the block diagram characterizing a reactor with feedback as shown in Figure 6-5. In particular, it should be recalled that we have already analyzed the "black box" describing the reactor kinetics, since this is just given by the point reactor kinetics equation without feedback, which can be most conveniently written in the form Eq. (6-72). This equation can be regarded as determining $p(t)$ for any $\rho(t)$. Of course we commonly analyze this equation under one of a variety of approximations, for example: (a) ignoring delayed neutrons ($D \equiv 0$) for very large reactivity insertions, (b) prompt jump approximation, and (c) linearization for small reactivity insertions, in which case we can solve Eq. (6-73) in terms of the open loop or zero-power transfer function to find

$$p[\rho] = P_0 \int_0^t d\tau \, \mathcal{Z}(t - \tau)\rho(\tau).$$
(6-90)

We therefore turn our attention to the study of the black box describing the feedback functional $\delta\rho_f[p]$.

## B. Models of Temperature Feedback

### 1. TEMPERATURE COEFFICIENT OF REACTIVITY

Of most concern in the study of short-term reactivity feedback is the effect of the core temperature $T$ on the multiplication of the core. One usually expresses this in terms of a *temperature coefficient of reactivity* $\alpha_T$ defined as

$$\alpha_T \equiv \frac{\partial\rho}{\partial T}.$$
(6-91)
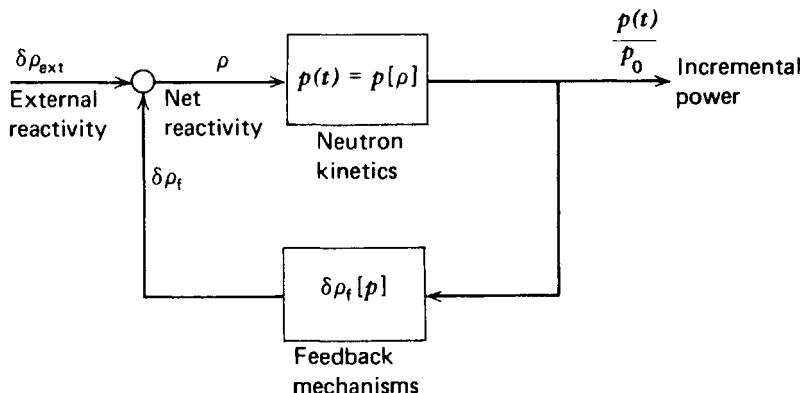


FIGURE 6-5.    Closed-loop block diagram

This should more properly be referred to as an *isothermal* temperature coefficient, since it assumes that the core can be characterized by a single uniform temperature $T$.

Such a simple model illustrates quite clearly the effect of temperature feedback on reactor stability. For if a reactor were to possess a *positive* $\alpha_T$, then an increase in temperature would produce an increase in $\rho$, hence the power would increase, causing a further increase in temperature, and so on. In this sense, the reactor would be unstable with respect to temperature or power variations. The more desirable situation is that in which $\alpha_T$ is *negative*, since then an increase in temperature will cause a decrease in $\rho$, hence a decrease in reactor power and temperature which tends to stabilize the reactor power level.

The temperature coefficient of reactivity depends on a great many processes occurring within the core. Since the details of these processes depend on the specific reactor type under consideration, we will defer a discussion of just how such temperature coefficients are evaluated to Chapter 14.

However we should remark at this point that the concept of such an isothermal temperature coefficient has a very limited range of usefulness in reactor analysis. In a heterogeneous reactor, most of the fission energy release is confined to the fuel elements. This energy must then be transferred by thermal conduction through the fuel element, the clad, and then into the coolant before it can be withdrawn from the core. Hence one has a very nonuniform temperature distribution. For example, fuel centerline temperatures may range as high as 2700°C, while coolant temperatures are as low as 250°C.

Hence one usually introduces several such temperature coefficients of reactivity, each of which characterizes the reactivity feedback due to a variation in the effective or average temperatures of each major component of the core, such as fuel, moderator, and structure

$$\alpha_T = \sum_j \alpha_j \equiv \sum_j \frac{\partial \rho}{\partial T_j}. \tag{6-92}$$

However one must also keep in mind that the various thermal processes in the core are characterized by widely different time behaviors. The fuel temperature responds relatively rapidly to any power level changes. However it takes an appreciable amount of time to transfer this energy to the coolant, and hence its temperature response is much slower. For this reason, it is convenient to divide up the temperature coefficient of reactivity into prompt and delayed components.

Effects that depend on the instantaneous state of the fuel—for instance, resonance absorption (Doppler effect) or thermal distortion of fuel elements—may be regarded as prompt, while effects that depend primarily on the moderator or coolant—neutron energy spectrum and thermal expansion of moderator material—are delayed. Prompt feedback mechanisms are of particular importance in reactor safety studies, since they play a very important role in limiting any reactor transients that may occur.

For these reasons, the isothermal temperature coefficient of reactivity is not really a very useful quantity. A more useful quantity is the change in reactivity caused by a change in reactor power. We will consider this in detail in the next section.

There is one instance in which the concept of an isothermal temperature coefficient is of some use, however. When the reactor is at zero power, there is no

fission energy being released in the fuel, and hence the entire reactor core can essentially be characterized by a single temperature. As the temperature of the core is increased, say by heating the primary coolant, there will be a decrease in core multiplication due to temperature feedback. One defines the so-called *temperature defect* of reactivity, $\Delta\rho_{TD}$, as the change in reactivity that occurs in taking the reactor core from the fuel-loading temperature (i.e., the ambient temperature) to the zero power operating temperature

$$\Delta\rho_{TD} = \int_{T \text{ ambient}}^{T \text{ zero power}} \frac{\partial\rho}{\partial T} \, dT. \tag{6-93}$$

The magnitude of $\Delta\rho_{TD}$ is primarily determined by the coolant temperature coefficient of reactivity, and depends sensitively on the moderator-to-fuel ratio and soluble poison concentration. In a LWR $\Delta\rho_{TD} \sim .02 - .04(\Delta k/k)$.

## 2. POWER COEFFICIENTS OF REACTIVITY

A far more useful parameter characterizing feedback is the power coefficient of reactivity defined by

$$\alpha_P \equiv \frac{d\rho}{dP} = \sum_i \left( \frac{\partial\rho}{\partial T_i} \right) \left( \frac{\partial T_i}{\partial P} \right), \tag{6-94}$$

where the $T_i$ are again the effective temperatures associated with each core component. Such a parameter takes account of the temperature differences occurring in a reactor while it is operating at power. The reactivity due to power feedback can then be written as

$$\rho = \int_0^P dP \, \alpha_P(P). \tag{6-95}$$

Obviously if a reactor is to be inherently stable against power-level fluctuations, it must be designed with $\alpha_P < 0$.

A closely related quantity is the *power defect*, which is defined to be the change in reactivity taking place between zero power and full power

$$\Delta\rho_{PD} \equiv \int_0^{P_{\text{full power}}} \frac{\partial\rho}{\partial P} \, dP. \tag{6-96}$$

The power defect can be quite sizable. For example, in the LWR the power defect is typically of the order $\Delta\rho_{PD} \rightarrow .01 - .03(\Delta k/k)$.

Thus far we have only discussed how the reactivity depends on temperature. The remaining problem of how the temperature depends on the power level is strongly related to the reactor type and involves a thermal–hydraulics analysis of the core. For slow power changes, one can use the steady-state analysis developed in Chapter 12 to determine the core temperatures for a given power level and hence the power coefficient of reactivity in terms of the temperature coefficients of the various components of the core.

Such a steady-state thermal analysis will no longer be valid for more rapid power transients. For example, the thermal time constant of the fuel is frequently as large

as 10 seconds. For power transients on shorter time scales the fuel temperature coefficient of reactivity (principally determined by the Doppler effect) will be the dominant factor in determining the power coefficient of reactivity.

Although a realistic description of temperature feedback involves a transient thermal–hydraulics model of the reactor core such as those we will develop in Chapter 12, several alternative lumped parameter models of the reactor temperature dependence are occasionally used for qualitative studies of reactor dynamics.

One common model assumes a single effective coolant temperature $T_c$, and models the fuel temperature $T_F$ by *Newton's law of cooling*

$$\frac{dT_F}{dt} = KP(t) - \gamma(T_F - T_c), \tag{6-97}$$

where $K$ and $\gamma$ are thermal constants characterizing the core. At the opposite extreme would be an *adiabatic* model, in which the heat loss is assumed to be negligible (such as in a very rapid transient)

$$\frac{dT_F}{dt} = KP(t). \tag{6-98}$$

Still another model assumes *constant power removal* such that

$$\frac{dT_F}{dt} = K(P - P_0). \tag{6-99}$$

All of these models can be considered as special cases of a general linear feedback functional:

$$\rho_f(t) = \int_{-\infty}^{t} d\tau \, h(t - \tau)[P(\tau) - P_0]. \tag{6-100}$$

A little inspection should convince you that the feedback kernel $h(t)$ in each of these cases takes the form:

Newton's law of cooling:    $h(t) = \alpha K e^{-\gamma t}$

Adiabatic model:    $h(t) = \alpha K [P_0 = 0]$      (6-101)

Constant power removal:    $h(t) = \alpha K$.

If more reliable design information is required, then one is usually forced to go to a multigroup diffusion calculation coupled with a detailed thermal–hydraulic analysis of the core. One can then calculate the multiplication for several different power levels, and hence determine directly the dependence of reactivity on power level. The corresponding power and temperature coefficients are frequently precalculated and stored in tabular form for use in determining the reactivity feedback to use in point reactor kinetics models.

## C. The Transfer Function of a Reactor with Feedback

### 1. CLOSED-LOOP TRANSFER FUNCTION

Let us now return to consider the dynamic behavior of a reactor with feedback. In particular we will consider the effects of feedback on the reactor

response to an external reactivity insertion. First we will consider the power oscillations resulting from a periodic reactivity insertion of small amplitude, since this in effect measures the reactivity-to-power transfer function.

A typical series of reactivity power transfer function gain measurements[10,11] is shown in Fig. 6-6. In particular notice how different the transfer function at power is from the zero power transfer function. The marked resonance behavior in the vicinity of .03 cps at $P_0 = 550$ kW in the first plot is apparent. Such behavior is due to the presence of feedback. As the power level increases, the resonance peak becomes narrower and higher. As we shall see, this implies that for sufficiently large powers, the reactor is unstable.

Let us go back and develop a mathematical expression for the transfer function characterizing a reactor with feedback.[1] We will restrict ourselves to small power variations about the equilibrium level $P_0$ so that the feedback can be adequately represented as a linear functional similar to Eq. (6-100)

$$\delta\rho_f[p] = \int_0^\infty d\tau\, h(\tau)p(t-\tau). \qquad (6\text{-}102)$$

Note that with this sign convention the negative feedback necessary for reactor
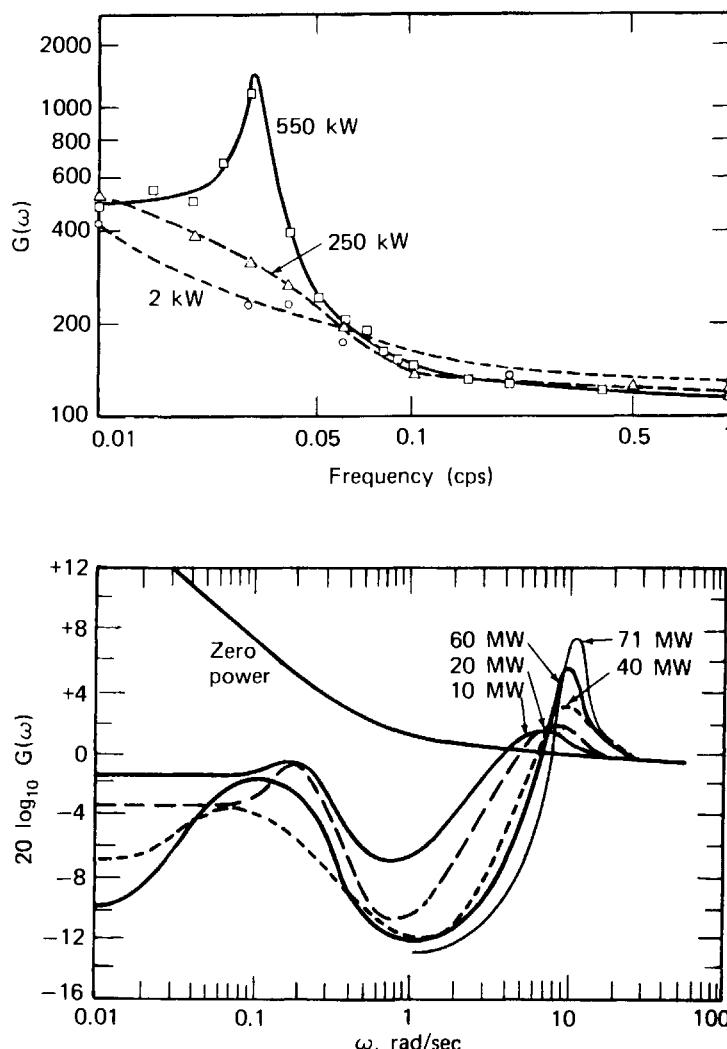


FIGURE 6-6.   Examples of measured closed-loop transfer functions[10,11]

stability will imply that $h(\tau) < 0$. It should also be kept in mind that the feedback kernel $h(t)$ actually depends on the equilibrium power level $P_0$.

If we substitute Eq. (6-102) into Eq. (6-72), we find

$$\frac{dp}{dt} = \frac{1}{\Lambda}\left[ \delta\rho_{\text{ext}}(t) + \int_0^\infty d\tau\, h(\tau)p(t-\tau) \right][P_0 + p(t)]$$

$$+ \frac{\beta}{\Lambda}\int_0^\infty d\tau\, D(\tau)[p(t-\tau) - p(t)]. \qquad (6\text{-}103)$$

Of course this equation is still nonlinear. We will consider only small power variations $p(t) \ll P_0$ such that we can linearize Eq. (6-103) to write

$$\frac{dp}{dt} = \frac{1}{\Lambda}P_0\delta\rho_{\text{ext}}(t) + \frac{1}{\Lambda}\int_0^\infty d\tau[\,\beta D(\tau) + P_0 h(\tau)\,]p(t-\tau) - \frac{\beta}{\Lambda}p(t). \qquad (6\text{-}104)$$

Now, as before, we will assume the reactor is operating at a steady state power level $P_0$ prior to $t = 0$. Then by Laplace transforming Eq. (6-104) we find

$$s\tilde{p}(s) = \frac{1}{\Lambda}P_0\delta\tilde{\rho}_{\text{ext}} + \frac{\beta}{\Lambda}\tilde{D}(s)\tilde{p}(s) + \frac{1}{\Lambda}P_0 H(s)\tilde{p}(s) - \frac{\beta}{\Lambda}\tilde{p}(s),$$

or

$$\frac{\tilde{p}(s)}{P_0} = \left\{ \frac{Z(s)}{1 - P_0 H(s)Z(s)} \right\}\delta\tilde{\rho}_{\text{ext}}(s) \equiv L(s)\delta\tilde{\rho}_{\text{ext}}(s), \qquad (6\text{-}105)$$

where $Z(s)$ is the usual zero power transfer function given by Eq. (6-76) while $H(s) = \mathcal{L}\{h(t)\}$ is the *feedback transfer function*. We have further defined the *reactivity-to-power* or *closed-loop* transfer function $L(s)$

$$L(s) \equiv \frac{Z(s)}{1 - P_0 H(s)Z(s)}. \qquad (6\text{-}106)$$

Notice that as $P_0 \to 0$, $L(s) \to Z(s)$, the zero power transfer function. This notation is consistent with our earlier block diagram that has been relabeled in Figure 6-7. Just
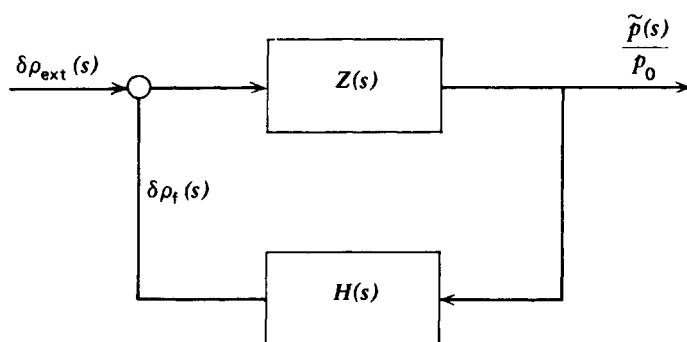


FIGURE 6-7.   Closed-loop Transfer function

as in the zero power case, the inverse of $L(s)$, $l(t) \equiv \mathcal{L}^{-1}\{L(s)\}$, is the Green's function for the point-reactor kinetics equation with feedback

$$p(t) = P_0 \int_0^t d\tau\, l(t-\tau)\delta\rho_{ext}(\tau). \tag{6-107}$$

Let us examine $L(s)$ in a bit more detail. Unlike $Z(s)$, $L(s)$ is analytic at $s = 0$ with a value

$$L(0) = -[P_0 H(0)]^{-1} = \int_0^\infty l(t)dt. \tag{6-108}$$

Hence the long time response to a positive step reactivity insertion of magnitude $\delta\rho_{ext} \rightarrow \delta\rho_0$ is just

$$p(t) = P_0 \delta\rho_0 \int_0^t d\tau\, l(\tau) \rightarrow P_0 \delta\rho_0 L(0). \tag{6-109}$$

This implies that the reactor approaches a new equilibrium power level

$$P(t \rightarrow \infty) = P_0[1 + \delta\rho_0 L(0)]. \tag{6-110}$$

This is in sharp contrast to the zero power (i.e., no feedback) reactor whose power level grew exponentially for long times. The equilibrium state occurs when the power level reaches a value such that the feedback reactivity just compensates for the step reactivity insertion

$$\delta\rho_f(t) = \int_0^t d\tau\, h(t-\tau)p(\tau) \rightarrow p(\infty)H(0) = -\delta\rho_0. \tag{6-111}$$

## 2. RESPONSE TO A SINUSOIDAL REACTIVITY INSERTION

Let us once again consider a sinusoidal reactivity variation

$$\delta\rho_{ext}(t) = \delta\rho_0 \sin \omega t. \tag{6-112}$$

Then the long time response is given in analogy to the zero feedback case [Eq. (6-84)] by

$$\frac{p(t)}{P_0} = |L(i\omega)|\sin(\omega t + \phi), \qquad \phi(\omega) = \arg\{L(i\omega)\}. \tag{6-113}$$

Now if we recall the form for $L(s)$ given by Eq. (6-106), we can see that a resonance in the gain $G(\omega) = |L(i\omega)|$ will occur when

$$1 - P_0 H(i\omega)Z(i\omega) = 1 + P_0|H(i\omega)Z(i\omega)|\exp i\theta \rightarrow 0, \tag{6-114}$$

where

$$\theta(\omega) = \arg\{-H(i\omega)Z(i\omega)\}. \tag{6-115}$$

However for the resonance condition [Eq. (6-122)] to be satisfied, we require that both of the conditions

$$\theta(\omega) = 180° \quad \text{and} \quad P_0 |H(i\omega)Z(i\omega)| = 1 \quad\quad (6\text{-}116)$$

be simultaneously satisfied. These two conditions will determine a critical power level $P_{crit}$ and a resonance frequency $\omega_{crit}$ at which a true resonance situation will arise. As long as the reactor power $P_0$ is kept below $P_{crit}$, only a finite resonance peak such as those illustrated in Figure 6-6 will occur. At this peak, the gain $|L(i\omega)|$ will assume a value

$$|L(i\omega_{crit})| = \frac{|Z(i\omega_{crit})|}{1 - (P_0/P_{crit})}. \quad\quad (6\text{-}117)$$

In the light of this discussion we can more readily understand the transfer function gain measurements given in Figure 6-6.

In almost all cases of reactor design, the critical power level $P_{crit}$ above which the reactor is susceptible to such instabilities is always quite far above actual or design operating levels. Nevertheless it is important to be able to anticipate such inherent instabilities in the design so that effective countermeasures can be taken (such as by modification of the original design or by the addition of stabilizing feedback control). Such considerations arise in reactor stability analysis.

## 3. LINEAR STABILITY ANALYSIS

The stability of a reactor with feedback can be investigated by examining the singularities of the closed-loop transfer function

$$L(s) = \frac{Z(s)}{1 - P_0 H(s)Z(s)} \qu\quad\quad (6\text{-}118)$$

in the complex s-plane. First notice that since $Z(s)$ appears both in the numerator *and* denominator, its poles $s_j$ [that is, the roots of the inhour equation $Y(s_j)$ $= Z^{-1}(s_j) = 0$] "cancel." Hence the poles of $L(s)$ are simply the zeros of

$$1 - P_0 H(s)Z(s) = 0. \quad\quad (6\text{-}119)$$

Now suppose that Eq. (6-119) were to have a simple root at $s = s_0$ [i.e., a pole of $L(s)$]. Then when we invert the Laplace transform, this pole will contribute a term in $p(t)$ of the form $\exp(s_0 t)$. Hence if $s_0$ is in the right half s-plane (RHP), then $p(t)$ will grow exponentially in time. This would imply an unstable response to an applied reactivity perturbation (within the linear approximation, of course). If the root $s_0$ lies in the LHP, then terms of the form $\exp(s_0 t)$ will decay in time. Hence to study reactor stability, it is obviously important to determine if any of the poles of $L(s)$ [i.e., zeros of Eq. (6-119)] lie in the RHP.

Instabilities may arise for sufficiently large power levels $P_0$ even with negative reactivity feedback, as the sequence of diagrams in Figure 6-8 indicate. For $P_0 = 0$, we can identify the poles of $L(s)$ as just those of $Z(s)$ [i.e., the inhour equation roots]. Then, for the case in which $\alpha_P = H(0) < 0$, increasing $P_0$ will provide more

negative feedback and hence shift the pole $s_1$ to the left and into the LHP. However the other poles will also shift. In particular, the pole $s_2$ will shift to the right. For some sufficiently large power level $P_0$, the poles $s_1$ and $s_2$ will coalesce, forming a complex conjugate pair that moves off of the real axis and into the complex plane. For still larger $P_0$, this pair moves back to the right, until for some critical power level $P_0 = P_{crit}$ the poles move into the RHP and the reactor becomes unstable. When the poles cross the imaginary axis, we observe a "resonance" in the transfer function gain $|L(i\omega)|$ as we have already noted. Hence the problem of the linear stability of our equilibrium state reduces to the problem of determining the sign of the real parts of the poles of $L(s)$. In particular, we have found that a reactor is linearly "strictly stable" when the poles of $L(s)$ all have negative real parts. The response of the power in the critical case, when any of these poles have real parts equal to zero, is not correctly described by linear analysis and depends on nonlinearities of the point reactor kinetics equation.
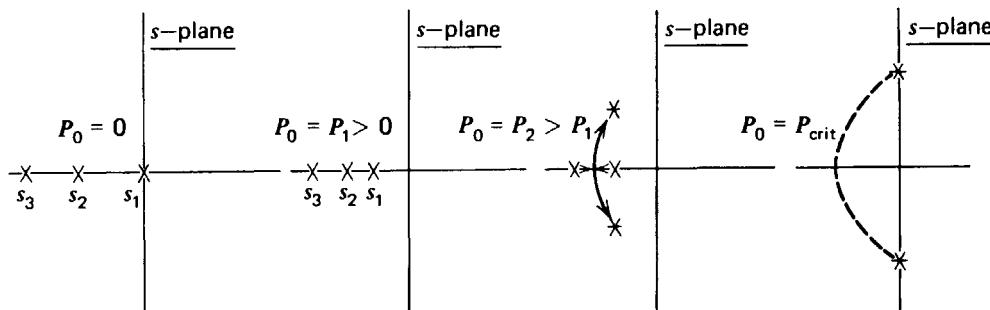


FIGURE 6-8.   Shifting of poles of the closed-loop transfer function with increasing reactor power level $P_0$

There are numerous tricks for determining the signs of these poles. These include methods[12] such as those utilizing Nyquist diagrams, root-locus plots, and Routh–Hurwitz criteria. However such subjects are more properly the concern of linear system analysis or control theory, so we will simply refer the interested reader to the references listed at the end of the chapter.[1,8,9]

## 4. NONLINEAR POINT REACTOR KINETICS

Thus far our study of the point reactor kinetics equations with feedback has been restricted to situations in which the reactivity changes and corresponding power changes are sufficiently small that these equations can be linearized. In particular our study of the stability of the reactor has been restricted to the consideration of *stability in the small*—that is, to the study of perturbations and responses sufficiently small for a linear analysis. However for larger perturbations nonlinear effects must be taken into account. In these cases, the resulting conclusions about stability may be quite different.

For example, we have seen that the linearized point reactor kinetics equation predicts that the reactor will be unstable if the power exceeds some critical value

$P_{\text{crit}}$. However even though the reactor is linearly unstable, it may be stable in the nonlinear description. Hence it is of some interest to study the significance of linear stability theory within the more general framework of nonlinear stability theory.

It should be remarked, however, that there are many different approaches to nonlinear point reactor kinetics—none of which is completely satisfactory. Furthermore such results as do exist provide only *sufficient* (as opposed to *necessary*) conditions for stability. Sufficiency conditions are usually much too restrictive for practical application. Furthermore, the very limited validity of the models investigated by nonlinear stability methods usually discount their value for practical reactor design. And of course there is also the more pragmatic philosophy adopted in most nuclear reactor design favoring an ultraconservative design that guarantees linear stability under all conceivable operating conditions, hence obviating the need for a nonlinear stability analysis.

## 5. SOME FINAL COMMENTS ON REACTOR STABILITY ANALYSIS

It might seem that an integral part of any reactor safety analysis would be an investigation of the stability of the reactor design. In particular such an analysis should consider the possibility that the reactor might become unstable under some feasible combination of operating conditions. In practice, however, such stability studies do not play near as significant a role in reactor design as one might expect. Reactor instabilities usually can occur only if one of the temperature feedback coefficients happens to be positive over some range of operating conditions. However it is usually quite easy to design a power reactor so that it will always be characterized by large, negative temperature coefficients (as we will see in Chapter 14). Indeed all power reactor designs tend to be ultraconservative in this respect (as they do with respect to all safety considerations). Hence there has been relatively little motivation to perform detailed stability analyses of reactor core designs. And in those instances in which methods of stability analysis have been applied to practical reactor designs, investigations have usually been limited to the linear domain.

## IV. EXPERIMENTAL DETERMINATION OF REACTOR KINETIC PARAMETERS AND REACTIVITY

From our earlier development of the point reactor kinetics equations, we have found that the three most important parameters characterizing the kinetic behavior of a nuclear reactor are the reactivity $\rho$, the prompt generation time $\Lambda$, and the effective delayed neutron fraction $\beta$. A variety of experimental techniques have been developed to measure both these as well as dynamic (i.e., feedback) characteristics of the reactor. Such methods can be classified as either static or dynamic measurement techniques.

### A. Static Techniques for Reactivity Determination

#### 1. NEUTRON MULTIPLICATION MEASUREMENT (RECIPROCAL MULTIPLICATION METHOD)

Perhaps the most common measurement is the so-called *critical loading experiment* or *reciprocal multiplication method*, in which the steady-state neutron

flux resulting from a source in a subcritical assembly is measured as fuel is added to the assembly. If the reactor is characterized by a multiplication factor $k$, then one can crudely think of the amplification of the original source neutrons by the assembly as given by

$$\mathcal{R} = S_0 + kS_0 + k^2S_0 + \cdots$$

$$= (1 - k)^{-1}S_0 \equiv MS_0, \tag{6-120}$$

where $S_0$ is the rate at which source neutrons are emitted in the reactor. The usual procedure for a safe approach to delayed critical in core loading consists of plotting $M^{-1}$ (or the reciprocal neutron counting rate) as a function of some parameter that controls reactivity (e.g., fuel mass) and then extrapolating this $M^{-1}$ plot to zero to determine the critical loading (as sketched in Figure 6-9). During a stepwise approach to delayed critical by the reciprocal multiplication method, the neutron level following each addition of reactivity must be allowed to stabilize in order to obtain an accurate indication of the asymptotic multiplication before proceeding with the next reactivity addition. As one approaches delayed critical, the buildup of the precursor concentrations can become bothersome.
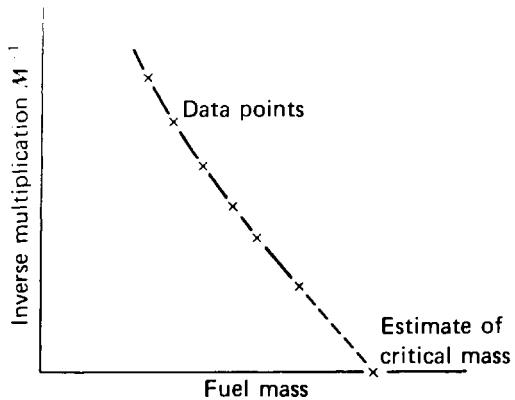


FIGURE 6-9.    Critical loading measurements

## 2. FUEL SUBSTITUTION TECHNIQUES[4]

One can determine reactivity by uniformly substituting a p₋ison for a small fraction of the fuel. The poison is usually chosen such that it has the same scattering and absorption properties as the fuel (or as closely as possible). Then first-order perturbation theory yields a reactivity change due to the substituted poison of

$$\Delta\rho = \frac{\int_{\text{poison}} d^3r \phi^\dagger(\mathbf{r}) \delta\Sigma_f(\mathbf{r})\phi(\mathbf{r})}{\int_{\text{core}} d^3r \phi^\dagger(\mathbf{r})\Sigma_f(\mathbf{r})\phi(\mathbf{r})}. \tag{6-121}$$

This substitution method can be used for control-rod calibration by balancing the effect of a given rod movement by adding a proper amount of distributed poison.

## B. Dynamic Techniques for Reactivity Measurements

### 1. ASYMPTOTIC PERIOD MEASUREMENTS

Perhaps the simplest type of kinetic measurement one can perform is to make a small perturbation in the core composition of a critical reactor, and then to measure the stable or asymptotic period of the resultant reactor transient. Using the inhour equation, one can then infer the reactivity "worth" of the perturbation from a measurement of the asymptotic period. It should be noted that the period method for all practical purposes applies only to positive periods, since negative periods are dominated by the longest delayed neutron precursor decay and hence provide very low sensitivity to negative reactivity.

### 2. ROD DROP METHOD

Let us consider a reactor operating at some equilibrium power level $P_0$ when it is suddenly shut down by the introduction of a negative reactivity $-\delta\rho$ (the "rod drop"). From our earlier studies of the point reactor kinetics equations we know that after a few prompt neutron lifetimes, the reactor power level drops to a lower level $P_1$, determined by the amount of reactivity insertion and remains at this "quasistatic" level until it is ultimately decreased by delayed neutron precursor decay. We can use our earlier result [Eq. (6-64)] from the prompt jump approximation to write

$$\frac{P_1}{P_0} = \frac{\beta}{\beta + \delta\rho}. \tag{6-122}$$

Hence we can solve for the reactivity insertion in dollars in terms of the power levels $P_0$ and $P_1$ as

$$\frac{\delta\rho}{\beta} = \frac{P_0}{P_1} - 1. \tag{6-123}$$

To determine $P_1$, one need only extrapolate back the asymptotic behavior following the rod drop to $t = 0$.

### 3. SOURCE JERK METHOD

A very similar technique can be used to measure the multiplication of a subcritical assembly. Suppose we consider such a subcritical system maintained at a power level $P_0$ by a neutron source of strength $S_0$. One can express the equilibrium power level $P_0$ using the point reactor kinetics equation as

$$P_0 = \frac{\Lambda}{\delta\rho + \beta}\left[\sum_i \lambda_i C_{i0} + S_0\right], \tag{6-124}$$

where $\delta\rho$ is the degree of subcriticality of the system. Suppose the source is now jerked out of the core. Once again the prompt jump approximation can be used to express the lower "quasistatic" power level $P_1$ as

$$P_1 = \frac{\Lambda}{\delta\rho + \beta}\left[\sum_i \lambda_i C_{i0}\right]. \tag{6-125}$$

Using Eqs. (6-124) and (6-125), along with the equilibrium forms of the point-reactor kinetics equation prior to the source jerk, one can find

$$\frac{P_0}{P_1} = 1 + \frac{\delta\rho}{\beta}.$$

(6-126)

Hence the dollars subcritical of the assembly is given very simply by

$$\frac{\delta\rho}{\beta} = \frac{P_0}{P_1} - 1.$$

(6-127)

The source jerk method is very similar to the rod drop method in concept. However it is somewhat simpler to perform since it requires only the removal of a small mass of material (the source) in contrast to the rapid release of one or more control rods.

## 4. ROD OSCILLATOR METHOD

If one oscillates a control rod in a sinusoidal fashion in a critical reactor, there will be a corresponding oscillation in the reactor power. By measuring the gain and magnitude of the phase shift characterizing the power oscillations, one can measure the reactor transfer function, either at zero power or operating power:

$$\frac{\delta P}{P_0} = L(i\omega)\delta\rho.$$

(6-128)

For low powers, $L(i\omega) \rightarrow Z(i\omega)$. In this case, the high-frequency behavior of the transfer function

$$Z(i\omega) \sim \frac{1}{\omega\Lambda}$$

(6-129)

can be used to measure either the prompt generation time $\Lambda$ or the reactivity worth of the oscillating rod,

$$\delta\rho = \omega\Lambda \frac{\delta P}{P_0}.$$

(6-130)

Such oscillator measurements can also be used to determine the stability characteristics of the reactor.

## 5. PULSED NEUTRON METHODS

By measuring the transient behavior of the neutron population following a burst of neutrons injected into an assembly, one can measure a variety of important parameters. Suppose we first consider a pulse of neutrons injected at $t = 0$ into a nonmultiplying assembly. Then according to one-speed diffusion theory, the flux satisfies

$$\frac{1}{v}\frac{\partial\phi}{\partial t} = D\nabla^2\phi - \Sigma_a\phi(\mathbf{r}, t)$$

(6-131)

subject to the initial condition applying to the pulsed source, $\phi(\mathbf{r},0) = \phi_0(\mathbf{r})$. For long times, the flux in the assembly will approach the asymptotic form

$$\phi(\mathbf{r},t) \sim a_1 \psi_1(\mathbf{r}) \exp - \left( v\Sigma_a + vDB_g^2 \right) t, \tag{6-132}$$

where $\psi_1(\mathbf{r})$ is the fundamental mode of the assembly geometry. Hence the asymptotic behavior of the flux is governed by the decay constant

$$\alpha_0 \equiv v\Sigma_a + vDB_g^2. \tag{6-133}$$

If one measures $\alpha_0$ for various assembly sizes, then plotting $\alpha_0$ against $B_g^2$ will yield $v\Sigma_a$ (the intercept at $B_g^2 = 0$) and $vD$ (the slope). (See Figure 6-10.) Actually, there are higher order terms in $B_g^2$ due to both transport and energy-dependent corrections

$$\alpha_0 = v\Sigma_a + vDB_g^2 + CB_g^4 + \cdots \tag{6-134}$$

which add a curvature to the $\alpha_0(B_g^2)$ plot.

In multiplying assemblies if one assumes that both the pulse injection and measurement are performed on a time scale short compared to delayed neutron lifetimes, then one can use

$$\frac{1}{v}\frac{\partial \phi}{\partial t} = D\nabla^2 \phi - (\Sigma_a - \nu\Sigma_f)\phi(\mathbf{r},t) \tag{6-135}$$

to find decay constants of the form

$$\alpha_0 = v(\Sigma_a - \nu\Sigma_f) + vDB_g^2. \tag{6-136}$$
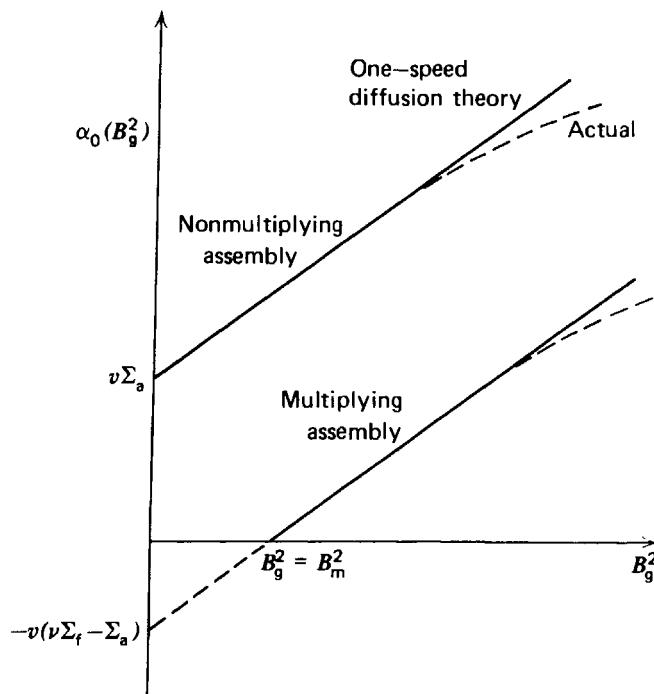


FIGURE 6-10. The fundamental decay constant versus geometric buckling in a pulsed neutron experiment

In this case, the $\alpha_0$ versus $B_g^2$ curve appears as that shown in Figure 6-10.

One can use this technique to directly measure reactivity. For a rapid pulse, the time behavior of the flux or power will be determined by prompt neutron kinetics such as

$$\alpha_0 = \frac{1}{P}\frac{dP}{dt} = \frac{\rho - \beta}{\Lambda}.$$  (6-137)

Hence $\alpha_0$ can be used to infer $\rho$, provided $\beta$ and $\Lambda$ are known. If the core is maintained at delayed critical, then $\rho = 0$ and the pulsed neutron method measures

$$\alpha_0 = -\Lambda/\beta.$$  (6-138)

## C. Noise Analysis in Nuclear Reactors[13,14]

Thus far we have been analyzing the reactor as essentially a deterministic system. Yet we know that all of the dynamic variables describing the reactor (power level, flux, temperature, etc.) actually fluctuate in a statistical fashion about some mean value. We are unable to predict with certainty the future values of these variables but rather can only specify the *probability* that they will assume a certain value.

The statistical nature of the neutron diffusion process has been stressed repeatedly. Moreover the concept of a cross section, and, indeed, even the quantum mechanical description of the neutron interactions, must be interpreted in a probabilistic sense. There are numerous other sources of such statistical fluctuations or *noise* in a reactor, such as in fluid flow, coolant boiling, and mechanical vibration. In fact, statistics enters even into the measurement of the reactor state due to detector noise.

At low power levels the statistical fluctuations associated with the fundamental *nuclear processes* occurring in the core will be dominant. However at higher power levels, the reactor noise will be predominantly due to disturbances of a *nonnuclear* nature (e.g., coolant flow). Regardless of its origin, reactor noise is important in reactor dynamics for at least two reasons. First, it *interferes* with the precision with which a desired quantity can be measured in a reactor; that is, one must extract the signal of interest out of the background noise. Second, however, since the noise originates from various processes occurring in the reactor, it can actually serve as a source of *information* about the system. The latter of these properties is of most interest to us here. We will study how noise analysis can be used to measure the transfer function of the reactor.

### 1. CROSS CORRELATION METHODS

Let us begin by introducing two definitions. We will define the *autocorrelation* of a function $x(t)$ by

$$\varphi_{xx}(\tau) = \lim_{T \to \infty} \frac{1}{2T}\int_{-T}^{T} x(t)x(t+\tau)dt,$$  (6-139)

and the *cross correlation* of two functions, $x(t)$ and $y(t)$ by

$$\varphi_{xy}(\tau) = \lim_{T \to \infty} \frac{1}{2T}\int_{-T}^{T} x(t)y(t+\tau)dt.$$  (6-140)

If the functions $x(t)$ and $y(t)$ are periodic, then the limit process can be omitted provided $T$ is chosen as the period. In general, however, $x(t)$ and $y(t)$ will not be periodic. In fact we will later consider them to be *random variables* in the sense that only their probability distribution can be specified.

Now we will set up the cross correlation between reactivity and power (using a notation in which the limit process $T \to \infty$ is to be understood)

$$\varphi_{\rho P}(\tau) = \frac{1}{2T} \int_{-T}^{T} \delta\rho_{\text{ext}}(t) \frac{p(t+\tau)}{P_0} dt. \tag{6-141}$$

If we substitute in our expression for $p(t)/P_0$ from Eq. (6-107) (after extending the time domain to $-\infty < t' < t$), we find

$$\varphi_{\rho P}(\tau) = \frac{1}{2T} \int_{-T}^{T} \delta\rho_{\text{ext}}(t - \tau) \left[ \int_0^\infty du\, \delta\rho_{\text{ext}}(t - u) l(u) \right] dt$$

$$= \int_0^\infty l(u) \left[ \frac{1}{2T} \int_{-T}^{T} \delta\rho_{\text{ext}}(t - \tau) \delta\rho_{\text{ext}}(t - u) dt \right] du$$

$$= \int_0^\infty l(u) \varphi_{\rho\rho}(\tau - u) du, \tag{6-142}$$

where we have identified the autocorrelation function of reactivity

$$\varphi_{\rho\rho}(\tau) = \frac{1}{2T} \int_{-T}^{T} \delta\rho_{\text{ext}}(t) \delta\rho_{\text{ext}}(t + \tau) dt. \tag{6-143}$$

As a final step, we take the Fourier transform of Eq. (6-142), defined as

$$\tilde{\varphi}_{\rho P}(\omega) = \int_{-\infty}^{\infty} d\tau\, e^{i\omega\tau} \varphi_{\rho\rho}(\tau) \equiv \mathcal{F}\{\varphi_{\rho\rho}\} \tag{6-144}$$

to find

$$\tilde{\varphi}_{\rho P}(\omega) = \mathcal{F}\{l(u)\} \tilde{\varphi}_{\rho\rho}(\omega); \tag{6-145}$$

but $\mathcal{F}\{l(u)\}$ is just the closed loop transfer function $L(i\omega)$. Hence we find that we can write

$$L(i\omega) = \frac{\mathcal{F}\{\varphi_{\rho P}\}}{\mathcal{F}\{\varphi_{\rho\rho}\}}. \tag{6-146}$$

Here $\tilde{\varphi}_{\rho P} \equiv \mathcal{F}\{\varphi_{\rho P}\}$ is referred to as the *cross-spectral density*, while $\tilde{\varphi}_{\rho\rho} \equiv \mathcal{F}\{\varphi_{\rho\rho}\}$ is referred to as the *reactivity* (or *input*) *spectral density*.

To apply this result in a practical measurement, one varies the reactivity of the reactor in a random or pseudorandom fashion and then measures the corresponding variations in the reactor power or flux. In this sense, the measurement is very similar to that involved in a rod oscillator experiment. To construct the time-correlation function, one measures both $\delta\rho_{\text{ext}}(t)$ and $p(t)$ at the time $t$ and at various delayed times $t \to t + \Delta\tau, t + 2\Delta\tau, \ldots$ . Using these measurements, one can

then construct both the time-correlation functions $\varphi(t)$ and their Fourier transforms numerically. For example, if measurements are taken at delay intervals of $\Delta\tau$, then the cross-spectral density is given by

$$\mathcal{F}\{\varphi_{\rho P}(\tau)\} \cong \sum_n \varphi_{\rho P}(n\Delta\tau)\exp(i\omega n\Delta\tau)\Delta\tau. \tag{6-147}$$

Then by taking the ratio of $\mathcal{F}\{\varphi_{\rho P}\}$ and $\mathcal{F}\{\varphi_{\rho\rho}\}$, one can obtain both the gain and phase of the closed-loop transfer function $L(i\omega)$. This experiment becomes particularly simple if one can use a so-called "white" noise source as the reactivity input. Such sources are characterized by a spectral density that is constant in frequency, that is, $\mathcal{F}\{\varphi_{\rho\rho}\} = \text{constant} = A$. Then

$$\mathcal{F}\{\varphi_{\rho P}\} = AL(i\omega). \tag{6-148}$$

Hence by merely measuring the cross correlation, one can determine both the amplitude and phase of the transfer function.

This experiment serves, then, as an alternative to a reactor oscillator transfer-function measurement. Unlike the latter, it does not suffer from background noise (rather taking advantage of such random fluctuations), and hence does not require nearly so large an input signal. However both of these experiments suffer from the fact that one must perturb the reactor by introducing an externally controlled reactivity signal in order to perform the measurement. It is possible to bypass this difficulty and measure the amplitude of $L(i\omega)$ directly from the inherent noise naturally present in the reactor.

## 2. AUTOCORRELATION MEASUREMENTS

Consider the autocorrelation of the fluctuations in the reactor power

$$\varphi_{PP}(\tau) = \frac{1}{2T} \int_{-T}^{T} \frac{p(t)}{P_0} \frac{p(t+\tau)}{P_0} dt. \tag{6-149}$$

If we substitute in Eq. (6-107) for $p(t)/P_0$ and again take a Fourier transform in time, we find

$$\mathcal{F}\{\varphi_{PP}\} = L(-i\omega)L(i\omega)\mathcal{F}\{\varphi_{\rho\rho}\}, \tag{6-150}$$

or

$$|L(i\omega)|^2 = \frac{\mathcal{F}\{\varphi_{PP}\}}{\mathcal{F}\{\varphi_{\rho\rho}\}}. \tag{6-151}$$

Hence the square of the magnitude (i.e., the gain) of the transfer function can be determined as the ratio of the power and reactivity spectral densities.

Although we can easily measure the power spectral density, the reactivity spectral density characterizing inherent reactivity noise is not experimentally accessible. If one has reason to believe that such fluctuations are truly random in nature, then $\mathcal{F}\{\varphi_{\rho\rho}\} = \text{constant}$, and the measurement of the power autocorrelation function by itself will yield the amplitude of the transfer function (although phase information will have been lost).

Such a measurement of $|L(i\omega)|$ is extremely simple. It has the advantage that it does not perturb the reactor. Indeed it can be used in a real time mode to obtain an instantaneous measurement of the reactor transfer function. Its only significant disadvantage is its limited accuracy.

Such noise measurements have been used to measure a large variety of nuclear reactor parameters, and have proven to constitute a valuable diagnostic technique in determining reactor kinetic behavior.

## V. SPATIAL EFFECTS IN REACTOR KINETICS

Thus far our analysis of time-dependent nuclear reactor behavior has been based on the point reactor kinetics model in which the neutron flux was assumed to be the product of a time-independent spatial shape factor $\psi_1(r)$ and a time-dependent amplitude factor $P(t)$ [cf. Eq. (6-7)]. However this assumption will obviously be invalid in many cases of interest. For example, one of the most important safety questions concerning reactor analysis involves the reactor kinetic behavior following the postulated ejection of the control rod with highest reactivity worth. Such a strongly localized perturbation in the core composition would certainly cause a considerable deviation from the spatial shape factor $\psi_1(r)$ and would invalidate the point reactor kinetics model.

Furthermore most modern power reactor cores are quite large from a neutronic point of view, being as much as 200 diffusion lengths in diameter. Hence the neutronic behavior in such cores tends to be quite loosely coupled from point to point. This means that a change in the flux or power density (or core multiplication) at one point in the core will not be felt at other points until after an appreciable time delay. For example, one frequently finds rather significant "tilts" in the spatial power distribution across the core due to nonuniform coolant temperature or fission product buildup. The phenomenon of such loose spatial coupling can be seen rather vividly by measuring the reactor transfer function, say, under zero power conditions, at several points in a large power reactor core. That is, one inserts a sinusoidal or pseudorandom reactivity variation at one point r in the core (say, by moving a control rod in and out of the core), and then measures the amplitude and phase of the resulting power or flux oscillations by locating a neutron detector at various other points r' in the core. If the reactor were truly described by the point reactor kinetics equation, then the transfer function $Z(i\omega;$ r,r') measured at various points r would be the same. And for low frequencies, one does indeed find that $Z(i\omega; r, r')$ is essentially spatially independent. However for higher frequencies in large reactor cores, one finds that actual measurements will yield different results, depending on where the oscillator and detector are placed. Such measurements reveal that the transfer function is actually spatially dependent for higher frequencies, because of the time it takes to propagate a disturbance in the neutron flux from one point to another in the core. This implies a breakdown in the point reactor kinetics model that characterizes every point in the reactor by the same time-dependence $P(t)$.

As a general rule, one finds that the point reactor kinetics equations are incapable of predicting the detailed behavior of reactor transients initiated by rapid local changes in reactivity. More precisely, if the neutron flux changes rapidly on a

time scale of the order of the effective neutron lifetime $\langle l \rangle$, the point reactor kinetics equation should be regarded as suspect.

In these instances, one must take explicit account of the spatial dependence of the neutron flux. In fact one is frequently forced to perform a brute force numerical solution of the time-dependent neutron diffusion equation and precursor equations. Unfortunately in most cases in which such spatial effects are significant, one cannot rely on the one-speed approximation to provide an adequate description of the neutron energy-dependence. Hence a direct numerical study of nuclear reactor kinetics[15] usually involves the solution of the multigroup, time-dependent diffusion equations—at a considerable computational expense.

For such finite difference solutions of the multigroup diffusion equations to be feasible, it is necessary to employ a variety of numerical techniques to accelerate the computation. These calculations are usually coupled with transient thermal-hydraulic calculations and can become quite involved. In general they are only used as a last resort to describe situations in which detailed spatial behavior is of paramount importance in a rapid transient (such as the rod-ejection accident analysis).

A variety of less direct methods exist. These can generally be classified as nodal, quasistatic, or modal techniques. The *nodal* approach[16] is very similar to that discussed in Section 5-II in that the core is divided into a number of regions or nodes. As in the static case, the primary difficulty in this approach is determining the parameters that couple the flux at various nodal points. This is usually accomplished by a variety of approximate schemes adjusted by numerous empirical fits to either experimental or benchmark calculation data.

So-called *quasistatic* methods[17] essentially work within the framework of the point reactor model, performing periodic static spatial calculations to obtain the shape functions necessary for evaluating the point kinetics parameters $\rho$, $\beta$, and $\Lambda$. The practical utilization of this method has been rather limited to date.

Perhaps the most popular alternative[18] to direct finite difference schemes involves expanding the flux in a *finite* series of known spatial functions or modes, $\psi_j(\mathbf{r})$, and then obtaining a set of equations for the time-dependent expansion coefficients $\varphi_j(t)$:

$$\phi(\mathbf{r},t) = \sum_{j=1}^{N} \varphi_j(t)\psi_j(\mathbf{r}). \tag{6-152}$$

Of course the ideal scheme would be to choose $\psi_j(\mathbf{r})$ as the spatial eigenfunctions of the perturbed reactor. Unfortunately one usually does not know these modes. Instead it is common to expand in an alternative finite set of spatial functions and then use either weighted residual or variational methods (recall Section 5-III-C) to determine the appropriate set of *modal equations* for the $\varphi_j$. Such schemes are referred to as *synthesis methods* and will be discussed in more detail in Chapter 13.

Although such spatially dependent kinetics problems are of importance in the very rapid transients arising in postulated accident analysis, they also arise in the study of much longer term fuel depletion and fission product buildup phenomena. In these latter cases, however, one can treat the neutron flux in a quasi steady-state manner by performing a sequence of criticality calculations as the core composition changes with time. We will devote considerable attention to the analysis of such fuel depletion or burnup problems in Chapter 15.
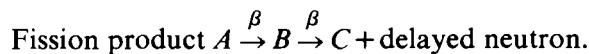
## REFERENCES

1. A. Z. Akcasu, G. S. Lellouche, and L. M. Shotkin, *Mathematical Methods in Nuclear Reactor Dynamics*, Academic, New York (1971).
2. R. Scalletar, in Proceedings of Conference on Neutron Dynamics and Control, D. L. Hetrick and L. E. Weaver Eds., USAEC CONF-650413 (1966).
3. W. M. Stacey, Jr., *Space-Time Nuclear Reactor Kinetics*, Academic, New York (1969).
4. G. R. Keepin, *Physics of Nuclear Kinetics*, Addison-Wesley, Reading, Mass. (1965).
5. A. Z. Akcasu, G. S. Lellouche, and L. M. Shotkin, *Mathematical Methods in Nuclear Reactor Dynamics*, Academic, New York (1971), p. 91.
6. R. Goldstein and L. M. Shotkin, *Nucl. Sci. Eng.* 38, 94 (1969).
7. P. H. Hammond, *Feedback Theory and its Applications*, English Universities Press, London (1958); J. L. Bower and P. M. Schultheiss, *Introduction to the Design of Servomechanisms*, Wiley, New York (1958).
8. D. L. Hetrick, *Dynamics of Nuclear Reactors*, University of Chicago Press (1971).
9. L. E. Weaver, *Reactor Dynamics and Control*, Elsevier, New York (1968).
10. F. W. Thalgott, et al., Proceedings of Second U. N. Conf. on Peaceful Uses of Atomic Energy, Vol. 12, 242 (1958).
11. J. A. Deshong, Jr., and W. C. Lipinski, USAEC Document ANL-5850 (1958).
12. A. Z. Akcasu, G. S. Lellouche, and L. M. Shotkin, *Mathematical Methods in Nuclear Reactor Dynamics*, Academic, New York (1971), Chapter 6.
13. J. A. Thie, *Reactor Noise*, Rowman and Littlefield, Totowa N.J. (1963).
14. G. I. Bell and S. Glasstone, *Nuclear Reactor Theory*, Van Nostrand, Princeton, N. J. (1970), pp. 511–514.
15. D. R. Ferguson and K. F. Hansen, *Nucl. Sci. Eng.* 51, 189 (1973).
16. W. M. Stacey, Jr., *Space-Time Nuclear Kinetics*, Academic, New York (1969), Section 1.4.
17. K. O. Ott, *Nucl. Sci. Eng.* 26, 563 (1966).
18. J. B. Yasinsky and A. F. Henry, *Nucl. Sci. Eng.* 22, 171 (1965).

## PROBLEMS

6-1 At time $t=0$, a decaying point source emitting $S_0 e^{-\lambda t}$ neutrons per second is placed at the center of a homogeneous bare spherical reactor which is being maintained in a subcritical state. Determine the time-dependence of the neutron flux that would be measured by a detector placed outside of the reactor. Use one-speed diffusion theory and ignore delayed neutrons.

6-2 Consider a spherical assembly operating at a critical steady-state power level at time $t=0$. At this instance a neutron burst is suddenly inserted at the center of the reactor. Derive an expression for the length of time before the reactor flux will once again assume its fundamental mode shape to within 10%. Plot this time versus assembly radius $R$ for a thermal assembly moderated with $H_2O$. Ignore delayed neutrons.

6-3 (a) What is the maximum possible reactivity insertion capable in a $^{235}U$ fueled reactor? (Express your answer in $.)
    (b) What is the maximum possible reactivity of a $^{235}U$-fueled reactor having a nonleakage probability of 0.6 for fission neutrons and 0.7 for delayed neutrons?

6-4 Estimate the prompt neutron lifetime in a large thermal reactor fueled with $^{235}U$ and moderated with: (a) $H_2O$, (b) graphite, and (c) $D_2O$.

6-5 Calculate the effective neutron lifetime $\langle l \rangle$ for a thermal reactor fueled with either $^{233}U$ or $^{235}U$ and a fast reactor fueled with $^{239}Pu$.

6-6 Give a physical discussion of the difference between the prompt neutron lifetime and mean neutron generation time $\Lambda$ for both an infinite and finite reactor. (Refer to Keepin,[4] p. 166, for a more thorough discussion.)

6-7 In our development of an equation describing the delayed neutron precursor concentration, we assumed that these precursors did not migrate from the point of fission. This is a reasonable assumption in solid-fueled reactors. Consider, however, a reactor core in which the fuel is in gaseous form. Then the precursors may diffuse from the point of fission before decaying. If the diffusion coefficient characterizing a given precursor migration is $D_j$, develop a generalization of the precursor concentration equations to account for this process.

6-8 Derive an expression for the effective delayed neutron yield fractions $\bar{\beta}_i$ characterizing a mixture of several fissile isotopes.

6-9 Rederive the inhour equation for the case of a fast reactor fueled with $^{239}$Pu and $^{238}$U treating delayed neutrons from both isotopes explicitly.

6-10 Repeat the solution of the point reactor kinetics equations with one effective delayed group for a constant reactivity insertion $\rho_0$ using Laplace transform methods (see Appendix G).

6-11 Demonstrate that for small reactivity insertions and $(\beta - \rho_0 + \lambda\Lambda)^2 \gg 4\Lambda\lambda\rho_0$ the reactor power $P(t)$ is given by the approximate form [Eq. (6-40)].

6-12 Estimate the reactor period induced by a positive reactivity insertion of 1 $ in an infinite $^{235}$U-fueled thermal reactor moderated with water and a fast $^{239}$Pu-fueled reactor.

6-13 Prove that for six groups of delayed neutrons, the inhour equation has seven roots $s_i$ of which six have negative values.

6-14 Consider a two-stage delayed neutron production process as sketched below:

$$\text{Fission product } A \xrightarrow{\beta} B \xrightarrow{\beta} C + \text{delayed neutron.}$$

Assuming that $B$ is the only delayed neutron precursor of interest, write the point reactor kinetics equations including both rate equations for $A$ and $B$. By then deriving the corresponding inhour equation, demonstrate that such a two-stage decay process can actually yield a *negative* effective delayed neutron fraction.

6-15 Initially a reactor is operating at a steady-state power level $P_0$. Using the point reactor kinetics equation with one equivalent group of delayed neutrons, determine the stable reactor period $T$ for a positive step reactivity insertion of 1 $. Use the fact that $\lambda\Lambda/\beta \ll 1$ to simplify your answer. Calculate a numerical value for $T$ in the case in which $\lambda = 0.1$ sec$^{-1}$ and $\Lambda = 0.001$sec$^{-1}$.

6-16 According to the point kinetics equations with one equivalent group of delayed neutrons, how long should a steady source of $S_0$ neutrons per second be left on in order to raise the steady state reactor power level from $P_1$ to $P_2$? Assume $\lambda\Lambda/\beta \ll 1$. Roughly plot $P(t)$ against $t$.

6-17 Using the point kinetics equations with one equivalent group of delayed neutrons, derive an expression for $\rho(t)$ such that $P(t) = P_0 + at$.

6-18 Use the one-speed, one equivalent delayed neutron group form of the point reactor kinetics equation to analyze the following situation: A reactor operator wishes to reduce the power level of a reactor from $P_1$ to $P_2$. He therefore takes the reactor subcritical to a reactivity $\rho_0$, where $\rho_0$ is a negative number, and after a time $T$, he restores the reactivity to zero, whereupon the reactor levels out to $P_2$. In terms of $P_1$, $P_2$, $\rho_0$, and the other constants of the system, how long must he choose the time $T$ to be? (Assume $\lambda\Lambda/\beta \ll 1$ for convenience.)

6-19 Repeat the derivation of the integrodifferential form [Eq. (6-51)] of the point reactor kinetics equation for the case in which $P(t)$ and $C_j(t)$ are specified at an initial time, chosen at $t = 0$.

6-20 Demonstrate that for a periodic power variation $P(t) = P_0 + P_1 \sin \omega t$, one requires a periodic reactivity insertion of the form given by Eq. (6-54). Demonstrate that this reactivity insertion has a negative bias in the sense that its average over a period is negative.

6-21 Compute the time-dependence of the reactivity insertion for a positive power excursion of very short duration compared to delayed neutron lifetimes. Express this result in terms of the total energy released in the excursion.

6-22 By considering the point reactor kinetics equation with one effective delayed group, determine the time-dependence of the reactor power for a ramp reactivity insertion of $\rho(t) = -\gamma\beta t$. Compare this with the result predicted by the prompt jump approximation, Eq. (6-68).

6-23 Demonstrate that following a reactivity change from $\rho_1$ to $\rho_2$, the power levels before and after the reactivity step are given by $P_2/P_1 = (\beta - \rho_1)/\beta - \rho_2)$ in the prompt jump approximation.

6-24 Provide the details omitted in the derivation of the alternative form of the point-reactor kinetics equation given by Eq. (6-72).

6-25 In reactor kinetics problems in which reactivity is inserted at a very rapid rate, important changes occur in the neutron density while the delayed neutron emission changes only slightly. Assuming under this approximation that for short times after reactivity insertion Eq. (6-59) is applicable, determine the reactor power level $P(t)$ if the time-dependence of reactivity is $\rho(t) = \rho_0 \exp(t/\tau)$.

6-26 Explicitly perform the Laplace transform inversion of the zero power transfer function $Z(s)$ to obtain the impulse response function $\mathfrak{X}(t)$.

6-27 Prove that a necessary and sufficient condition for stability of a linear system is that

$\int_0^\infty |\mathfrak{X}(t)|\,dt < \infty$. [Hint: To prove sufficiency, show that this condition implies that the reactor power will be bounded for any bounded reactivity input. To prove necessity, consider the specific reactivity input $\rho(-t) = \mathfrak{X}(t)/|\mathfrak{X}(t)|$ and show that for this bounded input, the output $p(t)$ is unbounded if the above condition does not hold.]

6-28 Calculate the amplitude and phase angle for the zero-power transfer function and plot these as functions of frequency. Assume one group of delayed neutrons with $\bar{\beta} = .0065$, $\lambda = 0.08$ sec$^{-1}$, and $\Lambda = 10^{-4}$ sec.

6-29 Write and run a simple computer program that solves the point reactor kinetics equations numerically. Assume only one effective delayed group of neutrons, and use either a Runge–Kutta or predictor–corrector scheme to integrate the equations. In particular, study the time-step magnitude necessary to handle step reactivity insertions of $\rho_0 = 0.2$ \$, 1 \$, and 5 \$.

6-30 Set up the point reactor kinetics equations, including temperature feedback but no delayed neutrons. Assume that the power removal rate is proportional to the deviations of the temperature from some steady-state operating condition. Linearize the equations, solve them, and discuss the solutions. Assume step reactivity input at $t = 0$.

6-31 A reactor operating at steady state with constant heat removal rate experiences a step insertion of positive reactivity of 3 \$.

(a) Assuming a prompt negative temperature coefficient of reactivity, a heat removal rate during the excursion that remains constant at the steady-state value, and a constant delayed neutron contribution, give an expression for the maximum temperature reached during the excursion. (Make any necessary assumptions and state what they are.)

(b) Approximately what is the power level when this maximum temperature is reached?

6-32 In a prompt critical reactor excursion a large amount of reactivity (measured above prompt critical) $\rho_0$ is instantaneously inserted in an equilibrium reactor at $t = 0$. Assume that: (a) the effect of delayed neutrons is negligible on the time scales under consideration and (b) the reactor shuts itself down by thermal expansion of the core in such a way that negative reactivity is "added" proportional to the total heat energy generated up to time $t$, that is, $\rho = \rho_0 - \gamma \int_0^t dt' P(t')$. Find the power level $P(t)$ where $t$ is measured from the time of reactivity insertion and in units of the prompt neutron lifetime. [This is known as the Fuchs–Hansen model of a reactor excursion.]

6-33   Determine the total energy generated in the excursion modeled in Problem 6-32 in terms of the reactivity insertion, delayed neutron fraction, and reactivity feedback coefficient $\gamma$. Also determine the peak power generated in the excursion. Discuss the implications of these results for reactor safety.

6-34   A homogeneous fuel-moderator mixture is assembled as an unreflected critical reactor. No cooling is provided. Suddenly a control rod is removed, bringing $k$ to 1.02. Estimate the maximum temperature that results. The thermal conductivity is high enough that the core can be treated isothermally. As data, use: $\alpha_T = -2.5 \times 10^{-4}/°C$, $\beta = 0.0075$, and $\Lambda = 10^{-5}$ sec.

6-35   An interesting alternative to the pulsed neutron experiment is a modification of the diffusion length experiment in which an oscillating source of thermal neutrons is placed against one end of a long column of the material to be studied, and then the oscillating component of the resulting neutron flux in the column is measured at various positions. Determine expressions for the attenuation and phase shift (relative to the source) of the flux as functions of frequency $\omega$ for a nonmultiplying column as described by one-speed diffusion theory. [This is known as the *neutron wave* experiment.]

6-36   Derive the expression obtained for the system gain in terms of the autocorrelation functions in Eq. (6-151).

# 3

# The Multigroup Diffusion Method

# 7
## Multigroup Diffusion Theory
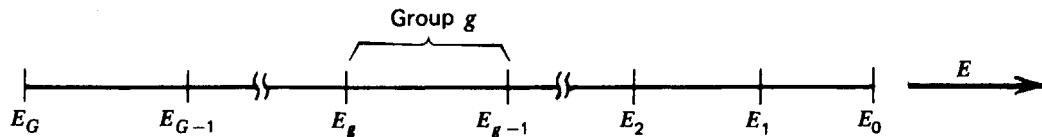
Thus far we have based our study of nuclear reactor theory on a particularly simple model of neutron transport, one-speed diffusion theory. This model certainly suffices to introduce most of the important concepts of reactor analysis as well as many of the computational methods used in modern reactor design. It can even be used on occasion to provide useful qualitative information such as in preliminary survey design studies. However for most of the problems encountered in practical nuclear reactor design the one-speed diffusion model is simply not adequate.

Two very significant assumptions were made in deriving the one-speed diffusion model. We first assumed that the angular flux was only weakly dependent on angle (linearly anisotropic, in fact) so that the diffusion approximation was valid. Usually this assumption is reasonably well satisfied in large power reactors provided we take care to modify the analysis a bit in the vicinity of strong absorbers, interfaces, and boundaries to account for transport effects.

The principal deficiency of the model is the assumption that all of the neutrons can be characterized by only a single speed or energy. As we have seen, the neutrons in a reactor have energies spanning the range from 10 MeV down to less than 0.01 eV—some nine orders of magnitude. Furthermore, we have noted that neutron–nuclear cross sections depend rather sensitively on the incident neutron energy. Hence it is not surprising that practical reactor calculations will require a more realistic treatment of the neutron energy dependence. (Indeed it is surprising that the one-speed diffusion equation works at all. Its success depends on a very judicious choice of the one-speed cross sections that appear in the equation.)

We will now allow the neutron flux to depend on energy, but rather than treat the neutron energy variable $E$ as a continuous variable, we will immediately

discretize it into energy intervals or groups. That is, we will break the neutron energy range into $G$ *energy groups*, as shown schematically below:



Notice that we are using a backward indexing scheme, corresponding physically to the fact that the neutron usually loses energy during its lifetime (and mathematically to the fact that one always solves the discretized equations starting at high energies and working successively to lower energies).

As in our earlier discrete ordinates approach, it would be possible to discretize $\phi(\mathbf{r}, E, t)$ by considering it only to be defined at each energy mesh point $E_g$. However it is more convenient to define the discretized fluxes instead to be the integrals of $\phi(\mathbf{r}, E, t)$ over the energies of each group, such that the *multigroup fluxes* $\phi_g(\mathbf{r}, t)$, represent the total flux of all neutrons with energies $E$ in the group $E_g < E < E_{g-1}$. Then our task is to determine equations for $\phi_g(\mathbf{r}, t)$. We will find that these equations take the form of a set of diffusion equations describing the neutrons in each energy group. The equations are coupled to one another since neutrons may experience changes in energy and hence pass from group to group. For example fission neutrons will usually be born in the highest energy groups and then cascade downward in energy from group to group as they are moderated by scattering collisions.
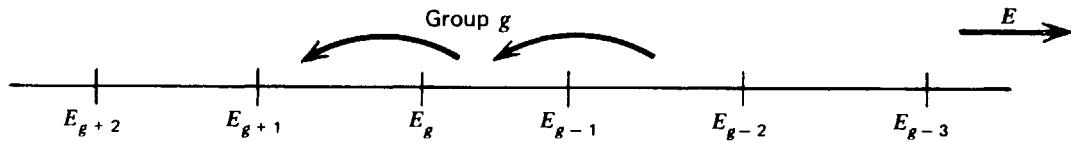
Recalling the rather detailed dependence of neutron cross sections on neutron energy $E$, one might expect that a great many such energy groups would be necessary to adequately describe a nuclear reactor. Surprisingly enough, however, most nuclear reactor calculations achieve sufficient accuracy using only *few-group diffusion* descriptions. The ability to describe a reactor adequately with a relatively small number of energy groups is not simply fortuitous, but rather is a consequence of a careful choice of the energy-averaged cross sections that characterize the neutrons in each group. Since the calculation of such group-averaged cross sections or *multigroup constants* is the key to the successful implementation of multigroup diffusion theory, we will consider it in some detail in Chapters 8 and 9.

In this chapter, we will first give a heuristic derivation of the multigroup diffusion equations based on the concept of neutron balance. We will then rederive these equations in a more rigorous (and useful) fashion and illustrate their application using several important examples. Finally we will discuss the common calculational strategies useful for solving this set of coupled partial differential equations.

## I. A HEURISTIC DERIVATION OF THE MULTIGROUP DIFFUSION EQUATIONS

Perhaps the most straightforward manner in which to arrive at the form of the multigroup diffusion equations is to apply the concept of neutron balance to a given energy group by balancing the ways in which neutrons can enter or leave this

group. Consider then a typical energy group $g$:



After a bit of reflection, it should be apparent that such a balance would read as follows:

$$
\begin{bmatrix} \text{Time rate of} \\ \text{change of} \\ \text{neutrons in} \\ \text{group } g \end{bmatrix} = - \begin{bmatrix} \text{change due} \\ \text{to} \\ \text{leakage} \end{bmatrix} - \begin{bmatrix} \text{absorption} \\ \text{in} \\ \text{group } g \end{bmatrix} + \begin{bmatrix} \text{source} \\ \text{neutrons} \\ \text{appearing} \\ \text{in group } g \end{bmatrix}
$$

$$
- \begin{bmatrix} \text{neutrons} \\ \text{scattering} \\ \text{out of} \\ \text{group } g \end{bmatrix} + \begin{bmatrix} \text{neutrons} \\ \text{scattering} \\ \text{into} \\ \text{group } g \end{bmatrix} . \qquad (7\text{-}1)
$$

It should be noted that we have taken explicit account of the fact that a scattering collision can change the neutron energy and hence either remove it from the group $g$, or if it is initially in another group $g'$, scatter it to an energy in the group $g$. We will characterize the probability for scattering a neutron from a group $g'$ to the group $g$ by something akin to the differential scattering cross section $\Sigma_s(E_{g'} \to E_g)$ (a so-called *group-transfer cross section*), $\Sigma_{sg'g}$. Note that the cross section characterizing the probability that a neutron will scatter out of the group $g$ is then given by

$$
\Sigma_{sg} = \sum_{g'=1}^{G} \Sigma_{sgg'}. \qquad (7\text{-}2)
$$

We will similarly define an absorption cross section characterizing the group $g$, $\Sigma_{ag}$, and a source term $S_g$ giving the rate at which source neutrons appear in group $g$. Finally we will define a diffusion coefficient $D_g$ so that the leakage from group $g$ can be written within the diffusion approximation as $\nabla \cdot D_g \nabla \phi_g$. If we combine all of these terms, we find a mathematical representation of the balance relations [Eq. (7-1)]

$$
\frac{1}{v_g} \frac{\partial \phi_g}{\partial t} = \nabla \cdot D_g \nabla \phi - \Sigma_{ag} \phi_g + S_g - \Sigma_{sg} \phi_g + \sum_{g'=1}^{G} \Sigma_{sg'g} \phi_{g'}, \qquad g = 1, 2, \ldots, G. \qquad (7\text{-}3)
$$

If we separate out that component of the source due to fissions, then we can write

$$
S_g = \chi_g \sum_{g'=1}^{G} \nu_{g'} \Sigma_{fg'} \phi_{g'} + S_g^{ext}, \qquad (7\text{-}4)
$$

where $\chi_g$ is the probability that a fission neutron will be born with an energy in

group $g$, while $\Sigma_{fg'}$ is the fission cross section characterizing a group $g'$ and $\nu_{g'}$ is the average number of fission neutrons released in a fission reaction iduced by a neutron in group $g'$.

Hence we now have a set of $G$ coupled diffusion equations for the $G$ unknown group fluxes $\phi_g(r,t)$. It shouldn't take much imagination to see that many of the same techniques that we used for the one-speed (or in our present terminology, *one-group*) model will also hold for the $G$-group system. In fact, we will see later in this chapter that the specific structure of the multigroup equations makes their solution extremely simple in most cases—provided one can handle the diffusion equation characterizing each individual group.

The more serious problem concerns just how one determines the *group constants* that appear in these equations:

$$v_g, D_g, \Sigma_{ag}, \Sigma_{sg}, \Sigma_{sg'g}, \chi_g, \Sigma_{fg}, \nu_g. \tag{7-15}$$

We have only given a very vague definition of these constants in our heuristic derivation of the multigroup equations. Hence before we can concern ourselves with just how these equations are to be solved, we must go back and give a more careful derivation of these equations in an effort to obtain a more explicit and useful definition of the group constants.

## II. DERIVATION OF THE MULTIGROUP EQUATIONS FROM ENERGY-DEPENDENT DIFFUSION THEORY

Perhaps the most satisfying manner in which to derive the multigroup diffusion equations characterizing the average behavior of neutrons in each energy group is to integrate (i.e., average) the equation for the energy-dependent neutron flux, $\phi(r, E, t)$, over a given group, $E_g < E < E_{g-1}$. We will assume that this flux can be adequately described by the energy-dependent diffusion equation:

$$\frac{1}{v} \frac{\partial \phi}{\partial t} - \nabla \cdot D \nabla \phi + \Sigma_t \phi(r, E, t) = \int_0^\infty dE' \Sigma_s(E' \to E) \phi(r, E', t)$$

$$+ \chi(E) \int_0^\infty dE' \nu(E') \Sigma_f(E') \phi(r, E', t)$$

$$+ S_{ext}(r, E, t). \tag{7-6}$$

Notice that we have inserted the explicit form for the fission source developed earlier in Eq. (4-50).

We might mention that other energy-dependent equations could be used as a starting point for the development of the multigroup diffusion equations.[1,2] For example, we could have first developed the multigroup form of the transport equation and then introduced the diffusion approximation for each group. We will consider an alternative approach based upon the $P_1$ equations in Chapter 8. However all of these approaches yield very similar forms for the multigroup diffusion equations, with only some minor variations in the expressions for the group-averaged cross sections.

We will begin by eliminating the energy variable in the energy-dependent diffusion equation by integrating Eq. (7-6) over the $g$th energy group characterized

by energies $E_g < E < E_{g-1}$:

$$\frac{\partial}{\partial t} \int_{E_g}^{E_{g-1}} dE \frac{1}{v}\phi - \nabla \cdot \int_{E_g}^{E_{g-1}} dE \, D\nabla\phi + \int_{E_g}^{E_{g-1}} dE \, \Sigma_t\phi$$

$$= \int_{E_g}^{E_{g-1}} dE \int_0^\infty dE' \, \Sigma_s(E' \to E)\phi(\mathbf{r}, E', t) + \int_{E_g}^{E_{g-1}} dE \, S. \qquad (7\text{-}7)$$

We will proceed further by making some formal definitions. First define the neutron flux in group $g$ as

$$\phi_g(\mathbf{r}, t) \equiv \int_{E_g}^{E_{g-1}} dE \, \phi(\mathbf{r}, E, t). \qquad (7\text{-}8)$$

Next define the total cross section for group $g$ as

$$\Sigma_{tg} \equiv \frac{1}{\phi_g} \int_{E_g}^{E_{g-1}} dE \, \Sigma_t(E)\phi(\mathbf{r}, E, t), \qquad (7\text{-}9)$$

the diffusion coefficient for group $g$ as

$$D_g \equiv \frac{\int_{E_g}^{E_{g-1}} dE \, D(E)\nabla_j\phi(\mathbf{r}, E, t)}{\int_{E_g}^{E_{g-1}} dE \, \nabla_j\phi(\mathbf{r}, E, t)}, \qquad (7\text{-}10)$$

and the neutron speed characterizing group $g$ as

$$\frac{1}{v_g} \equiv \frac{1}{\phi_g} \int_{E_g}^{E_{g-1}} dE \frac{1}{v}\phi(\mathbf{r}, E, t). \qquad (7\text{-}11)$$

The scattering term requires a bit more work. If we break up the integral over $E'$ to write

$$\int_{E_g}^{E_{g-1}} dE \int_0^\infty dE' \, \Sigma_s(E' \to E)\phi(\mathbf{r}, E', t)$$

$$= \sum_{g'=1}^{G} \int_{E_g}^{E_{g-1}} dE \int_{E_{g'}}^{E_{g'-1}} dE' \, \Sigma_s(E' \to E)\phi(\mathbf{r}, E', t), \qquad (7\text{-}12)$$

then it becomes evident that we want to define the group-transfer cross section as

$$\Sigma_{sg'g} \equiv \frac{1}{\phi_{g'}} \int_{E_g}^{E_{g-1}} dE \int_{E_{g'}}^{E_{g'-1}} dE' \, \Sigma_s(E' \to E)\phi(\mathbf{r}, E', t). \qquad (7\text{-}13)$$

A very similar procedure is followed for the fission term by writing

$$\int_{E_g}^{E_{g-1}} dE \, S_f(\mathbf{r}, E, t) = \int_{E_g}^{E_{g-1}} dE \, \chi(E) \left[ \sum_{g'=1}^{G} \int_{E_{g'}}^{E_{g'-1}} dE' \, \nu(E')\Sigma_f(E')\phi(\mathbf{r}, E', t) \right], \qquad (7\text{-}14)$$

and then defining the fission cross section for group $g'$ as

$$\nu_{g'}\Sigma_{fg'} \equiv \frac{1}{\phi_{g'}} \int_{E_{g'}}^{E_{g'-1}} dE' \, \nu(E')\Sigma_f(E')\phi(\mathbf{r},E',t), \tag{7-15}$$

while defining

$$\chi_g \equiv \int_{E_g}^{E_{g-1}} dE \, \chi(E). \tag{7-16}$$

If we now use these purely formal definitions to rewrite Eq. (7-7), we arrive directly at the *multigroup diffusion equations*:

$$\frac{1}{v_g}\frac{\partial \phi_g}{\partial t} - \nabla \cdot D_g \nabla \phi + \Sigma_{tg}\phi_g(\mathbf{r},t) = \sum_{g'=1}^{G} \Sigma_{sg'g}\phi_{g'} + \chi_g \sum_{g'=1}^{G} \nu_{g'}\Sigma_{fg'}\phi_{g'} + S_g,$$

$$g = 1,2,\dots,G. \tag{7-17}$$

Several comments concerning these equations are necessary. The multigroup diffusion equations (7-17) are still quite exact (within the diffusion approximation, that is), but they are also quite formal in the sense that the group constants are as yet undetermined. While it is true that our derivation has yielded explicit expressions for these group constants, it is apparent that in order to calculate them we would need to know the flux $\phi(\mathbf{r},E,t)$, and this is just the function we were trying to calculate in the first place by discretizing the energy-dependent diffusion equation (7-6). Hence it seems as if our development has been a bit circular.

In fact the multigroup "constants" as we have defined them still depend on space and time. They will be rigorously constant only in the case in which the neutron flux is of the separable form

$$\phi(\mathbf{r},E,t) = \psi(\mathbf{r},t)\varphi(E), \tag{7-18}$$

in which case they reduce to group averages over the neutron flux *energy spectrum* $\varphi(E)$. Unfortunately the flux in a nuclear reactor is usually *not* separable in energy, and in general we will find that the group constants do indeed depend on space and time (although in a manner somewhat more subtle than the above discussion might indicate).

However perhaps you have already guessed the game we will play now, for we will, in fact, attempt to guess or approximate the *intragroup fluxes*,

$$\phi(\mathbf{r},E,t) \cong \phi_{approx}(\mathbf{r},E,t), \tag{7-19}$$

in our calculation of the group constants, e.g.,

$$\Sigma_{tg} \cong \frac{\int_{E_g}^{E_{g-1}} dE \, \Sigma_t(E)\phi_{approx}(\mathbf{r},E,t)}{\int_{E_g}^{E_{g-1}} dE \, \phi_{approx}(\mathbf{r},E,t)} \tag{7-20}$$
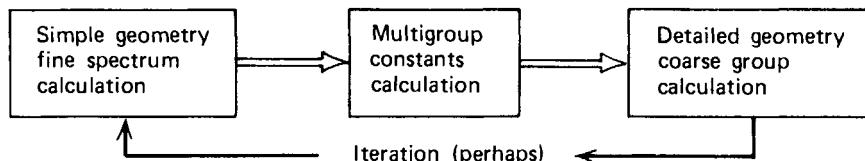
as averages over these approximate intragroup fluxes.

In the next two chapters we will develop a number of schemes for approximating

the flux $\phi(\mathbf{r},E,t)$ within a group—usually by first neglecting its spatial and time dependence. The accuracy required of this flux estimate is primarily dictated by the group structure itself. Of course for an extremely fine group structure, the cross sections and hence the flux would tend to be smoothly varying over a given group, and hence even a very crude approximation to the flux would be sufficient. For example, in Chapter 8 we will demonstrate that in a thermal reactor the flux behaves very roughly as $\phi(E) \sim 1/E$ for energies between 1 eV and $10^5$ eV. Hence this functional form could be inserted into our definitions to calculate the group constants characterizing groups in this energy range. However when we remember the very complicated dependence of the cross sections on energy (in particular, their resonance structure), it becomes apparent that the groups would have to be very finely divided indeed for such a crude approximation to the intragroup fluxes to yield meaningful results.

In actual practice, one usually works with from two to 20 groups in reactor calculations. Such few group calculations can only be effective with reasonably accurate estimates of the group constants (and hence the intragroup fluxes). The most common approach is to actually perform two multigroup calculations. In the first of these calculations, the spatial and time dependence is ignored (or very crudely approximated), and a very finely structured multigroup calculation is performed to calculate the intragroup fluxes (usually relying on various models of neutron slowing down and thermalization). The group constants for this *fine spectrum calculation* are frequently taken to be just the tabulated cross section data averaged (with, for example, a $1/E$ weighting) over each of the fine groups.

These intragroup fluxes are then used to calculate the group constants for a *coarse group calculation* (including spatial dependence):



This scheme of first calculating a neutron flux spectrum and then *collapsing* the cross section data over this spectrum to generate few group constants is the most common method in use today. It should be noted that in a calculation of this type, the spectrum calculation (and hence the few-group constants) will depend sensitively on the particular reactor being analyzed and its operating conditions (e.g., fuel loading, isotopic composition, temperature, and coolant conditions). In fact such group constants will have to be calculated in each region of the reactor in which the core composition varies appreciably, for example, because of variations in fuel enrichment or moderator density. Furthermore these group constants will have to be recalculated whenever these regionwise core properties change, such as during fuel burnup or reactivity adjustment via the movement of control rods. Hence spectrum calculations and the generation of few-group constants must be performed repeatedly in reactor design.

It is usually necessary to take some account of the spatial dependence of the flux in the generation of group constants. This is frequently done by performing the calculation of the neutron spectrum for a typical cell of the reactor core lattice, using a variety of approximate techniques to account for flux variation throughout

the cell. The flux spectrum $\varphi(E)$ that one then uses to generate group constants will be a *spatial average* of the true flux $\phi(\mathbf{r}, E)$ over the cell. Such cell calculations are essential for an adequate description of thermal reactors in which the neutron mfp is relatively short, and we will devote considerable attention to them in Chapter 10.

The above discussion illustrates a very important feature of nuclear reactor analysis: the separation of the treatment of energy- and space-dependence in multigroup diffusion theory. That is, one first utilizes a rather crude description of the flux spatial dependence (say, for only a given cell of the reactor lattice) to generate a detailed representation of the energy spectrum $\varphi(E)$ suitable for the generation of accurate multigroup constants. One then uses these group constants in a few-group diffusion equation analysis of the reactor. In this latter calculation, the energy dependence of the flux is treated rather coarsely (only a few energy groups), while more emphasis is directed toward adequately describing the spatial variation via the diffusion equation. We will find that this procedure of separating the treatment of the various independent variables $\mathbf{r}$, $E$, and $t$ arises very frequently in nuclear reactor analysis. If performed properly, it will allow a rather detailed study of the reactor for only a modest amount of computational effort.

How many groups are necessary for a reactor calculation? This will depend on the problem one is considering. For example, in very crude survey calculations of thermal reactors, two groups (one to characterize fast neutrons and the other to characterize thermal neutrons) may be sufficient. Most LWR calculations are performed using a four-group diffusion model[3] (three fast groups, one thermal group) while gas-cooled reactor analysis typically uses seven to nine groups.[4] For fine detail, one may have to go as high as 20 groups (this is particularly true in fast-reactor calculations)[5], and in spectrum calculations, the number of groups can range as high as 1000 (so-called microgroup structure), which is almost as detailed as the tabulated cross section data itself.[6]

Let us look now in a bit more detail at the structure of the multigroup diffusion equation. In particular, consider the scattering term in the equation. Recall that in our study of the kinematics of neutron scattering collisions in Chapter 2, we noted that if the incident neutron energy $E$ was substantially greater than the thermal energy of the target nuclei (typically less than 0.1 eV), the neutron could never *gain* energy in a scattering collision. Such "fast" neutrons will only slow down in a scattering collision. Hence in these fast groups, we can set

$$\Sigma_{sg'g} = 0, \quad \text{for } g' > g. \tag{7-21}$$

Since most few-group diffusion calculations utilize only one thermal group to describe the neutrons with $E < 1$ eV (assuming that neutrons cannot scatter up out of the thermal group), we can generally simplify the scattering term to write

$$\sum_{g'=1}^{G} \Sigma_{sg'g}\phi_{g'} = \sum_{g'=1}^{g-1} \Sigma_{sg'g}\phi_{g'} + \Sigma_{sgg}\phi_g. \tag{7-22}$$

Here we have taken care to separate out the *in-group scattering* term $\Sigma_{sgg}$ which characterizes the probability that a neutron can suffer a scattering collision and lose sufficiently little energy that it will still remain within the group. It is customary to transfer this term to the left-hand side of the multigroup equation (7-17) and to define a *removal cross section*,

$$\Sigma_{Rg} \equiv \Sigma_{tg} - \Sigma_{sgg}, \tag{7-23}$$

which characterizes the probability that a neutron will be removed from the group $g$ by a collision. Note that the removal cross section is sometimes defined such that it does not contain absorption $\Sigma_{ag}$. We will use the above definition in our development, however. We will see later that the neglect of upscattering (that is, the assumption that the neutron can never gain or scatter up in energy in a collision) greatly simplifies the solution of the multigroup diffusion equations.

One frequently achieves an additional simplification of the multigroup equations by choosing the group spacing such that neutrons will only scatter to the next lowest group—that is, such that

$$\sum_{g'=1}^{G} \Sigma_{sg'g}\phi_{g'} = \Sigma_{sg-1,g}\phi_{g-1} + \Sigma_{sgg}\phi_{g}. \tag{7-24}$$

In this case, one refers to the multigroup equations as being *directly coupled*. If we recall from Section 2-II-D that a neutron of energy $E$ cannot scatter to an energy below $\alpha E$ in a single elastic scattering collision, then it is apparent that to achieve direct coupling we should choose our group spacing such that $E_{g-1}/E_g > 1/\alpha$. For heavier moderators (e.g., $^{12}C$), this is easy to do. Unfortunately in hydrogeneous moderators $\alpha_H = 0$, and hence direct coupling cannot be strictly achieved. However, if one chooses $E_{g-1}/E_g > 150$, then the probability of the neutron "skipping" the next lowest group in a scattering collision with hydrogen is less than 1%, and hence direct coupling is effectively achieved. We might mention as well that one typically chooses a group structure such that the ratio, $E_{g-1}/E_g$, is kept constant from group to group. The motivation for this choice will become apparent in Chapter 8.

We will most frequently be concerned with situations in which both the time-dependence and the presence of an external source can be ignored (e.g., criticality



No upscattering       Directly coupled       Nondirectly coupled
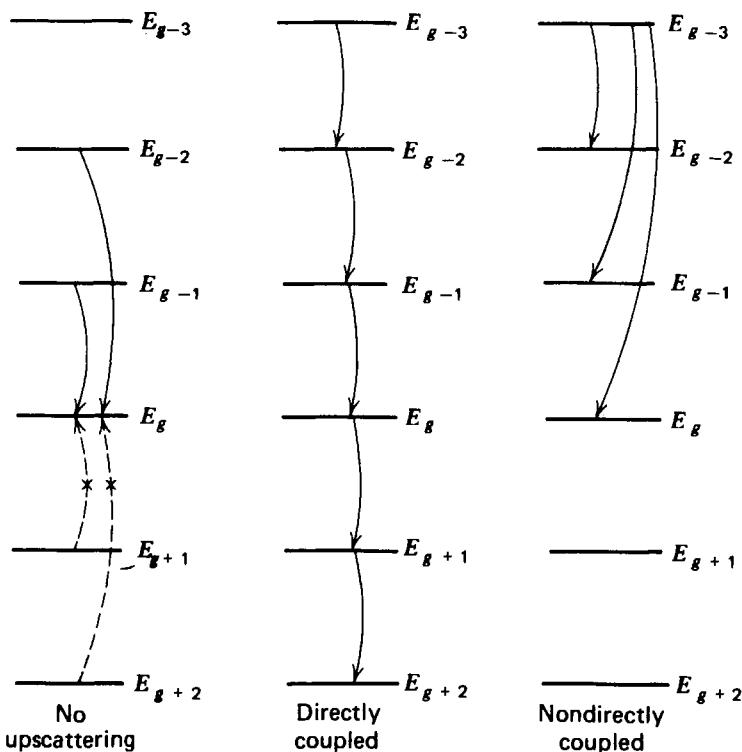
FIGURE 7-1.    Alternative types of multigroup coupling

calculations). In this case the multigroup equations can be written as

$$-\nabla \cdot D_g \nabla \phi_g + \Sigma_{R_g} \phi_g = \sum_{g'=1}^{g-1} \Sigma_{sg'g} \phi_{g'} + \frac{1}{k} \chi_g \sum_{g'=1}^{G} \nu_{g'} \Sigma_{fg'} \phi_{g'}. \qquad (7\text{-}25)$$

The structure of these equations can be seen more clearly in matrix form

$$\underbrace{\begin{pmatrix} -\nabla \cdot D_1 \nabla + \Sigma_{R_1} & 0 & 0 & \cdots \\ -\Sigma_{s_{12}} & -\nabla \cdot D_2 \nabla + \Sigma_{R_2} & 0 & \cdots \\ -\Sigma_{s_{13}} & -\Sigma_{s_{23}} & -\nabla \cdot D_3 \nabla + \Sigma_{R_3} & \cdots \\ \vdots & \vdots & \vdots & \end{pmatrix}}_{\underline{\underline{M}}} \underbrace{\begin{pmatrix} \phi_1 \\ \phi_2 \\ \phi_3 \\ \vdots \end{pmatrix}}_{\underline{\phi}}$$

$$= \frac{1}{k} \underbrace{\begin{pmatrix} \nu_1 \chi_1 \Sigma_{f_1} & \nu_2 \chi_1 \Sigma_{f_2} & \cdots \\ \nu_1 \chi_2 \Sigma_{f_1} & \nu_2 \chi_2 \Sigma_{f_2} & \cdots \\ \nu_1 \chi_3 \Sigma_{f_1} & \nu_2 \chi_3 \Sigma_{f_2} & \cdots \\ \vdots & \vdots & \end{pmatrix}}_{\underline{\underline{F}}} \underbrace{\begin{pmatrix} \phi_1 \\ \phi_2 \\ \phi_3 \\ \vdots \end{pmatrix}}_{\underline{\phi}}, \qquad (7\text{-}26)$$

where we have inserted the usual criticality eigenvalue $k$. Notice in particular that the neglect of upscattering has led to a lower triangular form for the "diffusion" matrix $\underline{\underline{M}}$. The fission matrix $\underline{\underline{F}}$ is full, however, since fission neutrons induced by a neutron absorption in a lower group will appear distributed among the higher energy groups.

In the case of directly coupled groups, $\underline{\underline{M}}$ becomes a simple bidiagonal matrix of the form

$$\underline{\underline{M}} = \begin{pmatrix} \blacktriangle \end{pmatrix} \longrightarrow \begin{pmatrix} \diagdown \end{pmatrix} \qquad (7\text{-}27)$$

By way of contrast, if one chooses to assign several groups to the thermal energy range in which appreciable upscattering occurs, there will be a full submatrix within $\underline{\underline{M}}$ corresponding to $\Sigma_{sg'g}$ for $g'$ or $g$ in the thermal range:

$$\underline{\underline{M}} = \begin{pmatrix} \blacktriangle \boxtimes \end{pmatrix} \qquad (7\text{-}28)$$

Thermal groups

We will return in a later section to discuss a general strategy for solving such systems of diffusion equations. Before doing so, however, it is useful to consider several simple applications of the multigroup diffusion equations.

## III. SIMPLE APPLICATIONS OF THE MULTIGROUP DIFFUSION MODEL

### A. One-Group Diffusion Theory

First suppose we set up the "one-group" diffusion equation by defining $E_0 = \infty$ and $E_1 = 0$. Then if we note that

$$\int_0^\infty dE \, \chi(E) = 1, \tag{7-29}$$

and

$$1 \text{ group} \begin{cases} \text{---------} E_0 = \infty \\ \text{---------} E_1 = 0 \end{cases}$$

$$\int_0^\infty dE' \, \Sigma_s(E \to E') = \Sigma_s(E), \tag{7-30}$$
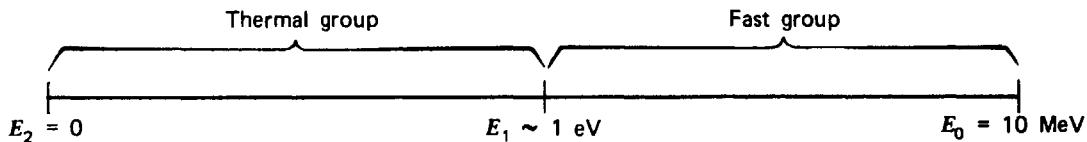
we find that the multigroup equations yield an old friend, the one-speed diffusion equation

$$\frac{1}{v} \frac{\partial \phi}{\partial t} - \nabla \cdot D \nabla \phi + \Sigma_a \phi(\mathbf{r}, t) = \nu \Sigma_f \phi. \tag{7-31}$$

Of course it should be stressed that this equation is still of only formal significance until we provide some prescription for calculating the group constants [that is, the intragroup flux—which, in this case, is $\phi(\mathbf{r}, E, t)$]. Nevertheless it is comforting to know that if we chose the group constants properly, even one-speed diffusion theory could give an accurate description of nuclear reactor behavior.

### B. Two-Group Diffusion Theory

A more enlightening application involves the case of two energy groups, one chosen to characterize fast neutrons and a second for thermal neutrons. The cutoff energy for the thermal group is chosen sufficiently high such that upscattering out of the thermal group can be ignored. This corresponds to an energy of 0.5–1.0eV in water moderated reactors, but may range as high as 3 eV in high-temperature gas-cooled reactors. If we choose the group structure as shown below:

Thermal group                        Fast group

$E_2 = 0$                               $E_1 \sim 1 \text{ eV}$                       $E_0 = 10 \text{ MeV}$

then we can identify:

$$\phi_1(\mathbf{r},t) = \int_{E_1}^{E_0} dE\, \phi(\mathbf{r},E,t) \equiv \text{fast flux},$$ (7-32)

$$\phi_2(\mathbf{r},t) = \int_{E_2}^{E_1} dE\, \phi(\mathbf{r},E,t) \equiv \text{thermal flux}.$$ (7-33)

We can simplify the group constants for this model somewhat. Consider first the fission spectrum. Since essentially all fission neutrons are born in the fast group (recall the fission spectrum $\chi(E)$ illustrated in Figure 2-21), we can write

$$\chi_1 = \int_{E_1}^{E_0} dE\, \chi(E) = 1, \qquad \chi_2 = \int_{E_2}^{E_1} dE\, \chi(E) = 0.$$ (7-34)

Hence the fission source will only appear in the fast group equation:

$$S_{f_1} = \nu_1 \Sigma_{f_1}\phi_1 + \nu_2 \Sigma_{f_2}\phi_2 \qquad \text{(fast)},$$ (7-35)

$$S_{f_2} = 0 \qquad \text{(thermal)}.$$ (7-36)

We can proceed to calculate the scattering and removal cross section. First since there is no upscattering out of the thermal group,

$$\int_{E_2=0}^{E_1 \sim 1\,\mathrm{eV}} dE\, \Sigma_s(E' \rightarrow E) = \Sigma_s(E'), \qquad E_2 \leqslant E' \leqslant E_1.$$ (7-37)

Hence we find

$$\Sigma_{s_{22}} = \frac{1}{\phi_2} \int_{E_2}^{E_1} dE \int_{E_2}^{E_1} dE'\, \Sigma_s(E' \rightarrow E)\phi(\mathbf{r},E') = \frac{1}{\phi_2} \int_{E_2}^{E_1} dE'\, \Sigma_s(E')\phi(\mathbf{r},E') = \Sigma_{s_2}.$$

(7-38)

Thus the removal cross section for the thermal group is just

$$\Sigma_{R_2} = \Sigma_{t_2} - \Sigma_{s_{22}} = \Sigma_{t_2} - \Sigma_{s_2} = \Sigma_{a_2},$$ (7-39)

as we might have expected. The remainder of the group constants are defined as before in the previous section. In practice they would be calculated by first performing a fine spectrum calculation for the group of interest, and then averaging the appropriate cross section data over this spectrum to obtain the group constants. For example, a *fast spectrum calculation* would be performed to calculate the *fast group constants* $\nu_1$, $\Sigma_{f_1}$, $\Sigma_{R_1}$, $\Sigma_{s_{12}}$, and $D_1$ (as described in Chapter 8) while a *thermal spectrum calculation* would be performed to calculate the *thermal group constants* $\nu_2$, $\Sigma_{f_2}$, $D_2$, and $\Sigma_{a_2}$ (as described in Chapter 9).

We will consider the application of two-group diffusion theory to a reactor criticality calculation.[7] Then we can set both the time derivatives and the external

source terms equal to zero to write the two-group diffusion equation as

$$-\nabla \cdot D_1 \nabla \phi_1 + \Sigma_{R_1} \phi_1 = \frac{1}{k} [\nu_1 \Sigma_{f_1} \phi_1 + \nu_2 \Sigma_{f_2} \phi_2],$$

$$-\nabla \cdot D_2 \nabla \phi_2 + \Sigma_{a_2} \phi_2 = \Sigma_{s_{12}} \phi_1. \tag{7-40}$$

Notice that we have inserted a multiplication factor $(1/k)$ in front of the fission source term since we are eventually going to be performing a criticality search. Also notice that while the source terms in the fast group correspond to fission neutrons, the source term in the thermal group is due only to slowing down from the fast group.

As a specific illustration, we will apply the two-group diffusion equations, Eq. (7-40), to analyze the criticality of a bare, uniform reactor assuming that both fast and thermal fluxes can be characterized by the same spatial shape $\psi(\mathbf{r})$:

$$\nabla^2 \psi + B^2 \psi(\mathbf{r}) = 0, \quad \psi(\tilde{\mathbf{r}}_s) = 0. \tag{7-41}$$

We have omitted the subscript $g$ from the geometric buckling $B_g^2 = B^2$ so as not to confuse it with the group index $g$. Then if we substitute

$$\phi_1(\mathbf{r}) = \phi_1 \psi(\mathbf{r}), \qquad \phi_2(\mathbf{r}) = \phi_2 \psi(\mathbf{r}) \tag{7-42}$$

into Eq. (7-40), we find the algebraic equations

$$\left(D_1 B^2 + \Sigma_{R_1} - k^{-1} \nu_1 \Sigma_{f_1}\right) \phi_1 - k^{-1} \nu_2 \Sigma_{f_2} \phi_2 = 0,$$

$$-\Sigma_{s_{12}} \phi_1 + \left(D_2 B^2 + \Sigma_{a_2}\right) \phi_2 = 0. \tag{7-43}$$

However this algebraic system has a solution if and only if

$$\left(D_1 B^2 + \Sigma_{R_1} - \frac{\nu_1 \Sigma_{f_1}}{k}\right)\left(D_2 B^2 + \Sigma_{a_2}\right) - \frac{\nu_2 \Sigma_{f_2} \Sigma_{s_{12}}}{k} = 0. \tag{7-44}$$

We can now solve for the value of the multiplication factor $k$, which will yield a nontrivial solution of the two-group equations:

$$k = \frac{\nu_1 \Sigma_{f_1}}{\Sigma_{R_1} + D_1 B^2} + \frac{\Sigma_{s_{12}}}{\left(\Sigma_{R_1} + D_1 B^2\right)} \frac{\nu_2 \Sigma_{f_2}}{\left(\Sigma_{a_2} + D_2 B^2\right)}. \tag{7-45}$$

It is of interest for us to see if we can relate this expression to our earlier expressions for $k$—notably the six-factor formula. First notice that the first term in Eq. (7-45) represents neutron multiplication due to fissions occurring in the fast group, whereas the second term represents multiplication due to thermal fission. Since we expect the thermal fission contribution to be dominant in those situations

in which such a two-group analysis makes sense, let us first examine

$$k_2 = \frac{\Sigma_{s_{12}}}{\left(\Sigma_{R_1} + D_1 B^2\right)} \frac{\nu_2 \Sigma_{f_2}}{\left(\Sigma_{a_2} + D_2 B^2\right)}$$

$$= \frac{\Sigma_{s_{12}}/\Sigma_{R_1}}{\left(1 + L_1^2 B^2\right)} \frac{\nu_2 \left(\Sigma_{f_2}/\Sigma_{a_2}\right)}{\left(1 + L_2^2 B^2\right)} \, . \tag{7-46}$$

From our earlier discussion in Section 5-III-D, it is evident that

$$P_{NL_1} = \left(1 + L_1^2 B^2\right)^{-1}, \quad P_{NL_2} = \left(1 + L_2^2 B^2\right)^{-1} \tag{7-47}$$

are just the fast and thermal nonleakage probabilities. Notice that the diffusion length $L_1$ characterizing the fast group is defined somewhat differently as

$$L_1^2 \equiv \frac{D_1}{\Sigma_{R_1}} = \frac{D_1}{\Sigma_{a_1} + \Sigma_{s_{12}}} \, , \tag{7-48}$$

but this is consistent with our earlier definition of the diffusion length, since both $\Sigma_a$ and $\Sigma_{s_{12}}$ act to remove neutrons from the fast group. The only unidentified term is the ratio $\Sigma_{s_{12}}/\Sigma_{R_1}$. However for a homogeneous reactor we know that this ratio is just:

$$\frac{\text{Rate at which neutrons slow down to thermal group}}{\text{Rate at which neutrons are removed from fast group}} = \frac{\int d^3 r \, \Sigma_{s_{12}} \phi_1(\mathbf{r})}{\int d^3 r \, \Sigma_{R_1} \phi_1(\mathbf{r})} = \frac{\Sigma_{s_{12}}}{\Sigma_{R_1}} = p, \tag{7-49}$$

which we can identify as the resonance escape probability $p$ characterizing slowing down from group 1 to group 2. Hence

$$k_2 = \eta_2 f_2 p P_{NL_1} P_{NL_2}. \tag{7-50}$$

In a very similar manner we can identify the fast multiplication factor as

$$k_1 = \frac{\nu_1 \Sigma_{f_1}/\Sigma_{R_1}}{\left(1 + L_1^2 B^2\right)} = \eta_1 f_1 P_{NL_1}, \tag{7-51}$$

where $\eta_1 = \nu_1 \Sigma_{f_1}^F/\Sigma_{a_1}^F$ and we have defined a "fast utilization factor" $f_1 = \Sigma_{a_1}^F/\Sigma_{R_1}$ in analogy to the thermal utilization factor $f_2$.

To complete our identification with the usual six-factor formula, we evidently must identify the fast fission factor $\epsilon$ as just

$$\epsilon = \left(1 + \frac{k_1}{k_2}\right) = \left[1 + \left(\frac{\nu_1 \Sigma_{f_1}}{\nu_2 \Sigma_{f_2}}\right)\left(\frac{\Sigma_{a_2} + D_2 B^2}{\Sigma_{s_{12}}}\right)\right]. \tag{7-52}$$

Then we find

$$k = k_1 + k_2 = \epsilon k_2 = \eta_2 f_2 p \epsilon P_{NL_1} P_{NL_2} = \eta_{th} f_{th} p \epsilon P_{FNL} P_{TNL}, \tag{7-53}$$

which is the usual six-factor formula. Of course, this definition of $\epsilon$ is somewhat awkward, since it depends upon quantities such as the thermal utilization, the thermal nonleakage probability, and the resonance escape probability.

The identification of the various components of the six-factor formula in terms of two group-constants is not unique, and alternative schemes can be found in the literature.[1,7] Such arbitrariness is indicative of the limited usefulness of the six-factor formula for more realistic reactor analysis. In fact the two-group expression for $k$ [Eq. (7-45)] is far more appropriate for the description of most thermal power reactor types which are characterized by a somewhat harder neutron energy spectrum than the natural uranium, graphite-moderated reactors which motivated the development of the six-factor formula.

The two-group diffusion model can be used to demonstrate a number of the various applications of the multigroup formalism. For example, one frequently wishes to generate the group constants for a few-group calculation using the neutron spectrum generated by a many-group calculation. Such a procedure is known as *group collapsing*, since it expresses few-group constants in terms of many-group constants.

To illustrate this, we can derive expressions for the one-group constants in terms of two-group constants. For example,

$$\Sigma_a = \frac{\int_{E_2}^{E_0} dE \, \Sigma_a(E) \phi(E)}{\int_{E_2}^{E_0} dE \, \phi(E)} = \frac{\int_{E_1}^{E_0} dE \, \Sigma_a(E) \phi(E) + \int_{E_2}^{E_1} dE \, \Sigma_a(E) \phi(E)}{\int_{E_1}^{E_0} dE \, \phi(E) + \int_{E_2}^{E_1} dE \, \phi(E)}$$

$$= \frac{\Sigma_{R_1} \phi_1 + \Sigma_{a_2} \phi_2 - \Sigma_{s_{12}} \phi_1}{\phi_1 + \phi_2}, \tag{7-54}$$

or using Eq. (7-43) to eliminate $\phi_2$ in terms of $\phi_1$:

$$\Sigma_a = \frac{(\Sigma_{R_1} - \Sigma_{s_{12}})(D_2 B^2 + \Sigma_{a_2}) + \Sigma_{a_2} \Sigma_{s_{12}}}{D_2 B^2 + \Sigma_{a_2} + \Sigma_{s_{12}}}. \tag{7-55}$$

The remaining one-group constants can be given as

$$D = \frac{D_1 \phi_1 + D_2 \phi_2}{\phi_1 + \phi_2} = \frac{(D_2 B^2 + \Sigma_{a_2}) D_1 + \Sigma_{s_{12}} D_2}{D_2 B^2 + \Sigma_{a_2} + \Sigma_{s_{12}}}, \tag{7-56}$$

$$\nu \Sigma_f = \frac{\nu_1 \Sigma_{f_1} \phi_1 + \nu_2 \Sigma_{f_2} \phi_2}{\phi_1 + \phi_2} = \frac{(D_2 B^2 + \Sigma_{a_2}) \nu_1 \Sigma_{f_1} + \nu_2 \Sigma_{s_{12}} \Sigma_{f_2}}{D_2 B^2 + \Sigma_{a_2} + \Sigma_{s_{12}}}. \tag{7-57}$$

(These relations can be generalized to the case of collapsing from $G$ groups, but we will leave this development to the problem set at the end of the chapter.)

## C. Modified One-Group Diffusion Theory

In the analysis of large thermal reactors it is sometimes possible to simplify the two-group diffusion equations even further by ignoring thermal leakage. If we note that in a large LWR, $D_2 \sim 0.5$ cm, $B^2 \cong 10^{-4}$ cm$^{-2}$, while $\Sigma_{a_2} \cong 0.1$ cm$^{-1}$, then we find

$$\frac{-D_2 \nabla^2 \phi_2}{\Sigma_{a_2} \phi_2} = \frac{D_2 B^2}{\Sigma_{a_2}} \cong 5 \times 10^{-4} \ll 1. \tag{7-58}$$

Hence the neglect of $-D_2 \nabla^2 \phi_2$ in the second of Eqs. (7-40) may occasionally be valid for the investigation of problems in which thermal neutron diffusion does not have a significant reactivity effect.

If we now solve the simplified equation for the thermal group flux

$$\phi_2(\mathbf{r}) = \frac{\Sigma_{s_{12}}}{\Sigma_{a_2}} \phi_1(\mathbf{r}) \tag{7-59}$$

and substitute this into the fast-group equation, we find the modified one-group diffusion model

$$-\nabla \cdot D_1 \nabla \phi_1 + \Sigma_{R_1} \phi_1 = \nu_1 \Sigma_{f_1} \phi_1 + \nu_2 \Sigma_{f_2} (\Sigma_{s_{12}} / \Sigma_{a_2}) \phi_1, \tag{7-60}$$

or rearranging for the case of a homogeneous reactor

$$\nabla^2 \phi_1 + \left( \frac{k_\infty - 1}{L_1^2} \right) \phi_1(\mathbf{r}) = 0, \tag{7-61}$$

where

$$k_\infty = \frac{\nu_1 \Sigma_{f_1}}{\Sigma_{R_1}} + \frac{\nu_2 \Sigma_{f_2}}{\Sigma_{a_2}} \frac{\Sigma_{s_{12}}}{\Sigma_{R_1}} = k_{\infty_1} + k_{\infty_2} p, \tag{7-62}$$

where we recall $L_1^2 = D_1 / \Sigma_{R_1}$. This model is sometimes referred to as one- and one-half-group diffusion theory, since it is midway between the one- and two-group schemes.

A very useful (and common) modification of this scheme which takes some account of both fast and thermal leakage within a one-group treatment is obtained by replacing $L_1^2$ in Eq. (7-61) by the so-called *migration area* $M^2$ defined as

$$M^2 = L_1^2 + L_2^2 = D_1 / \Sigma_{R_1} + D_2 / \Sigma_{R_2}. \tag{7-63}$$

We will show in Chapter 9 that $M^2$ is essentially just $1/6$ the mean square distance traveled by a neutron from its birth in fission to its eventual demise via thermal absorption.

We have developed these very simple few-group models to demonstrate how

multigroup techniques can be used to evaluate many of the quantities of interest in reactor analysis. (Still further examples are included as exercises at the end of this chapter.) We could continue our discussion by considering more elaborate multigroup diffusion models, such as the four-group model customarily used in LWR analysis, or the ultrafine group structure required in fast reactor studies. However we will defer such topics until we have studied schemes for the generation of multigroup constants.

Thus far our illustrations of multigroup diffusion calculations have been extremely simple. They usually ignored spatial dependence (or at best, assumed only a fundamental mode dependence). In any realistic calculation, one must take into account the inhomogeneous nature of the reactor core by actually solving the multigroup diffusion equations in detail. Hence we now turn our attention to the strategy for solving these more general equations.

## IV. NUMERICAL SOLUTION OF THE MULTIGROUP DIFFUSION EQUATIONS

### A. Successive Solution of the Multigroup Equations

We now consider a strategy for solving the multigroup diffusion equations on digital computers. Suppose we begin by writing these equations (7-26) out in detail as

$$-\nabla \cdot D_1 \nabla \phi_1 + \Sigma_{R_1} \phi_1 = \frac{1}{k} \chi_1 S$$

$$-\nabla \cdot D_2 \nabla \phi_2 + \Sigma_{R_2} \phi_2 = \frac{1}{k} \chi_2 S + \Sigma_{s_{12}} \phi_1$$

$$-\nabla \cdot D_3 \nabla \phi_3 + \Sigma_{R_3} \phi_3 = \frac{1}{k} \chi_3 S + \Sigma_{s_{13}} \phi_1 + \Sigma_{s_{23}} \phi_2 \tag{7-64}$$

$$\vdots \qquad \qquad \vdots$$

$$-\nabla \cdot D_G \nabla \phi_G + \Sigma_{R_G} \phi_G = \frac{1}{k} \chi_G S + \Sigma_{s_{1G}} \phi_1 + \cdots + \Sigma_{s_{G-1,G}} \phi_{G-1}.$$

Notice that here we have assumed that there is no upscattering and also defined the fission source as

$$S(\mathbf{r}) \equiv \sum_{g'=1}^{G} \nu_{g'} \Sigma_{f_{g'}} \phi_{g'}(\mathbf{r}). \tag{7-65}$$

It is very important to note that the *spatial* dependence of the fission source is identical in each group diffusion equation.

Now the essential scheme is just as before. We begin by guessing a fission source, $S(\mathbf{r})$ and a multiplication eigenvalue $k$:

$$S(\mathbf{r}) \sim S^{(0)}(\mathbf{r}), \qquad k \sim k^{(0)}. \tag{7-66}$$

Next, we calculate the flux in the first group:

$$-\nabla \cdot D_1 \nabla \phi_1^{(1)} + \Sigma_{R_1} \phi_1^{(1)} = \frac{1}{k^{(0)}} \chi_1 S^{(0)}(\mathbf{r}).$$

(7-67)

Having obtained this flux, we can then proceed to the diffusion equation characterizing the next lowest energy group

$$-\nabla \cdot D_2 \nabla \phi_2^{(1)} + \Sigma_{R_2} \phi_2^{(1)} = \frac{1}{k^{(0)}} \chi_2 S^{(0)}(\mathbf{r}) + \Sigma_{s_{12}} \phi_1^{(1)},$$

(7-68)

and solve this for $\phi_2^{(1)}(\mathbf{r})$ since the right-hand side is now known. We can continue on in this fashion to determine all of the group fluxes:

$$\phi_1^{(1)}(\mathbf{r}), \quad \phi_2^{(1)}(\mathbf{r}), \quad \phi_3^{(1)}(\mathbf{r}), \quad \phi_4^{(1)}(\mathbf{r}), \ldots, \phi_G^{(1)}(\mathbf{r}).$$

(7-69)

Having done so, we can then calculate a new fission source

$$S^{(1)}(\mathbf{r}) = \sum_{g'=1}^{G} \nu_{g'} \Sigma_{f_{g'}} \phi_{g'}^{(1)}(\mathbf{r}),$$

(7-70)

and a new value of $k$

$$k^{(1)} = \frac{\int d^3 r \, S^{(1)}(\mathbf{r})}{\frac{1}{k^{(0)}} \int d^3 r \, S^{(0)}(\mathbf{r})}.$$

(7-71)

We can then proceed to perform each source iteration by solving down the multigroup equations toward increasingly lower energies. This scheme of solving successively the equations in the direction of lower energies is enabled by the assumption that there is no upscattering. This implies that the flux in the higher energy groups always determines the source term in the lower energy groups. In effect, we are merely inverting a lower triangular matrix (as the matrix formulation in the previous section made apparent).

If one chooses a multigroup structure in which more than one group is assigned to the thermal energy range in which appreciable upscattering can occur, then such a *successive* groupwise solution of the multigroup diffusion equations is no longer possible. One must solve the equations characterizing the thermal group *simultaneously*. If the number of such fully coupled groups in which both upscattering as well as downscattering occurs is small (e.g., in HTGR calculations,[4] it is common to use three to four thermal groups), a direct simultaneous solution (i.e., matrix inversion) can be accomplished. However if the number of thermal groups is large, as it may be in thermal spectrum calculations, then iterative solution schemes will be necessary (similar to the inner iterations used in multidimensional diffusion calculations).

A great deal is known about the mathematical nature of such multigroup diffusion eigenvalue problems.[8,9] Under rather weak restrictions on the group fluxes and their boundary conditions, one can show that there will always exist a

maximum eigenvalue $k_{\text{eff}}$ that is real and positive. The corresponding eigenfunction is unique and nonnegative everywhere within the reactor. These features are reassuring, because we would anticipate that the largest eigenvalue will characterize the multiplication of the system, and the corresponding eigenfunction will describe the flux distribution within the core (which cannot be negative). One can also demonstrate that the above source iteration will converge to this "positive dominant" eigenvalue $k_{\text{eff}}$ and the corresponding eigenfunction.

Such formal considerations are interesting in their own right, as well as being useful in the investigation of algorithms devised for the solution of the multigroup diffusion equations. In actual practice, however, one must also discretize the spatial dependence in order to solve the group-diffusion equations. That is, one chooses a spatial mesh and finite difference scheme, just as we did in Chapter 5, and then discretizes the diffusion equations for each group. We now turn to a brief discussion of several more practical aspects of the solution of such equations.

## B. Strategies for Solving the Finite-Differenced Multigroup Diffusion Equations

If we recall the general discussion of finite difference representations of the neutron diffusion equations given in Section 5-II-B, it is apparent that the general structure of the finite-differenced multigroup diffusion equations takes the form:[11]

$$\left[\Sigma_{R_i}^g + \sum_j^J \frac{D_{ij}^g}{\Delta_{ij}^2}\right]\phi_{ig} - \sum_j^J \frac{D_{ij}^g}{\Delta_{ij}^2}\phi_{jg} - \sum_{g'=1}^{g-1}\Sigma_{s_i}^{g' \to g}\phi_{ig'} = \frac{\chi^g}{k}\sum_{g'=1}^{G}\nu_{g'}\Sigma_{f_i}^{g'}\phi_{ig'}. \quad (7\text{-}72)$$

(Note here that we will occasionally write the group index $g$ as a superscript in order to avoid confusing it with the spatial mesh indices $i$ and $j$.) Notice that in addition to the coupling to different energy group fluxes at a given mesh point due to the fission source and scattering, the finite difference equation is coupled as well to the flux at adjacent spatial mesh points because of the effect of spatial diffusion.

If we denote the number of spatial mesh points by $N$ and the number of groups by $G$, then Eq. (7-72) represents a set of $G \times N$ simultaneous linear algebraic equations. One usually normalizes the flux at one energy group-space mesh point (since the overall normalization of the flux is arbitrary in a criticality calculation). Hence we have $G \times N$ equations available to determine the $G \times N - 1$ fluxes and the multiplication eigenvalue $k_{\text{eff}}$. As before, it is convenient to rewrite this set of equations as a matrix eigenvalue problem

$$\underline{M}\,\underline{\phi} = \frac{1}{k}\,\underline{F}\,\underline{\phi}. \quad (7\text{-}26)$$

EXAMPLE: Consider four energy groups with a five by four two-dimensional spatial mesh. Then each matrix has $(4 \times 5 \times 4)^2 = 6400$ elements and the flux vector $\underline{\phi}$ has 80 elements. One typically allows fission neutrons to appear only in the uppermost energy group, $\chi_1 = 1$, $\chi_g = 0$, $g > 1$. Furthermore, we will assume directly coupled groups such that $\Sigma_{sg'g} = 0$ if $g' \neq g - 1$. We can explicitly exhibit the structure of the matrix eigenvalue problem in this case as shown in Figure (7-2).[11]

$$\left(-\Sigma_{s_i}^{1\to2}\right)\left(-\frac{D_{i,i-5}^2}{(\Delta_{i,i-5})^2}\right)\left(-\frac{D_{i,i-1}^2}{(\Delta_{i,i-1})^2}\right)\left(\Sigma_{R_i}^2 + \frac{D_{i,i-5}^2}{(\Delta_{i,i-5})^2} + \frac{D_{i,i-1}^2}{(\Delta_{i,i-1})^2} + \frac{D_{i,i+1}^2}{(\Delta_{i,i+1})^2} + \frac{D_{i,i+5}^2}{(\Delta_{i,i+5})^2}\right)\left(-\frac{D_{i,i+1}^2}{(\Delta_{i,i+1})^2}\right)\left(-\frac{D_{i,i+5}^2}{(\Delta_{i,i+5})^2}\right)\phi_i^2$$

$$\frac{1}{k} =$$

$$x^1\nu\Sigma_{f_{20}}^2$$
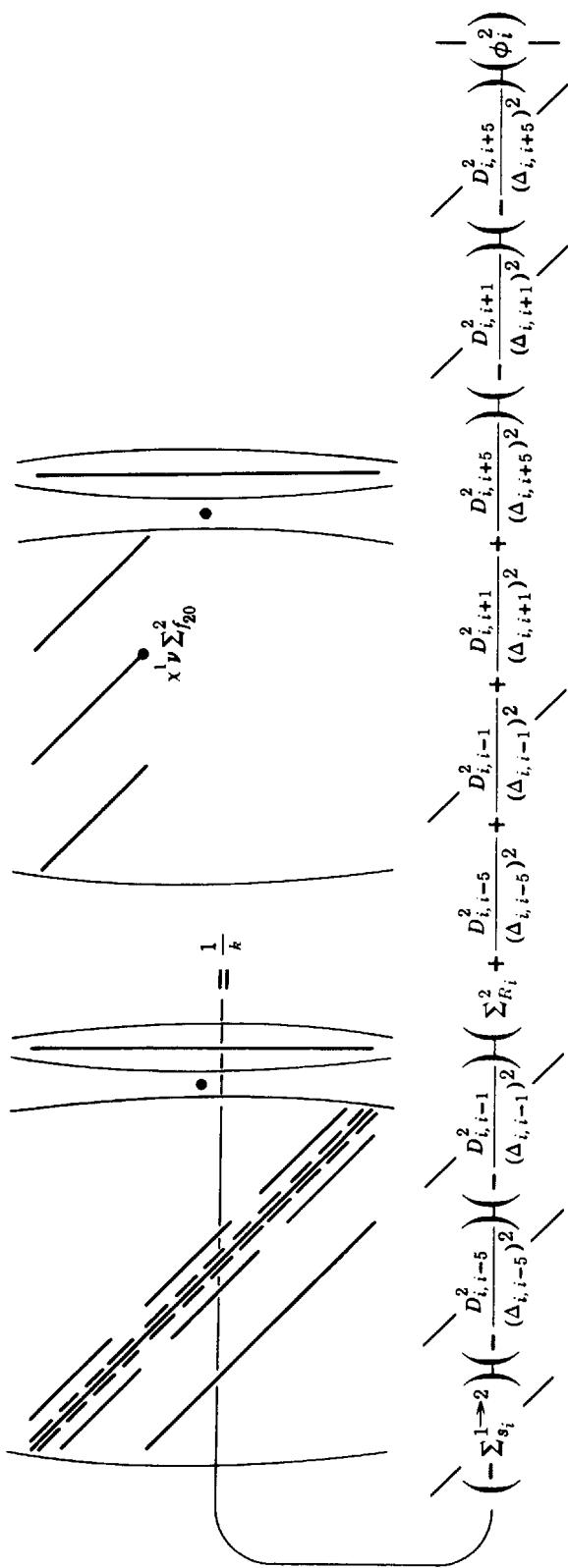
**FIGURE 7-2.** The matrix structure of a four-group, 5×4 spatial mesh point criticality calculation

Let us now review the general iterative strategy for solving this eigenvalue problem.

① One first makes an initial guess of the source vector $\underline{S}^{(0)}$ and the multiplication eigenvalue $k^{(0)}$.

② At this point one proceeds to solve the inhomogeneous matrix equation

$$\underline{\underline{M}}\,\underline{\phi}^{(n+1)} = \frac{1}{k^{(n)}}\,\underline{S}^{(n)} \qquad (7\text{-}73)$$

for the next flux iterate, $\underline{\phi}^{(n+1)}$. This solution involves a number of substeps:

2-1 One solves the inhomogeneous diffusion equation characterizing each of the energy groups $g$

$$\underline{\underline{A}}_g\,\underline{\phi}_g^{(n+1)} = \frac{1}{k^{(n)}}\,\underline{S}_g^{(n)} + \underline{\underline{R}}_{g-1}\,\underline{\phi}_{g-1}^{(n)} \equiv \underline{Q}_g^{(n)} \qquad (7\text{-}74)$$

by solving first for the highest energy group, $g = 1$ (noting $\underline{\underline{R}}_0 \equiv 0$, $\underline{\phi}_0^{(n)} \equiv 0$), and then using $\underline{\phi}_1^{(n+1)}$ to solve for $\underline{\phi}_2^{(n+1)}$, and so on, solving successively down the groups.

EXAMPLE: If we return for a moment to our earlier four-group, five-by-four spatial mesh problem, we find that each matrix in the group inhomogeneous equation [Eq. (7-74)] has $(5 \times 4)^2 = 400$ elements while the flux and source vectors have 20 elements. Note that the fission source $\underline{S}_g^{(n)}$ vanishes for all but the highest energy group since $\chi_g \equiv 0$, $g > 1$. Furthermore the highest energy group obviously has no slowing down source. The matrix form of the group diffusion equation [Eq. (7-74)] is shown in Figure 7-3 for this example.[11]

2-2 Of course, solving even the inhomogeneous diffusion equation [Eq. (7-74)] for a single group is no trivial matter. For multidimensional problems, iterative techniques will be necessary such as those discussed in Chapter 5 (e.g., SOR). Such inner iterations usually take the previous flux estimate $\underline{\phi}_g^{(n-1)}$ as their first guess in solving Eq. (7-74). It should be mentioned that a variety of schemes have been proposed (and utilized) for coupling such inner iterations to the outer (source) iterations to accelerate convergence.

③ Having obtained the flux estimate $\underline{\phi}^{(n+1)}$, one can now determine the next multiplication eigenvalue estimate. A variety of weighting schemes can be used to determine the ratio of fission source estimates. One such scheme can be derived by taking the scalar product of the fission source vector $\underline{\underline{F}}\,\underline{\phi}^{(n+1)}$ with the equation defining the iterative scheme

$$\underline{\underline{M}}\,\underline{\phi}^{(n+1)} = \frac{1}{k^{(n)}}\,\underline{\underline{F}}\,\underline{\phi}^{(n)}, \qquad (7\text{-}75)$$

and then noting that presumably

$$\underline{\underline{M}}\,\underline{\phi}^{(n+1)} \cong \frac{1}{k^{(n+1)}}\,\underline{\underline{F}}\,\underline{\phi}^{(n+1)} \qquad (7\text{-}76)$$

to find

$$k^{(n+1)} = k^{(n)}\,\frac{\left(\underline{\underline{F}}\,\underline{\phi}^{(n+1)},\,\underline{\underline{F}}\,\underline{\phi}^{(n+1)}\right)}{\left(\underline{\underline{F}}\,\underline{\phi}^{(n)},\,\underline{\underline{F}}\,\underline{\phi}^{(n+1)}\right)}. \qquad (7\text{-}77)$$

$$\left(-\frac{D_{7,2}^g}{(\Delta_{7,2})^2}\right)\left(-\frac{D_{7,6}^g}{(\Delta_{7,6})^2}\right)\left(\Sigma_{R_7}^g + \frac{D_{7,2}^g}{(\Delta_{7,2})^2} + \frac{D_{7,6}^g}{(\Delta_{7,6})^2} + \frac{D_{7,8}^g}{(\Delta_{7,8})^2} + \frac{D_{7,12}^g}{(\Delta_{7,12})^2}\right)\left(-\frac{D_{7,8}^g}{(\Delta_{7,8})^2}\right)\left(-\frac{D_{7,12}^g}{(\Delta_{7,12})^2}\right)\left(\phi_7^{g(n)}\right)$$

$$= \left(S_7^{1(n-1)}\right) \begin{pmatrix} 0 \\ 0 \end{pmatrix} \quad \text{if } g=1$$

$$\begin{pmatrix} 0 \\ 0 \end{pmatrix} \left(\Sigma_{s_7}^{g-1\to g}\right) \left(\phi_7^{g(n)}\right) \quad \text{if } g>1$$
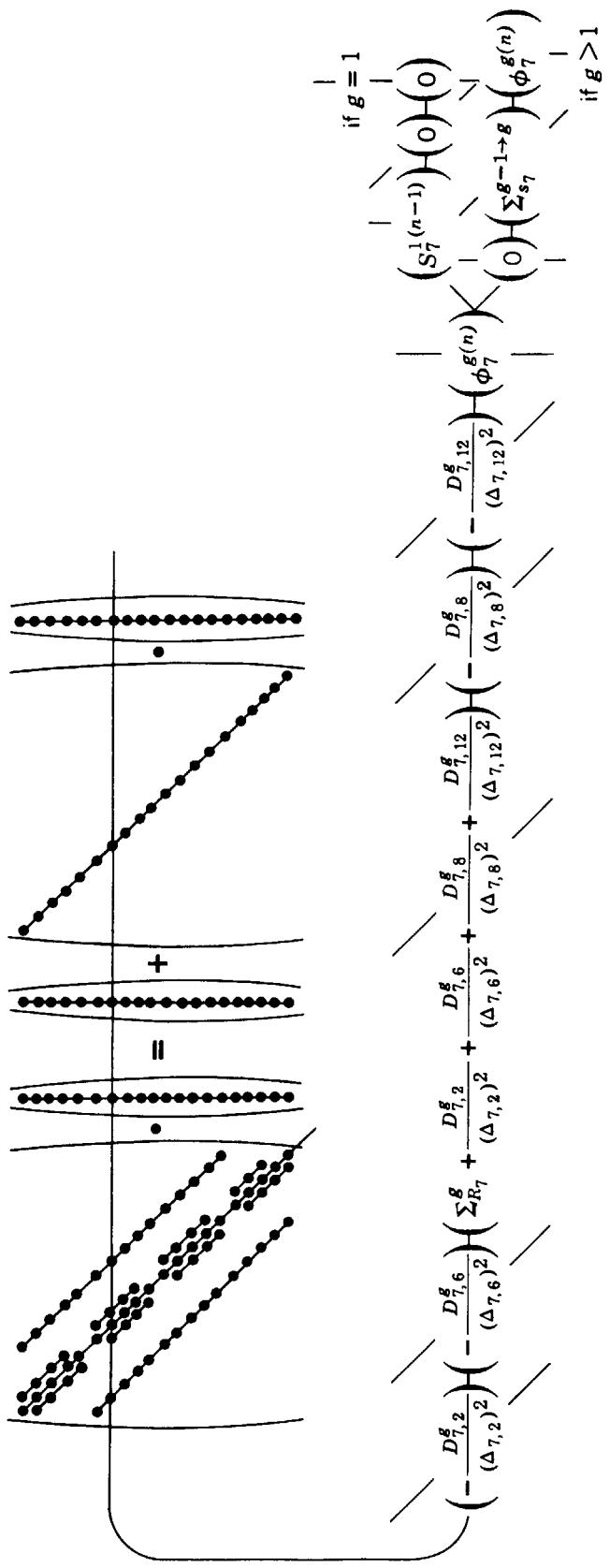
**FIGURE 7-3.** The matrix structure of the group-diffusion calculation

④ At this point one tests the source iteration for convergence, such as by comparing

$$\left| \frac{k^{(n+1)} - k^{(n)}}{k^{(n+1)}} \right| \overset{?}{<} \epsilon_1,$$ (7-78)

or a pointwise criterion

$$\max \left| \frac{S_{g_i}^{(n+1)} - S_{g_i}^{(n)}}{S_{g_i}^{(n+1)}} \right| \overset{?}{<} \epsilon_2$$ (7-79)

(or both). If the changes in $k^{(n)}$ or the elements of $\underline{S}^{(n)}$ or $\phi^{(n)}$ are sufficiently small, one assumes that convergence has been achieved, and the iterative procedure is ended. If not, then a new fission source is calculated and the iteration continues.

⑥ Usually the fission source $\underline{S}^{(n)}$ used in the next iteration is chosen via an extrapolation scheme (cf. Section 5-IV-C) to accelerate convergence of the source iterations, for example,

$$\underline{S}^{(n)} = S^{(n-1)} + \alpha \left[ \frac{1}{k^{(n)}} \underline{F} \underline{\phi}^{(n)} - \underline{S}^{(n-1)} \right].$$ (7-80)

The positive nature of the multigroup diffusion operators implies similar properties for the matrices resulting from finite-differencing these equations. Hence many of the formal conclusions concerning convergence to the positive dominant eigenvalue and eigenfunction can also be shown to hold for the finite-differenced multigroup diffusion equations. The theory of such numerical procedures has been placed on firm ground by Varga[10] and Wachpress,[8] and the interested reader is referred to their treatises for more detail.

Thus far we have only concerned ourselves with the usual criticality calculation for $k_{eff}$. Actually a variety of different types of criticality searches are typically conducted in an effect to achieve a desired core multiplication (which is frequently not equal to 1.0). For example, two such schemes are: (a) core size searches (usually the size of a given core region is varied, say by varying the position of one boundary, until the desired value of $k_{eff}$ is achieved) and (b) composition search (the atomic density of a specific fuel isotope, or several such isotopes, is varied, perhaps only in a given subregion of the core).

The multigroup diffusion equations can also be used for a variety of other applications. For example, one can use these equations to determine the neutron flux maintained in a subcritical assembly by a steady-state source (by retaining the source term in the multigroup diffusion equations). They can also be used to calculate the time eigenvalues $\alpha$ occurring in solutions of the form $e^{\alpha t}$ by inserting an effective absorption term $(\alpha/v_g)\phi_g$ into the equations, and then solving for $\alpha$ as a matrix eigenvalue problem. Such "$\alpha$-searches" are of use in studying reactor kinetic behavior.

## V. MULTIGROUP PERTURBATION THEORY

Before we conclude this general discussion of the multigroup diffusion equations, it is useful to redevelop the procedure of perturbation theory as it applies to the multigroup equations as written in matrix form:

$$\underline{M}\,\underline{\phi} = \frac{1}{k}\,\underline{F}\,\underline{\phi}.\qquad(7\text{-}81)$$

In order to determine the change in reactivity induced in the core by a small perturbation, we must generalize somewhat our concept of inner products and adjointness to account for the matrix nature of the multigroup eigenvalue problem [Eq. (7-81)]. To this end, define the inner product between two $G$-dimensional vectors $\underline{f}(\mathbf{r})$ and $\underline{g}(\mathbf{r})$ as

$$(\underline{f},\underline{g}) \equiv \int_V d^3r\,[f_1^*(\mathbf{r})\,g_1(\mathbf{r}) + f_2^*(\mathbf{r})\,g_2(\mathbf{r}) + \dots].\qquad(7\text{-}82)$$

We can now use this inner product to construct the adjoint of the operators $\underline{M}$ and $\underline{F}$:

$$\left(\underline{M}^\dagger\underline{f},\,\underline{g}\right) = \left(\underline{f},\,\underline{M}\,\underline{g}\right).\qquad(7\text{-}83)$$

Since the adjoint of a matrix is obtained by first taking the transpose of the matrix and then complex-conjugating each of its elements, it is evident that

$$\underline{M}^\dagger = \begin{pmatrix} -\nabla\cdot D_1\nabla + \Sigma_{R_1} & -\Sigma_{s_{12}} & \cdots \\ 0 & -\nabla\cdot D_2\nabla + \Sigma_{R_2} & \cdots \\ \vdots & \vdots & \end{pmatrix},\qquad(7\text{-}84)$$

and similarly

$$\underline{F}^\dagger = \begin{pmatrix} \nu_1\chi_1\Sigma_{f_1} & \nu_1\chi_2\Sigma_{f_1} & \cdots \\ \nu_2\chi_1\Sigma_{f_2} & \nu_2\chi_2\Sigma_{f_2} & \cdots \\ \vdots & \vdots & \end{pmatrix}.\qquad(7\text{-}85)$$

Note in particular that $\underline{M}^\dagger \neq \underline{M}$ and $\underline{F}^\dagger \neq \underline{F}$—that is, the multigroup criticality problem is not self-adjoint. Hence we find $\phi^\dagger \neq \phi$.

We can use our earlier expressions for the reactivity change corresponding to perturbations in the core composition, if we recognize that such perturbations will now have a matrix character—for example,

$$\underline{M}' = \underline{M} + \underline{\delta M},\qquad(7\text{-}86)$$

and

$$\underline{F}' = \underline{F} + \underline{\delta F}.\qquad(7\text{-}87)$$

For example, one could imagine a perturbation in the absorption cross section characterizing the second group as being represented by

$$\underline{\delta M} = \begin{pmatrix} 0 & 0 & 0 & \\ 0 & \delta\Sigma_{a_2} & 0 & \cdots \\ 0 & 0 & 0 & \\ & \vdots & & \end{pmatrix}. \tag{7-88}$$

The corresponding reactivity change is then given by

$$\Delta\rho = \frac{\left(\underline{\phi}^{\dagger}, [\,\underline{\delta F} - \underline{\delta M}\,]\,\underline{\phi}\right)}{\left(\underline{\phi}^{\dagger}, \underline{F}\,\underline{\phi}\right)}. \tag{7-89}$$

To make these ideas more precise, let us consider the particularly simple example of two-group diffusion theory as described by Eq. (7-40). In matrix form, these equations become

$$\underbrace{\begin{pmatrix} -\nabla\cdot D_1\nabla + \Sigma_{R_1} & 0 \\ -\Sigma_{s_{12}} & -\nabla\cdot D_2\nabla + \Sigma_{a_2} \end{pmatrix}}_{\underline{M}}\underbrace{\begin{pmatrix} \phi_1 \\ \phi_2 \end{pmatrix}}_{\underline{\phi}} = \underbrace{\frac{1}{k}\begin{pmatrix} \nu_1\Sigma_{f_1} & \nu_2\Sigma_{f_2} \\ 0 & 0 \end{pmatrix}}_{\frac{1}{k}\underline{F}}\underbrace{\begin{pmatrix} \phi_1 \\ \phi_2 \end{pmatrix}}_{\underline{\phi}}. \tag{7-90}$$

The adjoint equations are

$$\underbrace{\begin{pmatrix} -\nabla\cdot D_1\nabla + \Sigma_{R_1} & -\Sigma_{s_{12}} \\ 0 & -\nabla\cdot D_2\nabla + \Sigma_{a_2} \end{pmatrix}}_{\underline{M}^{\dagger}}\underbrace{\begin{pmatrix} \phi_1^{\dagger} \\ \phi_2^{\dagger} \end{pmatrix}}_{\underline{\phi}^{\dagger}} = \underbrace{\frac{1}{k}\begin{pmatrix} \nu_1\Sigma_{f_1} & 0 \\ \nu_2\Sigma_{f_2} & 0 \end{pmatrix}}_{\frac{1}{k}\underline{F}^{\dagger}}\underbrace{\begin{pmatrix} \phi_1^{\dagger} \\ \phi_2^{\dagger} \end{pmatrix}}_{\underline{\phi}^{\dagger}}. \tag{7-91}$$

Note that $\underline{M}^{\dagger} \neq \underline{M}$ and $\underline{F}^{\dagger} \neq \underline{F}$, hence $\underline{\phi}^{\dagger} \neq \underline{\phi}$.

Suppose we consider the reactivity change induced by perturbing the thermal absorption cross section by an amount $\delta\Sigma_{a_2}$. Then

$$\underline{\delta F} = 0,$$

$$\underline{\delta M} = \begin{pmatrix} 0 & 0 \\ 0 & \delta\Sigma_{a_2} \end{pmatrix}. \tag{7-92}$$

Hence we can compute

$$\left(\underline{\phi}^{\dagger}, \underline{\delta M}\,\underline{\phi}\right) = \int_V d^3r\ \overbrace{\phi_1^{\dagger}\phi_2^{\dagger}}\begin{pmatrix} 0 & 0 \\ 0 & \delta\Sigma_{a_2} \end{pmatrix}\begin{pmatrix} \phi_1 \\ \phi_2 \end{pmatrix} = \int_V d^3r\ \phi_2^{\dagger}\delta\Sigma_{a_2}\phi_2 \tag{7-93}$$

to find

$$\Delta\rho = -\frac{\int_V d^3r\ \phi_2^{\dagger}\delta\Sigma_{a_2}\phi_2}{\left(\underline{\phi}^{\dagger}, \underline{F}\,\underline{\phi}\right)} = -\frac{1}{c}\int_V d^3r\ \phi_2^{\dagger}\delta\Sigma_{a_2}\phi_2. \tag{7-94}$$

In analogy with our earlier one-speed calculation, suppose we set

$$\delta \Sigma_{a_2} = \alpha \delta (r - r_0). \tag{7-95}$$

Then

$$\Delta \rho = -\frac{\alpha}{c} \phi_2^\dagger(r_0)\phi_2(r_0). \tag{7-96}$$

Thus we find

$$\phi_2^\dagger(r_0) = -\frac{c\Delta\rho}{\alpha\phi_2(r_0)} = \begin{array}{l}\text{fractional change in} \\ \text{reactivity per neutron} \\ \text{absorbed per unit time.}\end{array} \tag{7-97}$$

In particular, if $\phi_2^\dagger$ is large at $r_0$, then the change in $\rho$ introduced by a thermal absorber at $r_0$ will be large. That is, $\phi_2^\dagger(r)$ measures the "importance" of the point $r$ with respect to reactivity changes induced by perturbing the thermal absorption at that point.

For the more general multigroup problem, $\phi_g^\dagger(r)$ can be identified as the neutron importance function for group $g$, since $\phi_g^\dagger(r)$ is proportional to the gain or loss in reactivity of a reactor due to the insertion or removal of one neutron per second in the group $g$ at point $r$.

In general, one finds that the multigroup neutron importance (or adjoint fluxes) differs substantially from the multigroup fluxes. This is shown for a two-group calculation for a reflected slab geometry core in Figure 7-4.



Core: $U^{235} + H_2O$

$$\frac{N^{25}}{N^W} = \frac{1}{300}$$

Reflector: $H_2O$

Two—group calculation
Infinite slab core
Infinite reflector
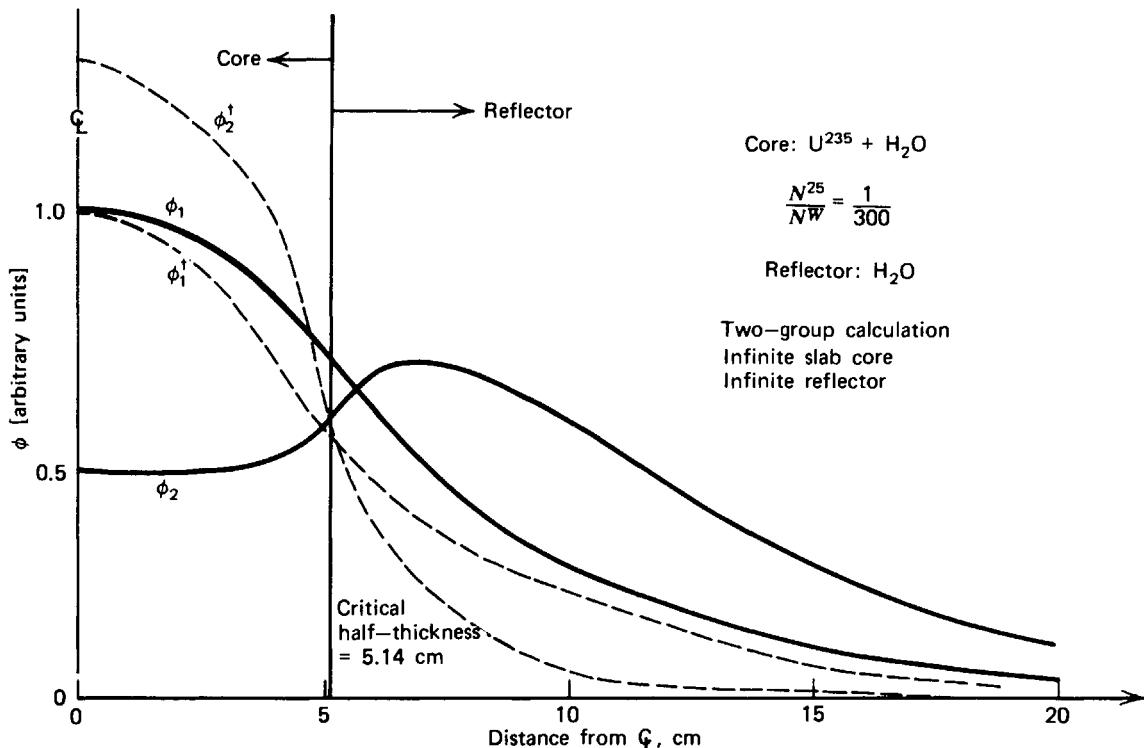
**FIGURE 7-4.** The two-group fluxes and adjoint fluxes for a reflected slab reactor

## VI. SOME CONCLUDING REMARKS

We have now developed the multigroup diffusion equations and outlined a strategy for solving them. The major uncertainty at this point concerns just how one determines the group constants. These latter calculations rely on clever guesses or approximations for the intragroup fluxes, and more specifically on one's ability to determine the neutron energy spectrum characterizing fast and thermal neutrons. This is the subject to which we will next turn our attention as we study the slowing down and thermalization of neutrons.

## REFERENCES

1. A. M. Weinberg and E. P. Wigner, *The Physical Theory of Neutron Chain Reactors*, University of Chicago Press, (1958), p. 509.
2. G. I. Bell and S. Glasstone, *Nuclear Reactor Theory*, Van Nostrand, Princeton, N. J. (1970), p. 181.
3. R. L. Hellens, The Physics of PWR Reactors, in New Developments in Reactor Physics and Shielding, USAEC CONF-720901 (1972).
4. M. H. Merrill, Nuclear Design Methods and Experimental Data in Use at Gulf General Atomic, GULF-GA-A12652 (GA-LTR-2), 1973.
5. R. Avery, Review of FBR Physics, in New Developments in Reactor Physics and Shielding, USAEC CONF-720901 (1972).
6. B. J. Toppel, A. L. Rago, and D. M. O'Shea, $MC^2$, A Code to Calculate Multigroup Cross Sections, ANL-7318, Argonne National Laboratory, 1967.
7. P. F. Zweifel, *Reactor Physics*, McGraw-Hill, New York (1973).
8. E. L. Wachspress, *Iterative Solution of Elliptic Systems and Applications to the Neutron Diffusion Equation of Reactor Physics*, Prentice-Hall, Englewood Cliffs, N. J. (1966).
9. G. J. Habetler and M. A. Martino, Proceedings of Symposium on Applied Mathematics, Vol. XI, American Mathematical Society (1961), p. 127.
10. R. S. Varga, *Matrix Iterative Analysis*, Prentice-Hall, Englewood Cliffs, N. J. (1962).
11. R. G. Steinke, A Review of Direct and Iterative Strategies for Solving Multi-Dimensional Finite Difference Problems, University of Michigan Nuclear Engineering Report (1971).
12. J. R. Lamarsh, *Introduction to Nuclear Reactor Theory*, Addison-Wesley, Reading, Mass. (1966).

## PROBLEMS

7-1 Estimate the fast-group constants characterizing $H_2O$ if the fast group is taken from $E_1 = 1 \text{eV}$ to $E_0 = 10 \text{MeV}$ and the neutron energy spectrum over this group is taken as $\phi(E) \sim 1/E$.

7-2 Estimate the minimum group spacing that will yield directly coupled multigroup equations for $^{12}C$, $^2D$, $^9Be$, and $^{22}Na$.

7-3 What percentage of the neutrons slowing down in hydrogen will tend to skip groups if the group structure is chosen such that $E_{g-1}/E_g = 100$?

7-4 Write out the detailed form of the multigroup diffusion equations, $\underline{M}\phi = k^{-1}\underline{F}\phi$, for a four-group model in which: (a) there is direct coupling, (b) the fission source exists only in the upper two groups, and (c) only the lowest group contains thermal neutrons.

7-5 Repeat Problem 7-4 for the case in which the lowest two groups correspond to thermal neutrons (which will be characterized by appreciable upscattering).

7-6 Calculate the critical size and mass of a bare sphere of pure $^{235}U$ metal using the group constants characterizing groups 1 and 2 in Table 7-1.

**TABLE 7-1   ANL Four-Group Microscopic Cross Sections (in barns)[†]**

| $g$ | Lower Energy $E_L$ | $u$ $[\ln E_0/E_L]$ | Fission Spectrum | $H_2O$ | | |
|---|---|---|---|---|---|---|
| | | | | $\sigma_{tr}$ | $\sigma_\gamma$ | $\sigma_{g \to g+1}$ |
| 1 | 1.353 MeV | 2 | 0.575 | 3.08 | 0 | 2.81 |
| 2 | 9.12 keV | 7 | 0.425 | 10.52 | 0 | 4.04 |
| 3 | 0.4 eV | 17.03 | 0 | 16.55 | 0.035 | 4.14 |
| 4 | 0 | — | 0 | 68.6 | 0.57 | 0 |

| $g$ | $U^{235}$ | | | | | | $U^{238}$ | | | | | |
|---|---|---|---|---|---|---|---|---|---|---|---|---|
| | $\sigma_{tr}$ | $\nu$ | $\sigma_f$ | $\sigma_\gamma$ | $\sigma_{inR}$ | $\sigma_{eR}$ | $\sigma_{tr}$ | $\nu$ | $\sigma_f$ | $\sigma_\gamma$ | $\sigma_{inR}$ | $\sigma_{eR}$ |
| 1 | 4.7 | 2.65 | 1.3 | 0.1 | 1.4 | 0 | 4.7 | 2.65 | 0.53 | 0.04 | 2.1 | 0 |
| 2 | 7.0 | 2.55 | 1.4 | 0.3 | 0 | 0 | 7.0 | — | 0 | 0.18 | 0 | 0 |
| 3 | 51.0 | 2.5 | 23.0 | 18.0 | 0 | 0.01 | 11.0 | — | 0 | 0.8 | 0 | 0.01 |
| 4 | 597.0 | 2.5 | 490 | 97 | 0 | 0 | 13.0 | — | 0 | 2.4 | 0 | 0 |

[†]From *Reactor Physics Constants*, ANL-5800 (1963). [Here, $\sigma_{inR}$ and $\sigma_{eR}$ refer to the inelastic and elastic scattering removal cross sections for the group similar to the definition given in Eq. (7-23).]

7-7 Compare the critical radius of a $^{235}U$ sphere as given by one-group, two-group, and modified one-group (1-1/2 group) diffusion models. Again use the data from groups 1 and 2 of Table 7-1.

7-8 Determine the thermal flux due to an isotropic point source emitting $S_0$ fast neutrons per second in an infinite moderating medium. Use two-group diffusion theory. In particular, discuss the solution to this problem for the case in which $L_1 > L_2$ and $L_1 < L_2$.

7-9 Consider a plane source emitting $S_0$ fast neutrons/cm² sec at the center of a subcritical slab of thickness $a$. Determine the two-group fluxes established in the assembly.

7-10 We have listed in Table 7-2 typical group constants characterizing a PWR (in both two-group and four-group forms). Calculate the multiplication factor of a PWR core of height 370 cm and diameter 340 cm using two-group diffusion theory.

**TABLE 7-2   Few-Group Diffusion Theory Constants for a Typical PWR Reactor Core**

| Group Constant | Two-Group | | Four-Group | | | |
|---|---|---|---|---|---|---|
| | 1 of 2 | 2 of 2 | 1 of 4 | 3 of 4 | 3 of 4 | 4 of 4 |
| $\nu\Sigma_f$ | .008476 | .18514 | .009572 | .001193 | .01768 | .18514 |
| $\Sigma_f$ | .003320 | .07537 | .003378 | .0004850 | .006970 | .07527 |
| $\Sigma_a$ | .01207 | .1210 | .004946 | .002840 | .03053 | .1210 |
| $D$ | 1.2627 | .3543 | 2.1623 | 1.0867 | .6318 | .3543 |
| $\Sigma_R$ | .02619 | .1210 | .08795 | .06124 | .09506 | .1210 |

7-11 Using the group constants of Table 7-2, calculate each of the terms in the six-factor formula for the core described in Problem 7-10.

7-12 The neutron "age" $\tau$ is defined as $1/6$ of the mean-square distance a fast neutron will travel before it slows down or is absorbed. Derive an expression for the age $\tau$ in terms of two-group constants. In particular, compute the age for the group constants characterizing a LWR in Table 7-2.

7-13 Recall that we defined the conversion ratio CR characterizing a reactor as the ratio of the production rate of fissile nuclei to the destruction rate of fissile nuclei. Derive an expression for the conversion ratio in a slightly enriched uranium-fueled reactor (such as a LWR) at the beginning of core life (i.e., such that the plutonium density is zero).

7-14 One important method of controlling reactivity in a PWR is to dissolve a poison such as boron in the coolant. If we assume that boron only affects the thermal absorption, $\Sigma_{a_2}$, derive an estimate of the critical boron concentration that will render $k_\infty = 1$. Use this expression to estimate the boron concentration necessary to render the reactor described in Problem 7-10 critical. Take $\sigma_{a_1}^B \cong 0$, $\sigma_{a_2}^B = 2207$ b.

7-15 Calculate the one-group constants corresponding to collapsing the two-group set given in Table 7-2.

7-16 Derive a general group collapsing expression for $N$-group constants in terms of $N \times M$-group constants (e.g., 2-group in terms of 4-group).

7-17 Calculate the two-group constants corresponding to collapsing the four-group constants in Table 7-2 by assigning groups 1, 2, and 3 to group 1 and group 4 to group 4, respectively. Compare these with the two-group constants listed in Table 7-2.

7-18 Using two-group theory, determine the critical core width of a slab reactor with core composition similar to that of a PWR and surrounded by an infinite water reflector. Use the two-group constants of Table 7-2 supplemented with group constants characterizing the water reflector: $D_1 = 1.13$ cm, $D_2 = 0.16$ cm, $\Sigma_{R_1} = 0.0494$ cm$^{-1}$ $\cong \Sigma_{s_{12}}$, $\Sigma_{a2} = 0.0197$ cm$^{-1}$, $\Sigma_{a_1} = .0004$ cm$^{-1}$.

7-19 A beam of $J_{in}$ *fast* neutrons/cm$^2$/sec is incident on the plane face of an infinite homogeneous nonmultiplying half-space. Use two-group diffusion theory and partial current boundary conditions to calculate $J_{out}$, the partial current of *thermal* neutrons going back toward the fast source.

7-20 Consider a thin slab of fuel surrounded by an infinite moderator. Suppose that the slab is thin enough that it is essentially transparent to nonthermal neutrons. However because of its large thermal absorption cross section, *all* thermal neutrons striking the surface of the slab are absorbed. Suppose further that every thermal neutron absorbed in the fuel results in the net production of $\eta$ fission neutrons. Using the two-group diffusion theory model, develop an equation for the effective multiplication factor for this system.

7-21 Assuming that *two*-group diffusion theory with one group of delayed fission neutrons represents a valid description of the reactor, write the three coupled differential equations for the time and spatial dependence of the neutron precursor fragment concentration $C(\mathbf{r},t)$ and the fast and slow group fluxes $\phi_1(\mathbf{r},t)$ and $\phi_2(\mathbf{r},t)$ respectively. The average speed, diffusion constants, and removal (by all types of collision) cross sections in the fast and slow groups are $v_1$, $D_1$, $\Sigma_{R_1}$ and $v_2$, $D_2$, and $\Sigma_{R_2}$ respectively. Fission can be produced only by slow group neutrons, and the cross section is $\Sigma_{f_2}$. There are $\nu$ neutrons emitted per fission, all into the fast group, with a fraction $\beta$ delayed. The decay constant of the neutron precursor is $\lambda$, and the cross section for transfer of neutrons from the fast group to the slow group is $\Sigma_{s_{12}}$. By assuming that the spatial shapes of $\phi_1$, $\phi_2$ and $C$ are that of the fundamental mode with geometric buckling $B^2$, find an equation for the transient and stable periods (i.e., the inhour equation). How many transient terms are there?

7-22 Write out the explicit form of the matrix equations $\underline{M}\phi = k^{-1}\underline{F}\phi$ and $\underline{A}_g\phi_g = \underline{S}_g + \underline{R}_{g-1}\phi_{g-1}$ for a four-group, $4 \times 4 \times 3$ three-dimensional spatial mesh problem in which the lowest two groups are both taken in the thermal range in which significant upscatter can occur.

7-23 Write a simple two-group, one-dimensional diffusion code (similar to the one-group code written in Problem 5-27). Then treating the LWR described in Problem 7-10 as a slab geometry, calculate the width necessary for reactor criticality.

7-24 Using ANL-7411, list and contrast various multigroup diffusion codes. In particular, compare their group structure, inner–outer iteration strategy, source-extrapolation methods, criticality search options, and estimated running times.

7-25 Calculate $\phi_1, \phi_2$ and the adjoint fluxes, $\phi_1^\dagger, \phi_2^\dagger$ for a bare, spherical reactor of radius $R$.

7-26 Compute and sketch both the two-group fluxes and adjoint fluxes for the reflected slab reactor described in Problem 7-18.

7-27 A critical system consisting of a slab surrounded on both sides by infinite reflectors is to be described by two-group diffusion theory. The center third of the core suddenly has its thermal group absorption cross section increased slightly. Find the change in core multiplication by perturbation theory. Then to demonstrate that the work saved over directly calculating the multiplication factor for the perturbed system is very great, carry out the latter calculation until as many pages are filled as were required to perform the perturbation calculation.

# 8

# Fast Spectrum Calculations
# and
# Fast Group Constants

The principal tool of nuclear reactor analysis is multigroup diffusion theory. In Chapter 7 we developed the general form of the multigroup diffusion equations and prescribed a strategy for their solution. However these equations contained various parameters known as group constants formally defined as averages over the energy-dependent intragroup fluxes $\phi(r, E)$ which must be determined before these equations assume more than a formal significance. The determination of suitable approximations for the intragroup fluxes, that is, the neutron energy spectrum, is the key to the generation of group constants that will yield an accurate few-group description of nuclear reactor behavior.

Hence our goal in this chapter and Chapter 9 is to develop methods for generating few-group constants by averaging fundamental microscopic cross section data over suitable approximations to the neutron energy spectrum. Of course there are two aspects to this problem, since both the energy and the spatial dependence of the intragroup fluxes must be estimated. Because of the extremely complicated dependence of microscopic neutron cross sections on energy, it is necessary to provide a rather careful treatment of the energy dependence of the intragroup flux. Of course if the number of groups is very large ($>50$), one can frequently get by with rather crude estimates of this energy dependence. For example, for energies above 1 MeV, one might approximate $\phi(E)$ by the fission spectrum $\chi(E)$; for intermediate energies, $1 \text{ eV} < E < 1 \text{ MeV}$, we will see that $\phi(E)$ behaves very roughly as $1/E$; while for energies below 1 eV, we might model $\phi(E)$ by a Maxwell–Boltzmann distribution characterizing neutrons in thermal equilibrium with the reactor core material at a temperature $T$.

Unfortunately, for the generation of few-group constants, one requires a far better treatment of the energy dependence of the intragroup flux. In fact one is

usually required to perform a detailed multigroup calculation of the neutron energy spectrum using a fine-group structure (with a crude treatment of spatial dependence) which can then be used to average or "collapse" fundamental cross section data to generate few-group constants.

The methods used to generate the neutron energy spectrum vary, depending on the range of neutron energies of interest. For example, at high energies the dominant process is neutron slowing down via both elastic and inelastic scattering. At intermediate energies, resonance absorption becomes quite important. At low energies, upscattering becomes appreciable as the neutrons tend to approach thermal equilibrium with the nuclei comprising the reactor core. Hence it is customary to divide the range of neutron energies into three different regions, each characterized by these different types of interaction, as indicated below:

| Upscattering<br><br>Chemical binding<br><br>Diffraction | Elastic scattering from stationary, free nuclei (isotropic in CM, s-wave)<br><br>No upscattering resonance absorption (resolved resonances) | Elastic scattering (anisotropic in CM, p-wave)<br><br>Inelastic scattering<br><br>No upscattering resonance absorption (unresolved resonances) fission sources |
|---|---|---|

0                          1 eV                          $10^5$ eV                          $10^7$ eV

Neutron Thermalization     Neutron moderation or slowing down     Fast fission

In this chapter we will be concerned with the calculation of the neutron energy spectrum characterizing fast neutrons. Hence our study of the calculation of *fast neutron spectra* and the generation of *fast group constants* will be dominated by a development of the theory of neutron slowing down and resonance absorption. In Chapter 9 we then consider the calculation of *thermal neutron spectra* and *thermal group constants* involving the development of the theory of neutron thermalization.

One must also account for the spatial dependence of the intragroup fluxes, as well as the spatial variation of the reactor core composition. Of course a detailed treatment of this spatial dependence in the generation of multigroup constants would be impractical—indeed the primary motivation for the generation of *few*-group constants is to yield a sufficiently coarse treatment of neutron energy dependence to allow such a detailed spatial calculation. Instead we must introduce a very approximate treatment of the spatial dependence of the intragroup fluxes.

Of course the most drastic such approximation is simply to ignore the spatial dependence altogether in the calculation of the neutron spectrum. That is, one effectively assumes that the intragroup fluxes can be calculated by assuming that neutron slowing down and thermalization occur in an infinite medium in which there is no spatial dependence. We will begin our study of both fast and thermal spectra for this situation because of its simplicity.

In most cases, however, one cannot so cavalierly ignore the spatial dependence of the intragroup fluxes. Hence we will modify our study of infinite medium spectrum calculations to include a very simple treatment in which the intragroup flux spatial and energy dependence are assumed to be separable, and this spatial dependence is then characterized by a single parameter (an effective value of the geometric buckling $B_g^2$).

However even this extended treatment is inadequate for many situations in which the detailed geometry of the reactor lattice must be taken into account. This is particularly true for an adequate treatment of both resonance and thermal neutron absorption. The few-group constants must be modified to account for the variation of both the neutron flux and the material composition in a small subregion or cell of the reactor core. In effect one must *spatially average* the few-group constants over a unit cell of the core lattice (much as the microscopic group constants have been averaged over *energy* to generate the few-group constants) before they can be used in a few-group diffusion calculation. We will consider such cell-averaging techniques in Chapter 10.

Therefore the generation of appropriate few-group constants usually involves a sequence of both energy and spatial averages of the microscopic cross section data over approximate estimates of the neutron energy spectrum and spatial dependence characterizing the neutron flux in a given subregion of the reactor of interest. As such, these group constants are dependent on the reactor design of interest, and also the region of the reactor core under investigation, its present operating conditions (e.g., coolant densities, temperatures), as well as its past history (e.g., fuel depletion, fission product buildup). The generation of multigroup constants is an extremely important (and usually time consuming) facet of nuclear design since it is the key to the successful implementation of the multigroup diffusion technique.

## I. NEUTRON SLOWING DOWN IN AN INFINITE MEDIUM

### A. Introduction

Our initial goal is the calculation of the energy dependence of the neutron flux $\phi(\mathbf{r}, E)$ in the fast energy range, $E \gtrsim 1$ eV, in which upscattering can be ignored. To simplify this calculation, we will first consider neutron slowing down from sources uniformly distributed throughout an infinite, uniform medium.[1,2,4] In this case, all spatial dependence disappears, and the neutron continuity equation, Eq. (4-79), reduces to an equation for the neutron energy spectrum $\phi(\mathbf{r}, E) \rightarrow \phi(E)$ of the form

$$\Sigma_t(E)\phi(E) = \int_0^\infty dE' \, \Sigma_s(E' \rightarrow E)\phi(E') + S(E). \qquad (8\text{-}1)$$

That is, the neutron transport equation simplifies rather dramatically to an *integral equation* in the single variable $E$, which we will refer to as the *infinite-medium spectrum equation*.

Of course the neglect of all spatial dependence may seem very drastic, and we will later study schemes for reincluding it in our analysis. In most large reactors, however, leakage is a relatively minor effect in comparison to neutron energy variation. Furthermore even spatial effects due to core heterogeneities are usually

of secondary importance, particularly in the fast neutron energy range. Hence we are certainly justified in focusing our initial attention on the energy dependence of the neutron flux.

Before we can proceed further, we must provide more information concerning the energy dependence of the neutron cross sections $\Sigma_t(E)$ and $\Sigma_s(E' \to E)$. Consistent with our present concern with fast neutron spectra, we will assume that the scattering nuclei are initially at rest and free to recoil. That is, we will consider only fast neutron energies much greater than the thermal energy of the nuclei $E \gg kT$ so that upscattering in collisions can be ignored.

We will further restrict our initial investigation by considering only the process of elastic scattering that is isotropic in the center of mass system. In this case, our earlier study of two-body collision kinematics has indicated that the differential scattering cross section is of the form

$$\Sigma_s(E' \to E) = \begin{cases} \dfrac{\Sigma_s(E')}{(1-\alpha)E'}, & E < E' < \dfrac{E}{\alpha} \\ 0, & \text{otherwise}, \end{cases} \qquad (8\text{-}2)$$

where $\alpha \equiv (A - 1/A + 1)^2$. This form is sufficiently simple to enable us to obtain analytical solutions to the *neutron slowing down equation*

$$[\Sigma_s(E) + \Sigma_a(E)]\phi(E) = \int_E^\infty dE' \Sigma_s(E' \to E)\phi(E') + S(E) \qquad (8\text{-}3)$$

in many cases of interest, even without specifying the detailed forms of the cross sections $\Sigma_s(E)$ and $\Sigma_a(E)$. Of course it will be necessary to use more general numerical methods in solving Eq. (8-3) for most practical situations. However those analytical results we will develop are of considerable use in formulating efficient numerical schemes, as well as in checking their accuracy.

By restricting our attention to s-wave elastic scattering, we have limited the applicability of our initial analysis to neutron energies below 1 MeV in light moderators, and below 0.1 MeV in heavier materials,[3] since the average scattering angle cosine $\bar{\mu}_0$ in the CM system is given roughly by $\bar{\mu}_0 = 0.07 \, A^{2/3} E$ [MeV]. More specifically, in hydrogen, s-wave scattering is dominant below several MeV. By way of contrast, for heavier nuclei such as $^{16}O$, p-wave scattering becomes significant above roughly 50 keV. We will justify our restricted study of only s-wave scattering by noting that in thermal reactors, most neutron moderation is due to light elements such as $^1_1H$, $^2_1D$, or $^{12}_6C$.

For neutron energies above 0.1 MeV, inelastic scattering from heavy nuclei becomes important and cannot be ignored. Unfortunately the complexities of inelastic processes severely limits the extent to which one can use analytical methods to investigate neutron slowing down. Hence our consideration of inelastic scattering will be deferred until our discussion of the numerical solution of the neutron slowing down equations.

We will begin our study of Eq. (8-3) for the particularly simple case of neutron slowing down in an infinite medium of hydrogen. This study is of particular importance since hydrogen is a very common moderator, and moreover this analysis will serve to introduce a number of concepts which prove useful in the study of more general neutron slowing down problems.

We will then turn to the study of neutron slowing down via elastic scattering from nonhydrogeneous moderators. The reader should be cautioned that while the detailed analysis of neutron slowing down in this section may look lengthy and complicated, the actual results of this analysis are extremely simple. We will find that the neutron flux will usually behave essentially as $\phi(E) \sim 1/\Sigma_s(E)E$, provided one is not near energies characterizing a neutron source or a strong cross section resonance. However, as is characteristic of so much of physics, the analysis necessary to derive and justify this result is considerably more complex than the result itself.

## B. Neutron Moderation in Hydrogen

### 1. SLOWING DOWN IN THE ABSENCE OF ABSORPTION

We will first examine the very simple case in which all absorption is ignored. Actually such an assumption is not too drastic in hydrogen, since $\sigma_a^H/\sigma_s^H \sim .014$. However we are more generally concerned with neutron slowing down in a hydrogeneous moderator containing in addition a heavy mass absorber (such as $^{238}U$). Even in this case, most neutron absorption occurs in fairly narrow energy ranges corresponding to absorption resonances, and for energies far from these resonances, the neglect of absorption will yield the correct quantitative behavior of the neutron spectrum $\phi(E)$.

For hydrogen we set $A = 1$ and hence $\alpha_H = 0$. Then in the absence of absorption, Eq. (8-3) becomes

$$\Sigma_s(E)\phi(E) = \int_E^\infty dE' \, \frac{\Sigma_s(E')\phi(E')}{E'} + S(E). \tag{8-4}$$

We will begin by determining the neutron energy spectrum $\phi(E)$ resulting from a monoenergetic source of strength $S_0$ emitting neutrons of energy $E_0$. It proves convenient to introduce a change of dependent variable in Eq. (8-4) by identifying the collision rate density $F(E) = \Sigma_s(E)\phi(E)$, so that we can rewrite the slowing down equation (8-4) as

$$F(E) = \int_E^{E_0} dE' \, \frac{F(E')}{E'} + S_0\delta(E - E_0). \tag{8-5}$$

Here we have set the upper limit of integration at $E_0$ since no neutrons can achieve energies higher than the source energy if only downscattering is possible.

We could solve this problem as we did the plane source diffusion problem of Chapter 5, by restricting our attention to energies $E < E_0$ and using the source as a boundary condition as $E \rightarrow E_0$. However it is more convenient in this case to solve Eq. (8-5) directly. First note that because of the singular source, the solution $F(E)$ must contain a term proportional to $\delta(E - E_0)$. Hence we will seek a solution of the form

$$F(E) = F_c(E) + C\delta(E - E_0), \tag{8-6}$$

where $C$ is an undetermined constant and $F_c(E)$ is the nonsingular component of $F(E)$. Substituting this form into Eq. (8-5), one finds

$$F_c(E) + C\delta(E - E_0) = \int_E^{E_0} dE' \frac{F_c(E')}{E'} + \frac{C}{E_0} + S_0\delta(E - E_0). \qquad (8\text{-}7)$$

However the singular contributions must be equal. Hence we demand $C = S_0$. Then we find that $F_c(E)$ satisfies the remaining nonsingular equation

$$F_c(E) = \int_E^{E_0} dE' \frac{F_c(E')}{E'} + \frac{S_0}{E_0}, \qquad E \leqslant E_0. \qquad (8\text{-}8)$$

Notice something rather interesting here. $F_c(E)$ satisfies an equation in which the source term is just that corresponding to source neutrons making a single collision at the source energy $E_0$—that is, the effective source presented by "once-collided" neutrons

$$S(E) = S_0 P(E_0 \to E) = \frac{S_0}{E_0}. \qquad (8\text{-}9)$$

Thus $F_c(E)$ can be interpreted as the collision density due to neutrons that have suffered at least one collision (hence the subscript "c"). In a similar sense, we now identify the singular component of $F(E)$, $S_0\delta(E - E_0)$, as simply the contribution due to uncollided source neutrons (present only at the source energy $E_0$).

We now must solve the remaining equation (8-8) for $F_c(E)$. We can solve this integral equation by first differentiating it to convert it into an ordinary differential equation (refer to Appendix B):

$$\frac{dF_c}{dE} = \frac{d}{dE}\left[ \int_E^{E_0} dE' \frac{F_c(E')}{E'} \right] + \frac{d}{dE}\left( \frac{S_0}{E_0} \right) \qquad (8\text{-}10)$$

or

$$\frac{dF_c}{dE} = -\frac{1}{E} F_c(E). \qquad (8\text{-}11)$$

The general solution to Eq. (8-11) is of the form $F_c(E) = C/E$. To determine the constant $C$, note that we can infer an initial condition at $E = E_0$ directly from the integral equation (8-8):

$$F_c(E_0) = \frac{S_0}{E_0}. \qquad (8\text{-}12)$$

Hence we must choose $C = S_0$ to find the total solution

$$F(E) = \frac{S_0}{E} + S_0\delta(E - E_0), \qquad (8\text{-}13)$$

or

$$\phi(E) = \frac{S_0}{\Sigma_s(E)E} + \frac{S_0}{\Sigma_s(E)}\delta(E-E_0). \tag{8-14}$$

It should be observed that if the scattering cross section is only weakly dependent on energy (which it usually is), then below the source energy $E_0$ the flux assumes a $1/E$ form. This functional form could in fact be used as a crude estimate of the flux in generating group constants characterizing neutron slowing down, but we will proceed to develop more sophisticated models.

A very similar analysis can be used to construct the solution corresponding to a distributed source $S(E)$. In this case, one finds (see Problem 8-2) that

$$\phi(E) = \frac{1}{\Sigma_s(E)E}\int_E^\infty dE' \, S(E') + \frac{S(E)}{\Sigma_s(E)}. \tag{8-15}$$

Once again we note that below the source energies, the flux behaves essentially as $1/E$.

## 2. SOME USEFUL DEFINITIONS

### (a) THE SLOWING DOWN DENSITY

It is useful to introduce several new definitions at this point in order to facilitate our later analysis. We first want to define the neutron *slowing down density* $q(E)$ describing the rate at which neutrons slow down past a given energy $E$. To be more general, we define

$$q(\mathbf{r},E)d^3r = \begin{array}{l}\text{number of neutrons slowing down past energy} \\ E \text{ per sec in } d^3r \text{ about } \mathbf{r}.\end{array} \tag{8-16}$$

If we recall that the differential scattering cross section describes the probability that a neutron will scatter from an initial energy $E'$ to a final energy $E''$ in $dE''$, then we can write

$$\begin{array}{l}\text{Rate at which neutrons} \\ \text{that suffer collision} \\ \text{at energy } E' \text{ in } dE' \\ \text{slow down past } E\end{array} = \left[\int_0^E \Sigma_s(E'\to E'')\phi(\mathbf{r},E')dE''\right]dE'. \tag{8-17}$$

Hence the total slowing down density resulting from all initial energies $E' > E$ is given by

$$q(\mathbf{r},E) = \int_E^\infty dE' \int_0^E dE'' \Sigma_s(E'\to E'')\phi(\mathbf{r},E'). \tag{8-18}$$

We can apply this definition to calculate the slowing down density in our infinite,

nonabsorbing, hydrogeneous moderator as

$$q(E) = \int_0^E dE'' \left[ \int_E^\infty dE' \frac{\Sigma_s(E')\phi(E')}{E'} \right]$$

$$= \int_0^E dE'' \left[ \int_E^\infty \frac{dE'}{E'} \left( F_c(E') + S_0 \delta(E' - E_0) \right) \right]$$

$$= E \left[ \int_E^\infty dE' \frac{F_c(E')}{E'} + \frac{S_0}{E_0} \right] = EF_c(E) = S_0. \qquad (8\text{-}19)$$

Hence for this simple problem, the slowing density is constant and equal to the source. This is of course understandable, since in the absence of absorption and leakage, *all* source neutrons must eventually slow down below the energy $E$.

### (b) THE NEUTRON LETHARGY

The energy range spanned by neutron slowing down is extremely large, ranging from $10^7$ eV down to 1 eV. Furthermore we have found that in elastic scattering the neutron tends to lose a fraction of its incident energy rather than a fixed amount of energy. These considerations suggest that it would be more convenient to use as an independent variable, the logarithm of the neutron energy $E$. To this end, we define the *neutron lethargy*

$$u \equiv \ln \frac{E_0}{E}. \qquad (8\text{-}20)$$

Here the energy $E_0$ is chosen to be the maximum energy that neutrons can achieve in the problem. It is usually set either at the source energy for a monoenergetic source problem, or chosen as 10 MeV for a reactor calculation.

Notice that as a neutron's energy $E$ decreases, its lethargy $u$ increases. That is, as a fast neutron loses energy via scattering collisions, it moves more slowly, becoming more "lethargic." The neutron lethargy is such a convenient variable that it is customary to perform fast spectrum calculations in terms of $u$ rather than $E$. Hence we must convert all of our earlier equations over to this new independent variable. To accomplish this, we first compute the relationships between differentials

$$du = \left( \frac{E}{E_0} \right) \left( \frac{-E_0}{E^2} \right) dE = \frac{-dE}{E}. \qquad (8\text{-}21)$$

Then, for example, we can calculate the collision density in terms of lethargy by writing

$$F(u)du = -F(E)dE \qquad (8\text{-}22)$$

or

$$F(u) = EF(E).$$

(The minus sign appears because lethargy increases as energy decreases.) If we apply this to our earlier example of slowing down in an infinite, nonabsorbing medium of hydrogen, we find for this case, the collision rate density is a constant in the lethargy variable

$$F(u) = EF(E) = S_0. \tag{8-23}$$

In more general cases, we will find that the collision density $F$ is usually a much more slowly varying function of $u$ than $E$ and hence is easier to approximate in the lethargy variable.

As a second example, we can compute the elastic scattering probability function $P(E' \to E)$ in lethargy by noting

$$P(u' \to u)du = -P(E' \to E)dE. \tag{8-24}$$

Thus

$$P(u' \to u) = -\frac{dE}{du} P(E' \to E) = EP(E' \to E)$$

$$= \frac{1}{(1-\alpha)} \left( \frac{E}{E'} \right) = \frac{e^{u'-u}}{(1-\alpha)}. \tag{8-25}$$

Also

$$E < E' < E/\alpha \Rightarrow u - \ln(1/\alpha) < u' < u. \tag{8-26}$$

Hence we find

$$P(u' \to u) = \begin{cases} \dfrac{e^{u'-u}}{(1-\alpha)}, & u - \ln(1/\alpha) < u' < u \\ 0, & \text{otherwise.} \end{cases} \tag{8-27}$$

We can now rewrite our slowing down equation for hydrogen in terms of the lethargy variable as

$$\Sigma_s(u)\phi(u) = \int_0^u du' \, e^{u'-u} \Sigma_s(u')\phi(u') + S(u). \tag{8-28}$$

Now notice something rather interesting; from Eqs. (8-18) and (8-27), it is apparent the slowing down density in the lethargy variable is given by

$$q(u) = \int_0^u du' \, \Sigma_s(u')\phi(u')e^{u'-u}. \tag{8-29}$$

Now suppose we differentiate this expression with respect to $u$

$$\frac{dq}{du} = -\int_0^u du' \, \Sigma_s(u')\phi(u')e^{u'-u} + \Sigma_s(u)\phi(u). \tag{8-30}$$

Hence we can reidentify $q(u)$ from Eq. (8-29) to write

$$\frac{dq}{du} + q(u) = \Sigma_s(u)\phi(u). \tag{8-31}$$

These equations relating the slowing down density to the flux are peculiar to slowing down in hydrogen, but we will later find that they also hold when absorption and spatial dependence are included. They will prove to be of considerable use in numerical studies of neutron slowing down.

As a final exercise involving the lethargy variable, let us compute the average lethargy gain (corresponding to the average logarithmic energy loss) of a neutron in a collision with a nucleus of arbitrary mass number:

$$\xi \equiv \langle \Delta u \rangle = \int_{\alpha E_i}^{E_i} \left[ \ln\left(\frac{E_0}{E_f}\right) - \ln\left(\frac{E_0}{E_i}\right) \right] \frac{1}{(1-\alpha)E_i} dE_f \tag{8-32}$$

or

$$\xi = 1 + \frac{\alpha}{1-\alpha} \ln \alpha = 1 - \frac{(A-1)^2}{2A} \ln\left(\frac{A+1}{A-1}\right). \tag{8-33}$$

By way of example, the mean lethargy gain per collision, $\xi$, is tabulated for several moderators of interest in Table 8-1.

**TABLE 8-1    Slowing Down Parameters of Typical Moderators**

| Moderator | $A$ | $\alpha$ | $\xi$ | $\rho[g/cm^3]$ | Number of collisions from 2 MeV to 1 eV | $\xi\Sigma_s[cm^{-1}]$ | $\xi\Sigma_s/\Sigma_a$ |
|---|---|---|---|---|---|---|---|
| H | 1 | 0 | 1 | gas | 14 | — | — |
| D | 2 | .111 | .725 | gas | 20 | — | — |
| $H_2O$ | — | — | .920 | 1.0 | 16 | 1.35 | 71 |
| $D_2O$ | — | — | .509 | 1.1 | 29 | 0.176 | 5670 |
| He | 4 | .360 | .425 | gas | 43 | $1.6 \times 10^{-5}$ | 83 |
| Be | 9 | .640 | .209 | 1.85 | 69 | 0.158 | 143 |
| C | 12 | .716 | .158 | 1.60 | 91 | 0.060 | 192 |
| $^{238}U$ | 238 | .983 | .008 | 19.1 | 1730 | 0.003 | .0092 |

An interesting application of this quantity is to compute the average number of collisions necessary to thermalize a fission neutron, that is, to slow it down from 2 MeV to 1.0 eV. This is given by

$$\langle \# \rangle = \frac{\ln \dfrac{2 \times 10^6}{1.0}}{\xi} = \frac{14.5}{\xi} \tag{8-34}$$

and is compared for several moderators of interest in Table 8-1. We can see rather dramatically how much more effective low mass-number nuclei are at moderating fast neutrons.

### (c) MODERATING POWER AND MODERATING RATIO

The above analysis has indicated that the number of scattering collisions necessary to slow a neutron to thermal energies is inversely proportional to $\xi$. Certainly the better moderators will be characterized by large values of $\xi$. However they must also be characterized by large scattering cross sections $\Sigma_s$ since otherwise the probability of a scattering collision occurring will be too small. Hence a more appropriate measure of the *moderating* or *slowing down power* of a material is the product $\xi\Sigma_s$. To this end, one defines:

$$\text{Moderating power} \equiv \xi\Sigma_s. \tag{8-35}$$

However, even this parameter is not sufficient in itself to describe the effectiveness of a material for neutron moderation, because obviously one also wishes the moderator to be a weak absorber of neutrons. Thus it is customary to choose as a figure of merit the *moderating ratio*, defined as

$$\text{Moderating ratio} \equiv \frac{\xi\Sigma_s}{\Sigma_a}. \tag{8-36}$$

The moderating power and moderating ratio are given for several materials of interest in Table 8-1. From this comparison it is evident that $D_2O$ is the superior moderator. Indeed the moderating ratio of $D_2O$ is sufficiently large that it can be used to construct a reactor fueled with natural uranium. Unfortunately it is also very expensive. Hence most thermal reactor designs choose to use somewhat poorer, but cheaper, moderators such as light water or graphite, although this usually requires the use of enriched uranium fuels.

### 3. SLOWING DOWN WITH ABSORPTION

.We will now include an absorption term in our infinite medium slowing down equation. Actually the absorption cross section of hydrogen is negligible. The physical situation we want to describe is that of a strongly absorbing isotope mixed in hydrogen (such as $^{238}U$). However this isotope can also scatter, and since its mass number is not unity, it would invalidate our analysis. For simplicity, therefore, we will assume the absorber to be "infinitely massive" so that it does not slow down neutrons—it only absorbs them. We will also ignore inelastic scattering. Then the appropriate slowing down equation (again with a monoenergetic source at energy $E_0$) is just

$$[\Sigma_a(E) + \Sigma_s(E)]\phi(E) = \int_E^{E_0} dE' \frac{\Sigma_s(E')\phi(E')}{E'} + S_0\delta(E - E_0). \tag{8-37}$$

As in our earlier analysis, we seek the solution for the total collision density $F(E) = \Sigma_t(E)\phi(E)$ as the sum of a collided and uncollided contribution, similar to

Eq. (8-6). Then we find that the collided contribution $F_c(E)$ must satisfy

$$F_c(E) = \int_E^{E_0} \frac{dE'\,\Sigma_s(E')F_c(E')}{E'\,\Sigma_t(E')} + \frac{\Sigma_s(E_0)}{\Sigma_t(E_0)}\frac{S_0}{E_0}. \tag{8-38}$$

Note that again the effective source term in this equation corresponds to once-collided source neutrons, suitably scaled down to account for neutron absorption at the source energy $E_0$.

We again solve this equation by first differentiating to find

$$\frac{dF_c}{dE} = -\left[\frac{\Sigma_s(E)}{E\Sigma_t(E)}\right]F_c(E). \tag{8-39}$$

We can easily integrate this ordinary differential equation using the initial condition at $E = E_0$ implied by Eq. (8-38) to find

$$F_c(E) = \frac{\Sigma_s(E_0)}{\Sigma_t(E_0)}\frac{S_0}{E}\exp\left[-\int_E^{E_0}\frac{dE'\,\Sigma_a(E')}{\Sigma_t(E')E'}\right]. \tag{8-40}$$

Notice in particular that if we were to set $\Sigma_a \equiv 0$ we would return to our earlier solution $F_c(E) = S_0/E$. We can compute the slowing down density as before to find

$$q(E) = EF_c(E) = \frac{\Sigma_s(E_0)}{\Sigma_t(E_0)}S_0\exp\left[-\int_E^{E_0}\frac{dE'\,\Sigma_a(E')}{\Sigma_t(E')E'}\right]. \tag{8-41}$$

If we now note that

$S_0 = $ rate at which source neutrons are emitted at energy $E_0$

$q(E) = $ rate at which neutrons slow down past $E$,

then we can identify

$$\frac{q(E)}{S_0} \equiv \begin{array}{l}\text{probability that a source neutron is not absorbed while}\\ \text{slowing down from } E_0 \text{ to } E.\end{array} \tag{8-42}$$

Since most absorption in the slowing down energy range is due to resonances in the absorption cross section, it is natural to identify the resonance escape probability to energy $E$ in hydrogen as just

$$p(E) = \frac{q(E)}{S_0} = \exp\left[-\int_E^{E_0}\frac{dE'\,\Sigma_a(E')}{E'\Sigma_t(E')}\right]. \tag{8-43}$$

To proceed further we need explicit forms for $\Sigma_a(E)$ and $\Sigma_t(E)$. We will develop these later in this chapter when we return to consider resonance absorption. First, however, we will generalize these results to the case of $A > 1$.

## C. Neutron Moderation in Media with $A > 1$

### 1. SLOWING DOWN WITHOUT ABSORPTION

We now turn our attention to the more general case in which neutrons slow down via elastic scattering in an infinite medium of arbitrary mass number $A \geqslant 1$. Once again we first consider the situation in which absorption is ignored. Then the slowing down equation for the collided flux resulting from a monoenergetic source at energy $E_0$ is just

$$\Sigma_s(E)\phi_c(E) = \int_E^{\frac{E}{\alpha}} dE' \, \frac{\Sigma_s(E')\phi_c(E')}{(1-\alpha)E'} + \frac{S_0}{(1-\alpha)E_0}, \qquad E < E_0. \qquad (8\text{-}44)$$

If we once again write this equation in terms of the collision density $F_c(E)$ and differentiate with respect to $E$, we arrive at

$$\frac{dF_c}{dE} = \frac{1}{(1-\alpha)E}\left[ F_c(E/\alpha) - F_c(E) \right] \qquad (8\text{-}45)$$

The appearance of the first term corresponding to the upper limit of integration is what fouls us up, since this term depends not on $E$ but rather on $E/\alpha$. This equation is related to a *differential-difference equation*[20, 21] and requires an alternative method of solution. Its solution is complicated because the collision density is in fact discontinuous (or possesses discontinuous derivatives) at energies $\alpha^n E_0$ (corresponding to the minimum energy a neutron can slow down to in $n$ collisions). These discontinuous "transients" in the collision density will eventually smooth out to an asymptotic solution far below the source energy of the form $F_c(E) \sim 1/E$ (indeed, one can readily verify that such a function is a solution of Eq. (8-44) when the source term is not present). Fortunately this asymptotic behavior is sufficient for most slowing down studies, since one is usually concerned with either hydrogen-dominated slowing down (such as in a LWR) in which the transients do not arise or with the behavior of the neutron flux far below the fission source energies. Only for intermediate mass number moderators such as deuterium do the transients cause difficulties.

However for completeness we will sketch the detailed solution[1] of the slowing down equation for arbitrary mass number $A$. It is most convenient to recast Eq. (8-44) in terms of lethargy. However we must be careful in our study of this equation since a neutron can only gain a maximum lethargy of $\ln(1/\alpha)$ in a collision. Hence the source term will disappear from the equation for lethargies $u > \ln(1/\alpha)$. We first consider only the lethargy range $0 < u < \ln(1/\alpha)$, in which case Eq. (8-44) becomes

$$\Sigma_s(u)\phi_0(u) = \frac{1}{1-\alpha}\int_0^u du' \, \Sigma_s(u')\phi_0(u')e^{u'-u} + \frac{S_0 e^{-u}}{(1-\alpha)}, \qquad 0 < u < \ln\frac{1}{\alpha}. \qquad (8\text{-}46)$$

We have denoted the solution in this range as $\phi_0(u)$. Notice that to gain a lethargy below $u = \ln(1/\alpha)$, the neutron would have to experience at least two collisions.

Hence we refer to $0 < u < \ln(1/\alpha)$ as the "first collision interval". We will introduce the collision density to write

$$F_0(u) = \frac{1}{1-\alpha} \int_0^u du' \, F_0(u') e^{u'-u} + \frac{S_0 e^{-u}}{(1-\alpha)}, \qquad 0 < u < \ln\frac{1}{\alpha}. \qquad (8\text{-}47)$$

Now differentiate with respect to $u$ to find

$$\frac{dF_0}{du} - \left(\frac{\alpha}{1-\alpha}\right) F_0(u) = 0. \qquad (8\text{-}48)$$

The corresponding boundary condition is found, as usual, by examining Eq. (8-47) as $u \to 0$ to find

$$F_0(0) = \frac{S_0}{1-\alpha}. \qquad (8\text{-}49)$$

Hence we can readily solve for

$$F_0(u) = S_0 \frac{\exp\left[\left(\frac{\alpha}{1-\alpha}\right)u\right]}{(1-\alpha)}. \qquad (8\text{-}50)$$

[Note that in terms of energy variables

$$F_0(E) = \frac{S_0}{(1-\alpha)E} \left(\frac{E_0}{E}\right)^{\frac{\alpha}{1-\alpha}}. \qquad (8\text{-}51)$$

To handle higher order collision intervals—say between $(n-1)\ln(1/\alpha) < u < (n+1)\ln(1/\alpha)$ one must split up the range of integration to write

$$F_n(u) = \frac{1}{1-\alpha} \int_{n\ln\frac{1}{\alpha}}^u du' \, F_n(u') e^{u'-u} \qquad\qquad \underline{\qquad\qquad}(n-1)\ln\frac{1}{\alpha}$$

$$\underline{\qquad\qquad}n\ln\frac{1}{\alpha}$$

$$+ \frac{1}{1-\alpha} \int_{u-\ln\frac{1}{\alpha}}^{n\ln\frac{1}{\alpha}} du' \, F_{n-1}(u') e^{u'-u}. \qquad \underline{\qquad\qquad}(n+1)\ln\frac{1}{\alpha}$$

$$(8\text{-}52)$$

Again we differentiate to find

$$\frac{dF_n}{du} - \left(\frac{\alpha}{1-\alpha}\right) F_n(u) = -\left(\frac{1}{1-\alpha}\right) F_{n-1}(u - \ln 1/\alpha). \qquad (8\text{-}53)$$

We can integrate this to write

$$F_n(u) = F_n(n\ln 1/\alpha) \exp\left[\left(\frac{\alpha}{1-\alpha}\right)\left(u - n\ln\frac{1}{\alpha}\right)\right]$$

$$- \frac{1}{1-\alpha} \int_{n\ln\frac{1}{\alpha}}^u du' \, F_{n-1}(u' - \ln 1/\alpha) \exp\left[\left(\frac{\alpha}{1-\alpha}\right)(u-u')\right]. \qquad (8\text{-}54)$$

Since we know $F_0(u)$, we can use this expression to generate higher order $F_n(u)$. For example

$$F_1(u) = S_0 \left( \frac{1 - \alpha^{\frac{1}{1-\alpha}}}{1 - \alpha} \right) \exp\left[ \left( \frac{\alpha}{1-\alpha} \right) u \right] - S_0 \frac{\alpha^{\frac{\alpha}{1-\alpha}}}{(1-\alpha)^2} \left( u - \ln \frac{1}{\alpha} \right) \exp\left[ \left( \frac{\alpha}{1-\alpha} \right) u \right].$$

(8-55)

Note that there is a discontinuity between $F_0(u)$ and $F_1(u)$ at $u = \ln 1/\alpha$:

$$F_0(\ln 1/\alpha) - F_1(\ln 1/\alpha) = \alpha/(1 - \alpha).$$

(8-56)

In a similar manner, one can generate the higher order collision densities $F_n(u)$. These functions (so-called "Placzek functions") are illustrated in Figure 8-1.[5] Notice in particular how these functions appear to be smoothing out as the neutrons suffer increasingly more collisions. In fact for $u \gg \ln 1/\alpha$, we can use an asymptotic solution to equation (8-46) in which the source term is neglected

$$F_c(u) = \int_{u - \ln \frac{1}{\alpha}}^{u} du' \frac{F_c(u')}{(1 - \alpha)} e^{u' - u}.$$

(8-57)

It is evident that $F_c(u) = \text{constant} = C$ is a solution to this equation. However it is
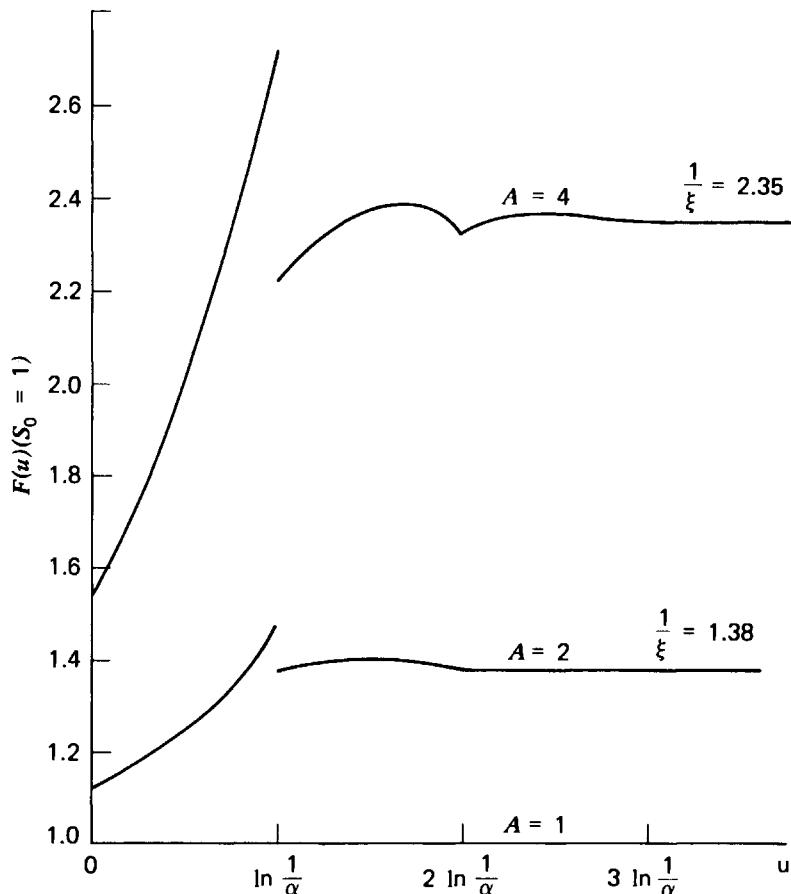


FIGURE 8-1.  The collision density $F(u)$ for $A = 2$ and 4.

not evident just what relationship this solution has to $F_n(u)$ for large $n$. Furthermore, this homogeneous equation provides no prescription for determining $C$.

Perhaps the most direct way to generate the asymptotic solution is to solve Eq. (8-47) using Laplace-transform methods.[6] We will adopt a somewhat more pedestrian approach by noting that the slowing down density in the lethargy variable is given by

$$q(u) = \int_{u - \ln \frac{1}{\alpha}}^{u} du' \, F_c(u') \int_{u}^{u' + \ln \frac{1}{\alpha}} du'' \, \frac{e^{u' - u''}}{(1 - \alpha)}. \tag{8-58}$$

If we substitute in our asymptotic form $F_c(u) = C$, we find

$$q(u) = \frac{C}{1 - \alpha} \int_{u - \ln \frac{1}{\alpha}}^{u} du' \, e^{u'} \int_{u}^{u' + \ln \frac{1}{\alpha}} du'' \, e^{-u''} = C\left[1 + \frac{\alpha}{1 - \alpha} \ln \alpha\right] = C\xi. \tag{8-59}$$

However in a nonabsorbing medium, we know that $q(u)$ must be constant and equal to the source rate $S_0$ (since there is nothing to prevent the neutrons from slowing down). Hence we must choose $C = S_0/\xi$, or

$$F_c(u) = \frac{S_0}{\xi}, \tag{8-60}$$

or

$$\phi(u) = \frac{S_0}{\xi \Sigma_s(u)}. \tag{8-61}$$

We can also write this asymptotic solution in terms of the energy variable as

$$\phi(E) = \frac{S_0}{\xi E \Sigma_s(E)}. \tag{8-62}$$

Hence asymptotically at least the flux characterizing neutron slowing down in a nonabsorbing medium of mass number $A$ is very similar to that found in hydrogen, with the exception of an additional factor, the mean lethargy gain per collision, $\xi$. As we have noted, the primary qualitative difference in the more general solution is the occurrence of irregular (discontinuous) behavior near energies at which source neutrons appear or strong absorption occurs. As one moves down in energy (up in lethargy) these transients damp out, leaving the smooth asymptotic behavior given by Eq. (8-62). The rapidity with which this asymptotic behavior is reached decreases with the mass number of the moderating material (although such behavior is always present in hydrogen).

More frequently one is concerned with neutron slowing down in a mixture of nuclides. Although we will treat this situation in some detail in later sections, we will note here that our earlier analysis can be easily generalized to a mixture of nuclides by writing

$$\phi(E) = S_0/\bar{\xi} E \Sigma_s(E), \tag{8-63}$$

where $\Sigma_s(E)$ is the total scattering cross section and $\bar{\xi}$ is the average lethargy gain per collision

$$\bar{\xi} \equiv \sum_{i=1}^{N} \xi_i \Sigma_s^{(i)}(E) \Big/ \sum_{i=1}^{N} \Sigma_s^{(i)}(E). \tag{8-64}$$

It should be noted that $\bar{\xi}(E)$ is in general energy (or lethargy)-dependent because of the energy dependence of the scattering cross section.

## 2. SLOWING DOWN WITH ABSORPTION

We could now introduce absorption (again assuming an infinitely massive absorber) into Eq. (8-44):

$$[\Sigma_a(E) + \Sigma_s(E)]\phi(E) = \int_E^{\frac{E}{\alpha}} dE' \frac{\Sigma_s(E')\phi(E')}{(1-\alpha)E'} + S(E), \tag{8-65}$$

or in terms of the collision density,

$$F(E) = \int_E^{\frac{E}{\alpha}} dE' \left[ \frac{\Sigma_s(E')}{\Sigma_t(E')} \right] \frac{F(E')}{(1-\alpha)E'} + S(E). \tag{8-66}$$

The presence of the factor $[\Sigma_s(E)/\Sigma_t(E)]$ makes it very difficult to make much progress toward an analytical solution to this equation, with the exception of very special cross section behaviors and elaborate approximation techniques.[1,2] Rather than discuss such techniques here, we will recognize that one is usually most interested in the effects of resonance absorption, and so we will proceed directly to a discussion of the various methods used to calculate the resonance escape probability. We will return later to discuss approximate treatments of slowing down when we consider as well how one treats spatial effects in neutron slowing down.

## D. Inelastic Scattering

Thus far we have concerned ourselves with neutron moderation via elastic collisions in which a neutron merely bounces off of a nucleus in billiard-ball fashion, losing some energy in the process. However for higher energy neutrons (>50 keV), inelastic scattering processes are possible in which an appreciable fraction of the incident neutron energy goes into exciting the nucleus into a higher nuclear quantum state. Such scattering is extremely important in heavy mass nuclei in which slowing down by elastic scattering is negligible. For example, if we consider a 1 MeV neutron incident on a $^{238}$U nucleus, the average energy lost in an elastic scattering collision would be $(1-\alpha)E_0/2 = 0.0085$ MeV. By way of contrast, the average energy lost in an inelastic scattering collision is about 0.6 MeV.

Of course for such inelastic scattering processes to occur, the incident neutron energy must be above the threshold corresponding to the lowest excited state of the target nucleus. For light nuclei, this threshold is quite high (4.4 MeV in $^{12}$C and 6.1 MeV in $^{16}$O, for example). However in heavier nuclei the inelastic scattering

thresholds are much lower (450 keV in $^{23}$Na and 45 keV in $^{238}$U), and inelastic processes become quite important.

Since inelastic scattering is much more significant for fast neutrons in high mass-number materials, it might be expected to be of considerable consequence in fast reactors. Indeed inelastic scattering in materials such as sodium is the dominant slowing down mechanism in fast reactors and must be carefully accounted for in any realistic reactor analysis.

Unfortunately the details of the inelastic scattering cross sections are quite complicated, and analytical investigations such as those we have applied to elastic scattering are restricted to very simple nuclear models (e.g., the Weisskopf evaporation model[2] or few level models[20]). Instead, one must usually proceed in practice with a brute force fine-structure multigroup calculation. That is, one writes the slowing down equation in multigroup form and solves it directly for many groups in order to obtain the intragroup fluxes for calculating the few-group constants. Such fine spectrum calculations may require as many as a thousand or more microgroups to adequately treat the details of inelastic scattering. Furthermore because of the rather large energy loss experienced by a neutron in an inelastic scattering event, several energy groups are usually coupled together (indirect group coupling). Later in this chapter we will consider in detail how inelastic scattering is treated in the generation of fast group constants.

## II. RESONANCE ABSORPTION (INFINITE MEDIUM)

### A. Introduction

As neutrons slow down from fission energies in a nuclear reactor, they experience an appreciable probability of being absorbed in the numerous sharp capture resonances which characterize heavy nuclei such as $^{238}$U or $^{232}$Th. Such resonance absorption of neutrons is an extremely important phenomenon in nuclear reactors. It not only affects reactor multiplication, but fuel burnup and breeding performance and reactor control characteristics as well.

One can distinguish several different types of resonance absorption in nuclear reactors. Of paramount importance in thermal reactors is absorption in the well-resolved low-energy resonances of fuel materials such as $^{238}$U or $^{232}$Th. The analysis of neutron absorption in such well-separated resonances is straightforward, and we will consider it in detail in this section.

Above several keV in fertile materials (and as low as 50 eV in fissile isotopes), one finds that the resonance structure becomes so finely detailed that resonances can no longer be individually resolved. The treatment of resonance absorption in the region of such unresolved resonances is considerably more complicated, since it requires the use of nuclear models to describe the resonance structure. Although this subject is of some importance in fast reactor analysis, its complexity induces us to refer the interested reader to more advanced studies of resonance absorption for a detailed discussion.[7]

An accurate treatment of resonance absorption is essential to reactor criticality calculations, since this is one of the primary neutron loss mechanisms in both thermal and fast reactors. Such a process enters into a multigroup diffusion calculation through the fast multigroup absorption cross sections $\Sigma_{ag}$, and the

accurate estimate of these group constants will be one of our principal concerns. In general, there will be a depression in the neutron flux at those energies in the vicinity of a strong resonance, and the analysis of such flux depressions is of considerable importance in determining multigroup constants.

Since resonance absorption in fertile material ($^{238}$U, $^{232}$Th) can lead to the production of fissile material ($^{239}$Pu, $^{233}$U), an accurate analysis of resonance absorption is also of importance in predicting conversion or breeding ratios. Indeed small inaccuracies in the treatment of resonance absorption can propagate sizable errors in the estimate of both fuel depletion and fertile-to-fissile conversion[8].

Resonance absorption is also extremely important in determining the kinetic behavior of the reactor. The amount of such absorption depends sensitively on the fuel temperature through the Doppler broadening mechanism. In fact the dominant reactivity feedback mechanism of significance in very rapid power transients is usually that due to the Doppler effect.

A rigorous treament of resonance absorption would attempt to determine the neutron flux $\phi(\mathbf{r},E)$ in a fuel lattice cell either by solving the transport equation directly or using Monte Carlo techniques. Although such calculations are occasionally performed, they are far too expensive for use in routine design analysis.

Instead one usually removes the spatial and angular dependence to arrive at an equation for the energy-dependent neutron flux similar to the slowing down equation (8-3). A direct numerical solution of this equation can be, and is, commonly performed. However the large number of calculations typically required in a reactor design preclude the extensive use of such direct methods in favor of simpler approximate solutions of the slowing down equation to determine the neutron flux in the vicinity of a resonance. Such approximate methods are usually analytical in nature, although various aspects of the solution may require numerical evaluation. When used for appropriate problems, they provide reasonable accuracy with considerably less calculational effort than the more rigorous methods.

In this section we will attempt to introduce some of the more elementary concepts and approximations useful in the study of resonance absorption. We will confine our discussion to resonance absorption in an infinite medium (consistent with our earlier study of neutron slowing down) and develop the principal approximations useful in the calculation of the resonance escape probability and fast group constants. However the results of such infinite medium calculations are of only limited utility, since spatial variations of the neutron flux in a fuel lattice can strongly influence resonance absorption. We defer the study of spatially dependent effects until we consider cell calculation techniques in Chapter 10.

Our general approach is to consider neutron slowing down in an infinite, homogeneous mixture of a heavy isotope characterized by absorption and scattering resonances and a moderator material having a constant scattering cross section (at least over the resonance) and a negligible absorption cross section. In particular we will study the solution of the neutron slowing down equation in the vicinity of a well-isolated resonance.

To illustrate the essential ideas involved, we will begin by considering the situation in which the moderating material is hydrogen and scattering from the absorber nuclei is neglected. This case is particularly simple, since the neutron slowing down equation can be solved exactly when the mass number of the scatterer is unity.

## B. Resonance Absorption in Hydrogen Plus An Infinitely Massive Absorber

We will begin by studying resonance absorption due to an infinitely massive absorber distributed uniformly through an infinite medium of hydrogen. The infinite absorber mass implies that all neutron slowing down due to elastic scattering will be due to hydrogen. We will also ignore inelastic scattering processes. We have already solved the neutron slowing down equation (8-37) for this case in Section 8-II-A to find the flux

$$\phi(E) = \frac{\Sigma_s(E_0)}{\Sigma_t(E_0)} \frac{S_0}{E\Sigma_t(E)} p(E), \tag{8-67}$$

where the resonance escape probability to energy $E$, $p(E)$, is given by

$$p(E) = \exp\left[ -\int_E^{E_0} dE' \frac{\Sigma_a(E')}{E'\Sigma_t(E')} \right]. \tag{8-68}$$

We will apply this exact expression to calculate the resonance escape probability for a single resonance at energy $E_0$. For convenience we will ignore scattering from the infinitely massive absorber and absorption in hydrogen, by assuming $N_H\sigma_s^H \gg N_A\sigma_s^A$, $\sigma_\gamma^H \ll \sigma_\gamma^A$. If we denote the resonance escape probability for this particular resonance as $p$, then we find

$$p = \exp\left[ -\int_{E_0} \frac{dE'}{E'} \frac{N_A\sigma_\gamma^A(E')}{N_H\sigma_s^H + N_A\sigma_\gamma^A(E')} \right]. \tag{8-69}$$

The notation $\int_{E_0}$ indicates that the integral is to be performed over energies in the neighborhood of the resonance.

To proceed further, we must introduce an explicit form for the capture cross section $\sigma_\gamma^A(E)$. We will use the Doppler-broadened Breit–Wigner cross section developed in Section 2-I-D:

$$\sigma_\gamma^A(E) = \sigma_0 \frac{\Gamma_\gamma}{\Gamma} \psi(\zeta, x), \qquad \zeta = \Gamma\left(\frac{A}{4E_0kT}\right)^{1/2}, \qquad x = 2\left(\frac{E - E_0}{\Gamma}\right). \tag{8-70}$$

We will first evaluate $p$ in the limit in which the absorber concentration is sufficiently dilute that the scattering from hydrogen is dominant even at the resonance energy, that is, $N_A\sigma_0 \ll N_H\sigma_s^H$. This is known as the *infinite dilution approximation*, and it is equivalent to assuming that the absorber concentration is so dilute that the absorption resonance does not perturb the slowing down form of the flux. Using this approximation in Eq. (8-69), we find that

$$p \rightarrow \exp\left[ -\frac{N_A}{N_H\sigma_s^H} \int_{E_0} \frac{dE'}{E'} \sigma_\gamma^A(E') \right] \equiv p^\infty. \tag{8-71}$$

To proceed further, we note that the major contribution to the integral comes from those energies close to resonance, $E' \sim E_0$. Hence we can extract $1/E' \sim 1/E_0$ to find

$$\int_{E_0} \frac{dE'}{E'} \sigma_\gamma^A(E') \cong \frac{1}{E_0} \int_{E_0} dE' \, \sigma_\gamma^A(E') \cong \frac{\sigma_0 \Gamma_\gamma}{2E_0} \int_{-\infty}^{\infty} dx \, \psi(\zeta, x) = \frac{\sigma_0 \Gamma_\gamma \pi}{2E_0}, \quad (8\text{-}72)$$

where the limits of integration have been extended to infinity since only a minor contribution comes from the wings of the resonance. Hence in the infinite dilution limit

$$p^\infty = \exp\left[ -\frac{\pi N_A \sigma_0 \Gamma_\gamma}{2N_H \sigma_s^H E_0} \right]. \quad (8\text{-}73)$$

Several features of this result are of interest. First note that the resonance escape probability increases with increasing moderator density (or cross section), since then the neutrons slow down through the resonance more rapidly. This effect is particularly important in water moderated reactors because it leads to large negative power coefficients of reactivity. That is, increasing power and hence moderator temperature will decrease moderator density (usually via steam formation). Hence the resonance escape probability will decrease, thereby decreasing reactivity.

Next it should be noted that the resonance is more effective in absorbing neutrons if the resonance energy $E_0$ is lower. This is easily understood when it is recalled that the asymptotic collision density behavior is as $F(E) \sim 1/E$. Hence lower energy neutrons will experience more collisions with absorber nuclei and therefore a higher probability of being absorbed. For this reason, the most significant resonance absorption in thermal reactors occurs in the lower lying resonances of fertile materials such as the 6.67 eV resonance in $^{238}$U. The resonance parameters characterizing several of the lower lying resonances of $^{238}$U which are significant in thermal reactor design are listed in Table 8-2.

**TABLE 8-2: Low-Lying Resonance Data for $^{238}$U**

| $E_0$ | $\Gamma_n$(eV) | $\Gamma_\gamma$(eV) | $\sigma_0$(b) | $\Gamma_p$(eV) | $\frac{1}{2}(1 - \alpha_A)E_0$(eV) |
|---|---|---|---|---|---|
| 6.67 | .00152 | .026 | $2.16 \times 10^5$ | 1.26 | .055 |
| 20.90 | .0087 | .025 | $3.19 \times 10^4$ | 1.95 | .174 |
| 36.80 | .032 | .025 | $3.98 \times 10^4$ | 3.65 | .306 |
| 66.54 | .026 | .022 | $2.14 \times 10^4$ | 2.26 | .554 |
| 102.47 | .070 | .026 | $1.86 \times 10^4$ | 3.98 | .850 |
| 116.85 | .030 | .022 | $1.30 \times 10^4$ | 1.32 | .966 |
| 165.27 | .0032 | .018 | $2.41 \times 10^3$ | 0.98 | 1.37 |
| 208.46 | .053 | .022 | $8.86 \times 10^3$ | 2.63 | 1.73 |

Finally we should note that although $\sigma_\gamma^A(E)$ is temperature-dependent through the Doppler-broadening mechanism, the infinite dilution limit $p^\infty$ has no tempera-

ture dependence. However this might have been anticipated since we have already noted that in this approximation the neutron flux is not perturbed by the resonance.

Therefore we turn to the more general case of finite dilution. Unfortunately we are now hampered in our ability to obtain a closed form evaluation of the relevant integrals. If we substitute the form Eq. (8-70) for $\sigma_\gamma^A(E)$ into Eq. (8-69) and extend the limits of integration, we find that the general result for the resonance escape probability

$$p = \exp\left[ -\frac{\Gamma}{E_0} J(\zeta,\beta) \right]$$

(8-74)

must be written in terms of a tabulated function[9] $J(\zeta,\beta)$,

$$J(\zeta,\beta) \equiv \int_0^\infty dx \frac{\psi(\zeta,x)}{\beta + \psi(\zeta,x)}$$

(8-75)

where

$$\beta \equiv N_H \sigma_s^H \Gamma / N_A \sigma_0 \Gamma_\gamma.$$

(8-76)
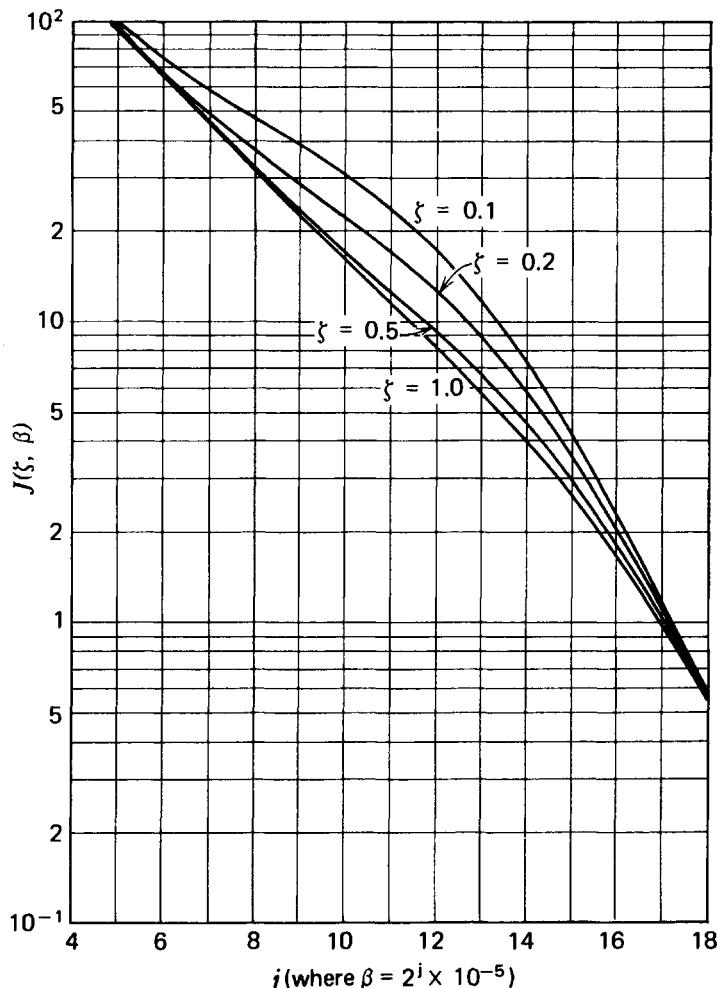


FIGURE 8-2. The function $J(\zeta,\beta)$ [L. Dresner, *Resonance Absorption in Nuclear Reactors*, Pergamon, New York (1960)].

It is apparent from this form that the finite dilution resonance integral is indeed temperature-dependent. In Figure 8-2 we have shown the function $J(\zeta,\beta)$ plotted versus $\beta$ for various values of the temperature parameter $\zeta$. From this plot it is apparent that as temperature $T$ increases, $\zeta$ decreases, implying that $J(\zeta,\beta)$ increases and hence that the resonance escape probability $p$ decreases. That is, resonance absorption increases with increasing temperature. This is the so-called *Doppler effect* referred to earlier in our discussion of temperature coefficients of reactivity.

**TABLE 8-3   The Function $J(\zeta,\beta)$ for $\zeta = 0.1$–$1.0$ and $\beta = 2^j \times 10^{-5\dagger}$**

| $j$ | $J(\zeta,\beta)$ | | | | | | | | | |
|---|---|---|---|---|---|---|---|---|---|---|
| | $\zeta=0.1$ | $\zeta=0.2$ | $\zeta=0.3$ | $\zeta=0.4$ | $\zeta=0.5$ | $\zeta=0.6$ | $\zeta=0.7$ | $\zeta=0.8$ | $\zeta=0.9$ | $\zeta=1.0$ |
| 0 | 4.979(2*) | 4.970(2) | 4.969(2) | 4.968(2) | 4.968(2) | 4.968(2) | 4.967(2) | 4.967(2) | 4.967(2) | 4.967(2) |
| 1 | 3.532 | 3.517 | 3.514 | 3.513 | 3.513 | 3.513 | 3.513 | 3.513 | 3.513 | 3.513 |
| 2 | 2.514 | 2.491 | 2.487 | 2.485 | 2.485 | 2.484 | 2.484 | 2.484 | 2.484 | 2.484 |
| 3 | 1.801 | 1.767 | 1.761 | 1.759 | 1.758 | 1.757 | 1.757 | 1.757 | 1.757 | 1.757 |
| 4 | 1.307 | 1.257 | 1.248 | 1.245 | 1.244 | 1.243 | 1.243 | 1.243 | 1.242 | 1.242 |
| 5 | 9.667(1) | 8.993(1) | 8.872(1) | 8.831(1) | 8.812(1) | 8.802(1) | 8.796(1) | 8.792(1) | 8.790(1) | 8.788(1) |
| 6 | 7.355 | 6.501 | 6.335 | 6.278 | 6.252 | 6.238 | 6.230 | 6.225 | 6.221 | 6.218 |
| 7 | 5.773 | 4.777 | 4.562 | 4.485 | 4.450 | 4.430 | 4.419 | 4.412 | 4.407 | 4.403 |
| 8 | 4.647 | 3.589 | 3.328 | 3.230 | 3.183 | 3.158 | 3.143 | 3.133 | 3.126 | 3.121 |
| 9 | 3.781 | 2.759 | 2.471 | 2.354 | 2.297 | 2.265 | 2.245 | 2.232 | 2.223 | 2.217 |
| 10 | 3.045 | 2.153 | 1.867 | 1.741 | 1.675 | 1.638 | 1.614 | 1.598 | 1.587 | 1.579 |
| 11 | 2.367 | 1.676 | 1.423 | 1.301 | 1.235 | 1.194 | 1.168 | 1.151 | 1.138 | 1.129 |
| 12 | 1.730 | 1.268 | 1.074 | 9.718(0) | 9.119(0) | 8.739(0) | 8.484(0) | 8.304(0) | 8.174(0) | 8.077(0) |
| 13 | 1.164 | 9.081(0) | 7.815(0) | 7.087 | 6.629 | 6.322 | 6.107 | 5.950 | 5.833 | 5.744 |
| 14 | 7.172(0) | 6.014 | 5.342 | 4.914 | 4.624 | 4.419 | 4.268 | 4.154 | 4.066 | 3.997 |
| 15 | 4.088 | 3.658 | 3.371 | 3.169 | 3.022 | 2.911 | 2.826 | 2.759 | 2.706 | 2.663 |
| 16 | 2.204 | 2.067 | 1.966 | 1.889 | 1.829 | 1.781 | 1.743 | 1.712 | 1.687 | 1.666 |
| 17 | 1.148 | 1.109 | 1.078 | 1.053 | 1.033 | 1.016 | 1.002 | 9.904(-1) | 9.805(-1) | 9.722(-1) |
| 18 | 5.862(-1) | 5.757(-1) | 5.671(-1) | 5.599(-1) | 5.539(-1) | 5.488(-1) | 5.445(-1) | 5.408 | 5.376 | 5.348 |
| 19 | 2.963 | 2.936 | 2.913 | 2.894 | 2.877 | 2.863 | 2.851 | 2.840 | 2.831 | 2.823 |
| 20 | 1.490 | 1.483 | 1.477 | 1.472 | 1.468 | 1.464 | 1.461 | 1.458 | 1.455 | 1.453 |
| 21 | 7.468(-2) | 7.452(-2) | 7.437(-2) | 7.424(-2) | 7.413(-2) | 7.403(-2) | 7.395(-2) | 7.388(-2) | 7.381(-2) | 7.375(-2) |
| 22 | 3.739 | 3.735 | 3.732 | 3.728 | 3.726 | 3.723 | 3.721 | 3.719 | 3.718 | 3.716 |
| 23 | 1.871 | 1.870 | 1.869 | 1.868 | 1.868 | 1.867 | 1.867 | 1.866 | 1.866 | 1.865 |
| 24 | 9.358(-3) | 9.356(-3) | 9.355(-3) | 9.352(-3) | 9.350(-3) | 9.349(-3) | 9.348(-3) | 9.346(-3) | 9.345(-3) | 9.344(-3) |
| 25 | 4.680 | 4.680 | 4.679 | 4.679 | 4.678 | 4.678 | 4.678 | 4.677 | 4.677 | 4.677 |
| 26 | 2.340 | 2.340 | 2.340 | 2.340 | 2.340 | 2.340 | 2.340 | 2.340 | 2.340 | 2.340 |
| 27 | 1.170 | 1.170 | 1.170 | 1.170 | 1.170 | 1.170 | 1.170 | 1.170 | 1.170 | 1.170 |
| 28 | 5.851(-4) | 5.851(-4) | 5.851(-4) | 5.851(-4) | 5.851(-4) | 5.851(-4) | 5.851(-4) | 5.851(-4) | 5.851(-4) | 5.851(-4) |
| 29 | 2.925 | 2.926 | 2.926 | 2.926 | 2.926 | 2.926 | 2.926 | 2.926 | 2.926 | 2.926 |
| 30 | 1.463 | 1.463 | 1.463 | 1.463 | 1.463 | 1.463 | 1.463 | 1.463 | 1.463 | 1.463 |
| 31 | 7.314(-5) | 7.314(-5) | 7.315(-5) | 7.315(-5) | 7.315(-5) | 7.315(-5) | 7.314(-5) | 7.314(-5) | 7.314(-5) | 7.314(-5) |

$\dagger$L. Dresner, *Resonance Absorption in Nuclear Reactors*, Pergamon, New York (1960).
*Numbers in parentheses are powers of 10, which multiply the entry next to which they stand and all unmarked entries below it.

To understand this behavior, recall that our earlier analysis indicated that increased temperature causes a resonance to broaden. However since the area under the resonance is essentially (almost) temperature-independent, the resonance peak drops with temperature. However the broadened resonance increases the energy range over which absorption occurs. This effect outweighs the slight lowering of the resonance peak and gives rise to an enhanced absorption with increasing temperature.

This effect arises because of the phenomenon of *self-shielding*. We will show later that the neutron flux is depressed (see Figure 8-3) for those energies in the neighborhood of the resonance. This effect is known as *energy* self-shielding since the strong absorption of the resonance tends to shield the absorber nuclei from neutrons with energy $E \sim E_0$ (the flux depression). (We will later study a related phenomenon known as *spatial* self-shielding.) As temperature increases, the resonance peak decreases, thereby decreasing self-shielding and the flux depression, and increasing resonance absorption [i.e., the energy-integrated reaction rate $\Sigma_a(E)\phi(E)$].
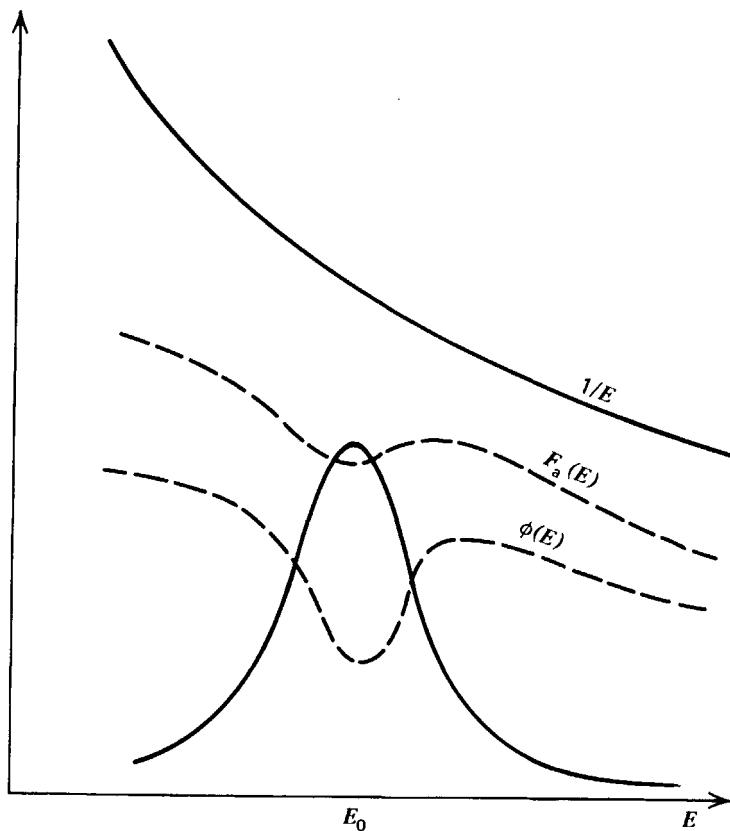


**FIGURE 8-3.    Flux depression in the neighborhood of a resonance.**

This latter interpretation also explains why the infinite dilution limit shows no temperature dependence, since in this case there is no flux depression (the absorber concentration is too low to perturb the flux) and hence no self-shielding.

## C. Resonance Integrals

We now turn our attention to the more general case of neutron slowing down in an infinite, homogeneous mixture of absorber and moderator. It is possible to cast the resonance escape probability characterizing this problem into a form very similar to that for hydrogeneous moderators, Eq. (8-68). If we imagine the neutrons being produced by a source of strength $S_0$ at energy $E_0$, then the total absorption rate experienced by neutrons while slowing down from energies $E_0$ to $E$ is just

$$\int_E^{E_0} dE' \, \Sigma_a(E')\phi(E').$$

Hence the resonance escape probability is just

$$p(E) = \frac{S_0 - \text{neutron absorption rate}}{S_0} = 1 - \frac{1}{S_0} \int_E^{E_0} dE' \, \Sigma_a(E') \phi(E'). \quad (8\text{-}77)$$

In a very similar manner we can define the resonance escape probability $p_i$ for any single, well-isolated resonance located at an energy $E_i$. To do so, we will assume that all absorption occurs in a number of well-separated resonances lying below the source energy $E_0$. If the individual resonances are sufficiently widely separated, then the flux occurring just above a given resonance at energy $E_i$ will have assumed the asymptotic form,

$$\phi(E) \sim \phi_{\text{asym}}(E) = \frac{S_{\text{eff}}^{(i)}}{\xi \Sigma_s E}, \qquad \bar{\xi} = \frac{\xi_A \Sigma_s^A + \xi_M \Sigma_s^M}{\Sigma_s^A + \Sigma_s^M}, \qquad (8\text{-}78)$$

where $S_{\text{eff}}^{(i)}$ is the original source strength $S_0$ reduced by the resonance-escape probabilities for all higher energy resonances—that is,

$$S_{\text{eff}}^{(i)} = S_0 \prod_j p_j, \qquad \text{where} \quad E_j > E_i. \qquad (8\text{-}79)$$

(See Figure 8-4.) Hence we can identify the absorption probability for the resonance at $E_i$ as just

$$\text{Absorption probability} = \frac{1}{S_{\text{eff}}^{(i)}} \int_{E_i} dE \, \Sigma_a^A(E) \phi(E), \qquad (8\text{-}80)$$
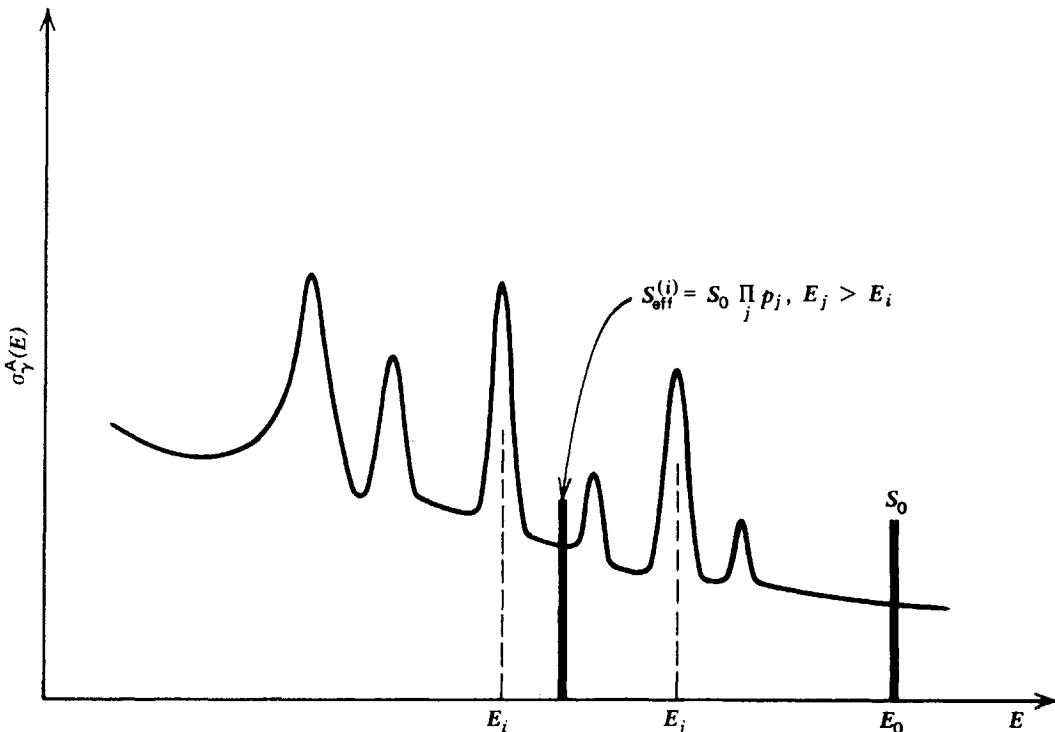


FIGURE 8-4. Definition of effective source for a well-separated resonance.

and thus the resonance escape probability for this particular resonance becomes just

$$p_i = 1 - \frac{1}{S_{\text{eff}}^{(i)}} \int_{E_i} dE\, \Sigma_a^A(E)\phi(E). \tag{8-81}$$

To write this in a more useful form, suppose we normalize the flux $\phi(E)$ so that far above the resonance it behaves as

$$\phi(E) \sim \frac{1}{E} \qquad \text{for} \quad E \gg E_i. \tag{8-82}$$

Then the resonance escape probability for the resonance is just

$$p_i = 1 - \frac{N_A}{\xi\Sigma_s} \int_{E_i} dE\, \sigma_\gamma^A(E)\phi(E), \qquad [\phi(E) \sim 1/E]. \tag{8-83}$$

This is still not sufficiently convenient for our purposes, since to compute the total resonance escape probability for a series of resonances, we would have to multiply the corresponding $p_i$ together as

$$p_{\text{total}} = \prod_i p_i. \tag{8-84}$$

To facilitate this calculation, we first note that in general the absorption probability $1 - p_i$ is quite small. Hence we can use the expansion

$$\exp[-(1-p_i)] \sim 1 - (1-p_i) + \cdots \sim p_i \tag{8-85}$$

to rewrite

$$p_i \cong \exp\left[-\frac{N_A}{\xi\Sigma_s} I_i\right], \tag{8-86}$$

where we have defined the *effective resonance integral* for the $i$th resonance as

$$I_i \equiv \int_{E_i} dE\, \sigma_\gamma^A(E)\phi(E), \qquad \left[\phi(E) \sim \frac{1}{E}\right]. \tag{8-87}$$

Then to compute the total resonance escape probability, we need only add the resonance integrals for each resonance

$$p_{\text{total}} = \prod_i p_i = \exp\left[-\frac{N_A}{\xi\Sigma_s} \sum_i I_i\right]. \tag{8-88}$$

The resonance integral $I_i$ is a very useful quantity for characterizing a resonance.

We first should note that $I_i$ has the dimensions of a microscopic cross section (barns), if we remember the normalization condition, $\phi(E) \sim 1/E$ for $E \gg E_i$. In effect, $I_i$ represents the average absorption cross section characterizing the resonance, averaged over the flux within the resonance. We will find that $I_i$ is largely independent of the properties of the moderator.

The resonance integral $I_i$ has yet another extremely important practical application since it can be used directly in the generation of multigroup constants. To see this, first recall the definition of the multigroup absorption cross section for a given group $g$:

$$\Sigma_{ag} \equiv \frac{\int_{E_g}^{E_{g-1}} dE\, \Sigma_a(E)\phi(E)}{\int_{E_g}^{E_{g-1}} dE\, \phi(E)}. \tag{8-89}$$

Now since the resonances are quite narrow, over most of the group energy range the flux behaves asymptotically as $\phi(E) \sim 1/E$ such that

$$\int_{E_g}^{E_{g-1}} dE\, \phi(E) = \ln(E_{g-1}/E_g). \tag{8-90}$$

Furthermore essentially all neutron absorption will occur in those resonances contained in group $g$. Hence using our earlier definition of the effective resonance integral, we find

$$\Sigma_{ag} = \frac{N_A \sum_{i \in g} I_i}{\ln(E_{g-1}/E_g)} = \frac{N_A \sum_{i \in g} I_i}{\Delta u_g}, \tag{8-91}$$

where $i \in g$ is written to indicate that only those resonances contained in the group $g$ contribute to $\Sigma_{ag}$, and $\Delta u_g$ represents the lethargy width of group $g$. Hence we can generate multigroup constants characterizing absorption directly by using resonance integrals. (We will later provide an alternative prescription using $p_i$.)

Therefore "all" we need to do is figure out a way to calculate or measure the resonance integrals themselves. We will now turn our attention toward several approximate schemes for doing this.

## D. Approximate Calculations of Resonance Integrals

We will now consider in more detail neutron slowing down through a single resonance characterizing an absorber (denoted by "A") distributed uniformly throughout a moderator ("M"). We will assume that the neutron flux has achieved its asymptotic behavior $\phi(E) \sim 1/E$ before reaching the resonance energy. We will furthermore assume that the moderator has a constant scattering cross section and a negligible absorption cross section.

The appropriate form of the neutron slowing down equation characterizing this

situation is

$$\Sigma_t(E)\phi(E) = \int_E^{\frac{E}{\alpha_M}} dE' \frac{\Sigma_s^M \phi(E')}{(1-\alpha_M)E'} + \int_E^{\frac{E}{\alpha_A}} dE' \frac{\Sigma_s^A(E')\phi(E')}{(1-\alpha_A)E'}. \qquad (8\text{-}92)$$

It is possible to solve this equation numerically.[10] However we will develop several simple approximate solutions based on assumptions concerning the width of the resonance.

Let us begin by noting several features of the cross sections that appear in this equation. We can effectively ignore the absorption cross section of the moderator over the range of the resonance to write

$$\Sigma_t^M(E) \sim \Sigma_s^M(E) = \Sigma_p^M, \qquad (8\text{-}93)$$

where we have further noted that scattering from the moderator is characterized by the potential scattering cross section $\Sigma_p^M$ which is essentially constant over the narrow range of the resonance.

The resonance absorber is characterized by a more complicated cross section dependence

$$\Sigma_t^A(E) = \Sigma_a^A(E) + \Sigma_{s,res}^A(E) + \Sigma_p^A, \qquad (8\text{-}94)$$

where we have separated the resonance and potential scattering components of the cross section. We can now characterize the effective width of the resonance by defining the *practical width* $\Gamma_p$ as the energy range over which the resonance cross section exceeds the nonresonance component (which is essentially just $\Sigma_p^A + \Sigma_p^M = \Sigma_p$). To estimate $\Gamma_p$, we can use the Breit–Wigner formula to compare

$$\Sigma_0 \left[ 4\left( \frac{E-E_0}{\Gamma} \right)^2 + 1 \right]^{-1} \sim \Sigma_p \qquad (8\text{-}95)$$

or

$$\Gamma_p = 2(E - E_0) \sim \sqrt{\frac{\Sigma_0}{\Sigma_p}}\ \Gamma. \qquad (8\text{-}96)$$

Typically for low-lying resonances in $^{238}$U, $\Sigma_0/\Sigma_p \sim 10^3$. Thus $\Gamma_p \rightarrow 30\Gamma \gtrsim .7$ eV which is much larger than the actual width of the resonance.

Nevertheless for all resonances of interest in reactor analysis, the practical width is much smaller than the average energy lost in a collision with a moderator nucleus

$$\overline{\Delta E}\,|_M = \frac{1}{2}(1 - \alpha_M)E_0 \gg \Gamma_p. \qquad (8\text{-}97)$$

This means that most of the range of integration, $E < E' < E/\alpha_M$, in the moderator integral in Eq. (8-92) will be sufficiently far from the resonance that the flux assumes its asymptotic form, $\phi(E) \rightarrow 1/E$, and hence we can replace the flux in the

integral with this asymptotic form with negligible error:

$$\int_E^{\frac{E}{\alpha_M}} \frac{dE'\Sigma_s^M\phi(E')}{(1-\alpha_M)E'} \cong \frac{\Sigma_s^M}{(1-\alpha_M)} \int_E^{\frac{E}{\alpha_M}} \frac{dE'}{E'}\left(\frac{1}{E'}\right) = \frac{\Sigma_s^M}{E}. \qquad (8\text{-}98)$$

If we substitute this into Eq. (8-92), we find that our slowing down equation becomes

$$\left[\Sigma_s^M + \Sigma_a^A(E) + \Sigma_s^A(E)\right]\phi(E) = \int_E^{\frac{E}{\alpha_A}} dE' \frac{\Sigma_s^A(E')\phi(E')}{(1-\alpha_A)E'} + \frac{\Sigma_s^M}{E}. \qquad (8\text{-}99)$$

The major approximation we will make in our solution of this equation will involve our treatment of the *absorber* scattering integral. This approximation will again be based on the relative width of the resonance, but now compared to the energy loss suffered in a collision with an absorber nucleus.

## 1. NARROW RESONANCE (NR) APPROXIMATION

We will first assume that the practical width $\Gamma_p$ of the resonance is small compared to the average energy loss suffered in a collision with the *absorber* nucleus:

$$\overline{\Delta E}\,|_A = \left(\frac{1-\alpha_A}{2}\right) E_0 \gg \Gamma_p. \qquad (8\text{-}100)$$

Then we can approximate the absorber scattering integral as we did that for the moderator by replacing $\phi(E)$ in the integrand by its asymptotic form

$$\int_E^{\frac{E}{\alpha_A}} dE' \frac{\Sigma_s^A(E')\phi(E')}{(1-\alpha_A)E'} \cong \frac{\Sigma_p^A}{(1-\alpha_A)} \int_E^{\frac{E}{\alpha_A}} \frac{dE'}{E'}\left(\frac{1}{E'}\right) = \frac{\Sigma_p^A}{E}. \qquad (8\text{-}101)$$

In the second integral we have noted that the absorber scattering cross section over most of this range is essentially just that for potential scattering $\Sigma_p^A$.

Using these results in Eq. (8-99), we find

$$\Sigma_t(E)\phi(E) = \frac{(\Sigma_s^M + \Sigma_p^A)}{E}. \qquad (8\text{-}102)$$

Hence the *narrow resonance approximation* to the flux is

$$\phi_{NR}(E) = \frac{(\Sigma_s^M + \Sigma_p^A)}{\Sigma_t(E)E}. \qquad (8\text{-}103)$$

We can calculate the corresponding expression for the resonance integral in the NR approximation as

$$I^{NR} = \int_{E_0} dE\sigma_\gamma^A(E)\phi_{NR}(E) = \int_{E_0} \frac{dE}{E}\sigma_\gamma^A(E)\left[\frac{\Sigma_s^M + \Sigma_p^A}{\Sigma_t(E)}\right]. \qquad (8\text{-}104)$$

This integral can now be computed using our Doppler-broadened resonance shapes, just as it was for hydrogen. Since the average energy loss per collision $(1 - \alpha_A)E_0/2$ increases with increasing energy $E_0$, we might expect the NR approximation to be valid for higher energy resonances. For lower energy resonances, the energy loss in collisions with absorber nuclei will no longer be larger than the practical width of the resonance $\Gamma_p$ and we must then consider an alternative approximation.

## 2. NARROW RESONANCE INFINITE MASS ABSORBER (NRIM) OR WIDE RESONANCE (WR) APPROXIMATION

We now consider the other limit in which the practical width of the resonance is very wide compared to the energy loss suffered in a collision with an absorber nucleus

$$\overline{\Delta E}\,|_A = \left(\frac{1 - \alpha_A}{2}\right)E_0 \ll \Gamma_p, \tag{8-105}$$

(although we continue to treat the resonance width as narrow compared to moderator energy loss $\overline{\Delta E}\,|_M$). This is occasionally known as the *wide resonance* case, although more frequently one obtains the corresponding approximation to the absorber scattering integral by assuming the absorber to be infinitely massive such that neutrons suffer no energy loss in a collision with the absorber. That is, we take the limit as $A \to \infty$ or $\alpha_A = (A - 1/A + 1)^2 \to 1$ to find

$$\lim_{\alpha_A \to 1} \int_E^{\frac{E}{\alpha_A}} \frac{dE'\,\Sigma_s^A(E')\phi(E')}{(1 - \alpha_A)E'} \to \Sigma_s^A(E)\phi(E) \lim_{\alpha_A \to 1} \frac{1}{E} \int_E^{\frac{E}{\alpha_A}} \frac{dE'}{(1 - \alpha_A)} = \Sigma_s^A(E)\phi(E).$$

$$\tag{8-106}$$

Then our slowing down equation [Eq. (8-99)] becomes

$$\Sigma_t(E)\phi(E) = \Sigma_s^A(E)\phi(E) + \frac{\Sigma_s^M}{E}. \tag{8-107}$$

We can then solve for the flux in the NRIM approximation as

$$\phi_{NRIM}(E) = \frac{\Sigma_s^M}{[\Sigma_t(E) - \Sigma_s^A(E)]E}, \tag{8-108}$$

and the corresponding resonance integral as

$$I^{NRIM} = \int_{E_0} \frac{dE}{E}\,\sigma_\gamma^A(E)\left[\frac{\Sigma_s^M}{\Sigma_t(E) - \Sigma_s^A(E)}\right]. \tag{8-109}$$

Notice that the NR and NRIM approximations differ only in the way in which scattering from the absorber nuclei is treated. If we note that usually the absorber density is sufficiently low that $\Sigma_s^M \gg \Sigma_p^A$ then in fact the only difference between the two forms for $I$ lies in the subtraction of the absorber scattering cross section $\Sigma_s^A(E)$ from the total cross section in the denominator of the NRIM expression for $I$.

If the absorber concentration is very small, $\Sigma_t(E) \sim \Sigma_s^M$, and we pass to the infinite dilution form of the resonance integral

$$I^\infty = \int_{E_0} \frac{dE}{E} \sigma_\gamma^A(E). \tag{8-110}$$

By comparing Eqs. (8-104) and (8-109) with (8-110), one finds that $I^\infty$ is larger than either $I^{NR}$ or $I^{NRIM}$. This is due to the *self-shielding* effect. If we examine either of the approximate forms, Eq. (8-103) or (8-108), for the flux $\phi(E)$ within the resonance, we note that the flux decreases as $\Sigma_a^A(E)$ increases—that is, *flux depression* occurs. This flux depression lowers the effective absorption in the resonance and hence $I$ is similarly decreased. We will find later in Chapter 10 that *spatial* self-shielding due to fuel lumping has the same effect on resonance absorption since it also reduces $I$.

One can go further and introduce the Doppler-broadened Breit–Wigner line shapes to calculate these resonance integrals in terms of resonance parameters. It is customary (although not always correct[11]) to neglect interference scattering such that our cross sections become

$$\sigma_s^A(E) \cong \sigma_0 \frac{\Gamma_n}{\Gamma} \psi(\zeta, x) + \sigma_p$$

$$\sigma_\gamma^A(E) \cong \sigma_0 \frac{\Gamma_\gamma}{\Gamma} \psi(\zeta, x). \tag{8-111}$$

Then inserting these into our expressions for the resonance integrals yields

$$I^{NR} = \frac{(\Sigma_s^M + \Sigma_p^A)\Gamma_\gamma}{N_A E_0} J(\zeta, \beta), \quad \beta \equiv \frac{\Sigma_s^M + \Sigma_p^A}{N_A \sigma_0}, \tag{8-112}$$

and

$$I^{NRIM} = \frac{\Sigma_s^M \Gamma}{N_A E_0} J(\zeta, \beta'), \quad \beta' \equiv \frac{\Sigma_s^M \Gamma_\gamma}{N_A \sigma_0 \Gamma}, \tag{8-113}$$

where the definition of the $J(\zeta, \beta)$ is given in Eq. (8-75).

Here $\beta$ is the parameter essentially characterizing the dilution of the absorber, while $\zeta$ characterizes the temperature. As $\beta$ or $\beta'$ becomes large, both the NR and NRIM forms approach the infinite dilution limit

$$I^{NR}(\beta \to \infty) = I^{NRIM}(\beta' \to \infty) = I^\infty = \frac{\sigma_0 \Gamma_\gamma \pi}{2E_0}. \tag{8-114}$$

As in the case of hydrogeneous moderators, we find that there is no temperature-dependence in this limit. If we recognize that the temperature range of most interest in reactor applications corresponds to $0.1 < \zeta < 1.0$, then we find that unless $1.6 \times 10^{-4} < \beta < 2.6$, there will be no temperature dependence of $I$ (and hence of $p$). For the range $\Sigma_s^M / N_A \sim 10{-}10^3$ b per absorber atom encountered in thermal reactor design, one can estimate the derivative of $I$ with respect to temperature as

$$\frac{\partial I}{\partial T} \sim 10^{-4}/^\circ C \Rightarrow \frac{\partial p}{\partial T} \sim -10^{-5}/^\circ C. \tag{8-115}$$

Hence in this parameter range, Doppler broadening will cause a significant decrease in $p$ with increasing temperature.

The NR approximation is commonly used for all but the lowest lying resonances for which the NRIM approximation is more satisfactory. In Table 8-4 we have given examples[12] of such calculations for several resonances in $^{238}$U. These are compared with direct numerical calculations of the resonance integral. Although neither approximation seems to yield satisfactory results for the resonances at intermediate energy,[13] when large numbers of resonances are accounted for, the errors tend to average out. For convenience, we have also summarized the results of these various schemes for handling resonance absorption in Table 8-5.

**TABLE 8-4:** Resonance Absorption Calculations[12]

| Resonance Energy $E_0$(eV) | $(1-p_i)$ NR | $(1-p_i)$ NRIM | $(1-p_i)$ Exact |
|---|---|---|---|
| 6.67 | 0.2376 (21%) | 0.1998 (1.8%) | 0.1963 |
| 21.0 | 0.07455 (+10.4%) | 0.07059 (+4.5%) | 0.06755 |
| 36.9 | 0.04739 (−18.6%) | 0.06110 (+5.0%) | 0.05820 |
| 81.3 | 0.010163 (+5.9%) | 0.008109 (−15.5%) | 0.009596 |
| 90. | 0.001114 (+0.9%) | 0.000998 (−9.6%) | 0.001104 |
| 117.5 | 0.009035 (−1.5%) | 0.009500 (+3.6%) | 0.009170 |
| 192. | 0.005086 (−28.6%) | 0.01228 (73.0%) | 0.007119 |
| 212. | 0.004440 (−11.6%) | 0.007689 (+53.1%) | 0.005021 |

**TABLE 8-5:** Resonance Integrals for Single Resonances

| | Hydrogen + Infinite Mass Absorption | NR Approximation | NRIM Approximation |
|---|---|---|---|
| Homogeneous Infinite dilution Zero temperature | $I = \dfrac{\sigma_0 \Gamma_\gamma \pi}{2E_0}$ | $I = \dfrac{\sigma_0 \Gamma_\gamma \pi}{2E_0}$ | $I = \dfrac{\sigma_0 \Gamma_\gamma \pi}{2E_0}$ |
| Homogeneous | $I = \dfrac{\sigma_0 \Gamma_\gamma \pi}{2E_0 a}$ | $I = \dfrac{\sigma_0 \Gamma_\gamma}{2E_0} \dfrac{\pi}{\sqrt{ac - b^2/4}}$ | $I = \dfrac{\sigma_0 \Gamma_\gamma \pi}{2E_0 a}$ |
| Finite dilution | | $a \equiv 1 + \dfrac{N_A \sigma_p^A}{N_M \sigma_s^M}$ | |
| Zero temperature | $a^2 \equiv 1 + \dfrac{N_A \sigma_0 \Gamma_\gamma}{N_H \sigma_s^H \Gamma}$ | $b = \dfrac{N_A \sigma_0}{N_M \sigma_s^M} \sqrt{\sigma_p^A / \pi \chi}$ | $a^2 \equiv 1 + \dfrac{N_A \sigma_0 \Gamma_\gamma}{N_M \sigma_s^M \Gamma}$ |
| | | $c \equiv a + \dfrac{N_A \sigma_0}{N_M \sigma_s^M}$ | |
| Homogeneous | $I = \dfrac{\Sigma_s^M \Gamma}{N_A E_0} J(\zeta, \beta)$ | $I = \dfrac{(\Sigma_s^M + \Sigma_p^A)}{N_A} \dfrac{\Gamma_\gamma}{E_0} J(\zeta, \beta)$ | $I = \dfrac{\Sigma_s^M}{N_A} \dfrac{\Gamma}{E_0} J(\zeta, \beta')$ |
| Finite dilution | | | |
| Finite temperature | $J(\zeta, \beta) \equiv \displaystyle\int_0^\infty \dfrac{\psi(\zeta, x)\,dx}{\beta + \psi(\zeta, x)}$ | $\beta \equiv \dfrac{\Sigma_s^M + \Sigma_p^A}{N_A \sigma_0}$ | $\beta' \equiv \dfrac{N_M \sigma_s^M \Gamma}{N_A \sigma_0 \Gamma_\gamma}$ |
| | $\beta \equiv \dfrac{N_H \sigma_s^H \Gamma}{N_A \sigma_0 \Gamma_\gamma}$ | | |

We will return later in Chapter 10 to discuss the modifications required in these results in order to account for heterogeneities (i.e., fuel lumping). Now, however, we will continue with our study of neutron slowing down in an effort to take account of spatial effects (i.e., finite media).

## III. NEUTRON SLOWING DOWN IN FINITE MEDIA

### A. The Lethargy-Dependent $P_1$ Equations

We now turn our attention to the determination of fast neutron spectra when the spatial dependence of the neutron flux must be considered. Since the effects of anisotropic scattering are usually significant, we will begin our study with the $P_1$ equations (4-153) and (4-154) rather than the energy-dependent diffusion equation. This will allow a far more consistent treatment of the spatial and energy variables than that provided by energy-dependent diffusion theory. It will be sufficient to consider the steady-state form of these equations in only a single spatial variable $x$ since our intent is to develop a rather simple treatment of the spatial dependence that we can use in the generation of fast group constants. It will prove convenient to rewrite the $P_1$ equations in the lethargy variable $u$ as

$$\frac{\partial J}{\partial x} + \Sigma_t(u)\phi(x,u) = \sum_{i=1}^{N} \int_0^u du' \, \Sigma_{s_0}^i(u' \to u)\phi(x,u') + S_0(x,u),$$

$$\frac{1}{3}\frac{\partial \phi}{\partial x} + \Sigma_t(u)J(x,u) = \sum_{i=1}^{N} \int_0^u du' \, \Sigma_{s_1}^i(u' \to u)J(x,u'), \qquad (8\text{-}116)$$

where $\Sigma_{s_0}^i(u' \to u)$ and $\Sigma_{s_1}^i(u' \to u)$ are the isotropic and linearly anisotropic components of the differential cross section characterizing *elastic* scattering from isotopic species "i." (Unless otherwise indicated, we will always use the cross section notation $\Sigma_s$ to refer only to elastic scattering in this section.) It should be noticed that we have restricted these equations to the description of neutron slowing down by truncating the upper limit of integration at $u' = u$ (that is, ignoring upscattering).

For the moment, we will include the effects of inelastic scattering and fission in the source term

$$S_0(x,u) \equiv \sum_{i=1}^{N} \int_0^u du' \, \Sigma_{in}^i(u' \to u)\phi(x,u') + \sum_{i=1}^{N} \chi_i(u) \int_0^\infty du' \, \nu_i \Sigma_f^i(u')\phi(x,u') + S_{ext}(x,u),$$

$$(8\text{-}117)$$

and focus our attention on approximate treatments of slowing down via elastic scattering. Although inelastic scattering can play a very important role in neutron slowing down (particularly in fast reactors), it is not nearly as susceptible to approximate treatments as elastic scattering and usually requires a direct multigroup treatment, discussion of which will be deferred until later in this section. It should also be noted that we have explicitly ignored any anisotropic components of inelastic scattering or fission by setting the source term $S_1(x,u) \equiv 0$ in the second $P_1$

equation (8-116). Our neglect of this anisotropic source component is motivated by recalling that both of these reactions involve compound nucleus formation in heavy nuclei and hence should be adequately described as processes that are isotropic in the LAB system.

To proceed further, we will now introduce the slowing down densities characterizing elastic scattering from each isotopic species by rewriting Eq. (8-18) in terms of the lethargy variable as

$$q_0^i(x,u) \equiv \int_0^u du' \int_u^\infty du'' \Sigma_{s_0}^i(u' \to u'') \phi(x,u'). \qquad (8\text{-}118)$$

We have inserted the subscript "0" to distinguish $q_0^i(x,u)$ from a closely related quantity defined in terms of the current density $J(x,u)$:

$$q_1^i(x,u) \equiv \int_0^u du' \int_u^\infty du'' \Sigma_{s1}^i(u' \to u'') J(x,u'). \qquad (8\text{-}119)$$

We can make these definitions a bit more explicit by recalling that the elastic scattering processes of greatest concern in nuclear reactor analysis involve s-wave scattering, for which we can write

$$\Sigma_{s_0}^i(u' \to u) = \begin{cases} \dfrac{\Sigma_s^i(u') e^{u'-u}}{(1-\alpha_i)}, & u - \ln\dfrac{1}{\alpha_i} < u' < u \\ 0, & \text{otherwise.} \end{cases} \qquad (8\text{-}120)$$

One can similarly show that for s-wave scattering,

$$\Sigma_{s_1}^i(u' \to u) = \begin{cases} \dfrac{\Sigma_s^i(u') e^{u'-u}}{(1-\alpha_i)} \left[ \left(\dfrac{A+1}{2}\right) e^{\frac{u'-u}{2}} - \left(\dfrac{A-1}{2}\right) e^{-\frac{u'-u}{2}} \right], & u - \ln\dfrac{1}{\alpha_i} < u' < u \\ 0, & \text{otherwise.} \end{cases}$$

$$(8\text{-}121)$$

Thus we can use these cross sections to write the slowing down densities in more explicit form. For example,

$$q_0^i(x,u) = \int_{u-\ln\frac{1}{\alpha_i}}^u du' \int_u^{u'+\ln\frac{1}{\alpha_i}} du'' \frac{\Sigma_s^i(u') e^{u'-u''}}{(1-\alpha_i)} \phi(x,u')$$

$$= \int_{u-\ln\frac{1}{\alpha_i}}^u du' \Sigma_s^i(u') \phi(x,u') \left[ \frac{e^{u'-u} - \alpha_i}{1-\alpha_i} \right]. \qquad (8\text{-}122)$$

To implement these definitions, we will differentiate the slowing down densities with respect to $u$:

$$\frac{\partial q_0^i}{\partial u} = \int_u^\infty du'' \Sigma_{s_0}^i(u \to u'') \phi(x,u) - \int_0^u du' \Sigma_{s_0}^i(u' \to u) \phi(x,u'), \qquad (8\text{-}123)$$

or noting that

$$\int_u^\infty du'' \Sigma_{s_0}^i(u \to u'') = \Sigma_s^i(u),$$
(8-124)

we find

$$\frac{\partial q_0^i}{\partial u} = \Sigma_s^i(u)\phi(x,u) - \int_0^u du' \Sigma_{s_0}^i(u' \to u)\phi(x,u').$$
(8-125)

In a very similar manner we can find

$$\frac{\partial q_1^i}{\partial u} = \bar{\mu}_{0_i}\Sigma_s^i(u)J(x,u) - \int_0^u du' \Sigma_{s_1}^i(u' \to u)J(x,u'),$$
(8-126)

where we have noted that

$$\int_u^\infty du'' \Sigma_{s_1}^i(u \to u'') = \bar{\mu}_{0_i}\Sigma_s^i(u).$$
(8-127)

We can now use Eqs. (8-125) and (8-126) to replace the elastic scattering terms in the $P_1$ equations (8-116) with the derivatives of the elastic slowing down densities:

$$\frac{\partial J}{\partial x} + \Sigma_{ne}(u)\phi(x,u) = -\sum_{i=1}^N \frac{\partial q_0^i}{\partial u} + S_0(x,u),$$

$$\frac{1}{3}\frac{\partial \phi}{\partial x} + \Sigma_{tr}(u)J(x,u) = -\sum_{i=1}^N \frac{\partial q_1^i}{\partial u}.$$
(8-128)

Here we have defined the *nonelastic* cross section

$$\Sigma_{ne}(u) \equiv \Sigma_t(u) - \Sigma_s^{el}(u) = \Sigma_t(u) - \sum_{i=1}^N \Sigma_s^i(u)$$
(8-129)

and the *transport* cross section

$$\Sigma_{tr}(u) \equiv \Sigma_t(u) - \bar{\mu}_0\Sigma_s^{el}(u) = \Sigma_t(u) - \sum_{i=1}^N \bar{\mu}_{0_i}\Sigma_s^i(u).$$
(8-130)

The $P_1$ equations in the form (8-128) will serve as our point of departure for the study of neutron slowing down in finite media. We would stress that the only essential approximation used in deriving these equations involves the assumption that the angular neutron flux $\phi(x,\mu,u)$ can be adequately represented by only a linearly anisotropic dependence on the angular variable $\mu$—that is, the $P_1$ approximation.

By introducing the slowing down densities, we have eliminated the integral terms characterizing elastic scattering. However in the process we have of course introduced additional dependent variables, $q_0^i(x,u)$ and $q_1^i(x,u)$. Although these

variables are formally defined in terms of the flux and current by Eqs. (8-118) and (8-119), it will prove convenient to seek alternative approximate equations for the slowing down densities that can be used to augment the $P_1$ equations (8-128).

## B. Approximate Treatments of Neutron Slowing Down—Continuous Slowing Down Theory

In most schemes used to generate fast neutron spectra, elastic scattering is treated using approximate methods that are usually referred to collectively as *continuous slowing down theory*. In such methods, an approximate differential equation is developed for each slowing down density by expanding the collision densities $\Sigma_s^i(u') \phi(x,u')$ and $\Sigma_s^i(u')J(x,u')$ which appear in the integrals of the exact definitions [Eqs. (8-118) and (8-119)] of the slowing down densities as Taylor series expansions about $u' = u$ and retaining only one or two terms of these expansions. This in effect replaces the original integral equation by a set of coupled first-order differential equations in the lethargy variable.

The motivation behind such an approximate treatment might be questioned when it is recognized that a direct solution of the multigroup representation of the original fast spectrum equations could be performed on any modern digital computer—particularly since the absence of upscattering would allow a direct successive solution of the multigroup equations for successively higher lethargies. However to generate such a fine-group representation, it is necessary to calculate fine-group constants by making a simple estimate of the intragroup flux, say $\phi(u) \sim$ constant. We have noted, however, that the scattering cross sections $\Sigma_s^i(u' \rightarrow u)$ characterizing elastic scattering vanish discontinuously outside of the collision interval, $u - \ln 1/\alpha_i < u' < u$. Such a stepwise behavior is difficult to approximate accurately by a multigroup representation. Hence it is to our advantage to replace the scattering integrals by smoothly varying terms more susceptible to a multigroup representation by seeking approximate equations for the slowing down densities, $q_0^i(x,u)$ and $q_1^i(x,u)$.

### 1. SLOWING DOWN IN HYDROGEN ($A = 1$)

We will begin by examining the particularly simple case of slowing down from hydrogen in which $A = 1$ and hence $\alpha = 0$. This case is a particularly appropriate starting point since it can be treated exactly. If we set $\alpha = 0$ in Eqs. (8-118) and (8-119), we find

$$q_0^H(x,u) = \int_0^u du' \, \Sigma_s^H(u')e^{u'-u}\phi(x,u'),$$

$$q_1^H(x,u) = \frac{2}{3} \int_0^u du' \, \Sigma_s^H(u') e^{3(u'-u)/2} J(x,u'). \tag{8-131}$$

However of more relevance is the fact that by differentiating these expressions, we can identify two simple differential equations,

$$\frac{\partial q_0^H}{\partial u} + q_0^H(x,u) = \Sigma_s^H(u)\phi(x,u),$$

$$\frac{\partial q_1^H}{\partial u} + \frac{3}{2}q_1^H(x,u) = \frac{2}{3}\Sigma_s^H(u)J(x,u), \tag{8-132}$$

which can be used to supplement the $P_1$ slowing down equations (8-128). It should be stressed that while these equations are *exact*, they only apply to the case of hydrogen.

## 2. THE AGE APPROXIMATION

For the more general case of nonhydrogeneous moderators, one can not obtain such differential equations exactly characterizing the slowing down densities. However essentially all treatments of elastic scattering attempt to obtain approximate differential equations for $q_0^i(x,u)$ and $q_1^i(x,u)$ in the form

$$\lambda_{0_i}\frac{\partial q_0^i}{\partial u} + q_0^i(x,u) = \beta_{0_i}\phi(x,u),$$

$$\lambda_{1_i}\frac{\partial q_1^i}{\partial u} + q_1^i(x,u) = \beta_{1_i}J(x,u). \tag{8-133}$$

To accomplish this one first notes that in many cases the elastic scattering collision density $\Sigma_s^i(u)\phi(u)$ is a slowly varying function of lethargy. For example, for zero absorption in an infinite medium far below source energies, we know that the asymptotic form of the collision density is in fact constant, $\Sigma_s^i(u)\phi(u) = S_0/\xi_i$. Thus if the system of interest is not too strongly absorbing, and if the collision interval is not too large—that is, if $A$ is large—we are tempted to expand the collision density appearing in the integrals of Eqs. (8-118) and (8-119) as Taylor expansions about $u' = u$ and retain only low-order terms:

$$\Sigma_s^i(u')\phi(x,u') \cong \Sigma_s^i(u)\phi(x,u) + (u'-u)\frac{\partial}{\partial u}\left[\Sigma_s^i(u)\phi(x,u)\right],$$

$$\Sigma_s^i(u')J(x,u') \cong \Sigma_s^i(u)J(x,u) + (u'-u)\frac{\partial}{\partial u}\left[\Sigma_s^i(u)J(x,u)\right]. \tag{8-134}$$

If we substitute the first of these expansions into Eq. (8-118), we find

$$q_0^i(x,u) \cong \xi_i\Sigma_s^i(u)\phi(x,u) + a_i\frac{\partial}{\partial u}\left[\Sigma_s^i(u)\phi(x,u)\right], \tag{8-135}$$

where we have identified

$$\xi_i \equiv \int_{u-\ln\frac{1}{\alpha_i}}^{u} du'\left[\frac{e^{u'-u}-\alpha_i}{1-\alpha_i}\right] = 1 - \frac{\alpha_i\ln\frac{1}{\alpha_i}}{1-\alpha_i}, \tag{8-136}$$

$$a_i \equiv \int_{u-\ln\frac{1}{\alpha_i}}^{u} du'\left[\frac{e^{u'-u}-\alpha_i}{1-\alpha_i}\right](u'-u) = \frac{\alpha_i\left(\ln\frac{1}{\alpha_i}\right)^2}{2(1-\alpha_i)} - \xi_i. \tag{8-137}$$

It is common to truncate Eq. (8-135) after only one term to write

$$q_0^i(x,u) \cong \xi_i\Sigma_s^i(u)\phi(x,u). \tag{8-138}$$

This result is known as the *age approximation* or sometimes as *continuous slowing*

*down theory*. The former name will only become apparent in Section 8-IV-C. The latter name arises because the neglect of higher order terms in the expansion of the collision density effectively implies that neutrons lose only an infinitesimal amount of energy in each collision.

To proceed further, we will assume that we can rather arbitrarily set

$$q_1^i(x,u) \equiv 0, \qquad (8\text{-}139)$$

that is, we will neglect anisotropic energy exchange. Then the second of equations [Eq. (8-128)] can be solved for

$$J(x,u) = -[3\Sigma_{tr}(u)]^{-1} \frac{\partial \phi}{\partial x} \equiv -D(u) \frac{\partial \phi}{\partial x}, \qquad (8\text{-}140)$$

which yields just Fick's law. This can then be substituted into the first equation (8-128) to find

$$-\frac{\partial}{\partial x} D(x,u) \frac{\partial \phi}{\partial x} + \Sigma_{ne}(u)\phi(x,u) = -\frac{\partial}{\partial u} \left[ \bar{\xi}(u)\Sigma_s(u)\phi(x,u) \right] + S_0(x,u), \qquad (8\text{-}141)$$

where we have used the age approximation for all isotopes in the system. This is known as the *age-diffusion equation*. It is sometimes also referred to as *inconsistent $P_1$ theory* since we have not treated the slowing density $q_1^i(x,u)$ in the same fashion as we treated $q_0^i(x,u)$.

The age-diffusion equation is primarily of historical importance in reactor analysis since it is restricted to slowing down in heavy mass moderators such as graphite and would certainly not apply to hydrogeneous moderators. It is of interest simply because it can be solved exactly in certain special cases (as we will see in Section 8-IV-C).

We can partially alleviate the restriction to heavy mass moderators by using the exact equations (8-132) to describe hydrogen moderation and then use the age approximation (inconsistent $P_1$) only to describe nonhydrogeneous species ($A > 1$). This scheme, which is one of the common methods used in computing fast spectra in LWRs, is known as the *Selengut–Goertzel method*.

It is a relatively simple matter to remove the inconsistency present in the age approximation [i.e., Eq. (8-139)] by substituting Eq. (8-134) into the definition of $q_1^i(x,u)$ given by Eq. (8-119) to find

$$q_1^i(x,u) \cong \zeta_i \Sigma_s^i(u) J(x,u) \qquad (8\text{-}142)$$

where

$$\zeta_i \equiv \frac{(1+\gamma_i)^2}{\gamma_i^2} \left\{ \frac{1+\gamma_i}{9} \left( 1 - \alpha^{3/2} \left( \frac{3}{2} \ln 1/\alpha + 1 \right) \right) - (1-\gamma_i) \left( 1 - \alpha^{1/2} \left( \frac{1}{2} \ln 1/\alpha + 1 \right) \right) \right\},$$

$$\gamma_i \equiv A_i^{-1}. \qquad (8\text{-}143)$$

If Eqs. (8-138) and Eq. (8-142) are both used in the $P_1$ equations, one arrives at the *consistent $P_1$ approximation*.

One other modification occasionally encountered in the treatment of neutron slowing down in weakly absorbing systems involves retaining both terms in the expansion (8-135) to write

$$q_0(x,u) \cong \xi\Sigma_s(u)\phi(x,u) + a\frac{\partial}{\partial u}[\Sigma_s(u)\phi(x,u)]$$

$$\cong \xi\Sigma_s(u)\phi(x,u) + \frac{a}{\xi}\frac{\partial}{\partial u}[q_0(x,u)] \qquad (8\text{-}144)$$

where we have reintroduced Eq. (8-138) into the second term to achieve a consistent second-order expansion. Now in an infinite, sourceless medium, Eq. (8-128) can be written as

$$-\frac{\partial q_0}{\partial u} = \Sigma_{ne}(u)\phi(u). \qquad (8\text{-}145)$$

If we substitute Eq. (8-144) into Eq. (8-145), we can solve for

$$q_0(x,u) \cong \left(\xi\Sigma_s(u) - \frac{a}{\xi}\Sigma_{ne}(u)\right)\phi(x,u). \qquad (8\text{-}146)$$

However we can approximate $a/\xi \sim -\xi$ (see Problem 8-29) to write

$$q_0(x,u) \cong \xi\Sigma_t(u)\phi(x,u). \qquad (8\text{-}147)$$

This form of the age approximation is frequently used instead of our earlier form given by Eq. (8-138). For weak absorption, both expressions yield very similar results.

## 3. THE GRUELING–GOERTZEL APPROXIMATION

Thus far we have provided prescriptions for handling neutron slowing down in either very heavy (age theory) or hydrogeneous (exact) moderators. However neither of these schemes is adequate for light, nonhydrogeneous materials—with deuterium $^2D$ being a prime villian. Hence we are motivated to construct an alternative to the age approximation for nonhydrogeneous media.

To accomplish this, we will use the Taylor expansion of the collision densities to write approximate equations for $q_0^i(x,u)$ and $q_1^i(x,u)$ in the forms Eq. (8-133). To illustrate how this may be accomplished, suppose we use the expansion Eq. (8-135) to calculate

$$\lambda_{0i}\frac{\partial q_0^i}{\partial u} + q_0^i \cong \lambda_{0i}\left[\xi_i\frac{\partial}{\partial u}(\Sigma_s^i\phi) + a_i\frac{\partial^2}{\partial u^2}(\Sigma_s^i\phi)\right] + \left[\xi_i\Sigma_s^i\phi + a_i\frac{\partial}{\partial u}(\Sigma_s^i\phi)\right]. \qquad (8\text{-}148)$$

To cast this into the form of Eq. (8-133), we can ignore terms in $\partial^2\phi/\partial u^2$ as being of higher order and choose $\lambda_{0i}$ so that terms in $\partial\phi/\partial u$ cancel. This yields

$$\lambda_{0i} \equiv \frac{1 - \alpha_i\left(1 + \ln\frac{1}{\alpha_i} + \frac{1}{2}\ln^2\frac{1}{\alpha_i}\right)}{1 - \alpha_i\left(1 + \ln\frac{1}{\alpha_i}\right)} , \quad \beta_{0i} \equiv \xi_i\Sigma_s^i(u). \qquad (8\text{-}149)$$

A very similar calculation will yield the second of equations (8-133) with the choice

$$\lambda_{1i} = -\left(\frac{(1+\gamma_i)^2}{4\gamma_i}\left\{\frac{(1+\gamma_i)}{3}\left[\frac{8}{9} - \alpha_i^{3/2}\left(\ln^2 1/\alpha_i - \frac{4}{3}\ln 1/\alpha_i + \frac{8}{9}\right)\right]\right.\right.$$

$$\left.\left. -(1-\gamma_i)\left[8 - \alpha_i^{1/2}\left(\ln^2 1/\alpha_i - 4\ln 1/\alpha_i + 8\right)\right]\right\}\zeta_i^{-1}, \quad \beta_{1i} = \zeta_i\Sigma_s^i. \quad (8\text{-}150)$$

Augmenting the set of $P_1$ equations (8-128) with Eq. (8-133) yields what is known as the *Greuling–Goertzel approximation*. Since higher order terms in the collision density expansion have been retained in this scheme, the Greuling–Goertzel approximation will provide a far more accurate treatment of intermediate mass moderators such as $^2D$ or $^4Be$ than that provided by age theory. This approximation also has the property that it reduces to the exact equations describing hydrogen in the limit $A \to 1$.

## 4. SUMMARY OF THE $P_1$ SLOWING DOWN EQUATIONS

It is convenient to summarize these various approximate treatments of neutron slowing down by writing the $P_1$ equations as

$$\frac{\partial J}{\partial x} + \Sigma_{ne}(u)\phi(x,u) = -\frac{\partial q_0^H}{\partial u} - \sum_i \frac{\partial q_0^{NH_i}}{\partial u} + S_0(x,u),$$

$$\tag{8-151}$$

$$\frac{1}{3}\frac{\partial\phi}{\partial x} + \Sigma_{tr}(u)J(x,u) = -\frac{\partial q_1^H}{\partial u} - \sum_i \frac{\partial q_1^{NH_i}}{\partial u},$$

where the slowing down densities are given by the equations

$$\frac{\partial q_0^H}{\partial u} + q_0^H(x,u) = \Sigma_s^H\phi(x,u),$$

$$\frac{2}{3}\frac{\partial q_1^H}{\partial u} + q_1^H(x,u) = \frac{4}{9}\Sigma_s^H J(x,u), \text{ (exact treatment of H)}$$

$$\tag{8-152}$$

$$\lambda_{0i}\frac{\partial q_0^{NH_i}}{\partial u} + q_0^{NH_i}(x,u) = \beta_{0i}\phi(x,u),$$

$$\lambda_{1i}\frac{\partial q_1^{NH_i}}{\partial u} + q_1^{NH_i}(x,u) = \beta_{1i}J(x,u), \text{ (approximate treatment of NH)}.$$

Note we have separated the treatment of hydrogenous (H) from nonhydrogeneous (NH) slowing down. The various approximations we have discussed can then be characterized by a particular choice of the coefficients $\lambda_{0i}$, $\lambda_{1i}$, $\beta_{0i}$, and $\beta_{1i}$. We have summarized these choices in Table 8-6 below:

**TABLE 8-6:** Choice of Parameters for Continuous Slowing Down Models

|  | $\lambda_{0i}$ | $\lambda_{1i}$ | $\beta_{0i}$ | $\beta_{1i}$ |
|---|---|---|---|---|
| Age approximation Selengut–Goertzel | 0 | 0 | $\xi_i \Sigma_s^{(i)}$ | 0 |
| Consistent age approximation | 0 | 0 | $\xi_i \Sigma_s^{(i)}$ | $\gamma_i \Sigma_s^{(i)}$ |
| Greuling–Goertzel (s-wave scattering) | Eq. (8-149) | Eq. (8-150) | $\xi_i \Sigma_s^{(i)}$ | $\gamma_i \Sigma_s^{(i)}$ |

These equations can be rather easily solved on a digital computer provided the spatial dependence can be simplified.

## 5. TREATMENT OF THE SPATIAL DEPENDENCE IN THE $P_1$ SLOWING DOWN EQUATIONS

Recall that we are going to use the solution of the $P_1$ slowing down equations to generate fast group constants. Hence we only need a crude method to account for gross leakage effects. In particular we will assume that the lethargy and spatial dependence of the flux are separable and furthermore characterize the spatial dependence of each of the variables by a simple buckling mode. For example, the flux would be written as

$$\phi(x,u) = \phi(u)\exp(iBx), \qquad (8-153)$$

with similar expressions for current, source, and slowing down densities. That is, we approximate the spatial dependence by a single Fourier mode, $\exp(iBx)$. (This turns out to be somewhat more convenient than choosing a slab geometry mode such as $\cos Bx$ since it results in different spatial variation for the flux and the current when the real part of the solutions is taken.) Here the parameter $B$ will characterize the leakage in each region of the core in which the neutron spectrum $\phi(u)$ is to be calculated, and must be chosen from other considerations. For example, if we were considering a bare, homogeneous reactor we know the flux would indeed be separable, and $B$ would be determined by

$$\nabla^2 \psi(\mathbf{r}) + B^2 \psi(\mathbf{r}) = 0. \qquad (8-154)$$

More generally, the flux will not be separable in $\mathbf{r}$ and $u$, but $B^2$ can be regarded as characterizing the average core leakage. In the event that an accurate estimate is required, one could first estimate $B^2$, calculate group constants, use these in a multigroup diffusion calculation of the flux, and then use this flux to calculate a new $B^2 \sim \langle \nabla^2 \phi / \phi \rangle$. This improved estimate of $B^2$ could then be used to regenerate the group constants. Fortunately multigroup constants are rarely sufficiently sensitive to the choice of $B^2$ to require such an iterative approach.

Assuming for the moment that we have specified $B^2$, we can then substitute the

separable forms Eq. (8-153) into the $P_1$ equations to arrive at

$$iBJ(u) + \Sigma_{ne}(u)\phi(u) = -\frac{dq_0^H}{du} - \sum_i \frac{dq_0^{NH_i}}{du} + S_0(u),$$

(8-155)

$$\frac{iB}{3}\phi(u) + \Sigma_{tr}(u)J(u) = -\frac{dq_1^H}{du} - \sum_i \frac{dq_1^{NH_i}}{du}$$

augmented by the set

$$\frac{dq_0^H}{du} + q_0^H(u) = \Sigma_s^H \phi(u),$$

$$\frac{2}{3}\frac{dq_1^H}{du} + q_1^H(u) = \frac{4}{9}\Sigma_s^H J(u),$$

(8-156)

and

$$\lambda_{0i}\frac{dq_0^{NH_i}}{du} + q_0^{NH_i}(u) = \beta_{0i}\phi(u),$$

$$\lambda_{1i}\frac{dq_1^{NH_i}}{du} + q_1^{NH_i}(u) = \beta_{1i}J(u).$$

Hence we now have arrived at a set of simple, first-order differential equations that we can integrate numerically. We should recall here that inelastic scattering and fission have been included in the source term as

$$S_0(u) = \sum_{i=1}^N \int_0^u du' \Sigma_{in}^i(u' \rightarrow u)\phi(u') + \sum_{i=1}^N \chi_i(u)\int_0^\infty du' \nu_i\Sigma_f^i(u')\phi(u') + S_{ext}(u).$$

(8-157)

## 6. AN ALTERNATIVE TREATMENT OF SPATIAL DEPENDENCE—THE $B_1$ METHOD[15]

Thus far we have considered approximating the spatial dependence of the solutions to the $P_1$ slowing down equations by a single mode of the form $\exp(iBx)$. There is an alternative scheme that bypasses the $P_1$ equations entirely, and for completeness we will sketch its derivation here. To do so, we must return to the steady-state transport equation, written in its one-dimensional form, Eq. (4-48), as

$$\mu\frac{\partial\varphi}{\partial x} + \Sigma_t(u)\varphi(x,\mu,u) = \int_{-1}^{+1}d\mu'\int_0^u du'\Sigma_s(u' \rightarrow u, \mu' \rightarrow \mu)\varphi(x,\mu',u') + S(x,\mu,u).$$

(8-158)

Now assume an angular flux and source spatial dependence of the form similar to that in Eq. (8-153):

$$\varphi(x,\mu,u) = \varphi(\mu,u)e^{iBx},$$

$$S(x,\mu,u) = \frac{S(u)}{2}e^{iBx}.$$

(8-159)

(Note that we have assumed an isotropic source consistent with our earlier assumptions concerning fission and inelastic scattering.) Then we find

$$[\Sigma_t(u) + iB\mu]\varphi(\mu, u) = \int_{-1}^{+1} d\mu' \int_0^u du' \Sigma_s(u' \to u, \mu' \to \mu)\varphi(\mu', u') + \frac{S(u)}{2}. \quad (8\text{-}160)$$

At this point, if we multiplied by 1 or $\mu$ and integrated over $\mu$ and then expanded $\varphi = 1/2\phi(u) + 3/2\mu J(u)$, we would rederive the $P_1$ equations. Instead suppose we first divide by $(\Sigma_t + iB\mu)$ and furthermore assume only linearly anisotropic scattering to write:

$$\varphi(\mu, u) = (\Sigma_t + iB\mu)^{-1} \left[ \frac{1}{2} \int_0^u du' \Sigma_{s0}(u' \to u)\phi(u') \right.$$

$$\left. + \frac{3\mu}{2} \int_0^u du' \Sigma_{s1}(u' \to u) J(u') + \frac{S(u)}{2} \right]. \quad (8\text{-}161)$$

Now multiply by 1 and $\mu$ and integrate over $\mu$ to find the coupled pair of equations:

$$\phi(u) = \frac{A(u)}{\Sigma_t(u)} \left[ \int_0^u du' \Sigma_{s0}(u' \to u)\phi(u') + S_0(u) \right]$$

$$+ \frac{3i}{B} [1 - A(u)] \int_0^u du' \Sigma_{s1}(u' \to u) J(u'),$$

$$J(u) = \frac{i}{B} [1 - A(u)] \left[ \int_0^u du' \Sigma_{s0}(u' \to u)\phi(u') + S_0(u) \right]$$

$$+ \frac{3\Sigma_t(u)}{B^2} [1 - A(u)] \int_0^u du' \Sigma_{s1}(u' \to u) J(u'),$$

$$A(u) \equiv \frac{\tan^{-1}[B/\Sigma_t(u)]}{B/\Sigma_t(u)}. \quad (8\text{-}162)$$

After some rearranging, one can rewrite these equations as

$$iBJ(u) + \Sigma_t(u)\phi(u) = \int_0^u du' \Sigma_{s0}(u' \to u)\phi(u') + S_0(u),$$

$$\frac{iB}{3}\phi(u) + \gamma(u)\Sigma_t(u)J(u) = \int_0^u du' \Sigma_{s1}(u' \to u) J(u'), \quad (8\text{-}163)$$

where

$$\gamma(u) = \frac{\left(\frac{B}{\Sigma_t}\right)^2 \tan^{-1}\left(\frac{B}{\Sigma_t}\right)}{3\left[\frac{B}{\Sigma_t} - \tan^{-1}\left(\frac{B}{\Sigma_t}\right)\right]} \cong 1 + \frac{4}{15}\left(\frac{B}{\Sigma_t}\right). \quad (8\text{-}164)$$

Upon rewriting the scattering integrals in terms of slowing down densities, one can recognize that the $B_1$ *equations* above are very similar to the $P_1$ equations, except for the appearance of the factor $\gamma$. For bare slab geometries, the $B_1$ equations are found to yield slightly more accurate spectra. In fact, if only linearly anisotropic scattering is present, the $B_1$ equations provide an exact treatment of angular effects. However for more complicated geometries, as well as for large thermal reactor cores in which leakage is relatively small, both methods yield very similar results. The more recent tendency has been to generate group constants using the $B_1$ equations. However because of their simplicity (and mathematical similarity), we will continue our discussion using the $P_1$ equations for the calculation of fast neutron spectra.

## IV. FAST SPECTRUM CALCULATIONS AND FAST GROUP CONSTANTS

We now turn our attention toward the application of the $P_1$ and $B_1$ equations to the calculation of fast neutron spectra suitable for the generation of fast group constants to be used in few-group diffusion codes. We will study three different schemes that can be used to generate fast group constants. The first such scheme will be the numerical solution of the $P_1$ (or $B_1$) equations by discretizing these equations on a fine group mesh (typically 50–100 groups). This scheme was originally developed for the analysis of LWRs, and when applied to the generation of group constants for hydrogeneous systems, it is known as the MUFT technique.[16] For many years it and its various modifications such as the GAM codes[17] have been the mainstay of thermal reactor design. For this reason, and also because the techniques used in the MUFT-GAM codes to solve the $P_1$ (or $B_1$) equations are common to other fast spectrum codes, we will consider this scheme in some detail.

We will also consider the calculation of fast reactor spectra in which inelastic scattering is of primary importance and for which a direct solution of the $P_1$ equations over an ultrafine group structure is required. Then finally for completeness (and historical sentiment), we will briefly develop the analytical age-diffusion model (although such a model has very little relevance to modern day reactor calculations).

## A. MUFT–GAM TYPE FAST SPECTRUM CALCULATIONS

Let us begin by considering the $P_1$ equations applied to describe neutron slowing down in a mixture of hydrogen plus a single heavier isotope of mass number $A$. (The modifications of the method we will describe to handle more general mixtures of moderators is straightforward.) To be specific, we will utilize the age approximation to describe slowing down from this heavy isotope coupled with an exact treatment of hydrogen—that is, we will use the Selengut–Goertzel description. It should be stressed that the procedure we will outline would apply equally well to the other approximate treatments of slowing down that we have discussed (e.g., the consistent $P_1$ approximation or the Goertzel–Greuling method).

The $P_1$ equations characterizing a single spatial mode can then be written as

$$iBJ + \left[ \Sigma_a^S + \Sigma_a^R + \Sigma_{in} \right]\phi = - \frac{dq_0^H}{du} - \frac{dq_0^A}{du} + \int_0^u du' \, \Sigma_{in}^A(u' \to u)\phi(u') + \chi \,,$$

$$\frac{iB}{3}\phi + \Sigma_{tr}J = - \frac{dq_1^H}{du} \,,$$

$$\frac{dq_0^H}{du} + q_0^H = \Sigma_s^H \phi, \tag{8-165}$$

$$\frac{2}{3} \frac{dq_1^H}{du} + q_1^H = \frac{4}{9} \Sigma_s^H J,$$

$$q_0^A = \xi_A \Sigma_s^A \phi.$$

Here we have found it convenient to separate the removal cross section into three parts:

$$\Sigma_a^S = \text{``smooth'' absorption cross section,}$$

$$\Sigma_a^R = \text{``resonance'' absorption cross section,}$$

$$\Sigma_{in} = \int_0^\infty du' \, \Sigma_{in}^A(u \to u') \equiv \text{inelastic scattering cross section.}$$

Remember that removal due to elastic scattering has already been accounted for in the terms involving the slowing down density.

To solve these equations, we will now discretize them into multigroup form. We will choose a fine group structure in the lethargy variables as shown in Figure 8-5. We will label these fine groups with a subscript $n$ to avoid confusion with the coarse group structure denoted earlier by $g$.

The set of equations (8-165) will now be averaged over the fine group structure in a manner very similar to the multigroup equations developed in Chapter 7. For example, the group averages of dependent variables such as $\phi(u)$, $J(u)$, or $q(u)$ are defined as:

$$\phi_n \equiv \frac{1}{\Delta u_n} \int_{u_{n-1}}^{u_n} du \, \phi(u). \tag{8-166}$$

Simple difference expressions can be used for derivatives:

$$\int_{u_{n-1}}^{u_n} du \frac{dq}{du} = q_n - q_{n-1}. \tag{8-167}$$

The fine group constants characterizing smoothly varying (nonresonant) cross sections are determined by simple averaging:

$$\Sigma_{a_n}^S \equiv \frac{1}{\Delta u_n} \int_{u_{n-1}}^{u_n} du \, \Sigma_a^S(u), \tag{8-168}$$

or

$$\Sigma_{n'n}^A \equiv \frac{1}{\Delta u_n} \frac{1}{\Delta u_{n'}} \int_{u_{n-1}}^{u_n} du \int_{u_{n'-1}}^{u_{n'}} du' \, \Sigma_{in}^A(u' \to u). \tag{8-169}$$
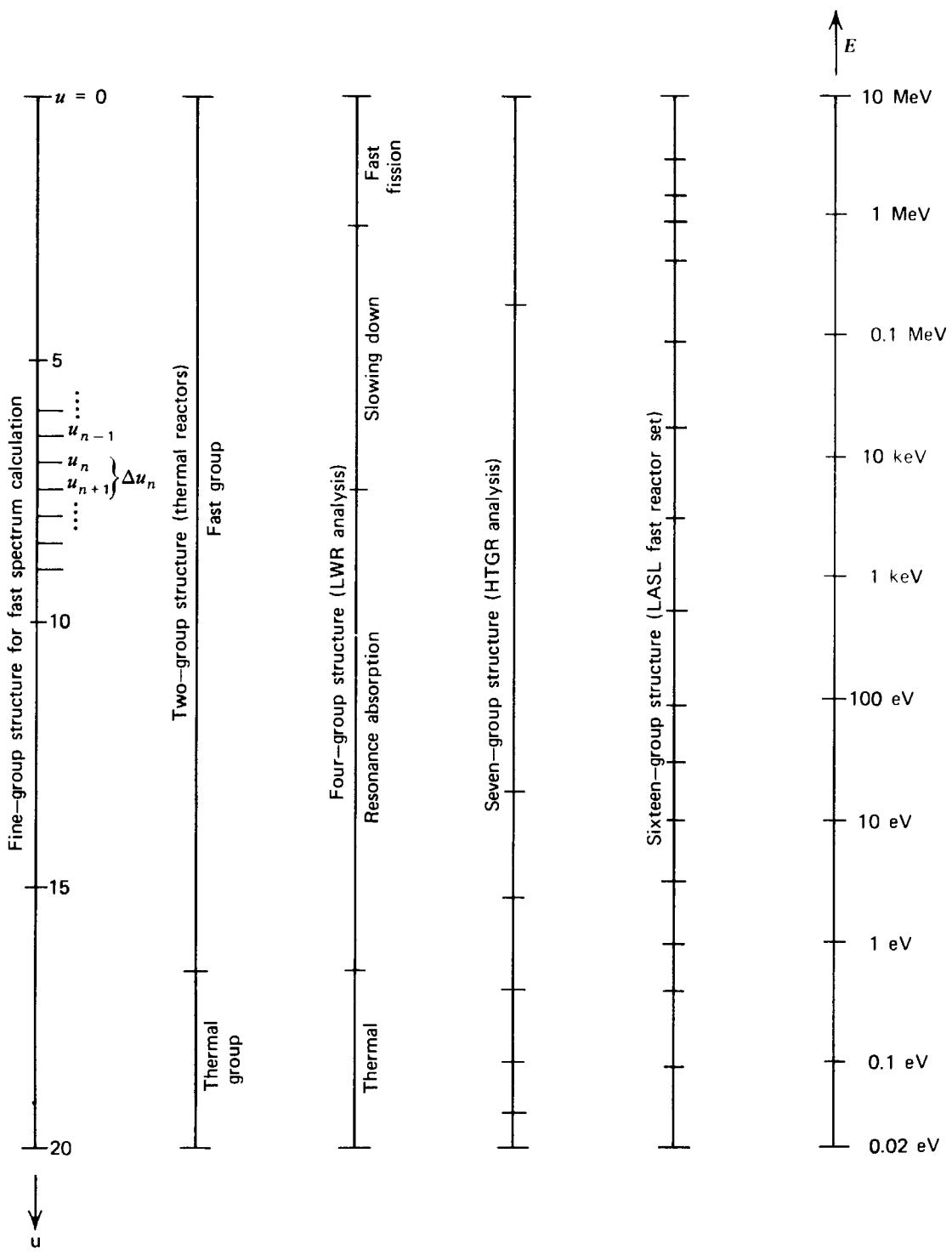
**FIGURE 8-5.** Typical few-group structures.

The group constants representing resonance absorption in the group can either be calculated in terms of the resonance integrals characterizing resonances in the group:

$$\Sigma_{a_n}^R = \frac{N_A}{\Delta u_n} \sum_{i \in n} I_i,$$

(8-170)

or in terms of the resonance escape probability $p_n$ for the group by noting:

$$\int_{u_{n-1}}^{u_n} du\, \Sigma_a^R(u)\phi(u) = (1 - p_n)\big(q_{0_{n-1}}^H + q_{0_{n-1}}^A\big).$$

(8-171)

Hence the multigroup form of the slowing down equations (8-165) can be written as:

$$iBJ_n\Delta u_n + \Sigma_{a n}^S \phi_n \Delta u_n + \Sigma_{\text{in}_n}\phi_n\Delta u_n + (1 - p_n)\left[ q_{0_{n-1}}^H + q_{0_{n-1}}^A \right]$$

$$= \chi_n\Delta u_n + \Delta u_n \sum_{n'=1}^{n-1} \Sigma_{n'n}^A \phi_{n'}\Delta u_{n'} - \left(q_{0_n}^H - q_{0n-1}^H\right) - \left(q_{0_n}^A - q_{0_{n-1}}^A\right),$$

$$\frac{iB}{3}\phi_n\Delta u_n + \Sigma_{\text{tr}_n}J_n\Delta u_n = -\left(q_{1_n}^H - q_{1_{n-1}}^H\right),$$

$$\left(q_{0_n}^H + q_{0_{n-1}}^H\right)\Delta u_n/2 + \left(q_{0_n}^H - q_{0_{n-1}}^H\right) = \Sigma_{s_n}^H \phi_n\Delta u_n,$$

$$\left(q_{1_n}^H + q_{1_{n-1}}^H\right)\Delta u_n/2 + \frac{2}{3}\left(q_{1_n}^H - q_{1_{n-1}}^H\right) = \frac{4}{9}\Sigma_{s_n}^H J_n\Delta u_n, \qquad (8\text{-}172)$$

$$\left(q_{0_n}^A + q_{0_{n-1}}^A\right)\Delta u_n/2 = \left(\xi_A\Sigma_s^A\right)_n\phi_n\Delta u_n, \qquad n = 1,\ldots,N$$

We have now arrived at a set of $5N$ algebraic equations for the unknowns $J_n$, $\phi_n$, $q_{0n}^H$, $q_{1n}^H$, and $q_{0n}^A$. To solve these equations, we begin by noting $q_{0_0}^H = q_{1_0}^H = q_{0_0}^A = 0$ (since no neutrons can slow down into the uppermost group). We can then solve for $J_1$ and $\phi_1$ using the $P_1$ equations (8-172) for $n = 1$. Having determined these, we then solve the remaining equations (8-172) for $q_{0_1}^H$, $q_{1_1}^H$, and $q_{0_1}^A$. We can proceed in this manner, solving successively for the variables characterizing increasingly higher lethargy groups (i.e., increasingly lower energy groups).

Once we have obtained $\phi_n$, we can then use it to generate few-group constants. For example, if we utilized a 54-group MUFT calculation to generate one-fast-group constants, we would find

$$\Sigma_{a_1} = \frac{\displaystyle\int_0^{u_{\text{thermal}}}\Sigma_a(u)\phi(u)\,du}{\displaystyle\int_0^{u_{\text{thermal}}}\phi(u)\,du} = \frac{\displaystyle\sum_{n=1}^{54}\Sigma_{an}\phi_n\Delta u_n}{\displaystyle\sum_{n=1}^{54}\phi_n\Delta u_n}, \qquad (8\text{-}173)$$

or

$$D_1 = \frac{\displaystyle\sum_{n=1}^{54}\frac{1}{3\Sigma_{\text{tr}_n}}\phi_n\Delta u_n}{\displaystyle\sum_{n=1}^{54}\phi_n\Delta u_n}. \qquad (8\text{-}174)$$

Sometimes an alternative scheme is used to calculate the group-diffusion coefficients. This procedure comes from requiring that $D_g$ be defined such that for a group of lethargy width $\Delta u$

$$\int_{\Delta u_g} du\, J(x,u) = -D_g\frac{d}{dx}\int_{\Delta u_g} du\,\phi(x,u). \qquad (8\text{-}175)$$

If we use our single buckling mode forms for $J(x,u)$ and $\phi(x,u)$, we find that $D_g$ is then defined by

$$D_g = \frac{1}{iB}\frac{\displaystyle\sum_{n=1}^{54}J_n\Delta u_n}{\displaystyle\sum_{n=1}^{54}\phi_n\Delta u_n}. \qquad (8\text{-}176)$$

In summary then, MUFT–GAM-type schemes generate a fast neutron spectrum and calculate few-group constants by using the $P_1$ (or $B_1$) slowing down equations, approximating the spatial dependence by a single spatial mode characterized by an "equivalent bare core buckling" $B^2$, treating elastic scattering by a continuous slowing down model (an exact treatment for hydrogen and either the age approximation or the Goertzel–Greuling model for materials with mass number $A > 1$), and handling inelastic scattering using a multigroup transfer matrix. We have not dwelt in detail on the treatment of resonance absorption, because such calculations will usually correct the infinite medium resonance escape probabilities we considered earlier for fuel lumping (heterogeneous) effects. We will return to discuss this in some detail in Chapter 10.

Most typically the MUFT scheme is used to generate either one-fast-group or three-fast-group constants for LWR calculations with the group structure as shown in Figure 8-5 (we have also indicated the thermal group, which must be handled by methods to be discussed in the next chapter).

An alternative to the MUFT fast spectrum procedure is that utilized in the GAM code and its offspring, in which a direct fine-group solution of the slowing down equation (in the $B_1$ or $P_1$ approximation is solved). Typically of the order of 100 lethargy groups are used, varying in width $\Delta u$ from 0.1 to 0.25. In most respects (aside from its direct multigroup treatment of elastic scattering), GAM spectrum codes are very similar to MUFT codes and are commonly used to generate fast group constants for HTGRs.

## B. Fast Group Constant Generation for Fast Reactor Calculations

The generation of few-group constants for fast reactor applications involves much more in the way of direct or brute force techniques than comparable thermal reactor calculations. To a large degree this is because of the relatively limited experience in fast reactor design and hence the desire for as accurate a calculation as possible. It also arises, however, because of the increased complexity of the variety of nuclear processes that influence a fast reactor spectrum—particularly the effects of resonance absorption and inelastic scattering. In a thermal reactor, the strong elastic scattering present in the system and the fact that most fissions are induced by thermal neutrons will tend to wash out many of these details. However in a fast reactor essentially all fissions are induced by neutrons with energies in just those ranges in which inelastic scattering and resonance absorption are most important.

At the present time, the most general class of codes for generating few-group constants for fast reactor calculations includes the $MC^2$ code and its variants.[18] This code begins with evaluated cross section data (ENDF/B) and proceeds to perform a sequence of group averages from ultrafine groups with $\Delta u \sim 1/120$, to fine groups with $\Delta u \sim 1/4$, and finally to broad groups with $\Delta u \sim 1/2$ to 1. In the more advanced versions of this code, a direct multigroup spectrum calculation is performed at higher energies, whereas a continuous slowing down calculation is used to handle elastic scattering at lower energies. The continuous slowing down calculation uses an improved Goertzel–Grueling approximation similar to that we discussed in the previous section. Spatial dependence is handled in either the $P_1$ or $B_1$ approximation with again a single spatial mode characterizing leakage with an effective buckling $B^2$. A number of rather sophisticated techniques are used to handle resonance absorption—particularly for the overlapping or unresolved res-

onance regions [the isolated resonances are most typically handled by the narrow resonance (NR) approximation].

As we have mentioned, codes such as $MC^2$ are much too elaborate for daily use in reactor design and are intended more for the evaluation of calculational techniques and comparison with critical experiments. As more experience is acquired in the design of cores for commercial fast reactors, less elaborate (although sufficiently accurate) techniques will evolve in a manner similar to the MUFT-GAM schemes used in thermal reactor design.

We have noted that in thermal reactors the multigroup constants are sensitive functions of core composition and core operating conditions and hence must be recalculated many times in a core design. In fast reactors the expense of a direct calculation of the multigroup constants coupled with a somewhat lower sensitivity to core environment has motivated the development of sets of universal microscopic multigroup constants which can be used for any fast reactor core design. The most well-known of such sets of fast group constants include the YOM set,[22] the Hansen-Roach or LASL 16-group set,[23] and the Bondarenko or ABN set.[24]

The effects of core environment on the multigroup constants are then taken into account by using so-called "$f$-factors"[25] (sometimes also referred to as Bondarenko self-shielding factors) which are defined in such a way that if $\sigma_{eff}$ is the group constant characterizing the particular core of interest, while $\sigma_{av}$ is the universal group constant, then

$$\sigma_{eff} = f\sigma_{av} .$$

Here, $\sigma_{av}$ would essentially correspond to the infinite dilution cross section (similar to the infinite dilution resonance integral). The set of universal microscopic group constants is typically calculated using a very simple intragroup flux—for example, a $1/E$ collision density. The $f$-factor then takes into account the detailed intragroup flux behavior due to resonance self-shielding, for example. The $f$-factors are usually tabulated as functions of concentration and temperature and included with the cross section sets.

## C. Age-Diffusion Theory

For historical completeness, let us return to consider the age-diffusion equation in a bit more detail. Recall that this equation takes the form

$$- D(u)\nabla^2\phi(\mathbf{r},u) + \Sigma_a(u)\phi(\mathbf{r},u) = -\frac{\partial q}{\partial u} + S(\mathbf{r},u) \tag{8-177}$$

where

$$q(\mathbf{r},u) \cong \xi\Sigma_s(u)\phi(\mathbf{r},u). \tag{8-178}$$

Now we know that this equation is only valid for neutron slowing down in moderators with reasonably large mass numbers (such as graphite). Nevertheless, age-diffusion theory has been thoroughly studied in the past because one can obtain an explicit solution of this equation in certain simplified cases.

For convenience, we will first consider the solution of the age-diffusion equation in the absence of a source. If we then substitute Eq. (8-178) into (8-177), we find

$$\frac{D(u)}{\xi\Sigma_s(u)}\nabla^2 q - \frac{\Sigma_a(u)}{\xi\Sigma_s(u)}q(\mathbf{r},u) = \frac{\partial q}{\partial u}. \tag{8-179}$$

Let us introduce an integrating factor to eliminate the absorption term by defining a new dependent variable, $\hat{q}(\mathbf{r}, u)$:

$$\hat{q}(\mathbf{r}, u) \equiv q(\mathbf{r}, u) \exp\left[ \int_0^u du' \frac{\Sigma_a(u')}{\xi \Sigma_s(u')} \right].$$
(8-180)

Then if we substitute this form into Eq. (8-179), we find

$$\frac{D(u)}{\xi \Sigma_s(u)} \nabla^2 \hat{q} = \frac{\partial \hat{q}}{\partial u}.$$
(8-181)

To solve this equation, we next make a change of independent variable by defining

$$\tau(u) \equiv \int_0^u du' \frac{D(u')}{\xi \Sigma_s(u')}$$
(8-182)

and note

$$\frac{\partial}{\partial u} = \frac{\partial \tau}{\partial u} \frac{\partial}{\partial \tau} = \frac{D(u)}{\xi \Sigma_s(u)} \frac{\partial}{\partial \tau}.$$
(8-183)

If we now use this new independent variable in Eq. (8-181), we find that $\hat{q}(\mathbf{r}, \tau)$ satisfies

$$\nabla^2 \hat{q}(\mathbf{r}, \tau) = \frac{\partial \hat{q}}{\partial \tau}.$$
(8-184)

Notice that the form of this equation is very similar to that of the time-dependent diffusion equation. For this reason, $\tau$ is known as the *Fermi age* in analogy to the time variable $t$ even though its units are $cm^2$ rather than sec.

By noting the similarity between the age equation (8-184) and the time-dependent diffusion equation, we can adapt our entire earlier analysis to solve this equation. We won't do this here, however, because age theory is primarily of historical interest and is only of limited utility in present-day reactor design. We will, however, generalize our results to include absorption by noting

$$q(\mathbf{r}, \tau) = \hat{q}(\mathbf{r}, \tau) \exp\left[ -\int_0^u du' \frac{\Sigma_a(u')}{\xi \Sigma_s(u')} \right] \equiv \hat{q}(\mathbf{r}, \tau) p(u),$$
(8-185)

where we have identified the exponential factor as just the resonance escape probability $p(u)$ to lethargy $u$.

To illustrate these ideas more clearly, let us consider the example of an infinite planar source emitting neutrons of energy $E_0$ at the center of a nonabsorbing slab of width $a$ (as we have seen, absorption can be easily included) [see Figure 8-6]. We will define the lethargy variable with respect to the source energy $E_0$ so that $u = 0$ corresponds to the source energy. If we also note

$$\tau(u) = \int_E^{E_0} \frac{dE}{E} \frac{D(E)}{\xi \Sigma_s(E)},$$
(8-186)

$S_0 \delta(x)\delta(\tau)$



$0 < \tau_1 < \tau_2 < \tau_3$

$q(x, \tau_1)$

$q(x, \tau_2)$

$q(x, \tau_3)$
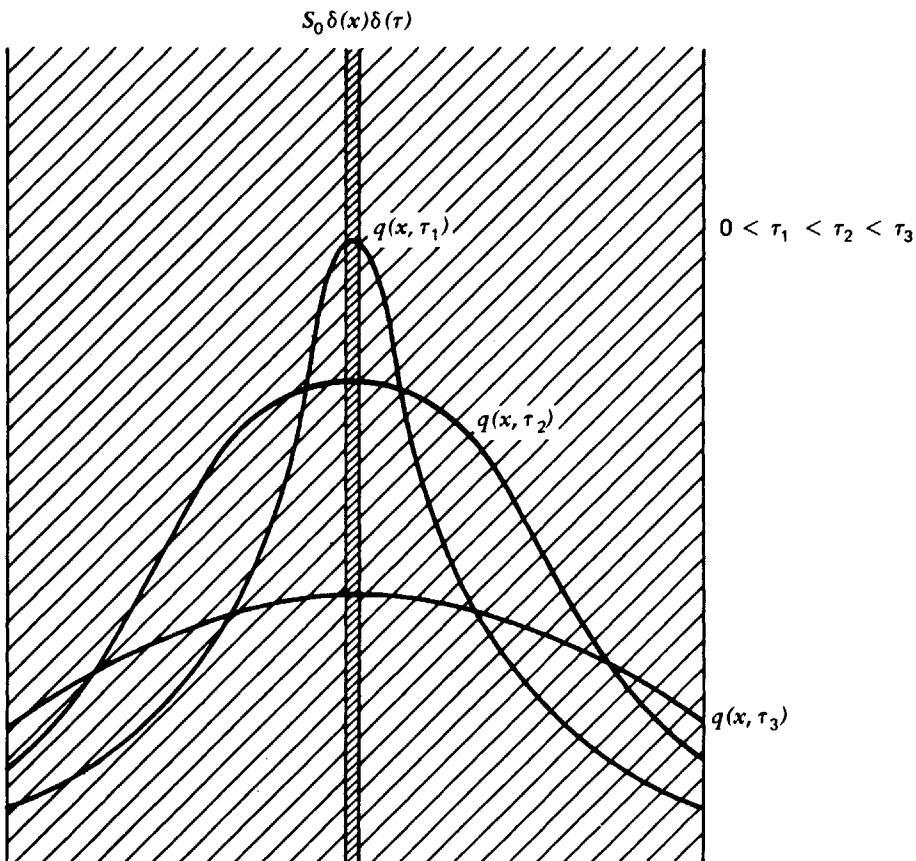
FIGURE 8-6. The slowing down density $q(x,\tau)$, resulting from a monoenergetic plane source at the origin of a slab.

then we can write the appropriate form of the age equation as

$$\frac{\partial^2 q}{\partial x^2} = \frac{\partial q}{\partial \tau}$$

(8-187)

subject to:    (a) initial condition:        $q(x,0) = S\delta(x)$

(b) boundary conditions:    $q(-\tilde{a}/2,\tau) = 0 = q(\tilde{a}/2,\tau)$

To solve this, we will try an eigenfunction expansion (noting by symmetry that only even eigenfunctions need be used)

$$q(x,\tau) = \sum_n f_n(\tau) \cos B_n x, \quad B_n = \frac{n\pi}{\tilde{a}}.$$

(8-188)

If we substitute this into the age equation

$$-\sum_n B_n^2 f_n(\tau) \cos B_n x = \sum_n \frac{df_n}{d\tau} \cos B_n x,$$

(8-189)

and use orthogonality we find

$$\frac{df_n}{d\tau} = - B_n^2 f_n(\tau).$$

(8-190)

The solution to this equation is just

$$f_n(\tau) = A_n \exp - B_n^2 \tau. \tag{8-191}$$

Hence the general solution to Eq. 8-187 is

$$q(x,\tau) = \sum_n A_n \exp\left(- B_n^2 \tau\right) \cos B_n x. \tag{8-192}$$

Now using the initial condition at $\tau = 0$, we require

$$q(x,0) = \sum_n A_n \cos B_n x = S\delta(x). \tag{8-193}$$

In the usual manner we can now multiply by $\cos B_m x$, integrate over $x$, and use orthogonality to evaluate all $A_n$ to find the solution

$$q(x,\tau) = \frac{2S}{\tilde{a}} \sum_n \exp\left(- B_n^2 \tau\right) \cos B_n x. \tag{8-194}$$

Just as the fundamental mode $(n = 1)$ will dominate the solution of the time-dependent diffusion equation, we find that for large values of $\tau$, that is, for neutron energies far below the source energy $E_0$, the solution of the age-diffusion equation approaches

$$q(x,\tau) \sim \frac{2S}{\tilde{a}} \exp\left(- B_g^2 \tau\right) \cos B_g x, \quad B_g \equiv B_1. \tag{8-195}$$

This is a very useful expression, since it essentially describes the spatial distribution of neutrons slowing down to thermal energies in a bare, homogeneous assembly from fission sources. Since there is no absorption in our modeled problem, we can interpret the decrease in $q(x,\tau)$ with increasing age as being due to neutron leakage while slowing down.

Note in particular that if all of the source neutrons had initially been distributed in the fundamental mode $\cos B_g x$ shape (which would correspond, for example, to the appearance of fission neutrons in a bare, critical slab reactor), then the loss of neutrons during slowing down would be described by the $\exp(- B_g^2 \tau)$ factor. That is, we can identify the fast nonleakage probability $P_{FNL}$ introduced earlier (Chapter 3) in the six-factor formula for $k$ as just

$$P_{FNL} = \exp\left(- B_g^2 \tau_{th}\right), \tag{8-196}$$

where $\tau_{th}$ is the age corresponding to thermal energies (usually taken as $\sim 1$ eV):

$$\tau_{th} = \int_{E_{th}}^{E_0} dE \frac{D(E)}{\xi \Sigma_s(E) E}. \tag{8-197}$$

Of course this expression for $P_{FNL}$ is valid only in the age approximation as applied to a bare, uniform reactor.

The age-diffusion equation can also be solved in several other standard

geometries. For example, the slowing down density resulting from a plane source in an infinite, nonabsorbing medium is

$$q_{pl}(x,\tau) = \frac{S\exp\left(-\dfrac{x^2}{4\tau}\right)}{\sqrt{4\pi\tau}}, \qquad (8\text{-}198)$$

while that resulting from a point source in such a medium is

$$q_{pt}(r,\tau) = \frac{S\exp\left(\dfrac{-r^2}{4\tau}\right)}{(4\pi\tau)^{3/2}}. \qquad (8\text{-}199)$$

This last result can be used to demonstrate that

$$\tau = \frac{1}{6}\langle r^2 \rangle = \quad \text{1/6 the average (crow-flight distance)}^2$$

from the point where a neutron enters
a system with $E_0$ to the point at which
it slows down to an age $\tau$. $\qquad (8\text{-}200)$

One usually calculates or measures the age-to-thermal energies $\tau_{th}$ or more commonly, the age-to-indium resonance at 1.45 eV, $\tau_{IN}$ (since this is the most common experimental measurement). In Table 8-7, we have listed the age $\tau_{th}$ for several common moderators, along with other parameters characterizing thermal neutron behavior in these moderators.

**TABLE 8-7:** Diffusion Parameters for Some Common Moderators

| Moderator | Density (g/cm$^3$) | D(cm) | $\Sigma_a$(cm$^{-1}$) | $L$(cm) | $\tau_{th}$(cm$^2$) | $M$(cm) |
|---|---|---|---|---|---|---|
| $H_2O$ | 1.00 | 0.16 | 0.0197 | 2.85 | 26 | 5.84 |
| $D_2O$ | 1.10 | 0.87 | $2.9\times10^{-5}$ | 170 | 131 | 170 |
| Be | 1.85 | 0.50 | $1.0\times10^{-3}$ | 21 | 102 | 23 |
| Graphite | 1.60 | 0.84 | $2.4\times10^{-4}$ | 59 | 368 | 62 |

| Reactor Type | $\langle L \rangle$(cm) | $\tau_{th}$(cm$^2$) | $\langle M \rangle$(cm) | Diameter $\langle M \rangle$ | Diameter $\langle L \rangle$ |
|---|---|---|---|---|---|
| PWR | 1.8 | 40 | 6.6 | 56 | 190 |
| BWR | 2.2 | 50 | 7.3 | 50 | 180 |
| HTGR | 12.0 | 300 | 21 | 40 | 63 |
| LMFBR | 5.0 | - | - | - | 35 |
| GCFR | 6.6 | - | - | - | 35 |

If we recall that the thermal nonleakage probability is $P_{TNL} = (1 + L^2 B_g^2)^{-1}$, and note further that for most larger power reactors, $B_g^2$ is sufficiently small that both $L^2 B_g^2$ and $\tau B_g^2$ are much less than one, then we can write the total nonleakage

probability as

$$P_{NL} = P_{TNL} P_{FNL} = \frac{1}{\left(1 + L^2 B_g^2\right)} \exp\left(-\tau B_g^2\right)$$

$$\cong \frac{1}{\left(1 + L^2 B_g^2\right)} \frac{1}{\left(1 + \tau B_g^2\right)} \cong \frac{1}{\left(1 + L^2 B_g^2 + \tau B_g^2\right)} \equiv \frac{1}{\left(1 + M^2 B_g^2\right)} \qquad (8\text{-}201)$$

where we have defined the *neutron migration area* $M^2$ as

$$M^2 = L^2 + \tau. \qquad (8\text{-}202)$$

The *migration length* $M$ can be interpreted as $1/\sqrt{6}$ of the rms distance a neutron travels from its appearance as a fast fission neutron to its capture as a thermal neutron (see Problem 8-42). We have listed the migration lengths for typical moderators in Table 8-7. The migration length proves useful as a scale with which to characterize the size of a reactor core. For example, a modern LWR is typically $\sim$50 $M$ in diameter, whereas a comparable HTGR core is about 40 $M$. In this sense, even though the physical size of the HTGR is two to three times that of a LWR, its "neutronic" size is actually somewhat smaller. Both reactor types are certainly far more loosely coupled in a neutronic sense than fast reactor cores ($\sim$30 $L$) and hence are more susceptible to spatial power transients.

## D. Some Additional Comments on Fast Spectrum Calculations

As we have seen, most schemes for generating fast group constants first perform a fine multigroup solution of the neutron slowing down equations (in the $P_1$ or $B_1$ approximation) to obtain the fast neutron spectrum, and then average microscopic cross section data over this spectrum to obtain the desired few-group constants. Microscopic cross section data enter this calculation in two different ways. First, the microscopic cross sections available from nuclear data files such as ENDF/B must be converted into fine multigroup constants in order to allow the calculation of the fast neutron spectrum. Then these data must be averaged over this spectrum to generate the few group constants themselves.

Such basic nuclear data are usually given in the form of pointwise data along with various interpolation specifications in a data set such as ENDF/B. Hence the first step in a fast spectrum calculation is to prepare a library of fast fine-group constants by averaging these basic cross section data over the groups to be used in the fast spectrum calculation. Usually either a $1/E$ or a fission spectrum is used as a weighting function. These fast libraries are typically supplied as part of a given fast spectrum code, since their generation from a basic nuclear data set can be rather expensive. A schematic of this procedure is shown in Figure 8-7.

A rather important aspect of such cross section libraries involves the preparation of resonance cross section data. In the resolved resonance region, the techniques we have discussed (e.g., the NR or NRIM methods) can be used to calculate the resonance integrals characterizing the resonances in each of the fine groups. However in the region of unresolved resonances more elaborate schemes must be used. Although a rather crude treatment of the unresolved resonance region is usually sufficient in thermal reactor calculations, in a fast reactor as much as 40% of the resonance absorption can occur in unresolved resonances, and hence a detailed calculation is required.
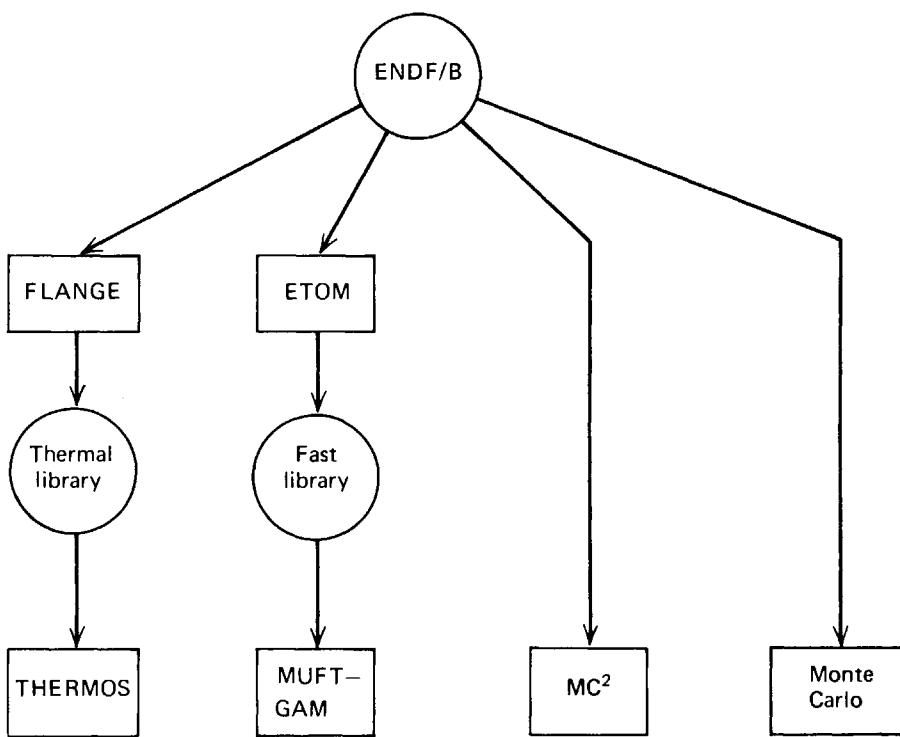
FIGURE 8-7.    Generation of cross section libraries from ENDF/B.

In most fast spectrum codes, one has the option of specifying the group structure characterizing the few-group constants that he wishes to generate. In general one wishes to use the smallest number of coarse groups consistent with the desired accuracy in the corresponding multigroup diffusion calculation. In fact, the necessary group structure will usually depend on the type of calculation of interest. For example, the calculation of integral quantities such as the core multiplication factor can usually be accomplished with fewer groups than an estimate of the power-peaking in a fuel assembly.

The lower cutoff of the fast spectrum is usually chosen high enough so that upscattering out of the thermal groups can be neglected. In a LWR, this cutoff is typically chosen at around 0.6 eV. However in an HTGR, it must be chosen somewhat higher (typically 2.38 eV) because the higher moderator temperature in such reactors causes appreciably larger upscattering. The remaining group structure is usually chosen such that different physical phenomena tend to be isolated within a given group. For example, in a three-fast-group calculation, the highest energy group is usually chosen to contain all of the fission spectrum, the middle group is characterized by elastic slowing down, and most of the resonance absorption is confined to the lowest energy group. (See Figure 8-5).

A fast spectrum calculation not only supplies fast few-group constants and the fast neutron spectrum, but also will provide the rate at which neutrons slow down into the thermal energy range. This latter information is needed to complete the determination of few-group constants by generating a thermal neutron spectrum and then averaging cross section data over this spectrum to obtain thermal group constants.

## REFERENCES

1. J. H. Ferziger and P. F. Zweifel, *The Theory of Neutron Slowing Down in Nuclear Reactors*, M.I.T. Press, Cambridge (1966).

2. M. M. R. Williams, *The Slowing Down and Thermalization of Neutrons*, North-Holland, Amsterdam (1966).

3. Ibid., Chapter VIII.

4. A. Radowsky, (Ed.), *Naval Reactors Physics Handbook*, Vol. I, *Selected Techniques*, USAEC Report (1964), Chapter 2.

5. A. M. Weinberg and E. P. Wigner, *The Physical Theory of Neutron Chain Reactors*, University of Chicago Press (1958), p. 290.

6. J. H. Ferziger and P. F. Zweifel, *The Theory of Neutron Slowing Down in Nuclear Reactors*, M.I.T. Press, Cambridge (1966) pp. 73–78; R. E. Marshak, *Rev. Mod. Phys.* **19**, 185 (1947).

7. G. I. Bell and S. Glasstone, *Nuclear Reactor Theory*, Van Nostrand, Princeton, N.J., (1970), pp. 439–443.

8. P. E. Meyer and P. F. Zweifel, *Trans. Am. Nucl. Soc.* **13**, 305 (1970).

9. M. E. Rose, W. Miranker, P. Leak, and G. Rabinowitz, A Table of the Integral $\psi(x,t)$, BNL-257 (T-40), (1953); WAPD-SR-506 (1954); K. K. Seth and R. H. Tabony, USAEC Document TID-21304 (1964).

10. L. W. Nordheim, *Nucl. Sci. Eng.* **12**, 457 (1962).

11. Y. Ishiguro, *Nucl. Sci. Eng.* **49**, 526 (1972); R. Goldstein, *Nucl. Sci. Eng.* **49**, 526 (1972).

12. K. T. Spinney, BNL-433 (1960).

13. P. E. Meyer, Approximate Methods for the Calculation of Resonance Absorption, University of Michigan Ph.D. Dissertation, 1974.

14. G. Goertzel and E. Greuling, *Nucl. Sci. Eng.* **7**, 69 (1960).

15. H. Hurwitz and P. F. Zweifel, *J. Appl. Phys.* **26**, 923 (1956).

16. H. Bohl, Jr., E. M. Gelbard, and G. H. Ryan, MUFT-4, A Fast Neutron Spectrum Code, Report WAPD-TM-22 (1957).

17. G. D. Joanou, E. J. Leshan, and J. S. Dudek, GAM-1 a Consistent $P_1$ Multigroup Code for the Calculation of Fast Neutron Spectra and Multigroup Constants, General Atomic Report GA-1850 (1961).

18. B. J. Toppel, A. L. Rago, and D. M. O'Shea, $MC^2$ A Code to Calculate Multigroup Cross Sections, ANL-7318 (1967).

19. J. R. Lamarsh, *An Introduction to Nuclear Reactor Theory*, Addison-Wesley, Reading, Mass. (1966).

20. M. Lineberry and N. Corngold, *Nucl. Sci. Eng.* **53**, 153 (1974).

21. R. Bellman and K. Cooke, *Differential-Difference Equations*, Academic, New York (1962).

22. S. Yiftah, D. Okrent, and P. A. Moldauer, *Fast Reactor Cross Sections*, Pergamon, New York (1960).

23. I. I. Bondarenko, et. al., *Group Constants for Nuclear Reactor Calculations*, Consultants Bureau, New York (1964).

24. *Reactor Physics Constants*, 2nd Ed., USAEC Document ANL-5800 (1963), pp. 568–579.

25. M. Segev, *Nucl. Sci. Eng.* **56**, 72 (1975).

## PROBLEMS

8-1 The lower cutoff energy $E_c$ for the fast region is usually chosen such that there is negligible upscattering above this energy. If the moderator is modeled as a free proton gas [cf. Eq. (2-107)], compute the cutoff energy $E_c$ such that less than 0.1% of the thermal region neutrons will be upscattered above $E_c$. Plot this cutoff energy versus moderator temperature $T$.

8-2 Determine the neutron flux $\phi(E)$ resulting from an arbitrary source in an infinite hydrogeneous medium by: (a) solving the infinite medium slowing down equation with this general source term, and then (b) using the solution obtained for a monoenergetic source as a Green's function for the more general problem.

8-3 (a) Derive an expression for the neutron balance in a nuclear reactor in terms of the

scalar flux $\phi(r, E, t)$, and the net current $J(r, E, t)$.

(b) Derive an expression for the neutron slowing down density $q(r, E, t)$ in terms of $\phi(r, E, t)$.

(c) Prove that in a purely hydrogeneous medium and in the steady state one may write

$$q = E(\Sigma_t \phi + \nabla \cdot J - S),$$

where $S$ represents the sources. You may use the lethargy variable $u$ rather than the energy $E$ if you prefer. Throughout, assume $E \gg kT$.

8-4 Transform the infinite medium slowing down equation (assuming only elastic scattering) from the energy variable to the lethargy variable.

8-5 Repeat the derivation of an expression for the neutron slowing down density in an infinite moderating medium by first calculating $P(E' > E)$, the probability that a neutron with energy $E'$ scatters below an energy $E$ in a collision. Then integrate the product of this quantity with the collision density $\Sigma_s(E')\phi(E')$ over all $E' > E$ to find $q(E)$.

8-6 Show that the neutron continuity equation can be written quite generally in terms of the slowing down density $q(r, E, t)$ as

$$\frac{1}{v} \frac{\partial \phi}{\partial t} + \nabla \cdot J + \Sigma_a(E)\phi(r, E, t) = \frac{\partial q}{\partial E} + S(r, E, t).$$

8-7 Solve the coupled slowing down equations for an infinite hydrogeneous medium $\Sigma_a(u)\phi(u) = -\frac{dq}{du} + S(u); \quad \frac{dq}{du} + q(u) = \Sigma_s(u)\phi(u)$ for a monoenergetic source at lethargy $u = 0$.

8-8 Calculate the mean lethargy loss per collision $\xi$, the moderating power, and the moderating ratio for $H_2O$ and $D_2O$ at energies of 1 eV and 100 eV. Estimate the necessary cross section data from BNL-325.

8-9 Consider neutrons slowing down in an infinite medium with no absorption.

(a) By equating the number of collisions in a lethargy interval $du$ with the number of collisions in a time $dt$, obtain an expression for the time required for neutrons to slow down to thermal energies.

(b) Calculate the time required for fission neutrons to slow down to thermal in graphite and water. Assume $\Sigma_s^C = 0.385$ cm$^{-1}$ while $\Sigma_s^{H_2O} = 0.528$ cm$^{-1}$ (constant in energy).

8-10 Demonstrate that for large mass numbers, $\xi \sim \frac{2}{A + 2/3}$.

8-11 Show that the average increase in lethargy $\xi$ in an elastic (s-wave) collision is one-half the maximum lethargy increase.

8-12 Calculate the multigroup transfer scattering elements $\Sigma_{sg'g}$ for hydrogen under the assumption that $\Sigma_s(u)$ and the intragroup flux $\phi(u)$ can be taken as constant. Assume the groups are equally spaced with a lethargy width $\Delta u$.

8-13 Demonstrate that the multigroup transfer scattering elements characterizing elastic scattering for directly coupled groups of lethargy width $\Delta u_g$ are given by $\Sigma_{sg \to g+1}$ $= \Sigma_{sg} \xi_g / \Delta u_g$ (Hint: Balance the scattering rates into and out of each group.)

8-14 As an example of a nondirectly coupled multigroup calculation, consider a scheme in which all groups are of the same lethargy width $\Delta u$ and in which neutrons are able to skip at most one group. Assume that only s-wave elastic scattering need be considered and that the scattering cross section $\Sigma_s(u)$ can be treated as lethargy-independent. Calculate the elements of the scattering transfer cross section $\Sigma_{sg'g}$ for all $g'$ and $g$, assuming a constant intragroup flux $\phi(u) = \phi$. Also verify that the sum of these transfer cross sections is indeed equal to the group-averaged scattering cross section $\Sigma_{sg}$.

absorber whose absorption cross section is infinite over the range $E_1$ to $E_2$ and zero at all other energies. The resonance region is several orders of magnitude below the source energy.

(b) What is the resonance escape probability when $E_2 = \alpha E_1$?

8-25 Calculate the escape probabilities for $T = 300°K$, $600°K$, and $1200°K$ for both the 6.67 eV and 208 eV resonances in $^{238}U$, assuming that $\Sigma_s^M / N_A = 10$ and 1000 b per $^{238}U$ atom. Use the NRIM approximation for the lower resonance and the NR approximation for the higher resonance. (Ignore interference scattering terms.)

8-26 Estimate the probability that a 2 MeV neutron emitted in an infinite medium of water will not be absorbed while slowing down to 1 eV.

8-27 Demonstrate explicitly that for any capture resonance, $\partial I / \partial T > 0$ and hence $\partial p / \partial T < 0$. (Use either the NR or NRIM expression for the effective resonance integral.)

8-28 Derive the equations (8-132) for the slowing down densities $q_0^H(x,u)$ and $q_1^H(x,u)$ in hydrogen.

8-29 Show that $a/\xi \sim -\xi$ by plotting both parameters as functions of $\alpha$ for $0 < \alpha < 1$.

8-30 Explicitly derive the expressions for $\lambda_0$, $\lambda_1$, $\beta_0$, and $\beta_1$ in the Goertzel–Greuling approximation.

8-31 Derive the $B_1$ equations by explicitly calculating the first two angular moments of the transport equation as described in Section 8-III-B and then rearranging these results into the form of Eq. (8-163).

8-32 Using the group-averaging schemes discussed in Section 8-IV, develop in detail the fine multigroup slowing down equations (8-172) from the set (8-165).

8-33 Determine the following quantities in terms of the fine-group MUFT representation: (a) source rate, (b) slowing down rate to thermal, (c) leakage rate, and (d) absorption rate. Then calculate the slowing down probability, leakage probability, and absorption probability. Verify that these latter probabilities all add to unity.

8-34 Consider an infinite slab of thickness $L$ composed of pure atomic hydrogen with a number density $N_H$. The slab contains an external source of the form $S(x,u)$ $= \chi(u) \exp(iBx)$ where $\chi(u)$ is the $^{235}U$ fission spectrum and $x = 0$ denotes the midplane of the slab.

Write a computer program that will solve the $P_1$ equations for this problem. Your program should tabulate $\phi(u)$, $J(u)$, $q_0(u)$, and $q_1(u)$; it should also calculate the fast leakage and absorption probabilities and the age to thermal. Run your program for several slab thicknesses and compare the results.

Use the MUFT 54 group scheme and a pointwise representation of the fission spectrum as given by Eq. (2-112), and use BNL-325 to obtain a pointwise representation of $\Sigma_s^H(u)$.

8-35 Determine the slowing down spectrum of fission neutrons slowing down in an infinite medium of water using a MUFT-type fast spectrum code. Repeat this calculation for an infinite medium of $D_2O$.

8-36 Determine the slowing down density established by a monoenergetic plane source at the origin of an infinite moderating medium as given by age-diffusion theory.

8-37 Determine the slowing down density resulting from a point source in an infinite moderating medium (using age-diffusion theory).

8-38 Sources of monoenergetic fast neutrons are distributed in a moderating slab as $S(x) = S_0 \cos(\pi x/a)$, where $a$ is the width of the slab. Using age-diffusion theory, determine the slowing density in the slab. Then calculate the average probability that a source neutron leaks out of the slab while slowing down.

8-39 Age theory for hydrogen fails principally because the collision density may not be slowly varying over the limits of the scattering integral. Why not?

8-40 Consider a "zero-temperature" reactor, namely, a reactor in which all nuclei are at rest and thus slowing down theory is valid for all lethargies. Assume that the reactor is bare with a geometric buckling $B_g^2$, and that all fission neutrons are born with zero lethargy. Then using age-diffusion theory, derive the criticality relation for this reactor

in the form:

$$1 = \int_0^\infty du \frac{\nu(u)\Sigma_f(u)}{\xi\Sigma_t(u)} p(u)\exp\left[-B_g^2\tau(u)\right].$$

8-41 Estimate the fast and thermal nonleakage probabilities for each of the reactor types listed in Table 8-7. Use core sizes from Appendix H.

8-42 Demonstrate that $M^2 = L^2 + \tau$ is indeed $1/6$ the mean-square distance a neutron will travel from its origin in fission to its eventual absorption as a thermal neutron.

8-43 Consider an effectively infinite medium in which a monoenergetic pulse of fast neutrons is instantaneously injected at time $t = 0$ uniformly throughout the medium. Using age theory, determine the time-dependent slowing down density $q(u,t)$.

# 9

---

# Thermal Spectrum Calculations
# and
# Thermal Group Constants

---

We now turn our attention to the generation of multigroup constants characterizing low-energy neutrons. Once again the general approach will be to develop methods for determining the detailed energy dependence or spectrum of such neutrons in those situations in which the spatial dependence can be ignored (or treated in a crude manner) and then to average microscopic cross section data over this energy spectrum.

A detailed investigation of the neutron energy spectrum below several eV becomes quite involved due to the complicated nature of the neutron scattering process. For at such low energies we can no longer ignore the thermal motion of the nuclei, as we did in the study of neutron slowing down. The energy of such slow or thermal neutrons is comparable as well to the binding energy of the atoms in molecular or crystalline materials, and hence the neutron will tend to interact with an aggregate of atoms rather than with a single nucleus. These features greatly complicate the determination of cross sections characterizing the scattering of thermal neutrons, and such cross sections will exhibit a rather involved dependence on both neutron energy and scattering angle. Moreover thermal neutron cross sections depend, in a detailed manner, on the temperature and physical state (i.e., solid, liquid, or gas) of the scattering medium, unlike fast neutron cross sections, which depend primarily on the nuclear species. The complicated nature of such cross sections renders the determination of thermal neutron spectra rather involved, and one usually must resort to direct numerical methods.

The study of thermal neutron behavior is customarily referred to as *neutron thermalization*.[1-4] Actually, however, the subject of neutron thermalization can be classified into two separate problems: (a) the calculation of cross sections characterizing thermal neutron scattering in various materials and (b) the use of these cross sections in the determination of the energy spectrum characterizing

low-energy neutrons (e.g., for use in determining thermal group constants for few-group diffusion calculations). These subjects are quite interrelated since those features characteristic of thermal neutron cross sections may have a rather significant influence on the determination of thermal spectra.

For example, the fact that the kinetic energy of a low-energy neutron is comparable to the thermal energy of atomic motion means that microscopic thermal neutron cross sections actually must be regarded as averages over the thermal distribution of nuclear speeds and hence are temperature-dependent, as we saw in Chapter 2. Furthermore, it will be possible for the neutron to gain energy—that is, to upscatter—in a scattering collision with a moving nucleus. This will complicate the numerical solution of the fine-structure multigroup equations used to determine thermal spectra.

Of similar importance is the fact that the energy of thermal neutrons is comparable to the chemical binding energy of the scattering nuclei (e.g., in a molecule or a crystal lattice). Hence the nucleus will no longer recoil freely, and thus binding will become significant in determining the energy and angle change of a neutron in a collision. In fact one can show that the scattering cross section of a bound nucleus is somewhat larger than that of a free nucleus by an amount that is roughly $\sigma_{bound} = (1 + 1/A)^2 \sigma_{free}$, where $A$ is the mass number of the scattering nucleus.[2] For example, in hydrogeneous materials for which $A = 1$, we would find that the actual low-energy scattering cross section is some four times larger than the free-atom scattering cross section $\sigma_{free}$.

Of related significance are inelastic scattering processes in which the internal states of the scattering system (e.g., molecular vibration and rotation or crystal lattice vibration) are excited by neutron scattering collisions. (Such thermal inelastic scattering processes should not be confused with nuclear inelastic scattering in which the nucleus itself is excited into a higher quantum state. The latter process is of little concern for the low energies characterizing thermal neutrons.) Inelastic scattering gives rise to a complicated cross section dependence on energy and angle.

For very low energies, the neutron wavelength is comparable to the interatomic spacing of the scattering material. Hence the neutron wave function experiences diffraction effects (just as light is diffracted). However, we should add that while such coherent interference effects can be quite important in determining the very low energy behavior of neutron scattering cross sections, they are rarely of importance in nuclear reactor behavior.

Needless to say, such considerations greatly complicate the subject of neutron thermalization. The determination of thermal neutron cross sections is extremely complicated and can be regarded as essentially a subfield of statistical mechanics and solid and liquid-state physics. Since the measurement and calculation of such cross sections can infer information about the microscopic structure and dynamics of materials, thermal neutron scattering (or *thermal neutron spectroscopy*) has received an exhaustive treatment in the scientific literature, and we will not attempt to duplicate that treatment in this text.[4-6]

Fortunately *most* of the complicated details of thermal neutron cross section behavior are of secondary concern in nuclear reactor analysis. Indeed in most large thermal power reactors the neutron energy spectrum is sufficiently well "thermalized" that rather crude models of the neutron scattering process are sufficient for the generation of thermal group constants. For example, in LWR

calculations, the core can frequently be modeled as an ideal gas of protons (totally ignoring binding and diffraction effects) seeded with a uniformly distributed absorber corresponding to the fuel. Such a model is particularly useful for generating the thermal group constants to be used in survey or parametric studies (e.g., core lifetime studies). Of course, more detailed studies of such large, heterogeneous reactor cores characterized by strong temperature gradients require more elaborate models of the scattering material. This is particularly true for the analysis of reactors utilizing solid moderators, such as the HTGR, which uses graphite as a moderator. However, in all cases the models of the physical and chemical structure of the scattering material used to calculate thermal neutron cross sections for nuclear reactor analysis are very crude indeed when compared to the sophisticated theories and measurements that exist for the interpretation of thermal neutron scattering data.

Hence our concern in this chapter will be to first illustrate some of the simple ideas involved in neutron thermalization and then to develop those tools forming the basis for thermal spectra calculations and used to generate thermal group constants.

# I. GENERAL FEATURES OF THERMAL NEUTRON SPECTRA

## A. Thermal Equilibrium

Although the detailed form of the cross section characterizing thermal neutron scattering is extremely complicated, depending as it does on the temperature and physical structure of the scattering material, there are several simple general features of such cross section behavior with important implications for thermal neutron spectra. Suppose we once again consider a situation in which we imagine sources of neutrons distributed uniformly throughout an infinite medium such that spatial and time dependence can be ignored. Then we recall that the neutron continuity equation (4-79) simplies to

$$[\Sigma_a(E) + \Sigma_s(E)]\phi(E) = \int_0^\infty dE' \Sigma_s(E' \to E)\phi(E') + S(E). \qquad (9\text{-}1)$$

Notice that we have allowed the range of integration to extend to $E = 0$, since we now wish to analyze the low energy behavior of the neutron flux.

The first useful property of thermal neutron cross sections—and indeed, *all* differential scattering cross sections—is essentially just a definition:

$$\Sigma_s(E) = \int_0^\infty dE' \Sigma_s(E \to E'). \qquad (9\text{-}2)$$

However even this familiar property tells us something interesting. For if we integrate Eq. (9-1) over all energy and use the relation Eq. (9-2), we find the balance relation

$$\int_0^\infty dE \Sigma_a(E)\phi(E) = \int_0^\infty dE S(E). \qquad (9\text{-}3)$$

That is, for a steady-state flux $\phi(E)$ to be possible in an infinite medium, we

require that the rate at which source neutrons appear be just equal to the rate at which neutrons are absorbed (since there is no leakage). If we recognize that in thermalization problems all source neutrons will appear as fission neutrons slowing down into the thermal energy range, and the absence of upscattering above the thermal cutoff energy $E_c$ implies that Eq. (9-1) holds with the upper limit truncated at $E_c$, then one can rewrite Eq. (9-3) as (see Problems 9-2 and 9-3)

$$\text{Total rate of absorption in thermal range/cm}^3 = \int_0^{E_c} dE \, \Sigma_a(E)\phi(E) = q(E_c) = \begin{array}{l} \text{rate at which} \\ \text{neutrons slow} \\ \text{down into thermal} \\ \text{range/cm}^3. \end{array} \quad (9\text{-}4)$$

The differential scattering cross section or scattering kernel $\Sigma_s(E' \to E)$ can be shown to possess another very important property:

$$v'\Sigma_s(E' \to E)M(E') = v\Sigma_s(E \to E')M(E), \quad (9\text{-}5)$$

where $M(E)$ is the Maxwell–Boltzmann distribution function characterizing the energies of the particles of an ideal gas at temperature $T$:

$$M(E) \equiv \frac{2\pi}{(\pi kT)^{3/2}} \sqrt{E} \, \exp\left(-\frac{E}{kT}\right). \quad (9\text{-}6)$$

Eq. (9-5) is known as the *principle of detailed balance*, and it must be satisfied by any neutron cross section characterizing neutron scattering from a system of nuclei in thermal equilibrium at a temperature $T$ (regardless of their structure or detailed dynamics). This property is essentially a consequence of the laws of statistical mechanics characterizing the scattering material.[7] It implies an extremely important consequence for the neutron energy spectrum in a reactor, as we will now demonstrate.

Suppose we consider the special case in which we set the absorption and source terms in our infinite medium equation, Eq. (9-1), to zero:

$$\Sigma_s(E)\phi(E) = \int_0^\infty dE' \, \Sigma_s(E' \to E)\phi(E'). \quad (9\text{-}7)$$

Then we claim that the solution to this equation, regardless of the detailed form of the scattering cross section, must be just the neutron flux characterizing neutrons in thermal equilibrium at the same temperature $T$ as the scattering medium:

$$\phi(E) \to \phi_M(E) \equiv vn_0 M(E) = \frac{2\pi n_0}{(\pi kT)^{3/2}} \left(\frac{2}{m}\right)^{1/2} E \exp\left(-\frac{E}{kT}\right), \quad (9\text{-}8)$$

where $n_0$ is the neutron number density in the medium. This result is a consequence of the principal of detailed balance, for we can use Eq. (9-5) to demonstrate that $\phi_M$ is indeed a solution of Eq. (9-7):

$$\Sigma_s(E)\phi_M(E) = \int_0^\infty dE' \, \Sigma_s(E' \to E)v'n_0 M(E')$$

$$= \int_0^\infty dE' \, \Sigma_s(E \to E')vn_0 M(E) = \Sigma_s(E)\phi_M(E). \quad (9\text{-}9)$$

Hence the principle of detailed balance ensures that the equilibrium spectrum of the neutrons (in the absence of absorption, sources, leakage, etc.) will be a "Maxwellian" characterized by the moderator temperature $T$—that is, that the neutrons will eventually come into thermal equilibrium with the moderator nuclei. In this sense, the neutrons behave as a very dilute gas that will gradually come into thermal equilibrium—namely, "thermalize"—with the system through which it is diffusing. From the properties of the Maxwell–Boltzmann distribution function we know that the most probable neutron energy and corresponding speed in such a situation are then given in terms of the system temperature $T$ as:

$$E_T = kT = 8.62 \times 10^{-5} T \text{ (eV)}$$

$$v_T = \sqrt{\frac{2kT}{m}} = 1.28 \times 10^4 \sqrt{T} \text{ (cm/sec)}. \tag{9-10}$$

For example, at $T = 293°K$, $E_T = .025$ eV while $v_T = 2.2 \times 10^5$ cm/sec. (Although at typical reactor core operating temperatures, $T = 590°K$ corresponds to $E_T = .051$ eV and $v_T = 3.1 \times 10^5$ cm/sec.)

The detailed balance property only guarantees that the neutrons will be in thermal equilibrium with the medium if there are no mechanisms present that tend to introduce nonequilibrium behavior. Of course, in a nuclear reactor core even for a very thermal reactor the neutron distribution will never be precisely in thermal equilibrium because of one of the following effects: (a) presence of absorption, (b) presence of sources, (c) leakage of neutrons, or (d) time dependence.

These effects all act to perturb the neutron distribution away from thermal equilibrium. In fact, neutron thermalization can physically be regarded as a competition process between the moderator atoms attempting to "thermalize" the neutron distribution into thermal equilibrium with them, and those effects tending to perturb or distort the thermal neutron spectrum from this equilibrium distribution.

## B. Nonequilibrium Thermal Spectra

The presence of absorption or leakage or a slowing down source can act to distort the thermal spectrum, that is, the solution $\phi(E)$ to Eq. (9-1), from a Maxwellian flux $\phi_M(E)$. We will consider later procedures for calculating thermal spectra to any desired accuracy by solving Eq. (9-1) directly in Section 9-III. However it is useful to give a somewhat more qualitative discussion of nonequilibrium neutron spectra at this point to lay the groundwork for this subsequent discussion.

Consider first the addition of an absorption term to Eq. (9-7). One then finds that the thermal neutron spectrum will be slightly shifted to higher energies, almost as if its temperature were effectively increased by the addition of absorption (see Figure 9-1). This "absorption heating" of the spectrum can be easily understood, however, when it is recalled that most absorption cross sections behave essentially as $1/E^{1/2}$ for low energies. Hence the lower energy neutrons in the spectrum will tend to be preferentially depleted by absorption, and this leads to an effective shift (at least in the normalized spectrum) to higher energies.

Exactly the opposite effect occurs when one accounts for neutron leakage. This can be modeled by adding a term of the form $D(E)B_g^2$ to the total cross section in
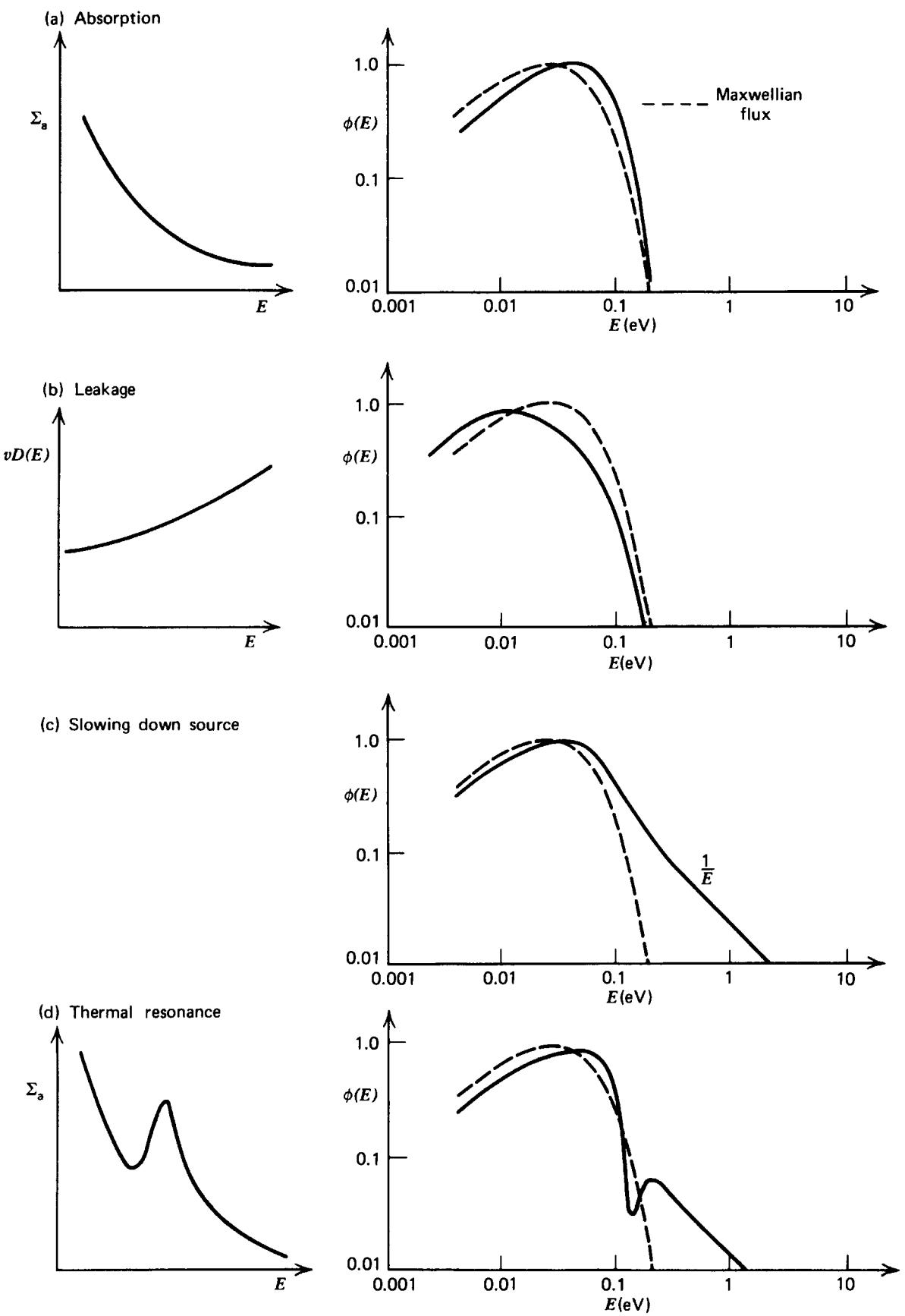
**FIGURE 9-1.** Effects of nonequilibrium perturbations on thermal neutron flux spectra.

380

Eq. (9-1). Note that this leakage term appears as an effective absorption. Now since $vD(E) = v[3\Sigma_{tr}(E)]^{-1}$ tends to increase with increasing energy, one finds that higher energy neutrons will tend to leak more rapidly from the system. This causes the equilibrium spectrum to shift to lower energies—that is, to a "diffusion cooling" effect.

Obviously the presence of a source term in Eq. (9-1) will also perturb the spectrum. For example, one is most commonly concerned with a source corresponding to neutron slowing down from higher energies. In this case one expects the neutron spectrum to behave as $1/E$ for energies above several eV.

Several other effects act to perturb the thermal spectrum away from equilibrium. For example, certain nuclides such as $^{135}$Xe, $^{235}$U, or $^{239}$Pu, have low-lying resonances in the thermal range. The neutron flux will be depressed in the vicinity of these resonances, as shown in Figure 9-1. Such low-lying resonance effects are particularly important toward the end of core life in reactors fueled with low-enrichment uranium, since the appreciable inventory of the plutonium produced can cause a strong distortion of the thermal spectrum.

## C. Effective Neutron Temperature Models

We have seen that the addition of absorption (or leakage) to a system tends to shift the equilibrium neutron spectrum to higher (or lower) energies, much as would occur if one were to change the temperature characterizing the Maxwell–Boltzmann distribution. For that reason, early studies of neutron thermalization represented the neutron spectrum by a Maxwellian with an effective temperature $T_n \neq T$:[8,9]

$$\phi(E) = \phi_M(E, T_n) = \phi_T \frac{E}{(kT_n)^2} \exp\left(-\frac{E}{kT_n}\right) \quad ,\phi_T \equiv n_0 \left(\frac{8kT_n}{\pi m}\right)^{1/2}. \quad (9-11)$$

Since absorption was the dominant loss mechanism in large thermal reactor cores, the *effective neutron temperature* $T_n$ was modeled as depending only on the relative absorption in the core

$$T_n = T[1 + A\Gamma], \qquad \Gamma \equiv \frac{\Sigma_a(kT)}{\xi\Sigma_s}, \quad (9-12)$$

where $T$ was the moderator temperature and $A$ was a dimensionless coefficient that had to be determined empirically by performing experimental spectrum measurements on the assembly of interest (typically, $A \sim 1.2$–$1.8$). It should be noted that the parameter $\Gamma$ that appears in this expression is just the inverse of the moderating ratio that measures the effective competition between absorption and scattering in determining the thermal spectrum.

The simple effective temperature model given by Eq. (9-11) is incorrect at high energies since it fails to yield the "$1/E$" behavior caused by a slowing down source. This can be easily corrected by adding to the model a slowing down term

$$\phi(E) = \phi_M(E, T_n) + \lambda \frac{\Delta(E/kT_n)}{E}, \quad (9-13)$$

where $\Delta(E/kT)$ is a "joining function" characterizing the transition between the

Maxwellian and the slowing down spectrum (see Figure 9-2) while $\lambda$ is a normalization factor given by

$$\lambda = \phi_T \frac{\sqrt{\pi}}{2} \frac{\Gamma}{1-\Gamma} . \tag{9-14}$$

The effective neutron temperature model played an important role in early reactor analysis and still is useful in obtaining a qualitative understanding of thermal reactor spectra. It is interesting to note that if indeed the neutron flux could be characterized by a Maxwellian $\phi_M(E, T_n)$ at a temperature $T_n$, then the total flux characterizing the thermal group would be just

$$\cdot \phi_T = \int_0^{E_c} dE\, \phi_M(E, T_n) \cong \int_0^{\infty} dE\, \phi_M(E, T_n) = \frac{2}{\sqrt{\pi}} v_T n_0, \tag{9-15}$$

where we have identified $v_T = \sqrt{2kT_n/m}$ . Hence we find that $\phi_T$ depends on the effective neutron temperature $T_n$.

An interesting application of this result is to the calculation of the reaction rates characterizing thermal neutrons. First recall that the effective cross sections which must be used would be averaged over a distribution of nuclear speeds at some temperature $T$. That is, the effective reaction rate depends both on the core temperature $T$ and the neutron temperature $T_n$:

$$F = \int_0^{E_c} dE\, \Sigma(E, T) \phi_M(E, T_n). \tag{9-16}$$

Now most thermal absorption cross sections behave as $1/v$ in the thermal neutron range. In Chapter 2, we found that when averaged over the distribution of nuclear speeds, the effective absorption cross section characterizing a $1/v$ absorber was independent of temperature and depended on neutron speed $v$ as

$$\Sigma_a(E, T) = \frac{\Sigma_a^0}{v} = \frac{\Sigma_a(E_0)v_0}{v} , \tag{9-17}$$
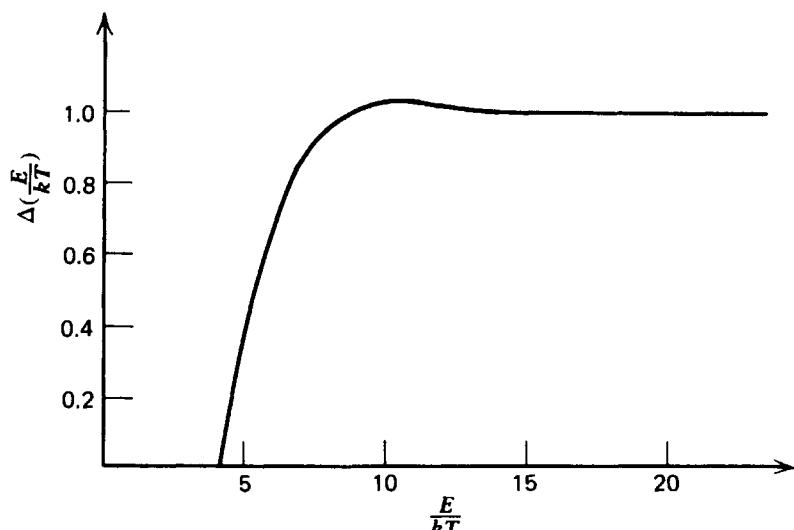


**FIGURE 9-2.** The joining function, $\Delta(E/kT)$.

where $\Sigma_a^0 = v_0 \Sigma_a(E_0)$ is just the absorption frequency evaluated at any reference speed $v_0$. Hence the absorption rate characterizing thermal neutrons is just

$$F_a = \int_0^{E_c} dE \, v \Sigma_a(E, T) n_0 M(E, T_n) = \Sigma_a(E_0) v_0 n_0$$

$$= \Sigma_a(E_0) \phi_0, \qquad (9\text{-}18)$$

where $\phi_0$ is the neutron flux evaluated at the reference speed $v_0$.

Since most neutron cross sections are measured in materials at the ambient temperature $T = 20.46°C$, it has become customary to tabulate thermal neutron cross section data at the corresponding speed $v_0 = (2kT/m)^{1/2} = 2200$ m/sec or energy $E_0 = kT = 0.025$ eV. That is, one tabulates $\Sigma_a(E_0)$. The reference flux $\phi_0$ is then referred to as the *2200 meter-per-second flux*. If we want to relate these quantities to the thermal flux $\phi_T$ characterizing a different temperature $T_n$, we first note

$$\phi_T = \frac{2}{\sqrt{\pi}} \left( \frac{T_n}{T_0} \right)^{1/2} \phi_0. \qquad (9\text{-}19)$$

We can also express the thermal group constant characterizing a $1/v$ absorber in a Maxwellian flux in terms of $\Sigma_a(E_0)$ as

$$\Sigma_{a_{th}} = \frac{\sqrt{\pi}}{2} \left( \frac{T_0}{T_n} \right)^{1/2} \Sigma_a(E_0). \qquad (9\text{-}20)$$

Note that one must take care to distinguish between the 2200 m/sec cross section $\Sigma_a(E_0)$ and the thermally-averaged cross section at ambient temperature, $\Sigma_{a_{th}} = (\pi/4)^{1/2} \Sigma_a(E_0)$, which differ by some 12%.

One can modify these results to calculate the Maxwellian-averaged thermal group constants of non-$1/v$ absorbers in this form by inserting a non-$1/v$ factor $g_a(T_n)$ to write

$$\Sigma_{a_{th}} = \frac{\sqrt{\pi}}{2} g_a(T_n) \left( \frac{T_0}{T_n} \right)^{1/2} \Sigma_a(E_0). \qquad (9\text{-}21)$$

Such non-$1/v$ factors have been tabulated for a number of isotopes of interest.[10] However, since we will make little use of the effective temperature model in our study of thermal neutron spectra, we will avoid a further discussion of such non-$1/v$ corrections.

There are several important reasons for abandoning the effective neutron temperature model in favor of a more sophisticated treatment of thermal neutron spectra. First, this rather simple model requires a good deal of empirical guess work in determining the absorption heating coefficient $A$ and the transition function $\Delta(E/kT)$. Furthermore one finds in practice that this model is inadequate when there is either strong absorption (i.e., $\Gamma \gtrsim 0.1$) or when the spectrum is appreciably influenced by resonance absorption in the thermal range. Since $\Gamma$ for a typical LWR ranges from a value of 0.2 for beginning of core life (with zero void fraction coolant) to as high as 0.6 at the end of core life (with high-quality steam

conditions), it is apparent that the effective temperature model has little relevance to this class of reactors. In addition, the presence of resonance absorbers in the thermal range (e.g., $^{239}$Pu) that can build up to appreciable levels near the end of core life also act to invalidate this model.

## D. An Overview of Techniques for Calculating Thermal Spectra

Most schemes for calculating thermal neutron spectra directly solve the infinite medium spectrum equation for the thermal energy range

$$\Sigma_t(E)\phi(E) = \int_0^{E_c} dE' \Sigma_s(E' \to E)\phi(E') + S(E), \quad 0 < E < E_c. \quad (9\text{-}22)$$

Here $S(E)$ is usually taken as a slowing down source, and the cutoff energy $E_c$ is taken sufficiently high that no appreciable upscattering out of the thermal range occurs.

If the cross sections are known, then Eq. (9-22) can be written in a fine-structure multigroup form and solved directly. There are several difficulties with such a brute force solution, however. First, the pointwise representation of the detailed cross section data in a nuclear data file such as ENDF/B is quite extensive and can require large amounts of data handling (particularly for the scattering kernels). In fact, it is sometimes preferable to directly generate the thermal cross section data from suitable theoretical models of the scattering material for the particular problem of interest. Furthermore the fact that appreciable upscattering occurs in the thermal range means that the multigroup representation of Eq. (9-22) involves full scattering matrices, rather than the lower triangular structures that appear when treating neutron slowing down. This implies that the multigroup thermalization equations must be solved simultaneously rather than successively from upper to lower energy groups, as were the multigroup slowing down equations. Such a solution usually requires iterative techniques (similar to those used in multidimensional diffusion calculations).

However in certain instances one can model the scattering material in such a way so as to reduce the integral equation (9-22) to a simple second-order differential equation, which is considerably easier to solve. One very popular such model represents the moderator as an ideal gas of unbound hydrogen atoms (or protons) which is in thermal equilibrium at a given temperature $T$. Because the proton gas model is extremely useful for modeling the thermal neutron behavior in LWRs, we will consider its development in some detail in this chapter.

## II. APPROXIMATE MODELS OF NEUTRON THERMALIZATION

### A. The Proton Gas (Wigner–Wilkins) Model[11,12]

Perhaps the simplest description of neutron thermalization yielding results of sufficient accuracy for use in reactor design is that which models the reactor core as a proton gas (mass number $A = 1$) in thermal equilibrium at a temperature $T$. Such a model obviously ignores both chemical binding and diffraction. However it does describe upscattering and has been proven remarkably successful for generating thermal spectra useful in LWR design.

To be more specific, we will consider the solution of the infinite medium spectrum equation (9-22) with the source term omitted. We will include the

presence of a source by demanding that $\phi(E)$ be properly normalized for large energies to yield the proper slowing down behavior. We will examine this equation for the case of a free proton gas under the assumptions:

(1) The microscopic scattering cross section $\sigma_s^H$ is independent of the relative velocity $v_r$ between neutron and proton.

(2) The absorption cross section behaves as $\sigma_a(v_r) = \gamma / v_r$. (This assumption can be relaxed in practice.)

(3) The proton gas is in thermal equilibrium at a temperature $T$. In this case we can use two-body kinematics to calculate the thermally averaged differential scattering cross section (cf. Section 2-I-D) as

$$\Sigma_s(E' \to E) = \frac{\Sigma_{fr}^H}{E'} \begin{cases} \operatorname{erf}\sqrt{\dfrac{E}{kT}} \ , & E' > E \\[2ex] \exp\left[\dfrac{(E'-E)}{kT}\right]\operatorname{erf}\sqrt{\dfrac{E'}{kT}} \ , & E' < E \end{cases} \qquad (9\text{-}23)$$

In Eq. (9-23) we have defined the *free atom scattering cross section* of hydrogen, $\Sigma_{fr}^H \equiv N_H \sigma_s^H$. We can calculate the macroscopic scattering cross section by integrating $\Sigma_s(E' \to E)$ over all final neutron energies to find

$$\Sigma_s(E) = \int_0^\infty dE' \, \Sigma_s(E \to E') = (\Sigma_{fr}^H / v) V(E), \qquad (9\text{-}24)$$

where we have defined

$$V(E) = \left(\frac{2kT}{M}\right)^{\frac{1}{2}}\left[\left(x + \frac{1}{2x}\right)\operatorname{erf} x + \pi^{-\frac{1}{2}}\exp(-x^2)\right], \quad x \equiv \left(\frac{E}{kT}\right)^{\frac{1}{2}}. \qquad (9\text{-}25)$$

We noted the form of the differential scattering cross section for a proton gas in Figure 2-15. In particular, we found that it approached the usual slowing down form

$$\Sigma_s(E' \to E) \to \frac{\Sigma_{fr}^H}{E'}, \qquad E' > E$$

$$0, \qquad E' < E \qquad (9\text{-}26)$$

for large $E$, $E' \gg kT$. It should also be noted from Eq. (9-23) that $\Sigma_s(E' \to E)$ has a discontinuous first derivative at $E = E'$. In fact, the structure of the scattering kernel $\Sigma_s(E' \to E)$ is very similar to that we encountered for the Green's functions of second-order differential equations (cf. Section 5-II). That is, Eq. (9-22) is of the form

$$\alpha(x)\phi(x) = \int_a^b dx' \, G(x, x')\phi(x') \qquad (9\text{-}27)$$

where $G(x, x')$ is the Green's function of a differential operator

$$LG(x, x') = a(x)\frac{d^2 G}{dx^2} + b(x)\frac{dG}{dx} + c(x)G(x, x') = \delta(x - x'). \qquad (9\text{-}28)$$

Hence if one can determine $L$, then by operating with $L$ on Eq. (9-27) as

$$L\alpha(x)\phi(x) = \int_a^b dx' \, LG(x,x')\phi(x') = \phi(x), \tag{9-29}$$

one can convert the original integral equation into a second-order ordinary differential equation:

$$a(x)\frac{d^2}{dx^2}(\alpha\phi) + b(x)\frac{d}{dx}(\alpha\phi) + [c(x)\alpha(x) - 1]\phi(x) = 0. \tag{9-30}$$

This procedure was utilized by Wigner and Wilkins[11] to convert Eq. (9-22) into a differential equation for $\psi \equiv \phi(E)/[EM(E)]^{\frac{1}{2}}$:

$$-\frac{d}{dx}\left\{ \frac{1}{P(x)}\frac{d}{dx}[V(x)+\Gamma]\psi(x) \right\} + \left\{ W(x)[V(x)+\Gamma] - \frac{4}{\sqrt{\pi}} \right\}\psi(x) = 0 \tag{9-31}$$

where

$$W(x) = \frac{x^2}{P(x)} - \frac{e^{-x^2}}{P^2(x)}, \qquad x \equiv \left(\frac{E}{kT}\right)^{\frac{1}{2}},$$

$$P(x) = e^{-x^2} + \sqrt{\pi}\, x\, \mathrm{erf}(x), \tag{9-32}$$

$$\Gamma = \frac{\Sigma_a(kT)}{\Sigma_{fr}^H} = \frac{N_A \gamma}{v_T N_H \sigma_s^H}.$$

Eq. (9-31) is known naturally enough as the *Wigner–Wilkins equation*. To it one appends the boundary conditions that the flux variable vanish as $x \to 0$ $[E \to 0]$ and be normalized to the slowing down source for $x \gg 1$ $[E \gg kT]$.

The Wigner–Wilkins equation has been studied analytically in exhaustive detail using a wide variety of approximation techniques—none of which really concern us here.[1] Of much more interest is the fact that such second-order ODEs can be very easily solved on a digital computer. To facilitate this solution, one first introduces a change of dependent variable to recast Eq. (9-31) into a nonlinear *first*-order differential equation (a *Ricatti* equation) more suitable for numerical integration:

$$\frac{dJ}{dE} = \frac{S(E)}{2kT} + \left[ \frac{1-2P(E)}{2E} \right]J(E) - \frac{P(E)}{2E}J^2(E), \tag{9-33}$$

where

$$\phi(E) = \frac{E}{Q(E)}\exp\left\{ \frac{1}{2}\int_0^E \frac{dE'}{E'}[P(E')[J(E')+1] - [1+E'/kT]] \right\}, \tag{9-34}$$

while

$$S(E) = \frac{1}{x^2}[1 - P(x)] + \frac{x^2}{P(x)} - \frac{e^{-x^2}}{P^2(x)} - \frac{4}{Q},$$

$$\tag{9-35}$$

$$Q(E) = P + \frac{1}{x}\frac{\sqrt{\pi}}{2}\mathrm{erf}\,x + \sqrt{\frac{\pi}{kT}}\left[ \frac{\Sigma_a(E) + DB^2}{\Sigma_{fr}^H} \right].$$

Here we have modified this derivation to include a non-$1/v$ absorption and modeled leakage with a $D(E)B^2$ term where

$$D(E) = (3\Sigma_{tr})^{-1} = [3(\Sigma_a + \Sigma_s(1 - \bar{\mu}_0))]^{-1}. \qquad (9\text{-}36)$$

Although the equation for $J(E)$ looks rather complicated it is in fact quite simple to solve numerically. Thermal spectrum codes based on solutions of the Wigner–Wilkins equation are occasionally referred to as SOFOCATE-type methods[12] (after the early thermal spectrum codes used for LWR calculations).

In most of these codes, Eq. (9-33) is first solved for $J(E)$ numerically using Milne's predictor–corrector method.[13] To get this method started, an asymptotic solution for $E \ll kT$ is used. Once $J(E)$ is known, $\phi(E)$ is then determined from Eq. (9-34) using a numerical integration (e.g., trapezoidal rule). Typically on the order of 50–60 mesh points are found to yield suffficient accuracy over the interval $0 < E < 1$ eV. (It is amusing to note that Eq. (9-33) is integrated from lower to higher energies, in contrast to fast spectrum calculations which always proceed downward in energy—or upwards in lethargy, the more convenient variable for slowing down calculations.)

The Wigner–Wilkins equation can be applied to mixtures of scattering isotopes by simply replacing the free atom cross section by an effective scattering cross section characterizing the mixture:

$$\Sigma_{fr}^H \to \sum_j \xi_j N_j \sigma_s^j = \bar{\xi}\Sigma_s. \qquad (9\text{-}37)$$

In fact sometimes (although very infrequently) the Wigner–Wilkins equation is applied by this modification to the analysis of nonhydrogeneous media in the hope that the actual spectrum will not be too sensitive to the details of the scattering process.

In Figure (9-3) we have illustrated the shape of the Wigner–Wilkins spectrum for a $1/v$ absorber, a slowing down source, and a thermal resonance (recall Figure 9-1). It should be noted that this model yields not only the correct solutions for $\Sigma_a \to 0[\phi \to \phi_M]$ and $E \ll kT[\phi \to 1/E]$, but also accounts for both absorption "heating" effects as well as flux depression in the vicinity of a thermal resonance.
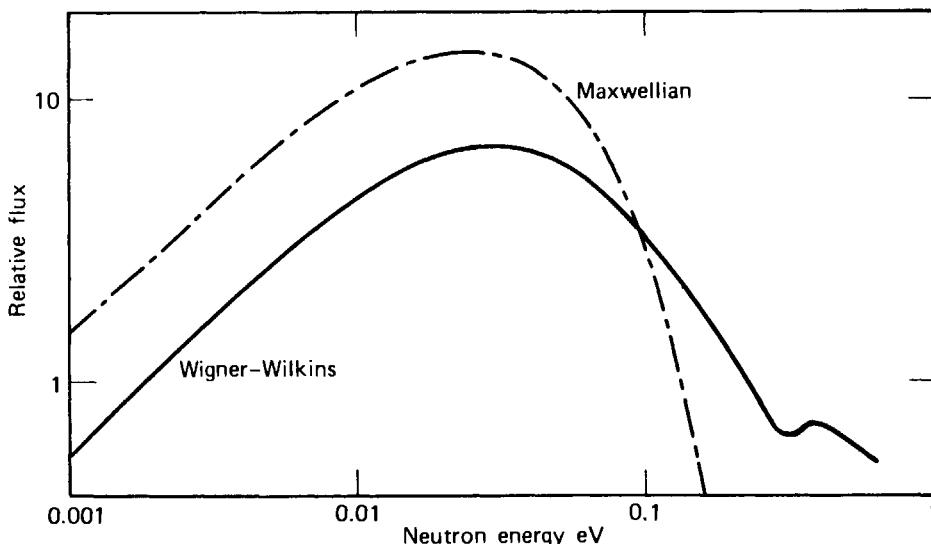


FIGURE 9-3.    Calculated thermal flux shapes.

One can now generate thermal group constants by simply performing numerically the averages of the microscopic cross section data over these computed thermal spectra.

It is very important to take into account the spatial heterogeneities present in a reactor core when generating thermal group constants because the thermal neutron mfp is frequently small compared to the distances characterizing the core lattice structure. Fortunately there are procedures available by which one can make simple modifications to infinite medium spectrum calculations to account for these spatial effects, thereby avoiding a detailed multigroup calculation of neutron diffusion. We will return to discuss these methods in more detail in Chapter 10.

It should be noted that the proton gas model effectively converts an integral equation (9-22) into an ordinary differential equation. Such a result is of some significance when considering numerical solutions, since these differential equations are considerably easier to solve than the full matrix equations that arise from discretizing the integral equation directly. In particular it allows us to calculate the numerical solution at one energy mesh point directly from the previous one or two mesh points, so that only a small computer memory is required and iterative methods are avoided.

There are other models of neutron thermalization that exploit the techniques of converting the integral equation (9-22) into a differential equation more suitable for machine calculations. We will next examine a model that can be utilized for survey estimates of the thermal spectrum when the moderator mass number $A$ is large (e.g., $^{12}C$).

## B. The Heavy Gas Model[14]

Obviously the proton gas model is of limited utility in analyzing neutron thermalization in nonhydrogeneous moderators. Alternative models are needed for heavier mass moderators such as graphite, which is used in gas-cooled reactors. One of the simplest thermalization models is based on expanding the cross section for a free gas of arbitrary mass number $A$ in powers of $1/A$, hence arriving at an approximation which should be valid for large mass numbers.

The differential scattering cross section for a free gas can be derived in a straightforward, if somewhat cumbersome, consideration of two-body kinematics (similar to that of Section 2-I-D). This cross section can be written as

$$\Sigma_s(E'\rightarrow E) = \frac{\Sigma_{fr}\theta^2}{2E'} e^{-(\epsilon-\epsilon')}\left\{\left[\mathrm{erf}(\theta\sqrt{\epsilon}'-\rho\sqrt{\epsilon})\pm\mathrm{erf}(\theta\sqrt{\epsilon}'+\rho\sqrt{\epsilon})\right]\right.$$

$$\left. +\mathrm{erf}(\theta\sqrt{\epsilon}-\rho\sqrt{\epsilon}')\mp\mathrm{erf}(\theta\sqrt{\epsilon}+\rho\sqrt{\epsilon}')\right\}, \qquad E'\lessgtr E, \quad (9\text{-}38)$$

where

$$\theta = \frac{(A+1)}{2\sqrt{A}}, \quad \rho = \frac{(A-1)}{2\sqrt{A}}, \quad \epsilon = \frac{E}{kT}. \qquad (9\text{-}39)$$

If we now expand in inverse mass number $A^{-1}$ and retain only lowest order terms,

we arrive at the *heavy gas model* of the scattering kernel

$$\Sigma_s(E' \to E) = \Sigma_{fr}\left(\frac{E}{E'}\right)^{\frac{1}{2}}\left\{\delta(E-E') + \frac{(E+E')}{A}\left[\delta'(E-E') + kT\delta''(E-E')\right]\right\}$$

(9-40)

Here $\delta'$ and $\delta''$ are the first and second derivatives of the Dirac $\delta$-function and are defined in Appendix C. The corresponding total scattering cross section for this model is

$$\Sigma_s(E) = \Sigma_{fr}\left(1 + \frac{kT}{2AE}\right).$$

(9-41)

If we now substitute this rather singular scattering kernel back into our integral equation and note that for large $A$, $\xi \sim 2/A$, such that

$$\int_0^\infty dE' \Sigma_s(E' \to E)\phi(E') = \xi\Sigma_{fr}\left[kTE\frac{d^2\phi}{dE^2} + E\frac{d\phi}{dE} + \phi\right] + \Sigma_s(E)\phi,$$

(9-42)

then we find that Eq. (9-2) becomes

$$\Sigma_a(E)\phi(E) = \xi\Sigma_{fr}\left[EkT\frac{d^2\phi}{dE^2} + E\frac{d\phi}{dE} + \phi(E)\right].$$

(9-43)

This simple second-order differential equation is known as the *heavy gas equation*. In many ways the heavy gas approximation is similar to the age approximation we developed to describe neutron slowing down in heavy mass moderators, and in the high-energy limit the heavy gas model just reduces to age theory.

Using the usual techniques from the theory of second-order ordinary differential equations, one can laboriously generate asymptotic solutions to this equation for different absorption cross section energy dependences—for example, $\Sigma_a(E)$ = constant = $\Sigma_a$, or $\Sigma_a(E) = \gamma/v$. It can also be integrated directly to generate thermal neutron spectra for moderators such as graphite. For example, the numerical solution of the heavy gas equation (assuming $1/v$ absorption) is shown in Figure 9-4 for several different values of the parameter $\Gamma = \Sigma_a(kT)/\xi\Sigma_{fr}$.

It should be noted that as the moderator mass becomes increasingly heavier (i.e., $\xi$ smaller), the moderator is increasingly less capable of slowing down neutrons and hence the spectrum hardens. In this model, then, a heavier gas is equivalent to the addition of absorption.

Unfortunately the heavy gas (or even free gas) model is far less effective at predicting thermal spectra in graphite moderated reactors (such as the HTGR) than is the proton gas model for the LWR[15] because of the significance of chemical binding effects. This has led to a rather limited use of this model in practice.

## C. Synthetic Scattering Kernel Models

In our two previous models of neutron thermalization we found that the scattering kernel $\Sigma_s(E' \to E)$ was of such a form that we could transform the
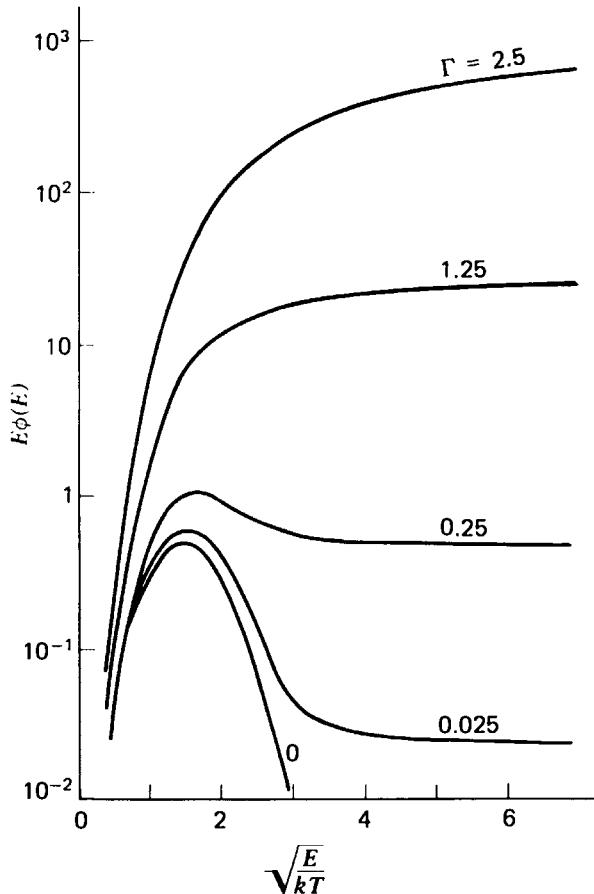
**FIGURE 9-4    The neutron spectrum predicted by the heavy gas model.**

integral form of the infinite medium spectrum equation (9-1) into a differential equation that was far better suited to machine computation.

It is natural to seek other models of neutron thermalization which also lead to differential equations. One such model is the *generalized heavy gas* or *primary model*[16] proposed by Horowitz in which the scattering terms in Eq. (9-1) are modeled by a differential equation very similar to the heavy gas model (9-42):

$$\int_0^\infty dE' \Sigma_s(E' \to E)\phi(E') - \Sigma_s(E)\phi(E) \cong \xi\Sigma_{fr}\frac{d}{dE}\left\{ f(E)\left[ EkT \frac{d\phi}{dE} + (E - kT)\phi \right]\right\}$$

$$(9\text{-}44)$$

Here $f(E)$ is an arbitrary function that must be determined either by fitting to experimental spectrum measurements or by a fit to an integral of the scattering kernel itself $\Sigma_s(E' \to E)$. The primary model satisfies the detailed balance condition and includes some accounting for chemical binding effects. Moreover the storage requirements and machine time required to solve the differential equation generated by Eq. (9-44) are quite small when compared to the machine labor involved in solving the integral equation (9-1) directly.

Unfortunately the primary model due to Horowitz fails to yield satisfactory results when strong absorption is present—particularly in the vicinity of thermal resonances. To circumvent this, Cadilhac[17] developed a slightly more elaborate

approximation known as the *secondary model* containing two (rather than one) free functions. One first writes the scattering kernel as the product of these two arbitrary functions $u(E)$ and $v(E)$ such that

$$M(E)\Sigma_s(E \rightarrow E') \cong \begin{cases} u(E)v(E'), & E > E' \\ u(E')v(E), & E < E'. \end{cases} \tag{9-45}$$

(Note again the discontinuous derivative at $E' = E$.) Then one finds that the infinite medium spectrum equation (9-1) can be written as the coupled set of differential equations

$$\Sigma_a(E)\phi(E) = \frac{dq}{dE} + S(E),$$

$$\frac{d}{dE}\left[\frac{\phi(E)}{M(E)}\right] = j(E)q(E) - \frac{d}{dE}\left[k(E)\frac{dq}{dE}\right], \tag{9-46}$$

where $j(E)$ and $k(E)$ are given in terms of the "free" functions, $u(E)$ and $v(E)$, as

$$j(E) = \frac{1}{v_1(E)} \frac{d}{dE}\left[v(E)k(E)\right], \quad v_1(E) \equiv \int_0^E dE' v(E'),$$

$$k(E) = \left[M(E)\Sigma_s(E)\right]^{-1}. \tag{9-47}$$
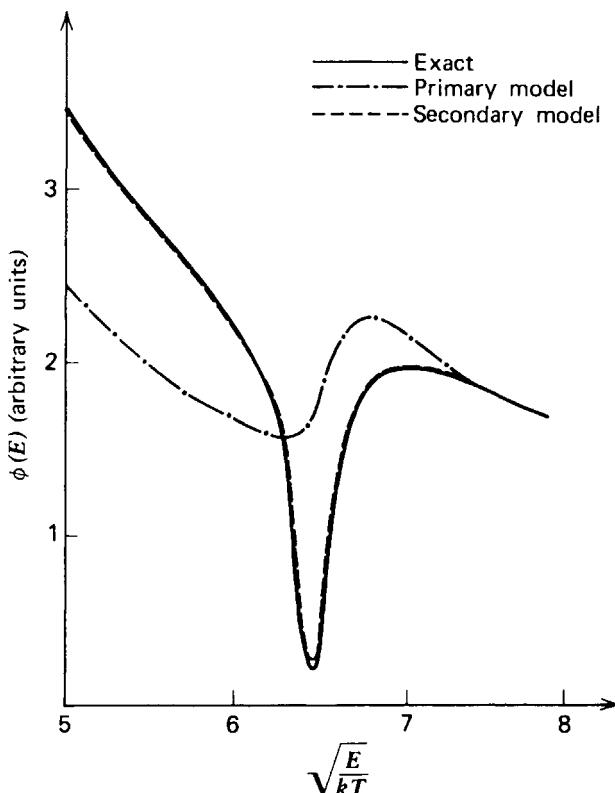


FIGURE 9-5.    Comparison of the primary and secondary synthetic kernel model predictions for the flux in the neighborhood of the $^{240}$Pu resonance (moderator is graphite).

This model is particularly interesting since for proper choices of $u(E)$ and $v(E)$ it will reduce to several of our earlier models including the proton gas model, the heavy gas (or primary) model, the Fermi age model, or the Goertzel–Greuling model. Hence the secondary model is evidently capable of bracketing the thermalization properties of the true scattering kernel $\Sigma_s(E' \to E)$.

One can choose the free functions $u(E)$ and $v(E)$ in any of a number of ways. For example, one can choose these functions by demanding that the first two energy moments of the true scattering kernel $\Sigma_s(E' \to E)$ be preserved by the approximate model [Eq. (9-45)]. The spectra predicted by the secondary model are frequently in excellent agreement with the results of a brute force numerical solution of Eq. (9-1) using the true scattering kernel $\Sigma_s(E' \to E)$. This is true even in the vicinity of thermal resonances, as illustrated in Figure 9-5.

Although the secondary model is usually not used for detailed thermal spectrum studies, it is frequently used to generate the initial guesses of the spectrum used in more elaborate iterative calculations necessary to solve the infinite medium spectrum equation (9-1) directly.

## III. GENERAL CALCULATIONS OF THERMAL NEUTRON SPECTRA

### A. Generation of Thermal Cross Section Data

As we have mentioned, thermal neutron cross sections are complicated by a sensitive dependence on the temperature and chemical state of the scattering material. Although such cross section information is tabulated and stored in nuclear data sets such as ENDF/B, it is useful to discuss briefly how these basic data are calculated. It is customary to express the differential scattering cross section $\sigma_s(E' \to E, \hat{\Omega}' \to \hat{\Omega})$ in terms of a quantity, $S(\alpha, \beta)^{1-6,15}$ known as the *scattering law* for the material of interest:

$$\sigma_s(E' \to E, \hat{\Omega}' \to \hat{\Omega}) = \frac{1}{4\pi kT} \left( \frac{E}{E'} \right)^{\frac{1}{2}} \exp\left( -\frac{\beta}{2} \right) \sigma_b S(\alpha, \beta). \tag{9-48}$$

Here, $\sigma_b$ is the bound atom cross section, while $\alpha$ and $\beta$ are related to the neutron momentum and energy exchange in a scattering collision:

$$\alpha \equiv (E' + E - 2\sqrt{E'E}\ \hat{\Omega} \cdot \hat{\Omega}')/kT,$$

$$\beta \equiv (E' - E)/kT. \tag{9-49}$$

$S(\alpha, \beta)$ depends in a very complicated manner on the detailed structure and dynamics of the scattering material. Most commonly, however, one introduces several horrifyingly brutal approximations (at least to the solid-state physicist, although not to the nuclear engineer) in order to allow the calculation of $S(\alpha, \beta)$. First one accounts for only incoherent scattering (i.e., no diffraction) such that $S(\alpha, \beta)$ is replaced by the incoherent part of the scattering law, $S_s(\alpha, \beta)$. Then this

quantity is calculated in the so-called Gaussian approximation[18] in which

$$S_s(\alpha,\beta) = \frac{1}{2\pi} \int_{-\infty}^{\infty} d\tau\, e^{i\beta\tau} \exp\left[-\alpha w^2(\tau)\right],$$

$$w^2(\tau) \equiv \int_{-\infty}^{\infty} \frac{d\beta\, \rho(\beta)}{\beta \sinh(\beta/2)} \left[\cosh\left(\frac{\beta}{2}\right) - \cos\left(\frac{\beta_i}{\chi_i}\right)\right]. \tag{9-50}$$

The entire dependence of the neutron scattering on the motion of the moderator atoms is contained in the function $\rho(\beta)$ or equivalently, $\rho(\omega)$, $\omega = kT\beta/\hbar$. For a harmonic solid, one would identify $\rho(\omega)$ as the phonon frequency distribution.

All of the essential physics enters into modeling the form of the function $\rho(\omega)$. In liquid moderators such as water, one uses models that account for the vibrations, hindered rotations, and translations of the water molecule (this gives rise to the so-called Nelkin scattering kernel[1-6] used for water or the St. John–Brown[1-6] kernel for $D_2O$). For polycrystalline materials such as graphite, the details of lattice vibrations must be taken into account. (The usual model used to describe graphite is known as the Park's scattering kernel[1-6].) It is necessary to use these more elaborate models of the microscopic dynamics of the moderator in performing detailed reactor studies.

The generation of thermal cross section data usually begins with the calculation of the scattering law $S(\alpha,\beta)$ for a given phonon frequency distribution $\rho(\omega)$ using a computer program such as the GASKET code.[19] A supplementary calculation is then needed to generate the actual scattering kernel $\Sigma_s(E' \to E, \hat{\Omega}' \to \hat{\Omega})$ from the scattering law (e.g., the FLANGE code).[20] These data can then either be used to prepare a restricted thermal cross section library, or transferred into a complete nuclear data set such as ENDF/B.

## B. Thermal Spectrum Calculations

For accurate determination of thermal neutron spectra and the generation of thermal group constants, one must perform a direct solution of the infinite medium spectrum equation (9-1) by writing it in a discrete multigroup form

$$\Sigma_{t_n}\phi_n = \sum_{n'=1}^{N} \Sigma_{s_{n'n}}\phi_{n'} + S_n \tag{9-51}$$

where $n$ is the fine group index. Since the thermal energy range is rather narrow $(0 \leqslant E \lesssim 1 \text{ eV})$, and typically from 50 to 100 energy groups are used, one can usually just use input cross section data on a pointwise basis (evaluated at the center of a group, for example).

Actually Eq. (9-1) is a bit too simplified, since one usually adds in a crude spatial treatment using the $P_1$ or $B_1$ method in a manner similar to that used to calculate fast spectra. Then the thermal leakage is determined by specifying an equivalent geometric buckling $B_g^2$.

Such infinite medium spectrum calculations must also be corrected for core heterogeneities. In the next chapter we will develop several prescriptions for

modifying the thermal group constants to account for flux nonuniformities which arise in a fuel lattice cell.

## C. Coupling between Fast and Thermal Spectrum Calculations

In a rigorous determination of the fast and thermal neutron energy spectrum, the fast and thermal energy regions will be coupled together. Downscattering from higher energies provides the source term in the thermal range, while thermal neutron induced fission reactions will give rise to the fission source in the fast neutron region. In addition there may be some mild influence on the lower energy behavior of the fast spectrum due to upscattering of thermal neutrons.

Fortunately the coupling between fast and thermal spectrum regions is sufficiently weak that the calculation of fast and thermal neutron spectra are usually performed separately. However many fast spectrum codes will generate the $P_0$ and $P_1$ slowing down sources to be inserted into thermal spectrum calculations. Usually all downscattered neutrons from the fast region are assumed to go into the highest energy thermal group, except for hydrogeneous moderators in which the slowing down neutrons are distributed over all thermal groups. If upscattering out of the thermal region is allowed, these neutrons are usually assumed to go into the lowest energy fast group.

## REFERENCES

1. M. M. R. Williams, *The Slowing Down and Thermalization of Neutrons*, North-Holland, Amsterdam (1966).
2. G. I. Bell and S. Glasstone, *Nuclear Reactor Theory*, Van Nostrand, New York (1970), Chapter 7.
3. K. H. Beckurts and K. Wirtz, *Neutron Physics*, Springer, Berlin (1964).
4. *Neutron Thermalization and Reactor Spectra*, International Atomic Energy Agency, Vienna (1968), Vols. I–II.
5. I. I. Gurevich and L. V. Tarasov, *Low Energy Neutron Physics*, Wiley, New York (1968).
6. D. E. Parks, M. S. Nelkin, N. F. Wikner, and J. R. Beyster, *Slow Neutron Scattering and Thermalization with Reactor Applications*, Benjamin, New York (1970).
7. A. C. Zemach and R. L. Glauber, *Phys. Rev.* **101**, 118 (1956).
8. R. F. Coveyou, R. R. Bate, and R. K. Osborn, ORNL-1958 (1955).
9. E. R. Cohen, *Nucl. Sci. Eng.* **2**, 227 (1957).
10. C. H. Westcott, Effective cross section values for well-moderated thermal reactor spectra, AECL-1101, 1962 (3rd Edition).
11. E. P. Wigner and J. E. Wilkins, AECD-2275 (1944); M. M. R. Williams, *The Slowing Down and Thermalization of Neutrons*, North-Holland, Amsterdam (1966), p. 75.
12. H. Amster and R. Suarez, The calculation of thermal constants averaged over a Wigner Wilkins flux spectrum; SOFOCATE, WAPD-TM-39 (1957).
13. B. Carnahan, H. A. Luther, and J. O. Wilkes, *Applied Numerical Methods*, Wiley, New York (1969) p. 386.
14. J. E. Wilkins, USAEC Document CP-2481 (1944); *Ann. Math.* **49**, 189 (1948).
15. J. R. Beyster, N. Corngold, H. C. Honeck, G. D. Joanou and D. E. Parks, P/258 in Third U. N. Conference on Peaceful Uses of Atomic Energy (1964).
16. M. M. R. Williams, *The Slowing Down and Thermalization of Neutrons*, North-Holland, Amsterdam (1966), p. 273.
17. M. Cadilhac, J. Horowitz, J. L. Soule, and O. Tretiakoff, Proceedings BNL Conference on Thermalization 2, 1962; M. Cadilhac, et. al., Third U. N. Conference on Peaceful Uses

of Atomic Energy (1964); M. M. R. Williams, *The Slowing Down and Thermalization of Neutrons*, North-Holland, Amsterdam (1966), p. 292.

18. P. A. Egelstaff and P. Schofield, *Nucl. Sci. Eng.* **12**, 260 (1962).
19. J. U. Koppel, J. R. Triplett and Y. D. Naliboff, GASKET, a unified code for thermal neutron scattering, General Atomic Report GA-7417 (1966).
20. H. C. Honeck and D. R. Finch, FLANGII (Version 71-1), a code to process thermal neutron data from an ENDF/B tape, Savannah River Laboratory Report DP-1278 (1971).

## PROBLEMS

9-1 Show that the scattering cross section $\sigma_{fr}$ of a free nucleus is related to that characterizing a perfectly bound nucleus $\sigma_b$ by $\sigma_b = (1 + A^{-1})^2 \sigma_{fr}$. (Hint: First demonstrate that $\sigma_b = 4\pi \dfrac{d\sigma_b}{d\Omega}\bigg|_{\cos\theta = 1} = 4\pi \dfrac{d\sigma_{fr}}{d\Omega}\bigg|_{\cos\theta = 1}$. Then use the expression for $d\sigma_{fr}/d\Omega$ for $s$-wave scattering.)

9-2. Generalize the definition of the slowing down density $q(\mathbf{r}, E)$ given by Eq. (8-18) to account for *upscattering* as well as downscattering.

9-3 Using the definition of the slowing down density for energies $E > E_c$ in the infinite-medium spectrum equation (9-1), derive the balance condition Eq. (9-4).

9-4 Check by explicit calculation whether the detailed balance condition holds for the scattering kernels characterizing: (a) a free proton gas, (b) the heavy gas model, and (c) a free gas of arbitrary mass number $A$.

9-5 Give three reasons why the neutron energy distribution in a thermal homogeneous reactor is not Maxwellian. What specific physical effects cause deviations at high energies and what physical effects give rise to deviations at low energies?

9-6 Calculate the *average* energy and velocity of neutrons in a Maxwellian distribution at a temperature $T_n$.

9-7 Plot the behavior of $E\phi(E)$ against $E$ for the effective temperature model given by Eq. (9-13). In particular show that the peak of $E\phi(E)$ occurs at $E \sim 2kT_n$.

9-8 Suppose that a $1/v$ absorber is suddenly inserted uniformly into an infinite medium containing a well-established Maxwellian distribution of neutrons.

(a) Show that the total density of neutrons in the medium steadily decreases in time, but that the neutron energy distribution, and hence the effective neutron temperature, does not change.

(b) Discuss qualitatively the change in the energy distribution for a non-$1/v$ absorber.

[Hint: Solve the time-dependent infinite medium spectrum equation as an initial value problem subject to the initial condition, $\phi(E, t = 0) = \phi_M(E)$.]

9-9 A water-moderated thermal reactor operating at 300°C has a computed average thermal flux of $2 \times 10^{14}$ neutrons/cm²-sec. Compute the absorption rate density in the water in this reactor. [Take $\rho_{H_2O} = 0.72$ g/cm³ (at 155 bar).]

9-10 Demonstrate with equations how to measure the neutron temperature in the center of a reactor core by simultaneous activation of manganese ($1/v$ neutron absorber) and lutetium (.142 eV resonance absorber) foils in the core.

9-11 Sketch the dependence of the thermal group constants characterizing a $1/v$ absorber on $\Gamma = \Sigma_a/\xi\Sigma_s$ if the thermal spectrum is characterized by a Maxwellian flux $\phi_M(E, T_n)$ with an effective neutron temperature $T_n = T(1 + A\Gamma)$.

9-12 Demonstrate that the requirement expressed by equation (9-3) demands that we choose the "joining function" normalization as $\lambda = \sqrt{\pi} \, \phi_T \Gamma/2(1 - \Gamma)$ in the effective temperature model, if we assume a slowing down source into the thermal group of $q(E_c) = \xi\Sigma_s\lambda$.

9-13  Verify the expression given for $\Sigma_s(E)$ characterizing a free proton gas by explicitly integrating the form given in Eq. (9-23) for $\Sigma_s(E' \to E)$.

9-14  The second energy moment of the scattering kernel,

$$M_2 \equiv \frac{1}{(kT)^2} \int_0^\infty dE' \int_0^\infty dE \, M(E')(E'-E)^2 \sigma_s(E' \to E)$$

is a measure of the mean squared energy exchanged between the neutron and the scattering atoms. Demonstrate that for a free proton gas $M_2 = 2\sqrt{2}\ \sigma_{fr}$.

9-15  Derive the Wigner–Wilkins equation (9-31) from the infinite medium spectrum equation (9-22) characterizing a proton gas. [Refer to E. P. Wigner and J. E. Wilkins, AECD 2275 (1944) or M. Williams, *Thermalization and Slowing Down of Neutrons*, North Holland, Amsterdam (1967), p. 77 for assistance.]

9-16  Using the variable transformation defined by Eq. (9-34), derive the Ricatti equation (9-33) from the Wigner–Wilkins equation.

9-17  Write a computer program that integrates the nonlinear differential equation (9-33) characterizing a free proton gas. Use either a predictor–corrector or Runge–Kutta scheme with an energy mesh size of $\Delta E = 0.01$ eV. Determine the flux $\phi(E)$ from $J(E)$ by performing the integration indicated in Eq. (9-34) using trapezoidal quadrature. For convenience, choose a $1/v$ absorption cross section $\Sigma_a(E) = \Sigma_a^0/\sqrt{E}$. Allow $\Sigma_a^0$, $\Sigma_{fr}^H$, $B^2$, and $T$ to be read in as inputs to the code.

9-18  Use the computer code written in Problem (9-17) to determine the spectrum in water at room temperature. Compare this spectrum with that predicted by the effective temperature model.

9-19  Run a SOFOCATE-type thermal spectrum code to generate the thermal neutron spectrum for a typical PWR and BWR core using the parameters tabulated in Appendix H. Use exit coolant conditions.

9-20  Repeat the spectrum calculation in Problem 9-19 for the PWR with boron added to the water moderator in concentrations of 500, 1000, and 1500 ppm (parts-per-million).

9-21  Derive the heavy gas equation from the infinite medium spectrum equation (9-22) by expanding $\phi(E')$ in the scattering integral in a Taylor series about $E$, and then truncating all terms of order higher than $(E-E')^2$. It will be helpful to note that for $A \gg 1$,

$$\int_0^\infty dE \, \sigma_s(E' \to E)(E'-E) \cong \frac{2}{A} \sigma_{fr}(E'-2kT),$$

$$\int_0^\infty dE \, \sigma_s(E' \to E)(E'-E)^2 \cong \frac{4}{A} \sigma_{fr}E'kT.$$

9-22  Demonstrate that for $E \gg kT$, the solution to the heavy gas equation is just $\phi(E) \sim C/\xi\Sigma_{fr}E$.

9-23  Determine the choice of the functions $u(E)$ and $v(E)$ of the secondary model that will yield the proton gas model and the heavy gas model.

9-24  A very useful approximation to the thermal neutron scattering kernel $\Sigma_s(E' \to E)$ is the so-called *synthetic* or *simple degenerate kernel* (SDK) model

$$\Sigma_s(E' \to E) = \beta\Sigma_s(E')vM(E)\Sigma_s(E),$$

where

$$\beta^{-1} = \int_0^\infty dE \, vM(E)\Sigma_s(E).$$

[See N. Corngold, P. Michael, and W. Wollman, *Nucl. Sci. Eng.* **15**, 13 (1963).] Demonstrate that this kernel preserves the correct total scattering cross section $\Sigma_s(E)$ and also satisfies the principle of detailed balance.

9-25 Solve the infinite medium spectrum equation for the flux resulting from an arbitrary source $S(E)$ using the SDK model.

9-26 The SDK model can be used to study the time-dependent thermalization of a neutron pulse injected into a moderator at an energy $E_0$. To this end, consider the initial value problem

$$\frac{1}{v} \frac{\partial \phi}{\partial t} + \Sigma_t(E)\phi(E,t) = \int_0^\infty dE' \Sigma_s(E' \to E)\phi(E',t)$$

subject to the initial condition

$$\phi(E,0) = \phi_0 \delta(E - E_0).$$

Assuming an absorption $\Sigma_a(E) = \Sigma_a^0/v$ and the SDK model, solve this problem for $\phi(E,t)$. (Hint: Use a Laplace transform in time.)

9-27 Age-diffusion theory can be used to provide the effective slowing down source for the neutron diffusion equation characterizing the thermal group. In this manner, determine the distribution of thermal neutrons resulting from an isotropic point source of monoenergetic fast neutrons located at the origin. In particular, discuss the asymptotic behavior of your solution far from the source for $\sqrt{\tau} \gtrsim L$.

9-28 Describe possible experimental techniques for measuring: (a) the neutron age to thermal and (b) the thermal neutron diffusion length. Assume that the only available neutron source is a fast ($\sim 2$ MeV) source. Justify your discussion by simple calculations. Then discuss how your experiments would differ for graphite and for light water.

9-29 Neutrons of lethargy zero are produced uniformly throughout an infinite medium. Assume that they then slow down by elastic collisions until they reach $E_{th}$ and there enter a one-speed diffusion process. The medium is characterized by the macroscopic cross sections $\Sigma_s$, $\Sigma_a$, $\Sigma_f$, and $\Sigma_t$, which are all independent of neutron energy for all energies. Find the fraction of fissions caused by the thermal neutrons. Assume that the age approximation is valid, that is, $q(u) = \xi \Sigma_t \phi(u)$.

9-30 Demonstrate that when age-diffusion theory is used to describe neutron slowing down, and one-speed diffusion theory is used to describe thermal neutron diffusion, then the multiplication factor for a bare, homogeneous reactor is

$$k = \eta_{th} f_{th} p \epsilon \frac{\exp - B_g^2 \tau}{1 + L^2 B_g^2}.$$

9-31 Compute and plot the critical mass and the fast and slow nonleakage probabilities for a spherical assembly of $^{235}U$ and moderator as a function of the radius of the assembly for the following moderators: (a) $H_2O$, (b) $D_2O$, (c) Be, and (d) graphite. Determine the minimum critical mass in each case. (Use the parameters listed in Table 8-7.)

# 10

## Cell Calculations for Heterogeneous Core Lattices

Thus far we have restricted ourselves to the study of reactor cores in which fuel, moderator, coolant, and structural materials were assumed to be intimately and homogeneously mixed. However, nuclear reactor cores are of course constructed in a highly heterogeneous configuration to facilitate thermal design (coolant channels, heat-transfer surfaces), mechanical design (structural integrity, fuel fabrication and handling), and reactivity control (control rods, burnable poisons, instrumentation). For example, the reader should recall the rather detailed structure of the typical PWR core illustrated in Figures 3-6 and 3-7. Such heterogeneities in the reactor fuel array or *lattice* must be taken into account in nuclear design since they will cause a local spatial variation in the neutron flux which may strongly influence core multiplication.

The degree to which core lattice effects must be taken into account in reactor design depends on the characteristic dimensions of the lattice structure, for example, the diameter of a fuel pin or the spacing between fuel elements, compared to the mean free path of neutrons in the core. For example, in the LWR the thermal neutron mean free path is typically on the order of one cm, comparable to the fuel pin diameter. Hence the flux distribution in the fuel might be expected to be quite different from that in the moderator or coolant channel, thereby necessitating a detailed treatment of the heterogeneity. By way of contrast, the much longer mean free path characteristic of the neutrons in a fast reactor (typically tens of centimeters) allows a much grosser treatment of lattice effects.

Of course, a detailed treatment of the core lattice on a scale sufficiently fine to account for the spatial variation of the flux in the neighborhood of a given fuel element is clearly out of the question, since it would require an unmanageably large array of mesh points in a multigroup diffusion calculation (typical LWRs have over 50,000 fuel elements). Indeed due to their strongly absorbing nature, fuel and

control elements in the core frequently require a more accurate treatment of neutron transport than that provided by diffusion theory. Hence one must adopt a more piecemeal approach by seeking to selectively "homogenize" the analysis of the core, usually by providing prescriptions for including lattice effects into existing infinite medium neutron energy-spectrum calculations or by calculating few-group constants that have been spatially averaged over the finer details of the flux distribution in the lattice.

Of course, the type of treatment one chooses will depend on the purpose of the calculation. For example, one can contrast a hand calculation based on the six-factor formula suitable for a crude survey estimate with an extremely detailed transport calculation that might be used in a comparison with a critical experiment or perhaps as a benchmark for the testing of other calculational schemes. Our concern in this chapter is with more routine design calculations that must be performed very frequently and hence place a premium on calculational ease. For such schemes to yield sufficient accuracy, one is forced to rely on frequent cross calibration with experiment—that is, to accept a certain amount of empiricism (fudging) in the technique. And of course as in most fast yet accurate methods, one relies heavily on a cancellation of errors.

For example, in a LWR core study, one might attempt to generate group constants for a few-group diffusion analysis using a SOFOCATE–MUFT scheme similar to that discussed in Chapters 8 and 9. Yet of course these procedures perform calculations for a homogeneous medium in which only gross leakage effects are accounted for via the $P_1$ or $B_1$ approximation. Hence our objective here is to provide a prescription for modifying these homogeneous results to account for heterogeneous lattice effects. The general approach is to divide the periodic array of the reactor lattice into a number of identical *unit cells* and then calculate the effective group constants characterizing one such cell. The detailed analysis of a unit cell must account for the strong spatial variation of the neutron energy spectrum within the cell. The cell is homogenized by averaging the group constants characterizing materials in the cell over the spatial flux distribution within the cell to produce *cell-averaged* or so-called *self-shielded* group constants that can then be used in a multigroup diffusion analysis of the entire core.

In this chapter we develop several procedures applicable for performing such cell calculations and thereby generating cell-averaged group constants. The highly absorbing nature of the fuel region in a reactor lattice cell will necessitate a transport theory description of the neutron flux, based on either so-called collision probability methods or a direct solution of the transport equation itself (or perhaps a Monte Carlo calculation). Since the trend in recent years has been toward more detailed treatments of the heterogeneous effects in core lattices, we will include a brief discussion of both analytical and direct numerical techniques for studying neutron transport within lattice cells.

# I. LATTICE EFFECTS IN NUCLEAR REACTOR ANALYSIS

## A. A Qualitative Discussion of Heterogeneous Effects on Core Multiplication in Thermal Reactors

Before we launch into a detailed study of how lattice effects are included in reactor core analysis methods, it is useful to give a simple qualitative discussion of the effects of fuel lumping on core multiplication in thermal reactors, since this

reveals most of the relevant physics. To this end we will simply examine how each of the various terms in the six-factor formula are modified in passing from a homogeneous reactor core, in which the fuel and moderator are intimately mixed, to a heterogeneous lattice, in which the fuel is lumped separately from the moderator. This discussion actually has a rather interesting historical significance, since without fuel lumping it would have been impossible to achieve a critical assembly using natural uranium and graphite in Fermi's "pile" at the University of Chicago in 1942. More specifically, for a natural uranium system, $\eta = 1.33$ while $\epsilon = 1.05$. If one studies $f$ and $p$ for various homogeneous mixtures of natural uranium and graphite, then, at best one finds $fp = 0.59$.[1] Hence, for a homogeneous reactor core composed of these materials, $k_\infty < (1.33)\ (1.05)\ (0.59) = 0.85$. Obviously such a system could never be made critical.

Fermi and Szilard[2] noted that if the fuel were lumped into a heterogeneous lattice, then the resonance escape probability $p$ would increase dramatically. This occurs because neutrons that are slowed down to resonance energies in the moderator are primarily absorbed in the outer regions of the fuel element—hence leading to a depression in the neutron flux within the fuel at resonance energies (see Figure 10-1). That is, the outer layers of the fuel tend to shield its interior from resonance energy neutrons, thereby decreasing the net resonance absorption and
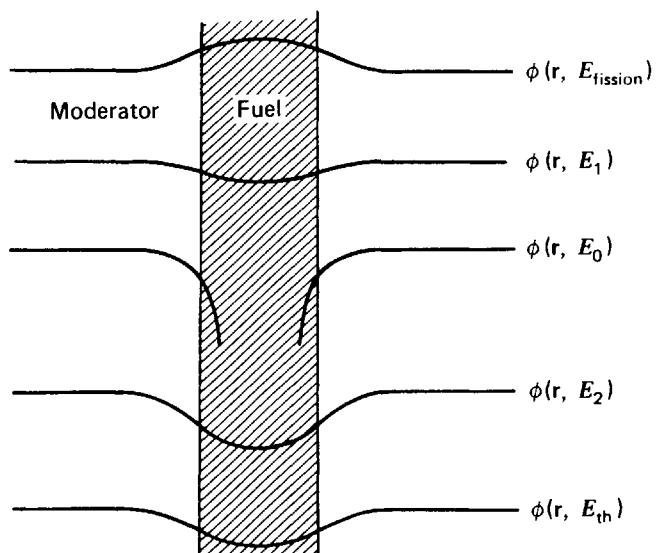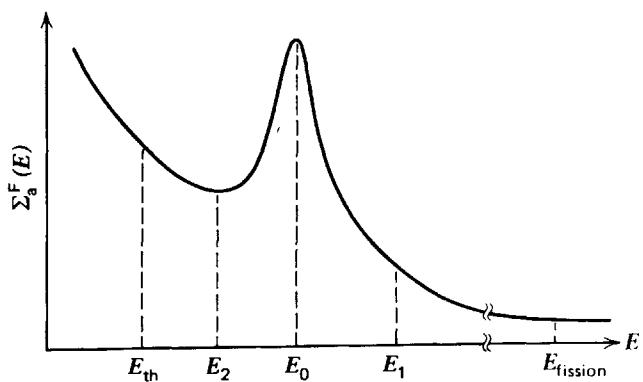


FIGURE 10-1. Flux behavior in the neighborhood of a fuel pin.

hence increasing the resonance escape probability $p$. This "self-shielding" effect is sufficiently strong that $k_\infty$ increases to a value of 1.08 in a graphite–natural uranium lattice. (It should be noted that this *spatial self-shielding* is in many ways analogous to the *energy self-shielding* we encountered in our discussion of the Doppler effect in resonance absorption. Both effects tend to decrease resonance absorption, thereby increasing the resonance escape probability.)

There are other effects due to fuel lumping, however. On the positive side, the fast fission factor $\epsilon$ will increase somewhat in a heterogeneous assembly because the probability of a fast neutron suffering a collision with a fuel nucleus while its energy is still above the fast fission threshold will increase. On the negative side, the thermal utilization $f$ will decrease somewhat because the thermal flux tends to be depressed in the fuel, hence yielding less absorption in the fuel at thermal energies (again due to self-shielding). Since thermal absorption in the fuel (in contrast to epithermal resonance absorption) usually leads to fission, the net result is a decrease in core multiplication due to $f$. Fortunately this decrease is far outweighed by the increase in $p$.

To examine these effects in somewhat more detail, we will now consider the influence of fuel lumping on each term in the six-factor formula. Then in later sections of this chapter, we will turn to the more practical problem of just how such effects are included in core neutronics analysis.

First recall that $\eta$ depends only on the macroscopic cross sections characterizing the fuel

$$\eta = \frac{\nu\sigma_f^F}{\sigma_a^F} \longrightarrow \frac{\sum_j \nu_j \Sigma_f^{(j)}}{\sum_j \Sigma_a^{(j)}} \tag{10-1}$$

(where the latter expression holds for a mixture of fuel isotopes). Hence one would not expect fuel lumping to appreciably affect this ratio. In actuality, however, the cross sections that appear in $\eta$ are group constants characterizing the thermal energy group. These are dependent, of course, on the thermal neutron energy spectrum, and this spectrum depends, in turn, on the fuel-moderator lattice configuration. Hence there will be a slight modification in $\eta$ when going to a heterogeneous lattice. This change is usually ignored in less sophisticated thermal spectrum codes that include heterogeneities via thermal disadvantage factors. More elaborate cell calculations accounting for space–energy effects within the cell will include this correction automatically.

In our earlier treatment of homogeneous systems we defined the thermal utilization $f$ as the ratio of the rate of thermal neutron absorption in the fuel to the total rate of thermal neutron absorption in all materials. This definition can be applied as well to a heterogeneous core by writing

$$f = \frac{\int d^3r\, \Sigma_a^F(\mathbf{r})\phi(\mathbf{r})}{\int d^3r\, \Sigma_a^F(\mathbf{r})\phi(\mathbf{r}) + \int d^3r\, \Sigma_a^M(\mathbf{r})\phi(\mathbf{r})}. \tag{10-2}$$

Here we are considering the core to be made up of only two types of material, fuel, denoted by the superscript "F", and moderator, denoted by "M". (The extension to

more than two regions will be given later.) Since the core is made up of a number of identical fuel cells, we can consider the average in Eq. (10-2) as being taken only over the volume $V_{cell}$ of one such cell. Now if we recognize that the macroscopic cross sections $\Sigma_a^F(\mathbf{r})$ and $\Sigma_a^M(\mathbf{r})$ are actually constant over the volume $V_F$ of the fuel and $V_M$ of the moderator respectively, and vanish elsewhere, we can limit the range of integration to each of these regions and pull the cross sections out of the integrals to write

$$f = \frac{\Sigma_a^F \int_{V_F} d^3r\,\phi(\mathbf{r})}{\Sigma_a^F \int_{V_F} d^3r\,\phi(\mathbf{r}) + \Sigma_a^M \int_{V_M} d^3r\,\phi(\mathbf{r})}. \tag{10-3}$$

Next, suppose we define the spatially averaged flux in each region as

$$\bar{\phi}_F \equiv \frac{1}{V_F} \int_{V_F} d^3r\,\phi(\mathbf{r}), \qquad \bar{\phi}_M \equiv \frac{1}{V_M} \int_{V_M} d^3r\,\phi(\mathbf{r}). \tag{10-4}$$

Then we can rewrite the thermal utilization $f$ in terms of these averages as

$$f = \frac{\Sigma_a^F V_F \bar{\phi}_F}{\Sigma_a^F V_F \bar{\phi}_F + \Sigma_a^M V_M \bar{\phi}_M}, \tag{10-5}$$

or, dividing both numerator and denominator by $\bar{\phi}_F V_F$,

$$f = \frac{\Sigma_a^F}{\Sigma_a^F + \Sigma_a^M (V_M/V_F)\zeta}, \tag{10-6}$$

where we have defined the *thermal disadvantage factor* $\zeta$ as the ratio of the average flux in the moderator to that in the fuel

$$\zeta \equiv \frac{\bar{\phi}_M}{\bar{\phi}_F}. \tag{10-7}$$

This terminology arises because the thermal flux tends to be depressed in the highly absorbing fuel region, leading to a value of $\zeta > 1$. Hence since the average flux is somewhat higher in the moderator than in the fuel, the fuel nuclei are at a relative
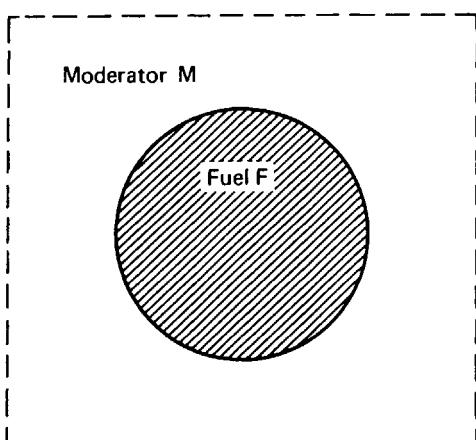


FIGURE 10-2  A two-region unit fuel cell.

disadvantage in competing with moderator nuclei for the capture of thermal neutrons.

The depression of the thermal flux in the fuel is again a consequence of the self-shielding effect. That is, neutrons born in fission events in the fuel will tend to thermalize in the moderator and then must eventually diffuse back into the fuel to induce a further fission. However the highly absorbing nuclei near the surface of the fuel pin tend to absorb the thermal neutrons diffusing back in from the moderator and hence in effect shield the fuel nuclei in the interior of the pin. This leads to the observed flux depression.

We can compare this more general definition of thermal utilization $f$ with our earlier expression for a homogeneous system

$$f^{\text{hom}} = \frac{\Sigma_a^{\text{Fhom}}}{\Sigma_a^{\text{Fhom}} + \Sigma_a^{\text{Mhom}}}, \tag{10-8}$$

if we consider the homogeneous system to consist of unit cells of the same volume $V_{\text{cell}} = V_F + V_M$ as our heterogeneous cell, but with the fuel and moderator now spread uniformly over the cell. Hence we would now find the fuel and moderator number densities in the homogeneous cell as

$$N_F^{\text{hom}} = \frac{N_F V_F}{V_{\text{cell}}}, \qquad N_M^{\text{hom}} = \frac{N_M V_M}{V_{\text{cell}}}. \tag{10-9}$$

If we now note that the macroscopic cross sections for the homogeneous cell are $\Sigma_a^{\text{Fhom}} = N_F^{\text{hom}} \sigma_a^F$, $\Sigma_a^{\text{Mhom}} = N_M^{\text{hom}} \sigma_a^M$, we find from Eq. (10-9)

$$f^{\text{hom}} = \frac{\Sigma_a^F}{\Sigma_a^F + \Sigma_a^M (V_M / V_F)}. \tag{10-10}$$

Comparing this with our more general definition for a heterogeneous system in Eq. (10-6), which we will now refer to as $f^{\text{het}}$, we note that in general $f^{\text{het}} \leqslant f^{\text{hom}}$, since $\zeta \geqslant 1$ (as the flux depression in the fuel would imply). Therefore lumping the fuel into a heterogeneous lattice will actually lower thermal utilization, thereby decreasing core multiplication.

One can generalize the concept of thermal utilization even further to account for a multiregion fuel cell. Consider, for example, a three-region fuel cell composed of fuel, clad, and moderator material. Then in analogy with our two-region example, we would write

$$f = \frac{\Sigma_a^F V_F \bar{\phi}_F}{\Sigma_a^F V_F \bar{\phi}_F + \Sigma_a^M V_M \bar{\phi}_M + \Sigma_a^C V_C \bar{\phi}_C}. \tag{10-11}$$

If we now divide through by the average flux in the fuel, we find that the thermal utilization $f$ involves two thermal disadvantage factors, one for the fuel to moderator, $\bar{\phi}_M / \bar{\phi}_F$, and one for the fuel to clad, $\bar{\phi}_C / \bar{\phi}_F$.

As yet we have said nothing concerning just how one calculates these thermal disadvantage factors. Of course, it might be argued that the concept of thermal utilization within the context of the six-factor formula has very limited utility aside from crude survey estimates. We will see later, however, that the disadvantage factor $\zeta$ can be used to spatially average thermal group constants over unit fuel cells, and hence plays an extremely important role in reactor design. Hence we will devote a considerable amount of attention toward its calculation in the next

section. We will examine both approximate ("quick and dirty") ways to estimate $\zeta$ as well as more elaborate schemes based on transport theory and collision-probability methods.

Since the fast neutron mfp is typically large compared to the scale of lattice dimensions, one usually need only consider the thermal nonleakage probability $P_{TNL}$. Lattice effects enter primarily through a change in the thermal group constants, which accounts for spatial flux variation within a cell. In particular one can show that the diffusion length characterizing a heterogeneous core is approximately just that characterizing a pure moderating medium decreased by the thermal utilization $L^2 \cong L_M^2 (1-f)$ (see Problem 10-3). However since leakage from a large thermal reactor core is a relatively minor effect, we will avoid an explicit discussion of heterogeneous effects on $P_{TNL}$ since it will have a small effect on core multiplication (and will be accounted for by using cell-averaged group constants in any event).

Perhaps the most significant effect due to heterogeneous arrangement of fuel in a thermal reactor is a significant increase in the resonance escape probability $p$. This modification occurs as a consequence of two phenomena. First there is a geometrical effect arising because the physical separation of the fuel and the moderator will allow some neutrons to slow down without ever encountering the fuel. This effect is of secondary importance to the phenomenon of self-shielding, however.

To understand this second effect more clearly, consider the diagram of the spatial dependence of the neutron flux at several different energies characterizing a resonance given in Figure 10-1. Of course at fission energies we might expect the flux to peak in the fuel since the fission sources are confined to the fuel. However once we have dropped in energy much below the fission energy, we will begin to see a flux depression in the fuel. This arises because the fission neutrons must escape the fuel pin into the moderator in order to be appreciably moderated. (Nuclear inelastic scattering from fuel isotopes as well as elastic scattering from light isotopes such as oxygen admixed into the fuel cause some moderation, but this is a secondary effect in thermal reactors.) Hence the moderator presents effectively a volumetric source of neutrons appearing at the lower energies. These neutrons must then either downscatter to even lower energies or diffuse into the fuel where they are absorbed.

The fuel presents a very highly absorbing medium to the neutrons of resonance energy diffusing in from the moderator. This absorption is sufficiently strong that many of the neutrons incident on the fuel are absorbed in the outer layers of the fuel pin. Hence the fuel nuclei in the pin interior see a somewhat depressed flux due to the effective shielding presented by the fuel nuclei near the fuel pin surface. Such self-shielding is present to a certain degree at all energies below fission energies. However it becomes much more pronounced when the fuel absorption cross section is large—such as at a resonance in the absorption cross section or in the thermal energy range.

This effect is quite pronounced. For example, the resonance integral characteristic of natural uranium uniformly mixed with moderating material is about 280 b; lumping the uranium, we can reduce the resonance integral to a value of 9 b—a 30-fold reduction. We will see later that one can usually write the effective resonance integral in the form

$$I = C_1 + C_2 \left( \frac{A_F}{M_F} \right) \tag{10-12}$$

where $A_F$ is the surface area of the fuel lump and $M_F$ is its mass (proportional to its

volume). As $(A_F/M_F)$ decreases—corresponding to more highly heterogeneous lattice configurations—the resonance integral decreases.

To treat the effects of heterogeneities in resonance absorption requires the use of several concepts from transport theory. Since this subject is of considerable importance in thermal reactor design, we will discuss it in some detail in Section 10-III.

The fast fission factor $\epsilon$ is also increased somewhat by going to a heterogeneous lattice. To understand why, one need only recall that the energy of a neutron must be above a certain threshold in order to induce a fast fission reaction in a fissionable isotope such as $^{238}U$. By lumping the fuel, one effectively increases the probability that a high-energy fission neutron will encounter a fuel nucleus before it is slowed down below the fast fission energy threshold, either by elastic scattering collisions with moderator nuclei or inelastic scattering from fuel nuclei.

In summary, then, lumping the fuel into a heterogeneous lattice can significantly increase $k_\infty$ for natural and slightly enriched ($\gtrsim 5\%$) uranium cores. The dominant effect is contained in the behavior of the thermal utilization $f$ and the resonance escape probability $p$. To illustrate these trends, we have indicated in Figure 10-3 the variation of each of the factors in the four-factor formula with heterogeneity (in this case measured by the fuel pin pitch/diameter ratio) for a typical PWR lattice.
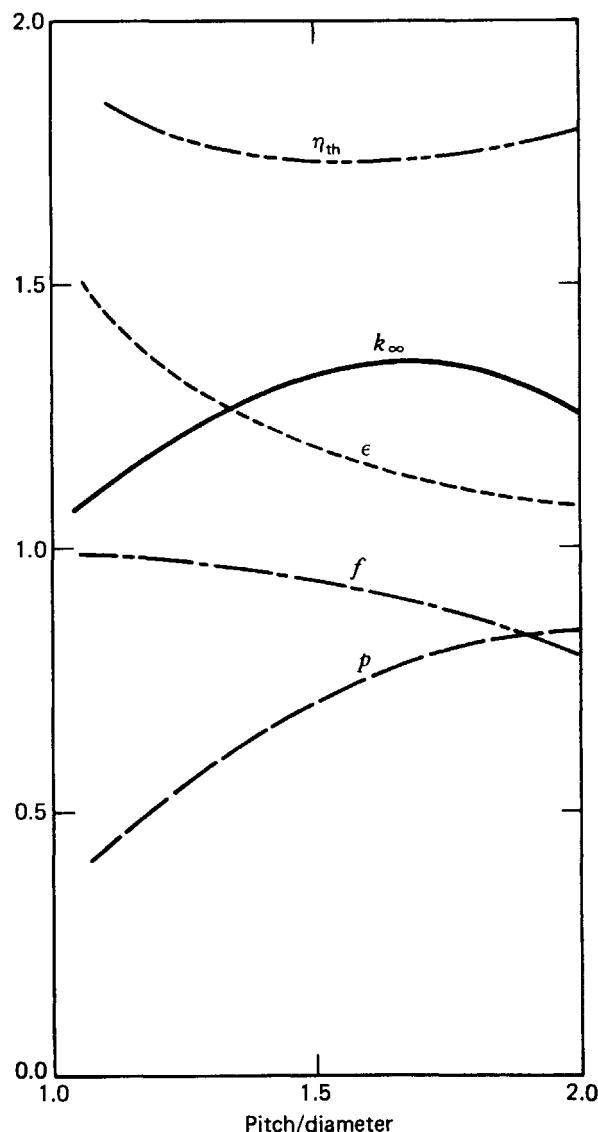


**FIGURE 10-3.** Effect of fuel lumping on $k_\infty$.

## B. Core Homogenization

To be more specific, let us outline one possible approach to the treatment of core lattice effects. We begin by noting that reactor cores have a regular or periodic lattice structure in which one subelement or so-called *unit cell* is repeated throughout the core. For example, a fuel subassembly or group of fuel subassemblies such as those sketched in Figure 10-4 could be regarded as a unit cell. On a more detailed scale, a given fuel element and adjacent coolant channel might be chosen as the unit cell (Figure 10-5). In fact, for reactor types using coated particle fuels, one is frequently required to consider a fuel microsphere or "grain" as a unit cell.

Of course the reactor lattice structure is not precisely regular because of control or instrumentation devices, nonuniform fuel loadings and coolant densities, core boundaries, and so on. These lattice irregularities are usually handled within the global multigroup diffusion calculation of the core flux distribution. For the purposes of our present analysis, we will ignore these gross lattice irregularities and assume that the core can be represented as an infinite array of identical lattice cells.

The essential scheme is then to perform a detailed calculation of the flux distribution in a given unit cell of the lattice—usually assuming that there is zero net neutron current across the boundary of the cell (using arguments based on the symmetry of the lattice). The various multigroup cross sections characterizing materials in the cell are then spatially averaged over the cell, using the flux distribution as a weighting function. In this way one can characterize the cell by effective group constants accounting for the inhomogeneous flux distribution in the cell. This scheme essentially replaces the actual unit cell by an equivalent *homogeneous* unit cell characterized by these effective cross sections.

For example, one usually begins by considering a typical fuel cell—namely, fuel plus clad plus coolant. The fuel cell is first reduced to an equivalent cell of simpler geometry to expedite calculations (see Figure 10-6a) (taking care to preserve volume fractions).

Our primary interest is usually concerned with the generation of effective fast and thermal group constants for such a cell. In the fast range, the heterogeneities enter primarily as modifications to the resonance escape probability and fast fission cross sections. Hence it is usually sufficient to simply perform the usual infinite medium fast spectrum calculation, taking care, however, to account for heterogeneous effects in resonance absorption and fast fission via techniques that will be discussed later in this chapter.

The much shorter mean free path characterizing thermal neutrons necessitates a somewhat more detailed treatment of heterogeneities in determining the thermal flux spectrum in a fuel cell. For less detailed core calculations, one can frequently get by with simply modifying the results of an infinite medium thermal spectrum calculation (e.g., SOFOCATE) to account for the variations in average flux in the fuel, $\bar{\phi}_F$, the moderator, $\bar{\phi}_M$, and the clad, $\bar{\phi}_C$. Of primary concern here is the calculation of the so-called *thermal disadvantage factors*, $\bar{\phi}_M/\bar{\phi}_F$ and $\bar{\phi}_C/\bar{\phi}_F$, which enter into modifying the infinite medium spectrum results. More detailed calculations of thermal spectra usually involve a direct solution of the neutron transport equation characterizing the cell. Both schemes will be discussed in Section 10-II.

Such fuel cell calculations are customarily performed under the assumption of zero net neutron leakage between cells (which decouples the fuel cells from one another). Actually such single fuel rod spectrum calculations are of questionable
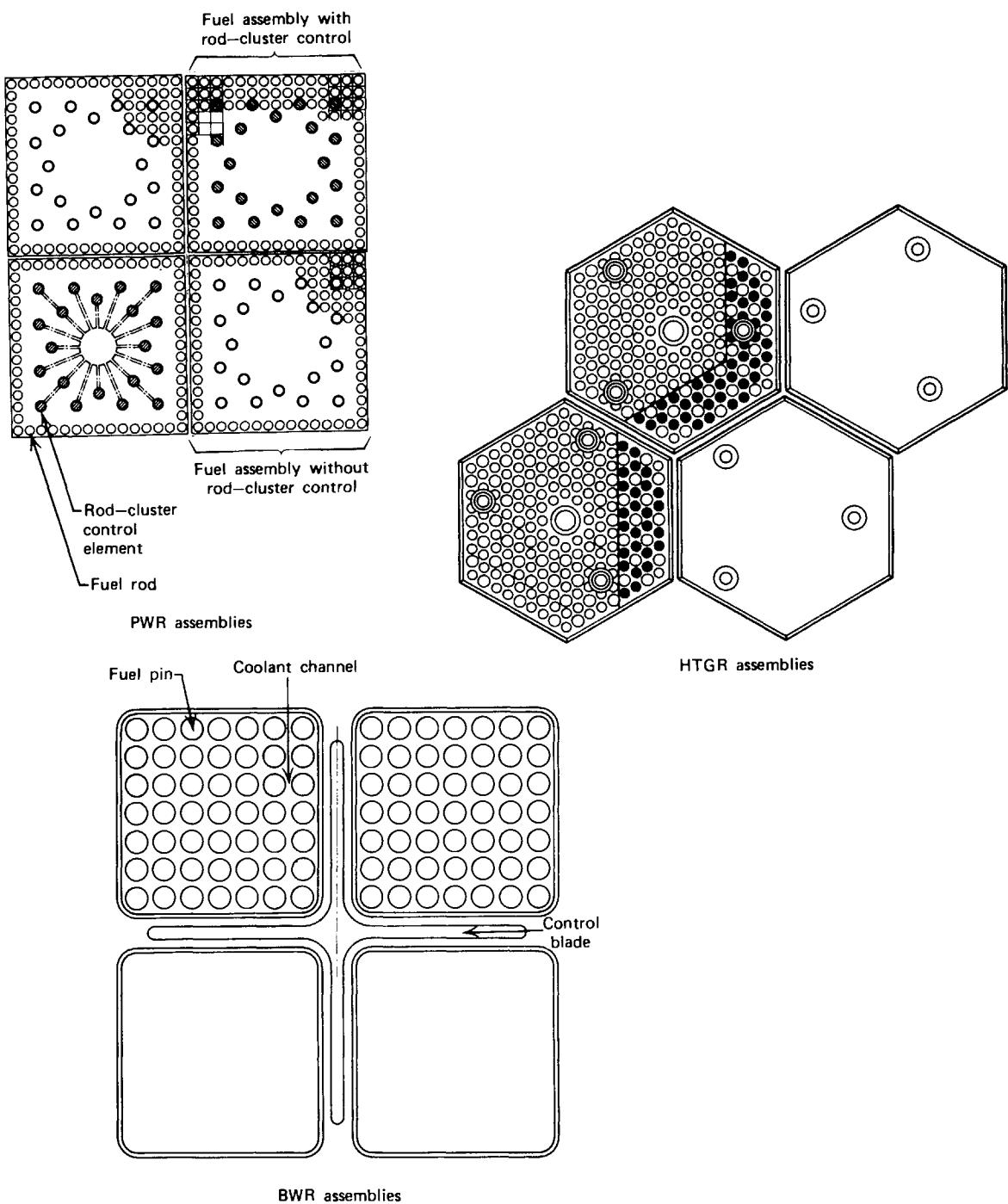
FIGURE 10-4. Typical fuel assemblies.

validity when rod neighbors include water holes, poison shims, control rods, or Pu-loaded fuel pins, since one then needs to account for cell-to-cell leakage.[3]

For coated particle fuels, such as those utilized in the HTGR, additional correction factors must be used to account for the heterogeneity represented by the microscopic grain structure of the fuel in the calculation of cell-averaged thermal spectra and group constants.[4]

The next step in the analysis of the core is to consider a typical fuel assembly or grouping of fuel assemblies, including control or shim elements (Figure 10-6b). The few-group constants calculated for the fuel cell can be used to describe most of the assembly, with the exception of control material which requires rather specialized

Square lattice                                      Hexagonal lattice
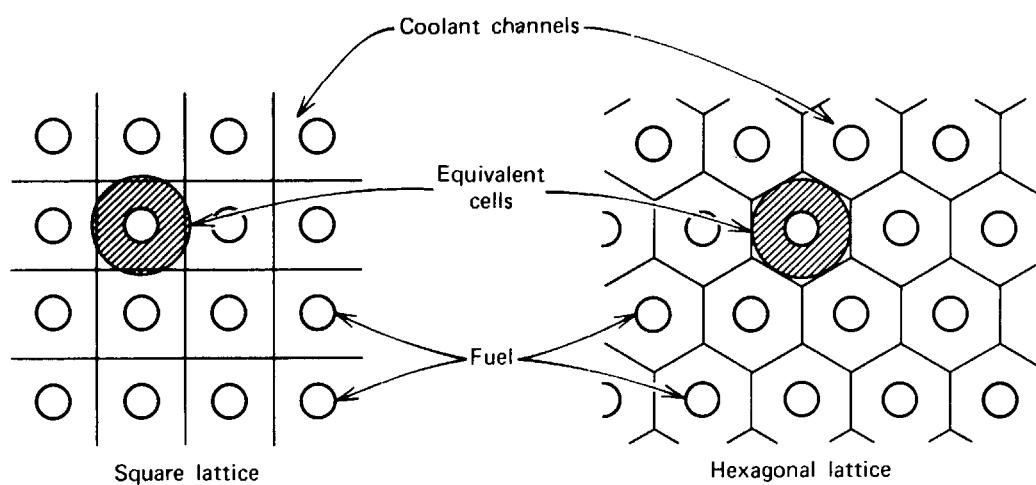
**FIGURE 10-5.    Typical unit fuel assemblies.**



(a) Fuel—cell homogenization



(b) Fuel—assembly homogenization



(c) Core homogenization
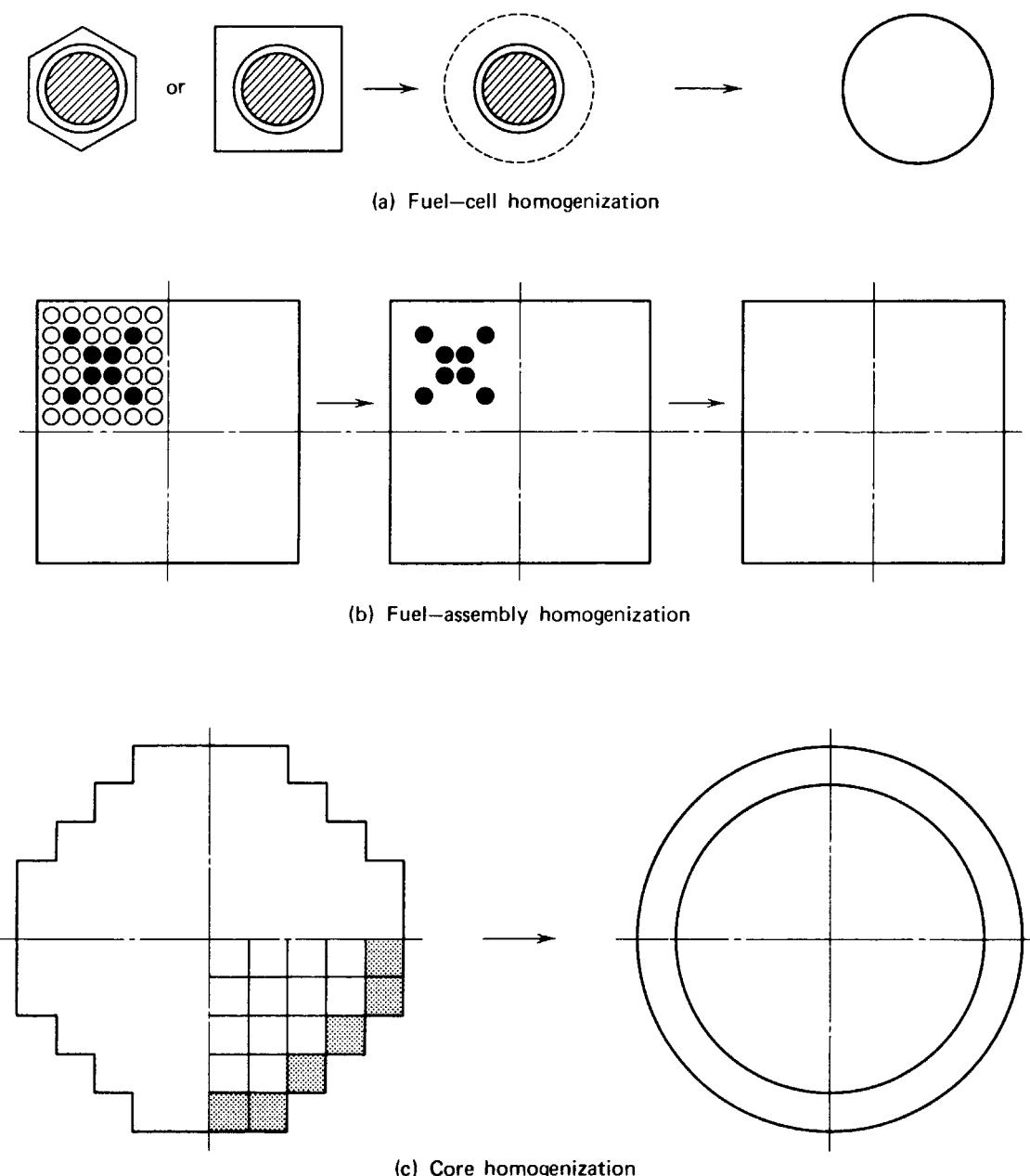
**FIGURE 10-6.    Reactor-core homogenization.**

techniques. Usually a detailed multigroup two-dimensional diffusion or transport code is used to determine the flux in such an assembly, and then once again these fluxes are used to generate assembly averaged group constants.

The final step is to use either these assembly-averaged group constants (or, in very detailed calculations, the original fuel cell group constants) to determine the flux and power distribution over the entire core. The symmetry of the core will frequently allow one to consider only one quadrant in detail. It may occasionally be desirable to homogenize the core still further to facilitate gross survey calculations (as in Figure 10-6c).

## C. Cell-Averaging Techniques

The goal of most of our analysis in this chapter will be to calculate effective group constants that have been spatially averaged over the flux distribution in a lattice cell and therefore can be used to characterize the cell in subsequent multigroup diffusion calculations in which the cell structure is ignored. To discuss this subject of cell averaging in more detail, let us consider the calculation of the cell-averaged group constant characterizing a two-region cell in which material composition is uniform in each region. We will again denote these regions by "M" and "F" for convenience (refer to Figure 10-2.)

The *cell-averaged group constant* characterizing a general cross section would then be defined as

$$\langle \Sigma_g \rangle_{\text{cell}} = \frac{\int_{E_g}^{E_{g-1}} dE \int_{V_{\text{cell}}} d^3 r \, \Sigma(\mathbf{r}, E) \phi(\mathbf{r}, E)}{\int_{E_g}^{E_{g-1}} dE \int_{V_{\text{cell}}} d^3 r \, \phi(\mathbf{r}, E)} \,. \tag{10-13}$$

Such cell-averaged group constants are frequently referred to as *self-shielded* or simply *shielded* group constants, since averaging over the spatial flux distribution in the cell accounts for the flux depression caused by self-shielding. We can use the fact that the cross section $\Sigma(\mathbf{r}, E)$ is constant within each region to rewrite $\langle \Sigma_g \rangle_{\text{cell}}$ as

$$\langle \Sigma_g \rangle_{\text{cell}} = \frac{V_M \int_{E_g}^{E_{g-1}} dE \, \Sigma^M(E) \bar{\phi}_M(E) + V_F \int_{E_g}^{E_{g-1}} dE \, \Sigma^F(E) \bar{\phi}_F(E)}{V_M \int_{E_g}^{E_{g-1}} dE \, \bar{\phi}_M(E) + V_F \int_{E_g}^{E_{g-1}} dE \, \bar{\phi}_F(E)} \,, \tag{10-14}$$

where we have defined the cell-averaged intragroup fluxes as

$$\bar{\phi}_M(E) \equiv \frac{1}{V_M} \int_{V_M} d^3 r \, \phi(\mathbf{r}, E), \qquad \bar{\phi}_F(E) \equiv \frac{1}{V_F} \int_{V_F} d^3 r \phi(\mathbf{r}, E). \tag{10-15}$$

Now if in fact the neutron flux in the cell were *separable* in space and energy such that

$$\phi(\mathbf{r}, E) = \phi(\mathbf{r}) \psi(E), \tag{10-16}$$

that is, if both regions of the cell were characterized by the same intragroup

spectrum, then one could collapse Eq. (10-14) to

$$\langle \Sigma_g \rangle_{cell} = \frac{V_M \Sigma_g^M \overline{\phi}_M + V_F \Sigma_g^F \overline{\phi}_F}{V_M \overline{\phi}_M + V_F \overline{\phi}_F}$$

$$= \frac{\Sigma_g^F + \Sigma_g^M (V_M / V_F) \zeta}{1 + (V_M / V_F) \zeta} . \tag{10-17}$$

where the regionwise group constants are defined as

$$\Sigma_g^F \equiv \int_{E_g}^{E_{g-1}} dE \, \Sigma^F(E) \psi(E) \Big/ \int_{E_g}^{E_{g-1}} dE \, \psi(E), \text{ etc.,} \tag{10-18}$$

while the spatial flux averages are defined as

$$\overline{\phi}_M = \frac{1}{V_M} \int_{V_M} d^3 r \, \phi(\mathbf{r}), \text{ etc.,} \tag{10-19}$$

and the cell-disadvantage factor is defined as before,

$$\zeta = \frac{\overline{\phi}_M}{\overline{\phi}_F} . \tag{10-20}$$

Of course the neutron flux in a typical lattice cell is rarely separable in space and energy. Nevertheless in many cell homogenization schemes such separability is assumed in order to separate the determination of the neutron spectrum $\psi(E)$ to be used as the weighting function in *energy* averaging from the calculation of the disadvantage factor $\zeta$ to be used as the weighting parameter in *spatial* cell-averaging. Such procedures begin by homogenizing fuel, coolant, clad and so on over the fuel cell volume and then calculating the neutron energy spectrum $\psi(E)$ for this homogenized cell using an infinite-medium spectrum code. Next this spectrum is used to calculate group constants for each region of the cell [e.g., $\Sigma_g^F$ and $\Sigma_g^M$]. An auxiliary one-speed spatial calculation of the cell disadvantage factor $\zeta$ is performed, usually at an average energy characterizing the group of interest, and finally the regionwise group constants $\Sigma_g^M$ and $\Sigma_g^F$ are combined using $\zeta$ to obtain the cell-averaged group constant $\langle \Sigma_g \rangle_{cell}$. This scheme is indicated schematically in Figure 10-7.

A minor modification of this scheme would be to calculate an energy-dependent disadvantage factor $\zeta(E)$ by simply allowing the one-speed cross sections appearing in formulas for $\zeta$ to be energy-dependent.[5] Then one can interchange the spatial and energy-averaging to first calculate the spatial average

$$\langle \Sigma(E) \rangle_{cell} = \frac{\Sigma^F(E) + \Sigma^M(E)(V_M / V_F) \zeta(E)}{1 + (V_M / V_F) \zeta(E)} \tag{10-21}$$
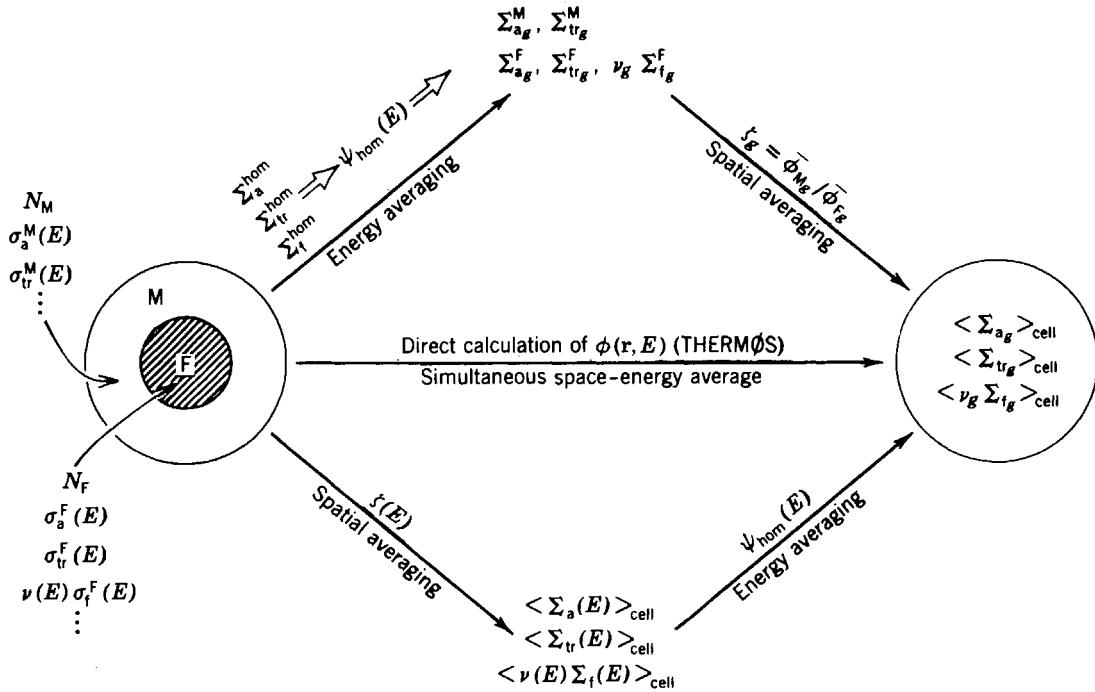
**FIGURE 10-7.** Various schemes for computing cell-averaged group constants.

and then the energy average over $\psi(E)$

$$\langle \Sigma_g \rangle_{cell} = \frac{\int_{E_g}^{E_{g-1}} dE \langle \Sigma(E) \rangle_{cell} \psi(E)}{\int_{E_g}^{E_{g-1}} dE \psi(E)} .$$

(10-22)

This latter scheme has also been sketched in Figure 10-7. It should be noted that in most cases the use of energy-dependent disadvantage factors $\zeta(E)$ for cell averaging yields results that are very comparable to those using the somewhat simpler disadvantage factor $\zeta$ simply calculated at the mean energy of the group.

The most serious limitation of both of the above schemes is the assumption of space–energy separability. One procedure for overcoming this is to first perform a spectrum calculation for a homogeneous mixture of cell constituents.[6] The few-group constants generated from this homogeneous spectrum calculation are then used in a few-group one-dimensional spatial calculation of the flux in the cell. The spatial flux distribution obtained in this calculation is then used to determine the appropriate disadvantage or shielding factors. These factors can then be used to adjust the fine-group cross section data used in the spectrum calculation. The spectrum obtained from these shielded or cell-averaged fine group constants will usually be much closer to the average spectrum in the cell, and averaging the shielded fine-group constants over this spectrum will usually provide adequate cell-averaged cross sections.

In certain cases it may be necessary to perform a detailed calculation of the spatially dependent spectrum $\phi(r, E)$ in the cell and calculate the cell-averaged group constants directly from the rigorous definition given by Eq. (10-13). Because this latter procedure is becoming increasingly common in providing cell-averaged

group constants for accurate multigroup diffusion estimates of core parameters, we will consider one such direct approach based on collision-probability methods in Section 10-II-C.

It is important to stress once again that the effect of fine-scale lattice heterogeneities enter reactor calculations through group constants that are adjusted to account for the spatial variation of the neutron flux within the lattice. Most frequently such group constants are modified by using disadvantage factors for the lattice cell of interest. Hence the primary effort involved in accounting for lattice effects involves the calculation of these disadvantage factors. As we will find, diffusion theory is usually inadequate for such calculations, and transport methods must be used.

We perhaps should mention that there are other prescriptions that prove very useful for defining cell-averaged absorption cross sections in the instance that the central region ("F") is very highly absorbing (as it would be for either a fuel pin or a control rod). Such schemes usually proceed by demanding that the rate of absorption calculated with the effective cell-averaged cross section be identical to the true absorption rate in the region F.

For example, if $\Sigma_a^{eff}$ is the effective cell absorption cross section, while $\bar{\phi}_{hom}$ is the average flux in the cell which has been homogenized, then obviously we require

$$\text{Cell absorption rate} \equiv \Sigma_a^{eff}\bar{\phi}_{hom}V_{cell} = \Sigma_a^F\bar{\phi}_F V_F. \qquad (10\text{-}23)$$

(Here we have neglected the absorption of the region M.) Hence the effective absorption cross section for the cell is given by

$$\Sigma_a^{eff} = \left(\frac{V_F}{V_{cell}}\right)\left[\frac{\bar{\phi}_F}{\bar{\phi}_{hom}}\right]\Sigma_a^F \equiv \left(\frac{V_F}{V_{cell}}\right)f_s\Sigma_a^F, \qquad (10\text{-}24)$$

where we have defined the *self-shielding factor*

$$f_s \equiv \frac{\bar{\phi}_F}{\bar{\phi}_{hom}}, \qquad (10\text{-}25)$$

which accounts for the flux depression in region $F$. Therefore to calculate $\Sigma_a^{eff}$ we need only scale the cross section for the fuel region by $(V_F/V_{cell})f_s$—that is, decrease $\Sigma_a^F$ by the volume fraction occupied by the fuel, as well as by the flux depression or self-shielding factor $f_s$. Since $\bar{\phi}_{hom} = (V_F/V_{cell})\bar{\phi}_F + (V_M/V_{cell})\bar{\phi}_M$ we can write

$$f_s = \frac{V_{cell}\bar{\phi}_F}{V_F\bar{\phi}_F + V_M\bar{\phi}_M} = \frac{(V_{cell}/V_F)}{1 + (V_M/V_F)(\bar{\phi}_M/\bar{\phi}_F)} = \frac{(V_{cell}/V_F)}{1 + (V_M/V_F)\zeta}. \qquad (10\text{-}26)$$

[Note that we can then identify Eq. (10-24) as equivalent to our earlier result for the case in which $\Sigma_a^M \sim 0$.]

Yet a third scheme frequently applied to situations in which the region $F$ is very highly absorbing (e.g., a control rod) is to equate:

$$\text{Absorption rate} \atop \text{in cell} = V_{\text{cell}}\Sigma_a^{\text{eff}}\bar{\phi}_{\text{hom}} = S_F J_F = \text{rate at which neutrons} \atop \text{enter the region F} \quad , \quad (10\text{-}27)$$

where $S_F$ is the surface area of region $F$, while $J_F$ is the average neutron current density into the absorbing region at this surface. Then

$$\Sigma_a^{\text{eff}} = \frac{S_F}{V_{\text{cell}}} \frac{J_F}{\bar{\phi}_{\text{hom}}} . \qquad (10\text{-}28)$$

Once again we are faced with determining a factor characterizing the spatial variation of the flux in the cell, $J_F/\bar{\phi}_{\text{hom}}$.

Hence all of these homogenization schemes require a detailed study of the spatial variation of the neutron flux in the cell. We will separate our study of the spatial transport of neutrons in a lattice cell into two parts. First we will concern ourselves with thermal neutrons and then later with fast neutrons. The physics of each of these problems is a bit different, since the dominant lattice effects on thermal neutron behavior enter as a decrease in the thermal utilization, while the dominant fast neutron effects are to enhance the resonance escape probability and the fast fission factor.

## II. HETEROGENEOUS EFFECTS IN THERMAL NEUTRON PHYSICS

### A. Thermal Utilization, Disadvantage Factors, and Cell-Averaged Thermal Group Constants

As we have seen, the core of a nuclear reactor is comprised of thousands of individual fuel cells, each characterized by the fuel element itself, usually some cladding material (separated from the fuel element by a gap), and an adjacent moderator that may also serve as a coolant (see Figure 10-5). We have also noted that it would be prohibitively expensive to perform a detailed few-group diffusion calculation taking into account the detailed configuration and composition of each fuel cell—indeed, the very high absorption present in the fuel element renders the use of the diffusion approximation itself highly questionable.

Instead the approach is to perform a detailed calculation of the flux in only one typical fuel cell and then to use this flux to spatially average the thermal group constants over the cell. Let us illustrate this by an example: Consider a typical square lattice fuel cell with a cylindrical fuel pin. One first replaces this geometry by an equivalent unit cell to simplify the calculations, taking care to preserve the same volume of fuel $V_F$ and moderator $V_M$.

We will now calculate the thermal group constants for this cell using the simplest of the cell-averaging techniques described in the previous section. That is, we first perform a thermal spectrum calculation for an infinite medium of identical composition as the cell, however, with the number densities of fuel and moderator (and clad) being uniformly distributed over the cell. Then using this homogeneous cell spectrum $\psi_{\text{hom}}(E)$, we compute the thermal group constants characterizing each

cell region, for example, $\Sigma_a^M$, $\Sigma_{tr}^M$, $\Sigma_a^F$, $\Sigma_{tr}^F$, and $\nu\Sigma_f^F$. (Here we have left the thermal group index as understood.) If we can then determine the disadvantage factors characterizing the cell $\zeta$, we can compute the cell-averaged thermal group constants (for a two-region cell) as

$$\langle\Sigma_a\rangle_{cell} = \frac{\Sigma_a^F + \Sigma_a^M(V_M/V_F)\zeta}{1+(V_M/V_F)\zeta},$$

$$\langle\Sigma_{tr}\rangle_{cell} = \frac{\Sigma_{tr}^F + \Sigma_{tr}^M(V_M/V_F)\zeta}{1+(V_M/V_F)\zeta}, \qquad (10\text{-}29)$$

$$\langle\nu\Sigma_f\rangle_{cell} = \frac{\nu\Sigma_f^F}{1+(V_M/V_F)\zeta}.$$

We could also calculate the thermal utilization for the cell as

$$f = \frac{\Sigma_a^F}{\Sigma_a^F + \Sigma_a^M(V_M/V_F)\zeta}. \qquad (10\text{-}30)$$

Thus we once again find that the key to including heterogeneities in the generation of thermal group constants rests on our ability to estimate the spatial dependence of the thermal flux in the cell—that is, to determine the thermal disadvantage factor $\zeta$.

For the large natural uranium–graphite moderated reactors of interest during the early years of the nuclear energy program, one could utilize one-speed diffusion theory to calculate $\zeta$. However in the more highly enriched and tightly packed core lattices utilized in today's modern power reactors, diffusion theory estimates are quite poor. Hence we will describe two alternative schemes useful for determining the thermal disadvantage factor, both of which are based on transport theory. The first method is an analytic scheme first proposed by Amouyal, Benoist, and Horowitz,[7] and referred to as the ABH method. It relies on the concept of an escape or collision probability characterizing neutron transport in the cell. The second scheme we shall discuss actually solves the energy-dependent neutron transport equation directly for the equivalent cell of interest to generate the thermal flux and perform spatial averaging over the cell. This scheme, known as THER-MOS[8], discretizes the integral form of the transport equation, thereby reducing it to a system of algebraic equations solvable on a computer.

There are still other methods for calculating spatially dependent thermal neutron spectra, ranging all the way from the assumption of a fundamental spatial mode (such as was used in the $B_N$ or $P_N$ methods discussed in Chapter 8) to direct $S_N$ solutions of the transport equation or Monte Carlo calculations. The choice of the method will depend on both the detail required in the design and computer

capability (and allowable expense). In recent years, the trend has been toward more careful treatment of the spatial detail of the lattice and more precise transport descriptions, with increasing use of Monte Carlo techniques.[9]

## B. Escape Probability Methods in Cell Calculations

We will first investigate an analytical approach for the determination of cell disadvantage factors that utilizes the concept of the probability that a neutron born in one region will escape the region before suffering a collision. The use of such "escape" probabilities is quite common in studying neutron transport in highly absorbing media (e.g., fuel).[10-12] We will outline the specific application of such concepts in a scheme, developed by Amouyal, Benoist, and Horowitz (the ABH method).

The ABH method combines aspects of transport theory, collision probability methods, and diffusion theory to calculate the thermal disadvantage factor characteristic of a unit fuel cell. More specifically, diffusion theory is used to describe the flux in the moderator, although a transport correction is introduced into the boundary condition at the moderator–fuel interface. Neutron transport in the fuel is described by multiple collision escape probabilities. All of these calculations are performed in the one-speed approximation and yield $\zeta$ in terms of the one-group constants characterizing materials in the cell.

Before we begin our description of the method, let us be a bit more precise in our definition of a unit fuel cell. We will make four assumptions concerning the treatment of the cell:

(1) There are no neutrons slowing to thermal energies in the fuel region. This assumption is quite reasonable in thermal power reactor lattices, since moderation in the fuel occurs only via inelastic scattering or elastic scattering from admixed materials such as oxygen or carbon, both of which yield inconsequential moderation when compared to the surrounding moderating region.

(2) We can treat the spatial distribution of neutrons slowing down within the moderator region as uniform. To motivate this assumption, notice that in most cases the distance required to slow a fission neutron to thermal energies $(\sqrt{6\tau})$ is quite large compared to the lattice spacing or pitch. For example, in a LWR the rms distance to slow down is roughly 15 cm, compared to a typical lattice pitch of 1–2 cm. Hence the neutrons slowing down within any moderating region come from a large number of the surrounding fuel pins. This tends to yield a more uniformly distributed slowing down source.

(3) We will finally assume that there is no net flow of neutrons between the cells. Surely this requirement would be true for an infinite lattice of identical fuel cells. It would be expected to break down only near the core boundaries or near to control elements or fuel pins of nonuniform enrichment or composition (e.g., Pu-loaded fuel pins, which are characterized by strong absorption resonances in the $\sim.5$ eV range).

(4) We will assume that a one-speed treatment of the neutron flux in the cell is sufficient. Actually, a one-speed calculation ignores the fact that the flux in the cell is frequently inseparable in space and energy, but provided

the proper thermal group constants are used in the one-speed treatment, this latter correction can frequently be ignored.

We will now use this model to calculate the thermal disadvantage factor $\zeta$ characterizing the cell. Actually the ABH method for calculating $\zeta$ proceeds somewhat indirectly by first calculating the thermal utilization $f$ for the cell, and then using this quantity and Eq. (10-6) to infer the disadvantage factor $\zeta$ as

$$\zeta = \left( \frac{\Sigma_a^F}{\Sigma_a^M} \right) \left( \frac{V_F}{V_M} \right) \left( \frac{1}{f} - 1 \right). \tag{10-31}$$

The key quantity involved in calculating the thermal utilization is the probability that a neutron appearing uniformly and isotropically in the moderator (i.e., slowing down source) will be absorbed in the fuel region. The calculation of such probabilities is far from trivial, particularly if one of the cell regions is sufficiently highly absorbing to invalidate diffusion theory. However approximate schemes can be used to calculate these probabilities that utilize the concepts of escape and collision probabilities.

## 1. ESCAPE PROBABILITIES

To be more specific, we will consider a two-region cell such as that illustrated in Figure 10-8. Then we define the *absorption probabilities* characterizing the two regions of the cell as

$$P_{FF} \equiv \begin{array}{l}\text{probability that a neutron appearing uniformly and isotropically}\\ \text{in region F will eventually be absorbed in region F,}\end{array}$$

$$\tag{10-32}$$

$$P_{FM} \equiv \begin{array}{l}\text{probability that a neutron, appearing uniformly and isotropically}\\ \text{in region F will eventually be absorbed in region M,}\end{array}$$

and similarly for $P_{MM}$ and $P_{MF}$. Notice that since the cell has only two regions which incorporate all space, we must have

$$P_{FF} + P_{FM} = 1$$

$$P_{MM} + P_{MF} = 1. \tag{10-33}$$
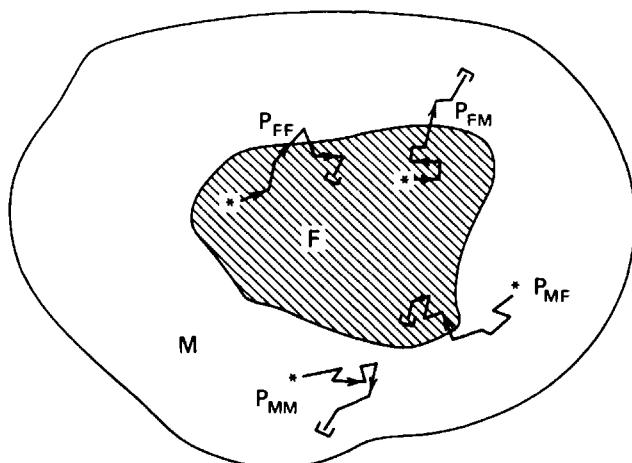


**FIGURE 10-8.** The absorption probabilities characterizing a two-region cell.

The calculation of these probabilities is complicated by the fact that they must account for scattering processes within each region as well as instances in which a neutron may scatter back and forth between the regions several times before finally being absorbed.

Although these absorption probabilities may be very difficult to calculate in practice, they do exhibit several simple and useful properties. The absorption probabilities characterizing cross-region transfer obey a reciprocity relation of the form:

$$V_F \Sigma_a^F P_{FM} = V_M \Sigma_a^M P_{MF}. \tag{10-34}$$

This very useful relation can be proven (see Problem 10-10) by noting that the Green's function characterizing the cell is symmetric such that $G(\mathbf{r}, \mathbf{r}') = G(\mathbf{r}', \mathbf{r})$ (whether described by one-speed diffusion or transport theory[11]).

This feature of absorption probabilities is particularly useful in the calculation of the thermal utilization $f$, for by definition $f$ is just the probability that a thermal neutron is absorbed by the fuel. That is, $f$ is just $P_{MF}$, since we have assumed that all thermal neutrons first appear as a slowing down source uniformly distributed in the moderator. We can therefore use Eq. (10-34) to write

$$f = P_{MF} = \left( \frac{V_F}{V_M} \right) \left( \frac{\Sigma_a^F}{\Sigma_a^M} \right) P_{FM}. \tag{10-35}$$

Thus we are now faced with calculating the absorption probability for the fuel region to moderator region $P_{FM}$. This quantity is somewhat easier to approximate, since the fuel is usually sufficiently highly absorbing that neutrons tend to make very few collisions in the fuel region before being absorbed.

So how do we calculate $P_{FM}$? We begin by breaking it up into two factors

$$P_{FM} = P_F \beta_M \tag{10-36}$$

where

$$P_F \equiv \begin{array}{l} \text{probability that a neutron born uniformly and isotropically} \\ \text{in the fuel escapes from the fuel before being absorbed,} \end{array}$$

$$\beta_M \equiv \begin{array}{l} \text{conditional probability that the neutron, having escaped} \\ \text{from the fuel, will then be absorbed in the moderator.} \end{array} \tag{10-37}$$

We will refer to $P_F$ as the *escape probability* characterizing the fuel region, since it gives the probability that a neutron eventually escapes the fuel (possibly after a number of scattering collisions) without being absorbed. In a similar manner we can identify $\beta_M$ as a measure of the blackness of the moderator region, since it measures the probability that a neutron entering this region will be absorbed. Our goal then is to calculate the escape probability $P_F$ for the fuel region and the conditional "absorption" probability $\beta_M$ for the moderator.

A word of caution at this point is advisable. There are a variety of different definitions of "escape probabilities" and "collision probabilities" floating around in the reactor physics literature. Since this concept was originally introduced to describe transport in purely absorbing media in which any collision within the fuel

resulted in neutron absorption,[10] the escape probability is occasionally defined as the probability that a neutron escapes the region without suffering any kind of a collision. We will denote this latter concept as the *first-flight escape probability*, however, since it characterizes the neutron streaming out of the fuel without interacting.

## 2. FIRST-FLIGHT ESCAPE PROBABILITIES AND COLLISION PROBABILITIES

Since the fuel is usually very highly absorbing, one can frequently calculate the escape probability $P_F$ in terms of a much simpler quantity $P_{FO}$, the *first-flight escape probability* defined by

$$P_{FO} \equiv \begin{array}{l} \text{probability that a neutron originating uniformly and iso-} \\ \text{tropically in the fuel will make its next collision in the} \\ \text{moderator (that is, will escape the fuel without making} \\ \text{a collision).} \end{array} \qquad (10\text{-}38)$$

The calculation of $P_{FO}$ is simply a geometrical problem, since one need only determine the probability that a neutron will stream out of the fuel region before it collides with anything. The first-flight escape probabilities $P_{FO}$ have been calculated[10] and tabulated[13] for most of the common fuel geometries and we will avoid wading through the solid geometry necessary to repeat these calculations here. It is useful to note several specific cases, however. For a very small fuel region we evidently must have

$$P_{FO} \xrightarrow[\substack{\text{fuel} \\ \text{lump}}]{\text{small}} 1 \qquad (10\text{-}39)$$

(since the probability of leaking out before suffering a collision must be almost
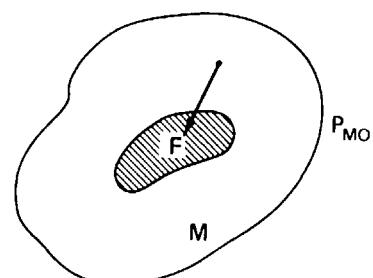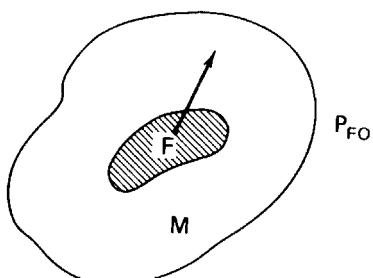


FIGURE 10-9.   The first-flight escape probabilities for a two-region cell.
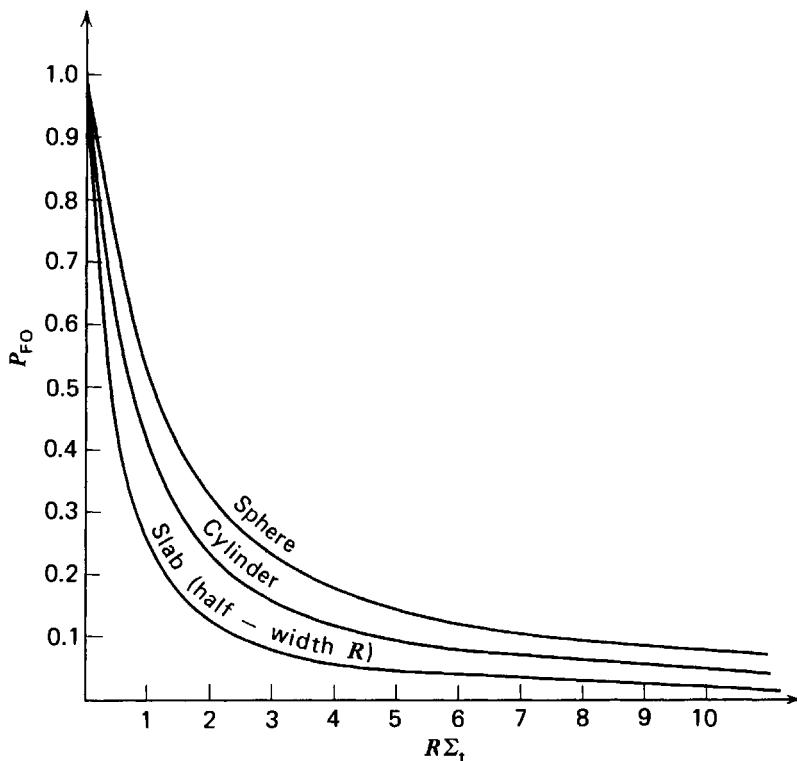
**FIGURE 10-10.** First-flight escape probability $P_{FO}$[10].

unity). For a large fuel region such that the fuel dimensions are large compared to a mfp, one finds[10]

$$P_{FO} \xrightarrow[\substack{\text{fuel} \\ \text{lump}}]{\text{large}} \frac{S_F}{4 V_F \Sigma_t^F} \qquad (10\text{-}40)$$

where $S_F$ is the surface area of the fuel region while $\Sigma_t^F$ is the total cross section of the fuel. The collision probability for intermediate size regions (size comparable to a mfp) is more complicated. We have included a plot of $P_{FO}$ for several common geometries in Figure 10-10.

A closely related concept is the *collision probability* characterizing a region

$$P_{FC} = \begin{array}{l} \text{probability that a neutron originating uniformly and iso-} \\ \text{tropically in the fuel will make first collision in the} \\ \text{fuel before escaping.} \end{array} \qquad (10\text{-}41)$$

From this definition it is apparent that

$$P_{FC} = 1 - P_{FO}. \qquad (10\text{-}42)$$

We will find it more convenient to work with the first-flight escape probability $P_{FO}$.

In the special case of a purely absorbing or "black" fuel lump, the escape probability $P_F$ is just equal to the first-flight escape probability $P_{FO}$, since any collision results in absorption. More generally, however, the neutron may scatter several times before being absorbed or escaping. Hence we should really write $P_F$

in terms of "multiple collision" escape probabilities

$$P_F = P_{FO} + P_{F1} + P_{F2} + \cdots = \sum_{n=0}^{\infty} P_{Fn}, \qquad (10\text{-}43)$$

where the $P_{Fn}$ are generalizations of the first flight escape probability $P_{FO}$ which describe the probability that the neutron escapes from the fuel lump after scattering $n$ times within the fuel. We can calculate these quantities in terms of $P_{FO}$ if we assume that the distribution of first, second, and further collisions is uniform. For example,

$$P_{F1} = (1 - P_{FO}) \frac{\Sigma_s^F}{\Sigma_t^F} P_{FO}. \qquad (10\text{-}44)$$

Similarly

$$P_{F2} = (1 - P_{FO}) \frac{\Sigma_s^F}{\Sigma_t^F} (1 - P_{FO}) \frac{\Sigma_s^F}{\Sigma_t^F} P_{FO}, \qquad (10\text{-}45)$$

and so on. Thus under the assumption of spatially uniform collision densities, we find the escape probability is given by

$$P_F = P_{FO} \left[ 1 + (1 - P_{FO}) \frac{\Sigma_s^F}{\Sigma_t^F} + (1 - P_{FO})^2 \left( \frac{\Sigma_s^F}{\Sigma_t^F} \right)^2 + \cdots \right]$$

$$= \left[ 1 + \frac{\Sigma_a^F}{\Sigma_t^F} \frac{(1 - P_{FO})}{P_{FO}} \right]^{-1}, \qquad (10\text{-}46)$$

where we have summed the geometric series. Actually in the ABH method this result is improved somewhat by accounting for a nonuniform distribution of first collisions.[7] In this case $P_F$ is given for a cylindrical fuel pin of radius $a$ by

$$P_F = \left\{ 1 + \frac{\Sigma_a^F}{\Sigma_t^F} \left[ \frac{(1 - P_{FO})}{P_{FO}} - a\Sigma_t^F \right] \left[ 1 + \alpha \left( \frac{\Sigma_s^F}{\Sigma_t^F} \right) + \beta \left( \frac{\Sigma_s^F}{\Sigma_t^F} \right)^2 \right] + a\Sigma_a^F \right\}^{-1} \qquad (10\text{-}47)$$

where the coefficients $\alpha$ and $\beta$ are given for cylindrical fuel in Figure 10-11. [Note that if $\alpha = \beta = 0$, this is identical to Eq. (10-46).]

### 3. THE ABH METHOD

Our final task is to calculate $\beta_M$, the probability that a neutron escaping the fuel will be absorbed in the moderator. In the ABH method, this is accomplished by combining Eqs. (10-35) and (10-36) to write

$$\beta_M = \left( \frac{V_M}{V_F} \right) \left( \frac{\Sigma_a^M}{\Sigma_a^F} \right) \frac{1}{P_F} P_{MF}. \qquad (10\text{-}48)$$
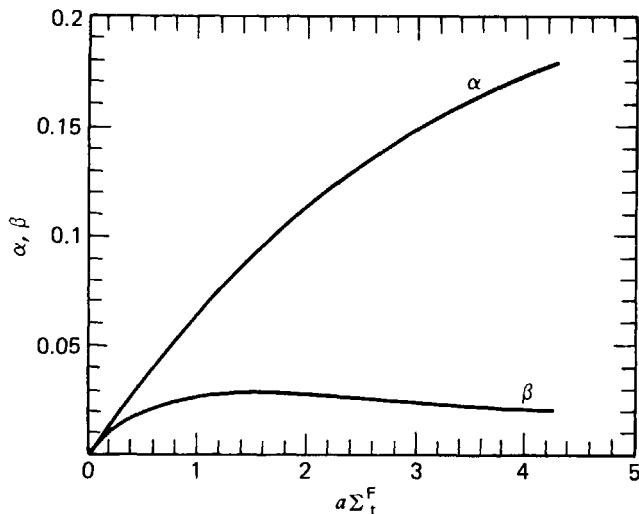
**FIGURE 10-11.   The ABH parameters $\alpha$ and $\beta$.[7]**

To calculate $\beta_M$, we now approximate $P_F$ by using its value for a large, purely absorbing fuel lump

$$P_F \sim P_{FO} \sim \frac{S_F}{4V_F\Sigma_a^F} . \qquad (10\text{-}49)$$

Then

$$\beta_M = \frac{4\Sigma_a^M V_M}{S_F} P_{MF}. \qquad (10\text{-}50)$$

Now all we need do is calculate $P_{MF}$, the transfer probability characterizing source neutrons born in the moderator escaping to the fuel where they are then absorbed.
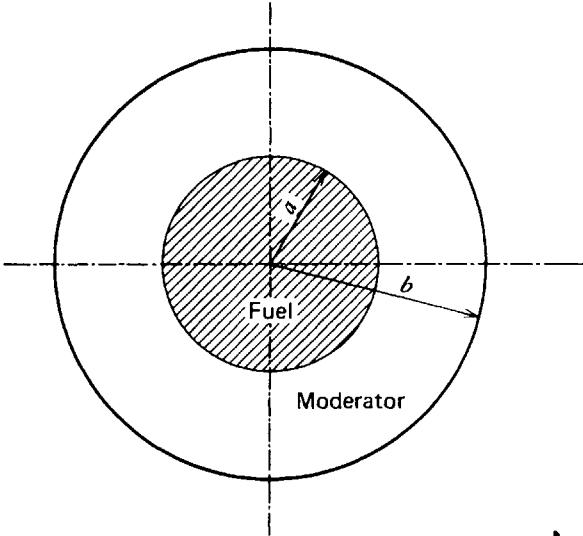
Ah, but isn't $P_{MF}$ just the thermal utilization, that we were trying to calculate originally? Yes, that is true. However the key idea in the ABH method is to note that one can use a relatively crude scheme to calculate $P_{MF}$ in obtaining $\beta_M$, provided the other quantities used in computing $f$ are treated adequately. That is, one can rewrite Eq. (10-35) as

$$\left(\frac{1}{f} - 1\right) = \left(\frac{\Sigma_a^M}{\Sigma_a^F}\right)\left(\frac{V_M}{V_F}\right)\frac{1}{P_F} + \frac{1 - f - \beta_M}{f} \qquad (10\text{-}51)$$

and then note that since the second term on the right-hand side is small, relatively crude approximations of it will suffice. If we rewrite Eq. (10-51) using $f \to P_{MF}$ and Eq. (10-49), we find

$$\left(\frac{1}{f} - 1\right) = \left(\frac{\Sigma_a^M}{\Sigma_a^F}\right)\left(\frac{V_M}{V_F}\right)\frac{1}{P_F} + \frac{1 - P_{MF}}{P_{MF}} - \frac{4\Sigma_a^M V_M}{S_F} . \qquad (10\text{-}52)$$

Hence we need only estimate $P_{MF}$. This can be done to sufficient accuracy using diffusion theory with a transport-corrected boundary condition at the fuel-

**FIGURE 10-12.** Fuel cell geometry for calculating $P_{MF}$.

moderator interface and assuming $P_{MF} \sim P_M$. That is, we solve

$$D_M \nabla^2 \phi_M(\mathbf{r}) - \Sigma_a^M \phi_M(\mathbf{r}) = -q_0$$

subject to boundary conditions:

$$(a) \quad \left. \frac{d\phi_M}{dr} \right|_{r=b} = 0 \tag{10-53}$$

$$(b) \quad \left. \frac{1}{\phi_M} \frac{d\phi_M}{dr} \right|_{r=a} = \frac{1}{d}$$

for the geometry indicated in Figure 10-12. Here we have used a transport-boundary condition at $r = a$, involving a parameter $d$ which is given in Figure 10-13 in terms of the fuel radius and the transport mean free path. We need only solve this diffusion problem, and then use the fact that

$$P_M = \left. \frac{2\pi a D_M}{q_0 V_M} \frac{d\phi_M}{dr} \right|_a \tag{10-54}$$

in order to determine $P_M$. Avoiding the details, we will only give the final result

$$P_M = \left\{ \frac{V_M a d}{2 V_F L_M^2} + E\left( \frac{a}{L_M}, \frac{b}{L_M} \right) \right\}^{-1} \cong P_{MF}, \tag{10-55}$$

where $L_M^2 = D_M / \Sigma_a^M$, and $E$ is a *lattice function*,[7] which for cylindrical geometries takes the form

$$E\left( \frac{a}{L_M}, \frac{b}{L_M} \right) = \frac{(b^2 - a^2)}{2a L_M} \left[ \frac{I_0\left( \frac{a}{L_M} \right) K_1\left( \frac{b}{L_M} \right) + K_0\left( \frac{a}{L_M} \right) I_1\left( \frac{b}{L_M} \right)}{I_1\left( \frac{b}{L_M} \right) K_1\left( \frac{a}{L_M} \right) - K_1\left( \frac{b}{L_M} \right) I_1\left( \frac{a}{L_M} \right)} \right]. \tag{10-56}$$
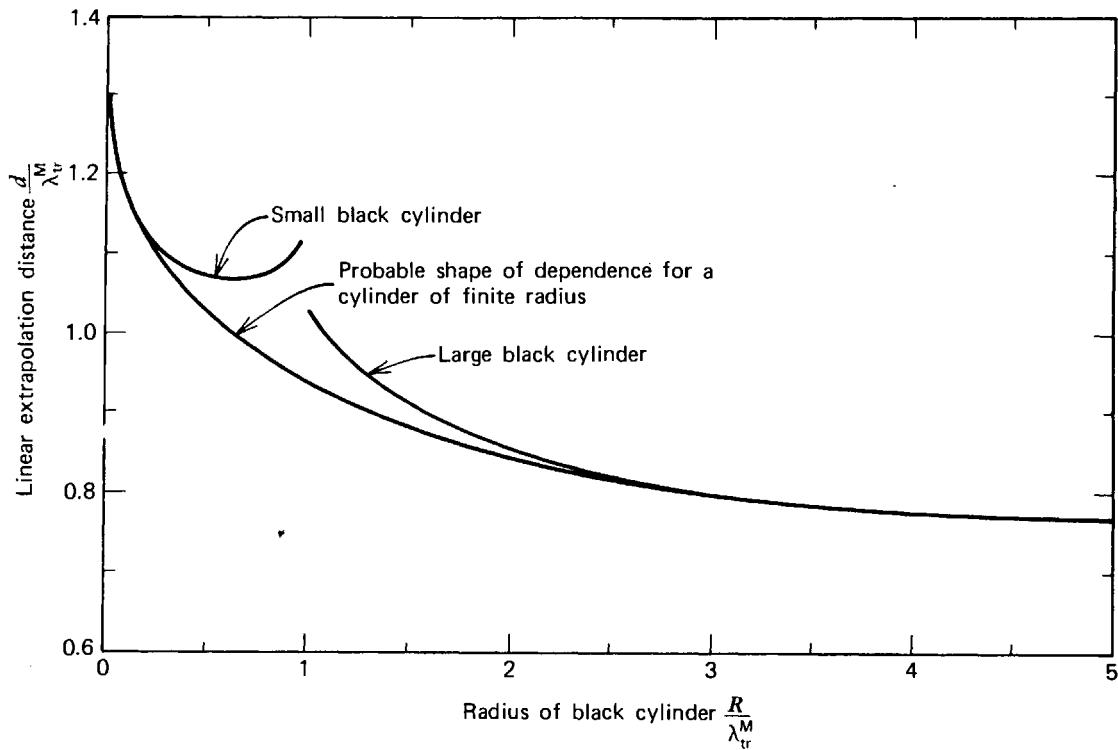
**FIGURE 10-13.** The transport boundary correction $d$.[13]

Hence our final expression becomes

$$\frac{1}{f} - 1 = \frac{\Sigma_a^M V_M}{\Sigma_a^F V_F} \left\{ 1 + \frac{\Sigma_a^F}{\Sigma_t^F} \left[ \frac{1 - P_{FO}}{P_{FO}} - a\Sigma_t^F \right] \left[ 1 + \alpha \left( \frac{\Sigma_s^F}{\Sigma_t^F} \right) + \beta \left( \frac{\Sigma_s^F}{\Sigma_t^F} \right)^2 \right] \right\}$$

$$+ \left( \frac{ad}{2L_M^2} - a\Sigma_a^M \right) \frac{V_M}{V_F} + E\left( \frac{a}{L_M}, \frac{b}{L_M} \right) - 1. \qquad (10\text{-}57)$$

Similar results for a three-region cell (including clad) can be obtained.[5,14]

The ABH method actually gives remarkably good results. For a range of fuel-to-moderator ratios, the values of $\bar{\phi}_M/\bar{\phi}_F$ calculated by the ABH method are within 0.5% of those calculated by a transport theory analysis. In Figure 10-14 we have compared the ABH method results for a cylindrical pin with the results of a more accurate transport calculation (THERMOS).

It should be noted that the disadvantage factors calculated by the ABH method depend on various macroscopic cross sections. The most common scheme is to consider these cross sections as being evaluated at the mean energy of the Maxwellian spectrum characterizing the moderator temperature. However it is possible to also regard the disadvantage factors as depending implicitly on energy via the energy-dependence of the cross sections that appear in them. That is, one can calculate a disadvantage factor for each energy point utilized in the thermal spectrum calculation. These energy-dependent disadvantage factors can then be utilized to determine cell-averaged group constants, as we indicated in Section 10-I-3.
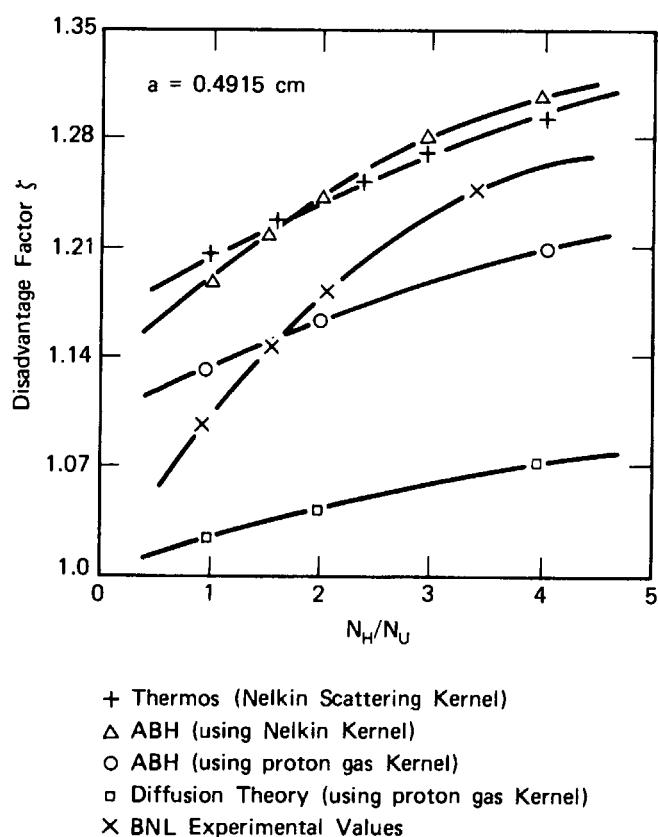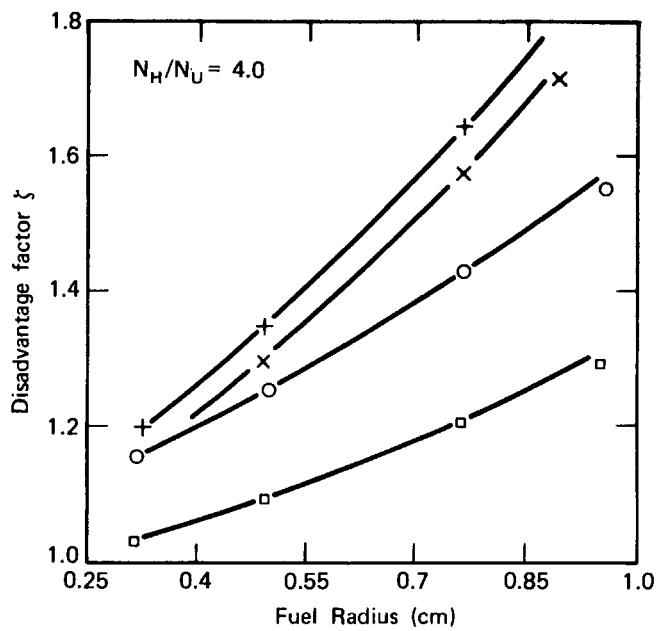
FIGURE 10-14.    Comparison of Disadvantage Factor Calculations for Cylindrical Fuel Pins of 1.3% Enrichment Fuel, H₂O Moderator.

## C. Integral Transport Methods for Thermal Cell Calculations (THERMOS)

Thus far we have described methods for including lattice heterogeneities in thermal spectrum calculations that essentially separate the treatment of the spatial and energy dependence of the neutron flux. That is, the spatial behavior of the flux in the unit cell is treated in the one-speed approximation (such as in the ABH method), and then the thermal disadvantage factors calculated from this spatial analysis are used to generate cell-averaged or "self-shielded" thermal group constants using the results of an infinite homogeneous medium thermal spectrum code. Such a scheme is characterized by a minimal calculational effort while still producing results of sufficient accuracy for many reactor design calculations.

However occasionally a more detailed analysis of the spatial dependence of the thermal spectrum in a fuel cell is required, for which the assumption of space–energy separability is inadequate. For such calculations it is usually also necessary to take into account the more detailed nature of thermal neutron scattering in the moderator using the scattering kernels generated by more elaborate methods (e.g., GASKET) than those such as the Wigner–Wilkins scheme.

Such an analysis usually requires a detailed solution of the energy-dependent transport equation characterizing the cell. Perhaps the most popular of such transport methods is the THERMOS code developed by Honeck,[8] which uses an integral form of the transport equation to calculate the spatially dependent thermal neutron spectrum in a cell characterized by a one-dimensional symmetry (usually cylindrical). The feasibility of the approach used in THERMOS relies heavily on the assumption of isotropic scattering.

To sketch the method, let us first recall the form of the energy-dependent transport equation, assuming isotropic sources and scattering:

$$\hat{\Omega} \cdot \nabla \varphi + \Sigma_t(\mathbf{r}, E)\varphi = \frac{1}{4\pi} \int_0^{E_c} dE' \int_{4\pi} d\hat{\Omega}' \Sigma_s(\mathbf{r}, E' \to E)\varphi(\mathbf{r}, E', \hat{\Omega}') + \frac{S(\mathbf{r}, E)}{4\pi},$$

$$0 \leqslant E \leqslant E_c, \qquad (10\text{-}58)$$

where we have noted that for such thermal spectrum problems, one is usually interested in energies $E$ below some cutoff energy $E_c$ (typically of the order of 1 eV). The source term actually represents neutrons slowing down below $E_c$ from higher energies:

$$S(\mathbf{r}, E) = \int_{E_c}^{\infty} dE' \Sigma_s(\mathbf{r}, E' \to E)\phi(\mathbf{r}, E'). \qquad (10\text{-}59)$$

Now notice that the transport Eq. (10-58) contains only a single derivative in space. Hence one can use standard integrating factor techniques (refer back to Section 4-IV-C) to integrate this equation over space. After a subsequent integration over angle, one arrives at the so-called "integral form" of the neutron transport equation

$$\phi(\mathbf{r}, E) = \int d^3r' \, T(\mathbf{r}, \mathbf{r}', E) \left[ \int_0^{E_c} dE' \Sigma_s(\mathbf{r}', E' \to E)\phi(\mathbf{r}', E') + S(\mathbf{r}', E) \right] \qquad (10\text{-}60)$$

where

$$T(\mathbf{r},\mathbf{r}',E) \equiv \frac{\exp\left[-\int_0^{|\mathbf{r}-\mathbf{r}'|} ds\, \Sigma_t\left(\mathbf{r}-s\frac{\mathbf{r}-\mathbf{r}'}{|\mathbf{r}-\mathbf{r}'|},E\right)\right]}{4\pi|\mathbf{r}-\mathbf{r}'|^2}. \tag{10-61}$$

Note here that $T(\mathbf{r},\mathbf{r}',E)$ is, in fact, the uncollided flux at $\mathbf{r}$ of energy $E$ from a unit point source at $\mathbf{r}'$ of the same energy $E$. It is sometimes known as the *transport* or *first-flight kernel*, and we will later see that it is closely related to an escape probability.

This equation is now solved numerically for a unit fuel cell, assuming zero net neutron current across cell boundaries and a uniformly distributed slowing down source only in the moderator. The integral transport equation is first written in multigroup form

$$\phi_g(\mathbf{r}) = \int d^3r'\, T(\mathbf{r},\mathbf{r}',E_g)\left[\sum_{g'=1}^{G} \Sigma_{s_{g'g}}(\mathbf{r}')\phi_{g'}(\mathbf{r}') + S_g(\mathbf{r}')\right],$$

$$1 \le g \le G. \tag{10-62}$$

To handle the spatial variable, the cell is divided into $N$ subregions. One then assumes that $\phi_g(\mathbf{r})$ is spatially independent within each subregion such that Eq. (10-62) can be written as

$$\phi_{ng} = \sum_{m=1}^{N} T_{mn}^g\left[\sum_{g'=1}^{G} \Sigma_{s_{g'g}}^m \phi_{mg'} + S_{mg}\right], \tag{10-63}$$

where

$$T_{mn}^g = \frac{1}{V_n}\int_{V_m} d^3r \int_{V_n} d^3r'\, T(\mathbf{r},\mathbf{r}',E_g). \tag{10-64}$$

Notice here that $T_{mn}^g$ can be interpreted as the transfer or coupling coefficient characterizing neutron transport between subregions $n$ and $m$. In fact, if we denote by $P_{mn}^g$ the probability that a neutron of energy $E_g$ appearing in region $m$ will suffer its next collision in region $n$, then the escape probabilities $P_{mn}^g$ are related to the coupling coefficients $T_{mn}^g$ by:

$$P_{mn}^g = \frac{V_n}{V_m}\Sigma_{t_g}^n T_{mn}^g. \tag{10-65}$$

The THERMOS method first calculates the coupling coefficients $T_{nm}^g$ for the cell of interest, usually by numerically performing the integration indicated in Eq. (10-61). Then the $N \times G$ multigroup, spatially discretized equations are solved using standard iterative techniques (e.g., overrelaxation). As one might expect, the calculation of the $T_{nm}^g$ is very time-consuming. Furthermore since we are actually solving a discretized integral equation in space (as opposed to a differential equation), it is not surprising to find that the matrices involved are full (that

restricts one in practice to using a small number of subregions).

THERMOS works best for tight, highly absorbing lattices with rapidly spatially varying properties. Once having obtained the spatially dependent flux in the cell $\phi(\mathbf{r}, E)$, one can directly calculate the cell-averaged or self-shielded cross sections as

$$\langle \Sigma^{(i)}(E) \rangle_{\text{cell}} = \frac{\int_{V_{\text{cell}}} d^3r \, N_i(\mathbf{r}) \sigma^{(i)}(E) \phi(\mathbf{r}, E)}{\int_{V_{\text{cell}}} d^3r \, \phi(\mathbf{r}, E)} . \tag{10-66}$$

Of course one can also calculate thermal disadvantage factors,

$$\zeta(E) = \frac{\frac{1}{V_M} \int_{V_M} d^3r \, \phi(\mathbf{r}, E)}{\frac{1}{V_F} \int_{V_F} d^3r \, \phi(\mathbf{r}, E)} . \tag{10-67}$$

The problem with codes such as THERMOS which attempt to calculate in some detail the spatial dependence of the flux in a unit fuel cell is one of cost relative to less sophisticated schemes such as the ABH method. Typical running times for such detailed transport codes are several orders of magnitude longer than those for schemes based on relatively simple estimates of the disadvantage factors. Hence the usual procedure is to calculate the fine structure within fuel cells using THERMOS only in detailed design studies. These results are then used to homogenize or self-shield group constants for a few group, two-dimensional diffusion or transport calculation performed on a fuel subassembly or group of subassemblies. The procedure is usually augmented by a few experimentally obtained corrections.

## III. HETEROGENEOUS EFFECTS IN FAST NEUTRON PHYSICS

### A. Resonance Escape Probabilities in Lumped Fuels

#### 1. THE SLOWING DOWN EQUATIONS FOR A TWO-REGION CELL

In our introductory discussion of lattice effects on core multiplication, it was stressed that fuel lumping can cause rather dramatic changes in resonance absorption due to self-shielding effects. Indeed the effective resonance integrals for the fuel can be decreased from their homogeneous values by as much as an order of magnitude. Hence it is essential that we discuss schemes for calculating the resonance integrals characterizing heterogeneous lattices. It is evident that such schemes must account for the spatial dependence of the flux in the fuel cell. Once again the method we will use is based on the concept of collision or escape probabilities—that is, the probability that a neutron originating in one region will make its next collision in another region.

For convenience, we will consider the fuel cell to be composed of only two species, fuel and moderator. (The extension to multiple isotopes or moderator admixed into the fuel is given in many of the standard references[15-17] on this

subject.) Our first task is to write a balance equation describing the neutron flux in the cell. Recall that the balance equation describing neutron slowing down in an infinite, *homogeneous* medium is

$$\Sigma_t(E)\phi(E)= \int_E^{\frac{E}{\alpha_A}} \frac{\Sigma_s^A(E')\phi(E')dE'}{(1-\alpha_A)E'} + \int_E^{\frac{E}{\alpha_M}} \frac{\Sigma_s^M(E')\phi(E')dE'}{(1-\alpha_M)E'}. \quad (10\text{-}68)$$

We will develop a generalization of this equation to account for a heterogeneous fuel cell by defining the energy-dependent first-flight escape probabilities:

$P_{FO}(E)$ = probability that a neutron of energy $E$ originating in the fuel will make its next collision in the moderator (that is, will escape the fuel without suffering a collision),

$P_{MO}(E)$ = probability that a neutron of energy $E$ originating in the moderator will make its next collision in the fuel.

We can now use these first flight escape probabilities to develop a generalization of Eq. (10-68). For suppose we interpret $\phi_F(E)$ and $\phi_M(E)$ as the volume-averaged flux in the fuel and moderator, respectively. Then for example,

$$V_M \int_E^{\frac{E}{\alpha_M}} \frac{\Sigma_s^M(E')\phi_M(E')dE'}{(1-\alpha_M)E'} \quad (10\text{-}70)$$

represents the average rate at which neutrons slow down to an energy $E$ in the moderator. Hence by multiplying this expression by $P_{MO}(E)$ we can compute the rate at which neutrons of energy $E$ are transferred from the moderator into the fuel. In a similar fashion, one can calculate the rate at which neutrons slowing down to energy $E$ in the fuel suffer their next collision in the fuel as

$$[1-P_{FO}(E)]V_F \int_E^{\frac{E}{\alpha_F}} dE' \frac{\Sigma_s^F(E')\phi_F(E')}{(1-\alpha_F)E'}. \quad (10\text{-}71)$$

The sum of these contributions must equal the total rate at which collisions are occurring in the fuel; hence we arrive at the balance relation for the fuel

$$V_F\Sigma_t^F(E)\phi_F(E) = V_F[1-P_{FO}(E)] \int_E^{\frac{E}{\alpha_F}} dE' \frac{\Sigma_s^F(E')\phi_F(E')}{(1-\alpha_F)E'}$$

$$+ V_M P_{MO}(E) \int_E^{\frac{E}{\alpha_M}} dE' \frac{\Sigma_s^M(E')\phi_M(E')}{(1-\alpha_M)E'}. \quad (10\text{-}72)$$

We can write a similar balance relation for the moderator region:

$$V_M \Sigma_t^M(E) \phi_M(E) = V_M[1 - P_{MO}(E)] \int_E^{\frac{E}{\alpha_M}} dE' \frac{\Sigma_s^M(E') \phi_M(E')}{(1 - \alpha_M) E'}$$

$$+ V_F P_{FO}(E) \int_E^{\frac{E}{\alpha_F}} dE' \frac{\Sigma_s^F(E') \phi_F(E')}{(1 - \alpha_F) E'} . \tag{10-73}$$

These two equations represent the generalization of the slowing down equation (10-68) to a heterogeneous two-region cell. As they stand, these coupled integral equations are exact. However they are only formal until the escape probabilities $P_{FO}(E)$ and $P_{MO}(E)$ have been specified (in much the same sense that the multigroup equations were also exact but of only a formal significance until the multigroup constants were determined). In practice, these escape probabilities are usually computed only approximately by assuming that the source neutrons in each region appear uniformly and isotropically. (This is referred to as the *flat source approximation*.)

These escape probabilities in effect allow us to separate the treatment of the spatial and energy variables in the study of neutron slowing down in the cell. The first-flight escape probabilities $P_{FO}(E)$ and $P_{MO}(E)$ will be calculated by considering spatial neutron transport at a given energy $E$. Once determined, these escape probabilities will be inserted into the slowing down equations involving only the energy variable. First we will proceed to apply Eqs. (10-72) and (10-73) to the study of resonance absorption in lattices, and defer until later the calculation of the escape probabilities.

It is possible to decouple these equations by making the narrow resonance approximation for the moderator

$$\Delta E|_M = \left(\frac{1 - \alpha_M}{2}\right) E_0 \gg \Gamma_p, \tag{10-74}$$

so that we can replace the average flux in the moderator by its asymptotic form

$$\phi_M(E) \sim \frac{1}{E} . \tag{10-75}$$

[Here we have again normalized the flux far above the resonance by removing the factor $\overline{\xi \Sigma_s}$ in $\phi(E) \sim 1/\overline{\xi \Sigma_s} E$, where for a heterogeneous cell, $\overline{\xi \Sigma_s} = (\xi_F \Sigma_p^F V_F + \xi_M \Sigma_s^M V_M)/V_{cell}$. Then in this region, $\phi_M(E) \sim \phi_F(E) \sim 1/E$.] If we now use this in the second term on the RHS of Eq. (10-72) corresponding to slowing down in the moderator, we find that it becomes

$$V_M P_{MO}(E) \int_E^{\frac{E}{\alpha_M}} dE' \frac{\Sigma_s^M(E') \phi_M(E')}{(1 - \alpha_M) E'} = V_M P_{MO}(E) \frac{\Sigma_s^M}{E} . \tag{10-76}$$

Hence by substituting this NR form into Eq. (10-72) we will have eliminated the appearance of the moderator flux in the equation for the fuel region, thereby decoupling this equation from the moderator region balance equation.

It is useful to make one further manipulation before inserting the NR approximation for the moderator into Eq. (10-72). One can demonstrate that the first-flight escape probabilities,[17] when calculated assuming a flat source in each of the fuel and moderator regions, must satisfy a reciprocity theorem similar to Eq. (10-34):

$$P_{FO}(E)\Sigma_t^F(E)V_F = P_{MO}(E)\Sigma_t^M(E)V_M. \tag{10-77}$$

If we furthermore assume that absorption is negligible in the moderator $[\Sigma_t^M(E){\sim}\Sigma_s^M(E)]$, we can rewrite Eq. (10-76) as

$$V_M P_{MO}(E) \int_E^{\frac{E}{\alpha_M}} dE' \frac{\Sigma_s^M(E')\phi_M(E')}{(1-\alpha_M)E'} = V_F P_{FO}(E)\frac{\Sigma_t^F(E)}{E}. \tag{10-78}$$

Hence our slowing down equation for the fuel region becomes

$$\Sigma_t^F(E)\phi_F(E) = [1 - P_{FO}(E)] \int_E^{\frac{E}{\alpha_F}} dE' \frac{\Sigma_s^F(E')\phi_F(E')}{(1-\alpha_F)E'} + \frac{P_{FO}(E)\Sigma_t^F(E)}{E}. \tag{10-79}$$

Once we know $P_{FO}(E)$ we can solve this equation for $\phi_F(E)$—either using analytical approximations or direct numerical methods—and thereby calculate the effective resonance integral for the resonance:

$$I = \int_{E_0} dE\, \sigma_\gamma^F(E)\phi_F(E) \tag{10-80}$$

(where once again we should keep in mind the normalization that $\phi_F(E){\sim}1/E$ far above the resonance).

## 2. APPROXIMATE CALCULATIONS OF THE RESONANCE INTEGRALS

We will now introduce the standard NR and NRIM approximations into our calculation of the resonance integral. First consider the narrow resonance approximation (NR) in which we can approximate

$$\int_E^{\frac{E}{\alpha_F}} dE' \frac{\Sigma_s^F(E')\phi_F(E')}{(1-\alpha_F)E'} {\sim} \frac{\Sigma_p^F}{E}. \tag{10-81}$$

If we substitute this into Eq. (10-79), we can immediately solve for the flux in the fuel as

$$\phi_F(E) = \frac{[1 - P_{FO}(E)]\Sigma_p^F + P_{FO}(E)\Sigma_t^F}{\Sigma_t^F E}. \tag{10-82}$$

Hence the NR approximation to the resonance integral becomes just

$$I^{NR} = \int \frac{dE}{E} \frac{\sigma_\gamma^F}{\sigma_t^F} \left[ \sigma_p^F + P_{FO}\left(\sigma_t^F - \sigma_p^F\right) \right],$$  (10-83)

where we have cancelled out the fuel number density $N_F$.

It is customary to express the first-flight escape probability $P_{FO}(E)$ in terms of a "pseudo" cross section $\sigma_e$ known as the *escape* cross section, which characterizes neutron removal from the fuel lump via leakage to the moderator:

$$P_{FO}(E) = \frac{\sigma_e}{\sigma_e + \sigma_t^F}, \quad \text{or} \quad \sigma_e \equiv \left( \frac{P_{FO}}{1 - P_{FO}} \right) \sigma_t^F.$$  (10-84)

That is, if $\sigma_e$ is proportional to the probability of a neutron leaking out of the fuel before suffering its next collision, then since $\sigma_e + \sigma_t^F$ characterizes neutron loss either via absorption or collisions with fuel nuclei, this physical interpretation of $\sigma_e$ is consistent with our earlier interpretation of the escape probability $P_{FO}(E)$. Of course, in order to determine $\sigma_e$ we must first calculate $P_{FO}(E)$ and then use Eq. (10-84). However $\sigma_e$ is particularly useful since it tends to be only weakly dependent on energy (much like a potential scattering cross section).

If we insert Eq. (10-84) into the resonance integral and note

$$\sigma_p^F + \frac{\sigma_e\left(\sigma_t^F - \sigma_p^F\right)}{\sigma_e + \sigma_t^F} = \frac{\sigma_t^F \sigma_p^F + \sigma_e \sigma_t^F}{\sigma_e + \sigma_t^F},$$  (10-85)

we find

$$I^{NR} = \int \frac{dE}{E} \frac{\left(\sigma_p^F + \sigma_e\right)\sigma_\gamma^F}{\sigma_t^F + \sigma_e}.$$  (10-86)

But recall that our earlier result for a homogeneous system was

$$I^{NR}\big|_{hom} = \int \frac{dE}{E} \left[ \frac{\sigma_p^F + \Sigma_s^M / N_F}{\sigma_t^F + \Sigma_s^M / N_F} \right] \sigma_\gamma^F.$$  (10-87)

Hence it is apparent that we can obtain the heterogeneous result [Eq. (10-86)] from the homogeneous resonance integral [Eq. (10-87)] by simply replacing

$$\frac{\Sigma_s^M}{N_F} \longrightarrow \sigma_e.$$  (10-88)

These results give rise to what are commonly referred to as the *equivalence relationships* for resonance absorption: (a) heterogeneous lattices with the same values of $\sigma_e$ will have the same resonance integral, regardless of the surrounding moderator and (b) a heterogeneous lattice with a given value of $\sigma_e$ will have the same resonance integral as a homogeneous reactor with $\Sigma_s^M / N_F \rightarrow \sigma_e$.

A very similar result can be obtained for the NRIM approximation. In this case, one finds

$$I^{\text{NRIM}} = \int \frac{dE}{E} \frac{P_{\text{FO}}\sigma_\gamma^F}{1 - (1 - P_{\text{FO}})(\sigma_s^F/\sigma_t^F)} = \int \frac{dE}{E} \frac{\sigma_e \sigma_\gamma^F}{\sigma_\gamma^F + \sigma_e}. \qquad (10\text{-}89)$$

Of course before proceeding further we must still determine how to calculate the escape cross section $\sigma_e$ or equivalently, the first-flight escape probability $P_{\text{FO}}(E)$. Recall that we had already assumed that $P_{\text{FO}}(E)$ and $P_{\text{MO}}(E)$ could be calculated using the flat source approximation. Although this approximation might be reasonable far from the resonance energy, it is certainly not strictly valid at this energy since the flux in the fuel element is quite strongly varying due to self-shielding. However such an approximation is found to be adequate in most applications of interest.

Hence we are now faced with calculating $P_{\text{FO}}(E)$, the probability that a neutron born uniformly and isotropically in the fuel makes its next collision in the moderator. Fortunately, the resonance integral is not overly sensitive to the detailed behavior of $P_{\text{FO}}(E)$. In fact, it is usually sufficient to introduce a particularly simple approximation for $P_{\text{FO}}(E)$ first suggested by Wigner.[18] First recall that we know the limiting behavior of $P_{\text{FO}}(E)$ for both small and large fuel lumps. For small fuel lumps, obviously

$$P_{\text{FO}}(E) \to 1 \quad \text{as} \quad \frac{V_F}{S_F} \to 0. \qquad (10\text{-}90)$$

For large fuel lumps, we can effectively use the black lump result

$$P_{\text{FO}}(E) \to \frac{S_F}{4V_F\Sigma_t^F} \quad \text{as} \quad \frac{V_F}{S_F} \to \infty. \qquad (10\text{-}91)$$

With these limits in mind, Wigner chose a simple interpolation formula between the limits (known as the *Wigner rational approximation*)

$$P_{\text{FO}}(E) = \frac{\left(S_F/4V_F\Sigma_t^F\right)}{1 + \left(S_F/4V_F\Sigma_t^F\right)}. \qquad (10\text{-}92)$$

This rather crude approximation is usually valid to within 10% in most lattices of interest. If we now compare Eq. (10-92) with our earlier definition of $\sigma_e$ given by Eq. (10-84), we can identify

$$\sigma_e \xrightarrow[\text{approximation}]{\text{Rational}} \frac{S_F}{4V_FN_F} = \frac{1}{N_F\langle R \rangle_F}. \qquad (10\text{-}93)$$

Here we have noted that $4V_F/S_F$ can be shown to be geometrically equal to the

average length of a chord drawn across the fuel region.[10,19] (See Problem 10-15.) Hence the only place that the fuel geometry enters is into the escape cross section $\sigma_e$. As we have seen, we can now adapt our earlier homogeneous resonance integral results to heterogeneous lattices by merely replacing $\Sigma_s^M / N_F \to \sigma_e \sim S_F / 4 V_F N_F$.

To proceed further, notice that we can rewrite Eq. (10-83) as two terms

$$I^{NR} = \int \frac{dE}{E} \frac{\sigma_\gamma^F \sigma_p^F}{\sigma_t^F} + \int \frac{dE}{E} \frac{P_{FO}(\sigma_t^F - \sigma_p^F)\sigma_\gamma^F}{\sigma_t^F} \tag{10-94}$$

where the first term is identical to the NR approximation for an infinite medium composed only of fuel, while the second term depends on geometry through $P_{FO}$.

From Eq. (10-92) it is apparent that $P_{FO} \sim S_F / V_F N_F \sim (S_F / M_F)$ in the rational approximation, where $M_F$ is the mass of the fuel lump. Hence Eq. (10-94) suggests that we can write the resonance integral in the form

$$I \sim a + b \left( \frac{S_F}{M_F} \right). \tag{10-95}$$

As we will see in a moment, this relationship is born out by experimental measurements.

If we now substitute in the Doppler-broadened resonance forms

$$\sigma_t^F = \sigma_\gamma^F + \sigma_s^F = \sigma_0 \frac{\Gamma_\gamma}{\Gamma} \psi(\zeta, x) + \sigma_0 \frac{\Gamma_n}{\Gamma} \psi(\zeta, x) + \sigma_p^F \tag{10-96}$$

(where we have again neglected interference scattering), we can write Eq. (10-94) as

$$I^{NR} = \frac{V_F}{V} \left\{ \frac{\sigma_p^F \Gamma_\gamma}{E_0} J(\zeta, \beta) + \frac{\sigma_0 \Gamma_\gamma}{E_0} L(t, \zeta, \beta) \right\}, \tag{10-97}$$

where we recall

$$\zeta = \frac{\Gamma}{\Gamma_D}, \qquad \beta = \frac{\sigma_p^F}{\sigma_0}, \qquad J(\zeta, \beta) = \int_0^\infty dx \frac{\psi(\zeta, x)}{\psi(\zeta, x) + \beta}, \tag{10-98}$$

while

$$L(t, \zeta, \beta) \equiv \int_0^\infty dx \frac{P_{FO}(x) \psi^2(\zeta, x)}{\psi(\zeta, x) + \beta}, \tag{10-99}$$

where

$$t \equiv \frac{4 V_F \Sigma_p^F}{S_F} = \Sigma_p^F \langle R \rangle_F. \tag{10-100}$$

We have encountered the $J(\zeta, \beta)$ function before. The $L(t, \zeta, \beta)$ function has been tabulated for common lattice geometries.[20]

A very similar result can be obtained for the NRIM approximation

$$I^{NRIM} = \frac{\Sigma_{pm}^F \Gamma}{N_F E_0} J(\zeta, \beta') + \frac{\Sigma_{pm}^F \Gamma}{N_F \beta' E_0} L(t', \zeta, \beta') \qquad (10\text{-}101)$$

where

$$\beta' \equiv \frac{\Sigma_{pm}^F \Gamma}{N_F \sigma_0 \Gamma_\gamma}, \qquad t' \equiv \frac{4 V_F \Sigma_{pm}^F}{S_F}. \qquad (10\text{-}102)$$

Since the NRIM approximation results in ignoring scattering from the absorber, we have chosen to generalize our result somewhat by including a moderator admixed into the fuel lump[15,16] (e.g., oxygen in $UO_2$ fuels) denoted by a potential scattering cross section $\Sigma_{pm}^F$.

### 3. ROD SHADOWING AND THE DANCOFF CORRECTION

Thus far we have treated resonance absorption in a fuel lump as if the unit fuel cell were truly isolated from other fuel cells. However, if the fuel rods in a lattice are in fact separated by a moderator that is not many mean free paths thick, it is possible for neutrons with energies in the resonance region to pass from one fuel lump to another. This invalidates our earlier calculation based on collision probabilities, for in that calculation we assumed that the escape probability from the fuel $P_{FO}$ implied that on escaping from the fuel, the neutron would suffer its next collision in the moderator. However if other fuel lumps are nearby, this next collision might also occur in the fuel. Hence we should try to calculate a modified escape probability $P_{FO}^*$ that a source neutron born in the fuel suffers its next collision in the moderator—even though there may be adjacent fuel elements. Then we can use our earlier analysis, merely replacing $P_{FO}$ by $P_{FO}^*$.

We shall not develop a detailed derivation[21,22] of a modified collision probability $P_{FO}^*$ including rod shadowing effects here, but merely indicate that the result of such a calculation is

$$P_{FO}^* = P_{FO} \frac{(1 - C)}{1 - C\left(1 - \Sigma_t^F \langle R \rangle_F P_{FO}\right)}, \qquad (10\text{-}103)$$

where $\langle R \rangle_F$ is the average chord length characterizing the fuel lump [$\langle R \rangle_F = 2R$ for an infinitely long cylinder] while $C$ is a tabulated parameter known as the Dancoff–Ginsberg factor[22] that depends on the fuel geometry and cross section. Actually this merely corresponds to increasing the average chord length in the fuel
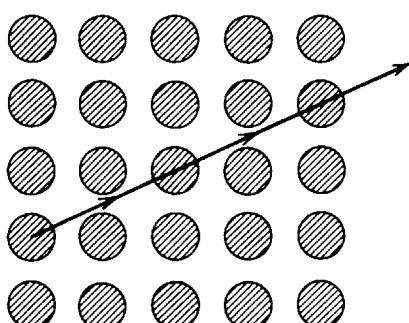


FIGURE 10-15.    Rod-shadowing effects.

lump by a factor $(1 - C)^{-1}$—that is,

$$N_F \sigma_e = \frac{1}{\langle R \rangle_F} \quad \longrightarrow \quad \frac{1-C}{\langle R \rangle_F} \quad . \qquad (10\text{-}104)$$

$$\text{(no shadowing)} \qquad \text{(shadowing)}$$

Hence the Dancoff–Ginsberg factor simply decreases the effective leakage from the lump (taking into account the possibility that the neutron might eventually be absorbed in a neighboring fuel lump).

One can now merely use $P_{FO}^*$ in place of $P_{FO}$ in the calculations of the resonance integrals for the lattice of interest. The effect of such a correction is to decrease the surface area of a single fuel element by a factor of $1 - C$. This fact is of particular use if one of the various correlations for the resonance integral is to be used. We have given a short table of the Dancoff factor $C$ in Table 10-1.

**TABLE 10-1  Dancoff Corrections $C$ for Two Parallel Circular Cylinders[22]**

| Pitch/radius | radius/$\lambda_{tr}$ | | | | | |
|---|---|---|---|---|---|---|
| | 0 | 0.25 | 0.50 | 1.0 | 1.5 | 2.0 |
| 2.0 | .182 | .170 | .160 | .144 | .132 | .123 |
| 2.25 | .155 | .132 | .114 | .086 | .067 | .0522 |
| 2.5 | .136 | .107 | .0849 | .0550 | .0364 | .0245 |
| 2.75 | .122 | .088 | .0649 | .0362 | .0208 | .0122 |
| 3.0 | .111 | .074 | .0505 | .0244 | .0122 | .0062 |
| 4.0 | .081 | .040 | .0205 | .0057 | .0016 | .0005 |
| 5.0 | .065 | .024 | .0091 | .0015 | .0003 | — |
| 6.0 | .054 | .015 | .0043 | .0004 | — | — |
| 7.0 | .046 | .0094 | .0021 | .0001 | — | — |
| 8.0 | .040 | .006 | .0011 | — | — | — |
| 9.0 | .036 | .004 | .0006 | — | — | — |
| 10.0 | .032 | .0028 | .0003 | — | — | — |

Notice that decreasing the surface area of a fuel lump will reduce the corresponding resonance integral from its value for an isolated fuel element. Hence one finds that the Dancoff correction for neighboring fuel elements corresponds effectively to a correction for the shadowing of one fuel element by another.

## 4. EMPIRICAL CORRELATIONS FOR RESONANCE INTEGRALS

A number of experimental measurements of resonance integrals have been performed that parameterize the data as empirical correlations of the form of Eq. (10-95). For example, the total resonance integral (i.e., over all resonances) in $UO_2$ at a temperature of 20°C can be written either[23] as

$$I^{28} = 11.6 + 22.8(S_F/M_F), \quad \text{or as} \quad I^{28} = 4.15 + 26.6\sqrt{S_F/M_F} \ .$$

[These forms can actually be derived from the expressions (10-97) and (10-101) in certain limits.] Both of these expressions are found to work equally well over the range of $S_F/M_F$ characteristic of $UO_2$ fuel lattices.

Experimental correlations have also been determined to characterize the temperature-dependence of the resonance integral. For example, in the temperature range from 20–600°C one can use[23]

$$I^{28} = I^{28}(300°\text{K})\left[1 + \beta(\sqrt{T} - \sqrt{300°\text{K}})\right] \tag{10-105}$$

where $\beta \sim .006-.008$, depending on fuel type and rod radius. A very convenient correlation has been proposed by Strawbridge and Barry[5] to characterize both lattice parameters and temperature effects:

$$I^{28} = 2.16x + 2.56 + \left[.0279x - .0537\right]\sqrt{T}$$

where

$$x = \left[\frac{\Sigma_p^F}{N_{28}}P_{\text{FO}} + \frac{(1-C)}{\langle R \rangle_F N_{28}}\right]^{1/2}, \tag{10-106}$$

while $C$ is the Dancoff-Ginsberg factor and $\langle R \rangle_F$ is the mean chord length of the fuel pin. Typical results from this correlation are shown for several different fuel temperatures in Figure 10-16.
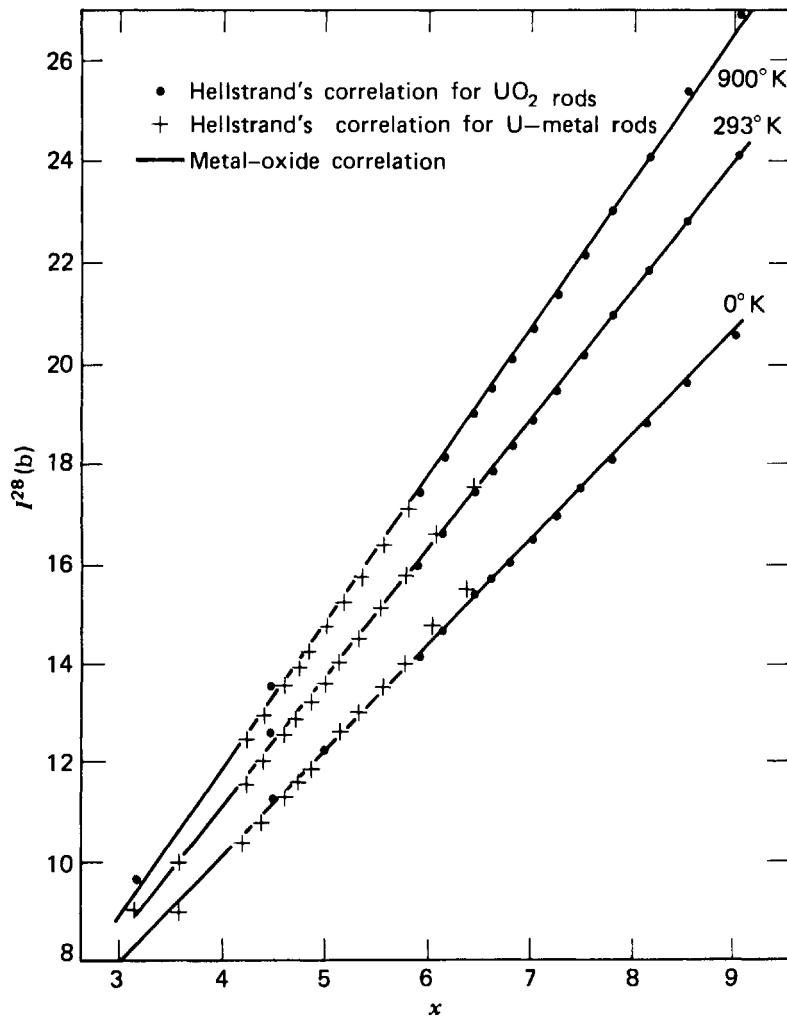


FIGURE 10-16. Comparison of metal-oxide resonance integral correlation with Hellstrand's correlations for isolated rods. [5]

Although such correlations cannot be used directly in reactor calculations (since the core lattice differs considerably from the pure $UO_2$ lattice described by the correlation), they do prove extremely useful in normalizing resonance integral calculations within fast spectrum codes, as we will see in Section 10-III-C.

## B. Modifications in the Treatment of Fast Fission

Although the number of fast fission events occurring in a thermal reactor is not large, such reactions can be quite significant since they can provide a sizable fraction of the excess reactivity of a core. It is particularly important to take some account of the enhancement of the probability of a fast fission reaction by fuel lumping. This will cause the fast fission factor $\epsilon$ to be increased from its value for a homogeneous reactor core.

The calculation of heterogeneous modifications to the fast fission factor is considered in detail in several of the standard references.[24,25] We will focus our attention instead on the more practical question of just how heterogeneous effects are included in the treatment of fast fission in conventional fast spectrum codes.

The rate at which fast fission reactions occur depends on the magnitude of the fast neutron flux in the fuel region. From our earlier discussion, we expect this fast flux (say, in the energy range .5–10 MeV) to be somewhat larger in the fuel than in the moderator, since once neutrons have entered the moderator, they are rapidly slowed down below the fast fission energy threshold. Hence we might expect that a homogeneous fast spectrum calculation will tend to underpredict the amount of fast fission occurring, since it will use the average flux characterizing a homogeneous system.

To correct this, one can follow a procedure very similar to that used in our treatment of thermal fission by defining a *fast utilization factor* (similar to the thermal utilization factor) which is the ratio of the neutron removal rate in the fuel to the total rate of fast neutron removal. Notice that we include in this definition all mechanisms for neutron removal, including neutron absorption, elastic and inelastic scattering. Then it is evident in analogy to out treatment of the thermal utilization that

$$f_F = \frac{\Sigma_R^F V_F \bar{\phi}_F}{\Sigma_R^F V_F \bar{\phi}_F + \Sigma_R^M V_M \bar{\phi}_M}. \tag{10-107}$$

Here $\Sigma_R$ is the removal cross section for fast neutrons. We will now introduce a flux *fast advantage factor*, defined as

$$\zeta_F \equiv \bar{\phi}_F / \bar{\phi}_M. \tag{10-108}$$

(Notice that at fission neutron energies, the fuel is now at an *advantage* in competing with the moderator for neutron absorption). Using this definition and our expression for $f_F$, we can solve for the fast advantage factor in terms of the fast utilization factor as

$$\zeta_F = \frac{\Sigma_R^M}{\Sigma_R^F} \frac{V_M}{V_F} \left( \frac{f_F}{1 - f_F} \right). \tag{10-109}$$

Once we have determined $\zeta_F$, we can calculate new group constants characterizing the fast range that include the effect of fast flux enhancement due to fuel lumping.

Of course the success of this technique is contingent on our ability to calculate $f_F$. One could always use brute force methods based on Monte Carlo calculations, but it is far more common to use alternative techniques[26] based on successive collision probabilities very similar to those used in the ABH method. This latter approach is particularly appropriate since the inclusion of lattice effects in fast fission is not nearly so critical as in thermal group constant generation. Indeed errors in the treatment of fast fission rarely lead to an error of over 0.1% in core multiplication. Hence rather crude methods are usually sufficient for accounting for lattice heterogeneities in fast fission for thermal reactor design. We will avoid a detailed discussion of the application of the techniques developed in Section 10-II-B and instead refer the interested reader to standard sources such as Strawbridge and Barry.[26]

## C. The Inclusion of Heterogeneous Effects in Fast Spectrum Codes

As we have seen, the most significant effects of a heterogeneous fuel arrangement on the calculation of fast group constants enter into the treatment of resonance absorption, although modifications are frequently also included in the treatment of fast fission.

The dominant heterogeneous effect in resonance absorption in thermal reactors is that of self-shielding, which substantially reduces the value of the resonance integral. One can include this effect in the calculation of resonance integrals by using collision probability methods. For crude treatments, one can simply use the rational approximation to calculate the effective escape cross section for the lattice geometry of interest, and then use $\Sigma_s^M / N_A \to \sigma_e$ in the usual homogeneous calculations. More accurate calculations based on a more realistic estimate of the escape probability $P_{FO}$ require an evaluation of both the $J(\zeta, \beta)$ and $L(t, \zeta, \beta)$ factors. Rod-shadowing effects are accounted for by using the Dancoff factor in the calculation of $I$.

The resonance integrals for each fine-spectrum group can then be calculated and used to calculate either the effective absorption cross section for the group

$$\Sigma_{a_n} = \frac{N_A^{hom} \sum_{i \in n} I_i}{\Delta u_n} \tag{10-110}$$

or the resonance escape probability for the group,

$$p_n = \exp\left[ -\frac{N_A^{hom}}{\xi \Sigma_s} \sum_{i \in n} I_i \right]. \tag{10-111}$$

Of course to perform a detailed calculation of the Doppler-broadened resonance integral for each resolved resonance would be prohibitively expensive. Hence one customarily only accounts for Doppler-broadening and heterogeneous effects in the more significant resonances. For example, in a slightly enriched uranium-fueled thermal reactor, one might only perform a detailed calculation for the lowest energy resonances of $^{238}U$ and $^{240}Pu$. The remaining resonances would then be characterized by their zero-temperature, homogeneous resonance integrals.

The resonance escape probabilities for each group are adjusted (fudged) so that the total resonance integral agrees with an empirical correlation (although the amount of resonance absorption assigned to each microgroup in the fast spectrum

code will vary with the details of the calculation). For example, one scheme might be to multiply every resonance escape probability $p_n$ for $^{238}U$ by the same fudge factor $L$, and then vary $L$ until $I^{28}$ when calculated assuming zero absorption for all other elements agrees with the Strawbridge and Barry correlation[5] [this is known as the "$\omega^*$-search," where $\omega^* = (1 - p^{28})/p^{28}$].

In fast reactor analysis, the small spacing between fuel elements and the large neutron mfp allows one to largely ignore heterogeneous effects in the calculation of resonance integrals. Furthermore for the high-energy resonances of importance to fast reactor behavior,[27] the NR approximation is usually valid. Other complications arise, however, such as unresolved resonances and p-wave resonances, somewhat complicating the analysis of resonance absorption in fast systems.

The cross sections characterizing the fast microgroups can be scaled to account for fast flux peaking, which tends to enhance fast fission. Such an effect can be included in both thermal and fast reactor analysis.

With these adjusted resonance integrals and fast cross sections, one can now continue on to calculate the fast neutron energy spectrum and generate the fast few-group constants. Hence as in the case of thermal neutron physics, one finds that the effects due to lattice heterogeneities enter the treatment of fast neutron physics via a simple modification of fast-group constants, which accounts for the spatial flux variation in the lattice cell (i.e., spatial self-shielding).

## IV. SOME CONCLUDING REMARKS ON THE MULTIGROUP DIFFUSION METHOD

In the past four chapters we have developed the principal tool of nuclear reactor analysis, multigroup diffusion theory. The multigroup diffusion equations are capable of yielding the neutron flux in a nuclear reactor core to an accuracy sufficient for most reactor design problems, provided adequate care is taken in the determination of the multigroup constants entering these equations.

Indeed we have found that the solution of the multigroup diffusion equations is rather straightforward. Most of our effort was expended in developing suitable prescriptions for calculating the group constants, for these group constants had to account for the rather complicated energy dependence of the intragroup fluxes used in averaging basic cross section data, as well as for spatial neutron transport effects arising in core lattices.

Hence a multigroup diffusion analysis of a reactor core really consists of two principal tasks: (a) generation of the multigroup constants, and (b) solution of the multigroup diffusion equations proper.

It should be noted that various input data are necessary in order to determine the group constants. For example, one obviously requires basic cross section data characterizing the various isotopes appearing in the reactor. This is usually provided in the form of fast and thermal cross section libraries which give these data as fine-group constants (just the basic cross section data averaged over each of the fine groups to be used in the fast and thermal spectrum calculations).

Next one requires information concerning the composition and geometry of the core. Since the core composition will vary throughout the core (e.g., in various zones of differing fuel enrichment or moderator density), one will usually be required to generate different group constants for each region of the core in which the gross core composition is significantly different. On a finer scale, one must provide the dimensions of the lattice unit cell for which the group constants are to

be generated. Finally one must input the temperatures of each of the major components of the cell (e.g., fuel temperature).

The basic dimensions of the lattice geometry can easily be provided at the beginning of the core analysis. However the necessary input describing the cell composition and temperature must first be calculated, since these will depend on considerations such as fuel depletion and isotope buildup, control insertion, and the thermal–hydraulic behavior of the core. As we will see later, this information is usually supplied by other computational modules in a reactor core analysis model (or computer code).

Now that we have developed the basic model used to describe the neutronic behavior of a nuclear reactor, it is appropriate that we turn to a discussion of how this model is applied in nuclear reactor analysis. The application of multigroup diffusion theory to reactor analysis will depend to some degree on the reactor type and the detailed information desired. In the remaining chapters of this text, we will concern ourselves with various examples of how such a model is applied to nuclear reactor analysis, and in particular, to how such applications interact with other facets of reactor core analysis and design.

## REFERENCES

1. S. Glasstone and M. C. Edlund, *The Elements of Nuclear Reactor Theory*, Van Nostrand, Princeton, N.J. (1952), Chapter 9.
2. H. D. Smyth, *Atomic Energy for Military Purposes*, Princeton University Press, Princeton, N.J. (1945).
3. R. L. Hellens, The physics of PWR reactors, *in* New Developments in Reactor Physics and Shielding, CONF-720901, (1972) Vol. I, p. 3.
4. M. H. Merrill, Nuclear design methods and experimental data in use at Gulf General Atomic, Gulf-GA-A12652 (1973).
5. L. W. Strawbridge and R. F. Barry, *Nucl. Sci. Eng.* 23, 58 (1965).
6. M. H. Merrill, Nuclear design methods and experimental data in use at Gulf General Atomic, Gulf-GA-A12652 (1973) Chapter 3.
7. A. Amouyal, P. Benoist, and J. Horowitz, *J. Nucl. Energy* 6, 79 (1957); J. R. Lamarsh, *Introduction to Nuclear Reactor Theory*, Addison-Wesley, Reading, Mass. (1966), pp. 382–389.
8. H. C. Honeck, THERMOS, a thermalization transport code for reactor lattice calculations, BNL-5826 (1961); *Nucl. Sci. Eng.* 8, 193 (1960).
9. R. L. Crowther, Physics of measurements of BWR reactors and comparison with theory, *in* New Developments in Reactor Physics and Shielding, CONF-720901, Vol. I. p. 114.
10. K. M. Case, F. de Hoffmann, and G. Placzek, *Introduction to the Theory of Neutron Diffusion*, Los Alamos Scientific Laboratory Report (1953).
11. P. F. Zweifel, *Reactor Physics*, McGraw-Hill, New York (1973).
12. G. C. Pomraning, Transport methods for the calculation of spatially dependent thermal spectra, in *Reactor Physics in the Resonance and Thermal Regions*, A. J. Goodjohn and G. C. Pomraning (Eds.), M. I. T. Press, Cambridge (1966), p. 207; D. R. Askew, Proceedings of Conference on Numerical Reactor Calculations, IAEA, Vienna (1972), pp. 185–196.
13. *Reactor Physics Constants*, USAEC Document ANL-5800 (2nd Edition) (1963).
14. A. Amouyal, P. Benoist, and J. Horowitz, *J. Nucl. Eng.* 23, 58 (1965).
15. L. Dresner, *Resonance Absorption in Nuclear Reactors*, Pergamon, New York (1960).
16. J. R. Lamarsh, *Introduction to Nuclear Reactor Theory*, Addison-Wesley, Reading, Mass. (1966), 390–401.
17. J. H. Ferziger and P. F. Zweifel, *The Theory of Neutron Slowing Down in Nuclear Reactors*, M. I. T. Press, Cambridge (1966).

18. E. P. Wigner, et al., *J. Appl. Phys.* **2**, 257 (1955).
19. G. I. Bell and S. Glasstone, *Nuclear Reactor Theory*, Van Nostrand, Princeton, N.J. (1970), Chapter 8.
20. F. T. Adler and L. W. Nordheim, Tables for the computation of resonance integrals, GA-377 (1958).
21. G. I. Bell and S. Glasstone, *Nuclear Reactor Theory*, Van Nostrand, Princeton, N.J. (1970), p. 123.
22. *Reactor Physics Constants*, USAEC Document ANL-5800 (2nd Edition) (1963), p. 280.
23. E. Hellstrand, P. Blomberg and S. Horner, *Nucl. Sci. Eng.* **8**, 497 (1960); E. Hellstrand, *J. Appl. Phys.*, **28**, 1493 (1957).
24. J. R. Lamarsh, *Introduction to Nuclear Reactor Theory*, Addison-Wesley, Reading, Mass. (1966), pp. 402–408.
25. R. V. Meghreblian and D. K. Holmes, *Reactor Analysis*, McGraw-Hill, New York (1960), pp. 692–698.
26. L. W. Strawbridge and R. F. Barry, *Nucl. Sci. Eng.* **23**, 58 (1965); R. L. Hellens and H. C. Honeck, IAEA Tech. Rep. Ser. No. **12**, 27 (1962).
27. J. Chernick, *Reactor Techn.* **13**, 368 (1971).
28. P. F. Zweifel, *Reactor Physics*, McGraw-Hill, New York (1973), p. 166.

## PROBLEMS

10-1  Determine the ratio of neutron mfp to lattice dimension (e.g., fuel-pin diameter or lattice pitch) in LWR, HTGR, and LMFBR cores for both fast and thermal neutrons. Also compare the ratio of core size to migration length in these reactors.

10-2  Derive an expression for the thermal utilization of a three-region lattice cell (including fuel, clad, and moderator) in terms of thermal disadvantage factors. Also derive an expression for the cell-averaged group constants characterizing this cell in terms of the appropriate disadvantage factors.

10-3  Show that the diffusion length characterizing a heterogeneous lattice cell can be written approximately as $L^2 \sim L_M^2(1-f)$, where $f$ is the thermal utilization for the cell. Does the nonleakage probability $P_{TNL}$ characterizing a bare, uniform core increase or decrease when going from a homogeneous to a heterogeneous lattice?

10-4  Calculate the disadvantage factor $\zeta$ characterizing a two-region slab geometry consisting of a fuel region of width $2a$, surrounded by moderating regions of width $b$. Use one-speed diffusion theory. (See Figure 10-17.)
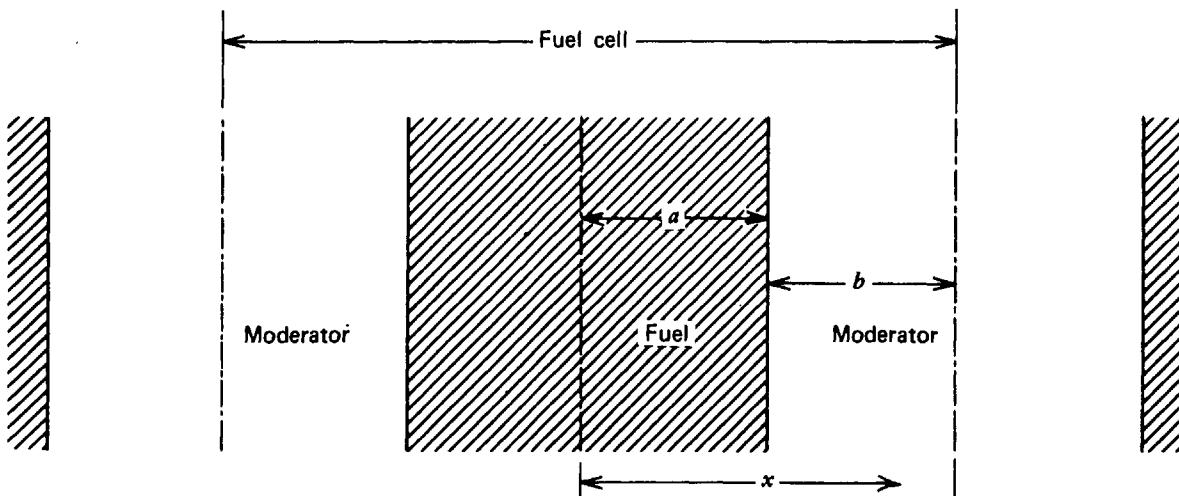


**FIGURE 10-17.  A two-region slab fuel cell.**

10-5 Calculate the self-shielding factor for the lattice cell of Figure 10-17. (Assume that one-speed diffusion theory is valid.)

10-6 Calculate the effective absorption cross section characterizing the cell of Figure 10-17 using the definition given by Eq. (10-28). Compare this with the cell-averaged absorption cross section calculated using the disadvantage factor or the self-shielding factor.

10-7 Derive the following formulas for the radius of the equivalent unit cell in terms of the *lattice pitch p* (i.e., the distance between fuel pin centerlines in the lattice):
(a) $r = 0.564\,p$, square lattice
(b) $r = 0.525\,p$, hexagonal lattice.

10-8 Prove that the Green's function characterizing a lattice cell has the property $G(\mathbf{r},\mathbf{r}') = G(\mathbf{r}',\mathbf{r})$ when described by one-speed diffusion theory.

10-9 Repeat Problem 10-8 for the case when $G(\mathbf{r},\mathbf{r}')$ is described by one-speed, isotropic scattering transport theory.

10-10 Using the symmetry of the Green's function $G(\mathbf{r},\mathbf{r}')$ for the cell, prove the reciprocity relation:

$$V_F \Sigma_a^F P_{FM} = V_M \Sigma_a^M P_{MF}.$$

10-11 Explain the physical difference between the absorption probability $P_{FM}$, the escape probability $P_F$, and the first-flight escape probability $P_{FO}$.

10-12 Calculate the absorption probability $P_{FM}$ for the simple slab cell of Figure 10-17. Use one-speed diffusion theory.

10-13 Calculate the escape probability $P_F$ for the slab cell of Figure 10-17 using one-speed diffusion theory.

10-14 Calculate the first-flight collision probability $P_{FO}$ for the cell of Figure 10-17.

10-15 Demonstrate that the average chord length characterizing a non-reentrant geometry volume is given by

$$\langle R \rangle = 4V/S.$$

(The reader might find it useful to refer to Case, de Hoffmann, and Placzek[10] or Meghreblian and Holmes[25] or Bell and Glasstone.[21])

10-16 Demonstrate that the first-flight escape probability for a non-reentrant volume can be written generally as

$$P_{FO} = \frac{1}{\langle R \rangle_F \Sigma_t^F} \int_{R_{min}}^{R_{max}} dR \,(1 - \exp - \Sigma_t^F R)\varphi(R),$$

where $R_{max}$ and $R_{min}$ are the maximum and minimum chord lengths of the volume and $\varphi(R)$ is the chord length distribution function such that $\varphi(R)dR$ is the probability that a chord length lies between $R$ and $R + dR$.[10,21,25]

10-17 Using the result of Problem 10-16 demonstrate that the first-flight escape probability characterizing a large lump is given by $P_{FO} = S/4V\Sigma_t^F$.

10-18 Derive an expression for the cell-averaged macroscopic absorption cross section $\langle \Sigma_a \rangle_{cell}$ characterizing a *three*-region fuel cell in terms of thermal disadvantage factors. Describe qualitatively how you might calculate these disadvantage factors.[5]

10-19 Find the escape probability for a slab of half-thickness $a$ and scattering and absorption cross sections $\Sigma_s$ and $\Sigma_a$ using one-speed diffusion theory.

10-20 Verify the ABH expression for $[1/f - 1]$ as given by Eq. (10-57) by solving the diffusion problem [Eq. (10-53)] to obtain $P_{MF}$.

10-21 Using the ABH method, compute the thermal utilization for one of the PWR core designs given in Appendix H assuming 2.8% enrichment fuel and a water density of $\rho_{H_2O} = 0.71$ g/cm$^3$. Also determine the thermal disadvantage factor for this lattice. (Use the thermal cross section data in Appendix A.)

10-22 Derive the integral form of the transport equation (10-60). [Hint: Follow the analysis of Section 4-IV-B.]

10-23 Prove the identity Eq. (10-65) relating the transfer coefficients $T_{mn}$ and the first-flight escape probabilities $P_{m \to n}$.

10-24 Prove that the first-flight escape probabilities satisfy the reciprocity relation:

$$V_F \Sigma_t^F (E) P_{FO}(E) = V_M \Sigma_t^M (E) P_{MO}(E).$$

10-24 Derive the expression (10-97) for the Doppler-broadened NR resonance integral.

10-25 Derive the expression (10-101) for the NRIM form of the resonance integral.

10-26 An improved rational approximation[28] is given by

$$P_{FO} = \frac{10 + 5 \langle R \rangle_F \Sigma_t^F + 5 (\langle R \rangle_F \Sigma_t^F)^2}{10 + 14 \langle R \rangle_F \Sigma_t^F + 5 (\langle R \rangle_F \Sigma_t^F)^2 + 5 (\langle R \rangle_F \Sigma_t^F)^3}.$$

Graphically compare this to the Wigner rational approximation for $\langle R \rangle_F \Sigma_t^F$ ranging from 0.1 to 10.0.

The following study (Problems 10-27–32) of a water-moderated reactor lattice will require the use of a MUFT-type fast-spectrum code and a SOFOCATE-type thermal spectrum code. The objective of these problems is to investigate the effects of enrichment, moderator-to-fuel ratio $(N_M / N_F)$, moderator temperature, and fuel temperature on the infinite lattice multiplication characteristics of a typical PWR core design. Use the core data for one of the PWR designs given in Appendix H.

10-27 Determine volume fractions of $H_2O$, $UO_2$, and Zr.

10-28 Calculate the thermal spectrum and spectrum-averaged 2-group constants for the reactor at zero power and operating temperature. Plot and compare with a Maxwellian distribution in pure water at 300°C.

10-29 Calculate the fast spectrum and spectrum-averaged group constants for the same conditions.

10-30 Determine the following parameters for the uncontrolled core: $k_\infty, p, p^{28}, \epsilon, f, \eta, \tau, L^2$, and CR (conversion ratio).

10-31 Estimate the concentration of boron in the coolant necessary for $k_\infty = 1$. Recalculate the thermal spectrum and compare with the spectrum for the zero boron concentration lattice.

10-32 Reevaluate the parameters in Problem 10-30 for the lattice containing the critical boron concentration.

# 4

# An Introduction to Nuclear Reactor Core Design

# 11

## General Aspects of Nuclear Reactor Core Design

The primary responsibility for the nuclear design of a reactor core rests with the nuclear engineer. He must determine that set of system parameters which will yield safe, reliable, and economical reactor operation at the rated power level over the desired core lifetime. The principal tools used by the nuclear engineer in this task consist of a number of models of neutron behavior in the reactor that are implemented by a multiplicity of computer programs or *codes* used to simulate the nuclear behavior of the reactor core. The nuclear analysis of the core cannot be performed in an independent manner (as we have developed it thus far in this text), but rather it must interact strongly with other aspects of core design, including thermal-hydraulic analysis of core cooling, structural analysis of core components, economic performance, and so on. Such "nonnuclear" design considerations will place a number of constraints on the nuclear design of the core. For example, the core size and geometry will usually be determined by thermal considerations, since one must insure that core power densities are sufficiently low to prevent temperatures in the core from becoming excessively high. As yet another example, the length of time that a fuel element can be utilized in a reactor core is usually determined not by the depletion of fissile material, but rather by the ability of the fuel element to withstand the radiation damage and thermal and mechanical stresses experienced in the reactor core environment.

The nuclear analysis of a given core configuration must be performed many times during the core design. Rather crude models are used initially to identify the major constraints that will be placed on the design. Usually in these preliminary design studies, one draws heavily on past design experience. Such studies are used to identify the range over which system parameters can be varied while still conforming to the constraints placed on core performance. Throughout this analy-

447

sis, the nuclear engineer will interact strongly with other design efforts, particularly with the thermal-hydraulic analysis.

As more information is accumulated, the design effort advances to increasingly detailed studies in an effort to narrow in on a reference design with which one can perform tradeoff studies in order to determine the best choice of system parameters to achieve the optimum core performance consistent with design constraints. Naturally during these latter stages of the design process the analytical models used to predict core behavior become more detailed (and much more expensive to apply).

It is convenient to separate the various aspects of nuclear reactor core design into several general areas including nuclear design, thermal–hydraulic design, structural and materials design, and, of course, economic and reliability (safety) evaluations of core performance. Although our primary concern is with the nuclear analysis and design of the core, it is important to present this topic within the more general framework of nuclear reactor core design to illustrate the strong interplay between the various aspects of the design procedure.

Of course, the specific details of core design will depend strongly on the reactor type under consideration (as well as past experience of the designer). More specific information concerning core design can be obtained from a number of sources, including several advanced monographs.[1–5] Although the specific details of many aspects of core design are regarded as proprietary information by reactor manufacturers, many of the general features of such design methods are available in a number of reports. An additional source of information is contained in the safety analysis reports (PSAR's or FSAR's) required of every nuclear power plant licensed in the United States.[6]

Our discussion here is of a much more introductory nature, with the primary intent of providing an appropriate atmosphere for illustrating how the fundamental concepts and models developed in the earlier portions of this text are applied in practice to nuclear reactor design. We first give a brief overview of the specific design problems faced by the nuclear engineer, then briefly consider how these problems are constrained by other facets of the nuclear core design, and finally, provide an overview of reactor calculational models usually implemented in the form of computer code packages capable of performing a variety of calculations of interest in reactor design.

## I. NUCLEAR CORE ANALYSIS

### A. Design Functions of the Nuclear Engineer

Since our primary concern is with the nuclear analysis of a reactor core, we will begin with a brief discussion of the principal design activities of the nuclear engineer, which can be conveniently grouped into three general areas:

#### 1. DETERMINATION OF CORE CRITICALITY AND POWER DISTRIBUTIONS

The calculation of the core multiplication and flux or power distribution is, of course, the most common type of analysis performed in nuclear core studies. [This explains our preoccupation with this subject during the earlier chapters of this text.] The nuclear engineer is concerned with the determination of the core power

distribution since it is of central importance to both the corresponding thermal analysis and fuel depletion studies of the core. For example, one would like to design a core that will result in a flat radial and axial power distribution throughout core life and also provide sufficient reactivity to yield adequate fuel burnups while maintaining adequate reactor control. The calculation of core power distributions will depend sensitively on parameters such as core enrichment, moderator-to-fuel ratio, core geometry, the location and types of reactivity control, and fuel element design. The core power density will also depend on both space and time (because of fuel burnup and isotope production over core life).

We will later find that the parameters of greatest interest to the core thermal designer are the ratios of the peak-to-average power densities in the core (so-called "hot channel" or "power peaking" factors) which, along with the axial core power profile, allow the determination of whether the thermal limitations on core performance will be exceeded by a given core design. We will also find that there is a strong feedback from the thermal core analysis. since the core temperature will strongly affect coolant density and resonance absorption, which, in turn, will affect reactivity.

The nuclear designer must also determine the fuel loading which will guarantee reactor criticality over the desired core lifetime. This requires compensating for fuel depletion as well as reactivity effects due to both temperature feedback and fission product buildup. At this point various details of the fuel design enter, such as the moderator-to-fuel ratio, the fuel element dimensions and configuration, and enrichment.

## 2. REACTIVITY AND CONTROL ANALYSIS

An analysis must be performed to determine the amount of negative reactivity or control required to compensate for the excess reactivity contained in the initial fuel loading as well as to allow for flexible and safe reactor operation. One must allocate this reactivity among several different control mechanisms, including movable control rods, soluble neutron poisons in the coolant ("chemical shim"), and neutron poisons that burn out over core life ("burnable poisons" or "mechanical shim"). It is important to study the interaction of such control elements with the nuclear behavior of the core, both in static and dynamic situations. Such calculations are necessary to perform the detailed design of individual control elements, as well as control rod patterns and withdrawal and insertion sequences during reactor operation (rod "programming").

One must also study the inherent reactivity changes that will occur in the core with power and temperature changes by calculating the various reactivity feedback coefficients that determine the short-time kinetic behavior of the core. Of particular concern are the reactivity coefficients characterizing coolant or moderator density and temperature changes, and the temperature coefficient of reactivity for the fuel (primarily determined by the Doppler effect).

There will also be longer term reactivity effects such as those due to the buildup of fission product poisons which must be studied.

## 3. DEPLETION ANALYSIS

During reactor operation the fuel composition will change as fissile isotopes are consumed and fission products are produced. The nuclear designer must monitor these processes over core life in an effort to ascertain fuel composition and

reactivity as a function of energy removal. This requires studying the depletion and production chains for the principal isotopes (e.g., $^{235}U-^{238}U$ or $^{233}U-^{232}Th$) coupled with the equations determining the neutron flux in the core. The calculation of the core multiplication and power distribution must be made many times over the operating lifetime of the core as the core composition changes. The study of the interaction of the core power distribution with the time-dependent production or depletion of nuclei in the core is known as *depletion* or *burnup analysis*. It is perhaps the most time-consuming and expensive aspect of nuclear reactor analysis—and also perhaps the most important (aside from reactor safety analysis), since it will indicate the economic performance of the nuclear reactor. Depletion analysis is closely related to the topic of nuclear fuel management in which one tries to optimize the fuel loading, arrangement, and reloading in order to achieve the most economical power generation within the design constraints (e.g., safety margins) placed on reactor operation.

From this discussion it is apparent that the responsibilities of the nuclear designer are quite varied and numerous. He must establish the limitations on and determine the values of the fuel-to-moderator volume ratio, the fuel rod diameter, and the fuel element arrangement. The fuel loading requirement must then be determined, taking into account temperature and power reactivity defects, fuel depletion, and fission product buildup. Control requirements must next be established, including reactivity requirements, control rod geometry and patterns, and the possible use of chemical shim and burnable poisons. The fuel distribution and refueling arrangement must then be studied in order to achieve economic fuel management within the constraints imposed by safe reactor operation. The kinetic characteristics of the reactor must be determined for safety analyses of core operation, including the various reactivity coefficients that arise, fission product poisoning, and the analyses of various hypothetical accidents.

All of these design functions rely on the basic theory of nuclear chain reactions that we have developed in the preceding chapters. However because of the accuracy and detail of the information required for actual reactor design, rather sophisticated applications of this theory are necessitated, which, in turn, require the extensive use of modern digital computers.

## B. Models of Core Nuclear Behavior

As we have mentioned, modern nuclear reactor design depends heavily on various mathematical models of the nuclear fission chain reaction applied to core analysis using digital computers. The computer programs or "codes" that represent these mathematical simulations of the reactor core are generally quite complex and are frequently the result of many years of extensive development and testing at the various nuclear laboratories in this country and abroad.[8] More recently, such codes have become the subject of various proprietary restrictions, and while their general features are usually common knowledge, the details of the codes used in present-day reactor design are classified as proprietary information by the reactor manufacturers. Hence our discussion here must be of a general nature. One can generally group such codes into one of four different types.

### 1. CROSS SECTION LIBRARY PROCESSING CODES

We noted in Chapter 2 that the basic source of nuclear cross section data for nuclear design in this country is the ENDF/B file, which contains data compiled and evaluated from all known cross section information. The amount of such data

requires that it be stored on magnetic tape and manipulated using complex data handling codes.[7] Such codes not only select the cross section data of interest and prepare them in a form suitable for input to reactor design codes, but also interpolate existing data to fill any gaps which may exist, as well as apply various theoretical models (such as the optical model of nuclear structure) to generate cross section data in those regimes in which no existing data exist. These library codes also generate differential scattering cross sections, resonance integrals, and thermal energy scattering kernels.

The differential scattering cross sections for elastic scattering are usually generated as a sequence of terms in a Legendre polynomial expansion. By way of contrast, inelastic scattering and $(n,2n)$ processes are usually assumed to be isotropic in the laboratory system and calculated using available data on the appropriate nuclear states or a theoretical model of the nucleus.

One of the more difficult aspects of cross section generation concerns the treatment of resonance cross sections. Because such resonances are usually quite large in magnitude and yet quite narrow compared to even the energy intervals characterizing the cross section data, it is necessary to make some attempt to account for flux depression in the resonances in order to include effective resonance integrals in the cross section data set. In the regime in which the resonances are isolated and measured, this can be accomplished using the standard techniques (e.g., the NR or NRIM approximations). Various nuclear models can be used to generate resonance parameters for the energy range in which the resonances are still isolated but not measured. The most difficult area to treat is the energy range in which the resonances are not only unresolved but overlap so appreciably that they cannot be considered independently. It is also usually necessary to account for heterogeneous effects (see Chapter 10), temperature effects on the resonance structure, and overlap of resonances of different materials.

## 2. MULTIGROUP CONSTANT (MGC) GENERATION CODES

As we have seen, the energy range spanned by the neutrons as they are born in fission and slow down to eventual capture or leakage at thermal energies (at least in thermal reactors) is enormous, covering some eight orders of magnitude. Since the cross sections themselves depend sensitively on energy, it is apparent that one must proceed rather carefully in generating few-group constants for use in multigroup diffusion calculations.

One usually proceeds in two steps. The energy range of interest is first divided up into a very fine multigroup structure, and the cross section data supplied by a library code are simply averaged over these groups (for example, in the slowing down range one might use a $1/E$ spectrum). Appropriate approximations to the effective resonance integrals of interest are also included in this set of "fine-group constants." These fine-group constants then serve as the microscopic cross section data used in fast and thermal spectrum codes that perform an approximate calculation of the neutron energy-dependence for the nuclear assembly of interest, and then average or collapse the fine-group constants into few-group constants over these approximate spectra. It should be noted that whereas fine-group constants are usually evaluated without reference to the detailed system under consideration, the spectrum generation codes generate few group MGC for the specific system of interest. These MGC are then used in static and kinetic design analysis.

Of course, the trick enabling one to perform a detailed study of the neutron energy spectrum is the temporary neglect of the detailed spatial dependence of the

neutron flux. It is customary to assume a simple single mode flux shape—that is, to assume a buckling that characterizes the region of the core under consideration. The angular flux dependence is simplified using either the $P_1$ or $B_1$ approximation (although sometimes higher order $B_N$ methods may be used).

However the success of MGC generation codes frequently depends on how these codes are corrected for the rather strong spatial dependence of the flux that occurs in the vicinity of the fuel rod or control rod. We have already examined several methods for correcting cross section group constants for these heterogeneous effects, such as disadvantage factors and collision probabilities. In the fast region, it is usually sufficient to merely correct the calculation of the resonance integrals for self-shielding effects using escape probabilities calculated for the cell geometry of interest. In the thermal range, one may use either approximate techniques such as the ABH method to determine disadvantage factors, or more elaborate cell-calculation techniques such as THERMOS[9] to directly calculate the self-shielded cross sections.

We have seen that these MGC are usually then spatially averaged over the fuel cell or perhaps a fuel assembly in order to generate "homogenized" cross sections most consistent with the spatial mesh to be used in the few-group multigroup diffusion calculation.

We have already referred to the various common schemes to generate few-group constants for LWRs–namely, MUFT–GAM-[10] type calculations for the fast spectrum, and SOFOCATE[11] or TEMPEST-[12]type calculations for the thermal spectrum, including perhaps a THERMOS calculation for cell analysis. The corresponding types of code for HTGRs include GAM[13] or MICROX[14] for the fast-group constants and GATHER[5] for thermal-group constants. The group structure necessary for fast reactor analysis must be considerably more detailed, and ultrafine group structures such as those employed in $MC^2$ are used to generate MGC for fast assembly analysis.

## 3. STATIC DESIGN CODES

Static design codes are used to obtain the global spatial dependence of the neutron flux throughout the reactor core. This information is required for accurate predictions of the fuel loading, power distributions, temperature dependence of reactivity, excess reactivity, shutdown margins, shielding requirements, and other quantities. These codes are usually few-group diffusion or transport codes that utilize the MGC generated by the spectrum codes discussed in the previous section. One customarily uses such codes to determine the multiplication factor (eigenvalue) and flux distribution in the system of interest. Usually multidimensional diffusion codes are sufficient for this task. However occasionally transport codes are necessary to determine cell-correction factors in the vicinity of strong absorbers or voids.

Indeed before a diffusion theory calculation can be performed the heterogeneities in the core must be homogenized. Although MGC generation codes augmented with prescriptions such as those provided by the ABH method usually provide sufficient accuracy for this purpose, it is occasionally necessary to use a transport code such as ANISN[15] or TWOTRAN[16]. With such corrections, multigroup diffusion codes are usually adequate for a wide class of problems, including the determination of the over-all flux and power distribution, the effects of fuel zoning, reactivity predictions, and so on.

Such codes can also be used to calculate temperature and power coefficients of reactivity. This is usually performed by merely calculating the core multiplication for several different core temperatures or power levels (using different MGC for each temperature, of course).

## 4. TIME-DEPENDENT DESIGN CODES

The fourth class of codes attempt to explicitly treat the time dependence of the nuclear behavior of the core. Of course by including this additional variable, one is usually forced to utilize a coarser description of the remaining variables–for example, space and energy. Such codes can themselves be broken into three separate classifications:

### (a.) *DEPLETION CODES*

In a depletion calculation, one is concerned with monitoring the core composition and flux distribution in the reactor over the core life. In particular one must take into account the time- and space-dependence of fissile material depletion, the transmutation of fertile to fissile material, fission product buildup, and the adjustment of control elements to maintain core criticality. Depletion codes involve the solution of the rate equations describing isotope concentrations, as well as the neutron balance equations describing core criticality. Because of the many variables involved, such as power density, reload frequency, excess reactivity requirements, and varying reload patterns, even the simplest depletion problem may require solutions at many points in time.

Because of their low computer cost and general flexibility, extensive use is made of zero-dimensional depletion codes for survey calculations. However, more detailed analyses will require the use of one- or two-dimensional depletion codes in order to account for the spatial flux variation and control-rod and reload patterns.

### (b.) *FUEL CYCLE ANALYSIS*

One of the major applications of fuel depletion codes is to the analysis of fuel cycle strategy—that is, a determination of the optimum fuel reloading strategy for minimizing the fuel cycle costs. Such estimates of initial core composition and reload fuel composition must take into account the requirements for heat removal, coolant pumping power, peak fuel temperatures, and so on, and hence are invariably a compromise between that core composition entailing the lowest fuel cycle cost and that composition resulting in acceptable system temperatures.

### (c.) *REACTOR KINETICS ANALYSIS*

In order to analyze the transient response of the reactor to both normal operating conditions and postulated accident situations, one must utilize codes based on the nuclear reactor kinetics equations discussed in Chapter 6. Such calculations differ dramatically from depletion calculations in two respects: (a) the time scale of reactor transient behavior is usually of the order of minutes or less, whereas depletion calculations are concerned with core behavior over times as long as several years and (b) in kinetics calculations, the reactor is usually subject to a nonzero net reactivity (due to control, operating conditions, etc.). In a depletion calculation, one always assumes that control is adjusted to hold the core critical at all times. Hence, in a depletion calculation, one is actually only concerned with the steady-state equations describing the neutronics.

Reactor kinetics analysis plays an important role in core design, since it is necessary to assess safety margins, to select and place control and safety instrumentation, to design the control and protective systems, and to determine the need and effectiveness of engineered safeguards.

Of course at the heart of such codes is a numerical solution of the reactor kinetics equations describing the neutron flux time behavior in the core. However one must also account for coolant flow and heat transfer in order to determine feedback reactivity. In addition, there is strong coupling to other dynamic processes in the NSSS, such as the primary coolant loop, steam generator, coolant pumps, and feedwater system. Hence the study of reactor dynamics can become quite complicated.

As input to such codes one requires not only basic nuclear data, such as cross sections, temperature coefficients, and so on, but thermal-hydraulic information as well. These latter quantities are frequently determined using static design codes.

The simplest level of description would be the use of point-reactor kinetics to describe the core neutronics. However, in many instances the spatial dependence of the flux is important, and then either time-dependent multigroup diffusion codes or hybrid schemes such as synthesis must be utilized for an adequate description.

## II. OTHER AREAS OF REACTOR CORE ANALYSIS

We have outlined the various types of calculation required in the nuclear analysis and design of a reactor core. These include the calculation of core criticality and power distributions, the determination of reactivity coefficients, fuel loading requirements and core arrangement, reactivity control calculations, fuel depletion studies, and reactor safety analysis. There are numerous constraints imposed on such nuclear design. Of course the core composition and configuration must be chosen such that sufficient excess reactivity is available for power generation over a reasonable time period (usually on the time scale of years). The reactivity control must be capable of ensuring the safe and reliable operation of the reactor over core life. And these requirements must be met while at the same time minimizing the economic cost of the power generation. These constraints are frequently in conflict with one another. For example, there is incentive to operate the reactor at the largest possible power density consistent with maintaining fuel and coolant temperatures below limits set by safety considerations. Yet such a high power density frequently does not lead to the optimum economic power generation over the entire core life, since the flux and hence power distribution will shift as the fuel is depleted.

The nuclear analysis and design of the core cannot be decoupled from other considerations such as the thermal behavior of the core or the behavior of the various materials that comprise the core. This can perhaps be understood more clearly by briefly describing the other types of analysis that arise in reactor core design.

### A. Thermal Core Analysis

The energy released in nuclear fission appears as kinetic energy of fission reaction products and eventually as heat generated in the reactor fuel elements. This heat must be removed from the reactor core and used to generate electrical

power. The study of the sequence of processes involved in the transport and utilization of fission heat energy is most properly the concern of the mechanical engineer. However since it has such a significant bearing on the nuclear design of the core, we will devote a considerable portion of Chapter 12 to a summary of the thermal analysis of nuclear reactor cores.

The primary objectives of thermal core design include achieving a high power density (to minimize core size), a high specific power (to minimize fuel inventory), and high coolant exit temperatures (to maximize thermodynamic efficiency). However these objectives are subject to several important constraints. For example, one must always ensure that the core temperatures remain below the melting points of core components (particularly for the fuel and the clad). There are also frequently limits on heat transfer rate between the fuel element and the coolant, since if this heat transfer rate becomes too large, film boiling of liquid coolants may occur which will result in a rapid rise in clad temperatures. Hydraulic considerations also enter. For example, the coolant pressure drop across the core must be kept low to minimize pumping requirements as well as hydraulic stresses on core components.

Such thermal–hydraulic constraints must be studied over core life, since as the power distribution in the core changes due to fuel burnup or core reloading, the temperature distribution will similarly change. Furthermore since the cross sections governing the neutronics of the core are strongly temperature- and density-dependent, there will be a strong coupling between the thermal–hydraulic and neutronic behavior of the reactor core. We will see in Chapter 12 that this coupling has a strong influence on the manner in which reactor criticality calculations must be performed.

## B. Mechanical Analysis of Reactor Cores

It is of vital importance to choose materials and design core components capable of withstanding the environment of intense radiation, high pressure, and high temperature of a nuclear reactor core. Of central concern is the structural design of fuel elements subject to rather severe mechanical stresses. For example, as the fuel produces energy via fission reactions, it will also produce fission product gases (roughly 27 atoms of such gases will be produced per 100 atoms fissioned).[17] These gases will diffuse through the fuel pin and into the fuel-clad gap, where they will accumulate, producing rather sizable pressures on the inner clad surface. Typically an attempt is made to keep these pressures below the design coolant pressures. However the internal fuel element gas pressure must not become too low, or else the clad may fail due to the outside coolant pressure (for example, should a gap appear between two fuel pellets). The fission events occurring in the fuel will also cause considerable swelling of the fuel pellets, which places additional internal stresses on the clad. There are other stresses on the fuel element, such as those from the external coolant pressure. The enormous thermal gradients across the fuel pin and clad, as well as the temperature changes (thermal cycling) accompanying changes in reactor power level, render the mechanical design[18] of the fuel element even more difficult, as do a number of other considerations involving radiation damage. These factors are discussed below.

The mechanical design of other core components must also be considered in core design. For example, the various internal structure required to support the fuel, flow baffles, and control rod assemblies must be designed to withstand the intense

core environment. And of course the reactor pressure vessel itself represents a formidable mechanical design problem, since it must withstand extremely high pressures and radiation intensity over the operating lifetime of the reactor (~30 years). One must keep in mind throughout the fabrication costs and maintenance of the mechanical assemblies in the core (with particular attention to movement of control rod assemblies and refueling operations).

## C. Materials Problems in Reactor Core Design

As we mentioned above, the environment of a nuclear reactor core is characterized by very high pressures, large thermal gradients, and intense nuclear radiation, which place very stringent demands on the materials comprising core components. The behavior of materials subjected to large mechanical and thermal stresses is not a new area of investigation (except possibly to the extremes encountered in modern reactor design), and a great deal is known about the fabrication of high-strength alloys and ceramics which can withstand these stresses. However the nuclear reactor core subjects materials to an additional demand, that posed by the intensive bombardment by nuclear radiation to which materials in the core are exposed. Over a period of time, such radiation can dramatically alter the properties of these materials.[19] For example metals will become brittle and swell and corrosion is enhanced. The reactor engineer must be very careful to anticipate such radiation damage in his design, as well as to adopt a sufficiently conservative design to compensate for the lack of experience available with the behavior of materials under very high irradiation fluences.

These effects of radiation on reactor materials have become particularly important in today's maturing nuclear reactor industry. In order to achieve the lowest possible power costs, nuclear fuel elements must be used in a reactor as long as possible (i.e., high burnup). Actually the principal limitation on the amount of burnup is not the loss of $^{235}U$ or $^{239}Pu$ nuclei through fission, but rather the attendant radiation damage to the fuel and the cladding material, which would lead to fuel element failure if the fuel is left in the core too long.[20] Hence whereas nuclear reactors were limited by nuclear considerations during the 1950s, and by thermal design during the 1960s, today's modern power reactors are primarily limited by the radiation damage which can be withstood by reactor materials.

This situation becomes even more difficult in fast-breeder reactors because of the intensity of fast neutron radiation. It has been found that stainless steel (a major structural component of the fast breeder) swells rather dramatically (several percent) when irradiated over long periods of time by fast neutrons.[21] Such swelling must be accounted for in the mechanical design of the fast reactor core (with a considerable associated economic penalty).

We have seen that there are several types of high-energy radiation present in a nuclear reactor core. Most of these result from the nuclear fission reaction itself, although lesser amounts arise from associated reactions such as radiative neutron capture. Of course, most fission energy is carried by the massive fission-fragment nuclei. These cause catastrophic damage to the adjacent fuel material, but because of their large electrical charge, the range of the fission fragments is extremely short ($<20\mu m$); and hence this damage is localized in the fuel within the immediate vicinity of the fission event. A potentially more serious type of radiation is that due to fast neutrons. Because of their neutrality, neutrons have rather long ranges (as

much as several meters). Hence they can damage material located anywhere in the reactor core. Gamma radiation is also characterized by large ranges, but is of secondary importance to fast neutron damage.

The actual effect of radiation on a material depends sensitively on the type of material, the type of radiation, and the conditions during the time of irradiation (such as temperature). However some general observations can be made. For example, for irradiated metals, hardness, tensile strength, and impact resistance increase, while ductility decreases (corresponding to an increase in brittleness).

The significance of radiation damage in reactor core design becomes particularly apparent when one examines nuclear fuel performance in the LWR. As we will see, the low cost of nuclear fuel (relative to fossil fuel) is the principal factor that leads to the economic advantages of nuclear power. That such costs are realizable is due in no small measure to the significant advances made in nuclear fuel design and performance since the mid-1960s. Nuclear fuel elements must be designed subject to several criteria[22] intended to guarantee the fuel performance up to the lifetime limit: (a) the fuel temperature at the hottest point always must be below the melting point, (b) any fuel displacement that might influence core temperature distribution and multiplication must be minimized, (c) the cladding must remain leak-proof, and (d) the outer geometry of the fuel pin (length, diameter, straightness) is subject to very small tolerances.

As we have seen, nuclear fuel elements are subjected to intensive irradiation. They are furthermore subject to extremely large temperature variations. This is caused to a large degree by the rather poor ability of the principal types of nuclear fuel, uranium oxide or carbide, to conduct heat. Such temperature variations place enormous thermal stresses on the fuel elements and interact strongly with the changes in the fuel induced by irradiation.

The principal radiation effects that must be accounted for in fuel element design include:[22] (a) fuel creep and swelling, fission gas release, pore migration, chemical changes, and change in radiation and axial fuel density profile, (b) cladding mechanical properties, swelling by void formation, and corrosion, (c) fuel pin radial heat transfer and temperature distribution, mechanical and chemical interaction between fuel and cladding, swelling and bowing of the pin, and (d) fuel bundle changes in component geometry and interaction of fuel pins and spacers.

Such considerations have led to a number of modifications in fuel element designs for modern power reactors. Current designs provide for increased void volume to accommodate fuel swelling and fission gas release associated with the higher burnups used in present-day power reactors. The excellent corrosion resistance of zirconium and stainless steel alloys has led to their almost exclusive use as a cladding material. As the nuclear power industry obtains more operating experience with fuel design and behavior under long-term irradiation, it will be more able to develop advanced designs capable of very high burnups and power densities.

The commercial success of the LMFBR will also be critically dependent on the attainment of low fuel cycle costs and therefore on the ability to run fuel elements to very high burnups. Only rather recently has any appreciable experience in the behavior of materials in high fast neutron flux environments been available. Perhaps the most dramatic effect thus far observed occurs in structural materials such as stainless steel. After long periods of irradiation by fast neutrons, the steel is observed to swell. Closer examination indicates the presence of small voids in the

irradiated material. Of course such swelling and void formation are highly undesirable in a reactor core in which mechanical and structural tolerances must be kept very refined over the lifetime of the core (up to 30 years).

The voids are caused by fast neutrons that rip through the crystal lattice, knocking atoms out of their lattice positions. These vacancies tend to migrate together to form voids and hence induce the swelling. By raising the steel to high temperatures the voids can be annealed out. Unfortunately at the anticipated operating temperatures of the LMFBR such swelling can be quite pronounced and must be accounted for in core design.

## D. Economic Analysis[23-25]

The justification for nuclear power plants must reside in their economic advantages over more conventional sources of electrical power. The cost of electrical power can be broken down into a number of factors, including the capital cost of constructing the plant, the annual cost of operating and maintaining the plant, and the annual costs for fuel. The capital investment required for the construction of nuclear power plants is usually greater than that required for conventional power plants. Furthermore, operating and maintenance costs account for only a small fraction of the total cost of producing electricity. Hence the primary advantage enjoyed by nuclear power is in the lower cost of its fuel.

It is important to recognize that nuclear fuels are totally different from fossil fuels, both in their processing and utilization, as well as in their costs. There are a large number of sophisticated and expensive processing operations required by the fuel before it is inserted into the reactor core. It is then "burned" in the reactor for several years before being removed. Even after several years of use in a reactor, the fuel possesses a sizable concentration of fissile material. Hence it must be removed from the core, reprocessed, and refabricated into new fuel elements. The byproduct waste from the reprocessed fuel is highly radioactive and must be disposed of with considerable care.

Those operations involved in the extraction, preparation, utilization, reprocessing and disposing of nuclear fuels are referred to as the *nuclear fuel cycle*. Such a cycle extends over a period of several years, and the costs associated with the nuclear fuel cycle must be monitored over this period of time. In this sense, nuclear fuel costs are much different than fossil-fuel costs, since a number of charges other than direct materials costs are involved which may either lead or lag utilization of the fuel material by several years. The primary costs associated with the nuclear fuel cycle include the following:

(1) Costs of net isotope consumption that result from the conversion of uranium and plutonium into fission products and from the reduction in the $^{235}$U-enrichment of the uranium remaining in the spent fuel. These costs are associated with the exploration, mining, and enrichment of the uranium.

(2) Processing costs, such as those incurred in uranium purification, conversion, fuel fabrication, and reprocessing.

(3) Financing costs associated with the large working-capital requirements of the nuclear fuel cycle.

The management of the various activities involved in obtaining, irradiating, and disposing of fuel materials is referred to as *nuclear fuel management* and is a principal concern of nuclear engineering.[26] Such activities must be performed

subject to several very important constraints. Of course one desires to minimize electrical generation costs, but must also ensure that the safety of the reactor is not compromised. For instance, the fuel temperature must always be kept below melting points and the control margin must be maintained within safe limits.

Needless to say, the complexity of accounting for nuclear fuel costs and capital plant investment requires a rather sophisticated economics analysis of the plant design. Nuclear power costs will depend on parameters that vary widely, depending on the location of the plant, the type of the reactor, and even the time at which the economic study is performed. Such considerations make it apparent that each reactor manufacturer and utility have access to a technical group capable of predicting the behavior of the nuclear fuel, performing an economic analysis of such fuel utilization and analyzing the total power system requirements involving the plant (including other conventional and nuclear plants in the system).

## E. Safety and Regulatory Considerations[27-29]

Of course, all reactor designs are subjected to extremely thorough studies to ensure that they are compatible with existing safety and regulatory standards. For example, the response of the reactor design to reactivity insertions resulting from severe disturbances that could arise only under the most extreme circumstances must be determined.

The principal safety concern inherent in nuclear reactor operation does not involve the possibility of a nuclear explosion. Such an event is quite impossible in thermal reactors, and it requires an agile mind to concoct a sufficiently fantastic scenario to initiate such an explosion even in a fast reactor. Rather, the problem is the large inventory of radioactive fission products that accumulate in the reactor fuel. As long as these fission products remain in the fuel, they represent no hazard to either plant personnel or nearby population. Yet should they be released and transported to populated areas, substantial dangers could arise.

Hence nuclear reactors must be designed such that under no credible—or even incredible—operating situation could such radioactive material be released from the core. To achieve this guarantee, not only must the reactor core and coolant system be carefully designed against every conceivable accident situation, but auxiliary systems must be incorporated into the core as well—so-called *engineered safeguards*—to ensure that fission products are contained in any foreseeable accident.

The subject of nuclear reactor safety is exceedingly complex, enmeshed in a labyrinth of complex technical, regulatory, political, philosophical, and even emotional issues. We will avoid a detailed discussion of these topics in this section, choosing instead to merely illustrate several of the considerations that arise in reactor safety.

As we have mentioned, the primary concern in nuclear reactor safety analysis is that the large fission product inventory produced in the reactor core is kept intact and not released in any conceivable accident situation. There are several barriers to such fission product release. The primary barrier is the metal clad of the fuel itself, which isolates the fuel pellets from the coolant. Should this clad be ruptured, the pressure vessel containing the reactor core and the coolant will then assume the role of a secondary barrier to fission product release. In the catastrophic event of failure of the primary coolant piping or pressure vessel, the containment structure itself provides yet a third barrier to fission product release.

It is the task of the nuclear reactor designer to dream up possible accident

situations in which one or more of these containment barriers might be breached, and then to design the nuclear reactor system so that if such situations did arise, there would still be no danger to the public. There are essentially three lines of defense against such accident.

First, of course, is the careful attention to design, component fabrication, construction, and plant operation. Such monitoring is referred to as *quality assurance* or *safety assurance* and is of central concern in nuclear power generation. Secondly there are separate safety systems designed to take protective action in the case of abnormal reactor behavior. Examples would include the scram control systems designed to shut the reactor down if abnormal operating conditions are encountered. Finally, nuclear plants are equipped with various engineered safeguards systems to protect against the consequences of highly unlikely but possible catastrophic accidents.
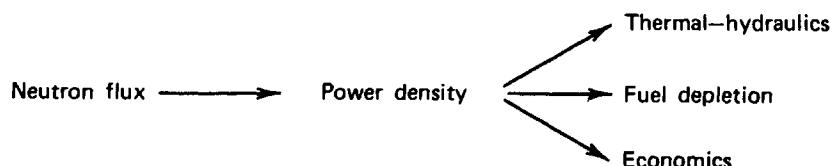
All nuclear reactors possess such engineered safeguards systems to prevent fission product release in the event of an accident. It is extremely important to thoroughly analyze the behavior of the reactor system in the event of an accident situation, not only to determine the appropriate engineered safeguards systems, but also to study the performance and interaction of these systems under postulated accident conditions. However since the particular type of safeguards required depend sensitively on the reactor type under consideration, we will avoid any detailed discussion of nuclear reactor safety systems here.

## III. REACTOR CALCULATION MODELS

As we have repeatedly stressed throughout this text, the complexities of modern nuclear reactor design require that the various theories of nuclear reactor behavior we have been studying be implemented in a form suitable for digital computer calculations. A variety of such computer programs or codes have been developed over the years to assist the engineer in all facets of nuclear reactor analysis.

Frequently, a number of such codes are grouped together into *code packages* which can be applied to a variety of design tasks. Since our primary concern is with the nuclear analysis of a reactor core, we will confine our attention to a general discussion of those code packages which usually comprise the calculational model for describing the nuclear behavior of the core.[30-32]

However, we should bear in mind that the nuclear behavior of the core frequently serves as the input to other aspects of core design. For example, the determination of the neutron flux in the core implies the core power distribution which is necessary for thermal-hydraulic analysis, fuel depletion studies, and the optimization of plant economic parameters:

$$\text{Neutron flux} \longrightarrow \text{Power density} \begin{array}{l} \nearrow \text{Thermal--hydraulics} \\ \longrightarrow \text{Fuel depletion} \\ \searrow \text{Economics} \end{array}$$

There will, of course, be considerable feedback from these latter design functions back to the nuclear analysis. For example, the thermal-hydraulic calculations will

determine both core temperatures and coolant densities essential to the generation of macroscopic group constants. The depletion calculation will determine the isotopic composition of the fuel throughout core life.

Although the details of such nuclear code packages or computer models will vary from one design group to another (or for one application or another), the general features are usually very similar. Of course all aspects of the neutronic analysis of the reactor can be traced back to the neutron transport equation, but as we have repeatedly emphasized, the direct solution of this equation is usually quite intractible. Hence numerous approximations are usually required in order to develop the mathematical models that serve as the basis of reactor design codes. Typically, these codes suppress certain independent variables in order to allow a detailed analysis of the process of interest. For example, multigroup constant generation codes usually suppress spatial dependence—either by assuming an infinite medium or an effective buckling mode—in order to facilitate a detailed treatment of the neutron energy. In a similar sense, static design codes employ a rather coarse multigroup structure in order to allow a detailed study of the spatial dependence of the neutron flux. In time-dependent codes one frequently ignores both spatial and energy dependence.

The proper utilization of such nuclear reactor codes requires not only a thorough knowledge of the various approximations that have entered into the development of the code, but a good deal of common sense, experience, and just plain old-fashioned good luck as well.

In Figure 11-1 we have illustrated the principal components (*code modules*) of a computational model (*code package*) suitable for the nuclear analysis of a reactor core. For purposes of reference we have indicated on this diagram the chapter of this text in which the underlying theory of each module has been developed. However, for completeness, we will review the function of each module here.

The basic structure of the model consists of a module to generate macroscopic group constants, followed by a module to utilize these group constants in a determination of the core multiplication, flux, and power distribution. The power distribution can then be used as the input to a thermal-hydraulics module which solves the equations of heat transfer and fluid flow to determine the temperature and coolant density distribution in the core. Of course, this latter information is required for the generation of macroscopic group constants; hence feedback to the earlier MGC module (and possible iteration) will be necessary.

At this point one has presumably calculated the core multiplication $k_{eff}$ and power distribution, but in general the core will not be critical ($k_{eff} \neq 1$). Hence a control adjustment module is necessary to calculate the degree of control element withdrawal or insertion to return the core to a critical state (again via an iterative process).

When a critical core configuration has been achieved, one passes to a depletion module that uses the resulting flux distribution as input for a solution of the rate equations describing fuel isotope depletion, fertile isotope transmutation, and fission product buildup for a given period of reactor operation. After this depletion step, the new isotopic composition of the fuel is returned to the group-constant module, and the entire calculation is repeated (since the core is now no longer critical).

After a series of depletion steps, the fissile inventory drops sufficiently low that the control system can no longer return the core to criticality. At this point, the
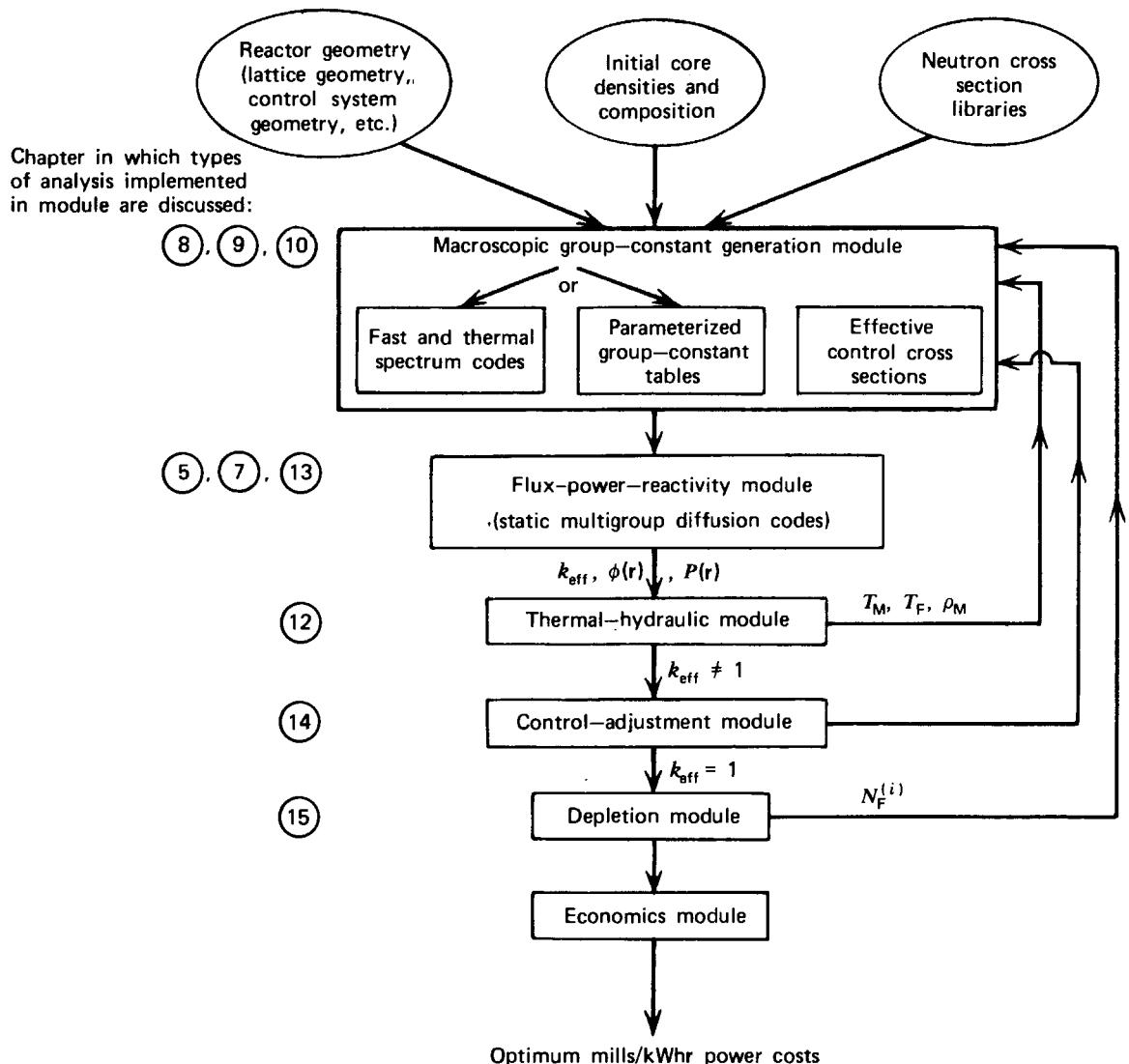
FIGURE 11-1.    Computational model of a nuclear reactor.

useful operating life of the core is deemed to have ended, and one passes on to an economics module that utilizes the total energy produced over the core lifetime and the amount of fissile material consumption (and production) to compute the fuel costs of the operating cycle.

Various different types of input data are needed for this sequence of calculations, including the geometry of the reactor core, lattice, and control system, the initial core loading (composition, etc.), inlet coolant conditions, as well as fundamental cross section data.

A somewhat more detailed description of each of the code modules follows.

## A. Macroscopic Cross Section Module

One of the most important aspects of calculations based on the multigroup treatment of the neutron energy dependence (as is essentially all nuclear design) is the generation of few-group constants. As we have seen, such group constants are formed by averaging the microscopic cross section information obtained from evaluated data sets such as ENDF/B over not only a neutron energy spectrum hopefully characterizing that in the reactor core of interest, but averaging these cross sections as well over the detailed spatial dependence of the flux in a unit fuel

cell in order to account for heterogeneous effects (such as self-shielding). As input, such modules require the number densities characterizing the materials in the fuel cell to be analyzed. The coolant density and average moderator, structure, and fuel temperatures are provided from a thermal-hydraulic module, while the fuel density (as well as fission product densities) are provided by a depletion module. The densities of other materials such as structure are provided by input specifications. The energy-averaged, self-shielded macroscopic group constants are then determined either by performing fast and thermal spectrum calculations for the fuel cell of the specified composition, or by computing a small number of descriptive parameters that can then be used to obtain the macroscopic group constants from suitable tables constructed for the reactor core of interest. (The business of group constant parameterization is a very useful and important topic in depletion calculations because of the large number of times such group constants must be generated over core life. We will return to consider it in greater detail later in Chapter 13.)

Such group constants must be generated for each region of the core in which the composition is different. One must also account for the contributions of fission products such as xenon and samarium and for control absorption which might be present in the cell of interest. As we will see in Chapter 14, the effect of control elements or burnable or soluble poisons in the cell are usually included by generating effective absorption cross sections characterizing the control absorber and then adding these to the absorption group constant characterizing the cell. These effective control cross sections can also frequently be parameterized at considerable computational savings.

## B. Flux-Power-Reactivity Module

At the heart of the neutronics code package is the module that solves the multigroup diffusion equations to determine the flux and power distribution in the core as well as the core multiplication. We have already examined this particular module in some detail in Chapters 5 and 7. In particular, we have studied two different approaches to this calculation: (a) that based on the conventional finite-difference solution of the multigroup diffusion equations and (b) that based on so-called nodal methods which decompose the core into "node cells" and then calculate only the average power or flux for each of these cells. The latter scheme is particularly useful when information is required about the three-dimensional flux distribution in the core, since a direct finite difference solution of the multigroup diffusion equations is extremely expensive.

## C. Thermal-hydraulic Module

The flux-power module provides the power distribution required by the thermal-hydraulic module which then calculates core temperatures and heat fluxes in order to make certain that the thermal limitations placed on core performance are not exceeded. The core temperatures and coolant density profiles are returned to the macroscopic cross section module. As we will see in more detail in Chapter 13, some iteration between the thermal–hydraulic and nuclear core analysis is usually necessary.

Since the thermal–hydraulic analysis of a reactor core plays such an important role in nuclear reactor design, we will describe in some detail the various models and concepts used in this module in Chapter 12.

## D. Control-Adjustment Module

The control-adjustment module takes the core multiplication calculated by the flux-power module and estimates the amount of control insertion or withdrawal necessary to return the reactor to a critical state. In determining how to adjust the control reactivity (e.g., movable rods or chemical shim), the control module may be guided by a prespecified control management scheme. The control appears in the nuclear analysis as effective control cross section group constants that are added to the absorption group constants characterizing those core regions in which a control element is present. We will develop the necessary theory for calculating these effective cross sections in Chapter 14 (although we might remark that the basic idea is very similar to that involved in calculating fuel-cell averaged group constants to permit the analysis of a heterogeneous reactor lattice). The control module then returns the effective control group constants for the new control pattern to the macroscopic cross section module for the next criticality calculation.

## E. Depletion Module

The depletion module solves the rate equations describing the isotopic changes in core composition during reactor operation. Such equations must account for fuel burnup, the conversion of fertile to fissile material, and the buildup of nonsaturating fission products. The input to the depletion module is the flux calculated by the flux-power-reactivity module, while the number densities calculated by the depletion module are returned as input to the macroscopic cross section module. We will discuss such depletion calculations in some detail in Chapter 15.

## F. Economics Module

Such code packages will frequently also contain a module that uses information from the depletion analysis to determine the cost of the power generation (i.e., fuel costs) for the period. Such modules must account for the various costs associated with the nuclear fuel cycle for the core under study. We will not discuss such fuel economics calculations here, but will instead refer the interested reader to a number of sources of additional information on this topic.[23-25]

## G. Concluding Remarks

Of course, this rather brief description of the general features of computer code models used to analyze nuclear reactor core behavior does not really do justice to the complex interactions existing among the various modules or with other aspects of the core design. Other nonnuclear aspects of the design such as mechanical design or materials limitations on fuel element performance usually enter the nuclear analysis model as constraints placed on core performance. For example, the extent to which a fuel element can suffer radiation damage without experiencing an appreciable probability of failure will usually be represented by a limit on fuel burnup. Clad strength requirements may appear in the calculation as a limitation on clad surface temperature (or clad surface heat flux).

Furthermore we have not described in any detail the enormous variety of design problems to which such a model can be applied. Some of these will be illustrated in

later chapters, when we try to "fill in the gaps" to complete our description of the models used in nuclear reactor analysis.

Finally we should stress once again that such mathematical or computer models of an extremely complex system such as a nuclear reactor "work" primarily because past experience (rather than elegant mathematical analysis) has indicated the validity of the approximations used in developing the model (although sometimes only because of a fortunate cancellation of errors), and, equally important, because such models have been "fine-tuned" by empirical adjustments of a number of parameters appearing in the model. For this reason we should stress once again that a given model (code package) will require considerable insight, ingenuity, and a dose of good fortune on the part of the user if it is to be extended into areas of application that depart considerably from the experience on which the model was constructed.

## REFERENCES

1. A. Sesonske, *Nuclear Power Plant Design Analysis*, USAEC TID-26241 (1973).
2. H. W. Graves, Jr., Nuclear Reactor Design, University of Michigan Lecture Notes (unpublished) (1969).
3. A. Radkowsky (Ed.) *Naval Reactors Physics Handbook*, Vol. I, USAEC (1964).
4. *Reactor Physics Constants*, USAEC Document ANL-5800, 2nd Edition (1963).
5. M. H. Merrill, Nuclear Design Methods and Experimental Data in use at Gulf General Atomic, Gulf-GA-A12652 (1973).
6. Standard Safety Analysis Reports, General Electric, Westinghouse, Combustion Engineering, Babcock and Wilcox, and Gulf General Atomics.
7. H. C. Honeck, ENDF/B: Specifications for an Evaluated Nuclear Data File for Reactor Applications, USAEC Report BNL-50066, 1966; revised by S. Pearlstein (1967).
8. J. Chernick, *Reactor Tech.* **13**, 368 (1971); *Reactor Physics Constants*, USAEC Document ANL-5800, 2nd Edition (1963).
9. H. C. Honeck, THERMOS, BNL-5826 (1961); *Nucl. Sci. Eng.* **8**, 193 (1960).
10. H. Bohl, Jr., E. M. Gelbard, and G. H. Ryan, MUFT-4, WAPD-TM-22 (1957).
11. H. Amster and R. Suarez, SOFOCATE, WAPD-TM-39 (1957).
12. R. H. Shudde and J. Dyer, TEMPEST, NAA Program 3W-354 (1960).
13. G. D. Joanou, E. J. Leshan, and J. S. Dudek, GAM-1, GA-1850 (1961).
14. P. Walti and P. Koch, MICROX—A Two-Region Flux Spectrum Code for the Efficient Calculation of Group Cross Sections, Gulf-GA-A10827 (1972).
15. W. W. Engle, Jr., A Users Manual for ANISN, A One Dimensional Discrete Ordinates Transport Code with Anisotropic Scattering, USAEC Report K-1693 (1967).
16. K. D. Lathrop, TWOTRAN, A Fortran Program for Two-Dimensional Transport, GA-8747 (1968).
17. W. B. Lewis, *Nucl. Appl.* **2**, 171 (1966).
18. N. J. Palladino, Mechanical Design of Components for Reactor Systems, in *The Technology of Nuclear Reactor Safety*, T. J. Thompson and J. G. Beckerley (Eds.), M.I.T. Press, Cambridge (1973), Vol. II.
19. R. B. Holden, *Ceramic Fuel Elements*, Gordon and Breach, New York (1966).
20. P. G. Shewmon, in *Education and Research in the Nuclear Fuel Cycle*, D. M. Elliot and L. E. Weaver (Eds.) Oklahoma University Press, Norman (1970).
21. C. M. Cox and F. J. Homan, *Nucl. Appl. Tech.* **9**, 317 (1970); P. R. Huebotter, *Reactor Techn.* **15**, 156 (1972).
22. A. Sesonske, *Nuclear Power Plant Design Analysis*, USAEC TID-26241 (1973), Chapter 7.
23. D. M. Elliott and L. E. Weaver (Eds.) *The Nuclear Fuel Cycle*, Oklahoma University Press, Norman (1972).

24. A. Sesonske, *Nuclear Power Plant Design Analysis*, USAEC TID-26241 (1973), Chapters 2 and 3.
25. M. M. El-Wakil, *Nuclear Energy Conversion*, Intext, Scranton (1971), Chapter 17.
26. D. M. Elliott and L. E. Weaver (Eds.) *The Nuclear Fuel Cycle*, Oklahoma University Press, Norman (1972).
27. *The Technology of Nuclear Reactor Safety*, T. J. Thompson and J. G. Beckerley (Eds.), M.I.T. Press, Cambridge (1973).
28. An Assessment of Accident Risks in U. S. Commercial Nuclear Power Plants, USAEC Document WASH-1400 (1974).
29. A. Sesonske, *Nuclear Power Plant Design Analysis*, USAEC TID-26241 (1973), Chapter 6.
30. B. J. Toppel, The Argonne Reaction Computation (ARC) System, ANL-7332 (1967).
31. H. C. Honeck, et. al., JOSHUA—Reactor Physics Computational System, in Proceedings of Conference on the Effective Use of Computers in the Nuclear Industry, Knoxville (1969), pp. 324–336.
32. Mathematical Models and Computational Techniques for Analysis of Nuclear Systems, USAEC Document CONF-730414, Vols. I and II (1973).

Several universities have developed simplified reactor design code packages which are far better suited for instructional use than the production codes utilized by the nuclear reactor industry. Two particularly flexible and comprehensive code packages are:

Nuclear Engineering Computer Modules, Department of Nuclear Engineering, Virginia Polytechnic Institute and State University, Blacksburg, Va. (1974)

UMNE Computer Code Library, Department of Nuclear Engineering, The University of Michigan, Ann Arbor, Mi. (1971)

.

# 12

## Thermal-Hydraulic Analysis of Nuclear Reactor Cores

## I. INTRODUCTION

### A. The Relationship of Thermal Core Analysis to Nuclear Reactor Design

A nuclear power reactor is designed to produce heat that can then be used to generate electrical energy, usually by way of an associated steam thermal cycle. Once we have acknowledged the fact that the primary function of the reactor is really just that of a rather exotic heat source for turning water into steam, it becomes apparent that the determination of core temperature distributions and heat transfer rates, namely, the *thermal analysis* of the reactor core, must play a very important role in reactor design. Indeed the design of a reactor core depends as much on thermal as nuclear considerations. For one must design the core in such a way that it can produce the desired thermal power without exceeding temperature limitations on core components that might lead to fuel failure and the release of radioactive material into the coolant.

Such thermal limitations constitute the primary factor in determining core size. For as we have seen, a critical mass of fissile material can theoretically operate at any power level if sufficient cooling can be provided. Hence one first determines the core power density that can be accommodated by the intended primary cooling system, and then determines the reactor core size necessary to meet the desired reactor thermal power output at this power density. The efficient cooling of the core also plays a very important role in the detailed fuel element design. For example, the desire for large contact area between fuel and coolant to enhance heat transfer will influence the choice of core volume ratios (e.g., coolant-to-fuel). Furthermore the hydrodynamic behavior of the coolant as it flows through the core

467

will play a role in determining the core lattice design. Since nuclear power reactors operate at far higher power densities than those characterizing fossil-fueled steam generators, a core design to optimize thermal performance is obviously of considerable importance.

After determining the basic fuel element geometry and core volume from thermal-hydraulic considerations, one then performs a nuclear analysis of the core to determine the fissile fuel concentration or loading necessary to allow this core to operate at rated power over the desired core lifetime. (Of course the required fuel loading is usually considerably larger than that which would be determined by purely nuclear considerations.) In this sense, then, the thermal analysis of the core usually determines the gross features of the core geometry prior to the actual nuclear core analysis.
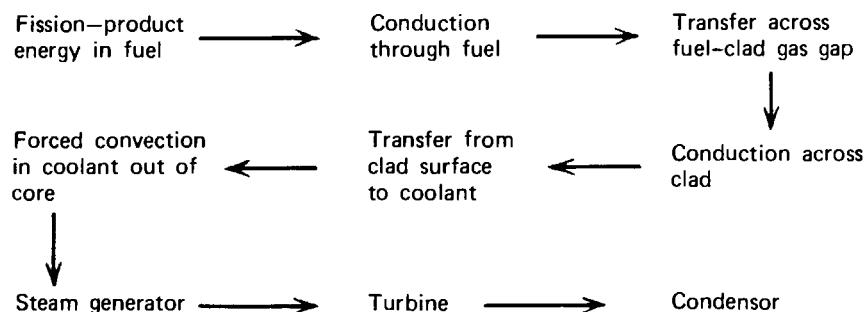
The nuclear analysis of a reactor core is rather intimately related to its thermal analysis in other ways. We have seen that nuclear cross sections that determine core multiplication depend sensitively on temperature (e.g., the Doppler effect). Furthermore the material composition of the core depends on thermal considerations because of the density changes accompanying the addition of heat energy to the coolant (e.g., expansion or vapor formation). On the other hand, since this heat energy is generated by the fission reactions induced by the neutron flux in the reactor, the temperature distribution in the core will depend sensitively on its neutronic behavior.

Thermal considerations also dominate the safety analysis of the reactor design. Indeed one of the most critical aspects of modern power reactor designs is that of providing auxiliary cooling systems that can continue to remove heat from the reactor core should the primary coolant system fail.

A nuclear designer will frequently require information concerning the thermal behavior of the reactor core. Hence he must be prepared to either interface with the mechanical engineers responsible for thermal core analysis or undertake this analysis himself.

Hence, we feel it advisable to include a rather brief overview of thermal core analysis in this text. Our intent is not to provide a complete development of this topic, but rather to indicate those areas in which thermal analysis will interact with nuclear design and hence drift into the domain of nuclear engineering.

Our presentation will essentially follow the path traced out by thermal energy in the reactor, from its origin as fission heat energy in the fuel until it is finally removed from the reactor core by the coolant.

Fission—product energy in fuel $\longrightarrow$ Conduction through fuel $\longrightarrow$ Transfer across fuel–clad gas gap $\downarrow$

Forced convection in coolant out of core $\longleftarrow$ Transfer from clad surface to coolant $\longleftarrow$ Conduction across clad

Steam generator $\longrightarrow$ Turbine $\longrightarrow$ Condensor

As we have seen, the energy released by the nuclear fission reactions appears

primarily as kinetic energy of the various fission reaction products. The bulk of this fission product energy is rapidly deposited as heat in the fuel material very close to the location of the fission event. This heat is then transported via thermal conduction across the fuel element, across the gap separating the fuel from the clad, and then across the clad to the clad surface. It is then transferred from the clad surface to the coolant by forced convection. The mass motion of the coolant then carries the thermal energy up and out of the reactor core, either as sensible heat (i.e., coolant temperature rise) or latent heat (i.e., thermally induced phase change—boiling). (See Figure 12-1.)

The direct concern of the nuclear core designer usually ceases at this point, although the power-plant engineer must continue to follow the heat energy as it is used to convert feedwater into steam, then as the steam is used to drive a turbogenerator, and then finally recondensed into feedwater. Actually the remainder of the thermal cycle will be very intimately coupled to the reactor core analysis since it will determine variables such as primary system pressure, inlet coolant temperature, and desired coolant exit conditions.
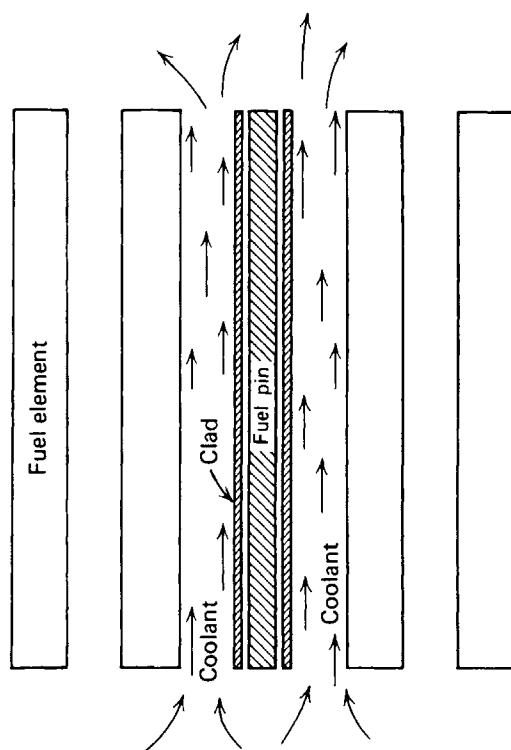


FIGURE 12-1.    Reactor core cooling.

## B. Objectives and Limitations of Thermal Design[1-5]

There are a number of obvious objectives for the thermal performance of a reactor core. For example, one wishes to achieve as high a core power density as possible since this will reduce the core volume required for a desired thermal output. Furthermore high fuel specific powers (power generated per unit mass of fuel) are desired in order to minimize the required fuel inventory. One also desires high coolant exit temperatures, since this not only leads to higher thermodynamic

efficiencies, but also to the production of higher temperature steam that will reduce the demands placed on the turbine.

Unfortunately one's ability to achieve these objectives is restricted by a number of limitations imposed by the thermal behavior of the core. It is useful to discuss briefly several of the more significant limitations on core thermal performance before we consider the thermal analysis of a nuclear reactor core.

## 1. FUEL TEMPERATURE LIMITATIONS

One of the principal limitations on allowable power densities in a reactor core arises from the desire to prevent the fuel temperature at any point in the core from exceeding its melting point. The melting point for the ceramic fuels used in most power reactors is extremely high, being roughly 2800°C for $UO_2$ and 2500°C for $UC$.[6] Nevertheless the power densities achieved in modern power reactors are sufficiently high that centerline fuel melting (maximum fuel temperatures normally occur at the fuel element centerline) represents an important limitation in reactor core design. It should be noted that such temperature limits are sensitive to fuel irradiation and tend to decrease with increasing fuel exposure. For example, the melting point of $UO_2$ fuel is commonly taken as 2800°C when first irradiated, and then reduced by 32°C for each 10,000 MWD/MTU burnup.[7]

There are other types of fuel thermal limitations. For example, in metallic fuels one must hold fuel temperatures below those points at which phase changes in the fuel occur (e.g., $T = 667°C$ in uranium metal). Furthermore, the low thermal conductivity of ceramic fuels leads to high temperature gradients that can cause fuel cracking and swelling.

Fuel elements subjected to temperatures sufficiently high to induce centerline melting will experience a significantly higher probability of failure. (By "failure" here we are referring to a loss in the functional behavior of the fuel element caused by a change in its physical properties.) Hence, although nothing catastrophic will happen if a few fuel elements in the core temporarily exceed centerline melting temperatures, considerable care is taken such that these limits will not be exceeded during normal core operating conditions.

We will find later that the maximum temperature achieved in the fuel is relatively insensitive to the diameter of the fuel rod and depends primarily on the thermal conductivity of the fuel and the linear power density in the core. Therefore one usually expresses the thermal limits imposed by fuel melting in terms of a limitation on the maximum achievable linear power density in the core. For example, in $UO_2$-fueled reactors this limitation is about 660 W/cm. Present power reactors of this type are usually designed to operate with a maximum linear power density of 460–500 W/cm under normal operating conditions.

## 2. CLAD THERMAL LIMITATIONS

Although the fuel element cladding in a nuclear reactor core will rarely experience temperatures approaching its melting point (unless critical heat flux or burnout conditions are exceeded), the clad thermal behavior does place limitations on the core power density. The clad serves as a containment barrier to prevent radioactive fission products produced in the fuel from being released into the coolant (and subsequently being swept out of the reactor core). The cladding is

subjected to rather severe stresses, both from the high-pressure coolant surrounding the fuel element, and by fission gas pressure and fuel swelling inside the fuel element. The buildup of fission gas pressure in the fuel pellet–clad gap and the cracking and swelling of the fuel pellet can both cause excessive cladding stresses and strains if not limited. Such phenomena not only depend on fuel irradiation, but also on thermal history (e.g., temperature variations due to reactor power level changes). Furthermore the clad is subjected to high thermal stresses due to the enormous thermal gradients across the clad thickness. Since clad strength is a sensitive function of temperature and thermal history, one must limit core thermal performance to avoid clad failure. (Such limitations constitute one of the motivations for using coated particle fuels such as in the HTGR in which the clad is actually a ceramic coating of a tiny fuel particle.)

A more critical thermal limitation is frequently placed on the heat flux that can be transferred from the clad to the coolant in liquid-cooled reactors (e.g., PWRs or BWRs). Above certain heat flux magnitudes, the heat transfer to the coolant will become unstable as a film of vapor forms to cover the fuel element surface. At this point the clad temperature will increase dramatically (several hundred degrees) leading to clad failure. This thermal limitation, known as the *critical heat flux*, is of primary concern in water-cooled reactor cores in which the coolant temperature is allowed to approach the boiling point.

## 3. COOLANT TEMPERATURE LIMITATIONS

In many reactor types, one wishes to limit the coolant temperature in order to achieve suitable coolant behavior. For example, in a PWR one desires to keep the bulk coolant temperature below its saturation temperature so that no bulk boiling occurs. Similarly in a LMFBR there is motivation to keep the sodium temperature sufficiently low that the heat transfer capability of the coolant is maximized.

There are also limitations on the allowable temperature rise of the coolant as it passes through the core. On one hand, one would like this temperature rise to be large enough to allow efficient heat transfer in the steam generator; but there is also strong motivation to minimize this temperature rise in order to lessen thermal shocks in the reactor core (such as during a reactor scram). The temperature rise in water-moderated reactors is kept quite small—for example, in a PWR, the coolant typically rises from an entrance temperature of 293°C to a exit temperature of 315°C—a temperature increase of only 22°C. In an LMFBR, this temperature rise is somewhat larger, amounting to some 140°C, while in a HTGR, the helium temperature rises by as much as 500°C. These coolant parameters are summarized for several reactor types in Appendix H.

It should be noted that while such temperature limitations set upper limits on the temperatures achieved in the core, there are also lower limits imposed on the inlet coolant temperature due to the available condensor cooling. The size of a reactor core will be determined primarily by the amount of heat transfer area necessary to transfer the desired thermal power utilizing the given temperature differences.

## 4. OTHER THERMAL LIMITATIONS

There are other types of thermal limitations placed on coolant behavior that have a more nuclear origin. We have seen that the core multiplication depends

sensitively on the coolant density. For example, in a LWR the coolant serves as a moderator. Decreasing the coolant density will reduce moderation and hence reactivity. By way of contrast, in a LMFBR, decreasing coolant density will cause a hardening of the neutron energy spectrum, which enhances reactivity. Since the coolant density depends sensitively on temperature, there is frequently a very strong coupling between the thermal and nuclear behavior of a reactor. It is essential to account for such coupling, both in static reactor design and reactor transient studies. Indeed stability considerations will frequently place restrictions on the allowable temperatures or heat fluxes achieved in the core.

In summary then, the principal limitations on core thermal performance include the avoidance of significant centerline fuel melting, maintaining the heat flux below the maximum value allowed by coolant conditions (burnout), and limiting the stresses due to fission gas release, fuel swelling, and thermal gradients on the clad. These limitations place constraints on the surface heat flux, the linear power density, and the volumetric power density in the fuel element. Usually one determines the maximum heat flux allowed by burnout considerations, and then adjusts the fuel rod diameter to achieve an optimum compromise between linear power density (i.e., fuel centerline temperature) and power density (fuel inventory, core size).[4]

It is apparent that the first goal in thermal analysis is to determine the temperature distribution throughout the core for a given fission power distribution and coolant inlet condition, since one must ensure that the maximum temperatures achieved in the core do not exceed any of the thermal limitations. In particular, one would want to determine the maximum allowable overpower at which the reactor could operate and still be within the thermal design constraints. It should be kept in mind that the fission power density is highly nonuniform. Hence the temperature distribution is similarly nonuniform—and, will depend on time, since the fission power distribution will shift over core life as the fuel burns nonuniformly. The usual procedure is to estimate the set of local operating conditions representing the most extreme case, (e.g., highest temperatures or heat fluxes), and then to design the core so as to guarantee satisfactory performance for this "hot spot,"[1-3] although it should be recognized that this may, in fact, yield an overconservative design.

The thermal analysis begins by determining the volumetric source of fission heat throughout the core. Since this is proportional to the fission rate density, one requires an initial estimate of the neutron flux distribution in the core. For the purpose of most thermal analysis, it is assumed that this fission heat source is confined to the fuel elements.

Since in the steady state this fission heat energy must be removed by the coolant, one can use a simple energy balance to calculate the coolant temperature as it passes up through the core using the inlet coolant temperature (presumed known). Then one can work backward to determine the temperature rise across the clad, gap, and fuel element to the fuel centerline using the equations of thermal conduction (Fourier's law) and forced convection (Newton's law of cooling). In simple analyses, one performs such a calculation only for an average coolant channel and a hot coolant channel chosen to represent the worst possible case. In more realistic analyses, one must also take into account flow conditions and the intermixing of flow between coolant channels.

One is also occasionally interested in the transient thermal behavior of a reactor when subjected to power level or coolant flow rate changes. Such transient studies

are of very considerable importance in reactor safety studies and in the modeling of nuclear reactor dynamics.

In this chapter we will sketch the basic concepts and procedures involved in the thermal analysis of a nuclear reactor core. Although we will usually try to relate these concepts and methods to well-known laws of thermodynamics, we will give very few derivations. We do not intend this chapter to be a thorough development of heat transfer and fluid flow, but rather a brief description of how standard concepts from these disciplines are applied to nuclear reactor analysis. We have attempted to include sufficient explanation and discussion of these methods to allow the reader with only rudimentary exposure to heat transfer and fluid flow to still benefit from the chapter. For more detailed treatments of many of these topics, we must refer the reader to one of several standard references.[8-10]

## II. POWER GENERATION IN NUCLEAR REACTOR CORES

The energy released in a nuclear fission reaction is distributed among a variety of reaction products characterized by different ranges and time delays. In thermal design, the energy deposition distributed over the coolant and structural materials is frequently reassigned to the fuel in order to simplify the thermal analysis of the core. We can determine the volumetric fission heat source in the core $q'''(\mathbf{r})$ by multiplying the fission reaction rate density for each isotope by $w_f^{(i)}$, the recoverable energy released per fission event, to find

$$q'''(\mathbf{r}) = \sum_i w_f^{(i)} N_i(\mathbf{r}) \int_0^\infty dE\, \sigma_f^{(i)}(E)\phi(\mathbf{r}, E). \tag{12-1}$$

Of course, since the flux and number density of the fuel vary across the reactor core, there will be a corresponding variation in the fission heat source.[†]

The simplest model of fission heat distribution would correspond to a bare, homogeneous core. In particular, we should recall the one-group flux distribution for several typical geometries given in Table 5-1. Of course, the geometry of most interest will be the cylindrical core, for which we have sketched in Figure 12-2 the radial and axial flux profiles. We have also indicated the modifications to these profiles resulting from the addition of reflectors (since most power reactor designs are reflected, either by coolant bypass flow, additional moderating material, or perhaps a blanket of fertile material).

To account for heterogeneities in the core lattice, one can use the gross flux profiles to determine the flux in each of the fuel elements of the core. Usually the fuel element cross section is so small compared to the core size that we can assume $q'''(\mathbf{r})$ to be constant across the width of the fuel rod for many calculations. For example, we would take the fission heat source in a rod at a radius $r_f$ in a bare,

[†]We will utilize the more or less conventional notation of mechanical engineers when referring to heat densities in which the number of primes on $q$ indicates the dimensionality of the density. Hence $q'''$ represents a volumetric heat source in units of $W/cm^3$; $q''$ represents a heat flux $(W/cm^2)$; while $q'$ represents a linear heat density $(W/cm)$ typically used to describe the heat generated per unit length of a fuel rod.
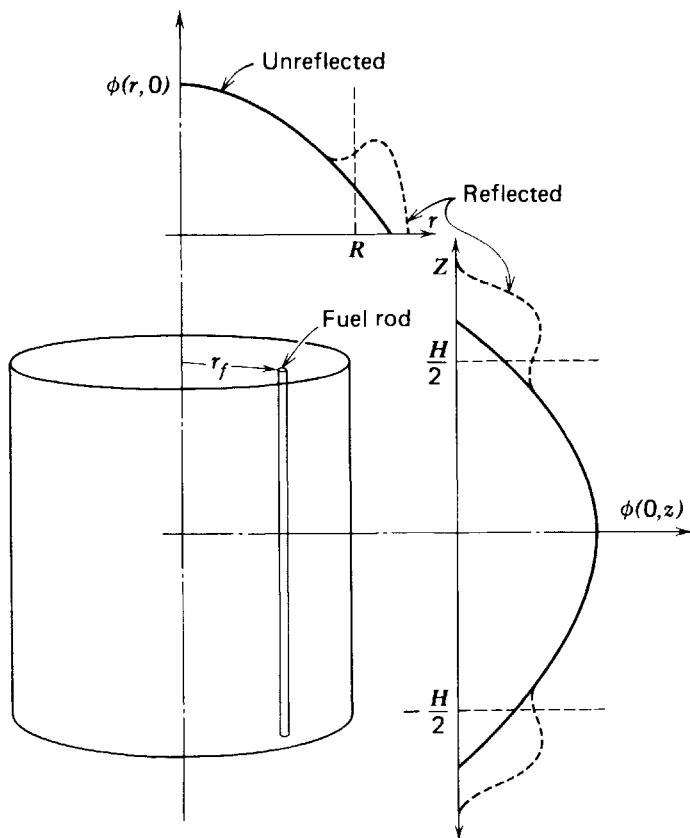
**FIGURE 12-2.** Flux distribution in a cylindrical core.

uniform cylindrical core to be

$$q'''(\mathbf{r}) = w_f \Sigma_f \phi_0 J_0 \left( \frac{2.405 r_f}{\tilde{R}} \right) \cos \left( \frac{\pi z}{\tilde{H}} \right) \tag{12-2}$$

(where, for convenience, we have assumed only one fuel isotope and used a one-group representation). Here $\tilde{R}$ and $\tilde{H}$ are to be regarded as effective core dimensions that include extrapolation lengths as well as an adjustment to account for a reflected core (i.e., reflector savings).

Notice that while we can frequently neglect the radial variations in the fission heat generation in the fuel rod, we cannot ignore the axial variation. In fact, if we remember that there is an appreciable depression of the thermal flux in the fuel rod due to self-shielding, then it is apparent that there may even be situations in which we may want to account for radial variation of the fission heat generated in the rod (such as in the calculation of the Doppler coefficient of reactivity).

There are numerous other factors that will perturb the power distribution of the reactor core. For example, the reactor is usually not loaded with fuel of uniform enrichment. At the beginning of core life, higher enrichment fuel is commonly loaded toward the edge of the core in order to flatten the power distribution. During core operation, the fuel will burn nonuniformly, leading to power nonuniformities that must be accounted for in thermal core analysis. Furthermore, subsequent refueling of the core will not be uniform and will lead to further variation in the power distribution.

Control rods will also have a major effect on the axial and radial flux profiles. There will also be local peaking of the flux, for instance in water gaps in LWRs or near reflectors. All of these variations in the flux and power distributions must be

predicted by the nuclear engineer and included in a subsequent thermal analysis of the core.

From the above discussion, it is apparent that the fission power density will vary considerably over the core. Such variations occur not only from the usual flux variations in a bare, homogeneous reactor core, but also due to the heterogeneous nature of the core, the nonuniformities of fuel burnup and fuel loading, the presence of coolant gaps and control elements, and small variations due to manufacturing tolerances of core components. These will cause corresponding variations in the temperature distribution in the core. A common technique for accounting for these variations is to estimate a set of local operating conditions for the "worst case" ("worst" in the sense of most closely approaching thermal limitations), and to evaluate the reactor performance for this set of conditions. Associated with such local conditions are so-called "hot channel" factors relating this extreme case to the average core behavior.

One most commonly defines the *hot channel* of the core as that coolant channel where the core heat flux and enthalpy rise is a maximum. Conditions in the hot channel are defined by several ratios of local conditions to average conditions, and these ratios, termed the *hot channel factors* or *power peaking factors*, are considered in some detail in Section 12-VII.

The major results of the nuclear calculations on a core can frequently be relayed to the thermal designer in terms of nuclear hot-channel factors. These factors, together with an estimate of the axial power distribution shape, can serve as the basis for the initial plant thermal design, although there will be later interaction between the thermal and nuclear designs.

Once we are given an axial flux or power distribution and the coolant inlet conditions (e.g., temperature and pressure), we can compute the conditions of the coolant as it passes up the coolant channel through the core of the reactor. Such a calculation involves only a simple energy balance equating the heat flux passing into the coolant from the fuel element to the change in temperature (or, more generally, the enthalpy) of the coolant as it absorbs this heat.

The more difficult analysis concerns the determination of the radial temperature rise from the coolant to the clad surface, then across the clad and the gap to the fuel itself. Such a calculation involves a study of heat conduction through the fuel element and forced convection heat transfer from the clad surface to the coolant. This analysis is frequently complicated by a phase change of the coolant as it passes up the channel. Finally, we are usually also concerned with the hydrodynamic flow conditions of the coolant, such as the pressure drop along the channel, flow mixing, and other characteristics of the coolant.

We will consider each of these topics in turn, first developing the relations between the temperature drop across the fuel, gap, and clad using the thermal conduction equation; then studying the transfer of heat from the clad surface to the coolant via forced convection considering both single phase and two-phase coolants; and finally giving a brief outline of the hydraulic analysis of the core.

## III. RADIAL HEAT CONDUCTION IN REACTOR FUEL ELEMENTS

### A. The Equation of Heat Conduction

Let us begin by quickly reviewing the topic of heat transfer in solids via thermal conduction.[8-10] If we perform a simple energy balance for an arbitrary

volume in the solid, we arrive at an equation expressing the time rate of energy change as the difference between energy addition due to distributed heat sources $q'''(\mathbf{r}, t)$ and energy loss due to heat transport:

$$\frac{\partial}{\partial t}(\rho c T) = q'''(\mathbf{r}, t) - \nabla \cdot \mathbf{q}''(\mathbf{r}, t), \tag{12-3}$$

where $T(\mathbf{r}, t)$ is the local temperature of the solid, $\rho(\mathbf{r}, t)$ and $c$ are its density and specific heat, respectively, and $\mathbf{q}''(\mathbf{r}, t)$ is the heat flux vector expressing the rate at which heat flows across a surface. This energy conservation equation is derived in a manner identical to that used in Chapter 5 to derive the neutron diffusion equation. And as in that case, the balance equation contains two unknowns, $T(\mathbf{r}, t)$ and $\mathbf{q}''(\mathbf{r}, t)$. We will now introduce an approximation that is the direct analog to the diffusion approximation used in neutron transport by assuming that the heat flux vector $\mathbf{q}''(\mathbf{r}, t)$ is proportional to the temperature gradient

$$\mathbf{q}''(\mathbf{r}, t) = -k\nabla T(\mathbf{r}, t). \tag{12-4}$$

This relationship, known as *Fourier's law of thermal conduction*, is a very good approximation for most materials. The coefficient of proportionality $k$ is referred to as the *thermal conductivity*. [Of course Eq. (12-4) is the analog to Fick's law.] When we substitute Eq. (12-4) into the energy conservation equation, we arrive at the *equation of thermal conduction*:

$$\frac{\partial}{\partial t}(\rho c T) - \nabla \cdot k\nabla T = q'''(\mathbf{r}, t). \tag{12-5}$$

We need both initial and boundary conditions to complete the mathematical description of heat conduction. These conditions can be derived in a general fashion using energy balance ideas, but we will use physical arguments to more directly motivate the conditions appropriate for the specific problems we will consider.

We will generally consider the case of time-independent heat transport, for which Eq. (12-5) simplifies to

$$-\nabla \cdot k\nabla T(\mathbf{r}) = q'''(\mathbf{r}). \tag{12-6}$$

It should be noted here that the thermal conductivity $k$ appearing in this equation is temperature-dependent in most materials. Although this temperature-dependence is usually ignored in studying thermal conduction in materials such as the gap or the clad in which a relatively small temperature drop occurs, it must be considered in treating thermal conduction through the fuel, since in this case we may have a temperature variation of several thousand degrees.

## B. Heat Transfer in Cylindrical Fuel Elements

Most modern power reactor cores are composed of cylindrical fuel elements that contain ceramic fuel pellets in metallic tubes (i.e., cladding) (although the HTGR is a notable exception). Our goal will be to calculate the temperature drop from the centerline of the fuel, where the maximum temperature normally occurs, to the surface of the clad in terms of the various physical properties of the fuel element. For the purposes of this calculation, we can regard the clad surface

temperature as a reference temperature, since it will be determined in terms of the coolant temperature and eventually in terms of the coolant inlet conditions and the reactor power level. To simplify this calculation, we will make several useful assumptions:

(1) We will assume that we can neglect thermal conduction in the axial direction. This is a valid assumption since the temperature gradient across the fuel element in the radial direction is several orders of magnitude larger than that in the axial direction. Axial heat transfer will occur outside the fuel element via forced convection in the coolant.

(2) The fission energy will be assumed to appear as a uniform heat source distributed through the fuel. Actually there is some variation in this heat source since it is proportional to the flux in the fuel, and we have seen in Chapter 10 that there is an appreciable flux depression in the fuel due to self-shielding effects. However neglect of this spatial variation is frequently adequate in thermal core analysis.

(3) Only steady-state heat transfer in the core will be considered.

We will now apply the equation of heat conduction to study the radial heat transfer in each region of the reactor fuel element (see Figure 12-3).
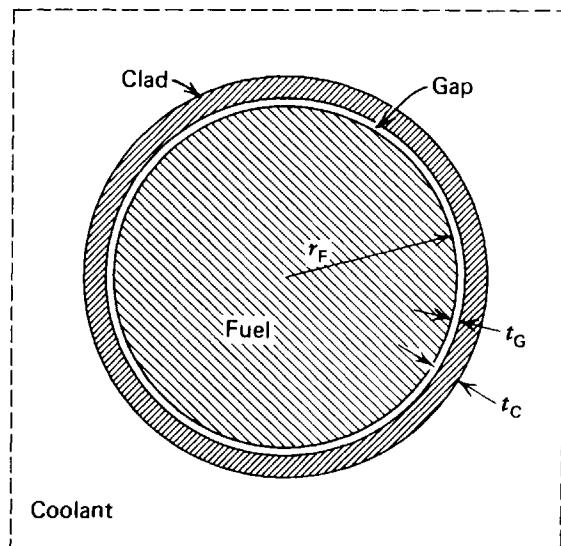


**FIGURE 12-3. Radial fuel element geometry.**

## 1. FUEL

The heat conduction equation for a cylindrical fuel pin with a uniform volumetric heat source $q'''$ in which axial heat conduction can be ignored takes the form

$$\frac{1}{r}\frac{d}{dr}k_F r \frac{dT}{dr} = -q''', \tag{12-7}$$

where we have used axial symmetry to omit the angular dependence.

If $k_F$ were constant, we could solve this equation immediately for $T(r)$. However we must recognize that $k_F$ will depend strongly on the fuel temperature. Hence we will follow a somewhat less direct path by first integrating Eq. (12-7) from the fuel

centerline at $r = 0$ to a radius $r$

$$k_F r \frac{dT}{dr} = -\frac{r^2}{2} q'''. \tag{12-8}$$

Now divide by $r$ and integrate once again, this time from $r = 0$ to the fuel pin surface $r = r_F$,

$$\int_{T_F}^{T_F} k_F(T) dT = -\int_0^{r_F} dr \frac{rq'''}{2} = -\frac{r_F^2}{4} q''', \tag{12-9}$$

where we have denoted the fuel centerline and surface temperatures as $T_{\ell} = T(0)$ and $T_F = T(r_F)$, respectively. If we now define an average thermal conductivity for the fuel

$$\bar{k}_F \equiv \frac{1}{T_{\ell} - T_F} \int_{T_F}^{T_{\ell}} dT \, k_F(T), \tag{12-10}$$

we can rewrite Eq. (12-9) to give the temperature drop across the fuel as

$$\Delta T|_{FUEL} \equiv T_{\ell} - T_F = \frac{q''' r_F^2}{4\bar{k}_F}. \tag{12-11}$$

In the situation where $k_F$ can be assumed constant, one can actually determine the functional form of $T(r)$ by integrating Eq. (12-7) directly to find a parabolic temperature profile

$$T(r) = T_{\ell} - \frac{q''' r^2}{4\bar{k}_F}. \tag{12-12}$$

Let us define the linear power density of the fuel element $q'$ as the power generated per unit length

$$q' \equiv \pi r_F^2 q'''. \tag{12-13}$$

Then Eq. (12-11) can be rewritten in terms of $q'$ as

$$\Delta T|_{FUEL} = \frac{q'}{4\pi \bar{k}_F}. \tag{12-14}$$

In particular we should note that the fuel temperature drop is not dependent on the fuel radius. This temperature drop depends only on the linear power density $q'$ and the thermal conductivity of the fuel. This explains why linear power density is a useful core parameter.

The fuel thermal conductivity is quite low for ceramics such as $UO_2$, for which $k_F$ is typically 0.020–0.030 W/cm°K.[11] [Although it should be noted that $k_F$ will change somewhat with fuel exposure.] This low thermal conductivity leads to rather large temperature differences across the fuel element. For example, a linear power density of 500 W/cm in a typical LWR would lead to a temperature difference of 1400°C.

Since the fuel centerline temperature $T_{\ell}$ is limited by the fuel melting point to about 2800°C for $UO_2$, it becomes apparent that one must limit the linear power density in order to avoid fuel centerline melting. For $UO_2$ fuel elements, the limit

on linear power density is roughly 660 W/cm. Most power reactors operate such that the maximum linear power density is 420–460 W/cm.

It should also be noted that the weak dependence of the temperature drop on the fuel radius suggests that, at least from a thermal standpoint, one can achieve the same linear power density without exceeding core temperature limitations by using smaller fuel rods. Since the use of smaller rods can reduce fuel inventory, this feature can have an important bearing on the economics of core design.

It is possible to repeat our analysis of the heat transfer in the fuel for the situation in which we explicitly account for the flux depression. Such an analysis indicates that the assumption of a uniform heat source $q'''$ actually implies a somewhat larger $\Delta T|_{\text{FUEL}}$ than that corresponding to a distributed heat source. Therefore our calculations above are somewhat on the conservative side.

## 2. GAP

In reactor types in which the ceramic fuel pellets are encased in a metallic tube or clad, there will be a small clearance or gap between the fuel and the clad several thousands of a cm in thickness which is usually filled with some inert gas such as helium. Although the thickness of the gap is quite small, the low thermal conductivities of gases will cause a rather large temperature drop across the gap. If the gap spacing were uniform, we could simply solve the equation of thermal conduction for the gas in the gap to find the temperature drop across the gap. More specifically since there is no heat production in the gap, we would solve

$$\frac{1}{r}\frac{d}{dr}k_{\text{G}}r\frac{dT}{dr}=0. \tag{12-15}$$

If we assume that the thermal conductivity of the gas $k_{\text{G}}$ is constant, and also note that at the fuel surface we must satisfy continuity of heat flux emerging from the fuel by requiring

$$-k_{\text{G}}\frac{dT}{dr}\bigg|_{r=r_{\text{F}}}=q''=\frac{q'}{2\pi r_{\text{F}}}=\frac{q'''r_{\text{F}}}{2}, \tag{12-16}$$

then we can integrate Eq. (12-15) to find the temperature drop across the gap as

$$\Delta T|_{\text{GAP}}\equiv T_{\text{F}}-T_{\text{C}}=\frac{q'''}{k_{\text{G}}}\frac{r_{\text{F}}^2}{2}\ln\left(\frac{r_{\text{F}}+t_{\text{G}}}{r_{\text{F}}}\right), \tag{12-17}$$

where $t_{\text{G}}$ is the gap thickness and $T_{\text{C}}$ is the inside surface temperature of the clad. Since $t_{\text{G}}$ is usually very small ($\sim$.005 cm), we can expand the log term to write

$$\Delta T|_{\text{GAP}}\cong\frac{q'''r_{\text{F}}}{2}\frac{t_{\text{G}}}{k_{\text{G}}}=\frac{q'}{2\pi r_{\text{F}}}\left(\frac{t_{\text{G}}}{k_{\text{G}}}\right). \tag{12-18}$$

After a period of operation, the gap will contain a mixture of the original fill gas and fission product gases such as Xe and Kr. Hence the thermal conductivity $k_{\text{G}}$ will change over core life. Typically $k_{\text{He}}=0.002$ W/cm°K, while $k_{\text{Xe}+\text{Kr}}=0.0001$ W/cm°K.[12] Hence a linear power density of 500 W/cm and a gap thickness of $t_{\text{G}}=.005$ cm would give rise to a temperature difference across the gap of 300°C or more.

There is another much more significant burnup effect, however. As fission events occur in the fuel, the fuel pellets will swell and crack and will actually come into contact with the clad in many places (see Figure 12-4). Such a phenomenon is very difficult to treat analytically, and hence one usually defines an effective coefficient of gap heat transfer $h_G$ such that the temperature drop across the gap is

$$\Delta T|_{GAP} = \frac{q''}{h_G} . \tag{12-19}$$

The empirical coefficient $h_G$ will be a function of the mean gap thickness, gas conductivity, the contact pressure between the fuel pellet and the clad, surface roughness, clad material, and, of course, burnup. It typically ranges in value between 0.5 to 1.1 $W/cm^2 °K$, depending on the material type, the fuel exposure, and the contact pressure between the clad and the pellet.[13]

If we recognize that the heat flux across the gap in the steady state must be just that amount of heat produced in the fuel divided by the surface area of the fuel

$$q'' = \frac{q'''(\pi r_F^2 H)}{2\pi r_F H} = \frac{q''' r_F}{2} = \frac{q'}{2\pi r_F} , \tag{12-20}$$

then we can calculate the temperature drop across the gap as

$$\Delta T|_{GAP} = \frac{q''' r_F}{2h_G} = \frac{q'}{2\pi r_F h_G} . \tag{12-21}$$
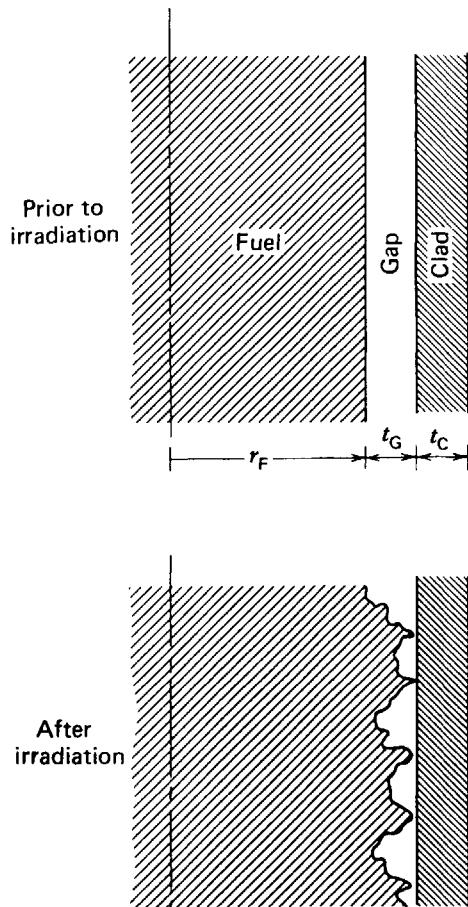


FIGURE 12-4.   The effect of irradiation on the fuel-clad gap.

For a linear power density of 500 W/cm this temperature difference can range from 140° to 280°C, depending on the value chosen for $h_G$.

## 3. CLAD

If we assume that the clad thermal conductivity $k_C$ is constant and that there is no heat production in the clad, we can solve

$$\frac{1}{r} \frac{d}{dr} r k_C \frac{dT}{dr} = 0 \qquad (12\text{-}22)$$

to find the temperature drop across the clad as

$$\Delta T|_{\text{CLAD}} \equiv T_C - T_S = \frac{q''' r_F^2}{2k_C} \ln \frac{r_F + t_C}{r_F}, \qquad (12\text{-}23)$$

where $T_S$ is the outer clad surface temperature and $t_C$ is the clad thickness. (We have ignored the gap thickness $t_G$ in this calculation.) In practice the clad thickness $t_C$ is quite small compared to the fuel rod diameter, and hence we are once again justified in expanding the log to write

$$\Delta T|_{\text{CLAD}} \cong \frac{q''' r_F}{2} \frac{t_C}{k_C} = \frac{q'}{2\pi r_F} \frac{t_C}{k_C} \qquad (12\text{-}24)$$

for the temperature drop across the clad. Clad materials are usually chosen to have large thermal conductivity (e.g., $k_{Zr} = 0.11$ W/cm °K). This fact, when combined with the small clad thickness $t_C$, leads to relatively small temperature drops across the clad. For example, at $q' = 500$ W/cm, a clad of thickness $t_C = .053$ cm would experience a temperature drop of 78°C.

## 4. CLAD SURFACE TO COOLANT

Heat transfer from the clad surface to the coolant is described by *Newton's law of cooling*

$$q'' = h_s(T_S - T_{fl}), \qquad (12\text{-}25)$$

where $h_s$ is the convective heat-transfer coefficient. This coefficient will depend upon the properties and flow conditions of the coolant, and its determination will be the subject of the next section of this chapter. For now, however, we will assume that it is known, and proceed to calculate the temperature drop to the coolant using Eq. (12-25) for $q''$ to find

$$\Delta T|_{\text{COOL}} \equiv T_S - T_{fl} = \frac{q''}{h_s} = \frac{q''' r_F^2}{h_s 2(r_F + t_C)} = \frac{q'}{h_s 2\pi (r_F + t_C)}. \qquad (12\text{-}26)$$

As we will later find, heat transfer from the clad surface to the coolant is an extremely efficient process and values of $h_s$ range as high as 4.5 W/cm² °K. In a LWR, $\Delta T|_{\text{COOL}}$ is typically only about 10–20°C.

## 5. TOTAL TEMPERATURE DROP ACROSS THE FUEL ELEMENT

We can sum all of these separate temperature drops from the fuel centerline to the coolant to write

$$T_q - T_{fl} = \frac{q'}{2\pi r_F} \left[ \frac{r_F}{2\bar{k}_F} + \frac{1}{h_G} + \frac{t_C}{k_C} + \frac{r_F}{h_s(r_F + t_C)} \right]. \tag{12-27}$$

Now, in general, the coolant temperature is essentially fixed by the remaining thermal components of the plant (such as the steam generator and condensor). Furthermore, regardless of where we are along the axis of the core, the coolant temperature varies comparatively little (e.g., in a LWR, the coolant rises from 293° to 315°C, while in a LMFBR it rises from 370° to 510°C). The fuel centerline temperature is constrained to remain below the melting point of the fuel (e.g., 2800°C). Hence the allowable temperature drop across the fuel element is limited by the fuel melting point; there will be corresponding limits on the allowable linear power density. This maximum allowable linear power density essentially determines the size of the reactor core for a desired power level. If we rewrite Eq. (12-27) as

$$q' = \frac{2\pi \left( T_q - T_{fl} \right)}{\left[ \dfrac{1}{2\bar{k}_F} + \dfrac{1}{r_F h_G} + \dfrac{t_C}{k_C r_F} + \dfrac{1}{h_s(r_F + t_C)} \right]}, \tag{12-28}$$

we can see that there is strong motivation to maximize the heat transfer coefficients $h_G$, $h_s$, $k_C$, and $k_F$ in order to maximize the allowable linear power density and hence minimize the required core size.

In Table 12-1 we have listed several thermal properties of the common fuel, clad, and coolant materials used in nuclear reactor cores.[3] By way of illustration, we have used these data to calculate the temperature drops across a LWR fuel element generating a linear power density of $q' = 500$ W/cm. The temperature profile across the fuel element is shown in Figure 12-5.

**TABLE 12-1:** Some Physical Properties of Interest in Fuel-Rod Design

| Material | Temperature °C | Density g/cm³ | Thermal Conductivity W/cm°K | Linear Thermal Expansion Coefficient m/m°K | Heat Capacity J/kg |
|---|---|---|---|---|---|
| UO₂-Unirradiated (95%ρ_T)† | 540–2700 | 10.4 | .024 | $1.75 \times 10^{-5}$ | 221 |
| UC-Unirradiated (92%ρ_T) | 540–1400 | 12.6 | .130 | $1.08 \times 10^{-5}$ | 140 |
| Stainless steel (Type 304) | 340 | 8.0 | .163 | $1.73 \times 10^{-5}$ | 325 |
| Zircaloy IV | 340 | 6.44 | .107 | $6.10 \times 10^{-6}$ | 183 |
| Water at 155 bar | 300 | 0.72 | .004 | — | 2930 |
| Sodium | 540 | 0.81 | .542 | — | 698 |
| Helium | 340 | — | .002 | — | — |
| Fission gas mixture (Xe + Kr) | 340 | — | $1.3 \times 10^{-4}$ | — | — |

†ρ_T-Theoretical density
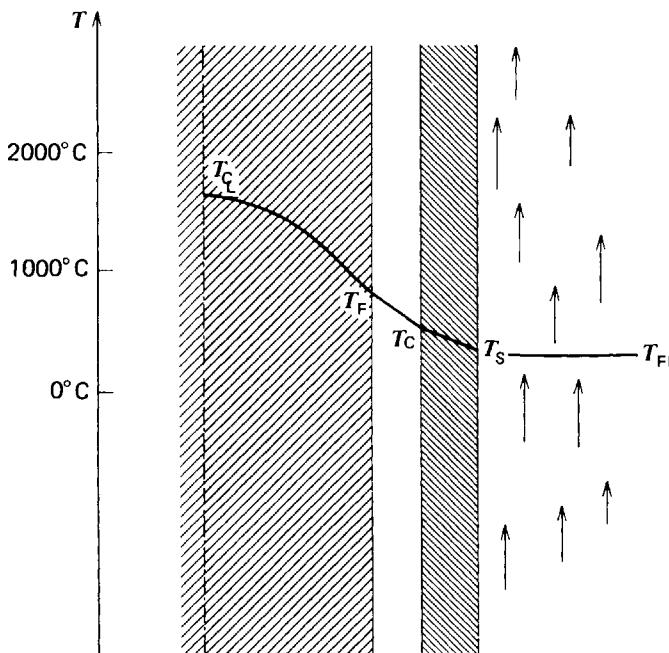
FIGURE 12-5.    Temperature distribution in a cylindrical fuel pin.

# IV. FORCED CONVECTION HEAT TRANSFER IN SINGLE-PHASE COOLANTS

In the preceding section we treated the transfer of heat from the clad surface to the coolant using Newton's law of cooling

$$q'' = h_s(T_S - T_{fl}) \qquad (12\text{-}29)$$

where $h_s$ is the coefficient of convective heat transfer. The magnitude of $h_s$ varies greatly for different types of coolants and flow conditions. For example, $h_s$ in water can range from .05 to as high as 4.5 $W/cm^{2\circ}K$ (if boiling occurs), while for a gas such as helium, $h_s$ is only .005–.05 $W/cm^{2\circ}K$. We will study how $h_s$ is determined for the case of forced convection heat transfer—namely, that situation in which heat is transported away from a surface by mass motion of a coolant adjacent to the surface maintained by an externally induced flow (e.g., coolant pumps), in contrast to natural convection, in which the density variation in a temperature gradient induces a flow (e.g., in a swimming-pool reactor).

## A. Hydraulic Flow in Channels

The determination of the convective heat transfer coefficient $h_s$ for various coolant and flow conditions characteristic of nuclear power reactors is intimately related to the subject of hydraulics, that is, the study of incompressible flow in channels.[14] We will avoid a detailed discussion of hydraulics and application of hydrodynamics equations to describe forced convection in reactor cores in favor of a brief survey of the principal results of significance for reactor analysis. Since the coolant flow in most power reactors is highly turbulent, the quantitative analysis of thermal–hydraulics in reactor cores has a highly empirical flavor in any event.

The pressure drop experienced by an incompressible fluid flowing in a channel of circular cross section can be written as

$$\Delta p = 2(L/D)\rho \bar{u}_z^2 f, \qquad (12\text{-}30)$$

where $L$ is the length of the channel, $D$ is its diameter, $\rho$ is the fluid density, and $\bar{u}_z$ is its mean flow velocity along the channel. An empirical factor $f$ known as the *Fanning friction factor*[†], has been inserted to account for the effect of turbulent flow. In general this factor will depend both on the roughness of the channel wall and the *Reynold's number* characterizing the flow which is defined by

$$\mathrm{Re} \equiv \rho \bar{u}_z D/\mu, \qquad (12\text{-}31)$$

where $\mu$ is the shear viscosity of the fluid. For turbulent flow, the friction factor $f$ must be measured experimentally as a function of both Re and channel surface roughness and is customarily plotted against these parameters on a chart known as a *Moody diagram* (see Figure 12-6). On this chart the transition from laminar to turbulent flow occurs at a critical Reynolds number of $\mathrm{Re}^* = 2100$.
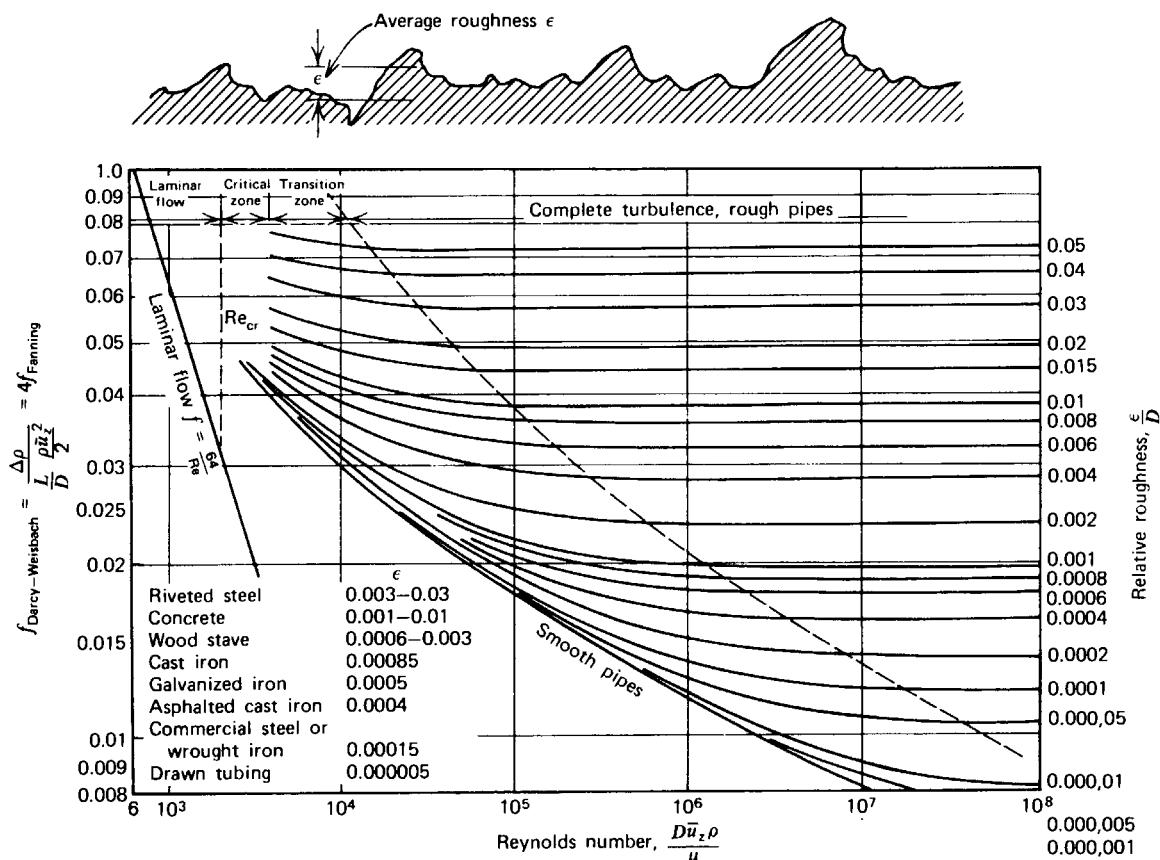


**FIGURE 12-6.** **The Moody diagram for the Fanning friction factor.** [L. F. Moody, Trans. ASME **66**, 671 (1944)].

For laminar flow ($\mathrm{Re} < 2100$), one can explicitly solve the equations of hydrodynamics characterizing incompressible flow in a circular pipe (so-called Hagen–Poiseuille flow) to obtain the friction factor as

$$f = 16/\mathrm{Re}, \qquad \mathrm{Re} < 2100 \ (\text{laminar flow}). \qquad (12\text{-}32)$$

For turbulent flow ($\mathrm{Re} \geqslant 2100$) one must use empirical correlations for the friction

[†]Note that one occasionally encounters an alternative factor known as the Darcy–Weisbach friction factor. The relationship between the two friction factors is $f_{\mathrm{Fanning}} = (1/4) f_{\mathrm{Darcey\text{-}Weisbach}}$.

factor. In particular for turbulent flow in smooth pipes (such as arise in reactor applications), one customarily uses the Blasius formula[10]

$$f = 0.0791 \, \mathrm{Re}^{-0.25}, \quad 2100 < \mathrm{Re} < 10^5 \text{ (turbulent flow).} \tag{12-33}$$

Frequently it becomes necessary to extend these results to flow in channels of noncircular cross section. For this purpose, one replaces $D$ by an *equivalent hydraulic diameter* $D_h$ defined by

$$D_h = 4S/Z \tag{12-34}$$

where $S$ is the flow area and $Z$ is the wetted perimeter of the flow.

As an example, suppose we consider flow through a bundle of circular fuel elements of diameter $d$ and square pitch $p$. Then one defines the equivalent hydraulic diameter by locating a unit cell and calculating $S$ and $Z$ for this cell as $S = p^2 - \pi d^2/4$, $Z = \pi d$ (see Figure 12-7). Hence for this geometry, we find

$$D_h = d\left[\frac{4}{\pi}\left(\frac{p}{d}\right)^2 - 1\right]. \tag{12-35}$$

The hydraulic diameter for triangular lattice geometries is given in Figure 12-7.



Square lattice

$$D_h = d\left[\frac{4}{\pi}\left(\frac{p}{d}\right)^2 - 1\right]$$

Triangular lattice

$$D_h = d\left[\frac{2\sqrt{3}}{\pi}\left(\frac{p}{d}\right)^2 - 1\right]$$
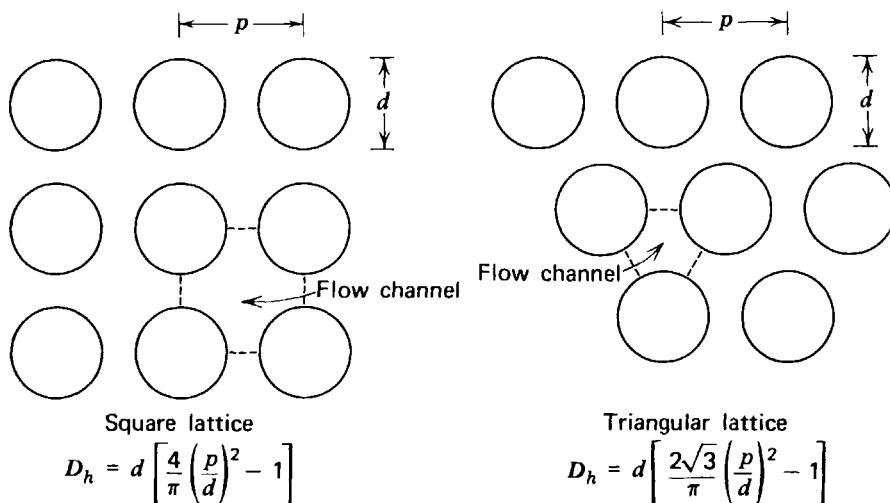
FIGURE 12-7. Typical coolant channels.

In summary then, one can use Eq. (12-30) and corresponding expressions for $f$ and $D_h$ to calculate the pressure drop for either laminar or turbulent flow of a fluid in a channel, such as for a coolant passing through a reactor core. We will utilize these results later when we discuss the hydraulic analysis of coolant flow in a reactor core. However we will first turn to an investigation of heat transfer from a surface to a moving fluid.

## B. Forced Convection Heat Transfer

We have indicated that coolant flow in nuclear reactor cores is highly turbulent. This turbulence tends to greatly enhance heat transfer from the clad surface to the coolant over that which would be present if the flow were laminar. However the complexity of fluid turbulence once again forces us to rely on various

empirical correlations for calculating quantities such as the convective heat transfer coefficient $h_s$.

The convective heat transfer coefficient $h_s$ is usually expressed in terms of the thermal conductivity of the fluid $k$, the hydraulic diameter of the channel $D_h$, and a dimensionless parameter Nu

$$h_s = (k/D_h)\text{Nu} \tag{12-36}$$

where Nu is known as the *Nusselt number* which characterizes both the physical properties of the fluid and the dynamical characteristics of its flow. For a flow that is laminar with a constant wall heat flux passing into the fluid, one can solve the equations of hydrodynamics[8-10] to calculate $\text{Nu} = 48/11 = 4.364$. For turbulent flow, one must again rely on empirical correlations to determine Nu (in the same fashion as we used the Blasius formula to determine the friction factor $f$). Fortunately one can use dimensional analysis to find that the Nusselt number can at most be a function of two other dimensionless parameters, the Reynolds number Re which characterizes the conditions of the flow, and a new parameter, the *Prandtl number* Pr,

$$\text{Pr} = \mu c / k, \tag{12-37}$$

which characterizes the physical properties of the coolant fluid.

Several of the more common correlations for the Nusselt number (and hence the convective heat transfer coefficient, $h_s$) are tabulated in Table 12-2 for various ranges of Prandtl numbers. The most common such correlations used in reactor analysis are the *Dittus-Boelter correlation*, which characterizes fluids with $\text{Pr} \sim 1$ such as water or helium

$$\text{Nu} = 0.023 \, \text{Pr}^{0.4} \, \text{Re}^{0.8}, \tag{12-38}$$

and the *Lyon-Martinelli correlation*, which characterizes liquid metals subject to a constant-wall heat flux:

$$\text{Nu} = 6.3 + 0.030 \, (\text{Re Pr})^{0.8}. \tag{12-39}$$

TABLE 12-2: Common Forced Convection Correlations[15]

| | |
|---|---|
| Pr < 0.1 (liquid metals) | |
| $\text{Nu} = 6.3 + 0.03 \, (\text{Re Pr})^{0.8}$ | (constant heat flux) |
| $\text{Nu} = 4.8 + 0.03 \, (\text{Re Pr})^{0.8}$ | (constant temperature) |
| 0.5 < Pr < 1.0 | |
| $\text{Nu} = 0.022 \, \text{Pr}^{0.6} \, \text{Re}^{0.8}$ | (constant heat flux) |
| $\text{Nu} = 0.021 \, \text{Pr}^{0.6} \, \text{Re}^{0.8}$ | (constant temperature) |
| 1.0 < Pr < 20 (water and light liquids) | |
| $\text{Nu} = 0.023 \, \text{Pr}^{0.4} \, \text{Re}^{0.8}$ | |
| Pr > 20 (oils and other viscous liquids) | |
| $\text{Nu} = 0.0118 \, \text{Pr}^{0.3} \, \text{Re}^{0.9}$ | |

## C. Choice of Reactor Coolants

With the preceding discussion of the analysis of fluid flow and heat transfer serving as a background, let us now turn briefly to the considerations involved in choosing a reactor coolant. From a nuclear standpoint, one desires coolants with low neutron absorption cross sections, low induced radioactivity, good radiation

stability, and, depending on whether one is concerned with thermal or fast reactors, strong or weak moderating properties. And, of course, one desires high heat transfer coefficients, low pumping losses, and low cost.

Clearly, two of the characteristics of greatest concern are the magnitude of the heat transfer coefficient $h_s$ and the size of the pumping power required to pump the coolant through the primary coolant loop (reactor core, piping, heat exchangers, etc.). The value of the heat transfer coefficient depends on many factors, such as the geometrical shape of the channel, the flow rate, the heat flux, the temperature, as well as the physical properties of the coolant itself. The pumping power can be estimated in terms of the pressure drop $\Delta p$ across the core as

$$\text{pumping power} = \Delta p A_c \bar{u}_z, \qquad (12\text{-}40)$$

where $A_c$ is the cross-sectional flow area and $\bar{u}_z$ is the mean flow velocity.

In order to evaluate the suitability of various candidates for reactor coolants, we have compared a number of thermal and hydraulic parameters characterizing typical coolants in Table 12-3.

TABLE 12-3:   Physical Properties of Some Typical Coolants

| Coolant | $T_{inlet}$ [°C] | $\Delta T_{core}$ [°C] | Pressure [bar] | $\Delta p_{core}$ [bar] | $\bar{u}_z$ [cm/sec] | Density [g/cm³] | $h_s$ [W/cm²°K] |
|---|---|---|---|---|---|---|---|
| $H_2O$ | 300 | 20 | 100 | 2 | 400 | .70 | 2.8–4.5 |
| He | 500 | 400 | 40 | 1 | 16,000 | .0024 | .005–.05 |
| Na | 400 | 150 | 10 | 10 | 400 | .85 | 2.2–5.5 |

Clearly in terms of these quantities, liquid metals would make the best coolants. However there are of course, a number of nuclear advantages in coolants such as water that often outweigh the heat transfer capability of liquid metals (e.g., moderating power). One should also note here the very high flow rates required in order for a gas coolant to achieve a heat-transfer capability comparable to that of a liquid. Such flow rates require rather large pumping powers. Indeed in an HTGR roughly 5–10% of the power output is required just to pump the coolant through the core. As another example, the height of an LMFBR core is to a large degree determined by the allowable pressure drop across the core ($\sim 10$ bar) which can be handled by the primary pumps.

We will return later to compare the more detailed thermal–hydraulic analysis of each of the principal reactor types. For now, however, we will proceed to discuss the determination of axial temperature distributions in a reactor core cooled by a single-phase coolant.

## D. Axial Temperature Distributions

Consider now the determination of the axial temperature distribution in a channel containing a single-phase coolant. For purposes of illustration, we will first assume that the axial power distribution is that characterizing a bare, homogeneous cylindrical core and given by Eq. (12-1). For more general axial power distributions, one will usually have to resort to numerical methods such as those discussed later in this chapter.

We will consider a *coolant channel* in the reactor to be defined as the flow area

associated with one fuel element. As Figure 12-7 indicates, such channels are rarely circular in cross-section. However by using an equivalent hydraulic diameter, we can apply our earlier analysis.

To compute the temperature of the coolant as it passes up the coolant channel, we simply perform an energy balance by equating the heat energy gained by the coolant to that produced in the fuel and passed through the channel walls over a small distance $dz$

$$w c_p dT = q''(2\pi r_F) dz = q'(z) dz, \tag{12-41}$$

where $w$ is the mass flow rate and the linear power density is just

$$q'(z) = q_0' \cos(\pi z / \tilde{H}) \tag{12-42}$$

$$\text{where} \quad q_0' = \pi r_F^2 w_f \Sigma_f \phi_0 J \, (2.405 \, r_f / \tilde{R}).$$

It should be noted that by restricting ourselves to a single-phase coolant we have assumed that all the heat is absorbed as sensible heat and that no coolant phase change is allowed to occur in the channel. In the more general case, we would use the specific enthalpy $h$ (or energy content per unit mass of coolant) to write the energy balance [Eq. (12-41)] as simply

$$w \, dh = q'(z) dz. \tag{12-43}$$

We can now integrate Eq. (12-41) up the channel from the coolant inlet at $z = -H/2$ to find

$$w c_p \int_{T_{\text{inlet}}}^{T_{fl}} dT = q_0' \int_{-H/2}^{z} dz' \cos\left(\frac{\pi z'}{\tilde{H}}\right), \tag{12-44}$$

or

$$T_{fl}(z) - T_{\text{inlet}} = \frac{q_0' \tilde{H}}{\pi c_p w} \left[ \sin\left(\frac{\pi z}{\tilde{H}}\right) + \sin\left(\frac{\pi H}{2 \tilde{H}}\right) \right]. \tag{12-45}$$

In particular, the exit coolant temperature is given by

$$T_{\text{exit}} - T_{\text{inlet}} = \frac{2 q_0' \tilde{H}}{\pi c_p w} \sin\left(\frac{\pi H}{2 \tilde{H}}\right) \sim \frac{2 q_0' \tilde{H}}{\pi c_p w} \quad \text{for } \tilde{H} \sim H. \tag{12-46}$$

[For example, in a LWR, $(\tilde{H} - H)/H \sim 20$ cm$/366$ cm$\sim .06$.] We have now evaluated the coolant temperature distribution at any point $z$ in the channel:

$$T_{fl}(z) = T_{\text{inlet}} + \frac{q_0' \tilde{H}}{\pi c_p w} \left[ \sin\left(\frac{\pi z}{\tilde{H}}\right) + \sin\left(\frac{\pi H}{2 \tilde{H}}\right) \right]. \tag{12-47}$$

Hence using our earlier work on thermal conduction in radial fuel elements, we can work back to calculate the temperatures in the clad and fuel by simply adding on the relevant temperature differences, say, as given by Eq. (12-27). We have plotted the axial temperature profile of the various fuel element temperatures in Figure

12-8. It should be noted that while the power density in a bare, uniform core peaks at the midplane ($z = 0$), the fuel element temperatures peak somewhat above this point for the simple cosine axial power distribution.
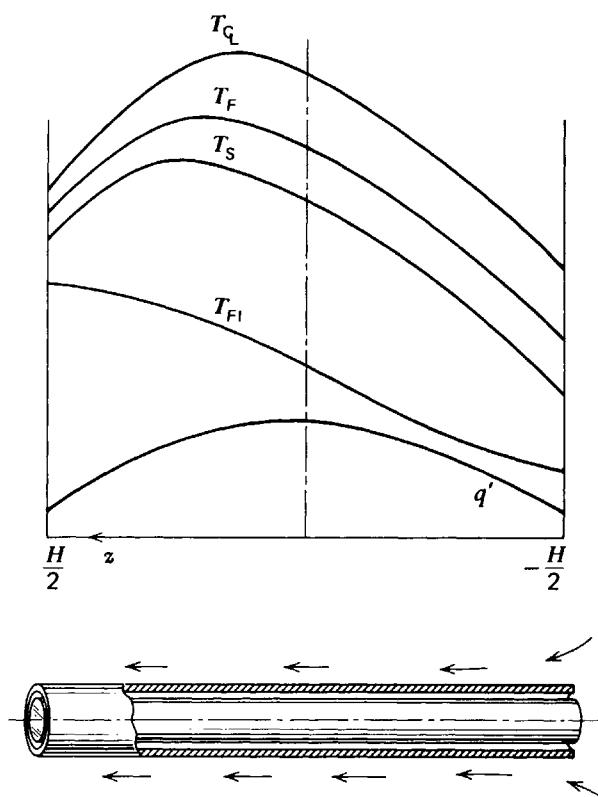


FIGURE 12-8. Axial temperature distributions for a cylindrical fuel element.

It is important to keep in mind the limited validity of the above calculations. In general, the axial power profile in a reactor core is not of the form given by Eq. (12-42) due to fuel and moderator density variations. Furthermore, we have assumed in our analysis that the thermal parameters such as $h_s$ and $c_p$ are constant when in fact they may vary considerably as one passes up the coolant channel. Finally, we have ignored the possibility of coolant phase change which can very strongly modify these temperature profiles.

# V. BOILING HEAT TRANSFER IN NUCLEAR REACTORS

## A. Introduction

Thus far we have restricted our analysis of heat transfer between the clad surface and the coolant to situations in which there is no phase change. However many types of power reactors are designed to operate so that there will, in fact, be localized boiling at the clad surface, since boiling heat transfer is usually the most efficient heat transfer mechanism. Such localized boiling does not necessarily lead to bulk boiling of the coolant, however. For example, in a PWR, the clad surface temperature is allowed to exceed the saturation temperature of the coolant. However although small vapor bubbles will form on the clad surface, they quickly

collapse as they leave this surface. This phenomenon, known as *subcooled boiling*, is an extremely efficient heat transfer mechanism.

By way of contrast, in a BWR the bulk coolant temperature is allowed to exceed the saturation temperature. *Bulk* or *saturated boiling* occurs and results in appreciable vapor (steam) formation within the core.

The primary form of boiling heat transfer used in nuclear reactors is so-called *nucleate boiling*, in which many small bubbles form around small nucleation points on the clad surface and then break away into the coolant. It is desirable to operate in the nucleate boiling regime since this is the most efficient form of heat transfer. Indeed the efficiency of heat transfer in the nucleate boiling regime is so high that the clad surface temperature will rise no more than 3–6°C above the fluid saturation temperature in a LWR.

There are disadvantages accompanying nucleate boiling heat transfer, however. The pressure drop associated with this mechanism is somewhat larger than that characterizing single-phase heat transfer. But even more serious is the fact that heat transfer instabilities may set in. One must take care that the heat flux does not become sufficiently large that the small bubbles formed in nucleate boiling coalesce into a vapor film that covers the surface, since then the heat transfer efficiency drops dramatically, and the clad surface temperature will rise by several hundred degrees. This situation is known as the *departure from nucleate boiling* (DNB) and will be discussed in greater detail later.

In this section we will briefly discuss several more general aspects of boiling heat transfer, and then we will introduce the various methods used to analyze this phenomenon in thermal core analysis.

## B. Boiling Heat Transfer

Suppose we first consider a heating element submerged in a pool of stationary fluid. A sketch of the heat flux transferred from the heating surface to the fluid versus the temperature difference between the surface and the bulk fluid temperature is shown in Figure 12-9.[15] From this sketch it is evident that one can distinguish several different regions of heat transfer.

0–a: There is little liquid superheat; heat transfer is by natural convection.

a–b: A few bubbles are formed but collapse after leaving the surface (although agitation will increase heat transfer).

a–c: The number of bubbles formed increases rapidly—this is the *nucleate boiling* regime.

c: "Burnout" point or DNB is reached.

c–d: Bubbles become so numerous that they begin to coalesce and clump near the heating surface (the vapor covering the surface acts as a heat insulator)—this is known as *partial nucleate boiling*.

d–e: A continuous blanket of vapor forms over the heating surface—*film boiling* regime.

e–f: Thermal radiation from the surface comes into play—*film* and *radiation* regime.

It should particularly be noted that if the heat flux $q''$ is the independent variable, then increasing $q''$ beyond the DNB point will result in a large increase in the surface temperature for a given coolant temperature (see Figure 12-9.) This phenomenon is known as *burnout* and must be avoided in reactor operation.
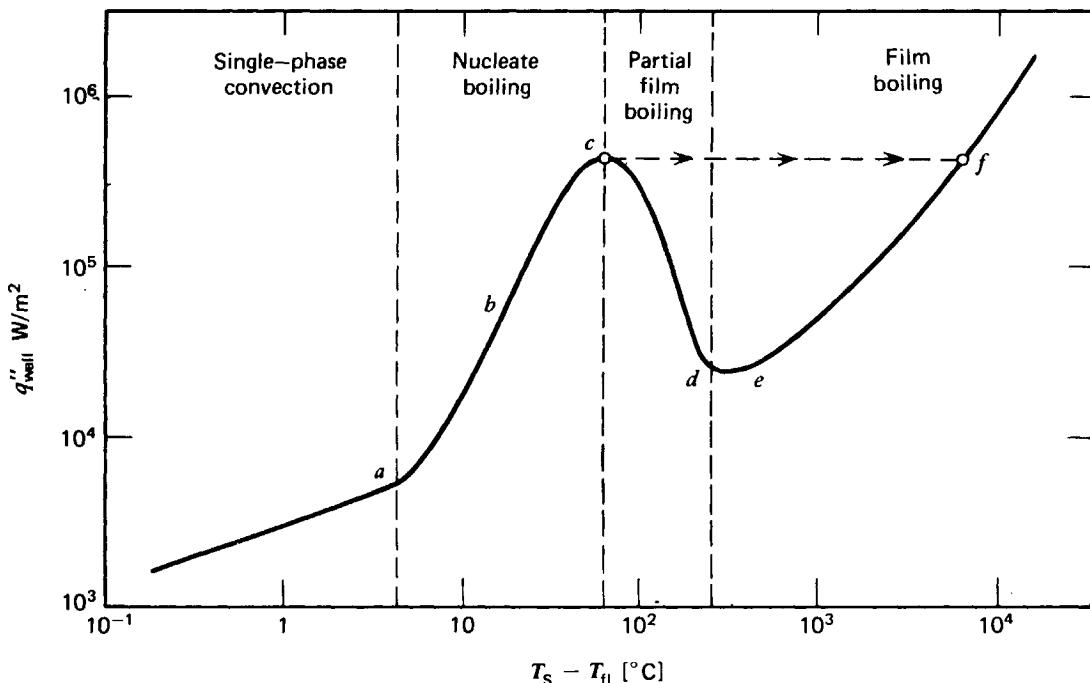
**FIGURE 12-9.**   Heat flux versus temperature difference for pool-boiling heat transfer.

These concepts also apply in a flowing channel. Suppose we consider a channel with a uniform wall heat flux $q''_{wall}$. Then one will find temperature profiles up the channel as shown in Figure 12-10. Once again we can distinguish several regions of heat transfer:
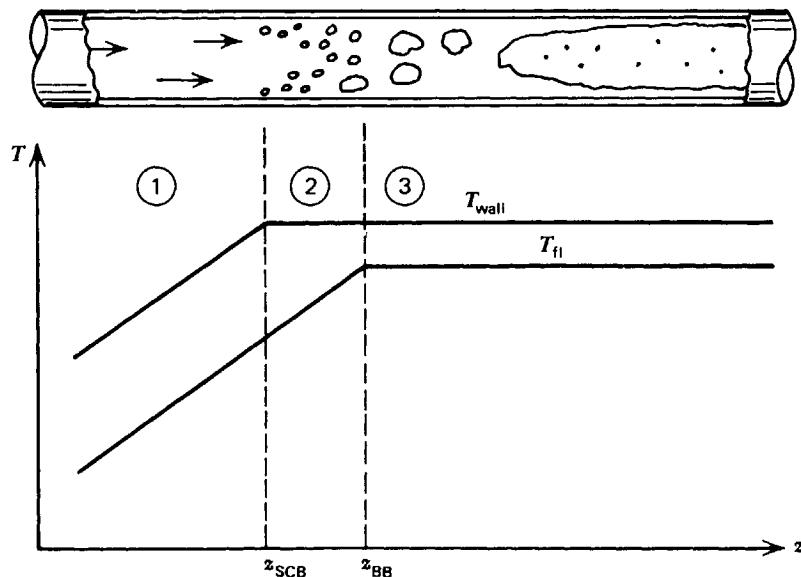


**FIGURE 12-10.**   Boiling-channel temperature profiles.

(1)  Region ①: Single-phase convection.

In this region, we can use the analysis we developed in the previous section to determine the convective heat-transfer coefficient $h_s$ arising in Newton's law of cooling

$$q'' = h_s(T_S - T_{fl}). \qquad (12\text{-}48)$$

For example, for turbulent flow one customarily would use the Dittus-Boelter equation (12-38) to determine Nu and hence $h_s$. For

such single-phase forced convection, $h_s$ is relatively constant for fixed values of coolant velocity, fuel geometry, and coolant properties. Since the coolant flow is outside and parallel to the fuel elements, one must use the equivalent hydraulic diameter in this expression.

(2) Region ②: Subcooled boiling: $T_S \geqslant T_{sat}$ but $T_{fl} < T_{sat}$.

Once the clad surface temperature reaches the saturation temperature of the coolant, the temperature drop is no longer linear in the heat flux. In this region, the heat transfer process is extremely efficient, and the temperature difference is quite small compared to the other temperature differences in the core. In LWRs it is customary to use an empirical correlation developed by Jens and Lottes[16] in order to calculate the temperature difference between the clad surface and the coolant:

$$\Delta T|_{COOL} = T_S - T_{fl} = 45 \exp\left(\frac{-p}{62}\right)(q'')^{0.25}, \qquad (12\text{-}49)$$

where $p$ is the pressure in units of bar and $q''$ is the heat flux in units of $MW/m^2$. This correlation is valid for pressures, temperatures, and coolant flow rates characteristic of both PWRs and BWRs. For example, in a PWR at 155 bar with a heat flux of $1.5 \times 10^6$ $W/m^2$, one would find a temperature difference of only $3°C$. There will be very little change in the temperature difference with heat flux in this boiling regime. Once the clad surface temperature reaches the saturation temperature of the coolant, it tends to remain near that level unless the heat flux reaches the DNB value.

One can use these relationships to determine the position $z_{SCB}$ at which subcooled boiling begins. We equate $T_{fl} = T_{sat}$ in Eq. (12-49):

$$T_S - T_{sat} = 45 \cdot \exp\left(\frac{-p}{62}\right)(q'')^{0.25}. \qquad (12\text{-}50)$$

Then noting also that

$$q'' = h_s(T_S - T_{fl}), \qquad (12\text{-}51)$$

we can find

$$T_{fl}|_{z_{SCB}} = T_S - \frac{q''}{h}$$

$$= T_{sat} + 45 \exp\left(\frac{-p}{62}\right)(q'')^{0.25} - \frac{q''}{h_s} \qquad (12\text{-}52)$$

and then solve this for the position $z_{SCB}$.

(3) Region ③: Saturated or bulk boiling: $T_{fl} = T_{sat}$.

Eventually sufficient heat is transferred to the coolant that it reaches its saturation temperature and begins bulk boiling. Subsequent heat addition will cause further boiling, and hence the coolant temperature will remain essentially constant and equal to $T_{sat}$ up the remainder of the channel.

## C. Two-Phase Flow

When the coolant is a two-phase mixture of liquid and vapor, the coolant flow pattern can become quite complicated. One can distinguish several types of two-phase flow, as shown in Figure 12-11. It is useful to introduce some definitions characterizing the vapor content of a coolant at rest:

$$\text{Static quality} \equiv \chi_s \equiv \frac{\text{mass of vapor in mixture}}{\text{total mass of mixture}},$$

$$\text{Void fraction} \equiv \alpha \equiv \frac{\text{volume of vapor in mixture}}{\text{total volume of liquid-vapor mixture}}. \tag{12-53}$$

We can compute these quantities in terms of the cross-sectional areas in the channels occupied by liquid $(A_l)$ and vapor $(A_g)$. The void fraction is given by

$$\alpha = \frac{A_g}{A_g + A_l}, \tag{12-54}$$
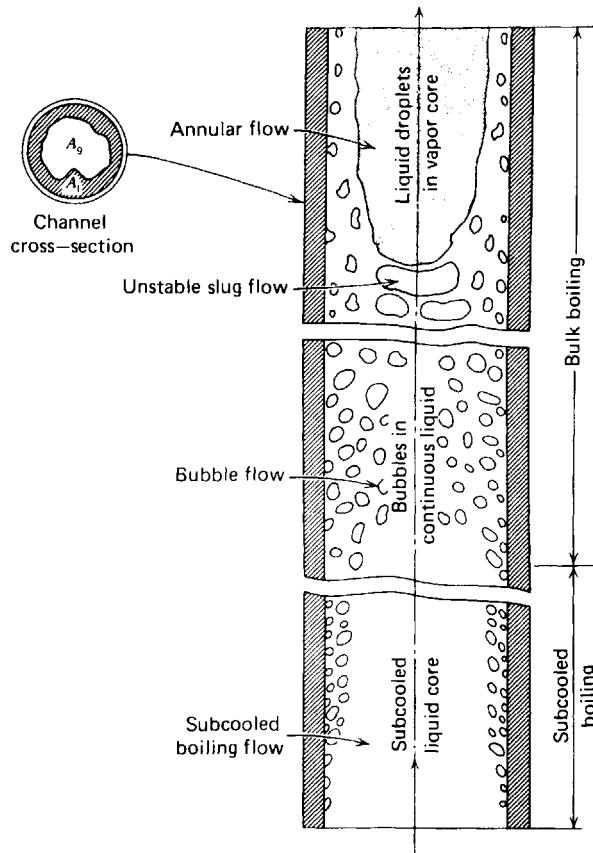


**FIGURE 12-11.   Flow patterns in a heated channel.**

while the static quality is

$$\chi_s = \frac{\rho_g A_g}{\rho_g A_g + \rho_l A_l} = \frac{1}{1 + \dfrac{\rho_l A_l}{\rho_g A_g}} = \frac{1}{1 + \dfrac{\rho_l}{\rho_g}\left(\dfrac{1-\alpha}{\alpha}\right)}. \tag{12-55}$$

For example, the void fraction is given for water at various qualities and pressures in Figure 12-12.
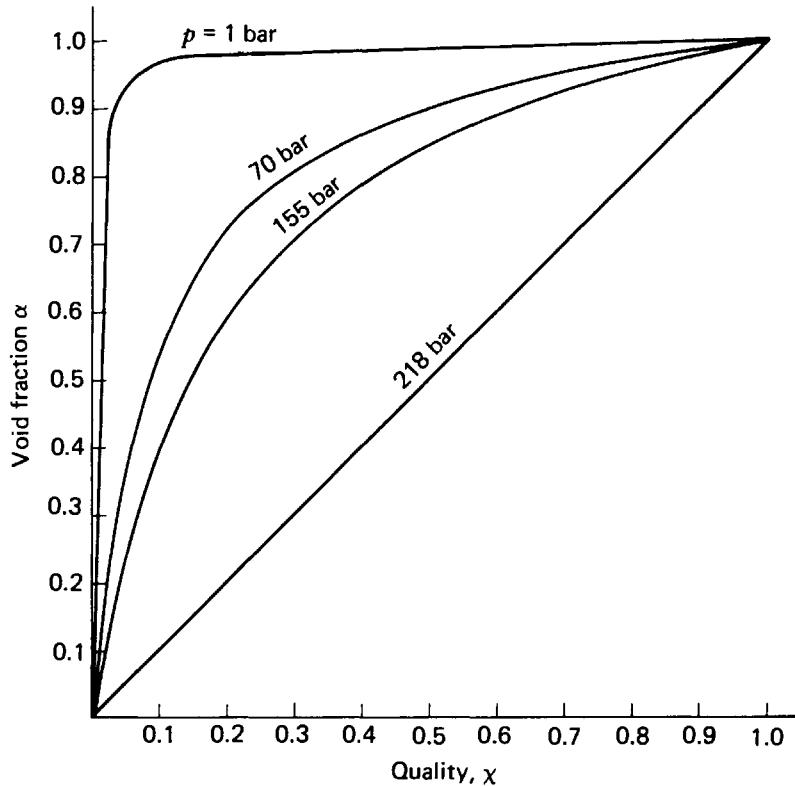
FIGURE 12-12.  Void fraction versus quality for bulk boiling.

It is also useful to express the specific enthalpy $h$ in terms of quality. First recall that for a single-phase fluid

$$h = h_f(T) = \int_{T_{melt}}^{T} dT' c_p(T').$$
(12-56)

If we denote the heat of vaporization of a liquid as $h_{fg}$, then the enthalpy of a saturated vapor at $T_{sat}$ is just

$$h_g(T_{sat}) = h_f(T_{sat}) + h_{fg}.$$
(12-57)

If we have a mixture of liquid and vapor, then the enthalpy of the mixture is just

$$h_{mixture} = (1 - \chi_s)h_f(T_{sat}) + \chi_s h_g(T_{sat})$$

$$= h_f(T_{sat}) + \chi_s h_{fg}.$$
(12-58)

We can actually turn this around to compute the quality in terms of the enthalpy as

$$\chi_s = \frac{h_{mixture} - h_f(T_{sat})}{h_{fg}}.$$
(12-59)

(Note Eq. (12-59) can be used to define a negative quality.) Typical values of enthalpy for various temperatures and pressures are given in Table 12-4 for illustration.[17]

**TABLE 12-4  Thermodynamic Data on Steam**

| $P$(bar) | $T_{sat}[°C]$ | $h_f[MJ/kg]$ | $h_{fg}[MJ/kg]$ | $c_p$ | $X_s$ | $\rho_l/\rho_g$ | $\alpha$ |
|----------|---------------|--------------|-----------------|-------|-------|-----------------|----------|
| 1 | 100 | .419 | 2.26 | 4.186 | .1 | 1602 | .995 |
| 70 | 285 | 1.26 | 1.51 | 5.44 | .1 | 20.6 | .7 |
| 155 | 345 | 1.68 | .96 | 7.95 | .1 | 5.9 | .4 |
| 218 | 373 | 2.10 | 0 | ~62 | .1 | 1 | .1 |

When the two-phase mixture is flowing, we must be more careful in our definitions since the vapor has a tendency to slip past the liquid because of its bouyancy. We then must define the quality in terms of a parameter $S$ known as the *slip ratio* which relates the different flow velocities:

$$\text{Slip ratio} \equiv S \equiv v_g/v_l. \tag{12-60}$$

Then we can define a *flow quality*

$$\chi = \frac{\text{mass flow rate of vapor}}{\text{total mass flow rate}} = \frac{w_g}{w_g + w_l}$$

$$= \frac{A_g\rho_g v_g}{A_g\rho_g v_g + A_l\rho_l v_l} = \frac{1}{1 + \dfrac{\rho_l}{\rho_g}\dfrac{A_l}{A_g}\dfrac{v_l}{v_g}} \tag{12-61}$$

or

$$\chi = \frac{1}{1 + \dfrac{\rho_l}{\rho_g}\left(\dfrac{1-\alpha}{\alpha}\right)\dfrac{1}{S}}. \tag{12-62}$$

One can invert this to write the void fraction $\alpha$ as

$$\alpha = \frac{1}{1 + \dfrac{\rho_g}{\rho_l}\left(\dfrac{1-\chi}{\chi}\right)S}. \tag{12-63}$$

This latter equation is sometimes known as the "$S - \alpha - \chi$" relationship.

## D. Heat Addition to Boiling Flow

Consider now a fluid flowing through a channel adjacent to a fuel element generating a linear power density $q'(z)$. Then we can write the energy balance for the fluid as

$$w\,dh = q'(z)dz. \tag{12-64}$$

If we integrate this in the usual manner, we can find the enthalpy at any point in the coolant channel as

$$h(z) = h_{inlet} + \frac{1}{w}\int_0^z q'(z)dz. \tag{12-65}$$

Now suppose that bulk boiling begins at a point $z_{BB}$ up the channel; that is, up to $z_{BB}$ the coolant temperature rises to $T_{sat}$. Above $z_{BB}$, there is no further temperature change, but instead vapor formation occurs. We can determine $z_{BB}$ from Eq. (12-65) by solving

$$h_f(T_{sat}) = h_{inlet} + \frac{1}{w} \int_0^{z_{BB}} q'(z)\,dz \qquad (12\text{-}66)$$

for $z_{BB}$. Now for $z > z_{BB}$, the heat addition will cause a phase change. Then one finds from Eq. (12-58) that the enthalpy can be expressed in terms of the flow quality as

$$h(z) = h_{mixture} = h_f(T_{sat}) + \chi(z)h_{fg}, \qquad z > z_{BB}. \qquad (12\text{-}67)$$

If we combine Eqs. (12-66) and (12-67), we find that the quality at any point $z > z_{BB}$ in the channel can be written as

$$\chi(z) = \frac{1}{w h_{fg}} \int_{z_{BB}}^{z} q'(z)\,dz, \qquad z > z_{BB}. \qquad (12\text{-}68)$$

Once we know $\chi(z)$, then we can determine the void fraction $\alpha(z)$ provided we know the slip ratio $S(z)$. In general, $S$ has a value of about 1 near $z_{BB}$ and tends to increase from this value to a maximum of about 3 as one passes up the channel.

A knowledge of the void fraction is essential to the nuclear analysis of the core, since $\alpha$ determines the coolant density and hence the macroscopic cross section of the coolant. We will later find that there is a very strong coupling between the thermal core behavior which determines $\alpha(z)$ and the axial flux profile in reactor cores in which boiling occurs. As we mentioned earlier, the void fraction is extremely important in the calculation of the void coefficient of reactivity. There is very strong coupling between the thermal core behavior which determines $\alpha(z)$ and the axial flux profile in boiling water reactors.

## E. Flow Boiling Crisis or DNB

Our earlier discussion of boiling heat transfer indicated that if the wall heat flux exceeded a certain magnitude, there would be an unstable transition from nucleate boiling to film boiling with a corresponding increase in wall surface temperature. This "boiling crisis," in which the clad surface temperature rises dramatically, corresponds to a sudden drop in the heat transfer coefficient $h_s$ due to a change in the boiling mechanism from nucleate to film boiling. The boiling crisis is known by a number of names, including *burnout, critical heat flux*, and DNB. Such a phenomenon in a flowing coolant is more complicated than a pool-boiling crisis due to the added effects of forced convention and bubble clouding that tend to shield the heat transfer surface. Flow instabilities can also complicate the situation. For example, a sudden drop in pressure can increase the local superheat and perhaps lead to DNB.

One should be a bit more careful in terminology here, since for low flow rates, one may not have nucleate boiling prior to exceeding the critical heat flux, and hence strictly speaking DNB does not occur. Furthermore the heat flux may be sufficiently low so that the subsequent temperature rise of the clad is still below melting or failure limits. (This might occur at high exit qualities in a BWR in which the wall heat flux was only of the order of $3 \times 10^5$ W/m$^2$.) However, in most power

reactors, the heat flux approaches $3 \times 10^6$ W/m$^2$, and exceeding the critical heat flux will almost certainly lead to clad failure.

The detailed mechanism involved in such a flow crisis is closely related to the flow pattern. There are basically two types of phenomenon of interest in nuclear reactor studies (see Figure 12-13):

(1) Subcooled or low-quality DNB: Here DNB can be caused by detachment of the bubble boundary layer. This is the type of DNB that one would design against in a PWR.

(2) Burnout in high-quality region: In this phenomenon, burnout occurs in a liquid film that covers the heat transfer surface. Such a process is of concern in BWRs. Burnout in the high-quality region will occur when the liquid film "dries out." This process is slow compared to subcooled DNB, since the high-velocity vapor core provides fairly good single-phase convection heat transfer.



Subcooled or low—quality DNB                    Burnout in high—quality regions
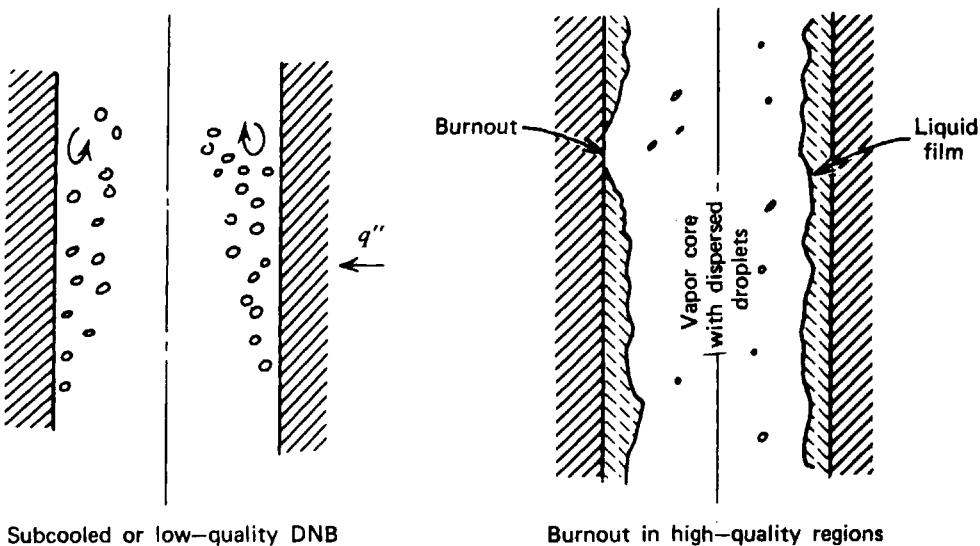
FIGURE 12-13.    Types of boiling-flow crisis.

It is extremely important to be able to determine the critical heat flux at which DNB will occur. Unfortunately this heat flux depends on a large number of factors, such as channel shape, surface condition, physical properties of the coolant, and flow conditions. Various empirical correlations based on experimental data have been developed for those ranges of conditions encountered in modern power reactors. However because of the complexity (and rapid obsolescence) of such correlations, we will refer the reader elsewhere for more information.[1,5,18,19]

The core designer must use such correlations to ensure that the critical heat flux is not exceeded during core operation. One usually defines the minimum ratio of the critical heat flux to the heat flux achieved in the core as the *DNB ratio* (DNBR) (see Figure 12-14),

$$\text{DNBR} \equiv \frac{q''_{\text{DNB}}(z)}{q''(z)} .$$                    (12-69)

One must design the reactor core so as to prevent the DNBR from dropping below
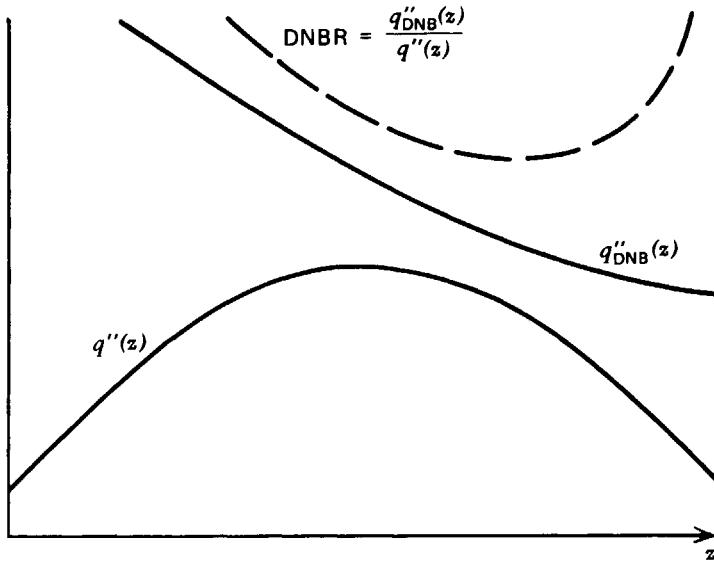
FIGURE 12-14. Critical heat flux in a uniformly loaded core.

a chosen value under a high heat flux transient condition for the most adverse set of mechanical and coolant conditions. For example, in PWRs a common constraint is to maintain $DNBR > 1.3$ in the event of a 115% overpower condition.[7]

## F. Axial Temperature Distributions

Thus far we have confined our discussion of axial temperature distributions to channels containing a single-phase coolant. Let us now consider how such temperature distributions would be altered when coolant boiling is present. First consider the "hot" channel of a PWR in which nucleate boiling occurs. The coolant enters the channel with a temperature $T < T_{sat}$. After passing some distance up the channel, the clad surface temperature reaches $T_{sat}$ (although the bulk coolant temperature $T_{fl}$ remains below $T_{sat}$ throughout the channel), and nucleate boiling heat transfer begins. Such heat transfer is so efficient that the clad surface temperature remains essentially constant the rest of the way up the channel (see Figure 12-15a).[3]

Consider now a coolant channel in a BWR. Once again the coolant enters below saturation temperature, and the clad surface temperature will eventually reach $T_{sat}$ before the bulk coolant temperature. However further up the channel the coolant reaches saturation, and additional heat added to the channel increases its quality (see Figure 12-15b)[3]. Both the coolant and clad surface temperatures will remain essentially constant after boiling begins.

We should again insert a disclaimer concerning these diagrams which have been sketched for a simple cosine power profile. As we have mentioned, the coolant density variations will affect core multiplication and hence the shape of the power profile. As we will see later, in LWRs the fact that the coolant density is higher near inlet tends to shift the axial power peak toward the bottom (inlet) of the core.

## VI. HYDRODYNAMIC CORE ANALYSIS

The thermal performance of a reactor core will depend strongly on coolant flow behavior. For example, higher coolant flow rates will lead to better heat

Temperature profiles in a PWR
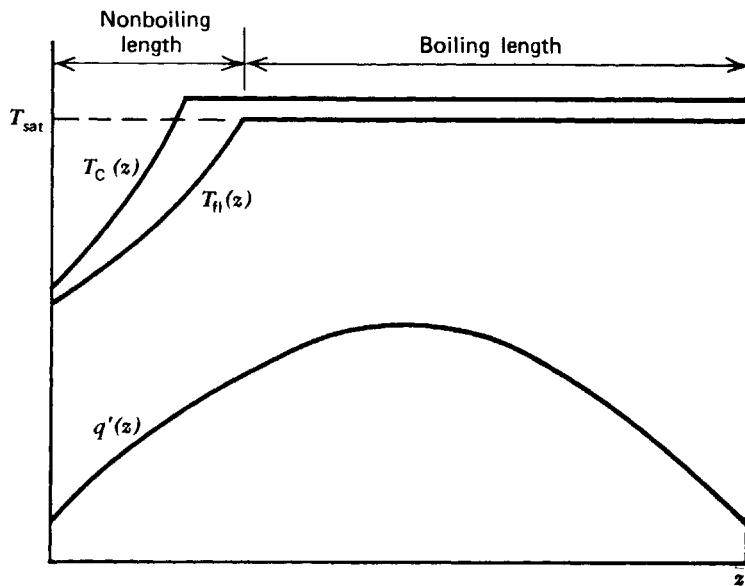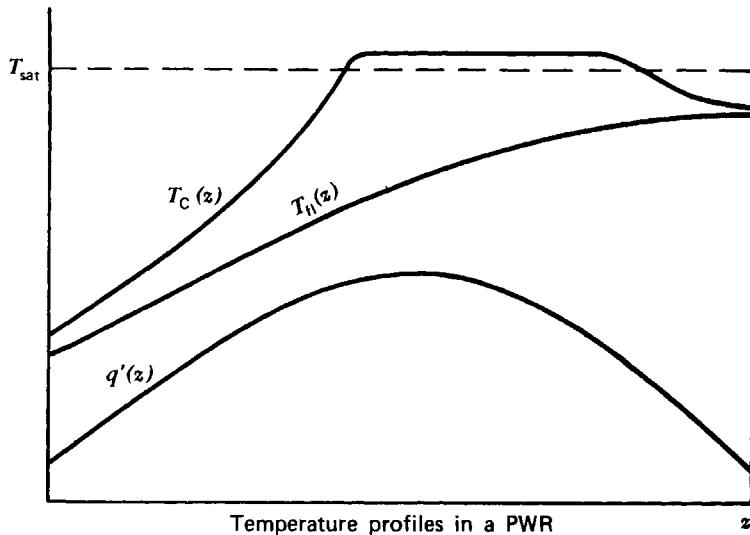


FIGURE 12-15. Temperature profiles in a BWR.

transfer coefficients and higher critical heat flux limits. However higher flow rates will also result in larger pressure drops across the core, hence larger required pumping powers and hydrodynamic stresses on core components.

A very important aspect of nuclear reactor core analysis involves the determination of the coolant flow distribution and pressure drop across the core. Since the flow in a reactor core is highly turbulent, we are forced to employ once again various empirical correlations in order to analyze the coolant hydrodynamic behavior.

## A. Single-Phase Coolant Pressure Drops

One can identify several mechanisms that will cause a pressure drop along the coolant channel: (a) friction losses from the fuel rod bundle (channel friction), (b) friction losses from the spacer grids used to maintain fuel assembly geometry, (c) friction losses at the core inlet and exit flow plenum (contraction or expansion), and (d) elevation. We will study each of these components in turn.

Consider first the pressure drop due to channel friction. Here we can use the result Eq. (12-30) involving the friction factor

$$\Delta p|_{\text{friction}} = 2\left(\frac{L}{D_{\text{h}}}\right)\rho \, \overline{u_z}^2 f, \tag{12-70}$$

where $L$ is the total channel length and $D_{\text{h}}$ is its hydraulic diameter. In most cases one can calculate $f$ using the Blasius formula, Eq. (12-33).

Another source of pressure drop important in most reactor types is caused by the spacer grids that bind the fuel elements into a fuel bundle (see Figure 3-7). There is an additional pressure loss associated with the coolant inlet and exit. Friction losses due to spacer grids or inlet or exit geometry are classified as *form losses*, since they correspond to a change in the coolant momentum due to a change in the coolant channel geometry. One usually writes

$$\Delta p|_{\text{form}} = \Delta p|_{\text{grids}} + \Delta p|_{\substack{\text{inlet} \\ +\text{exit}}} = \sum_i K_i \rho \frac{\overline{u_z}^2}{2} \tag{12-71}$$

where $K_i$ is a *form friction factor* due to a change in the coolant channel cross-sectional area of the $i$th type. $K_i$ is quite complicated for spacer grids and must be determined experimentally for each spacer grid design. The typical $K_{\text{TOTAL}}$ range is 0.6–1.2.

The final component is the pressure drop due to coolant elevation as it passes up the core

$$\Delta p|_{\text{elevation}} = \int_{-H/2}^{H/2} \rho(z) \, g \, dz. \tag{12-72}$$

For purposes of illustration, we have tabulated typical values of each of these pressure drop components for several reactor types in Table 12-5. We have also included in this table the pressure drop across the entire pressure vessel (which essentially determines the pumping power requirements in the primary loop).

**TABLE 12-5: Typical core pressure drops**

| Reactor Type | $\Delta p_{\text{friction}}$ | $\Delta p_{\text{form}}$ | $\Delta p_{\text{gravity}}$ | $\Delta p_{\text{acc}}$ | $\Delta p_{\text{core}}$ | $\Delta p_{\text{vessel}}$ |
|---|---|---|---|---|---|---|
| PWR | .40 bar | .61 | .16 | — | 1.45 | 3.40 |
| BWR | .40 | .61 | .16 | .05 | 1.49 | 3.40 |
| HTGR | .134 | .03 | — | — | .16 | |
| LMFBR | 5.4 | .81 | .30 | — | 6.51 | 9.5 |

## B. Boiling Channel Pressure Drops

The pressure drop occurring in a boiling channel is somewhat different because of the phenomena involved in two phase flow. There is first an additional pressure drop due to the acceleration which accompanies the coolant-vapor forma-

tion and expansion[1,3]

$$\Delta p\big|_{\text{acc}} = \rho_l \overline{u_z}^2 \left[ \frac{(1-\chi)^2}{1-\alpha} + \frac{\chi^2}{\alpha}\frac{\rho_l}{\rho_g} - 1 \right].$$ (12-73)

The hydrostatic pressure drop must also be computed somewhat differently as

$$\Delta p\big|_{\text{elevation}} = \int_{-H/2}^{H/2} \left[ \alpha\rho_g + (1-\alpha)\rho_l \right] g\, dz.$$ (12-74)

Finally for two-phase flow a somewhat different friction and form pressure drop must be used. It is customary to modify the friction pressure drop by inserting a parameter $R_{\text{MN}}$ to write

$$\Delta p\big|_{2\text{-}\phi\ \text{friction}} = 2\left( \frac{L}{D_h} \right)\rho\, \overline{u_z}^2 f R_{\text{MN}}$$ (12-75)

where $R_{\text{MN}}$ is known as the *Martinelli–Nelson friction multiplier*,[20] which is a tabulated function of pressure and flow quality. In a BWR, $R_{\text{MN}}$ ranges from 1.0 ($\chi = 0$) to as high as 4 ($\chi = 20\%$).

The form losses can be written as

$$\Delta p\big|_{2\text{-}\phi\ \text{form}} = K_g \frac{\rho\, \overline{u_z}^2}{2} \left[ \frac{(1-\chi)^2}{1-\alpha} + \frac{\chi^2}{\alpha}\frac{\rho_l}{\rho_g} \right],$$ (12-76)

where $K_g$ is the appropriate form factor for two-phase flow.

It should be stressed that there is a large degree of uncertainty in these methods used for estimating coolant hydrodynamic behavior. The predictions of such analyses must usually be confirmed by experimental testing before they are applied in making detailed core design decisions.

## C. Multichannel Analysis

Our earlier single-channel analysis has not accounted for phenomena such as flow mixing between channels, which is caused by both turbulence and pressure gradients. Such mixing can lead to energy transfer between channels as well as pressure losses.

One could characterize coupling between channels by writing a generalized energy balance equation for a channel $m$

$$\underbrace{w_m \frac{dh_m}{dz}}_{\substack{\text{(axial mass} \\ \text{flow rate)}}} = \underbrace{w_{n \to m}(h_n - h_m)}_{\substack{\text{(cross flow} \\ \text{rate/length)}}} + \underbrace{\rho\epsilon(h_n - h_m)}_{\substack{\text{(mixing} \\ \text{coefficient)}}} + q'.$$ (12-77)

Here the cross channel coupling coefficients $w_{n \to m}$ and $\epsilon$ must be evaluated from empirical correlations based on experiment.

One can also have flow redistribution effects in the inlet plenum causing a nonuniform inlet velocity to each channel. Such flow redistribution could, in fact, lead to instabilities, and must be accounted for in more detailed core hydraulic analysis.[21]

## VII. THERMAL-HYDRAULIC CORE ANALYSIS

### A. Hot Channel Factors

One of the principal goals of the reactor designer is to ensure that none of the thermal limitations on the core behavior are exceeded. Thus far we have discussed two such limitations. First one must design the core so that the fuel centerline temperature does not exceed the fuel melting point. This limitation is usually expressed as a restriction on the linear power density

$$q'(\mathbf{r}) < q'_{max}[\ \sim 660 \ W/cm \ in \ UO_2 \ fuel \ elements]. \qquad (12\text{-}78)$$

Yet another limitation arises from requiring that the clad surface heat flux always remains below its DNB limit:

$$q''(\mathbf{r}) < q''_{DNB}[\ \sim 300 \ W/cm^2 \ in \ LWRs]. \qquad (12\text{-}79)$$

There are usually other thermal limitations placed on core performance. For example, thermal and fission gas stresses on the clad can limit power generation. Furthermore, thermal–hydraulic performance is also frequently limited by nuclear stability considerations (particularly in BWRs that experience an appreciable variation in moderator density throughout the core).

Certainly one approach to thermal-hydraulic analysis of the core would be to first perform a detailed three-dimensional calculation of the core power distribution, taking into account the effects of fuel burnup, fission product buildup, control distributions, and moderator density variations over core life. This information could then be used to determine the coolant flow and temperature distribution throughout the core. However, such a calculation is usually prohibitively expensive for routine design applications.

A more common approach is to investigate how closely the "hot channel" in the core approaches the operating limitations. Then if one can ensure that the thermal conditions of this channel remain below the core limitations, the remaining channels in the core will presumably fall within design limitations. One usually defines the hot channel in the core as that coolant channel in which the core heat flux and enthalpy rise is maximum. Associated with this channel are various "hot channel" or "hot spot" factors relating the performance of this channel to the average behavior of the core.

More precisely, we will define the *hot assembly* in a reactor core as that fuel assembly having the maximum power output. The *hot spot* in the core is the point of maximum heat flux or linear power density, while the *hot channel* is defined to be that coolant channel in which the hot spot occurs, or along which the maximum coolant enthalpy increase occurs.

We first will introduce the concept of *nuclear* hot channel factors, which take into account the variation of the neutron flux and fuel distribution within the core.

First, we define the *radial nuclear hot channel factor*

$$F_R^N = \frac{\text{average heat flux of the hot channel}}{\text{average heat flux of the channels in core}}$$

$$= \frac{\int_{-H/2}^{H/2} q''(\mathbf{r}_{HC})dz}{\frac{1}{I}\sum_{i=1}^{I}\int_{-H/2}^{H/2} q''(\mathbf{r}_i)dz} \quad \begin{array}{c}\text{for } I \text{ channels}\\ \text{(pins)}.\end{array} \tag{12-80}$$

One can similarly define the *axial nuclear hot channel factor*:

$$F_Z^N = \frac{\text{maximum heat flux of hot channel}}{\text{average heat flux of hot channel}}$$

$$= \frac{\max_z q''(\mathbf{r}_{HC})}{\frac{1}{H}\int_{-H/2}^{H/2} q''(\mathbf{r}_{HC})dz}. \tag{12-81}$$

The *total nuclear hot channel factor* or *nuclear heat flux factor* is then just

$$F_q^N = \frac{\text{maximum heat flux in the core}}{\text{average heat flux in the core}} = F_R^N F_Z^N. \tag{12-82}$$

By way of example, consider a homogeneous, bare cylindrical core described by a power distribution given by Eq. (12-1). We can then calculate

$$F_R^N = \frac{J_0(0)\int_{-H/2}^{H/2}\cos\left(\frac{\pi z}{H}\right)dz}{\int_0^R J_0\left(\frac{2.405r}{R}\right)2\pi r\,dr\int_{-H/2}^{H/2}\cos\left(\frac{\pi z}{H}\right)dz} = 2.32, \tag{12-83}$$

and

$$F_Z^N = \frac{\cos(0)J_0(0)}{\frac{1}{H}\int_{-H/2}^{H/2}\cos\left(\frac{\pi z}{H}\right)dz\,J_0(0)} = 1.57. \tag{12-84}$$

This implies an overall nuclear hot-channel factor of

$$F_q^N = (2.32)(1.57) = 3.638. \tag{12-85}$$

This is actually quite conservative. A zone-loaded PWR[22] will typically have a nuclear hot channel factor of $F_q^N = 2.6$.

The nuclear heat flux hot channel factor is defined assuming nominal fuel pellet and rod parameters. However, there will be local variations in enrichment, fuel-pellet density and diameter, surface area of fuel rod and eccentricity of the

fuel-clad gap, and so on due to manufacturing tolerances. The more general *heat flux hot channel factor* or *total power peaking factor* $F_q$ is defined as the maximum heat flux in the hot channel divided by the average heat flux in the core, allowing for these manufacturing tolerances.[1-3] One relates $F_q$ to $F_q^N$ by defining an *engineering heat flux hot-channel factor* $F_q^E$

$$F_q^E = \frac{F_q}{F_q^N} \tag{12-86}$$

that specifically accounts for manufacturing tolerances. Typically $F_q^E$ is close to unity (in a modern PWR, $F_q^E \sim 1.03$).

One can next define an *enthalpy-rise hot channel factor*

$$F_{\Delta H} \equiv \frac{\text{maximum coolant enthalpy rise}}{\text{average coolant enthalpy rise}}. \tag{12-87}$$

This factor is a function of both variations in the power distribution and coolant flow. For example, some 3-10% of the coolant flow bypasses the fuel assemblies, due to leaks past mechanical seals or the presence of other core components.[1-3] There will be nonuniformities in the coolant flow from channel to channel, although these are reduced somewhat by the lower inlet plenum. Flow mixing between coolant channels can also occur, as well as flow redistribution in which pressure variations due to coolant expansion or variations in nucleate boiling cause flow nonuniformities.

By way of example, we can calculate the enthalpy hot channel factor taking into account only the power variation in a bare, homogeneous cylindrical core:

$$\Delta h(r) = \frac{1}{w} \int_{-H/2}^{H/2} q'(r,z) dz = \frac{2HA}{\pi w} J_0\left(\frac{2.405r}{R}\right), \tag{12-88}$$

or

$$\overline{\Delta h} = \frac{1}{\pi R^2} \int_0^R \Delta h(r) 2\pi r \, dr = .862 \frac{HA}{\pi w}$$

or

$$F_{\Delta H} = \frac{\Delta h|_{max}}{\overline{\Delta h}} = 2.32. \tag{12-89}$$

The third hot channel factor occasionally introduced is that characterizing the clad surface temperature

$$F_{CS} = \frac{(T_{clad} - T_{coolant})_{max}}{(T_{clad} - T_{coolant})_{ave}}. \tag{12-90}$$

Actually this factor is usually of little interest in LWRs in which nucleate boiling keeps the clad surface temperature quite close to the coolant temperature. However, it can be of more significance in HTGRs and LMFBRs in which the temperature jump from the coolant channel surface to the coolant is much larger.

The concept of such hot channel factors greatly simplifies thermal core analysis, since it provides a mechanism for accounting for nonuniformities in a crude

single-channel analysis of the reactor core. However the use of hot channel factors has only a limited validity, and will fail when a more precise knowledge of core temperature and flow distributions is required. Indeed one might almost regard the popularity of such an approach as evidence of the crude state of predictive theories of thermal–hydraulic core behavior that must depend on numerous empirical correlations and experimental measurements to achieve adequate results. (In comparison to methods used in thermal–hydraulic core analysis, the reader would probably agree that the methods we have developed for the nuclear analysis of a reactor core look very rigorous and elegant indeed!)

## B. Determination of Reactor Core Size

It is instructive to use some of these ideas to examine how the thermal design influences the determination of the reactor core size. Let us break this discussion into several steps:

1 One first determines the various hot channel factors characterizing the core, using both computer codes describing the core neutronics and thermal–hydraulic behavior, as well as experience from earlier designs.

2 Next one determines the maximum acceptable power level in the hot channel, taking into account both steady-state and transient operating conditions. This is usually expressed in terms of a limit on linear power density

$$q'(z) < q'_{MAX} = q'_{AVE} F_q^N.$$ (12-91)

Hence the average linear power density is given in terms of this limiting value and the nuclear hot channel factor $F_q^N$.

3 The fuel-to-moderator volume ratio in the core and the fuel element radius $r_{FE}$ are largely determined by nuclear considerations. For a square lattice (Figure 12-7) one notes that

$$\frac{V_M}{V_F} = \frac{p^2 - \pi r_{FE}^2}{\pi r_F^2}.$$ (12-92)

Here of course the fuel-element radius must take into account the gap and clad thickness

$$r_{FE} = r_F + t_G + t_C.$$ (12-93)

One usually specifies the lattice geometry in terms of the pitch to diameter ratio $(p/2r_{FE})$. Typically this ranges between 1.2–1.5 for both LWRs and LMFBRs.

4 The thermal power output of the core is given by

$$MWt = \frac{q'_{AVE} L N_R}{C_1},$$ (12-94)

where $N_R$ is the total number of fuel rods in the core, $L$ is the active fuel rod length, and $C_1$ is the fraction of the core power generated in the fuel

($\sim$95-97%). If one desires a fuel-assembly design with $N_A$ rods per assembly ($\sim$200), then the number of assemblies required by the core thermal limitations is just

$$\# \text{ assemblies} = \frac{MWt \, C_1 F_q^N}{q'_{\text{MAX}} L N_A}.$$ (12-95)

In a similar manner, if we note that the average core power density $q'''_{\text{AVE}} = q'_{\text{AVE}}/p^2$, we can compute the required core diameter $D_{\text{core}}$ by equating

$$MWt = q'''_{\text{AVE}} \left( \frac{\pi D^2_{\text{core}}}{4} \right) L = \frac{q'_{\text{AVE}}}{p^2} \left( \frac{\pi D^2_{\text{core}}}{4} \right) L.$$ (12-96)

Hence the required core diameter is just

$$D_{\text{core}} = \left[ \frac{4p^2 MWt \, F_q^N}{\pi q'_{\text{MAX}}} \right]^{1/2}.$$ (12-97)

Of course there are other thermal–hydraulic constraints on core design, such as the minimum allowable DNBR and maximum core pressure drop which we have not included in this simple analysis. It should be noted that in this analysis the allowable power densities and hence the core size are limited by the hot channel factor. It is obviously to one's advantage to obtain a $F_q^N$ as close to unity as possible. As we will see later, the power profile can be flattened considerably using zonal fuel loading and control element insertion.

It should be noted that hot channel factors such as $F_q^N$ and $F_{\Delta H}$ that account for nonuniformities in the core power profile and flow distributions can be augmented by engineering hot channel factors, $F_q^E$, which account for variations in flow and power due to effects such as component fabrication tolerances, fuel swelling and cracking during burnup, as well as uncertainties in thermal–hydraulic nuclear analysis. In a sense, these hot channel factors can be regarded as representing the conservatism in design.

A very major improvement in core thermal performance can be achieved by a more accurate estimate of these factors so as to eliminate excessive design conservatism. For example, the enthalpy rise hot channel factor $F_{\Delta H}$ was revised downward from 3.36 to 1.7 during PWR development during the 1960s based on both operating and design experience.[1] This allowed a considerable improvement in thermal performance. In a similar sense, the thermal design of advanced reactor cores such as the LMFBR tend to use considerably more conservative estimates of hot channel factors, and their designed performance usually falls well within thermal constraints.

We should mention at this point that the thermal–hydraulic analysis of the core is actually quite closely coupled to the nuclear analysis. For example, the neutron flux and hence power distribution over core life is necessary to calculate the nuclear hot channel factors. Furthermore the core nuclear design usually provides

the moderator-to-fuel ratio and fuel pin diameter required by the thermal analysis.

We have also noted that the thermal-hydraulic analysis must supply core densities and temperatures back to the nuclear analysis. For example, the coolant void distribution will strongly affect the power profile. Furthermore changes in core temperatures will cause reactivity feedback (e.g., the change in fuel temperature that leads to reactivity changes via the Doppler effect). Needless to say, such "neutronic-thermal-hydraulic" coupling is a very important facet of nuclear reactor analysis, and we will return to consider it in Chapter 13.

## C. Thermal-Hydraulic Design Codes

A variety of computer codes have been developed to analyze the thermal-hydraulic behavior of nuclear reactor cores.[23] In order to illustrate such models, we will consider only a very simple scheme designed to perform a single channel thermal-hydraulic analysis for the hot or average channel of a light water moderated core. In such a model, the hydrodynamic and thermodynamic equations describing one-dimensional axial flow are discretized and solved explicitly stepwise up the coolant channel for an arbitrary axial power profile. The model we will consider accounts for three flow regimes: (a) single-phase flow, (b) subcooled boiling two-phase flow, and (c) bulk boiling two-phase flow. Such a model is capable of predicting axial coolant, clad, and fuel temperature profiles, void fraction, pressure drop, the critical heat flux $q''_{DNB}$, and the DNB ratio for the core. Using the nuclear hot channel factors, one can also calculate the average thermal performance of the core.

We will divide the coolant channel into segments of length $\Delta z_i$ as shown in Figure 12-16. We will then consider the relevant equations describing each of the flow regions.

### 1. SINGLE-PHASE FLOW ($h_f < h_f(T_{sat})$ or $z < z_{SCB}$):

If we discretize the energy balance equation (12-43) for a given channel segment, we find

$$w[h_{i+1} - h_i] = \int_{z_i}^{z_{i+1}} q'(z)\,dz \cong \left[ \frac{q_i + q_{i+1}}{2} \right] \Delta z_i. \qquad (12\text{-}98)$$

Hence we can solve for the enthalpy at the point $z_{i+1}$ in terms of that at $z_i$ as

$$h_{i+1} = h_i + \frac{\Delta z_i}{2w}(q_i + q_{i+1}). \qquad (12\text{-}99)$$

Remember that the power profile $q_i$ is supplied as input to the model (perhaps from a nuclear criticality calculation).

Next one calculates the pressure drop up the segment as the sum of contributions

$$p_{i+1} = p_i - \underbrace{\Delta p_i^f}_{\text{friction}} - \underbrace{\Delta p_i^h}_{\text{hydrostatic}} - \underbrace{\Delta p_i^{form}}_{\text{form}}. \qquad (12\text{-}100)$$
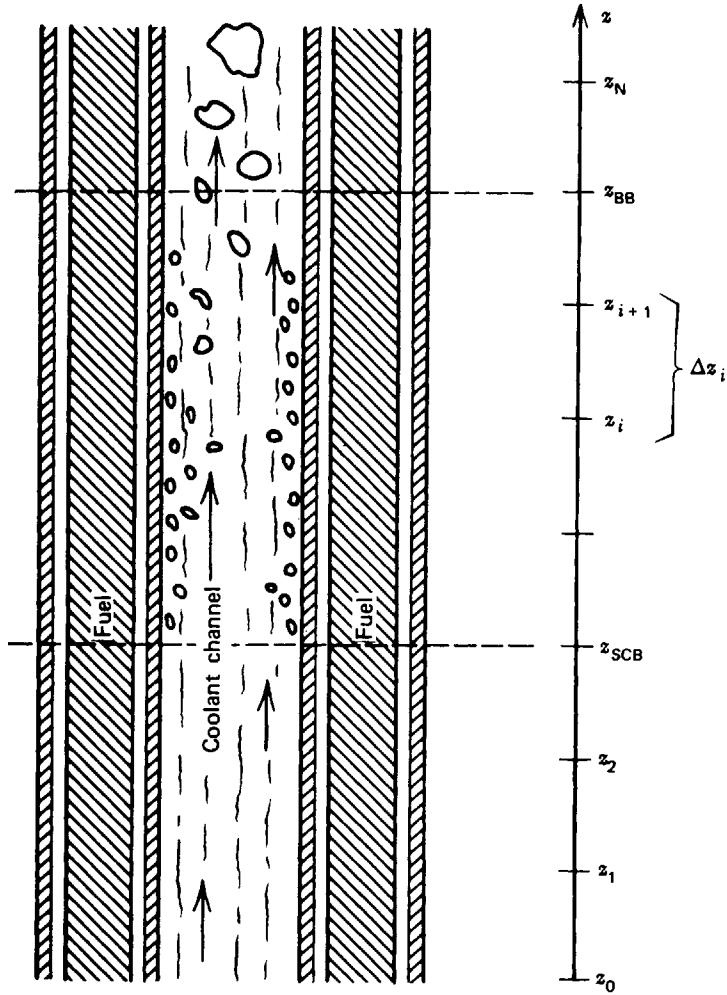
FIGURE 12-16.  Discretization of coolant channel.

If we recall our earlier hydrodynamic analysis, it is apparent that

$$\Delta p_i^f = \frac{2\Delta z_i}{D_h} \rho_i \overline{u_{z_i}}^2 f(\mathrm{Re}_i),$$ (12-101)

$$\Delta p_i^h = \rho_i g \Delta z_i,$$

$$\Delta p_i^{form} = \sum_i K_i \rho u_{z_i}^2 / 2.$$ (12-102)

Once we have determined the coolant enthalpy and pressure at $z_{i+1}$, we can go to thermodynamic tables (stored in computer memory or tape) to find the corresponding coolant density and temperature

$$\rho_{i+1} = \rho_{i+1}(h_{i+1}, p_{i+1}); \qquad T_{i+1} = T_{i+1}(h_{i+1}, p_{i+1}).$$ (12-103)

We can use these to compute quantities such as $\mathrm{Re}_{i+1}, \mathrm{Nu}_{i+1}, \mathrm{Pr}_{i+1}$. Next, we work inward to determine the fuel element temperatures at $z_{i+1}$. For instance, the clad surface temperature is

$$T_{s_{i+1}} = T_{i+1} + \frac{q_{i+1}}{h_{s_{i+1}}},$$ (12-104)

where $h_{s_{i+1}}(Nu_{i+1}, Re_{i+1})$ is usually determined from the Dittus–Boelter correlation (12-38) for single-phase flow. The fuel centerline temperature is then

$$T_{q_{i+1}} = T_{i+1} + \frac{q_{i+1}}{2\pi r_F}\left[\frac{r_F}{2\bar{k}_{F_{i+1}}} + \frac{1}{h_{G_{i+1}}} + \frac{t_C}{k_{C_{i+1}}} + \frac{r_F}{h_{s_{i+1}}(r_F + t_C)}\right]. \quad (12\text{-}105)$$

Finally the fluid velocity is determined by using mass flow conservation

$$w = \text{constant} = \rho_{i+1}\,\overline{u}_{z_{i+1}}A_c \quad (12\text{-}106)$$

to find

$$\overline{u}_{z_{i+1}} = w/\rho_{i+1}A_c. \quad (12\text{-}107)$$

## 2. TWO-PHASE FLOW $(h > h_f(T_{sat})$ or $z > z_{SCB})$

The energy balance relation giving the enthalpy at each point in the channel remains unchanged. The pressure drop is modified to account for two-phase flow effects. In particular, the Martinelli–Nelson correlation is used for $\Delta p_i^f$

$$\Delta p_i^f = 2\left(\frac{\Delta z_i}{D_h}\right)\rho_i\,\overline{u}_{z_i}^2 f(Re_i)R_{MN_i}, \quad (12\text{-}108)$$

where $R_{MN_i}$ is a tabulated function of $p_i$ and $\chi_i$. We also add in

$$\Delta p_i^a \cong \rho_i\,\overline{u}_{z_i}^2\left[\frac{r_i - r_{i-1}}{\Delta z_{i-1}}\right]\Delta z_i \quad (12\text{-}109)$$

where

$$r \equiv \frac{(1-\chi)^2}{(1-\alpha)} + \frac{\chi^2}{\alpha^2}\frac{\rho_l}{\rho_g}. \quad (12\text{-}110)$$

This will allow us to determine $h_{i+1}$ and $p_{i+1}$. Then using thermodynamic tables, we can generate

$$\begin{rcases}h_{i+1}\\p_{i+1}\end{rcases} \Longrightarrow \begin{matrix}h_{f_{i+1}}, h_{g_{i+1}}, \chi_{i+1}, T_{i+1} = T_{sat}(p_{i+1})\\ \rho_{l_{i+1}}, \rho_{g_{i+1}}.\end{matrix} \quad (12\text{-}111)$$

To determine the clad wall temperature, the Jens–Lottes correlation is used

$$T_{s_{i+1}} = T_{i+1} + 45\exp(-p_{i+1}/62)(q_{i+1}'')^{0.25}, \quad (12\text{-}112)$$

and then the fuel centerline temperature can be determined using Eq. (12-105)

If the slip ratio were known, one could then use the $S - \alpha - \chi$ relationship to determine the void fraction. However it is common practice instead to use a correlation (again due to Martinelli and Nelson) to determine $\alpha_{i+1}$ as a function of $\chi_{i+1}$ and $p_{i+1}$. Then the $S - \alpha - \chi$ relationship is used to determine the slip ratio

$$S_{i+1} = \frac{v_{g_{i+1}}}{v_{l_{i+1}}} = \left(\frac{\rho_{l_{i+1}}}{\rho_{g_{i+1}}}\right)\left(\frac{\chi_{i+1}}{1-\chi_{i+1}}\right)\left(\frac{1-\alpha_{i+1}}{\alpha_{i+1}}\right). \quad (12\text{-}113)$$

If we note that

$$w_g = v_g \rho_g A_g = v_g \rho_g \alpha A_c = \chi w, \qquad (12\text{-}114)$$

we can calculate

$$v_{g_{i+1}} = \frac{\chi_{i+1} w_{i+1}}{\rho_{g_{i+1}} \alpha_{i+1} A_c}, \qquad (12\text{-}115)$$

and then use the slip ratio to find

$$v_{l_{i+1}} = v_{g_{i+1}} / S_{i+1}. \qquad (12\text{-}116)$$

Finally, one can use these values of the flow parameters to compute the critical heat flux $q''_{DNB}$ at each point in the channel using an appropriate empirical correlation. The DNBR can similarly be calculated since the linear power density $q'$ and hence the heat flux $q''$ is known.

Thus the strategy for analyzing the channel is very simple. One merely takes the coolant inlet conditions and the power profile $q'(z)$ and marches up the channel, calculating the relevant hydrodynamic and thermodynamic parameters for the next channel mesh-point using conservation equations and tabulated thermodynamic data and correlations. The actual mechanics of such single-channel codes is quite simple (although thermodynamic data parameterization and storage may be more complicated).

### D. Some Additional Comments

Our illustration of thermal–hydraulic analysis in the previous section was specifically concerned with water-cooled reactors. However this model could also be used to analyze LMFBRs with only a minor modification in the correlations used to generate the coolant properties, since the fuel element lattice structure of a LMFBR is remarkably similar to that of a LWR. Indeed the thermal–hydraulic analysis of a liquid metal-cooled core is even a bit simpler since the coolant temperature is always kept well below the saturation point to permit only single-phase flow to occur. Since LMFBR fuel elements are frequently fabricated with a sodium bond between the fuel and the clad, a slightly different gap conductance would be used.

A very similar type of analysis would apply to the gas-cooled fast reactor (GCFR) that uses helium to cool a fuel lattice almost identical to that of the LMFBR. Again, the coolant is single phase (gas). However there is a slight complication since high-speed gas flow can be accompanied by compressible flow phenomena (flow choking, shock waves, etc.). At the level of our simple single-channel analysis, these effects can frequently be accommodated by a minor adjustment of correlations. However in more elaborate calculations (e.g., system depressurization), such effects would require a different type of analysis.

The HTGR can also be described by a similar single-channel analysis (with the appropriate adjustments for compressible flow), with one major difference. In the LWR, LMFBR, and GCFR, the coolant flows about the cylindrical fuel elements in a bundle. However the coolant in an HTGR flows through channels in a graphite block containing the fuel (see Figure 10-4). Although the description of axial flow through a circular channel is simple enough, the analysis of the radial

heat conduction from the fuel pins through the graphite block to the coolant channel wall is a complicated two-dimensional heat conduction problem.[24] Hence the calculation of the temperature distribution in HTGR fuel assemblies usually requires a direct two-dimensional numerical solution of the thermal conduction equation (a task beyond our present patience in this book, although it is obviously very similar to a two-dimensional neutron diffusion calculation).

## REFERENCES

1. L. S. Tong and J. Weisman, *Thermal Analysis of Pressurized Water Reactors*, American Nuclear Society, Hinsdale, Ill. (1970); L. S. Tong, *Nucl. Eng. Design* 6, 301 (1967).

2. M. M. El-Wakil, *Nuclear Heat Transport*, Intext, Scranton (1971).

3. H. W. Graves, Jr., *Nuclear Reactor Design*, University of Michigan Lecture Notes (unpublished), 1969.

4. A. Sesonske, *Nuclear Power Plant Design Analysis*, USAEC TID-26241 (1973).

5. H. Fenech and W. M. Rohsenow, Heat transfer, in *The Technology of Nuclear Reactor Safety*, T. J. Thompson and J. G. Beckerley (Eds.), M. I. T. Press, Cambridge (1973), Vol. II.

6. J. A. Christensen, R. J. Allio, and A. Biancheria, WCAP-6065 (1965).

7. Reference Safety Analysis Report (RESAR-3), Vol. II, Part 4.4, Westinghouse Nuclear Energy Systems (1973).

8. W. M. Rohsenow and H. Choi, *Heat, Mass, and Momentum Transfer*, Prentice-Hall, Englewood Cliffs, N.J. (1961).

9. F. Kreith, *Principles of Heat Transfer*, 3rd Ed., Intext, Scranton (1973).

10. R. B. Bird, W. E. Stewart, and E. N. Lightfoot, *Transport Phenomena*, Wiley, New York (1960).

11. L. S. Tong and J. Weisman, *Thermal Analysis of Pressurized Water Reactors*, American Nuclear Society, Hinsdale, Ill. (1970); L. S. Tong, *Nucl. Eng. Design* 6, 301 (1967).

12. See references contained in L. S. Tong and J. Weisman, *Thermal Analysis of Pressurized Water Reactors*, American Nuclear Society, Hinsdale, Ill. (1970); J. Weisman and R. W. Bowring, *Nucl. Sci. Eng.* 57, 255 (1975).

13. R. A. Dean, Thermal Contact Conductance, M. S. Thesis, University of Pittsburgh (1963).

14. L. D. Landau and E. M. Lifshitz, *Fluid Mechanics*, Pergamon, New York (1959).

15. M. M. El-Wakil, *Nuclear Heat Transport*, Intext, Scranton (1971).

16. W. H. Jens and P. A. Lottes, Analysis of heat transfer, burnout, pressure drop, and density data for high pressure water, USAEC Report ANL-4627 (1961).

17. J. H. Keenan and F. G. Keyes, *Thermodynamic Properties of Steam*, Wiley, New York (1937).

18. E. Janssen and S. Levy, Burnout limit curves for boiling water reactors, General Electric Company Report APED 3892 (1962).

19. J. Weisman and R. W. Bowring, *Nucl. Sci. Eng.* 57, 255 (1975).

20. R. C. Martinelli and D. B. Nelson, Prediction of pressure drops during forced circulation boiling of water, *Trans. ASME* 70 (1948).

21. Mathematical Models and Computational Techniques for Analysis of Nuclear Systems, USAEC Document CONF-730414-P2, Vol. I, Session III (1973).

22. L. S. Tong and J. Weisman, *Thermal Analysis of Pressurized Water Reactors*, American Nuclear Society, Hinsdale, Ill. (1970); L. S. Tong, *Nucl. Eng. Design* 6, 301 (1967).

23. D. S. Rowe, COBRA-II: A Digital Computer Program for Thermal-Hydraulic Subchannel Analysis of Rod-Bundle Nuclear Fuel Elements, BNWL-1229 (1970); BNWL-1695 (1973); J. Weisman and R. W. Bowring, *Nucl. Sci. Eng.* 57, 255 (1975).

24. Preliminary Safety Analysis Report, Summit Power Station, Delmarva Power, Vol. 3, Chapter 4 (1973), Section 4.4.2.2.

## PROBLEMS

12-1 Compare the average thermal power densities $(q',q'',q''')$ of each of the major reactor types (e.g., PWR, BWR, HTGR, LMFBR, GCFR, ...) along with that of the boiler of a fossil-fuel-fired plant. Use data from PSAR's for actual plants, if possible.

12-2 Derive the equation of heat conduction by considering an energy balance for an arbitrary volume (in analogy to the derivation of the neutron diffusion equation).

12-3 Determine the temperature profile in plate-type fuel elements composed of fuel of thickness $2r_F$ sandwiched between a clad of thickness $t_C$. Assume a gap thickness $t_G$.

12-4 Derive an expression for the average fuel temperature in a cylindrical fuel pellet as a function of the surface and centerline temperature. Assume a constant heat source and thermal conductivity.

12-5 Determine the temperature distribution in an infinitely long cylinder, assuming an internal source given by $q'''(r) = q_0 I_0(r/L)$, where the surface of the cylinder is at temperature $T_s$. Assume that the thermal conductivity depends on temperature through the relationship $k(T) = k_0[1 + a(T - T_s)]$. Sketch the temperature profile for the constant $a$ positive, zero, and negative.

12-6 The flux depression in a cylindrical fuel pellet can be modeled by assuming that the radial dependence of $q'''(r)$ is of the form $q'''(r) = q_0'''(1 + ar^2)$. Derive an expression for the temperature rise in the fuel in terms of the linear power density $q_0'$. In particular compare this temperature drop with that resulting from a uniform heat flux for a 12% flux depression (i.e., $ar_F^2 = 0.12$) for the case in which $q_0' = 500$ W/cm and $k_F = .0245$ W/cm °K.

12-7 Calculate the equivalent heat transfer coefficient, $h_G$, characterizing radial gas gaps between pellet and clad of 0.010 and 0.005 cm. Assume $r_F \gg t_G$ and constant gas properties with temperature for both helium and fission product gas.

12-8 Consider two cylindrical fuel rods of radii $a$ and $2a$ respectively which are to operate under the limitation that the maximum center-to-outer surface temperature difference is $\Delta T$. Assuming uniform heat generation in the rods, which rod would be able to supply more heat?

12-9 It is frequently of interest to determine the temperature distribution in shielding material being heated by incident radiation (e.g., photons or neutrons). Such a calculation can easily be performed in analogy to our study of thermal conduction in fuel elements, provided one uses a distributed heat source. Consider a slab shield of thickness $L$ with a radiation flux $\phi_0$ incident upon one face. If the radiation intensity is assumed to be attenuated as $\phi_0 \exp(-\Sigma_a x)$, determine the temperature distribution across the shield. Assume that we maintain the surfaces at $x = 0$ and $x = L$ at specified temperatures $T_0$ and $T_L$.

12-10 A 8 cm-thick flat-plate iron shield is subjected at one face to 3.0 MeV/photon $\gamma$ radiation of uniform $10^{13}$ flux. The absorption cross section for 3 MeV $\gamma$s in iron is 0.282 cm$^{-1}$. If the temperatures of both sides of the plate were to remain equal, find: (a) the temperature distribution in the plate, (b) the difference between maximum and surface temperatures, and (c) the surface cooling on each side of the plate necessary to maintain the above conditions.

12-11 Using the fuel element data for the BWR/6 core design given in Appendix H, estimate the fuel centerline temperature that occurs at the point of maximum heat flux if it is assumed that the coolant temperature at this point is 290°C with a convective heat transfer coefficient of $h_s = 5.0$ W/cm$^2$ °K.

12-12 Repeat the calculation of Problem 12-11 for the LMFBR core data assuming a sodium temperature of 500 °C and $h_s = 4.0$ W/cm$^2$ °K.

12-13 Consider water at 1 bar, 20°C flowing through a smooth, circular pipe of 2 cm I.D. and length 3m. If the flow velocity is 3 m/sec, determine the pressure drop along the pipe and the pumping power necessary to maintain the flow in this pipe.

12-14 Compute the equivalent hydraulic diameter $D_h$ for a hexagonal lattice such as that sketched in Fig. 12-7.

12-15 A cylindrical LMFBR core contains $N$ fuel elements of length $L$. Sodium coolant flows through the core in the axial direction with a total mass flow rate $w$ that is uniformly divided among the coolant channels in the core. It is found that this reactor core has a positive sodium void coefficient of reactivity. To correct this, a new design is proposed in which the cross-sectional area of the cylindrical core is doubled (i.e., twice as many fuel elements), while the core length is halved, thereby increasing neutron leakage and achieving a negative void coefficient. If the total coolant flow rate does not change in the new core design, estimate the pumping power required relative to that for the original core. (Assume turbulent flow.)

12-16 A reactor coolant loop may be hydrodynamically unstable if operated with a portion of the loop in the transition region between laminar and turbulent flow. Because the flow resistance changes when transition occurs from laminar to turbulent flow (and vice versa), conditions are favorable for flow oscillation. Consider a loop consisting of constant diameter piping and a constant pressure pump ($\Delta p$ across pump independent of flow rate).

   (a) Describe how this type of instability can occur in such a simplified loop.
   (b) If the transitions take place at a Reynolds number of approximately 2500, determine the ratio of the maximum to minimum flow rates in the pipe (i.e., $w_{max}/w_{min}$).

12-17 Compare the heat transfer coefficients and the pumping power per 100 m length of 2 cm I.D. smooth-drawn tubing for the following coolants: (a) air at 10 bar, 100 m/sec, and 200°C, (b) He at the same conditions, (c) water at 10 m/sec, 200°C, 1 bar. and (d) sodium at the same conditions.

12-18 A reactor is cooled by a gas that flows turbulently through its core. Its temperature rise is small compared to its absolute temperature, and the pressure drop is small compared to the absolute pressure. Suppose the coolant pressure is now doubled. The reactor is to require no more pumping power than before. The temperature rise of the coolant is to be held constant. No core modifications are to be made. Determine: (a) the maximum possible increase in reactor power and (b) assuming that this power increase is made, the extent of temperature rise across the gas film as the heat transfer increases.

12-19 Determine the axial clad surface and fuel centerline temperature distribution present in a bare, uniform cylindrical core. In particular determine those positions at which the maximum fuel centerline and clad surface temperatures occur.

12-20 As we have seen, one of the primary limitations on thermal performance is the avoidance of fuel centerline melting. However it is obviously to our advantage to run the fuel at all points in the reactor as close to this limit as possible (consistent with safety requirements).

   (a) Determine the axial power profile that would yield a uniform axial fuel temperature in the core.
   (b) Determine the axial fuel loading distribution that would yield this power profile (use one-speed diffusion theory).
   (c) Compare the feasibility of obtaining such profiles for a HTGR and a PWR.

12-21 Consider a channel of length $L$ in which there is a bottom-peaked power profile of the form

$$q'(z) = q'_0(\pi/\tilde{H})(\tilde{H} - z)\sin[(\pi/\tilde{H})(\tilde{H} - z)].$$

Determine: (a) the maximum/average heat flux in the channel, (b) $q'(z)$ in terms of the average channel heat flux, and (c) the enthalpy rise at any position in the channel.

12-22 Consider an LMFBR core with design parameters as given in Appendix H. If the linear power density in the core is assumed to be a uniform 300 W/cm up the core and the flow area per fuel rod is 1 cm², calculate: (a) the flow rate per rod, (b) the coolant transit time through the core, and (c) the core power density.

12-23 Water flows in a circular channel 3 m long by 1 cm I.D. The system pressure is 70

bar. The water enters the channel with average velocity 3 m/sec and temperature 260°C. The wall heat flux has a cosine distribution (no extrapolation lengths) with a peak value of 200 W/cm². Determine: (a) axial coolant temperature distribution, (b) axial quality distribution, (c) axial void fraction distribution, assuming a constant slip ratio of 2, (d) acceleration pressure drop in the channel, (e) friction pressure drop in the channel, and (f) graph $T_0$, $\chi$, $\alpha$, and $p$ versus $z$. Assume thermodynamic equilibrium exists at each axial position (i.e., neglect subcooled boiling).

12-24 For Problem 12-23 determine the axial position where subcooled boiling starts. What is the coolant temperature at this position? The wall temperature?

12-25 Consider a PWR operating in such a fashion that nucleate boiling occurs at the point of maximum power density. How might you expect the following changes to affect both the maximum fuel centerline temperature and the DNBR, assuming a constant average linear power density: (a) 10% reduction of coolant flow in the hot channel, (b) modification of the core analysis to account for nonuniform power generation in the fuel pellets, (c) radial fuel migration and densification producing a 4% void volume along the fuel pellet axis (d) the axial core power profile shifting from a centered to a bottom-peaked distribution (such that both the peak power and integrated power remain the same), and (e) the axial core power profile shifting to a top-peaked distribution. (See Tong and Weisman[1] for typical DNB correlations.)

12-26 The outlet quality of an average coolant channel of a BWR is 14.6%. The system pressure is 70 bar, and the inlet temperature is 220°C [$h$(220°C, 70 bar) = 1.23 MJ/kg]. Determine: (a) the exit void fraction for a slip ratio of 2.0, (b) the average heat generation (W/cm) of the fuel rods if the mass flow rate per fuel rod is 10,000 kg/hr and the core height is 375 cm, and (c) the nonboiling length for the bottom-peaked power profile of Problem 12-21.

12-27 Using the description provided in Section 12-VII-C, write a computer program capable of analyzing the hot channel of a LWR (either PWR or BWR).

The following problems will require the use of a simple single-channel thermal–hydraulics code suitable for a LWR.

12-28 Use the thermal–hydraulics code to evaluate the performance of any one of the PWR designs given in Appendix H. In particular: (a) compare a bottom-peaked and centered power profile from the standpoint of: (i) peak linear power density, (ii) peak fuel centerline temperature, and (iii) DNB ratio; (b) roughly plot the following for the hot channel of the bottom peaked profile: (i) coolant temperature, (ii) clad surface temperature, (iii) heat flux, and (iv) DNB heat flux; and (c) evaluate the effect of a simultaneous 10% reduction in flow and 10% increase in power level on DNB ratio and centerline fuel temperature.

12-29 Use the thermal–hydraulics code to evaluate the performance of the BWR-6 design in Appendix H. Use the bottom-peaked power profile and determine: (a) coolant temperature, fuel temperature, void fraction, and flow quality profiles; and (b) the recirculation ratio (mass ratio of recirculated coolant to coolant leaving the vessel as steam) and the reactor vessel inlet temperature (i.e., feedwater temperature).

# 13

## The Calculation of Core Power Distributions

The central component of most computational models of nuclear reactors consists of a group of calculational modules that analyze the static neutronic behavior in the reactor core. As we have repeatedly emphasized, these static calculations are usually based on a solution of the multigroup diffusion equations for the multiplication eigenvalue $k_{eff}$ and the multigroup fluxes $\phi_g(r)$ characterizing a given core configuration. One can then construct the corresponding core power distribution by calculating the local fission rate as in Eq. (12-1).

Such static calculations not only involve what we have referred to as a flux-power-reactivity module that solves the multigroup diffusion equations to generate the core flux and power, but also a module that generates the necessary macroscopic group constants and a thermal-hydraulics module analyzing heat transfer and fluid flow in the reactor core to determine core temperatures and coolant densities. Hence our consideration of the calculation of core power distributions cannot be confined to the flux-power module alone, but must instead consider this coupled group of three calculational components (see Figure 13-1).

We are of course already very familiar with most of the features of these components. For example, Chapters 8, 9, and 10 dealt with the generation of multigroup constants. In Chapters 5 and 7 we discussed in some detail various methods for solving the time-independent multigroup diffusion equations. In Chapter 12 we considered the various features of models of the thermal–hydraulic behavior of a nuclear reactor core. Our goal in this chapter will be somewhat different (and considerably briefer) since we now wish to examine several of the more practical details of the calculation of core power distributions and explore the various ways in which such calculations interact with other aspects of the core design.
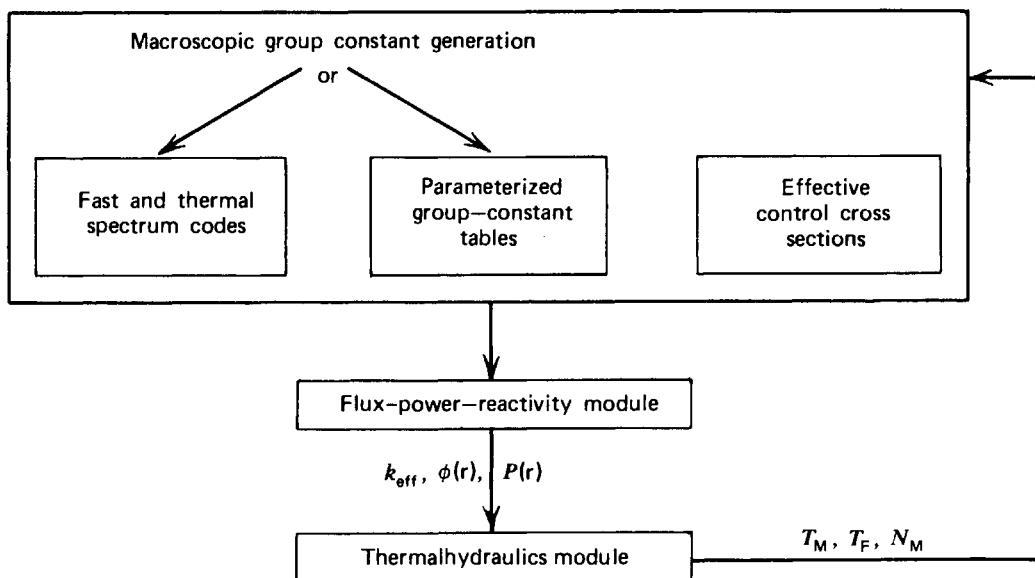
**FIGURE 13-1.** Modules involved in the calculation of core power distributions.

It is certainly not surprising that the calculation of core multiplication plays a very important role in nuclear reactor analysis. Of course such calculations are necessary in order to determine the fuel loading or control system adjustment necessary to achieve reactor criticality. However the calculation of the multiplication eigenvalue $k_{eff}$ for a sequence of different core configurations can also determine quantities such as control element worths, reactivity feedback coefficients (e.g., by calculating $k_{eff}$ for the core at various different temperatures), and reactivity changes accompanying various different fuel loading patterns.

The static reactor flux and power distributions are also of considerable importance in reactor design. In particular, we have found that the power distribution is essential for the subsequent thermal–hydraulic analysis of the core. For example, the nuclear hot channel factors and axial power profile determine how closely the core performance approaches thermal design limitations. Furthermore the neutron flux distribution is necessary for the determination of fuel burnup and isotope buildup. However since the thermal–hydraulic core behavior as well as its fuel depletion will affect both core composition and microscopic cross sections (i.e., through temperature effects), the coupling between these various components of a reactor model becomes very important. For example, the reactor designer would like to utilize the information provided by such core analysis to achieve a flat power profile (desirable from both a thermal as well as a fuel burnup viewpoint) while providing sufficient excess reactivity to yield long core lifetimes and hence high fuel exposures, but within the safety constraints imposed on core thermal and nuclear (i.e., control) performance.

## I. STATIC MULTIGROUP DIFFUSION CALCULATIONS

Perhaps the central problem in reactor analysis is the determination of the spatial flux and power distribution in a reactor core under steady-state operating conditions. There is, however, a considerable variation in the degree of accuracy and spatial detail of the power distribution required in different facets of reactor analysis and design. For example, in determining the optimum core thermal

performance one will require as accurate an estimate of the power distribution as possible in order to ensure that thermal constraints are not exceeded. In contrast, considerably less detail is required in the comparison of various fuel loading schemes involved in fuel cycle management. These two examples illustrate the contrast between absolute estimates of core power distributions required for ensuring that performance limitations are not exceeded, and relative estimates required in optimization or tradeoff studies.

The calculation of the global power distribution is most commonly accomplished by solving the few-group diffusion equations

$$-\nabla \cdot D_g(\mathbf{r})\nabla\phi_g(\mathbf{r}) + \Sigma_{R_g}(\mathbf{r})\phi_g(\mathbf{r}) = \sum_{g'=1}^{g-1} \Sigma_{s_{g'g}}\phi_{g'}(\mathbf{r}) + \frac{1}{k}\chi_g\sum_{g'=1}^{G} \nu_{g'}\Sigma_{f_{g'}}\phi_{g'}(\mathbf{r}). \quad (13\text{-}1)$$

These equations are solved by using finite-difference methods to discretize the spatial variable and then, following the usual inner–outer iteration strategy, solving for the criticality eigenvalue $k_{eff}$ and the corresponding multigroup flux $\phi_g(\mathbf{r})$. To be more precise, the reactor core is broken up into a spatial grid or mesh—for example, with $M$ mesh cells. Then the multigroup diffusion equation is integrated over a typical cell, and standard sum and difference formulas are used to represent the terms in the equation. Hence the multigroup diffusion equations are replaced by an $M \times G$ set of algebraic equations—that is, an $(M \times G)$ dimension matrix-eigenvalue problem

$$\underline{\underline{M}}\,\underline{\phi} = \frac{1}{k}\,\underline{\underline{F}}\,\underline{\phi}. \quad (13\text{-}2)$$

The elements of the matrices $\underline{M}$ and $\underline{F}$ are the few-group constants supplied by a macroscopic cross section module. The matrix eigenvalue problem can then be solved by standard power-iteration methods (usually accelerated by source extrapolation).

The complexity of such calculations depends sensitively on the nature of the design information required. During the early stages of the design process it is common to use very fast running one-dimensional survey codes. For core lifetime studies in which the power and flux distributions must be calculated at many time-steps during core life, one commonly uses one-dimensional diffusion codes (such as in the FEVER[1] depletion code) or even zero-dimensional descriptions (such as in the LEOPARD[2] code) for preliminary survey studies.

Most detailed design calculations of the core power distribution must be performed with two- and three-dimensional diffusion models, such as the PDQ[3] series of codes developed at the Naval Reactor Laboratories. An accurate description of the flux and power distribution in the reactor core using the finite-differenced multigroup diffusion equations requires that the mesh spacing be at least comparable (or less than) the minimum neutron diffusion length in the core ($\sim$0.5 cm in a LWR, $\sim$4–5 cm in an HTGR), even after core homogenization such as that described in Chapter 10 has been performed. For example, it is common in LWR analysis to assign one mesh point per fuel pin[4] in a two-dimensional radial calculation of the core power distribution (and even then some discrepancies arise in certain types of burnup studies).

Fortunately many thermal reactor cores are characterized by a rather weak coupling between the transverse and axial flux distributions. Hence one can frequently iterate back and forth between a two-dimensional transverse and a one-dimensional axial multigroup diffusion calculation to generate a three-dimensional "map" of the core power distribution, thereby avoiding the expense of a full three-dimensional treatment.

Although the use of such two-dimensional plus one-dimensional models of the core power distribution have been quite commonly used in reactor design, there is increasing tendency to go to direct three-dimensional diffusion calculations when detailed evaluations of a specific core design are required. For the large, loosely coupled cores characteristic of modern power reactors, such three-dimensional studies require rather fine mesh structures and hence considerable computer storage and calculational running time expenses are incurred (even for a core subregion such as an octant). This difficulty is aggravated when there is a strong coupling between the thermal–hydraulic and neutronic core behavior, as there is, for example, in a BWR or when core fuel depletion is of concern. It has been found that accurate multigroup diffusion calculations of the global power distribution typically require between four (LWR) and nine (HTGR) energy groups for thermal reactor analysis.

In fast reactor cores, the neutron mean free path is quite large. Hence fast reactors are more susceptible to a homogeneous analysis (except for a small fraction of neutrons with energies less than several keV). On the other hand, it is much more important to treat the energy-dependence accurately in fast reactor analysis. Hence one usually relies on many groups ($\sim$20) in a diffusion calculation for a few-region model of the core in fast reactor analysis.

In Table 13-1[27] we have summarized the computational requirements for a multigroup diffusion calculation of the core power distribution in various reactor types.

There has been strong motivation to develop alternatives to the standard finite-difference treatment of the multigroup diffusion equations. We have already examined one such scheme based on a *nodal* representation[5] of the neutron flux in the reactor core. Although such three-dimensional coarse nodal methods have customarily utilized a one-group description of the neutron flux (such as in the FLARE code[6]), more recent extensions to multigroup nodal schemes have been developed.[7]

Another alternative approach is to use so-called *finite element techniques*[8] to calculate the neutron flux at each of a number of ultracoarse mesh points. Such finite-element methods have been used for some time in performing calculations in mechanical stress analysis, and appear to have considerable (although not fully realized) potential for multidimensional neutron diffusion calculations.

Other coarse mesh techniques have been developed that utilize a mesh structure of the order of one mesh point per fuel assembly. However in order to ensure the stability of such techniques, it is usually necessary to alternate between coarse and fine mesh calculations in performing the source iterations required in a criticality calculation. This latter scheme, known as *coarse mesh rebalancing*[9], also appears to have considerable potential for accelerating multigroup diffusion calculations.

There is yet another alternative to a direct multidimensional diffusion calculation that has proven remarkably successful in reactor analysis, the so-called *flux synthesis*[10] method, in which a multidimensional flux is "synthesized" from a combination of one- or two-dimensional calculations. Because of the importance of

TABLE 13-1    Meshpoint Requirements for MGD Analysis of Various Reactor Types

| Reactor Type[†] | Core Volume $(m^3)$ | Core-Averaged Power Density $(W/cm^3)$ | Characteristic Diffusion Length $(cm)$ | Diameter of Reactor in Diffusion Lengths |
|---|---|---|---|---|
| PWR | 40 | 75.0 | 1.8 | 190 |
| BWR | 60 | 50.0 | 2.2 | 178 |
| HTGR | 430 | 7.0 | 12.0 | 63 |
| LMFBR | 5.7 | 530.0 | 5.0 | 36 |
| GCFR | 10.7 | 280.0 | 6.6 | 33 |

| Reactor Type[†] | Necessary Number of Mesh Points (One per Diffusion Length) 2-D | 3-D | Number of Groups (Thermal Groups) | Necessary Number of Group-Space Meshpoints (One per Diffusion Length) 1-D | 2-D | 3-D |
|---|---|---|---|---|---|---|
| PWR | 36,100 | 6,859,000 | 4 (1) | 760 | 144,400 | 27,436,000 |
| BWR | 31,666 | 5,635,000 | 4 (1) | 712 | 126,664 | 22,540,000 |
| HTGR | 3,947 | 247,969 | 7 (4) | 441 | 27,629 | 1,735,783 |
| LMFBR | 1,270 | 45,270 | 10 (0) | 360 | 12,700 | 452,700 |
| GCFR | 1,115 | 37,253 | 10 (0) | 330 | 11,150 | 372,530 |

[†]Based on a 3000 MWt core. [R. Froehlich, in USAEC CONF-730414-P2 (1973), p. VII-46-49]

this method in nuclear reactor design, we will consider it in some detail in Section 13-IV.

We should remark that most multigroup diffusion codes usually have the capability of computing not only the neutron fluxes $\phi_g(r)$ but also their adjoints $\phi_g^\dagger(r)$. These quantities are extremely useful in making perturbation theory estimates of reactivity changes due to changes in core composition or configuration. Although perturbation theory is capable of only limited accuracy, it can provide useful initial guesses for more detailed diffusion calculations. And since one can frequently calculate the adjoint fluxes with only slightly more effort than that involved in simply calculating the fluxes by themselves, many design codes have been developed with perturbation theory options.

## II. INTERACTION OF THERMAL-HYDRAULICS, NEUTRONICS, AND FUEL DEPLETION

We have noted that the power distribution found in a reactor will deviate considerably from that predicted for a bare, uniform cylindrical core. Such variations arise due to the presence of blankets or reflectors in most core designs, nonuniform fuel loading (or burnup), and nonuniform coolant densities.

Many nuclear reactors are characterized by a rather strong coupling between coolant density and neutronic behavior. As an example, consider first LWRs in which the water coolant also serves as a moderator. Since most LWR cores are "undermoderated," a local decrease in water density will cause a decrease in moderation and hence a decrease in local power density. As the coolant passes up through the core, it absorbs heat from the fuel elements and eventually will initiate

either subcooled (nucleate) or bulk boiling. Hence there will be an increase in coolant void fraction—that is, a decrease in coolant density—as it passes up through the core. Since the coolant density is maximum at the bottom core inlet, one would therefore expect a bottom peaked power profile (as sketched in Figure 13-2).

A similar thermal–hydraulic–neutronic coupling can arise in liquid metal-cooled fast breeder reactors. As we will find later, the liquid metal coolant (sodium) will cause appreciable moderation or softening of the neutron energy spectrum in a fast reactor. This will lead to a decrease in reactivity, since $\eta$ for a fast reactor increases with average neutron energy. Hence a local decrease in coolant density can lead to an increase in local reactivity and thereby an increase in the local power density (note that this effect is in the opposite direction of coolant void reactivity effects in LWRs). Although weaker than the coupling that arises in LWRs, this effect must nevertheless be accounted for in core calculations.

The coupling between coolant properties and core neutronic behavior is very much weaker in gas-cooled reactors such as the HTGR, because coolant phase
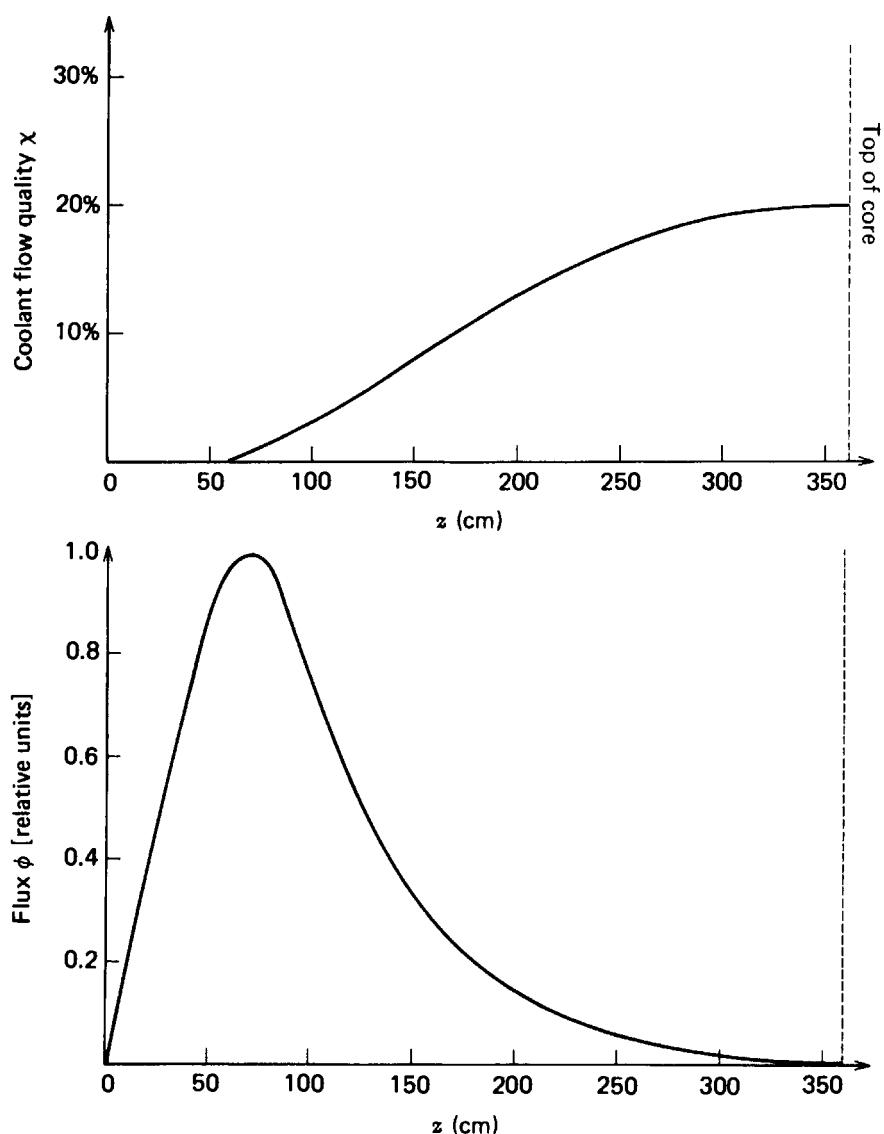


FIGURE 13-2. Bottom flux-peaking in a BWR.

change cannot occur, and also because the coolant does not provide appreciable moderation in the core due to its very low density.

To illustrate the interactions between thermal–hydraulic and neutronic calculations, let us examine the calculation of steady-state power distributions in LWRs. One usually begins such a calculation by supplying the thermal–hydraulics module with an initial estimate of the hot-channel factors and the axial flux profile in the core. This module will then calculate the core temperature distribution and coolant void fractions. (Actually, the thermal–hydraulics module may only calculate the conditions characterizing the hot channel and an average channel, but this thermal information is frequently sufficient for further core design purposes.) The core temperatures and coolant density variation are then returned to the macroscopic group constant generation module where they are used in the generation of group constants characterizing the core. In particular the average fuel temperature is used to determine the correct Doppler-broadened resonance integrals, while the moderator temperature will influence the thermal group constants. The coolant density is used in the generation of both microscopic (i.e., spectrum-averaged) and macroscopic group constants.

With this macroscopic group constant information, one can now use the flux-power-reactivity module to calculate the core power distribution and nuclear hot channel factors, which can then be used as an input to the thermal-hydraulics module for a second improved estimate of core temperatures and void distributions. Many code packages will automatically perform such an iteration back and forth between thermal-hydraulic and flux-power calculations until the calculated power distribution converges to its true shape. Such an iterative approach is extremely important in BWRs since the void fraction in a boiling channel varies quite dramatically from inlet to exit. In Figure 13-1, we have indicated the basic calculational procedure involved in performing coupled thermal-hydraulic-neutronic calculations, and in Figure 13-3, we have sketched typical coolant density variation and power distributions in a BWR. We have noted as well the typical convergence of these profiles as one iterates between thermal-hydraulic and neutronic calculations.

Such coupling effects can be troublesome, not only in the mathematical analysis of the reactor, but also in the actual reactor core design since they can lead to power peaking away from the optimally flat shape desired for the thermal design. This can be counteracted to a degree by control rod insertion. For example, if one inserts control rods into those regions in which power peaking is expected to occur, the negative reactivity of the control rod absorption should cancel the enhanced reactivity due to coolant density changes and eliminate the peaking. Such a scheme is commonly used in BWRs that use bottom-inserted control rods to inhibit the tendency toward bottom-peaked axial flux profiles.

These coupling effects are greatly complicated by nonuniform fuel depletion, however. The fission rate and hence the rate of fuel burnup is proportional to the neutron flux. Hence the fuel will deplete more rapidly in those assemblies exposed to higher fluxes, thereby leading to decreased local reactivity and hence, a modified flux distribution. As we will find in our discussion of core depletion calculations in Chapter 15, such nonuniform burnup effects on the flux and power profiles can become quite complicated when interactions with coolant density variations and control rod patterns are taken into account.
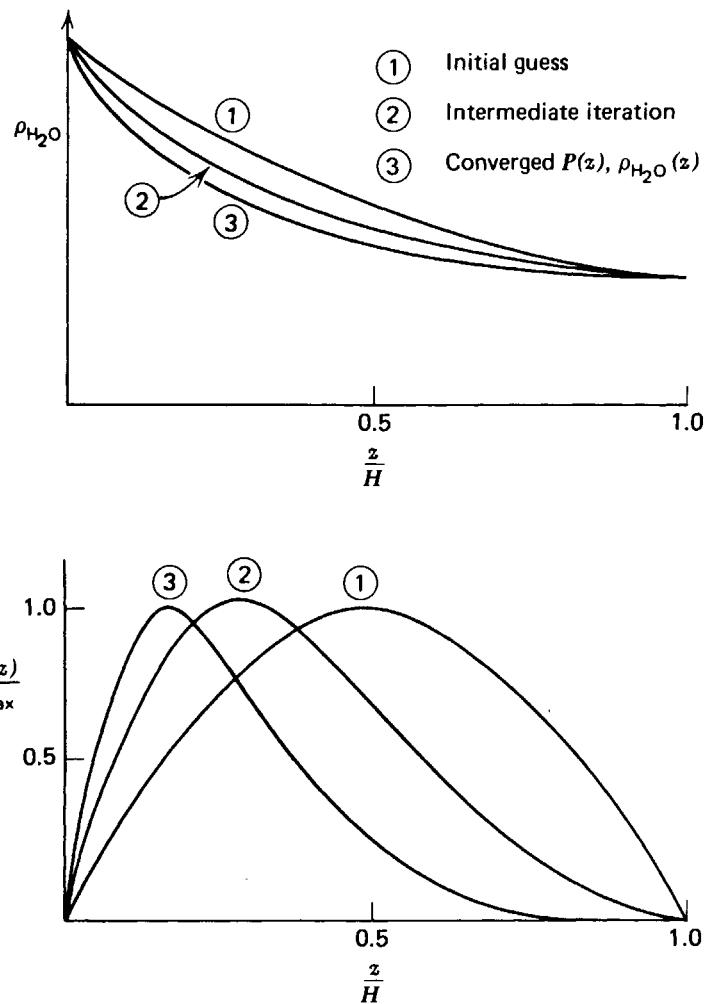
FIGURE 13-3.    Convergence of neutronics–thermal-hydraulics iteration.

## III. PARAMETERIZATION OF FEW-GROUP CONSTANTS

One of the most important and complex aspects of nuclear reactor analysis is the generation of suitable thermal and fast few-group constants characterizing absorption, scattering, removal, and fission cross sections and diffusion coefficients for each core region of interest. A variety of input data are necessary for this calculation. In particular, the fuel and moderator temperatures supplied by the thermal-hydraulics module are used in the generation of Doppler-broadened resonance integrals and thermal spectra. The moderator density is also supplied for the core region of interest by the thermal-hydraulics module. The composition of the fuel is provided either as direct input or by the depletion module. Using this information along with basic microscopic cross section libraries, one can then generate the fast and thermal spectra and hence compute the macroscopic few-group constants, using appropriate cell-averaging techniques to account for self-shielding. The absorption group constants are usually modified by adding an effective cross section characterizing any control elements in the region of interest. (These latter effective control cross sections are supplied by the control adjustment module.) The complete set of group constants for all core regions of interest are then passed along to the flux–power reactivity module.

The group constants necessary for a multigroup diffusion calculation must be generated hundreds or perhaps even thousands of times in a core lifetime study.

Not only must they be generated for each region (e.g., node cell) of the reactor core characterized by different composition, but also regenerated for each of these regions whenever the composition changes (e.g., via fuel burnup or moderator density changes). If detailed fast and thermal spectra had to be recalculated for each change in composition, the computing costs for group constant generation would be formidable.

In practice it is found that few-group constants frequently depend on relatively few parameters involving core temperatures and material densities. Hence it is far more efficient to construct tables of the values of the few-group constants for several values of these parameters, and then to use interpolation schemes to evaluate the group constants when necessary.[11] To provide an illustration of how such parameterization might work, we will give a very simple example of how one might generate group constants for LWRs within the MUFT–SOFOCATE approach[12].

First recall that thermal group constants were defined as averages of microscopic cross sections $\sigma_x^j(E)$ (characterizing reactions of type $x$ in material $j$) over the thermal neutron energy spectrum $\phi(E)$. In the SOFOCATE approach the thermal spectrum is obtained by solving the Wigner–Wilkins equation (9-31) characterizing a free proton gas. It should be noted that the only parameters that enter this equation are the temperature $T$ and the ratio of absorption to scattering $\Gamma = \Sigma_a(kT)/\xi\Sigma_s$. Hence we might expect that the microscopic thermal group constants generated by a SOFOCATE-type code will depend only on the parameters $\Gamma$ and $T$. This dependence is in fact rather smoothly varying, as shown, for example, in Figures 13-4 and 13-5, which show the dependence of $\bar{\sigma}_a^{25}$ on $\Gamma$ and $T$. In fact one can show, using the effective neutron temperature model (see Problem 9-11), that $1/v$ absorbers will yield group constants that behave as $\bar{\sigma}_a \sim C_1/(1 + C_2\Gamma)^{1/2}$.

The Wigner–Wilkins equation can also be applied for non-$1/v$ absorption, such as that due to resonances in the thermal range. However the above two parameters will not suffice in this more general situation. This is particularly relevant to high-burnup cores, which usually contain an appreciable amount of $^{239}$Pu, which is characterized by a strong thermal resonance. One can always introduce additional parameters to account for the presence of $^{239}$Pu such as

$$\psi \equiv \Sigma_a^{49}(kT)/\Sigma_a(kT).$$ (13-3)

The dependence of group constants on this parameter is essentially linear.

The above discussion suggests that it should be possible to construct tables of the dependence of thermal group constants on parameters such as $T$, $\Gamma$, and $\psi$. A macroscopic cross section module would then use data from thermal-hydraulic and depletion modules to compute these parameters and then use the precalculated group constant tables, along with appropriate interpolation schemes, to calculate the required thermal group constants.

For fast group constants, we should first recall that MUFT-type calculations solve the exact slowing down equation for hydrogen coupled with the age or Goertzel–Greuling approximation for mass numbers $A > 1$ to generate the fast spectrum. Inelastic scattering is treated by a direct microgroup approach, while resonance absorption is typically treated within the NR or NRIM approximations (with appropriate heterogeneous corrections).

Perhaps the key parameter of use in characterizing fast-group constants is the moderator-to-fuel density ratio in a homogenized lattice cell. (One occasionally
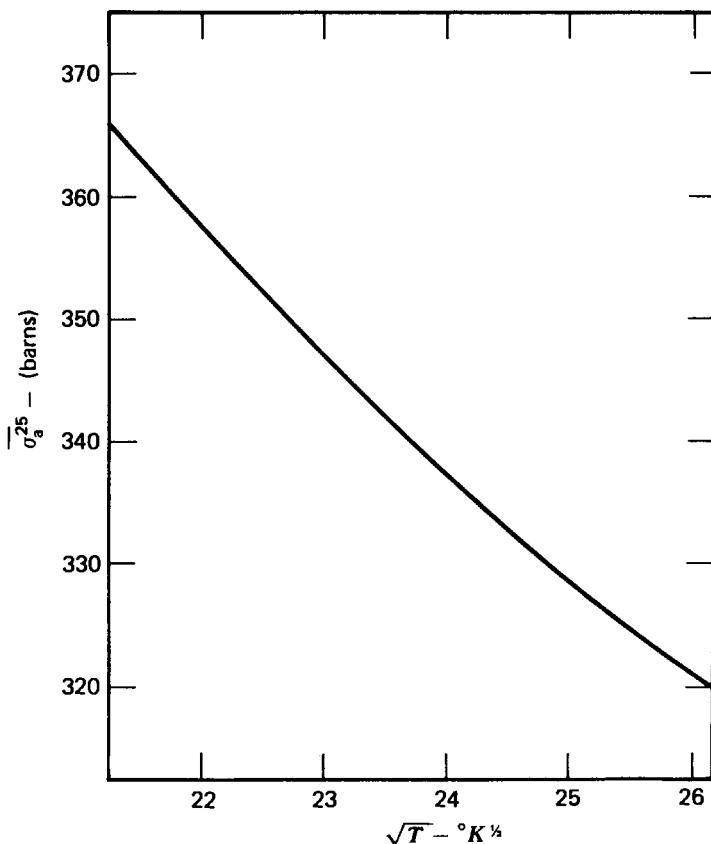
**FIGURE 13-4.** The dependence of $\bar{\sigma}_a^{25}$ on the moderator temperature.
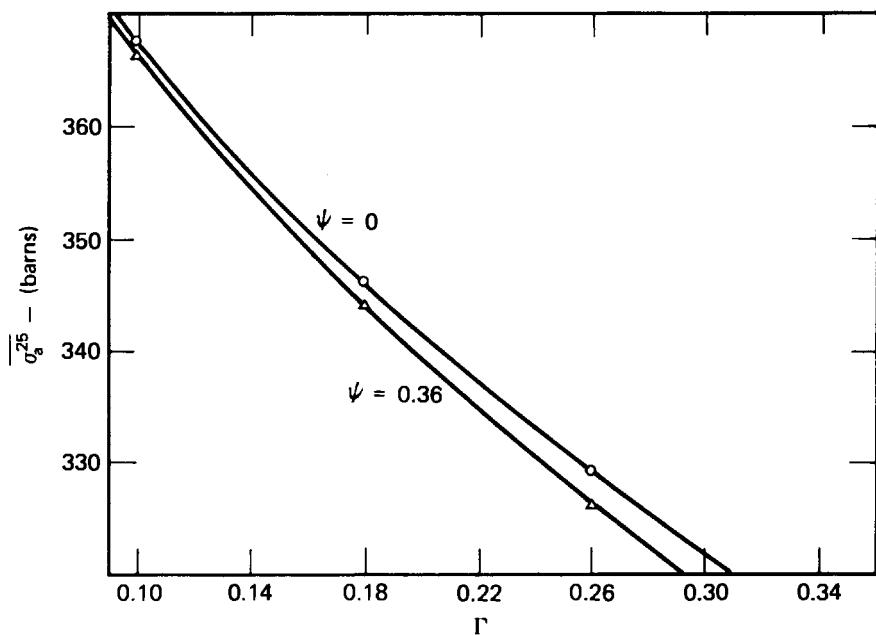


**FIGURE 13-5.** The dependence of $\bar{\sigma}_a^{25}$ on $\Gamma$, moderator temperature $= 303°C$.

also uses the ratio of moderator volume to fuel volume in a fuel cell, which gives essentially the same results.) Such a parameter characterizes the effectiveness of neutron moderation in the core. We have plotted the dependence of various fast group constants on this ratio in Figure 13-6. Such a parameterization works quite well, provided the moderator densities are not too low.

Unfortunately no truly satisfactory parameter exists for characterizing resonance integrals (aside from the fuel temperature). If such parameterizations are desired, it
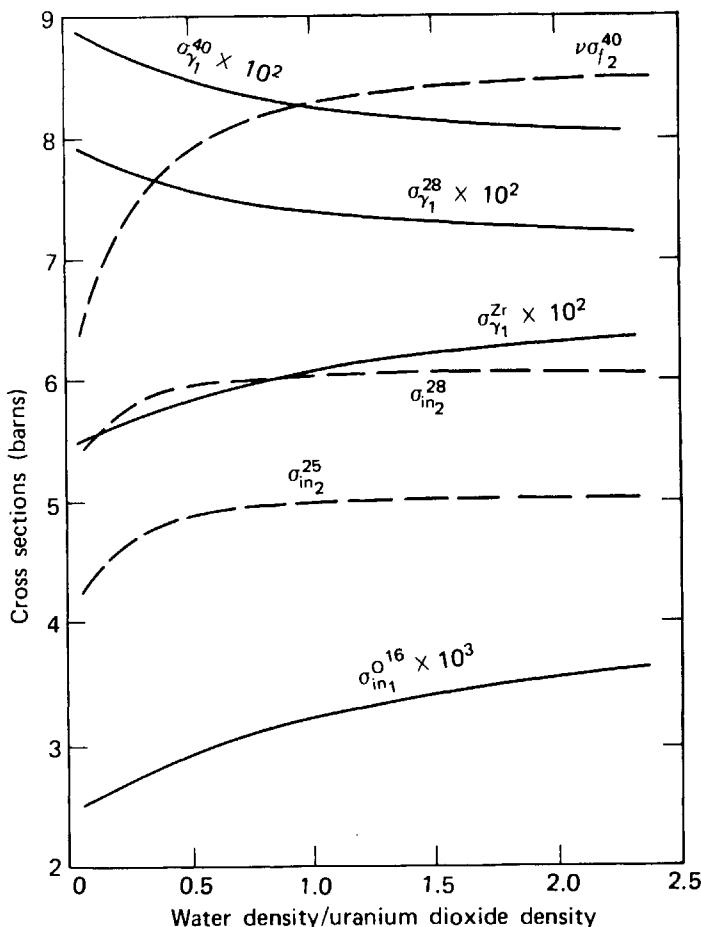
**FIGURE 13-6** Group 1 averaged cross sections (solid line); Group 2 averaged cross sections (dashed lines).

is usually necessary to rely on various empirical correlations for the resonance integrals, similar to those discussed in Section 10-III.

The above discussion has been intended as a very simple illustration of group constant parameterization. A variety of other parameters might be used, such as those characterizing burnup or control rod insertion. The specific parameterization scheme one chooses (if any) will depend on the accuracy desired from the calculation and the design problem of interest.

## IV. FLUX SYNTHESIS METHODS

### A. Spatial Synthesis

Spatial flux synthesis is a technique whereby one- or two-dimensional diffusion calculations are combined to yield a representation of a three-dimensional flux distribution. There are a variety of techniques, both heuristic and formal, for blending such lower dimensional calculations together. For purposes of illustration, let us first consider a simple example.[13]

Suppose we wish to analyze a cylindrical reactor core that has been partitioned into both radial and axial zones (denoted by indices $l$ and $m$ respectively) (see Figure 13-7) in which the core composition is presumably different. If the reactor core were of uniform composition (which it is not necessarily assumed to be), the flux would be separable in the axial and radial coordinates, and in particular would
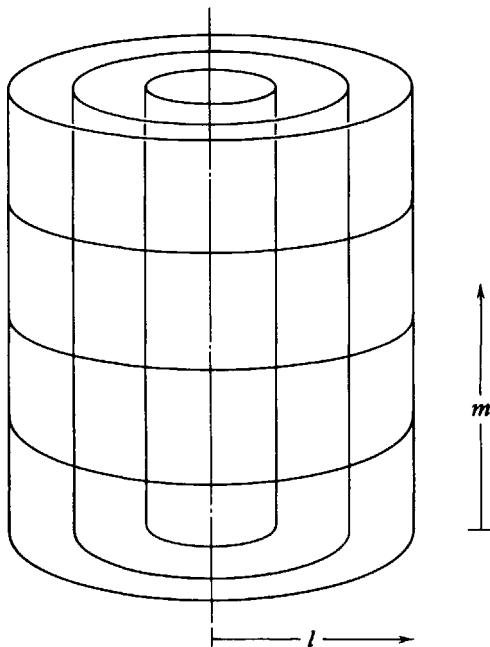
FIGURE 13-7. Axial and radial zoning.

have the form (for a given energy group)

$$\phi_g^m(\mathbf{r}) = \phi_g^m(r)\cos B_z z. \tag{13-4}$$

Of course the flux is more generally *not* of this separable form, but the idea of spatial synthesis is to represent it as such and then attempt to determine an appropriate radial shape factor $\phi_g^m(r)$ in each axial region $m$. Here the axial buckling $B_z$ is presumed known (or guessed).

If we substitute this separable flux shape into the multigroup diffusion equations, we arrive at a one-dimensional equation for the radial flux profile

$$-\frac{1}{r}\frac{d}{dr}D_g^m(r)\frac{d\phi_g^m}{dr} + \left[\Sigma_{R_g}^m(r) + D_g^m(r)B_z^2\right]\phi_g^m(r)$$

$$= \sum_{g'=1}^{g-1}\Sigma_{s_{g'g}}^m\phi_{g'}^m + \frac{1}{k}\chi_g\sum_{g'=1}^{G}\nu_{g'}\Sigma_{f_{g'}}^m\phi_{g'}^m, \tag{13-5}$$

which is characterized by an effective total cross section

$$\Sigma_{eff_g}^m \equiv \Sigma_{R_g}^m + D_g^m B_z^2. \tag{13-6}$$

Notice that here $D_g^m B_z^2$ represents removal of neutrons due to axial diffusion. We can now solve this one-dimensional problem to determine the radial flux profile $\phi_g^m$, and from this calculate the radial buckling for each region $(l,m)$ as

$$B_{r_{l,m}}^2 = \frac{\displaystyle\sum_g \int_{r_{l-1}}^{r_l} \nabla^2\phi_g^m(r)dr}{\displaystyle\sum_g \int_{r_{l-1}}^{r_l} \phi_g^m(r)dr}. \tag{13-7}$$

An analogous approach can be taken to determine the axial profile. That is, one solves the axial one-dimensional diffusion equation assuming an effective cross section

$$\Sigma_{\text{eff}_g}^l = \Sigma_{R_g}^l + D_g^l B_{r_l}^2(z),$$
(13-8)

where

$$B_{r_l}^2(z) = B_{r_{lm}}^2 \text{ for } z \text{ in region } m.$$
(13-9)

Having determined this axial profile, one can then calculate an axial buckling $B_{z_{lm}}^2$ for each region. This can be used to readjust the effective cross section in the radial multigroup diffusion equations and hence allow one to determine a new radial profile. By iterating back and forth between one-dimensional radial and axial profiles, one can eventually converge on a three-dimensional solution in each region of the form

$$\phi_g^{lm}(\mathbf{r}) = \phi_g^{lm}(r)\psi_g^{lm}(z).$$
(13-10)

To the extent that the flux in each region can be approximated as a separable function of $r$ and $z$, this scheme will yield adequate results. Although this procedure is actually a very primitive form of a flux-synthesis method, it is more commonly known as a *buckling-iteration* method.[13] It can be generalized by using a two-dimensional radial calculation and a one-dimensional axial calculation.

However a far more useful generalization is to choose a more elaborate representation or "synthesis" of the flux. Suppose we represent the flux in the core as a superposition of separable terms:

$$\phi_g(x,y,z) = \sum_{n=1}^{N} \phi_{g_n}(x,y)\psi_{g_n}(z).$$
(13-11)

The radial shape functions $\phi_{g_n}(x,y)$ are usually constructed by performing two-dimensional static flux calculations for $x$-$y$ slices at a small number ($N$) of axial locations. To determine the axial "blending" coefficients $\psi_{g_n}(z)$ one can use a variety of techniques. For example, a common scheme is to use *weighted residual* methods,[14] in which one requires that a weighted integral of the diffusion equation over the $x$-$y$ plane vanishes

$$\int dx \int dy \, w_j(x,y)\left[M\phi - \frac{1}{k}F\phi\right] = 0, \quad j=1,\dots,N,$$
(13-12)

for $N$ different weighting functions $w_j(x,y)$. Here $M$ and $F$ are the usual diffusion and fission operators (we have avoided using a multigroup notation for simplicity). It should be noted that relations such as Eq. (13-12) will lead to a set of $N$-coupled one-dimensional diffusion equations for the axial coefficients $\psi_n(z)$. A more satisfying approach is to use a variational principle to derive these one-dimensional problems, which can be regarded effectively as just the average of the three-dimensional diffusion equation over the $x$-$y$ plane (weighted by the transverse flux shapes $\phi_n(x,y)$).

All such schemes lead to very similar one-dimensional problems for the $\psi_{g_n}(z)$. Notice that as we have written Eq. (13-11), the flux synthesis applies to the entire

core. Such a scheme is known as *single-channel synthesis*,[10,15,16] since the axial coefficients $\psi_{g_n}(z)$ are the same across the core.

Yet in our earlier example we saw that it was useful to divide the core into both radial and axial regions. Hence we are led to generalize the expansion Eq. (13-11) such that we use different radial expansion functions in different radial regions ("channels").

$$\phi_g^I(x,y,z) = \sum_{n=1}^{N} \psi_{g_n}^I(z)\phi_{g_n}^I(x,y). \tag{13-13}$$

Such *multichannel synthesis* provides a great deal more flexibility in the choice of expansion functions.[17]

Single-channel synthesis methods are commonly used to synthesize three-dimensional fluxes from the results of both two- and one-dimensional calculations. The expansion functions are usually chosen, using physical insight, such that they bracket the expected flux behavior. They can be generated by performing static criticality calculations in one- or two-dimensional form for various transverse slices of the core. Such techniques have proven quite successful in many problems. (It might be noted that many synthesis codes synthesize the reactor power density rather than the flux itself,[16] for it is found that this gives a more accurate estimate of the three-dimensional core power distribution, which is of course usually the information one seeks.)

Experience with multichannel synthesis is far more limited. However in those cases in which the flux is highly nonseparable or in which it is difficult to choose the appropriate expansion functions, multichannel synthesis methods should prove superior.

## B. Spectral Synthesis

The general synthesis process of building up a complicated solution out of simpler, but not elementary, component parts has received a great deal of attention in other aspects of core analysis as well. There are, for example, problems in which significant details of the flux distribution can be predicted in advance, and in these situations the full calculation of the flux using standard multigroup finite-difference equations generates (at great expense) large amounts of redundant information. For example, an accurate calculation of the flux distribution in a fast reactor using the finite-difference multigroup equations would require the use of a great many groups (20–30) to treat the energy-dependence at each spatial point, when in fact it is known that the energy spectrum shifts fairly smoothly in space from one typical mode to another. The actual "information content" consists of these modal spectra and their relative strengths at each point, so effort is wasted in the finding of the multigroup solution. Synthesis techniques can be used to greatly simplify such calculations.

Thus far we have confined our attention to synthesis in the spatial variables, but the energy variable is also amenable to such a treatment.[18,19,20] In the sense that the multigroup approximation can be interpreted as a synthesis method, synthesis of the energy-dependence of the flux has been used for a long time. In the derivation of the multigroup equations it is implicitly assumed that the fine structure of the energy-dependence is fairly constant over larger spatial regions, and that it is only necessary to compute scale factors to be applied to precalculated spectra for each disjoint energy group. This proves very successful in applications to thermal

spectrum reactors, where indeed the dominant energy effect is the coupling of the neutron "birth" region through the resonance region to the thermal region, and usually only a few energy groups are sufficient. However things are not so simple in fast reactor analysis, where many groups would be required to adequately describe the energy-dependence.

Proper multigroup analysis of a fast reactor requires calculations in 20–30 groups primarily because of the effects of the resonances in the fast region. The spatial variations of the flux, however, are fairly smooth because the long mean free paths of fast neutrons make fine structural detail "invisible." This effect compensates somewhat, but not entirely, for the greater number of energy variables because the number of spatial variables can be reduced, but it does not alter the fact that the spectrum is everywhere in transition, so that many material regions should be used. Using 20 groups makes a two-dimensional diffusion code expensive to run and detailed three-dimensional analyses almost impossible.

*Spectral* or *energy synthesis* involving the use of overlapping, rather than disjoint, energy expansion functions seems to hold out the promise of solving the space and energy fast flux problem without doing all of the (diffusion theory) work. Spectral synthesis methods are implemented by expanding the flux as a linear combination of known functions of energy

$$\phi(\mathbf{r}, E) = \sum_m \psi_m(\mathbf{r}) \chi_m(E). \tag{13-14}$$

Just as in spatial synthesis methods, weighted residual or variational techniques can be used to obtain a set of coupled diffusion equations for the space-dependent combining functions $\psi_m(\mathbf{r})$. These equations are essentially equivalent in structure to the usual multigroup diffusion equations, except the functions $\psi_m(\mathbf{r})$ refer to the portion of the neutron flux characterized by a given energy spectrum $\chi_m(E)$ rather than a restricted range of energies $E_g \leqslant E \leqslant E_{g-1}$. Hence spectral synthesis is sometimes referred to as the *overlapping multigroup* technique.

Numerous studies have demonstrated that spectral synthesis methods do indeed provide an accurate alternative to multigroup diffusion calculations.[18,19] When combined with suitable numerical algorithms,[20] the spectral synthesis method can also yield very considerable savings in computation time over conventional multigroup techniques. Hence these methods are currently under active investigation and application, particularly to problems in fast reactor analysis.

## V. LOCAL POWER-PEAKING EFFECTS

In any heterogeneous core configuration there will be local variations in the neutron flux or power distribution that must be taken into account in reactor core design. We have already examined how the spatial variation of the flux in the vicinity of a fuel pin is treated by using collision probability methods to compute cell-averaged group constants. We will employ very similar techniques to analyze control elements in Chapter 14.

However there are other local spatial flux variations occurring due to variations in core composition and playing an important role in reactor design. Of major concern is the local power-peaking that occurs at the boundary between fuel and moderator regions. For example, in LWRs one is concerned with the power-peaking that occurs in water channels between fuel assemblies or the channels from

which control rods have been withdrawn. Since we have found that the moderator acts as an effective source of thermal neutrons (due to slowing down), we might expect that the fuel elements adjacent to such water channels will see a larger thermal flux and hence experience a higher power density. Since the local flux near the channel may be considerable higher than the average flux in the region, one must take care that constraints on core power densities (such as the critical heat flux limitations) are not exceeded. To this end, one would like to compute the local *power-peaking factor* for the channel that gives the peak-to-average flux.

Similar effects can occur at the boundaries between zones of different fuel loading, or between the reactor core and reflector regions (such as in HTGR cores characterized by axial fuel-loading zones). Although the detailed calculation of such local power-peaking factors generally involves multidimensional, multigroup diffusion calculations for the core region of interest, we can illustrate most of the physical ideas involved with a very simple modeled calculation.[21,22]

We will consider a one-dimensional slab geometry composed of two adjacent regions characterized by different composition (Figure 13-8). For example, one region might represent a water channel and the other region, a fuel assembly (in which fuel elements and coolant channels have been appropriately homogenized). For point of reference, we will assume that region 1 is characterized by a lower absorption than region 2 so that we can confine our attention to determining the power-peaking that occurs in region 2 due to the presence of region 1. For convenience, we will use a one-speed diffusion model:

$$-D_1 \frac{d^2\phi_1}{dx^2} + \Sigma_{a_1}\phi_1(x) = S_1,$$

$$(13\text{-}15)$$

$$-D_2 \frac{d^2\phi_2}{dx^2} + \Sigma_{a_2}\phi_2(x) = S_2,$$

where $S_1$ and $S_2$ represent spatially uniform slowing down sources within each region. Consistent with our interpretation of this modeled problem as representing a unit cell of the core lattice, we will use zero-current boundary conditions at $x = 0$
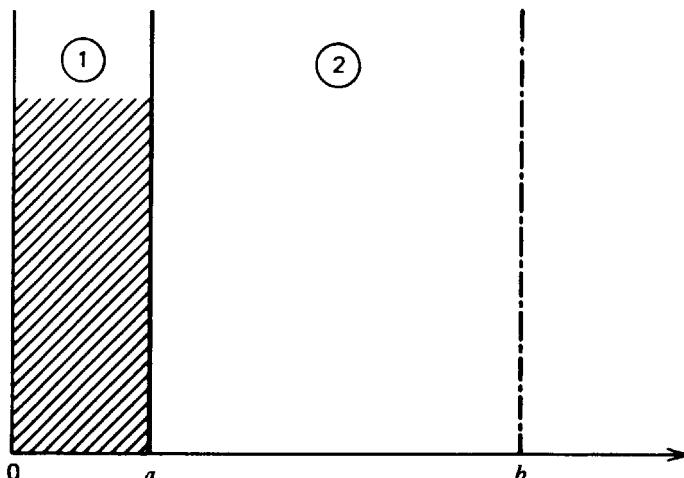


FIGURE 13-8.    Two-region slab-geometry model of power peaking.

and $x = b$, as well as the interface conditions at $x = a$:

$$J_1(0) = 0, \qquad J_2(b) = 0,$$
$$\phi_1(a) = \phi_2(a), \qquad J_1(a) = J_2(a). \tag{13-16}$$

We can easily solve Eq. (13-15) for the fluxes $\phi_1(x)$ and $\phi_2(x)$ in each region.

Actually we are not interested in the flux itself, but rather in the power-peaking factor $F_{pp}$ characterizing region 2, which is defined as the peak-to-average power ratio

$$F_{pp} = \frac{\phi_{max}}{\phi_{ave}} = \frac{\Sigma_{f_2}\phi_2(a)}{\dfrac{\Sigma_{f_2}}{b-a}\displaystyle\int_a^b \phi_2(x)\,dx}, \tag{13-17}$$

where we have noted here that the peak power will occur at the interface between the two regions. If we solve for $\phi_2(x)$ and then substitute into Eq. (13-17), we find the general result

$$F_{pp} = \frac{\dfrac{S_2}{\Sigma_{a_2}} + A_2 \cosh\left(\dfrac{b-a}{L_2}\right)}{\dfrac{S_2}{\Sigma_{a_2}} + \dfrac{A_2 L_2}{b-a}\sinh\left(\dfrac{b-a}{L_2}\right)}, \tag{13-18}$$

where

$$A_2 = \frac{\dfrac{S_1}{\Sigma_{a_1}} - \dfrac{S_2}{\Sigma_{a_2}}}{\cosh\left(\dfrac{b-a}{L_2}\right) + \dfrac{D_2 L_1}{D_1 L_2}\coth\dfrac{a}{L_1}\sinh\left(\dfrac{b-a}{L_2}\right)}. \tag{13-19}$$

Actually this result is a bit too complicated for our purposes. Instead we will assume that region 1 (e.g., the water channel) is narrow such that $a \ll L_1$, while region 2 (the fuel) is wide such that $b-a \gg L_2$. Then one can reduce Eq. (13-18) to the simpler approximate form

$$F_{pp} = \frac{S_2 + \dfrac{aS_1}{L_2}}{S_2 + \dfrac{aS_1}{(b-a)}}. \tag{13-20}$$

This simple result reveals several interesting aspects of local power-peaking. First, the peaking will increase as the width of the moderating region $a$ increases, or as the diffusion length $L_2$ in the fuel decreases (e.g., by using higher enrichment fuels). We can decrease the power-peaking by either decreasing the slowing down source $S_1$ in the channel (e.g., by using control rod followers characterized by weak moderating properties), increasing the slowing down source in the fuel region, or decreasing the fuel region width $b-a$.

There are other possible schemes for reducing such local power peaking that are not described by this model. For example, it is common practice in BWRs to use

fuel elements of somewhat lower enrichment near fuel assembly boundaries. One can also use distributed burnable poisions to flatten out the power-peaking.

The power-peaking in water channels in a LWR is mitigated by some extent by thermal-hydraulic coupling effects. This is particularly true in BWRs in which the very large negative void coefficient of reactivity due to boiling causes an inherent self-flattening of local power peaks.[23,26] We have sketched the power-peaking in a water channel adjacent to a BWR fuel assembly for several different coolant densities in Figure 13-9.

Yet another effect which gives rise to power-peaking is fuel densification, which can occur in metal clad fuel elements.[24] It has been found that ceramic fuel pellets can shrink both axially and radially when irradiated in a reactor core. This shrinkage gives rise to gaps in the fuel-pellet column within the fuel element. Because of decreased neutron absorption in the gap, there will be power-peaking in fuel elements adjacent to the gap.

The primary power peaking effect in HTGRs arises at boundaries between zones of differing fuel loading[25] (see Figure 13-10). Although the power-peaking factor is usually close to unity (typically $F_{pp} \sim 1.1$), such peaking effects must be accounted for in HTGR core design.
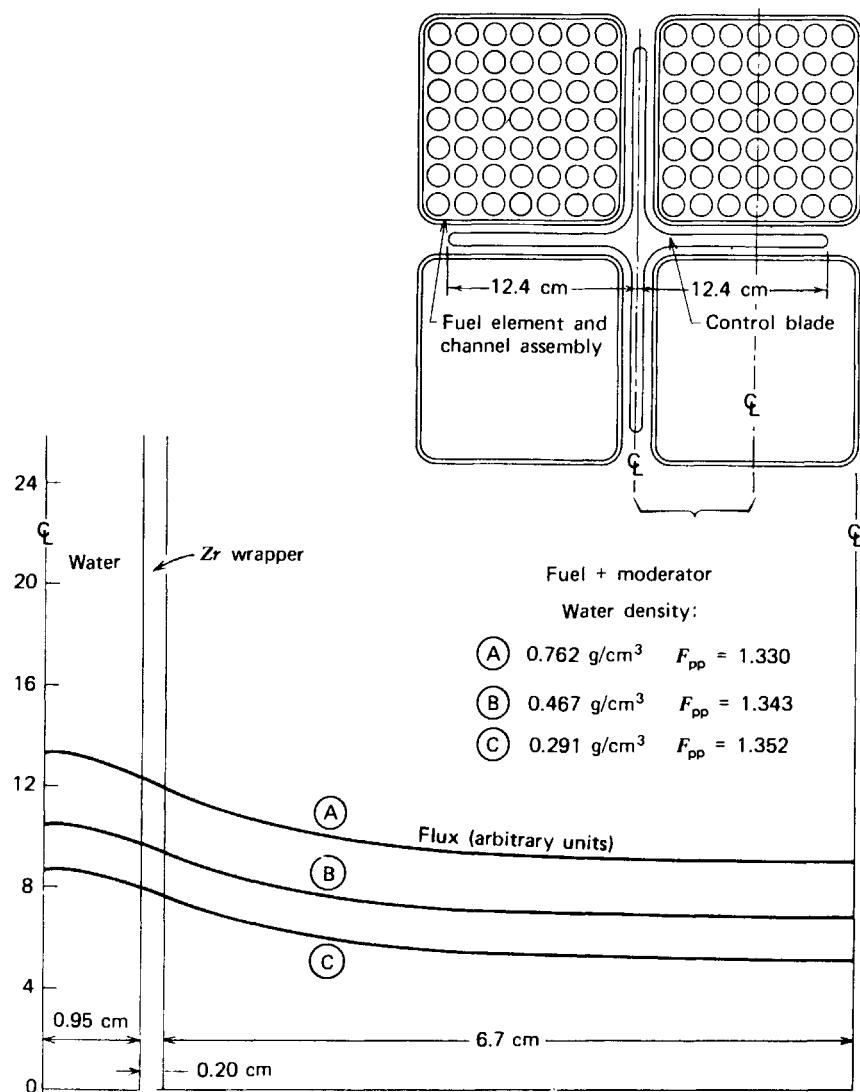


FIGURE 13-9.   Power-peaking in a water channel adjacent to a BWR fuel assembly.
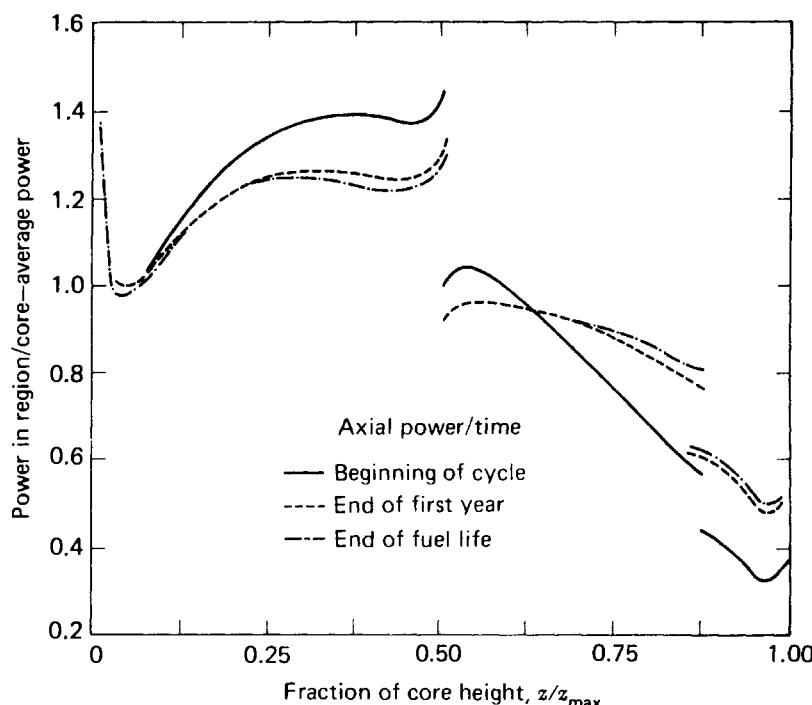
FIGURE 13-10. Power-peaking due to axial zones of different fuel loading in an HTGR.[25]

## REFERENCES

1. F. W. Todt and L. J. Todt, FEVER/M1–A One-Dimensional Depletion Program for Reactor Fuel Cycle Analysis, Gulf General Atomic Report GA-9780 (1969).

2. R. F. Barry, LEOPARD—a spectrum-dependent non-spatial depletion code for the IBM-7094, USAEC Report WCAP-6058 (1964).

3. W. R. Cadwell, PDQ-7—a program for the solution of the neutron diffusion equations in two dimensions, USAEC Report WAPD-TM-678 (1967).

4. R. L. Hellens, The physics of PWR reactors, New Developments in Reactor Physics and Shielding, CONF-720901, (1972), Vol. I., p. 3.

5. E. G. Adensam, et al., Reactor and Fuel Proc. Tech. 12, (2) (1969).

6. D. L. Delp, D. L. Fischer, J. M. Harriman, and M. J. Stedwell, FLARE, a three-dimensional boiling water reactor simulator, General Electric Report GEAP-4598 (1964).

7. R. G. Steinke, A coarse nodal method for solving the neutron diffusion equation, University of Michigan Ph.D. Dissertation (1972); H. W. Graves, Jr., Evaluation of power distribution in large reactors using a two-group nodal method, University of Michigan Ph. D. Dissertation (1973).

8. C. F. Kang and K. F. Hansen, Trans. Am. Nucl. Soc., 14, 199 (1971).

9. S. Nakamura, Nucl. Sci. Eng. 43, 116 (1971).

10. S. Kaplan, Nucl. Sci. Eng. 13, 22 (1962).

11. M. R. Bucker and H. C. Honeck, Mathematical Models and Computational Techniques for Analysis of Nuclear Systems, USAEC Report CONF-730414-P1 (1973), p. IX-42.

12. S. Karin, P. E. Meyer, and R. G. Steinke, An automated modular light water reactor calculation code package, Proceedings of Conference on New Developments in Reactor Mathematics and Applications, CONF 710302 (Vol. 2) (1971) p. 983.

13. A. Radkowsky (Ed.), Naval Reactors Physics Handbook, Vol. I, Selected Basic Techniques, USAEC Report TID-7030 (1964) p. 656.

14. W. M. Stacey, Jr., Modal Approximations: Theory and An Application to Reactor Physics, M.I.T. Press, Cambridge (1967).

15. J. B. Yasinsky and S. Kaplan, *Nucl. Sci. Eng.* **28**, 426 (1967); S. Kaplan, *Nucl. Sci. Eng.* **13**, 22 (1962).

16. R. D. Traylor, V. Malakhof, and S. Leighton, SCANAL, a single-channel synthesis depletion code with triangular mesh in the horizontal plane, Gulf General Atomic Report GA-9423 (1969).

17. E. L. Wachspress and M. Becker, Variational multichannel synthesis with discontinuous trial functions, USAEC Report KAPL-3095 (1965).

18. P. G. Lorenzini and A. H. Robinson, *Nucl. Sci. Eng.* **44**, 27 (1971).

19. R. J. Neuhold, *Nucl. Sci. Eng.* **43**, 74 (1971).

20. W. G. Price, Jr. and J. J. Duderstadt, *Nucl. Sci. Eng.* **55**, 98 (1974).

21. H. W. Graves, *Nuclear Reactor Design*, University of Michigan Nuclear Engineering Department Lecture Notes (unpublished) (1969).

22. R. W. Deutsch, Nucleonics **16**, 95 (1958).

23. R. L. Crowther, Physics measurements of BWR reactors and comparison with theory, New Developments in Reactor Physics and Shielding, USAEC CONF-720901 (1972), p. 114.

24. Technical session on fuel densification, *Trans. Am. Nucl. Soc.* **8**, 120 (1974).

25. GASSAR 6, General Atomic Standard Safety Analysis Report, GA-A13200 (1975).

26. N. McFarlane, *Nucl. Appl. Tech.* **9**, 634 (1970); E. Fuller, *Nucl. Appl. Tech.* **9**, 622 (1970).

27. R. Froehlich, *in* Mathematical Models and Computational Techniques for Analysis of Nuclear Systems, USAEC Document CONF-730414-P2 (1973), p. VII-1.

28. O. J. Marlowe, et al., WANDA, A One-Dimensional Few Group Diffusion Code, WAPD-TM-28 (1956), WAPD-TM-241 (1960); H. P. Flatt and D. C. Baller, AIM-5, A Multigroup One-Dimensional Diffusion Code, NAA-SR-4694 (1960).

## PROBLEMS

13-1 Numerous factors in a nuclear reactor core design depend on the moderator-to-fuel volume ratio $V_M/V_F$ in a fuel cell. Suppose we imagine decreasing this ratio in a LWR, by decreasing lattice pitch while keeping fuel rod radius fixed. Indicate qualitatively how and why each of the parameters below might be affected by such a change in the reactor core if the core is initially undermoderated.

(a) Nuclear factors: $\eta, f, p, \epsilon, P_{FNL}, P_{TNL}$, and $k_\infty$.

(b) Thermal-hydraulic factors: Core power density, coolant flow rate, core pressure drop, fuel and clad temperature, and DNBR.

(c) Safety factors: Temperature coefficient of reactivity and response to a loss of coolant accident.

(d) Economic factors: Fuel inventory, core size, and conversion ratio.

13-2 Using first-order perturbation theory, estimate the sign of the change in the thermal group constant $\bar{\sigma}_f^{25}$ due to the presence of [239]Pu. For convenience, model the thermal resonance of [239]Pu as a Dirac $\delta$-function such that

$$\Sigma_a^{49}(E) = \Sigma_a(kT)\psi\left[\left(\frac{E_T}{E}\right)^{1/2} + \alpha\delta(E - E_0)\right],$$

and, in particular, examine the cases of $E_0 \gtrless E_T = kT$.

13-3 Demonstrate that for small $\psi$, the thermal group constants $\bar{\sigma}$ depend linearly on $\psi$.

13-4 Provide a physical explanation for the dependence of the fast-group constants on the moderator-to-fuel ratio shown in Figure 13-6. (Remember that these results were generated using a MUFT scheme.)

13-5 The following problem will require the use of a very simple code package which includes: (a) a simple group constant generation code (e.g., SOFOCATE–MUFT), (b) a one-dimensional few-group diffusion code (e.g., WANDA[28] or AIM), and (c) a single-channel thermal–hydraulics code capable of analyzing a boiling water channel in a BWR. This problem demonstrates a number of topics in Chapter 13, including thermalhydraulic coupling and group constant parameterization. Consider the BWR/6 core design given in Appendix H. Idealize the reactor core as an infinite bare slab (Figure 13-11). Using a simple LWR code package, determine both $k_{eff}$ and the *axial* power distribution for the reactor. In your solution to the problem, carefully outline your calculational procedure as well as the reasoning that led to the procedure. Hints are as follow:

(a) The purpose of this problem is to demonstrate the strong coupling between the neutronic calculations and thermal-hydraulic calculations in reactor design.

(b) You will have a limited amount of computer funds, so give careful thought as to how you can best spend the money to get maximum accuracy in your solution.

(c) Do not treat this as a criticality search problem! Both composition and geometry are fixed.

Procedure:

(i) Run the thermal-hydraulics code to obtain representative water densities, fuel temperatures, and moderator temperatures. Use a bottom-peaked profile since $k_{\infty}$ (and power) are expected to be greater in a nonboiling region of the core.

(ii) Run the fast and thermal spectrum codes for high, low, and average water density, using average fuel and moderator temperature. Determine $\Sigma_x^j (\rho_{H_2O})$. Actually $\Sigma_x^j$ is a function of $T_{fuel}$ as well. Since there is not a direct correlation between $T_{fuel}$ and $\rho_{H_2O}$, one should plot $\Sigma_x^j$ versus both $T_{fuel}$ and $\rho_{H_2O}$. However to minimize computing costs, the same fuel temperature $T_{fuel}$ can be used for all $\Sigma_x^j$. Plot $\Sigma_x^j$ versus $\rho_{H_2O}$ so that the spectrum codes need not be run for other water densities. (Use the graph to obtain $\Sigma_x^j$ for other $\rho_{H_2O}$.)

(iii) Divide the core into suitable regions and find the average density in each region from the thermal-hydraulics code. From these densities determine all $\Sigma_x^j$ for each region as input to the diffusion code.

(iv) From the multigroup diffusion calculation, obtain $k_{eff}$ and the power profile for input to the thermal-hydraulics calculation.

(v) Since neutronics and thermal-hydraulics are coupled, iterate between the MGD and T-H codes until convergence of $k_{eff}$ and the power profile occurs.
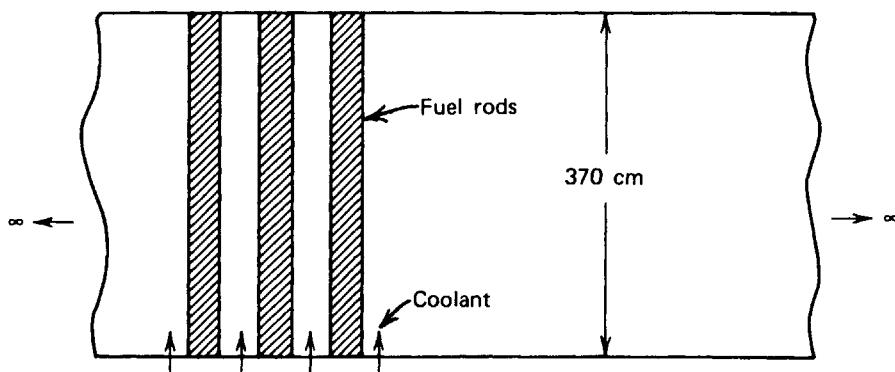


FIGURE 13-11. Slab model of axial BWR power calculation.

13-6 Use a one-dimensional code to perform a buckling iteration between axial and radial calculations on the BWR of Problem 13-5 similar to that described in Section 13-IV. For convenience, assume that the moderator density profile is fixed, obviating the necessity of performing a thermal-hydraulic calculation.

13-7 Using the weighted residual method, develop the general form of the equations describing the axial weighting coefficients in a single-channel synthesis scheme. For convenience, treat only the case of one-group diffusion theory.

13-8 Choose the energy-expansion functions in the spectral synthesis method to be disjoint step functions

$$\chi_m(E) = \begin{matrix} 1, & E_m \leqslant E \leqslant E_{m-1} \\ 0, & \text{otherwise}, \end{matrix}$$

$$m = 1, \ldots, M.$$

Then using the weighted residual method, verify that this choice indeed leads to the usual multigroup diffusion equations. For convenience, choose the weight functions $w_m(E)$ to be the $\chi_m(E)$ proper. (This is known as the Galerkin weighting scheme.)

13-9 Explicitly derive the form given for the power-peaking factor $F_{pp}$ in Eq. (13-20).

13-10 Repeat the derivation of the power-peaking factor for the slab geometry of Figure 13-8 by equating the current leaving the moderator region to the rate of thermal neutron production in this region.

13-11 Derive the power-peaking factor characterizing two adjacent fuel regions of differing enrichment.

13-12 In the BWR described in Problem 13-5, water slots are provided between fuel assemblies to accomodate the cruciform shaped control rods (see Figure 13-9). When the control rods are withdrawn from the water channels, power-peaking can occur in neighboring fuel rods. We will model the geometry by the one-dimensional representation shown in Figure 13-9.

(a) Use a one-dimensional, one thermal group diffusion model to determine: (i) shape of the flux in the unit cell, and (ii) the power-peaking factor $F_{pp}$ for the unit cell.

(b) What is the trend in $F_{pp}$ if: (i) the water channel thickness is increased, (ii) the fuel enrichment is increased, and (iii) stainless steel cladding is substituted for zircaloy cladding.

Justify your answers.

# 14

## Reactivity Control

## I. INTRODUCTION

Nuclear reactors must be initially loaded with a significantly larger amount of fuel than that required merely to achieve criticality, since the intrinsic multiplication of the core will change during core operation due to processes such as fuel burnup and fission product production. Sufficient excess reactivity must also be provided to compensate for negative reactivity feedback effects such as those represented by the temperature and power defects of reactivity. In contrast to the core geometry and volume, which are primarily determined by thermal considerations (i.e., achieving the required core thermal power output utilizing a power density consistent with thermal design limitations), the fuel loading or enrichment will be determined by the desire to build into the core sufficient excess reactivity to allow full power operation for a predetermined period of time.

To compensate for this excess reactivity, it is necessary to introduce an amount of negative reactivity into the core which one can adjust or control at will. This control reactivity can be used both to compensate for the excess reactivity necessary for long term core operation and also to adjust the power level of the reactor in order to bring the core to power, follow load demands, and shut the core down. The control reactivity is most often present in the form of strong neutron absorbers that can be inserted into or withdrawn from the core (although movable core reflector elements or fuel assemblies and coolant flow have also occasionally been used for reactivity control). The determination of the control reactivity requirements and the apportionment of control reactivity among various types of control elements is a very important aspect of nuclear reactor core design. In this introductory section we will classify the control requirements of nuclear reactor

cores, as well as the various control elements commonly used in power reactors. It is first useful to introduce several definitions characterizing reactivity control:

(1) *Excess reactivity* $\rho_{ex}$: The core reactivity present with all control elements withdrawn from the core. $\rho_{ex}$ will be a function of both time (due to fuel burnup and isotope production) and temperature (due to reactivity feedback). Larger values of $\rho_{ex}$ will generally imply longer core lifetimes, but at the expense of larger control requirements and poorer neutron economy (since with more control reactivity in the core, there will be more neutron absorption).

(2) *Shutdown margin* $\rho_{sm}$: The negative reactivity of the core present when all control elements have been fully inserted to achieve minimum core multiplication. Again the shutdown margin $\rho_{sm}$ is a function of time and temperature. For example, the shutdown margin for a "cold," "clean" core, that is, a core at ambient temperatures and with a fresh fuel composition in which no depletion or fission product buildup has occurred, will be quite different from the shutdown margin characterizing a core that has been operating at power for some time. Typically shutdown margins are chosen such that the core multiplication is below critical (e.g., $k = 0.99$) even with the most reactive control rod stuck in the full "out" position (the so-called *stuck-rod criterion*).[1]

The shutdown margin not only characterizes the core multiplication in its shutdown state, but is also related to the rate at which the reactor power level may be reduced in an emergency shutdown or "scram." In particular we recall that the prompt jump approximation implies that the fractional power level decrease achieved immediately after control insertion is given approximately by:

$$\frac{\text{Power before control insertion}}{\text{Power after control insertion}} = \frac{\beta - \rho_0}{\beta - \rho_1} = \frac{\beta}{\rho_{sm} + \beta}. \qquad (14\text{-}1)$$

For example, a shutdown margin of $\rho_{sm} = .030$ would imply that the reactor power level in a $^{235}$U-fueled thermal reactor ($\beta = .00655$) would drop to 18% of its initial value immediately following a scram.

(3) *Total control element worth* $\Delta\rho$: The difference between the excess reactivity and the minimum reactivity when all control elements are fully inserted. That is,

$$\Delta\rho = \rho_{ex} + \rho_{sm}. \qquad (14\text{-}2)$$

The precise definition of reactivity worth is occasionally given a slightly different characterization, depending on whether the control element of interest is intended for power-level changes or for longer term fuel burnup compensation.[2] We will utilize the simple definition implied by Eq. (14-2) above.

(4) *Control element worth* $\Delta\rho_i$: One can also define the reactivity worth of an individual control element as the reactivity change induced in the core by the full insertion of the element. In Table 14-1, we have listed typical values of the excess reactivity requirements, shutdown margins, and

control element worths for the principal reactor types. We will return later in this chapter to discuss how this reactivity control is allocated among various control elements. It should be noted that the amount of excess reactivity and hence control required for thermal reactors is considerably larger than that required for fast reactors (in which fuel breeding compensates for fuel depletion).

**TABLE 14-1:  Reactivity Requirements in Major Reactor Types**

| Reactivity $(\Delta k / k)$ | BWR | PWR | HTGR | LMFBR |
|---|---|---|---|---|
| Excess reactivity $\rho_{ex}$ of clean core: | | | | |
| at 68 °F | 0.25 | 0.293 | 0.128 | 0.050 |
| at op. temp | | 0.248 | | 0.037 |
| at eq. Xe, Sm | | 0.181 | 0.073 | |
| Total worth of control, $\Delta\rho$ | 0.29 | 0.32 | 0.256 | 0.074 |
| Control-rod worth | 0.17 | 0.07 | 0.156 | 0.074 |
| Burnable poison worth | 0.12 | 0.08 | 0.100 | |
| Chemical shim worth | | 0.17 | | |
| Shutdown margin $\rho_{sm}$ | | | | |
| Cold and clean | 0.04 | 0.03 | 0.028 | 0.024 |
| Hot and eq. Xe, Sm | | 0.14 | 0.082 | 0.037 |

One can distinguish several different types of control requirements:

(1) *Scram control*: The reactor control system must be capable of shutting the reactor down under any credible operating conditions. Elements used for such scram control purposes must be capable of inserting negative reactivity very rapidly and must operate with an extremely high degree of reliability.

(2) *Power regulation*: Certain control elements are designed to compensate for small reactivity transients caused by changes in load demand, core temperature, and for power-level maneuvering.

(3) *Shim control*: Shim control elements are designed to cover the excess reactivity necessary to compensate for long-term fuel depletion and fission product buildup, as well as to shape the power distribution in the core in order to obtain better thermal performance and more uniform fuel burnup. Although the reactivity worth of such elements must of necessity be quite large, shim control adjustments are made very gradually over long time periods.

There are several schemes used for introducing control absorption into a nuclear reactor core. One common method is to insert movable rods of absorbing material into the core. Such *movable control elements* not only can be used to adjust the core power, but because of their rapid response can also be used for scramming the reactor, as well as for shim and power shaping. Fixed absorbing materials are sometimes fabricated into the core, with the intent that such absorption will gradually burn out along with the fuel. These *burnable poisons* are useful for extending the initial core lifetime of reactors. A third very popular control mechanism in LWRs involves dissolving a poison such as boric acid in the coolant itself. Such a *soluble poison* provides a very uniformly distributed shim control which minimizes spatial power profile perturbations.

A large power reactor will contain many control elements distributed in a pattern about the core in an effort to achieve efficient reactivity control within flux-peaking limitations, as well as to facilitate power shaping. The grouping of such control rods, the determination of the control rod withdrawal sequence, and the coordination of movable control elements with burnable and soluble control poisons all fall within the realm of what is known as *control management*. Since the reactivity worth of control elements will change, due to both the depletion of control absorber nuclei and changes in the core power distribution, control management analysis must continually monitor the worth of the control system components throughout core life in order to maintain both an adequate shutdown margin and sufficient operating maneuverability.

## II. MOVABLE CONTROL RODS

### A. General Considerations Involved in Control Rod Design

Movable control rods are used for a variety of purposes—to control reactivity for power maneuvering, shim control, or reactor scram. In the early days of nuclear reactor development, control elements were typically cylindrical in shape. However in today's tightly packed fuel lattices, control elements are typically cruciform-shaped blades or clusters of narrow control rods, although larger cylindrical rods continue to be utilized in gas-cooled reactors. We have included illustrations of typical movable control rod assemblies in Figures 14-1, 14-2, and 14-3.
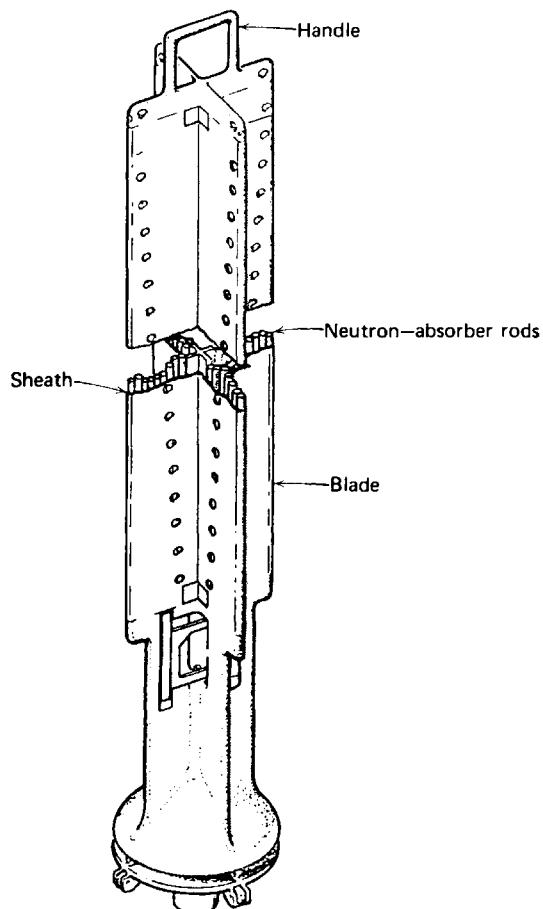


FIGURE 14-1. BWR control rod assembly.[15]
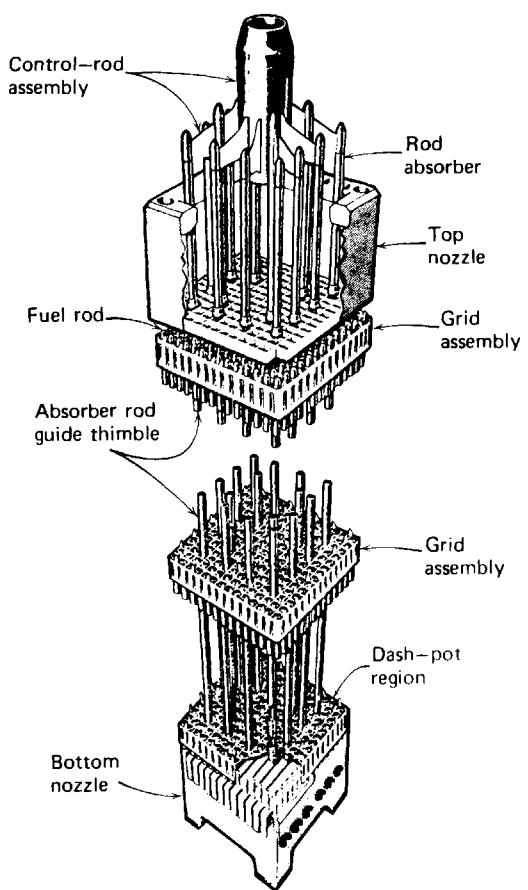
**FIGURE 14-2.** PWR rod cluster control assembly.[16]
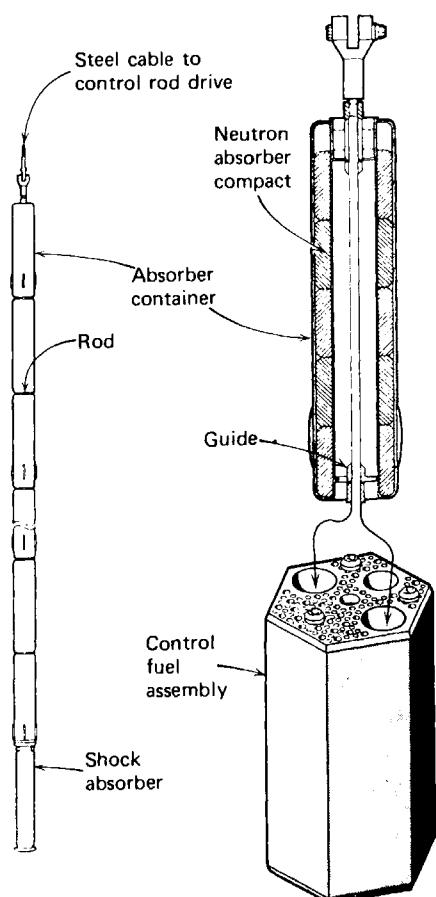


**FIGURE 14-3.** HGTR control rod and control fuel assembly.[21]

A number of factors are involved in the design of such control elements.[3] For example, one would desire to achieve the required reactivity worth with a minimum perturbation on the flux distribution in the core. Obviously if the control rod is too highly absorbing (too "black"), there will be a very pronounced flux depression in its vicinity. Hence one generally attempts to design rods such that their thickness is not much over several mean absorption lengths. Such considerations place a premium on high surface-to-volume ratios for control elements (such as those characterizing cruciform blades).

In thermal reactor control, most of the neutron absorption in control elements (some 60%–80%) occurs in the thermal energy range. However there will be an epithermal absorption effect due to resonance absorption. In an ideal design, a mixture of absorbing isotopes would be used to provide absorption over a range of neutron energies (e.g., the Ag–In–Cd alloy used in PWR control elements).

There are a number of other considerations involved in designing a control element. For example, one desires a composition and design having a long lifetime against absorber depletion. This requires a large number of absorbing atoms per unit volume. The depletion of absorber material is a prime factor in determining control rod thickness. The control element must also be designed with consideration given to mechanical performance. For example, the intense radiation environment in which the rod must function will cause high radiation damage. Furthermore the control element must exhibit good resistance to corrosion, as well as being able to tolerate the high operating temperatures in the core. Such temperatures are augmented by the heat generated within the element due to neutron capture. Finally the fabrication costs of the element will be an important factor in determining the design.

## B. The Calculation of Control Rod Worth

The calculation of the reactivity worth of individual control elements and groups of such control elements and the effects of such elements on the power distribution in the core of a nuclear reactor constitute a very important facet of nuclear reactor design. A variety of methods have been developed to calculate control rod worth.

One might be tempted to utilize perturbation theory to estimate the effect of a localized control absorber on core multiplication. Unfortunately, however, the strong absorption characterizing a control element causes a severe local distortion of the flux, particularly in those fuel assemblies adjacent to the rod. The control element is characterized by strong self-shielding, much as fuel pins are. Hence perturbation theory is of limited use in control studies, unless the control element is characterized by relatively weak absorption. (Although the control absorption is usually too strong to allow meaningful perturbation theory estimates in thermal reactors, the decrease of absorption cross sections and increase in mean free paths with increasing neutron energy allows some justification for use of perturbation methods in fast reactor control studies. And, as we saw earlier in Chapter 5, even though perturbation theory usually does not provide meaningful estimates of *absolute* control rod worths, it does in fact prove useful in studying the *relative* worth of various control element patterns and positions.)

A more common approach involves the use of one-speed diffusion theory treatments that utilize transport-corrected boundary conditions at the surface of the control rod. The literature[4] abounds with diffusion theory studies of cylindrical rods inserted into bare, homogeneous cylindrical reactor cores—either on or off

core axis. However such analyses are of little relevance to control studies of large power reactors with relatively tight fuel lattices in which large numbers of elements are distributed about the core in an effort to achieve a more uniform power distribution (see Figure 14-4).
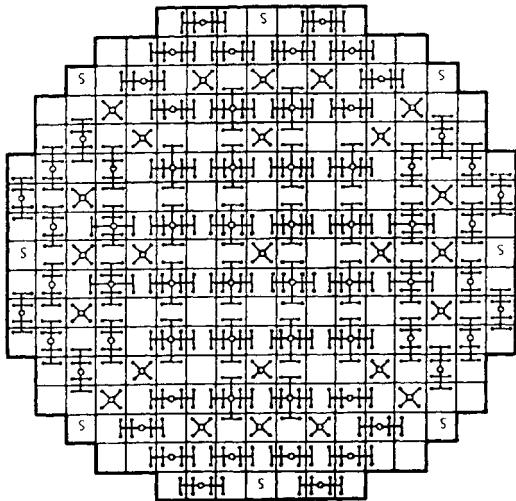


FIGURE 14-4. Location of control assemblies in a PWR core.[19]

We will instead approach the calculation of control rod worths in a manner very similar to that utilized for the inclusion of fuel lattice heterogeneities in the generation of thermal group constants. We will use the fact that modern power reactors contain large numbers of control elements which tend to be reasonably uniformly distributed across the core allowing division of the core into cells, each containing one control element. We will then perform a detailed analysis of one such control cell, similar to the analysis we presented earlier for a fuel cell, in an effort to determine an effective absorption cross section for the control element which, when multiplied by the average flux in the control cell, yields the correct absorption rate in the element. Such effective cross sections can then be included in the multigroup diffusion theory analysis of the overall core. Obviously such a scheme is very similar to the generation of "self-shielded" thermal group constants discussed in Chapter 10.

As in Chapter 10, our approach will be to isolate a local region in the vicinity of the control element from the remainder of the core and to analyze the neutron flux in the region in detail. Typical control cells for several reactor types are sketched in Figure 14-5 by way of illustration. As in our earlier analysis, we will decouple the control cell from the rest of the core by demanding that the net neutron current across the cell boundary is zero. The influence of adjacent cells can be represented by relaxing this boundary condition to allow nonzero flux gradients across the boundary.

Our approach will be to use diffusion theory with transport-corrected boundary conditions on the control element surface in order to determine the flux in the control cell.[5] We can then use this flux to determine an effective cross section $\Sigma_c^{\text{eff}}$ characterizing the control element by requiring that

$$V_{\text{cell}} \bar{\phi} \Sigma_c^{\text{eff}} = S_c J_c,$$

(14-3)

**PWR**

Rod—cluster control element

Fuel rod

Fuel assembly with rod—cluster control

Fuel element and channel assembly

Note:
Special corrected corner rods have different enrichment than standard rods
(1) Intermediate enrichment
(2) Low enrichment

Control blade

**BWR**



Reserve shutdown hole

Coolant hole

Control—rod channel

Fuel hole

Burnable poison hole

**HTGR**
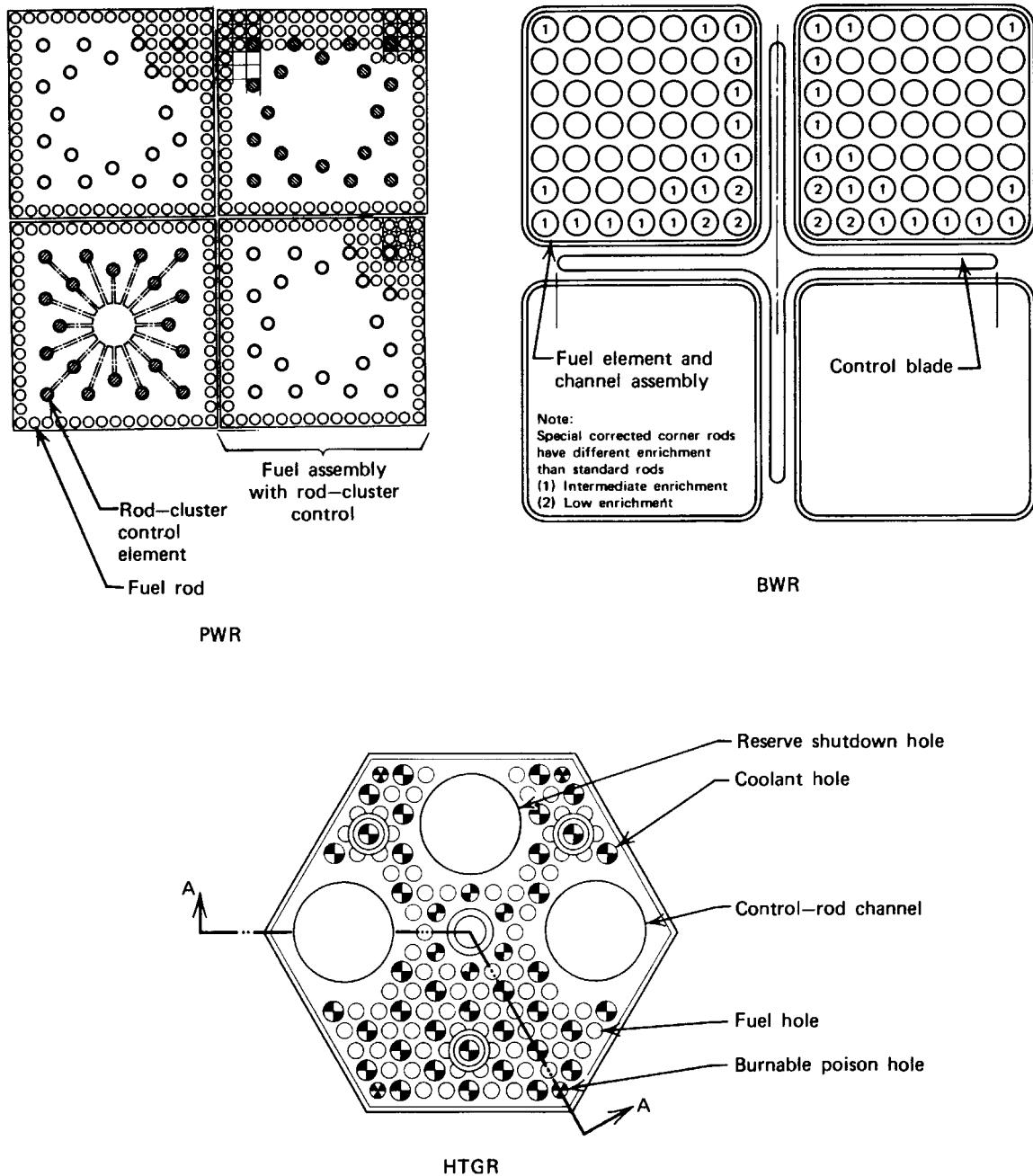
**FIGURE 14-5.** Control cells for several reactor types.

where $\bar{\phi}$ is the volume-averaged flux in the cell, $V_{cell}$ is the control cell volume, and $S_c$ the control element surface area, respectively, while $J_c$ is the average neutron current at the surface of the control element. This usually reduces to a two-dimensional geometry (such as those in Figure 14-5), in which case we can write

$$\Sigma_c^{eff} = \frac{P_c}{A_{cell}} \frac{J_c}{\bar{\phi}},$$

(14-4)

where $P_c$ is the exposed control element perimeter and $A_{cell}$ is the cross-sectional area of the control cell.

Hence our task is obviously to determine the ratio $J_c/\bar{\phi}$ since this will yield $\Sigma_c^{eff}$. The highly absorbing nature of the control element invalidates the direct application of diffusion theory. Instead, one uses a diffusion theory calculation outside the element, collision probability methods within it, and then couples these at the control element boundary using "blackness theory"[7] or effective transport-corrected boundary conditions (much as was done in the ABH method).

The advantage of this approach is that it yields a cell parameter $J_c/\bar{\phi}$ that is relatively insensitive to the material composition surrounding the control element. Hence the detailed calculation of $J_c/\bar{\phi}$ need be performed only once and can be reapplied regardless of the change in the cell composition (due to fuel depletion, moderator density changes, or fission product buildup).

To indicate more clearly just what is involved in such a calculation, let us consider the explicit example of a cruciform-shaped control blade inserted into a homogeneous cell.[6] We will not attack this two-dimensional problem directly, but rather will replace it by an equivalent one-dimensional problem that preserves the same ratio of control rod surface to fuel volume (see Figure 14-6). Such a scheme should give a reasonable estimate if the span $l$ of the control blade is substantially greater than the diffusion length $L$ characterizing the surrounding medium. The surface-to-volume ratio of the rod is

$$\frac{S_c}{V_{cell}} = \frac{8l}{4m^2 - 8tl + 4t^2} .$$

(14-5)

Our equivalent one-dimensional problem will be as shown in Figure 14-6 with a surface-to-volume ratio of $1/a$; hence we will demand

$$a = (m^2 - 2tl + t^2)/2l.$$

(14-6)

We will now use one-speed diffusion theory to determine the flux in the fuel

$$-D\frac{d^2\phi}{dx^2} + \Sigma_a\phi(x) = S_0,$$

(14-7)
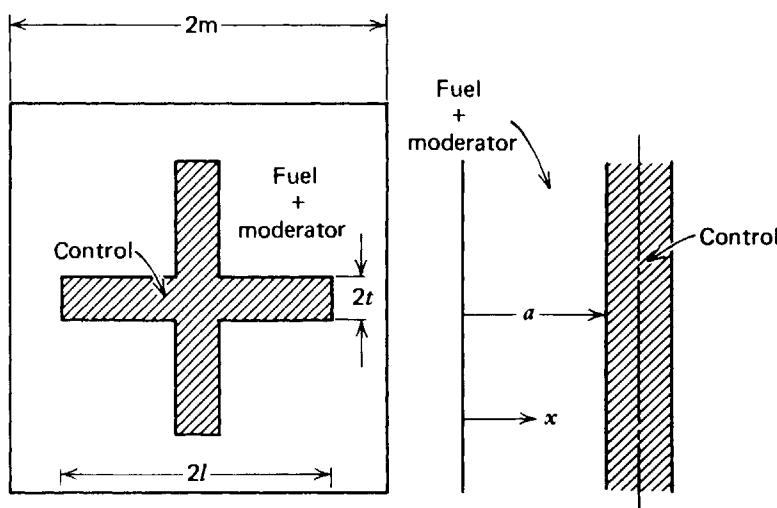


FIGURE 14-6. A one-dimensional model of a cruciform control blade cell.

where we assume a uniformly distributed source of neutrons $S_0$ slowing down in the fuel-moderator mixture. The boundary conditions corresponding to the cell are:

$$J(0) = 0$$

$$J(a)/\phi(a) = \alpha. \tag{14-8}$$

Notice that we have introduced a parameter $\alpha$ characterizing the ratio of the current to the flux at the surface of the control rod. Since the control rod is a strong absorber, $\alpha$ must be determined from a separate transport calculation— much as one determines the extrapolation length characterizing a free plane surface, $z_0 = .7104 \ \lambda_{tr}$. Indeed, by comparing Eq. (14-8) with Eq. (4-175), one can identify an effective extrapolation length as $d = D/\alpha$.

It is convenient to rewrite our expression for the effective control cross section as

$$\Sigma_c^{eff} = \frac{P_c}{A_{cell}} \frac{J_c}{\phi_c} \frac{\phi_c}{\bar{\phi}} = \left( \frac{P_c}{A_{cell}} \right) \alpha \left( \frac{\phi_c}{\bar{\phi}} \right). \tag{14-9}$$

We will solve the above diffusion equation in the fuel to determine the ratio of the surface flux $\phi_c$ to the average flux $\bar{\phi}$. This formulation is particularly enlightening because it stresses that the diffusion equation is only being used to describe the flux outside of the control element. We can easily solve this problem to find

$$\phi(x) = \frac{S_0}{\Sigma_a} \left[ 1 - \frac{\alpha \cosh \frac{x}{L}}{\alpha \cosh \frac{a}{L} + \Sigma_a L \sinh \frac{a}{L}} \right]. \tag{14-10}$$

Then we can compute the maximum-to-average flux ratio as

$$\frac{\phi(a)}{\bar{\phi}} = \frac{\Sigma_a}{\Sigma_a + \frac{\alpha}{L} \coth \frac{a}{L} - \frac{\alpha}{a}}. \tag{14-11}$$

If we note that $P_c/A_{cell} = 1/a$ for our one-dimensional problem, we can find

$$\Sigma_c^{eff} = \frac{\Sigma_a}{a \left( \frac{\Sigma_a}{\alpha} + \frac{1}{L} \coth \frac{a}{L} \right) - 1}. \tag{14-12}$$

In particular, notice that the control rod worth (which is proportional to $\Sigma_c^{eff}$) increases as the ratio of control rod surface to fuel volume increases (i.e., $a$ decreases) or as fuel absorption decreases, as we might have expected. Rod worth also increases with increasing fuel diffusion length, since more of the fuel volume is then sensitive to flux perturbations introduced by the rod.

The calculation of the transport correction parameter $\alpha$ involves the use of transport theory or collision probability methods. If the control element were a perfectly black absorbing slab, then a transport calculation[7] indicates that $\alpha = 0.47$. For gray elements, the result is more complicated and depends on the geometry of

the control element. For a slab element of width $t$, such an analysis yields

$$\alpha = \frac{1 - 2E_3(\Sigma_a t)}{2[1 + 3E_4(\Sigma_a t)]},$$  (14-13)

where $E_n(z)$ is the exponential integral

$$E_n(z) = \int_1^\infty e^{-zu} u^{-n} du.$$  (14-14)

For more complicated element geometries, such as sandwich or pin structures, more complex expressions for $\alpha$ must be used.[8,9] In a similar sense, one can calculate $\phi_c/\bar{\phi}$ for more complicated cell geometries.

A number of other considerations must be included in a more accurate determination of control rod worth. For example, most control blades have structural materials in their tips that protrude into high flux regions. The effective cross section of these regions must usually be calculated separately. Furthermore one finds a flux depression at the corner of the blade, with a corresponding flux-peaking at the opposite corner of the cell. The effective control cross section must be corrected for this effect.

## C. Control Rod Effects on Core Power Distributions

The primary function of movable control elements in a reactor core is to control core reactivity. However we have seen that the strongly absorbing nature of control elements will cause major perturbations in the neutron flux in the vicinity of the control element. Thus far we have confined our treatment to a consideration of such perturbations on a local scale, such as in a control cell. However as the control elements are inserted or withdrawn, they will of course also strongly affect the overall flux distribution and hence the power distribution of the reactor core. It is extremely important to predict the interaction of control elements on core power distributions in order to ensure that the power density limitations demanded by thermal considerations such as those discussed in Chapter 12 are not exceeded. Furthermore, control rod patterns can actually be used to shape the power distribution into a more favorable profile for core thermal performance and fuel burnup.

In determining the effects of control rod insertion patterns on core power distributions, one must be careful to include the many interactions that will affect the power profile. For example, suppose we consider the variation in the axial power profile of a core controlled by rod insertion from the top. At the beginning of core life, the rods must be inserted to compensate for the large excess reactivity of the fresh core loading. The region of the core in which the rods have been inserted will experience decreased multiplication and hence relatively lower fluxes. Hence since the overall reactor power will be kept constant, there will be a flux-peaking near the bottom of the core. As the fuel in the core is depleted, the control rods will be gradually withdrawn to compensate for the reduced reactivity of the fuel. During the early stages of core life, the fuel near the bottom of the core will have been exposed to relatively higher fluxes and hence experience larger burnups. Thus as the control rods are withdrawn, the flux peak will shift toward the top of the reactor core. Such interactions between rods and fuel burnup can be

minimized by using more uniformly distributed control such as burnable poisons and chemical shim.



Beginning of core life (BOL)

End of core life (EOL)
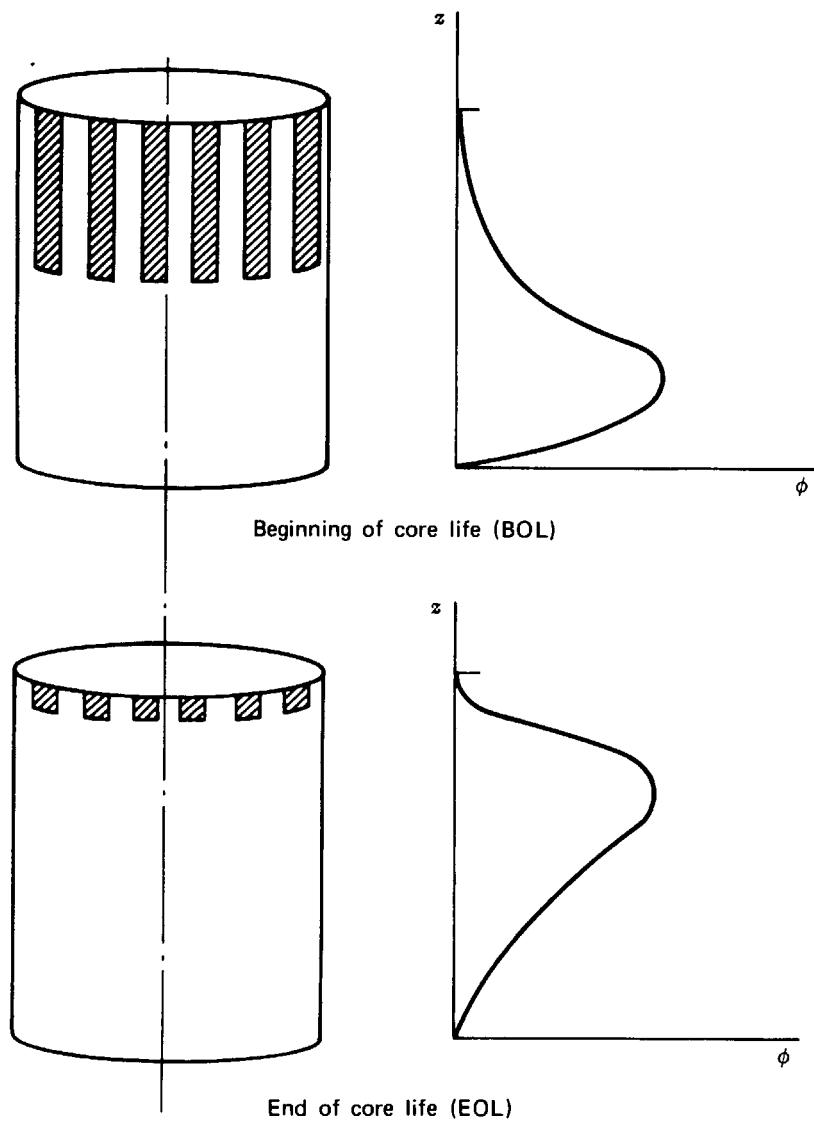
FIGURE 14-7.    Interaction between control rod insertion and flux profile.

Another area of concern is the interaction between control rod positions and the buildup of fission product poisons. The accumulation of fission products characterized by large absorption cross sections, such as $^{135}Xe$, can lead to spatial power oscillations in the core (as we will see in more detail when we study the topic of fission product poisoning in Chapter 15). In certain instances the incorrect management of control rod patterns can lead to instability of these spatial oscillations.

Yet a third type of interaction is found in BWR cores in which the large water density toward the bottom of the core leads to a bottom-peaked flux profile. By inserting control rods from the core bottom, one can compensate for the enhanced reactivity introduced by the higher moderator density and hence achieve a somewhat more uniform axial flux profile.

Of course there are some disadvantages in the use of control elements for power-profile shaping. For example, the achievement of favorable radial power

profiles is sometimes accomplished only at the expense of satisfactory axial profiles. Furthermore the achievement of optimal fuel burnup may be partially offset by the poor neutron economy of a core with high control insertion. These factors must be considered in devising an optimal control management scheme.

To more explicitly study the effects of rod insertion on core power distributions, let us consider a simple model of the interaction of a bank of control rods with an axial flux profile.[10] We will model the reactor as a cylinder and treat the "rodded" and "unrodded" regions of the core as homogeneous (see Figure 14-8). Hence the insertion or withdrawal of the control rod bank is represented by a shift of the boundary between the two regions (a so-called "windowshade" model).
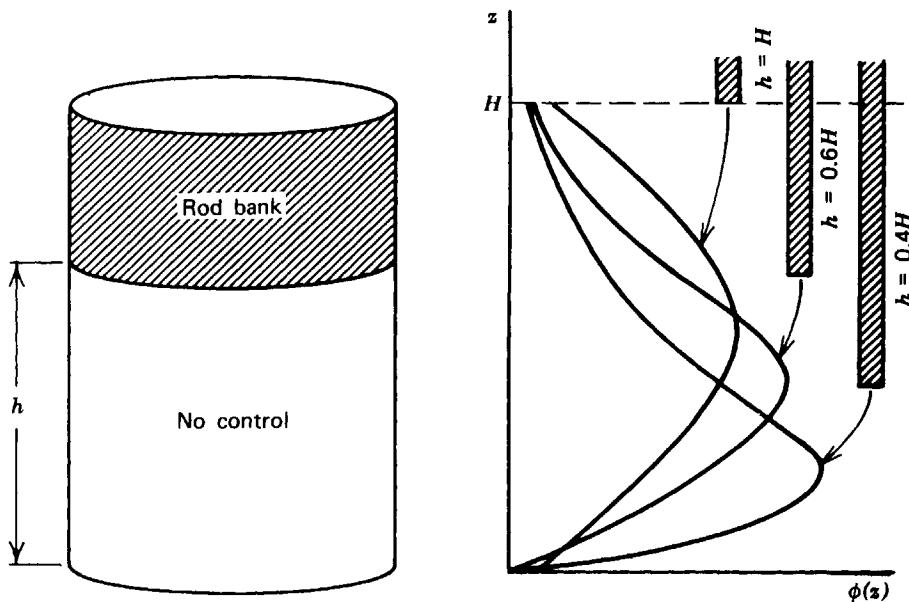


FIGURE 14-8. Insertion of a uniform rod bank into a bare uniform cylindrical core.

To simplify this analysis, we will assume that the flux is separable in $r$ and $z$ such that

$$\phi(r,z) = \mathfrak{X}(z)J_0(\nu_0 r / R).$$ (14-15)

Then the axial flux profile $\mathfrak{X}(z)$ satisfies

$$\frac{d^2 \mathfrak{X}_i}{dz^2} + B_{z_i}^2 \mathfrak{X}(z) = 0,$$ (14-16)

where the effective axial buckling $B_{z_i}^2$ is given by

$$B_{z_i}^2 = \frac{k_{\infty i} - 1}{L^2} - \left(\frac{\nu_0}{R}\right)^2$$ (14-17)

and the $i$ subscript has been included to distinguish between core compositions $(k_{\infty i})$ and hence flux profiles $(\mathfrak{X}_i)$ in the unrodded (region 1) and rodded (region 2) core regions.

We will seek solutions in each of these regions which vanish at the top and

bottom of the core,

$$\mathfrak{T}_1(z) = A_1 \sin B_{z_1} z, \qquad 0 \leqslant z \leqslant h$$

$$\mathfrak{T}_2(z) = A_2 \sinh\left[ B_{z_2}(H - z) \right], \qquad h \leqslant z \leqslant H$$

(14-18)

(where we have assumed the control bank absorption is sufficiently large that $B_{z_2}^2$ is negative) and require the usual interface boundary conditions:

$$\mathfrak{T}_1(h) = \mathfrak{T}_2(h), \qquad D_1 \frac{d\mathfrak{T}_1}{dz}\bigg|_h = D_2 \frac{d\mathfrak{T}_2}{dz}\bigg|_h.$$

(14-19)

Using these interface conditions to match the solutions at $z = h$, we find that the criticality condition becomes

$$\left( \frac{1}{B_{z_1}} \right) \tan B_{z_1} h = -\left( \frac{1}{B_{z_2}} \right) \tanh B_{z_2}(H - h),$$

(14-20)

(assuming $D_1 \sim D_2$) while the relationship between the axial flux amplitudes is

$$\frac{A_2}{A_1} = \frac{\sin B_{z_1} h}{\sinh\left[ B_{z_2}(H - h) \right]}.$$

(14-21)

The axial flux profile has been sketched for several different rod-bank insertion depths $h$ in Figure 14-8. As expected, this result indicates that rod insertion can be used to shift and shape the peak of the axial flux profile. Hence many core designs use *partial-length* control rods[11] containing absorbing material only over a limited fraction of their length in order to more effectively shape the axial profiles.

### D. Control-Adjustment Calculations

In our description of a general nuclear analysis code package, we indicated that a very important component was the *control adjustment module*, which adjusted the amount of control in the core to return the reactor to a critical state following a fuel depletion step. In this sense, the control adjustment module simulates the operation of an actual reactor in which shim control is slowly withdrawn to compensate for the loss of excess reactivity due to fuel burnup.

In many reactor models, one has the option of either adjusting the concentration of a dissolved absorbing isotope in the coolant (i.e., chemical shim) or adjusting the positions of movable control rods using a prescribed insertion-removal sequence scheme. Chemical shim adjustment can be modeled by merely adding a prescribed amount of absorption cross section $\Sigma_a^C$ uniformly across the core. The treatment of movable solid control elements is more complex, as we have seen, and requires the determination of an effective control cross section for each control cell in which the rod position has changed. Such effective control cross sections will depend not only on the rod insertion depth, but also on the coolant density and fuel composition of each cell. Since the frequent calculation of such cross sections can be rather expensive, it is customary to tabulate effective control cross sections versus coolant density and cell burnup so that a control adjustment step only requires a table reference and interpolation (much as is done with multigroup constants).

Since the amount of control necessary to return the core to critical is not known a priori, one must usually proceed iteratively by guessing a control adjustment, computing $k_{eff}$, and then readjusting control if $k_{eff}$ is not sufficiently close to unity. The convergence rate of such an iterative control adjustment procedure depends on one's ability to estimate the required control change. Such a procedure can be greatly accelerated by using perturbation theory to estimate the reactivity worth of a given control adjustment. Such perturbation estimates work quite well for adjustments of a uniformly distributed control absorber, such as chemical shim. However the limited validity of perturbation theory for strongly localized absorbers, such as movable control rods, frequently requires more elaborate treatments in which the local perturbation on the neutron flux in the vicinity of the control element is taken into account.[12]

## III. BURNABLE POISONS

The lifetime of a given core fuel loading, that is, the period during which the core has sufficient excess reactivity to permit startup and full power operation, is generally determined by the amount of fuel initially loaded into the reactor core. (Although it should be mentioned that a major factor in determining fuel element lifetime in today's modern power reactors is the amount of radiation damage a fuel element can withstand before experiencing an appreciable probability of failure.) Of course the amount of fuel loaded into the reactor will depend in part on the excess reactivity that can be conveniently compensated for by the reactor control elements.

In order to increase the allowable initial core fuel loading, it is common to load into the core materials characterized by high neutron absorption cross sections (poisons) that compensate for such excess reactivity during the early stages of core life.[13-15] Such absorbers are chosen such that they "burn out" (i.e., are transmuted by neutron capture into isotopes with low capture cross sections) somewhat faster than fuel burnup, so that later in core life they contribute negligible negative reactivity. Hence these burnable poisons can nearly match the time behavior of the excess fuel reactivity as it decreases over core life, thereby allowing larger initial fuel inventories without a corresponding increase in control requirements.

Burnable poisons thus possess a number of advantages. They increase core lifetime without any decrease in control safety, reduce the amount of mechanical control required, and if distributed in a proper fashion, can also improve core power distributions, for example, by suppressing reactivity in high flux regions, such as near coolant channels.

Such burnable poisons are usually fabricated into the initial core loading as either fixed control blades or curtains or mixed into certain fuel pins. For example, in present BWR designs,[15] gadolinium-loaded fuel pins with an initial reactivity worth of 0.12 $\Delta k/k$ are loaded into the core until an equilibrium fuel cycle is achieved. In PWRs, borosilicate glass tubes are placed in the core in the initial core loading.[16] The locations of such burnable poisons are shown in typical fuel assembly control cells in Figure 14-5.

From this discussion, several desirable characteristics of burnable poisons are apparent. Obviously they should be characterized by absorption cross sections somewhat higher than those of the fuel, since then they will burn out more rapidly

than the fuel, leaving minimal poison residue at the end of the fuel cycle. Furthermore the isotopes formed by neutron capture in the poison should have low absorption cross sections. Finally, the burnable poison, as well as its surrounding clad or structural material, should not affect the structural integrity of the core (such as by swelling).

In this section we will examine two approaches for loading burnable poisons into a reactor core. The first merely assumes a uniform distribution of the poison material among the fuel. As we will see by a simple analysis, such a homogeneous scheme encounters difficulties in matching control requirements. Hence a more desirable scheme is to load the poisons in a heterogeneous fashion to take advantage of self-shielding effects that can provide a closer match between poison burnout and fuel depletion.

## A. Uniform Distribution of Burnable Poisons

For convenience, consider an infinite medium of homogeneously mixed fuel and poison. Then the rate equations describing the burnup of fuel and poison nuclei are just

$$\frac{dN_F}{dt} = -\sigma_a^F \phi(t) N_F(t),$$

$$\frac{dN_P}{dt} = -\sigma_a^P \phi(t) N_P(t).$$

(14-22)

We can integrate each of these equations to find

$$N_F(t) = N_F(0) \exp\left[ -\sigma_a^F \Phi(t) \right]$$

$$N_P(t) = N_P(0) \exp\left[ -\sigma_a^P \Phi(t) \right]$$

(14-23)

where $\Phi(t)$ is the time-integrated neutron flux or *neutron fluence*

$$\Phi(t) \equiv \int_0^t dt' \, \phi(t').$$

(14-24)

Now the core multiplication can be estimated as

$$k = \frac{\nu \Sigma_f^F}{\Sigma_a^F + \Sigma_a^P} = \nu \sigma_f^F \frac{N_F(t)}{N_F(t) \sigma_a^F + N_P(t) \sigma_a^P}$$

$$= \eta \left[ 1 + \frac{N_P(0)}{N_F(0)} \frac{\sigma_a^P}{\sigma_a^F} \exp\left[ -(\sigma_a^P - \sigma_a^F) \Phi(t) \right] \right]^{-1}.$$

(14-25)

We can sketch the form of $k(t)$ for various choices of poison cross section as shown in Figure 14-9.

Initially the change in reactivity will be high due to poison burnup. This results in a reactivity mismatch. The mismatch will be less severe for a poison with a small $\sigma_a^P$, but then there will be a poison residue that will shorten core life. Thus there is a certain fuel loading and corresponding core life beyond which the reactivity rise
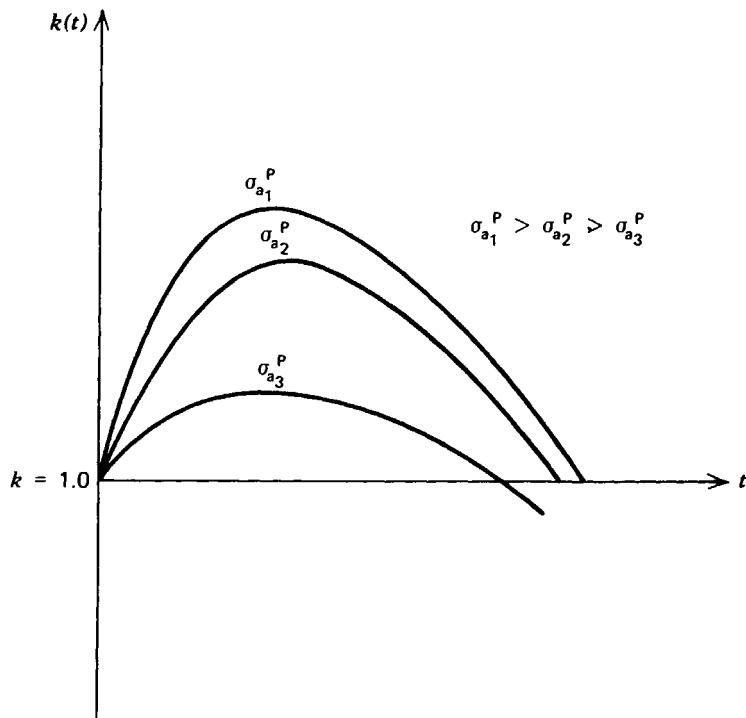
**FIGURE 14-9.** Core multiplication versus time for various uniform burnable poison loadings.

due to the relatively rapid depletion of the poison will be greater than that which can be handled by the available mechanical control. Ideally one would like to employ a poison of lower cross section early in core life (to reduce reactivity mismatch) and then switch to a poison of large cross section late in core life (to minimize poison residue). One can effectively achieve this by locating the poison in a region characterized by a different flux than that seen by the fuel.

## B. Heterogeneous Distributions of Burnable Poisons

The general idea underlying the use of heterogeneously lumped burnable poisons is to take advantage of the strong self-shielding that will occur in such poisons. Early in core life, the self-shielding will reduce the effective absorption cross section of the poison, thereby minimizing reactivity mismatch. As the poison depletes, however, the effective cross section of the poison relative to the fuel will increase, due to self-shielding, which is the desired behavior in order to maintain reactivity as high as possible near the end of core life.

To be a bit more precise, reconsider our equation describing the time rate of change of the poison concentration

$$\frac{dN_{\mathrm{P}}}{dt} = -f_s(t)\sigma_a^{\mathrm{P}}\phi(t)N_{\mathrm{P}}(t).$$

$$(14\text{-}26)$$
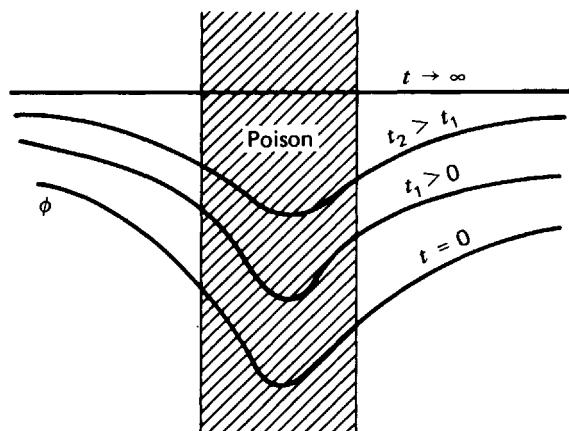
Here we have inserted a self-shielding factor $f_s(t)$ defined such that

$$f_s(t) = \frac{\text{average flux in poison}}{\text{average flux in fuel}}.$$

$$(14\text{-}27)$$

We have explicitly indicated that $f_s(t)$ will depend on time because of poison depletion, which will reduce the self-shielding as the poison burns out (see Figure

14-10). Initially the poison burnout is relatively slow due to strong self-shielding. However as poison depletion proceeds, self-shielding becomes less significant until eventually $f_s(t) \rightarrow 1$. Hence by using various self-shielded burnable poisons (e.g., boron or gadolinium), one can minimize the reactivity mismatch early in core life and still avoid a large residue of unburned poison that would shorten core lifetime.

Burnable poisons will also affect the reactivity coefficients of the reactor. Since most candidates for burnable poisons are $1/v$ absorbers, the microscopic absorption cross section of the poison will be larger in a cold core. Hence a lumped poison element will be more highly self-shielded and therefore less effective in a cold core than in a hot core. This enhances the negative behavior of the temperature coefficient of reactivity.



Change in flux depression as poison burns out
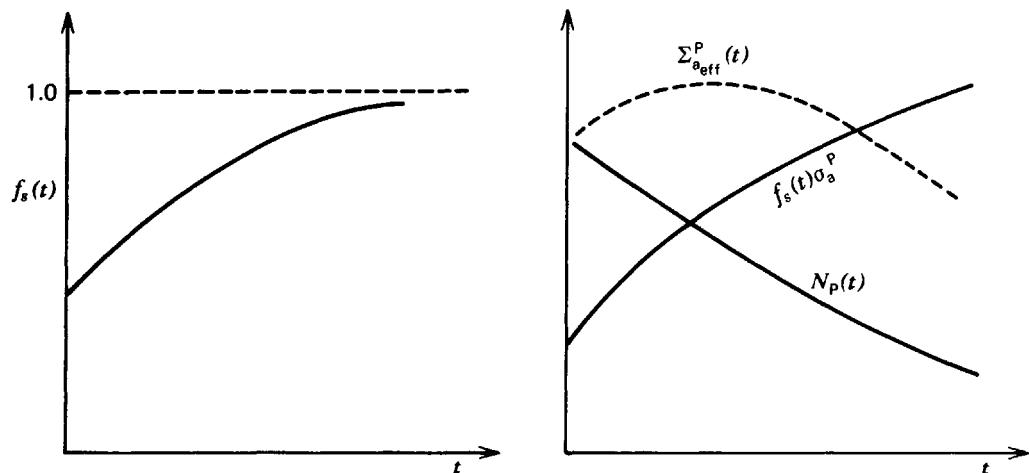


FIGURE 14-10. Effect of variable self-shielding on poison burnout.[18]

## IV. CHEMICAL SHIM

In light water reactors, boric acid is frequently dissolved in the coolant (to concentrations of $\sim 2000$ ppm) to act as shim control.[17,18] Such soluble poisons or chemical shim have several advantages. Since the poison distribution is uniform and independent of the amount of reactivity being controlled, the fuel loading can

be more easily distributed to yield a uniform power distribution, such as by zone-loading patterns. Chemical shim reduces the mechanical control rod requirements quite considerably. Since such rods are expensive and occupy a sizable fraction of the core volume, the elimination of mechanical control where possible is desirable.

In Table 14-1, the relative mechanical and chemical control requirements of a typical PWR are indicated. We have also sketched in Figure 14-11 the boron concentration required to compensate for excess reactivity over core life in a typical reactor design (comparing control requirements both with and without a burnable poison).
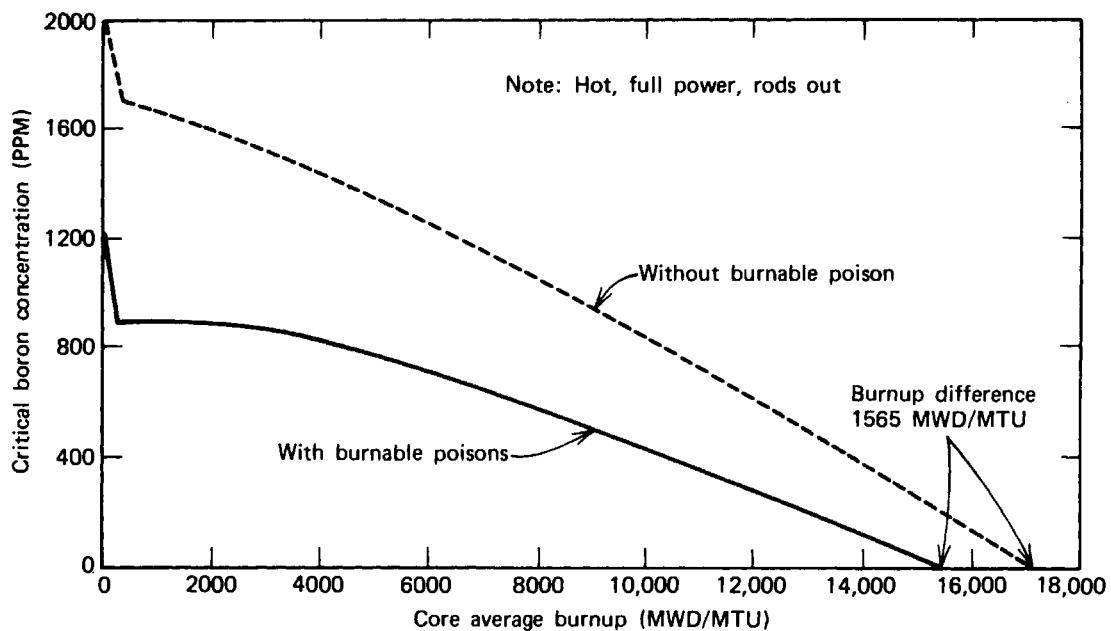


FIGURE 14-11.    Boron concentration versus first cycle burnup with and without burnable poison rods.[11]

A suitable soluble poison must be an isotope characterized by a large neutron absorption section which is soluble in the coolant. It should be of a noncorrosive nature and relatively stable so it will not adhere to core components. Boric acid possesses these requirements when used in LWRs.

Chemical shim does have several disadvantages, however. Since the rate at which one can inject or withdraw appreciable amounts of poison from the coolant is quite small, the reactivity insertion rates are correspondingly small (with maximum insertion rates of $\sim 3 \times 10^{-5}/\text{sec}$). Hence chemical shim is only of use to compensate for relatively slow reactivity changes such as those due to fuel burnup or conversion, fission product poisoning, and moderator temperature change (temperature defect).

Chemical shim can have a major effect on the moderator void coefficient of reactivity. We will find that in LWRs this void coefficient is usually quite negative, since a decrease in coolant density leads to a decrease in moderation and hence reactivity. However if a soluble poison is present, a decrease in coolant density will also lead to a decrease in poison concentration—a positive reactivity effect. The desire for a negative void coefficient will frequently limit the amount of chemical

shim allowed (typically to less than $\Delta\rho \sim 0.20 \; \Delta k / k$). We have shown this effect for a modern PWR core design in Figure 14-12.
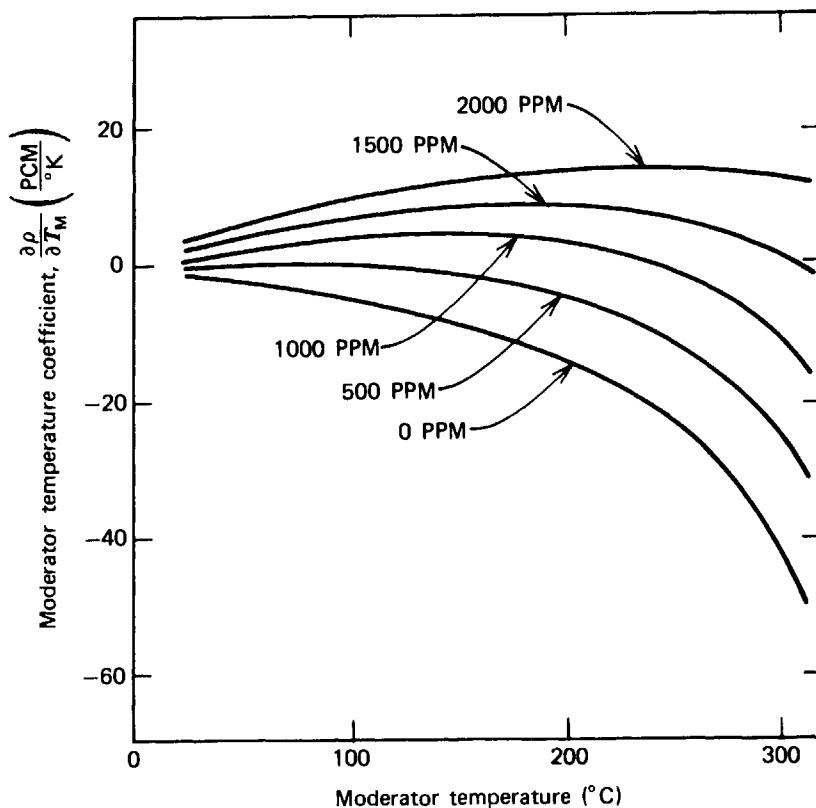


**FIGURE 14-12. The effect of chemical shim on the moderator temperature coefficient in a PWR.**[11]

There are other possible disadvantages, such as the possibility of sudden reactivity surges due to chemical shim that has been entrained in the core and suddenly breaks loose to escape. Chemical shim can also interact in an unfavorable way with fission product transients (xenon and samarium) toward the end of core life, as we will indicate in Chapter 15. Nevertheless the advantages of chemical shim make it a very attractive alternative to mechanical control in those reactor designs in which it can be utilized.

## V. INHERENT REACTIVITY EFFECTS

To complete our discussion of reactivity control, it is appropriate to consider some of the more common mechanisms that give rise to short-term reactivity changes in a nuclear reactor core. Perhaps the most important such mechanism is the variation of reactivity with core temperature. As we saw earlier in Chapter 6, this variation is usually expressed in terms of a temperature coefficient of reactivity defined as the derivative of the core reactivity with respect to temperature

$$\alpha_T \equiv \frac{\partial \rho}{\partial T} \rightarrow \sum_j \frac{\partial \rho}{\partial T_j} = \sum_j \alpha_T^{(j)}. \tag{14-28}$$

Here we have noted that more generally we must take into account the temperature variation in the reactor by computing separate temperature coefficients characteriz-

ing the fuel, coolant, moderator, and so on. It should also be noted that these coefficients are themselves functions of temperature.

Actually the more useful quantity is the power coefficient of reactivity $\alpha_P$ that describes the variation in reactivity due to a change in reactor power. This latter parameter is directly related to the inherent stability of the reactor, and must be kept negative for all conceivable operating conditions for a given reactor design. However, $\alpha_P$ is dependent on a very large number of different phenomena, including not only core neutronic behavior, but thermal–hydraulic phenomena as well. Thus in practice it is found to be far more convenient to analyze instead the temperature coefficients of reactivity that characterize the various components of the core. Of course, in principle, the power coefficient of reactivity could then be determined from the $\alpha_T^{(j)}$ as

$$\alpha_P = \frac{d\rho}{dP} = \sum_j \left( \frac{\partial \rho}{\partial T_j} \right)\left( \frac{\partial T_j}{\partial P} \right) = \sum_j \alpha_T^{(j)} \left( \frac{\partial T_j}{\partial P} \right), \tag{14-29}$$

provided one can perform a thermal–hydraulic analysis of the core to determine the change in core temperatures $T_j$ resulting from a change in power level.

Temperature variations in a reactor core will affect core multiplication, both because of the resulting density changes in core components (due to expansion or phase change) that change macroscopic cross sections, and because of a change in the thermal motion of core nuclei which changes microscopic cross sections (e.g., the Doppler effect). Although many introductory treatments attempt to study this phenomenon by calculating the isothermal temperature coefficient characterizing each component of the six-factor formula,[23] we will examine the temperature coefficients associated with each major component of the reactor core. In practice it is sufficient to consider the reactivity coefficients characterizing only the fuel, moderator (if any), coolant, and structure.

The two dominant temperature effects in most reactors are the change in resonance absorption (Doppler effect) due to fuel temperature changes, and the change in the neutron energy spectrum due to changing moderator or coolant density (due to temperature, pressure, or void fraction changes). One must also occasionally be concerned with core structure effects such as differential expansion and rod bowing. Fortunately in most cases of practical interest, these physical phenomena are sufficiently separable to allow an independent analysis of each reactivity coefficient.

For example, suppose we assume that the dominant contributions to the temperature coefficient of reactivity are due to Doppler-broadening of fuel resonances and the change in the spectrum due to moderator density changes. If we note that

$$\alpha_T \equiv \frac{\partial \rho}{\partial T} = \frac{1}{k^2} \frac{\partial k}{\partial T} \cong \frac{1}{k} \frac{dk}{dT}, \tag{14-30}$$

then we can write

$$\alpha_T = \frac{1}{k} \frac{\partial k}{\partial T_F} + \frac{1}{k} \frac{\partial k}{\partial T_M} = \alpha_T^F + \alpha_T^M. \tag{14-31}$$

Now changes in fuel temperature $T_F$ do not effect the shape of the thermal neutron energy spectrum. In reactor cores in which solid moderators are used (e.g.,

HTGRs), a change in moderator temperature will only affect the thermal spectrum and not the absorption rate in the resonance energy range, hence each temperature coefficient can be analyzed separately.[24] In liquid-moderated reactors (e.g., LWRs), a change in moderator temperature will change moderator density significantly, thereby influencing slowing down and hence resonance absorption. Even so, it is customary to analyze $\alpha_T^F$ and $\alpha_T^M$ separately, even when this interaction is present.

In this spirit, we will now examine each of the major reactivity feedback mechanisms of concern in nuclear reactor analysis. We will then consider the more practical problem of just how the corresponding reactivity coefficient for each mechanism is calculated.

## A. Fuel Temperature Coefficient of Reactivity

First we should recall from our study of resonance absorption that an increase in fuel temperature will lead to Doppler-broadening of resonances with a corresponding decrease in self-shielding, hence an *increase* in resonance absorption. We can estimate the effect of such Doppler broadening on reactivity by recalling that the resonance escape probability can be written in terms of the effective resonance integral $I$ as

$$p = \exp\left[ - \frac{N_F}{\xi \Sigma_p} I \right].$$
(14-32)

Hence we can calculate the Doppler coefficient of reactivity in terms of the resonance integral as

$$\alpha_T^F = \frac{1}{k} \frac{dk}{dT_F} = \frac{1}{p} \frac{dp}{dT_F} = \ln p \frac{1}{I} \frac{dI}{dT_F}.$$
(14-33)

We mentioned in Chapter 10 that a very useful correlation[25] for the temperature-dependence of the resonance integral was

$$I(T) = I(300°K)\left[ 1 + \beta (\sqrt{T} - \sqrt{300°K}) \right].$$
(14-34)

If we use this in Eq. (14-33), we find

$$\alpha_T^F = -\ln\left[ \frac{1}{p(300°K)} \right] \frac{\beta}{2\sqrt{T_F}}.$$
(14-35)

Here $\beta$ is a constant that depends only on fuel composition and geometry. For example, for $^{238}UO_2$,

$$\beta = 61 \times 10^{-4} + 47 \times 10^{-4}\left( \frac{S_F}{M_F} \right),$$
(14-36)

while for $^{232}ThO_2$

$$\beta = 97 \times 10^{-4} + 120 \times 10^{-4}\left( \frac{S_F}{M_F} \right).$$
(14-37)

In most thermal reactor types, the Doppler effect arises primarily from capture resonances in fertile material in the fuel. For example, in slightly enriched uranium

cores, $^{238}U$ is the principal contributor early in core life, although $^{240}Pu$ becomes important later in core life. In an HTGR, $^{232}Th$ is of primary concern. The contribution of other heavy metal isotopes such as $^{235}U$ or $^{239}Pu$ should be included in estimates of Doppler coefficients, but their contribution is usually quite small in low fissile-density cores.

This situation is modified somewhat in fast reactors,[26] since the neutron energy spectrum spans the resonance regions of both fertile and fissile materials. Hence increasing temperature will increase both $\Sigma_a\phi$ *and* $\Sigma_f\phi$. There may be a net increase in reactivity. Since the Doppler effect is a fast feedback mechanism, and since the prompt neutron lifetime of a fast core is so short, the sign of the Doppler coefficient is extremely important.

The Doppler coefficient will tend to be more positive in a core with a hard spectrum (such as in a metal-fueled core). To soften the spectrum, one uses oxide fuels. Here the oxygen will degrade the spectrum to yield a negative Doppler coefficient. Indeed several fast reactor core designs have actually considered adding small amounts of moderator (such as BeO) to the core to soften the spectrum and enhance the negative Doppler coefficient (although at considerable economic penalty).

Although the reactivity change caused by the Doppler effect is frequently small compared to other reactivity changes during normal operation, it becomes very important for the postulated power excursions of concern in reactor safety analysis. In such an excursion, rapid fuel temperature changes will lead to strong Doppler feedback, which becomes the principal mechanism acting to terminate the power excursion.

Since the Doppler coefficient depends sensitively on fuel composition, it will change due to fuel burnup and hence must be monitored over core life. For example, in a slightly enriched core, the Doppler coefficient becomes more negative as a function of core life due to buildup of $^{240}Pu$.

## B. Coolant or Moderator Reactivity Coefficients

### 1. SOLID MODERATORS

In solid moderator reactor cores, such as the graphite-moderated HTGR, the primary reactivity effect is due to a hardening of the thermal neutron spectrum with increasing temperature, which causes a change in the thermal group constants. The magnitude and sign of the associated moderator temperature coefficient depends on a number of complicated interactions, which leads to a rather complicated dependence on temperature (see Figure 14-13).

### 2. LIQUID-MODERATED REACTORS

The moderator coefficient of reactivity is a measure of the change in reactivity due to a change in moderator properties such as temperature, density, pressure, or void fraction. When the moderator is a liquid also functioning as a coolant, such as in a LWR, these reactivity coefficients may be quite sizable. We will consider the reactivity coefficient associated with each property of the moderator.

#### (a) MODERATOR TEMPERATURE COEFFICIENTS

An increase in moderator temperature, keeping density constant, will lead to a hardened neutron spectrum, resulting in increased resonance absorption in
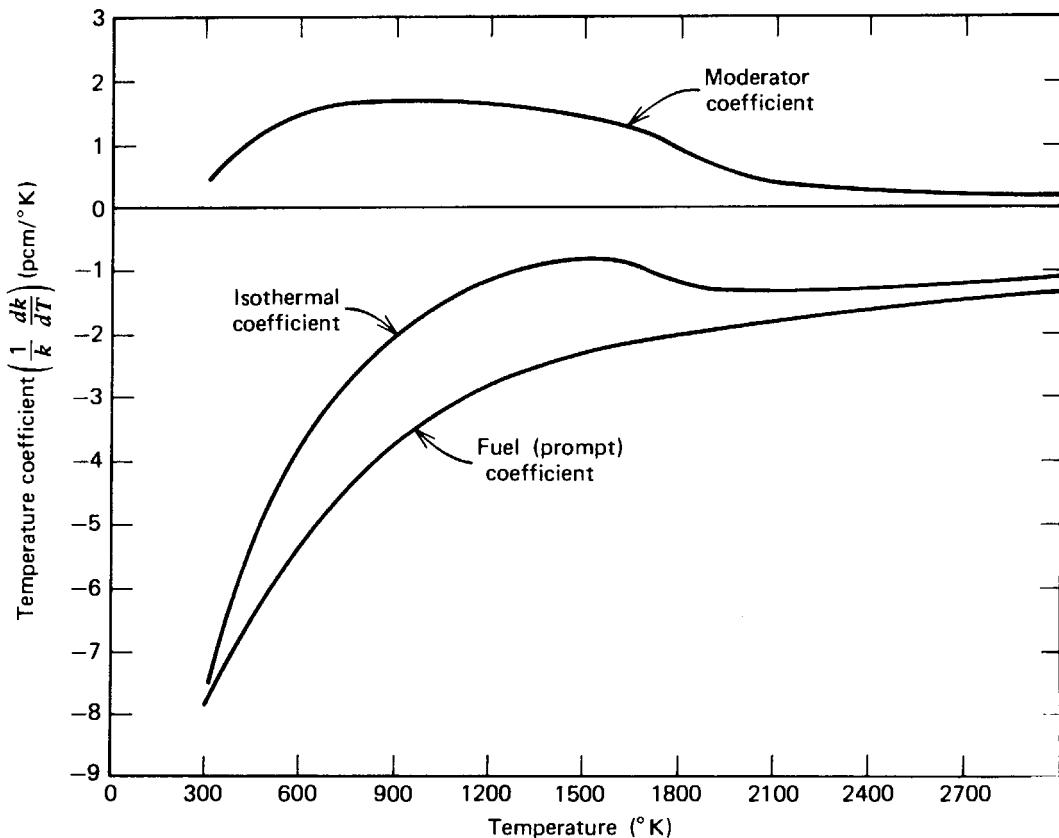
**FIGURE 14-13.** Temperature-dependence of temperature coefficients of reactivity for a large HTGR.[21]

low-lying resonances in isotopes such as $^{238}U$, $^{240}Pu$, or $^{232}Th$. The hardened spectrum will also cause an increase in the capture-to-fission ratio in $^{235}U$ and $^{239}Pu$, hence a decrease in $\eta$. Both of these effects render the moderator temperature coefficient more negative.

### (b) MODERATOR DENSITY CHANGES

The dominant reactivity effect in water-moderated reactors arises from changes in moderator density, due either to thermal expansion or void formation (steam production). The principal effect is usually the loss of moderation that accompanies a decrease in moderator density and causes a corresponding increase in resonance absorption.[27] To see this more clearly, let us return to our expression Eq. (14-32) for the resonance escape probability

$$p = \exp\left[ - \frac{N_F}{\xi N_M \sigma_p} I \right],$$  (14-38)

where we have specifically identified the moderator density. Hence the void or density coefficient of reactivity is just

$$\alpha_T^M = \frac{1}{k} \frac{dk}{dT_M} = \ln\left(\frac{1}{p}\right) \frac{dN_M}{dT_M}.$$  (14-39)

Since $dN_M / dT_M$ will be negative and may be quite large, particularly if the coolant is near saturation temperature, the void coefficient of reactivity can also be large (see Figure 14-14).
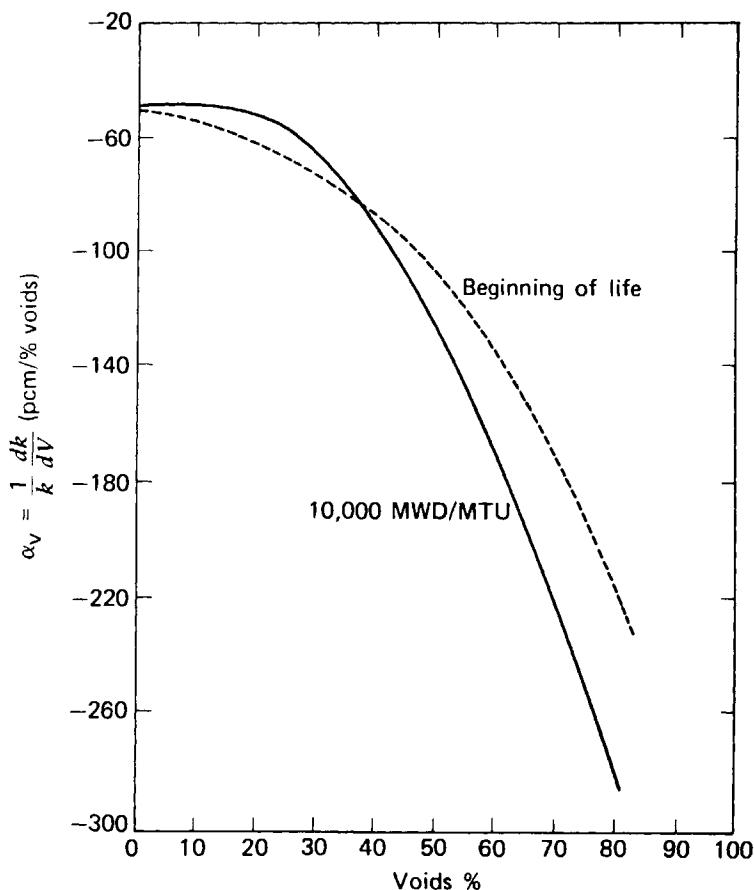
FIGURE 14-14.  Void coefficient of reactivity for a large BWR.[20]

In most cases, the void coefficient for a water-moderated core will be large and negative. However if appreciable chemical shim is used, this reactivity coefficient becomes more positive since then a decrease in coolant density will cause a decrease in poison concentration and hence macroscopic absorption cross section. In order to achieve a negative moderator coefficient, one must limit the concentration of soluble poison.

### (c) MODERATOR PRESSURE COEFFICIENT

The moderator pressure coefficient relates the change in moderator density that results from a coolant pressure change, to a change in reactivity. Since most reactor cores are operated at high pressure, this is a relatively small effect. For example, a change of 4 bar in a PWR has approximately the same reactivity effect as does a half-degree change in moderator temperature.[28]

### (d) COOLANT REACTIVITY COEFFICIENTS IN LMFBRS

In thermal reactors, the coolant void coefficient is negative, but in a large fast core, the sodium void coefficient $\alpha_V$ may in fact be positive. That is, an increasing temperature will increase the void fraction, hence increasing reactivity and thereby temperature. There are two competing effects which determine the sign of $\alpha_V$: (a) spectrum effects, where the coolant degrades the spectrum, lowering the effective $\bar{\eta}$; hence any loss of sodium hardens the spectrum, implying $\alpha_V > 0$ and (b) leakage effects, where loss of sodium near the edge of the core will increase leakage, hence implying $\alpha_V < 0$. These effects compete in such a way that the void coefficient is

positive in the center of the core and negative near the edge. One finds that this effect becomes more pronounced with larger cores. One can design around this effect by increasing leakage using a "spoiled" core geometry (e.g., pancake geometries) but this will incur penalties in large fuel inventory and poor core breeding ratios.

## C. Core Expansion Effects

An increase in core temperature can cause an expansion of core structural components with an attendant change in core configuration and hence reactivity. If the core were to expand uniformly, the dominant effects would be an increase in core size and coolant volume fraction. The latter would usually be the largest effect and would tend to decrease reactivity in a fast core (in which such expansion effects are most important).

Perhaps a more significant effect would be due to differential expansion leading to fuel rod bowing. Since the bowing would usually be in the direction of a thermal gradient, the fuel rods would bow in toward the center of the core, reducing coolant volume fraction and increasing reactivity. Such bowing effects led to instabilities in some of the early LMFBR core designs.[29] They can usually be eliminated by careful design of the fuel element support structure.

A somewhat different expansion effect that occurs in metal clad fuel reactor cores is differential fuel–clad expansion, which can lead to increased fuel–clad contact pressure and hence increased gap thermal conductance. The net result is a lowering of fuel temperatures and hence an increase in reactivity (although this is a second-order effect).

## D. Calculation of Reactivity Coefficients

Although the simple expressions we have developed for several of the temperature coefficients characterizing a reactor core are useful for a qualitative understanding of reactivity feedback effects, a practical calculation usually involves performing a sequence of static criticality calculations for different fuel or moderator temperatures, and then determining the appropriate reactivity coefficients directly from a table of $k_{eff}$ as a function of $T_F$ and $T_M$ or whatever other variable is of interest. Such calculations may be greatly expedited if the relevant physics determining the coefficient of interest can be isolated. For example, if the primary effect is known to be dependent on a change in the thermal neutron energy spectrum (such as the moderator temperature coefficient characterizing a HTGR), then an infinite medium spectrum calculation may be used to determine the reactivity coefficient.

There are a great many details involved in the accurate determination of reactivity coefficients. For example, one must determine just what temperatures to use in characterizing the fuel or moderator. Typically one uses a flux-weighted temperature average in determining the Doppler coefficient of a fuel pin to take into account the flux depression that results from self-shielding. Perhaps the most complete discussion of such calculations is given in the Safety Analysis Reports covering each reactor type,[15,16,21,22] and the reader should refer to these reports for further information.

For purposes of illustration, we have tabulated the principal reactivity coefficients characterizing several of the more common reactor types in Table 14-2.

TABLE 14-2: Temperature Coefficients

| | BWR | PWR | HTGR | LMFBR |
|---|---|---|---|---|
| Fuel-temperature coefficient | | | | |
| Doppler (pcm/°K) | $-4$ to $-1$ | $-4$ to $-1$ | $-7$ | $-0.6$ to $-2.5$ |
| Isothermal temperature coefficient | | | | |
| Coolant void (pcm/%void) | $-200$ to $-100$ | 0 | 0 | $-12$ to $+20$ |
| Moderator (pcm/°K) | $-50$ to $-8$ | $-50$ to $-8$ | $+1.0$ | |
| Expansion (pcm/°K) | $\sim 0$ | $\sim 0$ | $\sim 0$ | $-.92$ |
| Temperature defect (%$\Delta k/k$) | 2.0–3.0 | 2.0–3.0 | 0.7 | 0.5 |
| Power defect (%$\Delta k/k$) | 1.5–2.5 | 1.5–2.5 | 4.0 | 0.8 |
| Xe worth (%$\Delta k/k$) | 2.6 | 2.6 | 3.3 | 0.0 |
| Sm worth (%$\Delta k/k$) | 0.7 | 0.7 | 0.5 | 0.0 |

# REFERENCES

1. A. Sesonske, *Nuclear Power Plant Design Analysis*, USAEC Document TID-26241 (1973), Chapter 6.
2. J. R. Lamarsh, *Introduction to Nuclear Reactor Theory*, Addison-Wesley, Reading, Mass. (1966), pp. 499–503.
3. H. W. Graves, Jr., *Nuclear Reactor Design*, University of Michigan Nuclear Engineering Department Lecture Notes (unpublished) (1969).
4. J. R. Lamarsh, *Introduction to Nuclear Reactor Theory* Addison-Wesley, Reading, Mass. (1966), pp. 509–517; R. V. Meghreblian and D. K. Holmes, *Reactor Analysis*, McGraw-Hill, New York (1960). Ch. 11.
5. A. Radkowsky (Ed.), *Naval Reactors Physics Handbook*, Vol. I, Selected Basic Techniques, USAEC Report TID-7030 (1964).
6. J. R. Lamarsh, *Introduction to Nuclear Reactor Theory*, Addison-Wesley, Reading, Mass. (1966), pp. 518–519; H. W. Graves, Jr., *Nuclear Reactor Design*, University of Michigan Nuclear Engineering Department Lecture Notes (unpublished) (1969); A. F. Henry, USAEC TID-7532, Part 1 (1957).
7. C. W. Maynard, in *Naval Reactor Physics Handbook*, Vol. 1, A. Radkowsky (Ed.), USAEC Report TID-7030 (1964), pp. 409–447.
8. M. Michelini, *Nucl. Sci. Eng.* **42**, 162 (1970).
9. *Reactor Physics Constants*, USAEC Document ANL-5800, 2nd Edition (1963).
10. H. W. Graves, Jr., *Nuclear Control Management*, University of Michigan Nuclear Engineering Department Lecture Notes (unpublished) (1969).
11. RESAR, PWR Standard Safety Analysis Report, Westinghouse (1973) Chapter 4.
12. D. C. Wade, *Trans. Am. Nucl. Soc.* **11**, 314 (1968).
13. A. Radkowsky (Ed.), *Naval Reactors Physics Handbook*, Vol. I, Selected Basic Techniques, USAEC Report TID-7030 (1964), p. 800.
14. H. W. Graves, Jr., *Nuclear Reactor Design*, University of Michigan Nuclear Engineering Department Lecture Notes (unpublished) (1969).
15. BWR/6 Standard Safety Analysis Report, General Electric (1973).
16. Reference Safety Analysis Report, Westinghouse Nuclear Energy Systems (1973).
17. P. Cohen and H. W. Graves, Jr., *Nucleonics* **22**, 75 (1964).
18. H. W. Graves, Jr., *Nuclear Control Management*, University of Michigan Nuclear Engineering Department Lecture Notes (unpublished) (1969).
19. CESSAR, Standard Safety Analysis Report, System 80, Combustion Engineering (1973).
20. BWR/6 Standard Safety Analysis Report, General Electric (1973).
21. Preliminary Safety Analysis Report, Summit Power Station, Delmarva Power (1973).
22. Preliminary Safety Analysis Report, Clinch River LMFBR Demonstration Plant, Project Management Corporation (1975).

23. J. R. Lamarsh, *Introduction to Nuclear Reactor Theory*, Addison-Wesley, Reading, Mass. (1966), pp. 451–466.

24. M. H. Merrill, Nuclear design methods and experimental data in use at Gulf General Atomic, Gulf-GA-A12652 (1974).

25. E. Hellstrand, P. Blomberg, and S. Horner, *Nucl. Sci. Eng.* **8**, 497 (1960).

26. D. Okrent and H. Hummel, *Temperature Coefficients of Fast Reactors*, Am. Nucl. Soc., Hindsdale, Ill. (1968).

27. J. R. Lamarsh, *Introduction to Nuclear Reactor Theory*, Addison-Wesley, Reading, Mass. (1966) p. 458; H. W. Graves, Jr., *Nuclear Reactor Design*, University of Michigan Nuclear Engineering Department Lecture Notes (unpublished) (1969).

28. Reference Safety Analysis Report, Westinghouse Nuclear Energy Systems, Vol. 4 (1973).

29. T. J. Thompson and J. G. Beckerley, *The Technology of Nuclear Reactor Safety*, Vol. I, M.I.T. Press, Cambridge (1966).

## PROBLEMS

14-1 Calculate the effective control cross section $\Sigma_c^{eff}$ characterizing a circular control cell geometry in which the control rod is of radius $a$ and the cell is of radius $R$. The transport parameter $\alpha$ for this geometry is given in ANL-5800[9] as

$$\lambda = \frac{1}{3\alpha} = 0.7104 + \frac{0.2524}{\Sigma_a^C a} + \frac{0.0949}{\left(\Sigma_a^C a\right)^2} + \cdots$$

14-2 Demonstrate that for a perfectly black absorbing slab, the transport correction parameter is $\alpha = 0.47$.

14-3 Determine the effective control cross section $\Sigma_c^{eff}$ for the slab geometry control cell described in Section 14-II-B if the control rod is sufficiently weakly absorbing that diffusion theory is valid. (That is, calculate $\alpha$ using diffusion theory in the control rod.)

14-4 Compare $\alpha$ for a black rod ($\alpha = 0.47$) and the diffusion theory description (Problem 14-3) with the transport theory result given by Eq. (14-13) for various values of $\Sigma_a a$.

14-5 Suppose the shim rods of a power reactor are ganged together in such a way that they can be treated as a uniformly distributed absorption cross section inserted into a cylindrical core to a depth $h$. Using one-group perturbation theory, determine and sketch the relative distance of insertion of the rods as a function of time over the core life.

14-6 The measured thermal flux at the surface of the scram rods of a low power research reactor is approximately $3 \times 10^{12}$ neutrons/cm$^2$/sec. The rods are stainless steel with 2% (by weight) boron. How long will it take to produce 90% burnup of the boron at the rod surface. ($\sigma_a$ for naturally occurring boron at 0.025 eV is 796 barns).

14-7 Repeat the calculation of the effect of rod-bank insertion on the axial power distribution [i.e., resolve Eq. (14-16)] for partial length control rods of active length $l$, $l < H$.

14-8 Show that in a critical reactor, a small change in soluble poison concentration produces a change in reactivity that is approximately equal to the fractional change in poison concentration multiplied by the fraction of neutrons absorbed in the poison.

14-9 A reactor is to operate at constant power. The reactor is initially loaded with excess fuel plus a burnable poison. Neglecting fission product poisoning, determine: (a) the poison concentration as a function of time and (b) the reactivity as a function of time if it is zero at startup.

14-10 A reactor that is highly enriched in $^{235}U$ and contains a burnable poison is required to operate under the conditions that the excess reactivity never falls below $\rho_1$ and

never rises above $\rho_2$. Assume that a homogeneous model can be used to describe the reactor. Develop expressions for both the initial poisoning ratio and the maximum fluence for a core life $t_l$.

14-11 From the attached two-group constants for a typical low-power research reactor find the total worth of the shim rod using a two-group diffusion code. Run the code for four intermediate rod positions and plot the rod worth versus depth of insertion. Using perturbation theory, calculate the rod worth versus position, and compare with these results. Also plot the peak/average power ratio as a function of insertion depth and explain your results. (Model the core as a slab of width 50 cm and treat as a "windowshade" problem.)

The two-group constants for the core without the shim rod are:

| Group | $D$ | $\nu\Sigma_f$ | $\Sigma_f$ | $\Sigma_{s_{12}}$ | $\Sigma_a$ |
|---|---|---|---|---|---|
| 1 | 1.44440 | 0.001865 | 0.000763 | 0.028743 | 0.001905 |
| 2 | 0.24712 | 0.0780 | 0.0321 | — | 0.052200 |

When the shim rod is inserted, $\Sigma_{a_2} = 0.053606$; all other group constants remain unchanged.

14-12 Suppose that it were possible to choose a burnable poison whose effective microscopic cross section, $\sigma_a^P(t)$ were a controllable function of time (e.g., by careful design of self-shielding burnout). What time-dependence would be required to yield a uniform excess reactivity over core life?

14-13 Calculate the isothermal temperature coefficient of reactivity for the thermal and fast nonleakage probabilities $\alpha_T(P_{\text{TNL}})$ and $\alpha_T(P_{\text{FNL}})$, assuming that the primary temperature effect is core expansion. Assume a thermal expansion coefficient of $\beta$ for the core.

14-14 Consider a LWR fueled with slightly enriched uranium.
(a) Indicate how, for small void fractions, to calculate approximately the void coefficient of reactivity, i.e., the fractional change in multiplication per fractional change in void.
(b) In PWRs the water will frequently contain boron in solution. Indicate the effect this is likely to have on the void coefficient and explain.
(c) What is the effect of water temperature (at a given pressure) on the results of (a) and (b) above.

14-15 If a large BWR has a zero moderator density coefficient at operating temperature ($\rho_{\text{H}_2\text{O}} = 0.8$ g/cm$^3$) and zero power, what will the *sign* of the coefficient be: (a) at full power with 10% void fraction and (b) at refueling temperature ($\rho_{\text{H}_2\text{O}} = 1$ g/cm$^3$)? Give reasons for your answers.

# 15

# Analysis of Core Composition Changes

The atomic densities of various isotopes in a reactor core are continually changing due to nuclear processes such as fission, neutron capture, and radioactive decay. For example, fission events will reduce the concentration of fissile isotopes such as $^{233}U$, $^{235}U$, or $^{239}Pu$. Neutron capture will reduce fertile nuclide concentrations while building up the concentrations of transmutation products such as $^{239}Pu$. In addition we must remember that fission reactions will produce a large variety of fission product nuclides, most of which are radioactive and will subsequently decay into other isotopic species.

It is extremely important to monitor the isotopic composition in the core during reactor operation, since changes in core composition can affect core multiplication as well as flux and power distributions. Certainly the prediction of fuel depletion and conversion in the core is essential for the determination of fuel loading requirements. Furthermore certain of the fission product nuclei (or their progeny following radioactive decay) are characterized by extremely large absorption cross sections and hence may significantly affect the reactivity of the core. For example, $^{135}Xe$ has an enormous thermal neutron cross section of $\sigma_a = 2.7 \times 10^6$ barns. A very small amount of such fission product "poisons" may significantly affect the multiplication of the reactor, since as they accumulate they will absorb neutrons from the chain reaction.

The analysis of core composition changes is complicated by the fact that the time and spatial variation in isotopic composition will depend on the neutron flux distribution–which itself depends on core composition. Fortunately changes in core composition occur relatively slowly (on time scales of hours, days, or even months) so that the reactor core can always be kept in a critical state by control element adjustments. This means that although a time-dependent analysis of the rate

equations describing changes in isotopic number density is necessary, the neutronic behavior can be studied by performing a sequence of instantaneous static criticality calculations for each core composition encountered. Hence although the analysis of core composition changes does involve time-dependent phenomena, the neutronic part of the analysis involves only static calculations of core flux distributions and hence differs considerably from the treatment of nuclear reactor kinetics of Chapter 6.

Our intent in this chapter is to examine the procedures useful for analyzing such time-dependent changes in core composition. We will first examine short-term composition changes due to fission product buildup that affect the operation of the reactor. In particular we will apply these methods to an analysis of the very important problem of xenon and samarium transients in thermal power reactor cores.

We will then continue to consider the longer term process of fuel depletion and develop methods for core depletion analysis. This will allow us to examine the variables determining core lifetime and fuel loading requirements. Finally, we will illustrate these methods by considering the very important problem of in-core fuel management.

# I. FISSION PRODUCT POISONING

Certain fission products possess extremely large thermal neutron absorption cross sections. Of particular concern are $^{135}$Xe and $^{149}$Sm, whose absorption cross sections[1] are shown in Figure 2-4. The significance of these extremely strongly absorbing fission products is compounded by their relatively large fission yields. The buildup of such fission product poisons can appreciably affect core multiplication and hence reactor operation. It should be noted, however, that since these absorption cross sections fall off quite rapidly for neutron energies above 1 eV, *fission product poisoning* is primarily of concern in thermal reactors (and only of secondary importance in fast reactor operation).

In order to illustrate the importance of this phenomenon, let us make a very simple estimate of the reactivity change induced in a reactor core by the addition of a fission product poison. To first order, the effects of such poisons enter through the thermal utilization $f$. If we imagine introducing a poison characterized by a macroscopic cross section $\Sigma_a^P$ uniformly throughout a homogeneous reactor core, then we can write the thermal utilization characterizing the "poisoned" core as

$$f = \frac{\Sigma_a^F}{\Sigma_a^F + \Sigma_a^M + \Sigma_a^P}.$$

(15-1)

Hence we can compute the reactivity change from a critical reactor in which $\Sigma_a^P = 0$ as

$$\Delta\rho \equiv \rho(\Sigma_a^P) - \rho(\Sigma_a^P = 0) = \rho' - \rho.$$

(15-2)

Now if we recall our earlier definition of reactivity as given by the six-factor

formula

$$\rho = \frac{k-1}{k}, \qquad k = \eta p f \epsilon P_{\text{FNL}} P_{\text{TNL}} \tag{15-3}$$

and note that

$$P_{\text{TNL}} = \frac{1}{1 + L^2 B_g^2}, \qquad L^2 = \frac{D}{\Sigma_a} = \frac{1}{3\Sigma_{\text{tr}}\Sigma_a}, \tag{15-4}$$

will also change as $\Sigma_a^P$ changes, then we can compute

$$\Delta\rho = \frac{f'-f}{f'} + \frac{P'_{\text{TNL}} - P_{\text{TNL}}}{P'_{\text{TNL}}}. \tag{15-5}$$

If we use Eqs. (15-1) and (15-4), we find

$$\frac{f'-f}{f'} = -\frac{\Sigma_a^P}{\Sigma_a^F + \Sigma_a^M}, \tag{15-6}$$

and

$$\frac{P'_{\text{TNL}} - P_{\text{TNL}}}{P'_{\text{TNL}}} = \frac{L^2 B_g^2}{1 + L^2 B_g^2}\left[\frac{\Sigma_a^P}{\Sigma_a} + \frac{\Sigma_{\text{tr}}^P}{\Sigma_{\text{tr}}}\right]. \tag{15-7}$$

Hence

$$\Delta\rho = -\frac{\Sigma_a^P}{\Sigma_a}\frac{1}{1 + L^2 B_g^2}\left[1 - L^2 B_g^2 \frac{\Sigma_{\text{tr}}^P/\Sigma_a^P}{\Sigma_{\text{tr}}/\Sigma_a}\right] \cong \frac{\Sigma_a^P/\Sigma_a}{1 + L^2 B_g^2}. \tag{15-8}$$

Here we have noted that the second term in brackets is usually quite small ($< 10^{-3}$) and can be ignored. In fact for many large power reactor cores, leakage is sufficiently small that $L^2 B_g^2 \ll 1$ and to first order, the reactivity change due to such a poison is just the fraction of the total macroscopic absorption cross section due to the poison. (Here we must keep in mind the crude nature of this estimate which has totally ignored any spatial variation in the poison concentration—a variation that we will later find is rather important.)

Now recall that the macroscopic cross section for the poison is given by $\Sigma_a^P = N_P \sigma_a^P$, where $N_P$ is the number density of the poison while $\sigma_a^P$ is its thermal absorption cross section. Hence in order to estimate the reactivity change due to fission product poisoning, we must calculate the number density of the poisoning isotope $N_P$ at any time $t$.

The procedure is simple—at least in concept. To determine $N_P(t)$, we must solve the rate equations describing the various production and decay processes that can affect the poison concentration. We will illustrate this procedure with two simple (but nevertheless important) examples involving the buildup of [135]Xe and [149]Sm.

## A. Xenon Fission Product Poisoning

[135]Xe is the most significant fission product because of its enormous thermal neutron absorption cross section and its relatively large fission yield. Actually [135]Xe

can be produced not only directly as a fission product but may also result from the $\beta$-decay of $^{135}$Te. A portion of the production decay scheme of the A = 135 chain is shown in Figure 15-1. Fortunately this rather complicated decay scheme can be considerably simplified by assuming that the decay of $^{135}$Te to $^{135}$I is instantaneous (i.e., that $^{135}$I is produced directly as a fission product). Furthermore we will also ignore the short-lived isomeric state $^{135m}$Xe, and assume that all $^{135}$I nuclei will decay directly to the ground state $^{135}$Xe. Hence the effective decay scheme we will study is shown in Figure 15-2.

Thus, we now must write isotopic rate equations similar to those discussed in Chapter 2 to describe the atomic densities of $^{135}$I and $^{135}$Xe. Let us denote the atomic number densities of these two isotopes as $I(r,t)$ and $X(r,t)$ respectively. Furthermore let $\gamma_I$ and $\gamma_X$ denote the effective fraction of the fission products which are $^{135}$I and $^{135}$Xe, while $\lambda_I$ and $\lambda_X$ are the $\beta$-decay constants for these two isotopes. Using these parameters, we can then write the coupled rate equations describing the simplified decay scheme illustrated in Figure 15-2 as

*Iodine*

$$\frac{\partial I}{\partial t} = \underset{\substack{\text{direct}\\\text{from fission}}}{\gamma_I \Sigma_f \phi(r,t)} - \underset{\substack{\text{iodine}\\\text{decay}}}{\lambda_I I(r,t)}. \tag{15-9}$$

*Xenon*

$$\frac{\partial X}{\partial t} = \underset{\substack{\text{direct}\\\text{from fission}}}{\gamma_X \Sigma_f \phi(r,t)} + \underset{\substack{\text{iodine}\\\text{decay}}}{\lambda_I I(r,t)} - \underset{\substack{\text{xenon}\\\text{decay}}}{\lambda_X X(r,t)} - \underset{\substack{\text{xenon}\\\text{absorption}}}{\sigma_a^X \phi(r,t) X(r,t)} \tag{15-10}$$

Here the macroscopic cross sections and neutron flux are to be interpreted as one-group averages. Notice that we have included a loss term in the xenon balance equation to account for the fact that capture will deplete the $^{135}$Xe concentration (as well as the neutrons, of course). Strictly speaking, we should have included a similar term in the iodine equation, but the absorption cross section of $^{135}$I is sufficiently low that such a term would only be significant for extremely high flux levels ($\phi > 10^{16}$ cm$^{-2}$ sec$^{-1}$). The values of the yields and decay constants are tabulated in Table 15-1[2,3].
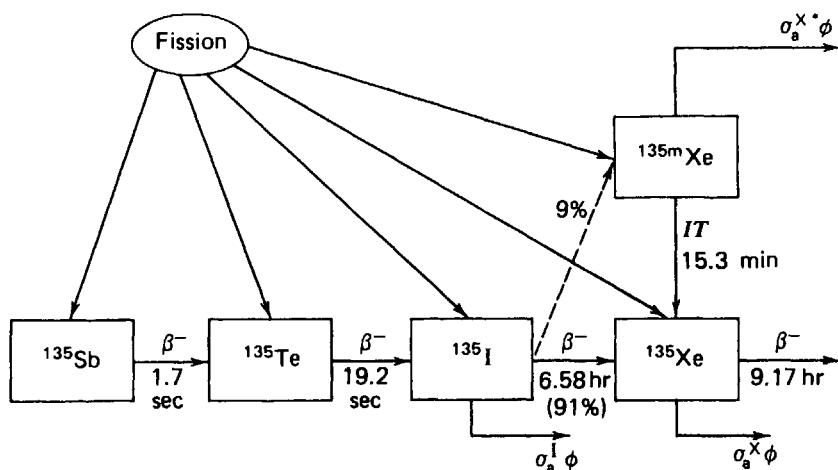


**FIGURE 15-1.** A portion of the decay scheme for A = 135.
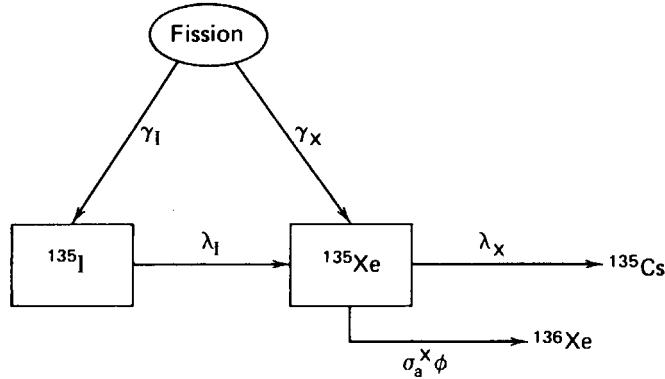
FIGURE 15-2.  A simplified decay scheme for $^{135}$Xe.

TABLE 15-1:  Fission Product Yields and Decay Constants

| Fission Product Yields | $^{233}$U | $^{235}$U | $^{239}$Pu | $^{241}$Pu | Decay constants |
|---|---|---|---|---|---|
| $\gamma_I(\%)$ | 4.884 | 6.386 | 6.100 | 7.694 | $\lambda_I = 0.1035$ hr$^{-1}$ |
| $\gamma_X(\%)$ | 1.363 | 0.228 | 1.087 | 0.255 | $\lambda_X = 0.0753$ hr$^{-1}$ |
| $\gamma_P(\%)$ | 0.66 | 1.13 | 1.9 | | $\lambda_P = 0.0128$ hr$^{-1}$ |

Before we can proceed further to solve these equations, we need information about the flux in the reactor $\phi(\mathbf{r},t)$. Suppose that we were to merely assume that the flux behavior was a known function of space and time. Then we could immediately integrate the iodine equation to find

$$I(\mathbf{r},t) = \left[ I(\mathbf{r},0) + \gamma_I \int_0^t dt' \, \Sigma_f(\mathbf{r},t')\phi(\mathbf{r},t') \exp(\lambda_I t') \right] \exp(-\lambda_I t) \qquad (15\text{-}11)$$

and then substitute this solution into the xenon equation and integrate it to determine the $^{135}$Xe concentration as a function of space and time:

$$X(\mathbf{r},t) = \left\{ X(\mathbf{r},0) + \int_0^t dt' \left[ \lambda_I I(\mathbf{r},t') + \gamma_X \Sigma_f(\mathbf{r},t')\phi(\mathbf{r},t') \right] \exp\left[ \int_0^{t'} dt'' \left[ \lambda_X + \sigma_a^X \phi(\mathbf{r},t'') \right] \right] \right\}$$

$$\times \exp\left[ -\int_0^t dt'' \left[ \lambda_X + \sigma_a^X \phi(\mathbf{r},t'') \right] \right]. \qquad (15\text{-}12)$$

Of course, for any complicated flux behavior, these solutions will require numerical integrations, and until we specify the form of $\phi(\mathbf{r},t)$, this formal solution is of little use in understanding the general behavior of the xenon concentration in the reactor. Hence we will examine the time-behavior of the xenon concentration for several particularly simple examples of flux behavior.

## 1. STARTUP OF A CLEAN CORE REACTOR

Suppose that we suddenly bring the reactor to a steady-state flux level $\phi_0$ at time $t = 0$. We will assume that prior to this time, the reactor core has been in a

shutdown state with zero fission product poison concentrations (i.e., a "clean" core). We need only substitute a time-independent flux $\phi(\mathbf{r},t) = \phi_0(\mathbf{r})$ into our general solutions, Eq. (15-11) and (15-12), and use the initial conditions $I(\mathbf{r},0) = 0 = X(\mathbf{r},0)$ to find the time behavior of the fission product concentrations following startup:

$$I(t) = \frac{\gamma_I \Sigma_f \phi_0}{\lambda_I}(1 - \exp - \lambda_I t),\tag{15-13}$$

and

$$X(t) = \frac{(\gamma_I + \gamma_X)\Sigma_f \phi_0}{\lambda_X + \sigma_a^X \phi_0}\left[1 - \exp\left(-(\lambda_X + \sigma_a^X \phi_0)t\right)\right]$$

$$+ \frac{\gamma_I \Sigma_f \phi_0}{\lambda_X - \lambda_I + \sigma_a^X \phi_0}\left[\exp\left(-(\lambda_X + \sigma_a^X \phi_0)t\right) - \exp(-\lambda_I t)\right].\tag{15-14}$$

The qualitative time behavior of these concentrations following a clean startup is shown in Figure 15-3. In particular, it should be noted that these concentrations eventually level off at equilibrium levels for long times following startup:

$$I(t)\xrightarrow[t \to \infty]{} I_\infty = \frac{\gamma_I \Sigma_f \phi_0}{\lambda_I},$$

$$X(t)\xrightarrow[t \to \infty]{} X_\infty = \frac{(\gamma_I + \gamma_X)\Sigma_f \phi_0}{\lambda_X + \sigma_a^X \phi_0}.\tag{15-15}$$

That is, the concentrations of these fission product poisons in a reactor operating at constant flux will eventually saturate at those equilibrium values for which the production of poisons from fission is just balanced by the decay and neutron capture losses of the poisons. These equilibrium concentrations could also have been determined directly from the rate equations (15-9) and (15-10) themselves by merely setting $dX/dt = 0 = dI/dt$.

The equilibrium concentration $X_\infty$ is of interest because we can substitute it into Eq. (15-8) to determine the negative reactivity which the xenon will contribute under steady-state power conditions.

$$\Delta\rho \cong -\frac{\Sigma_a^X}{\Sigma_a} = -\frac{\sigma_a^X}{\Sigma_a}\frac{(\gamma_I + \gamma_X)\Sigma_f \phi_0}{(\lambda_X + \sigma_a^X \phi_0)}.\tag{15-16}$$

In a critical reactor in which leakage can be ignored, $k = (\nu\Sigma_f/\Sigma_a)p\epsilon = 1$ implies that $\Sigma_f/\Sigma_a = (\nu p\epsilon)^{-1} \sim 1/\nu$ and therefore

$$\Delta\rho \cong -\frac{(\gamma_I + \gamma_X)\phi_0}{\nu\left(\dfrac{\lambda_X}{\sigma_a^X} + \phi_0\right)}.\tag{15-17}$$
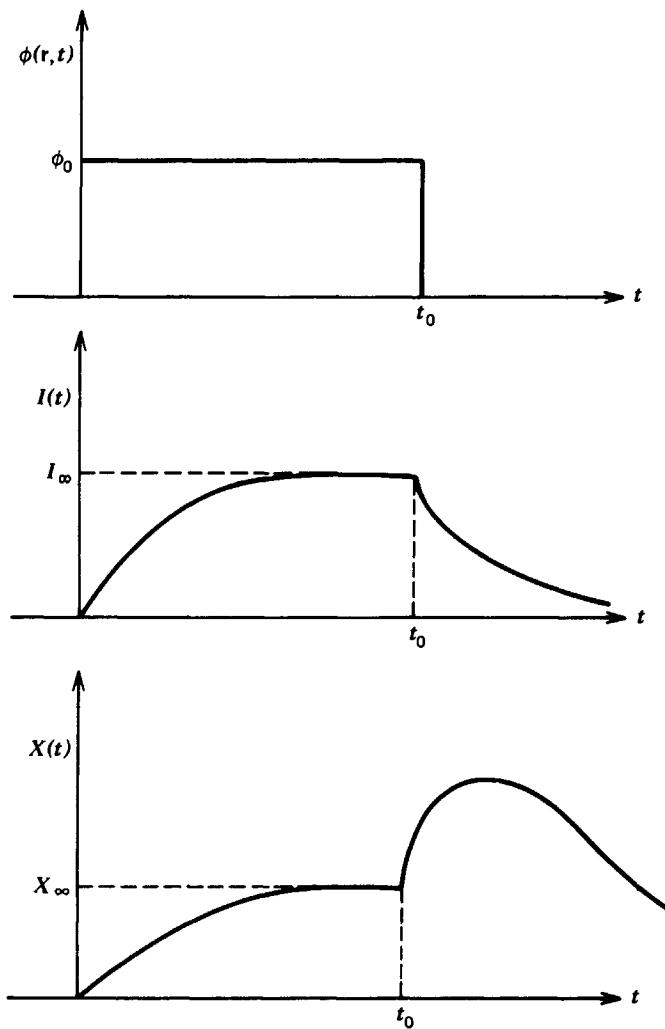
**FIGURE 15-3.** Qualitative behavior of $^{135}I$ and $^{135}Xe$ concentrations following a cold, clean startup and then shutdown.

Notice this reactivity will depend on the flux level $\phi_0$. However for large flux levels characteristic of those in power reactors,

$$\phi_0 \gg \frac{\lambda_x}{\sigma_a^x} = 0.756 \times 10^{13} \text{ cm}^{-2} \text{ sec}^{-1}, \tag{15-18}$$

and the xenon reactivity will approach a maximum value of

$$\Delta\rho \rightarrow - \frac{(\gamma_I + \gamma_x)}{\nu}. \tag{15-19}$$

This amounts to $\Delta\rho \cong -.026$ for both $^{233}U$ and $^{235}U$-fueled reactors, a rather sizable reactivity. This, of course, must be accounted for in determining excess reactivity and control system requirements.

## 2. REACTOR SHUTDOWN

Suppose now that after operating the reactor for a long period of time at a constant flux level $\phi_0$, we suddenly shut the reactor down. An examination of the rate equations (15-9) and (15-10) reveal several consequences of setting the flux $\phi$ suddenly equal to zero. First the removal of $^{135}Xe$ due to neutron capture ceases,

leaving $^{135}$Xe decay as the sole removal mechanism. However the production of $^{135}$Xe via decay of $^{135}$I will continue. Since the half-life of $^{135}$I is shorter than that of $^{135}$Xe, the $^{135}$Xe concentration may initially build up before decaying out. To study this more explicitly, suppose we solve the rate equations (15-9) and (15-10) characterizing the shutdown reactor:

$$\frac{\partial I}{\partial t} = -\lambda_I I(\mathbf{r}, t),$$

$$\frac{\partial X}{\partial t} = \lambda_I I(\mathbf{r}, t) - \lambda_X X(\mathbf{r}, t)$$

(15-20)

subject to the initial conditions that at the time of shutdown $(t = 0)$, the poison concentrations have attained their equilibrium values $I_\infty$ and $X_\infty$. The iodine equation is easy to solve

$$I(\mathbf{r}, t) = I_\infty(\mathbf{r}) \exp - \lambda_I t.$$

(15-21)

One can now insert this into the xenon equation and integrate to find

$$X(\mathbf{r}, t) = X_\infty(\mathbf{r}) \exp(-\lambda_X t) + \frac{\lambda_I I_\infty(\mathbf{r})}{\lambda_I - \lambda_X} \left[ \exp(-\lambda_X t) - \exp(-\lambda_I t) \right].$$

(15-22)

If we use the explicit forms for $X_\infty$ and $I_\infty$ in Eq. (15-8), we can find the negative reactivity introduced by the $^{135}$Xe buildup as

$$\Delta \rho(t) = -\frac{1}{\nu p \epsilon} \left[ \frac{(\gamma_I + \gamma_X)\phi_0}{\lambda_X / \sigma_a^X + \phi_0} \exp(-\lambda_X t) + \frac{\gamma_I \sigma_a^X \phi_0}{\lambda_I - \lambda_X} \left[ \exp(-\lambda_X t) - \exp(-\lambda_I t) \right] \right].$$

(15-23)

Some typical values are shown plotted in Figure 15-4. The maximum value of negative reactivity depends quite sensitively on the flux level prior to shutdown. In fact unless

$$\phi_0 > \frac{\gamma_X}{\gamma_I} \frac{\lambda_X}{\sigma_a^X},$$

(15-24)

no buildup of xenon following shutdown will occur. However since this ratio is quite small $(4 \times 10^{11}$ and $3 \times 10^{12}$ cm$^{-2}$ sec$^{-1}$ in $^{235}$U- and $^{233}$U-fueled reactors, respectively), a xenon transient buildup will occur following shutdown in most power reactors.

We can calculate the time at which the maximum negative reactivity occurs as

$$t_{max} = \frac{1}{\lambda_I - \lambda_X} \ln \left[ \frac{\lambda_I / \lambda_X}{1 + \frac{\lambda_X}{\lambda_I} \left( \frac{\lambda_I}{\lambda_X} - 1 \right) \frac{X_\infty}{I_\infty}} \right] \xrightarrow[\phi_0 \gg \lambda_X / \sigma_a^X]{} \frac{1}{\lambda_I - \lambda_X} \ln \left( \frac{\lambda_I}{\lambda_X} \right) = 11.6 \text{ h}$$

(15-25)

where we have also noted the value assumed by $t_{max}$ in the limit of large flux levels
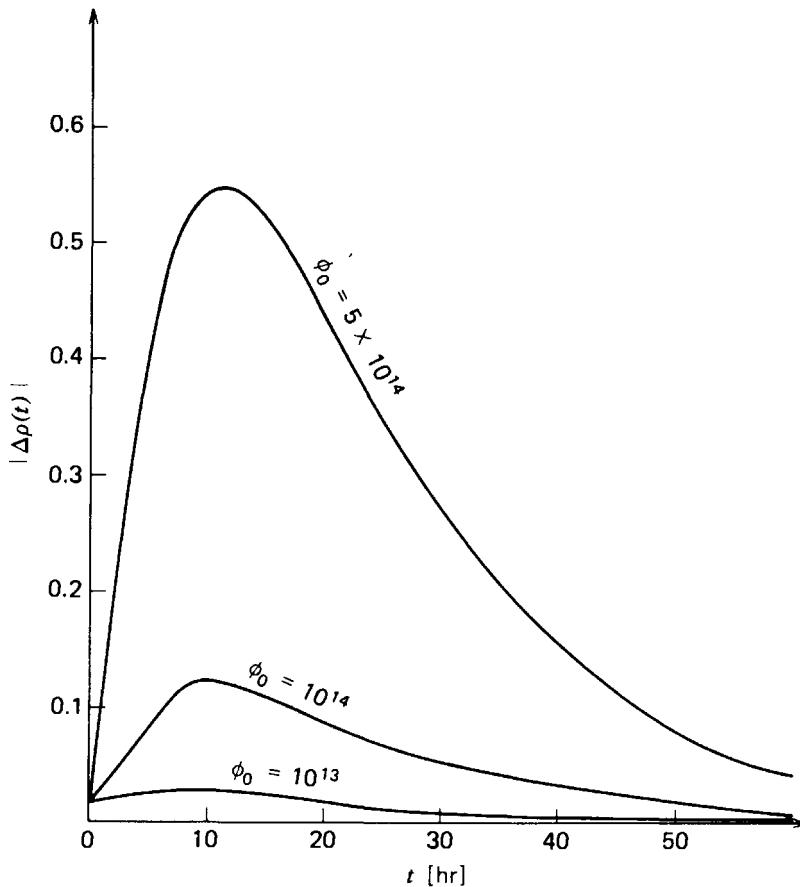
FIGURE 15-4. Negative reactivity due to $^{135}Xe$ buildup following shutdown at $t=0$.

$\phi_0$. In particular, one should note that for a period of about 30 hours after reactor shutdown, a rather sizable reserve of positive reactivity would be needed to restart the reactor. This, of course, is a major consideration in scheduling shutdown for short periods of time.

In large power reactors the xenon transients following shutdown are mitigated to a degree by several factors.[5] First the neutron fluxes in large power reactors are somewhat lower than in research or propulsion reactors (typically $\phi_0 \lesssim 10^{14}$ cm$^{-2}$ sec$^{-1}$). Furthermore the xenon buildup can be minimized by avoiding an abrupt shutdown and instead programming the shutdown in a gradual manner to burn out some of the xenon while shutting down. Finally, the existence of a power defect of reactivity means that the reactor can usually be brought to a low power level following shutdown and xenon buildup in order to burn out some of the xenon before increasing the flux to full power levels.

## 3. XENON TRANSIENTS FOLLOWING POWER LEVEL CHANGES

Let us calculate the xenon transient following a change in reactor flux level from $\phi_0$ to $\phi_1$. If we assume that this change occurs at $t=0$, we can solve the isotopic rate equations (15-9) and (15-10) as an initial value problem with $\phi \rightarrow \phi_1$ and $I(0)=I_\infty$, $X(0)=X_\infty$. In particular, we find that following the power-level change

$$I(t) = \frac{\gamma_I \Sigma_f \phi_1}{\lambda_I} \left[ 1 - \left( \frac{\phi_1 - \phi_0}{\phi_1} \right) \exp - \lambda_I t \right], \tag{15-26}$$

and

$$X(t) = \frac{(\gamma_I + \gamma_X)\Sigma_f \phi_1}{\lambda_X + \sigma_a^X \phi_1} \left\{ 1 - \left( \frac{\phi_1 - \phi_0}{\phi_1} \right) \left[ \frac{\lambda_X}{\lambda_X + \sigma_a^X \phi_0} \exp\left[ -(\lambda_X + \sigma_a^X \phi_1)t \right] \right. \right.$$

$$\left. \left. + \left( \frac{\gamma_I}{\gamma_X + \gamma_I} \right) \left( \frac{\lambda_X + \sigma_a^X \phi_1}{\lambda_X + \sigma_a^X \phi_1 - \lambda_I} \right) \left[ \exp(-\lambda_I t) - \exp\left( -(\lambda_X + \sigma_a^X \phi_1)t \right) \right] \right] \right\}. \quad (15\text{-}27)$$

As we have sketched in Figure 15-5, a flux level increase is followed by a xenon concentration decrease and vice versa. These xenon transients following flux level changes are characterized by times of the order of eight hours. Such xenon transients induce reactivity transients, which although slow enough to be compensated for by shim control, can nevertheless be troublesome.

For example, suppose we consider a PWR operating at some nominal power level toward the end of core life. Since the fuel will be relatively highly depleted,
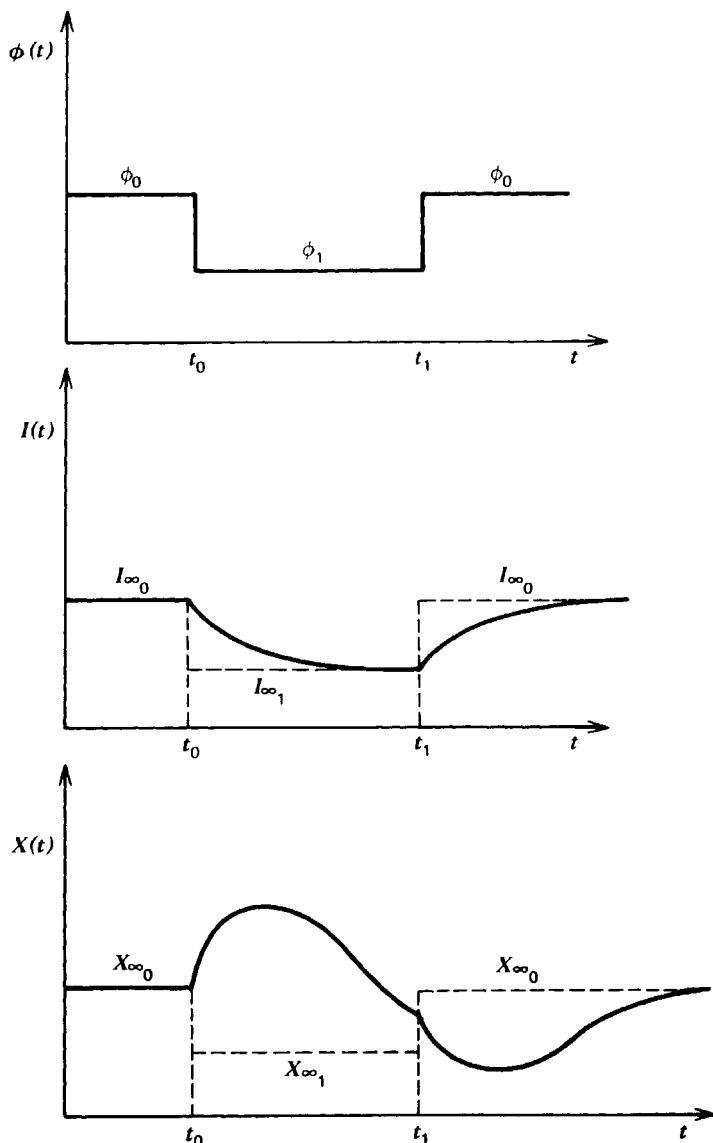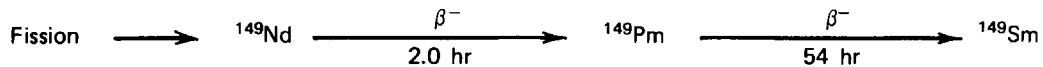


FIGURE 15-5.    Variation in $^{135}$Xe concentration following power level changes.

the amount of chemical shim present will be small. However since the rate at which reactivity can be changed is proportional to the soluble poison concentration, the reactivity response $d\rho/dt$ will also be small. Now suppose the reactor power level is suddenly reduced. Then, as we have just seen, the xenon concentration will begin to build up. One would then desire to decrease the chemical shim concentration to compensate for the negative reactivity introduced by the xenon transient, and there may be insufficient chemical shim present to allow this. One encounters a similar situation following a power increase, since now chemical shim must be rapidly inserted into the coolant to compensate for xenon burnup. Such considerations can place strong limitations on the allowable chemical shim concentrations in the core design.

## B. Samarium Fission Product Poisoning

A very similar analysis can be given for $^{149}$Sm, which is also characterized by large fission yields (see Table 15-1) and absorption cross sections ($\sigma_a^S = 58,500$ b). The appropriate decay scheme is

Fission $\longrightarrow$ $^{149}$Nd $\xrightarrow[\text{2.0 hr}]{\beta^-}$ $^{149}$Pm $\xrightarrow[\text{54 hr}]{\beta^-}$ $^{149}$Sm

Again, it is consistent to neglect the $^{149}$Nd and assume fission yields $^{149}$Pm directly. The corresponding rate equations are then

*Promethium*:

$$\frac{\partial P}{\partial t} = \gamma_P \Sigma_f \phi(\mathbf{r},t) - \lambda_P P(\mathbf{r},t), \tag{15-28}$$

*Samarium*:

$$\frac{\partial S}{\partial t} = \lambda_P P(\mathbf{r},t) - \sigma_a^S \phi(\mathbf{r},t) S(\mathbf{r},t). \tag{15-29}$$

The equilibrium concentrations can again be obtained by setting $\partial P/\partial t = 0$ $= \partial S/\partial t$ to find

$$P_\infty = \frac{\gamma_P \Sigma_f \phi_0(\mathbf{r})}{\lambda_P},$$

$$\tag{15-30}$$

$$S_\infty = \frac{\gamma_P \Sigma_f}{\sigma_a^S}.$$

The corresponding negative reactivity due to saturated samarium poisoning is then

$$\Delta \rho \cong -\frac{\gamma_P}{\nu} \cong 0.00463. \tag{15-31}$$

We can again study the shutdown behavior using $P_\infty$ and $S_\infty$ as initial conditions. Notice that since $^{149}$Sm is stable (unlike $^{135}$Xe), it can only be removed by neutron capture. Hence after shutdown it will build up to a steady level

$$S(t) = S_\infty + P_\infty(1 - \exp - \lambda_P t) \underset{t \to \infty}{\longrightarrow} S_\infty + P_\infty. \tag{15-32}$$
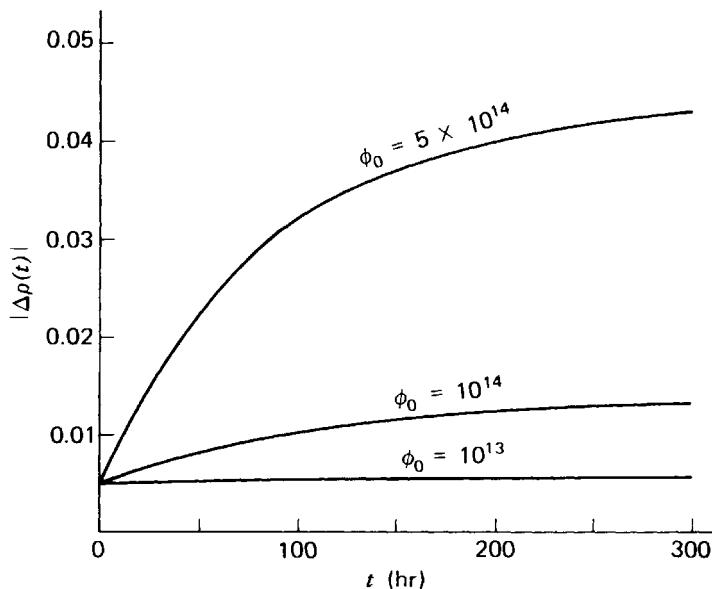
**FIGURE 15-6.** Negative reactivity due to $^{149}$Sm buildup following reactor shutdown at $t = 0$.

The corresponding reactivity is

$$\Delta\rho = -\frac{\gamma_P}{\nu}\left[1 + \frac{\phi_0\sigma_a^S}{\lambda_P}(1 - \exp -\lambda_P t)\right].$$  (15-33)

Typical plots of $\Delta\rho(t)$ are given for a $^{235}$U-fueled reactor in Figure 15-6. The much longer time scale characterizing $^{149}$Sm buildup should be noted. Indeed it takes roughly one week for the $^{149}$Sm concentration to approach saturation levels in a core.

The smaller absorption cross section and yield fraction and longer precursor half-life characterizing samarium imply that it will lead to far less severe reactivity effects than $^{135}$Xe. Nevertheless, $^{149}$Sm buildup must be accounted for in nuclear analysis.

## C. Other Fission Product Poisons

There are a great many fission product nuclides other than $^{135}$Xe and $^{149}$Sm that have appreciable neutron absorption cross sections. However the cross sections of these other isotopes are not sufficiently large in most cases for their concentration to be depleted by neutron capture. Hence these fission products do not saturate but rather tend to accumulate in a core indefinitely. Furthermore the fission yields of these isotopes are not as large as those of $^{135}$Xe or $^{149}$Sm. It has become customary[6] to account for these nonsaturating fission products in criticality calculations by lumping them together into several effective groups characterized by effective cross sections and yields. (For one-speed thermal calculations, one frequently assumes that each fission produces a permanent poison nucleus with effective absorption cross section $\sigma_a^P \sim 50$ b.) We will return later in this chapter to discuss how such considerations enter core lifetime and burnup studies.

Since the absorption cross sections of all nuclides drop off rapidly with increasing neutron energy, neutron capture will not appreciably affect fission-product concentrations in fast reactors. Hence all fission products can be lumped into nonsaturating groups characterized by effective absorption cross sections in fast reactor analysis.

## D. Spatial Effects in Fission Product Poisoning

### 1. A PERTURBATION THEORY ESTIMATE OF REACTIVITY WORTH

In our earlier estimate of the reactivity change caused by fission product poisoning, we merely computed the changes in the thermal utilization as the poison concentration built up. However such an estimate is actually only valid for a uniform concentration of poison in an infinite core. More generally, we know that the poison concentration will depend on the spatial variation of the flux in a finite core, and hence our estimate of reactivity worth of the poison is only of limited validity. We can improve this estimate by using perturbation theory.

Let us compute the reactivity due to the equilibrium xenon concentration in a core operating with a steady-state flux $\phi_0(\mathbf{r})$. Then we know

$$\Sigma_a^X(\mathbf{r}) = \sigma_a^X X_\infty(\mathbf{r}) = \frac{(\gamma_I + \gamma_X)\Sigma_f(\mathbf{r})\phi_0(\mathbf{r})}{(\lambda_X/\sigma_a^X) + \phi_0(\mathbf{r})}. \tag{15-34}$$

If we treat this as a perturbation in the absorption cross section, $\delta\Sigma_a \rightarrow \Sigma_a^X(\mathbf{r})$, then we can use the first-order perturbation result given by Eq. (5-306) to find the reactivity change due to the xenon as

$$\Delta\rho = -\frac{\int d^3r\,\phi_0^2(\mathbf{r})\Sigma_a^X(\mathbf{r})}{\nu\int d^3r\,\phi_0^2(\mathbf{r})\Sigma_f(\mathbf{r})} = -\frac{(\gamma_I + \gamma_X)}{\nu}\frac{\int d^3r\,\dfrac{\Sigma_f(\mathbf{r})\phi_0^3(\mathbf{r})}{\lambda_X/\sigma_a^X + \phi_0(\mathbf{r})}}{\int d^3r\,\phi_0^2(\mathbf{r})\Sigma_f(\mathbf{r})}. \tag{15-35}$$

This expression can be evaluated numerically to compute the equilibrium reactivity worth of the xenon poisoning in a core. Note that for large power levels, $\phi_0 \gg \lambda_X/\sigma_a^X$, this reduces to just our earlier approximate result for an infinite medium

$$\Delta\rho \xrightarrow[\phi_0 \gg \lambda_X/\sigma_a^X]{} -\frac{(\gamma_I + \gamma_X)}{\nu} \equiv \Delta\rho_\infty. \tag{15-36}$$

For low flux levels, $\phi_0 \ll \lambda_X/\sigma_a^X$, in an uniform core (e.g., a low-power research reactor)

$$\Delta\rho \xrightarrow[\phi_0 \ll \lambda_X/\sigma_a^X]{} -\frac{(\gamma_I + \gamma_X)}{\nu}\frac{\int d^3r\,\phi_0^3(\mathbf{r})}{\int d^3r\,\phi_0^2(\mathbf{r})}. \tag{15-37}$$

For example, in a slab, one finds that in this limit

$$\Delta\rho \rightarrow \tfrac{4}{3}\Delta\rho_\infty, \tag{15-38}$$

where $\Delta\rho_\infty$ is the reactivity change characterizing an infinite medium model. That is, the reactivity worth is some 33% larger when the spatial variation of the flux is taken into account. In a low-power reactor core, this spatial weighting factor is more typically between 2.5 and 3.0 (see Problem 15-12).[5]

### 2. XENON-INDUCED POWER OSCILLATIONS IN LARGE POWER REACTORS[7-10]

Thus far we have ignored the effect of the reactivity introduced by the fission product poisons on the neutronic behavior of the core. The interaction between

xenon fission product buildup and the changes in the neutron flux distribution that accompanies local changes in reactivity can lead to spatial oscillations in the power distribution in a large thermal reactor core.

To explain this phenomenon, let us first consider a point-reactor model in which the reactor has been operating at a steady-state flux level for a period of time. Then our earlier study of xenon fission product poisoning has indicated that there will be a saturation in the $^{135}Xe$ concentration resulting from the balance of $^{135}Xe$ production (via direct fission and $^{135}I$ decay) and loss due to decay to $^{135}Cs$ and transmutation (via neutron absorption) to $^{136}Xe$. (Recall Figure 15-2.) Now suppose a small perturbation increase in the flux occurs. Then $^{135}Xe$ will transmute more rapidly to $^{136}Xe$ (instantaneously), depleting the $^{135}Xe$ concentration, hence decreasing the absorption and increasing the reactivity and the flux. However the increased flux transmutes even more $^{135}Xe$, and hence the initial flux perturbation grows with time (unstable). Such an instability can only exist for power levels higher than a certain threshold value. For $^{235}U$-fueled reactors, this threshold is $3 \times 10^{11}$ neutrons/cm²·sec. Below this threshold the stabilizing effect of the direct xenon yield from fission is more important than the destabilizing effect of the xenon decaying from $^{135}I$.

Actually this type of instability is relatively unimportant in practical reactor operations, since it is easily controlled by normal control rod movement. A much more serious *spatial* xenon instability can arise, however, which requires a more complex control rod program. To understand this, consider the very simple model illustrated in Figure 15-7 consisting of two coupled xenon-unstable point reactors, separated by a region of nonmultiplying material. Suppose further that there is a control system keeping the *total* power of all three core regions constant (although the flux or power in an individual region is not constant).

A slight increase in the power level on one side of the core will give rise to the unstable xenon process described for a point reactor. Since the control system keeps the total power constant, the flux on the other side decreases. This process continues with an increasingly steeper tilt in the flux resulting. Two effects will
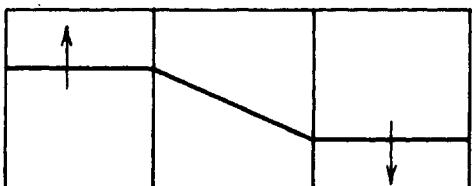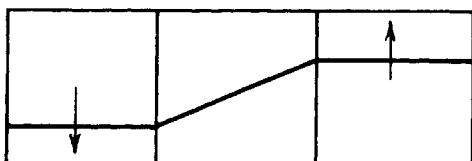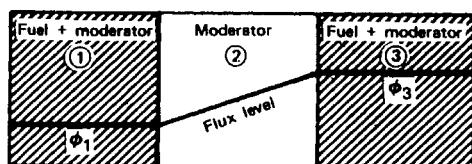


FIGURE 15-7. A simple model of xenon-induced power oscillations.

limit this tilt: (a) burnup of most of the xenon on the high flux side and (b) the steep flux tilt which creates a flux gradient and hence a current that carries all the excess neutrons being produced to the other side. The flux will remain tilted for several hours. Eventually the high flux side will have created an $^{135}$I concentration much greater than that originally present. Since the decay half-life of $^{135}$I is 6.7 hours, more xenon will be created after this delay period. Similarly on the low side less xenon will be created. This reverses the flux tilt eventually and produces a side-to-side oscillation with a period of 15–30 hours. Thus the xenon process tends to be self-limiting and produces the effect of a moving "hot spot" to the reactor operator.

The oscillation of the power distribution in a reactor can cause changes in the power-peaking factor $F_q^N$. However this can be easily accounted for in design to ensure that thermal performance constraints are not exceeded. Such xenon-induced power oscillations are more of an operational than a safety problem.

Although such oscillations can be controlled by control rod motion, there is strong motivation to design the reactor core in such a way that xenon oscillations are minimized, since the load-following requirements of a power reactor operating on a utility power grid imply that such control adjustments may incur considerable economic penalty. In general, negative feedback mechanisms such as moderator void formation or the Doppler effect will tend to suppress xenon-induced power oscillations. For example, the very large negative void coefficient in a BWR will usually suppress the oscillations within one or two cycles.

The stability of the spatial power distribution with respect to xenon-induced oscillations will decrease with increasing core size or decreasing neutron migration length. As a rule of thumb, xenon oscillations will be a problem if the reactor core is over 30 migration lengths in size.[10] Since this is the case with most large power reactor cores, xenon oscillations can represent a serious design and control consideration. Strong reactivity feedback, such as the moderator void coefficient in a BWR, will help to suppress such oscillations, however. In addition, partial length control rods can be used to damp out power oscillations by suitable rod programming.

## II. FUEL DEPLETION ANALYSIS

### A. Introduction

Fuel depletion analysis is concerned with predicting the long-term changes in reactor fuel composition caused by exposure to neutron flux during reactor operation. Such changes have an important bearing on the operating life of a reactor, as well as on its stability and control. One must first ensure that the shift in the core power distribution that accompanies fuel burnup does not result in the exceeding of core thermal limitations. Sufficient excess reactivity must be provided in the fresh core loading to achieve the desired fuel exposure (consistent with safety limitations). And, of course, a detailed analysis of core composition is necessary in order to optimize fuel exposure to achieve minimum power costs as well as to determine the value of discharged fuel. Since the fuel costs over the operating lifetime of the reactor can exceed those of the capital cost of the plant itself, the incentive for accurate analysis of fuel depletion is quite high.

A variety of nuclear processes must be monitored during a depletion study. These include, of course, the consumption of fissile nuclides (fuel burnup). However one must also account for the conversion of fertile isotopes into fissile isotopes
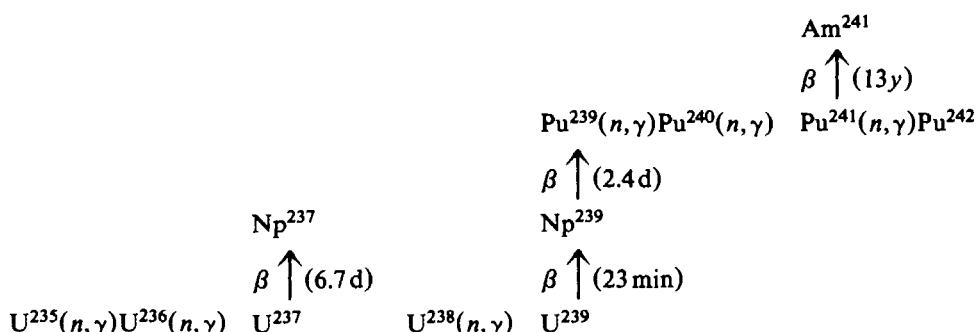
and the production of numerous fission products. Finally, one must monitor the reactivity balance to ensure core criticality (usually by determining the change in reactivity over a period of core operation and then adjusting control to compensate for this reactivity change).

A complete burnup calculation would involve the solution of the coupled reaction rate equations describing such processes for the hundreds of different types of isotopes in a reactor core. In practice, one usually introduces approximations that greatly simplify these calculations. For example, the only fission products that are usually treated explicitly are those with large capture cross sections and fission yields, namely, $^{135}Xe$ and $^{149}Sm$. The remaining fission products are lumped into one or several groups, each characterized by an effective cross section. Furthermore any nuclide with a short half-life is omitted from a burnup calculation.

The specific isotopes monitored depend on the particular fuel used in the core. The isotopes of interest in both uranium- and thorium-fueled reactors are indicated in Figure 15-8. In addition to fission products and the other isotopes produced during fuel irradiation, one must monitor concentrations of burnable poisons such as boron or gadolinium.

The general procedure is to solve the time-dependent rate equations describing isotopic concentrations together with the static multigroup diffusion equations describing the spatial flux profile in a reactor core that is kept critical by control adjustments while its core composition is changing due to fuel burnup and isotope production. As we indicated earlier, this analysis can become quite involved since one also may have to account for changes in core thermal–hydraulic behavior that accompany changes in the power distribution, as well as implement a prescribed control management scheme to maintain a critical core operating at rated power over core life. Hence before we consider in detail how such practical depletion studies are performed, we will first consider several extremely simple examples to illustrate the general ideas involved in such studies.

*Uranium-fueled cores*:

$$Am^{241}$$

$$\beta \uparrow (13y)$$

$$Pu^{239}(n,\gamma)Pu^{240}(n,\gamma) \quad Pu^{241}(n,\gamma)Pu^{242}$$

$$\beta \uparrow (2.4d)$$

$$Np^{237} \qquad\qquad Np^{239}$$

$$\beta \uparrow (6.7d) \qquad\qquad \beta \uparrow (23\,min)$$

$$U^{235}(n,\gamma)U^{236}(n,\gamma) \quad U^{237} \qquad U^{238}(n,\gamma) \quad U^{239}$$

*Thorium-fueled cores*:

$$U^{233}(n,\gamma) \qquad U^{234}$$

$$\beta \uparrow (27d) \qquad \beta \uparrow (6.7\,hr)$$

$$Pa^{233}(n,\gamma) \qquad Pa^{234}$$

$$\beta \uparrow (22\,min)$$

$$Th^{232}(n,\gamma) \quad Th^{233}$$
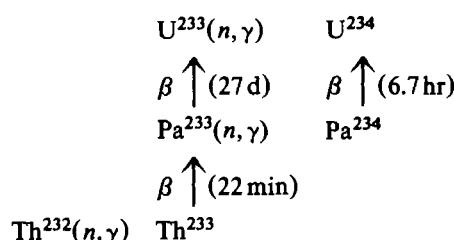
FIGURE 15-8.    Isotope chains of interest in fuel depletion analysis.

## B. Some Simple Examples of Fuel Depletion

### 1. THE DEPLETION OF A SINGLE ISOTOPE

Suppose a reactor were fueled with only a single isotope, characterized by an atomic number density $N_F(\mathbf{r}, t)$ and one-group absorption cross section $\sigma_a^F$. Then the fuel burnup would be described by the simple rate equation

$$\frac{\partial N_F}{\partial t} = -N_F(\mathbf{r}, t)\sigma_a^F \phi(\mathbf{r}, t). \tag{15-39}$$

Now if the flux were known in advance, we could easily solve this equation to find

$$N_F(\mathbf{r}, t) = N_F(\mathbf{r}, 0)\exp\left[-\sigma_a^F \int_0^t \phi(\mathbf{r}, t')dt'\right], \tag{15-40}$$

or in terms of the neutron fluence, $\Phi(\mathbf{r}, t)$, defined by Eq. (14-24),

$$N_F(\mathbf{r}, t) = N_F(\mathbf{r}, 0)\exp\left[-\sigma_a^F \Phi(\mathbf{r}, t)\right]. \tag{15-41}$$

Of course, this is still a formal solution since the flux $\phi(\mathbf{r}, t)$ depends on the fuel density $N_F(\mathbf{r}, t)$ through the equations describing reactor criticality (i.e., the multigroup diffusion equations).

We can use this result to illustrate the two standard approximations used in more elaborate depletion studies:

(a) CONSTANT FLUX APPROXIMATION:

Assume that over the time interval of interest, the flux can be treated as constant

$$\phi(\mathbf{r}, t) = \phi_0(\mathbf{r}). \tag{15-42}$$

Then we can solve for

$$N_F(\mathbf{r}, t) = N_F(\mathbf{r}, 0)\exp\left[-\sigma_a^F \phi_0(\mathbf{r})t\right]. \tag{15-43}$$

(b) CONSTANT POWER APPROXIMATION:

One assumes instead that the reactor power is constant

$$P(\mathbf{r}, t) = w_a N_F(\mathbf{r}, t)\sigma_a^F \phi(\mathbf{r}, t) = P_0(\mathbf{r}), \tag{15-44}$$

where $w_a$ is the energy released per neutron absorption in the fuel ($w_a = (\sigma_f^F/\sigma_a^F)w_f$). Then one can integrate

$$\frac{\partial N_F}{\partial t} = -\sigma_a^F N_F \phi = \frac{P_0}{w_a}, \tag{15-45}$$

to find

$$N_F(\mathbf{r}, t) = N_F(\mathbf{r}, 0) - \frac{P_0(\mathbf{r})}{w_a}t. \tag{15-46}$$

The isotopic depletion resulting from the assumptions of constant flux or constant power are quite different, as shown in Figure 15-9. However for short time intervals, these solutions are similar since for small $t$, Eq. (15-43) becomes

$$N_F(r,t) \cong N_F(r,0)\left[ 1 - \sigma_a^F \phi_0(r)t \right]$$

$$= N_F(r,0) - \frac{P_0(r)}{w_a}t. \tag{15-47}$$

This is significant because while we cannot rely on the assumption of constant power or flux over times as long as a core lifetime, we can use these approximations over very short time steps, since both yield the same result as a short-time Taylor expansion of the isotopic density

$$N_F(r,t) = N_F(r,0) + t\left.\frac{\partial N_F}{\partial t}\right|_{t=0} + \cdots$$

$$\cong N_F(r,0) - \frac{P_0(r)}{w_a}t. \tag{15-48}$$

That is, these two types of approximation will be used to characterize the flux or power over a time step or "depletion step" in a finite-difference solution of the time-dependent isotopic rate equations.
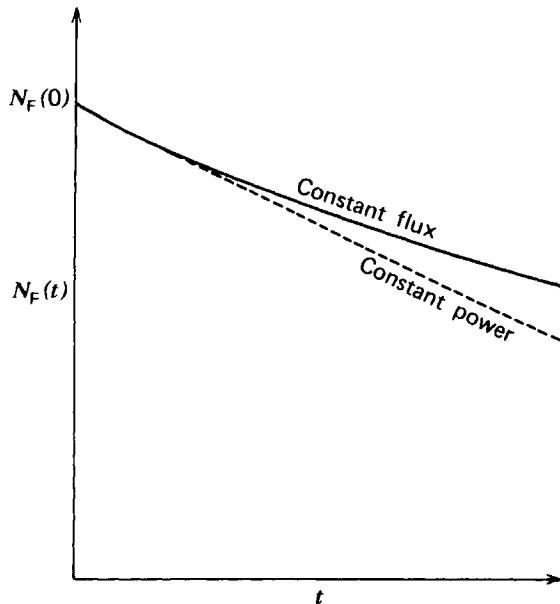


FIGURE 15-9. Depletion of a single fuel isotope in the constant flux or power approximation.

## 2. FUEL DEPLETION IN A SIMPLE REACTOR MODEL[11]

Of course, we cannot decouple fuel depletion from reactivity effects if the fuel concentrations change appreciably. In general, one must consider both the neutronic behavior and control adjustment of the core as fuel depletes over core life. It is of interest to illustrate the ideas involved in the solution of the isotopic depletion equations and control adjustment by considering a simple model in

which the neutronic analysis is bypassed by assuming an infinite one-speed reactor characterized by a multiplication $k = \eta f$. That is, we assume a simple model of an infinite, homogeneous, thermal reactor with a single fissile isotope (e.g., $^{235}U$) and no fertile material. We will represent the control rods used to balance the excess reactivity of the initial core loading by a uniformly distributed absorption cross section $\Sigma_C(t)$. The criticality condition for this simple model is just

$$k = \eta f = \frac{\eta \Sigma_a^F(t)}{\underset{\text{Fuel}}{\underbrace{\Sigma_a^F(t)}} + \underset{\text{Moderator}}{\underbrace{\Sigma_a^M}} + \underset{\text{Fission-product poison}}{\underbrace{\Sigma_a^P(t) + \Sigma_C(t)}}} = 1. \tag{15-49}$$

We can solve this for the required control

$$\Sigma_C(t) = (\eta - 1)\Sigma_a^F(t) - \Sigma_a^M - \Sigma_a^P(t). \tag{15-50}$$

Now as the core life proceeds, the fuel cross section $\Sigma_a^F(t)$ decreases, while the poison concentration increases. Hence $\Sigma_C(t)$ will drop to zero eventually at some time $t_l$, corresponding to the end of core life. It is possible to calculate $t_l$, provided the power history of the reactor is known.

For simplicity, we will suppose that the reactor is operated at constant power over the core life. This implies

$$\Sigma_a^F(t)\phi(t) = \Sigma_a^F(0)\phi(0), \tag{15-51}$$

where $\Sigma_a^F(0)\phi(0)$ characterizes the initial core loading. After a time $t$,

$$N_F(t) = N_F(0) - \Sigma_a^F(0)\phi(0)t$$

$$= N_F(0)\left[ 1 - \sigma_a^F\phi(0)t \right], \tag{15-52}$$

or

$$\Sigma_a^F(t) = \Sigma_a^F(0)\left[ 1 - \sigma_a^F\phi(0)t \right]. \tag{15-53}$$

If we substitute this into (15-51), we can solve for the flux

$$\phi(t) = \frac{\phi(0)}{1 - \sigma_a^F\phi(0)t}. \tag{15-54}$$

(Note how $\phi(t)$ must increase as the fuel is depleted in order to yield a constant power production.)

We can now use this flux history to compute the fission product poison concentrations. Recall from our earlier work that the equilibrium fission product concentrations are given by:

$$\Sigma_a^X(t) = \frac{(\gamma_I + \gamma_X)\Sigma_f\phi}{\lambda_X / \sigma_a^X + \phi} = \frac{(\gamma_I + \gamma_X)\Sigma_f(0)\phi(0)}{\lambda_X / \sigma_a^X + \phi(t)} \tag{15-55}$$

for xenon, and

$$\Sigma_a^S(t) = \gamma_P \Sigma_f(t) \tag{15-56}$$

for samarium. [Note here that $\Sigma_f(t) = \Sigma_a^F(t)/(1+\alpha)$.]

We must also worry about non-saturating or "permanent" poisons

$$\Sigma_{pp} = \sigma_{pp}\Sigma_f(t)\phi(t)t = \sigma_{pp}\Sigma_f(0)\phi(0)t. \tag{15-57}$$

Substituting Eqns. (15-53) to (15-57) into our expression for the control cross section, Eq. (15-50), we find

$$\Sigma_C(t) = (\eta - 1)\Sigma_a^F(0)\left[1 - \sigma_a^F\phi(0)t\right] - \Sigma_a^M - \frac{(\gamma_I + \gamma_X)\Sigma_f(0)\phi(0)}{\lambda_X/\sigma_a^X + \phi(t)}$$

$$- \gamma_P\Sigma_f(0)\left[1 - \sigma_a^F\phi(0)t\right] - \sigma_{pp}\Sigma_f(0)\phi(0)t. \tag{15-58}$$

If we now substitute Eq. (15-54) for $\phi(t)$, and then set $\Sigma_C(t_l) = 0$, we can solve for the core lifetime $t_l$ as

$$t_l \cong \frac{\eta\rho_{ex}(1+\alpha) - (\gamma_I + \gamma_X)\phi(0)\sigma_a^X/\lambda_X - \gamma_P}{\left[(\eta-1)(1+\alpha)\sigma_a^F - \gamma_P\sigma_a^F + \sigma_{pp}\right]\phi(0)} \quad \text{for } \phi(t) \ll \frac{\lambda_X}{\sigma_a^X}, \tag{15-59}$$

or

$$t_l \cong \frac{\eta\rho_{ex}(1+\alpha) - (\gamma_I + \gamma_X + \gamma_P)}{\left[(\eta-1)(1+\alpha)\sigma_a^F - (\gamma_I + \gamma_X + \gamma_P)\sigma_a^F + \sigma_{pp}\right]\phi(0)} \quad \text{for } \phi(t) \gg \frac{\lambda_X}{\sigma_a^X}, \tag{15-60}$$

where $\rho_{ex} = k_\infty(0) - 1/k_\infty(0)$ is the initial excess reactivity. Hence as we might expect, the core lifetime is essentially proportional to the excess reactivity loading $\rho_{ex}$. Indeed we must choose an initial excess reactivity sufficiently large to compensate for fission product buildup,

$$\rho_{ex} > \frac{\gamma_I + \gamma_X + \gamma_P}{\eta(1+\alpha)} = \frac{\gamma_I + \gamma_X + \gamma_P}{\nu} \tag{15-61}$$
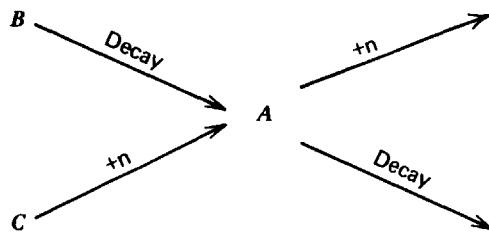
before criticality can be achieved. And of course the core lifetime is inversely proportional to the operating power or flux level $\phi(0)$.

## C. Calculational Methods of Depletion Analysis[12, 13]

We have noted that the analysis of fuel depletion involves a variety of nuclear processes. These can be roughly classified into calculations involving: (a) solution of the isotopic depletion equations, (solving for the nuclei densities as functions of time and position; this requires a knowledge of the neutron flux) and (b) solution of the static multigroup diffusion equations for the neutron flux (this task will usually also involve including thermal–hydraulic coupling, using as input the cross sections characterizing the depleting isotopes, and adjustment of the control representation to achieve core criticality). It is customary to decouple these calculations such that the depletion equations are solved over time intervals in which the flux or power is assumed to be constant. At the end of each time interval, the depleted densities are used to calculate new group constants, and the multigroup diffusion equations are solved to determine a new flux shape for the next time interval.

## 1. ISOTOPIC DEPLETION EQUATIONS

The reaction rate equations describing the number densities of nuclei in the core can be derived using simple balance ideas. If $N_A(r, t)$ is the number density characterizing a nuclide of type A, then the general rate equation characterizing a production-type decay scheme as shown below



takes the form

$$\frac{dN_A}{dt} = -\lambda_A N_A - \left[ \sum_g \sigma_{a_g}^A \phi_g \right] N_A + \lambda_B N_B + \left[ \sum_g \sigma_{\gamma_g}^C \phi_g \right] N_C. \qquad (15\text{-}62)$$

Here

$$\lambda_A N_A \qquad \text{loss due to radioactive decay of A,}$$

$$\left[ \sum_g \sigma_{a_g}^A \phi_g \right] N_A \qquad \text{loss due to neutron capture by A,}$$

$$\lambda_B N_B \qquad \text{gain due to decay of B to A,}$$

$$\left[ \sum_g \sigma_{\gamma_g}^C \phi_g \right] N_C \qquad \text{gain due to transmutation of C to}$$
$$\text{A via neutron capture.}$$

The fluxes and microscopic cross sections appearing in these equations are multigroup averages and must be generated by suitable group-constant generation codes and multigroup diffusion calculations.

These equations are nonlinear and inhomogeneous because the fluxes and microscopic cross sections not only vary in space and time, but depend on the densities of the depleting isotopes as well. Such equations must be written for each species of interest. In a detailed study of fuel depletion in a modern power reactor, some 15–24 heavy nuclides and 25–50 fission products are required for the analysis.[12] When one adds to this the fact that the differential equations describing isotopic depletion contain both long and short time constants (half-lives or large absorption cross sections) that complicate their numerical solution, it is apparent that fuel depletion calculations can become quite involved.

## 2. GENERATION OF GROUP CONSTANTS

A very important facet of any depletion calculation is the generation of the necessary group constants. These are required not only for the multigroup diffusion equations, but also for the isotopic rate equations. Our earlier discussion of a typical macroscopic cross section module illustrated several aspects of such calculations. We recall that these group constants consisted of two factors: (a) the number

densities supplied from the depletion module (or perhaps the thermal-hydraulic module or input) and (b) the microscopic group constants generated either by fast and thermal spectrum codes or by parameterization (where one of the parameters may be the burnup (MWD/MTU) or fluence):

$$\Sigma_{x_g}(\mathbf{r},t) = \sum_j N_j(\mathbf{r},t)\sigma^j_{x_g}(\mathbf{r},t). \tag{15-63}$$

The microscopic cross sections will change in time as the fuel depletes, since the neutron spectrum in the fuel cell will change, as will the effect of self-shielding. Many cross sections are sufficiently slowly varying with fuel depletion that they need only be recalculated at intervals of several time steps and can be interpolated at intermediate times. More rapidly varying cross sections which exhibit strong depletion-dependence of self-shielding factors or spectrum will require adjustment at shorter time intervals.

### 3. FLUX-POWER CALCULATIONS

One must use these few-group constants in the multigroup diffusion equations to determine the flux and power distribution in the core. Interaction with a control adjustment module is usually necessary in order to adjust core multiplication back to critical after a depletion time step. Such flux-power calculations may range from zero- to three-dimensional descriptions, and have already been described in detail in Chapter 13.

### 4. SOLUTION OF THE DEPLETION EQUATIONS

The direct solution of the coupled equations describing the number densities of core materials and the multigroup diffusion equations describing the neutron flux is impractical. Instead one must separate these calculations. The coupling between the depletion and neutronics calculations can be handled in one of several ways:

(a) *SPATIAL TREATMENT*:

The multigroup diffusion equations must be solved many times as depletion proceeds. Such solutions become very expensive if detailed spatial treatments are required. One can distinguish between two different classes of studies:

(i) Macroscopic burnup physics:

In *macroscopic* studies one is concerned with determining the global depletion behavior of the reactor core. In particular, such studies seek to determine the long-term behavior of reactivity variation (and the core lifetime), the core power and burnup distributions, and total core fuel material inventories.

(ii) Microscopic burnup physics:

In *microscopic* studies one is more concerned with an accurate calculation of reaction rates and fuel composition as functions of burnup at a point or in a cell representative of a given region of the core. That is, microscopic studies are usually concerned with the depletion analysis of a lattice unit cell. Such microscopic calculations are used to provide the homogenized or effective cross sections needed for the macroscopic global depletion studies.[14]

### (b) *TIME TREATMENT:*

The treatment of the time-dependence of the depletion and the changes in the flux distributions is usually handled by separating the depletion calculation from the neutronic calculation. To illustrate this approach, suppose that one knows the number densities in the clean, fresh core at time $t=0$. Then the macroscopic group constants can be generated, and the multigroup fluxes can be calculated (although a control adjustment will be required to achieve core criticality).

Next the depletion equations are solved for time $0 < t < \Delta t$ by assuming that over this time step either:

Constant flux for $0 < t < \Delta t$:

$$\phi_g(\mathbf{r}, t) = \phi_g(\mathbf{r}, 0).$$

Constant power density for $0 < t < \Delta t$:

$$\Sigma_{f_g}(\mathbf{r}, t)\phi_g(\mathbf{r}, t) = \sum_j N_j(\mathbf{r}, t)\sigma^j_{f_g}\phi(\mathbf{r}, t) = \Sigma_{f_g}(\mathbf{r}, 0)\phi(\mathbf{r}, 0). \qquad (15\text{-}64)$$

(One usually applies the constant flux approximation over the depletion step, since the assumption of constant power density is difficult to apply for more than one fissile isotope.) Under these assumptions, the isotopic depletion equations (written here in matrix notation for convenience)

$$\frac{d\underline{N}}{dt} = \underline{\underline{A}}\,\underline{N}(t) + \underline{F}(t) \qquad (15\text{-}65)$$

can be solved (in the constant flux approximation for purposes of illustration) as

$$\underline{N}(t + \Delta t) = (\exp \underline{\underline{A}}\Delta t)\,\underline{N}(t) + \underline{\underline{A}}^{-1}(\exp \underline{\underline{A}}\Delta t - 1)\,\underline{F}(t). \qquad (15\text{-}66)$$

Of course one must choose the depletion-time step size $\Delta t$ such that the variation of the flux over this time step is negligible. The solution of the depletion equations for a given time step can also be obtained by representing the system as a linear combination of linear decay chains and then using the analytic solutions for a given linear chain.[15]

Having determined the number densities $N_i$ at the later time $t = \Delta t$, one can now generate new multigroup constants (either by using parameterized cross sections or repeating spectrum calculations), and then use these to calculate a new multigroup flux distribution. Once again, control adjustment will be required to achieve core criticality, as will flux normalization to maintain the required core thermal power output.

This scheme can then be continued for another time step, $\Delta t < t < 2\Delta t$ (which may have a variable size), and so on until the excess reactivity of the core drops sufficiently low that core life is terminated.

A variety of depletion codes have been used in the analysis of core burnup. These range from zero-dimensional codes such as LEOPARD[16] used for survey calculations (such as those to determine the approximate fuel enrichment required to yield a desired burnup) to two- and three-dimensional codes such as PDQ–HARMONY[17] or CITATION,[18] which are used in final design calculations to give detailed nuclei densities and power distributions useful for the study of control management.
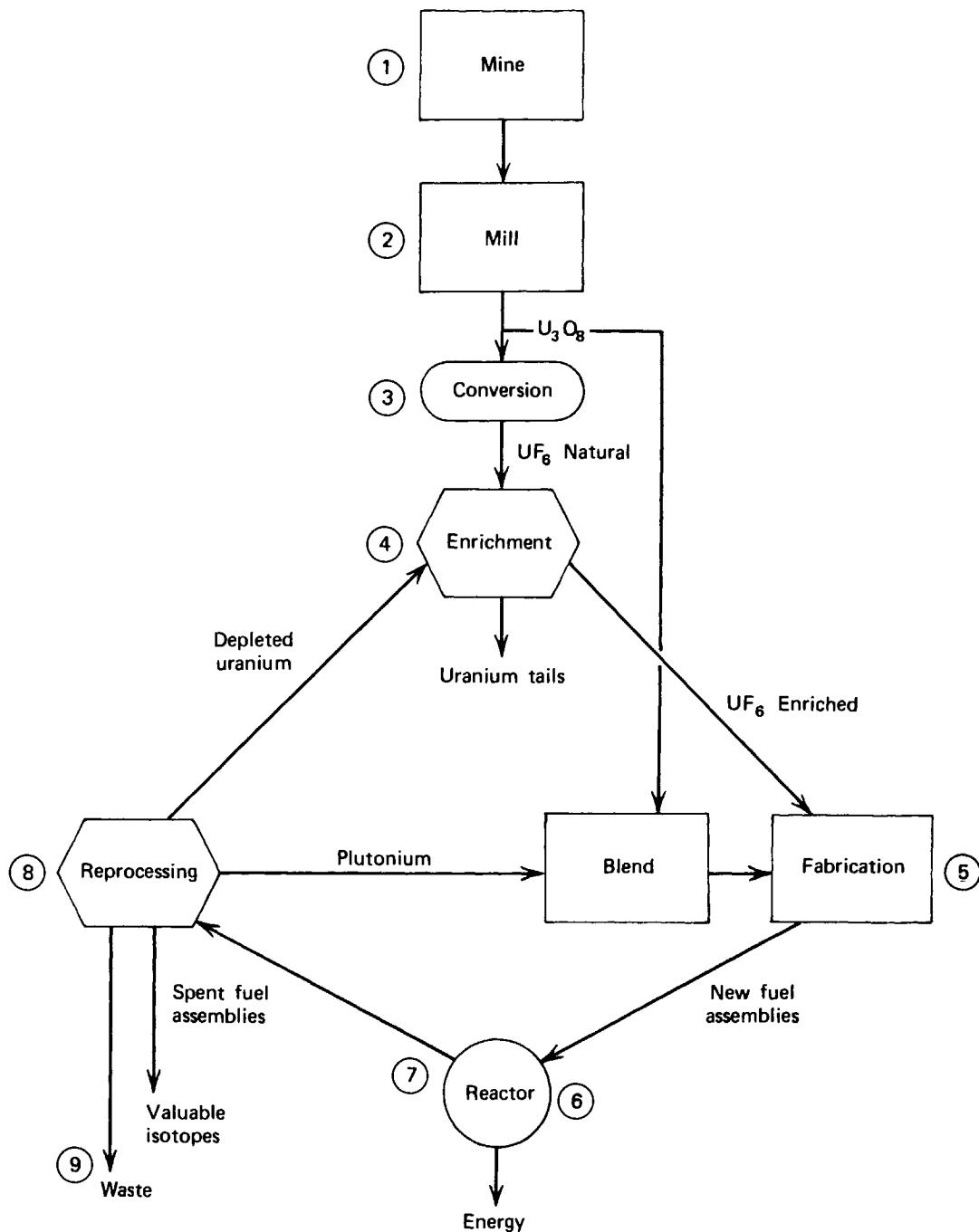
## III. NUCLEAR FUEL MANAGEMENT

We have stressed that the primary source of the economic advantages enjoyed by nuclear power over conventional power sources lies in the substantially lower fuel costs of nuclear power stations. An extremely important facet of nuclear engineering involves determining the parameters of both the initial reactor core as well as subsequent reload cores to minimize fuel costs. This topic is known as *in-core fuel management*, and it is perhaps the primary motivation behind depletion studies of fuel burnup. It is important to at least indicate the various considerations that arise in this particular aspect of reactor core design. However such a discussion is most appropriately imbedded within a brief overview of the nuclear fuel cycle in order to more properly understand the significance of each of the design variables that must be optimized by the nuclear engineer. [19-21]

### A. An Overview of the Nuclear Fuel Cycle

The various steps in obtaining, processing, using, and disposing of nuclear fuel are shown schematically in Figure 15-10 for a uranium fuel cycle[21] (thorium fuel cycles are very similar since they also must use a fissile-fuel feed involving $^{235}U$ or $^{233}U$):

(1) *Mining*: Both underground and open-pit techniques are used to mine uranium ore in a manner similar to that used in other low-grade ore mining. The ore obtained from mines in the United States averages only about 0.25% uranium oxide ($U_3O_8$).

(2) *Concentration*: Milling is necessary to extract uranium oxide from the raw ore. The ore is pulverized and leached with sulfuric acid to dissolve the $U_3O_8$. One then uses solvent extraction or ion exchange to recover the dissolved $U_3O_8$. Calcination (roasting) is then performed to produce *yellow cake*, a crude oxide containing some 70–90% $U_3O_8$. Yellow cake is the form of uranium most commonly traded in commodity markets. Further calcination and solvent extraction is used to refine the yellow cake to essentially pure $UO_3$.

(3) *Conversion*: Hydrogenation is first used to convert $UO_3$ to $UO_2$. Then reacting $UO_2$ with hydrogen fluoride produces $UF_4$, which can then be converted into a gas, uranium hexafluoride, $UF_6$, by adding fluorine salt. Such a gaseous form is most suitable for isotope separation and enrichment. Uranium hexafluoride is chosen because it is a gas at a lower temperature than any other uranium compound.

(4) *Enrichment*: Essentially all power reactors (with the exception of certain heavy-water reactors or the early gas-cooled, graphite-moderated reactors) utilize enriched uranium, that is, uranium with higher than the natural 0.7% concentration of $^{235}U$ (at least in their initial core loading). The enrichment of uranium is a very difficult and expensive process since it involves separating two isotopes, $^{235}U$ and $^{238}U$, with very little mass difference and essentially no chemical difference. A variety of separation techniques have been used or proposed:

    (a) Electromagnetic separation: Huge mass spectrometers were used for isotope separation during the Manhattan project, but this scheme was rapidly replaced by gaseous diffusion techniques.

    (b) Gaseous diffusion: Since the diffusion coefficient for a gas to

FIGURE 15-10.    Fuel cycle flow diagram.[21]

pass through a porous membrane is inversely proportional to the square-root of its mass, one can pass the $UF_6$ gas through thousands of porous barriers to separate the $UF_6$ ($^{235}U$) from the $UF_6$ ($^{238}U$).

(c)   Ultracentrifuges: This simply involves use of very high-speed centrifuges[26] or nozzle devices to separate the two isotopic forms of $UF_6$.

(d)   Laser excitation[27]: Of more recent consideration are schemes that use high-powered lasers to selectively excite $^{235}U$ in uranium vapor or $UF_6$ by tuning the laser wavelength to select the isotopic mass shift in the electronic or vibrational energy levels of the mixtures, thereby selectively exciting (i.e., "tagging") one isotopic

species in preference to another. A number of techniques then can be used to segregate the excited species including photoionization followed by electrical separation or chemical separation.

The gaseous diffusion method has been the primary technique used for uranium enrichment for the past 30 years. Recently, however, developments in ultracentrifuge design have indicated that these latter methods may, in fact, be superior to gaseous diffusion techniques. Most recently, advances in the development of high-powered tunable lasers has given rise to a large scale research effort in laser separation techniques.

(5) *Fabrication*: Following enrichment, the $UF_6$ is chemically converted into the form to be used in the fuel element. This is usually a ceramic such as $UO_2$ or UC. The resulting ceramic powder is then compacted (and sintered) into small pellets, which are then loaded into metallic tubes (the clad) or into the fuel-moderator matrix (as in the HTGR).

(6) *Fuel burnup in the reactor core*: The fuel assemblies are loaded into the reactor core for power production. These assemblies are typically irradiated in the core for a period of several years. The fuel burnup or lifetime can be limited by either reactivity considerations (i.e., the multiplication of the core drops too low for further power production) or by limitations on material stability under high radiation fluences. The latter limitation usually determines the lifetime of fuel in today's high-burnup designed cores.

(7) *Spent fuel storage and decay*: After being irradiated in the core, the fuel is intensely radioactive due to fission product buildup. The used or spent fuel is removed from the core and stored in water pools for several months to allow the short-lived fission products to decay out.

(8) *Reprocessing*: The spent fuel is then shipped to reprocessing facilities to reclaim unused uranium (which can then be recycled back as $UF_6$ for conversion or reenrichment) and plutonium.

(9) *Waste disposal*: The radioactive waste products remaining after reprocessing are then converted into either liquid or solid forms for storage and are shipped to various depositories for burial (and surveillance).

The above outline is a description of only the uranium–plutonium fuel cycle used in most modern power reactors. However other possible fuel cycles have been considered for future reactors, such as the thorium-$^{233}$U cycle proposed for HTGR operation. These latter fuel cycles are quite similar to the uranium fuel cycle we have considered above, since they usually employ $^{235}$U as fissile feed in addition to recycled $^{233}$U.

The management of the various activities involved in obtaining, irradiating, and disposing of fuel materials is referred to as *nuclear fuel management* and is a principal concern of nuclear engineering. Such activities must be performed subject to a number of important constraints. Of course, one desires to minimize electrical generation costs, but must also ensure that the safety of the reactor is not compromised—for example, the fuel temperature must always be kept below melting and the control margin must be maintained within safe limits.

The management of the processes involved in the nuclear fuel cycle can be classified into three types of activity: (a) head-end fuel management (mining, conversion, enrichment, and fuel fabrication), (b) in-core fuel management (evaluation of reactivity and control requirements, power distribution analysis, and core capability evaluation), and (c) tail-end fuel management (fuel storage, ship-

ping, reprocessing, and waste disposal). We will consider only in-core fuel management, since it most directly involves nuclear reactor analysis. However it is first useful to consider in greater detail the various fuel cycles of interest in power reactor operation.

## B. Power Reactor Fuel Cycles

### 1. LWR FUEL CYCLES

Fuel requirements for a typical LWR of the 1000 MWe class are shown in Figure 15-11 along with a LWR fuel cycle diagram in Figure 15-12.[21] We recall that such reactors are fueled with enriched uranium (from 2-3 w/o-weight percent). The spent fuel is discharged from the core with a $^{235}U$ concentration of roughly .8%. The conversion of $^{238}U$ results in a plutonium concentration of about the same magnitude. This plutonium is recovered by fuel reprocessing.

The recovered plutonium can then be recycled back into the LWR fuel cycle, as shown in Figure 15-13. This reduces the requirements for uranium feed by approximately 33%. There are several technical problems involved in plutonium recycling,[22] including the complications of fabricating plutonium (a very toxic and radioactive material) and matching the nuclear performance of a mixed oxide fuel ($PuO_2$ and $UO_2$) with enriched uranium fuel in a core. Such problems do not seem formidable, however, and the large inventory of plutonium that is beginning to accumulate from the existing generation of large power reactors (coupled with the lagging commercial development of the fast breeder reactor, which would provide an alternative market for this plutonium) provide strong incentives for implementing plutonium recycle in thermal power reactors.

### 2. HTGR FUEL CYCLES

The fuel cycle of the HTGR is quite different from that of light water reactors since it is based on a $^{232}Th$–$^{233}U$ conversion cycle.[23] As Figure 15-14 indicates, the initial loading of the HTGR core contains highly enriched uranium ($\sim$93% $^{235}U$) in the form of uranium carbide along with thorium oxide or carbide as the fertile material. The thorium is then converted to $^{233}U$, which is recovered and recycled back (eventually) to be mixed into reload fuel. The motivation behind using such a fuel cycle is primarily due to nuclear considerations. The number of neutrons per thermal neutron absorbed in $^{233}U$, $\eta^{23}$, is some 10% larger than that characterizing $^{235}U$. Hence it is possible to achieve much higher conversion ratios using $^{233}U$ (indeed, such "advanced converter" reactors are capable of operating with a conversion ratio as high as 0.8 compared with 0.6 for an LWR). The higher core temperature of the HTGR favors the use of $^{233}U$ over $^{239}Pu$ as a reload fuel, since $\eta^{49}$ tends to decrease with increasing core temperature.

As we have seen, the fuel design of the HTGR is much different from that of either the LWR or the LMFBR, in order to facilitate high temperature operation. The fuel composition is of small pellets of UC or $ThO_2$ coated with graphite and loaded into graphite blocks. Such a fuel design leads to much higher fabrication costs, however, and hence the fuel elements of an HTGR must be run to much higher burnups (some 80,000 MWD/MTU as compared to 30,000 MWD/MTU for a LWR or 100,000 MWD/MTU for the LMFBR).

The higher conversion ratio of the HTGR leads to a more efficient utilization of
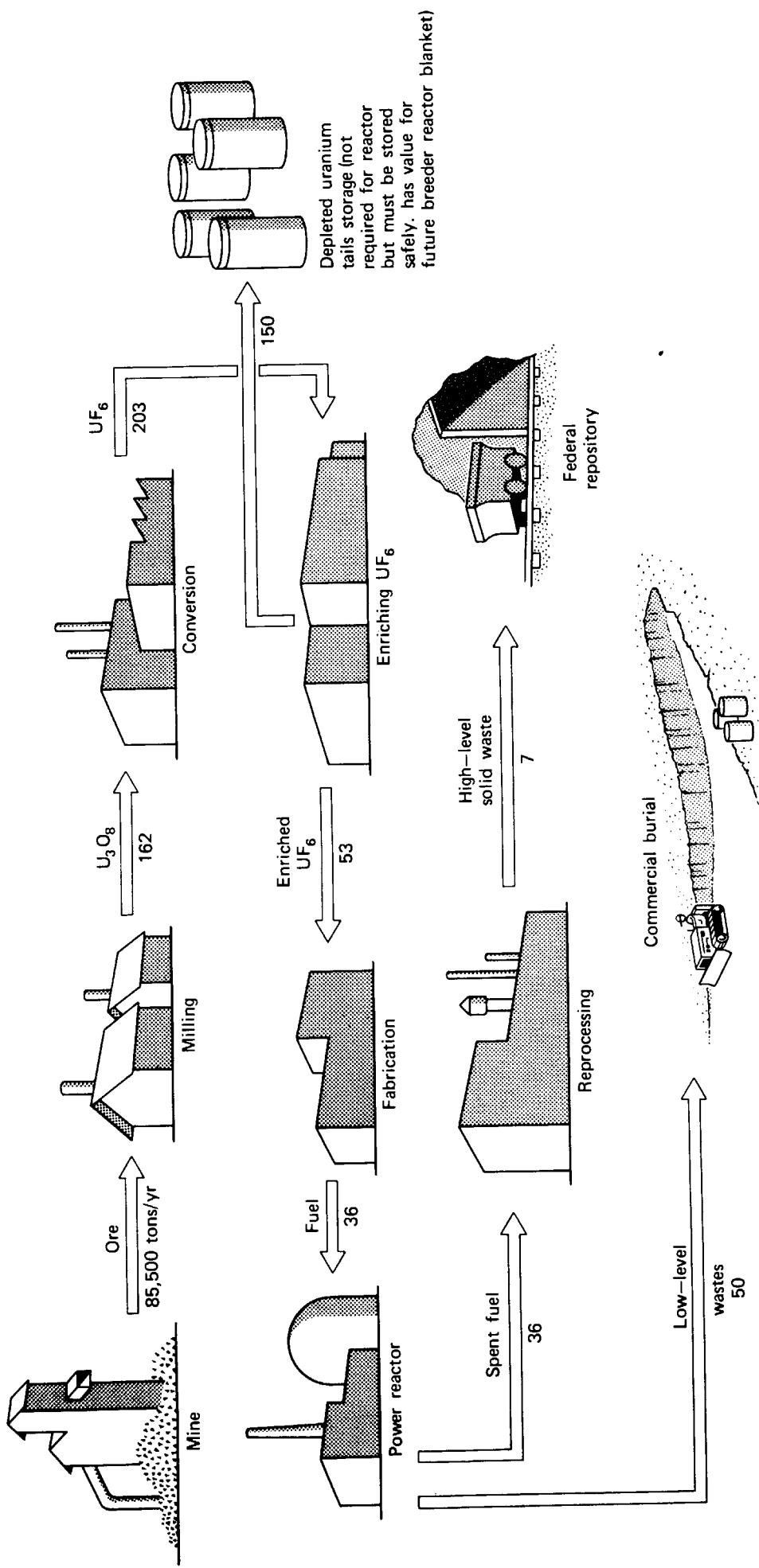
**FIGURE 15-11.** Uranium requirements for a 1000 MWe PWR. [*The Nuclear Industry*, USAEC Report WASH-1174-73 (1973)].

593
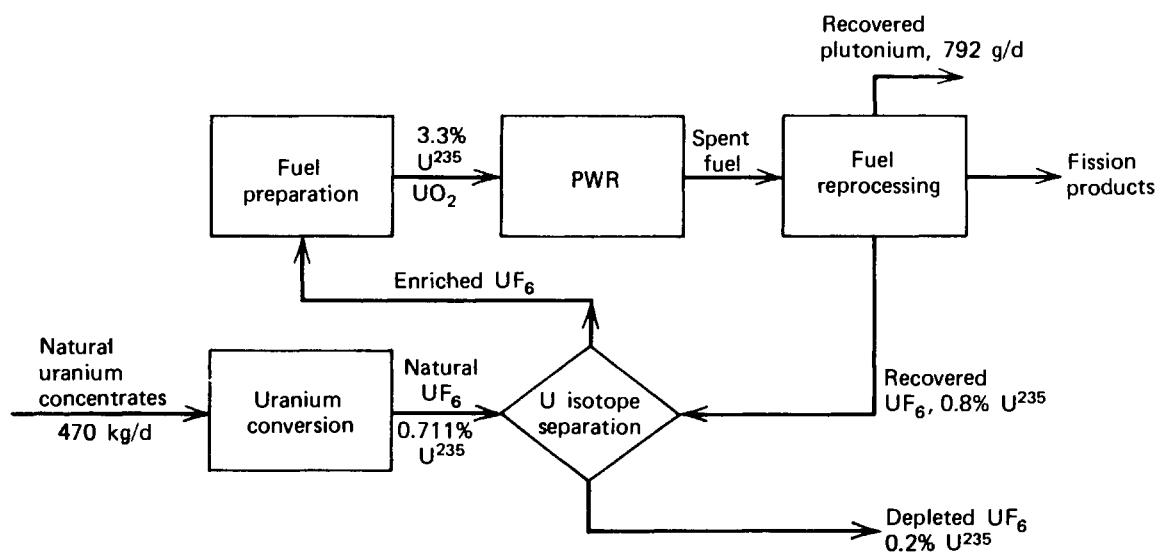
**FIGURE 15-12.** LWR fuel cycle (no Pu recycle).[21]
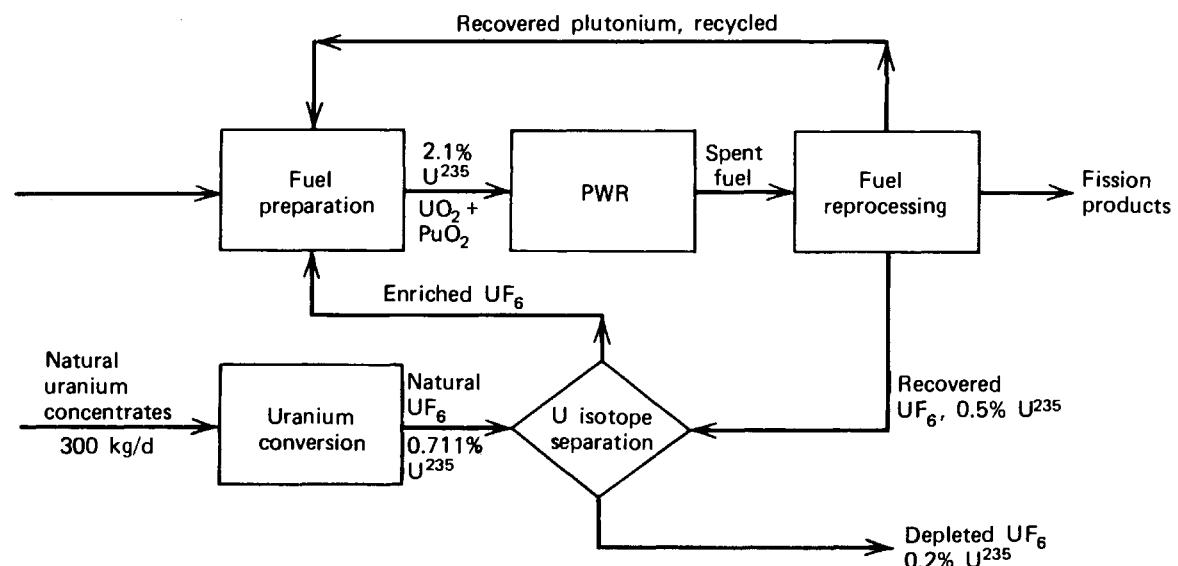


**FIGURE 15-13.** LWR fuel cycle (Pu recycle).[21]
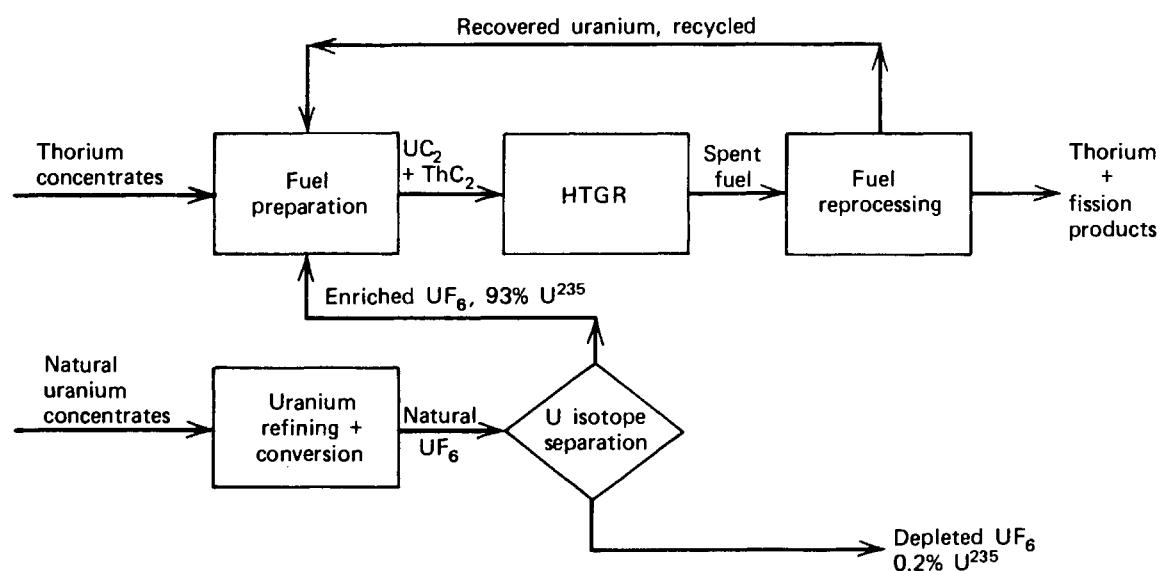


**FIGURE 15-14.** HTGR fuel cycle.[21]

uranium. In fact, an HTGR requires only about half the fuel feed $U_3O_8$ of an LWR of similar rating.[21]

## 3. LMFBR FUEL CYCLES

The fuel cycle of the fast breeder reactor differs from that of the LWR and HTGR in that the larger conversion ratio allows a net gain in the amount of fissile material produced during core operation. It is estimated that the LMFBR can utilize some 60–70% of the energy available in natural uranium (taking account of the transmutation of $^{238}U$ to $^{239}Pu$). The more efficient utilization of available fuel resources is the primary justification for the LMFBR, although there are side benefits such as higher coolant temperatures (and hence lower waste heat release) than for the LWR.

A typical fuel cycle for the LMFBR is shown in Figure 15-15, in which it is recognized that most of the transmutation of $^{238}U$ into $^{239}Pu$ will occur in the blanket, while the fuel burnup and power production will occur in the core. The LMFBR can use as fertile material either natural uranium or depleted uranium from the tails stream of the isotope-separation plants.
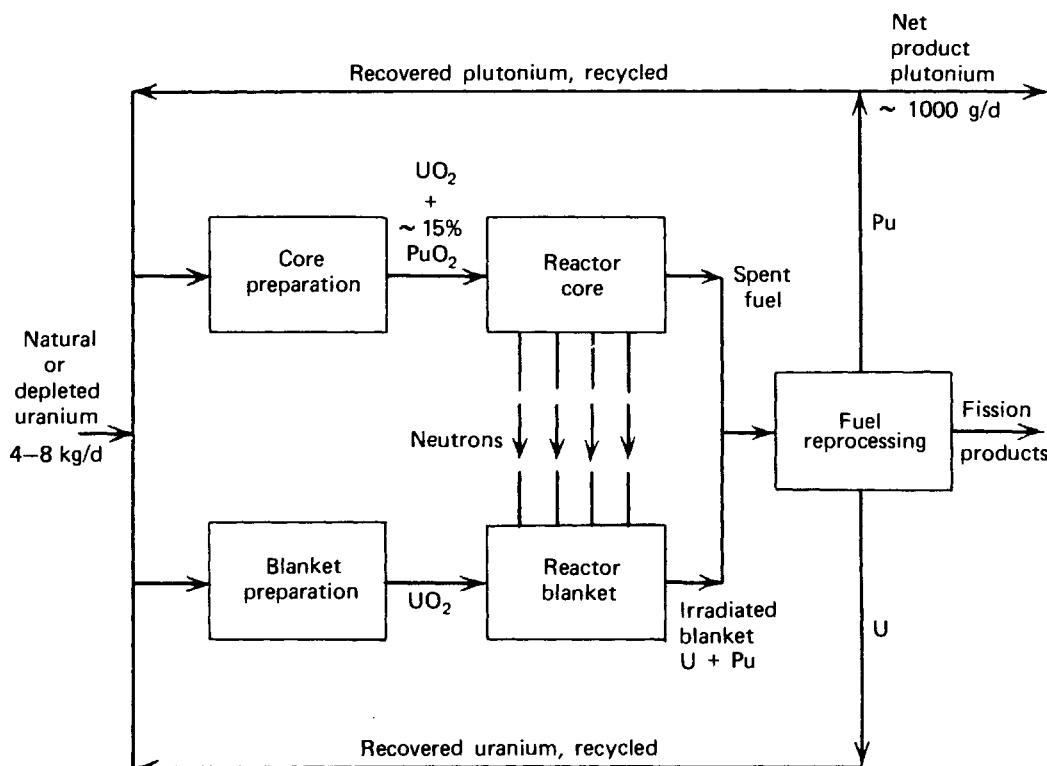


FIGURE 15-15.   LMFBR fuel cycle.[21]

## 4. INTERACTION AMONG FUEL CYCLES

It should be recognized that there will be a very substantial interaction among these various fuel cycles in a mature nuclear power industry. For example, the substantial amounts of plutonium produced by LWRs can be either directly recycled or used to fuel the first generation of fast breeder reactors. Similarly the excess plutonium produced by the LMFBR can be used to fuel either future LMFBRs or fed back into the LWR fuel stream.

There will also be strong interaction with the fuel cycle of advanced converter reactors such as the HTGR, which can be used to greatly stretch out the usefulness of available fuel, without, however, having to carry the high fissile fuel inventory of true fast breeders (since the relatively dilute fuel of the HTGRs can be run at around twice the fissile rating typical of fast breeder reactors).[24]

These interactions will determine to a very large degree the cost of the nuclear fuel cycle, since they not only influence the cost of the fresh fuel loading, but also determine the value of the spent fuel (i.e., the value of the plutonium produced in the core). Such interactions are quite complicated and no doubt will lead to even greater uncertainty in the future fuel costs of nuclear power reactors. It is apparent from this discussion, however, that the real incentive for developing new types of reactors such as the LMFBR is based almost entirely on expected improvements in the economics of their fuel cycles, rather than changes in their capital costs or operating costs.

TABLE 15-2 Enrichment Requirement of Various Reactor Types
(Thousands of kg SWU (or MT SWU) and short tons of $U_3O_8$ for 1000 MWe Power Plants at 0.25% Tails Concentration)

|  | BWR | PWR | HTGR | LMFBR |
|---|---|---|---|---|
| First core requirement |  |  |  |  |
| U-235 Enrichment, % | 2.0 | 2.6 | 93 |  |
| MT SWU | 229 | 233 | 347 | 240[†] |
| ST $U_3O_8$ | 580 | 500 | 420 | (70) |
| Annual reload requirements at 80% plant capacity factor |  |  |  |  |
| U-235 Enrichment, % | 2.7 | 3.2 | 93 |  |
| Early years—no recycle |  |  |  |  |
| MT SWU | 101 | 109 | 133 | 120[†] |
| ST $U_3O_8$ | 170 | 180 | 160 | (35) |
| Later years—full recycle |  |  |  |  |
| MT SWU | 62 | 73 | 82 | 0 |
| ST $U_3O_8$ | 110 | 110 | 100 | (1-2) |

[†]SWU equivalent of fissile Pu required: 1 kg Pu fissile ≈ 100 kg SWU

## C. In-Core Fuel Management

### 1. INTRODUCTION

#### (a) GENERAL FUEL MANAGEMENT CONSIDERATIONS[20]

Perhaps the most important responsibility of the nuclear engineer concerned with the nuclear fuel cycle is the management of the fuel in the core—including the selection of refueling schedules, fuel loading patterns, and the prediction (and measurement) of fuel burnup and isotope buildup, in an effort to satisfy both nuclear and economic constraints. In this section we will consider only a few of the many facets of in-core fuel management.

It is during fuel irradiation that many of the debit aspects of fuel economics occur (e.g., in the depletion of fissile material such as $^{235}U$). However the in-core portion of the fuel cycle is also where all of the credit aspects such as plutonium production occur.

The nuclear engineer would like to achieve minimum fuel costs consistent with nuclear and thermal constraints on the core performance. To this end, he must determine the optimum distribution of fuel enrichment for both the initial and reload cores. The refueling period and reload strategy must be specified, along with the control management of both movable rods and shim (soluble and burnable poisons). Hence the nuclear engineer has considerable flexibility (and considerable responsibility) in managing the incore utilization of the fuel.

### (b) CONSTRAINTS

The task of determining the optimum arrangement of fuel assemblies and loading is extremely complex, involving the core geometry and composition, neutronic–thermal-hydraulic coupling, reactivity control, and operational requirements. In a typical core design, the core size, fuel assembly design, control devices, and coolant conditions will be fixed before the detailed in-core fuel management scheme is determined. The variables at the nuclear engineer's disposal are then the enrichment of fresh fuel assemblies, the frequency of fuel reloading, the reloading pattern, and the associated control management program. A number of constraints on in-core fuel management must be considered.

We noted earlier that the two principal thermal limitations on core performance involved the requirements that the fuel centerline temperatures remain below melting point, and that the surface heat flux not exceed its DNB limit. Such requirements place limits on the local power density (in the case of the fuel centerline temperatures) and also on the integral of the power density or coolant enthalpy up each coolant channel (in the case of the critical heat flux limit). Such limitations must be kept in mind when determining a fuel arrangement, since the core must be capable of operating at its rated power level throughout the reactor cycle without exceeding these thermal limitations. Since the core power distribution will change over core life as fuel depletion occurs, one must be able to predict the local power density throughout the cycle. This is an extremely expensive and time-consuming aspect of fuel management.

The reactor control system must always be capable of controlling the excess reactivity loaded into the core to compensate for fuel depletion. Although this excess reactivity is usually larger in the initial core loading (since all of the fuel is fresh), one can use burnable poisons and/or chemical shim to adequately control it. In later reload cores, there are fewer alternatives available, since, for example, burnable poisons cannot be easily inserted into irradiated fuel assemblies. Such considerations impose serious upper limits on the allowable fuel burnup of a core.

The reactor should always be capable of responding to load-demand changes. Since the control rod worth is dependent on the flux profile, and since this flux profile will change over core life, one must ensure that adequate reactivity response is available for such power maneuvering.

Fuel burnup is also limited to a considerable degree by the amount of radiation damage the fuel can withstand without experiencing appreciable probability of failure. For example, fuel irradiation can induce swelling of the fuel, which places a strain on the cladding. Furthermore, the buildup of gaseous fission products within the element can cause a stress on the clad, which leads to a plastic deformation of the fuel rod at high temperature (high-temperature creep). The enormous thermal gradients across the fuel pin and cladding, combined with the variations in temperature which occur during reactor startup and shutdown (thermal cycling) can also lead to clad fracture in the intense radiation environment of the core. Such

fuel failure limitations on fuel burnup are particularly significant when very high burnups are required, such as in the LMFBR.

There are frequently external requirements placed on the scheduling of core refueling. For example, one wishes to avoid a reactor shutdown for refueling during periods of peak power demand (e.g., in the middle of the summer or winter months). In general, more frequent refueling leads to lower fuel inventory requirements (less excess reactivity is required for shorter core lifetimes), but at the expense of more reactor down time and enhanced thermal cycling.

## 2. REFUELING SCHEDULES

Rarely does one replace the entire core of a reactor in a refueling operation; only a fraction of the core is replaced with fresh fuel at any one time. The time period between such refuelings will be referred to as a *reactor cycle*, and in any partial refueling scheme, the complete fuel cycle consists of a number of such reactor cycles.

In general, the fuel inventory required for a given energy production decreases as the frequency of partial refueling increases. However, there is a tradeoff here, since more frequent core refueling can lead to increased shutdown time and hence increased costs due to power outage. For some time now, most reactors have been refueled on a yearly basis (although it should be noted that the pressure-tube design of the CANDU or SGHWR type reactors allows continuous or very rapid refueling). However recently alternative refueling cycles have been proposed.

For example, the development of rapid refueling systems for PWRs make possible refueling times of three to four days (compared to present down times of several weeks).[28] Such rapid refueling allows semiannual refueling at six-month intervals, with considerable savings in fuel inventory (estimated at some 10% of the annual fuel cycle costs). The tendency for BWRs has been to move in the direction toward longer reactor cycles, with refueling now proposed on an 18-month basis. This refueling frequency appears economically attractive to the BWR because of the ease with which its fuel lifetime can be stretched by adjusting coolant void fractions.[29]

Annual refueling schedules of LWRs tend to replace 1/4 to 1/3 of the core during each refueling operation. However, shifting to a semiannual schedule will allow the replacement of only 1/6 of the core at a time. The higher conversion ratio of the HTGR allows a refueling scheme in which only 1/6 of the core is replaced each year. This longer fuel residence time is facilitated by the coated particle fuel design for the HTGR which is capable of much higher burnups.

## 3. REFUELING PATTERNS

We now turn our attention to a consideration of how the fresh fuel is distributed in the reactor core during refueling, and just which spent fuel elements are withdrawn (assuming that partial refueling schemes will be used). Suppose we attempted to load the core with a uniform enrichment. Then, the flux peaking at the center of the core would lead to higher burnup of these fuel elements with a considerable flattening of the core power distribution toward the end of core life (see Figure 15-16). Unfortunately, such a uniform arrangement leads to a larger power-peaking factor $F_q^N$ early in core life. It also results in a very low burnup of fuel elements inserted toward the edge of the core.
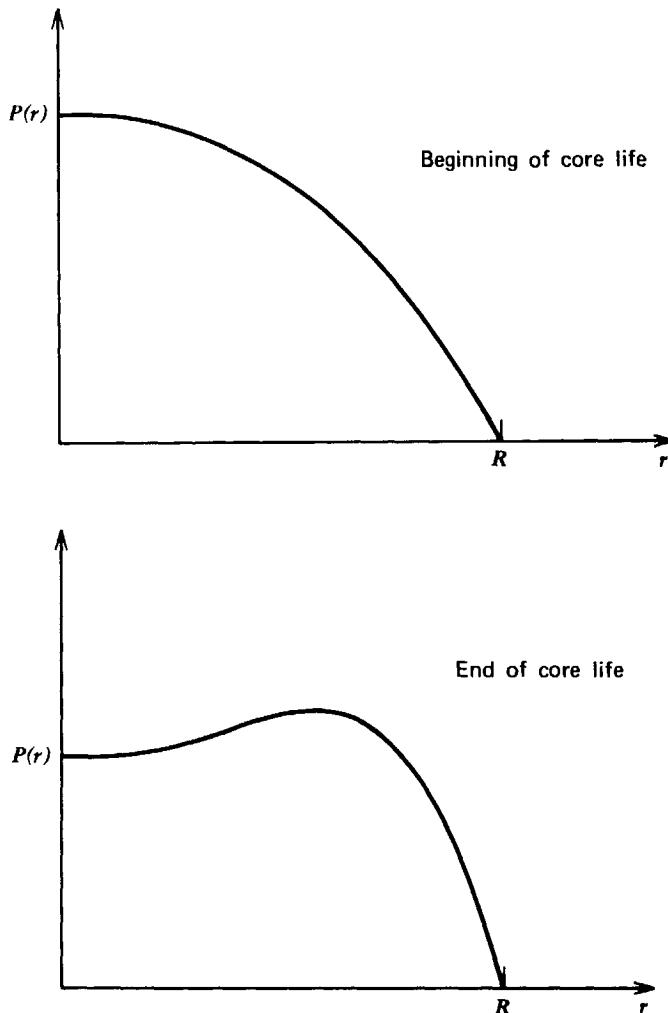
FIGURE 15-16. Shift in power distribution due to nonuniform burnup for batch refueling.

Hence a nonuniform core loading is clearly desirable—in both the initial core and subsequent replacement cores. There are two common refueling schemes.[13,20]

(a) ZONAL LOADING (IN-OUT CYCLING):

In this scheme, one loads unirradiated fuel in a zone on the periphery of the core. The irradiated fuel is shuffled in toward the inner zone, while the fuel in the central zone is withdrawn from the core. The motivation in this scheme is to make use of the inherent reduction in reactivity which accompanies fuel depletion as a power-flattening mechanism. By way of example, a three-cycle zonal pattern is shown in Figure 15-17. Such a pattern can even be implemented on the initial core loading by using fuel assemblies with varying enrichments.

Zonal loading does have disadvantages, however. In large cores subjected to high burnups, appreciable distortions in the flux distribution can arise which could lead to large power-peaking factors.

(b) SCATTER (ROUNDELAY) LOADING:

An alternative scheme loads fuel in a scatter or random pattern to achieve a more uniform fuel distribution. One still will find some power-flattening since the average burnup in the central zones of the core is more pronounced than near the

Zonal loading        Combination scatter—zonal loading
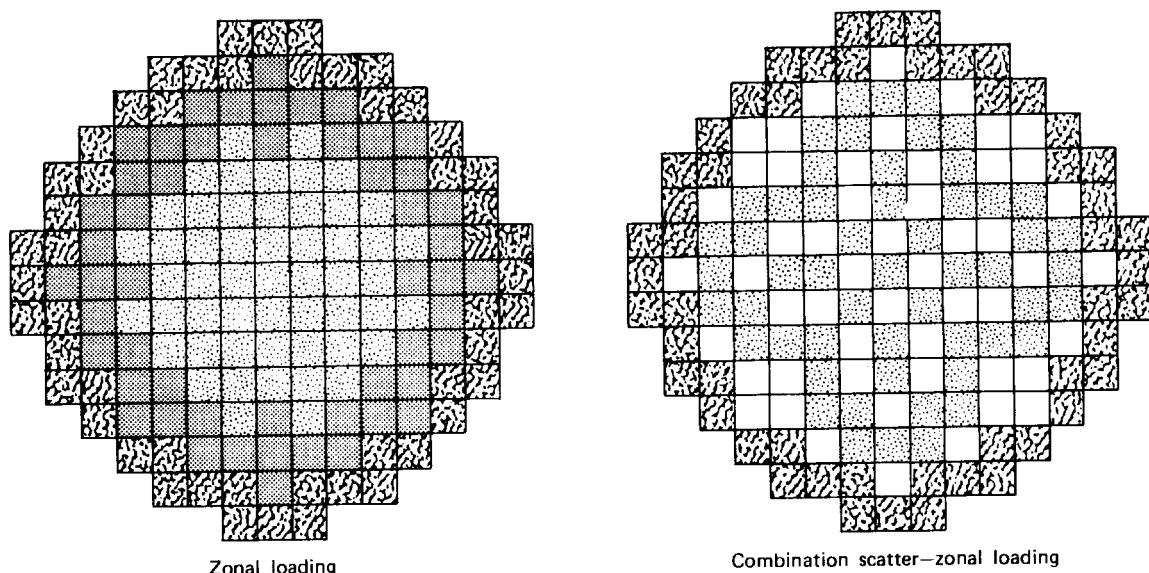
FIGURE 15-17. Alternative core loading schemes.

core periphery. The power distribution characterizing a scatter-loaded core has a somewhat flattened form of the distribution characterizing a uniformly loaded core. There is a fine-scale ripple in the local power density, however.

Scatter-loading has the additional advantage that no reshuffling of irradiated fuel is required.

In practice, most refueling schemes involve some combination of zonal and scatter loading techniques. For example, many PWRs are loaded in such a fashion that fresh fuel is loaded into the outer zone, while the fuel irradiated in the outer zone is scatter loaded into the center zones.

The detailed analysis and optimization of in-core fuel arrangement is a very complicated process. One must take into account core geometry, control management schemes, the coupling between core neutronics and thermal–hydraulic performance, and the constraints placed on core performance by operational requirements. Although this aspect of fuel management is still frequently performed by trial and error, using liberal dashes of physical intuition, there is now more of a tendency to attempt to implement more direct optimization methods[12] (e.g., linear programming) for in-core fuel management.

However, a very big headache with any elaborate fuel management scheme is the flexibility frequently required of a refueling program. For example, an unexpected alternation of a refueling pattern may be required to remove a fuel assembly leaking fission products which is discovered during a normal core reloading operation. Hence a capability is required to allow the rapid evaluation of a new loading pattern to ensure that various thermal-hydraulic, mechanical, and nuclear limitations are not exceeded during the subsequent core operation.

## REFERENCES

1. H. M. Summer, The neutron cross section of $^{135}$Xe, AEEW-R116 (1962).
2. R. Fleming, Xenon transients and their measurement, University of Michigan Nuclear Engineering Department Report (unpublished)(1973).

3. M. E. Meek and B. F. Rider, Compilation of fission product yields, NEDO-2154 (1972).

4. J. R. Lamarsh, *Introduction to Nuclear Reactor Theory*, Addison-Wesley, Reading, Mass. (1966).

5. H. W. Graves, Jr., Nuclear Reactor Control Management, University of Michigan Nuclear Engineering Department Lecture Notes (unpublished) (1969).

6. P. F. Zweifel, *Reactor Physics*, McGraw-Hill, New York (1973).

7. W. M. Stacey, *Reactor Tech.* **13**, 252 (1970).

8. G. I. Bell and S. Glasstone, *Nuclear Reactor Theory*, Van Nostrand, Princeton, N. J. (1970), pp. 555–562.

9. J. Canosa and H. Brooks, *Nucl. Sci. Eng.* **26**, 237 (1966).

10. D. Randall and D. St. John, *Nucleonics* **16**, 82 (1958); *Nucl. Sci. Eng.* **14**, 204 (1962).

11. J. R. Lamarsh, *Introduction to Nuclear Reactor Theory*, Addison-Wesley, Reading, Mass. (1966) pp. 481–484.

12. R. L. Crowther, Methods of fuel management analysis—an overview, *in* Mathematical Methods and Models in Reactor Calculations, CONF-730414-P1 (1973) p. II-1.

13. A. Sesonske, *Nuclear Power Plant Design Analysis*, USAEC TID-26241 (1973).

14. D. L. Delp, et al., FLARE, GEAP-4598 (1964); R. Goldstein, et al., *Trans. Am. Nucl. Soc.* **10**, 300 (1967).

15. T. R. England, CINDER, a one-point depletion and fission product program, WAPD-TM-334 (1962).

16. R. F. Barry, LEOPARD, a spectrum dependent non-spatial depletion code for the IBM-7094, WCAP-3741 (1963).

17. R. J. Breen, O. J. Marlowe, and C. J. Pfeifer, HARMONY: system for nuclear reactor depletion computation, WAPD-TM-478 (1965).

18. T. B. Fowler and D. R. Vondy, nuclear reactor core analysis code: CITATION, ORNL-TM-2496, Rev. 2 (1971).

19. D. M. Elliot and L. E. Weaver (Ed.), *Education and Research in the Nuclear Fuel Cycle*, Oklahoma U. P., Norman (1970).

20. H. W. Graves, Nuclear Fuel Management, University of Michigan Nuclear Engineering Department Lecture Notes (unpublished) (1969).

21. E. A. Mason, Overall view of the nuclear fuel cycle, in *Education and Research in the Nuclear Fuel Cycle*, D. M. Elliot and L. E. Weaver (Ed.), Oklahoma U. P., Norman (1970).

22. J. Haley, in *Education and Research in the Nuclear Fuel Cycle*, D. M. Elliot and L. E. Weaver (Ed.), Oklahoma U. P., Norman (1970); V. O. Uotinen, et al., *Nucl. Tech.* **18**, 129 (1973); R. Astley, et al., *Nucl. News* **14**, 29 (1971).

23. P. R. Kasten, in *Education and Research in the Nuclear Fuel Cycle*, D. M. Elliot and L. E. Weaver (Ed.), Oklahoma U. P., Norman (1970); USAEC Report WASH-1097 (1969).

24. P. Fortescue, A reactor strategy: FBR's and HTGR's, *Nucl. News* **15**, 36 (1972).

25. G. Gyorey, private communication (1974).

26. D. Olander, Technical basis of the gas centrifuge, *Advances in Nuclear Science and Technology*, Vol. **6**, (1972).

27. B. Snavely, Separation of uranium isotopes by laser photochemistry, USAEC Report UCRL-75725 (1974).

28. N. H. Andrews, C. A. Olmstead, H. G. Houser, *Nucl. News* **16**, 71 (1973).

29. E. D. Fuller, A. L. Phillips, and F. E. Wicks, *Nucl. News* **16**, 71 (1973).

# PROBLEMS

15-1  A thermal power reactor is shut down after an extended period of high-power operation. What happens to: (a) the power output of the reactor (you may ignore

the short-term transients if you wish), (b) the average reactor temperature, and (c) the ability of the reactor to be restarted.

15-2 Solve the isotopic rate equations to determine the buildup in xenon concentration following startup of a clean core to a steady-state flux level $\phi_0$.

15-3 Determine the ratio of atomic number densities of equilibrium $^{135}$Xe and $^{235}$U as a function of the steady-state thermal flux level of a reactor.

15-4 Consider a subcritical assembly in which a neutron flux of $\phi_0 = 10^6$ cm$^{-2}$ – sec$^{-1}$ is maintained by a source. How long must this source be left on before the xenon and samarium concentrations reach 90% of their saturation value, respectively?

15-5 Demonstrate that there will be no buildup of xenon following shutdown unless the flux prior to shutdown

$$\phi_0 > \frac{\gamma_X}{\gamma_I} \frac{\lambda_X}{\sigma_a^X} = 3.7 \times 10^{11} \text{ cm}^{-2} \text{ sec}^{-1}.$$
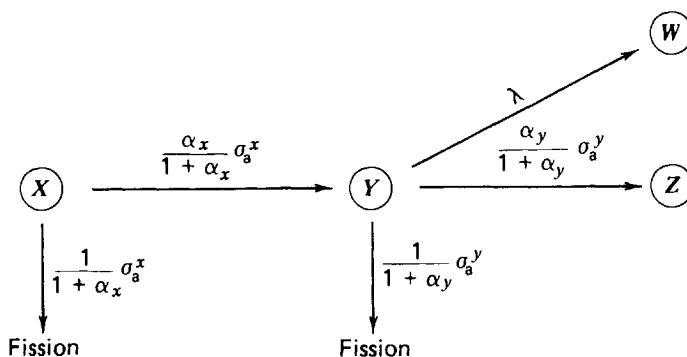
Explain this result physically.

15-6 Determine the time following shutdown at which the maximum xenon concentration occurs.

15-7 Consider a large power reactor operating at a thermal flux level of $\phi_0 = 10^{14}$ cm$^{-2}$ sec$^{-1}$ with a power defect of $\Delta\rho_{PD} = 0.04$ and an excess reactivity (in the cold, clean state) of $\rho_{ex} = 0.15$. Determine the length of time following a scram one has available to restart the reactor before xenon buildup will be sufficiently large to outweigh the excess reactivity available. How long will this deadtime period last during which the reactor cannot be restarted?

15-8 Determine the behavior of the samarium concentration in a reactor following a flux level change $\phi_0 \rightarrow \phi_1$.

15-9 Compare the effects of $^{135}$Xe and $^{149}$Sm buildup in thermal reactors fueled with $^{233}$U, $^{235}$U, and $^{239}$Pu, respectively.

15-10 Plot the trajectory of iodine and xenon buildup in the phase-plane with coordinates $I(t)$ and $X(t)$ following a clean core reactor startup and then a shutdown some time later.

15-11 A nuclear reactor is subcritical and operating at very low power level. Assume that no automatic control devices are operative. Reactivity is inserted (as by control rod withdrawal) continuously and infinitely slowly so that any short-lived transients induced come to rest. Making any further assumptions you require, discuss what happens as the reactivity increases over a wide range.

15-12 Using first-order perturbation theory, estimate the reactivity worth of equilibrium buildup in a bare cylindrical core in which a low flux level $\phi_0 \ll \lambda_X/\sigma_a^X$ is maintained.

15-13 Consider a slightly enriched uranium-fueled reactor operating at a constant flux level $\phi_0$. Determine the concentrations of $^{235}$U, $^{239}$Pu, and $^{241}$Pu as functions of time. (State carefully your assumptions concerning the particular nuclide chains you choose to consider.)

15-14 Determine the maximum possible burnup (MWD/MTU) achievable in a reactor with a given enrichment and conversion ratio (assume that CR < 1). Then compare this theoretical limit with the actual design burnup goals for each of the major reactor types (PWR, BWR, HTGR, CANDU, SGHWR) and comment on this comparison.

15-15 A high-temperature gas-cooled reactor is initially fueled with a mixture of $^{235}$U and $^{232}$Th. As the reactor is operated, the converted isotope $^{233}$U accumulates as the $^{235}$U is consumed. Develop the isotopic concentration equations for $^{235}$U, $^{233}$Pa, and $^{233}$U. Solve these equations, assuming that the flux and the thorium concentration remain constant.
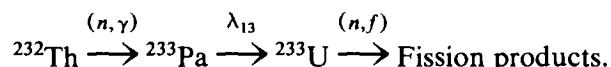
15-16 It has been proposed to fuel a batch-loaded reactor with transuranic nuclide $X$, which undergoes both fission and capture. Nonfission capture in $X$ results essentially instantaneously in nuclide $Y$, which is also fissionable. Nuclide $Y$ is also subject to radioactive decay and further capture reactions.

(a) If the reactor is just critical with an $X$ concentration of $X_0$, what is the condition that a non-zero reactivity lifetime be attainable with this loading and no initial excess reactivity?

(b) Assuming that $X$ and $Y$ are in secular equilibrium near the end of the reactivity lifetime of the fuel charge, what burnup fraction can be attained?

Neither nuclide undergoes resonance absorption. Neglect neutron absorption in nuclides $W$ and $Z$. Assume constant flux operation. The nuclear parameters of $X$, $Y$, and the fission products are to be assumed known.



15-17 Solve the differential equations for buildup of $^{240}$Pu and $^{241}$Pu in terms of $\Phi$ $= \int_0^t \phi(t')dt'$. Assume constant cross sections and zero initial concentration of all plutonium isotopes.

15-18 Give a qualitative discussion of the proposed fuel cycle for the LMFBR. In particular, discuss: (a) the interaction of the LMFBR fuel cycle with the LWR fuel cycle, (b) the relative advantages and disadvantages of different proposed fast reactor fuels (e.g., oxides versus carbides versus metal alloys), and (c) the economic advantages (if any) of the LMFBR.

15-19 The molten salt-breeder reactor (MSBR) is a fluid-fueled reactor designed to operate as a thermal breeder on pure $^{232}$Th feed. The most significant reactions that occur in the core are:

$$^{232}\text{Th} \xrightarrow{(n,\gamma)} {}^{233}\text{Pa} \xrightarrow{\lambda_{13}} {}^{233}\text{U} \xrightarrow{(n,f)} \text{Fission products.}$$

Steady-state operation at zero reactivity is maintained by continuous fission product removal at a rate proportional to the concentration.

$$\frac{\text{Rate of removal of fission}}{\text{products from core (atoms/sec)}} = CN_{\text{FP}}$$

where $N_{\text{FP}}$ is the concentration of fission products in the core in atoms/cm$^3$ and $C$ is a constant. The heavy elements are not removed. The volume of the core is $V$ and the average flux is $\phi_0$. The reactor is sufficiently well moderated to justify neglecting all fast effects. When fueled with pure $^{235}$U (but no thorium) the critical concentration is $N_{25}^*$. Determine: (a) the minimum value of constant $C$ and (b) the power

generated by the reactor for $C > C_{min}$. Assume all nuclear parameters are known and neglect xenon and samarium poisoning.

15-20 A bare cylindrical reactor, containing an initial loading of 100 kg of $^{235}U$ (no $^{238}U$) operates in batch irradiation. Because of radiation damage to the fuel elements, the maximum *local* depletion of $^{235}U$ due to neutron absorption is limited to 60%. Estimate the maximum thermal energy that can be produced from each fuel loading. What assumptions are involved? Use $\bar{\sigma}_\gamma / \bar{\sigma}_f = 0.18$.

15-21 A nuclear rocket may be required to operate for a period as short as a few minutes, but during this period it is desirable to obtain power at a constant and maximum rate. To accomplish this with an initially clean reactor core, it would be necessary to program the fission rate so that the total instantaneous power from prompt and delayed (fission product) energy sources is a constant. The time-dependence of the delayed sources can be determined from the Way–Wigner empirical correlation, which states that the rate of liberation of decay heat at a time $t$ after a single fission varies as $t^{-1.2}$. This correlation applies for all times greater than 10 sec after the fission. A fraction $f$ of the *total* recoverable energy from a single fission follows this decay law, and all other energy sources are assumed to be prompt. Assuming that the reactor power can be brought quickly (instantaneously) to the desired power $P$ at the time of startup, how should the fission rate $F(t)$ be programmed with respect to time so that $P$ remains constant?

15-22 An important isotope for power production in space is $^{238}Pu$.
  (a) Suggest a practical scheme whereby $^{238}Pu$ can be produced with the aid of a reactor.
  (b) Write down, but do not solve, the differential equations governing the concentration of $^{238}Pu$ and each of its precursors. Neglect resonance absorption effects.

# Appendix A
## Some Useful Nuclear Data

## I. MISCELLANEOUS PHYSICAL CONSTANTS

| | | |
|---|---|---|
| Avogadro's number, $N_A$ | $6.022045 \times 10^{23}$ mol$^{-1}$ | |
| Boltzmann constant, $k$ | $1.380662 \times 10^{-23}$ J K$^{-1}$ | |
| | $0.861735 \times 10^{-4}$ eV K$^{-1}$ | |
| Electron rest mass, $m_e$ | $9.109534 \times 10^{-31}$ kg | |
| | $0.5110034$ MeV | |
| Elementary charge, $e$ | $1.6021892 \times 10^{-19}$ C | |
| Gas constant, $R$ | $8.31441$ J mol$^{-1}$ K$^{-1}$ | |
| Neutron rest mass, $m_n$ | $1.6749544 \times 10^{-27}$ kg | |
| | $939.5731$ MeV | |
| Planck's constant, $h$ | $6.626176 \times 10^{-34}$ J Hz$^{-1}$ | |
| Proton rest mass, $m_p$ | $1.6726485 \times 10^{-27}$ kg | |
| | $938.2796$ MeV | |
| Speed of light, $c$ | $2.99792458 \times 10^8$ m sec$^{-1}$ | |

## II. SOME USEFUL CONVERSION FACTORS

| | |
|---|---|
| 1 eV | $1.6021892 \times 10^{-19}$ J |
| 1 MeV | $10^6$ eV |
| 1 amu | $1.6605655 \times 10^{-27}$ kg |
| | $931.5016$ MeV |
| 1 W | 1 joule/sec |
| 1 d | 86400 sec |
| 1 mean y | 365.25 d |
| | 8766 h |
| | $3.156 \times 10^7$ sec |
| 1 curie | $3.7000 \times 10^{10}$ disintegrations/sec |
| 1 °K | $8.617065 \times 10^{-5}$ eV |

## III. 2200m/sec CROSS SECTIONS FOR NATURALLY OCCURRING ELEMENTS
### [From *Reactor Physics Constants*, ANL-5800 (1963)].

| Atomic No. | Element or Compound | Atomic or Mol. Wt. | Density, g/cm³ | Nuclei per Unit Vol. ×10⁻²⁴ | $1-\bar{\mu}_0$ | $\xi$ | $\sigma_a$ | $\sigma_s$ | $\sigma_t$ | $\Sigma_a$ | $\Sigma_s$ | $\Sigma_t$ |
|---|---|---|---|---|---|---|---|---|---|---|---|---|
| | | | | | | | Microscopic Cross Section, b | | | Macroscopic Cross Section, cm⁻¹ | | |
| 1 | H | 1.008 | 8.9† | 5.3† ×... | 0.3386 | 1.000 | 0.33 | 38 | 38 | 1.7† | 0.002 | 0.002 |
| | H₂O | 18.016 | 1 | 0.0335‡ | 0.676 | 0.948 | 0.66 | 103 | 103 | 0.022 | 3.45 | 3.45 |
| | D₂O | 20.030 | 1.10 | 0.0331‡ | 0.884 | 0.570 | 0.001 | 13.6 | 13.6 | 3.3† | 0.449 | 0.449 |
| 2 | He | 4.003 | 17.8† | 2.6† | 0.8334 | 0.425 | 0.007 | 0.8 | 0.807 | 0.02† | 2.1† | 2.1† |
| 3 | Li | 6.940 | 0.534 | 0.0463 | 0.9047 | 0.268 | 71 | 1.4 | 72.4 | 3.29 | 0.065 | 3.35 |
| 4 | Be | 9.013 | 1.85 | 0.1236 | 0.9259 | 0.209 | 0.010 | 7.0 | 7.01 | 124‡ | 0.865 | 0.865 |
| | BeO | 25.02 | 3.025 | 0.0728‡ | 0.939 | 0.173 | 0.010 | 6.8 | 6.8 | 73† | 0.501 | 0.501 |
| 5 | B | 10.82 | 2.45 | 0.1364 | 0.9394 | 0.171 | 755 | 4 | 759 | 103 | 0.346 | 104 |
| 6 | C | 12.011 | 1.60 | 0.0803 | 0.9444 | 0.158 | 0.004 | 4.8 | 4.80 | 32† | 0.385 | 0.385 |
| 7 | N | 14.008 | 0.0013 | 5.3† | 0.9524 | 0.136 | 1.88 | 10 | 11.9 | 9.9† | 50† | 60† |
| 8 | O | 16.000 | 0.0014 | 5.3† | 0.9583 | 0.120 | 20† | 4.2 | 4.2 | 0.000 | 21† | 21† |
| 9 | F | 19.00 | 0.0017 | 5.3† | 0.9649 | 0.102 | 0.001 | 3.9 | 3.90 | 0.01† | 20† | 20† |
| 10 | Ne | 20.183 | 0.0009 | 2.6† | 0.9667 | 0.0968 | <2.8 | 2.4 | 5.2 | 7.3† | 6.2† | 13.5† |
| 11 | Na | 22.991 | 0.971 | 0.0254 | 0.9710 | 0.0845 | 0.525 | 4 | 4.53 | 0.013 | 0.102 | 0.115 |
| 12 | Mg | 24.32 | 1.74 | 0.0431 | 0.9722 | 0.0811 | 0.069 | 3.6 | 3.67 | 0.003 | 0.155 | 0.158 |
| 13 | Al | 26.98 | 2.699 | 0.0602 | 0.9754 | 0.0723 | 0.241 | 1.4 | 1.64 | 0.015 | 0.084 | 0.099 |
| 14 | Si | 28.09 | 2.42 | 0.0522 | 0.9762 | 0.0698 | 0.16 | 1.7 | 1.86 | 0.008 | 0.089 | 0.097 |
| 15 | P | 30.975 | 1.82 | 0.0354 | 0.9785 | 0.0632 | 0.20 | 5 | 5.20 | 0.007 | 0.177 | 0.184 |
| 16 | S | 32.066 | 2.07 | 0.0389 | 0.9792 | 0.0612 | 0.52 | 1.1 | 1.62 | 0.020 | 0.043 | 0.063 |
| 17 | Cl | 35.457 | 0.0032 | 5.3† | 0.9810 | 0.0561 | 33.8 | 16 | 49.8 | 0.002 | 80† | 0.003 |
| 18 | A | 39.944 | 0.0018 | 2.6† | 0.9833 | 0.0492 | 0.66 | 1.5 | 2.16 | 1.7† | 3.9 | 5.6† |
| 19 | K | 39.100 | 0.87 | 0.0134 | 0.9829 | 0.0504 | 2.07 | 1.5 | 3.57 | 0.028 | 0.020 | 0.048 |
| 20 | Ca | 40.08 | 1.55 | 0.0233 | 0.9833 | 0.0492 | 0.44 | 3.0 | 3.44 | 0.010 | 0.070 | 0.080 |
| 21 | Sc | 44.96 | 2.5 | 0.0335 | 0.9852 | 0.0438 | 24 | 24 | 48 | 0.804 | 0.804 | 1.61 |
| 22 | Ti | 47.90 | 4.5 | 0.0566 | 0.9861 | 0.0411 | 5.8 | 4 | 9.8 | 0.328 | 0.226 | 0.555 |

| Z | Element | At. wt. | | | | | | | | | | |
|---|---|---|---|---|---|---|---|---|---|---|---|---|
| 23 | V | 50.95 | 5.96 | 0.0704 | 0.9869 | 0.0387 | 5 | 5 | 10.0 | 0.352 | 0.352 | 0.704 |
| 24 | Cr | 52.01 | 7.1 | 0.0822 | 0.9872 | 0.0385 | 3.1 | 3 | 6.1 | 0.255 | 0.247 | 0.501 |
| 25 | Mn | 54.94 | 7.2 | 0.0789 | 0.9878 | 0.0359 | 13.2 | 2.3 | 15.5 | 1.04 | 0.181 | 1.22 |
| 26 | Fe | 55.85 | 7.86 | 0.0848 | 0.9881 | 0.0353 | 2.62 | 11 | 13.6 | 0.222 | 0.933 | 1.15 |
| 27 | Co | 58.94 | 8.9 | 0.0910 | 0.9887 | 0.0335 | 38 | 7 | 45 | 3.46 | 0.637 | 4.10 |
| 28 | Ni | 58.71 | 8.90 | 0.0913 | 0.9887 | 0.0335 | 4.6 | 17.5 | 22.1 | 0.420 | 1.60 | 2.02 |
| 29 | Cu | 63.54 | 8.94 | 0.0848 | 0.9896 | 0.0309 | 3.85 | 7.2 | 11.05 | 0.0326 | 0.611 | 0.937 |
| 30 | Zn | 65.38 | 7.14 | 0.0658 | 0.9897 | 0.0304 | 1.10 | 3.6 | 4.70 | 0.072 | 0.237 | 0.309 |
| 31 | Ga | 69.72 | 5.91 | 0.0511 | 0.9925 | 0.0283 | 2.80 | 4 | 6.80 | 0.143 | 0.204 | 0.347 |
| 32 | Ge | 72.60 | 5.36 | 0.0445 | 0.9909 | 0.0271 | 2.45 | 3 | 5.45 | 0.109 | 0.134 | 0.243 |
| 33 | As | 74.91 | 5.73 | 0.0461 | 0.9911 | 0.0264 | 4.3 | 6 | 10.3 | 0.198 | 0.277 | 0.475 |
| 34 | Se | 78.96 | 4.8 | 0.0366 | 0.9916 | 0.0251 | 12.3 | 11 | 23.3 | 0.450 | 0.403 | 0.853 |
| 35 | Br | 79.916 | 3.12 | 0.0235 | 0.9917 | 0.0247 | 6.7 | 6 | 12.7 | 0.157 | 0.141 | 0.298 |
| 36 | Kr | 83.80 | 0.0037 | 2.6† | 0.9921 | 0.0236 | 31 | 7.2 | 38.2 | 81† | 19† | 99† |
| 37 | Rb | 85.48 | 1.53 | 0.0108 | 0.9922 | 0.0233 | 0.73 | 12 | 12.7 | 0.008 | 0.130 | 0.138 |
| 38 | Sr | 87.63 | 2.54 | 0.0175 | 0.9925 | 0.0226 | 1.21 | 10 | 11.2 | 0.021 | 0.175 | 0.195 |
| 39 | Yt | 88.92 | 5.51 | 0.0373 | 0.9925 | 0.0223 | 1.313 | 4.3 | 4.3 | 0.049 | 0.112 | 0.160 |
| 40 | Zr | 91.22 | 6.4 | 0.0423 | 0.9927 | 0.0218 | 0.185 | 8 | 8.2 | 0.008 | 0.338 | 0.347 |
| 41 | Nb | 92.91 | 8.4 | 0.0545 | 0.9928 | 0.0214 | 1.16 | 5 | 6.16 | 0.063 | 0.273 | 0.336 |
| 42 | Mo | 95.95 | 10.2 | 0.0640 | 0.9931 | 0.0207 | 2.70 | 7 | 9.70 | 0.173 | 0.448 | 0.621 |
| 43 | Tc | 98.0 | — | — | 0.9932 | 0.0203 | 22 | — | — | — | — | — |
| 44 | Ru | 101.1 | 12.2 | 0.0727 | 0.9934 | 0.0197 | 2.56 | 6 | 8.56 | 0.186 | 0.436 | 0.622 |
| 45 | Rh | 102.91 | 12.5 | 0.0732 | 0.9935 | 0.0193 | 149 | 5 | 154 | 10.9 | 0.366 | 11.3 |
| 46 | Pd | 106.4 | 12.16 | 0.0689 | 0.9937 | 0.0187 | 8 | 3.6 | 11.6 | 0.551 | 0.248 | 0.799 |
| 47 | Ag | 107.88 | 10.5 | 0.0586 | 0.9938 | 0.0184 | 63 | 6 | 69 | 3.69 | 0.352 | 4.04 |
| 48 | Cd | 112.41 | 8.65 | 0.0464 | 0.9940 | 0.0178 | 2450 | 7 | 2457 | 114 | 0.325 | 114 |
| 49 | In | 114.82 | 7.28 | 0.0382 | 0.9942 | 0.0173 | 191 | 2.2 | 193 | 7.30 | 0.084 | 7.37 |
| 50 | Sn | 118.70 | 6.5 | 0.0330 | 0.9944 | 0.0167 | 0.625 | 4 | 4.6 | 0.021 | 0.132 | 0.152 |
| 51 | Sb | 121.76 | 6.69 | 0.0331 | 0.9945 | 0.0163 | 5.7 | 4.3 | 10.0 | 0.189 | 0.142 | 0.331 |
| 52 | Te | 127.61 | 6.24 | 0.0295 | 0.9948 | 0.0155 | 4.7 | 5 | 9.7 | 0.139 | 0.148 | 0.286 |
| 53 | I | 126.91 | 4.93 | 0.0234 | 0.9948 | 0.0157 | 7.0 | 3.6 | 10.6 | 0.164 | 0.084 | 0.248 |
| 54 | Xe | 131.30 | 0.0059 | 2.7† | 0.9949 | 0.0152 | 35 | 4.3 | 39.3 | 95† | 12† | 0.001 |
| 55 | Cs | 132.91 | 1.873 | 0.0085 | 0.9950 | 0.0150 | 28 | 20 | 48 | 0.238 | 0.170 | 0.408 |
| 56 | Ba | 137.36 | 3.5 | 0.0154 | 0.9951 | 0.0145 | 1.2 | 8 | 9.2 | 0.018 | 0.123 | 0.142 |

III. (*Continued*)

| Z | Element | $\bar{A}$ | $\rho$ | $N$ | $1-\bar{\mu}_0$ | $\xi$ | $\sigma_a$ | $\sigma_s$ | $\sigma_t$ | $\Sigma_a$ | $\Sigma_s$ | $\Sigma_t$ |
|---|---|---|---|---|---|---|---|---|---|---|---|---|
| 57 | La | 138.92 | 6.19 | 0.0268 | 0.9952 | 0.0143 | 8.9 | 15 | 24 | 0.239 | 0.403 | 0.642 |
| 58 | Ce | 140.13 | 6.78 | 0.0292 | 0.9952 | 0.0142 | 0.73 | 9 | 9.7 | 0.021 | 0.263 | 0.283 |
| 59 | Pr | 140.92 | 6.78 | 0.0290 | 0.9953 | 0.0141 | 11.3 | 4 | 15.3 | 0.328 | 0.116 | 0.444 |
| 60 | Nd | 144.27 | 6.95 | 0.0290 | 0.9954 | 0.0138 | 46 | 16 | 62 | 1.33 | 0.464 | 1.79 |
| 61 | Pm | 145.0 | — | — | 0.9954 | 0.0137 | 60 | — | — | — | — | — |
| 62 | Sm | 150.35 | 7.7 | 0.0309 | 0.9956 | 0.0133 | 5600 | 5 | 5605 | 173 | 0.155 | 173 |
|  | Sm₂O₃ | 348.70 | 7.43 | 0.0128‡ | 0.974 | 0.076 | 16,500 | 22.6 | 16,500 | 211 | 0.289 | 211 |
| 63 | Eu | 152.0 | 5.22 | 0.0207 | 0.9956 | 0.0131 | 4300 | 8 | 4308 | 89.0 | 0.166 | 89.2 |
|  | Eu₂O₃ | 352.00 | 7.42 | 0.0127‡ | 0.978 | 0.063 | 8740 | 30.2 | 8770 | 111 | 0.383 | 111 |
| 64 | Gd | 167.26 | 7.95 | 0.0305 | 0.9958 | 0.0127 | 46,000 | — | — | 1403 | — | — |
| 65 | Tb | 158.93 | 8.33 | 0.0316 | 0.9958 | 0.0125 | 46 | — | — | 1.45 | — | — |
| 66 | Dy | 162.51 | 8.56 | 0.0317 | 0.9959 | 0.0122 | 950 | 100 | 1050 | 30.1 | 3.17 | 33.3 |
|  | Dy₂O₃ | 372.92 | 7.81 | 0.0126‡ | 0.993 | 0.019 | 2200 | 214 | 2414 | 27.7 | 2.7 | 30.4 |
| 67 | Ho | 164.94 | 8.76 | 0.0320 | 0.9960 | 0.0121 | 65 | — | — | 2.08 | — | — |
| 68 | Er | 167.27 | 9.16 | 0.0330 | 0.9960 | 0.0119 | 173 | 15 | 188 | 5.71 | 0.495 | 6.20 |
| 69 | Tm | 168.94 | 9.35 | 0.0333 | 0.9961 | 0.0118 | 127 | 7 | 134 | 4.23 | 0.233 | 4.46 |
| 70 | Yb | 173.04 | 7.01 | 0.0244 | 0.9961 | 0.0115 | 37 | 12 | 49 | 0.903 | 0.293 | 1.20 |
| 71 | Lu | 174.99 | 9.74 | 0.0335 | 0.9962 | 0.0114 | 112 | — | — | 3.75 | — | — |
| 72 | Hf | 178.5 | 13.3 | 0.0449 | 0.9963 | 0.0112 | 105 | 8 | 113 | 4.71 | 0.0359 | 5.07 |
| 73 | Ta | 180.95 | 16.6 | 0.0553 | 0.9963 | 0.0110 | 21 | 5 | 26 | 1.16 | 0.277 | 1.44 |
| 74 | W | 183.86 | 19.3 | 0.0632 | 0.9964 | 0.0108 | 19.2 | 5 | 24.2 | 1.21 | 0.316 | 1.53 |
| 75 | Re | 186.22 | 20.53 | 0.0664 | 0.9964 | 0.0107 | 86 | 14 | 100 | 5.71 | 0.930 | 6.64 |
| 76 | OS | 190.2 | 22.48 | 0.0712 | 0.9965 | 0.0105 | 15.3 | 11 | 26.3 | 1.09 | 0.783 | 1.87 |
| 77 | Ir | 192.2 | 22.42 | 0.0703 | 0.9965 | 0.0104 | 440 | — | — | 30.9 | — | — |
| 78 | Pt | 195.09 | 21.37 | 0.0660 | 0.9966 | 0.0102 | 8.8 | 10 | 18.8 | 0.581 | 0.660 | 1.24 |
| 79 | Au | 197.0 | 19.32 | 0.0591 | 0.9966 | 0.0101 | 98.8 | 9.3 | 107.3 | 5.79 | 0.550 | 6.34 |
| 80 | Hg | 200.61 | 13.55 | 0.0407 | 0.9967 | 0.0099 | 380 | 20 | 400 | 15.5 | 0.814 | 16.3 |
| 81 | Ti | 204.39 | 11.85 | 0.0349 | 0.9967 | 0.0098 | 3.4 | 14 | 17.4 | 0.119 | 0.489 | 0.607 |
| 82 | Pb | 207.21 | 11.35 | 0.0330 | 0.9968 | 0.0096 | 0.170 | 11 | 11.2 | 0.006 | 0.363 | 0.369 |
| 83 | Bi | 209.0 | 9.747 | 0.0281 | 0.9968 | 0.0095 | 0.034 | 9 | 9 | 0.001 | 0.253 | 0.256 |

| | | | | | | | | | | | | |
|---|---|---|---|---|---|---|---|---|---|---|---|---|
| 84 | Po | 210.0 | 9.24 | 0.0265 | 0.9968 | 0.0095 | — | — | — | — | — | — |
| 85 | At | 211.0 | — | — | 0.9968 | 0.0094 | — | — | — | — | — | — |
| 86 | Rn | 222.0 | 0.0097 | 2.6† | 0.9970 | 0.0090 | 0.7 | — | — | — | — | — |
| 87 | Fr | 223.0 | — | — | 0.9980 | 0.0089 | — | — | — | 0.266 | — | — |
| 88 | Ra | 226.05 | 5 | 0.0133 | 0.9971 | 0.0088 | 20 | — | — | — | — | — |
| 89 | Ac | 227.0 | — | — | 0.9971 | 0.0088 | 510 | — | — | — | — | — |
| 90 | Th | 232.05 | 11.3 | 0.0293 | 0.9971 | 0.0086 | 7.56 | 12.6 | 20.2 | 0.222 | 0.369 | 0.592 |
| 91 | Pa | 231.0 | 15.4 | 0.0402 | 0.9971 | 0.0086 | 200 | — | — | 8.04 | — | — |
| 92 | U | 238.07 | 18.9 | 0.04783 | 0.9972 | 0.0084 | 7.68 | 8.3 | 16.0 | 0.367 | 0.397 | 0.765 |
| | UO$_2$ | 270.07 | 10 | 0.0223‡ | 0.9887 | 0.036 | 7.6 | 16.7 | 24.3 | 0.169 | 0.372 | 0.542 |
| 93 | Np | 237.0 | — | — | 0.9972 | 0.0084 | 170 | — | — | — | — | — |
| 94 | Pu | 239.0 | 19.74 | 0.0498 | 0.9972 | 0.0083 | 1026 | 9.6 | 1036 | 51.1 | 0.478 | 51.6 |
| 95 | Am | 242.0 | — | — | 0.9973 | 0.0082 | 8.000 | — | — | — | — | — |

† Value has been multiplied by 10$^5$.

‡ Molecules/cm$^3$.

## IV. 2200 m/sec CROSS SECTIONS OF SPECIAL INTEREST:

| | | |
|---|---|---|
| $^{10}$B: | $\sigma_a = 3837$b | |
| $^{11}$B: | $\sigma_a = 0.005$ | |
| $^{135}$Xe: | $\sigma_a = 2.7 \times 10^6$ | |
| $^{233}$U: | $\sigma_\gamma = 49$ | $\sigma_f = 524$ |
| $^{235}$U: | $\sigma_\gamma = 101$ | $\sigma_f = 577$ |
| $^{238}$U: | $\sigma_\gamma = 2.73$ | |
| $^{239}$Pu: | $\sigma_\gamma = 274$ | $\sigma_f = 741$ |
| $^{240}$Pu: | $\sigma_\gamma = 286$ | $\sigma_f = 0.03$ |
| $^{241}$Pu: | $\sigma_\gamma = 425$ | $\sigma_f = 950$ |
| $^{242}$Pu: | $\sigma_\gamma = 30$ | $\sigma_f < 0.2$ |

# Appendix B
## Some Useful Mathematical Formulas

(1) *Solution of First-Order Linear Differential Equations:*

$$\frac{df}{dx} + a(x)f(x) = g(x) \tag{B-1}$$

$$f(x) = e^{-A(x)}\left[\int^x dx'\, e^{A(x')} g(x') + C\right], \qquad A(x) \equiv \int^x dx'\, a(x'). \tag{B-2}$$
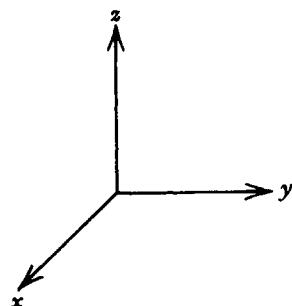
(2) *Differentiation of a Definite Integral:*

$$\frac{d}{dx} \int_{b(x)}^{a(x)} dx'\, F(x,x') = F(x,a)\frac{da}{dx} - F(x,b)\frac{db}{dx} + \int_{b(x)}^{a(x)} dx' \frac{\partial F(x,x')}{\partial x} \tag{B-3}$$

(3) *Representation of Laplacian $\nabla^2$ in Various Coordinate Systems:*
   (a) *Cartesian:*
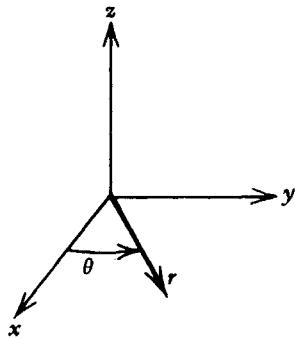
$$\nabla^2 = \frac{\partial^2}{\partial x^2} + \frac{\partial^2}{\partial y^2} + \frac{\partial^2}{\partial z^2} \tag{B-4}$$

**(b)** *Cylindrical:*
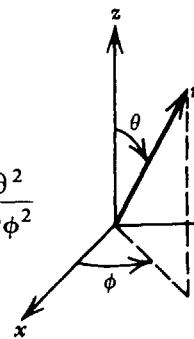
$$\nabla^2 = \frac{1}{r}\frac{\partial}{\partial r}r\frac{\partial}{\partial r} + \frac{1}{r^2}\frac{\partial^2}{\partial \theta^2} + \frac{\partial^2}{\partial z^2}$$

(B-5)

**(c)** *Spherical:*

$$\nabla^2 = \frac{1}{r^2}\frac{\partial}{\partial r}r^2\frac{\partial}{\partial r} + \frac{1}{r^2\sin\theta}\frac{\partial}{\partial \theta}\left(\sin\theta\frac{\partial}{\partial \theta}\right) + \frac{1}{r^2\sin^2\theta}\frac{\partial^2}{\partial \phi^2}$$

(B-6)

**(4)** *Gauss' Divergence Theorem:*

$$\int_V d^3r \nabla\cdot\mathbf{A} = \int_S dS\,\hat{\mathbf{e}}_s\cdot\mathbf{A}$$

(B-7)

where $\hat{\mathbf{e}}_s$ is the unit vector normal to the surface element $dS$.

**(5)** *Green's Theorem:*

$$\int d^3r \nabla\phi\cdot\nabla\psi = \int dS\,\phi\hat{\mathbf{e}}_s\cdot\nabla\psi - \int d^3r\phi\nabla^2\psi$$

(B-8)

$$\int d^3r(\phi\nabla^2\psi - \psi\nabla^2\phi) = \int dS\,\hat{\mathbf{e}}_s\cdot(\phi\nabla\psi - \psi\nabla\phi)$$

(B-9)

**(6)** *Taylor Series Expansion:*

$$f(x) = f(x_0) + (x - x_0)f'(x_0) + \frac{(x - x_0)^2}{2!}f''(x_0) + \cdots$$

(B-10)

**(7)** *Fourier Series Expansion:*

$$f(x) = \sum_{n=1}^{\infty} a_n\sin\frac{n\pi x}{l} + \frac{1}{2}b_0 + \sum_{n=1}^{\infty} b_n\cos\frac{n\pi x}{l}$$

(B-11)

where
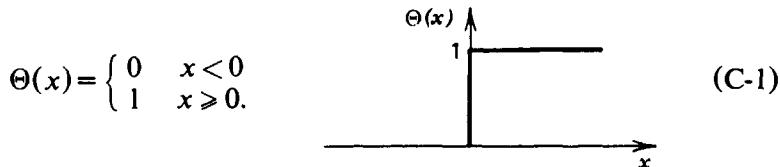
$$a_n \equiv \frac{1}{l}\int_{-l}^{l} dx' f(x')\sin\frac{n\pi x'}{l}, \qquad b_n \equiv \frac{1}{l}\int_{-l}^{l} dx' f(x')\cos\frac{n\pi x'}{l}.$$

(B-12)
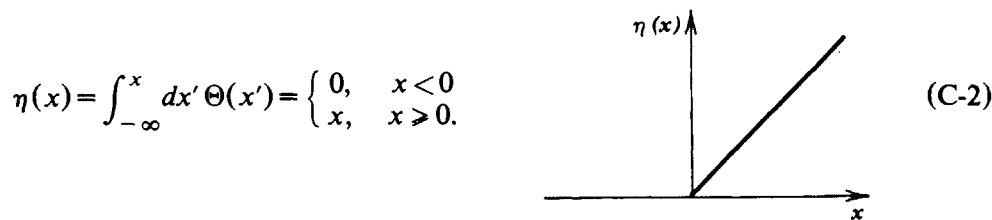
# Appendix C
# Step Functions, Delta Functions, and Other Exotic Beasts

## I. INTRODUCTION

Consider the discontinuous function $\Theta(x)$ defined by the properties

$$\Theta(x) = \begin{cases} 0 & x < 0 \\ 1 & x \geqslant 0. \end{cases}$$



$$(C-1)$$

$\Theta(x)$ is the unit "step function" introduced by Heaviside in his development of operational calculus (now known as integral transform analysis). One can perform numerous operations on $\Theta(x)$. In particular it can be integrated to yield the ramp function

$$\eta(x) = \int_{-\infty}^{x} dx' \, \Theta(x') = \begin{cases} 0, & x < 0 \\ x, & x \geqslant 0. \end{cases}$$



$$(C-2)$$

Let's try something a bit more unusual by taking the derivative of $\Theta(x)$. Clearly this is ridiculous, because this derivative, call it $\delta(x)$, is undefined at $x = 0$ because $\Theta(x)$ is discontinuous at this point:

$$\delta(x) = \Theta'(x) = \lim_{\epsilon \to 0} \left[ \frac{\Theta(x + \epsilon) - \Theta(x)}{\epsilon} \right] = \begin{cases} 0, & x \neq 0 \\ \infty, & x = 0. \end{cases} \qquad (C-3)$$

Nevertheless Dirac, Heaviside, and others have made very good use of this strange "function." To be more specific, the Dirac $\delta$-function, $\delta(x)$, has the properties

$$\delta(x - x_0) = \begin{cases} 0, & x \neq x_0 \\ \infty, & x = x_0 \end{cases}, \qquad \int_{-\infty}^{\infty} dx \, \delta(x - x_0) = 1. \qquad (C-4)$$

In a sense, it resembles a generalization of the Kronecker $\delta$-function

$$\delta_{mn} = \begin{cases} 0, & m \neq n \\ 1, & m = n. \end{cases}$$

The most useful property of the Dirac $\delta$-function occurs when it is integrated along with a well-behaved function, say $f(x)$:

$$\int dx f(x)\delta(x - x_0) = f(x_0).$$
(C-5)

This property not only is very interesting, but extremely useful in mathematical physics. Unfortunately the proof of this property—and, indeed, all of the *theory* of such generalized functions—requires a rather potent dose of mathematics. [Such generalized functions are really not functions at all, but rather a class of linear functionals[1] called "distributions" defined on some set of suitable test functions (which are "infinitely differentiable with compact support").]

Fortunately one does not need all of this high-powered mathematics in order to *use* $\delta$-functions. Only a knowledge of their properties is necessary.

## II. PROPERTIES OF THE DIRAC $\delta$-FUNCTION

### A. Alternative Representations

$$\delta(x - x_0) = \frac{1}{\pi} \lim_{\lambda \to \infty} \frac{\sin\lambda(x - x_0)}{(x - x_0)},$$
(C-6)

$$\delta(x - x_0) = \frac{1}{\pi} \lim_{\epsilon \to 0^+} \frac{\epsilon}{(x - x_0)^2 + \epsilon^2}.$$
(C-7)

### B. Properties

$$\delta(x) = \delta(-x),$$
(C-8)

$$\delta(ax) = \frac{1}{|a|}\delta(x), \qquad a \neq 0,$$
(C-9)

$$\delta[g(x)] = \sum_n \frac{1}{|g'(x_n)|}\delta(x - x_n), \quad [g(x_n) = 0, g'(x_n) \neq 0]$$
(C-10)

$$x\delta(x) = 0,$$
(C-11)

$$f(x)\delta(x - a) = f(a)\delta(x - a),$$
(C-12)

$$\int \delta(x - y)\delta(y - a)dy = \delta(x - a),$$
(C-13)

$$\delta(x) = \frac{1}{2\pi}\int_{-\infty}^{\infty} dk\, e^{ikx}.$$
(C-14)

Actually these properties only make sense when inserted in an integral. For example, property (C-8) really should be interpreted as

$$\int dx f(x)\delta(x) = \int dx f(x)\delta(-x) = f(0).$$
(C-15)

## C. Derivatives

One can differentiate a $\delta$-function as many times as one wishes. The $m$th derivative is defined by

$$\int_{-\infty}^{\infty} \delta^{[m]}(x-a)f(x)\,dx = (-1)^m \frac{d^m}{dx^m} f \bigg|_{x=a}.$$

(C-16)

One can show

$$\delta^{[m]}(x) = (-1)^m \delta^{[m]}(-x),$$

(C-17)

$$\int \delta^{[m]}(x-y)\delta^{[n]}(y-a)\,dy = \delta^{[m+n]}(x-a),$$

(C-18)

$$x^{m+1}\delta^{[m]}(x) = 0.$$

(C-19)

Perhaps of more direct use is the application of these properties to the first derivative

$$\int_{-\infty}^{\infty} \delta'(x)f(x)\,dx = -f'(0),$$

(C-20)

$$\delta'(x) = -\delta'(-x),$$

(C-21)

$$\int \delta'(x-y)\delta(y-a)\,dy = \delta'(x-a),$$

(C-22)

$$x\delta'(x) = -\delta(x).$$

(C-23)

One can generalize the concept of a $\delta$-function to several dimensions. For example, we would define the three-dimensional $\delta$-function by

$$\int d^3 r' \, \delta(\mathbf{r}' - \mathbf{r}) f(\mathbf{r}') = f(\mathbf{r}).$$

(C-24)

Note that we could write this in Cartesian coordinates as

$$\delta(\mathbf{r} - \mathbf{r}') = \delta(x - x')\delta(y - y')\delta(z - z').$$

(C-25)

Such multidimensional $\delta$-functions are of very considerable use in vector calculus.

More detailed discussions of the Dirac $\delta$-function and its relatives are found in the following references:

(1) J. W. Dettman, *Mathematical Methods in Physics and Engineering*, 2nd Edition, McGraw-Hill, New York (1969).

(2) M. J. Lighthill, *Fourier Analysis and Generalized Functions*, Cambridge U. P. (1959).

(3) A. Messiah, *Quantum Mechanics*, Vol. I, Wiley, New York (1965), pp. 468–470.

# Appendix D
## Some Properties of Special Functions

(1) *Legendre Functions*:
  (a) *Defining equation*:

$$(1 - x^2)f'' - 2xf' + l(l+1)f = 0, \qquad l = \text{integer.} \tag{D-1}$$

  (b) *Representation*:

$$P_l(x) = \frac{1}{2^l l!} \frac{d^l}{dx^l}(x^2 - 1)^l. \tag{D-2}$$

  (c) *Properties*:

$$P_0(x) = 1, \qquad P_1(x) = x, \qquad P_2(x) = \frac{1}{2}(3x^2 - 1), \qquad P_3 = \frac{1}{2}(5x^3 - 3x), \dots \tag{D-3}$$

$$\int_{-1}^{+1} P_l(x)P_{l'}(x)\,dx = \frac{2}{2l+1}\delta_{ll'}. \tag{D-4}$$

  (d) *Recurrence relations*:

$$P'_{l+1}(x) - xP'_l(x) = (l+1)P_l(x) \tag{D-5}$$

$$(l+1)P_{l+1}(x) - (2l+1)xP_l(x) + lP_{l-1}(x) = 0. \tag{D-6}$$

(2) *Associated Legendre Polynomials*:
  (a) *Defining equation*:

$$(1 - x^2)f'' - 2xf' + \left[ l(l+1) - \frac{m^2}{1-x^2} \right]f = 0. \tag{D-7}$$

(b) *Representation*:

$$P_l^m(x) = (1 - x^2)^{\frac{m}{2}} \frac{d^m}{dx^m} P_l(x).$$

(D-8)

(c) *Spherical harmonics*:

$$Y_{lm}(\hat{\Omega}) = \left[ \frac{(2l+1)(l-m)!}{4\pi(l+m)!} \right]^{1/2} P_l(\cos\theta)e^{im\phi}.$$

(D-9)

(d) *Properties*:

$$\int_{4\pi} d\hat{\Omega} \, Y_{lm}^*(\hat{\Omega}) \, Y_{l'm'}(\hat{\Omega}) = \delta_{ll'}\delta_{mm'}.$$

(D-10)

$$P_l(\hat{\Omega}\cdot\hat{\Omega}') = \frac{4\pi}{(2l+1)} \sum_{m=-l}^{l} Y_{lm}^*(\hat{\Omega}) Y_{lm}(\hat{\Omega}').$$

(D-11)

(3) *Bessel Functions*:
   (a) *Defining equation*:

$$x^2 f'' + xf' + (x^2 - n^2)f = 0$$

(D-12)

(b) *Solution*:  $J_n(x)$, Bessel function of first kind
                  $Y_n(x)$, Bessel function of second kind
(c) *Representation*:

$$J_n(x) = \sum_{k=0}^{\infty} \frac{(-1)^k}{\Gamma(k+1)\Gamma(k+n+1)} \left(\frac{x}{2}\right)^{n+2k}, \qquad Y_n(x) = \frac{J_n(x)\cos(n\pi) - J_{-n}(x)}{\sin n\pi}$$

(D-13)

(d) *Hankel functions*:

$$H_n^{(1)}(x) = J_n(x) + i\,Y_n(x)$$

(D-13)

$$H_n^{(2)}(x) = J_n(x) - i\,Y_n(x)$$

(D-14)

(4) *Modified Bessel Functions*:
   (a) *Defining equation*:

$$x^2 f'' + xf' - (x^2 + n^2)f = 0$$

(D-15)

(b) *Solution*:  $I_n(x)$, modified Bessel function of first kind
                  $K_n(x)$, modified Bessel function of second kind
(c) *Representation*:

$$I_n(x) = i^{-n}J_n(ix) = i^n J_n(-ix)$$

$$K_n(x) = \frac{\pi}{2}i^{n+1}H_n^{(1)}(ix) = \frac{\pi}{2}i^{-n-1}H_n^{(2)}(-ix)$$

(D-16)
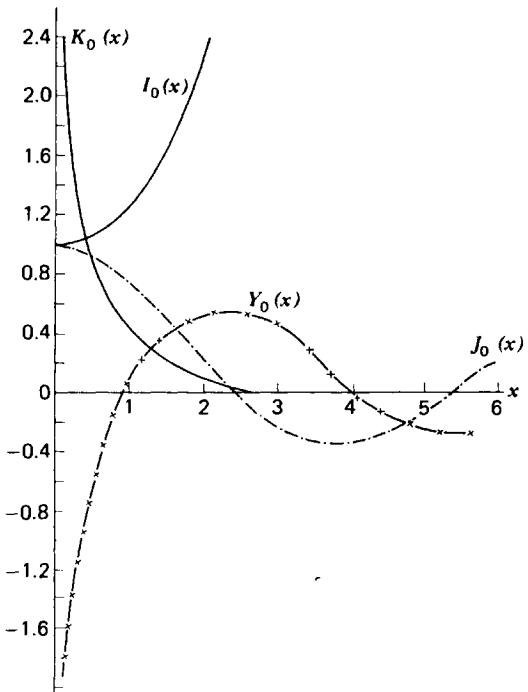
**FIGURE D-1.    The Bessel functions of zero order.**

(5)  *Useful Expansions of Bessel Functions for small x:*

$$J_0(x) = 1 - \frac{x^2}{4} + \frac{x^4}{64} - \frac{x^6}{2304} + \cdots \qquad \text{(D-17)}$$

$$J_1(x) = \frac{x}{2} - \frac{x^3}{16} + \frac{x^5}{384} - \cdots \qquad \text{(D-18)}$$

$$Y_0(x) = \frac{2}{\pi}\left[\left(\gamma + \ln\frac{x}{2}\right)J_0(x) + \frac{x^2}{4} + \cdots\right], \qquad \gamma \equiv 0.577216 \qquad \text{(D-19)}$$

$$Y_1(x) = \frac{2}{\pi}\left[\left(\gamma + \ln\frac{x}{2}\right)J_1(x) - \frac{1}{x} - \frac{x}{4} + \cdots\right] \qquad \text{(D-20)}$$

$$I_0(x) = 1 + \frac{x^2}{4} + \frac{x^4}{64} + \frac{x^6}{2304} + \cdots \qquad \text{(D-21)}$$

$$I_1(x) = \frac{x}{2} + \frac{x^3}{16} + \frac{x^5}{384} + \cdots \qquad \text{(D-22)}$$

$$K_0(x) = -\left(\gamma + \ln\frac{x}{2}\right)I_0(x) + \frac{x^2}{4} + \frac{3x^4}{128} + \cdots \qquad \text{(D-23)}$$

$$K_1(x) = \left(\gamma + \ln\frac{x}{2}\right)I_1(x) + \frac{1}{x} - \frac{x}{4} - \frac{5x^3}{64} + \cdots \qquad \text{(D-24)}$$

(a)  *Asymptotic expansions for large x:*

$$I_0(x) = \frac{e^x}{\sqrt{2\pi x}}\left(1 + \frac{1}{8x} + \cdots\right) \qquad \text{(D-25)}$$

$$I_1(x) = \frac{e^x}{\sqrt{2\pi x}}\left(1 - \frac{3}{8x} + \cdots\right) \qquad \text{(D-26)}$$

$$K_0(x) = \sqrt{\frac{\pi}{2x}}\; e^{-x}\left(1 - \frac{1}{8x} + \cdots\right) \qquad \text{(D-27)}$$

$$K_1(x) = \sqrt{\frac{\pi}{2x}}\; e^{-x}\left(1 + \frac{3}{8x} + \cdots\right) \qquad \text{(D-28)}$$

(b) *Recurrence relations*:

$$xJ_n' = nJ_n - xJ_{n+1} = -nJ_n + xJ_{n-1} \tag{D-29}$$

$$2nJ_n = xJ_{n-1} + xJ_{n+1} \tag{D-30}$$

$$xI_n' = nI_n + xI_{n+1} = -nI_n + xI_{n-1} \tag{D-31}$$

$$xK_n' = nK_n - xK_{n+1} = -nK_n - xK_{n-1} \tag{D-32}$$

$$J_0' = -J_1, \quad Y_0' = -Y_1, \quad I_0' = I_1, \quad K_0' = -K_1 \tag{D-33}$$

(c) *Integrals*:

$$\int x^n J_{n-1}(x)dx = x^n J_n, \qquad \int x^n Y_{n-1}(x)dx = x^n Y_n \tag{D-34}$$

$$\int x^n I_{n-1}dx = x^n I_n, \qquad \int x^n K_{n-1}dx = -x^n K_n. \tag{D-35}$$

(6) *Gamma Function*:
(a) *Definition*:

$$\Gamma(z) = \int_0^\infty dt\, e^{-t} t^{z-1} \tag{D-36}$$

(b) *Properties*:

$$\Gamma(z+1) = z\Gamma(z)$$

$$\Gamma(1/2) = \sqrt{\pi}, \quad \Gamma(0) = \infty, \quad \Gamma(1) = 1, \ldots, \Gamma(n) = (n-1)!. \tag{D-37}$$

(7) *Error Function*:
(a) *Definition*:

$$\mathrm{erf}(x) = \frac{2}{\sqrt{\pi}} \int_0^x dt\, e^{-t^2} \tag{D-38}$$

(b) *Complementary error function*:

$$\mathrm{erfc}(x) = 1 - \mathrm{erf}(x) = \frac{2}{\sqrt{\pi}} \int_x^\infty dt\, e^{-t^2} \tag{D-39}$$

(8) *Exponential Integrals*:
(a) *Definition*:

$$E_n(x) = \int_1^\infty dt\, \frac{e^{-xt}}{t^n}, \qquad E_1(x) = \int_1^\infty dt\, \frac{e^{-xt}}{t} = \int_x^\infty dt\, \frac{e^{-t}}{t} \tag{D-40}$$

(b) *Properties*:

$$E_0(x) = \frac{e^{-x}}{x} \tag{D-41}$$

$$E_n'(x) = -E_{n-1}(x) \tag{D-42}$$

$$E_n(x) = \frac{1}{n-1}[e^{-x} - xE_{n-1}(x)], \qquad n > 1 \tag{D-43}$$

$$E_1(x) = -\gamma - \ln x - \sum_{n=1}^\infty \frac{(-1)^n x^n}{nn!} \tag{D-44}$$

## REFERENCES

1. M. Abramowitz and I. Stegun (Eds.), *Handbook of Mathematica Functions*, Dover, New York (1965).
2. H. Margenau and G. M. Murphy, *The Mathematics of Physics and Chemistry*, 2nd Ed., Vol. I, Van Nostrand, Princeton, N.J. (1956).
3. I. S. Gradshteyn and I. M. Ryzhik, *Table of Integrals, Series, and Products*, 4th Ed., Academic Press, New York (1965).
4. P. M. Morse and H. Feshbach, *Methods of Theoretical Physics*, Vol. I and II, McGraw-Hill, New York (1953).

# Appendix E
## Some Assorted Facts on Linear Operators

## I. INNER PRODUCTS

We define the *inner product* or *scalar product* $(f,g)$ of two functions $f(x)$ and $g(x)$ as

$$(f,g) \equiv \int_a^b dx\, w(x) f^*(x) g(x), \tag{E-1}$$

[here $w(x)$ is frequently taken as 1] where $f^*(x)$ denotes the complex conjugate of $f(x)$. This inner product has the properties

(a) $(f,g) = (g,f)^*$,

(b) $(af_1(x) + bf_2(x), g) = a^*(f_1,g) + b^*(f_2,g)$,

(c) $(f,f) > 0$ if $f(x) \neq 0$.

[Note: Sometimes one defines a *real* inner product

$$(f,g) = \int_a^b dx\, w(x) f(x) g(x).$$

Such a form satisfies properties (a) and (b), but property (c) is satisfied only for real functions. Hence if one is concerned with complex valued functions, then it is necessary to use the more general form (E-1).]

We define the *norm* of a function $f(x)$ as

$$\|f\| \equiv [(f,f)]^{1/2}. \tag{E-2}$$

The norm is a real, positive number [by property (c) above] and characterizes the "magnitude" of the function $f(x)$.

Two functions, $f(x)$ and $g(x)$, are said to be *orthogonal* if their inner product vanishes,

$$(f,g) = 0. \tag{E-3}$$

## II. LINEAR OPERATORS

An *operator* refers to a mathematical operation by which we convert a function $f(x)$ into another function $g(x)$—that is,

$$Af(x) = g(x). \tag{E-4}$$

(In the more colorful language of functional analysis, an operator is "a *mapping* of a linear vector space into a linear vector space.")

## EXAMPLES:

Differential operator: $A \circ \equiv \dfrac{d}{dx}, \qquad Af = \dfrac{df}{dx}.$

Integral operator: $A \circ \equiv \displaystyle\int_a^b dx' \, k(x, x') \circ, \qquad Af = \displaystyle\int_a^b dx' \, k(x, x') f(x').$

Unit operator: $A \circ \equiv 1 \circ, \qquad Af = f(x).$

Null operator: $A \circ = 0 \circ, \qquad 0f = 0.$

Displacement operator: $A \circ = \exp(-\alpha \dfrac{d}{dx} \circ), \qquad Af = f(x - \alpha).$

$A \circ = (\circ)^2, \qquad Af = [f(x)]^2.$

If $A(af + bg) = aAf + bAg$, then we refer to $A$ as a *linear* operator. Note that the first five operators above are linear, while the sixth operator is a nonlinear operator.

Such operators can frequently be manipulated formally via ordinary algebra, much as one manipulates numbers or functions. However one must be very careful. In particular note that operators are generally not *commutative*

$$ABf(x) \neq BAf(x). \tag{E-5}$$

There is one other animal quite similar to an operator, that occasionally arises in mathematics. One refers to this mathematical operation, which converts a function into a scalar, as a *functional* $\mathcal{F}$

$$\mathcal{F}\{f(x)\} = a = \text{number} \tag{E-6}$$

(or, if you prefer, "a mapping of a vector space into a scalar field").

## EXAMPLE:   A definite integral

$$\mathcal{F}\{f(x)\} = \int_a^b dx \, f(x) = \text{number}. \tag{E-7}$$

In this sense, if we fix $f(x)$, then we can regard the inner product of $f(x)$ with $g(x)$ as a functional of $g(x)$, that is,

$$\mathcal{F}\{g(x)\} = (f, g) = \text{number}. \tag{E-8}$$

## III. LINEAR VECTOR SPACES

We have now defined the concept of an operator. Of course, such a definition is incomplete until we specify the types of functions we are going to let it act upon. For example, it makes no sense to let a differential operator $d/dx$ act on a discontinuous function, since $df/dx$ is not defined at the point of discontinuity.

Hence in practice one studies an operator $A$ by first specifying the class or type of function on which he will let $A$ operate. Such classes of functions usually possess the properties of a *linear vector space*, that is, a set of functions closed under the operations of addition and of multiplication by a scalar and containing a zero element.

## EXAMPLES

$C^0[a,b]$:    The set of all continuous functions $f(x)$ defined on the interval $x \in [a,b]$.

$C^n[a,b]$:    The set of all functions defined on $x \in [a,b]$ with $n$ continuous derivatives.

$L_2[a,b]$:    The set of all functions $f(x)$ defined on $x \in [a,b]$ such that

$$\int_a^b dx \, |f(x)|^2 < \infty.$$

(This is an example of a "Hilbert space".)

$L_p[a,b]$:    The set of all functions $f(x)$ defined on $x \in [a,b]$ such that

$$\int_a^b dx \, |f(x)|^p < \infty.$$

(This is an example of a "Banach space".) Note that for studying a differential operator of order $n$, we usually choose a corresponding space $C^{n-1}$. For an integral operator, the $L_p$ spaces are usually chosen.

The particular linear vector space or class of functions for which an operator $A$ is defined is referred to as its *domain* $\mathcal{D}$. Usually, $\mathcal{D}$ will be a subspace of a larger vector space $V$ (that is, the functions belonging to the class $\mathcal{D}$ will also belong to a more general class $V$). For instance, $A = d/dx$ is defined on the domain of all continuous functions $\mathcal{D} = C^0$. This class, however, is actually contained in the more general class of piecewise continuous functions $P$ (i.e., $\mathcal{D} \subset P$).

## IV. PROPERTIES OF OPERATORS

Consider now a linear operator $A$ defined on a domain of functions $\mathcal{D}$. Then we refer to $A$ as a *bounded* operator in this domain if

$$\frac{\|Af\|}{\|f\|} < \infty \qquad \text{for all } f(x) \in \mathcal{D}. \tag{E-9}$$

If $A$ is bounded on $\mathcal{D}$, then we can define its *norm* (an operator norm) as the largest of these values

$$\|A\| = \max_{f \in \mathcal{D}} \frac{\|Af\|}{\|f\|}. \tag{E-10}$$

Let us go one step further and associate an inner product $(f,g)$ with any two functions $f,g$ contained in the domain $\mathcal{D}$. Then we can define a *positive definite* operator as one for which

$$(f, Af) > 0 \qquad \text{for all } f \neq 0. \tag{E-11}$$

Using the inner product $(f,g)$, we can now introduce the very important concept of the operator $A^\dagger$ *adjoint* to $A$. We define the adjoint $A^\dagger$ of an operator $A$ as that operator $A^\dagger$ for which

$$(A^\dagger f, g) = (f, Ag) \qquad \text{for all } f,g \in \mathcal{D}. \tag{E-12}$$

Actually it may occur in practice that $A^\dagger$ and $A$ are defined over different domains—say $\mathcal{D}^\dagger$ and $\mathcal{D}$. Then this definition of the adjoint operator must be defined by

$$(A^\dagger f, g) = (f, Ag) \qquad \text{for all } g \in \mathcal{D}, \ f \in \mathcal{D}^\dagger. \tag{E-13}$$

Should

$$A^\dagger = A, \tag{E-14}$$

then we refer to the operator $A$ as *self-adjoint*. Self-adjoint operators are very popular in mathematics because they are easy to study, particularly with regard to their associated eigenvalue problem

$$A\psi_\lambda(x) = \lambda \psi_\lambda(x). \tag{E-15}$$

For instance, for self-adjoint operators the eigenvalues $\lambda$ are all real. Furthermore one can make statements regarding the eigenfunctions $\psi_\lambda(x)$, such as that they form a complete set. One reason for the preoccupation of mathematicians with self-adjoint operators concerns their role in quantum mechanics (all quantum mechanical observables correspond to self-adjoint operators).

## V. DIFFERENTIAL OPERATORS

Let's make a few more observations about the particular case of differential operators $L$, defined on some domain $\mathcal{D}$. For such operators, we can always construct the adjoint $L$ using integration by parts:

EXAMPLE: $L = d/dx$, $\mathcal{D} = C[a,b]$

$$(f, Lg) = \int_a^b dx \, f^*(x) \frac{dg}{dx} = f^*(b) g(b) - f^*(a) g(a) - \int_a^b dx \frac{df^*}{dx} g(x)$$

$$= f^*(b) g(b) - f^*(a) g(a) + \left( -\frac{df}{dx}, g \right). \tag{E-16}$$

Hence provided $J(f,g) \equiv f^*(b) g(b) - f^*(a) g(a) = 0$, we could identify the adjoint of $L$ as

$$L^\dagger = -\frac{d}{dx}. \tag{E-17}$$

How do we force $J(f,g)$ to vanish? (Here $J(f,g)$ is sometimes referred to as the *conjunct* of the operator $L$.) For a given problem, we will be given certain boundary conditions on $g(x)$ —say $g(a) = c_1$, $g(b) = c_2$. Hence by an appropriate choice of boundary conditions to be satisfied by $f(x)$ [in this case $f(a) = c_2^*$, $f(b) = c_1^*$] we can compel $J(f,g)$ to vanish. In general the boundary conditions we are required to place on $f(x)$ will not be the same as those we place on $g(x)$—that is, in the more abstract language developed earlier, the domain of definition of the adjoint operator $L^\dagger$, $f \in \mathcal{D}^\dagger$, will generally not be the same as the domain on which $L$ is defined.

A couple of definitions are useful here. If

$$L = L^\dagger, \tag{E-18}$$

then we refer to the operator $L$ as being *formally self-adjoint*. If the domains of definition are also identical

$$L = L^\dagger \qquad \text{and} \qquad \mathcal{D} = \mathcal{D}^\dagger, \tag{E-19}$$

then we refer to the operator $L$ plus the corresponding boundary conditions as being *self-adjoint*.

There are numerous fascinating problems and concepts that arise in the study of differential operators (which, of course, play the central role in most of physics). However it is most appropriate to refer the interested reader to one of the standard sources for more information:

(1) B. Friedmann, *Principles and Techniques of Applied Mathematics*, Wiley, New York, (1956).

(2) R. Courant and D. Hilbert, *Methods of Mathematical Physics*, Vol. I, Wiley-Interscience, New York (1956).

(3) J. W. Dettman, *Mathematical Methods in Physics and Engineering*, 2nd Edition, McGraw-Hill, New York (1969).

# Appendix F
## An Introduction to Matrices and Matrix Algebra

## I. SOME DEFINITIONS

One defines a *matrix of order* $(m \times n)$ to be a rectangular array of $m$ rows and $n$ columns

$$\underline{\underline{A}} = \begin{bmatrix} a_{11} & a_{12} & a_{13} & \cdots & a_{1n} \\ a_{21} & & \vdots & & \vdots \\ \vdots & & a_{ij} & & \vdots \\ a_{m1} & \cdots & \cdots & \cdots & a_{mn} \end{bmatrix}. \tag{F-1}$$

The *matrix elements* $a_{ij}$ will be identified by subscripts denoting their row $i$ and column $j$. If the matrix has the same number of rows as columns, it is said to be a *square matrix*; for example,

$$\underline{\underline{A}} = \begin{pmatrix} a_{11} & a_{12} & a_{13} \\ a_{21} & a_{22} & a_{23} \\ a_{31} & a_{32} & a_{33} \end{pmatrix}. \tag{F-2}$$

A *diagonal matrix* has nonzero elements only along its main diagonal:

$$\underline{\underline{A}} = \begin{bmatrix} a_{11} & 0 & 0 \\ 0 & a_{22} & 0 \\ 0 & 0 & a_{33} \end{bmatrix}. \tag{F-3}$$

A *tridiagonal matrix* would have nonzero elements only along its central three diagonals:

$$\underline{\underline{A}} = \begin{bmatrix} a_{11} & a_{12} & 0 & 0 & \cdots \\ a_{21} & a_{22} & a_{23} & 0 & \cdots \\ 0 & a_{32} & a_{33} & a_{34} & \cdots \\ \vdots & \vdots & \vdots & & \end{bmatrix}. \tag{F-4}$$

The *unit matrix* is the diagonal matrix with elements $a_{ij} = 1, i = j$:

$$\underline{I} = \begin{bmatrix} 1 & 0 & 0 & \cdots \\ 0 & 1 & 0 & \cdots \\ 0 & 0 & 1 & \cdots \\ \vdots & \vdots & \vdots & \end{bmatrix}.$$

(F-5)

For two matrices to be equal, each of their matrix elements must be equal:

$$\underline{A} = \begin{bmatrix} a_{11} & a_{12} & a_{13} & \cdots \\ a_{21} & a_{22} & \cdots & \\ \vdots & & & \end{bmatrix} = \begin{bmatrix} b_{11} & b_{12} & b_{13} & \cdots \\ b_{21} & b_{22} & \cdots & \\ \vdots & \vdots & & \end{bmatrix} = \underline{B}.$$

(F-6)

The *transpose* of a matrix is obtained by interchanging its rows and columns:

$$\left[\underline{A}^T\right]_{ij} = \left[\underline{A}\right]_{ji}$$

(F-7)

or

$$\underline{A}^T = \begin{bmatrix} a_{11} & a_{12} & a_{13} & \cdots \\ a_{21} & \ddots & & \\ a_{31} & & & \\ \vdots & & & \end{bmatrix}^T = \begin{bmatrix} a_{11} & a_{21} & a_{31} & \cdots \\ a_{12} & \ddots & & \\ a_{13} & & & \\ \vdots & & & \end{bmatrix}.$$

(F-8)

The *determinant* of a matrix is formed by taking the determinant of the elements of the matrix:

$$\det \underline{A} \equiv |\underline{A}| = \begin{vmatrix} a_{11} & a_{12} & a_{13} & \cdots \\ a_{21} & \vdots & & \\ a_{31} & \vdots & & \\ \vdots & & & \end{vmatrix}.$$

(F-9)

Of course, the determinant of a matrix is a scalar—that is, just a number.

One defines the *cofactor* of a square matrix for an element $a_{ij}$ by deleting the $i$th row and $j$th column, calculating the determinant of the remaining array, and multiplying by $(-1)^{i+j}$:

$$(\text{cof } \underline{A})_{23} = \text{cof} \begin{bmatrix} a_{11} & a_{12} & a_{13} & a_{14} & \cdots \\ a_{21} & a_{22} & a_{23} & a_{24} & \cdots \\ a_{31} & a_{32} & a_{33} & a_{34} & \cdots \\ a_{41} & a_{42} & a_{43} & a_{44} & \cdots \\ \vdots & \vdots & \vdots & \vdots & \end{bmatrix} = (-1)^{i+j} \begin{vmatrix} a_{11} & a_{12} & a_{14} & \cdots \\ a_{31} & a_{32} & a_{34} & \cdots \\ a_{41} & a_{42} & a_{44} & \cdots \\ \vdots & \vdots & \vdots & \end{vmatrix}.$$

(F-10)

We can construct the *adjoint* or *Hermitean conjugate* of a matrix by complex-conjugating each of its elements and then transposing as

$$\underline{A}^\dagger = (\underline{A}^*)^T \quad \text{or} \quad (a_{ij})^\dagger = (a_{ji}^*).$$

(F-11)

For example,

$$\underline{A}^\dagger = \begin{pmatrix} a_{11} & a_{12} \\ a_{21} & a_{22} \end{pmatrix}^\dagger = \begin{pmatrix} a_{11}^* & a_{12}^* \\ a_{21}^* & a_{22}^* \end{pmatrix}^T = \begin{pmatrix} a_{11}^* & a_{21}^* \\ a_{12}^* & a_{22}^* \end{pmatrix}.$$

If the determinant of a matrix vanishes, $\det(\underline{A}) = 0$, then the matrix $\underline{A}$ is said to be *singular*. If $\det(\underline{A}) \neq 0$, the matrix is said to *nonsingular*.

## II. MATRIX ALGEBRA

Two matrices of the same order may be *added* by adding their corresponding elements (the same holds for *subtraction*):

$$\underline{A} + \underline{B} = \begin{bmatrix} a_{11} & a_{12} & \cdots \\ a_{21} & & \\ \vdots & & \end{bmatrix} + \begin{bmatrix} b_{11} & b_{12} & \cdots \\ b_{21} & & \\ \vdots & & \end{bmatrix} = \begin{bmatrix} a_{11}+b_{11} & a_{12}+b_{12} & \cdots \\ a_{21}+b_{21} & & \\ \vdots & & \end{bmatrix}. \qquad \text{(F-12)}$$

In order for *matrix multiplication* to be possible, the number of columns of the first matrix must equal the number of rows of the second matrix. One then calculates the matrix elements of $\underline{C} = \underline{A} \cdot \underline{B}$ as

$$c_{ij} = \sum_{k=1}^{n} a_{ik} b_{kj}, \qquad \text{(F-13)}$$

or more explicitly

$$\underline{A} \cdot \underline{B} = \begin{bmatrix} a_{11} & a_{12} & a_{13} & \cdots \\ a_{21} & a_{22} & a_{23} & \cdots \\ a_{31} & a_{32} & a_{33} & \cdots \\ \vdots & \vdots & \end{bmatrix} \begin{bmatrix} b_{11} & b_{12} & b_{13} & \cdots \\ b_{21} & b_{22} & b_{23} & \cdots \\ b_{31} & b_{32} & b_{33} & \cdots \\ \vdots & \end{bmatrix} = \begin{bmatrix} a_{11}b_{11}+a_{12}b_{21}+\cdots \\ a_{21}b_{12}+a_{22}b_{22}+\cdots \\ \vdots \end{bmatrix}. \qquad \text{(F-14)}$$

Notice that matrix multiplication is not commutative—that is, $\underline{A} \cdot \underline{B} \neq \underline{B} \cdot \underline{A}$ in general.

A very important matrix concept is the *inverse* of a square matrix, $\underline{A}^{-1}$, which is defined by the relation

$$\underline{A}^{-1} \cdot \underline{A} = \underline{A} \cdot \underline{A}^{-1} = \underline{I}. \qquad \text{(F-15)}$$

The inverse can be calculated as

$$\underline{A}^{-1} = \frac{1}{|\underline{A}|} (\text{cof } \underline{A})^{T}. \qquad \text{(F-16)}$$

For example, consider

$$\underline{A} = \begin{pmatrix} 2 & 1 \\ -1 & 1 \end{pmatrix}.$$

Then

$$|\underline{A}| = 3,$$

while

$$(\text{cof } \underline{A})^{T} = \begin{pmatrix} 1 & 1 \\ -1 & 2 \end{pmatrix}^{T} = \begin{pmatrix} 1 & -1 \\ 1 & 2 \end{pmatrix}.$$

Hence

$$\underline{A}^{-1} = \frac{1}{3} \begin{pmatrix} 1 & -1 \\ 1 & 2 \end{pmatrix} = \begin{pmatrix} \frac{1}{3} & -\frac{1}{3} \\ \frac{1}{3} & \frac{2}{3} \end{pmatrix}.$$

Notice that if a matrix is singular, that is, $\det(\underline{A}) = 0$, then it has no inverse.
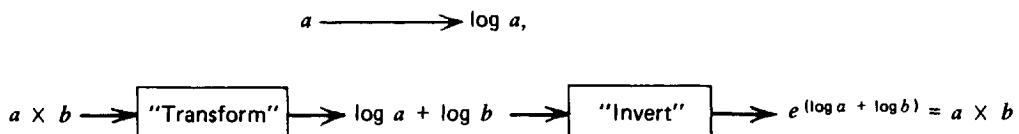
# Appendix G

# An Introduction to Laplace Transforms

## I. MOTIVATION

Differential equations play a central role in the description of most scientific phenomena. Moreover, in many cases these phenomena can be approximately described by a particularly simple type of differential equation—namely, those with constant coefficients. In this Appendix we will try to develop one of the most powerful tools for solving such equations: the application of integral transforms, and more specifically, the use of Laplace transforms to solve differential equations.

The analogy between the use of transform methods to solve differential equations and the use of logarithms to simplify arithmetic operations is quite striking. Suppose we wish to multiply two complicated numbers $a$ and $b$ together. Then an easy way to do this is to use logarithms

$$a \longrightarrow \log a,$$

$$a \times b \longrightarrow \boxed{\text{"Transform"}} \longrightarrow \log a + \log b \longrightarrow \boxed{\text{"Invert"}} \longrightarrow e^{(\log a + \log b)} = a \times b$$

That is, by first taking logs we have simplified the original problem, reducing it to a simple sum.

This is essentially the idea behind integral transform techniques. Suppose we symbolically represent the transform operation on a function as

$$f(t) \rightarrow \tilde{f}(s).$$

Then the idea is to transform the differential equation of interest

$$\frac{df}{dt} + \cdots \longrightarrow \boxed{\text{Transform}} \longrightarrow s\tilde{f}(s) + \cdots \longrightarrow \boxed{\text{Invert}} \longrightarrow f(t)$$

In this manner, the integral transform can be used to convert this differential equation into a simpler problem (frequently an algebraic equation) that can then be solved rather easily for the transformed solution. We then must somehow "invert" the transform to obtain the actual solution of interest.

**EXAMPLE:** Consider the very simple ordinary differential equation (familiar from prompt neutron reactor kinetics)

$$\frac{dn}{dt} - \left(\frac{\rho}{\Lambda}\right) n(t) = 0, \qquad n(0) = n_0. \tag{G-1}$$

Now define the Laplace transform of $n(t)$ as

$$\tilde{n}(s) = \int_0^\infty dt\, e^{-st} n(t) \equiv \mathcal{L}\{n\}. \tag{G-2}$$

To transform the ordinary differential equation (G-1), multiply by $e^{-st}$ and integrate over $t$

$$\int_0^\infty dt\, e^{-st} \frac{dn}{dt} - \left(\frac{\rho}{\Lambda}\right) \int_0^\infty dt\, e^{-st} n(t) = 0,$$

or using integration by parts

$$s\tilde{n}(s) - n(0) - (\rho/\Lambda)\tilde{n}(s) = 0,$$

but this is now just an algebraic equation which can be easily solved for

$$\tilde{n}(s) = \frac{n_0}{s - (\rho/\Lambda)}. \tag{G-3}$$

We must now "invert" $\tilde{n}(s)$ to find

$$n(t) = \mathcal{L}^{-1}\{\tilde{n}(s)\}. \tag{G-4}$$

By noting that

$$\mathcal{L}\{e^{-at}\} = \int_0^\infty dt\, e^{-st} e^{-at} = \frac{1}{s+a} \Rightarrow \mathcal{L}^{-1}\left\{\frac{1}{s+a}\right\} = e^{-at},$$

we find
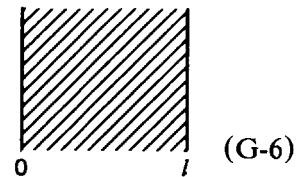
$$n(t) = n_0 \mathcal{L}^{-1}\left\{\frac{1}{s-(\rho/\Lambda)}\right\} = n_0 \exp[(\rho/\Lambda)t]. \tag{G-5}$$

**EXAMPLE:** Integral transforms can also be applied to the solution of partial differential equations. Consider, for example, the initial value problem for a nonmultiplying slab in one-speed diffusion theory

$$\frac{1}{v} \frac{\partial \phi}{\partial t} = D \frac{\partial^2 \phi}{\partial x^2} - \Sigma_a \phi(x,t)$$

Initial condition:     $\phi(x,0) = \phi_0(x)$

Boundary condition:   $\phi(0,t) = \phi(l,t) = 0.$



$$\tag{G-6}$$

Define the Laplace transform of $\phi(x,t)$ with respect to $t$ by

$$\tilde{\phi}(x,s) = \int_0^\infty dt\, e^{-st}\phi(x,t). \tag{G-7}$$

Now multiplying (G-6) by $e^{-st}$ and integrating over all times $t$, we find the transformed partial differential equation becomes

$$\frac{1}{v}[s\tilde{\phi}(x,s) - \phi(x,0)] = D\frac{d^2\tilde{\phi}}{dx^2} - \Sigma_a\tilde{\phi}(x,s).$$

Since the boundary conditions also depend on time, we must transform them to find:

$$\tilde{\phi}(0,s) = \tilde{\phi}(l,s) = 0.$$

Hence if we regard $s$ only as a parameter, the application of Laplace transforms has reduced our original *partial* differential equation (G-6) to an inhomogeneous *ordinary* differential equation in $x$

$$D\frac{d^2\tilde{\phi}}{dx^2} - \left(\Sigma_a + \frac{s}{v}\right)\tilde{\phi}(x,s) = \phi_0(x)$$

Boundary condition: $\quad \tilde{\phi}(0,s) = \tilde{\phi}(l,s) = 0 \tag{G-8}$

We can now solve this in any of the standard ways (e.g., eigenfunction expansions or Green's functions) to find $\tilde{\phi}(x,s)$, and then invert to find

$$\phi(x,t) = \mathcal{L}^{-1}\{\tilde{\phi}(x,s)\}. \tag{G-9}$$

Hence as should be apparent from these simple examples, Laplace transforms can be used to greatly simplify the solution of differential equations by: (a) transforming the original differential equation, (b) solving the transformed equation (which is now presumably a simpler equation such as an algebraic equation or ordinary differential equation) for the transformed solution, and (c) finally inverting the transformed solution to obtain the desired solution of the original equation. It is usually a straightforward task to complete the first two steps. The final step, that of inversion, can frequently be accomplished in a "cookbook" fashion by merely looking up the inverse in a table of Laplace transforms that some other fellow has had to work out. The general theory of how to perform such inversions from scratch is important, however, since the inverses of many of the functions one encounters in practice are not tabulated. However since it is heavily steeped in the theory of functions of a complex variable, we will avoid a detailed discussion of Laplace transform inversion via contour integration here and simply refer the reader to one of several standard texts.[1-3]

## II. "COOKBOOK" LAPLACE TRANSFORMS

We will now set up the recipes for solving differential equations with Laplace transforms. First we must determine just what types of equations we can consider:

(a) This can be any linear differential equation (ordinary or partial) in which the variable to be transformed runs from 0 to $\infty$. (Such as an initial value problem in time or a half-space problem in space.)

(b) We will further restrict ourselves to the study of differential equations with constant coefficients (i.e., the coefficients in the equation do not depend on the variable to which

we are applying the transform). This restriction can sometimes be relaxed; however we will not consider the more general problem of differential equations with variable coefficients here.

We will define the Laplace transform of a function $f(t)$ by

$$\tilde{f}(s) = \int_0^\infty dt\, e^{-st} f(t).$$ (G-10)

There are of course some restrictions on the type of function $f(t)$ and the ranges of values of $s$ for which this integral will be properly defined, but let's not worry about details at this stage of the game.

The general scheme for transforming the differential equation we are interested in solving is the same as before—namely, multiply by $e^{-st}$ and integrate over all $t$, using liberal integration by parts. One then solves the resulting transformed equation and attempts to invert the solution.

To facilitate in the preparation of a table of Laplace transforms (a cookbook), one merely takes the transforms of as many different functions as possible. Several useful transforms of general functions are:[4,5]

Derivatives: $\qquad\qquad \pounds\left\{\dfrac{df}{dt}\right\} = s\tilde{f}(s) - f(0).$ (G-11)

Recall that we obtained this by integration by parts. Further integration by parts yields

$$\pounds\left\{\frac{d^n f}{dt^n}\right\} = s^n \tilde{f}(s) - s^{n-1} f(0) - s^{n-2} f'(0) - \cdots - f^{[n-1]}(0).$$ (G-12)

Integration: $\qquad\qquad \pounds\left\{\displaystyle\int_0^t dt'\, f(t')\right\} = \dfrac{1}{s}\tilde{f}(s)$ (G-13)

Proof: $\quad \pounds\left\{\displaystyle\int_0^t dt'\, f(t')\right\} = \int_0^\infty dt\, e^{-st} \int_0^t dt'\, f(t') = -\dfrac{e^{-st}}{s}\int_0^t dt'\, f(t')\Big|_0^\infty + \dfrac{1}{s}\int_0^\infty dt\, e^{-st} f(t)$

$$= \frac{1}{s}\tilde{f}(s).$$

Differentiation by $s$: $\qquad\qquad \pounds\{tf(t)\} = -\dfrac{d\tilde{f}}{ds}$ (G-14)

Proof: $\qquad \dfrac{d\tilde{f}}{ds} = \displaystyle\int_0^\infty dt\, f(t)\dfrac{d}{ds}(e^{-st}) = -\int_0^\infty dt\, e^{-st}[tf(t)].$

Complex translation: $\qquad\qquad \pounds\{e^{at} f(t)\} = \tilde{f}(s-a)$ (G-15)

Proof: $\qquad \displaystyle\int_0^\infty dt\, e^{at} e^{-st} f(t) = \int_0^\infty dt\, e^{-(s-a)t} f(t) = \tilde{f}(s-a).$

Real translation: $\qquad\qquad \pounds\{f(t-a)\Theta(t-a)\} = e^{-as}\tilde{f}(s)$ (G-16)

where $\Theta(t)$ is the step function,

$$\Theta(t) = \begin{cases} 1 & t > 0 \\ 0 & t < 0 \end{cases}.$$

Several examples of more specific transform pairs are:

| $f(t)$ | $\tilde{f}(s) = \mathcal{L}\{f(t)\}$ |
|--------|--------------------------------------|
| $e^{-at}$ | $\dfrac{1}{s+a}$ |
| $\dfrac{t^n}{n!}$ | $\dfrac{1}{s^{n+1}}$ |
| $\sin \omega t$ | $\dfrac{\omega}{s^2 + \omega^2}$ |
| $\cos \omega t$ | $\dfrac{s}{s^2 + \omega^2}$ |
| $\Theta(t)$ | $\dfrac{1}{s}$ |
| $\delta(t)$ | $1$ |

Several other very useful relations[4,5] are

Convolution theorem:
$$\mathcal{L}\left\{ \int_0^t d\tau\, f(t - \tau)\, g(\tau) \right\} = \tilde{f}(s)\, \tilde{g}(s) \qquad \text{(G-17)}$$

(This result is useful for relating the inverse of the product of two transformed functions.)

Initial value theorem:
$$\lim_{t \to 0} f(t) = \lim_{s \to \infty} s\tilde{f}(s) \qquad \text{(G-18)}$$

Final value theorem:
$$\lim_{t \to \infty} f(t) = \lim_{s \to 0} s\tilde{f}(s) \qquad \text{(G-19)}$$

There are a number of reasonably complete tables of such transform pairs.[4,5] After obtaining the transformed solution, one can then turn to such tables in an effort to locate the desired inverse. However in many cases it will be necessary to proceed with a direct inversion calculation.

## REFERENCES

1. P. M. Morse and H. Feshbach, *Methods of Theoretical Physics*, Vol. 1, McGraw Hill, New York (1953), Chapter 4.
2. W. Kaplan, *Operational Methods for Linear Systems*, Addison-Wesley, Reading, Mass. (1962).
3. H. S. Carslaw and J. C. Jaegar, *Operational Methods in Applied Mathematics*, Dover, New York (1948).
4. P. A. McCollum and B. F. Brown, *Laplace Transform Tables and Theorems*, Holt, Rinehart, and Winston, New York (1965).
5. F. E. Nixon, *Handbook of Laplace Transforms*, Prentice-Hall, Englewood Cliffs, N. J. (1960).

# Appendix H

## Typical Nuclear Power Reactor Data

| General Data | PWR (W) | PWR (B&W) | PWR (CE) | BWR/6 | HTGR | LMFBR | GCFR | CANDU PHW |
|---|---|---|---|---|---|---|---|---|
| Thermal output (MWt) | 3411 | 3600 | 3800 | 3579 | 3000 | 2410 | 2530 | 1612 |
| Electrical output (MWe) | 1150 | 1200 | 1300 | 1200 | 1170 | 1000 | 1000 | 500 |
| Efficiency (%) | 33.7 | 33.3 | 34.2 | 33.5 | 39.0 | 39.0 | 39.5 | 31.0 |
| Fuel type | $UO_2$ | $UO_2$ | $UO_2$ | $UO_2$ | $UC, ThO_2$ | $PuO_2, UO_2$ | $PuO_2, UO_2$ | $UO_2$ |
| Coolant | $H_2O$ | $H_2O$ | $H_2O$ | $H_2O$ | He | Na | He | $D_2O$ |
| Structural material | Zircaloy | Zircaloy | Zircaloy | Zircaloy-2 | graphite | 316SS | 316SS | Zircaloy-4 |
| Moderator | $H_2O$ | $H_2O$ | $H_2O$ | $H_2O$ | graphite | — | — | $D_2O$ |
| **Core Data** | | | | | | | | |
| Active height (cm) | 366 | 363 | 381 | 376 | 634 | 91 | 148 | 410 |
| Equivalent active diameter (cm) | 337 | 352 | 363 | 366 | 844 | 222 | 270 | 680 |
| Height/diameter | 1.09 | 1.03 | 1.05 | 1.03 | 0.75 | 0.41 | 0.55 | 0.60 |
| Active core volume (l) | 32,800 | 37,600 | 40,000 | 63,910 | 354,000 | 6300 | 8510 | 130,000 |
| Average core power density (kW/l) | 104 | 95.7 | 95 | 56.0 | 8.4 | 380 | 297 | 12.4 |
| Fuel weight (kg) | 90,200 | 94,900 | 103,000 | 138,000 | 39,000 | 19,000 | 28,000 | 80,000 |
| Specific power (kW/kgU) | 37.8 | 37.9 | 36.9 | 25.9 | 77 | 126 | 90 | 20.4 |
| Burnup (MWD/MTU) | 33,000 | 33,000 | 33,000 | 27,500 | 98,000 | 100,000 | 100,000 | 10,000 |
| C.R. | 0.5 | 0.5 | 0.5 | 0.5 | 0.7 | 1.3 | 1.5 | 0.45 |
| **Fuel Assemblies** | | | | | | | | |
| Type | square bundles | square bundles | square bundles | canned-square bundles | hexagonal graphite prisms | hexagonal canned bundles | hexagonal canned bundles | pressure tube bundles |
| Number of Assemblies | 193 | 205 | 241 | 732 | 3944 | 394 | 347 | 473 |

| Fuel-element array | 17×17 | 17×17 | 16×16 | 8×8 | 132 pins | hex 12×12 | hex 17×17 | pressure tubes 8×50 |
|---|---|---|---|---|---|---|---|---|
| Assembly dimension (cm) | 21.4×21.4 | 21.7×21.7 | 20.3×20.3 | 14×14 | 35×79 | | | |
| Assembly pitch (cm) | 21.5 | 21.8 | 20.7 | 30.5 | 36.1 | 12.4 | 17.5 | 27.9 |
| Number of fuel elements/assembly | 264 | 264 | 236 | 63 | 132 | 217 | 225 | 28 |
| Total number of fuel locations | 50,952 | 54,120 | 56,876 | 46,116 | 35,496 | 85,464 | 77,031 | 13,244 |
| **Fuel Element Data** Type | Clad rod | Clad rod | Clad rod | Clad rod | Graphite UC, ThO$_2$ rod | Wire-wrap clad rod | Vented clad rod | Clad rod |
| Fuel-element pitch (cm) | 1.25 | 1.27 | 1.28 | 1.62 | | .725 | 1.14 | 1.65 |
| Fuel element O. D. (cm) | .94 | .96 | .97 | 1.25 | | .579 | .805 | 1.52 |
| Pitch/diameter | 1.32 | 1.32 | 1.33 | 1.30 | 1.56 | 1.25 | 1.41 | 1.08 |
| Clad thickness (cm) | .0572 | .0597 | .0635 | .0864 | | .038 | .0295 | .038 |
| Fuel-pellet diameter (cm) | .819 | .823 | .825 | 1.056 | 1.56 | .66 | .739 | 1.44 |
| Pellet-clad gap (cm) | .0082 | .010 | .0089 | .008 | | .012 | .012 | |
| Fuel enrichment | 2.1/2.6/3.1 | 2.91 | 1.9/2.4/2.9 | 2.2-2.7 | 93.5 | 10-15 | 10-15 | nat U |
| **Thermal Hydraulic Data** | | | | | | | | |
| System pressure (bar) | 155 | 155 | 155 | 72 | 50 | 14 | 86 | 89 |
| Coolant flow ($10^6$ kg/hr) | 62 | 68 | 72 | 47 | 5 | 50 | 10 | 23.9 |
| Average linear power density (W/cm) | 178 | 178 | 175 | 206 | 78.7 | 295 | 217 | 200 |
| Maximum linear power density (W/cm) | 426 | 483 | 410 | 440 | 229 | 492 | 390 | 528 |
| Average heat flux (W/cm$^2$) | 68.5 | 64 | 65 | 50.3 | 20.4 | 105 | 93 | 50 |
| Maximum heat flux (W/cm$^2$) | 183 | 168 | 173 | 111.5 | 58.3 | 237 | 168 | 115 |
| Minimum DNBR | 1.3 | 1.4 | 1.3 | 1.9 | — | — | — | |
| Inlet temperature (°C) | 300° | 300° | 296° | 269° | 337° | 380° | 332° | 249° |
| Outlet temperature (°C) | 332° | 333° | 328° | 286° | 755° | 552° | 642° | 293° |
| Maximum fuel temperature (°C) | 1788° | 2021° | 1882° | 1829° | 1410° | 2000° | 2200° | 1500° |

# Appendix I

## Units Utilized in Text

### BASE SI UNITS

| | | |
|---|---|---|
| length | meter | m |
| mass | kilogram | kg |
| time | second | s |
| thermodynamic temperature | kelvin | k |
| amount of substance | mole | mol |
| electric current | ampere | A |

### DERIVED SI UNITS

| | Derived SI Unit | SI Unit | British Unit |
|---|---|---|---|
| **Length** | | | |
| centimeter | cm | $10^{-2}$ m | 0.3937 in. |
| **Volume** | | | |
| cubic centimeter | $cm^3$ | $10^{-6}$ $m^3$ | 0.06102 $in.^3$ |
| liters | l | $10^{-3}$ $m^3$ | 0.03532 $ft^3$ |
| **Velocity** | | | |
| centimeter/second | cm/s | $10^{-2}$ $m \cdot s^{-1}$ | 0.03281 ft/s |
| **Mass** | | | |
| gram | g | $10^{-3}$ kg | $2.205 \times 10^{-3}$ lb |
| tonne | t(MT) | $10^3$ kg | 2205 lb |
| **Density** | | | |
| gram/cubic centimeter | $g/cm^3$ | $10^3$ $kg/m^3$ | 62.42 $lb/ft^3$ |
| **Force** | | | |
| newton | N | 1 $kg \cdot m \cdot s^{-2}$ | 0.2248 lbf |
| **Heat and energy** | | | |
| joule | J | 1 $N \cdot m$ | $9.478 \times 10^{-4}$ BTU |
| **Power** | | | |
| watt | W | 1 $J \cdot s^{-1}$ | 3.412 BTU/hr |

| | Derived SI Unit | SI Unit | British Unit |
|---|---|---|---|
| Pressure | | | |
| bar | bar | $10^5 \ N \cdot m^{-2}$ | 14.50 lbs/in$^2$ (psi) |
| Energy density | | | |
| joule/cubic centimeter | J/cm$^3$ | $10^6 \ J \cdot m^{-3}$ | 26.83 BTU/ft$^3$ |
| Power density | | | |
| watt/cm (linear) | W/cm | $10^2 \ W \cdot m^{-1}$ | 0.0305 kW/ft |
| watt/cm$^2$(energy flux) | W/cm$^2$ | $10^4 \ W \cdot m^{-2}$ | 0.930 kW/ft$^2$ |
| watt/cm$^3$ | W/cm$^3$ | $10^6 \ W \cdot m^{-3}$ | 28.35 kW/ft$^3$ |
| Temperature | | | |
| degree Celsius | °C | °K + 273.15 | °F = 1.8°C + 32 |
| Thermal units | | | |
| thermal conductivity | | W/m·K | 6.933 BTU/h·ft-°F |
| heat transfer coefficient | | W/m$^2$·K | 0.1761 BTU/h·ft$^2$-°F |
| specific heat capacity | | J/kg·K | $2.388 \times 10^{-4}$ BTU/1bm-°F |
| Electric charge | | | |
| coulomb | C | A·s | |

### NON-SI UNITS*

| | | |
|---|---|---|
| Electron volt (energy) | eV | $1.60219 \times 10^{-19}$J |
| Atomic mass unit (mass) | u | $1.66053 \times 10^{-27}$ kg |
| Bar (pressure) | bar | $10^5$ N/m$^2$ |
| Barn(cross section) | b | $10^{-24}$ cm$^2 = 10^{-28}$ m$^2$ |

*Recognized by the International Organization for Standardization

# Index